

# **Synthesis and Investigation of Novel p38 MAPK and DDR Kinase Inhibitors**

**Dissertation**

zur Erlangung des Doktorgrades  
der Naturwissenschaften

vorgelegt beim Fachbereich 14  
Biochemie, Chemie und Pharmazie  
der Johann Wolfgang Goethe-Universität  
in Frankfurt am Main

von

Sandra Röhm  
geboren in Seeheim-Jugenheim

Frankfurt am Main, 2020

(D30)

vom Fachbereich Biochemie, Chemie und Pharmazie der  
Johann Wolfgang Goethe-Universität Frankfurt als Dissertation angenommen

Dekan: Prof. Dr. Clemens Glaubitz  
Gutachter: Prof. Dr. Stefan Knapp  
Prof. Dr. Eugen Proschak

Datum der Disputation: 19.08.2020

„Was immer du tun kannst oder wovon du träumst – fange es an.  
In der Kühnheit liegt Genie, Macht und Magie“

- Johann Wolfgang von Goethe -

Für meine Familie

## Table of Contents

1	Introduction .....	1
1.1	An introduction to protein kinases .....	1
1.2	Kinase inhibitor design strategies .....	5
1.2.1	Canonical inhibitor binding modes .....	5
1.2.2	Non-canonical inhibitor binding modes .....	7
1.2.3	Allosteric kinase inhibitors .....	9
1.2.4	Covalent kinase inhibitors .....	12
1.3	Resistance to kinase inhibition .....	14
1.4	p38 MAPK structure function and regulation .....	15
1.4.1	Mitogene-activated protein kinase (MAPK) cascade .....	16
1.4.2	Activation and regulation of p38 MAPK signaling pathway .....	19
1.4.3	Downstream substrates of p38 MAPK and disease relation .....	20
1.5	A survey of p38 MAPK inhibitors in clinical trials .....	23
2	Selectivity guided inhibitor design approaches for p38 MAPK .....	32
2.1	Targeting a glycine-flipped mode .....	32
2.2	Targeting a leucine-flipped mode .....	34
2.3	Targeting rarely seen amino acid variations such as Ala157 .....	35
2.4	Targeting the switch-control residues .....	36
2.5	Targeting of folded P-loop conformations .....	40
2.6	The selection of the lead structure .....	43
2.6.1	Retrosynthetic analysis .....	44
3	Developing a chemical type-II inhibitor probe for p38 MAPK .....	46
3.1	Investigation of the p38 $\alpha$ / $\beta$ isoform selectivity .....	48
3.2	Discovery of a p38 MAPK type-II chemical probe and synthesis of a negative control .....	56
3.3	Conclusion .....	63
4	Exploring the $\alpha$ C-out and DFG-out pocket region .....	64
4.1	Biological testing .....	66
4.1.1	DSF Assay .....	66
4.1.2	NanoBRET <sup>TM</sup> assay .....	67
4.2	Synthesis of BIRB-fragment library .....	68
4.3	Results .....	71
4.3.1	Allosteric BIRB fragments .....	71
4.4	Convergent synthetic approach for back-pocket optimization .....	79
4.4.1	Description of steps i and ii .....	79
4.4.2	Description of steps iii and iv .....	80
4.4.3	Description of steps v and vi .....	83
4.4.4	Description of final step vii .....	88

4.5	Investigation of back-pocket modified VPC-00628 derivatives .....	89
4.5.1	Aliphatic moieties.....	89
4.5.2	Aromatic moieties.....	92
4.6	Kinome profiling and in cellulo off-target activity.....	96
4.7	Biological evaluation .....	97
4.7.1	Inhibitory effect on endogenous substrates .....	98
4.7.2	Metabolic stability and TNF- $\alpha$ release .....	99
4.8	Conclusion .....	100
5	Optimization of SR43 for DDR1/2 inhibition .....	101
5.1	Discoidin domain receptor kinase.....	101
5.1.1	Structure, function and regulation.....	101
5.1.2	DDR1/2 kinase inhibitors.....	103
5.2	Choosing the optimal building block.....	105
5.3	Chemistry .....	112
5.4	Results .....	115
5.4.1	Structure-activity relationship.....	115
5.4.2	Selectivity profiling.....	122
5.4.3	Further biological evaluation .....	126
5.5	Conclusion .....	127
6	Summary .....	128
7	Zusammenfassung.....	130
8	Experimental part.....	135
8.1	General and measuring instruments.....	135
8.1.1	General.....	135
8.1.2	Chemicals and solvents .....	135
8.1.3	Chromatographic methods .....	135
8.2	Biological Methods.....	137
8.2.1	Differential scanning fluorometrie (DSF)-assay .....	137
8.2.2	NanoBRET <sup>TM</sup> assay.....	137
8.2.3	Crystallization and structure determination .....	137
8.2.4	In silico studies .....	137
8.2.5	Selectivity screen.....	137
8.2.6	TNF- $\alpha$ release assay in human whole blood.....	138
8.2.7	In vitro metabolism studies.....	138
8.2.8	Western-blot analysis.....	138
8.2.9	E-cadherin staining.....	139
8.3	Experimental part of Chapter 3.....	139
8.3.1	VPC-00628 derivatives .....	139

8.3.2	Probe candidate and negative control compound .....	144
8.3.3	Synthesis of precursors .....	144
8.3.4	Synthesis of final compounds .....	149
8.4	Experimental part of Chapter 4 .....	151
8.4.1	Synthesis of BIRB-796 fragment library intermediates .....	151
8.4.2	Synthesis of final BIRB-796 fragment library compounds .....	157
8.4.3	DSF-assay results kinase panel ( $\Delta T_m$ values).....	167
8.4.4	Synthesis of intermediate compounds .....	170
8.4.5	Fmoc deprotections .....	200
8.4.6	Synthesis of final compounds .....	202
8.5	Experimental part of Chapter 5 .....	235
8.5.1	Synthesis of intermediates .....	235
8.5.2	Synthesis of final compounds .....	249
8.6	Results selectivity profiling .....	260
9	Abbreviations .....	285
10	References .....	286
11	Spectral data .....	307
12	Acknowledgements .....	407
13	Publications.....	408
14	Curriculum Vitae .....	409
15	Eidesstattliche Erklärung .....	411

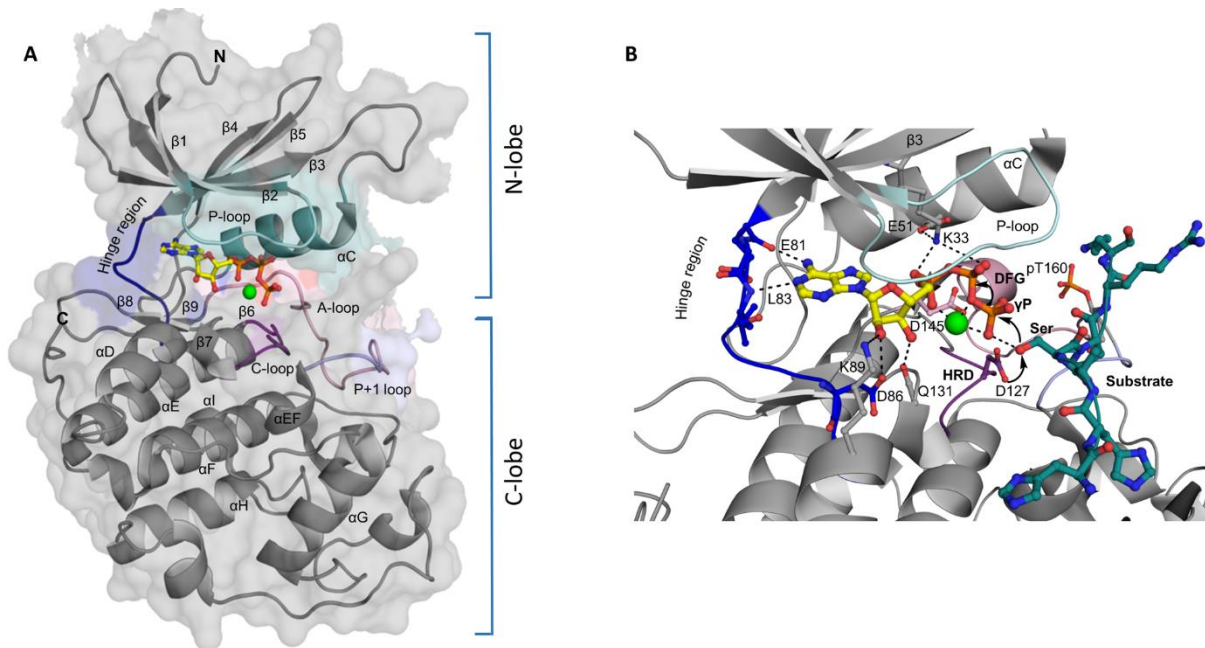
# 1 Introduction

## 1.1 An introduction to protein kinases

Posttranslational protein modifications, such as the protein phosphorylation, are of central importance for the regulation of fundamental cellular signaling processes, maintaining physiological functions of a cellular system. During signal transduction, proteins serve as molecular switches promoting signaling cascades or blocking their activation. In human cells, phosphorylation by a protein kinase is a common mechanism, important for turning signaling cascades on, whereas dephosphorylation by phosphatases is usually seen in terminating the signal.<sup>1</sup> With 518 proteins in total, kinases belong to one of the largest enzyme families in humans. About 2% of the human genes encode for protein kinases, which are responsible for 30% of all post translational protein modifications.<sup>2</sup> Protein kinases are evolutionary and structurally related enzymes that biochemically catalyze the transfer of the gamma-phosphate from adenosine triphosphate (ATP) to a corresponding substrate protein hydroxyl functionality and induce conformational changes that subsequently activate or inactivate their substrates. Depending on the type of hydroxyl moiety phosphorylated, kinases are divided in either serine/threonine- (Ser/Thr) or tyrosine- (Tyr) specific kinases. Upon primary sequence and conserved structural features, MANNING ET AL. classified the human kinome in 2002 in eight major kinase groups: 1) TK (tyrosine kinases), 2) CMGC (cyclin-dependant kinases, MAP kinases, glycogen synthase kinases, casein kinases, 3) CaMK (calcium/calmoduline dependent kinases), 4) AGC (protein kinase A, G, C), 5) CK1 (casein kinases), 6) STE (homologues of yeast sterile 7, sterile 11, sterile 20), 7) TKL (tyrosine kinase-like) and 8) RGC (receptor guanylate cyclases).<sup>2</sup> In addition, a large number of kinases share only weak sequence homology with any of these major groups and have been classified as “other” and atypical kinases. Around 10% of the human kinases are furthermore considered to be catalytically inactive pseudokinases. Pseudokinases share a typical kinase-domain fold, but they lack at least one conserved structural motif which is considered important for catalytic activity. Pseudokinases have essential signaling functions despite their lack of catalytic activity by acting as scaffolding proteins and allosteric regulators of catalytically active kinases.<sup>3</sup>

The overall protein kinase fold tertiary structure is highly conserved upon kinase family members and was first described in 1991 by the crystal structure of protein kinase A (PKA).<sup>2, 4, 5</sup> Commonly, protein kinases harbor two element core scaffolds, a conserved smaller N-terminal lobe (N-lobe) necessary mainly for ATP-binding and a larger C-terminal lobe (C-lobe) associated with peptide binding and catalysis (**Figure 1A**). Both, the N- and C-terminal lobes are connected to each other by a flexible linker, called hinge region, thus forming a hydrophobic cleft for ATP binding. The N-terminal part of a kinase consists of an assembly of five beta sheets, named  $\beta 1$ – $\beta 5$  and one alpha helix termed  $\alpha C$ . The most flexible part of a kinase is called P-loop, a glycine-rich region between sheets  $\beta 1$  and  $\beta 2$ . Structurally, the P-loop contains three conserved glycine residues in a common GXGX $\phi$ G motif, in which  $\phi$  is a hydrophobic, usually aromatic, residue and X refers to any amino acid. The flexibility of the P-loop is important for kinase-catalytic function, as it assists the binding of ATP by coordinating to the  $\gamma$ -phosphate moiety; positioning it right for phosphor transfer to a specific substrate. Another structurally conserved element, called AXK motif can be found in the  $\beta 3$  sheet, in which the lysine residue is crucial for catalysis. The active site lysine participates in a salt bridge with a conserved glutamate residue from the neighboring  $\alpha C$  helix, making further interactions with the  $\alpha$ - and  $\beta$ -phosphate groups of ATP, aligning these moieties for catalysis. Therefore, an intact lysine/glutamine salt bridge,

typically turning the  $\alpha$ C helix in an inward position ( $\alpha$ C-in), is a structural feature of an active kinase conformation and thus not seen in inactive kinases.<sup>6</sup>



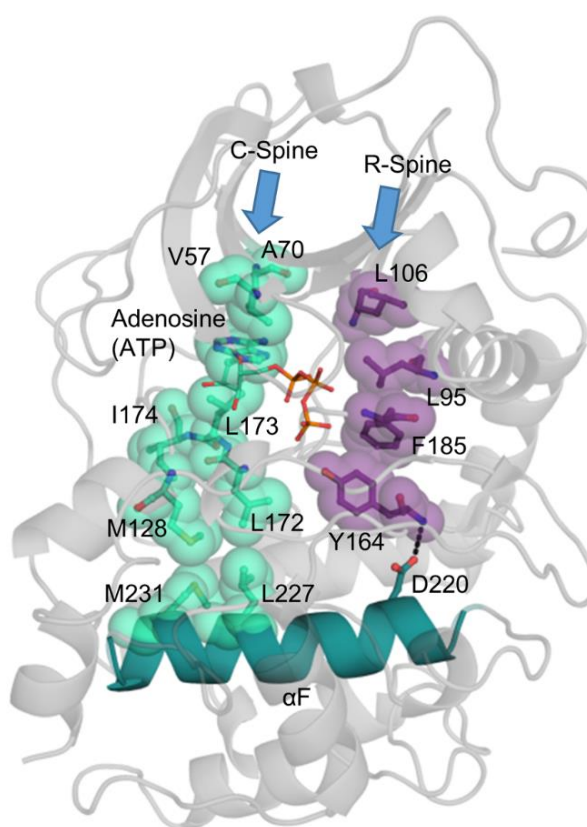
**Figure 1. Conserved kinase domain structure and catalytic center.** A) Kinase domain tertiary fold; important structural hallmarks are highlighted and exemplified by cyclin-dependent kinase 2 (CDK2, PDB: 1QMZ) in complex with ATP (stick-and-ball representation in yellow). The coordinated  $Mg^{2+}$  ion is shown as green sphere, whereas, the P-loop is highlighted in light teal,  $\alpha$ C helix in teal, hinge region in blue, A-loop in light pink, P+1 loop in light blue, C-loop in purple. B) catalytic machinery (PDB: 1QMZ). D127 acts as a base, deprotonating substrate serine residue, facilitating nucleophilic attack on  $\gamma$ -phosphate ( $\gamma$ P) of ATP. Substrate is highlighted in deep teal, phospho-tyrosine (pT160) residue in orange and important hydrogen bond interactions in black dashes.

The C-terminal part of the  $\alpha$ C helix is connected to sheet  $\beta$ 4 and  $\beta$ 5 of the C-lobe, which merges into the hinge region. Typically, the N-terminal beginning of the hinge region is marked by a single amino acid called “gatekeeper”, which controls the access to the hydrophobic back pocket of the enzyme. This gatekeeper residue is crucial for inhibitor binding and seen to be mutated in resistant kinases. Thus it will play a role in the development of kinase inhibitors and will be discussed in detail in the following sections. However, the hinge region recognizes the adenosine building block of ATP and connects it via two hydrogen bonds formed through the peptide backbone. Following this subdomain, the  $\alpha$ D helix marks the transition to the larger C-lobe of the kinase tertiary fold. In contrast to the N-lobe, the architecture of the C-lobe is mainly alpha helical and shares the conserved helices ( $\alpha$ D– $\alpha$ I), as well as the  $\beta$ -sheets ( $\beta$ 6– $\beta$ 9). The  $\alpha$ D helix is connected to the very hydrophobic  $\alpha$ E helix, further linked via  $\beta$ 6 to the catalytic loop with the essential Y/HRD motif. The conserved aspartate assists the catalysis by acting as base, deprotonating the hydroxyl functionality of either serine, threonine or tyrosine residue of a respective protein kinase substrate.<sup>7</sup> Therefore it facilitates the nucleophilic attack on the  $\gamma$ -phosphate of ATP, accelerating phosphate transfer and activation of kinase downstream targets. (**Figure 1B**) Following  $\beta$ 7– $\beta$ 9, a conserved DFG motif determines the beginning of the activation segment loop (A-loop). Depending on the activation state, the A-loop can adopt an open conformation, in which the DFG phenylalanine points outwards the ATP-binding pocket.<sup>8</sup> This conformation is also called DFG-in mode and allows substrate binding. However, the A-loop can also exist in a closed inactivated form, termed DFG-out, in which the phenylalanine residues directs inside the active binding side, prohibiting ATP binding. Further interactions are evident from the aspartate residue of the DFG motif, which coordinates to an  $Mg^{2+}$  ion that itself coordinates to the  $\beta$ - and  $\gamma$ -phosphates of ATP. The DFG motif



also builds up a hydrogen-bond network to the before described Y/HRD motif, linking these important regulatory elements. Overall the A-loop is part of a 20–40 residues long activation segment, which is accomplished by a short P+1 loop, important for docking of peptide substrates, typically ending with an APE-structure motif and the  $\alpha$ EF helix.<sup>8</sup> The activation segment contains also an important phosphorylation site, about 11 residues N-terminal to the APE motif, which is essential for enzyme activity of phosphorylation dependent Ser/Thr or Tyr kinases. The activation segment subdomain is connected to a very hydrophobic  $\alpha$ F helix, which is important in organizing the entire C-lobe. Finally, helix  $\alpha$ G,  $\alpha$ H and  $\alpha$ I are following which serve as docking site for substrate and regulatory proteins.

Kinases usually get activated by phosphorylation of each Ser/Thr or Tyr residues, accomplished by large structural rearrangements forcing ATP and substrate binding. Not obvious from sequence comparison, spatially related differences between active and inactive kinase forms are best described by the hydrophobic-spine concept introduced by TAYLOR ET AL.<sup>9-12</sup> By studying structure similarities between activated and inactivated kinase forms, they defined a conserved so-called hydrophobic regulatory spine (R-spine) and a catalytic spine (C-spine), found to be assembled in active kinases and to be interrupted in the inactive kinase state (**Figure 2**).



**Figure 2. Hydrophobic spine concept.** Important structural features of the kinase active state with assembled catalytic spine (C-spine) and regulatory spine (R-spine) are depicted by the crystal structure of PKA in complex with ATP (PDB: 1ATP). Hydrophobic residues of the R-spine and C-spine are highlighted in violet and cyan, respectively. The  $\alpha$ F helix is colored in deep teal.

The R-spine is made up of four non-contiguous residues each, one from  $\beta$ 4 and the  $\alpha$ C helix of the N-lobe as well as, each one residue from the DFG motif and the HRD motif of the C-lobe. The respective residues are of hydrophobic nature and align to a spatially well-defined motif conserved in every active kinase. In addition to the R-spine an aligned C-spine, was also found to be a structural hallmark of the catalytic active

kinase state. The C-spine consists of eight hydrophobic residues two from the N-lobe and six from the C-terminal lobe. Interestingly, the spine gets completed by the adenine ring of ATP, which set up a new coordination between the N- and C-lobe upon binding. In example of PKA, the R-spine is build up by Leu106 from  $\beta 4$  and Leu95 from the  $\alpha C$  helix of the smaller C-lobe as well as, by Phe185 from the DFG and Tyr164 from the Y/HRD motif of the N-lobe. The N-terminal part of the C-spine consists of Ala57 and Ala70 from  $\beta 2$  and  $\beta 3$ , respectively. It is bridged via adenosine ring of ATP to Leu173 from  $\beta 7$  and Ile174  $\alpha D$  from the C-lobe. The C-spine is further extended by Met128 ( $\alpha D$ ) interacting with Met231 from the  $\alpha F$  helix and in parallel by Leu172 ( $\beta 7$ ) networking with L227 ( $\alpha F$ ). The  $\alpha F$  helix is a very hydrophobic structure element, which spans the C-lobe and connects the C-spine to the R-spine, via hydrogen bond interaction by Asp220 to the backbone of Tyr164 (**Figure 2**). Therefore, it serves as a framework for assembling the active kinase state and is sometimes called  $S_2H$ -motif, or two spines and a helix motif.<sup>13</sup> The  $S_2H$ -motif is of fundamental architecture, which defines every kinase. However, when the kinase exists in its non-phosphorylated, inactive state the spines are interrupted in various feasible ways. In one example the active spine gets for instance broken by the DFG phenylalanine residue from the R-spine itself. In the non-phosphorylated state, the phenylalanine is able to protrude into the ATP binding site, filling the adenine pocket and disrupting the active spine.<sup>12</sup>

Overall, the inactive state of a kinase differs from the highly organized active conformation and displays a greater structural diversity.<sup>14, 15</sup> Whereas the active state is characterized mainly by an assembled R-spine and C-spine, in which the DFG motif adopts a DFG-in conformation and a salt bridge between the conserved lysine/glutamate pair is formed, heterogeneous conformations define the inactive kinase form.<sup>16</sup> The conformational plasticity and the activation state of a respective kinase can be influenced by the binding of substrates, inhibitors or regulatory proteins, as well as by posttranslational modifications.<sup>17</sup> Thus, the inactive state of a kinase can be described differently, but is mostly characterized by an inactive DFG-out conformation or by a DFG-in mode with the combination of an outward rotation of the  $\alpha C$  helix ( $\alpha C$ -out conformation), disrupting the catalytic lysine/glutamate salt bridge.<sup>16</sup>

Protein kinases are very important key players that control fundamental cellular processes, such as cell differentiation, migration and adhesion. They furthermore decide on the survival or apoptosis of a specific cellular system. Beside the physiological role in almost all signaling pathways, aberrant protein kinase activity, caused by transcriptional, mutational or post-translational protein modifications, is seen to play a role in carcinogenesis, tumor progression and in a diverse set of other diseases beyond cancer indications.<sup>18-23</sup> Thus, being interesting drug targets, kinases have been viewed long time as non-druggable because of the highly conserved ATP-binding side, prohibiting selective targeting of a single enzyme or even a small set of kinases. A breakthrough was achieved in 2001 when the first protein kinase inhibitor Imatinib (Gleevec®) was approved by the U. S. Food and Drug Administration (FDA) for the treatment of Philadelphia-chromosome-positive chronic myeloid leukemia (CML). Differently to the initial attempts, targeting the active ATP binding side of a kinase, this inhibitor interacts with an, at this time rarely seen, inactive conformation of cKIT, BCR-ABL and PDGFR kinases. As a result, Imatinib has good selectivity, by participating in contacts to less conserved amino acids.<sup>24</sup> Since these important insights, obvious from crystal structures available, novel enzyme pockets close to the ATP binding site were unveiled. The research efforts drastically increased and inhibitors of higher specificity emerged, leading to the overall approval of 48 small molecule protein kinase inhibitors. Almost half of these inhibitors reached the market in the last five years, and nowadays almost all pharmaceutical companies participate in research projects to explore structure novelties. As the clinical development of such inhibitors is quite risky and costly,<sup>25</sup> the approved kinase inhibitors commonly are of similar therapeutic indication, e.g. various forms of cancer and are usually of

limited scaffold diversity.<sup>18</sup> Hence, only eight small-molecule kinase inhibitors were successfully approved for non-cancer indications, such as rheumatoid arthritis (Tofacitinib, Baricitinib), Crohn disease and ulcerative colitis (Tofacitinib), idiopathic pulmonary fibrosis (Nintedanib), myelofibrosis and polycythemia vera (Ruxolitinib), chronic immune thrombocytopenia (Fostamatinib), chronic graft versus host disease (Ibrutinib, Sirolimus) and glaucoma (Netarsudil).<sup>26</sup> From the approved kinase inhibitors today, 25 target Tyr-kinases, 13 target Ser/Thr-kinases and 10 target non-receptor Tyr-kinases, providing extensive opportunities for further hit and lead identifications and drug development projects.<sup>27, 28</sup>

Major inhibitor design approaches are currently focusing on the design of inhibitors targeting either distinctive non-conserved structure elements, such as allosteric sites adjacent to the ATP-binding pocket or trapping unique kinase conformations.<sup>29-31</sup> Very promising is also the covalent targeting of specific cysteine residues located within or near the ATP-binding pocket.<sup>32, 33</sup> As many efforts have been made to synthesize inhibitors with improved potencies and cleaner selectivity profiles, the next section will give an overview on the kinase inhibitor design strategies applied. However, as about only 20% of the kinome has been targeted successfully yet,<sup>28</sup> new selective inhibitors are powerful tools to investigate so far undisclosed targets and help to get a better understanding on signaling-related biological processes and diseases.

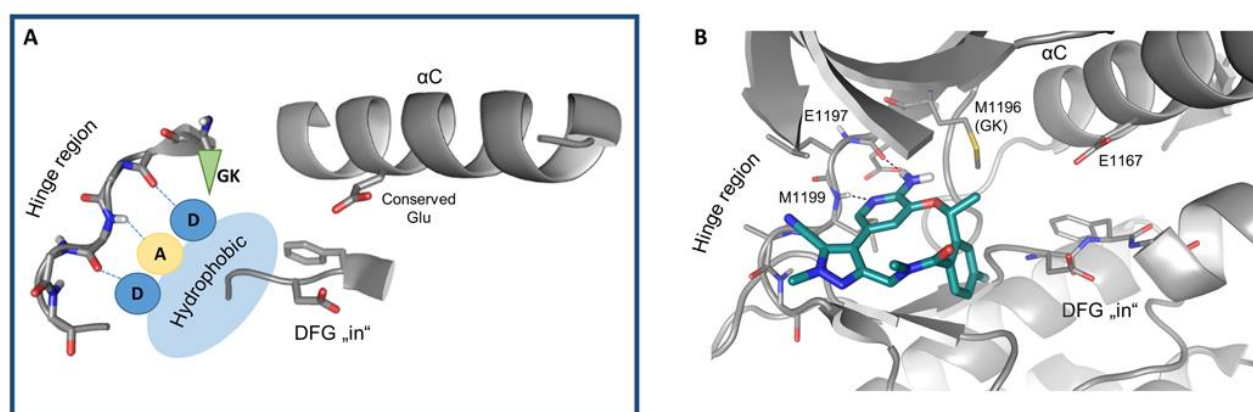
## 1.2 Kinase inhibitor design strategies

Stimulated by the success of the first approved small-molecule kinase inhibitor Imatinib, about two decades ago, different kinase inhibitor design strategies have been applied. However, the selective targeting of a respective kinase or even a set of kinases is challenging, because of the highly conserved ATP-binding site. In addition to selectivity issues, kinase inhibitors usually also have to compete with high intracellular ATP concentrations (about 1-5 mM) and therefore need to be of low nanomolar or picomolar potencies.<sup>34</sup> Different strategies targeting canonical and non-canonical binding modes have been described, as well as inhibitors targeting allosteric pockets distant from the ATP-binding site and novel approaches disclose also the covalent targeting of kinases. An overview on these interesting binding modes, successfully used for the synthesis of potent inhibitors is given in the following section. It further highlights chemical scaffolds typically used as pharmacophore, the advantages of targeting these inhibitor binding modes, as well as major drawbacks such as the resistance to kinase inhibitors.

### 1.2.1 Canonical inhibitor binding modes

The overall high plasticity of the kinase domain fold, opens the possibility to target different active or inactive states of a respective kinase, which have been first described by so-called canonical type-I inhibitors targeting the active state and by type-II inhibitors exclusively interfering with the kinase inactive state. A multitude of small molecule inhibitors found in the protein database (RCSB PDB, <http://www.rcsb.org/>),<sup>35</sup> bind in a canonical type-I mode to the ATP-binding region of the kinase (**Figure 3A**). The compounds are ATP mimetics, forming up between one to three hydrogen bonds with the conserved hinge-region amino acid backbone via hydrogen-bond donor or acceptor moieties. Similar to adenine in ATP, flat and hydrophobic residues such as heterocyclic structure moieties are preferred scaffolds. Type-I inhibitors directly compete with ATP and the displacement diminishes the catalytic activity of the kinase. Most frequently type-I inhibitors target the active state of a kinase with the DFG motif adopting a catalytically active DFG-in conformation. Examples of recognizing the inactive DFG-out form are also known, indicating the low

preference for the phosphorylated or non-phosphorylated state of the kinase.<sup>36, 37</sup> Although the design strategy is applicable to almost all kinases, the inhibitor selectivity is usually low because of the highly conserved nature of the kinase active site. The promiscuous binding of type-I compounds foster cross-reactivity with other kinases in different signaling pathways causing undesirable side effects. However, shape complementarity and sequence variations can be used for the development of inhibitors with high or restricted selectivity. Considering unique sequence features flanking the hinge, such as rare amino acids in hydrophobic regions I (HRI) and hydrophobic region II (HRII) and flexible structural elements, have been shown to provide selective inhibitors. Noteworthy is the gatekeeper residue, which controls the access to the hydrophobic back cavity. Small gatekeeper residues such as threonine give access to a larger back cavity and are present in only 5% of the kinome. Type-I inhibitors targeting this hydrophobic site have demonstrated to largely increase selectivity and potency over kinases with bulkier gatekeeper residues. Mutating this residue to glycine has further been used for the development of kinase specific ATP analogues.<sup>38</sup> A very promising macrocyclic compound, Lorlatinib (PF-06463922, **Figure 3B**), was approved in 2018 for the treatment of anaplastic lymphoma kinase (ALK)-positive metastatic non-small cell lung cancer.

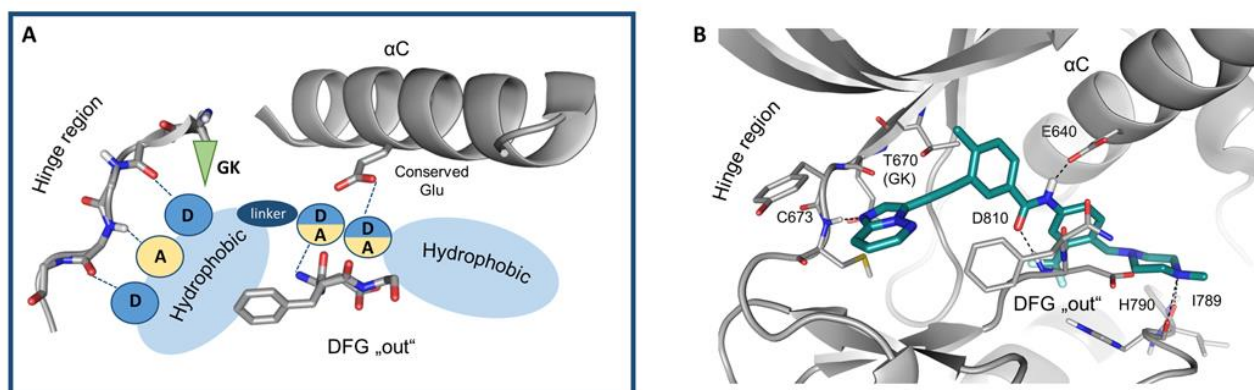


**Figure 3. Canonical type-I binding mode.** A) Pharmacophore model of type-I inhibitors. Important features of inhibitor binding to the hinge region (DFG-in mode) are depicted. Hydrogen bonds are highlighted in blue dashed lines, A = hydrogen bond acceptor (blue), D = hydrogen bond donor moieties (yellow), hydrophobic scaffold moieties (light blue), gatekeeper residue (GK, green). B) Macrocyclic type-I inhibitor Lorlatinib in complex with anaplastic lymphoma kinase (ALK, PDB: 4CLJ). Hydrogen bonds are shown as dashed lines (black).

The compound bound to the DFG-in/ $\alpha$ C-in state of ALK kinase and has further demonstrated to block Crizotinib-resistance in ROS1 mutations.<sup>39, 40</sup> In addition very interesting selective type-I inhibitors have been described by TAO ET AL., which shared a unique macrocyclic structure or bound covalent to the ATP-binding pocket as outlined in **Section 1.2.4**.<sup>32, 41</sup>

Canonical type-II inhibitors are ATP competitive and target the inactive state of a kinase targeting the more extended hydrophobic back pocket and allosteric sites. All type-II inhibitors also protrude into and stabilize the so-called deep pocket, which is accessible only in the inactive state of the kinase, e.g. the DFG-out or  $\alpha$ C helix-out state. The scaffold of a type-II small-molecule inhibitor can be viewed as an elongated version of a type-I inhibitor. The pharmacophore shares a common heterocyclic hydrophobic hinge-binding head group, which is connected with an amide, or urea-based linker group to a hydrophobic deep-pocket binding moiety. Besides the important hinge-binding interactions, donor/acceptor contacts with the highly conserved aspartate backbone from the DFG motif and glutamate, present in the  $\alpha$ C helix, are common.

**Figure 4A/B** highlights the binding mode and pharmacophore model of type-II inhibitors exemplified by the multikinase inhibitor Ponatinib in complex with the mast/stem cell growth factor receptor KIT.



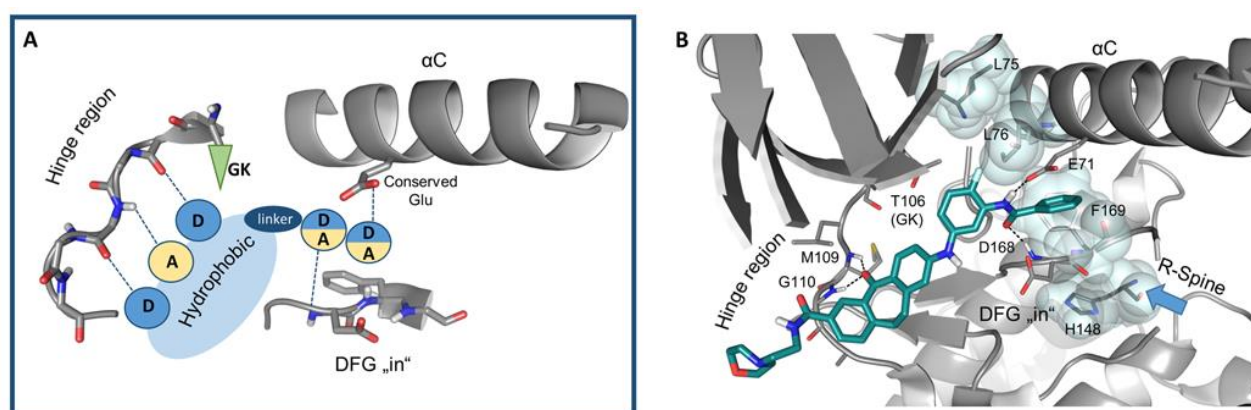
**Figure 4. Canonical type-II binding mode.** A) Pharmacophore model of type-II inhibitors. Important features of inhibitor binding to the hinge region and allosteric side (DFG-out mode) are depicted. Hydrogen bonds are highlighted in blue dashed lines, A = hydrogen bond acceptor (blue), D = hydrogen bond donor moieties (yellow), hydrophobic scaffold moieties (light blue), gatekeeper residue (GK, green). B) Type-II inhibitor Ponatinib in complex with KIT (PDB: 4U01). Hydrogen bonds are shown as dashed lines (black).

Designing type-II inhibitors provides access to more versatile scaffolds and helps to modulate the selectivity, as the allosteric region of a kinase is less conserved than the active site necessary for phosphotransfer catalysis. Furthermore, the inactive DFG-out state is not accessible in every kinase and inhibitors show a preference for kinases with small- and medium-sized gatekeeper residues. Studies demonstrated that type-II inhibitors show beneficial pharmacokinetics, such as slow off-rates and prolonged target-residence times.<sup>6</sup> Nonetheless, there are examples known in which type-I inhibitors are more efficient and selective than type-II inhibitors indicating that the general design strategy is not necessarily constructive.<sup>30, 42-47</sup> Targeting the DFG-in and DFG-out state are only two possible conformations, which can be targeted by small-molecule inhibitors. In the DFG-out state the aspartate of the DFG rotates  $\sim 180^\circ$  and moves  $\sim 5 \text{ \AA}$  away from the ATP-binding site, inactivating the kinase. The “in” and “out” state are only two extremes of a dynamic equilibrium of a multitude of possible conformations. Crystal structures highlight the intrinsic flexibility of the kinase domain, in complex with various inhibitors in different conformation states. However, the intracellular preferred conformation depending on the regulation and phosphorylation state of a given kinase is still unclear, as applicable experimental methods are lacking.<sup>3, 30, 45, 46</sup> Till now the type-II binding mode characterized by DFG-out conformation is the best studied inactive conformation that has been targeted by a large fraction of approved drugs such as the first approved inhibitor, Gleevec, for use in humans.<sup>24</sup>

### 1.2.2 Non-canonical inhibitor binding modes

Studies of the recent years came up with non-canonical binding modes broadening the spectra of selective inhibitor design. Type-I½ inhibitors (**Figure 5A**) have been described as a chimera of a type-I and a type-II inhibitor and share common features of both inhibitor types. Equivalent to type-I inhibitors, these compounds bind to the hinge region, pass the gatekeeper region and further target the hydrophobic back pocket.<sup>48</sup> They also show characteristic interactions seen for type-II inhibitors, for instance participating in donor and acceptor contacts with the DFG-glutamate residue and with the conserved aspartate residue from the  $\alpha C$  helix. Type-I½ inhibitors target the kinase either in the active DFG-in or the inactive DFG-out state, but have shown to preferentially shift the conformational equilibrium to the active “in” state.<sup>49</sup> Interestingly type-I½ inhibitors show similar pharmacokinetic features of type-II inhibitors, usually having

extended target residence times. The slow off-rates can be explained by the interaction with the back pocket and the higher degree of structural rearrangement necessary for adopting the DFG-out conformation.<sup>49</sup> A very promising type-I½ inhibitor is FS-694, a derivative of Skepinone-L, which induced a Gly110 backbone flip upon binding to the hinge region of p38 $\alpha$ . The phenyl residue further interferes with the R-spine and stabilizes the DFG-in conformation, greatly enhancing binding kinetics (**Figure 5B**).<sup>49</sup> Targeting the Gly110 flipped mode was accomplished with increased inhibitor selectivity and is described in detail in **Section 2.1**.



**Figure 5. Non-canonical type-I½ binding mode.** A) Pharmacophore model type-I½ inhibitor. Important features of inhibitor binding to the hinge region and allosteric side (DFG-in mode) are depicted. Hydrogen bonds are highlighted in blue dashed line, A = hydrogen bond acceptor (blue), D = hydrogen bond donor moieties (yellow), hydrophobic scaffold moieties (light blue), gatekeeper residue (GK, green). B) Type-I½ inhibitor FS694 in complex with p38 $\alpha$  (PDB: 4U01). Hydrogen bonds are shown as dashed lines (black).

In addition to the DFG-in and DFG-out state flexible structure elements in the kinase domain, e.g. the  $\alpha$ C helix, P-loop or the A-loop can adopt several inactive conformations, as confirmed by crystal structures and by small-molecule kinase inhibitors.<sup>3</sup> Besides canonical type-I, type-II and type-I½ binding, different ways of trapping inactive, high-energy conformations of a given kinase, creating less solvent exposed and more buried cavities can be found in diverse studies. For instance, the epidermal growth factor receptor (EGFR) receptor tyrosine kinase inhibitor Lapatinib binds to the DFG-in conformation of the kinase, interferes with the hydrophobic back pocket and simultaneously pushing the  $\alpha$ C helix out. As a consequence, the conserved lysine-glutamine ion pair, a hallmark of the active kinase state, gets interrupted. These large conformational rearrangements are unique to the EGFR kinase domain, finally turning the kinase catalytically inactive.<sup>50</sup> The same inactive-like conformation was not found in the before published EGFR inhibitor Erlotinib.<sup>50</sup> DFG-in inhibitor GSK2606414 targets a unique binding pocket created by an inactive activation segment conformation in the protein kinase R (PKR)-like endoplasmic reticulum kinase (PERK).<sup>51, 52</sup> Another interesting non-canonical binding mode was found for the Tyr-protein kinase Met (MET) inhibitor SGX523, which binds to a DFG-in conformation with excellent shape complementarity. In addition, SGX523 targets also a unique binding pocket created by an uncommon conformation of the activation segment.<sup>53</sup> Aromatic stacking interactions of the ligand with the conserved Tyr1248 residue moving the A-loop around 14 Å inside the phosphate-binding region of ATP thus inactivating the catalytic function of the kinase in a very specific mode. P-loop folded conformations have been found for a small set of kinases which share common aromatic amino acids such as tyrosine and phenylalanine at the tip.<sup>54</sup> In the active state of a particular kinase, these residues normally support the exact ATP binding required for catalysis. However, crystal structures disclosed that inhibitors could interact with these aromatic residues and capture the P-loop inside the ATP-binding active site. The folding of the P-loop allows the access to a less conserved enlarged pocket located between the P-loop and  $\alpha$ C helix.<sup>55</sup> It was exemplified that this allosteric pocket can be

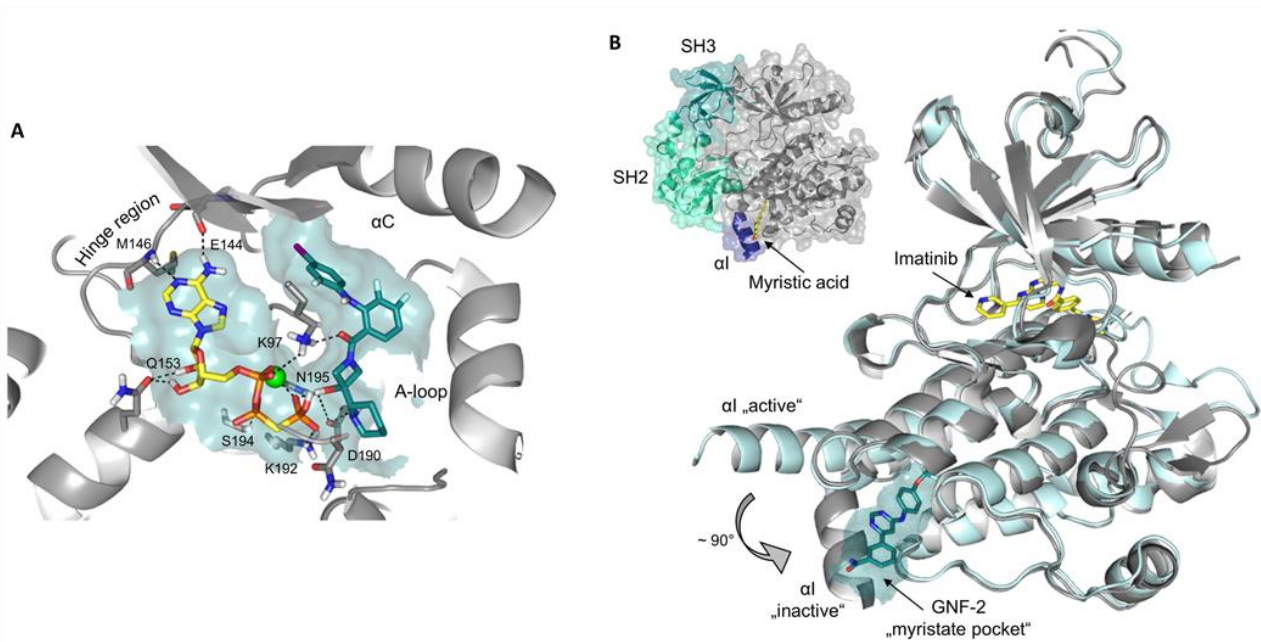
targeted in the case of the extracellular signal-regulated kinase 1/2 (ERK1/2) inhibitor SCH772984.<sup>56</sup> Although inhibitor binding is associated with high intrinsic ligand efficiency, no general design strategy for these very promising so-called type-IIB inhibitors has been established yet.<sup>31</sup> A more detailed discussion on these interesting folded P-loop binding modes, toward the selective inhibition of p38 MAPK, can be taken from **Section 2.5**. Overall inhibitors with non-canonical binding modes have demonstrated to deliver highly potent and selective compounds, which mostly benefit over canonical type-I and type-II inhibitors. However, as most of the compounds were found serendipitous, it stays a challenging task to find lead structures for the design of non-canonical inhibitors targeting a kinase of interest.

### 1.2.3 Allosteric kinase inhibitors

Allosteric inhibitors are classified according to the mode of action in type-III and type-IV inhibitors using topographically distant binding sites. Typically, type-III inhibitors target the allosteric back-pocket adjacent to the ATP-binding side, not participating in any hinge binding interaction. They are considered as steady-state ATP-uncompetitive or noncompetitive, as they can bind simultaneous with ATP to the active DFG-in conformation of a kinase, disrupting its catalytic function. Interestingly, for p38, focal adhesion kinase (FAK) and insulin-like growth factor 1 receptor (IGF1R) kinases, ATP competitive type-III inhibitors have been also reported, which interfere with and stabilize the inactive DFG-out state.<sup>57-59</sup> In this context, GOODWIN ET AL. reported about a *N*-phenylsulfonamide LIM domain kinase 2 (LIMK2) inhibitor, which shows high potency and exceptional selectivity binding allosterically to the DFG-out form of the tyrosine-like kinases (TKL).<sup>60</sup>

The most prominent example of an allosteric type-III inhibitor is the mitogen-activated protein kinase kinase 1/2 (MEK1/2) inhibitor Trametinib (GSK1120212). In clinical trials the compound demonstrated high efficiency, potency and target specific selectivity, and was the first allosteric kinase inhibitor approved by the FDA for the treatment of adult B-RafV600E and V600K mutated metastatic melanoma.<sup>61</sup> The tetrahydropyridopyrimidine derivative binds to the allosteric back pocket near the ATP-binding site, making hydrogen bonds to conserved  $\beta$ 3 lysine and hydrophobic contacts to the  $\beta$ 5 strand, the A-loop and the  $\alpha$ C helix. Upon inhibitor binding, the  $\alpha$ C helix gets displaced inhibiting of the kinase activity. The A-loop further adopts a closed conformation, prohibiting substrate binding.<sup>62, 63</sup> Encouraged by early successes, several allosteric MEK1/2 inhibitors have been synthesized, which are now being investigated in different phases of clinical trials, or are already approved, for various cancer indications, as non-small cell lung cancer (NSCLC), leukemia, thyroid and colon cancer (<https://clinicaltrials.gov/>).<sup>63, 64</sup> Approximately 30 MEK inhibitors in complex with a small molecule allosteric inhibitor and ATP have been crystallized so far, revealing important structural aspects of compound binding [<http://klifs.vu-compmedchem.nl/>]. **Figure 6A** exemplifies the allosteric pocket of Cobimetinib (GDC-0973) in complex with ATP (PDB: 4AN2). Cobimetinib and Trametinib, target the allosteric back cleft of MEK1/2 and both have been successfully used in combinatorial therapy with Vemurafenib in advanced melanoma patients, possessing BRAF V600E or V600K mutation.<sup>63, 65, 66</sup>

A potent and selective type-III tropomyosin receptor kinase A (TRKA) allosteric inhibitor has been recently published by BAGAL ET AL..<sup>67</sup> The inhibitor targets an allosteric pocket adjacent to the ATP-binding side accessible in the DFG-out conformation of the kinase. Hydrophobic interactions and hydrogen bonds stabilize the inhibitor, targeting also a less conserved juxtamembrane-domain region. As this structural feature and binding pocket is unique to TRKA, the compound showed superior selectivity over other TRK family members such as TRKB and TRKC.<sup>68, 69</sup> In addition, the compound has been demonstrated, to be effective in preclinical pain models and to benefit from fewer undesired off-target side-effects.<sup>67</sup>



**Figure 6. Examples of allosteric type-III and type-IV kinase inhibitors.** A) Type-III inhibitor Cobimetinib and ATP in complex with dual specificity mitogen-activated protein kinase kinase 1 (MEK1), view from N-terminal side (PDB: 4AN2). Inhibitor bound to the allosteric site is colored teal, ATP is shown in yellow, hydrogen bonds are depicted in black dashed lines,  $Mg^{2+}$  ion as green sphere. B) Overlay of active and inactive form of Abelson tyrosine-protein kinase (ABL) with Imatinib (yellow) bound to ATP-binding side and type-IV inhibitor GNF-2 (teal) bound to myristate pocket (PDB: 3K5V, 2Z6O). Movement of the  $\alpha 1$  helix is highlighted, image section on top shows autoinhibited ABL structure with SH2 (green cyan) and SH3 (teal) domain, myristic acid is shown in stick representation and colored yellow,  $\alpha 1$  in deep blue (PDB: 2FOO).

In contrast type-IV inhibitors bind reversibly to elements outside the active center, interfering with catalytic and regulatory domains at the interface of N- and C-terminal lobes.<sup>70</sup> These allosteric inhibitors are especially versatile, both from a structural point of view and from the different pockets and surfaces targetable. A unique binding mode has been observed for GNF-2, which binds to the myristate pocket located at the C-terminal lobe of ABL (**Figure 6B**).<sup>71</sup> The inactive form of ABL is typically stabilized by autoinhibition, which involves the binding of a myristoylated N-terminal residue of the SH3 domain of ABL to the allosteric myristate cleft of the kinase domain (**Figure 6B**, image section on top).<sup>72</sup> In the BCR-ABL fusion protein, found in chronic myelogenous leukemia (CML) and acute lymphoblastic leukemia (ALL), the autoinhibitory effect of the kinase gets lost, resulting in constitutive kinase activation.<sup>73, 74</sup> Thus, the allosteric inhibitor GNF-2 demonstrated to be beneficial, as it mimics the myristate residue disrupting the kinase catalytic function. The overall binding mode is very similar to the native autoinhibition state of ABL, as the N-terminal  $\alpha 1$  helix is rotated  $\sim 90^\circ$  inwards upon binding of GNF-2 and assembles the Src homology 2 (SH2) and Src homology 3 (SH3) domain.<sup>71, 72, 75-77</sup> In the active state this  $\alpha 1$  helix normally adopts an extended conformation, which was exemplified by the use of allosteric agonists.<sup>77</sup> Interestingly, GNF-2 binding can take place simultaneously with inhibitors targeting the ATP-binding pocket, e.g. the ATP-competitive inhibitors Nilotinib, Erlotinib or Imatinib. Numerous reports in oncology have therefore highlighted the benefits of a combinatorial drug therapy.<sup>71</sup> A very promising novel allosteric BCR-ABL inhibitor Asciminib (ABL001) has been published recently.<sup>78, 79</sup> The compound, similar to GNF-2, binds to the myristate pocket of BCR-ABL and is currently being studied in phase-I clinical trials, solely and in combination with Nilotinib, Dasatinib or Imatinib for the treatment of chronic myelogenous leukemia (CML) or Philadelphia chromosome-positive acute lymphoblastic leukemia (Ph+ ALL).<sup>78</sup> Besides the myristate pocket of BCR-ABL, differentially located allosteric sites in a diverse set of kinases have been targeted by allosteric



inhibitors.<sup>70</sup> Therefore, the following section should give an overview on interesting binding modes, published recently.

The activation of cyclin-dependent kinases (CDK's) is reliant on their regulatory proteins named cyclins and important for the cell cycle control.<sup>80, 81</sup> CDK's have been extensively studied as drug targets and their role in cancer and inflammatory diseases.<sup>81</sup> In the case of CDK2 it was shown that the kinase activity could be interrupted by targeting an allosteric pocket formed between the  $\alpha$ C helix and the  $\beta$ 3,  $\beta$ 4 and  $\beta$ 5 strand of the N-lobe.<sup>82</sup> The simultaneous binding of two 8-anilino-1-naphthalene sulfonate (ANS) inhibitors changed the orientation of the  $\beta$  strands, moving the  $\alpha$ C helix outwards which prohibited the binding of cyclins.<sup>83, 84</sup>

A different binding mode was found for PDK1 inhibitors RS1 and RS2, that targeted a hydrophobic motif called PDK1-interacting fragment (PIF) pocket, exclusively found at the N-terminal lobe of PDK1.<sup>85</sup> Upon binding, intrinsic kinase activity and the ability to phosphorylate downstream kinases got lost.<sup>86, 87</sup> Non-ATP competitive allosteric inhibitors of checkpoint kinase 1 (Chk1), such as the thioquinazolinones, have been reported to target an allosteric site adjacent to the  $\alpha$ D helix. As this pocket normally serves as substrate recognition site, the kinase cannot longer be activated.<sup>83, 88, 89</sup> AKT kinase (protein kinase B) is another interesting target for the design of allosteric inhibitors, as all previous described ATP-competitive inhibitors failed in clinical trials.<sup>77</sup> The complex architecture of AKT kinase opens the possibility to target the kinase in an allosteric way, as demonstrated by the antagonist MK-2206.<sup>90-92</sup> The compound bound via hydrogen bonds and  $\pi$ - $\pi$  interactions at the interface between AKT-kinase domain and its pleckstrin-homology (PH) domain and locked the kinase in an inactive conformation, which prohibited membrane association. In this closed so-called "PH-in" state the ATP binding pocket was no longer accessible.<sup>93-96</sup>

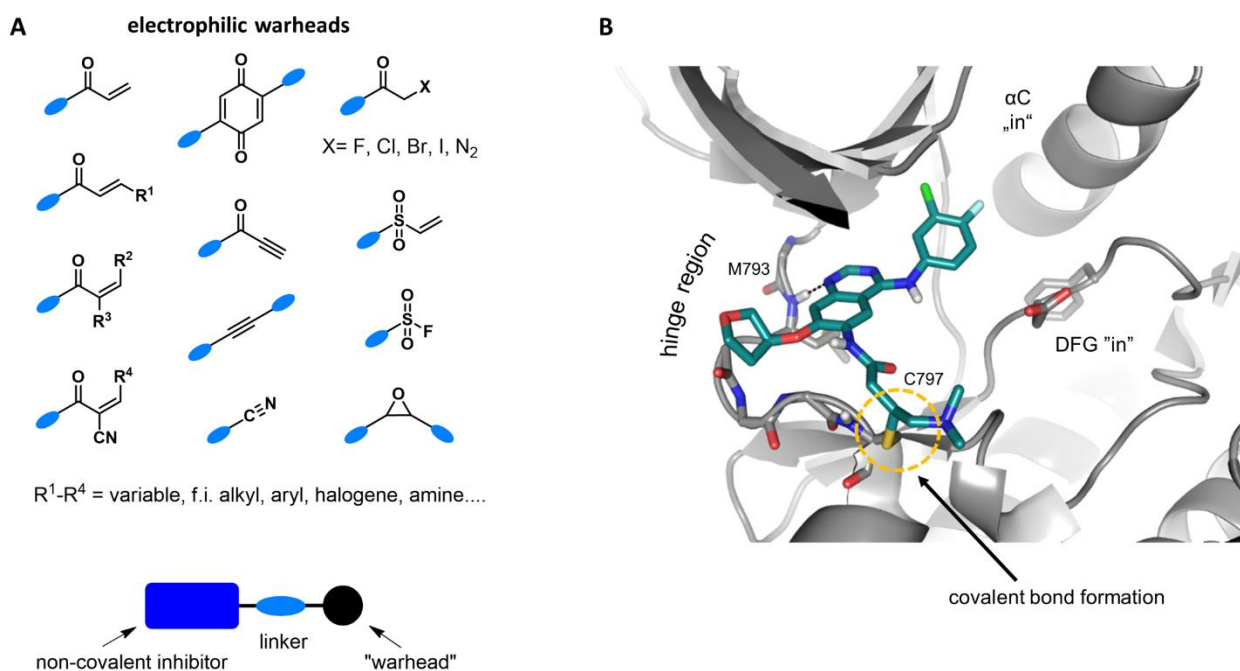
Epithelial growth factor receptor (EGFR) kinase gets activated by asymmetric dimerization in which the C-terminal lobe of the activator kinase activates the receiver kinase domain. EGFR can either build homo- or heterodimer-structures reminiscent on the cyclin-dependent activation of CDKs.<sup>97</sup> Thus, the recently published inhibitor EAI045 bound, similar CDK inhibitors did, to an allosteric pocket formed by the displacement of the  $\alpha$ C helix. The excellent selectivity of this allosteric inhibitor allowed the mutant selective targeting of EGFR with omission of the EGFR wild-type. In combination with Cetuximab, EAI045 potently inhibited the mutants EGFR(L858R/T790M) and EGFR(L858R/T790M/C797S), while all other available EGFR-kinase inhibitors developed resistance.<sup>98, 99</sup> Further allosteric EGFR inhibitors are in development and seem to open great opportunities for the treatment of non-small-cell lung cancer (NSCLC).<sup>100, 101</sup> The first potent and selective allosteric inhibitor of nuclear factor kappa-B kinase subunit beta (IKK $\beta$ ) which prevents IKK $\beta$  activation has been published by LIU ET AL. in 2018.<sup>102</sup> The inhibitor 3,4-dichloro-2-ethoxy-N-(2,2,6,6-tetramethylpiperidin-4-yl)benzenesulfonamide targets the inactive form of IKK $\beta$  by binding between the kinase domain and its ubiquitin-like domain, rendering the kinase unable for activation as suggested by molecular dynamic simulations. The compound also potently inhibited I $\kappa$ B $\alpha$  subunit phosphorylation and NF- $\kappa$ B activation in cells and opens the opportunity for the design of novel type-IV inhibitors.

In conclusion, allosteric inhibitors offer several advantages over canonical and non-canonical inhibitors. The compounds are usually highly selective, show slow-off rates and increase target-residence times by the occupation of less-conserved pockets. As the binding is mostly considered as ATP independent, compounds not necessarily require affinities in the low nanomolar or even picomolar range. Thus, even weak binders open great opportunities for a fast hit to lead generation. Unselective fragment hits are also considered as very useful research starting points. As binding more promiscuous to the kinome, novel kinase-drug targets

can be disclosed. Type-III and type-IV inhibitors are an alternative to overcome drug resistance, mainly occurring due to overexpression or mutations in the ATP site.<sup>61</sup> Drug resistance is the major issue in kinase-targeted therapies, as almost all FDA-approved kinase inhibitors lose their efficacy within several months or years.<sup>103</sup> The T315I gatekeeper mutation of BCR-ABL found in chronic-myelogenous leukemia (CML) for instance prohibited the binding of ATP-competitive inhibitors such as Imatinib.<sup>104-106</sup> Allosteric inhibitors represent a good therapeutic alternative as these target the kinase outside the ATP-binding site.<sup>107</sup> Furthermore, the minimal off-target pharmacology of allosteric inhibitors makes indications beyond cancer feasible.<sup>77</sup> Overall allosteric inhibitors are very useful alternatives to type-I, type-I½ and type-II inhibitors, although the design of novel lead structures remains a challenging task. As pharmacophore models and assay systems are missing, most allosteric inhibitors were found serendipitously in high-throughput screenings.<sup>30, 31</sup> Some examples of allosteric inhibitors were also predicted in molecular dynamic studies with the inactive apo-form of a given kinase. However, the lower availability of inactive apo-structures makes it difficult to identify new allosteric binding sites.

#### 1.2.4 Covalent kinase inhibitors

Current strategies for the design of selective ligands comprise, besides conventional inhibitors with a good shape complementarity and allosteric inhibitors, also covalent targeting of protein kinases. Typically, the scaffold of a reversible kinase inhibitor, which is known to bind with submicromolar affinity to the target of interest, is decorated with a flexible linker and an electrophilic “warhead” for covalent attachment.<sup>32, 108</sup> Covalent inhibitors can therefore be divided in type-I, type-II or allosteric inhibitors, as described above and have been designed mainly for covalent attachment to cysteine and lysine side-chain amino acids. Upon binding, the reversible part of the inhibitor first targets the kinase-binding site in a non-covalent manner. If a reactive cysteine or lysine residue is in proximity, covalent bond formation will take place in a second step, improving the selectivity over kinases having an equivalent side chain residue.<sup>32</sup> Numerous “warheads” have been explored acting as electrophiles either in a Michael reaction or in a nucleophilic addition or substitution reaction (**Figure 7A**). Thus,  $\alpha,\beta$ -unsaturated compounds such as substituted and unsubstituted acrylamides, acrylates, alkynyl amides, vinyl sulfonates, propargylic acids and quinones have been used for conjugated addition. For the nucleophilic displacement  $\alpha$ -haloketones were used frequently, together with alkynes, nitriles, oxiranes and sulfonyl halogenids.<sup>32, 109</sup> The different electrophiles allow, to adjust the reactivity with the appropriate cysteine residue targetable and to overcome competition with other cellular ubiquitous nucleophiles. The linker between the warhead and the reversible inhibitor moiety supports the selective binding to a given cysteine thiol group and should therefore display limited flexibility.<sup>33</sup> A common strategy applied is to target cysteine residues in vicinity to the ATP-binding site. Depending on the activation state of a kinase, cysteine residues in the P-loop, hydrophobic pocket, gatekeeper-, hinge- and DFG-region, as well as in the catalytic loop and front pocket are accessible. However, not every cysteine residue exhibits the same reactivity in covalent-bond formation, as solvating effects inside the binding pocket and the conformational orientation of the cysteine side-chain residue contribute to the overall binding.<sup>110</sup>



**Figure 7. Structural hallmarks of covalent kinase inhibitors.** A) Common electrophilic "warheads" used in the synthesis of covalent inhibitors (top) and schematic representation of inhibitor design (bottom). Non-covalent type-I, type-II or allosteric inhibitor colored in dark blue, linker depicted in light blue and warhead moiety in black. B) Crystal structure of Afatinib (BIBW2992) bound to EGFR kinase (PDB: 4G5J). Inhibitor is colored teal and shown in stick representation, covalent bond formation with C797 and hydrogen bond with hinge M793 are highlighted.

Covalent inhibitors offer the advantage to target a given kinase in a highly selective, potent and efficient way. In addition, they show prolonged pharmacodynamics, incapacitating kinase catalytic function till new protein is expressed.<sup>32, 111</sup> Studies on lung cancer patients with EGFR(L858R/T790M) kinase mutations have demonstrated that covalent inhibitors such as AZD-9291<sup>112</sup> can also help to overcome drug resistance, whereas first generation ATP-competitive inhibitors usually showed loss of efficacy after 12-18 months of treatment.<sup>113</sup> However, mutation of the targeted cysteine residue can also occur, prohibiting covalent attachment of the inhibitor.<sup>113</sup> Despite mayor concerns that covalent inhibitors might have more side effects and may be toxic, resulting from unwanted modification of off-target proteins, five covalent protein kinase inhibitors have been approved by the FDA currently and demonstrated an overall good *in vivo* efficacy. The first approved covalent inhibitor was Afatinib in 2013, for the treatment of metastatic non-small-cell lung cancer (NSCLC) patients. The aniline-quinazoline derivative covalently binds to C797 in the solvent exposed site of the ATP-binding pocket (**Figure 7B**, PDB: 4G5J), potent and selectively inhibiting the ErbB-family members: EGFR, HER2, ErbB4, as well as EGFR mutants, as the Leu858Arg/Thr790Met double mutant.<sup>32, 114-116</sup> Following these first successes, Ibrutinib was approved in the same year for the treatment of B-cell malignancies covalently targeting Bruton tyrosin kinase (BTK),<sup>117, 118</sup> Osimertinib was approved in 2015 to treat NSCLC with EGFR L858R and T790M mutations,<sup>119</sup> as well as Neratinib which demonstrated to be effective in the treatment of HER2 positive breast cancer.<sup>120-122</sup> Finally, Dacomitinib was approved in 2018 for the treatment of NSCLC, irreversible and covalently binding to EGFR kinase.<sup>123, 124</sup> Today, novel approaches focusing on the design of covalent reversible inhibitors, in which the initially covalent bond formed is destabilized, thus promoting reverse reaction after a specific on-target time. Typically, electronic deficient Michael acceptor groups, for instance carrying a nitrile at the  $\alpha$ -position, are in use. After conjugated addition of the cysteine thiol group, the covalent bond gets weakened due to the increased CH-acidity of the  $\alpha$ -position. Consequently, the corresponding proton can be easily deprotonated under

physiological conditions, promoting the reverse reaction by the conjugated base anion and thereby releasing the unmodified inhibitor.<sup>33, 125</sup> The concept of reversible covalent inhibitors is very promising to avoid potential toxic side effects and was successfully applied for instance for the design of Janus kinase 3 (JAK3) inhibitors.<sup>126</sup> In the latter study, the reverse reaction was confirmed experimentally and also the equilibrium state of covalently bound and unbound form of the inhibitor has been validated in crystal structures.<sup>126</sup>

In conclusion, the designs of allosteric and covalent kinase inhibitors are very useful alternatives to conventional canonical type-I and type-II inhibitors. Since these compounds are generally very potent and selective, and demonstrated to be effective in a cellular environment and *in vivo*, they show advantageous properties. Therefore, covalent inhibitors might broaden our understanding of kinase regulation mechanisms during inhibition and resistance and guide targeted cancer drug therapies in future.

### 1.3 Resistance to kinase inhibition

The last 30 years of kinase drug research lead to the approval of 48 kinase inhibitor drugs, mostly for the treatment of specific forms of cancer. However, the understanding of kinases involved in signaling cascades related to a multitude of cancers is still in its infancy, especially due to the heterogeneity of late-stage cancer cells, showing multiple mutations, genomic instability and chromosomal aberration.<sup>127</sup> Drug resistance to kinase targets turns out to be problematic, as nearly all FDA-approved inhibitors lose their efficacy within month or a few years of treatment.<sup>103</sup> The resistance occurs mainly due to changes in the expression rate of the protein target, which can also be bypassed by the upregulation of compensatory signaling pathways. In addition, mutations have been found frequently in the kinase domain and especially noteworthy is the gatekeeper point mutation found in several kinases targets, such as BCR-ABL,<sup>128</sup> fibroblast growth factor receptor 1 (FGFR1),<sup>129</sup> platelet-derived growth factor receptor alpha/beta (PDGFR $\alpha/\beta$ ),<sup>130</sup> Fms-like tyrosine kinase 3 (FLT3),<sup>131</sup> KIT<sup>132</sup> and ALK.<sup>133</sup> The gatekeeper is a unique structural hallmark of a kinase, which controls the access to the hydrophobic back pocket, depending on its shape and size. As the gatekeeper residue, as well as the back pocket, has been targeted commonly with different canonical type-I and type-II inhibitors, changes in the amino acid side chain mostly diminishes binding, while the kinase stays catalytically active.<sup>3, 127</sup> A classic example of this case is the gatekeeper mutation T315I found in BCR-ABL, responsible for Imatinib resistance.<sup>105</sup> Beside the steric clash with the inhibitor some examples are known, in which the gatekeeper mutation drastically increased the binding affinity of ATP. As a consequence, EGFR inhibitors were for instance no longer potent enough for the competitive displacement of ATP and lost their efficacy during treatment.<sup>134, 135</sup>

Research progress demonstrated the cancer dependence of kinase targets and revealed kinases, which are also associated with a large number of non-life threatening diseases.<sup>28</sup> Nevertheless, the function and regulation of many kinases is still unknown, as only a small fraction of the kinome has been studied successfully yet and selective inhibitors are largely missing. Small molecule chemical probes, showing exclusive selectivity for a target and are also effective *in vitro* are of interest, as a vulnerable tool to study kinase signaling processes.<sup>136</sup> Chemical probes will therefore help to explore kinase drug targets in a more promising way, assisting inhibitor development. An interesting target, seen to be associated with non-life threatening diseases, such as inflammatory, autoimmune or neuronal diseases, is mitogen-activated protein kinase 14 (p38 MAPK). Although being a very prominent kinase target, no p38 inhibitor has ever been successfully approved to the market and highly selective chemical probes are missing to study its implication

on signaling beyond its phosphotransferase activity. Therefore, the following sections will focus in more detail on the structure, function and regulation of this very promising target.

#### 1.4 *p38 MAPK structure function and regulation*

The mitogen-activated protein kinase (MAPK) p38 was first identified in 1994 as a 38 kDa protein which was phosphorylated on tyrosine upon stimulation with lipopolysaccharide (LPS) in bacterial cells by HAN ET AL.<sup>137</sup> Using sequence analysis, they disclosed, that p38 belongs to the family of mitogen-activated protein kinases and that it is a homologue of the osmosensing gene *Hog1*, found in *Saccharomyces cerevisiae*. At the same time, other researchers reported about a so-called reactivating kinase (RK) which activated MAPK-activated protein kinase 2 (MK2) upon stimulation with heat shock, osmotic stress, arsenite, IL-1 or TNF- $\alpha$ .<sup>138, 139</sup> Besides RK, p38 MAPK is also named as stress-activated protein kinase SAPK or cytokine suppressive anti-inflammatory drugs binding protein (CSBP), because of its ability to interact with pyridinyl-imidazole drug derivatives, e.g. SB203580, known to suppress the release of pro-inflammatory cytokines, such as IL-1 and TNF- $\alpha$  in LPS-stimulated human monocytes.<sup>140</sup>

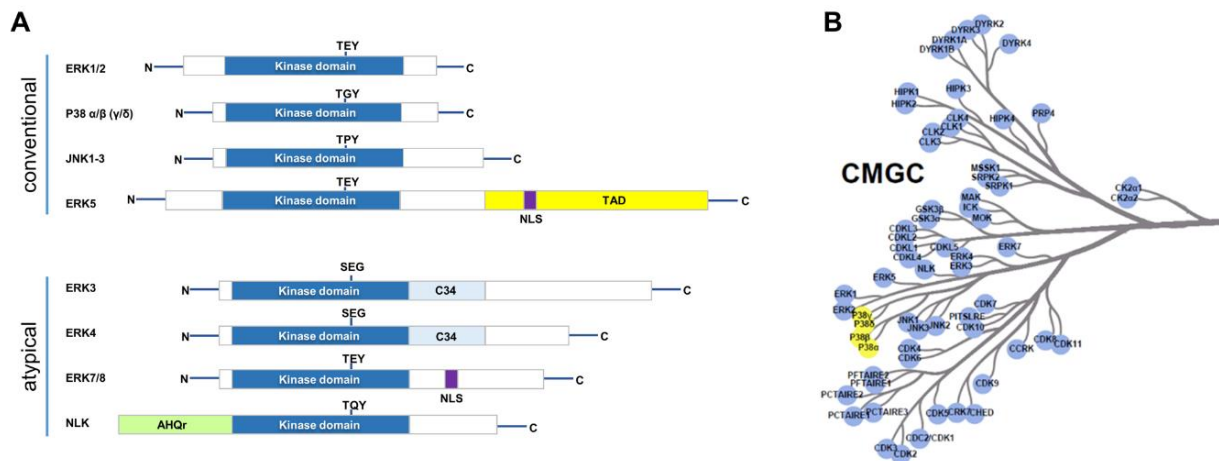
Since these initial studies four isoforms of mammalian p38 MAPK have been identified, namely p38 $\alpha$  (MAPK14, SAPK2a), p38 $\beta$  (MAPK11, SAPK2b),<sup>138, 141</sup> p38 $\delta$  (MAPK13, SAPK4)<sup>142, 143</sup> and p38 $\gamma$  (MAPK12, SAPK3).<sup>144, 145</sup> The isoforms are encoded by different genes and vary in their substrate specificities, tissue expression and cellular localization. p38 $\alpha$  is ubiquitously expressed and can be found for instance in tissues of brain, heart, muscle, placenta and pancreas. However, a lower expression level is found in liver, lung and kidneys. p38 $\alpha$  is localized mainly in the cytosol, but is also able to translocate to the nucleus thereby interfering with components of the transcriptions machinery. Furthermore, it is present in different subcellular compartments, e.g. the mitochondria. p38 $\alpha$  shows a sequence homology of 75% to its  $\beta$ -isoform, which is expressed in a lower content and is acting in a more tissue specific way. The highest levels of p38 $\beta$  exist in the brain and heart, whereas lower levels are detectable in tissues of lung, liver, placenta, muscle, pancreas and kidney. In general, isoforms p38 $\gamma$  and p38 $\delta$  are more similar to each other sharing 70% identity and only 60% in identity to p38 $\alpha$  and p38 $\beta$ . p38 $\gamma$  is tissue-specific expressed in the skeletal muscle and p38 $\delta$  in endocrine glands such as pancreas, testicles, as well as in the small intestine, kidney and lung.<sup>146-148</sup> High cellular levels of p38 $\delta$  exist also in neutrophils and CD4+ T-cells of the immune system and in endothelial cells.<sup>149</sup> The domain structure of p38 has a total length of 360 to 367 amino acids, a typical N-terminal MAPK signature and a kinase domain. Four variants produced by alternative splicing of p38 $\alpha$  exist and are listed on Uniprot (<https://www.uniprot.org/>), namely CSBP1, Mxi2, Exip and Isoform 5. For p38 $\beta$  one splicing variant, called p38 $\beta$ 2, was identified. The isoforms are mostly identical to p38 $\alpha$  or p38 $\beta$ , harboring unique differences in their amino acid structure that partially alter substrate specificities. In example the nuclear protein Mxi2 owns a special C-terminus of 17 amino acids in length and was reported to directly bind to the MAPK ERK1/2, assisting its nuclear import and activation.<sup>150-152</sup>

The p38 signal-transduction pathway is of central importance regulating fundamental cellular processes such as the biosynthesis of pro-inflammatory cytokines, cell migration and cellular differentiation. Therefore, p38 signaling contributes significantly to a normal physiological regulation of the immune system. A plethora of extracellular stimuli and cellular substrates upstream influence the activation and regulation of p38 MAPK, which is mainly organized in a so-called mitogen-activated protein kinase cascade. The following section gives an overview on the activation, function and regulation of p38 MAPK. It further

discusses important downstream targets effected by this pathway and how dysregulated and overexpressed p38 MAPKs transduce to inflammatory or autoimmune diseases.

### 1.4.1 Mitogene-activated protein kinase (MAPK) cascade

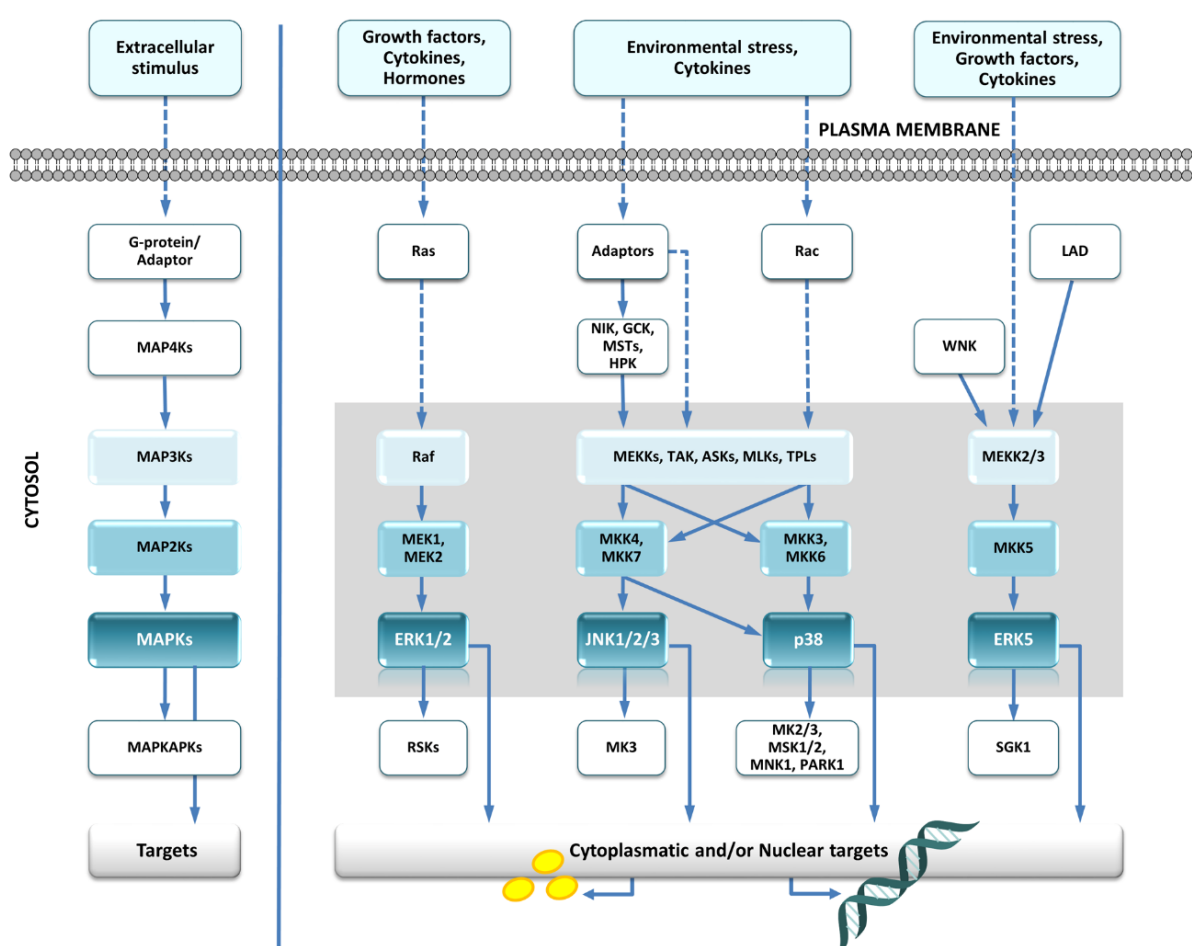
p38 is a Ser/Thr specific kinase and belongs to the kinase family of CMGC. Upon sequence similarities the CMGC family is subdivided in mitogen-activated protein kinases, of conventional and atypical MAPK domain structure (**Figure 8**). Conventional MAPKs comprise of extracellular signal-regulated kinases 1/2 (ERK1/2), p38 $\alpha/\beta/\gamma/\delta$ , c-Jun amino (N)-terminal kinases 1-3 (JNK1/2/3) as well as extracellular signal-regulated kinases 5 (ERK5) and are highly organized in an evolutionary conserved module of three kinases. In this three-tiered cascade, kinases phosphorylate each other in a sequentially well-defined order, which results in a rapid and directional signal transduction of extracellular stimuli to cellular and nuclear targets. In contrast to this, atypical MAPKs such as the extracellular signal-regulated kinases 3, 4, 7, 8 (ERK3, ERK4, ERK7/8) and Nemo-like kinase (NLK) differ in their activation, as they are not regulated in a MAPK cascade module. So far, atypical MAPKs are less well studied than ERK1/2, p38s and JNKs.<sup>153</sup>



**Figure 8. Domain structure of conventional and atypical mitogen-activated protein kinases (MAPKs).** A) Extracellular signal-regulated kinases 1-5, 7-8 (ERK1/2, ERK3, ERK4, ERK5, ERK7/8), p38 isoforms ( $\alpha$ ,  $\beta$ ,  $\gamma$ ,  $\delta$ ), c-Jun amino (N)-terminal kinases 1-3 (JNK1/2/3), Nemo-like kinase (NLK). Ser/Thr kinase domain with Thr-X-Tyr motif for activation via dual phosphorylation depicted for conventional kinases and Ser/Thr-X-Gly/Glu/Tyr motif for activation of atypical kinases. Transactivation domain (TAD), nuclear localization sequence (NLS) and Ala, His, Glu rich domain (AHQr), conserved region (CD34) are highlighted. B) Kinome-tree branch of CMGC-family, figure created with Coral.<sup>154</sup>

All conventional MAP kinases share a common domain structure with a N-terminal Ser/Thr kinase domain, and a TXY activation motif in the activation loop between subdomain VII and VIII. The length of the flexible loop differs between the family members, as well as the amino acid X and both are responsible for the different substrate specificities. Whereas ERK1/2 and ERK5 share a TEY motif, a TGY motif can be found in p38 $\alpha/\beta/\gamma/\delta$  and a TPY motif in JNK1/2/3. Typically, MAP kinases get activated by dual phosphorylation at each, threonine and tyrosine residue in this A-loop sequence. Following this event, conformational changes in the protein structure take place, which enables ATP binding. ERKs, p38s and JNKs get each activated as the last kinase in this three-tiered cascade and receive the cell signal from a plethora of upstream kinases and proteins of different type, which are partially specific for the different kinases and their isoforms. In general, the mitogen-activated protein kinase signaling pathway gets activated by extracellular stimuli such as mitogens, growth factors, inflammatory cytokines and various forms of cellular stress e.g. oxidative and osmotic stress, UV-irradiation, hypoxia or ischemia. The signal is usually then detected intracellularly by a

protein of the Ras or Rac family, which serves as switching station to induce the MAPK cascade (**Figure 9**). In this evolutionary conserved signaling cascade a MAP3K (mitogen activated protein kinase-kinase-kinase) receives the signal first. As a consequence, a second MAP2K (mitogen activated protein kinase-kinase) gets subsequently activated, by phosphorylation and transmits the signal to a third receiver kinase termed MAPK (mitogen activated protein kinase). Depending on the signal input and on sequence homology these Ser/Thr MAPKs are either named as ERKs, JNKs or p38s and get activated by dual phosphorylation on threonine and tyrosine residues on a conserved TXY motif in the A-loop of the kinase domain. Following activation, MAPKs transduce the signal to cytosolic and/or nuclear targets regulating elementary cellular functions such as gene expression, proliferation, differentiation, migration, cell survival and apoptosis. Components of the cascade are usually organized in a multiprotein complex, in which scaffold proteins additionally help to convey a fast and target directed signal transduction. Besides increasing the specificity and selectivity of the pathway, scaffold proteins can also function as adaptor proteins and prevent unwanted crosstalk between the different MAPK modules. It is assumed that the multiprotein complex of the entire MAPK system harbors nearby 200 distinct components, which are encoded by about 70 genes,<sup>155</sup> underlying the complexity on how cells communicate and respond to extracellular events in this important signaling pathway.



**Figure 9. Mitogene-activated protein kinase cascades.** Schematic representation of ERK1/2, JNK1/2/3, p38 and ERK5 kinase signaling pathways. The conserved three-tiered cascades, by MAP3Ks, MAP2Ks and MAPKs are highlighted by the gray box. Dashed arrows indicate indirect activation, and bold arrows indicate direct activation of specific downstream targets.

ERK1/2 was first identified as a receiver MAPK activated by growth factors such as epidermal growth factor (EGF), platelet-derived growth factor (PDGF), nerve growth factor (NGF) or insulin via the interaction with a respective transmembrane bound receptor-tyrosine kinase (RTK).<sup>156</sup> The signal is then transduced by Ras<sup>157, 158</sup> to Raf kinases<sup>159</sup> (Raf-1, A-Raf, B-Raf, Mos) and afterwards to the respective MAP2Ks, MEK1 and MEK2 downstream, which activates ERK1/2 by dual phosphorylation.<sup>160</sup> ERK1/2 can also be activated by hormones, cytokines or by ligands targeting G-protein-coupled receptors (GPCRs)<sup>161</sup> and is mainly known to induce cellular processes such as proliferation, differentiation and cell migration for instance via p90 ribosomal S6 kinases (RSKs).<sup>162</sup> As the Ras-Raf-MEK-ERK pathway also interferes with cell-cycle progression, cell metabolism and transcription of genes an upregulation or dysregulation of this pathway was observed in various cancer forms.<sup>156, 163, 164</sup> JNK and p38 signaling pathways are activated in response to chemical or physical stress, also known as stress-activated protein kinases (SAPKs), and partially share the same activator MAP3Ks (e.g. MEKKs, TAK, ASKs, MLKs and TPL2). In the JNK-signaling pathway<sup>165, 166</sup> extracellular stimuli are recognized either by related receptors as RTKs or GPCRs or by stress-induced membrane changes. The signal is typically recognized intracellularly by an adaptor protein and transferred to an activator kinase, sometimes referred to MAP4K (mitogen-activated protein kinase kinase kinase). Examples of MAP4Ks of the JNK signaling are NIK, GCK, MSTs, HPK, which demonstrated to activate MAP3Ks as the first kinase in the three-tiered cascade. In addition to the MAP3Ks shared with p38, some JNK signaling specific kinases such as ASK2, LZK1, MLK1 and MEKK4 have been reported exclusively. Despite several crosstalk between both signaling pathways, making it difficult to differentiate cell communication, specific MAP2K proteins for the activation of each JNK, namely MKK4 and MKK7,<sup>167</sup> as well as MKK3 and MKK6<sup>168</sup> for the activation of p38 have been described. MKK4 and MKK7 are kinases of dual specificity and get activated by phosphorylation at each serine and threonine residue in a conserved SXAXS/T motif in the activation loop. Subsequently, JNK1/2/3 isoforms receive the signal differently, after dual phosphorylation of the TPY motif and activate different cellular or nuclear targets. Since both the JNK and p38 signaling pathways are highly related, inflammatory marker production, growth/cell cycle arrest, apoptosis or cell differentiation are usually the response to extracellular stress. The interplay between both pathways is well documented in various cell lines and animal models, such as an antagonistic effect between JNK and p38 pathways during cell proliferation and survival.<sup>169</sup> Comprehensive details regarding the activation mechanisms and the regulation of the p38 MAPK signaling pathway are described in **Section 1.4.2**.

In homology, another so-called ERK5 pathway has been described that is activated by both environmental stress and by mitogen stimuli such as growth factors and by cytokines.<sup>169-171</sup> The mechanism of ERK5 activation by upstream kinases and other proteins is not yet fully understood.<sup>172</sup> It was found that the ERK5 cascade gets activated by WNK<sup>173</sup> and Lad1<sup>174</sup> proteins, which transduce the received extracellular signal to MEKK2/3<sup>175, 176</sup> and on to MKK5.<sup>177, 178</sup> So far it is known, that ERK5 is then activated by phosphorylation on Tyr220 and Thr218 in the TGY motif of the kinase domain, sharing high sequence similarity with the activation motif of ERK1/2 and its way of activation. In contrast to the other canonical MAP Kinases, ERK5 comprises a non-catalytically proline-rich transactivation domain (TAD) and a nuclear localization sequence (NLS) in the C-terminal part of the protein. Depending on the cell-line used, it was demonstrated that ERK5 can activate the serum and glucocorticoid-activated kinase-1 (SGK1)<sup>179</sup> as MAPKAPK or translocate to the nucleus, phosphorylating substrates such as c-Myc,<sup>180</sup> c-Fos<sup>181</sup> or MEF2 family<sup>182, 183</sup> members. Due to the TAD-domain ERK5 can participate in protein-protein interactions with transcription co-regulators e.g. MEF2C,<sup>183</sup> influencing the transcription of specific target genes. In a further study an intrinsic transcriptional activity of the C-terminal domain was also highlighted, making this cascade unique in comparison to the before mentioned ERK1/2, JNK and p38 MAPK signaling pathways.<sup>184</sup> Stimulation of the ERK5 cascade effects physiological functions such as proliferation, differentiation as well as survival of cells.<sup>185</sup>



### 1.4.2 Activation and regulation of p38 MAPK signaling pathway

The mammalian p38 MAPK gets activated by extracellular stimuli including various forms of environmental stress, e.g. oxidative stress, hypoxia and UV irradiation. In a similar way, growth factors and inflammatory cytokines have been found to regulate p38 activity by binding to its respective transmembrane receptors of the receptor tyrosine kinase (RTK) or cytokine family. In example stimulators, such as various interleukins (IL-1, IL-6, IL-8), tumor necrosis factor alpha (TNF- $\alpha$ ) and growth factors such as fibroblast growth factor (FGF), vascular endothelia growth factor (VEGF), insulin-like growth factor (IGF), platelet-derived growth factor (PDGF) or nerve growth factor (NGF) have been studied as activators of the p38 MAPK cascade. As p38 was also recognized to regulate the biosynthesis of these pro-inflammatory cytokines, a plethora of studies have been reviewed by different authors, investigating the role of p38 in inflammatory response and autoimmune diseases.<sup>146, 147, 186, 187</sup> It was further reported, that GPCRs can mediate the activation of the canonical p38 MAPK signaling pathway.<sup>188</sup> In this MAP3K/ MAP2K dependent pathway a diverse set of kinases with dual specificity (ASK1, DLK1, MEKK3/4, MLK3, TAK1, TAO1/2, TPL2 and ZAK1) activate its downstream substrates MKK3 and MKK6 in a more precise way.<sup>146</sup> In example, stimulation of GPCRs lead to the activation of the heterotrimeric G protein (G $\alpha$ 0), which activates the MAP3K TAO1/2, exclusively transferring the signal to MKK3/6.<sup>189</sup> The regulation of MAP3K is highly complex and not fully clarified yet. Thus, MAP3K activation is sometimes dependent on extracellular stimuli leading to phosphorylation of specific kinases, the binding of small GTP-binding proteins of the Rho family or on ubiquitination.<sup>190</sup> Overall, the p38 MAPK signaling pathway and the JNK pathway in parallel, are able to detect a diverse set of external stimuli and transduce the signal in a direct way to specific members within each cascade. The MAP2Ks, MKK3 and MKK6 downstream, are the major activators of p38 and substrate specificity is strongly dependent on cellular stimuli, tissue distribution and expression levels. Therefore, MKK3 is a known activator of the isoforms p38 $\alpha$ , p38 $\gamma$  and p38 $\delta$  with no influence on p38 $\beta$  phosphorylation. In contrast MKK6 is an activator of all p38 isoforms, as observed in MKK3 and MKK6 knock-out studies in mice.<sup>191, 192</sup> However, under certain conditions, such as UV irradiation, members of the highly related JNK signaling pathway, such as MKK4 and MKK7, may cross-react with the p38 cascade, which was demonstrated by phosphorylation of p38 $\alpha$  and p38 $\delta$ , respectively.<sup>192-194</sup>

As described earlier in **Section 1.4.1**, MAPK signaling pathways are organized in functional modules for a fast and directed signal transduction, in which scaffold proteins play important regulatory roles.<sup>195</sup> A small number of scaffold proteins were also found for p38, e.g. the osmosensing scaffold for MEKK3 (OSM) and the JNK-interacting proteins 2 and 4 (JIP2, JIP4). Compensatory osmoregulatory pathways help cells to adapt to prolonged exposure to hyperosmotic stress, whereas p38 plays a central role. In response to osmotic shock the OSM scaffold protein forms a complex with the GTPase Rac, MEKK3 and MKK3 upstream of p38.<sup>196</sup> Therefore, OSM indirectly regulates the gene transcription and post-translational modification of cytoskeletal remodeling proteins via p38 in response to osmotic stress. JIP2 and JIP4 scaffold proteins were originally identified as components of the JNK cascade.<sup>197</sup> However, it was recognized that JIP2 can also form a complex with MKK3, p38 $\alpha$  and p38 $\beta$ . The family member JIP4 exclusively activates the p38 isoforms  $\alpha$  and  $\beta$ , due to stabilizing the upstream proteins MKK3 and MKK6.<sup>198</sup>

Beside the described mechanism of p38 activation via the MAP kinase cascade, different researchers have reported additional MAP3K/MAP2K independent ways.<sup>199-201</sup> One alternative mode of activation was for instance found during myocardial ischemia, accomplished by the transforming growth factor  $\beta$  (TFG- $\beta$ ).

Upon stimulation of the TGF- $\beta$  cytokine receptor the signal gets further transduced to the downstream TGF- $\beta$  activated kinase 1 (TAB1). The scaffold protein TAB1 is then able to bind p38 at a bipartite docking site at the C-terminal kinase lobe, facilitating autophosphorylation and activation of p38.<sup>202</sup> Binding of TAB1 triggers large structural rearrangements of the N- and C-terminal lobes of the p38-kinase domain, in which the activation loop with the TGY motif moves toward the ATP-binding side. Autophosphorylation of each Thr180 and Tyr182 in p38 can take place, which is prompted by a network of hydrogen bond interactions between Thy185 of the catalytic loop and by Asp150 from the HRD motif.<sup>203</sup>

Another interesting mechanism on the autoactivation of p38 was observed in T-cells of the immune system.<sup>200, 204</sup> Upon activation through the T-cell-receptor (TCR) in T-lymphocytes, downstream targets such as the lymphocyte-specific protein tyrosine kinase (Lck) and  $\zeta$ -chain-associated protein kinase of 70 kDa (Zap70) get activated successively. Once activated, Zap70 demonstrated to phosphorylate p38 on a non-canonical activating residue Tyr323.<sup>205</sup> Following this event, conformational changes in the protein structure catalyze p38 autophosphorylation and subsequent activation of the signaling pathway.

### **1.4.3 Downstream substrates of p38 MAPK and disease relation**

Activated p38 MAPK stimulates different kinases such as the MAPKAPs, or other cytosolic and nuclear targets downstream. The family of the human MAPKAPs consists of 11 subfamilies, divided in MAPK-activated protein kinases 2 and 3, (MK2, MK3), mitogen- and stress-activated kinases 1 and 2 (MSK1, MSK2), MAPK-interacting kinases 1 and 2 (MNK1, MNK2), ribosomal protein S6 kinases 1-4 (RSK1-4) and p38-regulated/activated protein kinase (PRAK) also named MK5.<sup>206</sup> MAPKAPs belong to the calcium/calmodulin-dependent protein kinase (CAMK) family and can be activated by conventional and atypical MAPK pathways as described earlier.<sup>153</sup> Typically, MAPKAPs contain a D-domain docking motif for the recognition and interaction with their respective MAPK.<sup>207</sup> The D-domain is of basic nature due to arginine and lysine residues, commonly sharing a LX<sub>2</sub>K/RK/RX<sub>2-6</sub> $\phi$ X $\phi$  motif in which  $\phi$  is of hydrophobic nature and often a leucine, isoleucine or valine residue.<sup>208</sup> MAPKAP family members slightly differ in their docking side sequence, which allows to specify between different MAPK substrates such as ERKs, JNKs and p38s.<sup>209</sup> Overlapping substrate specificities were also found for MSK1, MSK2 and MNK1 regarding to p38 and ERK1/2 interaction. MAPKs recognize their MAPKAPs substrates by a C-terminal common docking (CD) domain, which consists of acidic and hydrophobic residues for stable electrostatic and hydrophobic van-der-Waals interaction with the D-domain.<sup>210</sup> The CD domain of ERK1/2 and p38 is extended by a two amino acid long residue, which is basic in the case of ERK1/2 and of acidic nature in p38s, and further help to exclusively interfere with its interaction partners.<sup>210</sup> Common MAPKAPs which are activated by p38s are MK2, MK3, MSK1/2, MNK1 and PARK. MK2 and MK3 were the first MAPKAP substrates described for p38, in which a specific lysine residue interacts exclusively with the acidic CD-domain of p38.<sup>153</sup> In quiescent cells, such as the heart, skeletal muscle and kidney, in which both MAPKAPs are most frequently expressed, MK2 and MK3 are predominately located inside the nucleus owing to a nuclear localization signal (NLS) sequence.<sup>211</sup> Interestingly, it was observed, that MK2 and MK3 can also translocate to the cytoplasm with an intrinsic nuclear export signal (NES) domain next to the NLS sequence.<sup>211, 212</sup> As taken from crystal structures of MK2 in complex with p38 $\alpha$ , the NES sequence gets exposed upon phosphorylation of Thr334 by activated p38.<sup>213</sup> It is therefore suggested, that under environmental stress conditions p38 $\alpha$  is controlling the nuclear import and export of MK2 via phosphorylation.<sup>213, 214</sup> However, it needs to be elucidated if the docking event and complex formation of p38 with MK2 also has an effect on the cellular localization. MK2 and MK3 play a key role in the p38 mediated signaling pathway and have been found to regulate a number of substrates

necessary for cytokine production, actin remodeling, cell migration, regulation of transcription and cell-cycle control.<sup>215, 216</sup> Thus, MK2 and MK3 have demonstrated to phosphorylate heat shock protein (Hsp27), which controls actin polymerization of the cytoskeleton to maintain cell motility upon heat shock and oxidative stress.<sup>217</sup> MK2 also regulates the translation and transcriptional stability of various mRNAs, which is considered essential in the LPS-stimulated upregulation of cytokines.<sup>153</sup> Therefore, p38 mediated MK2 activation is crucial for the biosynthesis of pro-inflammatory cytokines as IL-6, IL-8, IL-1 $\beta$ , TNF- $\alpha$  and interferon- $\gamma$  (IFN- $\gamma$ ) and therefore of central importance in inflammatory diseases.<sup>218, 219</sup> In response to UV-irradiation, MK2 further phosphorylates CDC25B/C, a phosphatase related to cell-cycle control, promoting entry into the G<sub>2</sub>/M checkpoint, which results in cell-cycle arrest.<sup>220</sup> An influence on the cell-cycle was also found for MK2, during the degradation of the cell-cycle regulator and tumor suppressor p53.<sup>221</sup> After phosphorylation and activation of MK2 by p38, HDM2 (a E3-ubiquitin ligase of p53) gets activated, promoting degradation of p53 and dampening its effect during stress response and DNA-damage.<sup>222</sup> Although the underlying mechanism needs to be clarified in more detail, an interesting study on skin carcinoma development in MK2-deficient mice showed decreased levels of HDM2 phosphorylation, accomplished by increased p53 levels.<sup>223</sup> It was therefore concluded, that MK2 plays a pivotal role in early stages of skin tumor promotion by regulating inflammatory responses as well as apoptosis of damaged cells.

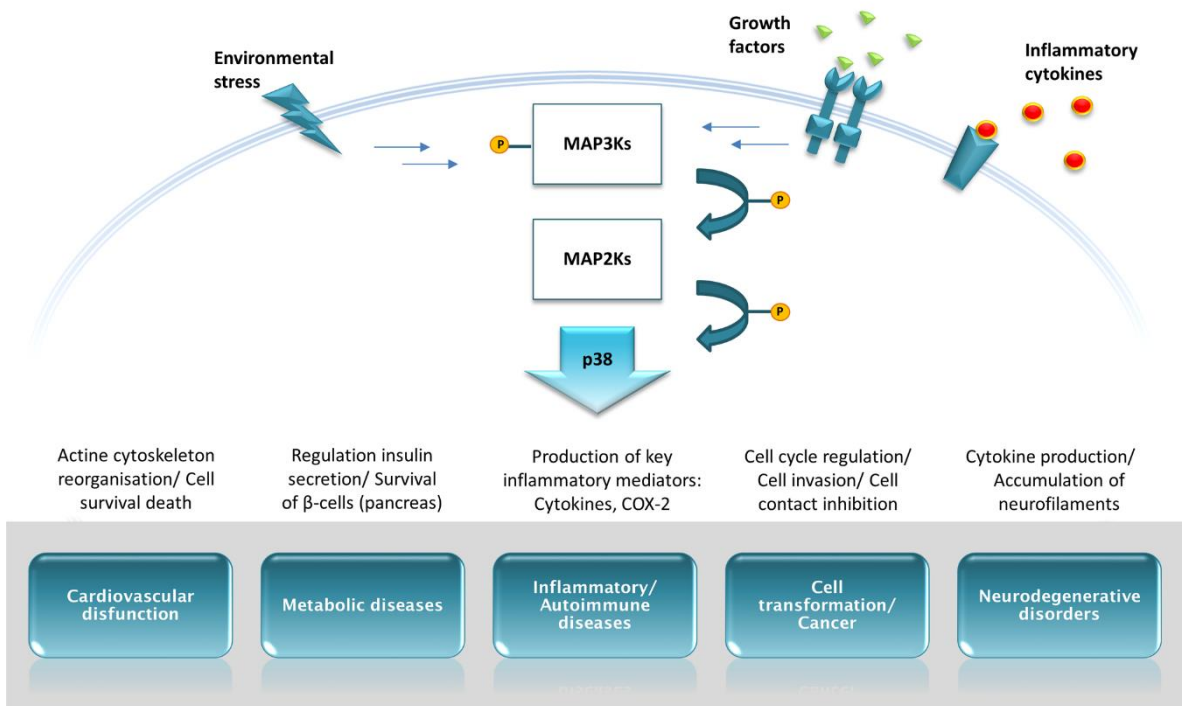
Although MK2/3 have been studied most extensively, further important signaling functions downstream of p38 MAPKs are also mediated by the ubiquitously expressed kinases MSK1 and MSK2. MSK1/2 are sharing 63% in identity and exhibit key domains also correspondingly found for RSKs, targeted exclusively by ERK1/2.<sup>153</sup> In homology to the latter MAPKAPKs, MSKs have two kinase sequences that belong to the N-terminal AGC family and to the CAMK family at the C-terminus. In total, four phosphorylation sites are responsible for the complex mechanism of activation.<sup>224</sup> Because of this, MSKs can be targeted by both p38s and ERKs. The physiological role of MSKs is not fully understood yet, but it is assumed that MSKs might play a role during cytokine production in the innate immune system and for the plasticity of neuronal synapses.<sup>224</sup> Furthermore, MSKs play a fundamental role in gene transcription, or in the nucleosomal response.<sup>225</sup>

Another downstream target of p38 MAPK is the kinase MNK1, which exerts an effect on the nuclear translation machinery via eukaryotic factors 4E and 4G (eIF4E and eIF4G).<sup>226-228</sup> It is therefore assumed that under cellular stress conditions MNK1 contributes to the promotion of tumor formation and the activation of oncogenes.<sup>229</sup> Interestingly, MNK1, as well as MSK1 and MK5/PARK, have each demonstrated to phosphorylate cytosolic phospholipase A<sub>2</sub> (cPLA<sub>2</sub>) *in vivo*. The phospholipase cPLA<sub>2</sub> is a key enzyme of the arachidonic acid cascade and triggers the release of arachidonic acid from the plasma membrane. The activation of MNK1, MSK1 and MK5 via p38 therefore has an indirect influence on the production of inflammatory mediators such as prostaglandins.<sup>230</sup>

As indicated before, activated p38 MAPK can also translocate to the nucleus, phosphorylating transcription factors, or directly interfering with regulators of chromatin remodeling exemplified by ATF-2 (cAMP-dependent transcription factor), GADD153 (growth arrest and DNA damage inducible gene 153), p53 (cellular tumor antigen p53), ELK (ETS domain-containing protein), C/EBP $\beta$  (CCAAT/enhancer-binding protein beta), MEF2A/C, (monocyte enhance factor 2A/C).<sup>186</sup> p38 MAPK can also indirectly influence transcription factors such as ATF-1, NF $\kappa$ B (nuclear factor NF-kappa-B), p65 (transcription factor p65), ER81 (ETS-related protein 81) and targets as histone 3, HMGN1 (non-histone chromosomal protein HMG-14) and RAR $\alpha$  (retinoic acid receptor RXR-alpha) via activation of MSK1/2. In example SACCANI ET AL. demonstrated the indirect phosphorylation of histone 3 caused by MSK1 in LPS-stimulated myeloid cells and the

consequent recruitment of NFκB.<sup>231</sup> They concluded, that genes involved in inflammatory response, as the interleukins IL-6, IL-8 and MCP-1 (monocyte chemoattractant protein 1), are responsible for p38 recruitment and the indirect phosphorylation of histone 3 on Ser10. The latter event is known to also create specific docking sides for proteins, regulating transcription or chromatin folding.<sup>232, 233</sup>

From the large studies undertaken, investigating the *in vitro* and *in vivo* functions of p38 MAPK, it is assumed that p38 MAPK influences about 200–300 substrates in total.<sup>146</sup> Thereof, a diverse set of functions can be ascribed to p38, regulating fundamental processes such as protein transcription and translation, mRNA stability, protein localization and degradation, endocytosis, apoptosis, cytoskeleton reorganization and cell migration (**Figure 10**).



**Figure 10. Physiological and pathophysiological roles of p38 MAPK.** Schematic representation of p38 kinase cascade. Growth factors are depicted in green binding to their corresponding tyrosine kinase receptor and cytokines in red binding to the respective cytokine receptor. Phosphate groups are highlighted in yellow.

The influence of p38 MAPK on specific targets gets further complicated by the fact, that the signaling outcome by p38 activation varies depending on stimuli, expression level of upstream and downstream proteins, as well as on the tissue system under investigation. Moreover, the strength and duration of p38 signaling itself significantly contributes to the effect detectable. A strong p38 activation was observed e.g. during stress stimuli or during apoptotic events. In contrast, less stimulation of p38 was observed during the regulation of homeostatic functions that promoted cell survival.<sup>234</sup> A diverse set of studies disclosed, that the four p38 isoforms identified also differ in their substrate specificities, by variations in its substrate binding domains and/or by targeting of precise docking-domain amino acids of substrate proteins.<sup>148</sup> Whereas p38α and p38β, share more or less similar physiological substrates such as components of the transcriptional and translational machinery, metabolic enzymes e.g. the glycogen synthase or phospholipase A<sub>2</sub> (PLA<sub>2</sub>), p38γ and p38δ are identified to be unable to phosphorylate the MAPKAP kinases MK2 and MK3, which are well known substrates of the former isoforms.<sup>235, 236</sup> However, the greatest difference in substrate specificity was observed for p38γ, which exhibits a C-terminal PDZ binding domain

KETXL sequence. The PDZ domain allows p38 $\gamma$  to make protein-protein interactions for instance with  $\alpha$ 1-syntrophin,<sup>237</sup> with the PDZ domain of protein-tyrosine phosphatase 1 (PTPH1)<sup>238</sup> and the scaffold protein human disc large hDlg/SAP97.<sup>239</sup> Usually hDlg/SAP97 forms multiprotein complexes and is located at the cytoskeleton by associating with the guanylate kinase-associated protein (GKAP), in which it regulates cell shape and cell volume, as well as intercellular-junctional complexes. However, under osmolar stress conditions p38 $\gamma$  demonstrated to phosphorylate hDlg/SAP97, releasing GKAP and thus promoting dissociation from the cytoskeleton.<sup>239</sup> Besides p38 $\gamma$ , substrates exclusively to p38 $\delta$  have also been described, e.g. the microtubule-associated protein tau, linked to Alzheimer disease<sup>240-242</sup> and the cytoplasmic protein stathmin responsible for microtubule dynamics.<sup>243</sup> Another substrate of p38 $\delta$  is protein kinase D1 (PKD1), which plays a role in insulin secretion, glucose homeostasis and survival of pancreatic beta cells in diabetes mellitus.<sup>244</sup> In addition, p38 $\delta$  interacts with the eukaryotic elongation factor 2 (eEF2)<sup>245, 246</sup> important for the regulation of the cytoskeleton.

In conclusion, p38 MAPK is a pivotal kinase that regulates a highly diverse set of fundamental cellular processes, such as differentiation, migration, apoptosis or cell-survival. By the plethora of substrates and targets investigated and found today, it seems to be obvious that aberrant expression of p38 MAPK is associated with a variety of inflammatory, as well as autoimmune diseases or several forms of cancer (**Figure 10**). Therefore, extensive research has been conducted by scientists and pharmaceutical companies to investigate the role of p38 MAPK in, for example, neuropathic pain, chronic obstructive pulmonary disease (COPD), Alzheimer disease, acute coronary syndrome/coronary heart disease, atherosclerosis, rheumatoid arthritis, systemic lupus erythematosus (SLE), atopic dermatitis, contact eczema and psoriasis as well as in Crohn's disease or multiple myeloma. Since p38 MAPK appeared to be a beneficial target in the treatment of these diseases, several dozen inhibitors have been synthesized and studied in clinical trials. However, as the mechanism on the function and regulation of p38 MAPK signaling pathways is quite complex under physiological conditions, compensatory mechanism upregulated by the inhibition of p38 are even more complex and less understood yet. Hence, today neither one inhibitor has successfully passed large-scale phase-III clinical trials, nor has it ever been approved by the FDA for the market.

### **1.5 A survey of p38 MAPK inhibitors in clinical trials**

Positive and negative feedback loops are triggered by p38 MAPK activation and demonstrate to be highly activated during immune response for instance in rheumatoid arthritis, multiple sclerosis, systemic lupus erythematosus (SLE) and psoriasis. As this MAPK is moreover well known to transduce extracellular stress and cytokine stimuli to the cell nucleus, thus helping the cells to trigger inflammatory answers, dysregulated p38 MAPK is collectively seen in almost all inflammatory diseases such as Crohn's disease, asthma bronchiale and chronic obstructive pulmonary disease (COPD). p38 MAPK has been intensively investigated in connection to these diseases in academia and by the pharmaceutical industry over 20 years. The enormous effort of scientists is documented in over 10,000 publications related to p38 MAPK inhibition and donated highly potent and selective compounds. However, only a limited number of specific kinase inhibitors entered clinical trials. Most of these clinical trials focused on inflammatory events and up to date no clinical candidate has been successfully applied to the market. The reasons for abandoning the clinical studies were different. On the one hand the trials stopped due to toxic side effects, such as liver or neuronal toxicity, and on the other hand to non-specific effects. In general, the interpretation of physiological and pathophysiological results was difficult, since p38 MAPK is ubiquitously expressed tissue-wide. Off-target inhibition effects not related to p38 and the contribution of responses due to cross-talk between the

signaling pathways were sometimes not known or hitherto misunderstood. The following section provides a brief overview of the p38 kinase inhibitors that have been clinically tested. It further highlights the outcome and reasons for which clinical studies were discontinued.

Although patients with inflammatory diseases, such as rheumatoid arthritis, have been successfully treated with immunosuppressants and monoclonal antibodies directly targeting pro-inflammatory cytokines, such as TNF- $\alpha$ , IL-1 and IL-6,<sup>247</sup> with approved drugs such as Infliximab, Adalimumab, Etanercept, Anakinra and Tocilizumab, kinase inhibitors might offer several therapeutic advantages. Of central importance is the non-peptidic nature of kinase inhibitors, which allow an oral instead of a parenteral administration. As the dose titration of immunosuppressants is difficult to adjust, side effects such as fever, urticariae and allergic reactions and anaphylactic shock reactions, are not uncommon. With an oral administered drug there is no need for patients to see the hospital for infusion, thus the costs for therapy and production are saved.<sup>247</sup> Small-molecule kinase inhibitors may also be an useful alternative for patients who no longer respond to previous therapies due to resistance. An overview of 26 small-molecule p38 MAPK inhibitors, which advanced into clinical trials, is shown in **Table 1**. Information is given, available from <https://clinicaltrials.gov>, for the highest reached clinical phase and referenced by its NCT accession code. In the case of preclinical and very early studies data were taken from <https://adisinsight.springer.com> and referenced by its drug ID number, respectively. However, it should be noted, that not all clinical studies, which have been taken place, or are currently ongoing, are listed in these public databases.

**Table 1.** p38 MAP Kinase inhibitors in clinical trials

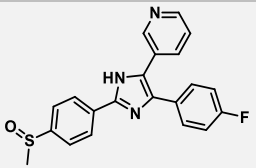
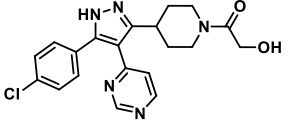
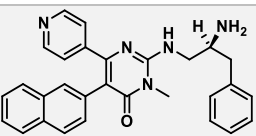
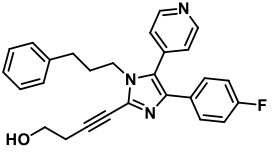
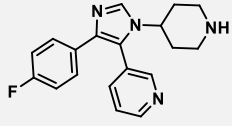
Compound	Originator/ Company	Conditions/ Disease	Structure/ Highest clinical phase	Ref.
SB203580	Glaxo Smith Kline	Arthritis/ Inflammatory bowel disease	 preclinical	Adis Insight (Drug ID 800007147)
SD-0006 (SC-409)	Pfizer	Asthma, chronic obstructive pulmonary disease, rheumatoid arthritis	 preclinical	Adis Insight (Drug ID 800024618)
AMG-548	Amgen	Rheumatoid arthritis	 preclinical	Adis Insight (Drug ID 800019881)
RWJ-67657	Johnson & Johnson	Rheumatoid arthritis	 preclinical	Adis Insight (Drug ID 800020786)
SB235699 (HEP689)	Glaxo Smith Kline/ LeoPharm	Psoriasis	 Phase I	Adis Insight (drug ID 800012315)

Table 1. (continued)

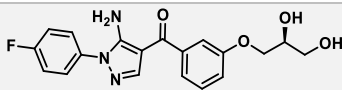
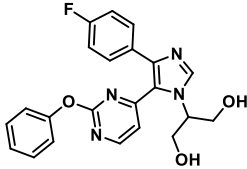
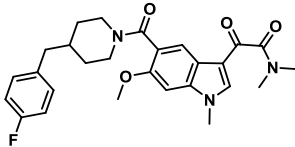
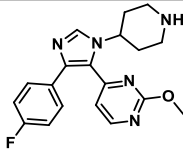
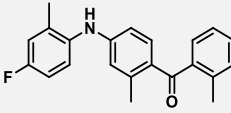
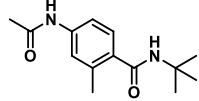
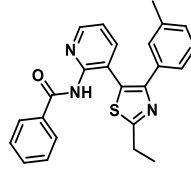
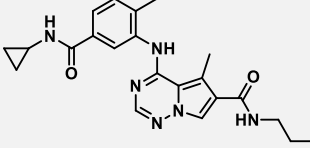
Compound	Originator/ Company	Conditions/ Disease	Structure/ Highest clinical phase	Ref.
RO3201195	Roche Palo Alto LLC	Rheumatoid arthritis	 Phase I	Adis Insight (Drug ID 800016371)
SB281832	GlaxoSmith Kline	Inflammatory bowel disease	 Phase I	Adis Insight (Drug ID 800016500)
"	"	Rheumatoid arthritis	Phase I	Adis Insight (Drug ID 800016500)
SCIO-323	Scios	Rheumatoid arthritis	 Phase I	Adis Insight (Drug ID 800018225)
GSK610677 (D0T2IH)	Glaxo Smith Kline	Chronic obstructive pulmonary disease	- Structure not available - Phase I	NCT00694902
SB242235	Glaxo Smith Kline	Rheumatoid arthritis	 Phase I	Adis Insight (Drug ID 800010787)
EO1606	LEO Pharma	Dermatitis	 Phase II	Adis Insight (Drug ID 800016127)
CPI1189 (REN-1654)	Renovis	Sciatica pain	 Phase II	NCT00107055
"	"	Post-herpetic neuralgia	Phase II	NCT00099528
TAK-715	Takeda	Rheumatoid arthritis	 Phase II	NCT00760864
PS540446 (BMS-582949)	Bristol-Myers Squibb	Psoriasis	 Phase II	NCT00399906
"	"	Rheumatoid arthritis	Phase II	NCT00605735
"	"	Vascular diseases	Phase II	NCT00570752

Table 1. (continued)

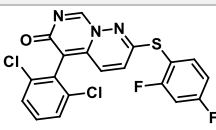
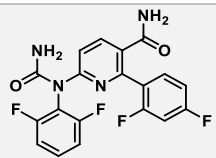
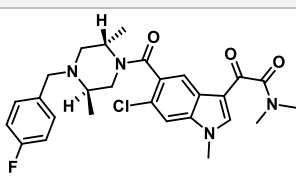
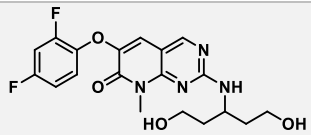
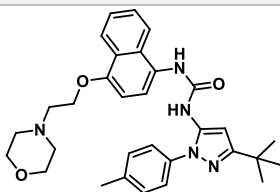
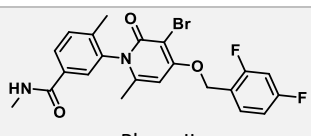
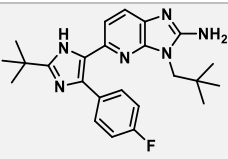
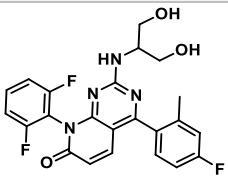
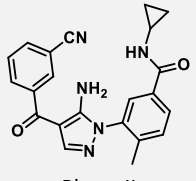
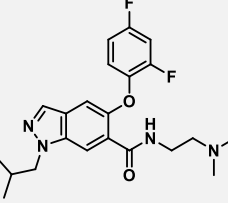
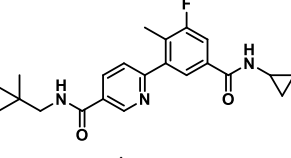
Compound	Originator/ Company	Conditions/ Disease	Structure/ Highest clinical phase	Ref.
KC706	Kemia	Pemphigus vulgaris	- Structure not available - Phase II	NCT00606749
Neflamapimod (VX-745)	Vertex Pharmaceuticals	Alzheimer's disease	 Phase II	NCT02423200 NCT02423122 NCT03435861 NCT03402659
VX-702	Vertex Pharmaceuticals	Rheumatoid arthritis	 Phase II	NCT00395577 NCT00205478
Talmapimod (SCIO-469)	Scios	Multiple myeloma	 Phase II	NCT00095680 NCT00087867
"	"	Rheumatoid arthritis	Phase II	NCT00043732
"	"	Myelodysplastic syndromes	Phase II	NCT00113893
Pamapimod (RO-4402257)	Roche	Rheumatoid arthritis	 Phase II	NCT00303563 NCT00316771
Doramapimod (BIRB-796)	Boehringer Ingelheim	Rheumatoid arthritis	 Phase II	NCT02214888 NCT02209779
"	"	Psoriasis	Phase II	NCT02209753
"	"	Crohn's disease	Phase II	NCT02209792
PH-797804	Pfizer	Chronic obstructive pulmonary disease	 Phase II	NCT00559910 NCT01321463 NCT01543919
"	"	Post-herpetic neuralgia	Phase II	NCT00614705
"	"	Rheumatoid arthritis	Phase II	NCT00620685 NCT00383188
"	"	Osteoarthritis	Phase II	NCT01102660



Table 1. (continued)

Compound	Originator/ Company	Conditions/ Disease	Structure/ Highest clinical phase	Ref.
<b>Ralimetinib (LY2228820)</b>	<i>Eli Lilly</i>	Postmenopausal metastatic breast cancer	 Phase II	NCT02322853
"	"	Adult glioblastoma	Phase II	NCT02364206
"	"	Epithelial ovarian cancer, fallopian tube cancer, primary peritoneal cancer	Phase II	NCT01663857
<b>Dilmapimod (SB681323)</b>	<i>Glaxo Smith Kline</i>	Rheumatoid arthritis	 Phase II	NCT00134693 NCT00320450
"	"	Neuropathic pain	Phase II	NCT00390845
"	"	Chronic obstructive pulmonary disease	Phase II	NCT00144859
"	"	Acute lung injury	Phase II	NCT00996840
"	"	Coronary heart disease	Phase II	NCT00291902
<b>Acumapimod (BCT-197)</b>	<i>Novartis/Mereo BioPharma</i>	Chronic obstructive pulmonary disease	 Phase II	NCT01332097 NCT02700919
"	"	Acute kidney injury	Phase II	NCT01336959
<b>Arry797 (ARRY-371797)</b>	<i>Array BioPharma</i>	Dilated cardiomyopathy	 Phase III	NCT03439514
<b>Losmapimod (GW-856553)</b>	<i>Glaxo Smith Kline</i>	Acute coronary syndrome	 Phase III	NCT02145468

Research toward the inhibition of p38 MAPK started in the early 90s, were *Smith Kline Beecham* (later *Glaxo Smith Kline*) reported about their pyridinyl-imidazole based inhibitor SB203580.<sup>248, 249</sup> First studies in 1993 demonstrated that this compound potently suppressed the phosphorylation of Hsp27, due to an, at this time called, reactive kinase 1, later renamed as p38 MAPK because of its size of 38kDa. These initial findings<sup>140</sup> stimulated intensive investigations by various research groups in industry and academia on a variety of structurally related derivatives, while *N*-substituted pyridinyl-imidazoles,<sup>250, 251</sup> pyrimidinyl-

imidazoles<sup>252</sup> and triarylpyrroles<sup>253</sup> can be cited as examples. Although SB203580 never reached phase-I clinical trials,<sup>254, 255</sup> because of severe liver toxicity caused by the interaction with cytochrome P450 enzymes necessary for the biotransformation and excretion of drugs,<sup>252</sup> it is one of the most used type-I inhibitor for studying the role of p38 MAPK in physiology and pathophysiology. SB203580 has demonstrated to be effective *in cellulo* as well as in animal models. For example, the compound potently inhibits the TNF- $\alpha$  release in LPS-stimulated THP-1 cells with an IC<sub>50</sub> value of 0.16  $\mu$ M,<sup>256</sup> as well as the IL-1 release in PBMC cells with an IC<sub>50</sub> value of 0.037  $\mu$ M.<sup>257</sup> Animal models have proven the efficacy of the compound against ischemic injury in an *in vivo* pig myocardium model.<sup>258</sup> In further studies SB203580 showed to improve renal disease when administered to MRL/lpr mice as a model system of systemic lupus erythematosus (SLE).<sup>259</sup>

The early studies around the pyridinyl-imidazole inhibitors and SB203580 led to the discovery of efficient derivatives, e.g. the *N*-alkyl substituted imidazole derivative SB235699,<sup>260</sup> which entered phase-I clinical trials, as a topical anti-inflammatory remedy for the treatment of atopic dermatitis, contact eczema and psoriasis. The compound interfered to a lower extent with CYP450 enzymes and benefited from an improved potency toward p38 MAPK.<sup>261</sup> A pyrimidine substituted structure homolog of the latter compound is SB2422335,<sup>262, 263</sup> which demonstrated its usefulness in anti-inflammatory models and reached phase-I clinical trials for studying rheumatoid arthritis.<sup>264</sup>

Tremendous efforts were made in the initial studies, focusing on inhibitors aimed at the selectivity around the ATP-binding site of p38 MAP kinase. However, it took about ten years for the researchers to make a breakthrough and find the first potent inhibitor, targeting the enzyme pocket adjacent to the ATP-binding site. The type-II inhibitor BIRB-796 (Doramapimod)<sup>265</sup> was first published in 2002 by *Boehringer Ingelheim*, who investigated the structure-activity-relationship around a series of, at this time novel, allosteric *N,N'*-diarylurea fragments obtained as a screening hit. BIRB-769 showed excellent picomolar potency toward p38 $\alpha$  ( $K_d = 0.045$  nM), inhibiting also the other p38 isoforms with nanomolar IC<sub>50</sub> values (IC<sub>50</sub> [p38 $\alpha$ / $\beta$ / $\gamma$ / $\delta$ ] = 38/ 65/ 200/ 520 nM, on isolated enzyme).<sup>266</sup> The compound showed good pharmacokinetic properties such as slow-off rate binding, and a good *in cellulo* and *in vivo* activity.<sup>265, 267-269</sup> After oral administration to mice (30 mg/kg), having a collagen-induced arthritis, BIRB-769 potently inhibited the LPS-stimulated TNF- $\alpha$  release to 84%.<sup>267</sup> BIRB-796 completed clinical phase-I trials on healthy subjects, already between the years 1999 and 2002. The clinical candidate was then tested on patients, investigating the dose finding and therapeutic effect in psoriasis, rheumatoid arthritis and Crohn's disease<sup>270</sup> in phase-II clinical trials. Whereas studies with low doses up to 30 mg of BIRB-796, administered twice a day over four weeks, were completed successfully, studies with higher drug doses and longer time of treatment were terminated. Reasons for discontinuation of studies were either inefficient clinical response or to an increase in alanine-transaminase levels, which are an indicator of hepatic toxicity. In 2011, IWANO ET AL. suggested that the hepatotoxicity is predominately caused by the biotransformation with CYP-enzymes, in which a highly reactive and toxic naphthalene epoxide intermediate is formed.<sup>271</sup> Interestingly, an initial dose-dependent decrease in the acute-phase protein CRP (C-reactive protein), an unspecific biomarker of inflammations, was detected. The values, however, returned to baseline after only one week of treatment, thereby relieving initial hopes.<sup>270</sup>

Researchers at *Scios* have used a different scaffold for the inhibition of p38 MAP kinase and developed the indole-based compounds SCIO-323 and SCIO-469 (Talmapimod). Both inhibitors have reached phase-I clinical trials, whereas SCIO-469 solely entered phase-II trials in 2002.<sup>272</sup> SCIO-496 was tested in rheumatoid arthritis patients, also receiving methotrexate in a 30-day study. In this multicenter, randomized, double-blind and placebo-controlled study, SCIO-496 was administered to 120 subjects, which were divided into

subgroups, obtaining each 30 mg, 60 mg or 90 mg of the drug. In another group the dose was continuously increased, from 60 mg, to 120 mg and to 180 mg after each a week of treatment in which the highest dose was kept constant till the end of the experiment. After completing this phase-II clinical trial the compound was further studied in patients with myelodysplastic syndromes and in multiple myeloma, administered for a longer time interval and with changed oral doses. Although, studies completed in 2007, Talmapimod did not enter in phase-III clinical trials properly because of the inefficient outcome. For example, no statistical significant reduction of the number of sensitive, swollen and painful joints (ARC20 response, American College of Rheumatology Response Criteria) was detectable in subjects with rheumatoid arthritis, as compared to placebo group.<sup>273</sup> Similar to BIRB-796, an initial effect, such as decreased levels of CRP, was found in the first two weeks of administration but did not persist over the whole time of treatment.

A comparable study on rheumatoid arthritis was also reported for VX-702 and VX-745 (Neflamapimod) reported by *Vertex Pharmaceuticals*.<sup>274, 275</sup> For example, VX-702 was investigated in a comprehensive study involving 315 subjects without treatment with methotrexate and 118 patients treated with methotrexate. Similar to the clinical trials described above, a rapid decrease in CRP levels at baseline and a remission after a short period of treatment were observed. The rheumatic criteria such as ARC20 responses varied between 22% and 40% in the patient group compared to the placebo-controlled group.<sup>274, 276</sup> For VX-745 an interesting study on Alzheimer disease and the  $\beta$ -amyloid plaque burden was completed in 2016. In this small study, 16 patients received either 40 mg or 125 mg of the orally-active and selective p38 kinase inhibitor twice daily for a period of 12 weeks. The effect on the  $\beta$ -amyloid plaque levels was followed by positron-emission tomography (PET) using 11C-PiB (carbon-11-labeled pittsburgh compound B) as tracer. PET images were taken each before and after the therapy with VX-745.<sup>277</sup> However, a slightly reduction on  $\beta$ -amyloid plaque levels was detected in three patients only, receiving 40 mg and questioning the outcome of this study. Therefore, a more comprehensive study with a larger group of subjects administered VX-745 and a placebo-controlled group is needed to further investigate how inhibition of p38 affects amyloid plaque load and episodic memory in Alzheimer's patients. Currently, patients are being recruited to investigate the effect of the compound on disease-related brain inflammation in Alzheimer's disease in a phase II study.<sup>278</sup>

Of a comparable ketone based pyrido[2,3-*d*]pyrimidine-7-one structure is Dilmapimod (SB-681323) investigated by *Glaxo Smith Kline*. The compound was examined for a diverse set of inflammatory and autoimmune diseases in phase-II clinical trials, such as rheumatoid arthritis, neuropathic pain, acute lung injury,<sup>279</sup> COPD and coronary heart disease.<sup>280</sup> In 2008 investigation on 50 patients with neuropathic pain following nerve trauma by injury or due to compression were administered to 15 mg/kg of Dilmapimod twice a day.<sup>281</sup> In this double-blind and placebo controlled study over two weeks, a statistical significant reduction in neuropathic pain symptoms by an overall good compatibility was observed at this dose, in comparison to the placebo-controlled group.

The role of p38 MAPK inhibitors in inflammatory diseases such as COPD is well known and documented.<sup>282</sup> Thereof Dilmapimod, Losmapimod and PH-797804 have entered clinical phase-II trials in COPD patients. PH-797804 is a *N*-aryl pyridinone, which was first published by *Pfizer* in 2011.<sup>283</sup> The compound is a potent inhibitor of p38 $\alpha$  ( $K_i$  = 5.8 nM), binding also very selective due to the stabilization of a non-conserved, glycine flipped conformation in the hinge region.<sup>284, 285</sup> In three randomized, double-blind and placebo-controlled phase-II studies on COPD patients, PH-797804 demonstrated to be well tolerated and safe at the different administered doses.<sup>286</sup> Lung function parameters, such as the FEV1 (forced expiratory volume in 1s) and dyspnea index scores, increased significantly within 6 weeks during drug intake. In contrast to other clinical trials with p38 MAPK inhibitors, CRP-levels decreased and remained low during this study. Further

investigations will be necessary to clarify the reason for this uncommon feature of PH-797804 and its influence on the p38 signaling cascade in COPD patients.

From the p38 inhibitors listed on <https://clinicaltrials.gov> the most advanced compounds are Arry797 from *Array BioPharma* and Losmapimod from *Glaxo Smith Kline*, which successfully entered phase-III clinical trials. In 2015 Losmapimod completed a multinational phase-III clinical trial, in which the anti-inflammatory features of p38 MAPK inhibition were tested on 3503 patients suffering from acute coronary syndrome, such as heart attack.<sup>287</sup> Since the inflammatory response is related to the formation of atherosclerotic plaques and these are known to induce ruptures via forming of blood clots, the incidence of severe cardiovascular complications was examined under the treatment with Losmapimod compared to placebo.<sup>280, 288, 289</sup> Therefore, in addition to conventional drug therapy, 7.5 mg Losmapimod or placebo was administered twice daily to patients suffering from myocardial infarction twice daily over 3 months. Interestingly, upon treatment with Losmapimod no reduction in ischemic cardiovascular events was detectable, in comparison to the placebo-controlled group, as assumed from former preclinical and clinical trials.<sup>290</sup> Based on these findings, no further studies with Losmapimod in acute coronary syndrome will be conducted in a larger patient population. However, in previous clinical trials, Losmapimod has been shown to be safe and well tolerated with fewer side effects on other organs, such as low reversible liver transaminase levels.<sup>289-293</sup> Arry797 has been investigated in six phase-II clinical trials for ankylosing spondylitis, dental pain<sup>294</sup> and osteoarthritis.<sup>295, 296</sup> The potent ( $IC_{50} = 4.5$  nM) and selective p38 MAPK inhibitor demonstrated to be efficient also in cardiomyopathy<sup>297</sup> and is currently recruiting for a phase-III clinical trial on patients with symptomatic dilated cardiomyopathy due to a lamin A/C gene mutation.<sup>298</sup> First results are expected in April 2020. Besides the mentioned p38 inhibitors, many other compounds have been studied in clinical trials, as depicted in **Table 1**. However, this compilation is only a small selection of a large number of p38 MAPK inhibitors that have been investigated by industry and whose results are not available to the public.<sup>299</sup>

In conclusion, potent inhibitors of p38 MAPK have been assessed and demonstrated its influence in blocking the transcription and translation of genes encoding for pro-inflammatory cytokine production. Although preliminary studies revealed a beneficial effect on chronic inflammatory diseases, many compounds failed during phase-II clinical trials. Reasons for discontinuation are reported, as caused either due to liver and/or CNS toxicity or general inefficacy. A preliminary reduction in unspecific inflammation CRP-levels was detectable in almost all studies, but did not persist over the time of treatment. While it is known that IL-1 and IL-6 each regulate the production of CRP in the liver via p38-MAPK pathway,<sup>300</sup> it stays unclear if p38 independent mechanism play a significant role. Since IL-6 is produced by activation of the toll-like receptor 4 (TLR4),<sup>300</sup> hepatocytes could also be stimulated to produce acute phase proteins by this process. Furthermore, it is known that glial cells in the CNS are able to produce CRP themselves,<sup>301</sup> which makes the actual contribution to the increase in CRP plasma levels difficult to interpret. For the lack of efficacy and the failure of the compounds under investigation different explanations, such as dose limitations by toxicity, biodistribution and targeting of the wrong p38 isoform are likely.<sup>302</sup> Furthermore, it is suggested that initial effects triggered by the inhibition of the p38 MAPK signaling cascade, get compensated by the upregulation of related upstream or downstream signaling pathways. Positive and negative feedback loops can set off, such as the upregulation of phosphatases, and the upstream kinases TAK1 and MLKs.<sup>226, 303, 304</sup> The latter are suggested to be able to cross-activate other pro-inflammatory signaling pathways such as JNK. So far only little is known about the complex regulation and cross-reactivity of pathways influenced by the escape from the blocked p38 MAPK signaling pathway and the transient reduction in inflammation.

As initial hopes in p38 as useful a target against inflammatory diseases are being damped, scientists are now beginning to rethink other upstream signaling pathways, which can be used alternatively.<sup>305</sup> However, it remains a question of whether these disappointing results can be transferred to other diseases associated to p38 MAPK inhibition. To pursue this issue, it would be interesting to design and use inhibitors with very high selectivity, to gain a better understanding of the regulation of p38 MAPK as well as how related signaling cascades escape through inhibition. Therefore, the following work focused on the synthesis and development of novel highly selective p38 kinase inhibitors by targeting less conserved allosteric binding pockets.

## 2 Selectivity guided inhibitor design approaches for p38 MAPK

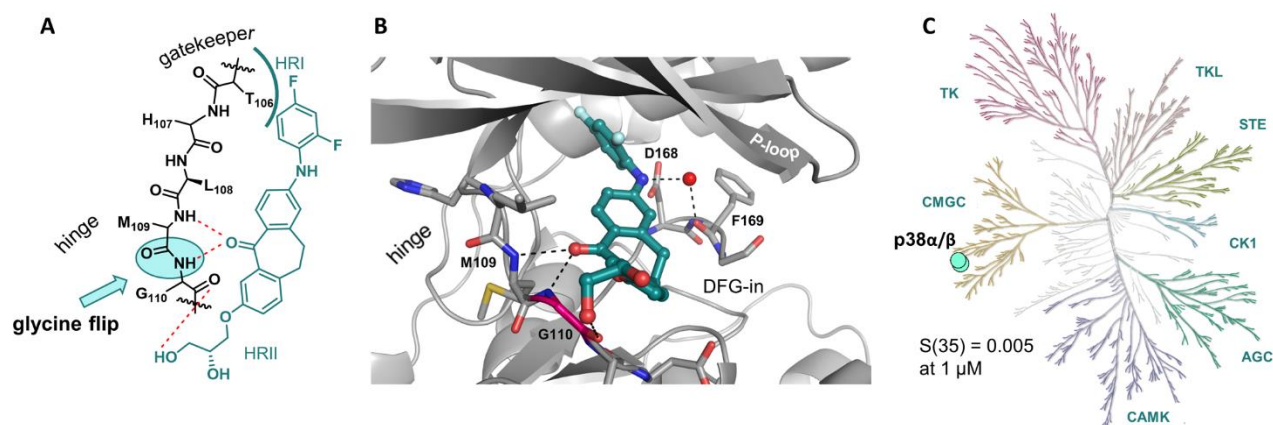
The research efforts of the last 20 years have produced a wealth of small-molecule inhibitors which, in addition to cancer treatment, have also shown to be efficacious in various non-life-threatening diseases. The stress-activated p38 MAPK regulates the production of pro-inflammatory cytokines such as TNF- $\alpha$  and IL-1 $\beta$  and is, therefore, an interesting target for inflammatory diseases such as rheumatoid arthritis, COPD and autoimmune diseases such as multiple sclerosis and psoriasis. While small molecules that inhibit p38 MAPK have entered clinical trials, no inhibitor has ever been approved by the FDA or other regulators. Although most of the compounds showed excellent *in vitro* potency as well as good cellular activity and have been shown to be effective in animal models, they failed in clinical trials due to, among other things, lack of selectivity. Although the targeting of different disease-related kinases has been shown to be partially helpful in cancer therapy, the associated side effects of the active substances are unacceptable for a, sometimes lifelong, therapy of non-life-threatening diseases. In order to contribute to the improvement of therapeutic options, new selective kinase inhibitors are needed that more precisely allow the investigation of the biological function of these targets. Different strategies have been developed to selectively target the highly conserved ATP-binding pocket in the 518 kinases (**Chapter 1.2**). For the development of selective p38 MAPK kinase inhibitors, canonical (type-I, type-II) and non-canonical binding strategies (type-I½) were applied and allosteric inhibitors (type-III and type-IV) were evaluated. These design approaches, which target differently localized binding pockets and unique, non-conserved structural elements in the kinase domain, have shown that the synthesis of selective compounds is possible. For p38 MAPK, five main strategies for the design of highly selective compounds can be proposed. Two strategies attempt to induce either a Gly110 or a Leu108 backbone flip in the hinge region which usually does not contain flexible glycine residues in protein kinases. The other three strategies either target Ala157 in the front pocket, the switch control residues Arg67, Arg70 and Arg149, or they try to capture the P-loop in a folded, inactive conformation. Since p38 MAPK has no cysteine residues in or in close proximity of the active site, the design of covalent inhibitors, which often shows a large increase in selectivity in other kinases (**Section 1.2.4**), is not possible.

The following section provides an overview of inhibitor design strategies that can be used to solve selectivity issues in p38 MAPK. Structural features that are important for the inhibition are discussed and approaches that could be used to design new selective p38 inhibitors in future research. For the synthesis of new selective p38 inhibitors in this doctoral work, a lead structure was selected which interacts with the P-loop as described in **Section 2.6**.

### 2.1 Targeting a glycine-flipped mode

The targeting of the small and not very common gatekeeper residue Thr106 in p38 $\alpha$ , which provides access to the hydrophobic pocket I formed by the N-terminal strands  $\beta$ 3,  $\beta$ 4,  $\beta$ 5 and the  $\alpha$ C helix, has delivered potent inhibitors (**Sections 1.2 and 1.5**). This design approach is well documented and has been one of the first to be used to synthesize selective p38 inhibitors, since access to the hydrophobic region I of other kinases is usually blocked by larger, space-occupying side chains. A second general design approach for the development of selective p38 inhibitors was outlined in 2003 by FITZGERALD ET AL. from Merck research laboratories, who were surprised by the selectivity of a number of quinazolinone and pyrido-pyrimidine

inhibitors that were not likely inhibitors based on docking studies.<sup>306</sup> Crystal structures of p38 $\alpha$  in complex with those compounds revealed an unprecedented binding mode in which Gly110 in the hinge region was rotated 180° relative to its orientation in the enzyme's apo- or ATP-bound structure. The flip of Gly110 was attributed to changes in the polarity of the inhibitor. The refined structure revealed that the carbonyl oxygen of the ligand induced the peptide main-chain flip, resulting in the formation of two hydrogen bonds with the backbone NH of Met109 and Gly110. These residues, crucial for facilitating the rotation, are poorly conserved and only found in a total of 46 kinases (9.2%) of the kinome. Other than in p38 $\alpha$ , the neighborhood of Gly110 and Met109 is present for instance in p38 $\beta/\gamma$ , but interestingly not in p38 $\delta$  and the closely-related MAP kinases JNKs and ERKs. The latter kinases have bulkier residues at this position that make the rotation energetically unfavorable.<sup>2, 284</sup> In general, compounds binding to the Gly110-flipped mode of p38 have shown to enhance kinome-wide selectivity, as concluded from mutational studies.<sup>306</sup> If Gly110 is replaced by an alanine or an aspartate residue, the ligand affinity for quinazolinones and pyrido-pyrimidines is significantly decreased, whereas the affinity of inhibitors not inducing a glycine flipped conformation remains unaffected. Since 2003, this design approach has been studied frequently and was successfully applied to synthesize selective compounds of different scaffolds. To date, the KLIFS database lists around 30 crystal structures, covering type-I, type-I½ and type-II inhibitors in complex with p38 $\alpha$ , highlighting this very versatile method. While *Merck* focused on dihydroquinazolinones, quinazolinones and pyrido-pyrimidines, *Vertex Pharmaceuticals* introduced the pyrimido-pyridazine scaffold for targeting the Gly110-flipped mode and established VX-745 (Neflamapimod).<sup>278</sup> As described already in **Section 1.5**, this compound is a very potent inhibitor of p38 $\alpha$  (IC<sub>50</sub> = 10 nM), showing also selectivity over the p38 $\beta$ -isoform (IC<sub>50</sub> = 220 nM).<sup>278</sup> X-ray structure analysis by AZEVEDO ET AL. highlighted an elongated conformation of the P-loop, where Tyr35 points into the allosteric site directing Arg67 from the  $\alpha$ C helix. At the same time, Phe169 from the A-loop DFG motif extends outside the DFG-out pocket, making a rarely seen face-to-edge  $\pi$ -interaction with Tyr35.<sup>307, 308</sup> VX-745 potently inhibited TNF- $\alpha$  and IL-1 $\beta$  release in isolated human peripheral blood mononuclear cell (PBMCs) and in human whole blood (IC<sub>50</sub> [TNF- $\alpha$ /IL-1 $\beta$ ] = 51/ 45 nM).<sup>278</sup> Furthermore, the compound demonstrated to be effective in a rheumatoid-arthritis model in mice and is currently in phase-II clinical trials on brain inflammations in Alzheimer disease. A set of highly selective inhibitors using this design approach has been published by LAUFER ET AL., with research focusing on the benzophenone<sup>309</sup>, dibenzepinone, dibenzoxepine and dibenzosuberone scaffold.<sup>49, 310-316</sup> In 2012 KÖBERLE ET AL. published Skepinone-L (**Figure 11A/B**), which is one of the first p38 type-I inhibitors showing an outstanding selectivity profile as well as a good cellular activity and *in vivo* potency.<sup>317</sup>



**Figure 11. Highly selective type-I inhibitor Skepinone-L adopting a glycine-flipped mode.** A) Schematic drawing of main hinge interactions. B) Crystal structure of Skepinone-L in complex with p38 $\alpha$  (PDB: 3QUE). Gly110 is highlighted in pink, hydrogen bonds in black and a structural water molecule is depicted as a red sphere. C) Selectivity profile of Skepinone-L screened at 1  $\mu$ M against 402 kinases. Selectivity score  $S(35)$  is given for compound comparison.

Skepinone-L was screened in a kinome-wide assay from *Ambit* against 402 kinases (**Figure 11C**) and exhibited a >1000-fold increased selectivity, only inhibiting p38 $\alpha$  and p38 $\beta$  at 1  $\mu$ M ( $K_d$ (p38 $\alpha$ )= 1.5 nM). The compound potently inhibited the production of IL-6, IL-8, IL-13, IL-17A and INF $\gamma$ , in agreement with the role of p38 MAPK in human peripheral blood mononuclear cells (hPBMCs).<sup>317</sup> However, no inhibition of IL-4, IL-5, MCP-1, IP-10 release was detected, although studies with the unselective inhibitor SB203580 suggested involvement in the p38 MAPK pathway. In further studies they analyzed the cellular selectivity due to phosphorylation of specific downstream signaling substrates for p38, JNK, ERK using either TNF- $\alpha$  or PMA treated THP-1 cells. The effect of Skepinone-L was compared with the ATP-competitive type-I inhibitor SB203580 and the type-II inhibitor BIRB-796, and the phosphorylation of Hsp27 (p38 substrate), CREB (ERKs substrate) and c-Jun (JNKs substrate) were analyzed by SDS-PAGE and Western blotting.<sup>317</sup> The results showed that Skepinone-L solely suppresses the phosphorylation of Hsp27, whereas BIRB-796 interferes also with the JNK signaling pathway, inhibiting phosphorylation of Hsp27 and c-Jun. However, the very unselective inhibitor SB203580 even diminishes the phosphorylation of all substrates. Although only a small group of MAPK substrates were examined in this study, the results clearly showed that non-selective inhibitors might trigger a variety of unpredictable signaling pathways. To increase the knowledge of the function and regulation of a protein of interest and to interpret results from previous biological studies, high quality probes are needed.

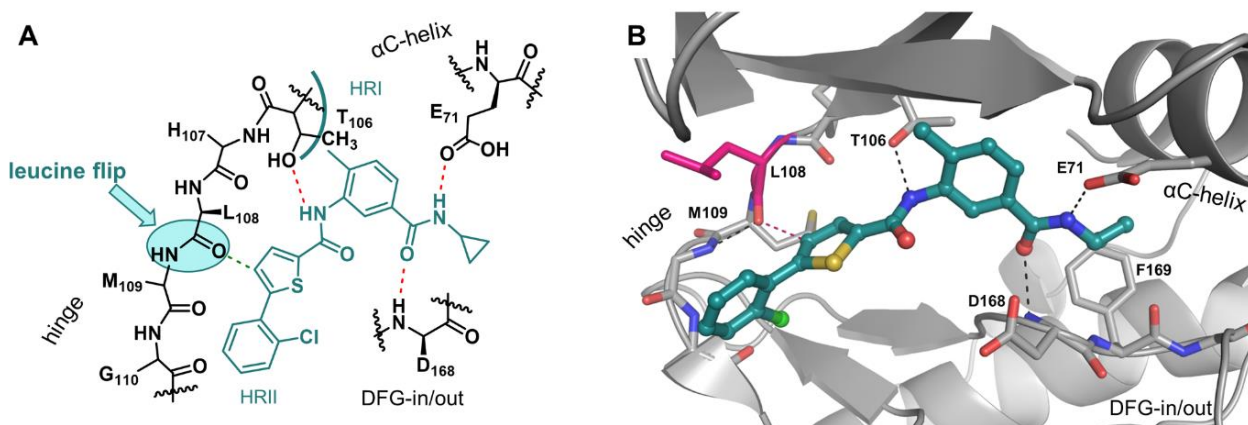
While most of the inhibitors use a carbonyl decoration at the hinge-binding head group to induce the Gly110 back-bone flip, JEROME ET AL. from *Pfizer* designed a triazolopyridine scaffold, in which neighboring nitrogen atoms each accept either a hydrogen bond from the main chain amide of Gly110 or Met109.<sup>318</sup> The usefulness of this hinge-binding heterocycle has been demonstrated in several studies and successfully used for the synthesis of type-I, type-I $\frac{1}{2}$  and type-II inhibitors.<sup>282</sup> A very similar binding mode was also found for the arylphthalazine scaffold synthesized by HERBERICH ET AL. in 2008.<sup>319</sup> In addition to the moieties described above, a rather uncommon aminopyridine *N*-oxid functionality was successfully exploited by LUMERAS ET AL., which delivered improved selectivity against a panel of 54 kinases as well as a good *in vivo* efficacy in an acute murine model of inflammation.<sup>320, 321</sup>

## 2.2 Targeting a leucine-flipped mode

Besides the already described Gly110 flip, *Bristol-Myers Squibb* reported an exceptional binding mode of potent p38 MAPK inhibitors in 2013.<sup>322</sup> While canonical inhibitors usually bind via the Met109 backbone amide NH to the hinge region, *Bristol-Myers Squibb* compounds induced a unique peptide backbone flip between Leu108 and Met109 in p38 MAPK. Intriguingly, these inhibitors, which don't seem to have an appropriate hinge binder at first glance, interacted with the hinge region by forming a non-classical aryl CH — O bond. As evident from the crystal structures solved (PDB: 4KIN, 4KIQ), each a thiophene or an indole C-4 aryl hydrogen bound to the carbonyl oxygen of Leu108. This binding mode was so far not seen in any other kinase and greatly enhanced the p38 $\alpha$ -isoform selectivity of these compounds. **Figure 12** illustrates the binding mode of BMS-5c in complex with p38 $\alpha$ . Besides the peculiar CH — O hydrogen bonding interaction (distance approx. 3 Å) from the thiophene carbon to the carbonyl oxygen atom of Leu108, the compound is stabilized in the binding pocket by a hydrogen bond with the gatekeeper-residue Thr106. The methyl group of the *ortho*-tolyl moiety targets the selectivity pocket of the hydrophobic region I (HRI) and further hydrogen bonds are formed between the terminal amide and the conserved Glu71/Asp168 pair. Thus, the cyclopropyl residue was placed in the back-pocket region, as is also the case with many other



type-I½ inhibitors. Lastly the sulphur atom of the thiophene stabilized the conformation of the inhibitor via an intramolecular  $n_o \rightarrow \sigma_s^*$  interaction.<sup>322</sup>



**Figure 12.**  $\alpha$ -Isoform selective type-I½ inhibitor BMS-5c adopting a leucine (Leu108) main chain flip. A) Schematic drawing of main hinge interactions CH — O interaction (green), hydrogen bonds (red). B) Crystal structure of BMS-5c in complex with p38 $\alpha$  (PDB: 4KIN). Leu108 is highlighted in pink with CH — O interaction in red, hydrogen bonds in black, and a structural water molecule is depicted as a red sphere.

The inhibitor showed a 55 times higher selectivity for the  $\alpha$ -isoform of the kinase, as determined by the  $IC_{50}$  values on isolated enzyme, which are 4.8 nM for p38 $\alpha$  and 265 nM for p38 $\beta$ . However, the compound showed only low activity in inhibiting the TNF- $\alpha$  release in human whole blood, which was explained by the low water solubility of BMS-5c and the associated high plasma protein binding (>99%) in whole blood. In these studies, the initial lead structure was also derivatized, and the thiophene ring system replaced by various substituted indole derivatives. In addition to the induction of Leu108/Met109 back-bone rearrangement, the p38 $\alpha$ / $\beta$  selectivity was significantly improved. In one particular case, a 625 times higher selectivity was determined for the p38 $\alpha$ -isoform ( $IC_{50}$  [p38 $\alpha$ /p38 $\beta$ ] = 35 nM/ 21920 nM), which represents the highest isoform selectivity achieved for p38 $\alpha$  to date. Furthermore, some selected hits were profiled in an Ambit kinome scan against more than 200 kinases and also showed excellent selectivity profiles.

### 2.3 Targeting rarely seen amino acid variations such as Ala157

Targeting non-conserved structural elements in kinases has proven to overcome selectivity issues and to deliver potent compounds. Advantageous inhibitor design approaches might therefore focus on the targeting of single amino acid variations in a kinase of interest. For p38 MAPK, targeting Ala157 has been described to improve the selectivity of inhibitors, as this residue is only present in seven kinases of the kinome. The small side chain of Ala157 is located at the bottom of the hydrophobic front pocket and selects between inhibitor binding to other kinases, since 98% of them have a bulkier amino acid at this position.<sup>2</sup> The beneficial effect of this design approach was first demonstrated by Amgen, who synthesized a series of arylphthalazine,<sup>319, 323</sup> pyrazolopyridinone,<sup>324, 325</sup> pyrazolopyridazine<sup>326</sup> and triazolopyridazinone<sup>327</sup> type-I½ inhibitor derivatives between 2008 and 2011. All inhibitors bound to the hinge region and used either a substituted 2-haloaryl residue, or in the case of the first published arylphthalazine series by WURZ ET AL. a 2-methyl substituted phenyl ring for tight hydrophobic van-der-Waals interactions with Ala157.<sup>319</sup> Interestingly, the phthalazine nitrogens also captured the kinase in a Gly110-flipped conformation and formed two hydrogen bonds with the hinge region, as shown by crystallographic studies (e.g. PDB: 3DS6).

In addition, the P-loop adopted a different conformation as a consequence of aromatic face-to-edge interaction with Tyr35 from the P-loop and the 2-methylphenyl residue of the inhibitor. Although the pyrazolopyridinones<sup>324</sup> (PDB: 3GFE) and the pyrazolopyridazines<sup>326</sup> (PDB: 3ITZ) did not adopt a Gly110-flipped conformation, these inhibitors showed similar or even higher selectivity compared with the already very selective phthalazines.<sup>319</sup> The latter was attributed to the additional interaction with the small gatekeeper-residue Thr106.

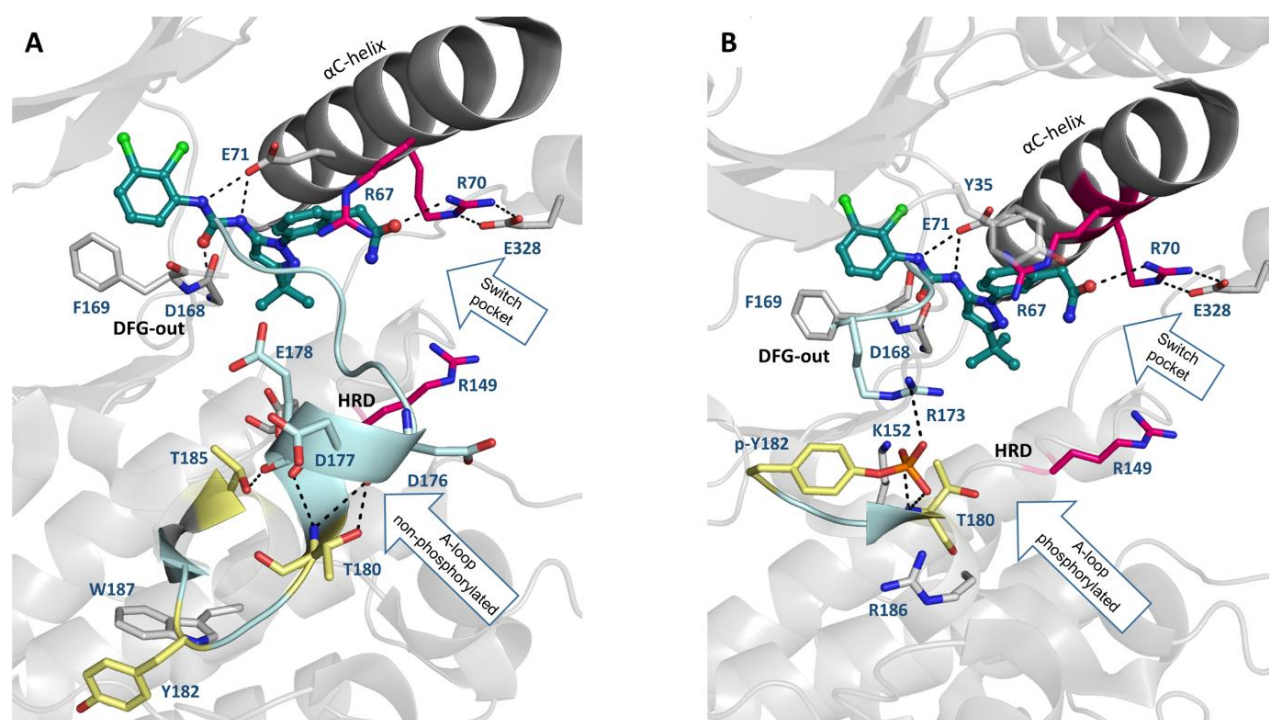
In 2011, SOTH ET AL. from *Roche* reported on the type-I inhibitor RO6226 (molecule in **Figure 15**), a pyrazolopyrimidine derivative that showed excellent selectivity in an *Ambit kinome scan* against a panel of 363 kinases and only inhibited p38 $\alpha/\beta$  at a concentration of 10  $\mu\text{M}$ .<sup>328</sup> The compound showed a good *in vitro* potency ( $\text{IC}_{50}$  [p38 $\alpha$ / p38 $\beta$ ] = 1 nM/ 25 nM) and inhibited the *ex vivo* LPS-induced TNF- $\alpha$  release in rats ( $\text{ED}_{50}$  = 1.5 mg/kg,  $\text{EC}_{50}$  = 0.76  $\mu\text{M}$ ). The superb features of this inhibitor are explainable by the crystal structure solved in complex with p38 $\alpha$  (PDB: 3FMM). The compound engaged the kinase in a folded P-loop conformation, formed hydrogen bonds with the hinge region Met109 and the gatekeeper-residue Thr106, and the methyl group of the sulphonamide side chain made van-der-Waals contacts to Ala157 as previously shown by the inhibitors from *Amgen*.

## 2.4 Targeting the switch-control residues

p38 is activated through dual phosphorylation at Thr180 and Tyr182 in the activation segment. The change in polarity triggers huge structural rearrangements, in which the A-loop adopts an active, open DGF-in conformation allowing access to the ATP-binding pocket and subsequent binding of ATP. During this event, the phosphorylated and hence negatively charged amino acids are stabilized by basic arginine residues, which are therefor called switch-control residues. After dephosphorylation and inactivation of the kinase, these arginine residues typically get repelled from the phosphorylation site, allowing structural rearrangements necessary to adopt an inactive, closed DFG-out form. The switch-control mechanism is a common structural hallmark found in many kinases and reflects the evolutionarily highly conserved activation mechanism of these enzymes, although the structure and location of the switch pocket differs between family members. In the case of p38 MAPK the conformational flexibility is controlled by Arg67, Arg70 from the  $\alpha\text{C}$  helix and Arg149 from the HRD segment located at the catalytic loop, which interfere with phosphorylated Thr180. The phospho-state of Tyr182 is controlled by the interaction with Arg186 and Arg189 from the A-loop.<sup>329</sup>

Targeting the switch-pocket residues of p38 MAPK has been first described in patents from *Deciphera Pharmaceuticals LLC* in 2004 as a new allosteric approach to generate highly effective inhibitors.<sup>330-332</sup> Allosteric BIRB-796 fragments were used as starting point for the investigation of the switch pocket, which is located opposite to the ATP binding site.<sup>265</sup> Interestingly, the developed compounds displayed excellent selectivity profiles, which was not only due to the allosteric binding mode but also due to a hydrogen bond with Arg70. The latter is a non-conserved amino acid, which is only accessible in the inactive state in p38 $\alpha/\beta$ . In 2010 AHN ET AL. from *Deciphera Pharmaceuticals LLC* published the first crystal structures from a series of compounds decorated with cyclic and linear polar moieties for targeting Arg70.<sup>329</sup> Besides the various residues introduced, such as pyrazolidinediones, triazolinediones, acyclic and cyclic sulfonylureas, *para*-thiomorpholino-*S*-dioxide amide, aminomethyl, hydroxymethyl and carboxyethyl, a *meta*-acetamide substituted phenyl residue delivered the potent and selective compound DP802. Crystal structures of DP802 in complex with p38 $\alpha$  were determined with both the inactive non-phosphorylated (PDB: 3NNW) and the active phosphorylated form of the kinase (PDB: 3NNX), revealing a unique mechanism of the inhibition.<sup>329</sup>

In the inactive unphosphorylated form of p38 MAPK (**Figure 13A**), the *meta*-acetamide carbonyl oxygen atom interacted with Arg70 via a hydrogen bond, whereas hydrophobic interactions with Arg67 also took place inside the switch pocket. Arg70 itself was further stabilized by Glu328, and Arg67 by an edge-to-face  $\pi$ -stacking interaction with Tyr35 from the P-loop (not shown, see **Figure 13B**). The *tert*-butyl residue of the compound bound to the DFG-out deep pocket, whereas the chloro-decorated phenyl residue protruded into the hydrophobic pocket II (HRII). The central urea moiety of DP802 formed a hydrogen bond with the conserved Glu71 ( $\alpha$ C helix) and Asp168 (DFG motif). The unphosphorylated amino acid, Thr180, interacted with the acidic amino acids Asp176, Asp177 and Glu178, resulting in a network of stabilizing hydrogen bonds. The unphosphorylated Tyr182 residue was stabilized by hydrophobic  $\pi$ -stacking interactions with Trp187. Furthermore, Glu178 stabilized Thr185, which was suggested to act as a pseudo-substrate, making hydrophobic contacts with Asp150 from the catalytic machinery (HRD segment).



**Figure 13. Inactive and active phosphorylated state of p38 $\alpha$  MAPK.** A) DP802 (teal) in complex with unphosphorylated p38 $\alpha$  (PDB: 3NNW). B) DP802 (teal) bound to the active DFG-in kinase conformation (PDB: 3NNX) with distorted A-loop. Switch pocket residues are shown in pink, the A-loop in light blue, and the phosphorylation site in light yellow.

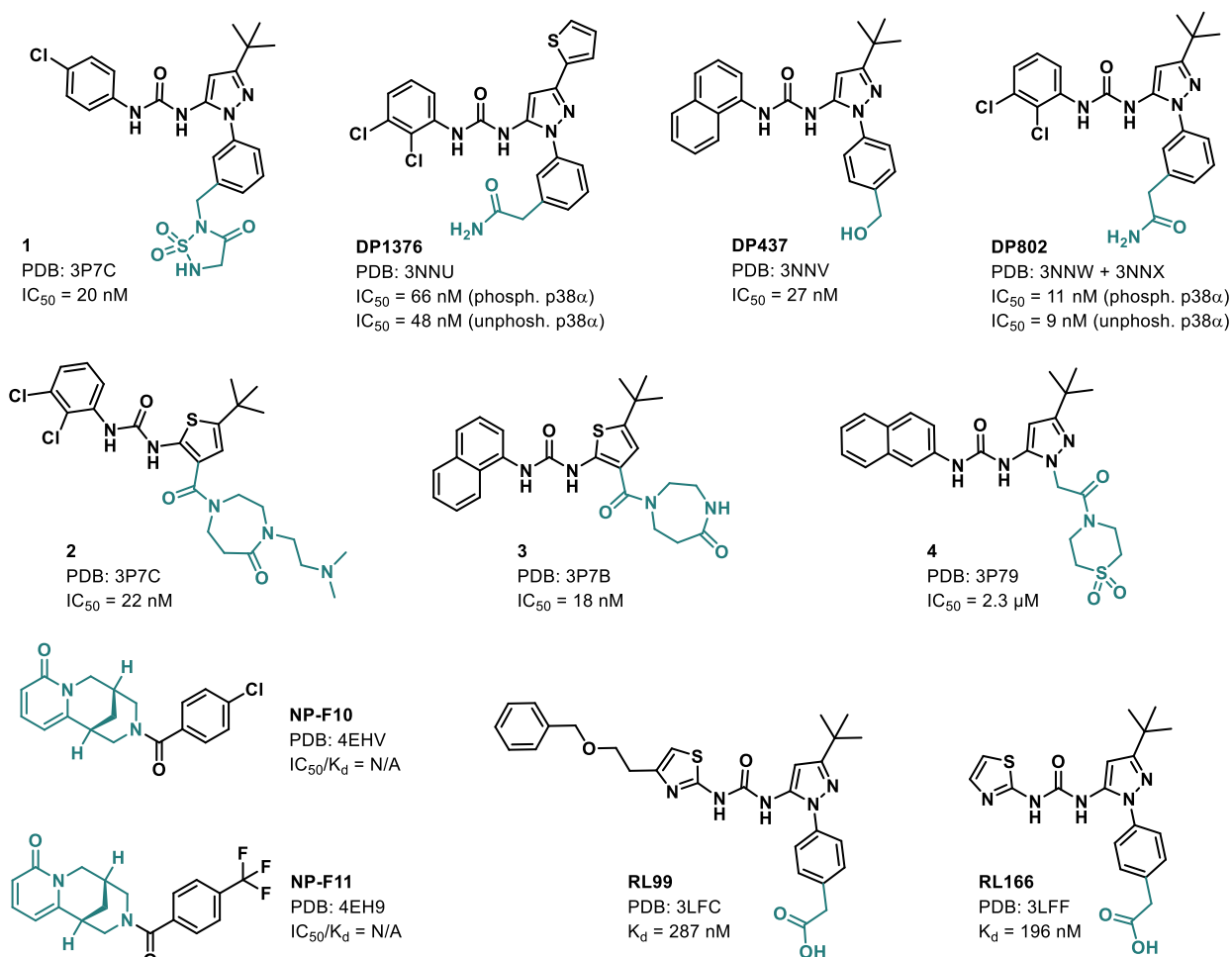
In contrast, the active state of p38 $\alpha$  (**Figure 13B**) was characterized by double phosphorylation at Thr180 and Tyr182. The binding of the inhibitor DP802 led to a structural rearrangement within the kinase domain, which was very similar to the inactive DFG-out form. In this phosphorylated active state, charge repulsion occurred between the negatively charged phospho-Thr180 and Asp176, Asp177 and Glu178, which were disordered in the crystal structure. In contrast, phospho-Tyr182 formed a salt bridge with Arg173, and the negative charge was additionally shielded by Arg186 from the A-loop and to Lys152 from the C-loop. The unusual binding mode of DP802 had a dramatic effect on the *in vivo* stability of the protein in HeLa cells.<sup>329</sup> In this study, the dephosphorylation of double phosphorylated p38 $\alpha$  by cellular phosphatases was investigated. DP-802 dose-dependently inhibited the cellular phosphorylation of p38 $\alpha$  (IC<sub>50</sub> = 19 nM), which was attributed to Thr180 and the reordered Tyr182 being more accessible to phosphatases upon inhibitor binding.<sup>329</sup> The *in vivo* potency of DP802 was further investigated in Lewis rats, and the compound also potently inhibited LPS-stimulated TNF- $\alpha$  release (ED<sub>50</sub> = 3.6 mg/kg).<sup>329</sup> Targeting the switch-control residues of p38 with inhibitors similar to DP802 might therefore have a particularly beneficial therapeutic effect, as

the compounds not only efficiently inhibit p38 signaling, but also recruit cellular phosphatases, which then rapidly dephosphorylate the kinase. The latter would have an additional damping effect on the signaling pathway upstream of p38 MAPK.

Two independent working groups from *Abbott Laboratories* and *Ansaris*, a division of *Locus Pharmaceuticals*, have published their work on p38 switch pocket inhibitors in 2010 and 2011.<sup>333, 334</sup> Interestingly, all researchers used BIRB-796 as lead structure, in which the switch pocket partially overlaps with the DFG-out deep pocket binder of BIRB-796, but different approaches were applied for the generation of highly selective compounds. In the publication by SWANN ET AL. the switch pocket area around the tolyl residue of BIRB-796 was explored using a model created from a patent-derived compound **1**.<sup>333</sup> The compounds shared the common pyrazole urea scaffold of BIRB-796 and did not make any contacts to the hinge region. The tolyl residue was replaced by a phenyl residue with a cyclic sulfonylurea in the *meta*-position. Several amide-based *meta*-substitutions targeting Arg70 and Asp168 of the DFG-motif have been proposed by docking into the switch pocket, whose shape is mainly controlled by the conformation of the P-loop, the  $\alpha$ C helix and the A-loop DFG segment. The on-target potency of the synthesized compounds was investigated by a TR-FRET assay on isolated enzyme, which further revealed that alkyl- and aryl-substituted amides with polar side-chain moieties were advantageous structures, while compounds with non-polar aromatic decorations interacted only weakly ( $K_i > 1 \mu\text{M}$ ) with p38. Although the compounds were not as potent ( $K_i$  between  $0.09 \mu\text{M}$  and  $0.9 \mu\text{M}$ ) as the type-I inhibitor SB203580 ( $K_i = 0.06 \mu\text{M}$ ), type-II inhibitor BIRB-796 ( $K_i = 0.02 \mu\text{M}$ ) and the lead compound ( $K_i = 0.10 \mu\text{M}$ ), selectivity profiles with very narrow off-target activity were obtained. Kinetic measurements also showed that the synthesized compounds and **1** exhibited slow-on rates, indicating that these inhibitors, similar to the type-II inhibitor BIRB-796, bound to the inactive DFG-out form of the kinase.

MOFFETT ET AL. used a virtual fragment-based drug design approach (vFBDD) to identify new non-aromatic fragments that form hydrogen-bond interactions with Arg70 to achieve selectivity.<sup>334</sup> Based on the crystal structure of BIRB-796 in complex with p38 $\alpha$  (PDB: 1KV2), 800 fragments were simulated by a grand canonical Monte Carlo simulation (GCMC), which predicted the dynamic movement of the ligand in the binding site. The free energies of binding to the protein of the small organic molecules found were calculated, and fragments with similar computed free energy were clustered into corresponding groups. A representative collection of seven compounds was selected as most drug-like and chosen for synthesis. Fragments with non-aromatic character, which carried polar groups such as cyclic amides and sulfoxides, and which were partially hydrophobic in structure, were preferably selected to achieve sufficient interaction with the tolyl (switch pocket) site. Further SAR studies finally led to compound **2**, which showed low nanomolar potency against p38 $\alpha$  ( $\text{IC}_{50} = 22 \text{ nM}$ ) and p38 $\beta$  ( $\text{IC}_{50} = 50 \text{ nM}$ ). In a selectivity screening against 150 kinases, besides p38 $\alpha$  and p38 $\beta$  no other kinases were targeted by compound **2**.<sup>334</sup> This behavior was underlined by the crystal structure in complex with p38 $\alpha$  (PDB: 3P7C), in which a hydrogen bond interaction between the lactam carbonyl group and the non-conserved Arg70 residue was formed, and hydrophobic interactions with the diazepamone ring in the tolyl pocket were observed. In addition to its efficacy and high selectivity, compound **2** has also been shown to be effective in *in vitro* and *in vivo* studies. Depending on the dose, compound **2** inhibited the release of TNF- $\alpha$  and IL-1 $\beta$  in an LPS-stimulated mouse model and showed good oral bioavailability when administered to rats (33% at 4 mg/kg). In addition, the compound displayed low micromolar activity toward CYP3A4 and showed high binding affinity in an hERG screen.<sup>334</sup> At present, the KLIFS database (<http://klifs.vu-compmedchem.nl>)<sup>335, 336</sup> lists eleven crystal structures with compounds that target the switch pocket and form specific interactions with the positively charged guanidinium group of Arg70 (PDB: 3NNU, 3NNV, 3NNW, 3NNX by AHN ET AL. PDB: 3P79, 3P7B, 3P7C by

MOFFETT ET AL.; PDB: 3LFC, 3LFF by RAUH ET AL.; PDB: 4EH9, 4EHV by OVER ET AL.) Those compounds were investigated between 2010 and 2013 (**Figure 14**).<sup>329, 334, 337</sup>



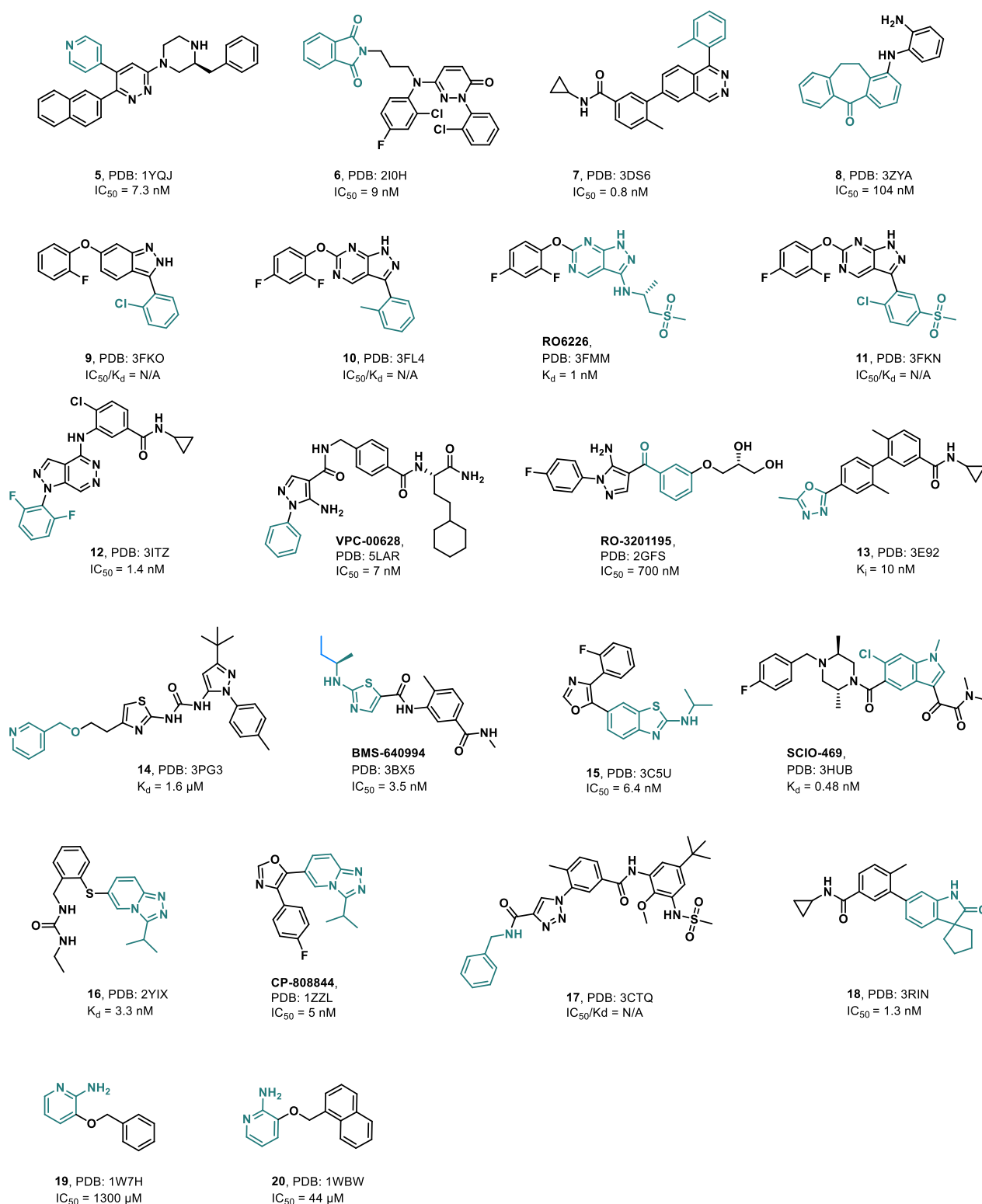
**Figure 14. Overview of selected p38α switch control pocket inhibitors.** Functional groups interacting with switch pocket colored in blue. IC<sub>50</sub> or K<sub>d</sub> values on isolated enzyme p38α (non-cellular assay) are given from ChEMBL database (<https://www.ebi.ac.uk/chembl/>) if available.<sup>338, 339</sup>

With the exception of the structures published by OVER ET AL., all inhibitors shared a common core scaffold derived from BIRB-796,<sup>265</sup> with a *tert*-butyl or thiophene moiety for targeting the DFG-out pocket. Since the DFG-out pocket of p38α has a unique isoleucine (Ile141) residue at the bottom of the pocket, bulky residues can easily enter. The latter offers a selectivity advantage over related kinases, with more space occupying amino acids at this position.<sup>306</sup> In this study, the tolyl moiety of BIRB-796 was replaced by a *para*- or *meta*-substituted phenyl residue to form hydrophobic interactions within the allosteric binding pocket. For interaction with the basic arginine residues, such as Arg70, the hydrophobic moieties were each equipped with a linker that had a free terminal amide, carboxylic acid or carbonyl group. A hinge-binding motif was not used in these studies. Interestingly, in 2013 OVER ET AL. reported two natural product derived cytosine inhibitors, NP-F10 and NP-F11, found in a fragment-based ligand discovery study.<sup>57</sup> Although, they share a weak *in vitro* potency (IC<sub>50</sub> [NP-F10] = 5.1 μM, IC<sub>50</sub> [NP-F11] = 5.5 μM), the crystal structures in complex with p38α (PDB: 4EH9 and 4EHV) revealed a unique binding mode that targeted the switch-pocket residues and participated in hydrogen bond interactions with Arg70. The cytosine scaffold can therefore be used as a unique lead structure to generate highly selective and potent inhibitors of p38 MAPK in future studies.

## 2.5 Targeting of folded P-loop conformations

A beneficial approach to the design of inhibitors with narrow selectivity profiles was demonstrated by a series of kinase inhibitors that captured the glycine-rich loop in an energetically less-favored conformation. The glycine-rich or phosphate-binding loop (P-loop) is a very flexible structural element typically found in kinases possessing a GXGX $\phi$ G sequence motif. In addition to the small glycine residues (G), tyrosine and phenylalanine residues ( $\phi$ ) are commonly found at the tip of this loop region, which supports the binding of the cofactor ATP. In the active form of a kinase, the P-loop usually adopts an extended, rather flat geometry in which the aromatic side chains of phenylalanine and tyrosine point away from the ATP-binding site. Interestingly, inhibitors of p38 MAPK have shown to engage the tyrosine residue (Tyr35) via aromatic stacking interactions and led to the rotation and folding of the P-loop inside the ATP binding site.<sup>54</sup> Ligand-induced folding of the P-loop has so far been rarely observed in other kinases.

Currently, the KLIFS database lists 78 PDB structures of 15 different kinase targets with a P-loop rotation of  $\leq 20^\circ$  (folded) namely: ABL1/2, AURA, EPHA3, FGFR1/4, p38 $\alpha$ , MAP4K4, MET, PIM1, PLK4, SLK, TYK2, VRK1 and ZAK. From these structures, 23 inhibitors were crystallized in complex with p38 $\alpha$ , showing that the inhibitors form both aromatic stacking interactions and hydrophobic interactions with Tyr35 (**Figure 15**). A collectively shared structural hallmark of these inhibitors for capturing the P-loop is an aromatic or heteroaromatic head group, such as a substituted phenyl,<sup>319, 326, 340, 341</sup> benzyl,<sup>342</sup> pyridine,<sup>343</sup> picoline or phthalimide,<sup>344</sup> adjacent to the hinge-binding moiety and protruding into the hydrophobic pocket (HR-I) or extending to the solvent-exposed region of the front cleft. Furthermore, various hinge-binding motifs such as 2-aminopyridines,<sup>345, 346</sup> oxadiazoles,<sup>347</sup> thiazoles,<sup>348</sup> benzothiazoles,<sup>349</sup> indoles,<sup>350, 351</sup> dibenzosuberone,<sup>317</sup> pyrazolo[3,4-*d*]pyrimidines,<sup>328</sup> and [1,2,4]triazolo[4,3-*a*]pyridines<sup>282, 352</sup> can interact directly with Tyr35 via  $\pi$ -stacking contacts (**Figure 15**). Although these decorations are quite common, the folding of the P-loop cannot be easily predicted for other kinases, since most of these folded conformations were found coincidentally. Presumably, a specific combination of these heteroaromatic head groups, functionalized with different structural moieties, might form the basis to successfully engage the P-loop. The intrinsic ability of the P-loop to fold is most likely of secondary importance, since this region has a high sequence similarity within the kinase family.<sup>54</sup> Almost all p38 $\alpha$  inhibitors that induced a folded P-loop conformation bound to the DFG-in form of the kinase, while the  $\alpha$ C helix adopted an out-like structure. However, this was not seen in the crystal structures of inhibitors with a type-II binding mode (**14**, **17** and VPC-00628). While **17** (PDB: 3CTQ) and VPC-00628 (PDB: 5LAR) occupy a DFG-out/ $\alpha$ C-in conformation in p38, compound **14** (PDB: 3PG3) stabilized a DFG-out/ $\alpha$ C-out conformation. Interestingly, SCIO-469 (Talmapimod, PDB: 3HUB) was the only inhibitor among the above search criteria that bound to the active DFG-in form of the kinase and simultaneously pushed the  $\alpha$ C helix away from the active center (DFG-in/  $\alpha$ C-out).



**Figure 15. Inhibitors in complex with p38 $\alpha$  found in the KLIFS database (<http://klifs.vu-compmedchem.nl>)<sup>335, 336</sup> with folded P-loop conformation. Cut-off value: P-loop rotation of  $\leq 20^\circ$ , structure moieties that induce aromatic face-to-face, face-to-edge interactions or hydrophobic interactions with Tyr35 are highlighted in teal. IC<sub>50</sub> or K<sub>d</sub> values on isolated enzyme p38 $\alpha$  (non-cellular assay) are given from ChEMBL database (<https://www.ebi.ac.uk/chembl>).<sup>338, 339</sup>**

In 2005, TAMAYO ET AL. from Amgen reported a set of pyridine-substituted pyridazine inhibitors.<sup>343</sup> The heteroaromatic core scaffold of the compounds participated in a face-to-face and face-to-edge as well as hydrophobic interaction with Tyr35, as shown by a representative crystal structure (compound 5, PDB: 1YQJ). In this noteworthy folded P-loop conformation, the glycine-rich element was found in a strongly

rotated arrangement (rotation  $\sim 15.3^\circ$ ), which was in sharp contrast to a typically found extended P-loop, such as in the type-I inhibitor SB203580 (P-loop rotation  $\sim 41.6^\circ$ ). The initial dibenzosuberone lead structure **8** (PDB: 3ZYA),<sup>312, 316</sup> which was used for the design of Skepinone-L<sup>317</sup> (see **Section 2.1**) by KOEBERLE ET AL., showed a very similar aromatic face-to-face and aromatic face-to-edge contact with Tyr35. In the this folded P-loop conformation, the loop was rotated by  $9.1^\circ$  compared with Skepinone-L adopting an extended P-loop conformation (P-loop rotation =  $57.2^\circ$ ). Although **8** and other monosubstituted dibenzosuberone derivatives bound potently to p38 $\alpha/\beta$ , *in vivo* efficacy in whole blood was low due to the high lipophilicity of these compounds.<sup>326</sup>

A comparable case, in which a compound bound to a folded P-loop conformation, concurrently inducing a Gly110 main-chain peptide flip, was found in the SCIO-469/p38 $\alpha$  complex (PDB: 3HUB).<sup>307, 353</sup> While the carbonyl group of this indole-based piperazinyl ketone targeted the amide (NH) back bone of Met109 and Gly110, respectively, the substituted piperazine made hydrophobic van-der-Waals contacts with Tyr35. Additionally, polar interactions from the nitrogen atom of the piperazine ring supported the folding of the glycine-rich loop. SCIO-469 showed a potent inhibition of p38 $\alpha$  ( $K_i = 9$  nM), with a 10-fold isoform selectivity over p38 $\beta$  ( $K_i = 98$  nM). Furthermore, it also displayed selectivity against the near relative MAP kinases ERK2 and JNK1, as well as LCK, each having a  $K_i$  value of  $>5000$  nM.<sup>354</sup> The very promising inhibitor SCIO-469 completed clinical phase II studies in 2004, in which the compound was tested in patients with rheumatoid arthritis and multiple myeloma. A highly distorted P-loop was furthermore found in the indonlin-2-one derivative **18** published by EASTWOOD ET AL.<sup>351, 355, 356</sup> in complex with p38 $\alpha$  (PDB: 3RIN). Obvious from this structure, the spiro-cyclopentyl moiety formed hydrophobic contacts to Tyr35 and to several other amino acids in the front cleft. During profiling against a panel of 50 kinases and 50 different receptor types, only c-Raf ( $IC_{50} = 200$  nM) was inhibited at  $10 \mu\text{M}$  in addition to p38 $\alpha$  ( $IC_{50} = 1.3$  nM), and the activity of the serotonin receptor, 5HT1B, was inhibited by 87%.<sup>351</sup> An explanation for the high selectivity and potency of the compound can be derived from the crystal structure in complex with p38 $\alpha$ , where, in addition to the folded P-loop conformation, the carbonyl group of the indoline scaffold induced a Gly110 flip upon binding to the hinge. The cyclopropyl amide decoration further interacted with the hydrophobic back pocket II (HRII) and formed hydrogen bond contacts with the conserved Asp167 (DFG) and Glu71 ( $\alpha\text{C}$  helix), as typically seen in type-I $\frac{1}{2}$  inhibitors.

In 2005, researchers at *Pfizer* were interested in replacing the hinge-binding benzimidazolone head group of their previously published p38 inhibitors with alternative bioisosteres.<sup>352</sup> To address this issue, they used a computational approach to calculate descriptors to predict useful hydrogen bond acceptor fragments. The most interesting bioisosteres were selected for synthesis and were subsequently tested on the isolated enzyme for their inhibition of p38 $\alpha$ . Interestingly, in these studies, they discovered the [1,2,4]triazolo[3,4-*a*]pyridine derivative CP-808844, which bound potently ( $IC_{50} = 5$  nM) to p38 $\alpha$  MAPK and coincidentally induced the rarely seen folded P-loop conformation (PDB: 1ZZL). In addition, the compound also triggered the Gly110 main-chain flip as seen for the indonlin-2-one inhibitor **18** described before. In a follow-up study, they continued to be interested in a type-II inhibitor of this scaffold type and synthesized urea-substituted [1,2,4]triazolo[3,4-*a*]pyridine derivatives, such as **16** (PDB: 2YIX), with which they investigated the influence on chronic obstructive pulmonary disease (COPD) in 2011.<sup>282</sup>

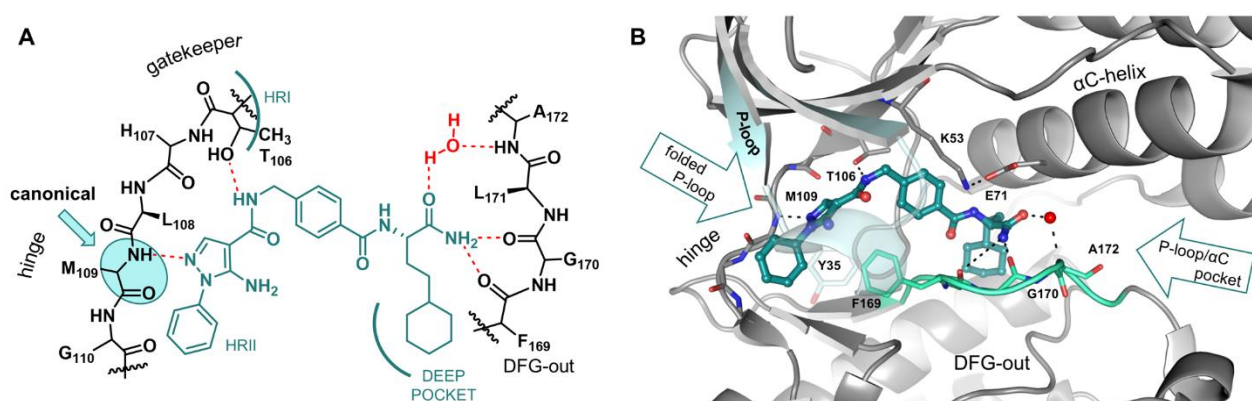
A unique binding mode can also be found in the crystal structure of p38 $\alpha$  with the 2-arylpyridazin-3-one derivative **6** (PDB: 2iOH) published by NATARAJAN ET AL. in 2006.<sup>344</sup> While the carbonyl oxygen of the former scaffold contacts Met109 in the hinge region, a phthalamide decorated with a flexible propyl linker formed strong, attractive face-to face  $\pi$ - $\pi$  interactions (distance  $\approx 3.8$  Å) with Tyr35, whereby the P-loop was folded



inside the adenine binding pocket (P-loop rotation =  $8.6^\circ$ ). The strongly bend conformation of the inhibitor was additionally reinforced by the weak aromatic stacking and hydrophobic interaction with the 2-chlorophenyl decoration perpendicular to the hinge binding functionality. Changing the propyl linker to a shorter ethyl linker prohibited the favorable engagement of the glycine-rich loop.<sup>344</sup> Therefore, the flexibility and length of the linker in this case had a decisive contribution to the strength of ligand binding to p38 MAPK. The p38 MAPK inhibitor VPC-00628, published in 2016 by PETERSEN ET AL., has, among the inhibitors described so far, a unique three-peptide like scaffold.<sup>340</sup> Due to its rarely seen type-II binding mode, also inducing a folded P-loop conformation, the compound was selected as very promising lead structure in the following work. The next section therefore focusses in more detail on this interesting binding mode.

## 2.6 The selection of the lead structure

The lead structure VPC-00628 was originally identified from a 12.6 million member DNA-encoded small molecule library using yoctoReactor and binder trap enrichment technology.<sup>340, 357, 358</sup> During this screen, p38 $\alpha$  was used as the first model system to demonstrate the performance of the binder trap enrichment technology, previously developed by *Vipergen* in Copenhagen. The homogeneous screening method is unique in that it uses a water-in-oil emulsion system to trap DNA-encoded small molecules (e.g. from a yoctoReactor library) bound to a DNA-tagged protein of interest. By ligating the DNA strands in the formed emulsion droplets, followed by amplification and sequencing, molecules that bound to the target of interest are easily disclosed. The method is very powerful, as the most affine 97 hits for p38 $\alpha$  from a library of 12.6 million compounds were identified after a single screen. The detected hits were then clustered by Tanimoto similarities, and the most interesting 24 compounds were selected for synthesis. To confirm the binding of the compounds to p38 $\alpha$ , IC<sub>50</sub> values were determined on isolated enzyme, with VPC-00628 identified as the most potent hit (IC<sub>50</sub> = 7 nM). VPC-00628 has a three-peptide-like structure and harbors a lipophilic cyclohexyl decoration linked via substituted amides to a pyrazole heterocycle, as frequently seen, for example, in BIRB-796 and its allosteric derivatives (**Figure 16A**). Since VPC-00628 did not appear to have a hinge-binding motif at the first glance, a crystal structure in complex with p38 $\alpha$  was solved and several unexpected key features of the binding mode were discovered (PDB: 5LAR, **Figure 16B**).



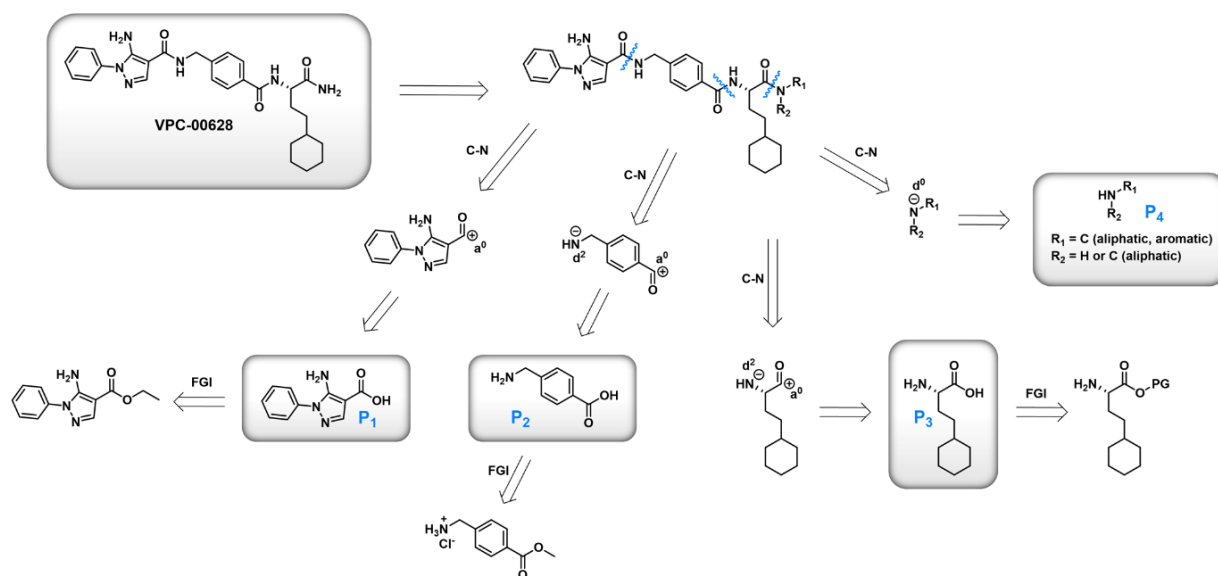
**Figure 16. Unique folded P-loop binding mode of VPC-00628.** A) Schematic binding of the lead structure VPC-00628 in p38 $\alpha$ . B) Crystal structure of VPC-00628 (PDB: 5LAR) in complex with p38 $\alpha$ . Folded P-loop (light blue), DFG-motif (cyan) and P-loop/ $\alpha$ C pocket are highlighted. A structural water molecule interacting with the ligand is depicted as a red sphere.

Interestingly, the amino-pyrazole decoration of VPC-00628 did not interact with the allosteric site as anticipated but showed an orientation rotated by  $180^\circ$ , in which the pyrazole nitrogen atom made contact

with the hinge region via Met109. In addition, the compound bound to the inactive DFG-out state, as seen in type-II inhibitors, in which the cyclohexyl moiety entered tightly into the DFG-out deep pocket. Besides the formation of hydrogen bonds with the conserved Phe169 and Gly170 from the DFG-motif, a water-mediated hydrogen bond was formed with Ala172. Another unexpected feature was an altered folded conformation of the P-loop. The phenyl-decorated amino-pyrazole hinge binder of VPC-00628 interacted with Tyr35, located at the tip of the P-loop, through aromatic face-to-face interactions that led to the folding of the glycine-rich loop inside the ATP-binding pocket. The folding process was further supported by a face-to-edge interaction with Phe169 from the DFG-motif. The movement of the P-loop exposed an enlarged allosteric pocket (P-loop/ $\alpha$ C pocket) that was originally believed to serve as a channel to tether the linker from the DNA-encoded library to the terminal amide of the inhibitor.<sup>340</sup> Although VPC-00628 did protrude into this pocket area, it was previously shown that targeting of this specific pocket in ERK1/2 by the inhibitor SCH772984 was possible and greatly enhanced the inhibitor selectivity and ligand efficacy.<sup>56</sup> Since this allosteric site in p38 $\alpha$  features His64, Arg67 and Arg70 from the  $\alpha$ C helix, an extension of the terminal amide could create favorable stacking interactions within this area. Additionally, Arg70 is a non-conserved amino acid that is only found in p38 $\alpha/\beta$  and also belongs to the switch-pocket residues described above (Section 2.4). Therefore, a very interesting selectivity profile of such VPC-00628 derivatives can be expected.

### 2.6.1 Retrosynthetic analysis

VPC-00628 was selected for the design, synthesis and preliminary evaluation of derivatives aimed at studying the binding mode of type-II inhibitors, isoform selectivity and interactions in the allosteric P-loop/ $\alpha$ C pocket in p38 MAPK. Therefore, a novel synthesis route for the preparation of VPC-00628 derived library compounds was established. By analyzing the lead structure retrosynthetically (Scheme 1), the three amide bonds in VPC-00628 were disconnected, delivering the respective negatively charged donor and positively charged acceptor synthons each. Four synthetic equivalents (P1 to P4) were then formulated, and reagents were selected to enable the reaction using the FGI (functional group interconversion) approach.



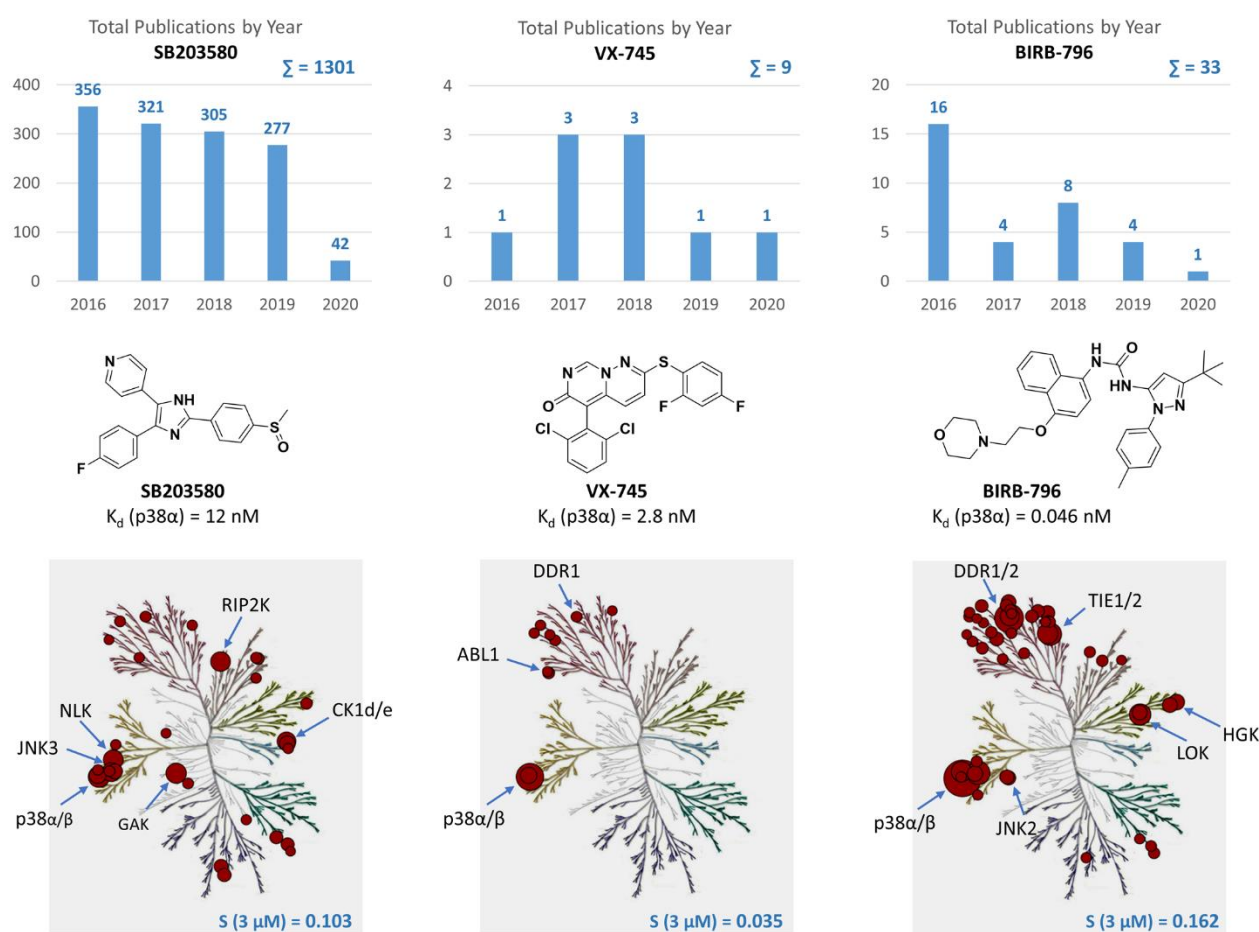
**Scheme 1. Retrosynthetic analysis of VPC-00628.** C–N disconnections are marked with jagged lines (blue), donor (d) and acceptor (a) synthons are classified. Synthetic equivalents and building blocks P1, P2, P3 and P4 are highlighted, FGI (functional group interconversion), PG (protecting group).

The following **Chapter 3** describes the fast iterative synthesis approach applied for the synthesis of a highly selective type-II inhibitor probe for p38 MAPK. In this study, the hinge-binding building block (P1), the linker (P2) and allosteric back-pocket motif (building block P3) of VPC-00628 were each varied. Besides the elucidation of structural features for the P-loop folding process and the identification of optimal pocket decorations, the  $\alpha/\beta$ -isoform selectivity of the compound library was monitored.

VPC-00628 derivatives were subsequently used for targeting the allosteric back and P-loop/ $\alpha$ C pockets of p38 MAPK, by adding a fourth building block (P4) to the core scaffold of VPC-006. In this study, a second highly selective p38 compound was identified and extensively evaluated (**Chapter 4**). The latter was then also used for the synthesis of a highly selective and potent dual DDR/p38 MAPK inhibitor probe (**Chapter 5**). In this study the P1 and P4 building blocks were each varied and optimized for the inhibition of DDR1/2 kinases.

### 3 Developing a chemical type-II inhibitor probe for p38 MAPK

p38 MAPK is a very prominent target that has attracted much attention because it is of central importance in inflammatory events. Years of research, documented in over 10,000 publications, have led to the development of a diverse set of inhibitors that show excellent potencies *in vitro* on the isolated enzyme and in a cellular environment, and they are also effective *in vivo* in animal models. Unfortunately, however, the most commonly used inhibitors have low selectivity, making it difficult to study the signaling pathway in detail. Upon reviewing the literature, it quickly becomes apparent that the selectivity profiles of many p38 inhibitors have either not been determined or are incomplete, since the compounds were characterized only against a small number of kinases (**Figure 17**).<sup>136</sup>



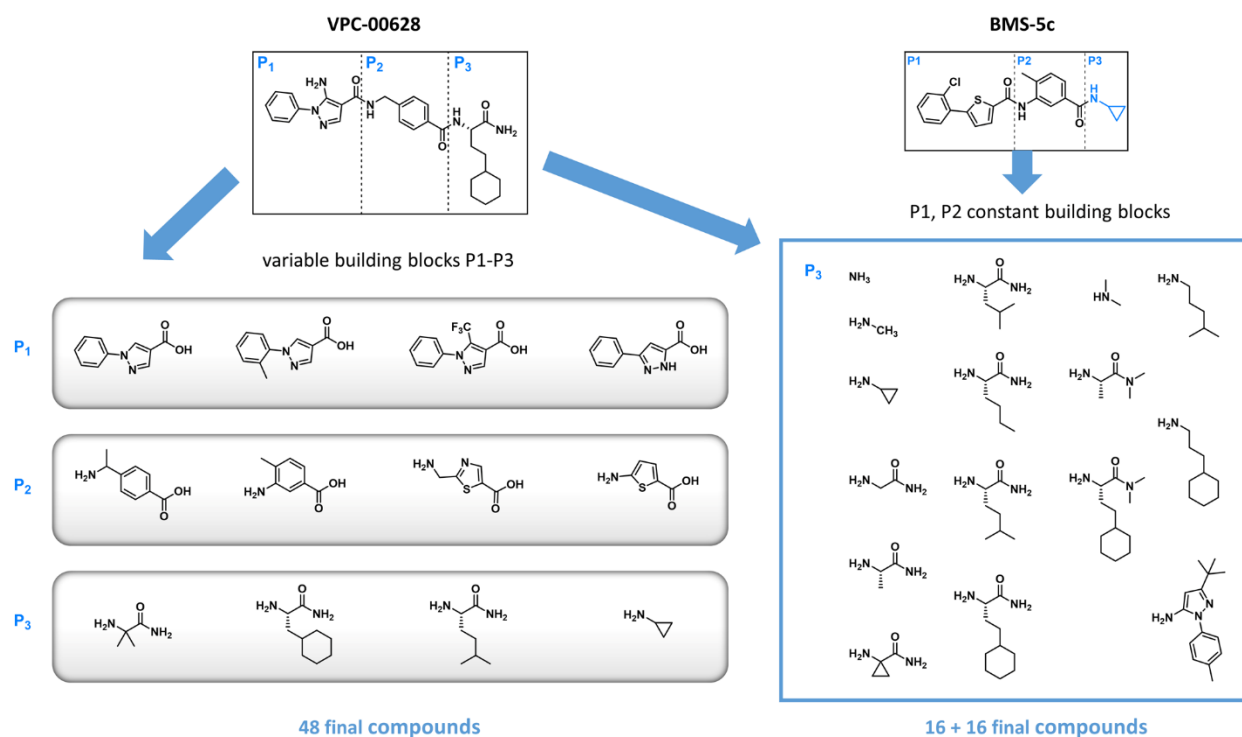
**Figure 17. Commonly used p38 inhibitors lack selectivity.** Screen by KARAMAN ET AL. covering 317 kinases at 10  $\mu$ M.<sup>44</sup> Interactions  $K_d < 3 \mu$ M are mapped in red, and kinase names are highlighted when  $K_d < 1 \mu$ M. Selectivity score  $S$  (3  $\mu$ M) is given for compound comparison ( $S = \text{number of hits } < 3 \mu\text{M}$ , divided by total number of kinases in the assay panel). The number of publications refers to the years between 2014 and 2019, and data are taken from Web of Science (<http://apps.webofknowledge.com/>). Kinome tree created with KinMAP (<http://kinhub.org/>).<sup>359</sup>

The existence of potent and selective inhibitors for p38 of type-I and type-I½ has already been reported earlier, e.g. by LAUFER ET AL. (Skepinone-L).<sup>49, 317</sup> Although some of these inhibitors are commercially available, they are very rarely used to study the MAPK pathway.<sup>360</sup> Analyzing the literature of the last five years on commercially available p38 inhibitors, the very unselective type-I inhibitor SB203580<sup>361-370</sup> is the

most frequently used for study purposes and has been reported in 1301 publications. To study the inactive conformation of the kinase, the type-II inhibitor BIRB-796 was used in 33<sup>371-380</sup> studies. Studies with more selective inhibitors, such as VX-745<sup>381-389</sup> and Skepinone-L<sup>313, 390-397</sup> (for details see **Figure 11** in **Section 2.1**) were reported each only 9 times in the literature of the last five years.

The data on the function of p38 MAPK by the use of non-selective compounds are difficult to interpret or could lead to false conclusions. As described in **Section 1.5**, due to the failure of clinical trials, it would be advisable to take a step back in the development of new p38 inhibitors and focus on the development of highly selective inhibitors. Within the scope of the "Donated-chemical-probe" program of the *Structural Genomics Consortium* (SGC), a p38 chemical probe package<sup>28, 136</sup> was developed during this PhD thesis, which allows detailed mechanistic studies on p38. The probe package was developed in collaboration with the *Lauffer Group* in Tübingen, Germany, and *Mercachem* in Nijmegen, Netherlands, and contains a potent and highly selective type-I, type-I½- and type-II inhibitor. The p38 probe package is further complemented by two inactive control substances and meets the strict quality criteria of a high-quality probe as defined by the SGC community.<sup>136</sup> Due to their different chemical scaffolds, these compounds allow the study of the kinase in both the active and inactive conformation, which enables more precise monitoring of changes in the phenotypic response to the signaling pathway. The latter would be of fundamental interest, as it has already been speculated in various publications that this type of ATP-competitive inhibitor can trigger an altered cellular signal.<sup>398</sup> For the p38 MAPK cascade this was described by HARI ET AL. in 2014, who observed different effects on activators, such as MAP2Ks, or inactivators, such as DUSPs, when using a type-I and type-II inhibitor.<sup>399</sup> So far it is unclear whether a similar phenomenon can be observed in other kinases of the kinome. Therefore, the p38 probe package could serve as a first example to reassess more efficient inhibitor design strategies in future science and to study kinases beyond their phosphotransferase activity. While the type-I and type-I½ inhibitor and a corresponding negative control compound was donated by LAUFER ET AL, VPC-00628 was used for the development of a potent and highly selective type-II inhibitor for p38 MAPK during this doctoral work. Targeting the inactive DFG-out conformation is a known strategy, as explained in more detail in **Section 1.2.1** for the development of inhibitors like the BCR-ABL inhibitor Imatinib.<sup>400, 401</sup> However, as it became obvious that many kinases can adopt a similar inactive state achieving selectivity, the design of type-II inhibitors seems to be challenging.<sup>42</sup> This is exemplified by the p38 type-II inhibitor BIRB-796 that exhibits picomolar on-target affinity but only a poor kinome-wide selectivity.<sup>44</sup>

To investigate the conformational space available for ligand binding within the inactivated p38 MAPK and to provide a type-II probe, the building blocks of VPC-00628 were each varied by a fast iterative synthetic approach by collaborators from *Mercachem*. In this combinatorial approach, the three different building blocks P1, P2, and P3, described in **Section 2.6.1**, were used for the synthesis of new VPC-00628 derivatives, with each individual building block initially kept constant. Following this approach, the P1 and P2 building blocks of VPC-006028 were kept invariant and a total of sixteen different motifs was introduced as the P3 structural motif. In summary, a panel of 64 compounds was synthesized and structural novelties were introduced for the hinge-bond head group, the hydrophobic region I and the DFG-out deep pocket (**Scheme 2**). In this study, we were further interested in whether this approach could help in the development of isoform-selective inhibitors of p38 MAPK. The latter is a challenge because the active sites of p38 $\alpha$  and its  $\beta$ -isoform have a sequence identity of 97%. Therefore, the allosteric P3 structural moieties used were also fused with the scaffold of the  $\alpha$ -isoform selective compound BMS-5c, which was previously described by WROBLESKI ET AL. (**Section 2.2**).<sup>322</sup>



**Scheme 2.** Building blocks (P1–P3) for the synthesis of new derivatives of VPC-00628 and BMS-5c. Synthesis done by Mercachem, Netherlands.

BMS-5c achieves isoform selectivity by inducing an energetically unfavorable Leu108 backbone flip in the hinge region. However, it could be deduced from the SAR studies that the leucine-flipped mode is not alone responsible for kinase inhibitor selectivity and that the allosteric backbone decoration could also make an important contribution. The crystal structure alignment of VPC-00628 (PDB: 5LAR) and BMS-5c (PDB: 4KIN) showed high shape similarities in the linker and allosteric P2 and P3 regions. Therefore, the terminal cyclopropylamide of BMS-5c was considered for P3 building block variations. Using the invariant building blocks P1 and P2, 16 compounds based on a thiophene-core structure with the previously used P3 decorations, as highlighted in **Scheme 2**, were successfully synthesized. A structural overview of the entire compound library is given in the experimental part, **Section 8.3.1**. The established synthetic route can be taken from the recent publication "Fast Iterative Synthetic Approach toward Identification of Novel Highly Selective p38 MAP Kinase Inhibitors", which was submitted as part of this PhD thesis.<sup>402</sup> The latter also describes the effects of the compound on protein stability, measured by differential scanning fluorimetry (DSF), and their potency against the two isoforms p38 $\alpha$  and p38 $\beta$ , using an orthogonal radiometric activity-based assay. In the following section, the investigation of the  $\alpha/\beta$  selectivity and the development of a type-II p38 MAPK probe with corresponding negative control are described.

### 3.1 Investigation of the p38 $\alpha/\beta$ isoform selectivity

All synthesized compounds were screened against p38 $\alpha$  and p38 $\beta$  by DSF assay (described in **Section 4.1.1**) and further characterized by a radiometric protein kinase assay (<sup>33</sup>PanQinase® Activity Assay, performed by Mercachem), in which the *in vitro* IC<sub>50</sub> values for binding to recombinantly produced enzyme were determined. Monitoring differences in affinity for both isoforms revealed that most compounds showed slightly higher potencies for p38 $\alpha$ .<sup>402</sup> Surprisingly, increased p38 $\alpha/\beta$  ratios were found for a number of VPC-

00628 derivatives that do not share a thiophene-core scaffold, typically providing  $\alpha$ -isoform selectivity by induction of a Leu108 flip in the hinge region. Selected representatives that showed isoform selectivity in the SAR study are listed in **Table 2** below for structural comparison. Using the  $IC_{50}$  values determined in the enzyme kinetic assay for each p38 $\alpha$  and p38 $\beta$ , selectivity ratios were calculated for each compound. VPC-00628 with an  $IC_{50}$  value of 39/250 nM for p38 $\alpha/\beta$ , showed a 6.5-fold selectivity over the  $\alpha$ -isoform. Intriguingly, increased isoform selectivity ratios were found for compounds sharing the VPC-00628 hinge-binding aminopyrazole moiety. An exception among these are compounds MCP-040 and MCP-044, which lack the free amine at the pyrazole. The latter is assumed to contribute to the folding of the P-loop in addition to the phenyl residue. Compounds MCP-004, MCP-012 and MCP-007 with medium sized, bulky P3 residues increased the p38 $\alpha/\beta$  ratios compared with MCP-003 without aliphatic P3 moiety and compound MCP-011 with extended cyclohexyl decoration. Within this P1, P2 invariant series, the highest isoform selectivity was found for compound MCP-081 (ratio [p38 $\alpha/\beta$ ] = 29.1-fold), which can be described as a chimera of VPC-00628 and BIRB-796. A similar size-dependent selectivity of the DFG-out aliphatic moiety was found for compounds MCP-078, MCP-079 and MCP-044 with methyl-decorated benzyl linkers. Although the potency for p38 $\alpha/\beta$  was reduced, compound MCP-012, which has a very similar structure to MCP-004, showed an about 3 times higher selectivity for the  $\alpha$ -isoform. By introducing a bulky, methylene-linked cyclohexyl moiety in compound MCP-078, a more than 40 times higher potency was determined for p38 $\alpha$ . In contrast, an ethylene-linked cyclohexyl moiety in compound MCP-044 resulted in a significant loss of isoform selectivity (ratio [p38 $\alpha/\beta$ ] = 18.1-fold). Isoform-selective binding, with nanomolar potency for p38 $\alpha$ , was also found for VPC-00628 derivatives with an *ortho*-tolyl linker. As previously observed, the compound with the bulkiest residue in the allosteric pocket region, MCP-040, showed the highest selectivity ratio in this series. The fast iterative synthetic approach applied also covered hinge-binding moieties, such as pyrazole isomers and various linker groups, such as thiophene or thiazole. However, isoform-selective binding was generally observed only for VPC-00628 derivatives that are most similar in their active site directed part. An exception was compound MCP-069 with a thiazole-linker moiety. The scaffold of MCP-069 is identical in the P1 and P3 building blocks to compounds MCP-073 and MCP-012, and comparable p38 $\alpha/\beta$  ratios were determined for these. Therefore, it can be concluded that the linker region is of minor importance to achieve isoform-selective binding toward p38 MAPK.

**Table 2.** Selection of VPC-00628 derivatives showing increased p38 $\alpha$ -isoform selectivity. Potency for p38 $\alpha/\beta$  determined by DSF- and enzyme kinetic assays for p38 $\alpha/\beta$  inhibition.

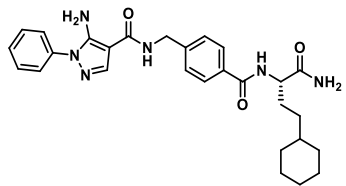
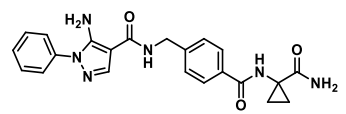
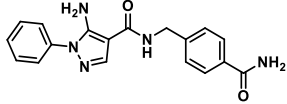
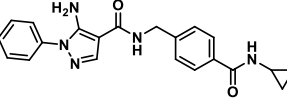
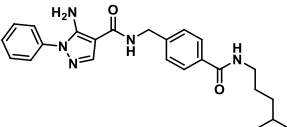
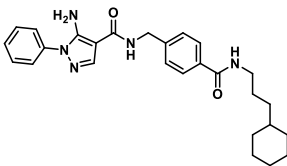
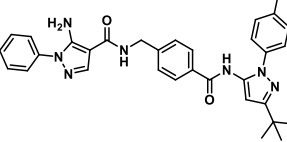
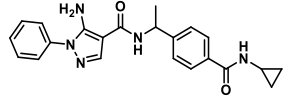
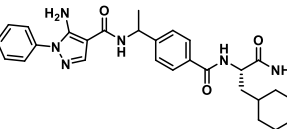
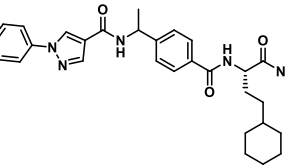
No.	Structure	$\Delta T_m^a$ [°C] ± SD p38 $\alpha$	$\Delta T_m^a$ [°C] ± SD p38 $\beta$	$IC_{50}^b$ [ $\mu$ M] p38 $\alpha$	$IC_{50}^b$ [ $\mu$ M] p38 $\beta$	ratio <sup>c</sup> [fold] p38 $\alpha/\beta$
VPC-00628		13.0 ± 0.7	12.5 ± 0.6	0.039	0.25	6.5
MCP-007		2.6 ± 0.3	2.1 ± 0.2	0.48	6.18	12.8

Table 2. (continued)

No.	Structure	$\Delta T_m^a$ [°C] ± SD p38 $\alpha$	$\Delta T_m^a$ [°C] ± SD p38 $\beta$	IC <sub>50</sub> <sup>b</sup> [ $\mu$ M] p38 $\alpha$	IC <sub>50</sub> <sup>b</sup> [ $\mu$ M] p38 $\beta$	ratio <sup>c</sup> [fold] p38 $\alpha$ / $\beta$
MCP-003		2.3 ± 0.4	1.4 ± 1.4	0.37	2.97	8.0
MCP-004		3.9 ± 0.6	3.0 ± 0.4	0.25	3.83	15.1
MCP-012		6.8 ± 0.4	5.2 ± 1.7	0.047	0.73	15.6
MCP-011 (SR318)		15.4 ± 0.4 <sup>e</sup>	n.d.	0.005	0.032	6.1
MCP-081		8.3 ± 0.9	5.5 ± 1.3	0.055	1.60	29.1
MCP-079		2.9 ± 0.4	1.6 ± 0.2	0.4	7.3	18.4
MCP-078		4.1 ± 0.6	1.6 ± 0.2	0.21	8.7	40.8
MCP-044		4.2 ± 0.8	2.5 ± 0.4 <sup>d</sup>	0.28	5.05	18.1



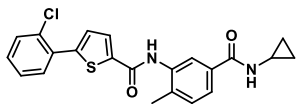
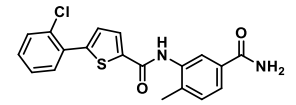
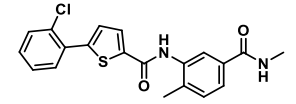
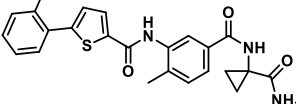
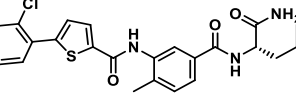
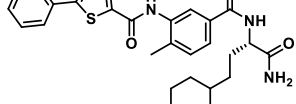
**Table 2.** (Continued)

No.	Structure	$\Delta T_m^a$ [°C] ± SD p38 $\alpha$	$\Delta T_m^a$ [°C] ± SD p38 $\beta$	IC <sub>50</sub> <sup>b</sup> [ $\mu$ M] p38 $\alpha$	IC <sub>50</sub> <sup>b</sup> [ $\mu$ M] p38 $\beta$	ratio <sup>c</sup> [fold] p38 $\alpha$ / $\beta$
MCP-072		2.7 ± 0.4	2.1 ± 0.3	0.044	0.96	21.6
MCP-073		5.6 ± 0.7	7.0 ± 0.6	0.053	0.736	13.8
MCP-040		12.6 ± 0.7 <sup>d</sup>	12.0 ± 1.2 <sup>d</sup>	0.013	0.209	16.3
MCP-069		3.6 ± 0.5	3.9 ± 0.3	0.12	1.7	14.7

<sup>a</sup>  $\Delta T_m$  average derived from seven replicates for p38 $\alpha$  and six replicates for p38 $\beta$  at a compound concentration of 10  $\mu$ M. DSF measured by Martin Schröder, SGC Frankfurt. <sup>b</sup> IC<sub>50</sub> values determined by a radiometric protein kinase assay (<sup>33</sup>PanQinase<sup>®</sup> activity assay, 1  $\mu$ M ATP, measured by Mercachem, Netherlands), <sup>c</sup> calcd. from IC<sub>50</sub> values. Standard deviation (SD) is given when  $n > 2$ , <sup>d</sup>  $\Delta T_m$  average of three measurements, <sup>e</sup>  $\Delta T_m$  average of six measurements, n.d. = not determined.

The previously described p38 $\alpha$ -isoform selective compound BMS-5c achieves a preferential binding of this isoform through its thiophene moiety. In the crystal structure of p38 $\alpha$  in complex with BMS-5c (PDB: 4KIN), inhibitor binding induced a backbone flip in the hinge region by a CH — O hydrogen bonded interaction between thiophene and the backbone oxygen of Leu108. This structural element and the *ortho*-tolyl linker were thus retained to study changes in isoform selectivity caused by the decoration of the backbone pocket (**Table 3**). In the enzymatic assay, BMS-5c showed very potent binding with an IC<sub>50</sub> value of 5 nM for p38 $\alpha$  and an about 55 times lower affinity for p38 $\beta$  (IC<sub>50</sub> = 265 nM). Interestingly, the shortening of the cyclopropyl moiety to a methyl group and a primary amide drastically increased the selectivity ratios of p38 $\alpha$ / $\beta$  by impairing the binding of p38 $\beta$ . Compound MCP-016, as the best candidate of this series, exhibited an excellent 115.3-fold increase in p38 $\alpha$  isoform binding selectivity, with a potency of IC<sub>50</sub> = 17 nM. In contrast to the VPC-00628 derivatives described above, the bulky P3 groups that additionally contained an amide increased the ratio of p38 $\alpha$ / $\beta$  with a BMS-5c-like scaffold in the case of MCP-021, MCP-022, MCP-025. In the other BMS-5c derivatives investigated, the introduced P3 residues led to an almost total loss of binding affinity (IC<sub>50</sub> [p38 $\alpha$ / $\beta$ ] = >5/ >10  $\mu$ M) and are therefore not shown in **Table 3**. For a comprehensive overview of all data obtained, the reader is referred to the paper "A fast iterative synthetic approach towards the identification of novel highly selective p38 MAP kinase inhibitors", which was submitted in the context of this PhD thesis.<sup>402</sup>

**Table 3.** Selection of BMS-5c derivatives showing increased p38 $\alpha$ -isoform selectivity. Potency for p38 $\alpha$ / $\beta$  determined by DSF and enzyme kinetic assays for p38 $\alpha$ / $\beta$  inhibition.

No.	Structure	$\Delta T_m^a$ [°C] $\pm$ SD p38 $\alpha$	$\Delta T_m^a$ [°C] $\pm$ SD p38 $\beta$	IC <sub>50</sub> <sup>b</sup> [ $\mu$ M] p38 $\alpha$	IC <sub>50</sub> <sup>b</sup> [ $\mu$ M] p38 $\beta$	ratio <sup>c</sup> [fold] p38 $\alpha$ / $\beta$
BMS-5c		9.6 $\pm$ 1.1	3.6 $\pm$ 0.5	0.005	0.265	55.2
MCP-016		5.2 $\pm$ 0.5	1.2 $\pm$ 0.3	0.017	1.99	115.3
MCP-017		5.4 $\pm$ 0.4	1.6 $\pm$ 0.3	0.017	1.16	68.3
MCP-021		6.7 $\pm$ 0.8	2.5 $\pm$ 0.4	0.059	2.48	41.7
MCP-022		2.2 $\pm$ 0.8	1.0 $\pm$ 0.4	0.470	7.05	15.0
MCP-025		5.0 $\pm$ 1.2	3.6 $\pm$ 1.2	0.015	0.167	11.0

<sup>a</sup>  $\Delta T_m$  average derived from seven replicates for p38 $\alpha$  and six replicates for p38 $\beta$  at a compound concentration of 10  $\mu$ M. DSF measured by Martin Schröder, SGC Frankfurt. <sup>b</sup> IC<sub>50</sub> values determined by a radiometric protein kinase assay (<sup>33</sup>PanQinase® activity assay, 1  $\mu$ M ATP, measured by Mercachem, Netherlands), <sup>c</sup> calcd. from IC<sub>50</sub> values. Standard deviation (SD) is given when n>2.

Since isoform-selective binding was sometimes not obvious from the thermal shifts determined by DSF, it was of interest whether the results of the enzyme kinetic assay could be confirmed in an orthogonal assay. Therefore, the most interesting compounds BMS-5c, MCP-016 and MCP-017 were selected for testing in living cells by NanoBRET™ assay (assay description see **Section 4.1.2**, results in **Table 4**). In HEK293T cells, a 10-35 times weaker potency for p38 $\alpha$ / $\beta$  was determined, which is not unusual due to the necessary passage through the cell membrane and the interaction with cell components. In comparison with the enzyme kinetics assay on the isolated enzyme, the cellular system has a significantly higher ATP concentration with which the inhibitors must compete. Comparing the IC<sub>50</sub> values determined for both p38

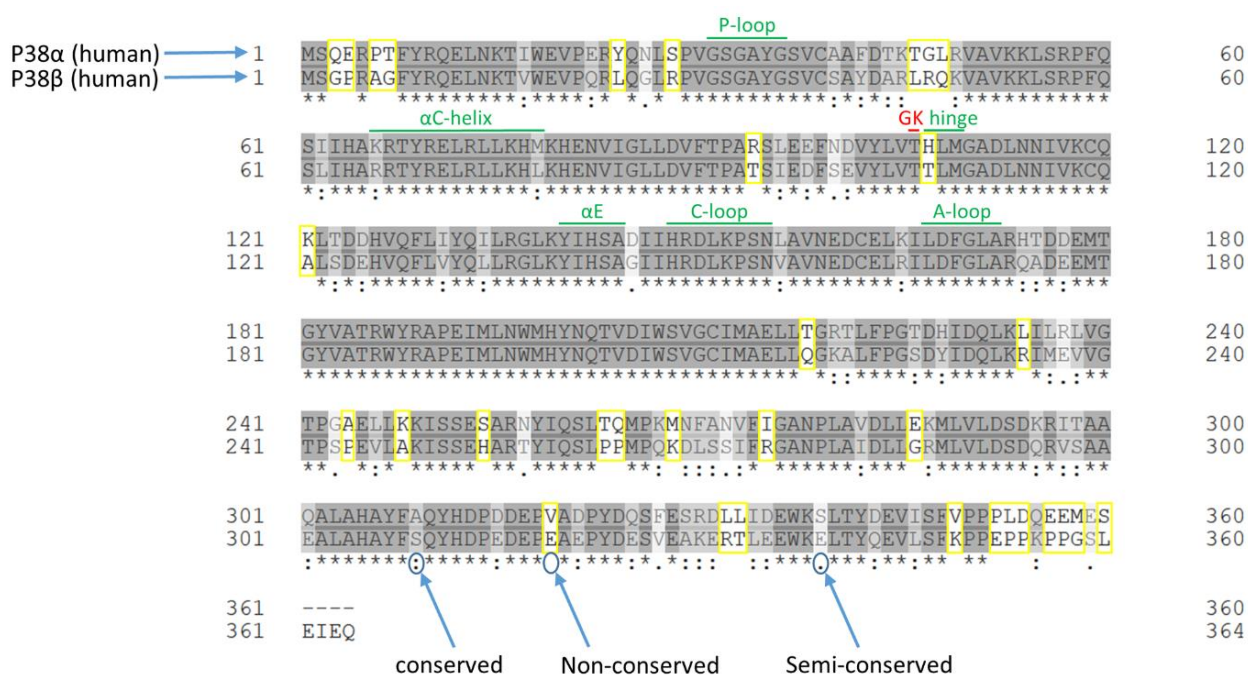
isoforms, it can be seen that the preference for binding to the  $\alpha$ -isoform is also maintained in the cellular system, albeit with slightly reduced ratios.

**Table 4.** Comparison of cellular potencies with the enzyme kinetics assay data

No.	NanoBRET™ assay <sup>a</sup>			Enzyme kinetics assay <sup>b</sup>		
	IC <sub>50</sub> [μM] ± SEM, p38α	IC <sub>50</sub> [μM] ± SEM, p38β	Ratio <sup>c</sup> [fold] p38α/p38β	IC <sub>50</sub> [μM] p38α	IC <sub>50</sub> [μM] p38β	Ratio <sup>c</sup> [fold] p38α/p38β
BMS-5c	0.056 ± 0.002	1.70 ± 0.002	31	0.005	0.265	55.2
MCP-016	0.583 ± 0.019	56.8 ± 4.36	97	0.017	1.99	115.3
MCP-017	1.02 ± 0.057	34.3 ± 1.77	34	0.017	1.16	68.3

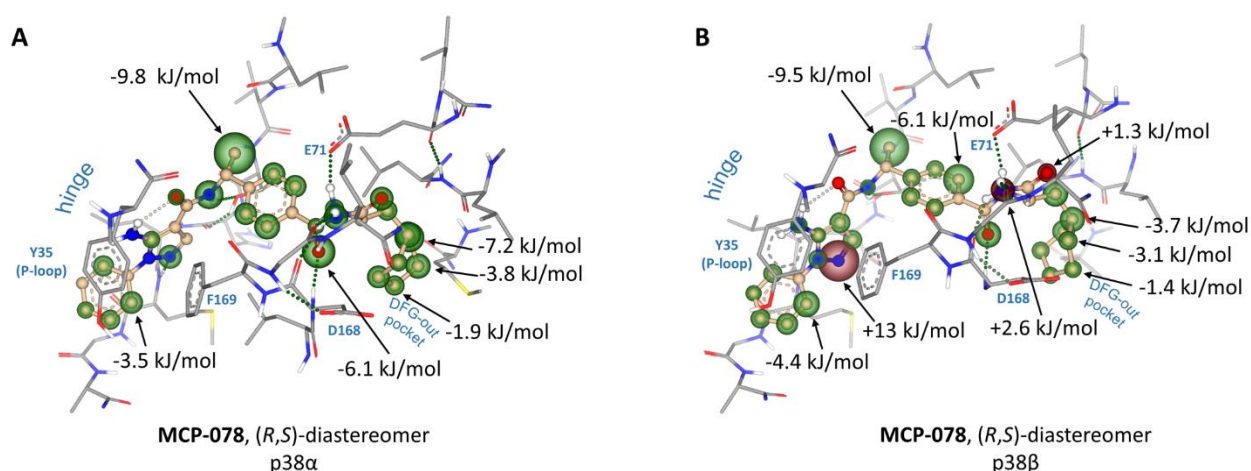
<sup>a</sup> IC<sub>50</sub> values are the mean of two experiments, experiment performed in HEK293T cells, <sup>b</sup> experiment on isolated enzyme, <sup>c</sup> calcd. from IC<sub>50</sub> values, ATP concentration 1 μM. NanoBRET measured by Benedict-Tilman Berger, SGC Frankfurt, enzyme kinetics assay by Mercachem, Netherlands.

To identify the cause of the surprising  $\alpha/\beta$  isoform selectivity, a sequence alignment of p38α and p38β was performed with the Uniprot alignment tool (<https://www.uniprot.org/align/>), as shown in **Figure 18**, to assess which amino acids might be responsible for the preferred inhibitor binding. Both isoforms share 72% sequence identity for residues 1-360. Not surprisingly, most amino acid changes are located distally to the conserved inhibitor binding site (region between amino acids 28 to 172), which displays an overall similarity of 97%.



**Figure 18.** Sequence alignment of human p38α (Q16539) and p38β (Q15759) MAPK. Sequence similarity is highlighted in gray. Non-conserved residues are depicted in yellow, important kinase domain regions are marked in green, and the gatekeeper residue (GK) is marked in red.

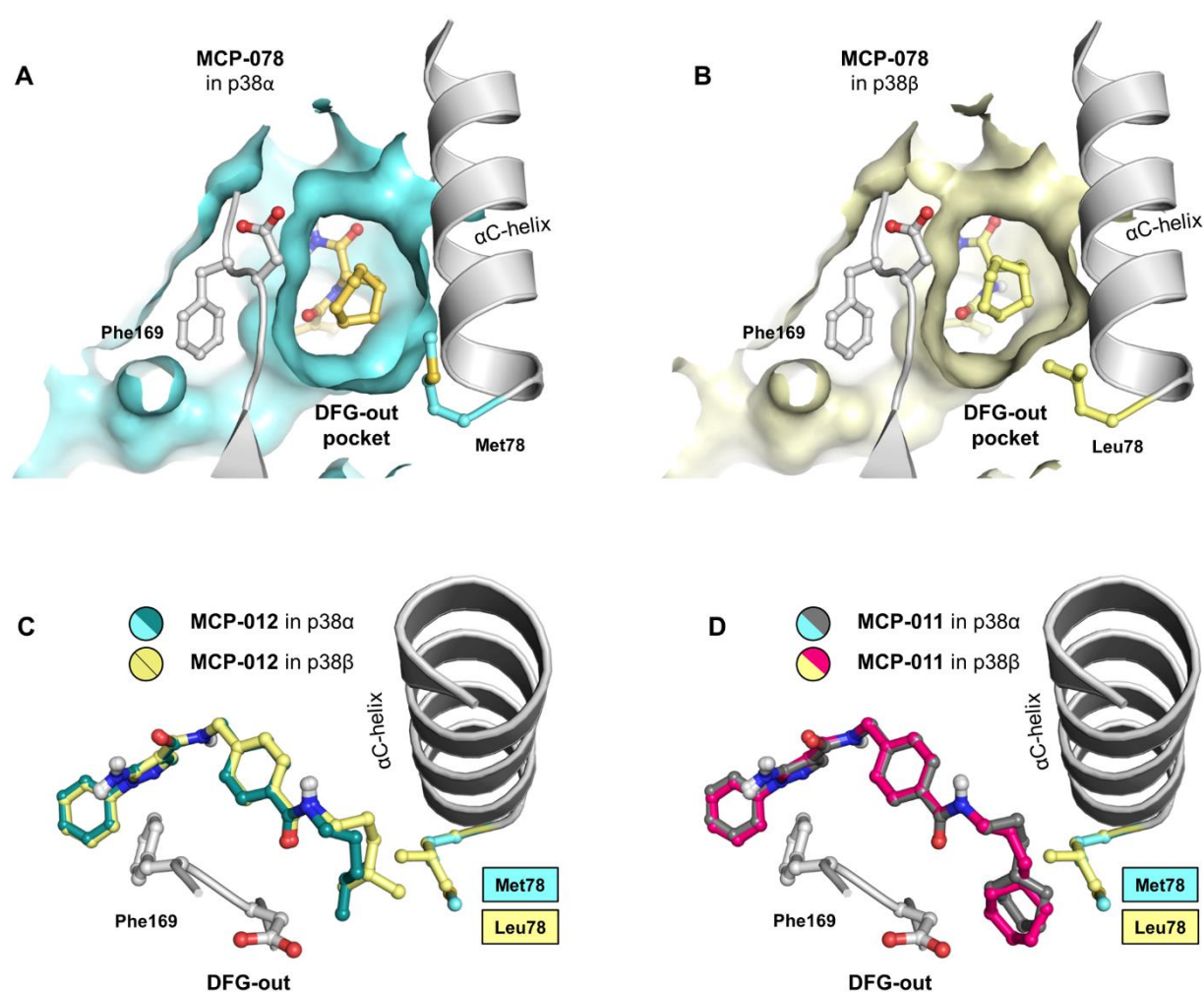
A total of seven non-conserved amino acid residues were found in the inhibitor binding site, for example at position 108 in the hinge region (histidine in p38 $\alpha$ , threonine in p38 $\beta$ ). Further differences in the amino acid sequence between the  $\alpha$ - and  $\beta$ -isoforms were observed in this region for a total of 19 additional amino acid residues. As shown in the SAR studies, isoform selectivity might be controlled by the allosteric pocket, a region between the activation loop DFG motif and the helix  $\alpha$ C. Interestingly, several conserved amino acids were found at the N- and C-terminal ends of the  $\alpha$ C helix (positions 66 and 78). In order to understand the structural role and location of these residues and to gain insights into which residues might influence the binding of the inhibitor to these kinases, a homology model of p38 $\beta$  was created using the Swiss-Model webserver (<https://swissmodel.expasy.org/>). The crystal structure of VPC-00628 in complex with p38 $\alpha$  (PDB: 5LAR) was used as a template for the model. Comparison of the structure of both isoforms revealed residue 78, a methionine in p38 $\alpha$  and a more bulky leucine in p38 $\beta$ , as a likely candidate for isoform specificity. In both isoforms, this residue at the end of the  $\alpha$ C helix protrudes into the DFG-out pocket. To assess the effect of this particular residue on the binding of inhibitors to the DFG-out pocket, *in silico* studies with the program SeeSAR v8.1 from *BioSolveIT GmbH* (Sankt Augustin, Germany, 2019, [www.biosolveit.de/SeeSAR](http://www.biosolveit.de/SeeSAR)) were performed in collaboration with Roberta Tesch. For the investigation of the  $\alpha/\beta$ -isoform selectivity different compounds, which previously showed an increased preference for binding to p38 $\alpha$  in **Table 2**, were selected and docking in both isoforms was performed. VPC-00628 was used as center point and ten poses were generated for each compound. For every inhibitor pose, binding affinities were calculated with the program and the best pose was selected for visual inspection with PyMol 4.4.0. An example of this study is given in **Figure 19** for compound MCP-078, which showed the highest isoform selectivity (p38 $\alpha/\beta$  ratio = 40.8-fold) in this series.



**Figure 19.** *In silico* docking studies of the (R,S)-diastereomer of MCP-078 in p38 $\alpha$  (A) and p38 $\beta$  (B). Estimated binding affinities are highlighted as spheres, favorable binding is colored in green, unfavorable binding in red. Estimated  $\Delta G$  values are given in kJ/mol and are highlighted for the most interesting atoms. Predicted hydrogen bonds are shown as green dotted lines.

During the synthesis of Compound MCP-078, a racemic methyl group was introduced to metabolically stabilize the compound and to enhance the hydrophobic contacts in the gatekeeper region. Since the spatial orientation of the methyl group (*R*- or *S*-configured) makes a different contribution to the binding energy, the *R*- and *S*-configured methyl derivatives were used for docking instead of the racemic compound, and their binding affinities were predicted. The stereo information of the DFG-out pocket moiety (*S*-configured) was retained and the best pose obtained for MCP-078, with an *R*-configured methyl group in p38 $\alpha$  and p38 $\beta$ , is shown in **Figure 19**. Interestingly, for the *R*-configured derivative much better binding affinity was calculated ( $\Delta G$  [p38 $\alpha/\beta$ ] = -9.8/ -9.5 kJ/mol) than with a methyl group with *S*-configuration ( $\Delta G$  [p38 $\alpha/\beta$ ] =

-6.8/ -5.1 kJ/mol, figure not shown), since this group pointed into the pocket behind the gatekeeper. This allows a stronger hydrophobic interaction, which is significantly lower for the *S*-configured methyl group pointing away from the pocket and toward the solvent-exposed site. The total binding of the (*R,S*)-diastereomer MCP-078 to p38 $\alpha$  was simulated also in the hinge, linker and DFG-out binding pocket, where the cyclohexyl decoration binds. For the p38 $\beta$  isoform, an overall lower binding affinity was calculated and an unfavorable binding in the hinge region and at the entrance of the DFG-out pocket was predicted. Positive  $\Delta G$  values were determined for the pyrazole nitrogen atom ( $\Delta G$  [p38 $\beta$ ] = +13 kJ/mol) and the allosteric amide nitrogen ( $\Delta G$  [p38 $\beta$ ] = +2.6 kJ/mol), since the inhibitor clashed with the protein structure in these areas. Since the cyclohexyl decoration adopted a different geometric orientation in p38 $\beta$ , the binding affinity for the cyclohexyl-*CH* group was found to be significantly lower. Visual examination, of the allosteric binding pocket of p38 in complex with compound MCP-078 using PyMol, revealed a differently shaped DFG-out pocket in both isoforms (**Figure 20A, B**).



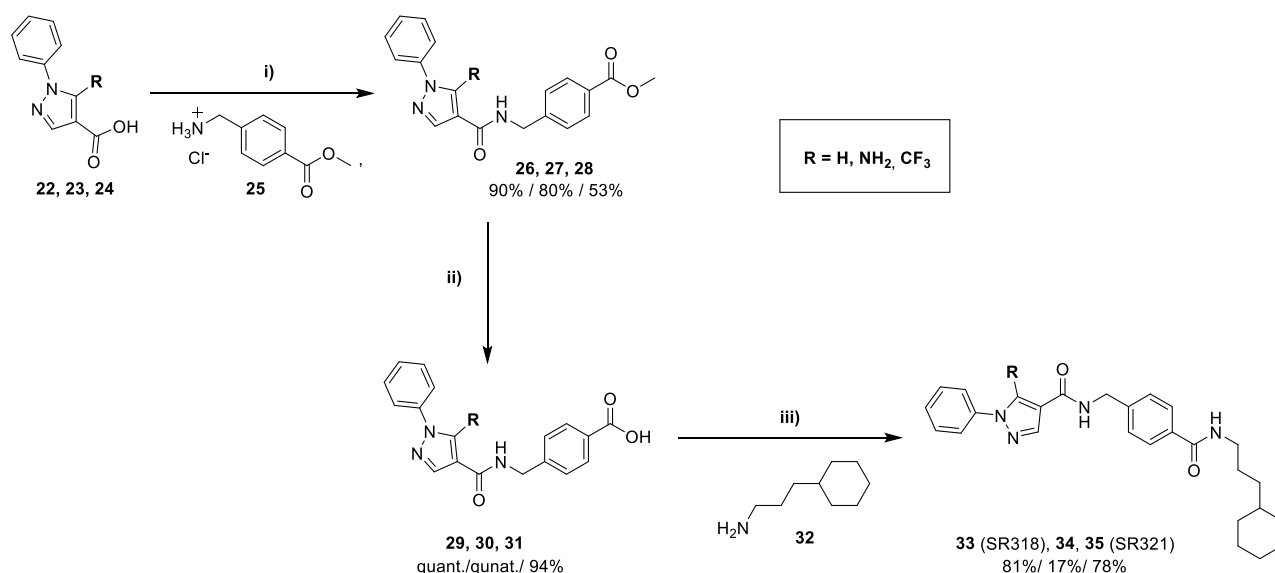
**Figure 20. Comparison of DFG-out pocket interactions in p38 $\alpha$  and p38 $\beta$ .** A) Model of (*R,S*)-diastereomer MCP-078 in p38 $\alpha$ . Pocket surface and Met78 are highlighted in light blue. B) Model of (*R,S*)-MCP-078 in p38 $\beta$ . Pocket surface and Leu78 are highlighted in light yellow. C) Alignment of compound MCP-012 in p38 $\alpha$  and p38 $\beta$ . D) Alignment of compound MCP-011 in p38 $\alpha$  and p38 $\beta$ .

Due to the more rigid and bulky Leu78 residue in the  $\beta$ -isoform, the allosteric pocket was slightly smaller than the  $\alpha$ -isoform, which has a more flexible Met78 residue at this position. The bulky leucine moiety induced a clash with the cyclohexyl residue, which could be the reason for the reduced potency of MCP-078 compared with p38 $\beta$  ( $IC_{50}$  [p38 $\alpha/\beta$ ] = 0.21/ 8.7  $\mu$ M). Compound MCP-078 was then compared with the most

potent compound MCP-011 of this series ( $IC_{50}$  [p38 $\alpha/\beta$ ] = 0.005/ 0.032  $\mu$ M, selectivity ratio = 6.1-fold), which has an elongated ethyl cyclohexyl DFG-out pocket decoration (**Figure 20D**). In addition, MCP-012 with a medium-sized back pocket decoration (ratio [p38 $\alpha/\beta$ ] = 15.6-fold) was considered for this analysis (**Figure 20C**). These studies suggested that the extended DFG-out pocket decoration of MCP-011 protrudes deeply into the pocket area below amino acid 78, thereby reducing potential repulsion with Leu78 in the  $\beta$ -isoform, which is reflected in the lower p38 $\alpha/\beta$  selectivity ratio measured. In contrast, shorter DFG-out P3 modifications, for example in compounds MCP-012 and MCP-078, bound at the entrance of this pocket region and therefore closer to Leu78. In summary, these studies suggest that amino acid 78 acts as a kind of "gatekeeper residue" that controls access to the allosteric DFG-out pocket in p38 $\alpha/\beta$  and the isoform-selective binding of inhibitors.

### 3.2 Discovery of a p38 MAPK type-II chemical probe and synthesis of a negative control

The applied fast optimization process led to the discovery of the very potent p38 $\alpha/\beta$  inhibitor, MCP-011 (SR318), with  $IC_{50}$  values of 5 nM and 32 nM in the enzyme kinetic assay on isolated enzyme. To further investigate the inhibitory effect of **33** (SR318), the compound was selected for resynthesis and scale up, using a synthetic pathway slightly different from the synthesis described in the publication.<sup>402</sup> For an in depth study of p38 $\alpha/\beta$  as a kinase drug target, a negative control compound would be of value to distinguish between on-target effects and non-specific effects, e.g., caused by cross-reactivity with other cellular proteins. Two compounds closely related to **33** (SR318) were considered for the synthesis of such a negative control (**Scheme 3**).



**Scheme 3.** Synthesis of the type-II p38 chemical probe **33** and both potential negative control compounds **34** and **35**. Reagents and conditions: i) Methyl 4-(aminomethyl)benzoate hydrochloride (**25**), HOBt, EDC-HCl, DIPEA, DMF, RT. ii) LiOH, THF/H<sub>2</sub>O, RT. iii) 3-cyclohexylpropan-1-amine (**32**), HATU, DIPEA, DMF, RT.

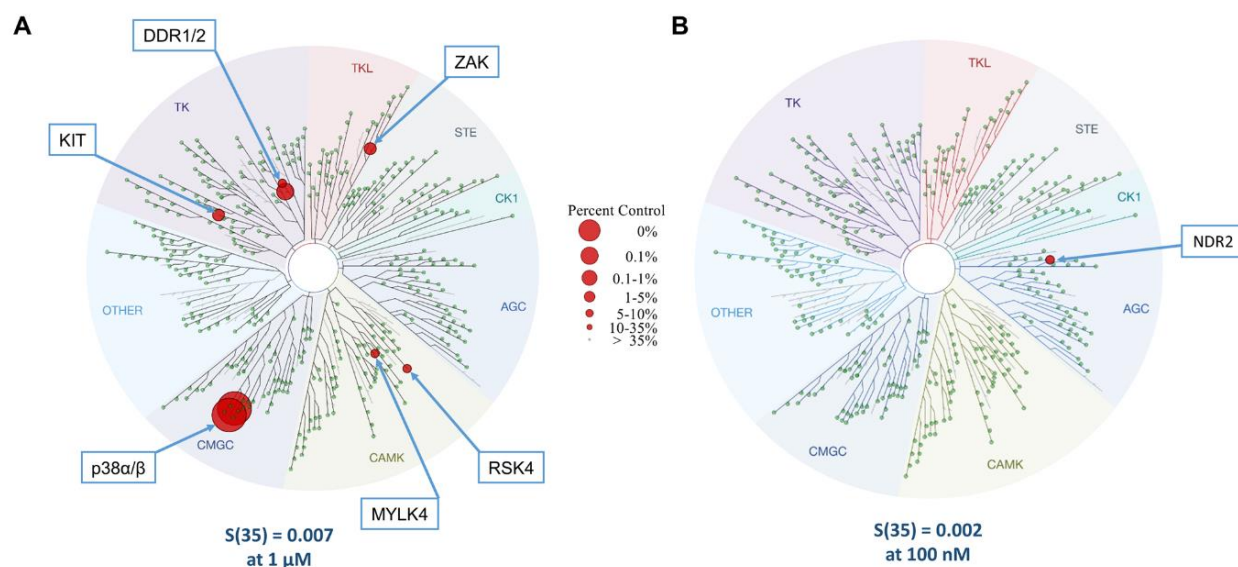
Since the hinge-binding P1 head group is involved in inhibitor binding, the free amine decoration on the pyrazole heterocycle was replaced by a CF<sub>3</sub> group or a hydrogen atom. These hinge-binding P1 groups, 1-phenyl-1H-pyrazole-4-carboxylic acid (**23**) and 1-phenyl-5-(trifluoromethyl)-1H-pyrazole-4-carboxylic acid (**24**), were also used as building blocks in the synthesis of *Merchachem* and showed an unfavorable binding toward p38 $\alpha/\beta$  as determined by DSF assays and the radiometric protein kinase assay.<sup>402</sup> Furthermore,

these hinge binding head groups are structurally more closely related to the other P1 building blocks used in this publication.<sup>402</sup> For the synthesis of both potential negative controls, a new synthetic route was established during this doctoral work, resembling the synthesis of **33** (SR318).

In the first step, an amide coupling reaction with the correspondingly decorated carboxylic acid derivative (**22-24**) was carried out with methyl 4-(aminomethyl)benzoate hydrochloride (**25**). In this reaction, the use of EDC-HCL as coupling reagent and HOBt as additive proved to be advantageous, and the corresponding compounds were obtained in fair to high yields. In order to add further amide functionality for back-pocket decoration, the ester functionality of the obtained compounds was subsequently hydrolyzed to the free acid using lithium hydroxide. The quantitatively obtained compounds **29**, **30** and **31** were then activated with the coupling agent HATU under basic conditions and reacted with 3-cyclohexylpropan-1-amine (**32**). The final compounds **33** and **35** were obtained in very good yields (81%, 78%), whereas for the potential negative compound **34** only a poor yield (17%) was obtained.

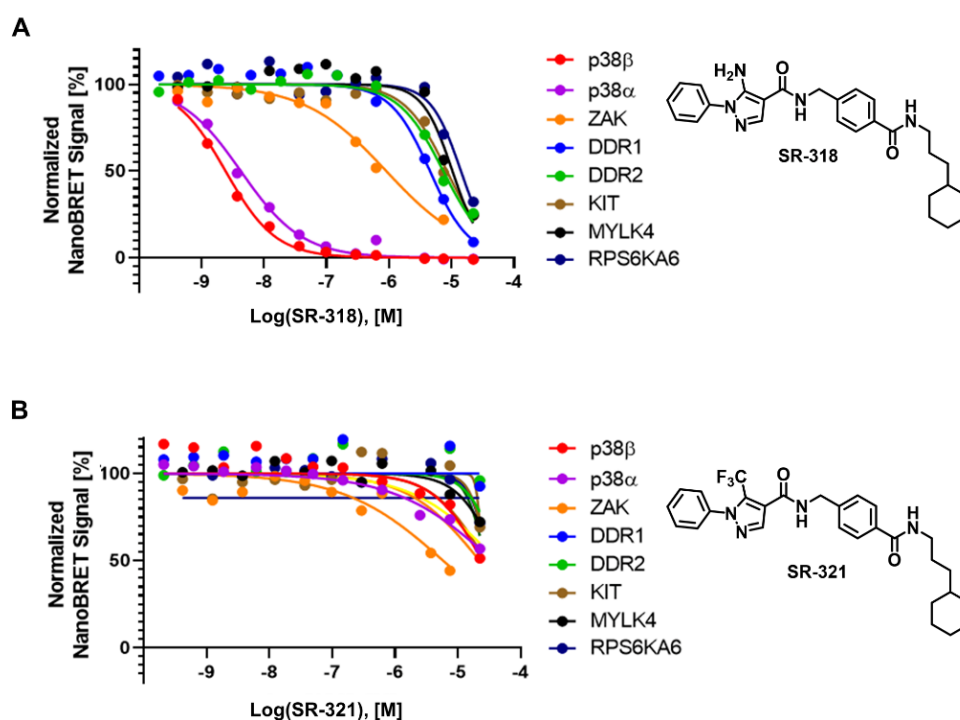
The compounds were then tested in the DSF assay for binding to p38 $\alpha$  at a concentration of 10  $\mu$ M ( $n = 6$ ). For the previously obtained potent p38 probe **33** (SR318,  $IC_{50}$  [p38 $\alpha$ ] = 5 nM), a temperature shift of  $\Delta T_m = 15.4 \pm 0.4$  °C was determined due to the favorable protein stabilization. As expected on the basis of the previous SAR studies, the melting temperatures for the possible negative control compounds with a CF<sub>3</sub> group (**35**) or a hydrogen atom (**34**) on the pyrazole ring were drastically lower. While compound **35** showed no change in melting behavior compared with the native protein ( $\Delta T_m$  [p38 $\alpha$ ] =  $0.2 \pm 0.8$  °C), a significantly reduced but still appreciably stabilization of p38 $\alpha$  was observed for **34** ( $\Delta T_m = 4.7 \pm 0.5$  °C). Therefore, **35** (SR321), which did not appear to bind to p38 $\alpha$  according to the DSF assay, was selected as a potential negative control compound for further characterization. In the following studies, compounds **33** (SR318) and **35** (SR321) were investigated for their cellular potency by NanoBRET™ assay in HEK293T cells. The potency of **33** (SR318) in the cellular system using the full-length protein was comparable to that of the isolated enzymes, with  $IC_{50}$  values of 3.7 nM and 10 nM for p38 $\alpha$  and p38 $\beta$ , respectively. For the potential negative control, **35** (SR321), an about 1000 times weaker potency was determined for the  $\alpha$  and  $\beta$  isoform, with  $IC_{50}$  values of 13 and 11  $\mu$ M, respectively.

In order to meet the criteria set by the *Structural Genomics Consortium* (SGC) for a chemical probe and its negative control, both compounds were subsequently tested for their selectivity toward the kinome. The profiling of **33** (SR318) and **35** (SR321) was performed with the ScanMax assay, a service provided by *DiscoverX*, which currently provides a panel of 468 kinases and mutants. Compound **33** (SR318) was screened at a concentration of 1  $\mu$ M and showed a remarkably high selectivity. Besides the main targets p38 $\alpha$  and p38 $\beta$ , only a few other targets, such as DDR1/2, KIT, ZAK, MYLK4, and RSK4 were found at a cut-off value of 35% of the remaining control (**Figure 21A**). Neglecting the mutants, an excellent selectivity score of  $S(35) = 0.007$  at a compound concentration of 1  $\mu$ M was calculated, from the quotient of targets identified <35% and the sum of non-mutated kinases in this panel ( $\Sigma = 403$ ). The standard selectivity score  $S(x)$  is a quantitative measure of compound selectivity and allows the direct comparison of compounds. The higher the selectivity of the compound, the lower the  $S(x)$  value, where  $x$  stands for the activity threshold.<sup>403</sup>



**Figure 21. Selectivity profile of type-II p38 MAPK probe and negative control compound.** A) DiscoverX screen against 468 kinases and mutants thereof with probe compound **33** (SR318) at 1  $\mu$ M and B) negative control **35** (SR321) at 100 nM. Kinases with <35% of control remaining are illustrated as red circles, only data for wild-type kinases are shown. Selectivity score  $S(35)$  is given for compound comparison.

For the negative control **35** (SR321), which was screened at a concentration of 100 nM, no activity against p38 MAPK was detected, and NDR2 was obtained as the only off-target in this assay (**Figure 21B**,  $S(35) = 0.002$  at 100 nM). Since the false positive rate in the kinome ScanMax assay is estimated to be about 1%, all off-targets were subsequently examined using NanoBRET to find out whether they play a role in the cellular system in the later use of **33** (SR318, **Figure 22**).



**Figure 22. In cellulo follow-up of main targets by NanoBRET™ assays.** A) Probe compound **33** (SR318), B) negative control **35** (SR321). Representative example of single measurement is depicted. Measured by Benedict-Tilman Berger, SGC Frankfurt.



In addition to the probe, the negative control **35** (SR321) was also used to investigate the off-target potencies on DDR1/2, KIT, ZAK, MYLK4 and RSK4. Interestingly, except for p38 $\alpha$ / $\beta$  (IC<sub>50</sub> = 3.7 nM/ 10 nM) and to some extent also ZAK (IC<sub>50</sub> = 910 nM), no other target was affected by **33** (SR318) on full-length protein in HEK293T cells. **33** (SR318) thus exceeds the requirements of the SGC<sup>136</sup> to have a selectivity of >30 fold within the target family. Not evident on the *DiscoverX* screen, **35** (SR321) showed low potency against DDR2 (IC<sub>50</sub> = 220 nM). However, the potencies against other targets investigated were slightly weaker with IC<sub>50</sub>s of 5.8  $\mu$ M for ZAK and 13  $\mu$ M for DDR1 or were determined as IC<sub>50</sub> = >20  $\mu$ M in this assay. The exact measured values are shown in **Table 5** below.

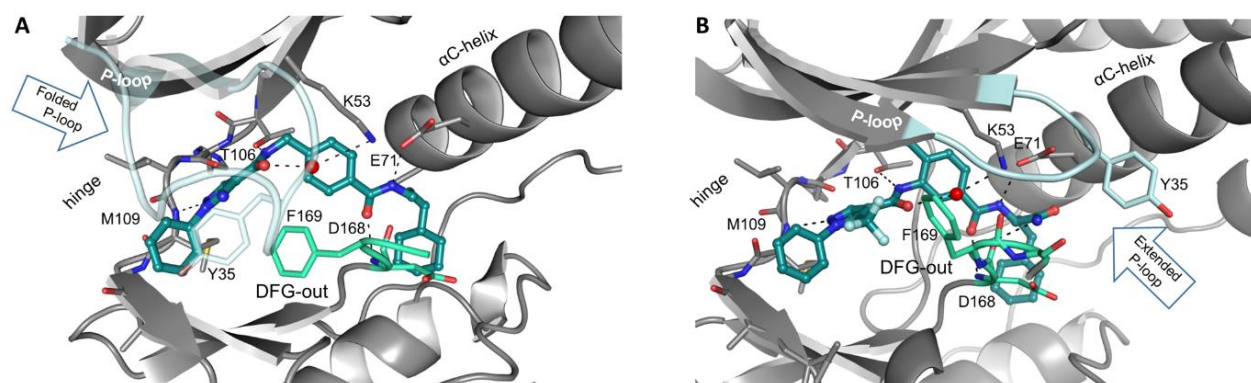
**Table 5.** Summary of potencies determined for main targets found in kinome scan for **33** (SR318) and **35** (SR321)

Kinome target	Percent of control at 1 $\mu$ M, <b>33</b> (SR318)	<b>33</b> (SR318) NanoBRET IC <sub>50</sub> $\pm$ SEM [ $\mu$ M]	<b>35</b> (SR321) NanoBRET IC <sub>50</sub> $\pm$ SEM [ $\mu$ M]
p38 $\alpha$	0.0%	0.0067 $\pm$ 0.0003 <sup>a</sup>	11.6 $\pm$ 3.2 <sup>d</sup>
p38 $\beta$	0.0%	0.014 $\pm$ 0.0004 <sup>b</sup>	20.9 $\pm$ 2.6 <sup>e</sup>
DDR1	3.0%	3.0 <sup>c</sup>	13 $\pm$ 2.8 <sup>e</sup>
KIT	7.7%	8.5 <sup>c</sup>	>20 <sup>c</sup>
ZAK	8.8%	0.91 <sup>c</sup>	5.8 <sup>c</sup>
RSK4	29.0%	14 <sup>c</sup>	>20 <sup>c</sup>
DDR2	31.0%	5.6 $\pm$ 1.7	0.22 <sup>a</sup>
MYLK4	31.0%	10 <sup>a</sup>	>20 <sup>a</sup>

<sup>a</sup> IC<sub>50</sub> values are the mean of seven experiments, <sup>b</sup> mean of four experiments, <sup>c</sup> IC<sub>50</sub> values from single experiment, <sup>d</sup> mean of five experiments, <sup>e</sup> mean of two experiments. NanoBRET measured by Benedict-Tilman Berger.

To confirm the inactive DFG-out binding mode of type-II, the crystal structure of the p38 $\alpha$ -SR318 (**33**) complex was determined (**Figure 23A**). However, the high degree of freedom of the cyclohexyl P3 building block, together with the flexibility inside the allosteric pocket region in this kinase, made it a challenging task to co-crystallize this structure. As expected, **33** (SR318) indeed stabilized p38 $\alpha$  in a type-II binding mode, with the DFG motif adopting an inactive DFG-out conformation that was targeted by the cyclohexyl decoration. Since the DFG-out pocket of p38 $\alpha$  has a unique isoleucine (Ile141) residue at the bottom of the pocket, bulky residues can easily enter, unlike in related kinases containing sterically demanding amino acids.<sup>329</sup> It can therefore be assumed that the cyclohexylpropyl P3 building block of **33** (SR318) contributes significantly to the selectivity and potency of the inhibitor. Similarly to its parent compound VPC-00628, **33** (SR318) engaged the glycine rich loop inside the adenine binding pocket by aromatic face-to-face and face-to-edge interactions between Tyr35, from the GXGX $\phi$ G motif of the P-loop, and the side chain of Phe169 from the DFG motif. This unique binding mode has rarely been described for other kinases and has been shown to greatly increase the selectivity of inhibitors, which also underlines the remarkable selectivity

profile found for **33** (SR318).<sup>54</sup> Besides these hydrophobic interactions, a network of hydrogen bonds supported the binding of the inhibitor, e.g., via the pyrazole *N*-atom and Met109 toward the hinge region. Further hydrogen bonds were formed with the small Thr106 gatekeeper-sidechain hydroxyl group and to the conserved Glu71 and Asp168 residues that are bound by both amide groups. Furthermore, the carbonyl *O*-atom next to the hinge binding head group interacted simultaneously with Lys53 and stabilized a water molecule inside the binding pocket.

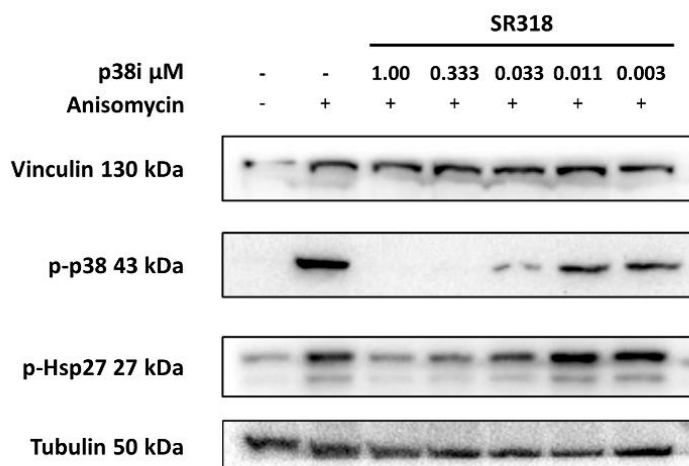


**Figure 23. Folding and unfolding of the P-loop.** A) Binding mode of **33** (SR318) in complex with p38 $\alpha$  with folded P-loop. B) MCP-042 in complex with p38 $\alpha$  showing an extended P-loop due to CF<sub>3</sub>-decoration. The inhibitor is highlighted in stick and ball representation (teal), the P-loop in light blue, and the DFG motif in cyan. Hydrogen bonds are indicated as black dotted lines and water molecule as red spheres. Crystal structures determined by Martin Schröder and Apirat Chaikuad, SGC Frankfurt.

Not directly evident from the crystal structure solved for **33** (SR318) in complex with p38 $\alpha$  is the fact that the exchange of the amine group by a CF<sub>3</sub> group in the hinge region, as present in the negative control **35** (SR321), resulted in an inactive compound. Reanalyzing the entire compound library of *Mercachem*, it was found that all eight compounds carrying the same CF<sub>3</sub>-decorated head group, with the exception of MCP-042 (IC<sub>50</sub> [p38 $\alpha$ /p38 $\beta$ ] = 0.071/0.55  $\mu$ M), were inactive in the <sup>33</sup>PanQinase<sup>®</sup> activity assay (IC<sub>50</sub> [p38 $\alpha$ /p38 $\beta$ ] = >5  $\mu$ M). In the following, a crystal structure with p38 $\alpha$  was determined to find out more about the binding mode of MCP-042 (**Figure 23B**). By comparing the binding mode of MCP-042 with that of **33** (SR318), it became apparent that both inhibitors bound to the inactive kinase in a type-II binding mode, but the P-loop adopted a completely different orientation. While **33** (SR318) interacted with the glycine-rich loop and forced it into a folded conformation, a more common closed conformation of the P-loop was found for compound MCP-042. Therefore, the free amine, in addition to the aromatic functionalities, seems to be of fundamental importance to capture the P-loop within the ATP-binding pocket. It can be assumed that the negative compound **35** (SR321), due to its high intrinsic flexibility, is not able to stabilize the P-loop in a folded conformation, and the allosteric back pocket of the protein.

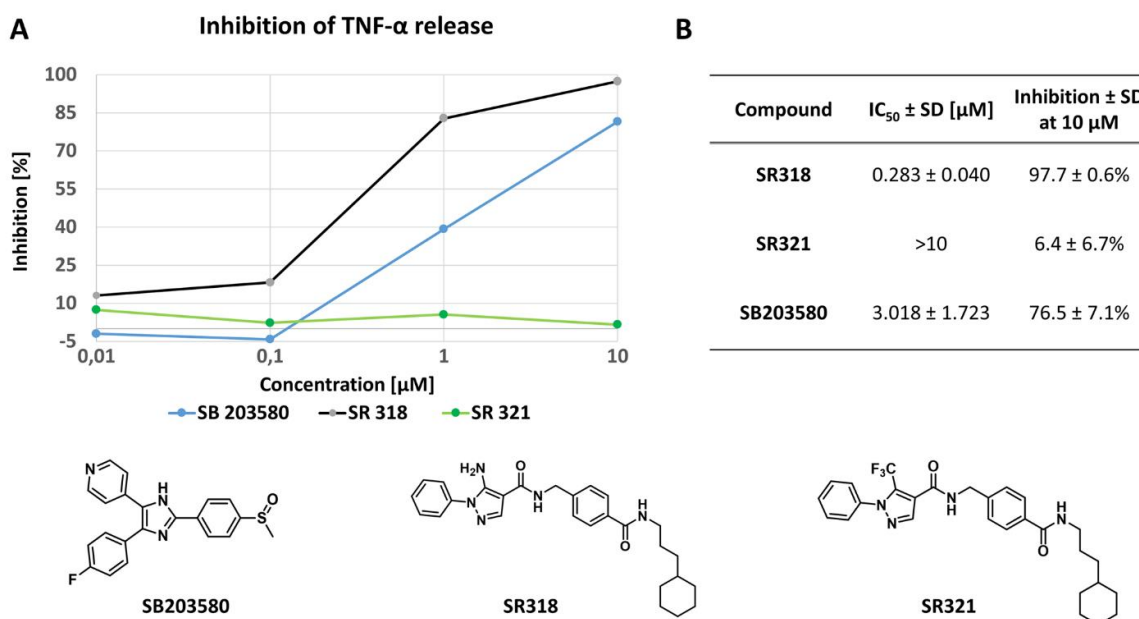
To further characterize the potent and highly selective probe candidate **33** (SR318), additional biological studies were performed to investigate the effect of p38 inhibition on endogenous substrates such as Hsp27. During p38-MAPK signaling, activated p38 phosphorylates its downstream substrate MK2, as described in **Section 1.4.3**. Activated MK2 is then able to phosphorylate and activate heat shock protein 27 (Hsp27), which is known to regulate actin remodeling of the cytoskeleton, prevent apoptosis and reduce reactive oxygen species (ROS) formed under stress conditions.<sup>404</sup> As a chaperone, Hsp27 is also known to assist in protein folding processes, such as the folding of the small protein Tau.<sup>405</sup> Therefore, over-expressed Hsp27 is frequently found in neurodegenerative and cardiovascular diseases and in renal fibrosis.<sup>406</sup> Several publications on Hsp27 also discuss its association with various cancers, such as breast, lung, liver and gastric cancer, and emphasize the poor prognosis in disease progression once this biomarker is upregulated.<sup>407-409</sup>

To study the inhibitory effect of **33** (SR318) on the phosphorylation of p38 and its downstream target Hsp27, the dose-dependent downregulation was analyzed by Western Blot. This study was performed in collaboration with Jule Harbig and Daniel Dauch (University Hospital, Tübingen). In this assay, **33** (SR318) inhibited the phosphorylation of p38 MAPK, with the greatest effect observed at inhibitor concentrations of 0.333  $\mu\text{M}$  and 1  $\mu\text{M}$ . SR318 also inhibited the phosphorylation of Hsp27 in a concentration-dependent manner, although phosphorylation was not completely impaired at the compound concentrations tested.



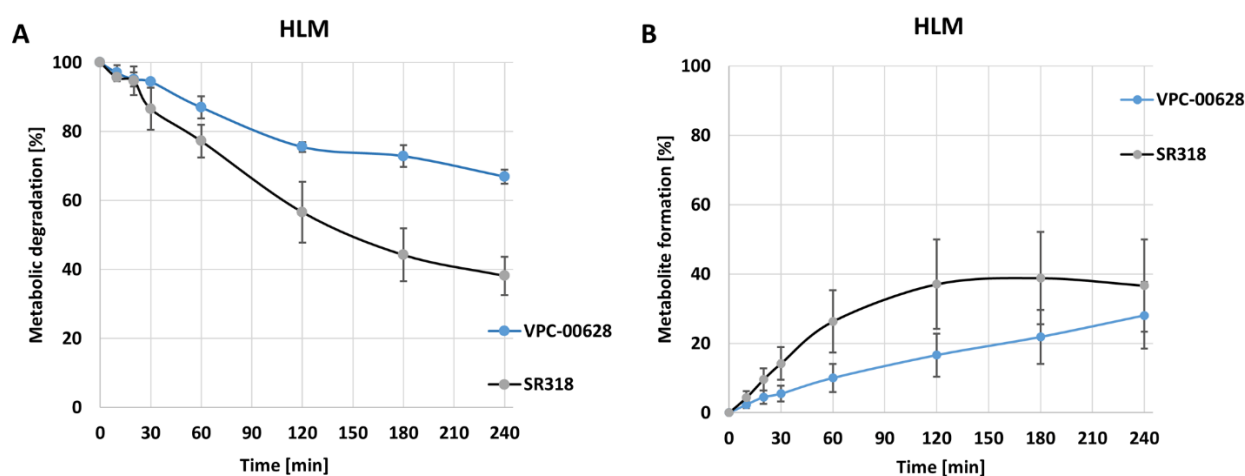
**Figure 24. Inhibitory effect of **33** (SR318) on endogenous substrates.** Inhibition of p38 and Hsp27 phosphorylation in HCT15 cells analyzed by Western Blot. Cells were treated with different inhibitor concentrations and stimulated with anisomycin. Vinculin and Tubulin were each used as loading control. Assay performed by Jule Harbig, Tübingen.

As described earlier in **Chapter 1.4**, p38 MAPK is also associated with inflammatory diseases, such as rheumatoid arthritis and COPD, as it regulates the production of proinflammatory cytokines such as IL-6, IL-8, IL-1 $\beta$ , TNF- $\alpha$  and interferon- $\gamma$  (IFN- $\gamma$ ). Therefore, the *in vitro* efficacy of **33** (SR318) was next investigated by determining the LPS-stimulated TNF- $\alpha$  release in whole blood.<sup>410</sup> The assay was performed in collaboration with Michael Forster (*Laufer Group*, University of Tübingen). To study the inhibition of TNF- $\alpha$  release, fresh whole blood from two donors was used, and, for comparison, the negative control **35** (SR321) and the commercially available type-I inhibitor SB203580 were tested (**Figure 25**). In summary, **33** (SR318) showed excellent *in vitro* efficacy, with LPS-stimulated TNF- $\alpha$  release quantitatively reduced at the highest test concentration of 10  $\mu\text{M}$  (inhibition of  $97.7 \pm 0.6\%$ ), and an  $\text{IC}_{50}$  value of  $0.283 \pm 0.040 \mu\text{M}$  was determined. The compound proved to be more effective than SB203580, with an overall inhibition of  $76.5 \pm 7.1\%$  at 10  $\mu\text{M}$  and an  $\text{IC}_{50}$  value of  $3.018 \pm 1.723 \mu\text{M}$ . As expected, no activity was observed for the negative control compound **35** (SR321).



**Figure 25. Inhibition of TNF- $\alpha$  release in human whole blood.** A) Dose-response curve of TNF- $\alpha$  release by compound **33** (SR318), negative control **35** (SR321) and commercial compound SB203580; single measurement is depicted. B) Calculated IC<sub>50</sub> values and percent of inhibition at highest compound concentration in the assay system (n=2). Assay performed in collaboration with Michael Forster, Tübingen.

The metabolic stability of **33** (SR318) was investigated in human liver microsomes (HLMs) and was done in collaboration by Mark Kudolo (*Laufer Group*, University of Tübingen). In this assay, the degradation of **33** (SR318) in HLMs was monitored together with the lead structure VPC-00628, and samples were analyzed after each 0, 10, 20, 30, 60, 120, 180, and 240 min by LC-MS. Interestingly, both compounds demonstrated to be metabolically stable and a total degradation of  $38.2 \pm 5.6\%$  for **33** (SR318) and  $66.9 \pm 2.1\%$  for VPC-00628 was detectable. Only a limited amount of metabolites was formed during this experiment for both compounds (**Figure 26**). The toxicity of the synthesized p38 probe compound **33** (SR318) and the negative control compound **35** (SR321) was studied by an XTT-assay<sup>411</sup> in HEK293T cells used also for the NanoBRET™ assays. These measurements were performed in collaboration by Haotian Wang and demonstrated that both compounds are not toxic at a concentration of 30  $\mu\text{M}$ .



**Figure 26. Metabolic stability in human liver microsomes (HLM).** A) Metabolic degradation and B) metabolite formation of **33** (SR318) and VPC-00628 over 240 min in HLM. Experiment was performed in triplicates. The values represent the mean with standard derivation. Assay by Mark Kudolo, Tübingen.

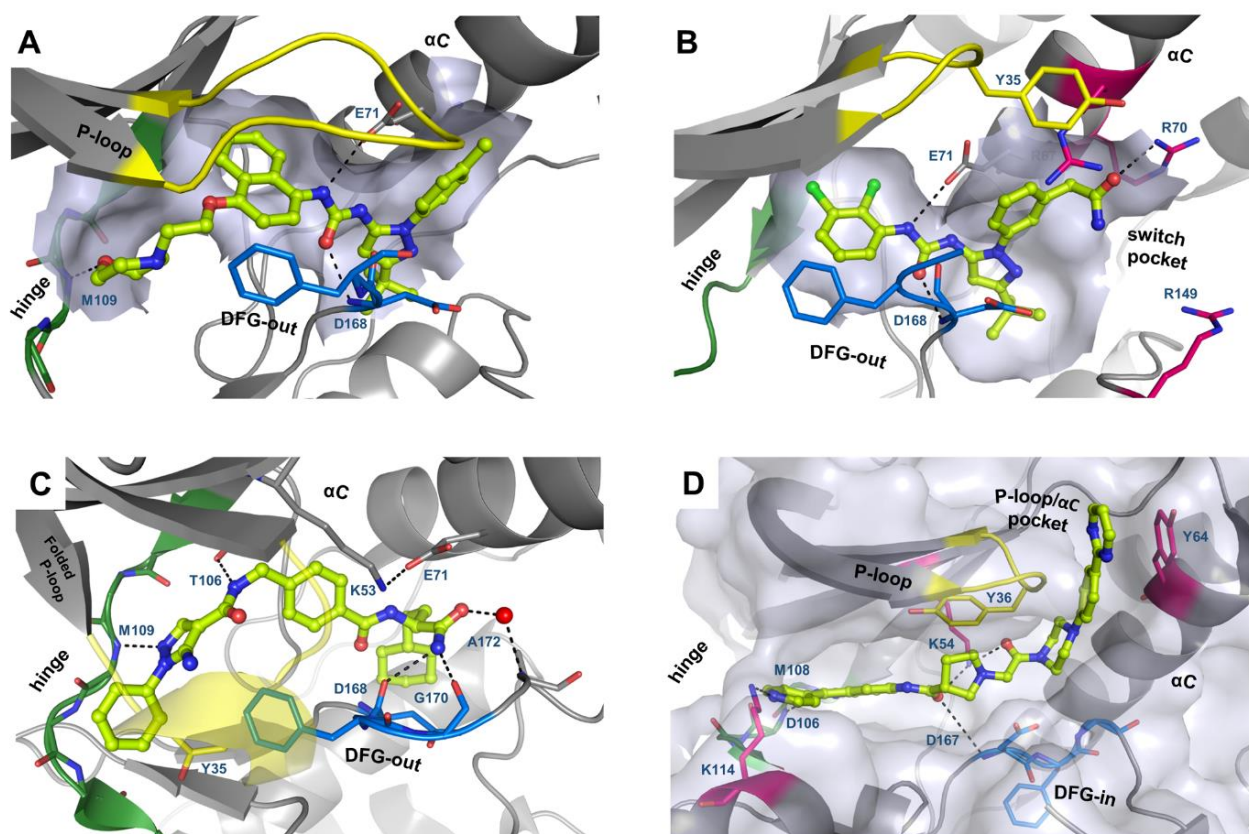
### 3.3 Conclusion

In summary, the fast iterative synthetic approach led to the development of a highly selective and very valuable type-II p38 $\alpha$ / $\beta$  probe, which fulfilled all probe criteria, namely to be potent, selective within the target family, active in cells as well as chemically stable and non-toxic. The same applies to the negative control compound **35** (SR321) synthesized during this work, which had a low activity on DDR2 kinase and was 100 times less potent than the probe.<sup>136, 412, 413</sup> Since no type-II p38 chemical probe was available until now, **33** (SR318) will fill this gap and allow a detailed mechanistic investigation of p38 MAPK. The latter can be profitably supported by using the entire p38-probe package, with the available type-I inhibitor Skepinone-L, the type-I½ inhibitor FS-694, and their negative control FM-743, and will contribute to a better understanding of the function of protein kinases in the future. For a complete overview of the designed p38-probe package, please visit the SGC website (<https://www.thesgc.org/donated-chemical-probes>).

During this work, further studies were conducted to investigate the  $\alpha$ / $\beta$ -isoform selectivity of p38 MAPK. Through docking studies structural characteristics within the DFG-out pocket, such as the amino acid at position 78, could be identified as likely reasons for the preferential binding of some compounds of the library to the  $\alpha$ -isoform of p38 MAPK. The synthesis of  $\alpha$ -isoform-selective inhibitors was previously reported by WOBLESKI ET AL., who observed a Leu108-backbone rearrangement in the hinge region induced by their inhibitors.<sup>322</sup> This leucine-flipped mode has so far been described as the only possibility to generate isoform selective inhibitors for p38 MAPK. The new findings from this work, therefore, offer a more general opportunity to develop  $\alpha$ -isoform-selective allosteric type-II inhibitors in the future.

## 4 Exploring the $\alpha$ C-out and DFG-out pocket region

Research over the past two decades has shown that a large proportion of human kinases can adopt an inactive DFG-out conformation.<sup>42, 43</sup> The type-II binding mode, which was originally exploited for the development of kinase inhibitors, is nowadays considered less suitable per se for achieving selective binding of compounds. In the case of p38 MAPK, this is exemplified by the aforementioned type-II inhibitor BIRB-796 (**Figure 27A**), which exhibits a very low nanomolar affinity toward p38, but lacks selectivity within the kinome (see also **Figure 17** in **Chapter 3**).<sup>44, 265, 414</sup> Based on the scaffold of BIRB-796, allosteric fragments have been extensively studied in the past and were used to explore the DFG-out lower selectivity site as well as the allosteric tolyl pocket higher selectivity site.<sup>265, 267, 415-417</sup> Although these fragments showed favorable pharmacokinetics, such as a very slow off-rate, the selectivity of these fragments has not yet been determined.<sup>265, 268, 418</sup> A more promising approach was developed by researchers at *Deciphera Pharmaceuticals*, in which the switch-pocket region of p38 was studied with urea-based allosteric fragments to improve the selectivity of the inhibitors.<sup>329</sup> By targeting the guanidinium groups of Arg67, Arg149 and of the non-conserved Arg70, located in the  $\alpha$ C helix and the HRD motif of p38 MAPK, selective type-III inhibitors such as DP802 were discovered (**Figure 27B**).<sup>329, 333, 334, 337</sup> However, most of these BIRB-796 derived compounds had low potency and poor pharmacological properties (see **Section 2.4**). Design approaches that aim at targeting non-conserved structural elements in kinases as well as unusual binding modes are therefore a more promising option for developing potent and selective inhibitors. The latter is also reflected in the p38 MAPK probe **33** (SR318) developed in **Chapter 3**, which combines a type-II binding mode with a folded P-loop conformation. A similar binding mode was already observed for the lead structure VPC-00628 (**Figure 27C**).<sup>340</sup> Although it is well known that some kinases, such as ABL1, ACK1, AURORA, cMET, ERK1/2, FGFR1, MAP4K4 and p38 can adopt a folded P-loop conformation,<sup>54</sup> the allosteric pocket enlarged by the movement of the P-loop was targeted only in one single case by the ERK1/2 inhibitor SCH772984 (**Figure 27D**). Initially, it was assumed that SCH772984 binds ERK1/2 kinase in a canonical type-II binding mode by protruding into the DFG-out deep pocket and in which the glycine-rich loop adopts a commonly found, extended orientation. However, after crystallization with ERK2, SCH772984 exposed a unique binding mode, in which the piperazine-phenyl-pyrimidine decoration adopts a bent conformation, aligning these residues inside the P-loop/ $\alpha$ C pocket. In this region, the compound is stabilized by hydrophobic and stacking interactions with Tyr64 from the  $\alpha$ C helix. The targeting of this pocket region proved beneficial, since it was associated with high inhibitor selectivity and favorable pharmacokinetics such as slow-off rates.<sup>56</sup> Interestingly, SCH772984 inhibited the ability of MEK1/2 to phosphorylate ERK1/2, at both Thr202/Tyr204 and Thr185/Thr187, and its subsequent activation, although it did not bind the MEK1/2 kinase upstream. Thus, a synergistic inhibitory effect on the RAF-MEK-ERK signaling cascade was observed, caused by large structural rearrangements in the N lobe, a region that normally serves as an interaction site with upstream MEKs.<sup>419-421</sup>



**Figure 27. Inhibitor binding to allosteric sites in p38 and ERK2.** A) Type-II p38 MAPK inhibitors BIRB-796 (PDB: 1KV2) targeting the inactive DFG-out conformation and the allosteric upper tolyl pocket. B) Type-III p38 inhibitor DP802 (PDB: 3NNW) interacting with switch pocket residues. C) Type-II inhibitor VPC00628 (PDB: 5LAR) stabilizing a folded P-loop conformation in p38 $\alpha$ . D) SCH772984 (PDB: 4QTA) targeting the allosteric P-loop/ $\alpha$ C pocket in the P-loop folded conformation of ERK2.

A similar conformation-selective inhibitory effect on p38 MAPK signaling was described by HARI ET AL. in 2014.<sup>398</sup> In this study, a type-I and a type-II inhibitor were used to investigate the non-catalytic functions during p38 inhibition and the impact on its upstream activator MEK6 as well as its inactivating phosphatase DUSP10. Different phenotypic responses were observed. Pyrazole-urea inhibitors of type-II, for example, stabilized the DFG-out form of the kinase and prevented the phosphorylation and activation by MEK6. In contrast, the type-I inhibitor SB203580, which stabilized the active form of p38, had no effect on A-loop phosphorylation and activation by its upstream kinase was unaffected. Furthermore, SB203580 allosterically increased the activity of the phosphatase DUSP10, thereby promoting dephosphorylation of the activated p38 MAPK. An opposite effect was found for the type-II inhibitor used, which negatively modulated DUSP10 activity.<sup>399</sup> SUVILLAN ET AL. reported that inhibitors targeting the DFG-out pocket selectivity sites, such as BIRB-796, concurrently inhibit p38 activation and phosphorylation by MEK6 with  $K_d$  values in the low nanomolar range, without directly binding to MEK6.<sup>418</sup> The detailed molecular mechanism of how P-loop folding effects the signaling on p38 MAPK is unknown. Even less is known on how conformation-selective inhibition translates to other signaling pathways and the rest of the kinome. Revealing the molecular basis of these effects would provide a platform for more efficient inhibitor design in future.

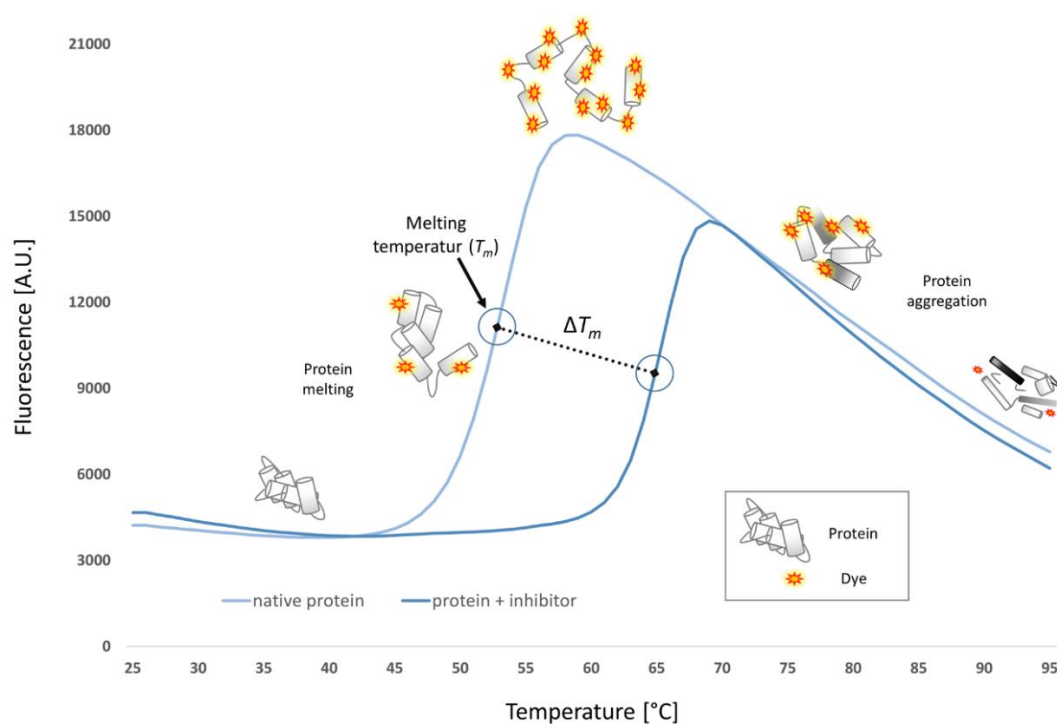
The following work focused on the exploration of the highly dynamic allosteric back pocket of p38 MAPK. Allosteric urea derivatives were synthesized and used to monitor off-target activities against a panel of 47 kinases with DSF assays. However, since these fragments retained selectivity issues, an improvement in selectivity was achieved after the allosteric part of BIRB-796 was fused with the hinge motif VPC-00628. Additional studies therefore focused on the optimization of the P-loop/ $\alpha$ C allosteric pocket interaction of

VPC-00628. Compounds were evaluated by DSF assays and by bioluminescence resonance energy transfer (NanoBRET™) assays *in cellulo*. Both assays will be briefly explained in the next section.

## 4.1 Biological testing

### 4.1.1 DSF Assay

For the studies in the present work, compounds were first evaluated using DSF assays<sup>422, 423</sup> to qualify the protein-ligand interaction against p38 $\alpha$ . The DSF assay, also called thermal-shift assay, monitors the temperature-dependent unfolding of a protein. The method measures changes in the intrinsic fluorescence of a dye upon binding to hydrophobic patches of the protein. Typically, SYPRO orange is used as a fluorescent dye that is highly fluorescence in a hydrophobic environment, whereas the fluorescence is quenched in aqueous solution. Upon heating the protein of interest in a thermocycler, the protein starts to unfold, thereby exposing hydrophobic patches. Successively, SYPRO orange dye binds in a larger proportion to the hydrophobic protein surface, thus leading to an overall increase in the fluorescence signal. After unfolding of the protein, heating to even higher temperatures result in protein aggregation, followed by dissociation of the fluorescence dye and decreasing the fluorescent signal. By plotting the fluorescence signal against the temperature, usually a sigmoidal curve is obtained that resembles a two-state transition, where the inflection point refers to the melting temperature of the protein under investigation (**Figure 28**). If a ligand is added to the solution of protein and dye, compound binding typically stabilizes the protein structure, and a shift of the melting curve toward higher temperatures can be observed. The differences in the melting points ( $\Delta T_m$ ) can therefore be used to get a quick estimate on relative protein-binding affinities and to easily sort out less suitable inhibitors.



**Figure 28.** Principle of a DSF assay for determining changes in protein melting temperatures.



DFS assays were used for an initial structure-activity relationship (SAR) study of the newly synthesized p38 compounds. Since this universal and label-free method is less protein consuming, it also proved to be very versatile in the high-throughput screening of drugs and fragments.<sup>424, 425</sup> In general, the results correlated well with the data obtained from other enzymatic binding assay, which are usually more time- and protein consuming, cost expensive and need to be optimized for each kinase first investigated.<sup>422, 426</sup> Since the SYPRO orange dye emits its highest fluorescence at  $\lambda=563$  nm, the signal-to-noise ratio of the assay is usually low. However, very hydrophobic inhibitors are able to interact with the dye itself and thereby raise the fluorescence signal in an unspecific way.

#### 4.1.2 NanoBRET™ assay

Following the  $\Delta T_m$  measurements, which provided a first ranking of inhibitor binding, the *in cellulo* potency of the newly synthesized compounds was determined using a NanoBRET™ assay from Promega.<sup>427</sup> This assay system was chosen for  $IC_{50}$  calculations as the initial lead compound VPC-00628 had already proven to be effective in the cellular environment by potent suppression of the TNF- $\alpha$  release in THP-1 cells ( $IC_{50} = 7$  nM).<sup>340</sup> Classically, a cellular assay is the preferred second step to investigate an already potent inhibitor under physiological conditions. However, assays on an isolated catalytic domain often do not reflect the binding of a compound to its full-length protein, and the potencies determined can differ up to 100-fold. In addition to the full-length protein, which influences inhibitor binding, cell permeability and solubility of the compounds, the intracellular concentration of ATP and cofactors, as well as the conformational state of the kinase are crucial for the efficacy of an inhibitor.<sup>428</sup> To quantify inhibitor binding to a respective protein, the NanoBRET™ assay uses the bioluminescence resonance energy transfer technique, which detects the proximity-dependent bioluminescence of a protein-fused donor and a corresponding acceptor pair (Figure 29).<sup>427</sup>

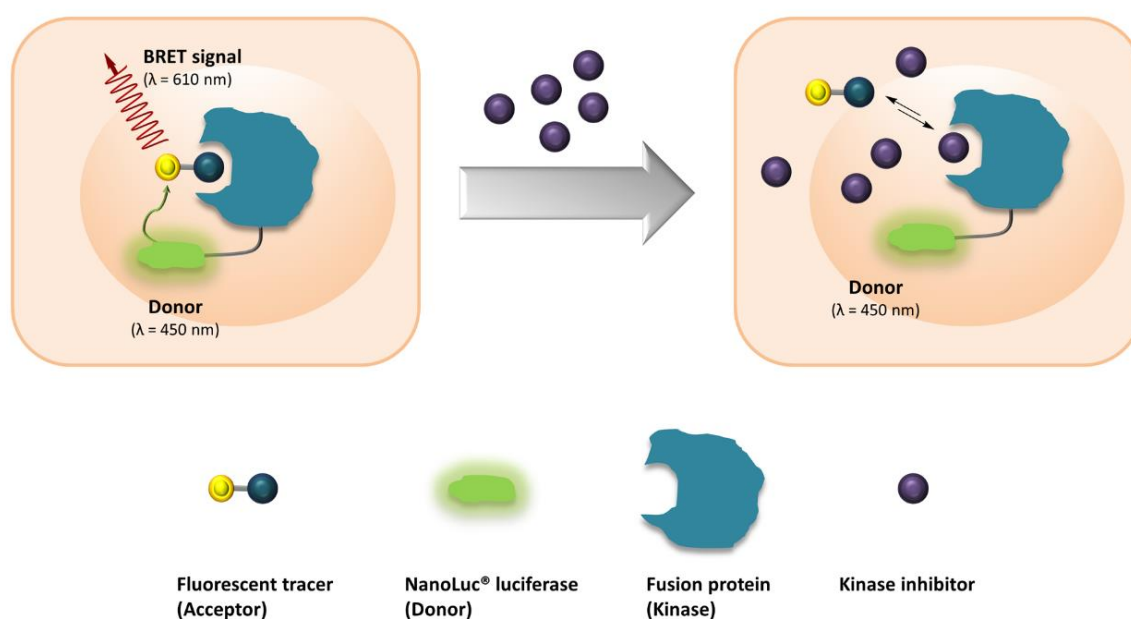
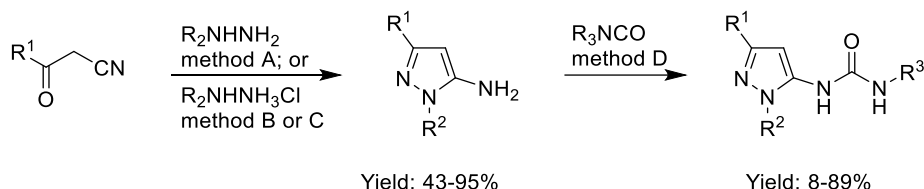


Figure 29. Principle of the NanoBRET™ assay for determining  $IC_{50}$  values in HEK293T cells.

Typically, the full-length kinase of interest is cloned with an N- or C-terminal NanoLuc luciferase fusion donor, transfected and expressed in HEK293T cells, and a fluorescent tracer is added as acceptor. Upon binding of the tracer to the fusion protein, an emission signal is detectable due to the proximity (maximally 10 nm) of the donor-acceptor pair, whereby the donor transmits its radiation-free energy to the fluorophore. The addition of an inhibitor to the assay system leads to a competitive displacement of the fluorescent tracer, resulting in a general decrease on the NanoBRET signal. The plotting of the NanoBRET signal against different compound concentrations of a dilution series results in sigmoidal curves, where the inflection point corresponds to the  $IC_{50}$  value of the compound of interest. For the current work, the NanoBRET™ assay was optimized for the specific targeting of p38 $\alpha/\beta$  (**Chapter 4**) and DDR1/2 (**Chapter 5**) in live cells and measured in collaboration with Benedict-Tillman Berger.

## 4.2 Synthesis of BIRB-fragment library

For exploring the allosteric back-pocket region of p38 $\alpha/\beta$  MAPK, a set of BIRB-796 fragment compounds was synthesized in a two-step reaction during this work (**Scheme 4**). The synthesis of the library compounds was a collaborative work that was carried out as part of this doctoral thesis in Frankfurt and by Jessica E. Dwyer and Caroline S. Widdowson from the Bagley Lab at the University of Sussex. The co-workers at Sussex University focussed mainly on a microwave-assisted synthesis of aminopyrazole derivatives<sup>429</sup> and optimized the aryl-urea part directed at the active center of p38 with invariant allosteric BIRB-796 pyrazole decorations or kept 3,5-di-fluoro-, 3,5-di- $CF_3$ - moieties facing the front pocket constant. The current work in Frankfurt focused on the optimization of the tolyl-pocket interactions. In contrast to the Bagley Lab, the synthesis of the respective aminopyrazoles was performed by non-microwave assisted heating. In both laboratories, the asymmetric urea formation was performed with isocyanate derivatives to obtain the compounds of interest.

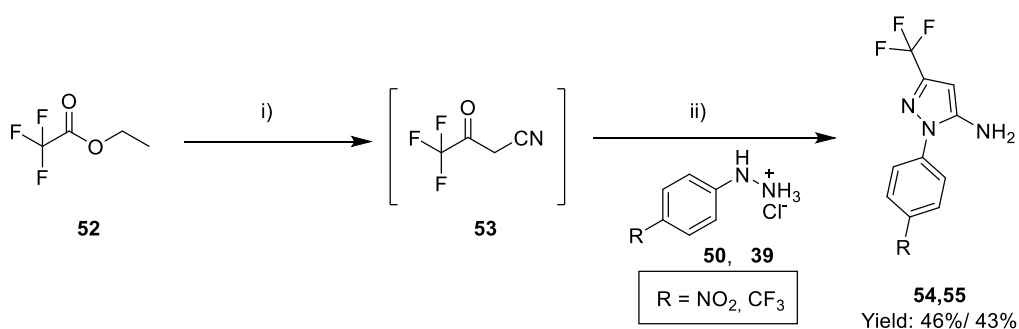


**Scheme 4. Synthetic route for the preparation of BIRB-fragment library compounds.** Reagents and conditions: Method A) hydrazine, toluene/AcOH (5:1), 120 °C (100 W), MW. Method B) hydrazine hydrochloride, HCl (cat.), EtOH, 130 °C (200 W), MW. Method C) hydrazine hydrochloride, HCl (cat.), EtOH, reflux. Method D) isocyanate,  $CH_2Cl_2$ , RT.  $R^1$ : tert-butyl, phenyl, cyclopropyl,  $CF_3$ .  $R^2$  = phenyl, 4-tolyl, tert-butyl, methyl, 4-X-phenyl (X =  $NO_2$ , Br, F,  $CF_3$ ,  $OCF_3$ , CN,  $SO_2CH_3$ ).  $R^3$  = 2-naphthyl, 1-naphthyl, 2-tolyl, m-xylol, 3-methoxy phenyl, O-tosyl 3-F-2-tolyl, 3,4-diF-phenyl, 3,5-di $CF_3$ -phenyl, 3,5-diF-phenyl, 4-Y-phenyl (Y = Me, OEt, F, Cl, O-benzyl). For final compounds see **Table 6**, **Table 7**, **Table 8**.

In the first step of the reaction to optimize the tolyl pocket, various para-substituted as well as 3,5-disubstituted hydrazine hydrochloride derivatives were reacted with 4,4-dimethyl-3-oxopentanitrile (**37**) or 3-cyclopropyl-3-oxopropanenitrile (**48**) in ethanol. The reaction followed the mechanism of a Knorr-pyrazole synthesis<sup>430</sup> using the 3-oxopentanenitrile derivative as 1,3-dicarbonyl analogue. Nucleophilic attack of the terminal nitrogen atom of hydrazine on the carbonyl atom was facilitated by the addition of hydrochloric acid. After hydrazone formation occurred, the less reactive second hydrazine nitrogen atom attacked the also protonated nitrile, which was facilitated by the formation of an electronically favored five-membered ring system. Finally, imine-enamine tautomerization regenerated the acidic catalyst and delivered the desired aminopyrazole product in fair to high yields.

In the second step, the respective aminopyrazole derivative was reacted with 1-chloro-4-isocyanatobenzene (**87**) to form the urea compounds of interest. Although there are several possibilities for forming urea compounds, such as the Curtius rearrangement<sup>431, 432</sup> in which acyl azides are reacted to form isocyanates *in situ*, or the synthesis via 1,1'-carbonyldiimidazole (CDI)<sup>433</sup>, which can be used as a reagent for the formation of ureas from two amines, the use of 1-chloro-4-isocyanatobenzene was chosen due to its good commercial availability and the higher yields to be expected. In addition, the direct use of isocyanates offers the advantage of avoiding very harsh and hazardous conditions, such as those typically applied in thermal decomposition of acyl azides in Curtius reactions, where the total yields for forming of ureas are often low due to incomplete rearrangement reactions.<sup>432, 434</sup> The use of CDI is a good alternative for a mild coupling reaction of two amine derivatives to form ureas by avoiding the use of toxic phosgene.<sup>433, 435</sup> However, depending on the nucleophilicity and the equivalents of the amines used, symmetrical ureas might be formed as a by-product, lowering the overall yield and also making the purification of compounds, for example by crystallization, more difficult.<sup>433</sup>

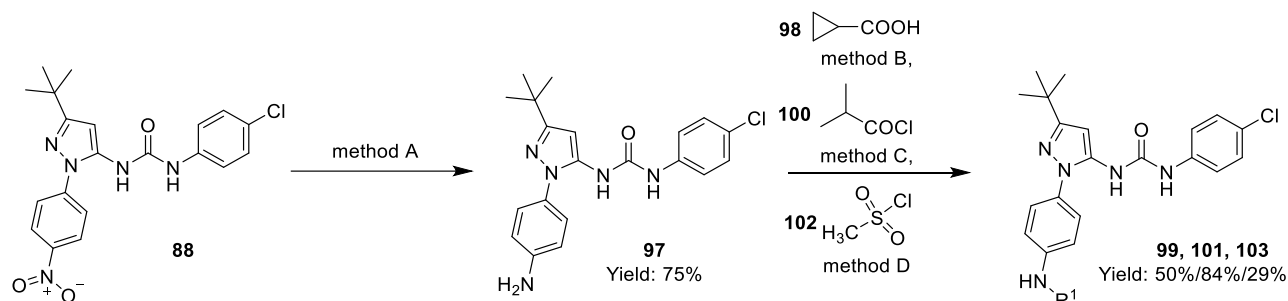
For the synthesis of a trifluoromethyl decorated pyrazole derivative, a one-pot synthesis was applied, using ethyl 2,2,2-trifluoroacetate (**52**) and acetonitrile as starting material (**Scheme 5**). The reaction was performed in a basic solution of potassium *tert*-butoxide in tetrahydrofuran, in which the nitrile compound 4,4,4-trifluoro-3-oxobutanenitrile (**53**), necessary for the Knorr-Pyrazole-like synthesis, was created *in situ*. Compared with the pyrazole formations described before, this one-pot synthesis was more convenient, since the trifluoro-decorated nitrile is very volatile and thus easier to handle. After a short work-up procedure, the nitrile intermediate formed was heated with (4-nitrophenyl)hydrazine hydrochloride (**50**) in ethanol to obtain 1-(4-nitrophenyl)-3-(trifluoromethyl)-1*H*-pyrazol-5-amine (**54**) in a fair yield of 46%. Subsequently, urea formation was performed by the use of 1-chloro-4-isocyanatobenzene (**87**) as described before in **Scheme 4**. The final product 1-(4-chlorophenyl)-3-(1-(4-nitrophenyl)-3-(trifluoromethyl)-1*H*-pyrazol-5-yl)urea (**96**) was obtained in a poor yield of 8%. The one-pot reaction was also successfully applied for the synthesis of 3-(trifluoromethyl)-1-(4-(trifluoromethyl)phenyl)-1*H*-pyrazol-5-amine (**55**, Yield: 43%). However, synthesis of a corresponding urea derivate failed, which might be due to solubility problems.



**Scheme 5.** One-pot synthesis for trifluoromethyl-decorated pyrazole derivatives. Reagents and conditions: i) Acetonitrile, *KOtBu*, THF, RT. ii) HCl, EtOH, reflux.

In order to synthetically extend the modification spectrum for the tolyl pocket, the nitro group of 1-(3-(*tert*-butyl)-1-(4-nitrophenyl)-1*H*-pyrazol-5-yl)-3-(4-chlorophenyl)urea (**88**) was reduced to a free amine functionality. Various methods have been applied to make the reaction feasible, such as reduction via tin(II) chloride or hydrogenation of the nitro group via hydrogen on palladium/charcoal. By performing the reaction with tin(II) chloride under gentle heating in ethyl acetate, product formation monitored by TLC was low and therefore no product was isolable. Under harsher conditions, reduction with hydrogen on charcoal quantitatively reduced the nitrogen group overnight at room temperature. However, the use of palladium

as a catalyst also led to a hydrogenolytic dehalogenation of the chloro-substituted phenyl residue. Therefore, a mild Fe-catalyzed Béchamp reduction with ammonium chloride was carried out instead in subsequent reactions, which resulted in the successful synthesis of 1-(1-(4-aminophenyl)-3-(*tert*-butyl)-1*H*-pyrazol-5-yl)-3-(4-chlorophenyl)urea (**97**), which was obtained in 75% yield (**Scheme 6**).



**Scheme 6. Synthesis of amino-functionalized compounds.** Reagents and conditions: Method A) Fe,  $\text{NH}_4\text{Cl}$ , EtOH/ $\text{H}_2\text{O}$  (4:1), 70 °C. Method B) HATU, DIPEA, DMF, RT. Method C) TEA, THF, 0 °C  $\rightarrow$  RT. Method D) TEA, DCM/THF, 0 °C  $\rightarrow$  RT.

The amino functionalized compound **97** is a very versatile building block that allows broad structural modifications. Therefore, the introduction of different functional groups and residues, such as amides, sulphonamides and secondary amines, was considered. For the formation of amides, two different methods were successfully applied: 1) For the synthesis of *N*-(4-(3-(*tert*-butyl)-5-(3-(4-chlorophenyl)ureido)-1*H*-pyrazol-1-yl)phenyl)isobutyramide (**101**) a Schotten-Baumann reaction with isobutyryl chloride under basic conditions. The reaction was carried out in dry tetrahydrofuran using one equivalent of amine (**97**) and two equivalents of triethylamine. The equivalents of the corresponding acid chloride were varied and the best yields were obtained by using two equivalents (1 eq., yield = 14%, 2 eq., yield = 84%). 2) For the synthesis of *N*-(4-(3-(*tert*-butyl)-5-(3-(4-chlorophenyl)ureido)-1*H*-pyrazol-1-yl)phenyl)cyclopropanecarboxamide (**99**) cyclopropanecarboxylic acid (**98**) was reacted with HATU and DIPEA to form an active ester. The amine 1-(1-(4-aminophenyl)-3-(*tert*-butyl)-1*H*-pyrazol-5-yl)-3-(4-chlorophenyl)urea (**97**) was added after a pre-activation time, and the product was isolated in 50% yield. To introduce a sulphonamide decoration, methanesulfonyl chloride (**102**) was added at 0 °C to a stirring solution of amine **97** in a basic solution of tetrahydrofuran. After purification, the final compound *N*-(4-(3-(*tert*-butyl)-5-(3-(4-chlorophenyl)ureido)-1*H*-pyrazol-1-yl)phenyl)methanesulfonamide (**103**) was obtained in 29% yield. For the synthesis of a secondary amine, which might form favorable hydrogen bonds in the allosteric region of p38 MAPK, an oxetane moiety was considered. Therefore 1-(1-(4-aminophenyl)-3-(*tert*-butyl)-1*H*-pyrazol-5-yl)-3-(4-chlorophenyl)urea (**97**) was stirred in a solution of tetrahydrofuran and cooled to 0 °C, after which 3-oxetanone and acetic acid were added to form an iminium intermediate. After a reaction time of two hours at room temperature, an excess of sodium triacetoxyborohydride was added to form the secondary amine of interest by reduction. After stirring overnight, product formation, which was monitored by TLC, was only low. Since sodium triacetoxyborohydride, compared to sodium borohydride which is also frequently used in reductive aminations, has the advantage of not reducing ketones and aldehydes, the equivalents of the ketone component, 3-oxetone, were increased 5 fold. Although product formation was subsequently observed by ESI-MS, isolation of the desired product was not possible.

Finally, a total of thirteen urea compounds were successfully synthesized that shared a 4-chloro-phenyl moiety. Depending on the synthetic route and the functional groups chosen, the overall yields varied from poor to very good yields (8-89%). All compounds were analyzed by  $^1\text{H-NMR}$ ,  $^{13}\text{C-NMR}$  and ESI-MS. In addition, a set of 31 BIRB-fragment library compounds was provided by the collaborators from Sussex

University. The chemical structures of all compounds synthesized and investigated are listed in **Table 6-8** in the following section, in which the selectivity against a panel of 47 kinase targets was monitored with differential scanning fluorimetry (DSF).

## 4.3 Results

### 4.3.1 Allosteric BIRB fragments

Kinase conformations are highly dynamic, allowing precise modulation of signaling cascades by catalytic as well as non-catalytic mechanisms. Allosteric pockets have been discovered coincidentally by trapping less conserved conformational states with small molecules, thereby providing insights into the conformational space available for ligand binding. In this section, p38 MAPK was used as a well-established model system for which a large diversity of allosteric and ATP-competitive inhibitors have been developed to study allosteric back-pocket interaction, including the DFG-out and the P-loop/ $\alpha$ C pocket. The previously synthesized allosteric urea-based fragments derived from the type-II inhibitor BIRB-796 (**Section 4.2**) were evaluated with respect to their selectivity profile against known BIRB-796 off-targets. Some of these allosteric fragments have been studied before, however, their selectivity profiles against BIRB-796 off-targets have not been determined.<sup>265, 267, 415-417</sup> Using DSF, activity of a set of 47 kinases, including a selection of BIRB-796 off-targets described by KARAMAN ET AL. and DAVIS ET AL., was monitored.<sup>37, 44</sup> The first library synthesized and investigated focused on the modification of the active-site directed aryllic urea moiety, with invariant allosteric pyrazole decoration (compounds **56-69**, **Table 6**). In this screen, the consistently highest activity was found for kinases like AURKB, BRAF, EPHA2, MAPK9, p38 $\alpha$ , p38 $\beta$ , SLK and STK10 (for the complete data set please see **Section 8.4.3**).

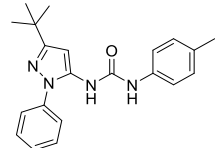
**Table 6.** Selectivity profiling by DSF assays; active site directed aryllic-urea modifications.

No.	Structure <sup>a</sup>	$\Delta T_m$ [°C] $\pm$ SEM <sup>b</sup>							
		AURKB	BRAF	EPHA2	MAPK 9	p38 $\alpha$	p38 $\beta$	SLK	STK10
BIRB 796		4.0 $\pm$ 0.1	22.1 $\pm$ 0.1	8.0 $\pm$ 0.0	6.7 $\pm$ 0.1	19.8 $\pm$ 0.1	19.9 $\pm$ 0.0	3.6 $\pm$ 0.6	10.0 $\pm$ 0.2
56		-3.0 $\pm$ 7.5	1.7 $\pm$ 0.1	2.9 $\pm$ 0.1	1.6 $\pm$ 0.4	13.1 $\pm$ 0.1	14.3 $\pm$ 0.5	2.7 $\pm$ 0.8	1.1 $\pm$ 0.2
57		2.7 $\pm$ 0.7	8.9 $\pm$ 0.3	1.2 $\pm$ 0.1	0.4 $\pm$ 0.1	10.3 $\pm$ 1.0	10.8 $\pm$ 0.0	7.1 $\pm$ 0.4	8.6 $\pm$ 0.1
58		4.3 $\pm$ 0.1	1.5 $\pm$ 0.1	1.6 $\pm$ 0.0	1.2 $\pm$ 0.1	5.3 $\pm$ 1.2	5.3 $\pm$ 0.8	1.8 $\pm$ 0.9	0.8 $\pm$ 0.0

Table 6. (continued)

No.	Structure <sup>a</sup>	$\Delta T_m$ [°C] $\pm$ SEM <sup>b</sup>							
		AURKB	BRAF	EPHA2	MAPK 9	p38 $\alpha$	p38 $\beta$	SLK	STK10
59		3.5 $\pm$ 0.2	3.1 $\pm$ 0.0	1.0 $\pm$ 0.0	0.6 $\pm$ 0.0	4.7 $\pm$ 0.8	7.0 $\pm$ 2.1	1.1 $\pm$ 0.3	0.8 $\pm$ 0.0
60		4.0 $\pm$ 0.0	10.1 $\pm$ 0.5	2.2 $\pm$ 0.0	2.6 $\pm$ 0.0	8.9 $\pm$ 0.3	8.9 $\pm$ 0.7	7.4 $\pm$ 0.0	6.5 $\pm$ 0.6
61		4.1 $\pm$ 0.1	0.6 $\pm$ 0.0	0.8 $\pm$ 0.1	0.3 $\pm$ 0.1	0.2 $\pm$ 0.0	0.0 $\pm$ 0.1	0.0 $\pm$ 0.0	-0.5 $\pm$ 0.2
62		3.9 $\pm$ 0.1	3.0 $\pm$ 0.2	1.5 $\pm$ 0.0	-0.1 $\pm$ 0.1	1.5 $\pm$ 0.4	1.5 $\pm$ 0.1	0.5 $\pm$ 0.0	0.4 $\pm$ 0.2
63		4.0 $\pm$ 0.0	2.1 $\pm$ 0.2	0.7 $\pm$ 0.0	0.3 $\pm$ 0.1	4.8 $\pm$ 1.4	4.5 $\pm$ 0.2	2.4 $\pm$ 0.8	-0.3 $\pm$ 0.2
64		4.2 $\pm$ 0.1	6.0 $\pm$ 0.4	1.6 $\pm$ 0.0	0.7 $\pm$ 0.1	9.6 $\pm$ 0.4	12.6 $\pm$ 0.6	6.0 $\pm$ 0.0	4.1 $\pm$ 0.0
65		2.3 $\pm$ 0.2	7.1 $\pm$ 0.0	2.2 $\pm$ 0.2	1.7 $\pm$ 0.0	10.2 $\pm$ 0.3	9.3 $\pm$ 0.2	5.5 $\pm$ 0.6	3.4 $\pm$ 0.2
66		4.4 $\pm$ 0.2	9.7 $\pm$ 0.2	1.6 $\pm$ 0.1	2.1 $\pm$ 0.0	10.6 $\pm$ 0.3	10.8 $\pm$ 0.6	7.7 $\pm$ 0.1	7.2 $\pm$ 0.2
67		3.0 $\pm$ 0.0	0.6 $\pm$ 0.1	0.2 $\pm$ 0.0	-0.3 $\pm$ 0.0	-0.4 $\pm$ 0.1	-1.3 $\pm$ 0.1	-0.3 $\pm$ 0.1	-0.9 $\pm$ 0.1
68		4.0 $\pm$ 0.1	8.7 $\pm$ 0.4	1.8 $\pm$ 0.1	1.4 $\pm$ 0.1	8.6 $\pm$ 0.2	9.8 $\pm$ 0.1	3.6 $\pm$ 0.6	3.7 $\pm$ 0.0

**Table 6.** (continued)

No.	Structure <sup>a</sup>	$\Delta T_m$ [°C] $\pm$ SEM <sup>b</sup>							
		AURKB	BRAF	EPHA2	MAPK 9	p38 $\alpha$	p38 $\beta$	SLK	STK10
69		3.6 $\pm$ 0.3	14.1 $\pm$ 0.3	1.7 $\pm$ 0.1	1.7 $\pm$ 0.1	10.6 $\pm$ 0.1	12.3 $\pm$ 0.1	4.6 $\pm$ 0.5	4.7 $\pm$ 0.3
Ctrl.	Staurosporine	9.9 $\pm$ 0.2	0.8 $\pm$ 0.0	7.0 $\pm$ 0.1	2.7 $\pm$ 0.1	0.4 $\pm$ 0.1	0.4 $\pm$ 0.1	16.9 $\pm$ 0.1	22.9 $\pm$ 0.3

<sup>a</sup> Compounds synthesized by Jessica E. Dwyer and Caroline S. Widdowson, Sussex. <sup>b</sup>  $\Delta T_m$  derived from two replicates at a compound concentration of 10  $\mu$ M. DSF measured by Andreas Krämer, SGC Frankfurt.

This limited screen showed that compounds potentially interacting with p38 $\alpha$ / $\beta$  largely retained activity on kinase targets known to bind to BIRB-796. Examples of such inhibitors are **57**, **60**, **65**, **66** and **69**. Besides p38 $\alpha$ / $\beta$ , the highest stabilization, and hence binding affinity, was found for the off-target BRAF, followed by SLK and STK10. Interestingly, the 3,5-di-CF<sub>3</sub> decorated compound **61** and **67** with a sulfonamide group had no stabilizing effect across the kinase panel, except for AURKB, suggesting that these fragments could be developed into chemical probes for this target. In the second library, 3,5-di-fluoro-, 3,5-di-CF<sub>3</sub>-phenyl decorations were kept constant and only the part of the ligand potentially interacting with the allosteric back was modified (compounds **70-86**, **Table 7**).

**Table 7.** Selectivity profiling by DSF; back-pocket modifications with invariant CF<sub>3</sub>- or F- decorations.

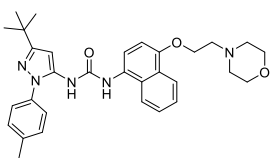
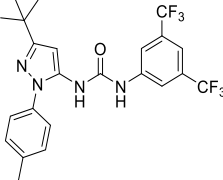
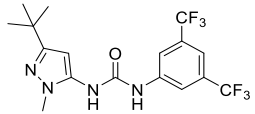
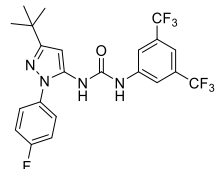
No.	Structure <sup>a</sup>	$\Delta T_m$ [°C] $\pm$ SEM <sup>b</sup>							
		AURKB	BRAF	EPHA2	MAPK 9	p38 $\alpha$	p38 $\beta$	SLK	STK10
BIRB 796		4.0 $\pm$ 0.1	22.1 $\pm$ 0.1	8.0 $\pm$ 0.0	6.7 $\pm$ 0.1	19.8 $\pm$ 0.1	19.9 $\pm$ 0.0	3.6 $\pm$ 0.6	10.0 $\pm$ 0.2
70		2.4 $\pm$ 1.5	1.0 $\pm$ 0.0	0.8 $\pm$ 0.0	0.3 $\pm$ 0.1	0.3 $\pm$ 0.1	-0.2 $\pm$ 0.1	0.0 $\pm$ 0.2	-0.5 $\pm$ 0.1
71		3.3 $\pm$ 0.4	1.0 $\pm$ 0.0	0.4 $\pm$ 0.1	0.1 $\pm$ 0.2	1.4 $\pm$ 0.1	1.4 $\pm$ 0.0	2.4 $\pm$ 0.2	1.1 $\pm$ 0.1
72		3.4 $\pm$ 0.6	0.4 $\pm$ 0.0	0.4 $\pm$ 0.1	-0.1 $\pm$ 0.1	0.2 $\pm$ 0.0	-0.1 $\pm$ 0.2	0.5 $\pm$ 0.0	-0.6 $\pm$ 0.2

Table 7. (continued)

No.	Structure <sup>a</sup>	$\Delta T_m$ [°C] $\pm$ SEM <sup>b</sup>							
		AURKB	BRAF	EPHA2	MAPK 9	p38 $\alpha$	p38 $\beta$	SLK	STK10
73		4.1 $\pm$ 0.1	0.9 $\pm$ 0.0	0.7 $\pm$ 0.0	0.1 $\pm$ 0.0	0.3 $\pm$ 0.0	-0.2 $\pm$ 0.1	-0.1 $\pm$ 0.1	-0.6 $\pm$ 0.1
74		4.0 $\pm$ 0.8	0.6 $\pm$ 0.1	0.5 $\pm$ 0.0	0.1 $\pm$ 0.0	0.1 $\pm$ 0.0	-0.4 $\pm$ 0.2	-0.2 $\pm$ 0.1	-0.7 $\pm$ 0.1
75		3.1 $\pm$ 0.5	0.0 $\pm$ 0.1	0.3 $\pm$ 0.0	0.0 $\pm$ 0.0	0.1 $\pm$ 0.0	0.3 $\pm$ 0.1	0.1 $\pm$ 0.0	-0.3 $\pm$ 0.0
76		4.1 $\pm$ 0.0	1.4 $\pm$ 0.0	0.9 $\pm$ 0.0	0.0 $\pm$ 0.1	2.2 $\pm$ 0.1	2.5 $\pm$ 0.3	1.9 $\pm$ 0.3	2.6 $\pm$ 0.1
77		3.9 $\pm$ 0.3	0.6 $\pm$ 0.1	0.5 $\pm$ 0.0	0.0 $\pm$ 0.0	0.1 $\pm$ 0.0	-0.4 $\pm$ 0.0	-0.2 $\pm$ 0.0	-0.7 $\pm$ 0.1
78		2.3 $\pm$ 2.3	5.4 $\pm$ 0.3	2.7 $\pm$ 0.2	2.7 $\pm$ 0.1	7.1 $\pm$ 1.0	8.6 $\pm$ 0.0	3.0 $\pm$ 0.3	2.5 $\pm$ 0.3
79		-0.1 $\pm$ 4.5	3.7 $\pm$ 0.1	1.9 $\pm$ 0.1	2.1 $\pm$ 0.0	7.0 $\pm$ 0.8	8.7 $\pm$ 0.5	2.8 $\pm$ 0.4	0.6 $\pm$ 0.1
80		3.4 $\pm$ 0.5	1.9 $\pm$ 0.1	0.4 $\pm$ 0.1	0.8 $\pm$ 0.0	3.8 $\pm$ 0.2	3.4 $\pm$ 0.3	1.2 $\pm$ 0.1	1.1 $\pm$ 0.1
81		4.5 $\pm$ 0.1	3.3 $\pm$ 0.0	1.9 $\pm$ 0.1	2.5 $\pm$ 0.0	5.2 $\pm$ 0.5	6.3 $\pm$ 1.8	2.7 $\pm$ 1.8	1.7 $\pm$ 0.1



Table 7. (continued)

No.	Structure <sup>a</sup>	$\Delta T_m$ [°C] $\pm$ SEM <sup>b</sup>							
		AURKB	BRAF	EPHA2	MAPK 9	p38 $\alpha$	p38 $\beta$	SLK	STK10
82		4.0 $\pm$ 0.1	1.3 $\pm$ 0.0	0.9 $\pm$ 0.0	1.2 $\pm$ 0.1	5.0 $\pm$ 0.8	6.9 $\pm$ 4.9	2.6 $\pm$ 0.7	0.6 $\pm$ 0.4
83		1.6 $\pm$ 1.3	0.0 $\pm$ 0.1	0.0 $\pm$ 0.0	-0.1 $\pm$ 0.0	0.1 $\pm$ 0.0	0.0 $\pm$ 0.1	0.2 $\pm$ 0.1	-0.2 $\pm$ 0.2
84		4.0 $\pm$ 0.2	2.0 $\pm$ 0.0	1.3 $\pm$ 0.0	1.1 $\pm$ 0.1	1.6 $\pm$ 0.0	1.8 $\pm$ 0.6	0.5 $\pm$ 0.0	0.2 $\pm$ 0.2
85		3.5 $\pm$ 0.1	0.4 $\pm$ 0.1	0.3 $\pm$ 0.0	-0.1 $\pm$ 0.1	0.1 $\pm$ 0.1	-0.2 $\pm$ 0.0	0.8 $\pm$ 0.4	-0.7 $\pm$ 0.1
86		4.2 $\pm$ 0.6	0.7 $\pm$ 0.1	1.1 $\pm$ 0.1	0.2 $\pm$ 0.1	2.8 $\pm$ 0.5	3.2 $\pm$ 0.3	2.6 $\pm$ 0.1	0.6 $\pm$ 0.2
Ctrl.	Staurosporine	9.9 $\pm$ 0.2	0.8 $\pm$ 0.0	7.0 $\pm$ 0.1	2.7 $\pm$ 0.1	0.4 $\pm$ 0.1	0.4 $\pm$ 0.1	16.9 $\pm$ 0.1	22.9 $\pm$ 0.3

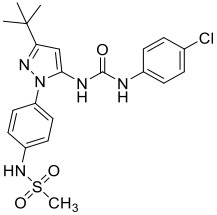
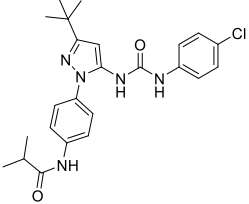
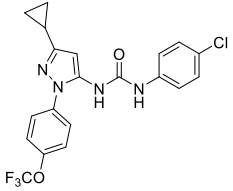
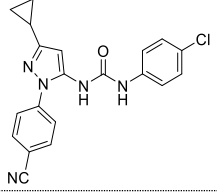
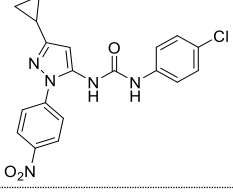
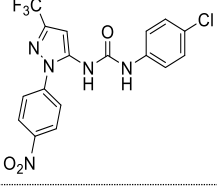
<sup>a</sup> Compounds synthesized by Jessica E. Dwyer and Caroline S. Widdowson, Sussex. <sup>b</sup>  $\Delta T_m$  average derived from two replicates at a compound concentration of 10  $\mu$ M. DSF measured by Andreas Krämer, SGC Frankfurt.

Most compounds harboring a 3,5-di CF<sub>3</sub> decoration (**70-77**), lost most of their binding activity for p38 compared with the parent compound, but, as indicated above some retained activity for AURKB. On the basis of the data for 3,5-difluoro-decorated compounds **78-86**, hydrophobic DFG-out pocket and tolyl-pocket interactions seem to be important for p38 activity. However, those compounds also had activity on AURKB, SLK and BRAF. Interestingly, allosteric fragments lost activity for EPHA2 and MAPK9, emphasizing the importance of an active-site directed moiety for potent inhibition of these kinases. Finally, in the third library, the 4-chlorophenyl decorations were kept unchanged and the tolyl-pocket directed moieties were modified (**Table 8**).

**Table 8.** Selectivity profiling by DSF; tolyl-pocket modifications.

No.	Structure <sup>a</sup>	$\Delta T_m$ [°C] $\pm$ SEM <sup>b</sup>							
		AURKB	BRAF	EPHA2	MAPK 9	p38 $\alpha$	p38 $\beta$	SLK	STK10
BIRB 796		4.0 $\pm$ 0.1	22.1 $\pm$ 0.1	8.0 $\pm$ 0.0	6.7 $\pm$ 0.1	19.8 $\pm$ 0.1	19.9 $\pm$ 0.0	3.6 $\pm$ 0.6	10.0 $\pm$ 0.2
88		3.6 $\pm$ 0.3	3.6 $\pm$ 0.3	0.4 $\pm$ 0.0	0.4 $\pm$ 0.1	1.3 $\pm$ 0.1	-0.2 $\pm$ 0.4	0.3 $\pm$ 0.2	0.0 $\pm$ 0.3
97		3.8 $\pm$ 0.4	3.8 $\pm$ 0.4	2.0 $\pm$ 0.2	2.7 $\pm$ 0.2	10.4 $\pm$ 0.9	9.4 $\pm$ 0.5	5.6 $\pm$ 0.8	2.0 $\pm$ 0.2
89		-3.8 $\pm$ 8.0	-3.8 $\pm$ 8.0	0.6 $\pm$ 0.0	0.0 $\pm$ 0.0	0.9 $\pm$ 0.2	0.3 $\pm$ 0.7	0.7 $\pm$ 0.8	-0.6 $\pm$ 0.2
90		4.1 $\pm$ 0.2	4.1 $\pm$ 0.2	0.9 $\pm$ 0.0	0.4 $\pm$ 0.0	0.9 $\pm$ 0.0	0.6 $\pm$ 0.0	0.2 $\pm$ 0.1	0.0 $\pm$ 0.1
91		4.5 $\pm$ 0.1	4.5 $\pm$ 0.1	0.8 $\pm$ 0.0	0.8 $\pm$ 0.0	3.6 $\pm$ 0.1	4.0 $\pm$ 0.9	1.6 $\pm$ 0.9	2.2 $\pm$ 0.1
92		3.7 $\pm$ 0.1	3.7 $\pm$ 0.1	1.2 $\pm$ 0.0	0.8 $\pm$ 0.1	5.6 $\pm$ 0.6	7.8 $\pm$ 0.3	5.2 $\pm$ 0.9	4.1 $\pm$ 0.1
99		4.1 $\pm$ 0.1	4.1 $\pm$ 0.1	3.0 $\pm$ 0.1	0.6 $\pm$ 0.0	2.4 $\pm$ 0.5	2.6 $\pm$ 0.4	4.1 $\pm$ 3.3	3.4 $\pm$ 0.1

Table 8. (continued)

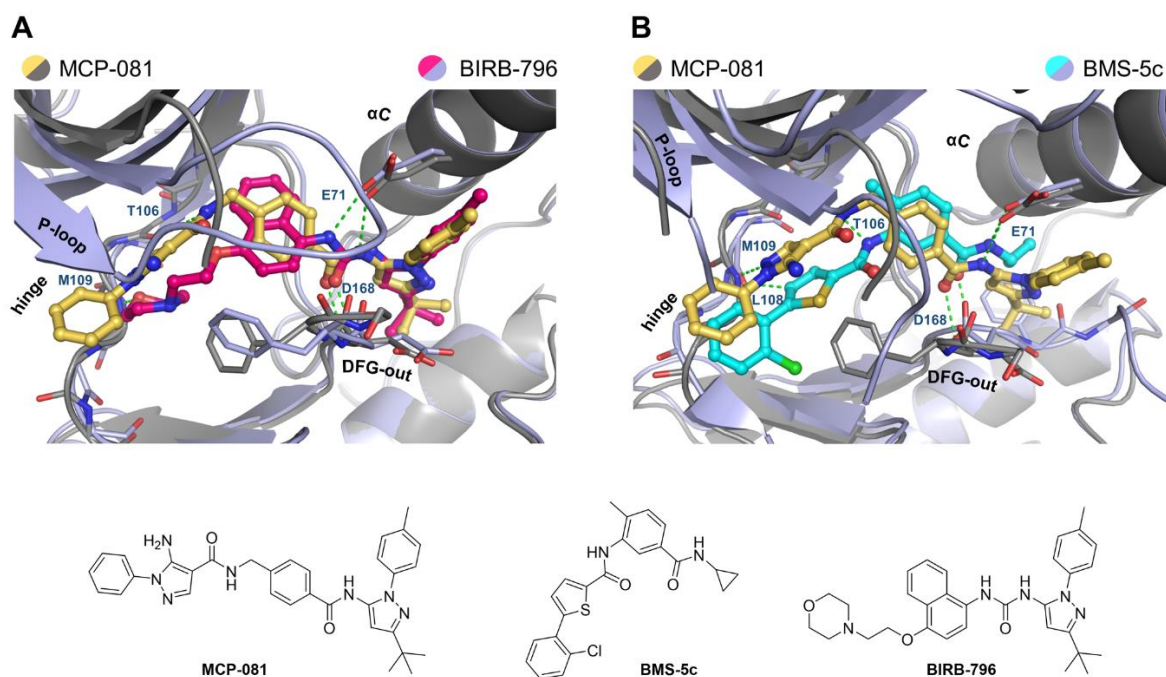
No.	Structure <sup>a</sup>	$\Delta T_m$ [°C] $\pm$ SEM <sup>b</sup>							
		AURKB	BRAF	EPHA2	MAPK 9	p38 $\alpha$	p38 $\beta$	SLK	STK10
103		3.7 $\pm$ 0.0	3.7 $\pm$ 0.0	2.8 $\pm$ 0.1	2.1 $\pm$ 0.1	6.7 $\pm$ 0.0	7.2 $\pm$ 0.6	7.3 $\pm$ 0.2	8.9 $\pm$ 0.2
101		3.9 $\pm$ 0.8	3.9 $\pm$ 0.8	2.8 $\pm$ 0.0	0.1 $\pm$ 0.0	1.5 $\pm$ 0.4	1.5 $\pm$ 0.4	6.8 $\pm$ 0.3	5.1 $\pm$ 0.8
93		2.2 $\pm$ 0.4	2.2 $\pm$ 0.4	0.2 $\pm$ 0.0	-0.2 $\pm$ 0.0	0.3 $\pm$ 0.1	0.3 $\pm$ 0.1	0.3 $\pm$ 0.0	0.0 $\pm$ 0.2
94		-2.3 $\pm$ 6.8	-2.3 $\pm$ 6.8	0.5 $\pm$ 0.1	0.0 $\pm$ 0.1	0.2 $\pm$ 0.1	-0.3 $\pm$ 0.3	0.7 $\pm$ 0.7	-0.7 $\pm$ 0.3
95		-2.5 $\pm$ 5.8	-2.5 $\pm$ 5.8	0.2 $\pm$ 0.0	-0.2 $\pm$ 0.0	0.1 $\pm$ 0.0	0.6 $\pm$ 0.5	0.1 $\pm$ 0.1	-0.9 $\pm$ 0.2
96		4.2 $\pm$ 0.0	4.2 $\pm$ 0.0	1.0 $\pm$ 0.0	0.6 $\pm$ 0.0	0.9 $\pm$ 0.0	0.6 $\pm$ 0.5	0.6 $\pm$ 0.4	0.5 $\pm$ 0.2
Ctrl.	Staurosporine	3.6 $\pm$ 0.3	3.6 $\pm$ 0.3	7.0 $\pm$ 0.1	2.7 $\pm$ 0.1	0.4 $\pm$ 0.1	0.4 $\pm$ 0.1	16.9 $\pm$ 0.1	22.9 $\pm$ 0.3

<sup>a</sup> Compounds synthesized as part of this PhD thesis. <sup>b</sup>  $\Delta T_m$  average derived from two replicates at a compound concentration of 10  $\mu$ M. DSF measured by Andreas Krämer, SGC Frankfurt.

This set of inhibitors showed that the tolyl-pocket decoration is important for inhibitor potency on p38 and also most off-targets. It seems that polar donor and acceptor groups present in **92**, **97** and **103** increase the potency for p38 MAPK. For targeting the DFG-out pocket of p38, the bulky *tert*-butyl decoration was preferred, as thermal stabilization was significantly smaller for compounds containing CF<sub>3</sub> and negligible for compounds with a cyclopropyl moiety. However, as observed in the first two fragment series, the most potent p38 fragments retained activity against BIRB-796 off-targets such as BRAF, SLK and STK10. Interestingly, some fragments showed selective binding to some off-targets, most notably to SLK and STK10

by compound **101**. Thus, the development of selective inhibitors based on these fragments might be possible.

In **Chapter 3**, a series of type-II p38 inhibitors with good p38 potencies was developed.<sup>402</sup> Some of those inhibitors showed selectivity for p38 $\alpha$  over the closely related isoform p38 $\beta$ , in particular when fusing the pyrazole-urea back-pocket decoration of BIRB-796 with the hinge-binding motif of the initial type-II hit VPC00628.<sup>340</sup> This compound, MCP-081, had an about 30-fold selectivity for p38 $\alpha$  over p38 $\beta$  ( $IC_{50}$  [p38 $\alpha$ /p38 $\beta$ ] = 0.055/ 1.60  $\mu$ M).<sup>402</sup> By screening this type-II inhibitor against the DSF kinase panel, a relatively clean selectivity profile was observed, with off-target activities for AURKB and BRAF only. In order to understand the remarkable  $\alpha$ -isoform selectivity of MCP-081 and its allosteric back pocket interactions, a crystal structure of MCP-081 in complex with p38 $\alpha$  was determined (PDB: 6Y6V). Superposition of this structure with the BIRB-796-p38 $\alpha$  (PDB: 1KV2) and the VPC-00628-p38 $\alpha$  complex (PDB: 5LAR, not shown) revealed similar back pocket interactions, while contacts to the hinge region varied (**Figure 30A**). This fact may, therefore, explain the reduced potency of MCP-081 against p38 MAPK that was previously observed. To gain further insights into the structural reasons for the remarkable  $\alpha$ -isoform selectivity of MCP-081, this structure was superimposed with the BMS-5c-p38 $\alpha$  complex (PDB: 4KIN, **Figure 30B**).<sup>322</sup> Good isoform selectivity for BMS-5c has been reported and rationalized based on a backbone flip between the methionine (Met109) and leucine residue (Leu108) in the hinge region<sup>322</sup> not observed in the MCP-081 structure. In **Chapter 3** it was speculated that a sequence variation in the back pocket between the p38 $\alpha$ /p38 $\beta$  isoforms could contribute to isoform selectivity.<sup>402</sup> In position 78 (p38 $\alpha$  numbering), the  $\alpha$ -isoform harbors a methionine, while p38 $\beta$  has a leucine. However, the similar binding mode described for BIRB-796, which shows no isoform selectivity, makes this difference as an explanation for the isoform selectivity of MCP-081 less plausible. Additional dissimilarities, e.g. differences in the water network, may also contribute to the observed selectivity.

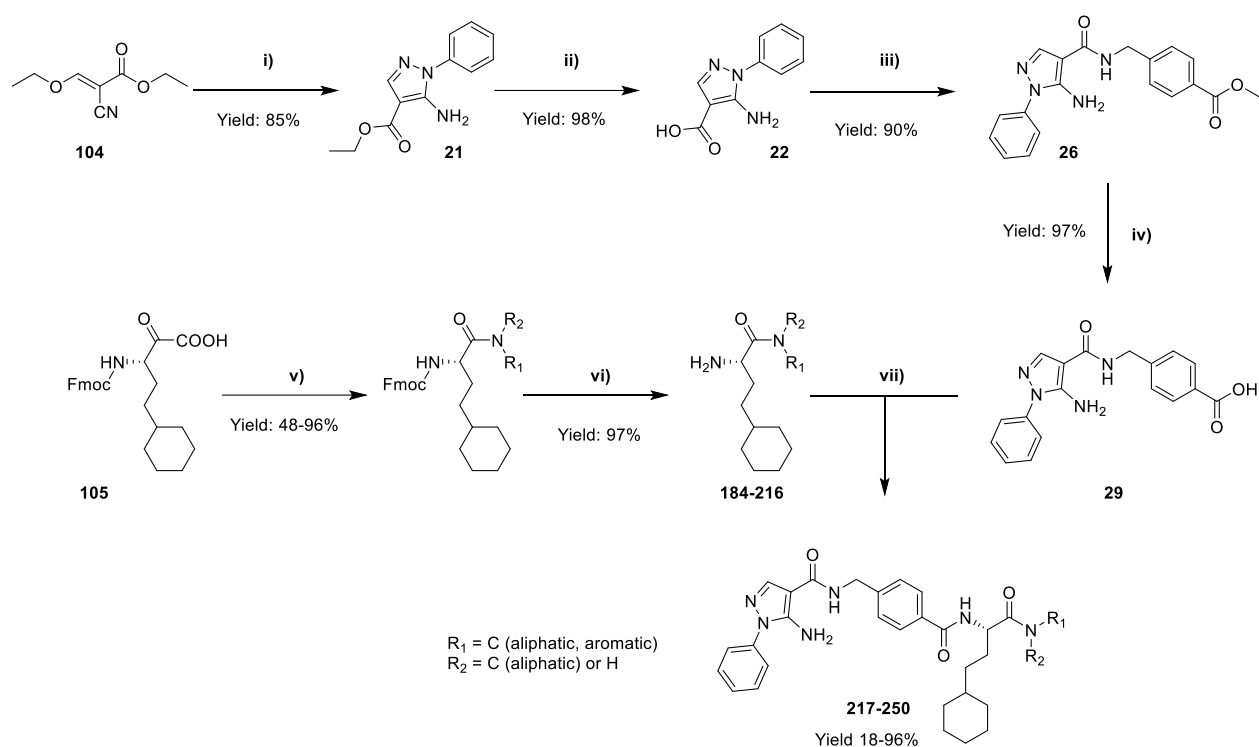


**Figure 30. Comparison of the binding modes of MCP-081 (PDB: 6Y6V), BMS-5c (PDB: 4KIN) and BIRB-796 (PDB: 1KV2) in complex with p38 $\alpha$ .** A) Superposition of the BIRB-796 fragment with the VPC-00628 hinge binding motif in MCP-081 reveals a different binding mode in the active-site region of p38 $\alpha$ . The P-loop in the MCP-081 complex is disordered in the crystal structure due to its high flexibility. B) Superposition of MCP-081 with the  $\alpha$ -isoform selective compound BMS-5c. Although both compounds shown exhibited an  $\alpha$ -isoform selectivity, a flip of the Leu108 backbone was induced by BMS-5c only, thereby questioning a key role of this backbone-flip induction in  $\alpha$ -isoform selectivity. Crystallization and structure determination of MCP-081 was done by Martin Schröder, Frankfurt.

Since structural variations of the BIRB-796 pyrazole-urea motif did not improve selectivity without loss of p38 activity, it was of interested whether the VPC-00628 DFG-out back-pocket binding moiety could be optimized by further expansion into the  $\alpha$ C-out pocket. Targeting this pocket had resulted in high target selectivity for the ERK1/2 inhibitor SCH772984.<sup>56</sup> In order to explore this pocket, the lead structure was expanded at the terminal primary amide with a diverse set of aliphatic and aromatic building blocks.

#### 4.4 Convergent synthetic approach for back-pocket optimization

In the following, a convergent synthetic approach was established for VPC-00628 derivatives to explore the allosteric back pocket. An overview of the complete synthetic route, optimized for the design of inhibitors is given in **Scheme 7**. A detailed synthetic description of the complete optimizing process follows below.

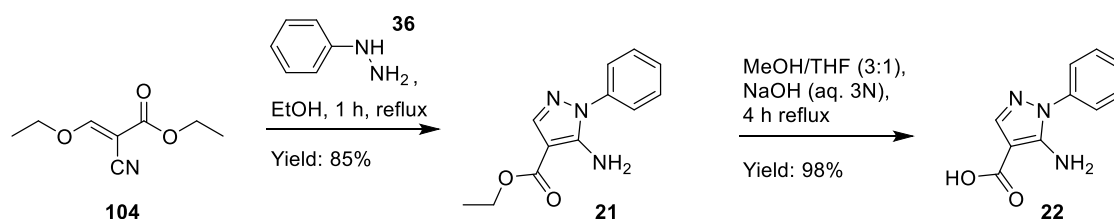


**Scheme 7.** Optimized convergent synthetic route for the back-pocket optimization of VPC-00628 derivatives. Reagents and conditions: i) Phenylhydrazine, EtOH, reflux. ii) MeOH/THF, NaOH aq., reflux. iii) Methyl 4-(aminomethyl)benzoate hydrochloride, HOBt, EDC-HCl, DIPEA, DMF, RT. iv) LiOH, THF/H<sub>2</sub>O, RT. v) Fmoc-homocyclohexyl-L-alanine, R<sub>1</sub>NH<sub>2</sub> or R<sub>2</sub>NH, HATU, DIPEA, DMF, RT. vi) Piperidine, DMF, RT. vii) HATU, DIPEA, DMF, RT. For R<sub>1</sub> and R<sub>2</sub> see **Table 11** and **Table 12**.

##### 4.4.1 Description of steps i and ii

In the first part of the synthetic route, the precursor 4-((5-amino-1-phenyl-1H-pyrazole-4-carboxamido)methyl)benzoic acid (**29**) was synthesized. To build the 5-aminopyrazole hinge-binding head group, the 1,3 biselectrophilic (*E*)-ethyl 2-cyano-3-ethoxyacrylate (**104**) was reacted with phenylhydrazine (**21**) to obtain ethyl 5-amino-1-phenyl-1H-pyrazole-4-carboxylate (**22**, **Scheme 8**). During this reaction, the hydrazine derivative most likely formed a hydrazone intermediate via nucleophilic attack on the carbonyl carbon atom. Subsequently, the 5-aminopyrazole was formed by the intramolecular addition of the hydrazine NH moiety to the nitrile functionality, by cyclization and tautomerization. The synthesis of **21** has already been described in various publications, whereby the reaction was mostly carried out under heating

(80 °C) for several hours in ethanol. In addition, some researchers also described the addition of trimethylamine as base<sup>436</sup>, the use of inorganic supports<sup>437</sup> or microwave assisted<sup>438</sup> reactions that yield about 60% of the desired product. In 2004, DYKMAN ET AL. published the synthesis of ethyl 5-amino-1-phenyl-1*H*-pyrazole-4-carboxylate (**21**) by heating (*E*)-ethyl 2-cyano-3-ethoxyacrylate (**104**) and phenylhydrazine (**36**) in ethanol as solvent solely, resulting in high yields even after a short reaction time of one hour.<sup>439</sup> Therefore, the synthesis of **21** was performed following this very promising procedure, and the desired product was obtained in a yield of 85%.

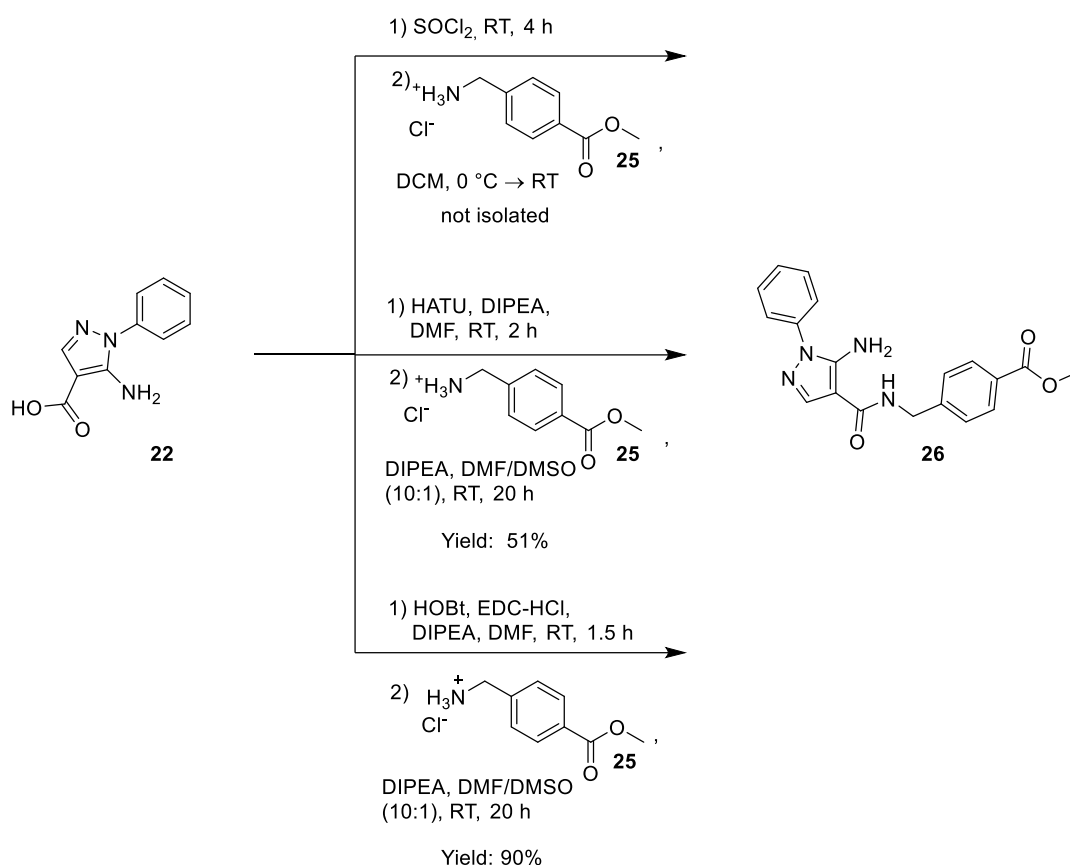


**Scheme 8. Step A and B, synthesis of the pyrazole building block P1.**

After the pyrazole synthesis, the ester functionality was hydrolyzed by heating **21** with an aqueous sodium hydroxide solution in a methanol-tetrahydrofuran mixture for four hours. The product 5-amino-1-phenyl-1*H*-pyrazole-4-carboxylic acid (**22**) precipitated after acidifying the reaction solution with hydrochloric acid and was obtained in an excellent yield, which is in accordance with the literature.<sup>439</sup>

#### 4.4.2 Description of steps iii and iv

After the synthesis of the hinge binding head group moiety, the benzyl linker moiety of VPC-00628 was introduced by an amide coupling reaction. Since the carboxylic acid group of the pyrazole heterocycle is deactivated and thus not electrophilic enough for direct reaction with methyl 4-(aminomethyl)benzoate hydrochloride (**25**), different conditions were applied to make the coupling reaction feasible and to improve the overall yields of the reaction (**Scheme 9**). In the first attempt the carboxylic acid was activated with an excess of thionyl chloride to form a more electrophilic acyl chloride. Various test reactions were carried out, in which the solvents were varied from methylene chloride to mixtures of methylene chloride and dimethyl sulfoxide and pyridine was added as a base. Usually, the pyrazole acyl chloride was prepared first, and the excess of thionyl chloride was removed under vacuum. The crude product obtained by this method was then resolved in methylene chloride. Subsequently, methyl 4-(aminomethyl)benzoate hydrochloride (**25**) was dissolved with pyridine in the solvent of choice, and the acid chloride was added dropwise under cooling with an ice bath. However, after stirring at room temperature overnight, none of the test reactions performed showed any product formation by TLC and ESI-MS, which may be due to solubility issues. The benzylic amine **25** has proved to be poorly soluble in the various solvents used, and the free amine on the pyrazole scaffold may have been protonated by hydrochloric acid that was released during the formation of the acid chloride in the first step. Several attempts were therefore made to protect the amine functionality on the pyrazole with a *tert*-butyloxycarbonyl (Boc) protective group, also with subsequent synthesis steps in mind. Product formation was only detectable in small amounts, though, by ESI-MS and raw <sup>1</sup>H-NMR, which highlights the poor nucleophilicity of the free amine, since these protecting reactions typically occur with fast conversion and high yields.<sup>440</sup> Presumably, the free electron pair is stabilized in an “amidine-like” resonance structure with the adjacent pyrazole nitrogen atom or deactivated by the electron withdrawing effect of the neighboring carboxylic acid group.



**Scheme 9.** Optimization of amide coupling reaction toward methyl 4-((5-amino-1-phenyl-1H-pyrazole-4-carboxamido)methyl)benzoate (**26**).

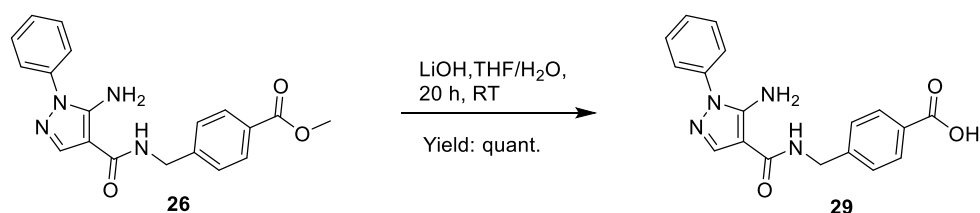
Since the synthesis via the corresponding acid chloride was not feasible, reactions using coupling reagents to form an amide bond were considered next. Therefore, 1-ethyl-3-(3-dimethylaminopropyl)carbodiimide hydrochloride (EDC-HCl) was selected as coupling agent with HOBt as additive. The reagent EDC-HCl is composed of a similar carbodiimide core scaffold as *N,N'*-dicyclohexylcarbodiimide (DCC),<sup>441</sup> which has been extensively used in classical amide-coupling reactions.<sup>442</sup> EDC-HCl proved to be more suitable than DCC, due to its water solubility, which is caused by its quaternary amine structure.<sup>443, 444</sup> During coupling reactions, ureas are typically formed as a by-product of the respective dicarbodiimide coupling reagent used, which are usually very insoluble and challenging to remove. The use of EDC-HCl is therefore beneficial as water-soluble ureas are formed as leaving group, simplifying the work-up procedures. In the course of the reaction, the carbodiimide typically activates the carboxyl functionality by forming an *O*-acyl urea intermediate, which can then easily react with an amine of interest. However, since these intermediates are highly electrophilic, reactive and thus unstable, *N*-acylureas are formed as side products or racemization via 5(4*H*)-oxazolone derivatives or enolates takes place under basic conditions.<sup>445, 446</sup> Furthermore, the use of an excess of the carboxylic acid derivative can lead to the formation of anhydrides, which can be converted into the desired amide, but lower the overall yield. To prevent the formation of these by-products and to improve the yield of the reaction, 1-hydroxybenzotriazole (HOBt) was used as an additive to trap the *O*-acyl urea intermediate and to form an *NO*-active ester.<sup>447</sup> In addition, the active ester formed *in situ* assists the nucleophilic attack of the corresponding amine via intermolecular hydrogen-bond interactions.

In the second attempt, 5-amino-1-phenyl-1*H*-pyrazole-4-carboxylic acid (**22**) was pre-activated with EDC-HCl under basic conditions with DIPEA, for 0.5-2 h at room temperature. Different polar aprotic solvents, such as *N,N*-dimethylformamide, dimethyl sulfoxide, methylene chloride, and the non-polar solvent 1,4-

dioxane were tested as pure solvents or mixtures. The highest yields were obtained using an *N,N*-dimethylformamide/dimethyl sulfoxide mixture (dry, 2:1). The amine methyl 4-(aminomethyl)benzoate hydrochloride (**25**) was deprotonated with DIPEA and added after pre-activation of the carboxylic acid, which worked best after 1.5 h. The maintenance of the pre-activation time is important, since the addition of the more nucleophilic primary amine to the carbodiimide EDC-HCl is faster than the required attack of the carboxylate anion. Otherwise a very stable guanidinium intermediate would be formed, which would consume the coupling agent and terminate the reaction. During the test reactions performed, it was further observed that the overall yields were lower when the amine was added later than 2 h after pre-activation, possibly due to the high reactivity and instability caused by hydrolysis of the active ester formed *in situ*. After optimizing the reaction conditions, methyl 4-((5-amino-1-phenyl-1*H*-pyrazole-4-carboxamido)methyl)benzoate (**26**) was obtained in excellent yields of 90%.

In a third experiment, the amide coupling reaction was performed with the uronium salt 1-[bis(dimethylamino)methylene]-1*H*-1,2,3-triazolo[4,5-*b*]pyridinium 3-oxide hexafluorophosphate (HATU). The coupling reagent HATU was already used in many amide forming reactions and has shown to advantageously accelerate the overall reaction speed.<sup>443, 448</sup> Typically, only small amounts of epimers were formed in these reactions, and products were obtained in high yields, even when sterically hindered carboxylic acids/amino acids were used.<sup>449</sup> The azabenzotriazole scaffold of HATU enables the formation of highly active *NO*-active ester *in situ*, and additives such as HOBT, which are thermally unstable and explosive, are no longer necessary. The promotional effect on the reaction rate can be attributed to the nitrogen atom in 7-position of the azabenzotriazole, which stabilizes the leaving group by its electron-withdrawing effect.<sup>445</sup> Furthermore, during the reaction, the nitrogen atom also stabilizes a seven-centered transition state, in which the neighboring-group effect facilitates the deprotonation and release of the final amide formed.

For the amide coupling via HATU, 5-amino-1-phenyl-1*H*-pyrazole-4-carboxylic acid (**22**) was first activated for two hours with HATU and DIPEA to form an active ester. Methyl 4-(aminomethyl)benzoate hydrochloride (**25**) was diluted in an *N,N*-dimethylformamide/dimethyl sulfoxide mixture with additional base and added to the pre-activated reaction solution. The concentration of the base and the mixing ratio of the solvents were varied in order to optimize the reaction conditions. The highest total yield of 52% was obtained with 1 eq. of carboxylic acid, 1.3 eq. of HATU, 1.2 eq. of amine as well as 4.4 eq. of DIPEA in an *N,N*-dimethylformamide/dimethyl sulfoxide mixture (2.6:1). After successful synthesis of methyl 4-((5-amino-1-phenyl-1*H*-pyrazole-4-carboxamido)methyl) benzoate (**26**), the ester functionality was cleaved in the next step of the convergent synthetic route developed. The reaction was performed under very mild condition using lithium hydroxide as base in a mixture of tetrahydrofuran in water (1:1). After three-day stirring at room temperature, the product was precipitated with hydrochloric acid to obtain 4-((5-amino-1-phenyl-1*H*-pyrazole-4-carboxamido)methyl)benzoic acid (**29**) in quantitative yield (**Scheme 10**).

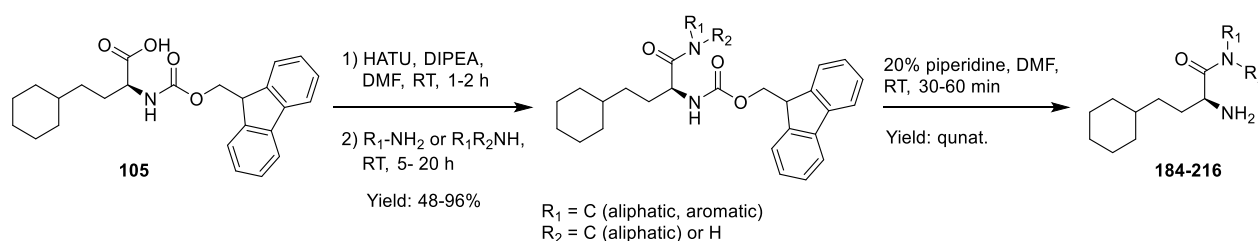


**Scheme 10.** Ester hydrolysis for the synthesis of 4-((5-amino-1-phenyl-1*H*-pyrazole-4-carboxamido)methyl)benzoic acid (**29**)



#### 4.4.3 Description of steps *van vi*

The second part of the convergent synthetic route developed introduced the unnatural amino acid building block of VPC-00628, which has been shown to target the DFG-out pocket of p38 MAPK via hydrophobic contacts (**Scheme 11**).<sup>340</sup> To explore the allosteric P-loop/ $\alpha$ C-out pocket region of p38 MAPK, different moieties were introduced by amide coupling reactions with the *N*-protected precursor Fmoc-homocyclohexyl-L-alanine (**105**). To find the optimal reaction conditions, the activation of the carboxylic acid group of **105** via the corresponding acid chloride was considered first. For this purpose, **105** was heated at 45 °C with an excess of thionyl chloride for three hours. The remaining thionyl chloride was then removed by distillation, and the crude product was resolved in methylene chloride. Subsequently, the mixture was added dropwise to a solution of methylamine in tetrahydrofuran and pyridine in methylene chloride under cooling and stirred overnight at room temperature. During the course of the reaction, however, no product formation was detected by TLC and ESI-MS. Therefore, in a second attempt, the amide coupling reaction was performed with the coupling agent HATU, which was previously used for the amide coupling reaction in **Section 4.4.2**.

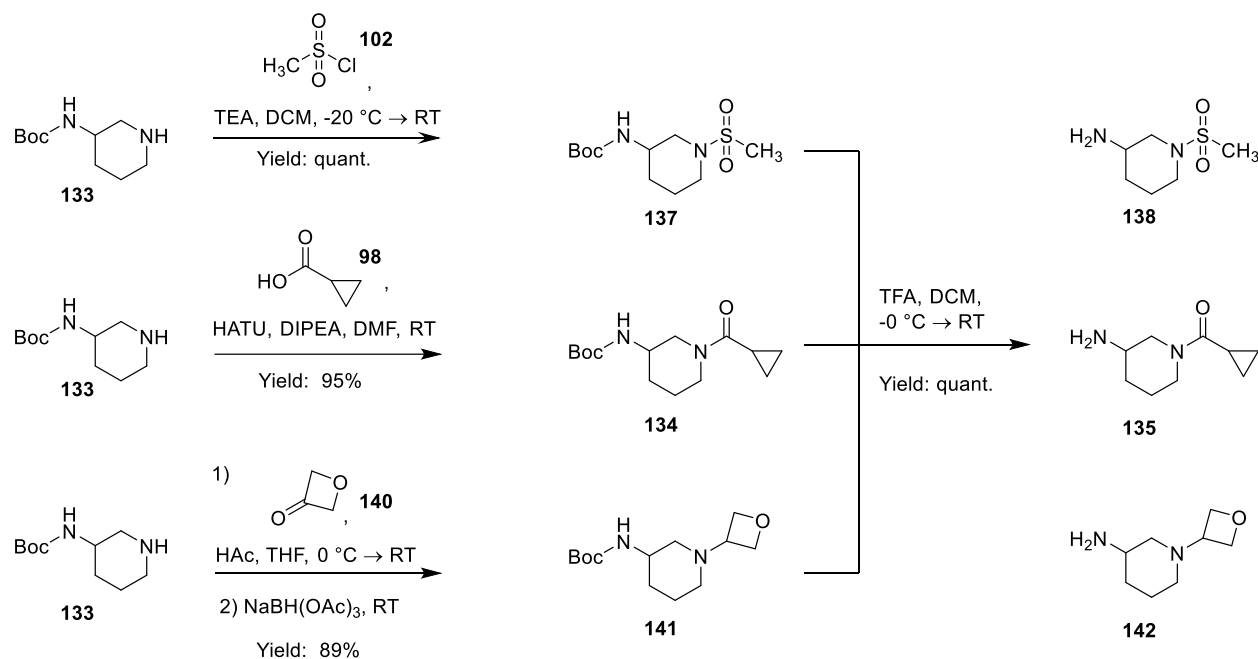


**Scheme 11.** Introduction of functional diversity for the exploration of the P-Loop/  $\alpha$ C-out pocket in p38 MAPK. For residues R<sub>1</sub>, R<sub>2</sub> see **Table 9**, **Table 10**.

To enable the reaction of a wide range of different amines in good to high yields, the optimal conditions for amide coupling were selected by using 1 eq. of carboxylic acid, 1.2 eq. of HATU, 1.2 eq. of amine and 1.2 eq. of DIPEA in *N,N*-dimethylformamide. To form an active ester, the carboxylic acid was usually stirred at room temperature for 1-2 hours, and the amine of interest was added afterwards. Using this method, different moieties including linear, branched, aliphatic, aromatic and hetero aromatic ones were introduced as summarized in **Table 9** and **Table 10**. The amines used were either purchased from commercial suppliers or were synthesized in advance in the case of the piperazine derivatives **132**, **177**, and **178**.

For the substituted piperidine derivatives **171**, **136**, and **143** a two-step synthesis route was developed to obtain the amine of interest. For the synthesis of 1-Boc-piperazine (**131**), piperazine (**130**) was dissolved in methylene chloride, and a solution of di-*tert*-butyl dicarbonate in methylene chloride was added dropwise under cooling. Since this reaction was performed with a one-fold excess of piperazine at low temperatures and within short reaction times, the formation of di-*tert*-butyl piperazine-1,4-dicarboxylate as a by-product is typically low. Thus, the desired compound **131** was obtained in a yield of 70%. To introduce 3-amino piperidine derivatives with distinct hydrogen-bond acceptor functionalities, three different synthetic routes were established (**Scheme 12**). For the synthesis of 1-(methylsulfonyl)piperidin-3-amine (**138**), a nucleophilic substitution reaction between methanesulfonyl chloride (**102**) and the respective amine *tert*-butyl piperidin-3-ylcarbamate (**133**) was considered. The reaction was performed under cooling in a basic solution of methylene chloride, in which the product *tert*-butyl (1-(methylsulfonyl)piperidin-3-yl)carbamate (**137**) was obtained in excellent yield. The Boc-protecting group was then removed under strongly acidic conditions by the use of trifluoroacetic acid to quantitatively yield **138**. Typically, the latter was done directly

before the coupling reaction with Fmoc-homocyclohexyl-L-alanine (**105**). For the synthesis of (3-aminopiperidin-1-yl)(cyclopropyl)methanone (**135**), cyclopropanecarboxylic acid was first activated with HATU and DIPEA in *N,N*-dimethylformamide. After that, the Boc-protected aminopiperidine derivative **133** was added to form an amide functionality in excellent yield. The protecting group of *tert*-butyl (1-(cyclopropanecarbonyl)piperidin-3-yl)carbamate (**134**) was then cleaved with trifluoroacetic acid to yield **135** quantitatively.



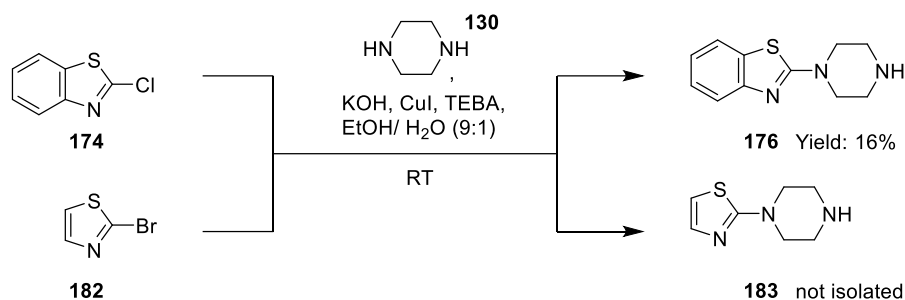
**Scheme 12.** Optimized synthetic route for the preparation of substituted 3-amino piperazine derivatives.

For the introduction of an oxetane functionality, a reductive amination reaction using *tert*-butyl piperidin-3-ylcarbamate (**133**) as amine and oxetan-3-one (**140**) as ketone functionality was performed. To obtain the desired tertiary amine, sodium triacetoxyborohydride was chosen as reagent for the reduction of the iminium ion formed *in situ*. Based on the three electron-withdrawing acetoxy groups, the boron-hydrogen bond gets stabilized, thus slowing down the hydride transfer to the imine or iminium intermediate. Therefore, sodium triacetoxyborohydride is a very mild reducing agent that typically does not reduce ketones, which are constantly present in the reaction equilibrium.<sup>450</sup> Compared with more reactive reagents such as sodium borohydride or sodium cyanoborohydride, pre-activation of amine and ketone to form an imine is not inevitably necessary, and yields are mostly higher.<sup>451</sup> Since reductive aminations work best in polar aprotic solvents, such as 1,2-dichloroethane, tetrahydrofuran, acetonitrile or *N,N*-dimethylformamide, tetrahydrofuran was chosen as a solvent.<sup>451, 452</sup>

In the first attempt, *tert*-butyl piperidin-3-ylcarbamate (**133**, 1.2 eq.) was dissolved in tetrahydrofuran, and oxetan-3-one (**140**, 1.0 eq.) was added while cooling at 0 °C. The mixture was then stirred at room temperature for 1.5 h to form an iminium ion. Sodium triacetoxyborohydride (2.0 eq.) was then added, and the mixture was stirred overnight to form the desired oxetane decorated tertiary amine. After quenching the reaction with a saturated sodium bicarbonate solution, the crude product was extracted with ethyl acetate and purified by column chromatography on silica to obtain *tert*-butyl (1-(oxetan-3-yl)piperidin-3-yl)carbamate (**141**) in a yield of 47%. To optimize the reaction conditions, the reaction was also performed with a 10-fold excess of the very reactive 4-membered cyclic ring ketone. However, by applying the reaction conditions described before, **141** was only obtained in a relatively low yield of 33%. Therefore, the addition

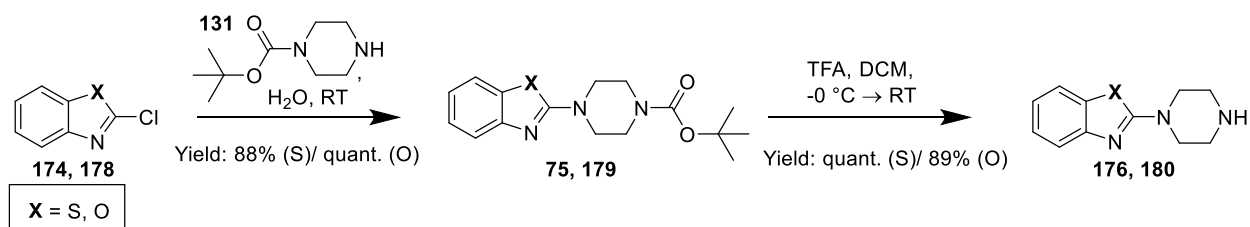
of acetic acid as catalyst was considered next, as it has proven its usefulness in previous studies by accelerating the reductive amination process of ketones.<sup>451</sup> The fact can be explained by the formation of a very electrophilic and, thus, more reactive oxonium ion intermediate, which is formed by the protonation of the ketone. In addition, acetic acid supports the dehydration process of the hemiaminal to the iminium intermediate, which is formed by the nucleophilic attack of the primary or secondary amine on the ketone of interest. In contrast, the use of strong acids such as hydrochloric acid or amines as hydrochloride salt has shown to prevent the actual reaction. The latter is due to the masking of the nucleophilicity of the amine, which is permanently protonated by the strong acid.<sup>451</sup> In the third attempt, 0.8 eq. of acetic acid were added to a stirring solution of *tert*-butyl piperidin-3-ylcarbamate (**133**, 1 eq.) in tetrahydrofuran. The reaction and the work-up were carried out as described before, and moderate amounts of oxetane-3-one (**140**, 4 eq.) and sodium triacetoxyborohydride (1.6 eq.) were used to obtain *tert*-butyl (1-(oxetan-3-yl)piperidin-3-yl)carbamate (**141**) in 89% yield. From this it can be concluded that the addition of acetic acid supported the reductive amination reaction with oxetan-3-one (**140**). Finally, the amine functionality was demasked by the use of trifluoroacetic acid in methylene chloride to quantitatively yield 1-(oxetan-3-yl)piperidin-3-amine (**149**).

The ERK1/2 inhibitor SCH772984, described previously (**Figure 27D**), achieved selective binding by targeting the P-loop/ $\alpha$ C-out pocket with a piperazine-phenyl-pyrimidine moiety. Therefore, different piperazine-aryl decorations were also considered for the extension of VPC-00628 toward this pocket area. For the synthesis of 2-(piperazin-1-yl)benzo[*d*]thiazole (**176**), an Ullmann coupling reaction was first selected using 10 mol% copper(I) iodide as catalyst, 10 mol% benzyltriethylammonium chloride (TEBA) as phase transfer *co*-catalyst and potassium hydroxide (1 eq.) in an ethanol/water (9:1) solution, and 1.3 eq. of each piperazine (**130**) and 1 eq. of aryl halide were used. The Ullmann coupling reaction with TEBA as phase transfer catalyst (PTC) proved to be very versatile for *N*-arylations of amines with heteroaryl halides, as demonstrated by SANJEEV ET AL. in 2011.<sup>453</sup> Compared with other *N*-arylation reactions, such as the Buchwald-Hartwig cross-coupling reaction with palladium as catalyst or the direct nucleophilic aromatic substitution, this ligand-free PTC-assisted coupling reaction takes place under very mild conditions (temperatures <40 °C).<sup>454</sup> Thus, heat-sensitive amines can also be used, water does not necessarily have to be avoided, and the reactants are usually inexpensive. Typically, the reaction is conducted in a heterogeneous two-phase system, e.g. containing chloroform/water or sometimes in a homogenous ethanol/water system, and high yields are obtainable even within short reaction times. To avoid the diarylation of piperazine (**130**), a homogenous ethanol/water system was chosen for the synthesis of 2-(piperazin-1-yl)benzo[*d*]thiazole (**176**), in which piperazine is highly soluble. Since the monoaryl product is of poor solubility in this polar solvent, the formation of the diaryl product is usually low. For forming an active copper-amine complex (oxidative addition), piperazine (**130**) and copper(I) iodide were suspended in water, stirred for 30 minutes at room temperature, and then potassium hydroxide was added. For the transmetalation and reductive elimination step to occur, TEBA and 2-chlorobenzothiazole (**174**) in ethanol were added, TEBA first and chlorobenzothiazole 30 min later. The reaction was stirred overnight at room temperature, and the product was obtained in 16% yield after purification by flash-chromatography on silica (**Scheme 13**). The same approach was applied for the synthesis of 2-(piperazin-1-yl)thiazole (**183**) from 2-bromothiazole (**182**). However, product formation was very low, and, therefore, no product could be isolated.



**Scheme 13.** PTC-assisted Ullmann C-N arylation reaction.

Since the overall yields were not satisfactory, various synthetic protocols from the literature were considered to make the reaction feasible also for other *N*-Aryl coupling reactions. Besides the *N*-arylation reaction by a Buchwald-Hartwig<sup>455</sup> or Goldberg<sup>456</sup> cross coupling, different nucleophilic substitution reactions applying a diverse set of different bases, such as K<sub>2</sub>CO<sub>3</sub>, K<sub>3</sub>PO<sub>4</sub>, Et<sub>3</sub>N, KOH, and LiO<sup>t</sup>Bu, with or without addition of metal catalysts, such as Fe, Mn, Ni, or Co, are described in the literature, delivering heteroarylamines in low to moderate or high yields.<sup>457</sup> Interestingly, a very mild environmentally friendly green chemistry protocol for the synthesis of *tert*-butyl 4-(benzothiazol-2-yl)piperazine-1-carboxylate (**175**) and for 2-(4-*tert*-butoxycarbonylpiperazin-1-yl)benzoxazole (**179**) was described by KUMAR ET AL. in 2016.<sup>457</sup> Although nucleophilic aromatic substitution reactions usually need to be heated for several hours or be microwave-assisted, the method described can be performed at room temperature in water without the need for additional reagents. Therefore, a 2:1 mixture of 2-chlorobenothiazole (**174**) and 1-Boc-piperazine (**131**), which was synthesized before from piperazine (**130**), was dispersed in water. The reaction was followed by TLC, and product formation was already observable after four hours of stirring at room temperature. After purification, *tert*-butyl 4-(benzothiazol-2-yl)piperazine-1-carboxylate (**175**) was obtained in a very good yield of 88%. The same protocol was also applied to the formation of 2-(4-*tert*-butoxycarbonylpiperazin-1-yl)benzoxazole (**179**) from 2-chlorobenzo[*d*]oxazole (**178**) and *tert*-butyl piperazine-1-carboxylate (**131**), which was obtained quantitatively (**Scheme 14**). However, by applying these conditions to synthesize *tert*-butyl 4-(thiazol-2-yl)piperazine-1-carboxylate from 2-bromothiazole (**182**) and 1-Boc-piperazine (**131**), no product was formed. The same phenomenon was observed for the microwave-assisted heating of 2-bromothiazole (**182**) and 1-Boc-piperazine (**131**) with triethylamine in tetrahydrofuran, which might be due to the poor leaving group, bromine, in aromatic nucleophilic substitution reactions.

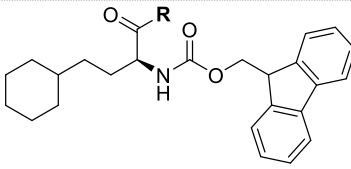
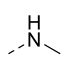
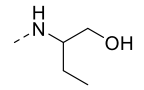
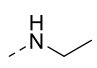
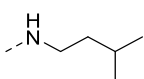
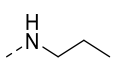
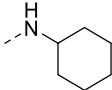
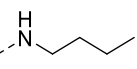
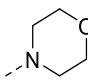
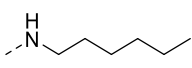
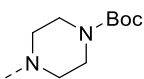
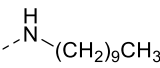
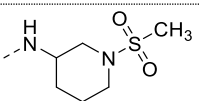
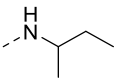
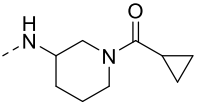
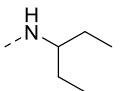
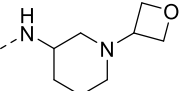


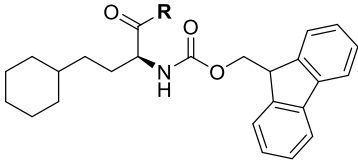
**Scheme 14.** Mild environmentally friendly C-N arylation reactions.

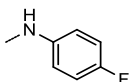
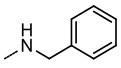
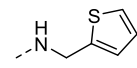
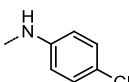
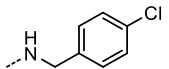
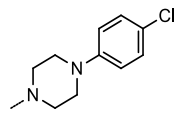
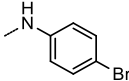
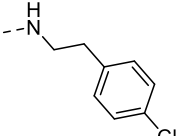
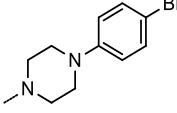
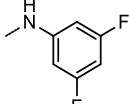
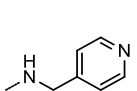
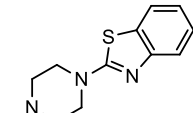
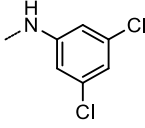
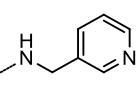
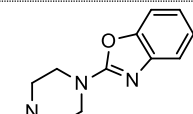
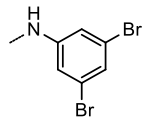
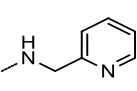
To make the amide coupling reaction to Fmoc-homocyclohexyl-L-alanine (**105**) feasible, the Boc-protecting group was afterwards cleaved under acidic conditions with trifluoroacetic acid to obtain the free amine 2-(piperazin-1-yl)benzo[*d*]oxazole (**180**) in 89% and 2-(piperazin-1-yl)benzo[*d*]thiazole (**176**) in quantitative yield.

In summary, using an optimized HATU coupling reaction, 33 different back-pocket decorations were introduced successfully in the precursor molecule Fmoc-homocyclohexyl-L-alanine (**105**), and compounds were obtained in fair to excellent yields of 48-91% (**Table 9**, **Table 10**). The Fmoc-protecting group of these compounds was then removed under basic conditions with 20% piperidine in *N,N*-dimethylformamide (**Scheme 11**). The respective amine was typically freshly prepared in quantitative yield and used directly for the synthesis of the final VPC-00628 derivatives.

**Table 9.** Aliphatic back-pocket decorations introduced and yields obtained in the coupling reaction with Fmoc-homocyclohexyl-L-alanine (**105**)

					
No.	R	Yield [%]	No.	R	Yield [%]
107		81	123		59
109		52	125		85
111		56	127		86
113		64	129		80
115		66	132		87
117		48	139		95
119		64	136		81
121		78	143		96

**Table 10.** Aromatic back-pocket decorations introduced and yields obtained in the coupling reaction with Fmoc-homocyclohexyl-L-alanine (**105**)


No.	R	Yield [%]	No.	R	Yield [%]	No.	R	Yield [%]
145		89	157		76	167		76
147		86	159		67	171		91
149		88	169		62	173		79
151		81	161		82	177		62
153		56	163		63	187		79
155		64	165		81			

#### 4.4.4 Description of final step vii

In the last step, 4-((5-amino-1-phenyl-1*H*-pyrazole-4-carboxamido)methyl)benzoic acid (**29**), synthesized in the first part of this convergent synthesis, was coupled to the amines (**184-216**) described in the previous section. Since the amide forming reaction with HATU proved to be very versatile for coupling a wide range of differently substituted amines, the reaction was also chosen for the preparation of the extended VPC-00628 derivatives (**217-250**). The final products were obtained in poor to excellent yields between 18% and 96%. For the synthesis of the final compound (*S*)-5-amino-*N*-(4-((4-cyclohexyl-1-oxo-1-(piperazin-1-yl)butan-2-yl)carbamoyl)benzyl)-1-phenyl-1*H*-pyrazole-4-carboxamide (**230**), the Boc-protected compound **229**, previously synthesized by the HATU coupling reaction, was treated with trifluoroacetic acid to yield 51% of **230**. The synthesized compounds were characterized by <sup>1</sup>H-NMR, <sup>13</sup>C-NMR, ESI-MS/ MALDI and HRMS. In some cases, 2D-NMR experiments, such as COSY, HSQC and HMBC, were performed or IR measurements were used in addition to determine the overall structure of the compounds. Unless otherwise stated, the purity of the compounds for biological testing was higher than 95% as determined by HPLC-MS.

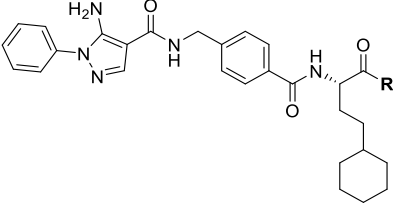
## 4.5 Investigation of back-pocket modified VPC-00628 derivatives

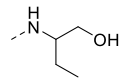
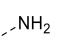
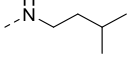
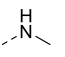
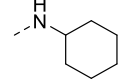
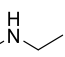
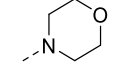
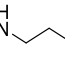
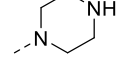
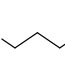
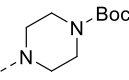
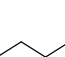
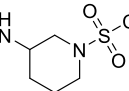
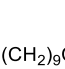
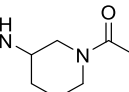
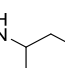
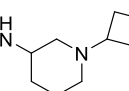
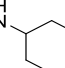
All compounds synthesized in **Section 4.4** targeting the P-loop/ $\alpha$ C pocket region of p38 MAPK were initially screened against p38 $\alpha$  by DSF according to the protocol described by FEDOROV ET AL. in 2012 at a compound concentration of 10  $\mu$ M each.<sup>422</sup> During these measurements, some of the more hydrophobic compounds, especially those having aniline back-pocket decorations, resulted in ambiguous melting curves that might indicate unspecific interference of the compound with the fluorescent dye used. Therefore, a background correction of all values was necessary by subtracting the fluorescence signal of buffer and dye without protein. The background correction led to a sharpening of the transition state for the previously ambiguous melting curves, while only minor differences in the melting curve were observed for compounds that already had a sharp sigmoidal fluorescence signal without background correction. Following the DSF assay, the *in cellulo* potency of the new compounds was measured in HEK293T cells by NanoBRET™ assay (described in **Section 4.1.2**). The well characterized lead structures VPC-00628 and BIRB-796, were added as controls. The DSF results are shown in **Table 11** and **Table 12**. Compounds were routinely co-crystallized with p38 $\alpha$  to elucidate the binding mode of the modified ligands and to guide the next round of compound optimization.

### 4.5.1 Aliphatic moieties

At first, linear and branched aliphatic residues were introduced, resulting in comparable or slightly better protein stabilization, in particular for short hydrophobic aliphatic chains compared with the parent compound VPC-00628 (**Table 11**). The increase in potency was also seen in the cellular assays. Overall, **218** (SR43) showed the highest potency, with an IC<sub>50</sub> value of 14.0  $\pm$  0.1 nM in cells and a thermal stabilization,  $\Delta T_m$ , of 16.4  $\pm$  0.2 °C in DSF assays, and was thus more potent than the lead structure VPC-00628 ( $\Delta T_m = 12.9 \pm 1.0^\circ\text{C}$ , IC<sub>50</sub> = 38.0  $\pm$  4.9 nM). Interestingly, extending the ethyl moiety of **218** by additional methylene groups resulted in a gradual loss of about 2.3 °C in  $\Delta T_m$  per additional methylene group, up to a total chain length of six carbon atoms. The lowest affinity was found for **222**, with a decyl residue, which bound to p38 $\alpha$  with only micromolar affinity ( $\Delta T_m = 4.6 \pm 0.6^\circ\text{C}$ , IC<sub>50</sub> = 2.1  $\pm$  0.2  $\mu$ M). Therefore, it can be assumed that the increased lipophilicity and flexibility of longer-chain ligands adversely affects the interaction within the more polar allosteric pocket in p38 $\alpha$ .

Next, branched aliphatic groups were introduced by the synthesis of a *sec*-butyl (**223**), a 3-pentyl (**224**) and an *iso*-pentyl derivative (**226**). While **223** ( $\Delta T_m = 14.0 \pm 0.4^\circ\text{C}$ ) showed a comparable temperature shift as the very similar unbranched ethyl derivative **219** ( $\Delta T_m = 13.7 \pm 0.5^\circ\text{C}$ ), additionally introduced carbon atoms had a destabilizing effect. Interestingly, when one of the methyl groups in the 3-pentyl moiety (**224**) was replaced by a hydroxyl group (**225**), an increase of 2.3 °C in  $\Delta T_m$  was detectable. The hydroxyl group presumably stabilized the ligand inside the binding pocket by interaction with the polar environment of this binding pocket. Larger branched decorations had an opposite effect on the binding affinity, which could be explained by their higher lipophilicity and their higher space requirement, which is not optimal for hydrophobic interactions within the binding pocket. Overall, the IC<sub>50</sub> values determined by NanoBRET showed nanomolar potencies, which was in good agreement with the  $\Delta T_m$  values.

**Table 11.** Activity of p38 back-pocket optimized aliphatic compounds **217-233** measured by DSF and cellular enzyme activity  $IC_{50}$  values determined by NanoBRET™ assay.


No.	R	$\Delta T_m^a$ [°C] ± SD p38 $\alpha$	$IC_{50}^b$ [nM] ± SEM p38 $\alpha$	No.	R	$\Delta T_m^a$ [°C] ± SD p38 $\alpha$	$IC_{50}^b$ [nM] ± SEM p38 $\alpha$
BIRB-796		20.1 ± 0.7	7.7 ± 0.4 <sup>c</sup>	225		12.7 ± 0.1	38.2 ± 4.1
VPC-00628		12.9 ± 1.0	38.0 ± 4.9	226		8.6 ± 0.5	93.7 ± 12.6
217		15.0 ± 0.2	21.9 ± 2.0	227		9.8 ± 0.2	47.0 ± 17.8
218 (SR43)		16.4 ± 0.2	14.0 ± 0.1 <sup>d</sup>	228		13.2 ± 0.3	44.8 ± 11.6
219		13.7 ± 0.5	17.7 ± 3.3	230		12.6 ± 0.3	81.3 ± 4.0
220		11.3 ± 0.5	40.1 ± 9.2	229		5.6 ± 0.3	n.d.
221		7.4 ± 0.7	9520 ± 321.0	232 (SR159)		14.1 ± 0.4	33.7 ± 2.4 <sup>e</sup>
222		4.6 ± 0.6	2070 ± 161.0	231		14.7 ± 0.5	92.7 ± 35.7 <sup>f</sup>
223		14.0 ± 0.4	20.0 ± 4.1	233		14.4 ± 0.2	56.7 ± 2.4 <sup>f</sup>
224		10.4 ± 0.4	37.6 ± 7.5				

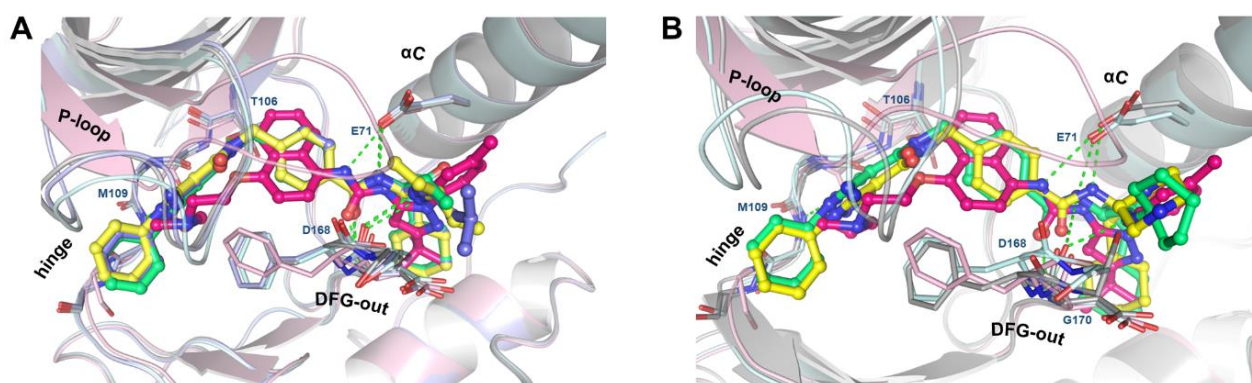
<sup>a</sup>  $\Delta T_m$  average of four measurements, compound concentration 10  $\mu$ M. <sup>b</sup>  $IC_{50}$  values were derived from duplicates ( $n = 2$ ). <sup>c</sup>  $n = 10$ ; <sup>d</sup>  $n = 6$ ; <sup>e</sup>  $n = 4$ ; <sup>f</sup>  $n = 3$ ; measurements n.d. not determined. NanoBRET™ assay performed by Benedict-Tilman Berger, DSF-assay assisted by Martin Schröder, SGC Frankfurt.

To study the influence of cyclic compounds on protein stabilization, six-membered aliphatic rings with different substitution patterns were synthesized. While the cyclohexyl-decorated compound (**227**) showed a thermal stabilization of  $\Delta T_m = 9.8 \pm 0.2$  °C, a comparatively higher affinity for p38 $\alpha$  was determined for the morpholine (**228**,  $\Delta T_m = 13.2 \pm 0.3$  °C) and the piperazine derivative (**230**,  $\Delta T_m = 12.6 \pm 0.3$  °C). This observation may be due to the altered electronic nature of the carbon versus oxygen and nitrogen atom or the changed lipophilicity or the conformation adopted by the cyclic systems. By masking the hydrogen-



donor group of piperazine with a Boc-protecting group, protein stabilization was decreased by around 7 °C, as exemplified by **229** ( $\Delta T_m = 5.6 \pm 0.3^\circ\text{C}$ ). From this it can be concluded that polar structural motifs, especially those having hydrogen-bond acceptor groups, preferentially stabilize the allosteric back pocket of p38 $\alpha$ .

The most interesting compounds of this series were co-crystallized with p38 $\alpha$ , and their binding mode was compared with BIRB-796 (**Figure 31**). The back-pocket modified VPC-00628 derivatives induced a folded conformation of the P-loop not observed in the p38 BIRB-796 complex. All compounds showed a type-II inhibitor binding mode, extending into the DFG-out pocket via their cyclohexyl decoration. As expected, all crystallized compounds formed hinge interactions with the backbone of Met109 and showed a conserved mode of binding. However, for residues targeting the tolyl pocket, the binding mode slightly differed. While the tolyl group of BIRB-796 bound near the  $\alpha\text{C}$  helix, the introduced linear and branched residues pointed toward the solvent-exposed region (**Figure 31A**). The latter observation may explain the difference in potency toward BIRB-796. For cyclic systems introduced at this position, interactions closer to the  $\alpha\text{C}$  helix were observed (**Figure 31B**).



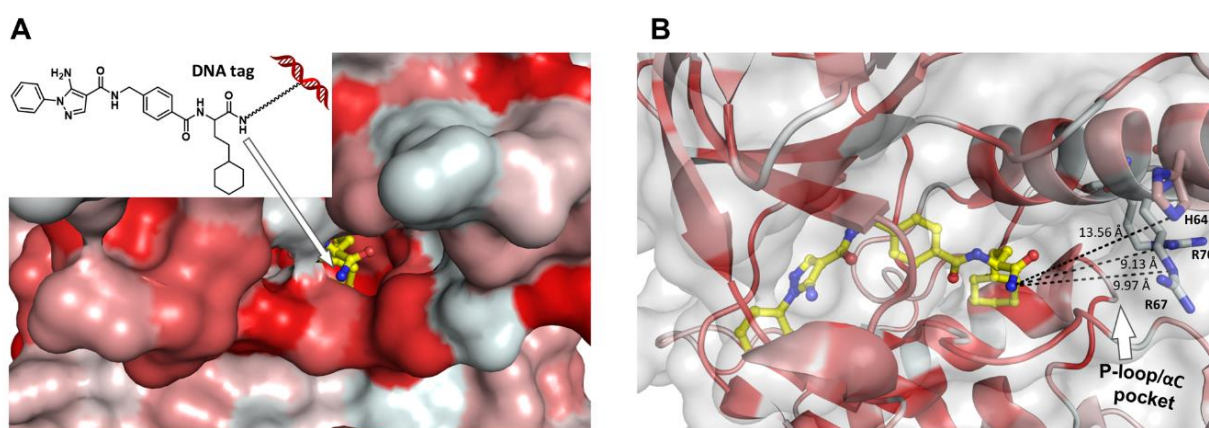
**Figure 31. Binding mode of back-pocket modified lead structures with aliphatic linear, branched and cyclic structures in complex with p38.** A) Overlay of the binding modes of linear and branched compounds **218** (SR43, lime, PDB: 6Y4T), **224** (yellow, PDB: 6Y4U) and **226** (violet, PDB: 6Y4V) with BIRB-796 (pink, PDB: 1KV2). B) Overlay of cyclic compounds **227** (lime, PDB: 6Y4W), **230** (yellow, PDB: N/A) and BIRB-796 (PDB: 1KV2). Hydrogen-bond interactions are highlighted in green. The extended P-loop conformation of p38 in the BIRB-796 complex is highlighted in light pink. Crystallization and structure determination was done by Apirat Chaikuad and Andreas Joerger.

A very promising strategy for the development of highly selective p38 MAPK inhibitors is the targeting of the switch pocket residues Arg67, Arg149 and Arg70, described by DECIPERA ET AL. and in **Section 2.4**.<sup>333, 334</sup> These less conserved structural elements are part of the  $\alpha\text{C}$  helix and the HRD segment and might be more accessible in the folded P-loop conformation of VPC-00628. So far, only a limited number of allosteric inhibitors, e.g. based on BIRB-796 fragments decorated with various substituents such as amides, sulfonamides and carboxylic acids, were used to study this pocket region.<sup>329</sup> The most potent and selective compounds of these studies interacted with these arginine side chains via a *meta*-substituted phenyl residue. In the crystal structure of **227** in complex with p38 $\alpha$  (**Figure 31B**), the cyclohexyl back-pocket decoration adopted a boat-shaped conformation in which the C-3 atom directed toward the switch-pocket residues. Therefore, 3-aminopiperidine derivatives were synthesized next and decorated either with cyclopropylamide, sulfonamide or oxetane moieties to engineer favorable interactions with these arginines. Analysis with DSF showed that all 3-aminopiperidine-substituted compounds actually increased the protein stabilization compared with **227** ( $\Delta T_m = 9.8 \pm 0.2^\circ\text{C}$ ) and the lead structure ( $\Delta T_m = 12.9 \pm 1.0^\circ\text{C}$ ). A  $\Delta T_m$  between 14.1 °C and 14.7 °C was determined for compounds **232** (SR159), **231** and **233**. Although slightly

less potent than VPC-00628, the cellular  $IC_{50}$  values of these compounds were determined as two-digit nanomolar (**232** [SR159]:  $IC_{50} = 33.7 \pm 2.4$  nM, **231**:  $IC_{50} = 92.7 \pm 35.7$  nM, **233**:  $IC_{50} = 56.7 \pm 2.4$  nM). The latter could be due to differences in the solubility and membrane permeability of these compounds. To confirm the switch-pocket directed binding mode, the crystal structure of **232** (SR159) in complex with p38 $\alpha$  was determined. As expected, **232** (SR159) bound in a type-II binding mode with the pyrazole head group directed toward the hinge region. The sulfonamide decoration pointed toward a solvent-exposed region, though, and no favorable interaction with the switch-pocket arginine residues could be detected. For further interest in the crystal structure of **232** (SR159) in complex with p38 $\alpha$ , please see **Section 5.2 (Figure 40B)** in which this compound was used for studies on a possible DDR1/2 kinase inhibitor.

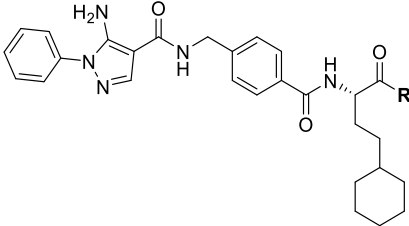
#### 4.5.2 Aromatic moieties

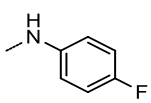
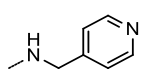
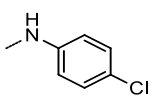
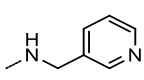
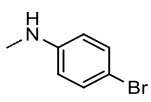
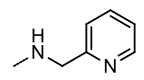
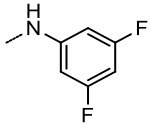
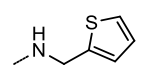
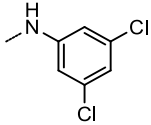
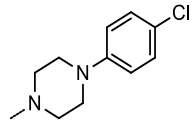
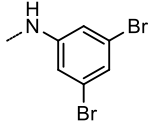
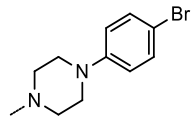
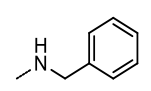
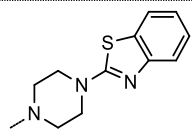
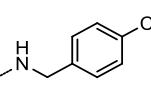
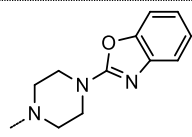
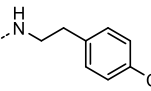
The P-loop/ $\alpha$ C pocket was initially suggested to serve as a channel for linking VPC-00628 to the DNA-tag in the DNA-encoded library approach used by PETERSEN ET AL. in 2016.<sup>340</sup> While the DFG-out deep pocket is mainly hydrophobic in nature, different polar amino acid side chains might be targetable in the allosteric region of p38 MAPK (**Figure 32**).



**Figure 32. Targeting the P-loop/ $\alpha$ C pocket in p38 MAPK.** A) Polar surface representation of VPC-00628 in complex with p38 $\alpha$  (PDB: 5LAR). The P-loop/ $\alpha$ C pocket served as a channel for VPC-00628 linked to DNA tag from initial DNA-encoded library.<sup>340</sup> Hydrophobic area (red), hydrophilic area (white). B) Amino acid residues that could be targeted in the P-loop/ $\alpha$ C pocket. Selected distances are highlighted (black dashes).

The P-loop/ $\alpha$ C pocket harbors an aromatic histidine residue, His64, at a distance of about 14 Å to the terminal amide of the lead structure, and the guanidinium groups of Arg70 and Arg67 are within a distance of 9 Å and 11 Å, respectively. Therefore, the introduction of an aromatic group at the terminal position of the lead structure might form favorable  $\pi$ - $\pi$  stacking and cation- $\pi$  stacking interactions with these residues. In addition, aromatic moieties with different substitution patterns typically contribute to the overall rigidity and lipophilicity of an inhibitor and might support binding in an entropically favored way. On the basis of these considerations, various mono- and di-substituted halogenated phenyl residues were introduced to extend the lead structure toward the allosteric back pocket. Subsequently, all compounds were examined again using DSF assays, and cellular potencies were determined by NanoBRET<sup>TM</sup> (**Table 12**).

**Table 12.** Activity of p38 back-pocket optimized aromatic compounds **234-250** measured by DSF ( $\Delta T_m$ ) and cellular NanoBRET™ assays.


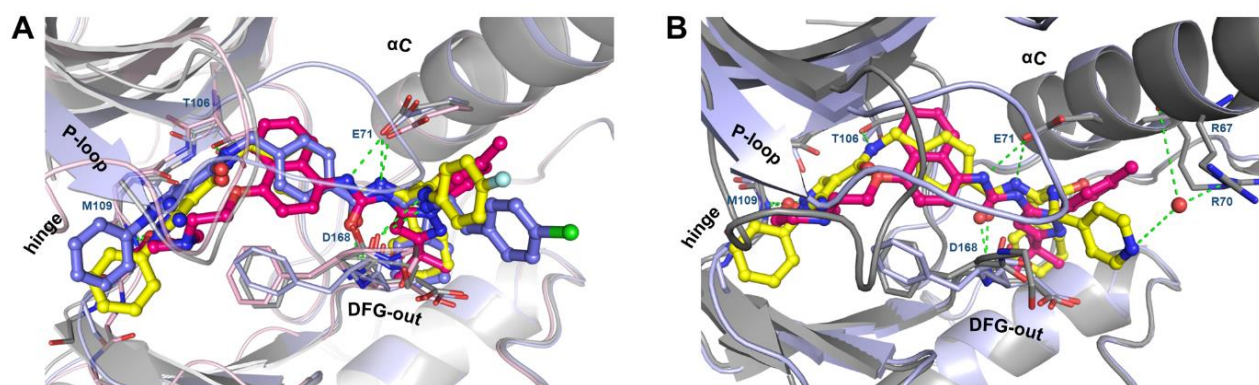
No.	R	$\Delta T_m^a$ [°C] ± SD p38 $\alpha$	IC <sub>50</sub> <sup>b</sup> [nM] ± SEM p38 $\alpha$	No.	R	$\Delta T_m^a$ [°C] ± SD p38 $\alpha$	IC <sub>50</sub> <sup>b</sup> [nM] ± SEM p38 $\alpha$
234		10.1 ± 0.5	22.1 ± 0.7	242 (SR92)		14.7 ± 0.5	21.7 ± 3.7
235		7.5 ± 1.1	107.0 ± 2.0	243		13.9 ± 0.4	32.9 ± 7.0
236		6.8 ± 0.1	94.4 ± 1.4	244		12.6 ± 0.3	25.2 ± 4.8
237		7.3 ± 0.2	41.1 ± 4.3	245		6.1 ± 2.1	81.3 ± 5.3
238		1.9 ± 0.5	1990 ± 90.9	247		4.8 ± 0.2	1770 ± 41.0
239		2.3 ± 0.3	2830 ± 9.9	248		3.1 ± 0.1	2390 ± 42.1
240		7.8 ± 1.2 <sup>d</sup>	543.0 ± 2.1	249		3.6 ± 0.1	1040 ± 29.0
241		3.5 ± 1.8	287.0 ± 5.2	250		6.0 ± 0.2	462.0 ± 41.0
246		5.1 ± 0.3	144.0 ± 56.4				

<sup>a</sup>  $\Delta T_m$  average of four measurements, compound concentration 10  $\mu$ M; <sup>b</sup> IC<sub>50</sub> values were derived from duplicates (n = 2); <sup>c</sup> n = 10; <sup>d</sup> n = 6; <sup>e</sup> n = 4; <sup>f</sup> n = 3; measurements n.d. not determined. NanoBRET™ assay performed by Benedict-Tilman Berger, DSF-assay assisted by Martin Schröder, SGC Frankfurt.

Thermal protein stabilization of *para*-substituted halogen compounds (**234-236**) decreased from fluorine over chlorine to bromine. The fluorine-substituted compound **234** seemed therefore most optimal within this series, with a  $\Delta T_m$  value of  $10.1 \pm 0.5$  °C and an  $IC_{50}$  value of  $22.1 \pm 6.7$  nM, which was comparable to the lead structure VPC-00628. For 3,5-dihalogen-substituted compounds (**237-239**), the  $\Delta T_m$  values were overall significantly lower but followed the same radius-dependent trend of halogen substitutions. The loss in affinity for the target protein might be due to the larger steric demand and the limited plasticity of the binding pocket.

To increase the flexibility of the aforementioned phenolic structures, either a methylene or ethylene bridge between the back-pocket terminal amide and a substituted aromatic or heteroaromatic moiety were introduced (**240-246**). A significantly decreased temperature shift was observed for chlorinated compounds **241** and **246**. Furthermore, various picoline derivatives were synthesized, as the introduction of a polar nitrogen atom can serve as a hydrogen-bond acceptor group, which may help targeting the histidine or arginine residues inside the allosteric pocket of p38 $\alpha$ . Interestingly, for all picoline compounds (**242-244**) an improved activity was observed in  $\Delta T_m$  assays, which was confirmed by cellular  $IC_{50}$  values showing low nanomolar potency. The *para*-substituted picoline derivative (**242** (SR92),  $\Delta T_m = 14.7 \pm 0.5$  °C,  $IC_{50} = 21.7 \pm 3.7$  nM) seemed to be slightly more potent compared with the *meta*-substituted (**243**,  $\Delta T_m = 13.9 \pm 0.4$  °C,  $IC_{50} = 32.9 \pm 7.0$  nM) and *ortho*-substituted (**244**,  $\Delta T_m = 12.6 \pm 0.3$  °C,  $IC_{50} = 25.2 \pm 4.8$  nM) compounds. Less potent binding was detected for the smaller, more-electron rich, five-membered thiophene compound **246**.

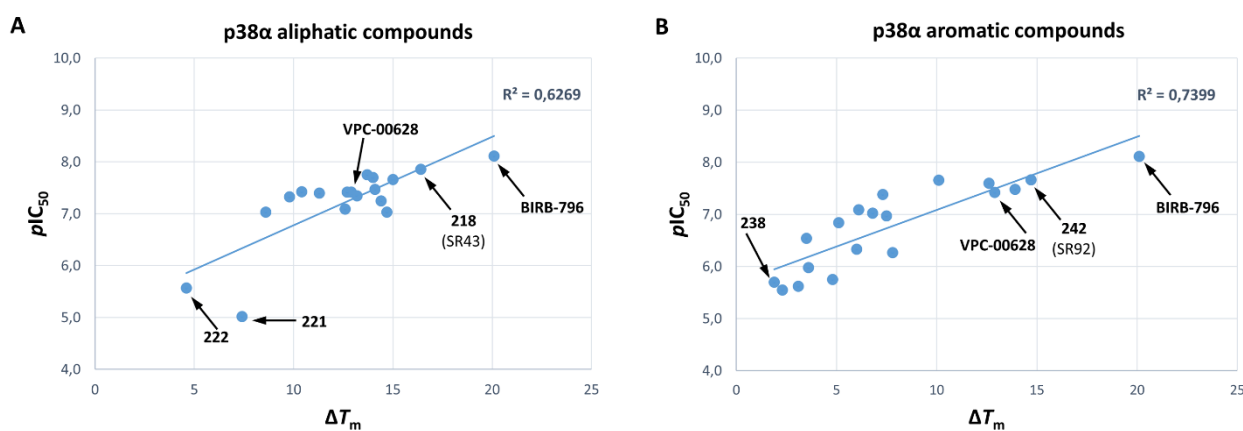
An overlay of the crystal structures of the p38 $\alpha$  complexes with chlorine-substituted **234** and **246** with the structure of the BIRB-796 complex illustrated the high plasticity of the allosteric pocket region (**Figure 33A**). Targeting unique residues such as the non-conserved Arg70 in p38 $\alpha$  MAPK is therefore a challenging task. The more rigid compound **234** bound in closer proximity to the  $\alpha C$  helix, and the structure in complex with **SR72** showed that the terminal decoration extended toward the solvent-exposed region. Interestingly, the picoline nitrogen atom of the potent inhibitor **242** (SR92) formed a water-mediated hydrogen bond with the guanidinium group of Arg70, which is unique to p38 $\alpha$  (**Figure 33B**). In addition, this water molecule was stabilized by the back-pocket carbonyl oxygen of the switch-pocket residue Arg67, which provides an explanation for the improved potency of this compound.



**Figure 33. Binding mode of back-pocket modified VPC-00628 derivatives with aromatic and heteroaromatic structures in complex with p38 $\alpha$ .** A) Overlay of the binding modes of aromatic compounds **234** (yellow, PDB: 6Y6W), **246** (violet, PDB: 6Y4X) with BIRB-796 (pink, PDB: 1KV2). B) Overlay of picoline derivative **242** (SR92, yellow, PDB: 6Y70) and BIRB-796 (pink, PDB: 1KV2). A structural water molecule bridging **242** (SR92) and the guanidinium group of Arg70 is depicted as a red sphere. Hydrogen-bond interactions are highlighted in green. The extended P-loop conformation of p38 $\alpha$  in the BIRB-796 complex is highlighted in light pink. Crystallization and structure determination was done by Apirat Chaikuad and Martin Schröder.

Targeting of the folded P-loop conformation of ERK2 with SCH772984 was possible because this inhibitor harbors a piperazine-phenyl-pyrimidine back-pocket decoration adopting a sharp bend conformation. As the P-loop/ $\alpha$ C pocket might be targetable in p38 as well, compounds with a back-pocket decoration similar to that of SCH772984 were synthesized. Therefore, space-occupying, elongated moieties were selected for the synthesis and extension of VPC-00628. To ensure, that the inhibitor is flexible enough to adopt a similar kinked conformation as seen for SCH772984, the piperazine moiety was kept and decorated with different aromatic and heteroaromatic structures. Compared with the piperazine derivative **230** ( $\Delta T_m = 12.6 \pm 0.3$  °C), substitution of the free NH-hydrogen atom by an aromatic residue led to a sharp decrease in thermal shift values for all compounds that were synthesized (**247-250**). Interestingly, a  $\Delta T_m$  value of  $6.0 \pm 0.2$  °C was measured for the benzoxazole derivative **250**, whereas replacement of the oxygen atom by a sulfur atom led to an overall loss of activity ( $\Delta T_m$  of 2.4 °C, **249**,  $\Delta T_m = 3.6 \pm 0.1$  °C). All piperazine-aryl derivatives showed cellular activity on p38 $\alpha$ , with IC<sub>50</sub> values in the low micromolar range. From these studies it became apparent that sterically demanding aromatic and heteroaromatic structures have a negative effect on protein stability and hence binding. It can therefore be concluded that more elongated moieties resembling the ERK2 inhibitor SCH772984 do not improve the binding interaction within the allosteric pocket of p38 and that a fundamentally different design strategy is required for efficiently targeting this allosteric pocket in p38.

To summarize all data and provide an overview the  $\Delta T_m$  data of p38 $\alpha$ , determined for both aliphatic and aromatic compounds, were each plotted against the calculated pIC<sub>50</sub> values (**Figure 34**). The overall data were in agreement for both assay formats and showed very good correlation for the most potent inhibitors.

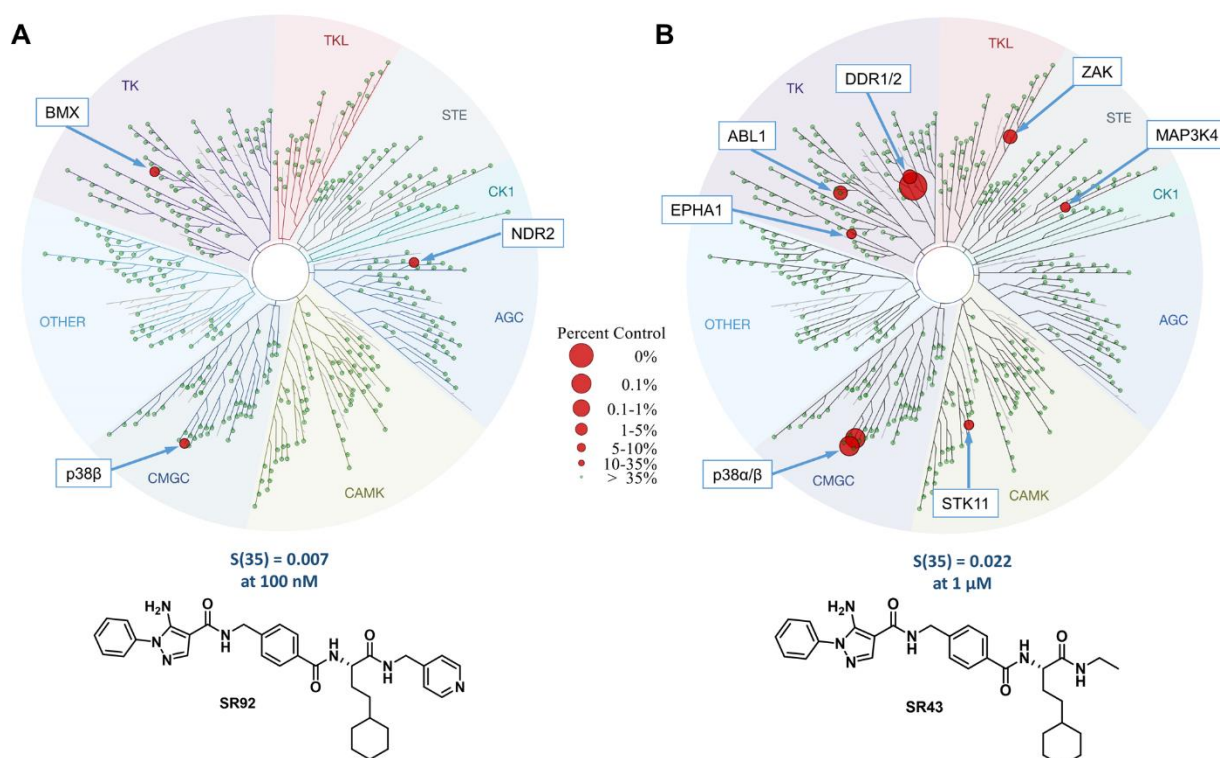


**Figure 34. Correlation between thermal shift and NanoBRET™ assay data.** A) Correlation for aliphatic compounds, B) correlation for aromatic compounds. Calculated pIC<sub>50</sub> values are depicted.

In summary, a set of ten inhibitors was synthesized that were more potent than the already potent lead structure VPC-00628, and although they did not achieve the excellent activity of BIRB-796, the strongest inhibitors were the aliphatic compound **218** (SR43) and the aromatic compound **242** (SR92). The worst correlation was found for the very hydrophobic compound **221**, which may be due to poor membrane permeability. The same could be a reason for the low potency of compounds **222** and **238**.

## 4.6 Kinome profiling and in cellulo off-target activity

The most potent and promising compounds of the series, **242** (SR92) and **218** (SR43), were chosen for a kinome wide selectivity screen. To evaluate their activity toward other kinases, compounds were screened against the largest kinase panel available by *DiscoverX* (*scanMAX*<sup>SM</sup>), covering a total 468 kinases and kinase mutants. An interesting selectivity profile was discovered for **242** (SR92), which interacts with non-conserved switch pocket residues via a water mediated-hydrogen. It was highly selective, targeting only p38 $\beta$ , NDR2 and BMX at a compound concentration of 100 nM, with <35% of control activity remaining in the assay (**Figure 35A**). The selectivity score was determined to be excellent,  $S(35) = 0.007$ , at this concentration and was calculated from the quotient of targets identified and the sum of 403 non-mutated kinases in this assay.<sup>403</sup> However, as the false-positive rate of this assay is typically around 1%, further confirmation of these targets would be necessary. As it was surprising that p38 $\alpha$  was not active in this assay, the most potent compound SR43 was screened again at a higher concentration of 1  $\mu$ M (**Figure 35B**).



**Figure 35. Selectivity profiling against 468 kinases and mutants.** A) SR92 (**242**) screened at 100 nM. B) SR43 (**218**) screened at 1  $\mu$ M. Main targets as percent of control are highlighted as red dots of different sizes reflecting inhibitor potency as indicated in the figure capture; only data for wild-type kinases are shown. Selectivity score  $S(35)$  is given for compound comparison.

At the higher compound concentration of 1  $\mu$ M, thirteen kinases and mutants were identified as targets (<35% activity of control) in the selectivity profiling assay. Neglecting the mutants, a selectivity score of  $S(35) = 0.022$  was calculated. All targets with <35% activity of the control remaining were confirmed by NanoBRET<sup>TM</sup> assay for *in cellulo* activity, and non-mutated targets with <10% activity of the control were additionally confirmed by  $K_d$  determination (*DiscoverX* service, **Table 13**). The  $K_d$  determinations revealed that **218** (SR43) binds highly selective to p38 $\alpha/\beta$  ( $K_d = 6.3/20$  nM), showing narrow selectivity for additional targets, such as DDR1/2 ( $K_d = 31/40$  nM), ZAK ( $K_d = 120$  nM) and ABL1 ( $K_d = 130$  nM). As a typical chemical probe might be used in a more complex cellular environment to study biological processes, knowledge of all potential targets inside the cell is a prerequisite. On the basis of the above data, compound **218** (SR43)

only inhibits p38 $\alpha$  and p38 $\beta$  *in cellulo* with nanomolar potencies ( $IC_{50}$  = 14.0/ 16.8 nM), whereas DDR1/2 ( $IC_{50}$  = 2.5/ 1.5  $\mu$ M), ZAK ( $IC_{50}$  = 1.7  $\mu$ M) and MAP3K4 ( $IC_{50}$  = 5.8  $\mu$ M) were inhibited with  $IC_{50}$  values in the low micromolar range. Interestingly, **218** (SR43) also potently inhibited FLT3 mutants K663Q and D835Y in the KinomeScan, which are the main mutants in chronic myeloid leukemia. However, only low affinity was measured on full-length protein in HEK293T cells (NanoBRET,  $IC_{50}$  FLT3(D835Y) = >20  $\mu$ M;  $IC_{50}$  FLT3(K663Q) = >20  $\mu$ M). No activity ( $IC_{50}$  = >20  $\mu$ M) was found for additional kinome targets such as ABL1 and EPHA1 in this cellular system. The differences in activity may be attributed to different  $K_m$  values for ATP and differences inhibiting full-length enzymes used in BRET assays compared with catalytic domains used in the KinomeScan as well as differences in the activation states of the screened kinases.

**Table 13.** Selectivity profiling of **218** (SR43) and target activity confirmed by  $K_d$  determination and *in cellulo*  $IC_{50}$  values.

Kinome targets	218 (SR43) percent of control at 1 $\mu$ M	218 (SR43) DiscoverX $K_d$ [ $\mu$ M]	218 (SR43) NanoBRET™ $IC_{50} \pm SEM^a$ [ $\mu$ M]
FLT3(K663Q)	0	n.d.	>20
FLT3(D835Y)	0	n.d.	>20
DDR1	0.1	0.031	2.5 $\pm$ 0.2
p38 $\alpha$	1.5	0.0063	0.0140 $\pm$ 0.0006
p38 $\beta$	3.4	0.02	0.0168 $\pm$ 0.0013
ABL1-nonphosphorylated	8.8	0.13	>20
ZAK	9.4	0.12	1.7 $\pm$ 0.5
DDR2	9.4	0.04	1.5 $\pm$ 0.8
MAP3K4	11.0	n.d.	5.80 <sup>b</sup>
EPHA1	11.0	n.d.	>20
STK11	18.0	n.d.	>20
FGFR3(G697C)	23.0	n.d.	10.0 $\pm$ 0.7
ABL1(Q252H)- nonphosphorylated	28.0	n.d.	>20

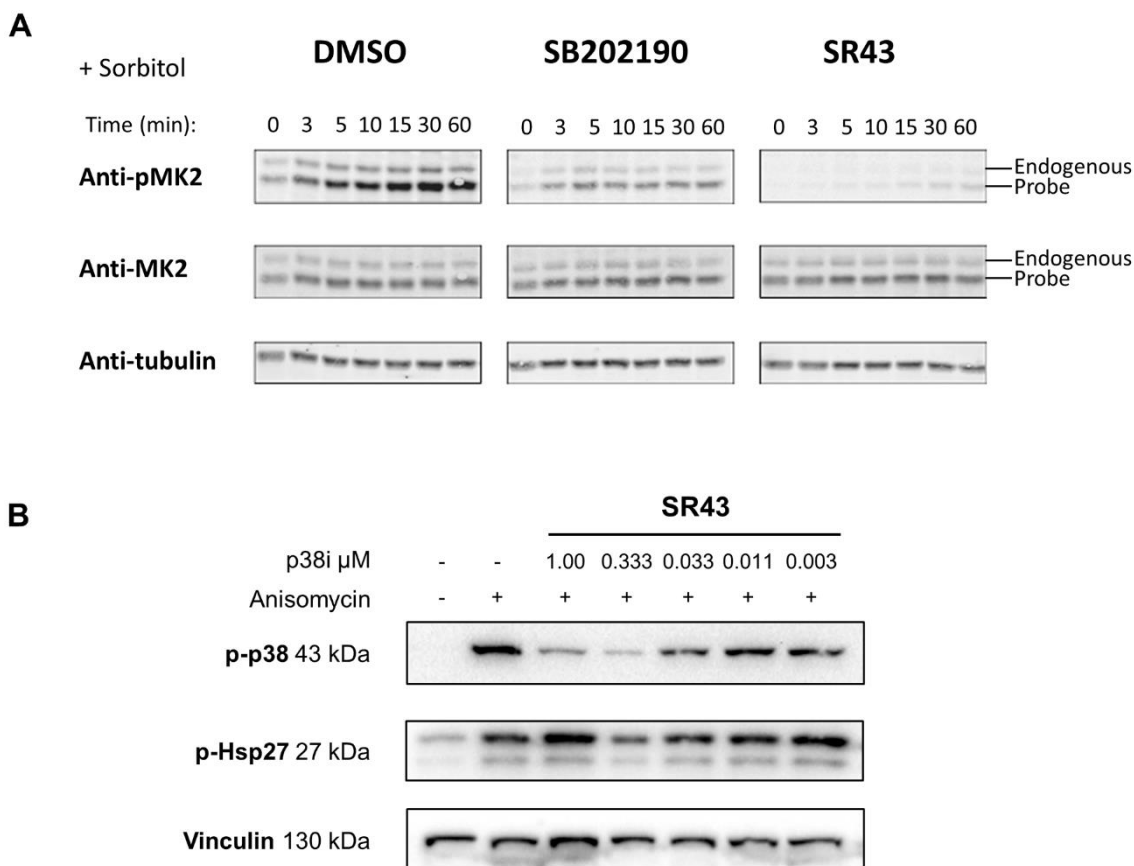
<sup>a</sup> $IC_{50}$  values listed are the mean of two experiments; <sup>b</sup> $IC_{50}$  value from single measurement; n.d. not determined.  $K_d$  values determined by DiscoverX service, NanoBRET™ assay performed by Benedict-Tilman Berger.

#### 4.7 Biological evaluation

After demonstrating the excellent selectivity of **218** (SR43) in cells, the inhibitor was evaluated further by probing its efficiency on endogenous p38 $\alpha$ / $\beta$ . Therefore, the phosphorylation state of endogenous p38 substrates MK2 and Hsp27 was measured by Western blot analysis as well as the TNF- $\alpha$  release in whole blood.

### 4.7.1 Inhibitory effect on endogenous substrates

MK2 plays a key role in the p38-mediated signaling pathway and was found to regulate a number of substrates necessary for cytokine production, actin remodeling, cell migration, regulation of transcription and cell-cycle control.<sup>215</sup> Therefore, the time-dependent impact on the MK2 phosphorylation was studied next, in sorbitol-stimulated HEK293T cells by dynamic luciferase complementation based probes. In addition to the inhibitory effect of the type-II inhibitor **218** (SR43), the effect on the phosphorylation of MK2 was monitored by the frequently used type-I inhibitor SB202190 (**Figure 36A**). The experiments were performed in collaboration by Anna Sebő and Attila Reményi (Research Center for Natural Sciences, Budapest, Hungary). Over 60 minutes, **218** (SR43) inhibited the phosphorylation of its downstream target MK2, with a stronger effect visible at the beginning of the experiment. Interestingly, the observed effect was higher for our type-II inhibitor compared with the type-I candidate SB202190, which may be attributed to the different kinase conformations trapped by these inhibitors.



**Figure 36. Analysis of p38 downstream targets MK2 and Hsp27.** A) Effects of SB202190 (type-I) and SR43 (**218**, type-II) on p38 activation and downstream MK2 substrate phosphorylation in HEK293T cells. The panels show the results of Western-blot analysis for samples taken at different time points after sorbitol treatment (endogenous – intact MK2 from HEK293T cells; probe – heterologously expressed MK2 tagged with the small bit, SmBiT, luciferase enzyme fragment). Note the similar levels of endogenous and heterologously expressed MK2. The MK2 probe appears smaller than the full-length endogenous MK2 because the former lacks its proline-rich N-terminal 40 amino acids. Anti-tubulin was used as control. Assay was performed by Anna Sebő, Hungary. B) Concentration-dependent effect on p38 autophosphorylation and Hsp27 phosphorylation by p38 inhibitor **218** (SR43). HCT-15 cells were treated for 2 h with inhibitors at different concentrations or vehicle (DMSO) and then stimulated with anisomycin (10  $\mu$ g/mL) for 30 min. Western blot analysis of whole cell lysates to detect p-Hsp27 (Ser82). Vinculin was used as loading control. Assay was performed by Jule Harbig, Tübingen.

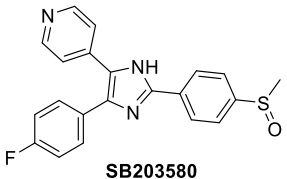


The phosphorylation of p38 and Hsp27 was determined by Jule Harbig and Daniel Dauch (University Hospital, Tübingen). After stimulation with the antibiotic anisomycin, analysis revealed that compound **218** (SR43) showed a dose-dependent inhibition of activating phosphorylation of p38 in HCT-15 cells and phosphorylation of its down-stream substrate Hsp27 (**Figure 36B**). However, while effects on p38 activation showed the expected dose response, there was no significant reduction of Hsp27 phosphorylation upon inhibitor treatment, probably due to phosphorylation of this protein by several stress-activated kinases.

As p38 MAPK is related to inflammatory diseases and regulates the expression of pro-inflammatory cytokines, the efficiency of **218** (SR43) in modulating the release of TNF- $\alpha$  was further tested in whole blood. This experiment was performed, as already described in **Section 3.2**, in collaboration with the Laufer Group at the University of Tübingen (**Table 14**).

**Table 14.** TNF- $\alpha$  release in whole blood. Calculated  $IC_{50}$  values and percent of inhibition at highest compound concentration in the assay system.

Compound	$IC_{50}$ [ $\mu$ M] $\pm$ SD (n=3)	Inhibition [%] $\pm$ SD at 10 $\mu$ M (n=3)
<b>218</b> (SR43)	0.484 $\pm$ 0.052	91.5 $\pm$ 1.39%
SB203580	1.360 $\pm$ 0.348	83.1 $\pm$ 0.40%

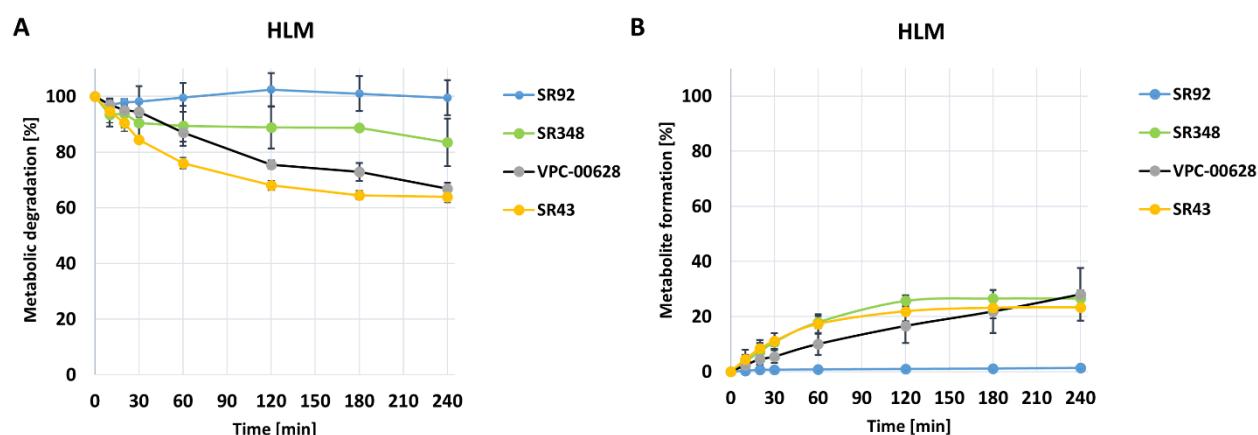


SB203580

Interestingly, the type-II inhibitor **218** (SR43) showed a significantly stronger inhibitory effect on the TNF- $\alpha$  release compared with compound SB203580,<sup>17-19</sup> which inhibits the active conformation of p38 via a canonical type-I binding mode. At the highest inhibitor concentration of 10  $\mu$ M used in this study, **218** (SR43) led to an almost complete inhibition of TNF- $\alpha$  release (92%), and an  $IC_{50}$  value of 0.48  $\pm$  0.05  $\mu$ M was calculated. In contrast, the type-I inhibitor with an  $IC_{50}$  value of 1.36  $\pm$  0.34  $\mu$ M and a total inhibition of 83% showed a significantly lower effect on the release of this pro-inflammatory marker.

#### 4.7.2 Metabolic stability and TNF- $\alpha$ release

The metabolic stability of compounds **218** (SR43), **234** (SR348), **242** (SR92) and the lead structure VPC-00628 was tested in human liver microsomes (HLM). The degradation and metabolite formation of the compounds was followed over 240 min, and each sample was analyzed after 0, 10, 20, 30, 60, 120, 180 and 240 min using LC-MS, ESI(+). The concentration of the protein was standardized to 1 mg/mL for all measurements (**Figure 37**). The assay was performed in collaboration with Mark Kudolo, University of Tübingen. All compounds showed good stability in human liver microsomes. After 240 min 99.5  $\pm$  6.3% of compound **242** (SR92), 83.5  $\pm$  8.5% of **234** (SR348) and 64.0  $\pm$  2.2% of **218** (SR43) remained in the media. Compounds **234** (SR348) and **218** (SR43) had a higher metabolic stability than the lead structure VPC-00628 (66.9  $\pm$  2.1% remaining), whereas **242** (SR92) showed a significant stability, with almost no metabolite formation during the 240 min time window that had been investigated.



**Figure 37. Study on the metabolic stability of selected compounds.** A) Metabolic degradation and B) metabolite formation of the lead compound VPC-00628, SR43 (**218**), SR92 (**242**), and SR348 (**234**) over 240 min in human liver microsomes (HLM). Experiments were performed in triplicates. The values represent the mean with standard deviation. Assay by Mark Kudolo, Tübingen.

## 4.8 Conclusion

In conclusion, a series of small molecules for targeting the allosteric  $\alpha$ C- and DFG-out pockets in p38 $\alpha$  MAPK were developed. First, pyrazole urea scaffolds derived from BIRB-796 were synthesized, and the activity of those fragments against a comprehensive set of 47 diverse kinases was tested using DSF. The results for this set of compounds were somewhat disappointing, though, as either off-targets described for BIRB-796 were retained or the activity for p38 $\alpha/\beta$  was significantly reduced. Revisiting the recently published compound MCP-081 that combines the allosteric part of BIRB-796 with the active-site directed part of VPC-00628, it could be shown that MCP-081 displays a clean selectivity profile in the DSF kinase panel. Intriguingly, a significant selectivity over the p38 $\beta$  isoform was also observed for this candidate. As the potency of MCP-081 was slightly reduced compared with VPC-00628 and the allosteric *tert*-butyl pyrazole moiety seemed suboptimal, a set of VPC-00628 derivatives for targeting the  $\alpha$ C-out pocket region was synthesized, inspired by the crystal structure of p38 $\alpha$  bound to MCP-081. Through structure-guided extension of the terminal amide of VPC-00628 toward this allosteric site, the potent and selective compound **218** (SR43) was developed, which showed excellent cellular activity on p38 MAPK in NanoBRET<sup>TM</sup> assays ( $IC_{50}$  [p38 $\alpha/\beta$ ] =  $14.0 \pm 0.1/ 16.8 \pm 0.1$  nM). The new type-II inhibitor **218** (SR43) also reduced phosphorylation of p38 downstream substrate MK2 in cells. In addition, **218** (SR43) induced an anti-inflammatory response by blocking TNF- $\alpha$  release in whole blood and displayed a high metabolic stability. Taken together, **218** (SR43) represents a valuable chemical probe for studying the structural plasticity of p38 MAPK and the phenotypic effects from targeting specific conformational states of kinases.

## 5 Optimization of SR43 for DDR1/2 inhibition

The studies in the previous chapters describe the development of two potent and highly selective p38 $\alpha$ / $\beta$  inhibitors, **218** (SR43) and **33** (SR318), which can be used to study the molecular mechanisms of p38 MAPK related signaling pathways. Selectivity profiling of these compounds was performed against the largest kinase panel available (468 kinases and mutations) and revealed narrow selectivity for additional targets. For **218** (SR43), additional high-affinity targets besides p38 $\alpha$ / $\beta$  ( $K_d$  = 6.3/ 20 nM) were DDR1/2 ( $K_d$  = 31/ 40 nM), ABL1 ( $K_d$  = 130 nM) and ZAK ( $K_d$  = 120 nM). Interestingly, DDR1/2 was also targeted by **33** (SR318) as well as by commercially available p38 inhibitors, such as BIRB-796 ( $K_d$  [DDR1/2] = 1.9/ 33 nM), VX-745 ( $K_d$  [DDR1] = 1100 nM) and SB203580 ( $K_d$  [DDR1/2] = 1000/ 5000 nM).<sup>44</sup> A set of approved drugs, such as Imatinib, Nilotinib or Ponatinib, are also potent inhibitors of this kinase.<sup>458</sup> Despite being a rather promiscuous target, there was not much focus on the development of selective DDR1/2 inhibitors so far. From the compounds mentioned above, BIRB-796 was the only candidate which was ever evaluated for DDR1/2 inhibition.<sup>459</sup> In these studies, a fluorescence-based direct binding assay (fluorescent labels in kinases, FliK-assay) for the detection of type-II and type-III DDR2 inhibitors was established.<sup>459</sup> By screening an 852-membered compound library, 81 potential DDR2 inhibitors were identified, from which 32 hits were chosen for a follow-up study. Although, nanomolar  $K_d$  values were determined for most of these compounds, the identified hits were of limited scaffold diversity as 21 compounds shared a similar pyrazole-urea BIRB-796-like core scaffold.

The discoidin domain receptor kinase (DDR) plays a central role in fibrotic-disorders, such as renal and pulmonale fibrosis, atherosclerosis and different forms of cancer, and is therefore an important therapeutic target.<sup>460, 461</sup> The design of selective inhibitors may also help to better understand the molecular mechanism of DDR1/2 kinase related processes.<sup>458</sup> For that reason, the previously obtained compound **218** (SR43) was chosen for the synthesis of DDR1/2 inhibitors with a novel chemical scaffold. The following sections describe the structure, function and regulation of discoidin domain receptor kinase (DDR, **Section 5.1.1**) and summarizes features of published DDR1/2 inhibitors (**Section 5.1.2**). Synthesis of an **218** (SR43)-derived compound library led to potent and selective DDR1/2 kinase inhibitors that are characterized in **Section 5.4**.

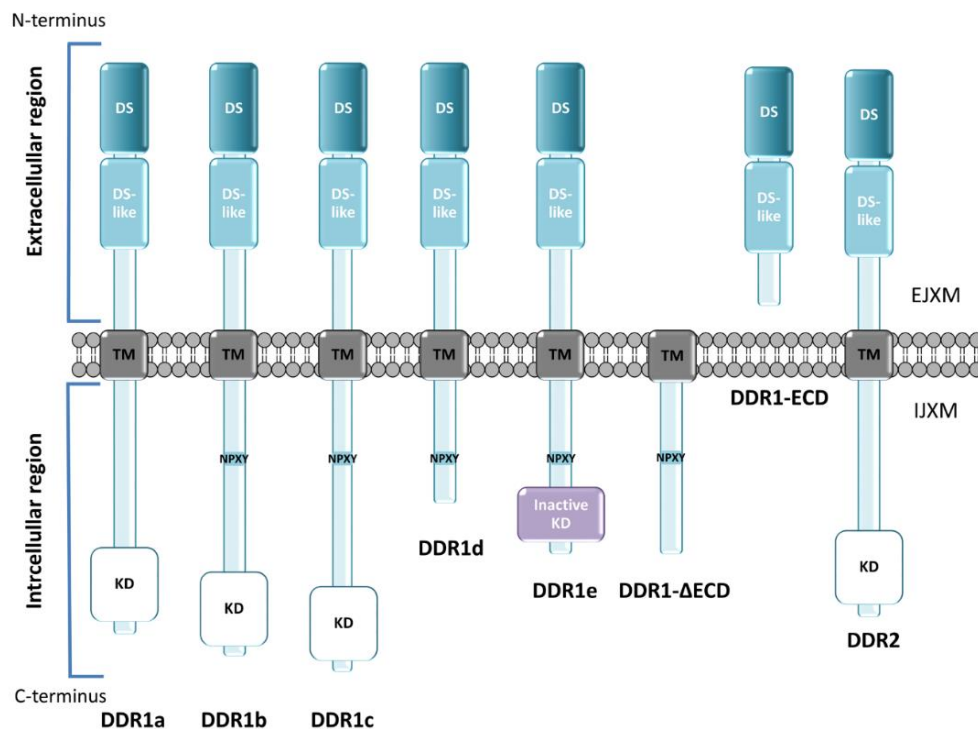
### 5.1 Discoidin domain receptor kinase

#### 5.1.1 Structure, function and regulation

Discoidin domain receptor kinase (DDR kinase) was discovered in in the early 90s by homology cloning of its catalytic kinase domain and was initially considered as orphan receptor. The type I transmembrane protein belongs to the family of receptor tyrosine kinases (RTK), which share a similar structure consisting of an extracellular domain, a transmembrane segment and an intracellular domain with intrinsic kinase function. In 1997, both SHRIVASTAVA ET AL. and VOGEL ET AL. reported that DDR can be activated by diverse types of fibrillar and non-fibrillar collagens.<sup>462, 463</sup> Normally, RTKs are activated by soluble, peptide-like growth factors, whereby ligand binding leads to rapid activation of the intracellular kinase function. While some of these receptors exist as a preformed dimer in the membrane, e.g. insulin receptor (IR) or epidermal growth factor receptor (EGFR), most of the 58 RTKs found in humans dimerize upon ligand binding.<sup>464</sup> Following this event, auto- and cross-phosphorylation occurs at several tyrosine residues in the intracellular domain, which triggers activation of the catalytic functions of the kinase. DDRs are unique members of the RTK family

because they are the only kinases that make use of collagens as extracellular ligands, which are the most abundant components of the extracellular matrix (ECM). Contrary to other RTKs, DDR preferentially exists in auto-inhibited preformed homo- and heterodimeric assemblies in the membrane before ligand binding. Although receptor clustering enhances collagen binding, activation of the inherent kinase function is exceptionally slow on the time scale of hours.<sup>464</sup> Thus, collagen-stimulated DDR kinase signaling is detectable even after several days and suggested to play an important role in long lasting and durable pathways.<sup>465</sup>

The DDR kinases subfamily consists of two members, named DDR1 and DDR2. Whereas DDR1 exists in five isoforms, namely DDR1a, DDR1b, DDR1c, DDR1d and DDR1e produced by alternative splicing, only one isoform of DDR2 was identified (**Figure 38**).<sup>466</sup> DDR1 kinase is further known to undergo ectodomain shedding by matrix metalloproteinases (MMPs), whereby a soluble N-terminal fragment, DDR1-ECD, and a membrane-anchored N-terminal intracellular fragment, DDR1- $\Delta$ ECD, is formed.<sup>464, 467</sup> Typically, the extracellular part of the transmembrane receptor consists of a C-terminal globular discoidin (DS) domain followed by a so-called DS-like domain. The DS domain is responsible for collagen binding and resembles the galactose-binding lectin discoidin 1 protein isolated from the slime mold *Dictyostelium discoideum*. While DDR1 binds to almost all triple-helical fibrillar and non-fibrillar collagens, DDR2 is preferentially activated by type I, II, III fibrillar as well as type X non-fibrillar collagens.<sup>468, 469</sup> The precise mechanism of ligand binding and receptor activation is complex and not fully understood yet, but a conserved GVMGFO motif (O = 4-hydroxyproline) on triple-helical collagens was identified to be specifically targeted by DDRs.<sup>470</sup>



**Figure 38. Domain structure of discoidin domain receptor DDR1, DDR2 and isoforms.** Discoidin domain (DS), discoidin domain-like (DS-like), transmembrane domain (TM), conserved NPXY motif, kinase domain (KD), inactive kinase domain, extracellular juxtamembrane (EJXM) and intracellular juxtamembrane (IJXM) are highlighted.

Despite very low sequence identity, the DS-like domain adopts a similar eight stranded  $\beta$ -sheet structure as found for the DS domain described above. DS-like domains contain a calcium binding site as well as several conserved *N*- and *O*-glycosylation sites that have been shown to be important for modulating non-covalent receptor dimerization and signaling.<sup>471</sup> Following these unique structural elements, an unstructured

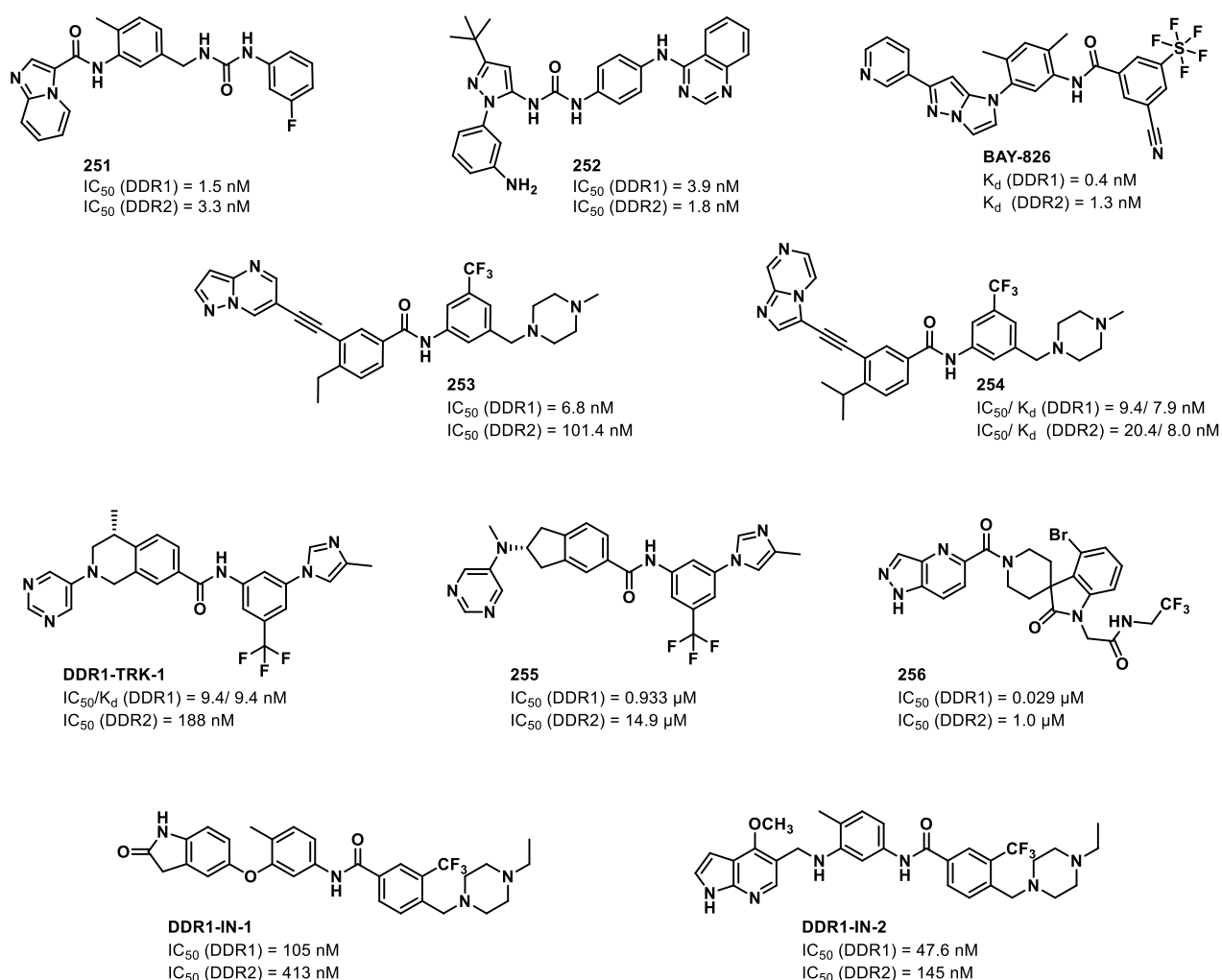
juxtamembrane region of 50 amino acids in DDR1 and 30 amino acids in DDR2 leads into the transmembrane region. The transmembrane region is characterized by repeated leucine zipper motifs, which are thought to be crucial for receptor self-association and, thus, for kinase activation.<sup>472, 473</sup> The intracellular part of DDR typically comprises a notably large intracellular juxtamembrane region (IJXM, 171 and 142 amino acids for DDR1 and DDR2, respectively), a kinase domain and a short C-terminal tail. The isoforms DDR1d and DDR1e are kinase-deficient, lacking the kinase domain due to alternative splicing. The tyrosine kinase domain is about 300 amino acids in size and has the typical N- and C-terminal lobe structure, whose activity is controlled by the phosphorylation of three tyrosine residues (Tyr792, Tyr740, Tyr797) in the activation loop. Interestingly, binding of the collagen ligand leads to the formation of linear homo- and heteromeric clusters of DDR1/2 and collagen fibrils. The latter proved to be a prerequisite for the phosphorylation of Tyr792 and Tyr740 as well as the subsequent activation of the catalytic functions of the kinase.<sup>474</sup> This event is supported by receptor cross-phosphorylation and followed by the autophosphorylation of additional tyrosine residues in the IJXM. The phosphotyrosine sites promote the binding and activation of various adaptor proteins via an intrinsic Src homology 2 (SH2) domain or a phosphotyrosine-binding domain (PTB).<sup>475</sup> Known DDR1/2 interacting proteins are the SH2 domain containing transforming protein (Shc1),<sup>476</sup> protein-tyrosine phosphatase SHP-2,<sup>477</sup> NFκB,<sup>478</sup> ERK1/2,<sup>479</sup> NCK2,<sup>480</sup> AP1<sup>479</sup> or signal transducers and activators of transcription (STAT) proteins.<sup>477</sup>

DDR kinases regulate fundamental processes such as proliferation, differentiation, adhesion, survival and matrix remodelling. The expression levels of the isoforms and the physiological effects triggered are tissue specific. While DDR1 is mainly expressed in epithelial cells, e.g. in lung, kidneys, colon and brain, DDR2 kinase is exclusively expressed in mesenchymal cells, smooth muscle cells and chondrocytes of kidney, skin, lung, heart and connective tissues. Beside the physiological DDR kinase functions, for instance during cell migration and wound healing, aberrant kinase activity was found to play a role in fibrotic disorders, atherosclerosis or during the invasion of cancer cells. In the early onset of osteoarthritis, DDR2 kinase, which is located on the surface of chondrocytes, binds to type II collagens that are released from mechanically injured cartilage, e.g., by age-related cartilage degradation process.<sup>481</sup> Typically, elevated levels of activated DDR2 kinases are detectable during this inflammatory event, whereby released TGF-β, integrin and collagen can no longer repair the damaged tissue.<sup>481, 482</sup> The high content of free collagen leads to aberrant DDR kinase activation, which in turn triggers the upregulation of matrix metalloproteinases (MMPs) and causes severe damage to the cartilage extracellular matrix.<sup>483</sup> Of particular note in this context is MMP13 (collagenase-3), which is overexpressed and known for its ability to efficiently cleave triple helical type II collagen, drastically promoting cartilage degeneration and disease progression.<sup>479, 484</sup> Now that the role of DDR2 kinase in osteoarthritis is known in more detail, selective DDR2 kinase inhibitors may help to protect cartilage and chondrocytes from degeneration and cell death. DDR2 kinase inhibitors could also be useful in combination therapy with current standard therapies to relieve disease symptoms.

### 5.1.2 *DDR1/2 kinase inhibitors*

Even 25 years after the discovery of DDR kinases, knowledge of the activation and inhibition mechanisms of DDR kinases is still insufficient and small-molecule inhibitors for this target are largely lacking. DDR1 and DDR2 kinase activity was frequently described as off-targets of various kinase inhibitors published. For example, the FDA approved kinase inhibitors Imatinib, Nilotinib and Dasatinib, originally developed for the inhibition of BCR-ABL protein in chronic myelogenous leukemia, are also known as potent inhibitors of DDR1/2 kinase. All inhibitors bound DDR1/2 kinase with nanomolar potencies, as determined by a TR-FRET

assay (100  $\mu$ M ATP), with  $IC_{50}$  values of 337/ 675 nM for Imatinib, 43/ 55 nM for Nilotinib and 0.5/ 1.4 nM for the multi-target protein kinase inhibitor Dasatinib, respectively.<sup>458</sup> BCR-ABL and DDRs show a high sequence similarity of about 60% in their active ATP-binding site, and crystal structures of these inhibitors for both kinase families have been determined to uncover specific binding characteristics. Interestingly, DDR kinase was not only found to be a prominent off-target when targeting its closest homologs but also of many promiscuous kinase inhibitors.<sup>485</sup> It is therefore surprising that so little attention has focused on the design of selective inhibitors for this important target so far. Accordingly, the landscape of DDR1/2 kinase inhibitors is of limited scaffold diversity (**Figure 39**), mainly from the last six years, and includes, for example, urea compounds designed by derivatizing inhibitors with known DDR1/2 kinase inhibitory activity, such as Imatinib, Dasatinib, and BIRB-796.<sup>459, 486, 487</sup> A similar approach focused on the Ponatinib scaffold, and a diverse set of pyrazolopyrimidine and imidazopyrazine derivatives were synthesized.<sup>488, 489</sup>



**Figure 39. Inhibitor landscape of potent DDR1/2 kinase inhibitors published.**

The pyrazolopyrimidines were synthesized and investigated by GAO ET AL. in 2013 as potent inhibitors of DDR1 isoforms. From this series, compound **253** was the most potent inhibitor, with an  $IC_{50}$  value of 6.8 nM for DDR1 kinase and reduced activity for DDR2 ( $IC_{50}$  = 101.4 nM). This compound suppressed the downstream signaling of DDR1 kinase on MMP2/3 or BCL-xL proteins in non-small cell lung cancer cells (NCI-H23) in a dose-dependent manner and also demonstrated anti-proliferative efficacy on a panel of eight cancer cell lines overexpressing DDR1 kinase. Although of value in biological studies, **253** was rather unselective when profiled against 396 kinases at a low concentration 100 nM. Under these screening

conditions, main target activity was found for twelve kinases >35% of control, ( $S(35) = 0.035$ ), covering kinases such as TRKB/C, TIE, LOK, ABL1 and ZAK. Therefore, even more kinase targets would have been detected upon screening at a higher, more commonly used concentration of 1  $\mu\text{M}$ . Therefore, **253** was derivatized to imidazopyrazines by WANG ET AL. in 2018. Although potency toward DDR2 was improved for **254**, inhibitors were of similar poor selectivity when tested against 468 kinases at an inhibitor concentration of 1  $\mu\text{M}$  ( $S(35) = 0.062$ ).<sup>489</sup>

KIM ET AL. screened a panel of 100 type-II kinase inhibitors, differing in their hinge-binding head group, linker region and back-pocket decoration, against 451 kinases.<sup>490</sup> This study led to two inhibitors, DDR1-IN-1 based on a indolin-2-one scaffold and DDR1-IN-2 based on a pyrrolopyridine core scaffold. Both inhibitors were tested in a Lanthascreen assay for their inhibitory effect on DDR1 and DDR2 activity, with  $\text{IC}_{50}$  values in the low nanomolar range (DDR1-IN-1:  $\text{IC}_{50}$  [DDR1/2] = 105/ 413 nM, DDR1-IN-2:  $\text{IC}_{50}$  [DDR1/2] = 47.6/ 145 nM). Both compounds also potently inhibited collagen-induced autophosphorylation of DDR1 in U2OS cells. Furthermore, the anti-proliferative effect of these inhibitors was studied on ten cancer cell lines overexpressing DDR kinase, covering different types of cancer. Interestingly, only DDR1-IN-2 had a significant effect on the proliferation in these cell, whereas DDR1-IN-1 showed no effect below a concentration of 10  $\mu\text{M}$ . Follow-up studies, which also examined the kinome-wide selectivity of these indolin-2-one inhibitors, suggested that the more unselective compound DDR1-IN-2 showed an antiproliferative effect solely due to multi-target rather than DDR1 inhibition.

Tetrahydroisoquinoline-7-carboxamides were described by different researchers as very potent and selective DDR1 inhibitors. However, these inhibitors showed undesired off-target activities on tropomyosin receptor kinases (TRKA-C), which is important for the development and normal function of the central and peripheral nervous systems.<sup>491-494</sup> To reduce TRKs activity, a follow-up study was recently reported by ZHU ET AL.<sup>495</sup> By docking the DDR-TRK-1 probe in TRKC and comparing the binding mode with the available crystal structure of DDR-TRK-1 in complex with DDR1 kinase, they provided important insights into inhibitor binding. Both compounds bound in the same orientation, but the methyl group fused to the tetrahydroisoquinoline scaffold targeted a small hydrophobic pocket in TRKC formed by Val552, Ala570, Lys572, and Phe617. Binding to this unique pocket was, therefore, suggested as the main driver of TRKs selectivity. This methyl group was therefore truncated and the core heterocycle replaced by a 2-amino-2,3-dihydro-1*H*-indene-5-carboxamide moiety (**255**).<sup>495</sup> The modified compound proved to be potent and efficient in pancreatic cancer *in vivo* with reduced activities ( $\text{IC}_{50}$  [TRKA/B/C] = >1  $\mu\text{M}$ / >1  $\mu\text{M}$ / 0.790  $\mu\text{M}$ ) on TRKs. Interestingly, a reduction in DDR2 activity was also detected ( $\text{IC}_{50} = 0.933 \mu\text{M}$ ), making compound **255** a very valuable selective DDR1 inhibitor. Recently, even more promising spiroindolinones were identified by Roche Pharma as potent DDR1 inhibitors with of novel scaffold using a DNA-encoded library. In SAR studies, compound **256** was discovered, which showed significant *in vivo* efficacy in renal Alport syndrome in mice. Interestingly, **256** is not only a very potent inhibitor of DDR1, as determined via binding competition assay on the isolated kinase domain ( $\text{IC}_{50}$  [DDR1/2] = 0.029/ 1.0  $\mu\text{M}$ ), but also showed the highest kinome-wide selectivity of any DDR1 inhibitor published to date ( $S(35) = 0.015$ , at 10  $\mu\text{M}$ ).<sup>496</sup>

## 5.2 Choosing the optimal building block

Since selective and potent DDR1/2 inhibitors are largely lacking and the existing inhibitors are of low scaffold diversity, the next study focused on optimizing **218** (SR43) toward DDR1/2 kinase inhibition. To obtain preliminary data on optimal building blocks, the previously synthesized compounds for exploring the

allosteric back pocket (**Chapter 4**), the BIRB-fragment library (**Chapter 4**) and the library donated by *Mercachem* (**Chapter 3**) were each screened with DSF against the most potent targets of **218** (SR43) in the selectivity profiling with *DiscoverX*. Thermal shift values were determined for DDR1/2, ABL1 as well as ZAK and compared with p38 $\alpha$ / $\beta$  (**Table 15**, **Table 16**). Since the  $\Delta T_m$  values typically correlate well with  $K_d$  values, potencies of new derivatives were estimated by comparing the corresponding thermal shift values. Compound **218** (SR43) with known  $K_d$  values was used as a standard in these experiments (p38 $\alpha$ / $\beta$  [ $K_d$  = 6.3/20 nM], DDR1/2 [ $K_d$  = 31 / 40 nM], ZAK [ $K_d$  = 120 nM], ABL1 [ $K_d$  = 130 nM]).

**Table 15.** Summary of thermal shift assays for the BIRB-fragment library compounds and back pocket modified compounds (**Chapter 4**), screened at 10  $\mu$ M against the main targets of **218** (SR43).

No.	$\Delta T_m^a$ [°C] $\pm$ SD, p38 $\alpha$	$\Delta T_m^b$ [°C] $\pm$ SD, p38 $\beta$	$\Delta T_m^b$ [°C] $\pm$ SD, DDR1	$\Delta T_m^b$ [°C] $\pm$ SD, DDR2	$\Delta T_m^c$ [°C] ZAK	$\Delta T_m^d$ [°C] $\pm$ SD, ABL1
88	1.3 $\pm$ 0.1 <sup>d</sup>	-0.2 $\pm$ 0.4 <sup>d</sup>	3.2 $\pm$ 0.7	1.9 $\pm$ 1.3	n.d.	0.1 $\pm$ 0.0
97	10.4 $\pm$ 0.9 <sup>d</sup>	9.4 $\pm$ 0.5 <sup>d</sup>	2.6 $\pm$ 0.1	1.3 $\pm$ 1.3	n.d.	0.2 $\pm$ 0.0
89	0.9 $\pm$ 0.2 <sup>d</sup>	0.3 $\pm$ 0.7 <sup>d</sup>	1.2 $\pm$ 0.6	0.9 $\pm$ 0.3	n.d.	0.1 $\pm$ 0.1
90	0.9 $\pm$ 0.0 <sup>d</sup>	0.6 $\pm$ 0.0 <sup>d</sup>	0.4 $\pm$ 0.7	0.6 $\pm$ 0.1	n.d.	0.5 $\pm$ 0.0
91	3.6 $\pm$ 0.1 <sup>d</sup>	4.0 $\pm$ 0.9 <sup>d</sup>	3.9 $\pm$ 0.2	2.1 $\pm$ 1.8	n.d.	0.3 $\pm$ 0.0
92	5.6 $\pm$ 0.6 <sup>d</sup>	7.8 $\pm$ 0.3 <sup>d</sup>	3.6 $\pm$ 0.2	1.9 $\pm$ 1.7	n.d.	0.1 $\pm$ 0.0
99	2.4 $\pm$ 0.5 <sup>d</sup>	2.6 $\pm$ 0.4 <sup>d</sup>	2.5 $\pm$ 0.3	1.4 $\pm$ 1.1	n.d.	0.8 $\pm$ 0.0
103	6.7 $\pm$ 0.0 <sup>d</sup>	7.2 $\pm$ 0.6 <sup>d</sup>	n.d.	n.d.	n.d.	0.8 $\pm$ 0.0
101	1.5 $\pm$ 0.4 <sup>d</sup>	1.5 $\pm$ 0.4 <sup>d</sup>	2.2 $\pm$ 0.3	1.3 $\pm$ 1.0	n.d.	0.5 $\pm$ 0.0
93	0.3 $\pm$ 0.1 <sup>d</sup>	0.3 $\pm$ 0.1 <sup>d</sup>	0.6 $\pm$ 0.4	0.5 $\pm$ 0.1	n.d.	0.2 $\pm$ 0.0
94	0.2 $\pm$ 0.1 <sup>d</sup>	-0.3 $\pm$ 0.3 <sup>d</sup>	0.9 $\pm$ 0.2	0.6 $\pm$ 0.4	n.d.	0.1 $\pm$ 0.0
95	0.1 $\pm$ 0.0 <sup>d</sup>	0.6 $\pm$ 0.5 <sup>d</sup>	0.8 $\pm$ 0.1	0.5 $\pm$ 0.3	n.d.	0.0 $\pm$ 0.2
96	0.9 $\pm$ 0.0 <sup>d</sup>	0.6 $\pm$ 0.5 <sup>d</sup>	2.4 $\pm$ 0.6	1.5 $\pm$ 0.9	n.d.	0.5 $\pm$ 0.2
217	15.0 $\pm$ 0.2	15.7 $\pm$ 0.1	3.5 $\pm$ 0.1	1.8 $\pm$ 0.3	6.3	3.5 $\pm$ 1.5
218 (SR43)	16.4 $\pm$ 0.2	16.2 $\pm$ 1.6	4.4 $\pm$ 0.0	2.2 $\pm$ 0.4	5.8	3.6 $\pm$ 0.6
219	13.7 $\pm$ 0.5	7.4 $\pm$ 1.6	2.8 $\pm$ 0.2	1.5 $\pm$ 0.3	5.1	1.4 $\pm$ 1.1
220	11.3 $\pm$ 0.5	4.2 $\pm$ 1.6	1.5 $\pm$ 0.9	1.2 $\pm$ 0.2	3.3	0.3 $\pm$ 1.1
221	7.4 $\pm$ 0.7	1.9 $\pm$ 1.7	-2.5 $\pm$ 1.3	-0.6 $\pm$ 0.0	n.d.	-0.2 $\pm$ 0.5
222	4.6 $\pm$ 0.6	-3.5 $\pm$ 0.6	-5.4 $\pm$ 3.3	-1.1 $\pm$ 0.3	n.d.	-2.6 $\pm$ 0.8
223	14.0 $\pm$ 0.4	8.9 $\pm$ 1.2	2.1 $\pm$ 0.1	1.1 $\pm$ 0.2	1.2	1.3 $\pm$ 0.7
224	10.4 $\pm$ 0.4	9.3 $\pm$ 0.2	1.0 $\pm$ 0.6	0.8 $\pm$ 0.1	0.0	0.5 $\pm$ 0.6
225	12.7 $\pm$ 0.1	9.3 $\pm$ 0.1	3.6 $\pm$ 0.3	2.0 $\pm$ 0.5	0.5	2.1 $\pm$ 0.5
226	8.6 $\pm$ 0.5	4.2 $\pm$ 0.9	-1.5 $\pm$ 1.6	0.0 $\pm$ 0.2	n.d.	-0.5 $\pm$ 1.5
227	9.8 $\pm$ 0.2	9.0 $\pm$ 0.5	2.0 $\pm$ 0.2	1.1 $\pm$ 0.4	-0.1	0.6 $\pm$ 0.5
228	13.2 $\pm$ 0.3	n.d.	2.1 $\pm$ 0.3	0.1 $\pm$ 0.2	2.3	1.6 $\pm$ 0.2
230	12.6 $\pm$ 0.3	n.d.	2.3 $\pm$ 0.1	1.2 $\pm$ 0.2	2.1	1.8 $\pm$ 0.5
229	5.6 $\pm$ 0.3	n.d.	0.1 $\pm$ 0.0	0.1 $\pm$ 0.0	0.4	-0.1 $\pm$ 0.3
232	14.1 $\pm$ 0.4	n.d.	4.6 $\pm$ 0.2	2.4 $\pm$ 0.4	4.8	2.7 $\pm$ 0.2
231	14.7 $\pm$ 0.5	n.d.	4.6 $\pm$ 0.2	2.4 $\pm$ 0.2	2.7	2.4 $\pm$ 0.8
233	14.4 $\pm$ 0.2	n.d.	4.9 $\pm$ 0.2	2.5 $\pm$ 0.0	n.d.	2.6 $\pm$ 0.3
234	10.1 $\pm$ 0.5	n.d.	1.5 $\pm$ 0.0	2.0 $\pm$ 0.2	n.d.	n.d.
235	7.5 $\pm$ 1.1	n.d.	0.9 $\pm$ 0.0	1.1 $\pm$ 0.1	n.d.	n.d.



Table 15. (continued)

No.	$\Delta T_m^a$ [°C] $\pm$ SD, p38 $\alpha$	$\Delta T_m^b$ [°C] $\pm$ SD, p38 $\beta$	$\Delta T_m^b$ [°C] $\pm$ SD, DDR1	$\Delta T_m^b$ [°C] $\pm$ SD, DDR2	$\Delta T_m^c$ [°C] ZAK	$\Delta T_m^d$ [°C] $\pm$ SD, ABL1
236	6.8 $\pm$ 0.1	n.d.	0.4 $\pm$ 0.2	0.7 $\pm$ 0.1	n.d.	n.d.
237	7.3 $\pm$ 0.2	n.d.	1.1 $\pm$ 0.2	1.1 $\pm$ 0.1	n.d.	n.d.
238	1.9 $\pm$ 0.5	n.d.	-0.2 $\pm$ 0.0	0.0 $\pm$ 0.1	n.d.	n.d.
239	2.3 $\pm$ 0.3	n.d.	-0.7 $\pm$ 0.2	-0.4 $\pm$ 0.1	n.d.	n.d.
240	7.8 $\pm$ 1.2 <sup>d</sup>	4.7 $\pm$ 0.1	1.0 $\pm$ 0.4	0.7 $\pm$ 0.1	0.8	0.5 $\pm$ 0.1
241	3.5 $\pm$ 1.8	6.3 $\pm$ 0.7	-0.8 $\pm$ 0.7	0.0 $\pm$ 0.0	n.d.	-0.3 $\pm$ 1.4
246	5.1 $\pm$ 0.3	6.8 $\pm$ 2.4	-0.7 $\pm$ 0.3	-0.2 $\pm$ 0.1	n.d.	0.2 $\pm$ 2.2
242	14.7 $\pm$ 0.5	14.1 $\pm$ 0.0	3.9 $\pm$ 0.2	2.1 $\pm$ 0.2	3.5	2.1 $\pm$ 0.1
243	13.9 $\pm$ 0.4	12.9 $\pm$ 0.5	3.6 $\pm$ 0.5	2.1 $\pm$ 0.1	2.9	1.9 $\pm$ 0.3
244	12.6 $\pm$ 0.3	11.1 $\pm$ 0.5	3.1 $\pm$ 0.5	1.8 $\pm$ 0.3	2.5	1.7 $\pm$ 0.5
245	6.1 $\pm$ 2.1	6.8 $\pm$ 0.2	0.8 $\pm$ 0.2	0.5 $\pm$ 0.2	n.d.	0.4 $\pm$ 0.7
247	4.8 $\pm$ 0.2	3.6 $\pm$ 0.5	-0.1 $\pm$ 0.2	0.0 $\pm$ 0.0	-0.1	0.1 $\pm$ 0.1
248	3.1 $\pm$ 0.1	3.4 $\pm$ 0.1	-0.3 $\pm$ 0.3	0.0 $\pm$ 0.1	-0.2	0.3 $\pm$ 0.1
249	3.6 $\pm$ 0.1	3.4 $\pm$ 0.2	-0.3 $\pm$ 0.2	0.0 $\pm$ 0.0	-0.2	0.1 $\pm$ 0.1
250	6.0 $\pm$ 0.2	5.4 $\pm$ 0.4	-0.4 $\pm$ 0.4	0.0 $\pm$ 0.1	0.1	0.1 $\pm$ 0.2

<sup>a</sup>  $\Delta T_m$  were derived from four measurements, <sup>b</sup>  $\Delta T_m$  average of three measurements, <sup>c</sup>  $\Delta T_m$  single measurement, <sup>d</sup>  $\Delta T_m$  average of two measurements, 10  $\mu$ M compound; n.d. not determined or not interpretable. Measurement assisted by Martin Schröder, Deep Chatterjee, SCG Frankfurt or performed by Sebastian Mathea at the SGC Oxford in the case of ZAK.

For the compound library synthesized for the back-pocket optimization of p38 in **Chapter 4**, thermal stabilization of DDR1/2 was highest for compounds also showing highest  $\Delta T_m$  values for p38 $\alpha$ . A similar behavior was found for targets such as ZAK and ABL1. Overall, thermal protein stabilization of DDR1/2 kinase was determined to be lower for allosteric BIRB-fragments (compounds between **88-103**) in comparison with the obtained hit **218** (SR43,  $\Delta T_m$  [DDR1/2] = 4.4/ 2.2 °C) with a  $K_d$  value of 1.9/ 33 nM for DDR1 and DDR2, respectively. In this experiment, the highest temperature shifts for DDR1 ( $\Delta T_m > 4$  °C) were seen for compounds **218** (SR43), **231-233**, showing slightly reduced affinity for p38 $\alpha$ . The amino-piperidine back-pocket decorations of compounds **231-233** (structures depicted in **Table 11**) were therefore considered as most useful for the synthesis of new DDR1/2 inhibitors.

Table 16. Summary of thermal shift assays for the Mercachem compound library (**Chapter 3**), screened at 10  $\mu$ M against the main targets of **218** (SR43).

No.	$\Delta T_m^a$ [°C] $\pm$ SD, p38 $\alpha$	$\Delta T_m^b$ [°C] $\pm$ SD, p38 $\beta$	$\Delta T_m^c$ [°C] DDR1	$\Delta T_m^c$ [°C] ZAK	$\Delta T_m^c$ [°C] ABL1
MCP-001	2.3 $\pm$ 0.4	1.4 $\pm$ 0.4	0.0	0.7	0.2
MCP-002	1.8 $\pm$ 0.3	0.5 $\pm$ 0.2	0.1	0.3	0.9
MCP-003	2.3 $\pm$ 0.4	1.6 $\pm$ 0.2	0.3	0.3	0.4
MCP-004	3.9 $\pm$ 0.6	3.0 $\pm$ 0.4	0.2	-0.1	0.6
MCP-005	1.1 $\pm$ 0.2	0.6 $\pm$ 0.3	0.4	0.1	0.2
MCP-006	1.5 $\pm$ 0.2	1.2 $\pm$ 0.2	0.5	0.3	0.5
MCP-007	2.6 $\pm$ 0.3	2.1 $\pm$ 0.2	0.3	0.1	0.5
MCP-008	1.9 $\pm$ 0.3	1.2 $\pm$ 0.2	0.6	0.2	0.9
MCP-009	2.8 $\pm$ 0.4	1.6 $\pm$ 0.2	1.3	0.9	1.4

Table 16. (continued)

No.	$\Delta T_m^a$ [°C] $\pm$ SD, p38 $\alpha$	$\Delta T_m^b$ [°C] $\pm$ SD, p38 $\beta$	$\Delta T_m^c$ [°C] DDR1	$\Delta T_m^c$ [°C] ZAK	$\Delta T_m^c$ [°C] ABL1
MCP-010	13.0 $\pm$ 0.7	12.5 $\pm$ 0.6	5.4	7.3	4.0
MCP-011	15.4 $\pm$ 0.4 <sup>b</sup>	n.d.	0.4	0.3	0.4
MCP-012	6.8 $\pm$ 0.4	5.2 $\pm$ 1.7	2.5	0.1	3.2
MCP-013	1.0 $\pm$ 0.3	0.2 $\pm$ 0.3	-0.1	0.4	0.2
MCP-014	1.3 $\pm$ 0.3	0.6 $\pm$ 0.3	-0.1	0.2	0.5
MCP-015	9.5 $\pm$ 1.1	8.0 $\pm$ 1.2	1.5	2.5	1.7
MCP-016	5.2 $\pm$ 0.5	1.2 $\pm$ 0.3	0.0	0.9	1.0
MCP-017	5.4 $\pm$ 0.4	1.6 $\pm$ 0.3	0.1	0.7	1.0
MCP-018	9.6 $\pm$ 1.1	3.6 $\pm$ 0.5	1.4	1.3	1.1
MCP-019	1.4 $\pm$ 0.3	0.2 $\pm$ 0.4	-0.2	0.3	0.7
MCP-020	2.7 $\pm$ 0.3	0.5 $\pm$ 0.3	0.4	0.2	0.8
MCP-021	6.7 $\pm$ 0.8	2.5 $\pm$ 0.4	0.0	0.1	0.7
MCP-022	2.2 $\pm$ 0.8	1.0 $\pm$ 0.4	0.4	0.1	0.7
MCP-023	2.1 $\pm$ 1.0	0.1 $\pm$ 1.0	1.3	0.7	-0.4
MCP-024	0.7 $\pm$ 1.0	-0.7 $\pm$ 0.7	3.3	1.8	-0.7
MCP-025	5.0 $\pm$ 1.2	3.6 $\pm$ 1.2	2.8	3.6	0.3
MCP-027	-0.4 $\pm$ 0.2	-0.6 $\pm$ 0.3	0.7	-0.9	0.1
MCP-028	4.7 $\pm$ 0.8	3.7 $\pm$ 0.8	0.5	1.2	1.1
MCP-029	1.1 $\pm$ 0.2	-0.3 $\pm$ 0.2	0.0	0.4	0.7
MCP-030	1.9 $\pm$ 0.2	0.5 $\pm$ 0.4	0.2	0.9	0.3
MCP-031	5.0 $\pm$ 0.6	3.5 $\pm$ 1.3	1.2	1.4	1.1
MCP-032	9.8 $\pm$ 0.6	10.6 $\pm$ 0.6	3.2	4.6	3.5
MCP-033	12.2 $\pm$ 0.6	13.0 $\pm$ 0.7	2.1	3.6	0.8
MCP-034	6.5 $\pm$ 0.5	7.2 $\pm$ 0.6	1.6	1.3	0.6
MCP-035	3.0 $\pm$ 0.5	3.0 $\pm$ 0.5	0.8	0.4	0.7
MCP-036	-0.1 $\pm$ 0.7	-1.0 $\pm$ 0.7	0.9	2.4	-0.3
MCP-037	0.1 $\pm$ 0.9	-0.9 $\pm$ 0.5	1.1	2.4	-0.7
MCP-038	0.0 $\pm$ 0.5	-0.8 $\pm$ 0.5	0.2	2.3	-0.3
MCP-039	n.d.	-1.0 $\pm$ 0.3	2.9	3.9	0.4
MCP-040	n.d.	n.d.	4.6	4.7	6.0
MCP-041	14.8 $\pm$ 0.6	n.d.	3.0	4.7	1.2
MCP-042	7.5 $\pm$ 1.7	6.7 $\pm$ 1.9	4.3	6.5	0.6
MCP-043	4.6 $\pm$ 1.5	n.d.	1.4	-0.9	1.3
MCP-044	4.2 $\pm$ 0.8	n.d.	2.0	1.4	0.0
MCP-045	6.7 $\pm$ 1.4	4.9 $\pm$ 0.7	3.3	2.1	0.1
MCP-046	1.6 $\pm$ 0.4	0.2 $\pm$ 0.8	0.3	0.7	0.1
MCP-047	0.5 $\pm$ 0.3	-0.1 $\pm$ 0.8	4.4	2.6	0.1
MCP-048	0.6 $\pm$ 0.2	0.1 $\pm$ 0.3	0.9	-0.1	0.0
MCP-049	1.5 $\pm$ 0.3	0.5 $\pm$ 0.3	2.2	0.4	0.3
MCP-050	0.7 $\pm$ 0.2	0.0 $\pm$ 0.2	-0.2	0.1	0.3
MCP-051	1.4 $\pm$ 0.2	0.7 $\pm$ 0.2	0.0	0.5	0.1

Table 16. (continued)

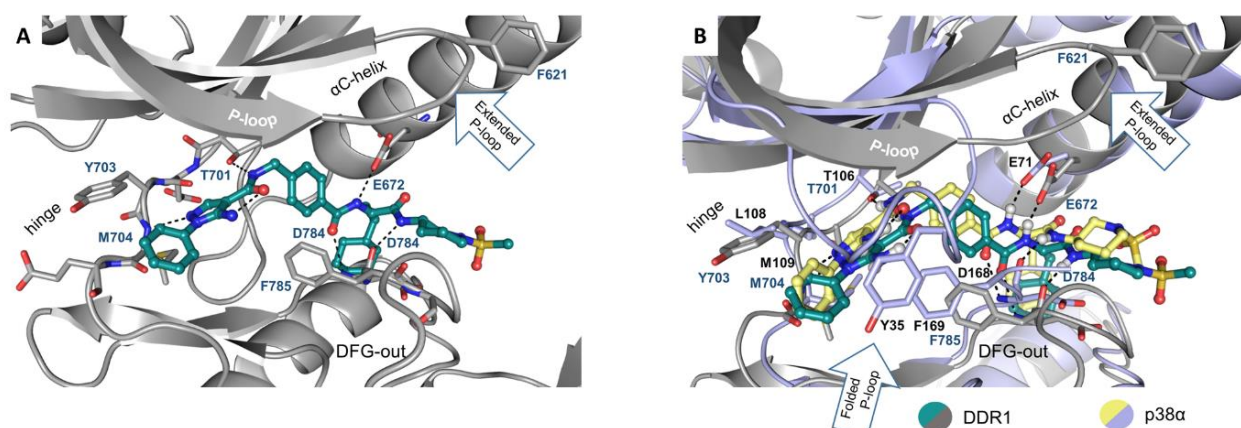
No.	$\Delta T_m^a$ [°C] $\pm$ SD, p38 $\alpha$	$\Delta T_m^b$ [°C] $\pm$ SD, p38 $\beta$	$\Delta T_m^c$ [°C] DDR1	$\Delta T_m^c$ [°C] ZAK	$\Delta T_m^c$ [°C] ABL1
MCP-052	3.6 $\pm$ 0.4	2.5 $\pm$ 0.3	0.4	0.6	0.2
MCP-053	3.0 $\pm$ 0.4	2.2 $\pm$ 0.3	0.4	0.1	0.1
MCP-054	0.0 $\pm$ 0.2	-0.2 $\pm$ 0.3	0.6	0.3	0.2
MCP-055	0.3 $\pm$ 0.1	-0.1 $\pm$ 0.2	0.4	0.5	0.1
MCP-056	0.4 $\pm$ 0.2	0.1 $\pm$ 0.4	0.4	0.0	0.1
MCP-057	0.6 $\pm$ 0.1	-0.1 $\pm$ 0.2	0.5	0.2	0.1
MCP-058	1.4 $\pm$ 0.3	0.5 $\pm$ 0.4	0.3	0.4	0.0
MCP-059	0.3 $\pm$ 0.1	0.0 $\pm$ 0.3	-0.1	-0.1	0.0
MCP-060	0.0 $\pm$ 0.1	0.0 $\pm$ 0.3	-0.2	-0.2	0.1
MCP-061	0.5 $\pm$ 0.2	0.2 $\pm$ 0.2	-0.2	0.0	0.1
MCP-062	0.0 $\pm$ 0.1	-0.3 $\pm$ 0.2	-0.4	0.3	0.1
MCP-063	0.2 $\pm$ 0.1	-0.1 $\pm$ 0.2	-0.5	-0.1	0.4
MCP-064	0.9 $\pm$ 0.1	0.0 $\pm$ 0.1	-0.2	0.0	0.1
MCP-065	0.8 $\pm$ 0.2	0.1 $\pm$ 0.3	0.2	0.7	0.3
MCP-066	1.1 $\pm$ 0.2	0.5 $\pm$ 0.1	0.5	1.0	0.6
MCP-067	1.4 $\pm$ 0.2	0.4 $\pm$ 0.3	0.4	0.0	0.2
MCP-068	0.6 $\pm$ 0.2	0.4 $\pm$ 0.3	0.5	0.0	0.3
MCP-069	3.6 $\pm$ 0.5	3.9 $\pm$ 0.3	1.8	1.7	1.9
MCP-070	8.6 $\pm$ 0.9	9.1 $\pm$ 0.5	3.1	3.7	3.8
MCP-071	9.8 $\pm$ 0.8	9.6 $\pm$ 0.5	0.1	-0.2	0.2
MCP-072	2.7 $\pm$ 0.4	2.1 $\pm$ 0.3	-0.2	0.2	0.1
MCP-073	5.6 $\pm$ 0.7	7.0 $\pm$ 0.6	3.8	2.4	6.2
MCP-074	10.9 $\pm$ 0.8	12.5 $\pm$ 0.8	5.3	4.3	8.8
MCP-075	14.8 $\pm$ 0.4	14.0 $\pm$ 0.7	-0.8	3.5	2.2
MCP-076	1.2 $\pm$ 0.1	0.7 $\pm$ 0.2	-0.5	0.1	0.2
MCP-077	2.5 $\pm$ 0.3	1.2 $\pm$ 0.1	0.5	0.7	0.4
MCP-078	4.1 $\pm$ 0.6	1.6 $\pm$ 0.2	1.1	0.9	0.5
MCP-079	2.9 $\pm$ 0.4	1.6 $\pm$ 0.2	0.3	-0.1	0.2
MCP-081	8.3 $\pm$ 0.9	5.5 $\pm$ 1.3	4.9	3.6	3.9
MCP-082	2.8 $\pm$ 0.7	1.4 $\pm$ 0.3	0.7	0.8	0.5

<sup>a</sup>  $\Delta T_m$  were derived from seven measurements, <sup>b</sup>  $\Delta T_m$  average of six measurements, <sup>c</sup>  $\Delta T_m$  single measurements, 10  $\mu$ M compound; n.d. not determined or strange curve. Measurement assisted by Martin Schröder, SCG Frankfurt or performed by Sebastian Mathea at the SGC Oxford in the case of DDR1, ZAK and ABL1.

For the compound library donated by *Mercachem* highest thermal shifts ( $\Delta T_m > 4$  °C) were each calculated for the lead structure VPC-00628 (MCP-010), MCP-040, MCP-042, MCP-047, MCP-074 as well as MCP-081 (for structures see experimental part **Section 8.3.1**). In this screen, VPC-00628 (MCP-010) and MCP-074 showed **218** (SR43)-like off-target activity on all five targets investigated. Besides DDR1 affinity, MCP-040 also displayed thermal stabilization of ZAK and ABL1. However,  $\Delta T_m$  values for p38 $\alpha/\beta$  could not be determined, because ambiguous curves were obtained. Compound MCP-042 led to a robust stabilization of DDR1 kinase ( $\Delta T_m = 4.3$  °C) and also showed the highest thermal shift for ZAK ( $\Delta T_m = 6.5$  °C). The affinity for p38 $\alpha/\beta$  was slightly reduced in comparison with **218** (SR43), which may be due to the CF<sub>3</sub>-decorated

pyrazole hinge-binding motif. The latter plays an important role in engaging the P-loop in a folded conformation, as confirmed by crystal structure determination of MCP-042 in complex with p38 $\alpha$  (Section 3.2, Figure 23). Interestingly, MCP-047 was the only compound in this library that showed improved stabilization of DDR1 ( $\Delta T_m = 4.4$  °C), with negligible temperature shifts for all other kinase targets investigated. MCP-047 and VPC-00628 are of similar back-pocket decoration, but differ in their hinge-binding head group, which is a 3-phenyl-1*H*-pyrazole-5-carboxamide moiety in the case of MCP-047. This building block might therefore be useful as hinge binding moiety to synthetically optimize **218** (SR43) toward DDR1/2 kinase. The chimera of VPC-00628 and BIRB-796, MCP-081, discussed in Chapter 3 and Section 4.3.1 because of its increased  $\alpha$ -isoform selectivity, showed a slight preference for DDR1 kinase in the thermal shift assays ( $\Delta T_m = 5.3$  °C). However, as BIRB-like fragments were evaluated in DSF assays before (Table 15) and appeared to be suboptimal for improving activity toward DDR1/2, the sulfonamide, cyclopropylamide or oxetane decorated 3-amino piperidines **231-233** might be better suited for targeting the back pocket of DDR1/2 kinase. Since the synthesis of the sulfonamide decoration (**232**) was carried out with excellent yields and purification procedures were more convincing, this moiety was considered as optimal building block for targeting the DDR1/2 back pocket.

Next, **232** (SR159) was crystallized in complex with DDR1 kinase in collaboration with Daniel Pinkas from SGC in Oxford (Figure 40A). To compare binding modes and reveal potential DDR1 kinase selectivity sites, this structure was superimposed onto the crystal structure of **232** (SR159, Section 4.5.1) in complex with p38 $\alpha$  (Figure 40B).

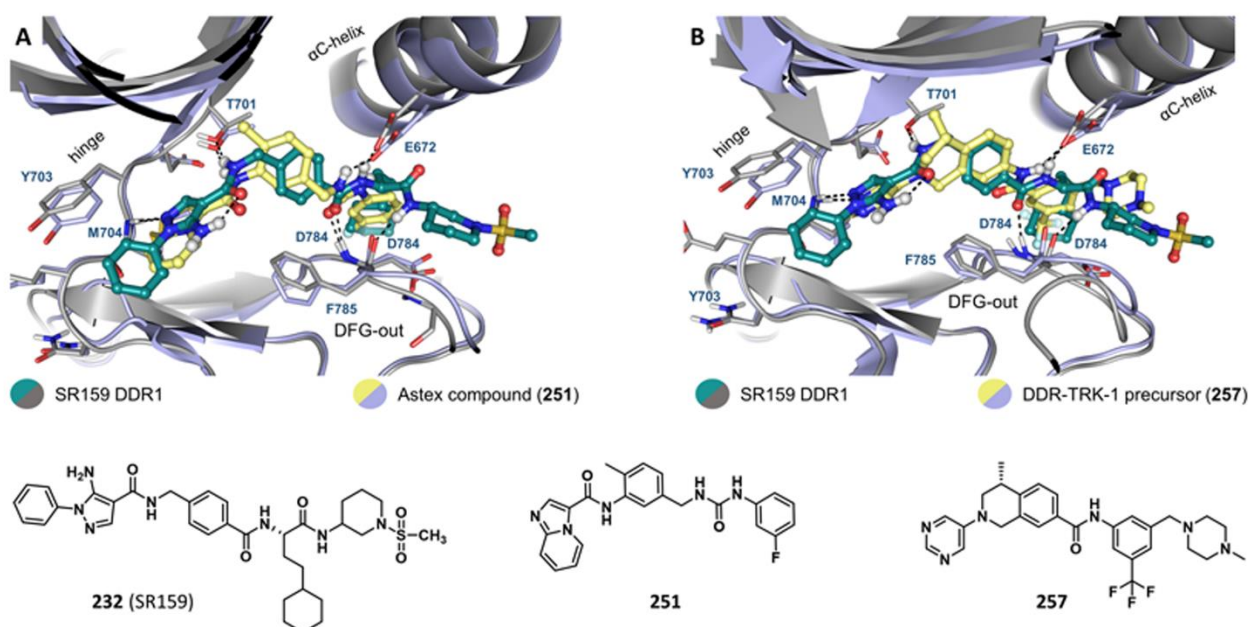


**Figure 40. Difference in binding mode of **232** (SR159) in DDR1 and p38 $\alpha$ .** A) **232** (SR159)/DDR1 kinase complex; inhibitor depicted in stick and ball representation (teal). B) Structure alignment of **232** (SR159)/DDR1 kinase complex (gray, inhibitor in teal) and **232** (SR159)/p38 $\alpha$  (light blue, inhibitor in yellow). Hydrogen bonds are highlighted as black dashes; important structural motifs are labeled (blue for DDR1 and black for p38 $\alpha$ ). Crystallization and structure determination of **232** (SR159) in p38 $\alpha$  was done by Martin Schröder and Andreas Joerger, Frankfurt and in DDR1 by Daniel Pinkas, Oxford.

Although, both kinases derive from different families (DDR1 = receptor tyrosine kinase, p38 $\alpha$  = CMGC family member) and thus share low sequence identity, key interactions with the inhibitor are conserved, e.g., the interaction with the methionine in the hinge, the conserved aspartate-glutamate pair in the allosteric site and the gatekeeper residue tyrosine. While **232** (SR159) engaged the P-loop in a folded conformation in p38 $\alpha$  via Tyr35, a typically found extended glycine-rich loop was observed in complex with DDR1. As Phe169 from the DFG-motif participated in the P-loop folding process in p38 $\alpha$  via aromatic site-on stacking interactions, the DFG-motif adopted a slightly different orientation in both kinases. However, inhibitor binding in a type-II mode, to the inactive DFG-out conformation, was observed for both structures determined, where the cyclohexyl moiety protruded into the allosteric deep pocket. There was only weak

electron density for sulfonamide moiety, suggesting that it is flexible and does not form specific interactions with the protein, or adopts alternative binding modes. When comparing differences in the protein structures that might be exploited for optimization of **232** (SR159), toward a stronger inhibitory effect on DDR1 kinase, the hinge region seemed to be attractive because of Tyr703 (p38 $\alpha$  has Leu108 at this position). The aromatic side chain can be targeted to improve hydrophobic interactions, e.g., by replacing the pyrazole moiety of **232** (SR159) by a better suited heterocycle. Furthermore, as the folded P-loop conformation in **232** (SR159) contributed to inhibitor potency and selectivity, diminishing  $\pi$ -stacking interactions between Tyr35, Phe169 and the phenyl moiety of **232** (SR159) might help to reduce the affinity for p38 $\alpha$  MAPK.

To identify the most promising hinge-binding building blocks, visual inspection of all inhibitors crystallized in complex with DDR1 kinase and published in the KLIFs database (<https://klifs.vu-compmedchem.nl/>), was performed. Thus, a set of 19 structures were compared with the **232** (SR159) structure to potentially reveal differences in inhibitor binding and shape complementarity. The published, most similar compounds were **251** from *Astex Pharmaceuticals* and the DDR-TRK-1 precursor **257** (Figure 41).



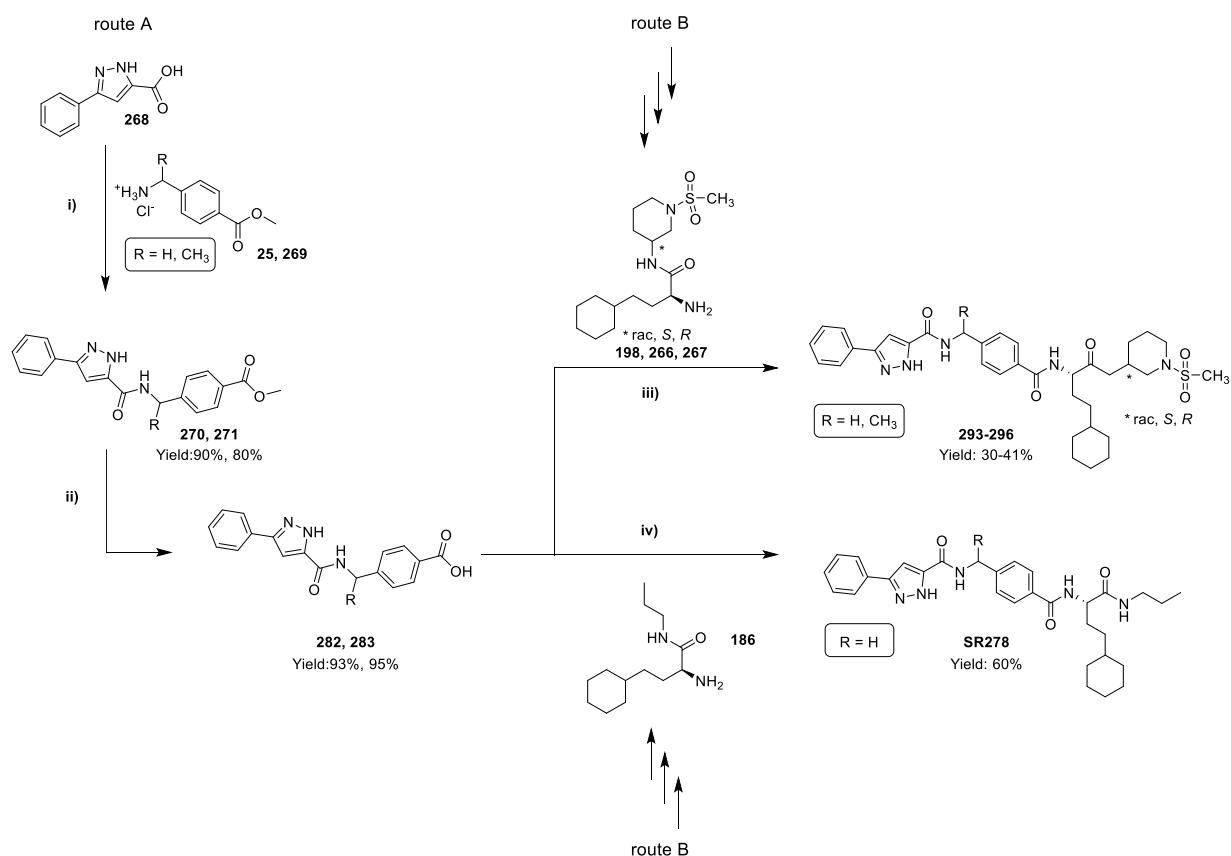
**Figure 41. Shape similarities of published DDR1 kinase inhibitors with **232** (SR159).** A) Alignment of **232** (SR159, teal) and Astex compound **251** (yellow, PDB: 5BVN). B) Alignment of **232** (SR159, teal) with DDR-TRK-1 precursor **257** (yellow, PDB: 5FDX). Hydrogen bonds are highlighted as black dashed lines. Important structural motifs are labeled. Crystallization and structure determination of **232** (SR159) in DDR1 kinase was done by Daniel Pinkas, Oxford.

Although of completely different scaffold, **251** showed very high shape similarities with **232** (SR159), such as in the hinge, linker and DFG-out pocket regions. Furthermore, **251** was of an overall smaller size and did not contain an allosteric solvent-exposed sulfonamide decoration. For polar contacts with Met704 in the hinge region, Astex compound **251** used a bicyclic imidazo[1,2-*a*]pyridine moiety. The flat geometry of the heterocycle enabled weak face-to-face  $\pi$ -interactions with Tyr703. In **232** (SR159) an orthogonal geometry between the pyrazol-phenyl decoration was observed, which partially extended into the front-pocket area. Changing the hinge-binding head group of **232** (SR159) to an imidazo[1,2-*a*]pyridine moiety might therefore help to improve potency toward DDR1 kinase. The alignment of DDR1-TRK-1 precursor **257** and **232** (SR159) highlighted shape similarities in the allosteric DFG-out pocket region and the solvent-exposed region. Although the 1,2,3,4-tetrahydroisoquinoline moiety in **257** is more rigid, both chemical scaffolds adopted a similar geometry in the linker and hinge region. The DDR1-TRK-1 precursor (**257**) formed hydrogen bonds

with Met704 via its pyrimidine heterocycle nitrogen atom. Similar to Astex compound **251**, **257** was also shorter than **232** (SR159) in this ATP-pocket region. Furthermore, both database-derived compounds harbored a methyl decoration in the linker part that targeted the hydrophobic pocket behind the gatekeeper residue Thr701. Thus, the introduction of a methyl group to the benzyl linker of **232** (SR159) may also improve DDR1/2 kinase activity.

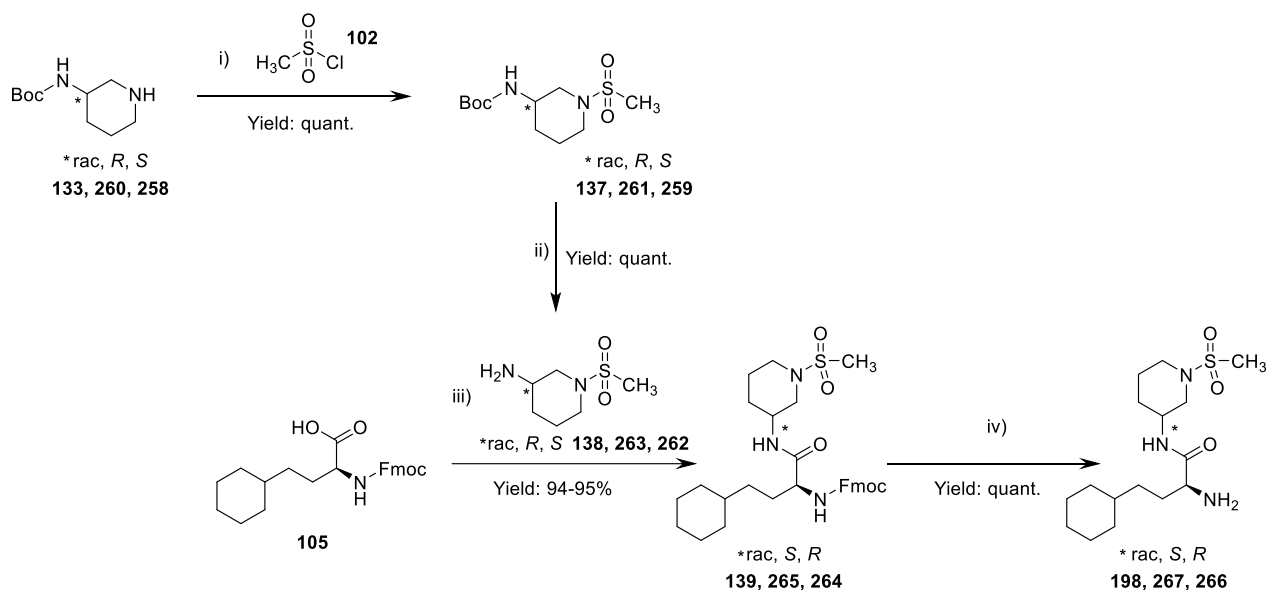
### 5.3 Chemistry

Similar to the synthesis of the modified VPC-00628 derivatives in **Section 4.4 (Scheme 15)**, a convergent synthesis route was developed for the preparation of various 3-phenyl-1*H*-pyrazole derivatives. In part A of the synthesis route, 3-phenyl-1*H*-pyrazole-5-carboxylic acid (**268**) was reacted with methyl 4-(aminomethyl)benzoate hydrochloride (**25**) or methyl 4-(1-aminoethyl)benzoate hydrochloride (**269**) in an amide coupling reaction. For this purpose, the optimized reaction described in **Section 4.4.2** using EDC-HCl and HOBT was selected. The reaction also proved to be optimal for these building blocks, since compounds **270** and **271** were obtained in a high yield of 90% and 80%, respectively. In the second step, the methyl ester was cleaved with LiOH in THF/H<sub>2</sub>O. The carboxylic acids **282** and **283** were obtained in excellent yields (93%, 95%) by the precipitation with hydrochloric acid. These molecules were then reacted with the corresponding building blocks for the allosteric back pocket (**198**, **266**, **267**, **186**), which were synthesized in part B of this convergent synthesis route. The previously modified amide coupling reaction with HATU and DIPEA in DMF (**Section 4.4.3**) was also used, and the compounds **293-297** were obtained in yields between 30% and 60%.



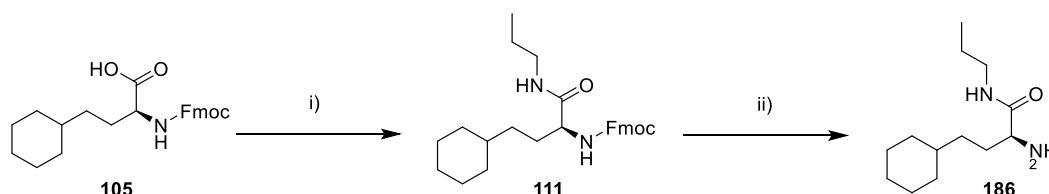
**Scheme 15. Convergent synthetic route for 3-phenyl-1*H*-pyrazole derivatives.** Reagents and conditions: i) EDC-HCl, HOBT, DIPEA, DMF, RT; ii) LiOH, THF/H<sub>2</sub>O, RT; iii) and iv) HATU, DIPEA, DMF, RT.

The components used to optimize the back pocket were prepared in four steps (route B) in the case of the 2-amino-4-cyclohexyl-*N*-(1-(methanesulfonyl)piperidin-3-yl)butanamide derivatives **198**, **267**, **266** (Scheme 16) or in two steps in the case of (*S*)-2-amino-4-cyclohexyl-*N*-propylbutanamide (**186**) (Scheme 17).



**Scheme 16.** Convergent synthetic route B for the preparation of the amines (**198**, **267**, **266**). Reagents and conditions: i) TEA, DCM,  $-20^{\circ}\text{C} \rightarrow \text{RT}$ . ii) TFA, DCM,  $0^{\circ}\text{C} \rightarrow \text{RT}$ ; iii) HATU, DIPEA, DMF, RT. iv) Piperidine, DMF, RT. Stereo center marked with an asterisk.

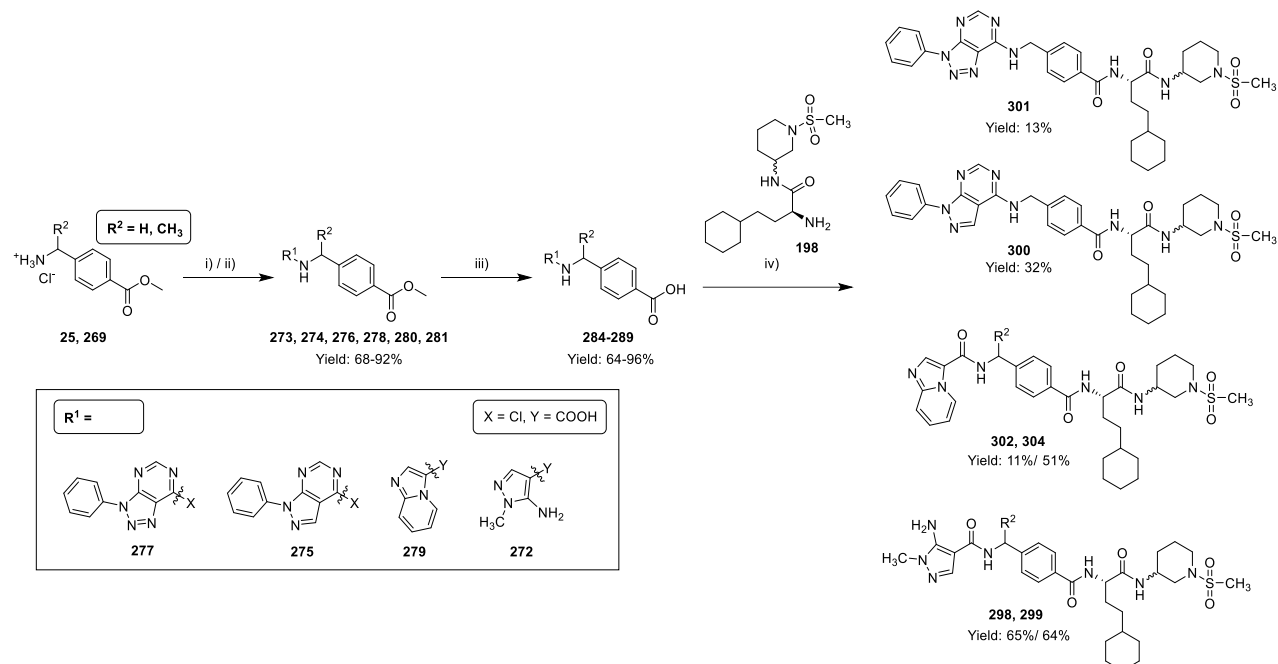
The corresponding substituted 3-amino piperidines used in amide coupling reaction were synthesized as described before (Section 4.4.3, Scheme 12). Besides racemic *tert*-butyl piperidin-3-ylcarbamate (**133**), enantiomeric pure (*R,S*) amines **260** and **258** were also used as starting material for optimizing DDR1/2 allosteric back-pocket interactions (Scheme 16). For introducing a sulphonamide decoration, **133**, **260** or **258** were each reacted with methanesulfonyl chloride (**102**) under basic conditions. After purifying and analyzing the compounds, the Boc-protecting group was removed with trifluoroacetic acid in methylene chloride. These building blocks were then reacted with Fmoc-homocyclohexyl-L-alanine (**105**). The carboxylic acid functionality was pre-activated with HATU and DIPEA, and the corresponding amine **138**, **263** or **262** was added. After purification, all compounds were obtained in excellent yields between 94-95%. In the fourth step, the Fmoc-protecting group was removed with piperidine, and the crude product was directly reacted with 4-(1-(3-phenyl-1*H*-pyrazole-5-carboxamido)ethyl)benzoic acid (**282**) or 4-((3-phenyl-1*H*-pyrazole-5-carboxamido)methyl)benzoic acid (**283**). The synthesis of (*S*)-2-amino-4-cyclohexyl-*N*-propylbutanamide (**111**) was analogously performed as described in Section 4.4.3 (Scheme 17).



**Scheme 17.** Convergent synthetic route B for the preparation of the amine (**186**). Reagents and conditions: i) HATU, DIPEA, DMF, RT. ii) Piperidine, DMF, RT.

For optimal hinge binding, various heterocycles were considered for the synthesis of new DDR1/2 inhibitors. In the following, the sulphonamide decoration was, therefore, retained, and compounds with heterocyclic head groups such as pyrazolo[3,4-*d*]pyrimidines, triazolo[4,5-*d*]pyrimidines, imidazo[1,2-*a*]pyridines or 5-

amino-1-methyl-1*H*-pyrazoles were synthesized (**Scheme 18**). To bridge the aminopyrazole functionality with the adjacent carbonyl carbon atom in **232** (SR159) and to stabilize the hinge binder in this region, 4-chloro-1-phenyl-1*H*-pyrazolo[3,4-*d*]pyrimidine (**275**) and 7-chloro-3-phenyl-3*H*-[1,2,3]triazolo[4,5-*d*]pyrimidine (**277**) were each reacted in a nucleophilic aromatic substitution with methyl 4-(aminomethyl)benzoates hydrochloride (**25**). The electron poor nature of the two heteroaromatics strongly favored the nucleophilic addition and subsequent elimination of chloride. As a result, compounds **276** and **278** were obtained in a very high yield of 92% and 83%, respectively.

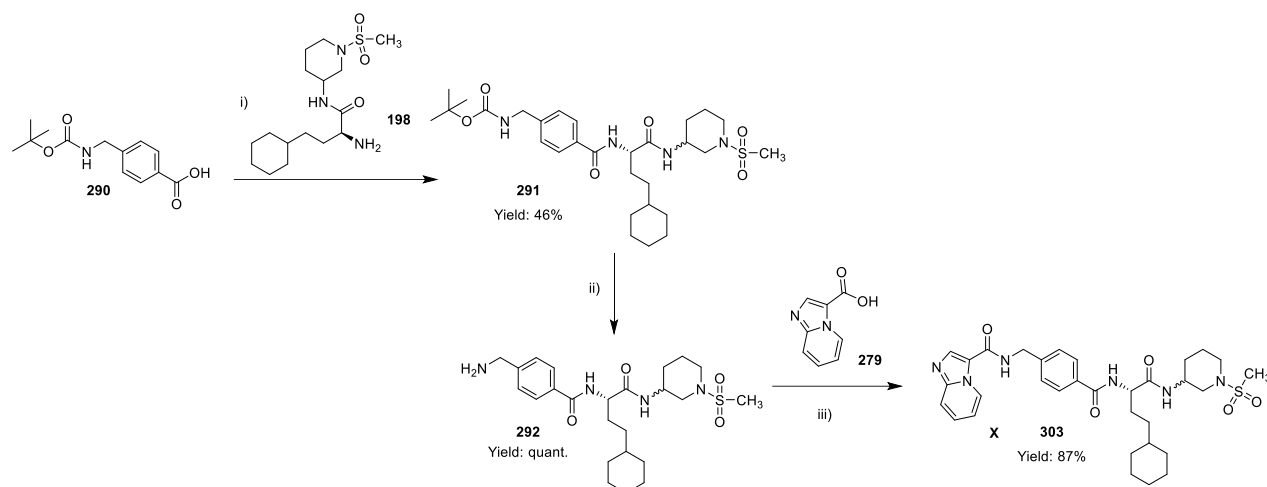


**Scheme 18.** Synthetic route for the preparation compounds (**298-302, 304**). Reagents and conditions: i) for nucleophilic substitution of  $X$ : DIPEA, THF, 60 °C. ii) For carboxylic acid  $Y$ : EDC-HCl, HOBT, DIPEA, DMF, RT. iii) LiOH, THF/H<sub>2</sub>O, RT; iv) HATU, DIPEA, DMF, RT.

In order to increase the potency against DDR1/2 kinase, the hinge-binding motif of the previously published *Astex* compound **251** was used for the synthesis of two imidazo[1,2-*a*]pyridine derivatives. The carboxylic acid of imidazo[1,2-*a*]pyridine-3-carboxylic acid (**279**) was first deprotonated with DIPEA and converted to an active ester with EDC-HCl and HOBT. After this pre-activation, the respective amine **25** or **269** was added to form an amide bond. After purification of the crude products, the two esters, methyl 4-((imidazo[1,2-*a*]pyridine-3-carboxamido)methyl)benzoate (**280**) and methyl 4-(1-(imidazo[1,2-*a*]pyridine-3-carboxamido)ethyl)benzoate (**281**), were obtained in a yield of 88% and 73%. For the synthesis of an aminopyrazole derivative, 5-amino-1-methyl-1*H*-pyrazole-4-carboxylic acid (**272**) was reacted analogously in an amide-coupling reaction with the aforementioned reagents as well as amines to the respective esters **274** and **273**. Following these syntheses, all previously prepared esters were hydrolyzed with LiOH to obtain the free carboxylic acids **284-289** in good to excellent yields (64%-96%). The synthesis of the final products **298-302** and **304** was performed as described for the amide coupling in **Scheme 15**. The corresponding carboxylic acids were pre-activated with HATU, and each was reacted with the previously synthesized amine (*S*)-2-amino-4-cyclohexyl-*N*-((*S*)-1-(methylsulfonyl)piperidin-3-yl)butanamide (**198**). After purification, the compounds **298-302** and **304** were obtained in poor to fair yields (11-65%). To improve the reaction and the overall yields, which were especially poor in the case of **301** and **302**, a different synthetic approach was established. In this synthetic route, the back-pocket decoration was synthesized first starting from 4-(((*tert*-butoxycarbonyl)amino)methyl)benzoic acid (**290**), which was coupled to (*S*)-2-amino-4-cyclohexyl-*N*-((*S*)-



1-(methylsulfonyl)piperidin-3-yl)butanamide (**198**). Amide-bond formation was again performed with HATU and DIPEA, and the final product **291** was obtained with a reasonable yield (46%).



**Scheme 19. Back-to-front approach for the preparation compound 303.** Reagents and conditions: i) HATU, DIPEA, DMF, RT. ii) TFA, DCM, 0 °C → RT. iii) HATU, DIPEA, DMF, RT.

The Boc-protecting group was removed with trifluoroacetic acid in methylene chloride to yield the amine, 4-(aminomethyl)-*N*-((*S*)-4-cyclohexyl-1-((*S*)-1-(methylsulfonyl)piperidin-3-yl)amino)-1-oxobutan-2-yl)benzamide (**292**), a very versatile building block allowing the introduction of various hinge-binding head groups. By performing an amide coupling reaction with imidazo[1,2-*a*]pyridine-3-carboxylic acid (**279**), HATU and DIPEA in *N,N*-dimethylformamide, compound **303**, synthesized before in **Scheme 18**, was obtained in a very good yield of 87%. To enrich the compound library, this method would therefore be the preferred choice for the synthesis of novel derivatives.

## 5.4 Results

### 5.4.1 Structure-activity relationship

To validate the  $\Delta T_m$  values determined for the inhibitors targeting the allosteric back pocket (**Section 5.2**), *in cellulo* IC<sub>50</sub> values of compounds **218**, **219**, **232**, **231** and **233** for p38 $\alpha$  as well as DDR1 and DDR2 kinase were determined (**Table 17**). Although nanomolar potencies were found for p38 $\alpha$ , IC<sub>50</sub> values for DDR1 and DDR2 were collectively higher in the cellular environment. For **218** (SR43) an about 43-fold and 60-fold higher IC<sub>50</sub> value was determined *in cellulo* compared with the K<sub>d</sub> values on isolated enzyme by DiscoverX. Differences in potency observed intracellularly compared with K<sub>d</sub> values determined on isolated enzyme are not surprising, given that NanoBRET™ assays usually measure kinase activity of the full-length proteins. While p38 MAPK is a soluble serine/threonine kinase, DDR kinase belongs to the family of receptor tyrosine kinases as described earlier. Enzyme activity of both kinases is dependent on the ATP concentration, which is typically about 10 mM intracellularly, and also on the stimulation by their upstream targets. DDR1/2 kinase was found to exist mostly in its inactive state if not stimulated by its extracellular collagen ligands. The low cellular activity of DDR1/2 kinase is also caused by its intrinsic autoinhibitory YxxxYY-motif, in which Tyr755 controls the autoinhibitory state by phosphorylation.<sup>465</sup> A similar structural motif has previously been described for the insulin-receptor tyrosine kinase, in which phosphorylation on tyrosine reverses autoinhibition and thus enables catalytic activity.<sup>474, 497</sup> Another molecular mechanism discussed for the

unexpected low DDR1/2 kinase activity inside the cell is a rarely seen salt bridge between Asp671 ( $\alpha$ D helix) and Arg752 (A-loop), which stabilizes the DFG-out conformation of these kinases.<sup>498</sup> The structural stabilization impairs the formation of a catalytically active DFG-in conformation and subsequent ATP-binding. The latter is probably also the reason why crystal structures of DDR1 kinase in complex with type-I inhibitors always showed the inactive DFG-out form. Interestingly, this salt bridge between Asp and Arg was seen also in six other kinases, such as KIT, CSF1R, MEK5, YSK4, and PDGFRa/b, and is suggested to play a role in inhibitor promiscuity.<sup>485</sup>

Besides **218** (SR43), which is characterized best and thus serving as a control, back-pocket targeting moieties such as propyl and the amino-piperidine derivatives **232** (SR159), **231** and **233** were investigated in this study. Although potency for p38 $\alpha$  kinase was retained mostly for compound **SR61**, potencies for DDR1/2 kinase increased 3.2-fold and 1.3-fold upon addition of an additional carbon atom to **218** (SR43). As expected from the very similar  $\Delta T_m$  values obtained for the sulfonamide, cyclopropanamide and oxetane decorated amino piperidines, low nanomolar binding of p38 $\alpha$  was determined. While **232** (SR159) and **233** inhibited both DDR1/2 kinases with micromolar potencies, **231** showed the best potency in this series, with  $IC_{50}$  values of 1.31  $\mu$ M and 1.75  $\mu$ M for DDR1/2 kinase, respectively.

**Table 17. Back-pocket optimization.** Potency of compounds **218**, **219**, **231-233** determined by thermal shift and in cellulo  $IC_{50}$  values for p38 $\alpha$  and DDR1/2.

No.	Structure	$\Delta T_m^a$	$\Delta T_m^a$	$\Delta T_m^a$	$IC_{50}^b$	$IC_{50}^b$	$IC_{50}^b$
		[°C] $\pm$ SD p38 $\alpha$	[°C] $\pm$ SD DDR1	[°C] $\pm$ SD DDR2	[ $\mu$ M] $\pm$ SEM p38 $\alpha$	[ $\mu$ M] $\pm$ SEM DDR1	[ $\mu$ M] $\pm$ SEM DDR2
<b>218</b> (SR43)		16.4 $\pm$ 0.2	4.4 $\pm$ 0.1	5.1 $\pm$ 0.4	0.014 $\pm$ 0.006 <sup>f</sup>	4.19 $\pm$ 0.84	4.00 $\pm$ 0.72
<b>219</b>		13.7 $\pm$ 0.5	2.8 $\pm$ 0.2	3.8 $\pm$ 0.3	0.017 $\pm$ 0.003 <sup>d</sup>	13.6 <sup>c</sup>	5.25 $\pm$ 2.84 <sup>d</sup>
<b>232</b> (SR159)		14.1 $\pm$ 0.4	4.6 $\pm$ 0.2	4.8 $\pm$ 0.4	0.033 $\pm$ 0.002 <sup>e</sup>	2.37 $\pm$ 0.28 <sup>e</sup>	3.46 $\pm$ 0.32 <sup>e</sup>
<b>231</b>		14.7 $\pm$ 0.5	4.6 $\pm$ 0.2	5.4 $\pm$ 0.2	0.092 $\pm$ 0.004	1.31 $\pm$ 0.12 <sup>e</sup>	1.75 $\pm$ 0.10 <sup>e</sup>
<b>233</b>		14.4 $\pm$ 0.2	4.9 $\pm$ 0.1	5.8 $\pm$ 0.0	0.057 $\pm$ 0.002	2.43 $\pm$ 0.66 <sup>d</sup>	3.72 $\pm$ 0.30 <sup>d</sup>

<sup>a</sup>  $\Delta T_m$  average derived from seven replicates for p38 $\alpha$  and three replicates for DDR1/DDR2 at a compound concentration of 10  $\mu$ M;

<sup>b</sup> Cellular  $IC_{50}$  values determined by NanoBRET™ assay in HEK293T cells,  $IC_{50}$  values were derived from duplicates ( $n = 3$ ); <sup>c</sup>  $n = 1$ ; <sup>d</sup>  $n = 2$ ; <sup>e</sup>  $n = 4$ ; <sup>f</sup>  $n = 6$ . DSF-assay assisted by Martin Schröder and Deep Chatterjee. NanoBRET™ assay performed by Benedict-Tilman Berger.

Since the previously used hinge-binding motif seemed to be less optimal for DDR1/2 inhibition, further heterocyclic compounds were considered as head group, synthesized and subsequently investigated (Table 18). The sulfonamide decoration was left unchanged, and the hinge binder of **232** (SR159) was replaced by a 3-phenyl-1H-pyrazole isomer (compounds **293-297**). This structural element was already used in Chapter 2 for the synthesis of VPC-00628 derivatives, and investigations of the off-targets found for **218** (SR43) in the DSF assay (Table 16) showed that this heterocycle in compound MCP-047 resulted in preferred thermal stabilization of the DDR1/2. In order to find out whether the exact stereochemistry of the racemic aminopiperidine derivative **232** (SR159) plays a role in the binding to DDR kinases, enantiomerically pure (S)- and (R)-configured derivatives were synthesized and investigated. Upon visual inspection of published DDR kinase inhibitors, such as the Astex compound **251**, DDR-1-IN-1, DDR-1-IN-2 and the DDR-TRK-1 probe, it became apparent that all compounds contain a free methyl group targeting the hydrophobic pocket behind the gatekeeper area. In order to investigate the influence of this moiety on the inhibition behavior, an additional methyl group was incorporated into the benzyl linker of compounds **293**, **294** and **295**. In compound **297**, the sulfonamide decoration was finally replaced by a propyl residue to investigate the actual contribution of 3-phenyl-1H-pyrazole as a hinge binder and to exclude combinatorial miss-match effects.

**Table 18. Hinge-binder optimization A.** Enzymatic activity of compounds **293-297** determined by  $\Delta T_m$  and in cellulo  $IC_{50}$  values for p38 $\alpha$  and DDR1/2.

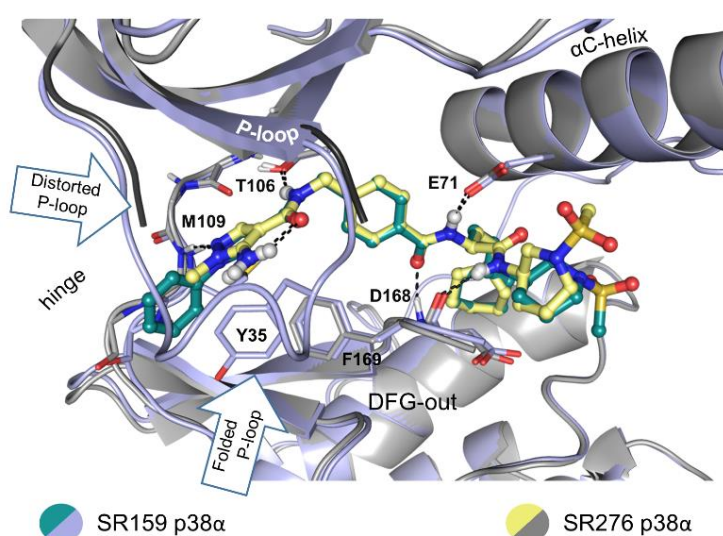
No.	Structure	$\Delta T_m^a$	$\Delta T_m^a$	$\Delta T_m^a$	$IC_{50}^b$	$IC_{50}^b$	$IC_{50}^b$
		[°C] $\pm$ SD p38 $\alpha$	[°C] $\pm$ SD DDR1	[°C] $\pm$ SD DDR2	[ $\mu$ M] $\pm$ SEM p38 $\alpha$	[ $\mu$ M] $\pm$ SEM DDR1	[ $\mu$ M] $\pm$ SEM DDR2
<b>296</b>		1.9 $\pm$ 0.4	1.3 $\pm$ 0.4	2.0 $\pm$ 0.1	12.5 $\pm$ 5.8	39.4 $\pm$ 19.2	21.5 $\pm$ 2.52
<b>293</b>		-0.3 $\pm$ 0.2	1.7 $\pm$ 0.2	1.7 $\pm$ 0.0	18.9 $\pm$ 0.9	16.5 <sup>c</sup>	27.7 $\pm$ 11.3
<b>294</b>		0.4 $\pm$ 0.3	1.1 $\pm$ 0.2	1.5 $\pm$ 0.0	6.0 $\pm$ 2.5	45.2 $\pm$ 17.9	22.0 $\pm$ 7.10
<b>295</b>		0.0 $\pm$ 0.3	1.7 $\pm$ 0.2	1.9 $\pm$ 0.1	6.9 $\pm$ 0.5	13.2 <sup>c</sup>	35.2 $\pm$ 9.4
<b>297</b>		1.0 $\pm$ 0.3	0.1 $\pm$ 0.3	1.1 $\pm$ 0.1	7.2 $\pm$ 0.4	10.4 <sup>c</sup>	59.2 $\pm$ 35.8

<sup>a</sup>  $\Delta T_m$  average derived from seven replicates for p38 $\alpha$  and three replicates for DDR1/DDR2 at a compound concentration of 10  $\mu$ M;

<sup>b</sup> Cellular  $IC_{50}$  values determined by NanoBRET™ assay in HEK293T cells,  $IC_{50}$  values were derived from duplicates ( $n = 2$ ); <sup>c</sup>  $n = 1$ ; <sup>d</sup>  $n = 3$ . DSF-assay assisted by Martin Schröder and Deep Chatterjee. NanoBRET™ assay performed by Benedict-Tilman Berger.

Consistent with the data presented in **Section 5.2**, the introduction of a 3-phenyl-1*H*-pyrazole decoration prevented binding of p38 $\alpha$ . However, micromolar potencies and negligible thermal shift values were determined also for DDR1/DDR2 kinase. For the amino piperidines with different stereo-configuration, very similar binding potencies were obtained, highlighting that the stereochemistry at this particular position is of minor importance for inhibitor potency. These observations are in agreement with the crystal structure solved for **232** (SR159) in complex with DDR1 kinase, showing that the (*S*)- and (*R*)-configured amino piperidine moieties are pointing toward the solvent. Comparing the  $\Delta T_m$  and  $IC_{50}$  values determined for all kinase targets of **293** with methyl- and **296** without methyl-decorated benzyl linker, no significant difference in binding potency was apparent. Due to the unfavorable 3-phenyl-1*H*-pyrazole hinge-binding building block, negligible inhibitory effects were also determined for compound **297** with a propyl back-pocket decoration.

From a literature search of inhibitors crystallized previously in complex with DDR1 kinases, similarities were obvious and several new heterocycles were tested (**Section 5.2**). The next synthetic approach focused, therefore, on the replacement of the amino-pyrazole moiety in **232** (SR159) by more versatile decorations (**Table 19**). In compounds **299** and **298**, the phenyl residue, thought to be crucial for P-loop folding in p38 MAPK and, hence, inhibitor selectivity and potency, was truncated. Consequently, affinity for this target might be lower with a methyl-substituted amino pyrazole decoration, while inhibitory effect on DDR1/2 kinase might be unaffected. Thermal stabilization of p38 $\alpha$  by **299** ( $\Delta T_m = 9.8$  °C) and **SR277** ( $\Delta T_m = 8.7$  °C) was significantly lower than that by **232** (SR159,  $\Delta T_m = 14.1$  °C), supporting the above assumption. Interestingly, thermal stabilization of DDR1/DDR2 kinase was even higher for the phenyl-truncated compounds, which was also in good agreement with their inhibitory effect in cellular environment. While **299** and **SR277** showed an about 58-fold/ 90-fold higher  $IC_{50}$  value for p38 $\alpha$  than **232** (SR159), favorable  $IC_{50}$  values of 1.33  $\mu$ M and 1.16  $\mu$ M were determined for **299** inhibiting DDR1/DDR2 kinases. For compound **SR277**, slightly higher  $IC_{50}$  values were obtained for all kinase targets, presumably due to unfavorable contacts of the methyl-stabilized benzyl linker. To study if the reduced affinity for p38 MAPK is caused by altered P-loop folding/interactions, a crystal structure of **299** in complex with p38 $\alpha$  kinase was determined (**Figure 42**).



**Figure 42. Mechanism of P-loop folding in p38 MAPK.** Alignment of **232** (SR159, teal) with **299** (SR276, yellow) in complex with p38 $\alpha$ . **232** (SR159) engages the P-loop in a folded conformation (light blue). Phenyl-deficient compound **299** (SR276) with distorted P-loop depicted in gray. Hydrogen bonds are highlighted by black dashed lines; important structural motifs are labeled. Crystallization and structure determination was done by Martin Schröder and Andreas Joerger, Frankfurt.

Upon superimposing the crystal structures of p38 $\alpha$  with compounds **232** (SR159) and **299**, remarkable differences in the P-loop region were visible. While **232** (SR159) engages the P-loop via its phenyl residue by a face-to-face stacking interaction with Tyr35 and side-on stacking interaction with Phe169 from the DFG-motif, the P-loop was disordered in complex with **299**. This observation confirmed the hypothesis that the p38 $\alpha$  hinge-targeting phenyl moiety of **299** is crucial for inhibitor potency and for trapping the P-loop inside the ATP-binding pocket. During the development of the p38 $\alpha$ / $\beta$  type-II probe **33** (SR318) and its negative control compound **35** (SR321) in Section 3.2, the free amine at the pyrazole ring system was also found to be important for the P-loop folding process (Figure 23), but the structural analysis above suggests that the phenyl-mediated interactions are the driving force for stabilizing the folded P-loop conformation.

Analysis of crystal structures revealed that an intramolecular hydrogen bond is typically formed between the pyrazole free amine and the neighboring carbonyl oxygen atom. This hydrogen bond stabilizes the heterocycle and amide group in a planar conformation, facilitating hinge-binding interaction with Met109 and the gatekeeper Thr106. Bridging of both groups was therefore considered next. Compounds **300** and **301** (SR301) were successfully prepared by the use of a 1-phenyl-1*H*-pyrazolo[3,4-*d*]pyrimidine or 3-phenyl-3*H*-[1,2,3]triazolo[4,5-*d*]pyrimidine building block.  $\Delta T_m$  and  $IC_{50}$  values were determined for both compounds, giving somewhat unexpected results. For compound **300** ( $IC_{50}$  (DDR1/2) = 1.04/ 2.06  $\mu$ M), the potency toward DDR1/2 was improved compared with inhibitor **232** (SR159), which has a higher intrinsic flexibility. However, affinity for p38 $\alpha$  remained unaffected, which is probably caused by the phenyl decoration in the hinge region. Interestingly, for **301** (SR301) binding toward p38 $\alpha$ , DDR1 and DDR2 was impaired, and only negligible thermal shift values and potencies inside the cell were determined. The latter finding was unexpected in so far as only a single carbon atom of the pyrazole was replaced by a nitrogen in the triazolo-decoration. These data suggested that the triazolo[4,5-*d*]pyrimidine in **301** (SR301) impairs binding due to altered electrostatic complementarity. **301** (SR301) might therefore be used as a potential negative control compound.

In compounds **302** (SR302) and **304**, the hinge-binding heterocycle was replaced by a bicyclic imidazo[1,2-*a*]pyridine decoration, reminiscent of Astex compound **251** for targeting DDR1/2 kinase. This modification was suggested using structure alignments of DDR compounds and **232** (SR159) as described in Section 5.2. Gratifyingly, the measured  $IC_{50}$  values of **302** (SR302) and **304** for DDR1/2 kinases were significant lower than  $IC_{50}$  values of earlier compounds. For **302** (SR302), an  $IC_{50}$  value of 23 nM and 18 nM was determined for DDR1/2 kinase, respectively. For compound **304** with a methyl-stabilized benzyl linker, potencies were slightly higher, highlighting that the methyl group minimally destabilized inhibitor binding to the target of interest. However, some target selectivity for p38 $\alpha$  kinase remained for both inhibitors, **302** (SR302) and **304**, with potencies 5-fold/ 6-fold higher for p38 $\alpha$  versus DDR1.

**Table 19. Hinge-binder optimization B.** Enzymatic activity of compounds **232**, **298-302** and **304** determined by  $\Delta T_m$ - and in cellulo  $IC_{50}$  values for p38 $\alpha$  and DDR1/2.

No.	Structure	$\Delta T_m^a$	$\Delta T_m^a$	$\Delta T_m^a$	$IC_{50}^b$	$IC_{50}^b$	$IC_{50}^b$
		[°C] $\pm$ SD p38 $\alpha$	[°C] $\pm$ SD DDR1	[°C] $\pm$ SD DDR2	[ $\mu$ M] $\pm$ SEM p38 $\alpha$	[ $\mu$ M] $\pm$ SEM DDR1	[ $\mu$ M] $\pm$ SEM DDR2
<b>232</b> (SR159)		14.1 $\pm$ 0.4	4.6 $\pm$ 0.2	4.8 $\pm$ 0.4	0.033 $\pm$ 0.002 <sup>e</sup>	2.37 $\pm$ 0.28 <sup>e</sup>	3.46 $\pm$ 0.32 <sup>e</sup>
<b>299</b> (SR276)		9.8 $\pm$ 0.3	6.9 $\pm$ 0.2	8.7 $\pm$ 0.1	1.93 $\pm$ 0.05	1.33 $\pm$ 0.27	1.16 $\pm$ 0.07
<b>298</b>		8.7 $\pm$ 0.2	6.1 $\pm$ 0.5	6.7 $\pm$ 0.5	2.97 $\pm$ 0.06	2.27 $\pm$ 0.16	7.46 $\pm$ 2.38
<b>300</b>		6.6 $\pm$ 0.3	5.7 $\pm$ 0.7	6.1 $\pm$ 0.7	0.24 $\pm$ 0.02	1.04 $\pm$ 0.17 <sup>e</sup>	2.06 $\pm$ 0.27 <sup>e</sup>
<b>301</b> (SR301)		0.5 $\pm$ 0.5	0.3 $\pm$ 0.1	0.6 $\pm$ 0.0	5.39 $\pm$ 3.10	21.9 $\pm$ 5.44	15.5 $\pm$ 5.08
<b>302</b> (SR302)		11.1 $\pm$ 0.5	7.1 $\pm$ 0.1	9.1 $\pm$ 0.6	0.125 $\pm$ 0.011 <sup>d</sup>	0.023 $\pm$ 0.002	0.018 $\pm$ 0.002
<b>304</b>		n.d.	7.3 $\pm$ 0.3	7.9 $\pm$ 0.3	0.284 $\pm$ 0.007 <sup>d</sup>	0.044 $\pm$ 0.001 <sup>d</sup>	0.032 $\pm$ 0.005 <sup>d</sup>

<sup>a</sup>  $\Delta T_m$  average derived from seven replicates for p38 $\alpha$  and three replicates for DDR1/DDR2 at a compound concentration of 10  $\mu$ M;

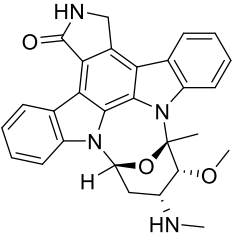
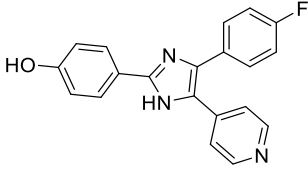
<sup>b</sup> Cellular  $IC_{50}$  values determined by NanoBRET<sup>TM</sup> assay in HEK293T cells,  $IC_{50}$  values were derived from duplicates ( $n = 3$ ); <sup>c</sup>  $n = 1$ ; <sup>d</sup>  $n = 2$ ; <sup>e</sup>  $n = 4$ . DSF-assay assisted by Martin Schröder and Deep Chatterjee. NanoBRET<sup>TM</sup> assay performed by Benedict-Tilman Berger.

To validate the NanoBRET<sup>TM</sup>-assay results and to see how the  $IC_{50}$  values translate to isolated enzymes of p38 $\alpha/\beta$ , MAPK and DDR1/2, the most potent compound **302** (SR302) was sent to the *Reaction Biology* service to perform enzyme kinetic assays (**Table 20**).

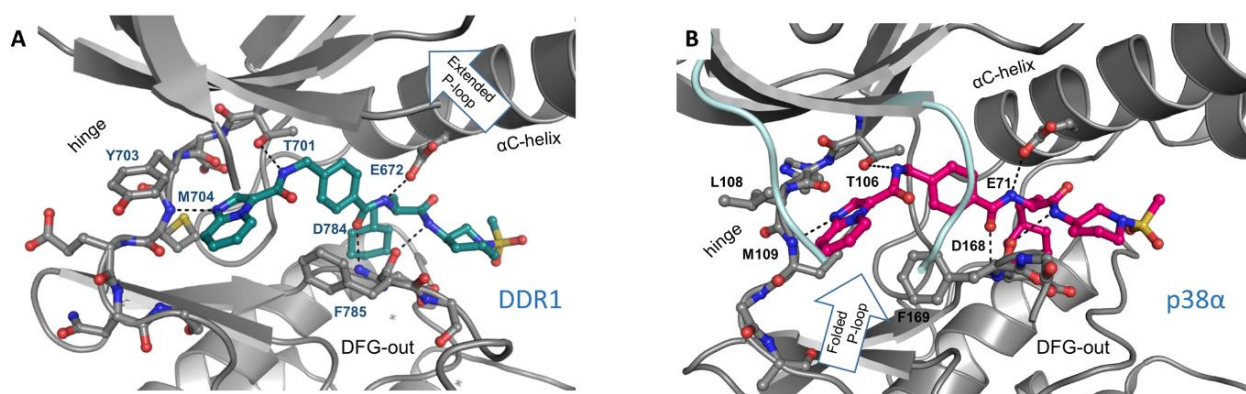
**Table 20. Enzyme kinetic assays on isolated enzymes.** Potencies of **302** (SR302) and appropriate control compound determined for DDR1/DDR2 kinase and p38 $\alpha$ / $\beta$  inhibition by Reaction Biology service.

Kinase	<b>302</b> (SR302) IC <sub>50</sub> (nM)	Ctrl. Cmpd. IC <sub>50</sub> (nM)	Ctrl. Cmpd.	ATP Conc. ( $\mu$ M)
DDR1	53.3	6.5	Staurosporine	100
DDR2	0.75	0.38	Staurosporine	5
p38 $\alpha$	6.2	11.8	SB202190	2.5
p38 $\beta$	45.1	67.9	SB202190	50

Staurosporine			SB202190	
---------------	---	--	----------	--

Compound **302** (SR302) was tested in a 10-point dose response IC<sub>50</sub> with 3-fold serial dilution starting at 10  $\mu$ M as highest assay concentration. To have maximum kinase activity, an ATP concentration higher  $K_m$ (ATP) was chosen for every kinase target, resembling the high ATP concentration inside the cellular system best. To validate the assay results, a control compound was used during this assay, which was Staurosporine in the case of DDR1/2 kinase and type-I inhibitor SB202190 for p38 $\alpha$ / $\beta$ . The results on the isolated enzymes clearly showed that **302** (SR302) inhibits all targets in the low nanomolar range. Especially remarkable was the high potency against DDR2 kinase with an IC<sub>50</sub> value of 0.75 nM. The inhibitor showed a 72-times weaker inhibition of the DDR1 kinase and thus DDR2 isoform selectivity. Isoform selectivity was also observed p38 $\alpha$ . **302** (SR302) tightly bound to p38 $\alpha$  (IC<sub>50</sub> = 6.2 nM) with a 7.3-fold reduced potency for p38 $\beta$ . To see if isoform-selective binding toward p38 $\alpha$  is additionally also observed in HEK293T cells, NanoBRET measurement on p38 $\beta$  was performed for **302** (SR302). In this single experiment, an IC<sub>50</sub> value of 219 nM was determined for **302** (SR302) and p38 $\beta$ , which does not suggest preferential binding to any of the isoforms in this cellular assay system. To understand the differences in inhibitor binding toward p38 $\alpha$  and DDR1 kinase, a crystal structure in complex with **302** (SR302) was solved for both kinase targets (**Figure 43**).



**Figure 43. Binding mode of dual DDR/p38 inhibitor 302 (SR302).** A) Crystal structure of **302** (SR302, teal) in complex with DDR1 kinase, showing an extended P-loop. B) **302** (SR302, pink) in complex with p38 $\alpha$  kinase, engaging the P-loop (light blue) in a folded conformation. Hydrogen bonds are highlighted as black dashed lines; important structural motifs are labeled. Crystallization and structure determination of **302** (SR302) in p38 $\alpha$  was done by Martin Schröder, Frankfurt and in DDR1 by Sebastian Mathea, Frankfurt.

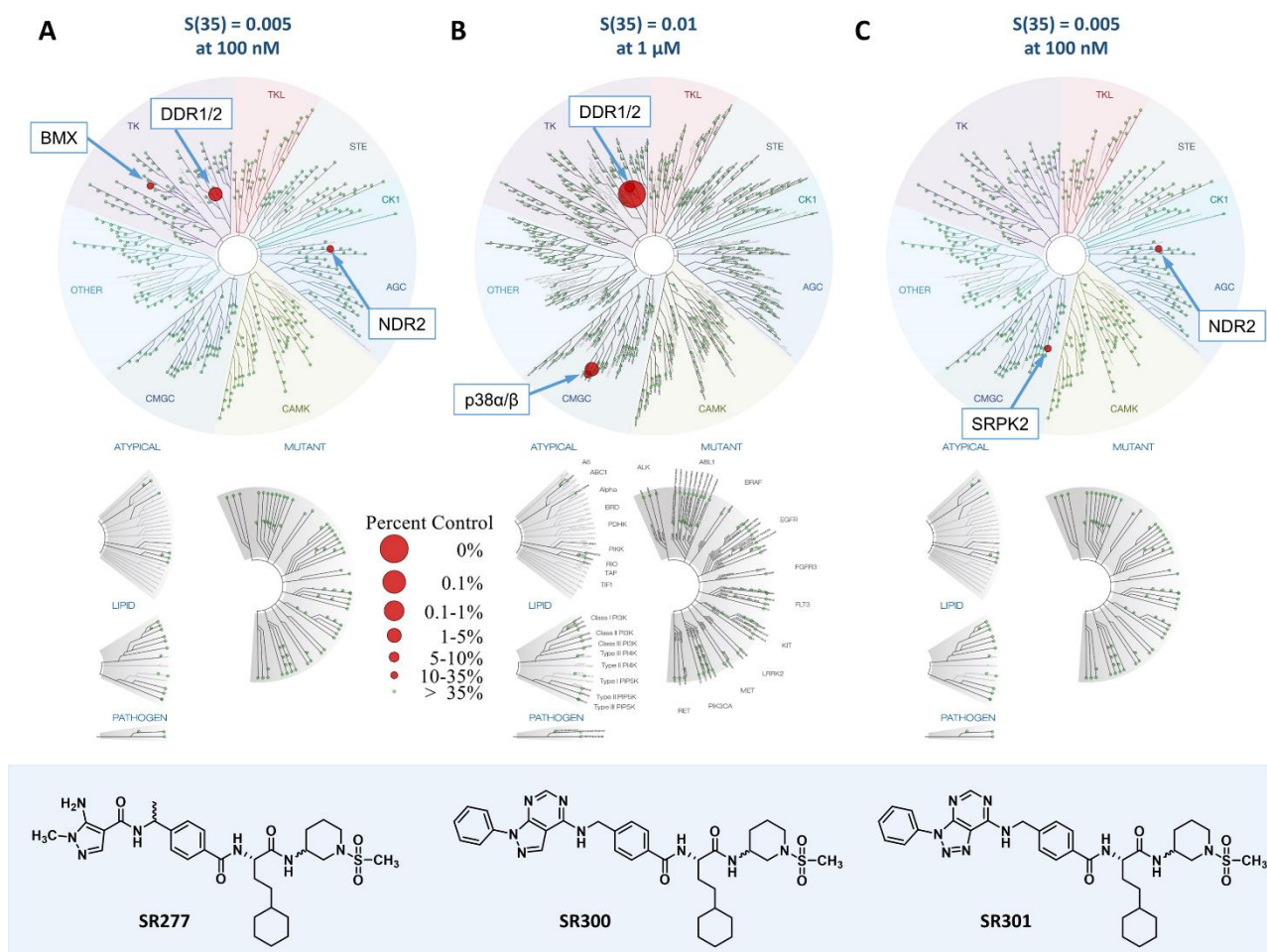
Overall, **302** (SR302) adopts the same binding mode in both kinases, targeting an inactive DFG-out state typically found for type-II inhibitors. While the cyclohexyl decoration reaches into the allosteric deep pocket, which is slightly smaller in DDR1 kinase, the sulfonamide moiety points toward the solvent exposed side. In both structures a similar hydrogen network is seen with the conserved Glu-Asp pair from the DFG-motif and the  $\alpha$ C helix, and an additional hydrogen bond via the DFG aspartate anchored the terminal amide inside the allosteric pocket region. In the ATP-binding site, DDR1 kinase as well as p38 $\alpha$  participated in the hydrogen-bond network with the same gatekeeper residue threonine and hinge contacts between the methionine and the N1-nitrogen of the imidazo[1,2-*a*]pyridine moiety. Although both kinases use the same residues for anchoring the inhibitor to the binding pocket, differences can be observed for instance in the hinge region and the P-loop. While in p38 $\alpha$  Met109 is followed by Leu109, an aromatic tyrosine residue (Tyr703) is found in DDR1 kinase. The side chain of Tyr703 is pointing toward the ATP-binding pocket and makes favorable face-to-face like  $\pi$ -stacking interactions with the imidazo[1,2-*a*]pyridine hinge-binding decoration (**Figure 43A**). The flat geometry of this hinge binder is probably the main driver for the improved potency for **302** (SR302) and DDR1/2 kinase. In the DDR1-**232** (SR302) complex (**Figure 40A**), an orthogonal orientation of amino-pyrazole and its phenyl decoration was found, negatively influencing aromatic interactions with Tyr703. In addition to the potency toward DDR1/2 kinase, **302** (SR302) also shows potent binding of p38 $\alpha$ / $\beta$ . The reason for this can also be explained based on the crystal structure, which shows that **302** (SR302) traps the P-loop of p38 $\alpha$  in a folded-like conformation. However, as electron density in this flexible P-loop region was not resolved completely,  $\pi$ -stacking interaction with Tyr35 and Phe169 from the DFG-motif were not visible in this structure (**Figure 43B**), indicating a certain degree of flexibility. As discussed above, **232** (SR159) shows a very low IC<sub>50</sub> value of 22.5 nM for p38 $\alpha$ , probably mainly due to favorable interactions with the folded P-loop, which was thus fully resolved in the crystal structure (**Figure 40**). As the hinge decoration of **302** (SR302) lacks the phenyl-extended hinge-binding head group, interactions with the P-loop Tyr35 are less pronounced, which might explain the about 4.8-fold reduced potency for p38 $\alpha$ .

#### 5.4.2 Selectivity profiling

The studies described above provided important information on the structure-activity relationship for the inhibition of DDR1 kinase and revealed a very potent dual DDR/p38 inhibitor **302** (SR302). Since the active center of kinases is highly conserved in the family of >500 members, selectivity is an important feature of a potent kinase inhibitor. From this series, the most interesting and potent compounds were therefore selected to study their kinome-wide selectivity. **298** (SR277), **300** (SR300), **302** (SR302), **304** (SR360) and the potentially negative control compound **301** (SR301) were selected and each profiled against 468 kinases and mutations in total by the *DiscoverX* service.

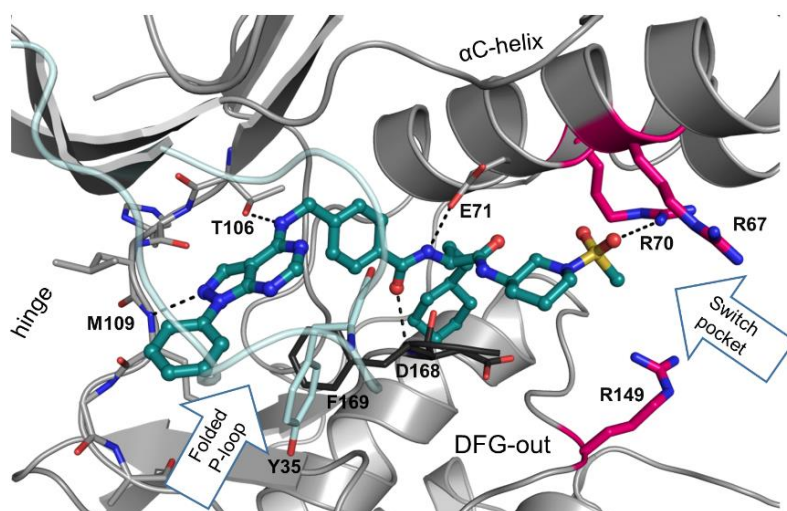
Interestingly, all compounds showed very clean selectivity profiles, as expected based on earlier studies on structurally related compounds (**Figure 44**). Compound **298** (SR277) with a truncated hinge-binding moiety was screened at a concentration of 100 nM to identify high-affinity targets (**Figure 44A**). In accordance with the previously determined IC<sub>50</sub> values, **298** (SR277) showed no affinity for p38 $\alpha$  at this concentration. In addition to inhibiting DDR1/2 kinases, off-target activities for BMX and NDR2 kinase were found at a cut-off value of >35% of control remaining in this assay (*S*-score (35) = 0.005). However, as the false-positive rate in this assay is typically around 1% and NDR2 was found as a target in other screens before as well (e.g. with **35**, SR321), it cannot be excluded that these kinases are false positives without additional control experiments.





**Figure 44. Selectivity profiling against 468 kinases and mutations.** A) 298 (SR277) screened at 100 nM; B) 300 (SR300) screened at 1  $\mu$ M, C) 301 (SR301) screened at 100 nM. Selectivity score  $S(35)$  is given for compound comparison.

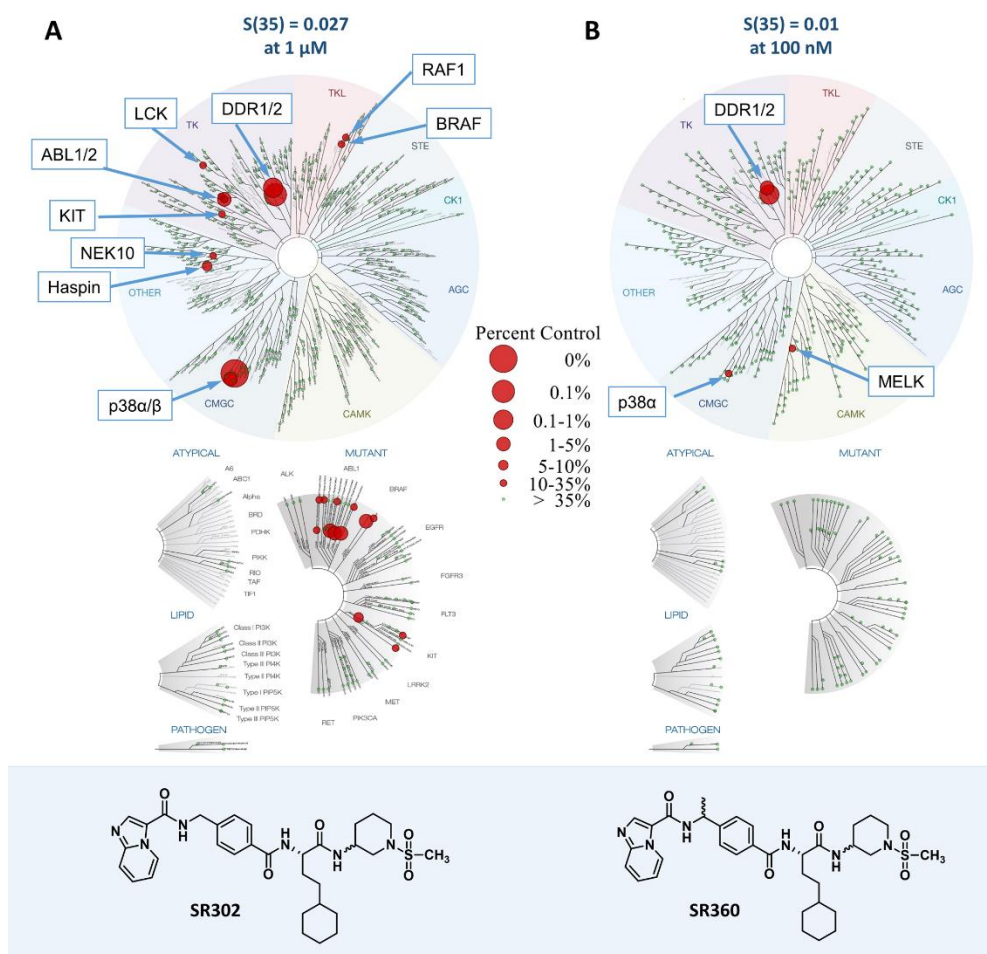
Compound **300** (SR300) which has a bridged pyridazo[3,4-*d*]pyrimidine structure was screened at a higher concentration of 1  $\mu$ M (**Figure 44B**). Although more off-targets were to be expected at this concentration, a remarkably clean selectivity profile was obtained for **300** (SR300). From the 468 kinases and mutations tested, **300** (SR300) inhibited only DDR1/2 and p38 $\alpha$ / $\beta$  kinases and, thus, a selectivity score of  $S(35) = 0.01$  was calculated. To understand the reason for the superior kinome-wide selectivity of this compound, a crystal structure in complex with p38 $\alpha$  was determined (**Figure 45**).



**Figure 45. Selectivity by targeting the switch-pocket residues in p38 $\alpha$ .** Compound **300** (SR300, teal) in complex with p38 $\alpha$  MAPK. Important structural elements are highlighted, such as the switch-pocket residues Arg70, Arg67 and Arg149. Folded P-loop is depicted in light blue, DFG-motif and hydrogen bonds in black. Crystallization and structure determination was done by Martin Schröder, Frankfurt.

In this crystal structure, **300** (SR300) bound like a typical type-II inhibitor to the DFG-out deep pocket and made contacts to the backbone amide of Met109 in the hinge region via its pyrazole nitrogen atom. Besides this canonical binding mode, **300** (SR300) engaged the P-loop in a folded conformation, which improves inhibitor selectivity as seen for other inhibitors crystallized in this study. However, none of those inhibitors had such a clean selectivity profile as **300** (SR300). Interestingly, the electron density for this inhibitor was very well resolved in the allosteric pocket region, which has not been the case with other sulfonamide-decorated compounds, e.g., **232** (SR159), **299**, **302** (SR302). The reason for this was a rather unexpected hydrogen bond formed between Arg70 from the  $\alpha$ C helix and one of the sulfonamide *O*-atoms. Like Arg67 ( $\alpha$ C helix) and Arg149 (HRD segment), Arg70 belongs to the so-called switch pocket residues, which are described in detail in **Section 2.4**. Targeting those amino acids was previously studied by *Deciphera*, which had provided highly selective p38 $\alpha$ / $\beta$  inhibitors.<sup>329</sup> Since Arg70 is a non-conserved amino acid found exclusively at p38 $\alpha$ / $\beta$ , the superior kinome-wide selectivity of **300** (SR300) is mainly caused by the additional interaction with this basic side-chain. However, the binding mode of **300** (SR300) is unique in that it is the first switch pocket inhibitor simultaneously making contacts with the hinge region. Another special feature is the interaction with the P-loop.

Compound **301** (SR301), which had no activity on p38 $\alpha$  and DDR1/2, was subsequently screened at a concentration of 100 nM (**Figure 44C**). Interestingly, **301** (SR301) also showed a very clean selectivity profile in the kinome scan. With a cut-off value of >35% of the control in the assay, only the two kinases SRPK2 and NDR2 were found ( $S(35) = 0.005$ ). After confirmation of both targets by NanoBRET, compound **301** (SR301) could therefore be used as a negative control of **300** (SR300) or **302** (SR302) in further functional studies on p38 MAPK and DDR1/2.



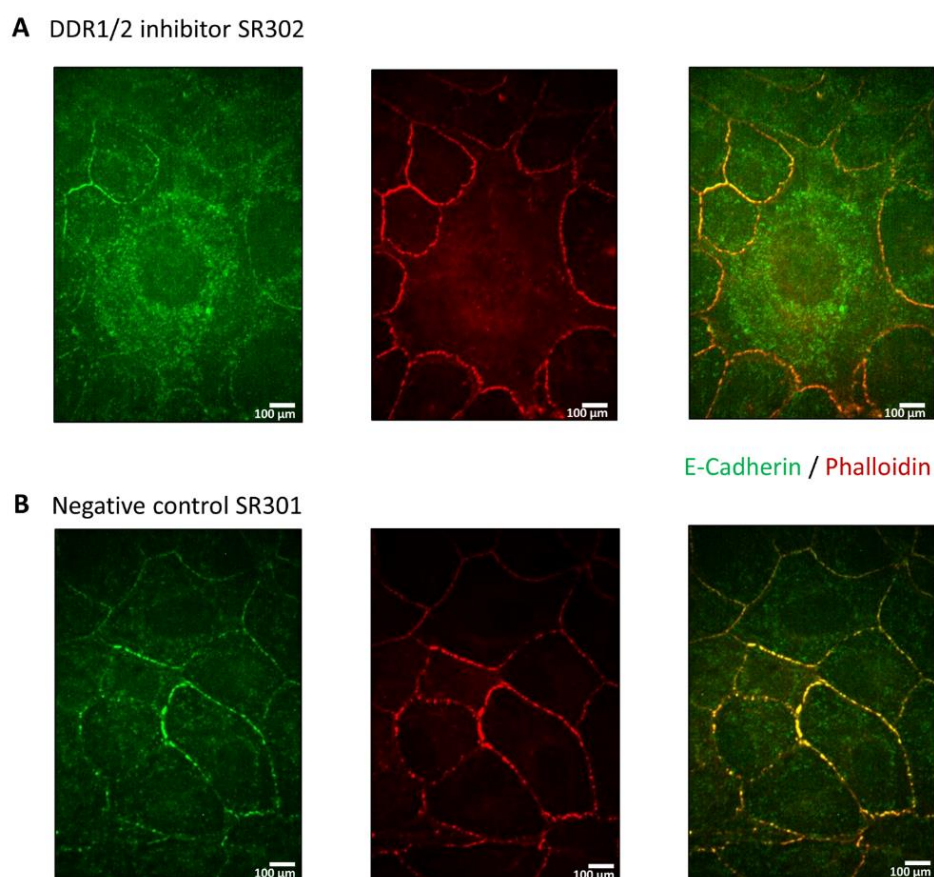
**Figure 46.** Selectivity profiling against 468 kinases and mutations. A) **302** (SR302) screened at 1  $\mu$ M; B) **304** (SR360) screened at 100 nM.

The most potent compound from this series **302** (SR302), was screened at a concentration of 1  $\mu$ M to obtain the most accurate insight for potential off-targets (**Figure 46A**). In comparison with **300** (SR300), which was previously investigated at 1  $\mu$ M, **302** (SR302) showed a significantly lower selectivity of  $S(35) = 0.027$ . In addition to DDR1/2 and p38 $\alpha/\beta$ , which were inhibited the strongest, eight other kinases were inhibited: BRAF, RAF1, LCK, ABL1/2, KIT, NEK10 and Haspin. Furthermore, a large number of BRAF, KIT and ABL1 mutants were targeted by the inhibitor. Based on the false positive rate usually observed in the assay, it can be assumed that **302** (SR302) is still significantly more selective than depicted in **Figure 46A**. In order to obtain an exact picture of the off-targets that play a role in the cell, it would therefore be useful to verify all kinase targets in a cellular assay. As in the previous chapters, this could be done using NanoBRET™ assays, for example, if a suitable constructs and tracers are available. In compound **304** (SR360), a methyl group was introduced in benzylic position to strengthen the interaction with the hydrophobic pocket behind the gatekeeper (Thr701) and to stabilize it metabolically. This methyl group is part of many previously published DDR1/2 kinase inhibitors such as DDR-TRK-1, DDR1-IN-1, as well as **251** and is believed to be responsible for the off-target inhibition of TRKs.<sup>495</sup> Since all previously synthesized compounds, based on the VPC-00628 scaffold, did show no inhibition of TRKs in the kinome scan, it was of interest whether a methyl group at this position in the molecule also leads to the aforementioned interaction. Compound **304** (SR360) was therefore investigated for its kinome wide selectivity at a concentration of 100 nM (**Figure 46B**). Interestingly, screening of **304** (SR360) revealed a very clean profile at this concentration, and high-affinity targets such as DDR1/2, p38 $\alpha$  and MELK were detected at a cut-off value of >35% of the control. The

presumed inhibition of TRKA, TRKB and TRKC was not confirmed for **304** (SR360) because 100% of the control was retained in the assay system (raw data see **Section 8.6**). It can therefore be assumed that the methyl group is not the only reason for the inhibition of TRKs as discussed by ZHU ET AL.<sup>495</sup> but this activity is rather depended on the hinge binding scaffold of the inhibitor used.

### 5.4.3 Further biological evaluation

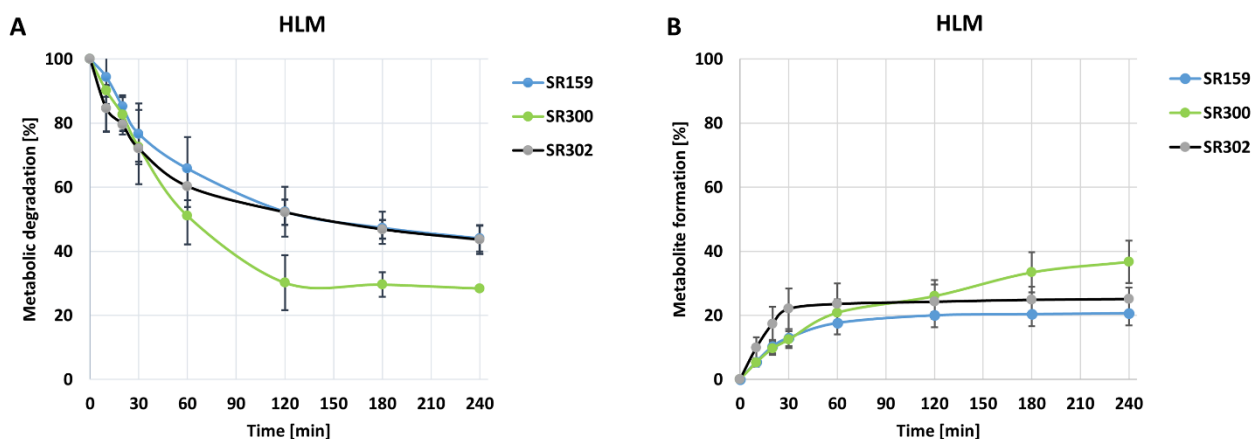
Previous studies highlighted that the receptor-tyrosine kinase DDR1 plays a fundamental role in the differentiation and adhesion of epithelial cells, where it also regulates the junctional stability of cell-cell contacts.<sup>499</sup> The overexpression of DDR1 kinase as well as collagen binding to the receptor stabilizes E-cadherins, by a process suggested to be mediated by SRC kinase which impairs the endocytosis of these cell-adhesion molecules. The latter is thought to be crucial for the formation of metastases in epithelial-cell cancer, in which aberrant expression levels of surface E-cadherins have been observed.<sup>500</sup> In 2016, CHEN ET AL. demonstrated that the knockdown of DDR1 promotes changes in the subcellular location of cell adhesion proteins such as E-cadherin.<sup>501</sup> In the next part of this work, epithelial cells (LLC-PK1 wild-type) were treated with the previously synthesized DDR1/2 inhibitor **302** (SR302) in order to investigate changes in epithelial plasticity. The experiment was performed in collaboration by Lohitesh Kovooru and Christian Pohl (BMLS Frankfurt). The negative control compound **301** (SR301) was also used as control in these studies and cells were treated for 24 h. The epithelial cells were then fixed and immunostaining of E-cadherin and phalloidin was performed to visualize cell-cell contacts (**Figure 47**).



**Figure 47. Immunofluorescence staining of E-cadherin in epithelial cells.** A) **302** (SR302) and B) negative control **301** (SR301) were treated at 100 nM for 24 h. LLC-PK1 wild-type (proximal tubule cell line) cells were then fixed and stained with E-cadherin (green, left) and phalloidin (red, middle). An overlay is depicted in the left figure. Images were captured using a confocal microscope, by Lohitesh Kovooru, BMLS Frankfurt.

Interestingly, cells treated with the potent DDR1/DDR2 inhibitor **302** (SR302) showed different morphology, and endocytosis of E-cadherin was clearly visible in the cytosol of treated cells (**Figure 47A**). In contrast, continuous cell-cell contacts were observed for cells treated with the negative control **301** (SR301), in which E-cadherin was located at the cell-cell adhesion sites (**Figure 47B**). It can therefore be concluded that the inhibition of DDR1/2 kinase indeed had a destabilizing effect on the epithelial surface adhesion protein E-cadherin. **302** (SR302) might therefore be a useful tool compound to study the DDR1/2 signaling pathway, e.g., in cancer cell-lines.

In the following, the metabolic stability of compounds **232** (SR159), **300** (SR300) and **302** (SR302) was investigated using human liver microsomes over a time interval of 240 min each (**Figure 48**). As already shown for **33** (SR318) and **218** (SR43) in the previous chapters, the derivatives modified for targeting DDR1/2 were also metabolically stable. In general, **300** (SR300) was metabolized slightly faster than **232** (SR159) and **302** (SR302), and a slightly higher proportion of metabolites was thus produced. After a reaction time of 240 min, only  $44.0 \pm 4.0\%$  of the compound remained unmetabolized for **232** (SR159),  $43.6 \pm 4.5\%$  for **302** (SR302) and  $28.4 \pm 0.8\%$  for **300** (SR300).



**Figure 48. Metabolic stability in human liver microsomes (HLM).** A) Metabolic degradation over 240 min. B) Metabolite formation over 240 min. Compound **232** (SR159) is highlighted in blue, **300** (SR300) in red and **302** (SR302) in black. Experiments were performed in triplicates. The values represent the mean with standard deviation. Assay by Mark Kudolo, Tübingen.

## 5.5 Conclusion

All compounds, previously synthesized in this work, were analyzed against **218** (SR43) main off-targets by DSF-assay and building blocks most useful for DDR1/2 inhibition were disclosed. The synthesis covered the optimization of the hinge-binding head group and allosteric part of **218** (SR43) toward DDR1/2 kinase inhibition. It further provided valuable insights in the P-loop folding process of p38 MAPK and showed that targeting of the switch-pocket residues can improve the kinome-wide selectivity of an inhibitor. The studies resulted in the very potent and selective dual p38/DDR inhibitor, **302** (SR302), with picomolar affinity for DDR2 in enzyme kinetic assay. **302** (SR302) demonstrated to be efficient *in vitro*, and showed a destabilizing effect on the surface adhesion protein E-cadherin in epithelial cells. A corresponding negative control, **301** (SR301), was synthesized for **302** (SR302) and both now provide a valuable tool set to study the phenotypic DDR1/2 signaling, e.g., in cancer cell-lines.

## 6 Summary

The p38 $\alpha$  mitogen-activated protein kinase (p38 $\alpha$  MAPK) is a Ser/Thr kinase that is activated through stress stimuli such as heat shock or hypoxia.<sup>502</sup> In the nucleus, p38 $\alpha$  modulates the activity of other kinases and transcription factors,<sup>503</sup> a process that regulates the expression of specific target genes, most importantly pro-inflammatory cytokines including the tumor necrosis factor alpha (TNF- $\alpha$ ) and interleukin 1 beta (IL-1 $\beta$ ).<sup>249</sup> Dysregulation of p38 $\alpha$  therefore plays a major role in the development of inflammatory diseases such as rheumatoid arthritis (RA), inflammatory bowel diseases, chronic obstructive pulmonary disease (COPD) and autoimmune diseases.<sup>504</sup> However, despite many years of intensive research and clinical efforts, no p38 small-molecule inhibitors have been approved yet, in many cases due to insufficient selectivity profiles leading to side effects<sup>505</sup> and activation of compensatory pathways.<sup>305, 506, 507</sup> The p38 MAPK family consists of four isoforms ( $\alpha$ ,  $\beta$ ,  $\delta$ , and  $\gamma$ ) with diverse physiological roles.<sup>508</sup> For example, several studies reported that p38 $\alpha$ , but not p38 $\beta$ , stimulates TNF- $\alpha$  release and other inflammatory cytokines.<sup>509</sup> In addition, inhibition of p38 $\beta$  may induce apoptosis<sup>510</sup> and stimulate the glycogen synthase pathway, potentially leading to undesirable side effects of p38 $\alpha$ / $\beta$  dual inhibitors.<sup>511</sup> Therefore, an isoform-selective inhibition of p38 $\alpha$  would be preferable. Several inhibitor design strategies have been reported, leading to >100-fold selective compounds for  $\alpha$ / $\beta$  over the  $\gamma$  and  $\delta$  isoforms. Achieving such a selectivity among the two structurally most related  $\alpha$  and  $\beta$  isoforms, however, remains a challenging task.<sup>512, 513</sup> This is due to their high sequence identity of 97%, with the only difference in the ATP-binding pocket being the substitution of His107 in the hinge region of the  $\alpha$  isoform by a threonine in the  $\beta$  counterpart. Recently, WROBLESKI ET AL. reported type-I 3-amino-4-methyl-*N*-cyclopropylbenzamide inhibitors that exhibited surprisingly high potencies for p38 $\alpha$  with a nearly 150-fold selectivity over the  $\beta$  isoform.<sup>322</sup> Dynamic changes in the hinge backbone have been suggested as structural mechanisms of inhibitor and isoform selectivity. In particular, the presence of a glycine residue in the hinge region (Gly110), which is a rare sequence variation in protein kinases, has been exploited for the development of highly selective type-I inhibitors such as Skepinone-L, whereas reorientation of the Leu108-Met109 peptide backbone is thought to contribute to p38 $\alpha$ / $\beta$  isoform selectivity (**Chapter 2**).<sup>322, 514, 515</sup> Targeting an inactive DFG-out conformation offers another strategy for the development of potent kinase inhibitors (type-II inhibitors), exemplified by the BCR-ABL-inhibitor Imatinib.<sup>401, 516</sup> Advantages of type-II inhibitors often include high potencies with a prolonged target residence time and potential targeting of non-catalytic functions of the kinases.<sup>268, 517, 518</sup> Achieving selectivity with type-II binders is challenging, though, given that many kinases can adopt an inactive DFG-out conformation.<sup>42</sup> This is exemplified by the p38 type-II inhibitor BIRB-796, which exhibits picomolar on-target affinity but only a poor kinome-wide selectivity.<sup>44</sup> A selective type-II chemical probe for p38 $\alpha$ / $\beta$  was still lacking at the start of this thesis.

To fill this gap for this well-studied target, the first aim of this PhD thesis was to develop a potent and selective type-II inhibitor of p38 (**Chapter 3**). The promising hit VPC-00628, which was identified by a large DNA-encoded library screen, was chosen for a combinatorial synthetic approach to develop such a chemical probe.<sup>340</sup> The studies covered the optimization of the hinge-binding head group, the hydrophobic region I and the DFG-out deep pocket of the lead compound VPC-00628. Selectivity for the p38 $\alpha$  and p38 $\beta$  isoforms was monitored during the optimization process, which identified several inhibitors with favorable isoform selectivity, providing valuable insights into the potential of isoform-selective inhibitor design for p38. The fast optimization process led to the discovery of a potent and highly selective p38 MAPK probe, **33** (SR318), which showed IC<sub>50</sub> values in the low nanomolar range in HEK293T cells for p38 $\alpha$  and p38 $\beta$  (IC<sub>50</sub> [p38 $\alpha$ / $\beta$ ] =

3.7 nM/ 10 nM). An unusual P-loop conformation induced upon binding of **33** (SR318) to p38 $\alpha$  contributed most likely to the impressive selectivity profile within the kinome that surpassed both the parent compound and BIRB-796. For an in-depth study of p38 $\alpha$ / $\beta$  as a kinase drug target, a negative control compound, **35** (SR321), was developed, to distinguish between on-target effects and non-specific effects due to cross-reactivity with other cellular proteins. Studies of the metabolic stability in human liver microsomes revealed a high stability of the compounds, with only a small amount of metabolites formed over several hours. Compound **33** (SR318) also exhibited a good *in vitro* efficacy, quantitatively reducing the LPS-stimulated TNF- $\alpha$  release in whole blood with an IC<sub>50</sub> in the nanomolar range. Taken together, **33** (SR318) is a highly potent and selective type-II p38 $\alpha$ / $\beta$  chemical probe, which will help to gain a better understanding of the catalytic and non-catalytic functions of these key signaling kinases in physiology and pathology.

The next studies focused on the exploration of the highly dynamic allosteric back pocket of p38 MAPK, and allosteric BIRB-796 derived compounds for targeting the  $\alpha$ C- and DFG-out pockets were synthesized (**Chapter 4**). Kinase activities of allosteric pyrazole-urea fragments were analyzed against a comprehensive set of 47 diverse kinases by differential scanning fluorimetry (DSF), revealing that BIRB-796 off-targets remain a problem when targeting this back-pocket binding motif. Revisiting the recently published compound MCP-081, which combines the allosteric part of BIRB-796 with the active-site directed part of VPC-00628, showed that it displays a clean selectivity profile in our kinase panel. Because the potency of MCP-081 was slightly reduced compared with VPC-00628 and the allosteric *tert*-butyl pyrazole moiety seemed suboptimal, a set of VPC-00628 derivatives for targeting the  $\alpha$ C-out pocket region was synthesized. Through structure-guided extension of the terminal amide of VPC-00628 toward this allosteric site, the potent and selective compound **218** (SR43) was developed, which showed excellent cellular activity on p38 MAPK in NanoBRET™ assays (IC<sub>50</sub> [p38 $\alpha$ / $\beta$ ] = 14.0 nM/ 16.8 nM). **218** (SR43) showed a dose-dependent inhibition of activating phosphorylation of p38 in HCT-15 cells and inhibition of phosphorylation of p38 downstream substrates MK2 and Hsp27. In addition, **218** (SR43) induced an anti-inflammatory response by blocking TNF- $\alpha$  release in whole blood and displayed a high metabolic stability.

Selectivity profiling of **218** (SR43) revealed a narrow selectivity for additional targets such as the discoidin domain receptor kinases (DDR1/2). DDR kinases play a central role in fibrotic disorders, such as renal and pulmonale fibrosis, atherosclerosis and different forms of cancer.<sup>460, 461</sup> Since selective and potent inhibitors for these important therapeutic targets are largely lacking and the existing inhibitors are of low scaffold diversity, the next study focused on the optimization of **218** (SR43) toward DDR1/2 kinase inhibition (**Chapter 5**). All compounds synthesized in this work were tested against the main off-targets of **218** (SR43) by DSF, revealing building blocks most useful for DDR1/2 inhibition. The synthetic work covered the optimization of the hinge-binding head group and the allosteric part of **218** (SR43) toward DDR1/2 kinase inhibition. These studies provided novel insights into the P-loop folding process of p38 MAPK and how targeting of non-conserved amino acids affects inhibitor selectivity. Importantly, they led to the development of a selective dual p38/DDR inhibitor, **302** (SR302), with picomolar affinity for DDR2 (IC<sub>50</sub> [DDR1/2] = 53.3 nM/ 0.75 nM, IC<sub>50</sub> [p38 $\alpha$ / $\beta$ ] = 6.2 nM/ 45.1 nM). **302** (SR302) was efficient *in vitro* and showed a destabilizing effect on the surface adhesion protein E-cadherin in epithelial cells. In summary, **302** (SR302) and its negative control **301** (SR301) provide a valuable tool set for studying the phenotypic effects of DDR1/2 signaling, e.g., in cancer cell lines.

## 7 Zusammenfassung

Die mitogen-aktivierte Proteinkinase (MAPK) p38 $\alpha$  ist eine Ser/Thr spezifische Kinase, die durch Stressreize wie Hitzeschock oder Hypoxie aktiviert wird.<sup>502</sup> Im Zellkern moduliert p38 $\alpha$  die Aktivität weiterer Kinasen sowie von Transkriptionsfaktoren,<sup>503</sup> wodurch die Expression spezifischer Zielgene, vor allem pro-inflammatorischer Zytokine wie dem Tumornekrosefaktor-alpha (TNF- $\alpha$ ) und dem Interleukin-1 beta (IL-1  $\beta$ ) reguliert wird.<sup>249</sup> Fehlerhaft reguliertes p38 $\alpha$  spielt daher eine wichtige Rolle bei der Entstehung von entzündlichen Erkrankungen wie rheumatoider Arthritis (RA), entzündlichen Darmerkrankungen, chronisch obstruktiver Lungenerkrankung (COPD) und Autoimmunerkrankungen.<sup>504</sup> Trotz jahrelanger intensiver Forschung und klinischer Bemühungen wurden bisher jedoch noch keine niedermolekularen p38-Inhibitoren zugelassen, in vielen Fällen aufgrund unzureichender Selektivitätsprofile, die zu Nebenwirkungen<sup>505</sup> sowie zur Aktivierung von kompensatorischen Signalwegen führen.<sup>305, 506, 507</sup> Die p38-MAPK-Familie besteht aus vier Isoformen ( $\alpha$ ,  $\beta$ ,  $\delta$  und  $\gamma$ ), die unterschiedliche physiologischen Funktionen besitzen.<sup>508</sup> Mehrere Studien berichteten beispielsweise, dass p38 $\alpha$ , aber nicht p38 $\beta$ , die Freisetzung von TNF- $\alpha$  und anderen entzündlichen Zytokinen stimuliert.<sup>509</sup> Darüber hinaus kann die Hemmung von p38 $\beta$  die Apoptose<sup>510</sup> induzieren und den Glykogensynthese-Weg stimulieren, was möglicherweise zu unerwünschten Nebenwirkungen von dualen p38 $\alpha/\beta$ -Inhibitoren führt.<sup>511</sup> Eine isoformselektive Hemmung von p38 $\alpha$  wäre daher wünschenswert. Verschiedene Studien haben Möglichkeiten zum Inhibitor-Design aufgezeigt, um Verbindungen mit >100-facher Selektivität für die p38 $\alpha/\beta$ -Isoformen gegenüber den p38 $\gamma/\delta$ -Isoformen zu synthetisieren. Das Erreichen einer Selektivität zwischen den beiden strukturell am engsten verwandten Isoformen  $\alpha$  und  $\beta$  bleibt aber eine schwierige Aufgabe.<sup>512, 513</sup> Dies ist auf ihre hohe Sequenzidentität von 97% zurückzuführen, wobei der einzige Unterschied in der ATP-Bindungstasche die Substitution von His107 in der Scharnierregion der  $\alpha$ -Isoform durch ein Threonin im  $\beta$ -Gegenstück ist. Kürzlich berichteten WROBLESKI ET AL. über 3-Amino-4-methyl-N-cyclopropylbenzamid Inhibitoren vom Typ-I, die für p38 $\alpha$  überraschend hohe Potenzen mit fast 150-facher Selektivität gegenüber der  $\beta$ -Isoform aufwiesen.<sup>322</sup> Als strukturelle Mechanismen der Inhibitor- und Isoformselektivität wurden dynamische Veränderungen des Scharnerrückgrats (hinge backbone) vorgeschlagen. Insbesondere wurde das Vorhandensein eines Glycinrests in der Scharnierregion (Gly110), einer seltenen Sequenzvariation bei Proteinkinasen, für die Entwicklung hochselektiver Typ-I-Inhibitoren wie Skepinone-L genutzt, während eine Neuorientierung des Leu108/Met109-Peptidrückgrats zur p38 $\alpha/\beta$ -Isoformselektivität beitragen soll (Kapitel 2).<sup>322, 514, 515</sup>

Die Adressierung einer inaktiven sogenannten DFG-out-Konformation der Kinasen stellt eine weitere Strategie für die Entwicklung potenter Typ-II-Inhibitoren dar, wie am Beispiel des BCR-ABL-Inhibitors Imatinib gezeigt wurde.<sup>401, 516</sup> Zu den Vorteilen von Typ-II-Inhibitoren gehören oft hohe Potenzen mit einer verlängerten Verweildauer am Zielmolekül (Target) und mögliche Effekte auf nicht-katalytische Funktionen der Kinasen.<sup>268, 517, 518</sup> Das Erzielen einer verbesserten Selektivität mit Typ-II-Inhibitoren hat sich jedoch als schwierig erwiesen, da eine inaktive DFG-out-Konformation von vielen Kinasen eingenommen werden kann.<sup>42</sup> Ein Beispiel hierfür ist der p38-Inhibitor BIRB-796, der zwar eine picomolare Affinität zum Target aber nur eine geringe Selektivität gegenüber dem restlichen Kinom aufweist.<sup>44</sup> Obwohl viele p38-Inhibitoren entwickelt wurden, ergab eine Analyse der Literatur der letzten fünf Jahre, dass vorwiegend ältere Inhibitoren mit unzureichender Selektivität in funktionellen Studien eingesetzt werden. Eine selektive chemische Sonde (Probe) vom Type-II für p38 $\alpha/\beta$ , welche eine gezielte Untersuchung der inaktiven Kinase ermöglichen würde, wurde bisher nicht publiziert.



Um diese Lücke für dieses gut untersuchte Target zu schließen, wurde im Rahmen dieser Doktorarbeit eine potente und selektive Typ-II-Inhibitor-Probe entwickelt (**Kapitel 3**). Die vielversprechende Verbindung, VPC-00628, welche während des Screenings einer insgesamt 12.6 Millionen großen DNA-kodierten Bibliothek an kleinen Molekülen identifiziert wurde, wurde für einen kombinatorischen Syntheseansatz zur Entwicklung dieser chemischen Sonde ausgewählt.<sup>340</sup> Die Arbeit entstand in einer Kollaboration mit Mitarbeitern von Mercachem BV (Niederlanden), welche ein Set von insgesamt 80 kleinen Molekülen synthetisiert und zur Untersuchung bereitgestellt haben. Biologische Daten wurden von Mercachem, Mitarbeitern am Structural Genomics Consortium (Frankfurt) und der Arbeitsgruppe Laufer (Universität Tübingen) generiert. Die Gesamtstudie umfasste die Optimierung der Scharnierbindungskopfgruppe (hinge binder), der hydrophoben Region I und der DFG-out-Tasche (deep pocket) der zuvor entdeckten Leitverbindung VPC-00628. Die Selektivität für die Isoformen p38 $\alpha$  und p38 $\beta$  wurde während des Optimierungsprozesses überwacht, wobei mehrere Inhibitoren mit günstiger Isoformselektivität identifiziert wurden. Durch Dockingstudien konnten strukturelle Merkmale innerhalb der DFG-out-Tasche, wie z.B. die Aminosäure an Position 78, als wahrscheinliche Gründe für die bevorzugte Bindung einiger Verbindungen der Bibliothek an die  $\alpha$ -Isoform von p38-MAPK identifiziert werden. Da der sogenannte „Leucin-flipped“-Modus von WROBLESKI ET AL.<sup>322</sup> bisher als die einzige Möglichkeit zur Generierung isoformselektiver Inhibitoren für p38-MAPK beschrieben wurde, stellen die neuen Erkenntnisse aus dieser Arbeit daher eine allgemeinere Möglichkeit dar, um in Zukunft p38 $\alpha$ -isoformselektive allosterische Inhibitoren zu entwickeln.

Der synthetische Ansatz führte zur Entwicklung einer hochselektiven und sehr wertvollen p38 $\alpha/\beta$  Probe (**33**, SR318) vom Typ-II, welche alle Probekriterien erfüllte, nämlich potent ( $IC_{50}$  [p38 $\alpha/\beta$ ] = 3.7 nM/ 10 nM), selektiv innerhalb der Zielfamilie, zellaktiv sowie chemisch stabil und ungiftig zu sein. Eine ungewöhnliche Faltung der glycinreichen Schleife (P-loop), die bei der Bindung von **33** (SR318) an p38 $\alpha$  induziert wurde, trug höchstwahrscheinlich zu dem erstaunlichen Selektivitätsprofil innerhalb des Kinoms bei, das sowohl das der Ausgangsverbindung als auch das von BIRB-796 übertrifft. Für eine eingehende Untersuchung von p38 $\alpha/\beta$  als Ziel für Kinase-Medikamente wurde weiterhin eine negative Kontrollverbindung während dieser Arbeit entwickelt, um zwischen spezifischen (on-target) Effekten und unspezifischen Effekten, z.B. durch Kreuzreaktivität mit anderen zellulären Proteinen, zu unterscheiden. Die Negativkontrollverbindung **35** (SR321) hatte eine geringe Aktivität gegenüber der DDR2-Kinase und war 100 mal weniger potent als die eigentliche Probe.<sup>136, 412, 413</sup> Weitere biologische Studien zur metabolischen Stabilität in menschlichen Lebermikrosomen zeigten die hohe Stabilität der Verbindungen, wobei nur eine geringe Menge an Metaboliten im Verlauf mehrerer Stunden gebildet wurde. Die Verbindung **33** (SR318) wies weiterhin eine gute Wirksamkeit *in vitro* auf, da sie bei höchster Testkonzentration zu einer quantitativen Reduzierung der LPS-stimulierten TNF- $\alpha$  Freisetzung im Vollblut führte und hierbei ein  $IC_{50}$ -Wert im nanomolaren Bereich bestimmt werden konnte. Mittels Western-Blot-Untersuchung wurde ferner eine konzentrationsabhängige hemmende Wirkung von **33** (SR318) auf endogene Substrate, wie der Phosphorylierung von p38 und Hsp27, in HCT15-Zellen festgestellt.

Zusammenfassend ist **33** (SR318) eine neue hochwirksame und selektive chemische Sonde vom Typ-II für p38 $\alpha/\beta$ , die zu einem besseren Verständnis der katalytischen und nicht-katalytischen Funktionen dieser wichtigen Signalkinasen in der Physiologie und Pathologie beitragen wird. Letzteres kann durch die Verwendung des gesamten während dieser Arbeit gemeinschaftlich entwickelten Pakets von p38-Inhibitor-Proben mit dem verfügbaren Typ-I-Inhibitor Skepinone-L, dem Typ-I $\frac{1}{2}$ -Inhibitor FS-694 und dessen Negativkontrolle FM-743 gewinnbringend unterstützt werden.

Die MAPK-p38 $\alpha$  und ihre eng verwandte Isoform p38 $\beta$  sind hochdynamische Proteinkinasen, die von Typ-II-Inhibitoren wie BIRB-796 adressiert werden. Ein Großteil der humanen Kinasedomänen kann eine inaktive DFG-out-Konformation annehmen,<sup>42, 43</sup> weshalb dieses Strukturmerkmal alleine als eher unwahrscheinlich angesehen wird, um selektive Inhibitoren zu erhalten.<sup>44, 265, 414</sup> Allosterische Fragmente, die vom Motiv der Bindung von BIRB-796 an p38 inspiriert sind, wurden auf ihre Interaktion innerhalb der allosterischen Toloyl-Tasche von höherer Selektivität und der DFG-out-Tasche von geringerer Selektivität untersucht.<sup>265, 267, 415-417</sup> Ein attraktives Merkmal der BIRB-796-Bindungsmotive für die sogenannte back-pocket ist, dass sie mit einer sehr langsamen off-rate-Bindungskinetik assoziiert wurden.<sup>265, 268, 418</sup> Ob die Selektivität dieser Fragmente gegenüber den für BIRB-796 gefundenen off-Targets verbessert werden kann, wurde bisher jedoch noch nicht ermittelt. Ein interessanter Ansatz wurde von Mitarbeitern bei *Deciphera Pharmaceuticals* entwickelt, welche über auf Harnstoff basierenden allosterischen Fragmente berichteten.<sup>329</sup> Während ihren Studien untersuchten sie die sogenannte switch-pocket-Region von p38, ein Bereich zwischen der  $\alpha$ C-Helix und dem HRD-Segment, in welchem sich die schwach konservierten Aminosäurereste Arg67, Arg149 und der nicht-konservierte Rest Arg70 befinden. Durch die Adressierung der Arginin Seitenketten konnte gezeigt werden, dass das Design von sehr selektiven Typ-III-Inhibitoren wie DP802 möglich ist.<sup>329, 333, 334, 337</sup> Die meisten dieser Inhibitoren verfügten jedoch nur über eine schwache Wirksamkeit und über schlechte pharmakologische Eigenschaften. Im Allgemeinen begünstigen ungewöhnliche Bindungsmodi, die auf nicht-konservierte Strukturelemente in Kinasen abzielen, nachweislich die Selektivität und Potenz der entsprechenden Inhibitoren (**Kapitel 2**). Ein Beispiel ist der ebenfalls veröffentlichte Typ-II p38 $\alpha$ -MAPK-Inhibitor VPC-00628, der eine einzigartig gefaltete Konformation des P-loops in p38 $\alpha$  stabilisiert, mit einem Cyclohexylrest gleichzeitig die DFG-out-Tasche adressiert und ein neuartiges Hinge-Bindemotiv besitzt.<sup>340</sup> Obwohl bekannt ist, dass einige Kinasen, wie ABL, ACK1, AURORA, cMET, FGFR1, MAP4K4 und p38, eine gefaltete (inaktive) Konformation des P-loops einnehmen können,<sup>54</sup> wurde die durch die Bewegung des P-loops vergrößerte allosterische Tasche (P-loop/ $\alpha$ C-Tasche) in der MAPK-Familie bisher nur durch den ERK1/2-Inhibitor SCH772984 adressiert.<sup>56</sup> Die Stabilisierung dieser Enzymtasche war mit hoher Inhibitorselektivität und langsamen Dissoziations-(off-)Raten verbunden. Interessanterweise hob SCH772984 dabei nicht nur die Aktivierung von den ERK1/2 nachgeschalteten Substraten auf, sondern auch dessen Phosphorylierung durch die stromaufwärts gelegene Kinase MEK1/2 an den Resten Thr202/Tyr204 sowie an Thr185/Thr187, ohne mit dieser selbst zu interagieren.<sup>56</sup> Aufgrund der großen strukturellen Veränderungen im N-Lobe, der normalerweise als Bindungsstelle für MEKs dient, wurde somit eine synergistische Hemmwirkung auf den Raf-MEK-ERK-Signalweg beobachtet.<sup>419-421</sup> Eine ausgeprägte konformationsselektive Hemmwirkung auf p38 und die MAPK-Signalkaskade wurde von HARI ET AL. im Jahr 2014 unter Verwendung kanonischer Typ-I- und Typ-II-Inhibitoren beschrieben.<sup>398</sup> Interessanterweise zeigte diese Studie auch unterschiedliche Effekte auf die Dephosphorylierung der Kinase durch die inaktivierende Phosphatase mit doppelter Spezifität (DUSP10) auf. Darüber hinaus berichteten SUVILLAN ET AL., dass Inhibitoren, die auf die Selektivität über die Stabilisierung der DFG-out-Tasche abzielen (z.B. BIRB-796) gleichzeitig die Aktivierung von p38 sowie Phosphorylierung durch MEK6 hemmen, mit  $K_d$ -Werten im niedrigen nanomolaren Bereich, ohne die Aktivität von MEK6 direkt zu beeinflussen.<sup>418</sup> Insgesamt liefern diese Berichte überzeugende Argumente dafür, dass konformationsselektive Kinaseinhibitoren sehr unterschiedliche Auswirkungen auf die zelluläre Signalübertragung und als Folge davon auch auf die phänotypischen Reaktionen haben können.

Die nächsten Studien dieser Doktorarbeit konzentrierten sich deshalb auf die Erforschung der hochdynamischen allosterischen back-pocket von p38-MAPK, und es wurden von BIRB-796 abgeleitete allosterische Verbindungen zur Adressierung der  $\alpha$ C- und DFG-out-Tasche synthetisiert (**Kapitel 4**). Diese Arbeit wurde in Kollaboration mit Mitarbeitern vom Bagley Lab (Sussex, UK), vom SGC (Frankfurt), der Arbeitsgruppe von Stefan Laufer (Universität Tübingen) und von Daniel Dauch (Universitätsklinikum

Tübingen) sowie der Biomolecular Interactions Research Group (Budapest, Ungarn) durchgeführt. Die Inhibitoreffekte der allosterischen Pyrazol-Harnstoff-Fragmente wurde mit Hilfe der Differential-Scanning-Fluorimetrie (DSF) für ein umfassendes Set von 47 verschiedenen Kinasen analysiert. Hierbei stellte sich heraus, dass die für BIRB-796 gefundenen off-Targets auch für die neu synthetisierten Fragmente, welche die back-pocket stabilisieren, weitgehend erhalten bleiben. Bei der erneuten Untersuchung der zuvor beschriebenen Verbindung MCP-081 (**Kapitel 3**), welche die allosterischen Komponente von BIRB-796 mit der auf das aktive Zentrum gerichteten Komponente von VPC-00628 kombiniert, zeigte sich, dass MCP-081 in unserem Kinasenset ein klares Selektivitätsprofil aufweist. Da die Potenz von MCP-081 im Vergleich zu VPC-00628 leicht reduziert war und das allosterische Pyrazol-Strukturmotiv suboptimal erschien, wurde ein Set von VPC-00628-Derivaten zur Ausrichtung auf die  $\alpha$ C-out-Taschenregion synthetisiert. Durch die kristallstrukturorientierte Erweiterung des terminalen Amids von VPC-00628 in Richtung dieser allosterischen Tasche wurde die potente und selektive Verbindung **218** (SR43) entwickelt, die im NanoBRET<sup>TM</sup>-Assay eine ausgezeichnete zelluläre Aktivität auf p38-MAPK zeigte ( $IC_{50}$  [p38 $\alpha/\beta$ ] = 14.0 nM/16.8 nM). Die Verbindung hemmte dosisabhängig die aktivierende Phosphorylierung von p38 in HCT-15 Zellen sowie die Phosphorylierung der nachgeschalteten Substrate MK2 und Hsp27. Darüber hinaus induzierte **218** (SR43) eine entzündungshemmende Wirkung durch Blockierung der TNF- $\alpha$ -Freisetzung im Vollblut und zeigte eine hohe metabolische Stabilität. Die Untersuchung des Selektivitätsprofils von **218** (SR43) ergab eine geringe Aktivität für zusätzliche Targets wie die Discoidin-Domain-Rezeptorkinasen (DDR1/2). DDR-Kinasen spielen eine zentrale Rolle bei fibrotischen Erkrankungen wie Nieren- und Lungenfibrose sowie bei Atherosklerose und Krebs. Da selektive und potente Inhibitoren für dieses wichtige therapeutische Target weitgehend fehlen und die vorhandenen Inhibitoren eine geringe chemische Diversität des Grundgerüsts aufweisen, konzentrierte sich die nächste Studie auf die Optimierung von **218** (SR43) zur Inhibition der DDR1/2-Kinasen (**Kapitel 5**). Die Arbeit entstand in einer Kollaboration mit Mitarbeitern vom SGC in Frankfurt und Oxford, der Universität in Tübingen sowie dem Buchmann Institute for Molecular Life Sciences (BMLS).

Die Discoidin-Domain-Rezeptorkinasen DDR1 und DDR2 wurden Anfang der 90er Jahre als Mitglieder der Rezeptortyrosinkinase-Familie (RTKs) identifiziert. Während DDR2 als einzelnes Typ-I-Transmembranprotein exprimiert wird, wurden fünf Isoformen von DDR1 entdeckt, die durch alternatives Spleißen erzeugt werden, nämlich DDR1a, DDR1b, DDR1c, DDR1d und DDR1e.<sup>462, 463</sup> DDR-Kinasen weisen eine hohe Strukturähnlichkeit in ihrer extrazellulären Discoidin-Domäne auf und unterscheiden sich deutlich stärker in ihrem intrazellulären Teilbereich. Während DDR1a-c und DDR2 eine gemeinsame intrazelluläre Kinasedomäne besitzen, besitzen die Isoformen DDR1d und DDR1e eine verkürzte, kinasedefiziente, intrazelluläre Domänenstruktur.<sup>469</sup> Der Vergleich von Struktur und Funktion dieser RTKs zeigte einzigartige Eigenschaften auf, wie die Aktivierung durch verschiedene dreifach helikale Kollagene der extrazellulären Matrix.<sup>462, 463, 468</sup> Typischerweise verwenden RTKs peptidähnliche Wachstumsfaktoren als extrazelluläre Liganden, gefolgt von einer Rezeptordimerisierung, Kreuzphosphorylierung und einer schnellen Aktivierung der Signalkaskade. Von einzelnen Ausnahmen wie bei der Aktivierung der Insulinrezeptorkinase (IRK) oder dem Epidermal Growth Factor Rezeptor (EGFR) wurde berichtet. Es wurde jedoch festgestellt, dass DDR-Kinasen in vorgeformten autoinhibierten Homo- oder Heterodimeren des Rezeptors in der Membran existieren, welche die Kollagenbindung forcieren.<sup>464</sup> Auf die Ligandbindung folgen typischerweise eine Reihe von Autophosphorylierungen in der intrazellulären Seite, die zu einer Aktivierung der intrinsischen Kinasedomäne mit untypisch langsamer Kinetik führen.<sup>464, 465</sup> Ein dauerhaftes Phosphorylierungssignal ist daher oft über Stunden nachweisbar und wird unter anderem durch Adaptorproteine wie dem SH2 domain containing transforming protein (Shc1) vermittelt.<sup>475</sup> In Verbindung mit der extrazellulären Matrix regulieren die DDR-Kinasen grundlegende physiologische Prozesse wie Adhäsion, Migration, Proliferation,

Differenzierung, den Umbau der Matrix sowie das Überleben.<sup>465</sup> Eine anomale Aktivierung der Kinase wurde bei fibrotischen Erkrankungen wie Lungen-, Nieren- und Leberfibrose, bei Krebserkrankungen wie dem Glioblastom und in der Frühphase der Entstehung einer Osteoarthritis nachgewiesen. Obwohl die DDR-Kinase als ein Enzym beschrieben wurde, welches Inhibitoren promiskuitiv bindet, und publizierte Kinaseinhibitoren diese deshalb sehr häufig als off-Target aufweisen, wurde der Entwicklung von selektiven DDR-Kinaseinhibitoren bisher wenig Aufmerksamkeit gewidmet.<sup>485</sup> Die Inhibitorlandschaft ist von begrenzter Gerüstvielfalt, die hauptsächlich in den letzten sechs Jahren entstanden ist und Harnstoffverbindungen umfasst, die durch Derivatisierung von Inhibitoren mit bekannter DDR1/2-Kinaseaktivität wie Imatinib, Dasatinib und BIRB-796 entwickelt wurden.<sup>459, 486, 487</sup> Ein ähnlicher Ansatz konzentrierte sich auf das Grundgerüst von Ponatinib, wobei eine Reihe von Pyrazolopyrimidin- und Imidazopyrazin-Derivaten entwickelt wurde.<sup>488, 489</sup> Des Weiteren wurden Tetrahydroisochinolin-7-carboxamide als sehr potente und selektive DDR1-Inhibitoren beschrieben. Letztere zeigten jedoch eine unerwünschte Inhibierung der Tropomyosin-Rezeptorkinasen (TrkA-C), die für die Entwicklung und normale Funktion des zentralen und peripheren Nervensystems von Bedeutung sind.<sup>491-494</sup> Eine vielversprechende Möglichkeit zur effektiven Inhibierung von DDR1 stellen die kürzlich von Roche Pharma entdeckten potenten Spiroindolinone dar, welche bereits positiv zur Behandlung des renalen Alport-Syndrom in Mäusen getestet wurden.<sup>496</sup>

Zur Entwicklung eines neuen DDR1/2-Kinaseinhibitors, der auf einem völlig neuen Grundgerüst basiert, wurden alle zuvor in dieser Arbeit synthetisierten und untersuchten p38-Inhibitoren mittels DSF-Assay auf die für **218** (SR43) gefundenen off-Targets wie DDR1/2, ZAK und ABL1 untersucht und mit p38 $\alpha/\beta$  verglichen. Anhand dieser Analyse wurde das vielversprechendste Derivat aus der Serie zur back-pocket-Optimierung (**Kapitel 4**) im Komplex mit der DDR1-Kinase kristallisiert und die erhaltene Kristallstruktur mit den publizierten Kristallstrukturen verglichen. Nach Evaluierung der geeignetsten Bausteine zur Entwicklung eines von **218** (SR43) abgeleiteten DDR1/2-Kinaseinhibitors wurde die Hinge-bindende Kopfgruppe sowie die allosterische Komponente von **218** (SR43) synthetisch verändert. Die Untersuchungen führten zur Entwicklung eines hochselektiven dualen p38/DDR-Inhibitors, **302** (SR302), mit picomolarer Affinität für DDR2 ( $IC_{50}$  [DDR1/2] = 53.3 nM/ 0.75 nM,  $IC_{50}$  [p38 $\alpha/\beta$ ] = 6.2 nM/ 45.1 nM). Weiterhin ermöglichten diese Studien interessante Einblicke in den Faltungsprozess des P-loops von p38-MAPK und zeigten auf, wie die gezielte Stabilisierung von nicht konservierten Aminosäuren die Selektivität eines p38-Inhibitors vom Typ-II beeinflussen kann. Im Rahmen dieser Arbeit wurde zudem eine entsprechende negative Kontrollsubstanz, **301** (SR301), synthetisiert, welche eine um drei Größenordnungen niedrigere Wirksamkeit für DDR1/2 in HEK293T Zellen als die Probe **302** (SR302) aufweist. Erste *in vitro* Studien zeigten, dass **302** (SR302) eine destabilisierende Wirkung auf das Oberflächenadhäsionsprotein E-Cadherin in Epithelzellen besitzt. Weiterführende Untersuchungen zur Quantifizierung des endozytierten E-Cadherins in Kollaboration mit der Zell-Biologie Gruppe von Christian Pohl (Buchmann Institute for Molecular Life Sciences (BMLS)) sind deshalb in Planung. Nach Abschluss entsprechender Studien könnte **302** (SR302) zusammen mit dessen Negativkontrolle **301** (SR301) als wertvolles Hilfsmittel zur eingehenden Untersuchung des DDR1/2-Signalwegs z.B. in Krebszelllinien eingesetzt werden.

## 8 Experimental part

### 8.1 General and measuring instruments

#### 8.1.1 General

Unless otherwise stated, all reactions in this work were carried out at 25 °C under an argon atmosphere. Distillations marked "removed under reduced pressure/in vacuo" were carried out with a rotary evaporator under membrane pump vacuum at 40 °C. Drying of the substances, for solids and high-boiling liquids, was performed in the high vacuum of an oil pump or in a vacuum drying oven at 40 °C. The molecular weights in brackets ( ) refer to the natural isotope distribution. The numerical values in square brackets [ ] refer to the masses of the most common isotopes <sup>1</sup>H, <sup>12</sup>C, <sup>14</sup>N, <sup>16</sup>O, <sup>23</sup>Na and <sup>32</sup>S.

#### 8.1.2 Chemicals and solvents

All chemicals and solvents used, were purchased from commercial suppliers as *Abcr*, *Acros Organics*, *Alfa Aesar*, *ChemPur*, *Carl Roth*, *Fischer Scientific*, *Fluka*, *Fluorochem UK*, *Merck*, *Santa Cruz Biotechnology*, *Sigma Aldrich*, *TCI Europe* and *VWR International*. The solvents were used in different degrees of purity: per analysis (p.a.), HPLC-grade and analytical grade. Unless otherwise indicated, all chemicals and solvents were used for synthesis without further purification. Deuterated solvents for NMR measurements were purchased from *Eurisotop*, France. Fmoc-homocyclohexyl-L-alanine (**105**) was purchased from *PolyPeptide Group*, France.

#### 8.1.3 Chromatographic methods

##### 8.1.3.1 Thin-layer chromatography (TLC)

For analytical thin-layer chromatography, silica gel coated aluminum plates with fluorescence indicator from *Merck KGaA* (TLC silica gel 60 F<sub>254</sub> plates) were used. The chromatographic zones were detected with UV light of the wavelength  $\lambda = 254$  nm (fluorescence quenching) and the wavelength  $\lambda = 365$  nm (autofluorescence). In addition, *p*-anisaldehyde, cerium molybdate, 2,4-dinitrophenylhydrazine (DNP) and ninhydrin solution were used as staining reagents for the detection:<sup>519</sup>

- *p*-Anisaldehyde solution: 3.7 mL *p*-Anisaldehyde, 5 mL concentrated sulfuric acid, 1.5 mL glacial acetic acid, 135 mL absolute EtOH.
- Dinitrophenylhydrazine (DNP) solution: 12 g 2,4-Dinitrophenylhydrazine, 60 mL concentrated sulfuric acid and 80 mL H<sub>2</sub>O in 200 mL of 95% EtOH.
- Ninhydrin solution: 1.5 g Ninhydrin, 15 mL glacial acetic acid, 500 mL MeOH.
- Cerium molybdate solution: 12 g Ammonium molybdate, 0.5 g ceric ammonium molybdate, and 15 mL concentrated sulfuric acid in 235 mL of H<sub>2</sub>O.

TLC plates were immersed in the respective solution and then developed under the action of heat using a heat gun. The solvent mixtures specified correspond to the volume ratios.

### 8.1.3.2 Preparative Column Chromatography

Column chromatographic purifications were performed on silica gel with a particle size of 0.040-0.063 mm from *Macherey-Nagel*, unless otherwise specified. Flash chromatographic purifications were carried out with a PuriFlash XS system from *Interchim* and with silica columns of 15  $\mu\text{m}$ , 30  $\mu\text{m}$  and 50  $\mu\text{m}$  particle size. Solvents were used in HPLC grade or technical grade purity. The noted solvent mixtures correspond to volume ratios.

### 8.1.3.3 High Performance Liquid Chromatography (HPLC)

The purity of the final compounds was determined to >95% using an HPLC system (LC-20A Prominence) from *Shimadzu*. The separations were performed on a C18 column (Luna 10 $\mu$  C18 (2) 100 Å. 250 mm x 4.6 mm) from *Phenomenex* using the following gradient profile: 0 - 2 min 95% B, 2 - 14 min 95% B, 14 - 21 min 10% B, 21 min 95% B. As solvent A) acetonitrile Ultra MS-Grade was used and as solvent B) MS-Grade H<sub>2</sub>O with 0.1% formic acid at a flow rate 1 mL/min. The detection was carried out with a LCMS-2020 mass spec detector from *Shimadzu* at a wavelength of 254 and 280 nm respectively.

### 8.1.3.4 NMR spectroscopy

All samples were dissolved in deuterated solvent and measured on one of the following devices:

- *Bruker* DPX 250: 250 MHz <sup>1</sup>H-NMR
- *Bruker* Avance 300: 300 MHz <sup>1</sup>H-NMR, 75 MHz <sup>13</sup>C-NMR
- *Bruker* Avance 400: 400 MHz <sup>1</sup>H-NMR, 101 MHz <sup>13</sup>C-NMR
- *Bruker* Avance 500: 500 MHz <sup>1</sup>H-NMR, 126 MHz <sup>13</sup>C-NMR
- *Bruker* DRX 600: 600 MHz <sup>1</sup>H-NMR, 150 MHz <sup>13</sup>C-NMR

The values given for the chemical shift ( $\delta$ ) refer to the signal of the particular deuterated solvent used in reference to the tetramethylsilane standard at  $\delta = 0$  ppm<sup>520</sup>

- CD<sub>2</sub>Cl<sub>2</sub>:  $\delta(^1\text{H}) = 5.32$  ppm,  $\delta(^{13}\text{C}) = 54.00$  ppm
- CDCl<sub>3</sub>:  $\delta(^1\text{H}) = 7.26$  ppm,  $\delta(^{13}\text{C}) = 77.16$  ppm
- CD<sub>3</sub>OD:  $\delta(^1\text{H}) = 3.31$  ppm,  $\delta(^{13}\text{C}) = 49.00$  ppm
- (CD<sub>3</sub>)<sub>2</sub>CO:  $\delta(^1\text{H}) = 2.05$  ppm,  $\delta(^{13}\text{C}) = 29.84$  ppm
- D<sub>2</sub>O:  $\delta(^1\text{H}) = 4.79$  ppm
- DMSO-d<sub>6</sub>:  $\delta(^1\text{H}) = 2.50$  ppm,  $\delta(^{13}\text{C}) = 39.52$  ppm

<sup>1</sup>H-broadband decoupling was performed on the <sup>13</sup>C-NMR-spectra. The obtained spectra were either evaluated with the software *TopSpin 3.2* from *Bruker* or *MestReNova* from *Mestrelab Research SL*.

### 8.1.3.5 Mass spectrometry

Mass spectrometry was measured as a service at the Faculty of Biochemistry, Chemistry and Pharmacy at Goethe University, D-60438 Frankfurt am Main, Germany.

- High resolution mass spectrometry (FTMS + p MALDI-HRMS) was performed using a MALDI LTQ XL Orbitrap spectrometer from *Thermo Scientific*. The samples were measured without solvent in a HCCA matrix.
- Mass spectrometry (ESI) was measured in solution on a Surveyor MSQ spectrometer from *ThermoFisher* or directly from TLC using TLC-MS interface 2 from *Camag*.

- Mass spectrometry (p MALDI) was measured without solvent in a HCCA matrix on a Voyager-DE STR spectrometer from *Perseptive Biosystems* (today: *Applied Biosystems*).

## 8.2 Biological Methods

### 8.2.1 Differential scanning fluorometrie (DSF)-assay

The differences in the melting temperature ( $\Delta T_m$ ) of proteins with and without ligand treatment were measured as described by FEDOROV ET AL.<sup>422</sup> The measurements were assisted by A. Krämer, M. Schröder, D. Chatterjee and S. Mathea from the Structural Genomics Consortium (SGC), Buchmann Institute for Life Sciences, Max-von-Laue-Str. 15, D-60438 Frankfurt am Main, Germany., who also provided the proteins.

### 8.2.2 NanoBRET™ assay

The assay originally developed by *Promega* was performed in HEK293T cells by B.T. Berger, from the Structural Genomics Consortium (SGC), Buchmann Institute for Life Sciences, Max-von-Laue-Str. 15, D-60438 Frankfurt am Main, Germany, as described previously.<sup>402, 427, 428</sup>

### 8.2.3 Crystallization and structure determination

Crystallization and structure determination of the compounds synthesized in this work in complex with p38 $\alpha$  and DDR1 kinase were performed in collaboration with A. Chaikuad, M. Schröder, A. Joerger, D. Chatterjee and S. Mathea from the Structural Genomics Consortium (SGC), Buchmann Institute for Life Sciences, Max-von-Laue-Str. 15, D-60438 Frankfurt am Main, Germany. The crystal structure of **232** (SR159) in complex with DDR1 kinase was solved in collaboration with D. Pinkas, Structural Genomics Consortium, University of Oxford, Old Road Campus Research Building, Roosevelt Drive, Oxford OX3 7DQ, U.K.

### 8.2.4 In silico studies

A comparative model of p38 $\beta$  was created with the server Swiss Model (<https://swissmodel.expasy.org/>), using the crystal structure of the lead compound VPC-00628 in complex with p38 $\alpha$  (PDB: 5LAR) as template. Docking studies on MCP-078, MCP-012 and MCP-011 were performed using the platform SeeSAR v8.1 (BioSolveIT GmbH, Sankt Augustin, Germany, 2019, [www.biosolveit.de/SeeSAR](http://www.biosolveit.de/SeeSAR)) for both p38 isoforms by the help of R. Tesch, Structural Genomics Consortium (SGC), Buchmann Institute for Life Sciences, Max-von-Laue-Str. 15, D-60438 Frankfurt am Main, Germany. The binding site was defined using VPC-00628 as center point and 10 poses were generated for each compound. The pose with the best estimated affinity for each compound was selected for visual inspection on PyMOL v4.4.0.<sup>402</sup>

### 8.2.5 Selectivity screen

Kinome wide selectivity screen was performed as a service of *DiscoverX* (today: *Eurofins*, Fremont, CA 94538, United States) using scanMAX<sup>SM</sup> kinase assay panel. The assay system covered 468 kinases from AGC, CAMK, CMGC, CK1, STE, TK, TKL, lipid and atypical kinase families, plus important mutant forms. Standard

selectivity scores (S) were calculated from non-mutated kinases, according the following equation:  $S(x) = \frac{\text{number of values } \leq x}{\text{total number of values}}$ , in which x represents the activity/%ctrl. threshold.

### **8.2.6 TNF- $\alpha$ release assay in human whole blood**

The assay was performed as published by BAUER ET AL. and done in collaboration with M. Forster from the Department of Pharmaceutical/Medicinal Chemistry, Eberhard Karls University Tübingen, Auf der Morgenstelle 8, 72076 Tübingen, Germany.<sup>521</sup> The assay principle is summarized here in brief: The tested compounds were pre-incubated in human whole blood from two different donors for 15 min before TNF- $\alpha$  release was stimulated by addition of LPS. After stimulation the samples were incubated at 37 °C and 6% CO<sub>2</sub> for 2.5 h followed by centrifugation to separate cells and plasma. The supernatant was separated and the TNF- $\alpha$  levels were determined using a sandwich ELISA.

### **8.2.7 In vitro metabolism studies**

The metabolism studies were performed in collaboration with M. Kudolo from the Department of Pharmaceutical/Medicinal Chemistry, Eberhard Karls University Tübingen, Auf der Morgenstelle 8, 72076 Tübingen, Germany. For this assay described in the recent publication by RÖHM ET AL. pooled male human liver microsomes (HLM) were used and samples were analyzed by LC-MS analysis.<sup>402</sup>

### **8.2.8 Western-blot analysis**

#### **8.2.8.1 Hsp27 phosphorylation**

Inhibition of Hsp27 phosphorylation in HCT15 cells was done by J. Harbig and D. Dauch from the Department of Medical Oncology and Pneumology, University Hospital Tuebingen. German Cancer Research Consortium (DKTK), German Cancer Research Center (DKFZ), 69120 Heidelberg, Germany iFIT Cluster of Excellence EXC 2180 „Image Guided and Functionally Instructed Tumour Therapies“, University of Tuebingen, Tuebingen, Germany. In brief: HCT15 cells were treated for 2 h with inhibitors at different concentrations or vehicle (DMSO) and then stimulated with 10  $\mu\text{g}/\text{mL}$  anisomycin (Merck, A9789) for 30 min. Levels of p-Hsp27 (antibody: Cell Signaling Technology, 2401) were determined via Western Blot analysis of whole cell lysates. Vinculin (antibody: Merck, V9131) was used as loading control. The chemiluminescence was measured with the Bio-Rad ChemiDoc MP Imaging System and recorded with the Image Lab 4.1 software for image acquisition.

#### **8.2.8.2 MK2 phosphorylation**

The assay was performed in collaboration with Anna Sebö and Attila Reményi, Biomolecular Interactions Research Group, Institute of Organic Chemistry, Research Center for Natural Sciences, Magyar Tudósok körútja 2, H-1117 Budapest, Hungary. In brief: Cells were treated with 0.33 M sorbitol and the phosphorylation of p38 and MK2 was monitored in time by Western-blot. Cells were incubated with DMSO or with the indicated inhibitors in 200 nM concentration 2 h prior to sorbitol stimulation. For Western-blot analysis, cells were lysed in SDS loading buffer after sorbitol treatment and samples were run on SDS PAGE. Western-blot results were analyzed using Odyssey CLx imaging system (Li-Cor) and fluorescently labeled secondary antibodies (IRDye 800 CW goat anti-Rabbit 925-32211 or IRDye 680 RD goat anti-Mouse 925-



68070. Li-Cor). Total p38 and MK2 and kinase phosphorylation levels - and tubulin as load control - were monitored by using the following antibodies: anti-p38 (Cell Signaling #9228), anti-MK2 (Cell Signaling #12155), anti-phosphop38 (Cell Signaling #9215), anti-phosphoMK2 (Phospho-MAPKAPK-2 (Thr334). Cell Signaling #3007) and anti-tubulin (Sigma-Aldrich T6199).

### 8.2.9 E-cadherin staining

The experiment was performed in collaboration by Lohitesh Kovooru and Christian Pohl, Buchmann Institute for Life Sciences, Max-von-Laue-Str. 15, D-60438 Frankfurt am Main, Germany. In brief: LLC-PK1 wildtype proximal tubule cells were treated with 100 nM of probe and negative control and incubated for 24 h. Cells were then fixed and stained with E-cadherin and Phalloidin. Images were captured using a confocal microscope (Leica DMI8 confocal microscope).

## 8.3 Experimental part of Chapter 3

### 8.3.1 VPC-00628 derivatives

Compounds synthesized for the development of highly selective p38 MAPK inhibitors in **Chapter 3**, were designed in cooperation with *Mercachem BV* in Kerkenbos 1013, 6546 BB, Nijmegen (The Netherlands). Detailed information on the synthesis of these compounds can be taken from the recent publication: "Fast iterative Synthetic Approach toward Identification of Novel Highly Selective p38 MAP kinase inhibitors", published as part of this PhD thesis in *Journal of Medicinal Chemistry*.<sup>402</sup> A structural overview of all compounds synthesized is given in the following Figures:

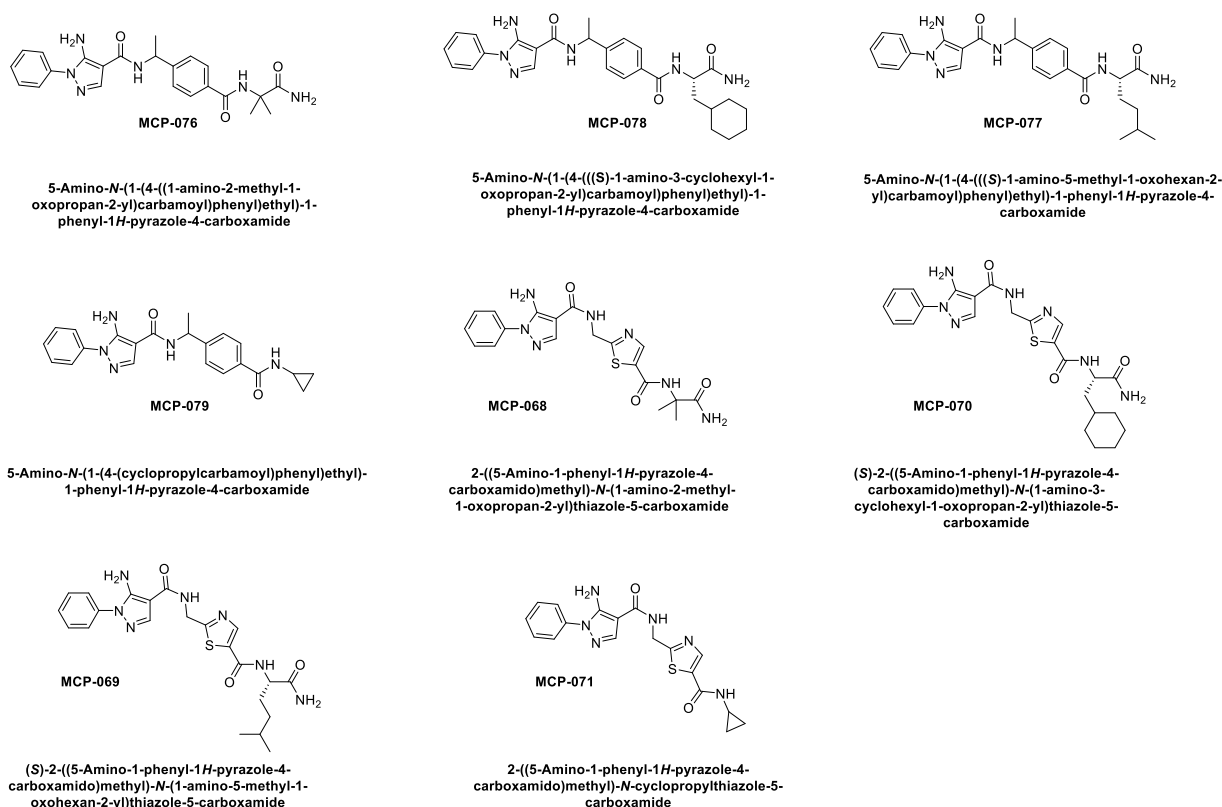
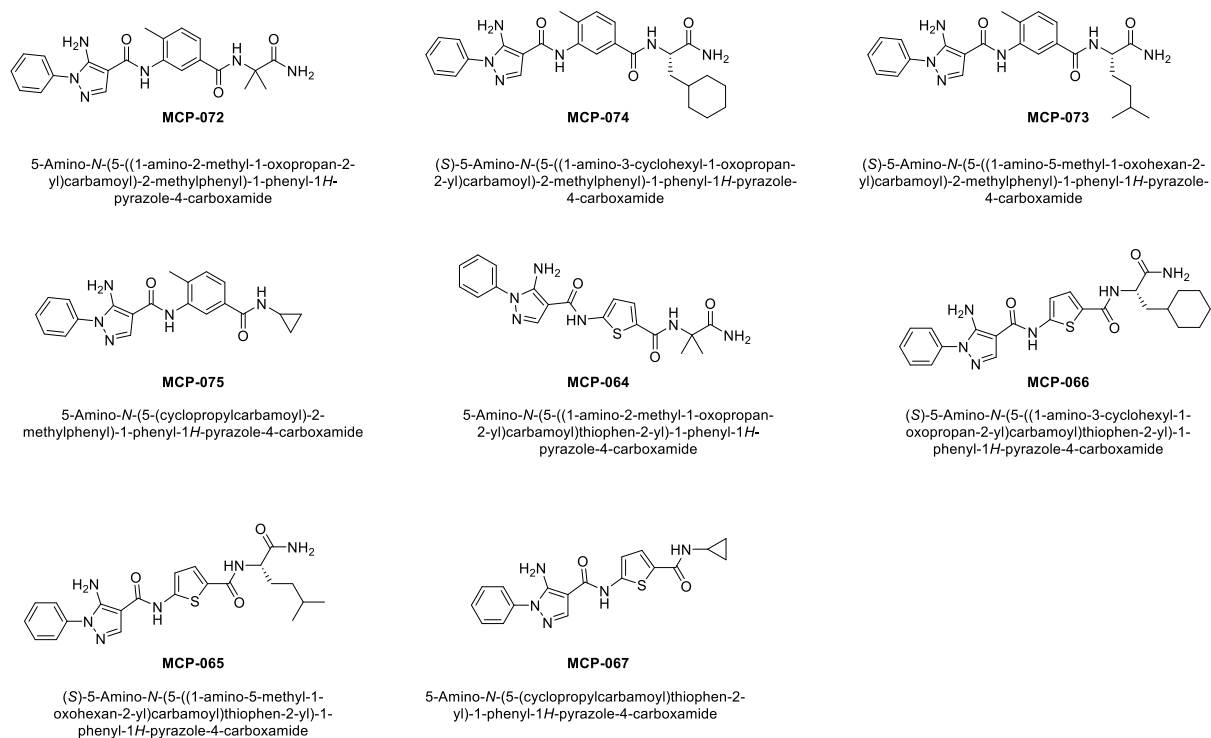
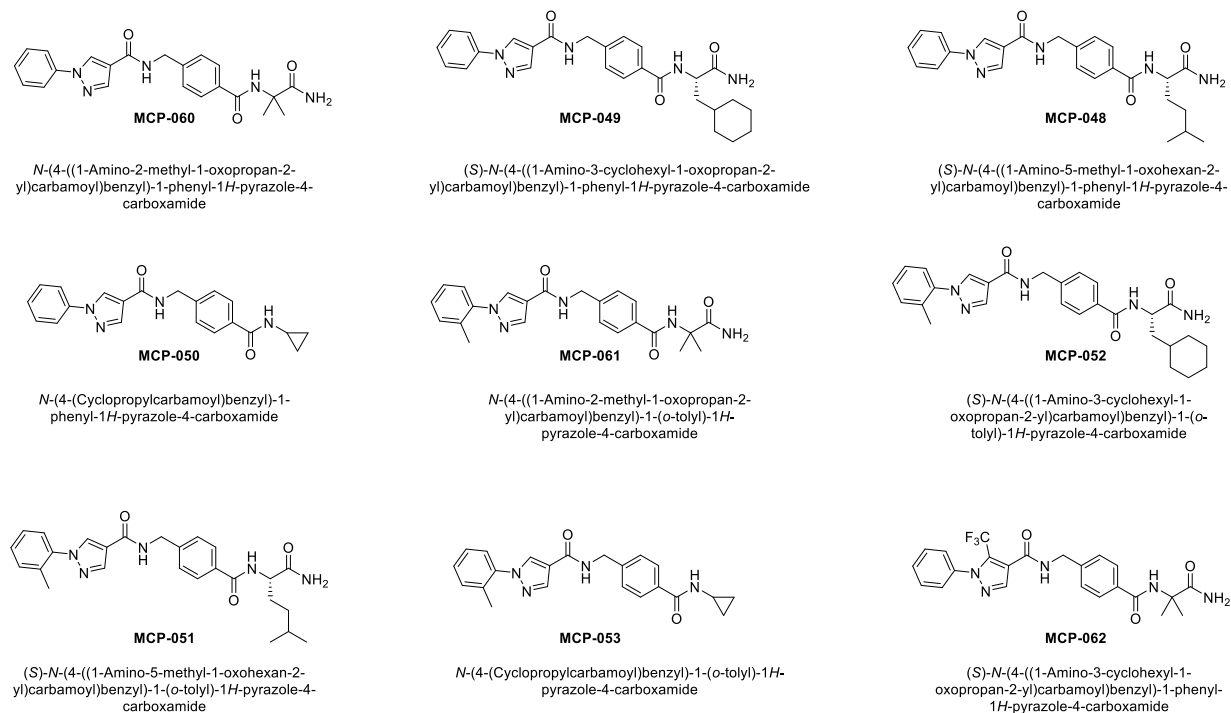


Figure 49. VPC-00628 derivatives by *Mercachem BV*, with P1 fixed building block, part A.



**Figure 50. VPC-00628 derivatives by Mercachem BV, with P1 fixed building block, part B.**



**Figure 51. VPC-00628 derivatives by Mercachem BV, with invariant P2 moiety, part A.**

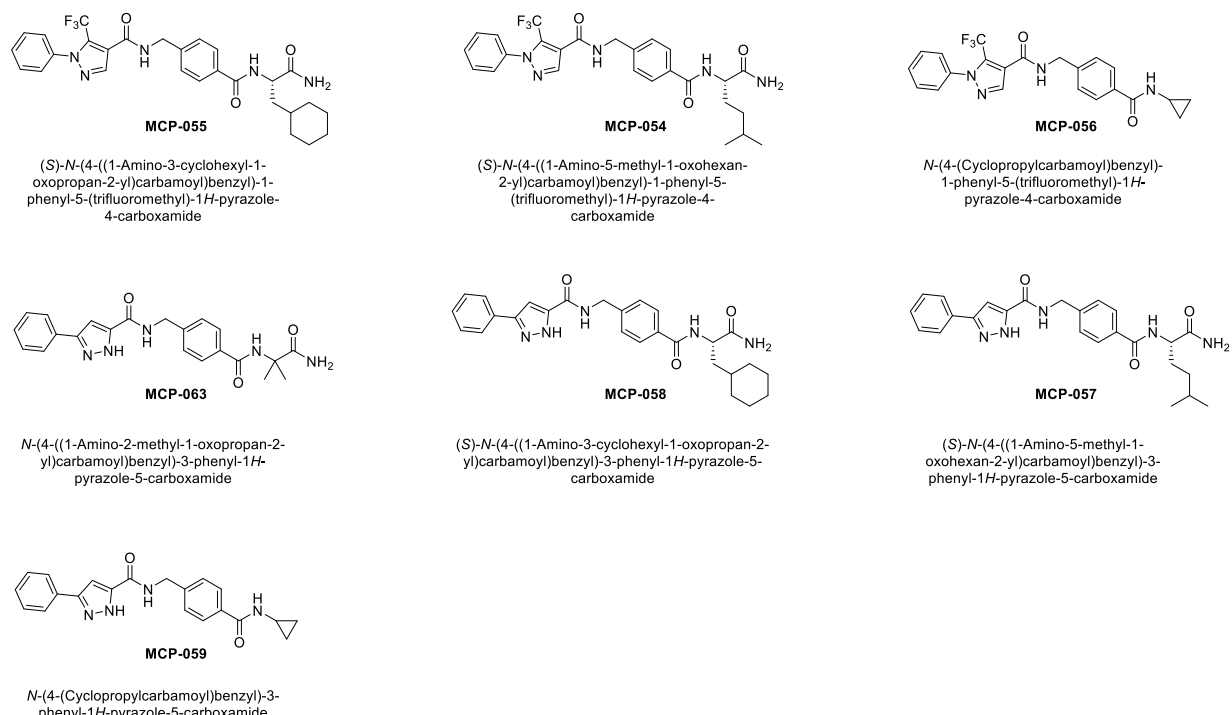


Figure 52. VPC-00628 derivatives by Mercachem BV, with invariant P2 moiety, part B.

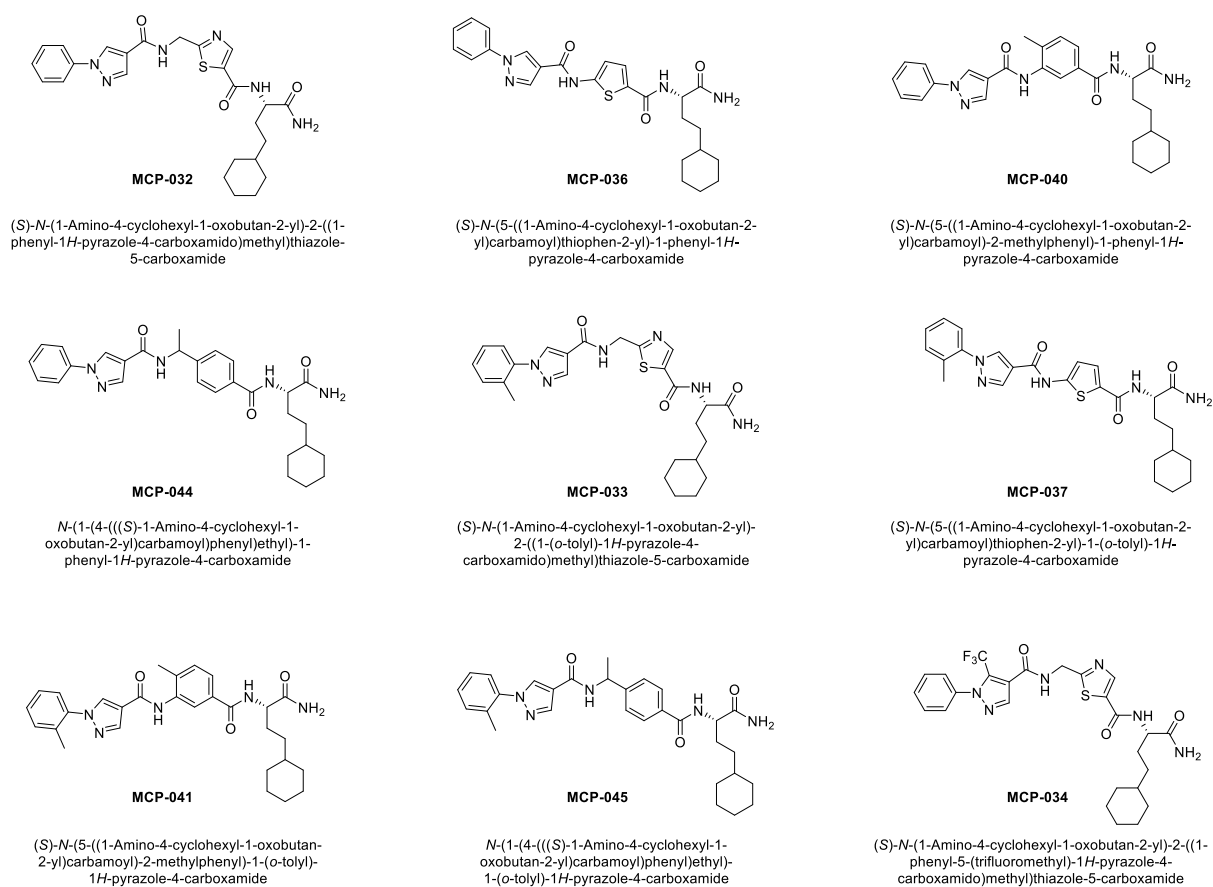
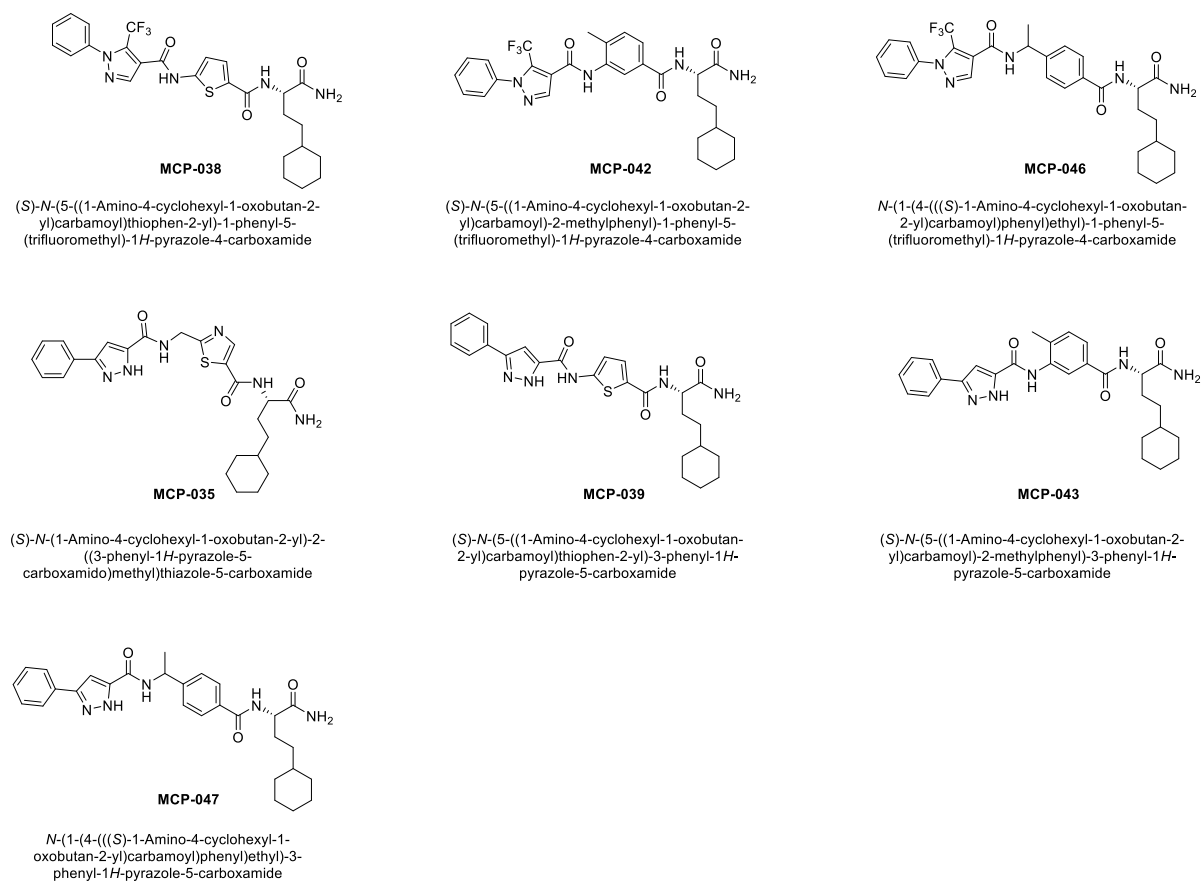
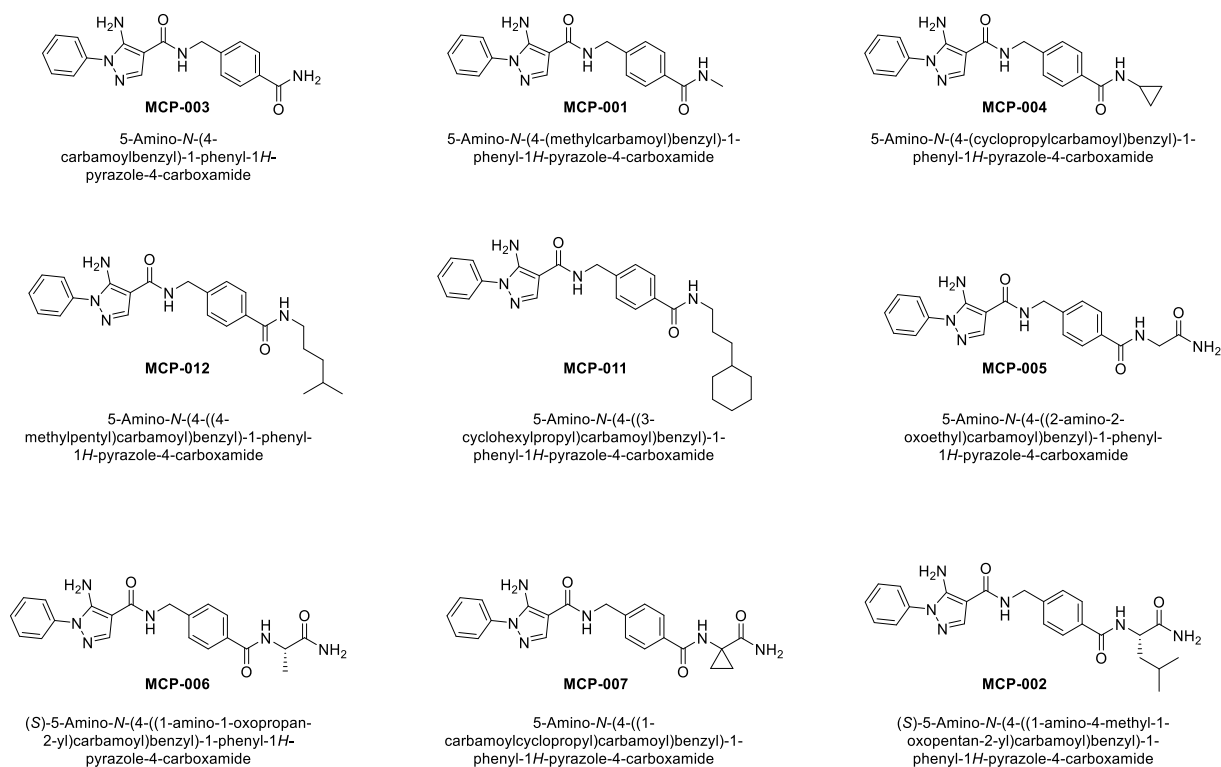


Figure 53. VPC-00628 derivatives by Mercachem BV, with P3 fixed building block, part A.



**Figure 54. VPC-00628 derivatives by Mercachem BV, with P3 fixed building block, part B.**



**Figure 55. VPC-00628 derivatives by Mercachem BV, with P1 and P2 invariant moieties, part A.**

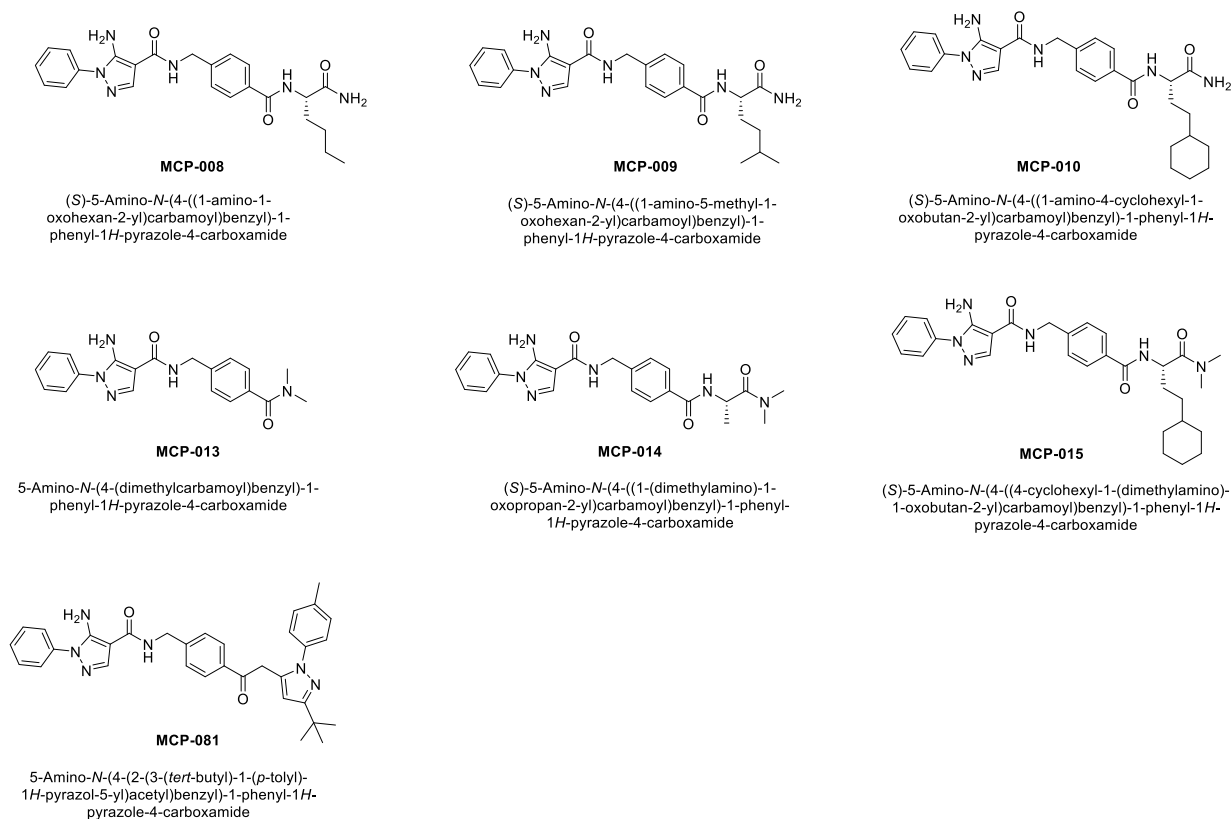


Figure 56. VPC-00628 derivatives by Mercachem BV, with P1 and P2 invariant moieties, part B.

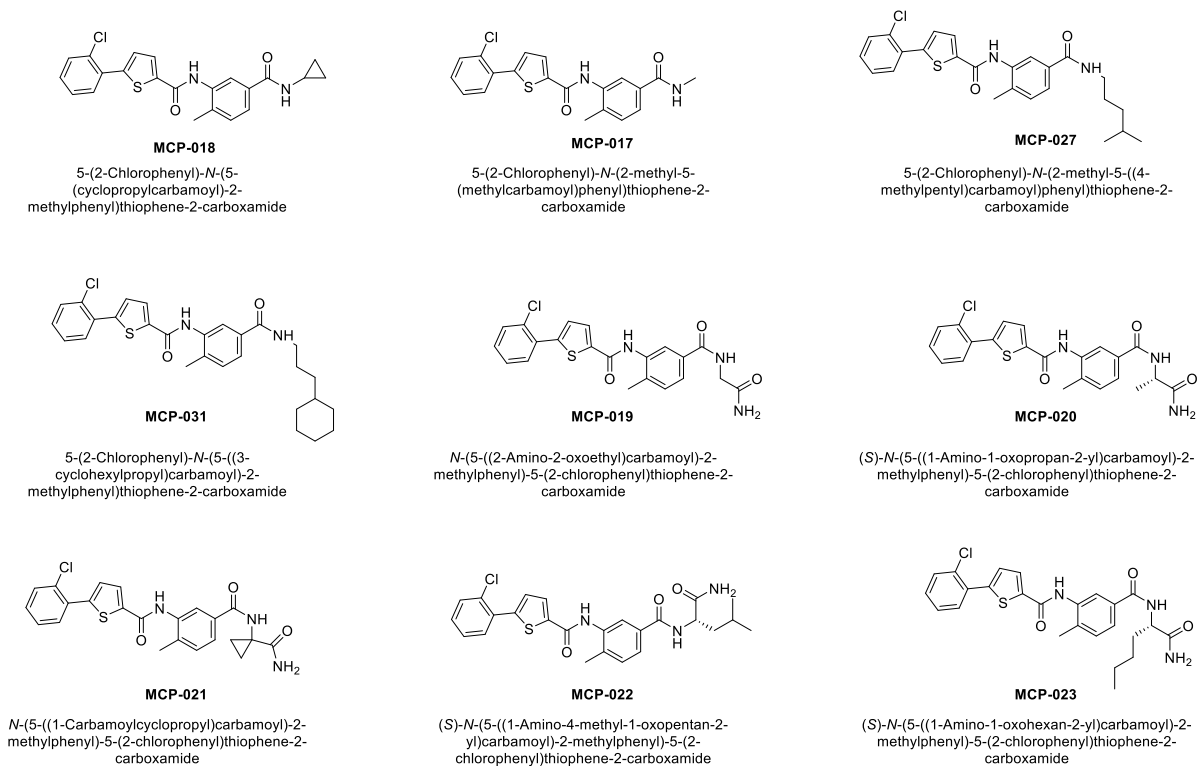


Figure 57. BMS-5c (MCP-018) and derivatives by Mercachem BV, with P1 and P2 invariant moieties, part A.

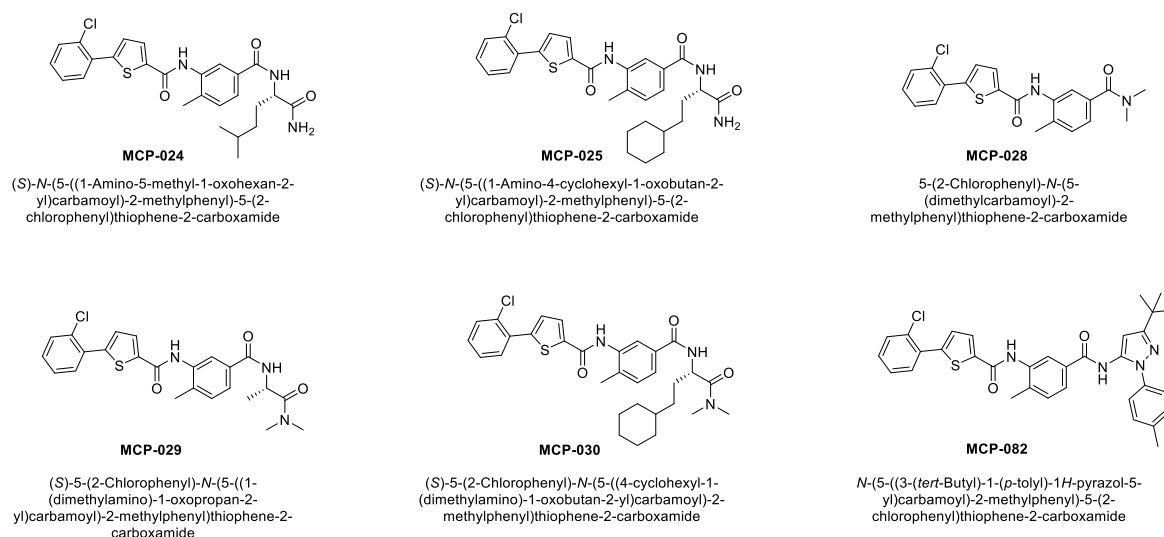


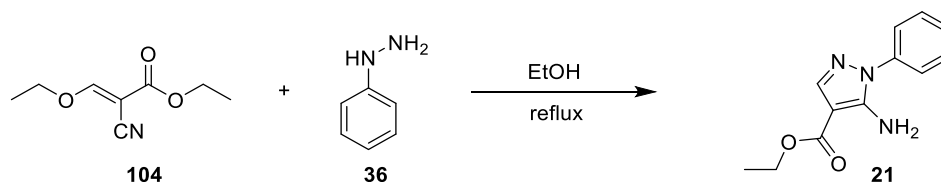
Figure 58. BMS-5c derivatives by Mercachem BV, with P1 and P2 invariant moieties, part B.

### 8.3.2 Probe candidate and negative control compound

The upscaling of compound MCP-011 (**33**, SR318) and the synthesis of potential negative control compounds was performed during this work by the following procedures:

### 8.3.3 Synthesis of precursors

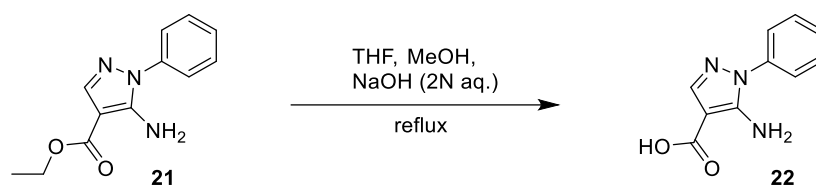
#### Ethyl 5-amino-1-phenyl-1*H*-pyrazole-4-carboxylate (**21**, SR8)



(*E*)-Ethyl 2-cyano-3-ethoxyacrylate (**104**, 35.0 g, 0.207 mol) and phenylhydrazine (**36**, 21.2 g, 0.169 mol) were dissolved in EtOH (abs., 200 mL). The reaction mixture was heated at reflux for 1 h and the solution was concentrated in vacuo to half of its starting volume. After cooling to RT the precipitate was filtered off and washed with EtOH. The crude product was recrystallized from EtOH.

**Yield:** 38.7 g (0.167 mmol, 85%), yellowish solid.

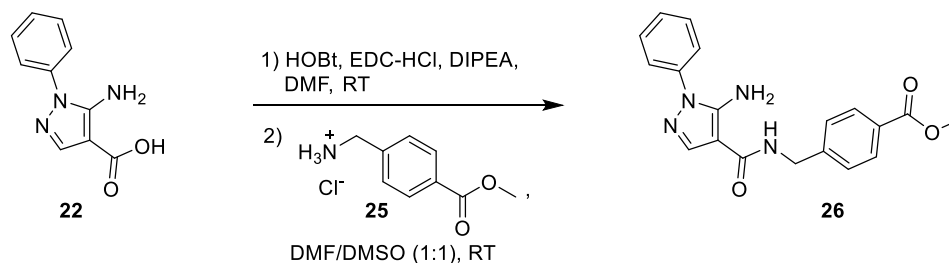
- **TLC:**  $R_f$  = 0.30 (SiO<sub>2</sub>, cyclohexane/EtOAc 4:1).
- **C<sub>12</sub>H<sub>13</sub>N<sub>3</sub>O<sub>2</sub>:** (231.25), [231.10].
- **<sup>1</sup>H-NMR (400 MHz, DMSO-*d*<sub>6</sub>, 300 K):**  $\delta$  = 7.70 (s, 1H, pyrazole), 7.57–7.50 (m, 4H, H-2-, H-3-, H-5-, H-6-phenyl), 7.46–7.37 (m, 1H, H-4-phenyl), 6.31 (s, 2H, NH<sub>2</sub>), 4.21 (q, <sup>3</sup>*J* = 7.1 Hz, 2H, CH<sub>2</sub>), 1.27 (t, <sup>3</sup>*J* = 7.1 Hz, 3H, CH<sub>3</sub>) ppm.
- **<sup>13</sup>C-NMR (101 MHz, DMSO-*d*<sub>6</sub>, 300 K):**  $\delta$  = 163.5, 149.7, 140.1, 137.9, 129.4, 127.5, 123.6, 94.7, 59.0, 14.5 ppm.
- **MS (ESI pos.):**  $m/z$  (%) = 232.15 (100) ([M+H]<sup>+</sup>, calcd. 232.10).

**5-Amino-1-phenyl-1H-pyrazole-4-carboxylic acid (22, SR11)**

Ethyl 5-amino-1-phenyl-1H-pyrazole-4-carboxylate (**21**, 22.1 g, 95.6 mmol) was dissolved in THF (25 mL), MeOH (75 mL) and NaOH (3 N, aq., 50 mL) was added. The reaction mixture was heated at reflux for 4 h. The reaction mixture was then concentrated under reduced pressure and HCl (1 N, aq., 150 mL) was added. After cooling to RT the precipitate was filtered and washed with H<sub>2</sub>O and dried under reduced pressure in a vacuum oven.

**Yield:** 19.0 g (93.5 mmol, 98%), colorless solid.

- **TLC:**  $R_f = 0.31$  (SiO<sub>2</sub>, cyclohexane/EtOAc 1:1).
- **C<sub>10</sub>H<sub>9</sub>N<sub>3</sub>O<sub>2</sub>:** (203.20), [203.07].
- **<sup>1</sup>H-NMR (500 MHz, DMSO-d<sub>6</sub>, 300 K):**  $\delta = 12.09$  (s, 1H, COOH), 7.69 (s, 1H, pyrazole), 7.58–7.51 (m, 4H, H-2-, H-3-, H-5-, H-6-phenyl), 7.43–7.38 (m, 1H, H-4-phenyl), 6.29 (br s, 2H, NH<sub>2</sub>) ppm.
- **<sup>13</sup>C-NMR (126 MHz, DMSO-d<sub>6</sub>, 300 K):**  $\delta = 166.4, 149.9, 140.6, 138.0, 129.5, 127.4, 123.5, 95.4$  ppm.
- **MS (ESI pos.):**  $m/z$  (%) = 204.08 (100) ([M+H]<sup>+</sup>, calcd. 204.07).

**Methyl 4-((5-amino-1-phenyl-1H-pyrazole-4-carboxamido)methyl)benzoate (26, SR32)**

5-Amino-1-phenyl-1H-pyrazole-4-carboxylic acid (**22**, 2.00 g, 9.84 mmol), HOBT (1.56 g, 11.8 mmol) and EDC-HCl (2.26 g, 11.8 mmol) were dissolved in DMF (dry, 20 mL) and DIPEA (1.91 g, 14.8 mmol) was added. The mixture was stirred for 30 min at RT and a solution of methyl 4-(aminomethyl)benzoate hydrochloride (**25**, 1.95 g, 11.8 mmol) in a DMF/DMSO mixture (dry, 20 mL, 1:1) and DIPEA (1.91 g, 14.8 mmol) was added. The reaction mixture was stirred for additional 20 h at RT. DCM (100 mL) was added and the mixture was washed with H<sub>2</sub>O (5x50 mL). The organic phase was separated, dried over MgSO<sub>4</sub> and the solvent was removed under reduced pressure. The crude product was purified using column chromatography on silica (DCM/MeOH, 98:2).

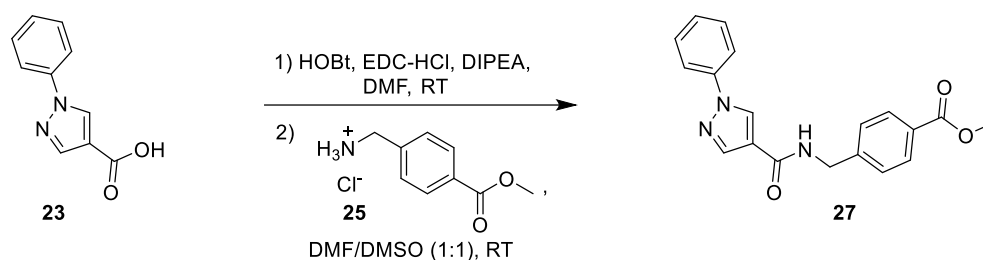
**Yield:** 3.10 g (8.85 mmol, 90%), yellowish solid.

- **TLC:**  $R_f = 0.33$  (SiO<sub>2</sub>, DCM/MeOH 10:1).
- **C<sub>19</sub>H<sub>18</sub>N<sub>4</sub>O<sub>3</sub>:** (350.37), [350.14].
- **<sup>1</sup>H-NMR (400 MHz, DMSO-d<sub>6</sub>, 300 K):**  $\delta = 8.54$  (t, <sup>3</sup>J = 6.1 Hz, 1H, NH), 7.99 (s, 1H, pyrazole), 7.94 (d, <sup>3</sup>J = 8.2 Hz, 2H, H-3-, H-5-benzyl), 7.60–7.49 (m, 4H, H-2-, H-3-, H-5-, H-6-phenyl), 7.45 (d, <sup>3</sup>J = 8.2

Hz, 2H, H-2-, H-5-benzyl), 7.42–7.36 (m, 1H, H-4-phenyl), 6.38 (s, 2H, NH<sub>2</sub>), 4.50 (d, <sup>3</sup>J = 6.1 Hz, 2H, CH<sub>2</sub>), 3.85 (s, 3H, CH<sub>3</sub>) ppm.

- **<sup>13</sup>C-NMR (101 MHz, DMSO-d<sub>6</sub>, 300 K):** δ = 166.1, 164.2, 149.2, 145.9, 138.4, 138.2, 129.3, 129.2, 128.0, 127.3, 127.1, 123.1, 97.3, 52.0, 41.3 ppm.
- **MS (ESI pos.):** m/z (%) = 351.13 (100) ([M+H]<sup>+</sup>, calcd. 351.15).

**Methyl 4-((1-phenyl-1H-pyrazole-4-carboxamido)methyl)benzoate (27, SR325)**

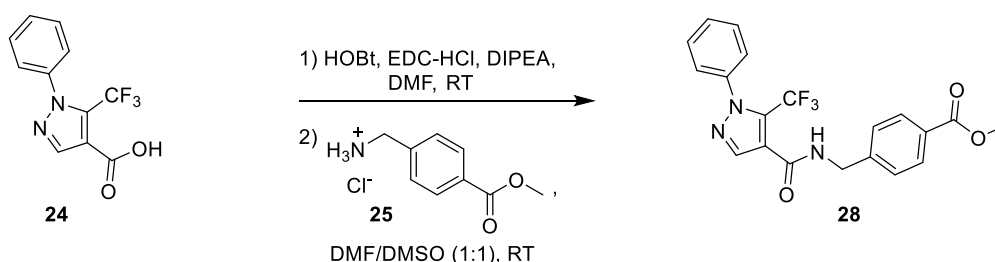


1-Phenyl-1H-pyrazole-4-carboxylic acid (**23**, 1.00 g, 5.31 mmol), HOBT (862 mg, 6.38 mmol) and EDC-HCl (1.22 g, 6.38 mmol) were dissolved in DMF (dry, 10 mL) and DIPEA (1.03 g, 7.97 mmol) was added. The mixture was stirred for 75 min at RT and a solution of methyl 4-(aminomethyl)benzoate hydrochloride (**25**, 1.05 g, 6.38 mmol) in DMSO (dry, 10 mL) and DIPEA (1.03 g, 7.97 mmol) was added. The reaction mixture was stirred for additional 4 h at RT. DCM (150 mL) was added and the mixture was washed 5 times with H<sub>2</sub>O (150 mL). The organic phase was separated, dried over MgSO<sub>4</sub> and the solvent was removed under reduced pressure. The crude product was purified using column chromatography on silica (cyclohexane/EtOAc 1:1 → EtOAc).

**Yield:** 1.43 g (4.25 mmol, 80%), yellowish solid.

- **TLC:** R<sub>f</sub> = 0.66 (SiO<sub>2</sub>, cyclohexane/EtOAc 1:3).
- **C<sub>19</sub>H<sub>17</sub>N<sub>3</sub>O<sub>3</sub>:** (335.36), [335.13].
- **<sup>1</sup>H-NMR (300 MHz, DMSO-d<sub>6</sub>, 300 K):** δ = 8.96 (s, 1H, H-5-pyrazole), 8.85 (t, <sup>3</sup>J = 6.0 Hz, 1H, NH), 8.19 (s, 1H, H-3-pyrazole), 7.97–7.91 (m, 2H, H-3-, H-5-benzyl), 7.88–7.83 (m, 2H, H-2-, H-6-phenyl), 7.57–7.44 (m, 4H, H-3-, H-5-phenyl, H-2-, H-6-benzyl), 7.37 (tt, <sup>3</sup>J = 7.4, 1.1 Hz, 1H, H-4-phenyl), 4.55 (d, <sup>3</sup>J = 6.0 Hz, 2H, CH<sub>2</sub>), 3.84 (s, 3H, CH<sub>3</sub>) ppm.
- **<sup>13</sup>C-NMR (75 MHz, DMSO-d<sub>6</sub>, 300 K):** δ = 166.1, 161.5, 145.3, 140.2, 139.2, 129.6, 129.3, 129.1, 128.2, 127.4, 127.0, 120.3, 118.8, 52.0, 41.8 ppm.
- **MS (ESI pos.):** m/z (%) = 336.01 (100) ([M+H]<sup>+</sup>, calcd. 336.14).

**Methyl 4-((1-phenyl-5-(trifluoromethyl)-1H-pyrazole-4-carboxamido)methyl)benzoate (28, SR319)**



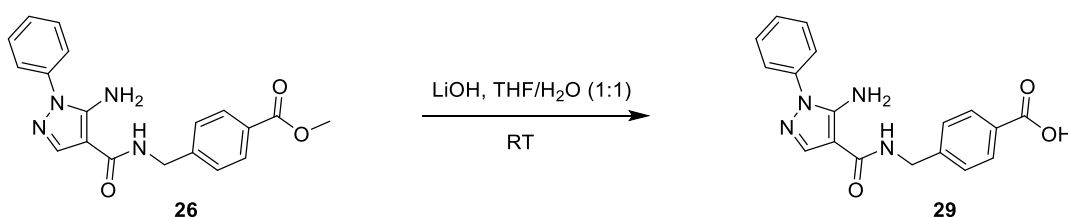


1-Phenyl-5-(trifluoromethyl)-1*H*-pyrazole-4-carboxylic acid (**24**, 1.00 g, 3.90 mmol), HOBt (633 mg, 4.68 mmol) and EDC-HCl (898 mg, 4.68 mmol) were dissolved in DMF (dry, 10 mL) and DIPEA (757 mg, 5.86 mmol) was added. The mixture was stirred for 75 min at RT and a solution of methyl 4-(aminomethyl)benzoate hydrochloride (**25**, 774 mg, 4.68 mmol) in DMSO (dry, 10 mL) and DIPEA (757 mg, 5.86 mmol) was added. The reaction mixture was stirred for additional 3 h at RT. DCM (100 mL) was added and the mixture was washed five times with H<sub>2</sub>O (100 mL). The organic phase was separated, dried over MgSO<sub>4</sub> and the solvent was removed under reduced pressure. The crude product was purified using column chromatography on silica (cyclohexane/EtOAc 1:1 → 1:3).

**Yield:** 839 mg (2.08 mmol, 53%), colorless solid.

- **TLC:** R<sub>f</sub> = 0.73 (SiO<sub>2</sub>, cyclohexane/EtOAc 1:3).
- **C<sub>20</sub>H<sub>16</sub>F<sub>3</sub>N<sub>3</sub>O<sub>3</sub>:** (403.35), [403.11].
- **<sup>1</sup>H-NMR (600 MHz, DMSO-d<sub>6</sub>, 300 K):** δ = 9.10 (t, <sup>3</sup>J = 5.9 Hz, 1H, NH), 8.22 (s, 1H, pyrazole), 7.95 (d, <sup>3</sup>J = 8.2 Hz, 2H, H-3-, H-5-benzyl), 7.61–7.57 (m, 3H, H-2, H-4-, H-6-phenyl), 7.54–7.50 (m, 2H, H-3-, H-5-phenyl), 7.48 (d, <sup>3</sup>J = 8.1 Hz, 2H, H-2-, H-5-benzyl), 4.54 (d, <sup>3</sup>J = 5.9 Hz, 2H, CH<sub>2</sub>), 3.85 (s, 3H, CH<sub>3</sub>) ppm.
- **<sup>13</sup>C-NMR (150 MHz, DMSO-d<sub>6</sub>, 300 K):** δ = 166.0, 160.4, 144.7, 139.5, 138.9, 129.9, 129.7 (<sup>2</sup>J<sub>CF</sub> = 38.9 Hz), 129.3, 129.2, 128.2, 127.3, 126.0, 121.0, 119.3 (<sup>1</sup>J<sub>CF</sub> = 270.6 Hz), 52.0, 42.2 ppm.
- **MS (ESI pos.):** m/z (%) = 404.14 (100) ([M+H]<sup>+</sup>, calcd. 404.12).

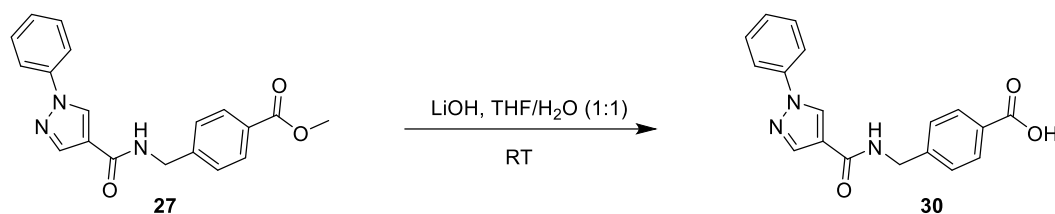
#### 4-((5-Amino-1-phenyl-1*H*-pyrazole-4-carboxamido)methyl)benzoic acid (**29**, SR29)



Methyl 4-((5-amino-1-phenyl-1*H*-pyrazole-4-carboxamido)methyl)benzoate (**26**, 1.50 g, 4.28 mmol) was dissolved in a THF/H<sub>2</sub>O mixture (100 mL, 1:1) and LiOH·xH<sub>2</sub>O (513 mg, 21.4 mmol) was added. The suspension was stirred for 20 h at RT and then acidified with HCl (aq., 100 mL, 1 M). The precipitate was filtered off, washed with H<sub>2</sub>O and dried under reduced pressure in a vacuum oven.

**Yield:** 1.40 g (4.16 mmol, 97%), colorless solid.

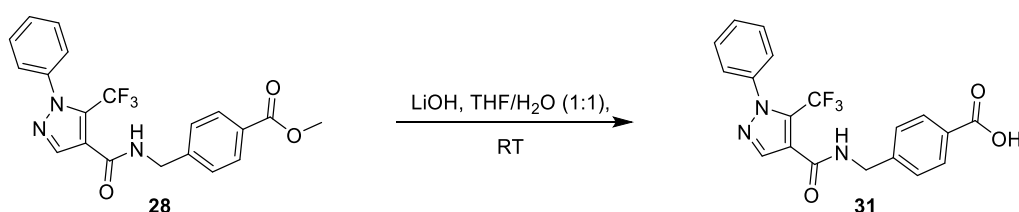
- **TLC:** R<sub>f</sub> = 0.48 (SiO<sub>2</sub>, DCM/MeOH 20:1).
- **C<sub>18</sub>H<sub>16</sub>N<sub>4</sub>O<sub>3</sub>:** (336.34), [336.12].
- **<sup>1</sup>H-NMR (400 MHz, DMSO-d<sub>6</sub>, 300 K):** δ = 12.84 (br s, 1H, COOH), 8.52 (t, <sup>3</sup>J = 6.0 Hz, 1H, NH), 7.99 (s, 1H, pyrazole), 7.92 (d, <sup>3</sup>J = 8.3 Hz, 2H, H-3-, H-5-benzyl), 7.60–7.49 (m, 4H, H-2-, H-3-, H-5-, H-6-phenyl), 7.45–7.35 (m, 3H, H-2-, H-5-benzyl, H-4-phenyl), 6.37 (br s, 2H, NH<sub>2</sub>), 4.49 (d, <sup>3</sup>J = 6.0 Hz, 2H, CH<sub>2</sub>) ppm.
- **<sup>13</sup>C-NMR (101 MHz, DMSO-d<sub>6</sub>, 300 K):** δ = 167.3, 164.2, 149.3, 145.5, 138.4, 138.2, 129.5, 129.4, 129.2, 127.2 (2x), 123.2, 97.4, 41.4 ppm.
- **MS (ESI pos.):** m/z (%) = 337.14 (100) ([M+H]<sup>+</sup>, calcd. 337.13).

4-((1-Phenyl-1H-pyrazole-4-carboxamido)methyl)benzoic acid (**30**, SR328)

Methyl 4-((1-phenyl-1H-pyrazole-4-carboxamido)methyl)benzoate (**27**, 780 mg, 2.43 mmol) was dissolved in a THF/H<sub>2</sub>O mixture (40 mL, 1:1) and LiOH·H<sub>2</sub>O (291 mg, 12.14 mmol) was added. The suspension was stirred for 4 d at RT and then acidified with HCl (aq., 10 mL, 1 M). The precipitate was filtered off, washed with H<sub>2</sub>O and dried under reduced pressure in a vacuum oven.

**Yield:** 746 mg (2.32 mmol, quant.), yellowish solid.

- **TLC:** R<sub>f</sub> = 0.10 (SiO<sub>2</sub>, cyclohexane/EtOAc 1:3).
- **C<sub>18</sub>H<sub>15</sub>N<sub>3</sub>O<sub>3</sub>:** (321.33), [321.11].
- **<sup>1</sup>H-NMR (300 MHz, DMSO-d<sub>6</sub>, 300 K):** δ = 8.95 (s, 1H, H-5-pyrazole), 8.84 (t, <sup>3</sup>J = 6.0 Hz, 1H, NH), 8.19 (s, 1H, H-3-pyrazole), 7.92 (d, <sup>3</sup>J = 7.9 Hz, 2H, H-3-, H-5-benzyl), 7.85 (d, <sup>3</sup>J = 7.9 Hz, 2H, H-2-, H-6-phenyl), 7.53 (t, <sup>3</sup>J = 7.8 Hz, 2H, H-3-, H-5-phenyl), 7.44 (d, <sup>3</sup>J = 8.0 Hz, 2H, H-2-, H-6-benzyl), 7.36 (t, <sup>3</sup>J = 7.4 Hz, 1H, H-4-phenyl), 4.54 (d, <sup>3</sup>J = 5.9 Hz, 2H, CH<sub>2</sub>) ppm.
- **<sup>13</sup>C-NMR (75 MHz, DMSO-d<sub>6</sub>, 300 K):** δ = 167.2, 161.6, 144.8, 140.3, 139.2, 129.7, 129.5, 129.4, 129.1, 127.3, 127.1, 120.3, 118.8, 41.9 ppm.
- **MS (ESI pos.):** m/z (%) = 322.09 (100) ([M+H]<sup>+</sup>, calcd. 322.12).

4-((1-Phenyl-5-(trifluoromethyl)-1H-pyrazole-4-carboxamido)methyl)benzoic acid (**31**, SR320)

Methyl 4-((1-phenyl-5-(trifluoromethyl)-1H-pyrazole-4-carboxamido)methyl)benzoate (**28**, 750 mg, 1.86 mmol) was dissolved in a THF/H<sub>2</sub>O mixture (40 mL, 1:1) and LiOH·H<sub>2</sub>O (223 mg, 9.30 mmol) was added. The suspension was stirred for 4 d at RT and then acidified with HCl (aq., 10 mL, 1 M). The precipitate was filtered, washed with H<sub>2</sub>O and dried under reduced pressure in a vacuum oven.

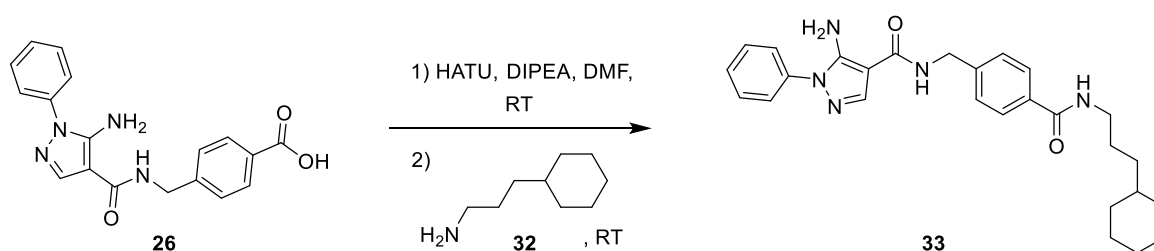
**Yield:** 678 mg (1.741 mmol, 94%), colorless solid.

- **TLC:** R<sub>f</sub> = 0.16 (SiO<sub>2</sub>, cyclohexane/EtOAc 1:3).
- **C<sub>19</sub>H<sub>14</sub>F<sub>3</sub>N<sub>3</sub>O<sub>3</sub>:** (389.33), [389.10].
- **<sup>1</sup>H-NMR (600 MHz, DMSO-d<sub>6</sub>, 300 K):** δ = 12.9 (br s, 1H, COOH), 9.18 (t, <sup>3</sup>J = 6.0 Hz, 1H, NH), 8.22 (s, 1H, pyrazole), 7.92 (d, <sup>3</sup>J = 8.1 Hz, 2H, H-3-, H-5-benzyl), 7.61–7.57 (m, 3H, H-2-, H-4-, H-6-phenyl), 7.54–7.49 (m, 2H, H-3-, H-5-phenyl), 7.45 (d, <sup>3</sup>J = 8.1 Hz, 2H, H-2-, H-6-benzyl), 4.53 (d, <sup>3</sup>J = 6.0 Hz, 2H, CH<sub>2</sub>) ppm.

- **$^{13}\text{C}$ -NMR (150 MHz, DMSO- $d_6$ , 300 K):**  $\delta$  = 167.1, 160.4, 144.2, 139.5, 138.9, 129.9, 129.8 ( $^2J_{\text{CF}}$  = 39.6 Hz), 129.4, 129.3, 128.2, 127.2, 126.0, 121.0, 119.3 ( $^1J_{\text{CF}}$  = 272.8 Hz), 42.3 ppm.
- **MS (ESI pos.):**  $m/z$  (%) = 390.09 (100) ( $[\text{M}+\text{H}]^+$ , calcd. 390.11).

### 8.3.4 Synthesis of final compounds

#### 5-Amino-*N*-(4-((3-cyclohexylpropyl)carbamoyl)benzyl)-1-phenyl-1*H*-pyrazole-4-carboxamide (**33**, SR318)

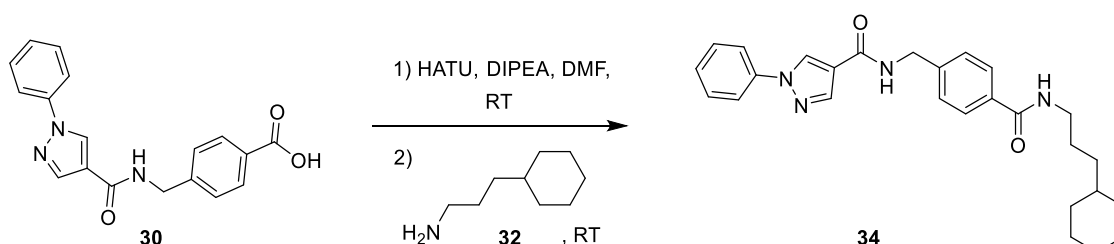


4-((5-Amino-1-phenyl-1*H*-pyrazole-4-carboxamido)methyl)benzoic acid (**26**, 200 mg, 0.595 mmol) and HATU (271 mg, 0.714 mmol) were dissolved in DMF (dry, 10 mL) and DIPEA (92 mg, 0.714 mmol) was added. The solution was stirred at RT for 1 h and 3-cyclohexylpropan-1-amine (**32**, 117 mg, 0.714 mmol) was added. The reaction was stirred for additional 3 h at RT. DCM (100 mL) was added, the organic phase was washed 5 times with H<sub>2</sub>O (100 mL) and dried over MgSO<sub>4</sub>. The solvent was removed under reduced pressure and the crude product was purified using column chromatography on silica (cyclohexane/EtOAc 1:1 → 1:3). The product was recrystallized from acetone.

**Yield:** 230 mg (0.500 mmol, 84%), colorless solid.

- **TLC:**  $R_f$  = 0.30 (SiO<sub>2</sub>, cyclohexane/EtOAc 1:3).
- **C<sub>27</sub>H<sub>33</sub>N<sub>5</sub>O<sub>2</sub>:** (459.58), [459.26].
- **$^1\text{H}$ -NMR (500 MHz, DMSO- $d_6$ , 300 K):**  $\delta$  = 8.51 (t,  $^3J$  = 6.1 Hz, 1H, NHCH<sub>2</sub>CH<sub>2</sub>), 8.39 (t,  $^3J$  = 5.7 Hz, 1H, NHCH<sub>2</sub>C<sub>Ar</sub>), 7.99 (s, 1H, pyrazole), 7.80 (d,  $^3J$  = 8.3 Hz, 2H, H-3-, H-5-benzyl), 7.59–7.49 (m, 4H, H-2-, H-3-, H-5-, H-6-phenyl), 7.41–7.34 (m, 3H, H-4-phenyl, H-2-, H-6-benzyl), 6.39 (br s, 2H, NH<sub>2</sub>), 4.47 (d,  $^3J$  = 6.0 Hz, 2H, CH<sub>2</sub>-benzyl), 3.21 (q,  $^3J$  = 7.4 Hz, 2H, NHCH<sub>2</sub>CH<sub>2</sub>), 1.71–1.56 (m, 5H, H-2<sub>eq</sub>-, H-3<sub>eq</sub>-, H-4<sub>eq</sub>-, H-5<sub>eq</sub>-, H-6<sub>eq</sub>-cyclohexyl), 1.52 (p,  $^3J$  = 7.4 Hz, 2H, NHCH<sub>2</sub>CH<sub>2</sub>CH<sub>2</sub>), 1.26–1.06 (m, 6H, H-1-, H-3<sub>ax</sub>-, H-4<sub>ax</sub>-, H-5<sub>ax</sub>-cyclohexyl, NH(CH<sub>2</sub>)<sub>2</sub>CH<sub>2</sub>), 0.90–0.79 (m, 2H, H-2<sub>ax</sub>-, H-6<sub>ax</sub>-cyclohexyl) ppm.
- **$^{13}\text{C}$ -NMR (126 MHz, DMSO- $d_6$ , 300 K):**  $\delta$  = 165.9, 164.2, 149.2, 143.3, 138.4, 138.2, 133.2, 129.4, 127.2, 127.1, 126.9, 123.1, 97.4, 41.3, 36.8, 34.3, 32.9, 26.5, 26.2, 25.8 ppm.
- **MS (ESI pos.):**  $m/z$  (%) = 460.30 (100) ( $[\text{M}+\text{H}]^+$ , calcd. 460.27), 482.28 (9) ( $[\text{M}+\text{Na}]^+$ , calcd. 482.25).
- **HRMS (FTMS + p MALDI):**  $m/z$  = 460.2702  $[\text{M}+\text{H}]^+$ , calcd. for [C<sub>27</sub>H<sub>34</sub>N<sub>5</sub>O<sub>2</sub>]<sup>+</sup> = 460.2713.

#### *N*-(4-((3-Cyclohexylpropyl)carbamoyl)benzyl)-1-phenyl-1*H*-pyrazole-4-carboxamide (**34**, SR329)

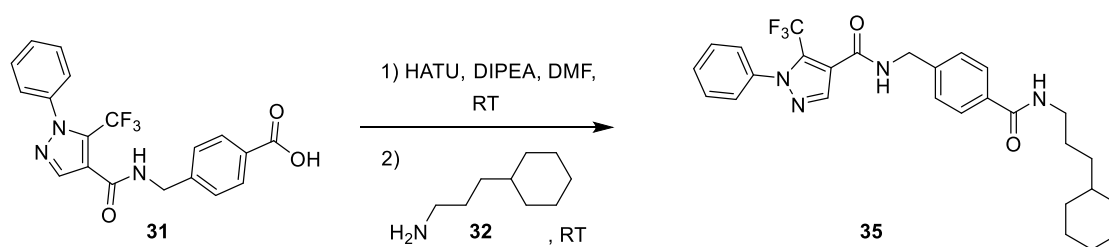


4-((1-Phenyl-1*H*-pyrazole-4-carboxamido)methyl)benzoic acid (**30**, 250 mg, 0.778 mmol) and HATU (355 mg, 0.934 mmol) were dissolved in DMF (dry, 10 mL) and DIPEA (121 mg, 0.934 mmol) was added. The solution was stirred at RT for 1 h and 3-cyclohexylpropan-1-amine (**32**, 132 mg, 0.934 mmol) was added. The reaction was stirred for additional 6 h at RT. DCM (150 mL) was added, the organic phase was washed 4 times with H<sub>2</sub>O (150 mL) and dried over MgSO<sub>4</sub>. The solvent was removed under reduced pressure and the crude product was purified using column chromatography on silica (cyclohexane/EtOAc 1:1 → 1:3).

**Yield:** 60 mg (0.135 mmol, 17%), colorless solid.

- **TLC:** R<sub>f</sub> = 0.52 (SiO<sub>2</sub>, cyclohexane/EtOAc 1:3).
- **C<sub>27</sub>H<sub>32</sub>N<sub>4</sub>O<sub>2</sub>:** (444.57), [444.25].
- **<sup>1</sup>H-NMR (500 MHz, DMSO-d<sub>6</sub>, 300 K):** δ = 8.96 (s, 1H, H-5 pyrazole), 8.82 (t, <sup>3</sup>J = 6.0 Hz, 1H, NH-benzyl), 8.40 (t, <sup>3</sup>J = 5.7 Hz, 1H, NH(CH<sub>2</sub>)<sub>3</sub>), 8.19 (s, 1H, H-3-pyrazole), 7.86 (d, <sup>3</sup>J = 7.4 Hz, 2H, H-3-, H-5-benzyl), 7.80 (d, <sup>3</sup>J = 8.3 Hz, 2H, H-2-, H-6-phenyl), 7.53 (t, <sup>3</sup>J = 8.1 Hz, 2H, H-3-, H-5-phenyl), 7.44–7.34 (m, 3H, H-2-, H-6-benzyl, H-4-phenyl), 4.51 (d, <sup>3</sup>J = 6.0 Hz, 2H, CH<sub>2</sub>-benzyl), 3.25–3.17 (m, 2H, NHCH<sub>2</sub>(CH<sub>2</sub>)<sub>2</sub>), 1.72–1.56 (m, 5H, H-2<sub>eq</sub>-, H-3<sub>eq</sub>-, H-4<sub>eq</sub>-, H-5<sub>eq</sub>-, H-6<sub>eq</sub>-cyclohexyl), 1.55–1.46 (m, 2H, NHCH<sub>2</sub>CH<sub>2</sub>CH<sub>2</sub>), 1.26–1.04 (m, 6H, H-1-, H-3<sub>ax</sub>-, H-4<sub>ax</sub>-, H-5<sub>ax</sub>-cyclohexyl, NH(CH<sub>2</sub>)<sub>2</sub>CH<sub>2</sub>), 0.90–0.78 (m, 2H, H-2<sub>ax</sub>-, H-6<sub>ax</sub>-cyclohexyl) ppm.
- **<sup>13</sup>C-NMR (126 MHz, DMSO-d<sub>6</sub>, 300 K):** δ = 165.8, 161.5, 142.7, 140.3, 139.2, 133.3, 129.7, 129.1, 127.2, 127.0 (2x), 120.4, 118.8, 41.8, 36.8, 34.3, 32.9, 26.5, 26.2, 25.8 ppm.
- **MS (ESI pos.):** *m/z* (%) = 445.26 (100) ([M+H]<sup>+</sup>, calcd. 445.26).
- **HRMS (FTMS + p MALDI):** *m/z* = 467.2416 [M+Na]<sup>+</sup>, calcd. for [C<sub>27</sub>H<sub>32</sub>N<sub>4</sub>NaO<sub>2</sub>]<sup>+</sup> = 467.2423.

***N*-4-((3-Cyclohexylpropyl)carbamoyl)benzyl)-1-phenyl-5-(trifluoromethyl)-1*H*-pyrazole-4-carboxamide (**35**, SR321)**



4-((1-Phenyl-5-(trifluoromethyl)-1*H*-pyrazole-4-carboxamido)methyl)-benzoic acid (**31**, 250 mg, 0.642 mmol) and HATU (293 mg, 0.771 mmol) were dissolved in DMF (dry, 10 mL) and DIPEA (100 mg, 0.771 mmol) was added. The solution was stirred at RT for 1 h and 3-cyclohexylpropan-1-amine (**32**, 127 μL, 0.771 mmol) was added. The reaction was stirred for additional 20 h at RT. DCM (100 mL) was added, the organic phase was washed 4 times with H<sub>2</sub>O (100 mL) and dried over MgSO<sub>4</sub>. The solvent was removed under reduced pressure and the crude product was purified using column chromatography on silica (cyclohexane/EtOAc 1:1 → 1:3). The product was recrystallized from acetone.

**Yield:** 250 mg (0.488 mmol, 76%), colorless solid.

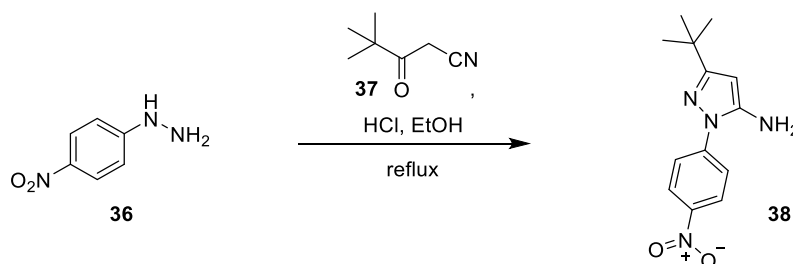
- **TLC:** R<sub>f</sub> = 0.51 (SiO<sub>2</sub>, cyclohexane/EtOAc 1:3).
- **C<sub>28</sub>H<sub>31</sub>F<sub>2</sub>N<sub>4</sub>O<sub>2</sub>:** (512.57), [512.24].

- **$^1\text{H-NMR}$  (300 MHz, DMSO- $d_6$ , 300 K):**  $\delta$  = 9.15 (t,  $^3J$  = 6.0 Hz, 1H,  $\text{NHCH}_2\text{CH}_2$ ), 8.39 (t,  $^3J$  = 5.7 Hz, 1H,  $\text{NHCH}_2\text{C}_{\text{Ar}}$ ), 8.20 (s, 1H, pyrazole), 7.81 (d,  $^3J$  = 8.0 Hz, 2H, H-3-, H-5-benzyl), 7.64–7.47 (m, 5H, H-2-, H-3-, H-4-, H-5-, H-6-phenyl), 7.39 (d,  $^3J$  = 8.0 Hz, 2H, H-2-, H-6-benzyl), 4.50 (d,  $^3J$  = 5.9 Hz, 2H,  $\text{CH}_2$ -benzyl), 3.21 (q,  $^3J$  = 7.4 Hz, 2H,  $\text{NHCH}_2\text{CH}_2$ ), 1.76–1.43 (m, 7H, H-2 $_{\text{eq}}$ -, H-3 $_{\text{eq}}$ -, H-4 $_{\text{eq}}$ -, H-5 $_{\text{eq}}$ -, H-6 $_{\text{eq}}$ -cyclohexyl,  $\text{NHCH}_2\text{CH}_2\text{CH}_2$ ), 1.32–1.03 (m, 6H, H-1-, H-3 $_{\text{ax}}$ -, H-4 $_{\text{ax}}$ -, H-5 $_{\text{ax}}$ -cyclohexyl,  $\text{NH}(\text{CH}_2)_2\text{CH}_2$ ), 0.96–0.77 (m, 2H, H-2 $_{\text{ax}}$ -, H-6 $_{\text{ax}}$ -cyclohexyl) ppm.
- **$^{13}\text{C-NMR}$  (126 MHz, DMSO- $d_6$ , 300 K):**  $\delta$  = 165.8, 160.4, 142.2, 139.6, 138.9, 136.6, , 133.4, 130.0, 129.7 ( $^2J_{\text{CF}}$  = 39.2 Hz), 129.4, 127.2, 126.9, 126.0, 121.1, 119.4 ( $^1J_{\text{CF}}$  = 271.8 Hz), 42.2, 38.3, 36.8, 34.3, 32.9, 26.5, 26.2, 25.9 ppm.
- **MS (ESI pos.):**  $m/z$  (%) = 513.28 (100) ( $[\text{M}+\text{H}]^+$ , calcd. 513.25), 372.12 (70) ( $[\text{M}_{\text{fr.}}]^+$ , calcd. 372.10), 545.29 (29) ( $[\text{M}+\text{MeOH}+\text{H}]^+$ , calcd. 545.28).
- **HRMS (FTMS + p MALDI):**  $m/z$  = 513.2466  $[\text{M}+\text{H}]^+$ , calcd. for  $[\text{C}_{28}\text{H}_{32}\text{F}_3\text{N}_4\text{O}_2]^+$  = 513.2477.

## 8.4 Experimental part of Chapter 4

### 8.4.1 Synthesis of BIRB-796 fragment library intermediates

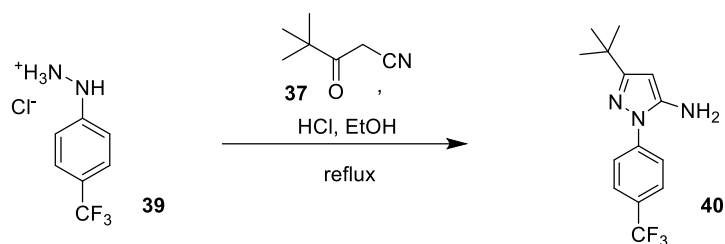
#### 3-(tert-Butyl)-1-(4-nitrophenyl)-1H-pyrazol-5-amine (**38**, SR224)



(4-Nitrophenyl)hydrazine (**36**, 3.67 g, 24.0 mmol) and 4,4-dimethyl-3-oxopentanenitrile (**37**, 3.00 g, 24.0 mmol) were dissolved in EtOH (abs., 100 mL) and HCl (conc., 6mL) was added. The reaction mixture was heated at reflux 20 h, the solvent was removed under reduced pressure and the residue dissolved in DCM (100 mL). The mixture was washed once with a  $\text{NaHCO}_3$  solution (sat., 100 mL), 2 times with  $\text{H}_2\text{O}$  (100 mL) and the organic phase was dried over  $\text{MgSO}_4$ . After removing the solvent under reduced pressure, the crude product was recrystallized from a cyclohexane/EtOAc mixture (1:1).

**Yield:** 4.90 g (18.7 mmol, 78%), orange solid.

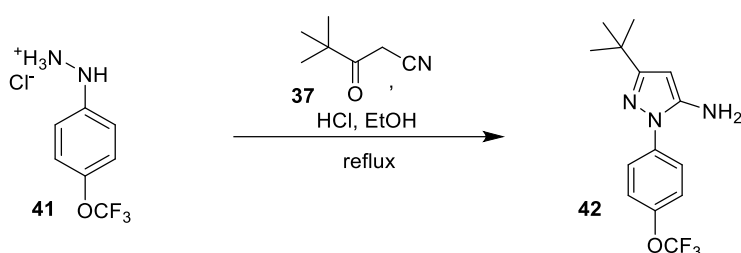
- **TLC:**  $R_f$  = 0.87 ( $\text{SiO}_2$ , hexane/EtOAc 1:3).
- **$\text{C}_{13}\text{H}_{16}\text{N}_4\text{O}_2$ :** (260.29), [260.13].
- **$^1\text{H-NMR}$  (500 MHz, DMSO- $d_6$ , 300 K):**  $\delta$  = 8.31 (d,  $^3J$  = 9.2 Hz, 2H, H-3-, H-5-phenyl), 7.94 (d,  $^3J$  = 9.2 Hz, 2H, H-2-, H-6-phenyl), 5.57 (br s, 2H,  $\text{NH}_2$ ), 5.49 (s, 1H, pyrazole), 1.23 (s, 9H, *t*Bu) ppm.
- **$^{13}\text{C-NMR}$  (126 MHz, DMSO- $d_6$ , 300 K):**  $\delta$  = 162.9, 148.5, 145.1, 143.6, 124.8, 121.3, 88.8, 32.0, 29.9 ppm.
- **MS (ESI pos.):**  $m/z$  (%) = 261.2 (100) ( $[\text{M}+\text{H}]^+$ , calcd. 261.1). 215.1 (45) ( $[\text{M}-\text{NO}_2]^+$ , calcd. 215.1).
- **MS (ESI neg.):**  $m/z$  (%) = 259.1 (100) ( $[\text{M}-\text{H}]^-$ , calcd. 259.1).

**3-(tert-Butyl)-1-(4-(trifluoromethyl)phenyl)-1H-pyrazol-5-amine (40, SR230)**

(4-(Trifluoromethyl)phenyl)hydrazine hydrochloride (**39**, 1.00 g, 4.70 mmol) and 4,4-dimethyl-3-oxopentanenitrile (**37**, 589 mg, 4.70 mmol) were dissolved in EtOH (abs., 15 mL) and HCl (conc., 2 mL) was added. The reaction mixture was heated at reflux for 20 h, the solvent was removed under reduced pressure and the residue dissolved in DCM (100 mL). The mixture was washed once with a NaHCO<sub>3</sub> solution (sat., 20 mL), 2 times with H<sub>2</sub>O (20 mL) and the organic phase was dried over MgSO<sub>4</sub>. After removing the solvent under reduced pressure, the crude product was recrystallized from a hexane/EtOAc mixture (1:1).

**Yield:** 613 mg (2.16 mmol, 46%), light yellow solid.

- **TLC:** R<sub>f</sub> = 0.81 (SiO<sub>2</sub>, hexane/EtOAc 1:1).
- **C<sub>14</sub>H<sub>16</sub>F<sub>3</sub>N<sub>3</sub>:** (283.29), [283.13].
- **<sup>1</sup>H-NMR (400 MHz, DMSO-d<sub>6</sub>, 300 K):** δ = 7.86 (d, <sup>3</sup>J = 8.7 Hz, 2H, H-3-, H-5-phenyl), 7.79 (d, <sup>3</sup>J = 8.7 Hz, 2H, H-2-, H-6-phenyl), 5.67–5.24 (m, 3H, pyrazole, NH<sub>2</sub>), 1.23 (s, 9H, tBu) ppm.
- **<sup>13</sup>C-NMR (101 MHz, DMSO-d<sub>6</sub>, 300 K):** δ = 161.9, 147.9, 142.9, 126.1 (<sup>3</sup>J<sub>CF</sub> = 3.9 Hz), 125.4 (<sup>2</sup>J<sub>CF</sub> = 32.0 Hz), 124.3 (<sup>1</sup>J<sub>CF</sub> = 271.7 Hz), 121.9, 88.0, 31.9, 30.0 ppm.
- **MS (ESI pos.):** m/z (%) = 284.2 (100) ([M+H]<sup>+</sup>, calcd. 284.1). 228.1 (45) ([M-tBu+H]<sup>+</sup>, calcd. 228.1).

**3-(tert-Butyl)-1-(4-(trifluoromethoxy)phenyl)-1H-pyrazol-5-amine (42, SR231)**

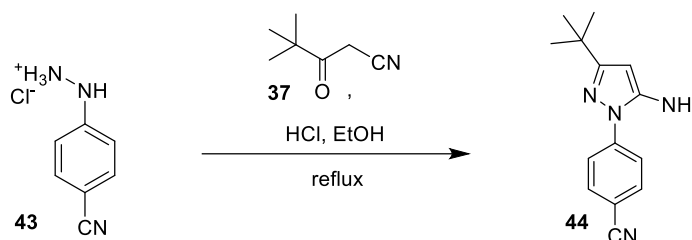
(4-(Trifluoromethoxy)phenyl)hydrazine hydrochloride (**41**, 1.00 g, 4.37 mmol) and 4,4-dimethyl-3-oxopentanenitrile (**37**, 548 mg, 4.37 mmol) were dissolved in EtOH (abs., 15 mL) and HCl (conc., 2 mL) was added. The reaction mixture was heated at reflux for 20 h, the solvent was removed under reduced pressure and the residue dissolved in DCM (100 mL). The mixture was washed once with a NaHCO<sub>3</sub> solution (sat., 20 mL), 2 times with H<sub>2</sub>O (20 mL) and the organic phase was dried over MgSO<sub>4</sub>. After removing the solvent under reduced pressure, the crude product was purified using column chromatography on silica (cyclohexane/EtOAc 4:1 → 1:1 → 1:3).

**Yield:** 761 mg (2.69 mmol, 61%), yellowish solid.

- **TLC:** R<sub>f</sub> = 0.53 (SiO<sub>2</sub>, DCM/MeOH 98:2).

- **C<sub>14</sub>H<sub>16</sub>F<sub>3</sub>N<sub>3</sub>O**: (299.29), [299.12].
- **<sup>1</sup>H-NMR (500 MHz, DMSO-d<sub>6</sub>, 300 K)**: δ = 7.71 (d, <sup>3</sup>J = 9.0 Hz, 2H, H-2-, H-6-phenyl), 7.44 (d, <sup>3</sup>J = 9.0 Hz, 2H, H-3-, H-5-phenyl), 5.41 (s, 1H, pyrazole), 5.31 (br s, 2H, NH<sub>2</sub>), 1.22 (s, 9H, tBu) ppm.
- **<sup>13</sup>C-NMR (126 MHz, DMSO-d<sub>6</sub>, 300 K)**: δ = 161.3, 147.4, 145.5, 138.8, 123.8, 121.8, 120.2 (<sup>1</sup>J<sub>CF</sub> = 258.3 Hz), 87.5, 31.8, 30.1 ppm.
- **MS (ESI pos.)**: *m/z* (%) = 300.2 (100) ([M+Na]<sup>+</sup>, calcd. 300.1). 244.1 (25) ([M-tBu+H]<sup>+</sup>, calcd. 244.1).

#### 4-(5-Amino-3-(tert-butyl)-1H-pyrazol-1-yl)benzonitrile (**44**, SR232)

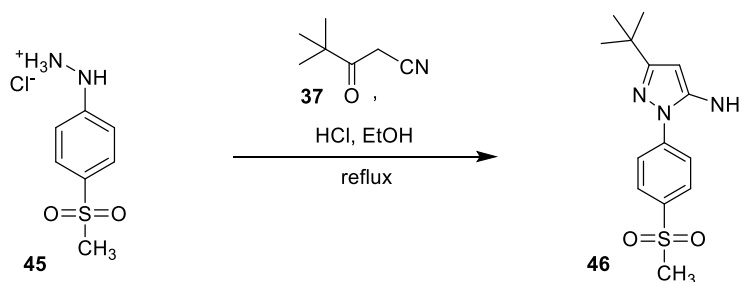


4-Hydrazinylbenzonitrile hydrochloride (**43**, 1.00 g, 5.90 mmol) and 4,4-dimethyl-3-oxopentanenitrile (**37**, 738 mg, 5.90 mmol) were dissolved in EtOH (abs., 30 mL) and HCl (conc., 2 mL) was added. The reaction mixture was heated at reflux for 20 h, the solvent was removed under reduced pressure and the residue dissolved in DCM (100 mL). The mixture was washed once with a NaHCO<sub>3</sub> solution (sat., 20 mL), 2 times with H<sub>2</sub>O (20 mL) and the organic phase was dried over MgSO<sub>4</sub>. After removing the solvent under reduced pressure, the crude product was recrystallized from a hexane/EtOAc mixture (1:1).

**Yield:** 790 mg (3.29 mmol, 56%), ochre solid.

- **TLC**: R<sub>f</sub> = 0.88 (SiO<sub>2</sub>, hexane/EtOAc 1:3).
- **C<sub>14</sub>H<sub>16</sub>N<sub>4</sub>**: (240.30), [240.14].
- **<sup>1</sup>H-NMR (400 MHz, DMSO-d<sub>6</sub>, 300 K)**: δ = 7.93–7.83 (m, 4H, H-2-, H-3-, H-5-, H-6-phenyl), 5.52–5.44 (m, 3H, pyrazole, NH<sub>2</sub>), 1.22 (s, 9H, tBu) ppm.
- **<sup>13</sup>C-NMR (101 MHz, DMSO-d<sub>6</sub>, 300 K)**: δ = 162.8, 148.1, 143.4, 133.3, 121.6, 118.8, 106.9, 88.5, 31.9, 29.9 ppm.
- **MS (ESI pos.)**: *m/z* (%) = 241.2 (100) ([M+H]<sup>+</sup>, calcd. 241.2). 185.1 (25) ([M-tBu+H]<sup>+</sup>, calcd. 185.1).

#### 3-(tert-Butyl)-1-(4-(methylsulfonyl)phenyl)-1H-pyrazol-5-amine (**46**, SR233)



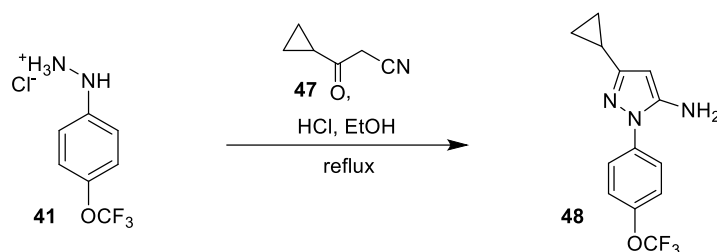
(4-(Methylsulfonyl)phenyl)hydrazine hydrochloride (**45**, 1.00 g, 4.49 mmol) and 4,4-dimethyl-3-oxopentanenitrile (**37**, 738 mg, 4.49 mmol) were dissolved in EtOH (abs., 30 mL) and HCl (conc., 2 mL) was added. The reaction mixture was heated at reflux for 20 h, the solvent was removed under reduced pressure

and the residue dissolved in DCM (100 mL). The mixture was washed once with a NaHCO<sub>3</sub> solution (sat., 20 mL), 2 times with H<sub>2</sub>O (20 mL) and the organic phase was dried over MgSO<sub>4</sub>. After removing the solvent under reduced pressure, the crude product was recrystallized from a hexane/EtOAc mixture (1:1).

**Yield:** 907 mg (3.09 mmol, 69%), yellowish solid.

- **TLC:** R<sub>f</sub> = 0.75 (SiO<sub>2</sub>, hexane/EtOAc 1:3).
- **C<sub>14</sub>H<sub>19</sub>N<sub>3</sub>O<sub>2</sub>S:** (293.38), [293.12].
- **<sup>1</sup>H-NMR (400 MHz, DMSO-d<sub>6</sub>, 300 K):** δ = 7.98 (d, <sup>3</sup>J = 8.9 Hz, 2H, H-3-, H-5-phenyl), 7.90 (d, <sup>3</sup>J = 8.9 Hz, 2H, H-2-, H-6-phenyl), 5.52–5.43 (m, 3H, pyrazole, NH<sub>2</sub>), 1.23 (s, 9H, tBu) ppm.
- **<sup>13</sup>C-NMR (101 MHz, DMSO-d<sub>6</sub>, 300 K):** δ = 162.2, 148.0, 143.7, 136.6, 128.1, 121.6, 88.2, 43.7, 31.9, 30.0 ppm.
- **MS (ESI pos.):** m/z (%) = 294.2 (100) ([M+H]<sup>+</sup>, calcd. 294.1). 238.1 (25) ([M-SO<sub>2</sub>CH<sub>3</sub>+Na]<sup>+</sup>, calcd. 185.1).

### 3-Cyclopropyl-1-(4-(trifluoromethoxy)phenyl)-1H-pyrazol-5-amine (48, SR257)

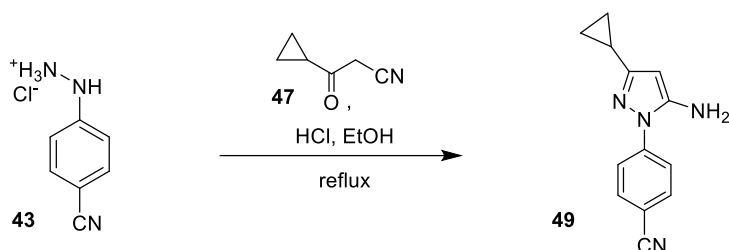


(4-(Trifluoromethoxy)phenyl)hydrazine hydrochloride (**41**, 1.00 g, 4.37 mmol) and 3-cyclopropyl-3-oxopropanenitrile (**47**, 643 mg, 4.37 mmol) were dissolved in EtOH (abs., 20 mL) and HCl (conc., 2 mL) was added. The reaction mixture was heated at reflux for 20 h, the solvent was removed under reduced pressure and the residue dissolved in EtOAc (100 mL). The mixture was washed once with a NaHCO<sub>3</sub> solution (sat., 20 mL), 2 times with H<sub>2</sub>O (20 mL) and the organic phase was dried over MgSO<sub>4</sub>. After removing the solvent under reduced pressure, the crude product was recrystallized from a cyclohexane/EtOAc mixture (1:1).

**Yield:** 956 mg (3.37 mmol, 77%), brownish solid.

- **TLC:** R<sub>f</sub> = 0.76 (SiO<sub>2</sub>, cyclohexane/EtOAc 1:1).
- **C<sub>13</sub>H<sub>12</sub>F<sub>3</sub>N<sub>3</sub>O:** (283.25), [283.09].
- **<sup>1</sup>H-NMR (500 MHz, DMSO-d<sub>6</sub>, 300 K):** δ = 7.69 (d, <sup>3</sup>J = 9.0 Hz, 2H, H-2-, H-6-phenyl), 7.43 (d, <sup>3</sup>J = 9.0 Hz, 2H, H-3-, H-5-phenyl), 5.35 (br s, 2H, NH<sub>2</sub>), 5.20 (s, 1H, pyrazole), 1.79–1.72 (m, 1H, CH(CH<sub>2</sub>)<sub>2</sub>), 0.85–0.78 (m, 2H, CH<sub>2(A)</sub>), 0.64–0.58 (m, 2H, CH<sub>2(B)</sub>) ppm.
- **<sup>13</sup>C-NMR (126 MHz, DMSO-d<sub>6</sub>, 300 K):** δ = 154.9, 147.7, 145.5 (2x), 138.6, 123.7, 121.8, 120.2 (<sup>1</sup>J<sub>CF</sub> = 256.1 Hz), 87.0, 9.4, 7.5 ppm
- **MS (ESI pos.):** m/z (%) = 284.0 (100) ([M+H]<sup>+</sup>, calcd. 284.3).
- **MS (ESI neg.):** m/z (%) = 328.0 (100) ([M+EtOH]<sup>-</sup>, calcd. 328.3). 199.2 (72) ([M<sub>fr</sub>-H]<sup>-</sup>, calcd. 199.1). 282.1 (77) ([M-H]<sup>-</sup>, calcd. 282.2).

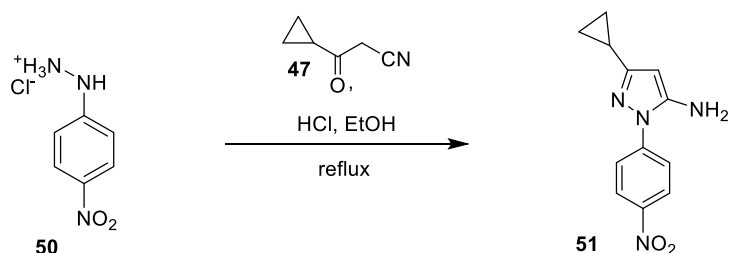


**4-(5-Amino-3-cyclopropyl-1H-pyrazol-1-yl)benzonitrile (49, SR256)**

4-Hydrazinylbenzonitrile hydrochloride (**43**, 1.00 g, 5.90 mmol) and 3-cyclopropyl-3-oxopropanenitrile (**47**, 643 mg, 5.90 mmol) were dissolved in EtOH (abs., 20 mL) and HCl (conc., 2 mL) was added. The reaction mixture was heated at reflux for 20 h, the solvent was removed under reduced pressure and the residue was dissolved in EtOAc (100 mL). The mixture was washed once with a NaHCO<sub>3</sub> solution (sat., 20 mL), 2 times with H<sub>2</sub>O (20 mL) and the organic phase was dried over MgSO<sub>4</sub>. After removing the solvent under reduced pressure, the crude product was recrystallized from a cyclohexane/EtOAc mixture (1:1).

**Yield:** 939 mg (4.19 mmol, 71%), maroon solid.

- **TLC:** R<sub>f</sub> = 0.73 (SiO<sub>2</sub>, cyclohexane/EtOAc 1:1).
- **C<sub>13</sub>H<sub>12</sub>N<sub>4</sub>:** (224.26), [224.11].
- **<sup>1</sup>H-NMR (500 MHz, DMSO-d<sub>6</sub>, 300 K):** δ = 7.93 (d, <sup>3</sup>J = 8.7 Hz, 2H, H-2-, H-6-phenyl), 7.83 (d, <sup>3</sup>J = 8.7 Hz, 2H, H-3-, H-5-phenyl), 5.97 (br s, 2H, NH<sub>2</sub>), 5.33 (s, 1H, pyrazole), 1.85–1.78 (m, 1H, CH(CH<sub>2</sub>)<sub>2</sub>), 0.92–0.87 (m, 2H, CH<sub>2(A)</sub>), 0.73–0.67 (m, 2H, CH<sub>2(B)</sub>) ppm.
- **<sup>13</sup>C-NMR (126 MHz, DMSO-d<sub>6</sub>, 300 K):** δ = 156.1, 149.0, 141.9, 133.5, 122.5, 118.7, 108.0, 88.0, 9.0, 8.0 ppm.
- **MS (ESI pos.):** m/z (%) = 225.1 (100) ([M+H]<sup>+</sup>, calcd. 225.1). 272.1 (14) ([M+EtOH-H]<sup>+</sup>, calcd. 271.2).
- **MS (ESI neg.):** m/z (%) = 259.1 (100) ([M+Cl]<sup>-</sup>, calcd. 259.6). 224.2 (53) ([M]<sup>-</sup>, calcd. 224.1). 303.0 (29) ([M+Br-H]<sup>-</sup>, calcd. 303.0).

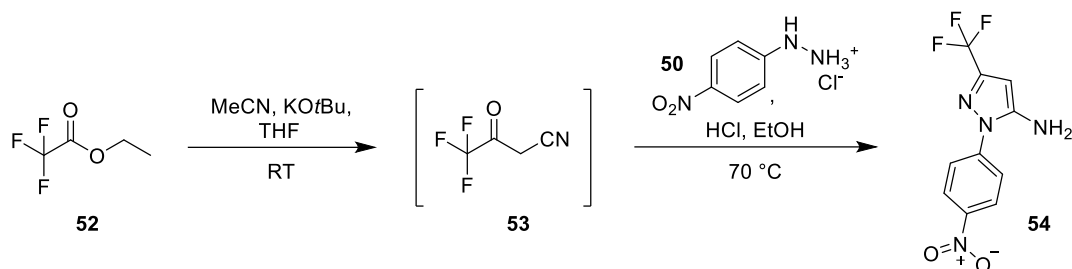
**3-Cyclopropyl-1-(4-nitrophenyl)-1H-pyrazol-5-amine (51, SR260)**

(4-Nitrophenyl)hydrazine hydrochloride (**50**, 1.00 g, 5.27 mmol) and 3-cyclopropyl-3-oxopropanenitrile (**47**, 643 mg, 5.27 mmol) were dissolved in EtOH (abs., 20 mL) and HCl (conc., 2 mL) was added. The reaction mixture was heated at reflux for 20 h, the solvent was removed under reduced pressure and the residue dissolved in EtOAc (100 mL). The mixture was washed once with a NaHCO<sub>3</sub> solution (sat., 20 mL), 2 times with H<sub>2</sub>O (20 mL) and the organic phase was dried over MgSO<sub>4</sub>. After removing the solvent under reduced pressure, the crude product was recrystallized from a cyclohexane/EtOAc mixture (1:1).

**Yield:** 631 mg (2.58 mmol, 49%), orange solid.

- **TLC:**  $R_f = 0.68$  ( $\text{SiO}_2$ , cyclohexane/EtOAc 1:1).
- **$\text{C}_{12}\text{H}_{12}\text{N}_4\text{O}_2$ :** (244.25), [244.10].
- **$^1\text{H-NMR}$  (600 MHz,  $\text{DMSO-d}_6$ , 300 K):**  $\delta = 8.29$  (d,  $^3J = 9.3$  Hz, 2H, H-3-, H-5-phenyl), 7.92 (d,  $^3J = 9.3$  Hz, 2H, H-2-, H-6-phenyl), 5.60 (br s, 2H,  $\text{NH}_2$ ), 5.28 (s, 1H, pyrazole), 1.82–1.76 (m, 1H,  $\text{CH}(\text{CH}_2)_2$ ), 0.88–0.82 (m, 2H,  $\text{CH}_{2(\text{A})}$ ), 0.68–0.83 (m, 2H,  $\text{CH}_{2(\text{B})}$ ) ppm.
- **$^{13}\text{C-NMR}$  (150 MHz,  $\text{DMSO-d}_6$ , 300 K):**  $\delta = 156.6, 148.7, 144.9, 143.6, 124.7, 121.1, 88.3, 9.3, 7.6$  ppm.
- **MS (ESI pos.):**  $m/z$  (%) = 245.04 (100) ( $[\text{M}+\text{H}]^+$ , calcd. 245.1).
- **MS (ESI neg.):**  $m/z$  (%) = 243.2 (100) ( $[\text{M}-\text{H}]^-$ , calcd. 243.1). 279.1 (14) ( $[\text{M}+\text{Cl}]^-$ , calcd. 279.6).

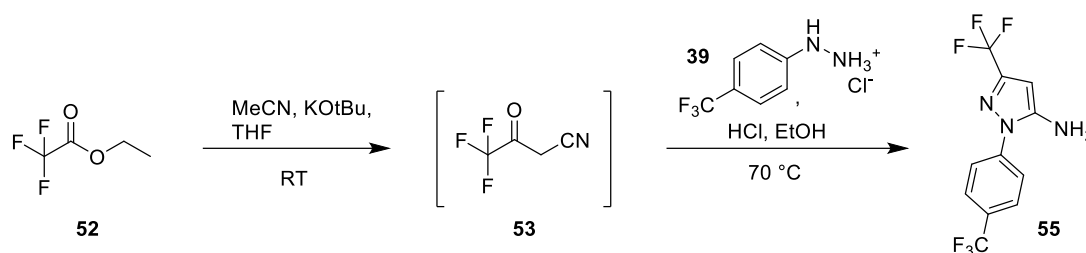
### 1-(4-Nitrophenyl)-3-(trifluoromethyl)-1H-pyrazol-5-amine (54, SR251)



Potassium *tert*-butoxide (3.25 g, 29.0 mmol) was dissolved in THF (dry, 30 mL) and acetonitrile (0.39 mg, 9.6 mmol). Ethyl 2,2,2-trifluoroacetate (**52**, 5.44 g, 38.3 mmol) was added dropwise and the mixture was stirred overnight at RT. The mixture was then acidified with HCl (conc., 3 mL) and  $\text{H}_2\text{O}$  (10 mL) was added. The solvent was removed under reduced pressure and the residue was extracted 3 times with EtOAc (20 mL). The organic extracts were combined, dried over  $\text{MgSO}_4$  and the solvent was removed under reduced pressure to give 4,4,4-trifluoro-3-oxobutanenitrile (**53**), as intermediate, which was used without further purification. The crude compound was dissolved in EtOH (abs., 20 mL) and (4-nitrophenyl)hydrazine hydrochloride (**50**, 1.81 g, 9.57 mmol) was added. The mixture was heated for 8 h at 70 °C and afterwards basified to  $\text{pH} \sim 12$  with aqueous NaOH solution (3 N, 10 mL). The mixture was extracted 4 times with EtOAc (50 mL) and the organic extracts were combined and dried over  $\text{MgSO}_4$ . After removing the solvent under reduced pressure, the crude product was purified by column chromatography on silica (cyclohexane/EtOAc 4:1  $\rightarrow$  1:1  $\rightarrow$  1:20  $\rightarrow$  EtOAc).

**Yield:** 1.19 g (4.37 mmol, 46%), orange solid.

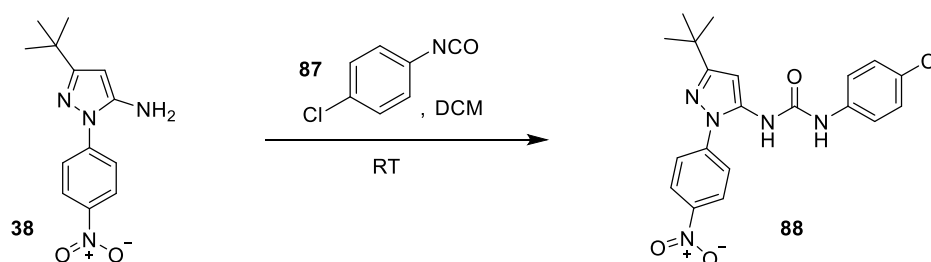
- **TLC:**  $R_f = 0.63$  ( $\text{SiO}_2$ , cyclohexane/EtOAc 1:1).
- **$\text{C}_{10}\text{H}_7\text{F}_3\text{N}_4\text{O}_2$ :** (272.18), [272.05].
- **$^1\text{H-NMR}$  (500 MHz,  $\text{DMSO-d}_6$ , 300 K):**  $\delta = 8.38$  (d,  $^3J = 9.1$  Hz, 2H, H-3-, H-5-phenyl), 7.94 (d,  $^3J = 9.1$  Hz, 2H, H-2-, H-6-phenyl), 6.10 (s, 2H,  $\text{NH}_2$ ), 5.88 (s, 1H, pyrazole) ppm.
- **$^{13}\text{C-NMR}$  (126 MHz,  $\text{DMSO-d}_6$ , 300 K):**  $\delta = 149.7, 145.6, 143.4, 142.6$  ( $^2J_{\text{CF}} = 36.9$  Hz), 126.4, 124.9, 123.7, 121.4 ( $^1J_{\text{CF}} = 269.2$  Hz), 112.4, 87.8 ppm.
- **MS (ESI pos.):**  $m/z$  (%) = 273.0 (100) ( $[\text{M}+\text{H}]^+$ , calcd. 273.1).
- **MS (ESI neg.):**  $m/z$  (%) = 271.1 (100) ( $[\text{M}-\text{H}]^-$ , calcd. 271.0). 307.0 (25) ( $[\text{M}+\text{Cl}]^-$ , calcd. 307.1).

**3-(Trifluoromethyl)-1-(4-(trifluoromethyl)phenyl)-1H-pyrazol-5-amine (55, SR252)**


The synthesis of 3-(trifluoromethyl)-1-(4-(trifluoromethyl)phenyl)-1H-pyrazol-5-amine (**55**) was performed according to the synthesis of 1-(4-nitrophenyl)-3-(trifluoromethyl)-1H-pyrazol-5-amine (**54**) described before. After preparing 4,4,4-trifluoro-3-oxobutanenitrile (**53**) as intermediate, (4-(trifluoromethyl)phenyl)hydrazine hydrochloride (**39**, 2.03 g, 9.57 mmol) was added and the mixture was heated for 6 h at 70 °C. The crude product was purified by column chromatography on silica (cyclohexane/EtOAc 4:1 → 1:1).

**Yield:** 1.21 g (4.11 mmol, 43%), colorless solid.

- **TLC:**  $R_f = 0.26$  (SiO<sub>2</sub>, cyclohexane/EtOAc 4:1).
- **C<sub>11</sub>H<sub>7</sub>F<sub>6</sub>N<sub>3</sub>:** (295.19), [295.05].
- **<sup>1</sup>H-NMR (500 MHz, DMSO-d<sub>6</sub>, 300 K):**  $\delta = 7.92\text{--}7.84$  (m, 4H, H-2-, H-3-, H-5-, H-6-phenyl), 5.99 (s, 2H, NH<sub>2</sub>), 5.85 (s, 1H, pyrazole) ppm.
- **<sup>13</sup>C-NMR (126 MHz, DMSO-d<sub>6</sub>, 300 K):**  $\delta = 149.3, 142.0$  (<sup>2</sup> $J_{CF} = 36.6$  Hz), 141.1, 127.6 (<sup>2</sup> $J_{CF} = 32.2$  Hz), 126.6, 126.5, 124.0 (<sup>1</sup> $J_{CF} = 272.2$  Hz), 123.9, 121.5 (<sup>1</sup> $J_{CF} = 268.0$  Hz), 87.5 ppm.
- **MS (ESI pos.):**  $m/z$  (%) = 295.95 (100) ([M+H]<sup>+</sup>, calcd. 295.05).

**8.4.2 Synthesis of final BIRB-796 fragment library compounds**
**1-(3-(tert-Butyl)-1-(4-nitrophenyl)-1H-pyrazol-5-yl)-3-(4-chlorophenyl)urea (88, SR225)**


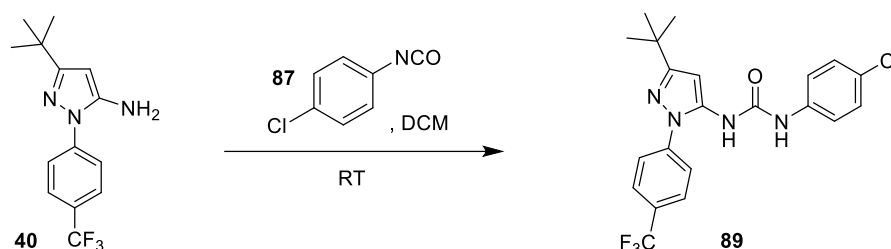
3-(*tert*-Butyl)-1-(4-nitrophenyl)-1H-pyrazol-5-amine (**38**, 2.00 g, 7.68 mmol) and 1-chloro-4-isocyanatobenzene (**87**, 1.07 g, 6.99 mmol) were dissolved in DCM (50 mL) and the mixture was stirred at RT for 20 h. The resultant solid was filtered and washed with hexane (30 mL). Subsequently, the filtrate was concentrated under reduced pressure to crystallize additional product, which was filtered and washed with hexane.

**Yield:** 1.83 g (4.41 mmol, 81%), yellowish solid.

- **TLC:**  $R_f = 0.89$  (SiO<sub>2</sub>, hexane/EtOAc 1:3).

- **C<sub>20</sub>H<sub>20</sub>ClN<sub>5</sub>O<sub>3</sub>**: (413.86), [413.13].
- **HPLC**:  $t_R$  = 16.83 min.
- **<sup>1</sup>H-NMR (500 MHz, DMSO-d<sub>6</sub>, 300 K)**:  $\delta$  = 9.20 (s, 1H, NH pyrazole), 8.67 (s, 1H, NH Cl-phenyl), 8.36 (d, <sup>3</sup>J = 9.2 Hz, 2H, H-3-, H-5-nitrophenyl), 7.88 (d, <sup>3</sup>J = 8.9 Hz, 2H, H-2-, H-6-nitrophenyl), 7.44 (d, <sup>3</sup>J = 8.9 Hz, 2H, H-3-, H-5-Cl-phenyl), 7.30 (d, <sup>3</sup>J = 8.9 Hz, 2H, H-2-, H-6-Cl-phenyl) 6.45 (s, 1H, pyrazole), 1.30 (s, 9H, tBu) ppm.
- **<sup>13</sup>C-NMR (126 MHz, DMSO-d<sub>6</sub>, 300 K)**:  $\delta$  = 162.5, 152.0, 145.0, 144.1, 138.3, 137.8, 128.7, 125.8, 124.9, 123.2, 119.9, 99.9, 32.2, 30.0 ppm.
- **MS (ESI pos.)**:  $m/z$  (%) = 414.2 (100) ([M+H]<sup>+</sup>, calcd. 414.2).
- **MS (ESI neg.)**:  $m/z$  (%) = 412.2 (73) ([M-H]<sup>-</sup>, calcd. 412.1). 259.1 (100) ([M<sub>fr.</sub>-H]<sup>-</sup>, calcd. 259.1).
- **HRMS (FTMS + p MALDI)**:  $m/z$  = 414.1345 [M+H]<sup>+</sup>, calcd. for [C<sub>20</sub>H<sub>21</sub>ClN<sub>5</sub>O<sub>3</sub>]<sup>+</sup> = 414.1327.

**1-(3-(tert-Butyl)-1-(4-(trifluoromethyl)phenyl)-1H-pyrazol-5-yl)-3-(4-chlorophenyl)urea (89, SR238)**

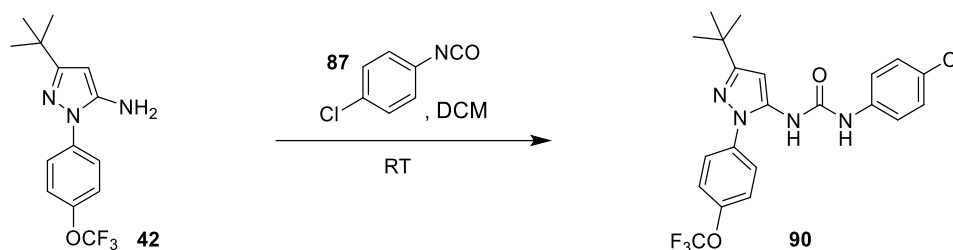


3-(tert-Butyl)-1-(4-(trifluoromethyl)phenyl)-1H-pyrazol-5-amine (**40**, 460 mg, 1.62 mmol) and 1-chloro-4-isocyanatobenzene (**87**, 340 mg, 2.21 mmol) were dissolved in DCM (10 mL) and the mixture was stirred at RT for 20 h. The resultant solid was filtered and washed with hexane (15 mL). Subsequently, the filtrate was concentrated under reduced pressure to crystallize additional product, which was filtered and washed with hexane. The combined crude product was recrystallized from hexane/EtOAc (1:1).

**Yield**: 226 mg (0.518 mmol, 32%), colorless solid.

- **TLC**:  $R_f$  = 0.91 (SiO<sub>2</sub>, cyclohexane/EtOAc 1:3).
- **C<sub>21</sub>H<sub>20</sub>ClF<sub>3</sub>N<sub>4</sub>O**: (436.86), [436.13].
- **HPLC**:  $t_R$  = 17.52 min.
- **<sup>1</sup>H-NMR (500 MHz, DMSO-d<sub>6</sub>, 300 K)**:  $\delta$  = 9.16 (br s, 1H, NH pyrazole), 8.59 (br s, 1H, NH Cl-phenyl), 7.89 (d, <sup>3</sup>J = 8.3 Hz, 2H, H-3-, H-5-CF<sub>3</sub>-phenyl), 7.81 (d, <sup>3</sup>J = 8.3 Hz, 2H, H-2-, H-6-CF<sub>3</sub>-phenyl), 7.45 (d, <sup>3</sup>J = 8.5 Hz, 2H, H-3-, H-5-Cl-phenyl), 7.31 (d, <sup>3</sup>J = 8.3 Hz, 2H, H-2-, H-6-Cl-phenyl), 6.43 (br s, 1H, pyrazole), 1.29 (s, 9H, tBu) ppm.
- **<sup>13</sup>C-NMR (126 MHz, DMSO-d<sub>6</sub>, 300 K)**:  $\delta$  = 161.8, 151.8, 142.0, 138.4, 137.5, 128.7, 127.0 (<sup>2</sup>J<sub>CF</sub> = 32.2 Hz), 126.4, 125.8, 124.6 (<sup>1</sup>J<sub>CF</sub> = 274.9 Hz), 123.9, 119.8, 97.5, 32.1, 30.0 ppm.
- **MS (ESI pos.)**:  $m/z$  (%) = 437.2 (100) ([M+H]<sup>+</sup>, calcd. 437.1). 310.2 (31) ([M<sub>fr.(1)}</sub>]<sup>+</sup>, calcd. 310.1). 284.2 (14) ([M<sub>fr.(11)}</sub>+H]<sup>+</sup>, calcd. 284.1).
- **MS (ESI neg.)**:  $m/z$  (%) = 282.2 (100) ([M<sub>fr.(11)}</sub>-H]<sup>-</sup>, calcd. 282.1). 435.2 (28) ([M-H]<sup>-</sup>, calcd. 435.1).
- **HRMS (FTMS + p MALDI)**:  $m/z$  = 437.1330 [M+H]<sup>+</sup>, calcd. for [C<sub>21</sub>H<sub>21</sub>ClF<sub>3</sub>N<sub>4</sub>O]<sup>+</sup> = 437.1351.

**1-(3-(tert-Butyl)-1-(4-(trifluoromethoxy)phenyl)-1H-pyrazol-5-yl)-3-(4-chlorophenyl)urea (90, SR239)**

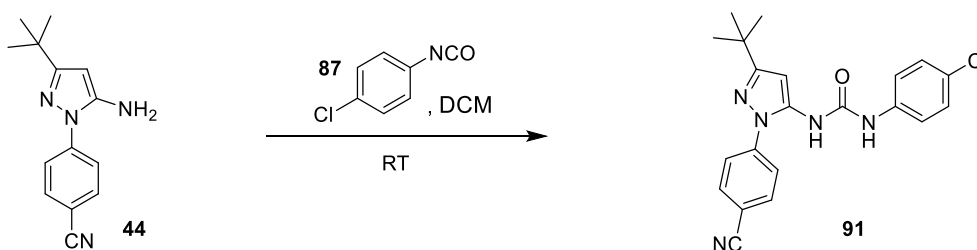


3-(tert-Butyl)-1-(4-(trifluoromethoxy)phenyl)-1H-pyrazol-5-amine (**42**, 505 mg, 1.69 mmol) and 1-chloro-4-isocyanatobenzene (**87**, 236 mg, 1.53 mmol) were dissolved in DCM (10 mL) and the mixture was stirred at RT for 20 h. The resultant solid was filtered and washed with hexane (15 mL). Subsequently, the filtrate was concentrated under reduced pressure to crystallize additional product, which was filtered and washed with hexane. The combined crude product was recrystallized from hexane/EtOAc (1:1).

**Yield:** 480 mg (1.06 mmol, 69%), colorless solid.

- **TLC:**  $R_f = 0.92$  (SiO<sub>2</sub>, cyclohexane/EtOAc 1:3).
- **C<sub>21</sub>H<sub>20</sub>ClF<sub>3</sub>N<sub>4</sub>O<sub>2</sub>:** (452.86), [452.12].
- **HPLC:**  $t_R = 17.57$  min.
- **<sup>1</sup>H-NMR (600 MHz, DMSO-d<sub>6</sub>, 300 K):**  $\delta = 9.12$  (br s, 1H, NH pyrazole), 8.51 (br s, 1H, NH Cl-phenyl), 7.67 (d,  $^3J = 8.9$  Hz, 2H, H-3-, H-5-OCF<sub>3</sub>-phenyl), 7.52 (d,  $^3J = 8.9$  Hz, 2H, H-2-, H-6-OCF<sub>3</sub>-phenyl), 7.44 (d,  $^3J = 8.8$  Hz, 2H, H-2-, H-6-Cl-phenyl), 7.31 (d,  $^3J = 8.8$  Hz, 2H, H-3-, H-5-Cl-phenyl), 6.39 (s, 1H, pyrazole), 1.28 (s, 9H, tBu) ppm.
- **<sup>13</sup>C-NMR (150 MHz, DMSO-d<sub>6</sub>, 300 K):**  $\delta = 161.3, 151.7, 146.8, 138.3, 137.7, 137.2, 128.6, 125.8$  (2x), 121.9, 120.1 ( $^1J_{CF} = 258.5$  Hz), 119.8, 96.6, 32.0, 30.1 ppm.
- **MS (ESI pos.):**  $m/z$  (%) = 453.2 (100) ([M+H]<sup>+</sup>, calcd. 453.1). 326.2 (37) ([M<sub>fr.(1)}</sub>]<sup>+</sup>, calcd. 326.1). 300.2 (11) ([M+H]<sup>+</sup>, calcd. 300.1).
- **MS (ESI neg.):**  $m/z$  (%) = 298.2 (100) ([M<sub>fr.(1)}</sub>-H]<sup>-</sup>, calcd. 298.2). 451.2 (28) ([M-H]<sup>-</sup>, calcd. 451.1).
- **HRMS (FTMS + p MALDI):**  $m/z = 453.1308$  [M+H]<sup>+</sup>, calcd. for [C<sub>21</sub>H<sub>21</sub>ClF<sub>3</sub>N<sub>4</sub>O<sub>2</sub>]<sup>+</sup> = 453.1300.

**1-(3-(tert-Butyl)-1-(4-cyanophenyl)-1H-pyrazol-5-yl)-3-(4-chlorophenyl)urea (91, SR240)**

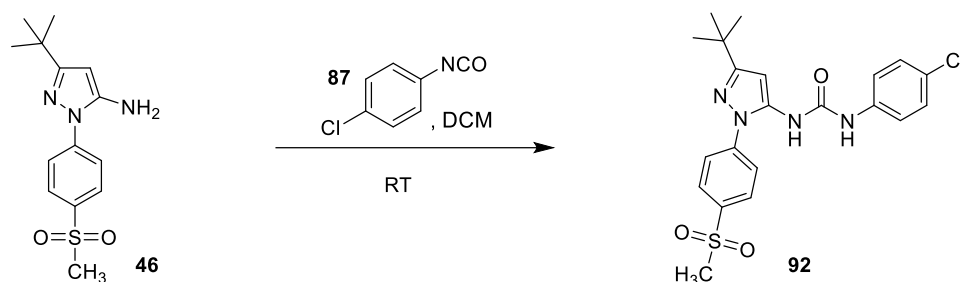


4-(5-Amino-3-(tert-butyl)-1H-pyrazol-1-yl)benzonitrile (**44**, 590 mg, 2.46 mmol) and 1-chloro-4-isocyanatobenzene (**87**, 514 mg, 3.35 mmol) were dissolved in DCM (30 mL) and the mixture was stirred at RT for 20 h. The resultant solid was filtered and washed with hexane (15 mL). Subsequently, the filtrate was concentrated under reduced pressure to crystallize additional product, which was filtered and washed with hexane. The combined crude product was recrystallized from a hexane/EtOAc mixture (1:1).

**Yield:** 539 mg (1.37 mmol, 56%), yellowish solid.

- **TLC:**  $R_f = 0.89$  (SiO<sub>2</sub>, cyclohexane/EtOAc 1:3).
- **C<sub>21</sub>H<sub>20</sub>ClN<sub>5</sub>O:** (393.87), [393.14].
- **HPLC:**  $t_R = 16.49$  min.
- **<sup>1</sup>H-NMR (600 MHz, DMSO-d<sub>6</sub>, 300 K):**  $\delta = 9.18$  (br s, 1H, NH pyrazole), 8.60 (br s, 1H, NH Cl-phenyl), 7.98 (d,  $^3J = 8.6$  Hz, 2H, H-3-, H-5-CN-phenyl), 7.80 (d,  $^3J = 8.6$  Hz, 2H, H-2-, H-6-CN-phenyl), 7.44 (d,  $^3J = 8.8$  Hz, 2H, H-3-, H-5-Cl-phenyl), 7.31 (d,  $^3J = 8.8$  Hz, 2H, H-2-, H-6-Cl-phenyl), 6.42 (s, 1H, pyrazole), 1.29 (s, 9H, tBu) ppm.
- **<sup>13</sup>C-NMR (150 MHz, DMSO-d<sub>6</sub>, 300 K):**  $\delta = 162.1, 151.9, 142.4, 138.3, 137.5, 133.5, 128.6, 125.8, 123.4, 119.9, 118.5, 108.8, 98.5, 32.1, 29.9$  ppm.
- **MS (ESI pos.):**  $m/z$  (%) = 394.2 (100) ([M+H]<sup>+</sup>, calcd. 349.2). 267.2 (32) ([M<sub>fr.(I)}</sub>+H]<sup>+</sup>, calcd. 268.1). 241.2 (29) ([M<sub>fr.(II)}</sub>+H]<sup>+</sup>, calcd. 241.2).
- **MS (ESI neg.):**  $m/z$  (%) = 239.2 (100) ([M<sub>fr.(I)}</sub>-H]<sup>-</sup>, calcd. 239.1). 392.2 (45) ([M-H]<sup>-</sup>, calcd. 392.1).
- **HRMS (FTMS + p MALDI):**  $m/z = 394.1409$  [M+H]<sup>+</sup>, calcd. for [C<sub>21</sub>H<sub>21</sub>ClN<sub>5</sub>O]<sup>+</sup> = 394.1429.

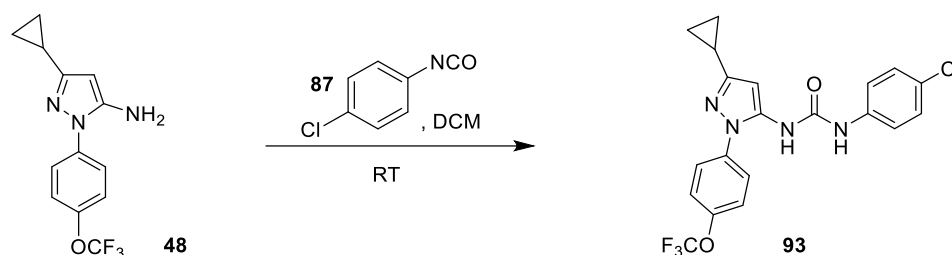
**1-(3-(tert-Butyl)-1-(4-(methylsulfonyl)phenyl)-1H-pyrazol-5-yl)-3-(4-chlorophenyl)urea (92, SR245)**



3-(tert-Butyl)-1-(4-(methylsulfonyl)phenyl)-1H-pyrazol-5-amine (**46**, 700 mg, 2.39 mmol) and 1-chloro-4-isocyanatobenzene (**87**, 333 mg, 2.17 mmol) were dissolved in DCM (15 mL) and the mixture was stirred at RT for 20 h. The resultant solid was filtered and washed with hexane (15 mL). Subsequently, the filtrate was concentrated under reduced pressure to crystallize additional product, which was filtered and washed with hexane. The combined crude product was recrystallized from a hexane/EtOAc mixture (1:1).

**Yield:** 761 mg (1.71 mmol, 78%), yellowish solid.

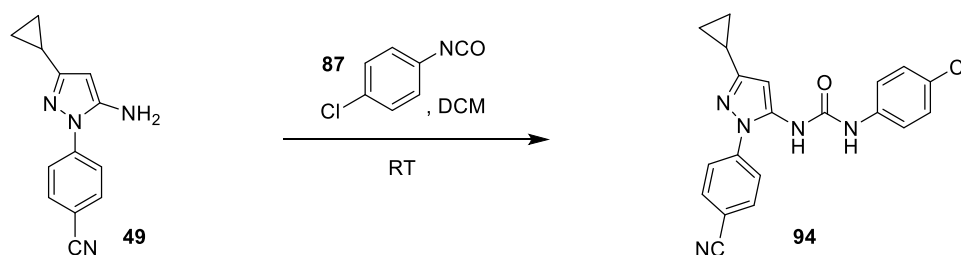
- **TLC:**  $R_f = 0.72$  (SiO<sub>2</sub>, cyclohexane/EtOAc 1:3).
- **C<sub>21</sub>H<sub>23</sub>ClN<sub>4</sub>O<sub>3</sub>S:** (446.95), [446.12].
- **HPLC:**  $t_R = 15.77$  min.
- **<sup>1</sup>H-NMR (600 MHz, DMSO-d<sub>6</sub>, 300 K):**  $\delta = 9.17$  (br s, 1H, NH pyrazole), 8.63 (br s, 1H, NH Cl-phenyl), 8.06 (d,  $^3J = 8.7$  Hz, 2H, H-3-, H-5-SO<sub>2</sub>CH<sub>3</sub>-phenyl), 7.84 (d,  $^3J = 8.7$  Hz, 2H, H-2-, H-6-SO<sub>2</sub>CH<sub>3</sub>-phenyl), 7.45 (d,  $^3J = 8.9$  Hz, 2H, H-3-, H-5-Cl-phenyl), 7.31 (d,  $^3J = 8.9$  Hz, 2H, H-2-, H-6-Cl-phenyl), 6.43 (s, 1H, pyrazole), 3.27 (s, 3H, SO<sub>2</sub>CH<sub>3</sub>), 1.29 (s, 9H, tBu) ppm.
- **<sup>13</sup>C-NMR (150 MHz, DMSO-d<sub>6</sub>, 300 K):**  $\delta = 162.0, 151.8, 142.7, 138.5, 138.3, 137.6, 128.6, 128.3, 125.8, 123.7, 119.8, 97.8, 43.5, 32.1, 30.0$  ppm.
- **MS (ESI pos.):**  $m/z$  (%) = 447.2 (100) ([M+H]<sup>+</sup>, calcd. 447.1). 294.2 (28) ([M<sub>fr.(I)}</sub>+H]<sup>+</sup>, calcd. 294.1). 320.2 (29) ([M<sub>fr.(II)}</sub>+H]<sup>+</sup>, calcd. 320.1).
- **MS (ESI neg.):**  $m/z$  (%) = 292.2 (100) ([M<sub>fr.(I)}</sub>-H]<sup>-</sup>, calcd. 292.1). 445.2 (24) ([M-H]<sup>-</sup>, calcd. 445.1).
- **HRMS (FTMS + p MALDI):**  $m/z = 469.1054$  [M+Na]<sup>+</sup>, calcd. for [C<sub>21</sub>H<sub>23</sub>ClN<sub>4</sub>NaO<sub>3</sub>S]<sup>+</sup> = 469.1072.

**1-(4-Chlorophenyl)-3-(3-cyclopropyl-1-(4-(trifluoromethoxy)phenyl)-1H-pyrazol-5-yl)urea (93, SR258)**

3-Cyclopropyl-1-(4-(trifluoromethoxy)phenyl)-1H-pyrazol-5-amine (**48**, 500 mg, 1.77 mmol) and 1-chloro-4-isocyanatobenzene (**87**, 407 mg, 2.65 mmol) were dissolved in DCM (20 mL) and the mixture was stirred at RT for 20 h. The solvent was removed under reduced pressure and the crude product was recrystallized from a hexane/EtOAc mixture (1:1).

**Yield:** 605 mg (1.39 mmol, 78%), colorless solid.

- **TLC:**  $R_f = 0.94$  (SiO<sub>2</sub>, cyclohexane/EtOAc 1:3).
- **C<sub>20</sub>H<sub>16</sub>ClF<sub>3</sub>N<sub>4</sub>O<sub>2</sub>:** (436.81), [436.09].
- **HPLC:**  $t_R = 16.44$  min.
- **<sup>1</sup>H-NMR (500 MHz, DMSO-d<sub>6</sub>, 300 K):**  $\delta = 9.09$  (br s, 1H, NH pyrazole), 8.53 (br s, 1H, NH Cl-phenyl), 7.65 (d,  $^3J = 9.0$  Hz, 2H, H-3-, H-5-OCF<sub>3</sub>-phenyl), 7.51 (d,  $^3J = 9.0$  Hz, 2H, H-2-, H-6-OCF<sub>3</sub>-phenyl), 7.43 (d,  $^3J = 8.9$  Hz, 2H, H-3-, H-5-Cl-phenyl), 7.30 (d,  $^3J = 8.9$  Hz, 2H, H-2-, H-6-Cl-phenyl), 6.19 (s, 1H, pyrazole), 1.93–1.86 (m, 1H, CH(CH<sub>2</sub>)<sub>2</sub>), 0.92–0.87 (m, 2H, CH<sub>2(A)</sub>), 0.73–0.68 (m, 2H, CH<sub>2(B)</sub>) ppm.
- **<sup>13</sup>C-NMR (126 MHz, DMSO-d<sub>6</sub>, 300 K):**  $\delta = 154.8, 151.7, 146.8, 138.3, 137.5$  (2x), 128.7, 125.8, 122.0, 120.1 ( $^1J_{CF} = 256.9$  Hz), 119.8, 96.4, 9.4, 7.8 ppm.
- **MS (ESI pos.):**  $m/z$  (%) = 436.9 (100) ([M+H]<sup>+</sup>, calcd. 437.1).
- **MS (ESI neg.):**  $m/z$  (%) = 435.0 (100) ([M-H]<sup>-</sup>, calcd. 435.1). 282.2 (11) ([M<sub>fr.</sub>]<sup>-</sup>, calcd. 282.1).
- **HRMS (FTMS + p MALDI):**  $m/z = 437.0978$  [M+H]<sup>+</sup>, calcd. for [C<sub>20</sub>H<sub>17</sub>ClF<sub>3</sub>N<sub>4</sub>O<sub>2</sub>]<sup>+</sup> = 437.0987.

**1-(4-Chlorophenyl)-3-(1-(4-cyanophenyl)-3-cyclopropyl-1H-pyrazol-5-yl)urea (94, SR261)**

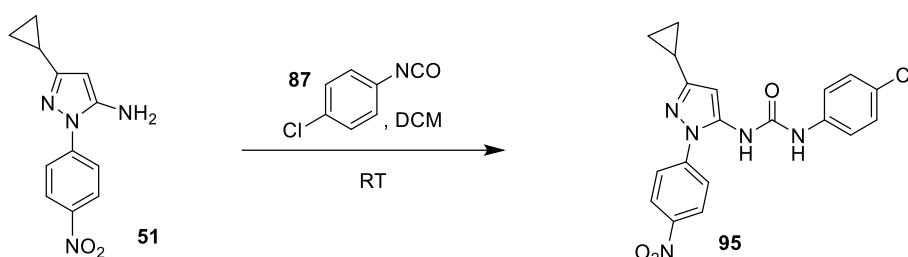
4-(5-Amino-3-cyclopropyl-1H-pyrazol-1-yl)benzonitrile (**49**, 500 mg, 2.23 mmol) and 1-chloro-4-isocyanatobenzene (**87**, 514 mg, 3.35 mmol) were dissolved in DCM (20 mL) and the mixture was stirred at RT for 20 h. The solvent was removed under reduced pressure and the crude product was recrystallized from a hexane/EtOAc mixture (1:1).

**Yield:** 110 mg (0.291 mmol, 13%), colorless solid.

- **TLC:**  $R_f = 0.86$  (SiO<sub>2</sub>, cyclohexane/EtOAc 1:3).
- **C<sub>20</sub>H<sub>16</sub>ClN<sub>5</sub>O:** (377.83), [377.10].

- **HPLC:**  $t_R = 15.25$  min.
- **$^1\text{H-NMR}$  (600 MHz,  $\text{DMSO-d}_6$ , 300 K):**  $\delta = 9.14$  (s, 1H, NH pyrazole), 8.62 (s, 1H, NH Cl-phenyl), 7.97 (d,  $^3J = 8.4$  Hz, 2H, H-3-, H-5-CN-phenyl), 7.77 (d,  $^3J = 8.4$  Hz, 2H, H-2-, H-6-CN-phenyl), 7.43 (d,  $^3J = 8.6$  Hz, 2H, H-3-, H-5-Cl-phenyl), 7.30 (d,  $^3J = 8.6$  Hz, 2H, H-2-, H-6-Cl-phenyl), 6.21 (s, 1H, pyrazole), 1.96–1.87 (m, 1H,  $\text{CH}(\text{CH}_2)_2$ ), 0.96–0.88 (m, 2H,  $\text{CH}_{2(\text{A})}$ ), 0.77–0.68 (m, 2H,  $\text{CH}_{2(\text{B})}$ ) ppm.
- **$^{13}\text{C-NMR}$  (150 MHz,  $\text{DMSO-d}_6$ , 300 K):**  $\delta = 155.8, 151.8, 142.4, 138.3, 137.7, 133.5, 128.6, 125.8, 123.4, 119.9, 118.4, 108.8, 98.4, 9.3, 7.8$  ppm.
- **MS (ESI pos.):**  $m/z$  (%) = 377.9 (100) ( $[\text{M}+\text{H}]^+$ , calcd. 378.1). 225.1 (63) ( $[\text{M}_{\text{fr.}}+2\text{H}]^+$ , calcd. 225.0).
- **MS (ESI neg.):**  $m/z$  (%) = 376.0 (100) ( $[\text{M}-\text{H}]^-$ , calcd. 376.1). 223.3 (13) ( $[\text{M}_{\text{fr.}}-\text{H}]^-$ , calcd. 223.1).
- **HRMS (FTMS + p MALDI):**  $m/z = 378.1100$   $[\text{M}+\text{H}]^+$ , calcd. for  $[\text{C}_{20}\text{H}_{17}\text{ClN}_5\text{O}]^+ = 378.1116$ .

**1-(4-Chlorophenyl)-3-(3-cyclopropyl-1-(4-nitrophenyl)-1H-pyrazol-5-yl)urea (95, SR263)**

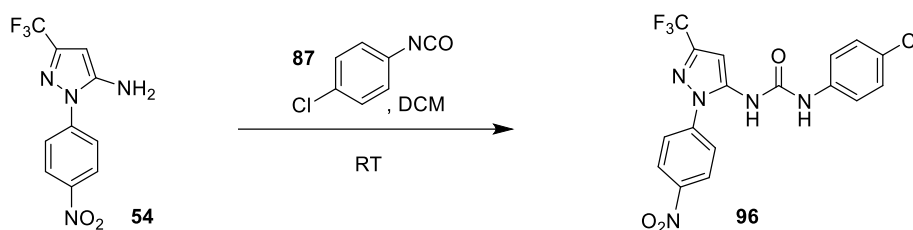


3-Cyclopropyl-1-(4-nitrophenyl)-1H-pyrazol-5-amine (**51**, 500 mg, 2.05 mmol) and 1-chloro-4-isocyanatobenzene (**87**, 314 mg, 2.05 mmol) were dissolved in DCM (20 mL) and the mixture was stirred at RT for 20 h. The solvent was removed under reduced pressure and the crude product was recrystallized from a hexane/EtOAc mixture (1:1).

**Yield:** 262 mg (0.659 mmol, 32%), colorless solid.

- **TLC:**  $R_f = 0.88$  ( $\text{SiO}_2$ , cyclohexane/EtOAc 98:2).
- **$\text{C}_{19}\text{H}_{16}\text{ClN}_5\text{O}_3$ :** (397.09), [397.82].
- **HPLC:**  $t_R = 15.65$  min.
- **$^1\text{H-NMR}$  (400 MHz,  $\text{DMSO-d}_6$ , 300 K):**  $\delta = 9.16$  (s, 1H, NH pyrazole), 8.69 (s, 1H, NH Cl-phenyl), 8.35 (d,  $^3J = 8.9$  Hz, 2H, H-3-, H-5-nitrophenyl), 7.87 (d,  $^3J = 8.9$  Hz, 2H, H-2-, H-6-nitrophenyl), 7.43 (d,  $^3J = 8.7$  Hz, 2H, H-3-, H-5-Cl-phenyl), 7.30 (d,  $^3J = 8.7$  Hz, 2H, H-2-, H-6-Cl-phenyl), 5.75 (s, 1H, pyrazole), 1.98–1.88 (m, 1H,  $\text{CH}(\text{CH}_2)_2$ ), 0.98–0.86 (m, 2H,  $\text{CH}_{2(\text{A})}$ ), 0.77–0.68 (m, 2H,  $\text{CH}_{2(\text{B})}$ ) ppm.
- **$^{13}\text{C-NMR}$  (101 MHz,  $\text{DMSO-d}_6$ , 300 K):**  $\delta = 156.2, 151.9, 145.0, 143.9, 138.3, 138.0, 128.6, 125.8, 124.8, 123.1, 119.9, 98.8, 39.5, 9.4, 7.9$  ppm.
- **MS (ESI pos.):**  $m/z$  (%) = 397.94 (100) ( $[\text{M}+\text{H}]^+$ , calcd. 398.10).
- **MS (ESI neg.):**  $m/z$  (%) = 396.07 (100) ( $[\text{M}-\text{H}]^-$ , calcd. 396.08). 243.24 (13) ( $[\text{M}_{\text{fr.}}]^-$ , calcd. 243.09).
- **HRMS (FTMS + p MALDI):**  $m/z = 398.1015$   $[\text{M}+\text{H}]^+$ , calcd. for  $[\text{C}_{19}\text{H}_{17}\text{ClN}_5\text{O}_3]^+ = 398.1014$ .

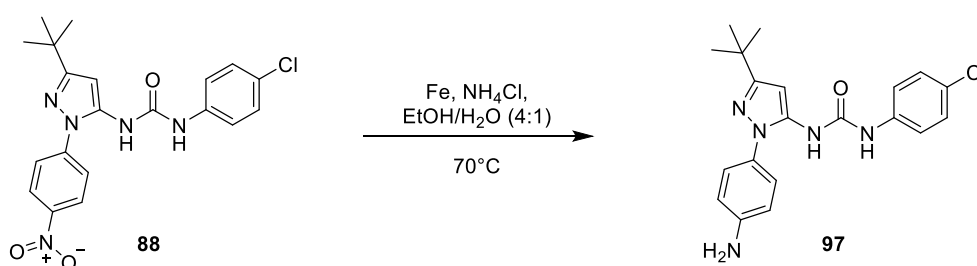


**1-(4-Chlorophenyl)-3-(1-(4-nitrophenyl)-3-(trifluoromethyl)-1H-pyrazol-5-yl)urea (96, SR266)**

1-(4-Nitrophenyl)-3-(trifluoromethyl)-1H-pyrazol-5-amine (**54**, 1.00 g, 3.67 mmol) and 1-chloro-4-isocyanatobenzene (**87**, 769 mg, 5.01 mmol) were dissolved in DCM (35 mL) and the mixture was stirred at RT for 20 h. The solvent was removed under reduced pressure and the crude product was recrystallized from a cyclohexane/EtOAc mixture (1:1).

**Yield:** 122 mg (0.287 mmol, 8%), brownish solid.

- **TLC:**  $R_f = 0.91$  (SiO<sub>2</sub>, cyclohexane/EtOAc 1:3).
- **C<sub>17</sub>H<sub>11</sub>ClF<sub>3</sub>N<sub>5</sub>O<sub>3</sub>:** (425.75), [425.05].
- **HPLC:**  $t_R = 16.32$  min.
- **<sup>1</sup>H-NMR (500 MHz, DMSO-d<sub>6</sub>, 300 K):**  $\delta = 9.26$  (s, 1H, NH pyrazole), 8.98 (s, 1H, NH Cl-phenyl), 8.44 (d,  $^3J = 8.9$  Hz, 2H, H-3-, H-5-nitrophenyl), 7.95 (d,  $^3J = 8.9$  Hz, 2H, H-2-, H-6-nitrophenyl), 7.43 (d,  $^3J = 8.7$  Hz, 2H, H-3-, H-5-Cl-phenyl), 7.33 (d,  $^3J = 8.7$  Hz, 2H, H-2-, H-6-Cl-phenyl), 6.95 (s, 1H, pyrazole) ppm.
- **<sup>13</sup>C-NMR (126 MHz, DMSO-d<sub>6</sub>, 300 K):**  $\delta = 151.3, 146.8, 142.4, 142.0$  ( $^2J_{CF} = 36.9$  Hz), 139.8, 137.9, 128.7, 126.1, 125.5, 125.0, 121.1 ( $^1J_{CF} = 267.6$  Hz), 120.0, 97.9 ppm.
- **MS (ESI pos.):**  $m/z$  (%) = 425.8 (17) ([M+H]<sup>+</sup>, calcd. 426.1). 357.1 (12) ([M<sub>fr.(I)}</sub>]<sup>+</sup>, calcd. 357.1). 256.9 (33) ([M<sub>fr.(II)}</sub>]<sup>+</sup>, calcd. 256.0).
- **MS (ESI neg.):**  $m/z$  (%) = 423.9 (100) ([M-H]<sup>-</sup>, calcd. 424.1). 271.2 (23) ([M<sub>fr.(III)}</sub>]<sup>-</sup>, calcd. 271.0).
- **HRMS (FTMS + p MALDI):**  $m/z = 426.0570$  [M+H]<sup>+</sup>, calcd. for [C<sub>17</sub>H<sub>12</sub>ClF<sub>3</sub>N<sub>5</sub>O<sub>3</sub>]<sup>+</sup> = 426.0575.

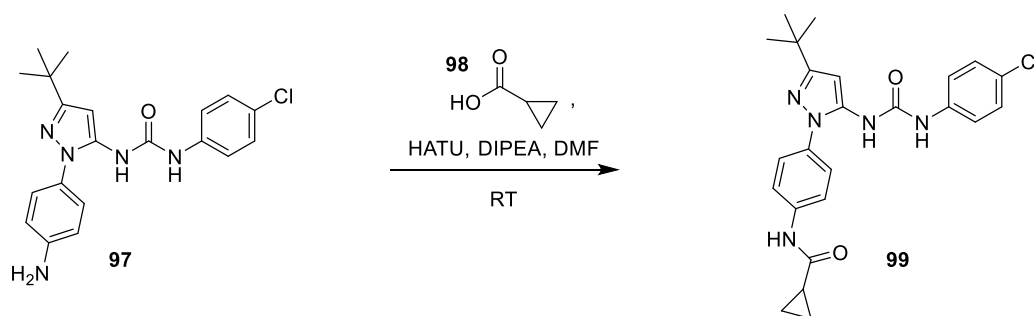
**1-(1-(4-Aminophenyl)-3-(tert-butyl)-1H-pyrazol-5-yl)-3-(4-chlorophenyl)urea (97, SR226)**

1-(3-(*tert*-Butyl)-1-(4-nitrophenyl)-1H-pyrazol-5-yl)-3-(4-chlorophenyl)urea (**88**, 1.14 g, 2.76 mmol) was dissolved in an EtOH/H<sub>2</sub>O mixture (4:1, 3 mL). Subsequently, Fe powder (1.54 g, 27.6 mmol) was sprinkled on, NH<sub>4</sub>Cl (1.47 g, 27.6 mmol) was added and the reaction was heated for 1 h at 70 °C. The mixture was filtered over Celite® and washed with EtOAc. The crude product was purified using column chromatography on silica (cyclohexane/EtOAc: 1:1 → 1:3).

**Yield:** 782 mg (2.03 mmol, 74%), colorless solid.

- **TLC:**  $R_f = 0.42$  ( $\text{SiO}_2$ , cyclohexane/EtOAc 1:3).
- **$\text{C}_{20}\text{H}_{22}\text{ClN}_5\text{O}$ :** (383.87), [383.15].
- **HPLC:**  $t_R = 15.23$  min.
- **$^1\text{H-NMR}$  (500 MHz,  $\text{DMSO-d}_6$ , 300 K):**  $\delta = 9.19$  (s, 1H, NH pyrazole), 8.20 (s, 1H, NH Cl-phenyl), 7.42 (d,  $^3J = 8.9$  Hz, H-3-, H-5-Cl-phenyl), 7.30 (d,  $^3J = 8.9$  Hz, 2H, H-2-, H-6-Cl-phenyl), 7.07 (d,  $^3J = 8.7$  Hz, 2H, H-2-, H-6-aminophenyl), 6.66 (d,  $^3J = 8.7$  Hz, 2H, H-3-, H-5-aminophenyl), 6.30 (s, 1H, pyrazole), 5.40 (br s, 2H,  $\text{NH}_2$ ), 1.25 (s, 9H, tBu) ppm.
- **$^{13}\text{C-NMR}$  (126 MHz,  $\text{DMSO-d}_6$ , 300 K):**  $\delta = 159.6, 151.1, 148.7, 138.5, 137.1, 128.7, 126.6, 126.5, 125.5, 119.5, 113.8, 92.8, 32.0, 30.3$  ppm.
- **MS (ESI pos.):**  $m/z$  (%) = 384.2 (100) ( $[\text{M}+\text{H}]^+$ , calcd. 384.2). 257.2 (49) ( $[\text{M}_{\text{fr.}(1)}]^+$ , calcd. 257.3). 231.1 (24) ( $[\text{M}_{\text{fr.}(1)}+\text{H}]^+$ , calcd. 231.2).
- **MS (ESI neg.):**  $m/z$  (%) = 382.2 (100) ( $[\text{M}-\text{H}]^-$ , calcd. 382.1). 255.2 (34) ( $[\text{M}_{\text{fr.}(1)}-\text{H}]^-$ , calcd. 256.3). 229.2 (46) ( $[\text{M}_{\text{fr.}(1)}-\text{H}]^-$ , calcd. 229.1).
- **HRMS (FTMS + p MALDI):**  $m/z = 384.1570$   $[\text{M}+\text{H}]^+$ , calcd. for  $[\text{C}_{20}\text{H}_{23}\text{ClN}_5\text{O}_3]^+ = 384.1586$ .

***N*-(4-(3-(*tert*-Butyl)-5-(3-(4-chlorophenyl)ureido)-1*H*-pyrazol-1-yl)phenyl)cyclopropanecarboxamide (99, SR246)**



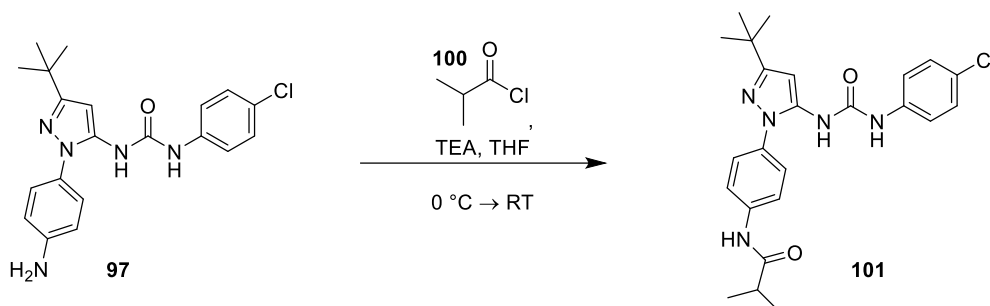
Cyclopropanecarboxylic acid (**98**, 28 mg, 0.33 mmol) and HATU (149 mg, 0.396 mmol) were dissolved in DMF (dry, 8 mL) and DIPEA (51 mg, 0.39 mmol) was added. The mixture was stirred at RT for 1.5 h and a solution of 1-(1-(4-aminophenyl)-3-(*tert*-butyl)-1*H*-pyrazol-5-yl)-3-(4-chlorophenyl)urea (**97**, 150 mg, 0.396 mmol) in DMF (dry, 2 mL) was added. The mixture was then stirred for additional 20 h at RT.  $\text{H}_2\text{O}$  (20 mL) was added, the precipitated solid was filtered, washed with  $\text{H}_2\text{O}$  (200 mL) and dried in a vacuum oven.

**Yield:** 89 mg (0.20 mmol, 50%), colorless solid.

- **TLC:**  $R_f = 0.64$  ( $\text{SiO}_2$ , cyclohexane/EtOAc 1:3).
- **$\text{C}_{24}\text{H}_{26}\text{ClN}_5\text{O}_2$ :** (451.95), [451.18].
- **HPLC:**  $t_R = 15.92$  min.
- **$^1\text{H-NMR}$  (300 MHz,  $\text{DMSO-d}_6$ , 300 K):**  $\delta = 10.37$  (br s, 1H, NH amide), 9.13 (br s, 1H, NH pyrazole), 8.35 (br s, 1H, NH Cl-phenyl), 7.73 (d,  $^3J = 8.9$  Hz, 2H, H-3-, H-5-NHCO-phenyl), 7.40–7.38 (m, 4H, H-2-, H-6-NHCO-phenyl, H-3-, H-5-Cl-phenyl), 7.30 (d,  $^3J = 8.9$  Hz, 2H, H-2-, H-6-Cl-phenyl), 6.35 (s, 1H, pyrazole), 1.86–1.73 (m, 1H,  $\text{CH}(\text{CH}_2)_2$ ), 1.27 (s, 9H, tBu), 0.90–0.74 (m, 4H,  $\text{CH}(\text{CH}_2)_2$ ) ppm.
- **$^{13}\text{C-NMR}$  (75 MHz,  $\text{DMSO-d}_6$ , 300 K):**  $\delta = 171.8, 160.5, 151.4, 138.6, 138.4, 137.0, 133.2, 128.7, 125.6, 125.1, 119.6, 119.4, 94.8, 32.0, 30.2, 14.6, 7.3$  ppm.
- **MS (ESI pos.):**  $m/z$  (%) = 452.18 (100) ( $[\text{M}+\text{H}]^+$ , calcd. 452.19).

- **MS (ESI neg.):**  $m/z$  (%) = 450.26 (100) ( $[M-H]^-$ , calcd. 450.17).
- **HRMS (FTMS + p MALDI):**  $m/z$  = 452.1836  $[M+H]^+$ , calcd. for  $[C_{24}H_{27}ClN_5O_2]^+$  = 452.1848.

***N*-(4-(3-(*tert*-Butyl)-5-(3-(4-chlorophenyl)ureido)-1*H*-pyrazol-1-yl)phenyl)isobutyramide (101, SR253)**

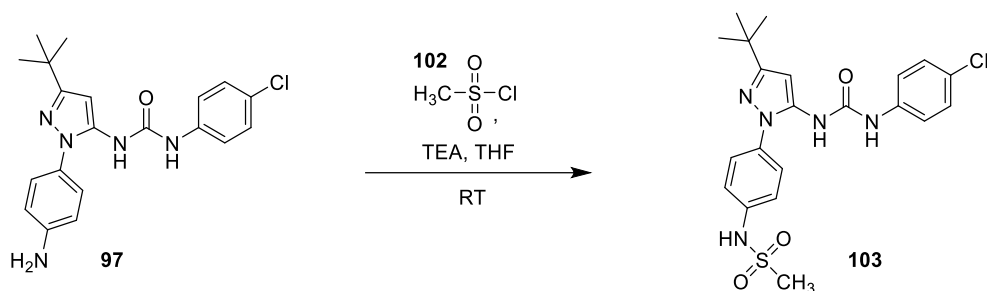


1-(1-(4-Aminophenyl)-3-(*tert*-butyl)-1*H*-pyrazol-5-yl)-3-(4-chlorophenyl)urea (**97**, 300 mg, 0.781 mmol) was dissolved in THF (dry, 10 mL) and TEA (158 mg, 1.56 mmol) was added. The mixture was cooled to 0 °C and isobutyryl chloride (**100**, 166 mg, 1.56 mmol) was added dropwise. After warming to RT, the mixture was stirred for 20 h at RT. Subsequently, the solvent was removed under reduced pressure and the residue was dissolved in EtOAc. The crude product was purified by column chromatography on silica (cyclohexane/EtOAc: 1:10 → EtOAc).

**Yield:** 298 mg (0.658 mmol, 84%), colorless solid.

- **TLC:**  $R_f$  = 0.75 (SiO<sub>2</sub>, cyclohexane/EtOAc 1:3).
- **C<sub>24</sub>H<sub>28</sub>ClN<sub>5</sub>O<sub>2</sub>:** (453.96), [453.19].
- **HPLC:**  $t_R$  = 16.12 min.
- **<sup>1</sup>H-NMR (500 MHz, DMSO-*d*<sub>6</sub>, 300 K):**  $\delta$  = 10.03 (br s, 1H, NH amide), 9.14 (br s, 1H, NH pyrazole), 8.33 (br s, 1H, NH Cl-phenyl), 7.75 (d, <sup>3</sup> $J$  = 9.0 Hz, 2H, H-3-, H-5-Cl-phenyl), 7.45–7.39 (m, 4H, H-2-, H-6-Cl-phenyl, H-3-, H-5-NHCO-phenyl), 7.30 (d, <sup>3</sup> $J$  = 9.0 Hz, 2H, H-2-, H-6-NHCO-phenyl), 6.35 (s, 1H, pyrazole), 2.68–2.57 (m, 1H, CH(CH<sub>3</sub>)<sub>2</sub>), 1.27 (s, 9H, *t*Bu), 1.11 (d, <sup>3</sup> $J$  = 6.7 Hz, 6H, CH(CH<sub>3</sub>)<sub>2</sub>) ppm.
- **<sup>13</sup>C-NMR (126 MHz, DMSO-*d*<sub>6</sub>, 300 K):**  $\delta$  = 175.4, 160.5, 151.4, 138.8, 138.4, 137.1, 133.2, 128.7, 125.6, 125.1, 119.6, 119.5, 94.7, 35.0, 32.0, 30.72, 19.5 ppm.
- **MS (ESI pos.):**  $m/z$  (%) = 454.2 (100) ( $[M+H]^+$ , calcd. 454.2). 327.2 (28) ( $[M_{fr.(I)}+H]^+$ , calcd. 327.2).
- **MS (ESI neg.):**  $m/z$  (%) = 452.3 (100) ( $[M-H]^-$ , calcd. 452.2). 299.2 (58) ( $[M_{fr.(II)}]^-$ , calcd. 299.2). 325.2 (42) ( $[M_{fr.(I)}-H]^-$ , calcd. 325.2).
- **HRMS (FTMS + p MALDI):**  $m/z$  = 545.2008  $[M+H]^+$ , calcd. for  $[C_{24}H_{29}ClN_5O_2]^+$  = 454.2004.

***N*-4-(3-(*tert*-Butyl)-5-(3-(4-chlorophenyl)ureido)-1*H*-pyrazol-1-yl)phenyl)methanesulfonamide (**103**, SR249)**



1-(1-(4-Aminophenyl)-3-(*tert*-butyl)-1*H*-pyrazol-5-yl)-3-(4-chlorophenyl)urea (**97**, 200 mg, 0.521 mmol) was dissolved in THF (dry, 8 mL) and TEA (53 mg, 0.52 mmol) was added. The mixture was cooled to 0 °C and methanesulfonyl chloride (**102**, 179 mg, 1.56 mmol) was added dropwise. After warming to RT, the mixture was stirred for 20 h at RT. The solvent was removed under reduced pressure and the residue was dissolved in EtOAc. The organic phase was washed 4 times with H<sub>2</sub>O and dried over MgSO<sub>4</sub>. The crude product was purified by column chromatography on silica (cyclohexane/EtOAc: 1:10 → 1:20).

**Yield:** 70 mg (0.15 mmol, 29%), colorless solid.

- **TLC:**  $R_f = 0.70$  (SiO<sub>2</sub>, cyclohexane/EtOAc 1:3).
- **C<sub>21</sub>H<sub>24</sub>ClN<sub>5</sub>O<sub>3</sub>S:** (461.96), [461.13].
- **HPLC:**  $t_R = 15.44$  min.
- **<sup>1</sup>H-NMR (400 MHz, DMSO-d<sub>6</sub>, 300 K):**  $\delta = 9.98$  (br s, 1H, NH amide), 9.12 (br s, 1H, NH pyrazole), 8.40 (br s, 1H, NH Cl-phenyl), 7.52–7.40 (m, 4H, H-3-, H-5-Cl-phenyl, H-3-, H-5-NHCO-phenyl), 7.38–7.30 (m, 4H, H-2-, H-6-Cl-phenyl, H-2-, H-6-NHCO-phenyl), 6.36 (s, 1H, pyrazole), 3.05 (s, 3H, CH<sub>3</sub>), 1.27 (s, 9H, *t*Bu) ppm.
- **<sup>13</sup>C-NMR (101 MHz, DMSO-d<sub>6</sub>, 300 K):**  $\delta = 160.6, 151.4, 138.4, 137.6, 137.1, 134.2, 128.7, 125.7, 125.6, 120.0, 119.7, 95.0, 32.0, 30.2$  ppm.
- **MS (ESI pos.):**  $m/z$  (%) = 461.97 (100) ([M+H]<sup>+</sup>, calcd. 462.12).
- **MS (ESI neg.):**  $m/z$  (%) = 460.04 (100) ([M-H]<sup>-</sup>, calcd. 460.12).
- **HRMS (FTMS + p MALDI):**  $m/z = 462.1348$  [M+H]<sup>+</sup>, calcd. for [C<sub>21</sub>H<sub>25</sub>ClN<sub>5</sub>O<sub>3</sub>S]<sup>+</sup> = 462.1361.

### 8.4.3 DSF-assay results kinase panel ( $\Delta T_m$ values).

DSF measured by Andreas Krämer, SGC Frankfurt.

No.	AAK1	ABL1	AKT3	AURKB	BMX	BRAF	CAMK1G	CAMK2	CASK	CDK2	CK2A1	CHEK2	CLK1	CSNK1D	DAPK3	DYRK1A
56	0.0	0.2	-0.1	-3.0	-1.7	1.7	0.2	0.4	0.5	0.2	0.4	0.7	-0.3	0.2	-1.2	-0.8
57	-0.1	0.5	0.2	2.7	-1.7	8.9	0.4	0.2	0.2	0.1	0.1	0.6	-0.1	0.0	-0.5	0.3
58	0.1	0.9	0.5	4.3	-1.4	1.5	0.6	0.4	0.0	0.7	0.7	0.9	1.8	0.2	-0.3	-0.4
59	-0.3	0.2	0.2	3.5	-1.6	3.1	0.4	0.2	0.0	0.1	0.1	0.7	-0.2	0.1	-1.3	-0.8
60	0.2	0.7	0.8	4.0	-3.7	10.1	0.8	1.0	-0.4	1.0	0.9	1.2	0.9	0.4	-0.4	0.1
61	0.0	0.5	0.5	4.1	-4.5	0.6	0.0	0.1	-0.4	0.4	0.4	0.6	0.1	0.3	-1.1	-1.1
62	0.0	0.6	0.4	3.9	-4.0	3.0	0.4	0.1	-1.4	0.4	0.4	1.1	-0.3	-0.2	-1.0	0.4
63	0.0	0.2	0.5	4.0	-1.2	2.1	-0.1	0.5	0.1	0.3	0.5	0.7	0.0	0.2	-1.3	-1.1
64	0.0	0.3	0.4	4.2	-1.8	6.0	0.3	0.3	-0.8	0.2	0.5	0.8	0.0	0.2	-1.3	-0.2
65	0.0	0.7	0.1	2.3	-1.8	7.1	1.4	1.5	-0.1	0.9	0.0	1.0	1.4	0.0	-0.4	0.6
66	0.0	0.4	0.5	4.4	-1.5	9.7	0.4	0.4	-0.8	0.6	0.8	1.0	0.0	0.3	-0.9	-0.4
68	0.1	0.6	0.5	4.0	-3.7	8.7	0.8	0.8	-0.2	0.7	0.6	1.1	0.2	0.5	-0.6	0.0
67	-0.2	0.0	0.2	3.0	-1.9	0.6	0.0	-0.1	0.0	-0.1	0.2	0.6	-0.5	0.0	-1.4	-1.0
69	0.0	0.4	0.5	3.6	-4.3	14.1	0.7	0.8	0.0	0.5	0.3	1.1	0.5	0.2	-0.6	-0.2
71	0.1	1.1	0.3	3.3	-1.8	1.0	2.4	2.8	0.9	0.8	0.6	0.7	1.3	0.0	1.1	1.5
72	-0.1	0.0	0.0	3.4	-1.8	0.4	0.2	0.2	0.0	0.2	0.3	0.5	-0.4	0.0	-1.4	-0.7
73	0.1	0.3	0.6	4.1	-1.6	0.9	0.0	0.2	0.2	0.4	0.5	0.7	-0.3	0.3	-1.2	-1.0
74	-0.1	0.1	0.5	4.0	-1.8	0.6	-0.2	-0.1	0.1	0.3	0.5	0.5	-0.6	0.3	-1.4	-1.2
75	-0.1	0.1	0.0	3.1	-1.8	0.0	0.3	-0.1	-0.1	0.1	0.0	0.3	-0.2	0.0	-0.4	-0.3
81	0.1	0.8	0.7	4.5	-0.8	3.3	1.3	0.6	0.0	1.3	0.8	1.7	0.5	0.1	0.0	0.1
73	0.6	2.4	0.6	4.1	-4.7	1.4	3.5	1.8	1.5	1.3	1.4	1.5	3.2	0.1	2.4	3.0
79	0.0	0.6	0.1	-0.1	-1.9	3.7	0.7	0.6	-0.1	0.9	0.5	1.6	1.2	0.2	-0.9	-0.3
70	0.1	0.7	0.7	2.4	-1.2	1.0	0.1	0.2	0.1	0.5	0.5	0.8	-0.2	0.1	-1.1	-0.8
77	-0.1	0.1	0.2	3.9	-4.4	0.6	-0.2	-0.1	-0.2	0.2	0.4	0.4	-0.6	0.0	-1.1	-1.1
80	0.0	-0.1	-0.2	3.4	-1.7	1.9	1.1	1.1	0.2	0.3	0.2	0.4	1.7	0.0	-0.6	-0.2
83	-0.1	0.2	0.0	1.6	-1.9	0.0	0.3	0.0	0.0	-0.1	-0.1	0.0	-0.1	0.0	-0.2	-0.3
76	0.2	0.8	0.8	2.3	-1.2	5.4	1.0	1.6	0.1	1.4	0.8	1.6	2.9	0.3	0.0	0.6
85	0.1	1.0	0.4	3.5	-4.4	0.4	-0.2	0.0	0.0	0.1	0.1	0.3	-0.4	0.0	-1.2	-1.1
83	0.1	1.1	0.8	4.2	-1.6	0.7	0.8	2.2	0.1	1.3	0.9	0.8	1.5	0.3	-0.1	0.5
84	0.1	1.0	0.6	4.0	-3.2	2.0	0.6	0.3	0.1	1.0	1.0	1.1	0.6	0.4	-0.5	-0.4
82	-0.2	0.1	0.1	4.0	-4.4	1.3	0.6	1.1	0.2	1.0	0.5	0.8	1.5	0.5	-0.7	1.1
BIRB796	0.0	0.2	0.6	4.0	-4.1	22.1	0.0	0.3	-0.3	0.4	0.5	2.5	0.8	0.4	-1.3	-1.0
MCP081	-0.1	-0.1	0.1	3.5	-2.1	6.3	0.0	0.0	0.5	-0.1	0.1	0.4	-0.5	-0.1	-1.4	-1.0
88	-0.1	-0.1	0.3	3.6	-4.3	0.8	0.2	0.3	0.0	0.4	0.2	0.4	-0.2	0.1	-0.6	-0.4
97	-0.1	0.2	0.4	3.8	-1.4	10.3	0.5	1.1	0.2	1.1	0.4	0.7	2.1	0.2	0.0	-0.9
89	-0.1	0.1	-0.2	-3.8	-2.1	1.1	0.0	0.1	-0.1	0.3	0.3	0.6	-0.5	0.0	-1.4	-1.0
90	0.2	0.5	0.7	4.1	-0.4	1.2	0.2	0.7	0.0	0.7	0.7	0.8	0.5	0.4	-1.0	-0.2
91	-0.1	0.3	0.6	4.5	-1.5	3.3	0.6	0.8	0.3	0.5	0.5	0.7	0.3	0.4	-0.3	-0.2
92	-0.1	0.1	0.2	3.7	-0.1	4.3	1.2	1.7	0.0	0.5	0.2	0.8	0.8	0.1	-0.5	0.3
99	0.1	0.8	0.6	4.1	-4.4	5.1	1.7	0.5	0.4	0.7	0.7	0.8	1.3	0.3	0.0	0.5
103	-0.1	0.8	0.4	3.7	-1.4	12.2	2.0	2.5	0.5	0.9	0.5	1.2	1.5	0.2	0.9	1.8
101	0.0	0.5	0.4	3.9	-4.0	2.2	0.8	1.6	0.2	0.4	0.4	0.6	1.0	0.2	-0.4	1.2
93	-0.1	0.2	0.0	2.2	-3.3	-0.2	0.4	0.2	0.0	0.1	0.1	0.1	0.0	0.1	0.3	0.3
94	0.0	0.1	0.4	-2.3	-0.4	0.7	-0.1	0.4	0.1	0.1	0.5	0.4	1.0	0.0	-1.4	-1.3
95	-0.1	0.1	-0.2	-2.5	-1.6	0.3	-0.1	0.2	0.1	0.0	-1.3	0.2	0.9	-0.1	-1.4	-1.1
96	0.1	0.5	0.8	4.2	-1.5	0.8	0.6	0.7	0.1	1.1	0.8	0.5	0.4	0.6	-0.3	0.5
Staurosporine	13.9	8.4	5.8	9.9	-4.0	0.8	11.9	25.4	4.0	14.1	3.8	16.2	13.0	1.6	12.7	10.7

DSF (continued)

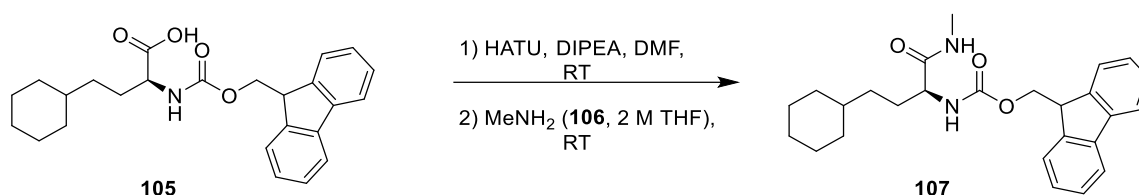
$\Delta T_m$  [°C], mean of duplicates

No.	EPHA2	FES	FGFR2	GAK	GPRK5	GSG2	GSK3B	MAP2K1	MAP2K6	MAPK11	MAPK14	MAPK1	MAPK8	MAPK9	MERTK	NEK2
56	2.9	0.3	0.1	-0.1	-0.3	-0.7	0.6	0.2	0.3	14.3	13.1	0.0	-1.6	1.6	0.3	-0.2
57	1.2	0.1	0.3	-0.1	0.1	-0.2	0.3	0.4	0.1	10.8	10.3	-0.4	0.7	0.4	0.4	0.8
58	1.6	0.4	0.3	0.1	0.3	-0.8	0.8	0.5	0.4	5.3	5.3	-0.4	0.4	1.2	0.1	1.0
59	1.0	0.4	-0.1	-0.4	-0.4	-0.9	0.3	0.0	0.0	7.0	4.7	-0.1	-1.6	0.6	-0.1	0.2
60	2.2	0.8	0.7	0.1	0.8	-0.5	1.4	0.7	0.6	8.9	8.9	0.3	0.0	2.6	0.5	0.3
61	0.8	0.3	0.0	0.1	0.6	-0.8	0.3	0.2	0.4	0.0	0.2	0.0	-0.4	0.3	0.2	-0.1
62	1.5	0.4	0.1	-0.2	0.4	-0.5	0.8	0.5	0.3	1.5	1.5	-0.3	0.8	-0.1	0.5	1.4
63	0.7	0.4	0.1	0.0	-0.4	-0.9	0.4	0.2	0.3	4.5	4.8	0.2	-1.9	0.3	0.3	-0.2
64	1.6	0.2	0.5	-0.1	-0.4	0.0	0.7	0.2	0.3	12.6	9.6	0.1	-1.2	0.7	0.4	-0.2
65	2.2	0.3	0.7	0.1	0.3	-0.2	1.0	0.6	0.2	9.3	10.2	0.0	0.3	1.7	0.1	1.5
66	1.6	0.5	0.4	-0.2	-0.3	-0.9	1.0	0.3	0.4	10.8	10.6	0.2	-0.9	2.1	0.3	-0.3
68	1.8	0.7	0.3	-0.2	0.9	-0.6	1.0	0.2	0.5	9.8	8.6	0.0	-0.6	1.4	0.3	0.7
67	0.2	0.0	-0.1	-0.3	-0.4	-0.8	0.2	-0.1	0.0	-1.3	-0.4	0.0	-1.0	-0.3	0.1	-1.1
69	1.7	0.4	0.2	-0.3	3.3	-0.7	1.0	0.2	0.3	12.3	10.6	-0.1	-1.1	1.7	0.1	-0.4
71	0.4	0.5	0.6	0.0	0.5	-0.1	0.2	0.8	0.3	1.4	1.4	0.2	0.1	0.1	0.0	2.1
72	0.4	0.2	0.0	-0.1	-0.3	-0.7	0.2	0.1	0.2	-0.1	0.2	-0.1	-0.9	-0.1	0.1	0.4
73	0.7	0.4	0.1	0.0	-0.3	-0.9	0.5	0.3	0.5	-0.2	0.3	0.3	-1.6	0.1	0.3	-0.2
74	0.5	0.2	-0.1	0.0	-0.6	-0.9	0.3	0.0	0.3	-0.4	0.1	0.0	-1.2	0.1	0.2	-1.1
75	0.3	0.0	-0.1	-0.1	0.1	-0.3	0.3	0.1	0.0	0.3	0.1	0.0	0.1	0.0	0.0	0.2
81	1.9	0.6	0.7	0.2	0.1	-0.5	1.2	0.7	0.5	6.3	5.2	0.4	0.4	2.5	0.2	0.7
73	0.9	0.8	1.0	0.4	1.7	0.7	0.6	1.2	0.6	2.5	2.2	0.3	0.9	0.0	1.3	4.7
79	1.9	0.5	0.6	0.1	-0.2	-0.8	0.8	0.3	0.3	8.7	7.0	0.3	-0.9	2.1	0.3	0.3
70	0.8	0.4	0.2	0.1	0.2	-0.8	0.7	0.3	0.4	-0.2	0.3	0.3	-2.8	0.3	0.3	-0.2
77	0.5	0.1	-0.1	-0.1	-0.1	-0.9	0.1	-0.1	0.2	-0.4	0.1	-0.1	-0.1	0.0	0.0	-0.2
80	0.4	0.2	0.2	-0.3	-0.2	-0.6	0.4	0.3	0.1	3.4	3.8	0.0	-1.0	0.8	-0.3	0.3
83	0.0	0.0	0.0	0.0	0.0	-0.2	0.2	0.1	0.0	0.0	0.1	0.0	-0.1	-0.1	0.0	-0.1
76	2.7	0.7	0.9	0.1	0.4	-0.5	1.4	0.7	0.5	8.6	7.1	0.3	-0.1	2.7	0.3	0.7
85	0.3	0.1	0.0	-0.2	0.3	-0.7	0.2	-0.1	0.1	-0.2	0.1	0.0	-0.4	-0.1	-0.1	-0.3
83	1.1	0.6	0.5	0.3	0.5	-0.4	0.8	0.8	0.4	3.2	2.8	0.4	-0.1	0.2	0.1	0.5
84	1.3	0.5	0.4	0.2	1.3	-0.7	0.7	0.5	0.4	1.8	1.6	0.2	0.1	1.1	0.2	-0.1
82	0.9	0.4	1.0	0.3	-0.1	-0.9	0.7	0.5	0.1	6.9	5.0	0.3	0.1	1.2	-0.1	-1.1
BIRB796	8.0	0.9	1.2	0.0	0.8	-0.9	1.5	0.2	0.4	19.9	19.8	0.3	-0.9	6.7	0.4	-0.7
MCP081	1.3	0.0	-0.2	-0.3	-0.5	-0.8	0.1	-0.2	0.1	8.0	8.5	-0.1	-1.4	-0.1	0.0	0.1
88	0.4	0.1	0.0	-0.1	0.1	-0.6	0.4	0.1	0.1	-0.2	1.3	0.1	-0.4	0.4	-0.2	0.1
97	2.0	0.4	0.6	-0.2	-0.2	-0.9	0.9	0.2	0.2	9.4	10.4	0.2	-2.2	2.7	-0.2	0.6
89	0.6	0.2	0.0	0.0	-0.3	-0.6	0.6	0.1	0.3	0.3	0.9	-0.1	-1.2	0.0	0.2	0.0
90	0.9	0.6	0.3	0.2	0.2	-0.6	0.9	0.7	0.5	0.6	0.9	0.3	-1.7	0.4	0.4	0.0
91	0.8	0.3	0.3	-0.1	0.0	-0.6	0.5	0.4	0.2	4.0	3.6	0.1	-0.3	0.8	0.0	0.5
92	1.2	0.3	0.3	-0.2	-0.2	-0.6	0.8	0.3	0.1	7.8	5.6	0.0	-0.4	0.8	-0.2	0.9
99	3.0	0.5	1.0	0.1	0.6	-0.6	0.8	0.7	0.4	2.6	2.4	0.3	0.5	0.6	0.1	0.3
103	2.8	0.7	0.9	0.1	0.2	-0.2	1.3	0.3	0.1	7.2	6.7	0.2	-0.3	2.1	0.0	2.1
101	2.8	0.5	0.9	-0.1	1.5	-0.7	0.4	0.4	0.3	1.5	1.5	0.0	0.4	0.1	0.2	-0.3
93	0.2	0.1	0.1	-0.1	0.8	-1.0	0.0	0.2	0.0	0.3	0.3	0.0	-0.8	0.0	-0.1	0.3
94	0.5	0.2	0.0	-0.1	-0.2	-1.0	0.3	0.2	0.2	-0.3	0.2	0.1	-0.8	0.0	0.3	-0.8
95	0.2	0.1	-0.2	-0.1	-0.4	-0.8	0.3	-0.2	0.1	0.6	0.1	-0.1	-2.0	-0.2	0.0	-0.2
96	1.0	0.5	0.7	0.4	0.0	-0.7	0.8	0.9	0.3	0.6	0.9	0.5	-1.0	0.6	0.1	0.2
Stauroporine	7.0	5.5	7.4	8.1	4.4	6.0	8.3	2.5	11.1	0.4	0.4	1.1	5.2	2.7	4.6	3.5

## DSF (continued)

No.	PAK4	PHK2	PIM1	RPS6KA1	RPS6KA5	SLK	SRC	STK10	STK17A	STK38L	STK39	STK3	TTK	ULK3	VRK1
56	-0.1	0.2	-1.2	-0.4	-0.5	2.7	0.2	1.1	0.1	0.4	-1.1	0.4	-0.8	0.4	0.2
57	0.1	0.2	-0.4	-0.9	-0.4	7.1	-0.3	8.6	0.1	0.4	0.2	0.6	0.4	0.2	0.1
58	0.0	0.3	-0.8	-0.5	-0.1	1.8	0.2	0.8	1.8	0.2	-0.5	0.7	0.7	0.8	0.5
59	-0.4	0.0	-0.7	-0.5	-0.4	1.1	0.0	0.8	0.0	0.1	-1.0	-0.2	-0.2	0.1	0.0
60	0.3	0.2	-0.6	-0.9	-0.2	7.4	0.4	6.5	0.5	0.8	-0.2	0.8	0.9	0.6	0.3
61	0.1	0.2	-0.8	0.1	-0.3	0.0	0.3	-0.5	0.5	0.3	-1.5	0.0	-0.1	0.4	0.2
62	0.3	0.4	-0.2	0.1	-0.4	0.5	-0.2	0.4	0.3	1.6	-0.4	0.4	0.0	0.4	0.2
63	-0.3	0.2	-1.3	-0.2	-0.4	2.4	0.3	-0.3	0.2	0.4	-0.9	0.1	-0.6	0.3	0.3
64	0.0	0.2	-1.2	-0.4	-0.5	6.0	0.2	4.1	0.1	0.4	-0.8	0.5	-0.4	0.5	0.2
65	0.5	0.1	0.2	-0.5	0.6	5.5	0.0	3.4	0.4	0.3	0.5	0.9	1.4	0.3	-0.2
66	-0.1	-0.1	-0.9	-1.4	0.0	7.7	0.3	7.2	0.2	0.7	-1.1	0.5	0.5	0.5	0.2
68	0.2	0.2	-0.5	-1.7	0.3	3.6	0.2	3.7	0.5	1.1	-0.4	0.4	0.7	0.5	0.3
67	-0.3	0.0	-1.2	-0.1	-0.9	-0.3	0.1	-0.9	-0.1	0.2	-1.3	-0.1	-0.6	0.1	0.0
69	0.0	0.1	-0.4	-2.2	-0.3	4.6	0.1	4.7	0.2	0.5	-1.1	0.1	0.0	0.5	0.1
71	1.0	0.6	1.5	-2.0	1.3	2.4	-0.5	1.1	1.1	0.5	1.1	0.8	2.2	0.0	0.2
72	-0.1	0.1	-0.9	0.1	-0.6	0.5	0.1	-0.6	0.2	0.1	-0.6	0.2	-0.8	0.2	0.1
73	-0.2	0.3	-1.6	0.0	-0.5	-0.1	0.3	-0.6	0.4	0.5	-1.1	0.0	-0.3	0.4	0.4
74	-0.3	0.2	-1.3	0.0	-0.6	-0.2	0.3	-0.7	0.1	0.1	-1.5	-0.1	-1.4	0.4	0.2
75	0.1	0.0	-0.3	0.1	-0.3	0.1	0.1	-0.3	0.1	0.1	-0.2	0.1	0.1	0.0	0.0
81	0.5	0.3	-0.4	-0.8	0.4	2.7	0.3	1.7	0.7	0.4	0.2	1.0	1.4	0.6	0.1
73	1.8	1.2	1.8	-1.6	3.2	1.9	-0.2	2.6	2.0	1.5	2.2	1.5	3.3	0.6	1.1
79	0.1	0.3	-0.7	-0.2	-0.2	2.8	0.2	0.6	0.4	0.4	-0.5	0.7	0.2	0.6	0.1
70	0.1	0.3	-0.9	0.4	-0.3	0.0	0.4	-0.5	0.4	0.5	-0.8	0.5	-0.3	0.5	0.3
77	-0.3	0.3	-0.9	0.1	-0.5	-0.2	0.1	-0.7	0.1	0.2	-1.1	-0.2	-0.3	0.2	0.1
80	0.1	0.2	0.0	-0.2	0.7	1.2	0.0	1.1	0.2	0.0	0.2	0.3	0.4	0.1	-0.3
83	0.3	0.0	0.0	0.1	-0.3	0.2	0.1	-0.2	0.0	0.0	-0.1	0.2	0.1	-0.1	0.0
76	0.5	0.2	-0.5	-0.8	0.6	3.0	0.4	2.5	0.8	0.7	0.2	1.0	1.2	0.7	0.2
85	-0.3	0.1	-0.8	-0.6	-0.2	0.8	0.2	-0.7	0.0	0.2	-0.9	-0.1	-0.3	0.3	0.1
83	0.3	0.3	-0.7	-0.2	0.8	2.6	0.2	0.6	0.8	0.5	0.1	1.0	1.2	0.6	0.1
84	0.1	0.2	-0.8	-0.5	0.0	0.5	0.3	0.2	0.7	0.4	-0.8	0.5	1.1	0.6	0.1
82	-0.3	0.2	-1.0	0.0	1.7	2.6	0.3	0.6	0.2	-0.4	-1.1	0.7	0.9	0.6	-0.3
BIR796	-0.2	0.2	-1.3	-0.1	-0.3	3.6	0.4	10.0	0.2	0.5	-1.1	0.4	0.6	0.3	0.4
MCP081	-0.1	0.0	-0.7	0.3	-0.7	0.1	-0.2	-0.6	0.0	0.3	-0.7	-0.2	-0.9	-0.1	0.1
88	0.0	-0.1	-0.5	0.1	-0.3	0.3	0.2	0.0	0.1	-0.1	-0.1	0.1	-0.5	0.2	-0.1
97	-0.1	-0.1	-0.9	-0.5	1.4	5.6	0.3	2.0	0.2	0.3	-0.9	0.1	-0.1	0.3	0.2
89	-0.3	0.2	-1.1	0.2	-0.5	0.7	0.2	-0.6	0.3	0.3	0.1	0.1	-0.2	0.4	0.1
90	0.0	0.3	-1.1	-0.1	-0.1	0.6	0.5	0.0	0.6	0.5	-0.6	0.5	0.4	0.6	0.3
91	0.2	0.0	-0.3	-0.4	0.5	1.6	0.3	2.2	0.3	0.1	-0.5	0.6	0.3	0.3	0.0
92	0.2	0.2	0.1	-0.8	0.6	5.2	0.0	4.1	0.1	0.1	0.2	0.4	0.8	0.1	-0.2
99	0.4	0.4	-0.1	-0.3	0.7	4.1	0.2	3.4	0.5	0.4	-0.1	0.8	1.1	0.4	0.1
103	1.1	0.9	1.0	-0.8	2.9	7.3	0.0	8.9	0.7	0.1	0.9	0.6	1.7	-0.1	0.1
101	0.2	0.3	-0.7	-0.7	0.2	6.8	0.1	5.1	0.3	0.2	0.0	0.6	-0.3	0.4	0.0
93	0.1	0.0	-0.2	0.0	0.1	0.3	0.0	0.0	0.1	0.0	0.3	0.1	0.2	0.0	0.0
94	-0.1	0.1	-0.7	0.0	-0.5	0.7	0.3	-0.7	0.2	0.4	-1.4	0.0	-0.6	0.3	0.3
95	-0.3	0.2	-1.1	-0.1	-0.7	0.1	0.2	-0.9	0.1	0.1	-1.0	-0.1	-0.7	0.2	0.1
96	0.2	0.1	-1.0	-0.2	0.7	0.6	0.5	0.5	0.7	0.0	0.3	0.9	0.7	0.7	-0.1
Stauroporine	11.8	21.7	9.1	2.3	10.7	16.9	5.0	22.9	12.2	7.7	7.3	14.2	5.3	16.8	2.1

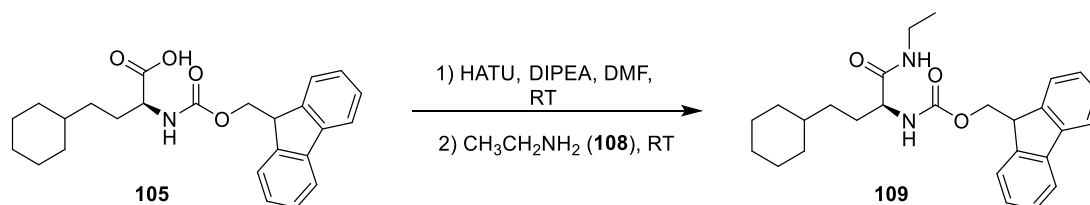
## 8.4.4 Synthesis of intermediate compounds

**(S)-2-(((9H-Fluoren-9-yl)methoxy)carbonyl)amino)-4-cyclohexyl-1-(methylamino)-1-oxobutan-2-yl)carbamate (107, SR34)**

(S)-2-(((9H-Fluoren-9-yl)methoxy)carbonyl)amino)-4-cyclohexylbutanoic acid (**105**, 400 mg, 0.982 mmol) and HATU (448 mg, 1.18 mmol) were dissolved in DMF (dry, 8 mL) and DIPEA (152 mg, 1.18 mmol) was added. The reaction mixture was stirred for 1.5 h at RT and methanamine (**106**, 596  $\mu$ L, 2 M in THF, 1.178 mmol) was added. The mixture was stirred for additional 3.5 h at RT. DCM (50 mL) was added and the organic phase was washed 5 times with H<sub>2</sub>O (20 mL) and dried over MgSO<sub>4</sub>. The solvent was evaporated under reduced pressure and the crude product was purified by column chromatography on silica (cyclohexane/EtOAc 1:1).

**Yield:** 334 mg (0.794 mmol, 81%), colorless solid.

- **TLC:** R<sub>f</sub> = 0.40 (SiO<sub>2</sub>, cyclohexane/EtOAc, 1:1).
- **C<sub>26</sub>H<sub>32</sub>N<sub>2</sub>O<sub>3</sub>:** (420.54), [420.24].
- **<sup>1</sup>H-NMR (500 MHz, CDCl<sub>3</sub>, 300 K):**  $\delta$  = 7.76 (d, <sup>3</sup>J = 7.5 Hz, 2H, H-4-, H-5-Fmoc), 7.62–7.54 (m, 2H, H-1-, H-8-Fmoc), 7.40 (t, <sup>3</sup>J = 7.5 Hz, 2H, H-3-, H-6-Fmoc), 7.30 (t, <sup>3</sup>J = 7.5 Hz, 2H, H-2-, H-7-Fmoc), 6.11 (s, 1H, NHCOO), 5.45 (d, <sup>3</sup>J = 8.0 Hz, 1H, CONHCH<sub>3</sub>), 4.46–4.33 (m, 2H, OCH<sub>2</sub>), 4.26–4.17 (m, 1H, NHCHCO), 4.11–4.01 (m, 1H, H-9-Fmoc), 2.81 (s, 3H, CH<sub>3</sub>), 1.89–1.79 (m, 1H, NHCHCH<sub>A</sub>H<sub>B</sub>CH<sub>2</sub>), 1.72–1.56 (m, 6H, NHCHCH<sub>A</sub>H<sub>B</sub>CH<sub>2</sub>, H-2<sub>eq</sub>-, H-3<sub>eq</sub>-, H-4<sub>eq</sub>-, H-5<sub>eq</sub>-, H-6<sub>eq</sub>-cyclohexyl), 1.30–1.05 (m, 6H, H-1-, H-3<sub>ax</sub>-, H-4<sub>ax</sub>-, H-5<sub>ax</sub>-cyclohexyl, NHCHCH<sub>2</sub>CH<sub>2</sub>), 0.93–0.78 (m, 2H, H-2<sub>ax</sub>-, H-6<sub>ax</sub>-cyclohexyl) ppm.
- **<sup>13</sup>C-NMR (126 MHz, CDCl<sub>3</sub>, 300 K):**  $\delta$  = 172.6, 156.4, 143.9, 143.8, 141.4, 127.9, 127.2 (2x), 125.2, 120.1, 67.1, 55.5, 47.3, 38.8, 37.6, 33.4, 33.3, 33.2, 30.2, 26.7, 26.4 (2x) ppm.
- **MS (ESI pos.):** m/z (%) = 421.35 (100) ([M+H]<sup>+</sup>, calcd. 421.24), 199.24 (66) ([M-Fmoc+H]<sup>+</sup>, calcd. 199.17), 179.21 (29) ([M<sub>fr</sub>+H]<sup>+</sup>, calcd. 179.08).

**(S)-2-(((9H-Fluoren-9-yl)methoxy)carbonyl)amino)-4-cyclohexyl-1-(ethylamino)-1-oxobutan-2-yl)carbamate (109, SR35)**

(S)-2-(((9H-Fluoren-9-yl)methoxy)carbonyl)amino)-4-cyclohexylbutanoic acid (**105**, 400 mg, 0.982 mmol) and HATU (448 mg, 1.18 mmol) were dissolved in DMF (dry, 8 mL) and DIPEA (152 mg, 1.18 mmol) was added. The reaction mixture was stirred for 1.5 h at RT and ethanamine (**108**, 589  $\mu$ L, 2M in THF, 1.18 mmol) was added. The mixture was stirred for additional 3.5 h at RT. DCM (50 mL) was added and the organic phase was washed 5 times with H<sub>2</sub>O (20 mL) and dried over MgSO<sub>4</sub>. The solvent was evaporated under

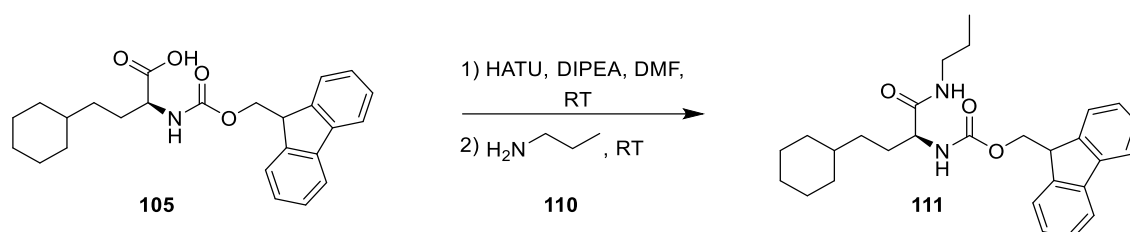


reduced pressure and the crude product was purified using column chromatography on silica (cyclohexane/EtOAc 1:1).

**Yield:** 224 mg (0.515 mmol, 52%), colorless solid.

- **TLC:**  $R_f = 0.68$  ( $\text{SiO}_2$ , cyclohexane/EtOAc, 1:1).
- **$\text{C}_{27}\text{H}_{34}\text{N}_2\text{O}_3$ :** (434.57), [434.26].
- **$^1\text{H-NMR}$  (500 MHz,  $\text{CDCl}_3$ , 300 K):**  $\delta = 7.76$  (d,  $^3J = 7.5$  Hz, 2H, H-4-, H-5-Fmoc), 7.58 (d,  $^3J = 7.5$  Hz, 2H, H-1-, H-8-Fmoc), 7.40 (t,  $^3J = 7.5$  Hz, 2H, H-3-, H-6-Fmoc), 7.31 (t,  $^3J = 7.5$  Hz, 2H, H-2-, H-7-Fmoc), 5.89 (s, 1H, NHCOO), 5.36 (d,  $^3J = 7.7$  Hz, 1H, CONHCH<sub>2</sub>), 4.46–4.35 (m, 2H, OCH<sub>2</sub>), 4.22 (t,  $^3J = 6.9$  Hz, 1H, NHCHCO), 4.08–3.99 (m, 1H, H-9-Fmoc), 3.36–3.22 (m, 2H, CH<sub>2</sub>CH<sub>3</sub>), 1.90–1.78 (m, 1H, NHCHCH<sub>A</sub>H<sub>B</sub>CH<sub>2</sub>), 1.74–1.56 (m, 6H, NHCHCH<sub>A</sub>H<sub>B</sub>CH<sub>2</sub>, H-2<sub>eq</sub>-, H-3<sub>eq</sub>-, H-4<sub>eq</sub>-, H-5<sub>eq</sub>-, H-6<sub>eq</sub>-cyclohexyl), 1.34–1.05 (m, 9H, CH<sub>3</sub>, H-1-, H-3<sub>ax</sub>-, H-4<sub>ax</sub>-, H-5<sub>ax</sub>-cyclohexyl, NHCHCH<sub>A</sub>H<sub>B</sub>CH<sub>2</sub>), 0.94–0.79 (m, 2H, H-2<sub>ax</sub>-, H-6<sub>ax</sub>-cyclohexyl) ppm.
- **$^{13}\text{C-NMR}$  (126 MHz,  $\text{CDCl}_3$ , 300 K):**  $\delta = 171.6, 154.3, 143.9, 141.4, 127.9, 127.2, 125.2, 120.1, 67.1, 55.5, 47.3, 37.6, 37.5, 34.6, 33.4, 33.3, 33.2, 30.2, 26.7, 26.4, 14.9$  ppm.
- **MS (ESI pos.):**  $m/z$  (%) = 435.26 (100) ( $[\text{M}+\text{H}]^+$ , calcd. 435.27), 213.29 (52) ( $[\text{M-Fmoc}+\text{H}]^+$ , calcd. 213.20), 179.29 (28) ( $[\text{M}_{\text{fr.}}+\text{H}]^+$ , calcd. 179.29).

**(S)-(9H-Fluoren-9-yl)methyl (4-cyclohexyl-1-oxo-1-(propylamino)butan-2-yl)carbamate (111, SR38)**



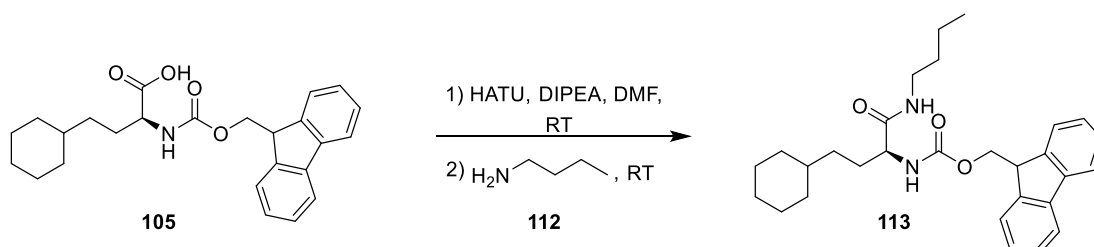
(S)-2-(((9H-Fluoren-9-yl)methoxy)carbonyl)amino-4-cyclohexylbutanoic acid (**105**, 400 mg, 0.982 mmol) and HATU (448 mg, 1.18 mmol) were dissolved in DMF (dry, 10 mL) and DIPEA (152 mg, 1.18 mmol) was added. The reaction mixture was stirred for 2 h at RT and propan-1-amine (**110**, 97  $\mu\text{L}$ , 1.18 mmol) was added. The mixture was stirred for additional 20 h at RT. DCM (50 mL) was added and the organic phase was washed 5 times with H<sub>2</sub>O (20 mL) and dried over MgSO<sub>4</sub>. The solvent was evaporated under reduced pressure and the crude product was purified by column chromatography on silica (cyclohexane/EtOAc 1:1).

**Yield:** 248 mg (0.553 mmol, 56%), colorless solid.

- **TLC:**  $R_f = 0.15$  ( $\text{SiO}_2$ , cyclohexane/EtOAc, 1:1).
- **$\text{C}_{28}\text{H}_{36}\text{N}_2\text{O}_3$ :** (448.60), [448.27].
- **$^1\text{H-NMR}$  (500 MHz,  $\text{CDCl}_3$ , 300 K):**  $\delta = 7.76$  (d,  $^3J = 7.5$  Hz, 2H, H-4-, H-5-Fmoc), 7.57 (d,  $^3J = 7.5$  Hz, 2H, H-1-, H-8-Fmoc), 7.39 (t,  $^3J = 7.4$  Hz, 2H, H-3-, H-6-Fmoc), 7.30 (t,  $^3J = 7.4$  Hz, 2H, H-2-, H-7-Fmoc), 6.13 (s, 1H, NHCOO), 5.48 (d,  $^3J = 7.9$  Hz, 1H, CONHCH<sub>2</sub>), 4.48–4.28 (m, 2H, OCH<sub>2</sub>), 4.20 (t,  $^3J = 7.0$  Hz, 1H, NHCHCO), 4.12–4.02 (m, 1H, H-9-Fmoc), 3.30–3.11 (m, 2H, CH<sub>2</sub>CH<sub>2</sub>CH<sub>3</sub>), 1.91–1.76 (m, 1H, NHCHCH<sub>A</sub>H<sub>B</sub>CH<sub>2</sub>), 1.73–1.58 (m, 6H, NHCHCH<sub>A</sub>H<sub>B</sub>CH<sub>2</sub>, H-2<sub>eq</sub>-, H-3<sub>eq</sub>-, H-4<sub>eq</sub>-, H-5<sub>eq</sub>-, H-6<sub>eq</sub>-cyclohexyl), 1.56–1.43 (m, 2H, CH<sub>2</sub>CH<sub>2</sub>CH<sub>3</sub>), 1.36–1.06 (m, 6H, H-1-, H-3<sub>ax</sub>-, H-4<sub>ax</sub>-, H-5<sub>ax</sub>-cyclohexyl, NHCHCH<sub>2</sub>CH<sub>2</sub>), 0.94–0.79 (m, 5H, CH<sub>3</sub>, H-2<sub>ax</sub>-, H-6<sub>ax</sub>-cyclohexyl) ppm.

- **$^{13}\text{C-NMR}$  (126 MHz,  $\text{CDCl}_3$ , 300 K):**  $\delta = 171.8, 156.3, 143.9, 141.4, 127.9, 127.2, 125.2, 120.1, 67.1, 55.5, 47.2, 41.3, 37.6, 33.4, 33.3, 33.1, 30.4, 26.7, 26.4, 22.9, 11.4$  ppm.
- **MS (ESI pos.):**  $m/z$  (%) = 897.62 (84) ( $[2\text{M}+\text{H}]^+$ , calcd. 897.54), 449.24 (92) ( $[\text{M}+\text{H}]^+$ , calcd. 449.27), 227.18 (100) ( $[\text{M-Fmoc}+\text{H}]^+$ , calcd. 227.20).

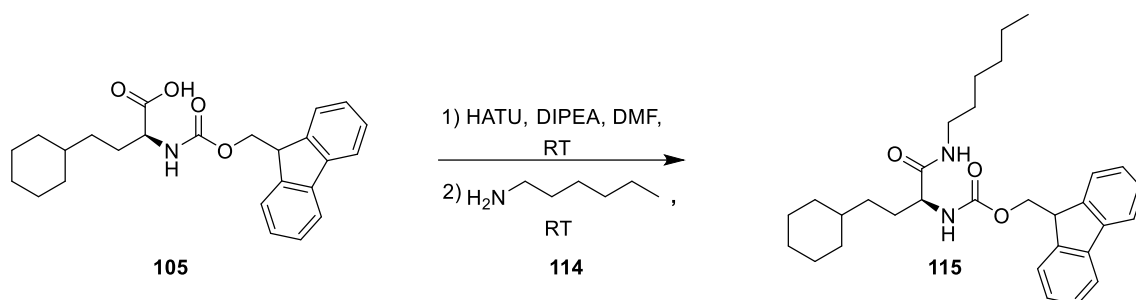
**(S)-(9H-Fluoren-9-yl)methyl (1-(butylamino)-4-cyclohexyl-1-oxobutan-2-yl)carbamate (113, SR40)**



(S)-2-(((9H-Fluoren-9-yl)methoxy)carbonyl)amino-4-cyclohexylbutanoic acid (**105**, 400 mg, 0.982 mmol) and HATU (448 mg, 1.18 mmol) were dissolved in DMF (dry, 10 mL) and DIPEA (152 mg, 1.18 mmol) was added. The reaction mixture was stirred for 2 h at RT and butan-1-amine (**112**, 120  $\mu\text{L}$ , 1.18 mmol) was added. The mixture was stirred for additional 3.5 h at RT. DCM (50 mL) was added and the organic phase was washed 5 times with  $\text{H}_2\text{O}$  (20 mL) and dried over  $\text{MgSO}_4$ . The solvent was evaporated under reduced pressure and the crude product was purified using column chromatography on silica (cyclohexane/ $\text{EtOAc}$  4:1  $\rightarrow$  1:1).

**Yield:** 301 mg (0.651 mmol, 66%), colorless solid.

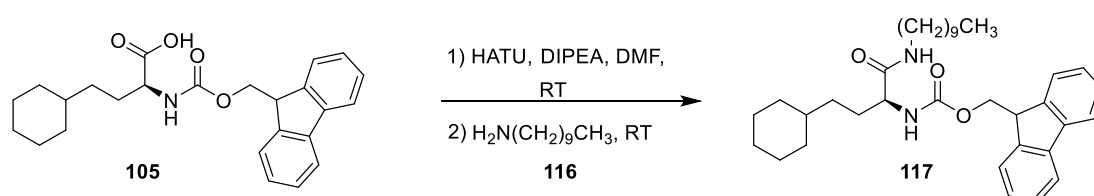
- **TLC:**  $R_f = 0.78$  ( $\text{SiO}_2$ , cyclohexane/ $\text{EtOAc}$ , 1:1).
- **$\text{C}_{29}\text{H}_{38}\text{N}_2\text{O}_3$ :** (462.62), [462.29].
- **$^1\text{H-NMR}$  (500 MHz,  $\text{CDCl}_3$ , 300 K):**  $\delta = 7.76$  (d,  $^3J = 7.5$  Hz, 2H, H-4-, H-5-Fmoc), 7.57 (d,  $^3J = 7.5$  Hz, 2H, H-1-, H-8-Fmoc), 7.40 (t,  $^3J = 7.3$  Hz, 2H, H-3-, H-6-Fmoc), 7.30 (t,  $^3J = 7.3$  Hz, 2H, H-2-, H-7-Fmoc), 6.03 (s, 1H,  $\text{NHCOO}$ ), 5.48–5.37 (m, 1H,  $\text{CONHCH}_2$ ), 4.45–4.32 (m, 2H,  $\text{OCH}_2$ ), 4.21 (t,  $^3J = 7.0$  Hz, 1H,  $\text{NHCHCO}$ ), 4.11–4.00 (m, 1H, H-9-Fmoc), 3.33–3.14 (m, 2H,  $\text{CH}_2\text{CH}_2\text{CH}_2\text{CH}_3$ ), 1.91–1.78 (m, 1H,  $\text{NHCHCH}_A\text{H}_B\text{CH}_2$ ), 1.74–1.56 (m, 6H,  $\text{NHCHCH}_A\text{H}_B\text{CH}_2$ , H-2 $_{\text{eq}}$ -, H-3 $_{\text{eq}}$ -, H-4 $_{\text{eq}}$ -, H-5 $_{\text{eq}}$ -, H-6 $_{\text{eq}}$ -cyclohexyl), 1.52–1.39 (m, 2H,  $\text{CH}_2\text{CH}_2\text{CH}_2\text{CH}_3$ ), 1.37–1.05 (m, 8H,  $\text{CH}_2\text{CH}_3$ , H-1-, H-3 $_{\text{ax}}$ -, H-4 $_{\text{ax}}$ -, H-5 $_{\text{ax}}$ -cyclohexyl,  $\text{NHCHCH}_2\text{CH}_2$ ), 0.93–0.79 (m, 5H,  $\text{CH}_3$ , H-2 $_{\text{ax}}$ -, H-6 $_{\text{ax}}$ -cyclohexyl) ppm.
- **$^{13}\text{C-NMR}$  (126 MHz,  $\text{CDCl}_3$ , 300 K):**  $\delta = 171.7, 156.3, 143.9, 141.4, 127.9, 127.2, 125.2, 120.1, 67.1, 55.5, 47.3, 39.4, 37.6, 33.4, 33.3, 33.1, 31.7, 30.4, 26.7, 26.4, 20.1, 13.8$  ppm.
- **MS (ESI pos.):**  $m/z$  (%) = 925.64 (12) ( $[2\text{M}+\text{H}]^+$ , calcd. 925.59), 463.21 (100) ( $[\text{M}+\text{H}]^+$ , calcd. 463.30), 241.23 (25) ( $[\text{M-Fmoc}+\text{H}]^+$ , calcd. 241.23), 179.21 (11) ( $[\text{M}_{\text{fr.}}+\text{H}]^+$ , calcd. 179.08).

**(S)-(9H-Fluoren-9-yl)methyl (4-cyclohexyl-1-(hexylamino)-1-oxobutan-2-yl)carbamate (115, SR46)**

(S)-2-(((9H-Fluoren-9-yl)methoxy)carbonyl)amino-4-cyclohexylbutanoic acid (**105**, 500 mg, 1.23 mmol) and HATU (560 mg, 1.47 mmol) were dissolved in DMF (dry, 10 mL) and DIPEA (190 mg, 1.47 mmol) was added. The reaction mixture was stirred for 2 h at RT and hexan-1-amine (**114**, 190  $\mu$ L, 1.47 mmol) was added. The mixture was stirred for additional 20 h at RT. DCM (50 mL) was added and the organic phase was washed 4 times with H<sub>2</sub>O (20 mL) and dried over MgSO<sub>4</sub>. The solvent was evaporated under reduced pressure and the crude product was purified using column chromatography on silica (cyclohexane/EtOAc 4:1  $\rightarrow$  1:1).

**Yield:** 396 mg (0.807 mmol, 66%), colorless solid.

- **TLC:**  $R_f$  = 0.87 (SiO<sub>2</sub>, cyclohexane/EtOAc, 1:1).
- **C<sub>31</sub>H<sub>42</sub>N<sub>2</sub>O<sub>3</sub>:** (490.68), [490.32].
- **<sup>1</sup>H-NMR (500 MHz, CDCl<sub>3</sub>, 300 K):**  $\delta$  = 7.76 (d, <sup>3</sup> $J$  = 7.5 Hz, 2H, H-4-, H-5-Fmoc), 7.57 (d, <sup>3</sup> $J$  = 7.5 Hz, 2H, H-1-, H-8-Fmoc), 7.40 (t, <sup>3</sup> $J$  = 7.4 Hz, 2H, H-3-, H-6-Fmoc), 7.30 (t, <sup>3</sup> $J$  = 7.4 Hz, 2H, H-2-, H-7-Fmoc), 6.05 (s, 1H, NHCOO), 5.45 (d, <sup>3</sup> $J$  = 7.5 Hz, 1H, CONHCH<sub>2</sub>), 4.46–4.31 (m, 2H, OCH<sub>2</sub>), 4.20 (t, <sup>3</sup> $J$  = 6.9 Hz, 1H, NHCHCO), 4.13–4.02 (m, 1H, H-9-Fmoc), 3.33–3.13 (m, 2H, NHCH<sub>2</sub>(CH<sub>2</sub>)<sub>4</sub>CH<sub>3</sub>), 1.92–1.76 (m, 1H, NHCHCH<sub>A</sub>H<sub>B</sub>CH<sub>2</sub>), 1.73–1.57 (m, 6H, NHCHCH<sub>A</sub>H<sub>B</sub>CH<sub>2</sub>, H-2<sub>eq</sub>-, H-3<sub>eq</sub>-, H-4<sub>eq</sub>-, H-5<sub>eq</sub>-, H-6<sub>eq</sub>-cyclohexyl), 1.53–1.40 (m, 2H, NHCH<sub>2</sub>CH<sub>2</sub>(CH<sub>2</sub>)<sub>3</sub>CH<sub>3</sub>), 1.35–1.05 (m, 12H, NHCH<sub>2</sub>CH<sub>2</sub>(CH<sub>2</sub>)<sub>3</sub>CH<sub>3</sub>, H-1-, H-3<sub>ax</sub>-, H-4<sub>ax</sub>-, H-5<sub>ax</sub>-cyclohexyl, NHCHCH<sub>2</sub>CH<sub>2</sub>), 0.94–0.79 (m, 5H, CH<sub>3</sub>, H-2<sub>ax</sub>-, H-6<sub>ax</sub>-cyclohexyl) ppm.
- **<sup>13</sup>C-NMR (126 MHz, CDCl<sub>3</sub>, 300 K):**  $\delta$  = 171.7, 156.3, 143.9, 141.4, 127.9, 127.2, 125.2, 120.1, 67.1, 55.5, 47.3, 39.7, 37.6, 33.4, 33.3, 33.1, 31.5, 30.4, 29.6, 26.7 (2x), 26.4, 22.7, 14.1 ppm.
- **MS (ESI pos.):**  $m/z$  (%) = 513.30 (18) ([M+Na]<sup>+</sup>, calcd. 513.31), 491.33 (100) ([M+H]<sup>+</sup>, calcd. 491.33), 269.33 (27) ([M-Fmoc+H]<sup>+</sup>, calcd. 269.25), 179.30 (20) ([M<sub>fr</sub>+H]<sup>+</sup>, calcd. 179.29).

**(S)-(9H-Fluoren-9-yl)methyl (4-cyclohexyl-1-(decylamino)-1-oxobutan-2-yl)carbamate (117, SR52)**

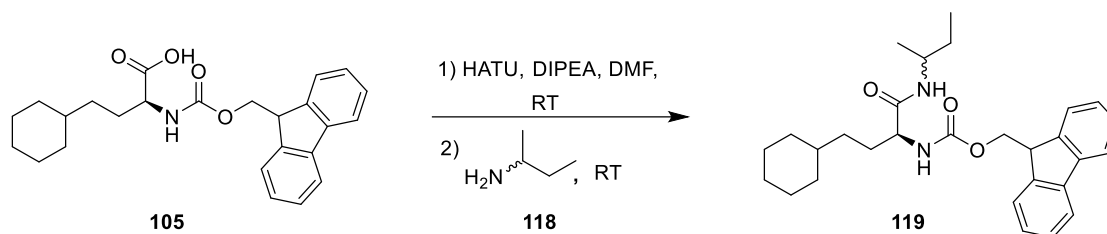
(S)-2-(((9H-Fluoren-9-yl)methoxy)carbonyl)amino-4-cyclohexylbutanoic acid (**105**, 500 mg, 1.23 mmol) and HATU (560 mg, 1.47 mmol) were dissolved in DMF (dry, 10 mL) and DIPEA (190 mg, 1.47 mmol) was added. The reaction mixture was stirred for 2 h at RT and decan-1-amine (**116**, 290  $\mu$ L, 1.47 mmol) was added. The mixture was stirred for additional 4 days at RT. DCM (50 mL) was added and the organic phase

was washed 4 times with H<sub>2</sub>O (20 mL) and dried over MgSO<sub>4</sub>. The solvent was evaporated under reduced pressure and the crude product was purified using column chromatography on silica (cyclohexane/EtOAc 4:1 → 1:1).

**Yield:** 565 mg (1.03 mmol, 84%), colorless solid.

- **TLC:** R<sub>f</sub> = 0.86 (SiO<sub>2</sub>, cyclohexane/EtOAc, 1:1).
- **C<sub>35</sub>H<sub>50</sub>N<sub>2</sub>O<sub>3</sub>:** (546.78), [546.38].
- **<sup>1</sup>H-NMR (500 MHz, CDCl<sub>3</sub>, 300 K):** δ = 7.76 (d, <sup>3</sup>J = 7.5 Hz, 2H, H-4-, H-5-Fmoc), 7.57 (d, <sup>3</sup>J = 7.5 Hz, 2H, H-1-, H-8-Fmoc), 7.40 (t, <sup>3</sup>J = 7.4 Hz, 2H, H-3-, H-6-Fmoc), 7.30 (t, <sup>3</sup>J = 7.4 Hz, 2H, H-2-, H-7-Fmoc), 6.00 (s, 1H, NHCOO), 5.42 (d, <sup>3</sup>J = 7.5 Hz, 1H, CONHCH<sub>2</sub>), 4.44–4.33 (m, 2H, OCH<sub>2</sub>), 4.21 (t, <sup>3</sup>J = 6.9 Hz, 1H, NHCHCO), 4.10–4.01 (m, 1H, H-9-Fmoc), 3.32–3.14 (m, 2H, NHCH<sub>2</sub>(CH<sub>2</sub>)<sub>8</sub>CH<sub>3</sub>), 1.90–1.96 (m, 1H, NHCHCH<sub>A</sub>H<sub>B</sub>CH<sub>2</sub>), 1.73–1.58 (m, 6H, NHCHCH<sub>A</sub>H<sub>B</sub>CH<sub>2</sub>, H-2<sub>eq</sub><sup>-</sup>, H-3<sub>eq</sub><sup>-</sup>, H-4<sub>eq</sub><sup>-</sup>, H-5<sub>eq</sub><sup>-</sup>, H-6<sub>eq</sub><sup>-</sup>-cyclohexyl), 1.51–1.40 (m, 2H, NHCH<sub>2</sub>CH<sub>2</sub>(CH<sub>2</sub>)<sub>7</sub>CH<sub>3</sub>), 1.33–1.07 (m, 20H, NHCH<sub>2</sub>CH<sub>2</sub>(CH<sub>2</sub>)<sub>7</sub>CH<sub>3</sub>, H-1-, H-3<sub>ax</sub><sup>-</sup>, H-4<sub>ax</sub><sup>-</sup>, H-5<sub>ax</sub>-cyclohexyl, NHCHCH<sub>2</sub>CH<sub>2</sub>), 0.93–0.80 (m, 5H, CH<sub>3</sub>, H-2<sub>ax</sub><sup>-</sup>, H-6<sub>ax</sub>-cyclohexyl) ppm.
- **<sup>13</sup>C-NMR (126 MHz, CDCl<sub>3</sub>, 300 K):** δ = 171.7, 156.3, 143.9, 141.4, 127.9, 127.2, 125.2, 120.1, 67.1, 55.5, 47.3, 39.7, 37.6, 33.4, 33.3, 33.1, 32.0, 30.4, 29.7 (2x), 29.6, 29.4 (2x), 27.0, 26.7, 26.4, 22.8, 14.3 ppm.
- **MS (ESI pos.):** m/z (%) = 569.32 (35) ([M+Na]<sup>+</sup>, calcd. 569.37), 547.34 (100) ([M+H]<sup>+</sup>, calcd. 547.39), 325.26 (11) ([M-Fmoc+H]<sup>+</sup>, calcd. 325.33).

**(9H-Fluoren-9-yl)methyl ((S)-1-((SR)-sec-butylamino)-4-cyclohexyl-1-oxobutan-2-yl)carbamate (119, SR44)**



(S)-2-(((9H-Fluoren-9-yl)methoxy)carbonyl)amino-4-cyclohexylbutanoic acid (**105**, 500 mg, 1.23 mmol) and HATU (560 mg, 1.47 mmol) were dissolved in DMF (dry, 15 mL) and DIPEA (190 mg, 1.47 mmol) was added. The reaction mixture was stirred for 2 h at RT and *rac*-butan-2-amine (**118**, 160 μL, 1.47 mmol) was added. The mixture was stirred for additional 20 h at RT. DCM (50 mL) was added and the organic phase was washed 4 times with H<sub>2</sub>O (20 mL) and dried over MgSO<sub>4</sub>. The solvent was evaporated under reduced pressure and the crude product was purified using column chromatography on silica (cyclohexane/EtOAc 4:1 → 1:1).

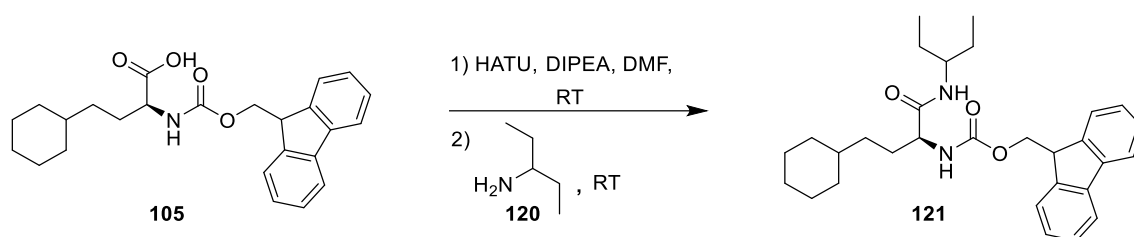
**Yield:** 363 mg (0.785 mmol, 64%), colorless solid.

- **TLC:** R<sub>f</sub> = 0.76 (SiO<sub>2</sub>, cyclohexane/EtOAc, 1:1).
- **C<sub>29</sub>H<sub>38</sub>N<sub>2</sub>O<sub>3</sub>:** (462.62), [462.29].
- **<sup>1</sup>H-NMR (500 MHz, CDCl<sub>3</sub>, 300 K):** (mixture of diastereomers) δ = 7.76 (d, <sup>3</sup>J = 7.5 Hz, 2H, H-4-, H-5-Fmoc), 7.58 (d, <sup>3</sup>J = 7.5 Hz, 2H, H-1-, H-8-Fmoc), 7.40 (t, <sup>3</sup>J = 7.4 Hz, 2H, H-3-, H-6-Fmoc), 7.30 (t, <sup>3</sup>J = 7.4 Hz, 2H, H-2-, H-7-Fmoc), 5.86–5.74 (m, 1H, NHCOO), 5.52–5.41 (m, 1H, CONHCH<sub>2</sub>), 4.43–4.32 (m, 2H, OCH<sub>2</sub>), 4.21 (t, <sup>3</sup>J = 7.1 Hz, 1H, NHCHCO), 4.12–4.00 (m, 1H, H-9-Fmoc), 3.95–3.84 (m,

1H, CHCH<sub>2</sub>CH<sub>3</sub>), 1.90–1.76 (m, 1H, NHCHCH<sub>A</sub>H<sub>B</sub>CH<sub>2</sub>), 1.74–1.57 (m, 6H, NHCHCH<sub>A</sub>H<sub>B</sub>CH<sub>2</sub>, H-2<sub>eq</sub>-, H-3<sub>eq</sub>-, H-4<sub>eq</sub>-, H-5<sub>eq</sub>-, H-6<sub>eq</sub>-cyclohexyl), 1.50–1.38 (m, 2H, CHCH<sub>2</sub>CH<sub>3</sub>), 1.30–1.04 (m, 9H, CHCH<sub>3</sub>, H-1-, H-3<sub>ax</sub>-, H-4<sub>ax</sub>-, H-5<sub>ax</sub>-cyclohexyl, NHCHCH<sub>2</sub>CH<sub>2</sub>), 0.94–0.79 (m, 5H, CH<sub>2</sub>CH<sub>3</sub>, H-2<sub>ax</sub>-, H-6<sub>ax</sub>-cyclohexyl) ppm.

- **<sup>13</sup>C-NMR (126 MHz, CDCl<sub>3</sub>, 300 K):** (mixture of diastereomers) δ = 171.7, 156.3, 143.9, 141.4, 127.9, 127.2, 125.2, 120.1, 67.1, 55.5, 47.2, 37.6, 33.4, 33.3, 33.1, 30.6, 30.4, 29.7, 26.7, 26.4, 20.6, 20.5, 10.5 ppm.
- **MS (ESI pos.):** *m/z* (%) = 925.68 (12) ([2M+H]<sup>+</sup>, calcd. 925.59), 463.25 (100) ([M+H]<sup>+</sup>, calcd. 463.30), 241.23 (25) ([M-Fmoc+H]<sup>+</sup>, calcd. 241.23), 179.15 (9) ([M<sub>fr.</sub>+H]<sup>+</sup>, calcd. 179.08).

**(S)-(9H-Fluoren-9-yl)methyl (4-cyclohexyl-1-oxo-1-(pentan-3-ylamino)butan-2-yl)carbamate (121, SR45)**

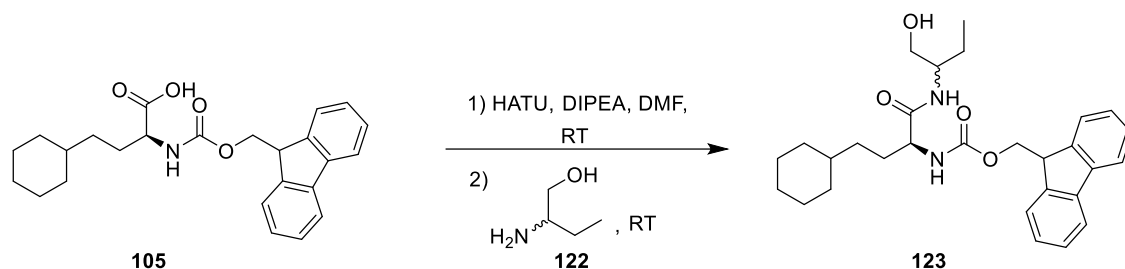


(S)-2-(((9H-Fluoren-9-yl)methoxy)carbonyl)amino-4-cyclohexylbutanoic acid (**105**, 500 mg, 1.23 mmol) and HATU (560 mg, 1.47 mmol) were dissolved in DMF (dry, 10 mL) and DIPEA (190 mg, 1.47 mmol) was added. The reaction mixture was stirred for 1.5 h at RT and pentan-3-amine (**120**, 170 μL, 1.47 mmol) was added. The mixture was stirred for additional 20 h at RT. DCM (50 mL) was added and the organic phase was washed 4 times with H<sub>2</sub>O (20 mL) and dried over MgSO<sub>4</sub>. The solvent was evaporated under reduced pressure and the crude product was purified by column chromatography on silica (cyclohexane/EtOAc 4:1 → 1:1).

**Yield:** 458 mg (0.961 mmol, 78%), colorless solid.

- **TLC:** R<sub>f</sub> = 0.82 (SiO<sub>2</sub>, cyclohexane/EtOAc, 1:1).
- **C<sub>30</sub>H<sub>40</sub>N<sub>2</sub>O<sub>3</sub>:** (476.65), [476.30].
- **<sup>1</sup>H-NMR (500 MHz, CDCl<sub>3</sub>, 300 K):** δ = 7.76 (d, <sup>3</sup>J = 7.5 Hz, 2H, H-4-, H-5-Fmoc), 7.58 (d, <sup>3</sup>J = 7.5 Hz, 2H, H-1-, H-8-Fmoc), 7.40 (t, <sup>3</sup>J = 7.4 Hz, 2H, H-3-, H-6-Fmoc), 7.30 (t, <sup>3</sup>J = 7.4 Hz, 2H, H-2-, H-7-Fmoc), 5.75 (d, <sup>3</sup>J = 8.5 Hz, 1H, NHCOO), 5.49 (d, <sup>3</sup>J = 7.9 Hz, 1H, CONHCH), 4.42–4.32 (m, 2H, OCH<sub>2</sub>), 4.21 (t, <sup>3</sup>J = 7.0 Hz, 1H, NHCHCO), 4.14–4.06 (m, 1H, H-9-Fmoc), 3.81–3.71 (m, 1H, CH(CH<sub>2</sub>CH<sub>3</sub>)<sub>2</sub>), 1.91–1.78 (m, 1H, NHCHCH<sub>A</sub>H<sub>B</sub>CH<sub>2</sub>), 1.76–1.60 (m, 6H, NHCHCH<sub>A</sub>H<sub>B</sub>CH<sub>2</sub>, H-2<sub>eq</sub>-, H-3<sub>eq</sub>-, H-4<sub>eq</sub>-, H-5<sub>eq</sub>-, H-6<sub>eq</sub>-cyclohexyl), 1.59–1.46 (m, 2H, CH(CH<sub>A</sub>H<sub>B</sub>CH<sub>3</sub>)<sub>2</sub>), 1.40–1.30 (m, 2H, CH(CH<sub>A</sub>H<sub>B</sub>CH<sub>3</sub>)<sub>2</sub>), 1.29–1.07 (m, 6H, H-1-, H-3<sub>ax</sub>-, H-4<sub>ax</sub>-, H-5<sub>ax</sub>-cyclohexyl, NHCHCH<sub>2</sub>CH<sub>2</sub>), 0.94–0.78 (m, 8H, CH(CH<sub>2</sub>CH<sub>3</sub>)<sub>2</sub>, H-2<sub>ax</sub>-, H-6<sub>ax</sub>-cyclohexyl) ppm.
- **<sup>13</sup>C-NMR (126 MHz, CDCl<sub>3</sub>, 300 K):** δ = 171.5, 156.3, 143.9, 141.4, 127.9, 127.2, 125.2, 120.1, 67.1, 55.5, 52.3, 47.2, 37.6, 33.4, 33.3, 33.1, 30.5, 26.7, 26.4, 10.4 ppm.
- **MS (ESI pos.):** *m/z* (%) = 499.21 (9) ([M+Na]<sup>+</sup>, calcd. 499.29), 477.25 (100) ([M+H]<sup>+</sup>, calcd. 477.31), 255.28 (7) ([M-Fmoc+H]<sup>+</sup>, calcd. 255.23).

**(9H-Fluoren-9-yl)methyl ((S)-4-cyclohexyl-1-(((S)-1-hydroxybutan-2-yl)amino)-1-oxobutan-2-yl)carbamate (123, SR96)**

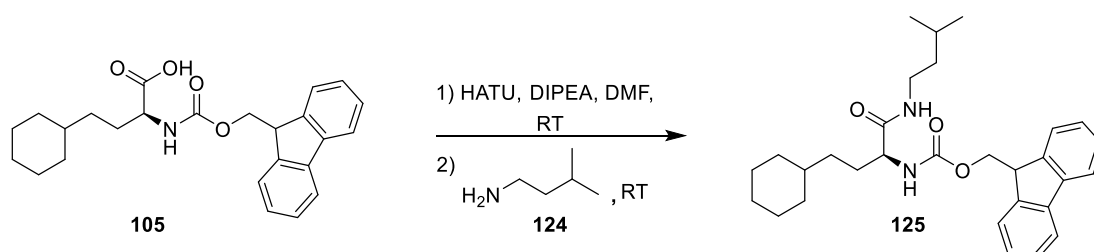


(S)-2-(((9H-Fluoren-9-yl)methoxy)carbonyl)amino-4-cyclohexylbutanoic acid (**105**, 500 mg, 1.23 mmol) and HATU (560 mg, 1.47 mmol) were dissolved in DMF (dry, 10 mL) and DIPEA (190 mg, 1.47 mmol) was added. The reaction mixture was stirred for 1.5 h at RT and *rac*-2-aminobutan-1-ol (**122**, 133 mg, 1.47 mmol) was added. The mixture was stirred for additional 20 h at RT. DCM (50 mL) was added and the organic phase was washed 5 times with H<sub>2</sub>O (50 mL) and dried over MgSO<sub>4</sub>. The solvent was evaporated under reduced pressure and the crude product was triturated with cyclohexane/DCM (1:1).

**Yield:** 345 mg (0.721 mmol, 59%), colorless solid.

- **TLC:** R<sub>f</sub> = 0.30 (SiO<sub>2</sub>, cyclohexane/EtOAc, 1:1).
- **C<sub>29</sub>H<sub>38</sub>N<sub>2</sub>O<sub>4</sub>:** (478.62), [478.28].
- **<sup>1</sup>H-NMR (400 MHz, DMSO-d<sub>6</sub>, 300 K):** (mixture of diastereomers) δ = 7.95–7.84 (m, 3H, H-4-, H-5-Fmoc, NHCOO), 7.77–7.69 (m, 2H, H-1-, H-8-Fmoc), 7.95–7.84 (m, 3H, H-3-, H-6-Fmoc, CONHCH), 7.36–7.28 (m, 2H, H-2-, H-7-Fmoc), 4.32–4.17 (m, 3H, NHCHCO, OCH<sub>2</sub>), 4.03–3.91 (m, 1H, H-9-Fmoc), 3.90–3.76 (m, 1H, NHCH(CH<sub>2</sub>)<sub>2</sub>), 3.66–3.51 (m, 2H, NHCHCH<sub>2</sub>OH), 1.72–1.49 (m, 8H, NHCHCH<sub>2</sub>CH<sub>3</sub>, NHCHCH<sub>A</sub>H<sub>B</sub>CH<sub>2</sub>, H-2<sub>eq</sub>-, H-3<sub>eq</sub>-, H-4<sub>eq</sub>-, H-5<sub>eq</sub>-, H-6<sub>eq</sub>-cyclohexyl), 1.48–1.37 (m, 1H, NHCHCH<sub>A</sub>H<sub>B</sub>CH<sub>2</sub>), 1.27–1.04 (m, 6H, NHCHCH<sub>2</sub>CH<sub>2</sub>, H-1-, H-3<sub>ax</sub>-, H-4<sub>ax</sub>-, H-5<sub>ax</sub>-cyclohexyl), 0.90–0.77 (m, 5H, H-2<sub>ax</sub>-, H-6<sub>ax</sub>-cyclohexyl, CH<sub>3</sub>) ppm.
- **<sup>13</sup>C-NMR (101 MHz, DMSO-d<sub>6</sub>, 300 K):** (mixture of diastereomers) δ = 172.0, 155.8, 143.9, 143.8, 140.7, 127.6, 127.0, 125.3, 120.1, 65.5, 55.0, 54.9, 51.4, 51.2, 47.2 (2x), 36.8, 36.7, 32.9 (2x), 32.7, 29.7, 29.6, 26.1, 25.7, 24.3, 24.1, 10.2 (2x) ppm.
- **MS (ESI pos.):** *m/z* (%) = 501.26 (100) ([M+Na]<sup>+</sup>, calcd. 501.27), 479.29 (95) ([M+H]<sup>+</sup>, calcd. 479.29).

**(S)-((9H-Fluoren-9-yl)methyl (4-cyclohexyl-1-(isopentylamino)-1-oxobutan-2-yl)carbamate (125, SR55)**



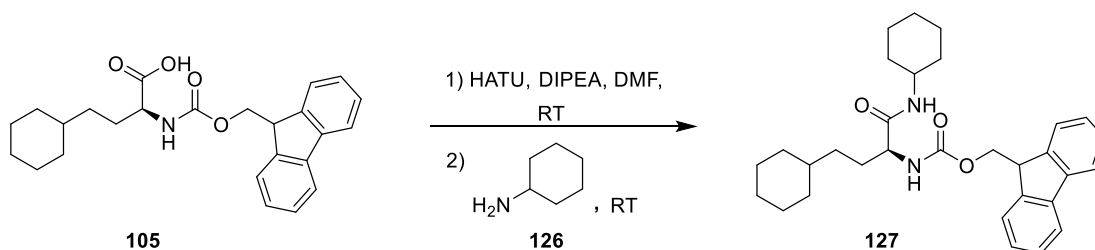
(S)-2-(((9H-Fluoren-9-yl)methoxy)carbonyl)amino-4-cyclohexylbutanoic acid (**150**, 500 mg, 1.23 mmol) and HATU (560 mg, 1.47 mmol) were dissolved in DMF (dry, 10 mL) and DIPEA (190 mg, 1.47 mmol) was added. The reaction mixture was stirred for 1.5 h at RT and 3-methylbutan-1-amine (**125**, 171 μL,

1.47 mmol) was added. The mixture was stirred for additional 20 h at RT. DCM (50 mL) was added and the organic phase was washed 5 times with H<sub>2</sub>O (20 mL) and dried over MgSO<sub>4</sub>. The solvent was evaporated under reduced pressure and the crude product was purified using column chromatography on silica (cyclohexane/EtOAc 4:1 → 2:1).

**Yield:** 498 mg (1.05 mmol, 85%), colorless solid.

- **TLC:** R<sub>f</sub> = 0.30 (SiO<sub>2</sub>, cyclohexane/EtOAc, 1:1).
- **C<sub>30</sub>H<sub>40</sub>N<sub>2</sub>O<sub>3</sub>:** (476.65), [476.30].
- **<sup>1</sup>H-NMR (500 MHz, CDCl<sub>3</sub>, 300 K):** δ = 7.76 (d, <sup>3</sup>J = 7.6 Hz, 2H, H-4-, H-5-Fmoc), 7.57 (d, <sup>3</sup>J = 7.6 Hz, 2H, H-1-, H-8-Fmoc), 7.40 (t, <sup>3</sup>J = 7.6 Hz, 2H, H-3-, H-6-Fmoc), 7.30 (t, <sup>3</sup>J = 7.6 Hz, 2H, H-2-, H-7-Fmoc), 6.03 (s, 1H, NHCOO), 5.44 (d, <sup>3</sup>J = 8.0 Hz, 1H, CONHCH<sub>2</sub>), 4.45–4.31 (m, 2H, OCH<sub>2</sub>), 4.20 (t, <sup>3</sup>J = 6.8 Hz, 1H, NHCHCO), 4.11–4.02 (m, 1H, H-9-Fmoc), 3.34–3.16 (m, 2H, NHCH<sub>2</sub>CH<sub>2</sub>CH(CH<sub>3</sub>)<sub>2</sub>), 1.91–1.77 (m, 1H, NHCHCH<sub>A</sub>H<sub>B</sub>CH<sub>2</sub>), 1.73–1.52 (m, 7H, NHCHCH<sub>A</sub>H<sub>B</sub>CH<sub>2</sub>, NHCH<sub>2</sub>CH<sub>2</sub>CH(CH<sub>3</sub>)<sub>2</sub>), H-2<sub>eq</sub><sup>-</sup>, H-3<sub>eq</sub><sup>-</sup>, H-4<sub>eq</sub><sup>-</sup>, H-5<sub>eq</sub><sup>-</sup>, H-6<sub>eq</sub>-cyclohexyl), 1.42–1.31 (m, 2H, NHCH<sub>2</sub>CH<sub>2</sub>CH(CH<sub>3</sub>)<sub>2</sub>), 1.28–1.06 (m, 6H, H-1-, H-3<sub>ax</sub><sup>-</sup>, H-4<sub>ax</sub><sup>-</sup>, H-5<sub>ax</sub>-cyclohexyl, NHCHCH<sub>2</sub>CH<sub>2</sub>), 0.94–0.79 (m, 8H, CH(CH<sub>3</sub>)<sub>2</sub>, H-2<sub>ax</sub><sup>-</sup>, H-6<sub>ax</sub>-cyclohexyl) ppm.
- **<sup>13</sup>C-NMR (126 MHz, CDCl<sub>3</sub>, 300 K):** δ = 171.7, 156.3, 143.9, 141.4, 127.9, 127.2, 125.2, 120.2, 67.1, 55.5, 47.2, 38.5, 38.0, 37.6, 33.4, 33.3, 33.1, 30.4, 26.7, 26.4, 25.9, 22.5 (2x) ppm.
- **MS (ESI pos.):** m/z (%) = 499.21 (37) ([M+Na]<sup>+</sup>, calcd. 499.29), 477.26 (100) ([M+H]<sup>+</sup>, calcd. 477.31), 186.20 (97) ([M<sub>fr.</sub>]<sup>+</sup>, calcd. 186.10).

**(S)-(9H-Fluoren-9-yl)methyl (4-cyclohexyl-1-(cyclohexylamino)-1-oxobutan-2-yl)carbamate (127, SR51)**



(S)-2-(((9H-Fluoren-9-yl)methoxy)carbonyl)amino-4-cyclohexylbutanoic acid (**105**, 500 mg, 1.23 mmol) and HATU (560 mg, 1.47 mmol) were dissolved in DMF (dry, 10 mL) and DIPEA (190 mg, 1.47 mmol) was added. The reaction mixture was stirred for 2 h at RT and cyclohexylamine (**126**, 170 μL, 1.47 mmol) was added. The mixture was stirred for 4 d at RT. DCM (50 mL) was added and the organic phase was washed 4 times with H<sub>2</sub>O (20 mL) and dried over MgSO<sub>4</sub>. The solvent was evaporated under reduced pressure and the crude product was purified using column chromatography on silica (cyclohexane/EtOAc 4:1 → 1:1).

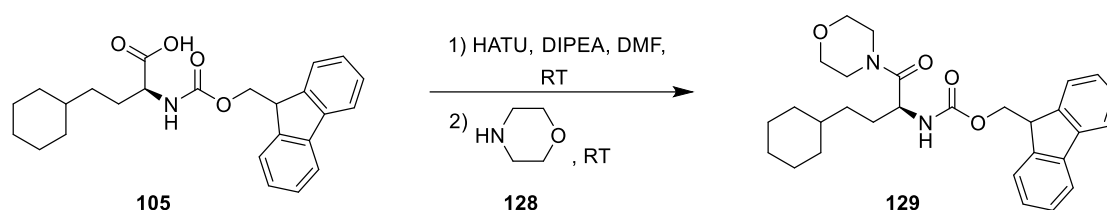
**Yield:** 513 mg (1.05 mmol, 86%), colorless solid.

- **TLC:** R<sub>f</sub> = 0.29 (SiO<sub>2</sub>, cyclohexane/EtOAc, 4:1).
- **C<sub>31</sub>H<sub>40</sub>N<sub>2</sub>O<sub>3</sub>:** (488.30), [488.66].
- **<sup>1</sup>H-NMR (500 MHz, CDCl<sub>3</sub>, 300 K):** δ = 7.76 (d, <sup>3</sup>J = 7.6 Hz, 2H, H-4-, H-5-Fmoc), 7.58 (d, <sup>3</sup>J = 7.5 Hz, 2H, H-1-, H-8-Fmoc), 7.40 (t, <sup>3</sup>J = 7.6 Hz, 2H, H-3-, H-6-Fmoc), 7.30 (t, <sup>3</sup>J = 7.5 Hz, 2H, H-2-, H-7-Fmoc), 5.90 (d, <sup>3</sup>J = 7.2 Hz, 1H, NHCOO), 5.47 (d, <sup>3</sup>J = 7.8 Hz, 1H, CONHCH), 4.43–4.31 (m, 2H, OCH<sub>2</sub>), 4.21 (t, <sup>3</sup>J = 7.1 Hz, 1H, NHCHCO), 4.10–4.01 (m, 1H, H-9-Fmoc), 3.80–3.70 (m, 1H, NHCH-cyclohexyl), 1.93–1.77 (m, 3H, NHCHCH<sub>A</sub>H<sub>B</sub>CH<sub>2</sub>, H-2<sub>eq</sub><sup>-</sup>, H-6<sub>eq</sub>-NH-cyclohexyl), 1.74–1.54 (m, 10H, NHCHCH<sub>A</sub>H<sub>B</sub>CH<sub>2</sub>, H-2<sub>eq</sub><sup>-</sup>, H-3<sub>eq</sub><sup>-</sup>, H-4<sub>eq</sub><sup>-</sup>, H-5<sub>eq</sub><sup>-</sup>, H-6<sub>eq</sub>-cyclohexyl, H-3<sub>eq</sub><sup>-</sup>, H-4<sub>eq</sub><sup>-</sup>, H-5<sub>eq</sub><sup>-</sup>, H-6<sub>eq</sub>-NH-

cyclohexyl), 1.40–1.28 (m, 2H, NHCHCH<sub>2</sub>CH<sub>2</sub>), 1.27–1.04 (m, 9H, H-1-, H-3<sub>ax</sub>-, H-4<sub>ax</sub>-, H-5<sub>ax</sub>-cyclohexyl, H-2<sub>ax</sub>-, H-3<sub>ax</sub>-, H-4<sub>ax</sub>-, H-5<sub>ax</sub>-, H-6<sub>ax</sub>-NH-cyclohexyl), 0.95–0.78 (m, 2H, H-2<sub>ax</sub>-, H-6<sub>ax</sub>-cyclohexyl) ppm.

- **<sup>13</sup>C-NMR (126 MHz, CDCl<sub>3</sub>, 300 K):** δ = 170.7, 156.3, 143.9 (2x), 141.4, 127.9, 127.2, 125.2 (2x), 120.1 (2x), 67.1, 55.5, 48.4, 47.2, 37.6, 33.4, 33.3, 33.2, 33.0, 30.6, 26.7, 26.4, 25.6, 24.9 ppm.
- **MS (ESI pos.):** *m/z* (%) = 511.24 (100) ([M+Na]<sup>+</sup>, calcd. 511.65).

**(S)-(9H-Fluoren-9-yl)methyl (4-cyclohexyl-1-morpholino-1-oxobutan-2-yl)carbamate (129, SR136)**



(S)-2-(((9H-Fluoren-9-yl)methoxy)carbonyl)amino-4-cyclohexylbutanoic acid (**105**, 500 mg, 1.23 mmol) and HATU (560 mg, 1.47 mmol) were dissolved in DMF (dry, 10 mL) and DIPEA (190 mg, 1.47 mmol) was added. The reaction mixture was stirred for 1.5 h at RT and morpholine (**128**, 128 mg, 1.47 mmol) was added. The mixture was stirred for additional 20 h at RT. DCM (50 mL) was added and the organic phase was washed 4 times with H<sub>2</sub>O (50 mL) and dried over MgSO<sub>4</sub>. The solvent was evaporated under reduced pressure and the crude product was purified using column chromatography on silica (cyclohexane/EtOAc 4:1 → 1:1 → 1:3).

**Yield:** 465 mg (0.976 mmol, 80%), colorless solid.

- **TLC:** R<sub>f</sub> = 0.55 (SiO<sub>2</sub>, cyclohexane/EtOAc, 1:1).
- **C<sub>29</sub>H<sub>36</sub>N<sub>2</sub>O<sub>4</sub>:** (476.61), [476.27].
- **<sup>1</sup>H-NMR (500 MHz, CDCl<sub>3</sub>, 300 K):** δ = 7.76 (d, <sup>3</sup>J = 7.5 Hz, 2H, H-4-, H-5-Fmoc), 7.65–7.53 (m, 2H, H-1-, H-8-Fmoc), 7.40 (t, <sup>3</sup>J = 7.4 Hz, 2H, H-3-, H-6-Fmoc), 7.31 (t, <sup>3</sup>J = 7.5 Hz, 2H, H-2-, H-7-Fmoc), 5.70 (d, <sup>3</sup>J = 8.5 Hz, 1H, NHCOO), 4.65–4.56 (m, 1H, NHCHCO), 4.42–4.31 (m, 2H, OCH<sub>2</sub>CH), 4.22 (t, <sup>3</sup>J = 7.1 Hz, 1H, H-9-Fmoc), 3.75–3.45 (m, 8H, CH<sub>2</sub>-2-, CH<sub>2</sub>-3-, CH<sub>2</sub>-5-, CH<sub>2</sub>-6-morpholine), 1.78–1.51 (m, 7H, NHCHCH<sub>2</sub>CH<sub>2</sub>, H-2<sub>eq</sub>-, H-3<sub>eq</sub>-, H-4<sub>eq</sub>-, H-5<sub>eq</sub>-, H-6<sub>eq</sub>-cyclohexyl), 1.34–1.07 (m, 6H, H-1-, H-3<sub>ax</sub>-, H-4<sub>ax</sub>-, H-5<sub>ax</sub>-cyclohexyl, NHCHCH<sub>2</sub>CH<sub>2</sub>), 0.95–0.81 (m, 2H, H-2<sub>ax</sub>-, H-6<sub>ax</sub>-cyclohexyl) ppm.
- **<sup>13</sup>C-NMR (126 MHz, CDCl<sub>3</sub>, 300 K):** δ = 170.7, 156.1, 144.1, 143.9, 141.4, 127.8, 127.2, 125.3, 120.1, 67.1, 67.0, 66.8, 50.8, 47.3, 46.2, 42.6, 37.7, 33.5, 33.3, 32.6, 30.8, 26.7, 26.4 (2x) ppm.
- **MS (ESI pos.):** *m/z* (%) = 499.26 (100) ([M+Na]<sup>+</sup>, calcd. 499.26), 477.31 (65) ([M+H]<sup>+</sup>, calcd. 477.28), 517.36 (23) ([M+K]<sup>+</sup>, calcd. 515.28).

**tert-Butyl piperazine-1-carboxylate (131)**



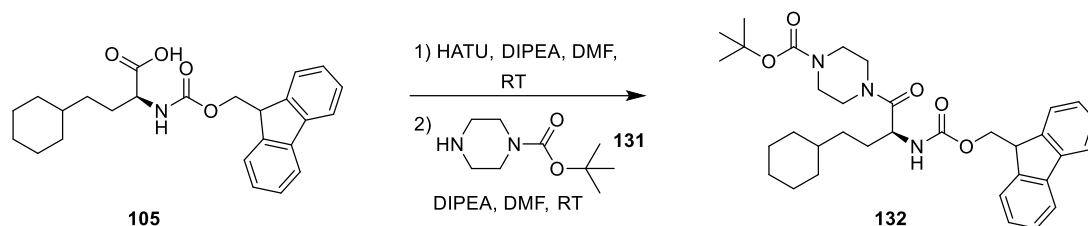
tert-Butyl piperazine-1-carboxylate was synthesized according to CARPINO ET AL.<sup>522</sup> Piperazine (**130**, 25 mmol) was dissolved in DCM (60 mL) and cooled to 0 °C. A mixture of Boc<sub>2</sub>O (12.5 mmol) in DCM (25 mL) was added dropwise and the mixture was stirred for 1 h at 0 °C. The reaction mixture was filtered and the



solvent was removed under reduced pressure. The residue was dissolved in H<sub>2</sub>O and washed once with K<sub>2</sub>CO<sub>3</sub> (sat., 80 mL) and extracted each 3 times with Et<sub>2</sub>O (80 mL). The organic phase was dried over Na<sub>2</sub>SO<sub>4</sub>, filtrated and the solvent was removed under reduced pressure to yield 70% of *tert*-butyl piperazine-1-carboxylate (**131**).

The analytical data are consistent with the literature.<sup>522</sup>

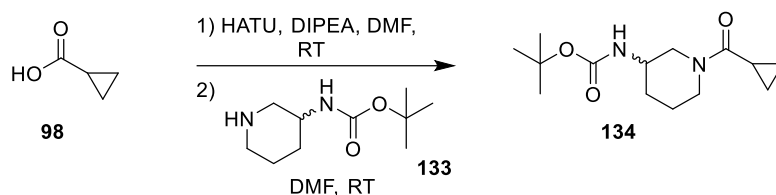
**(S)-*tert*-Butyl 4-(2-(((9H-fluoren-9-yl)methoxy)carbonyl)amino)-4-cyclohexylbutanoyl)piperazine-1-carboxylate (132, SR135)**



(S)-2-(((9H-Fluoren-9-yl)methoxy)carbonyl)amino)-4-cyclohexylbutanoic acid (**105**, 500 mg, 1.23 mmol) and HATU (560 mg, 1.47 mmol) were dissolved in DMF (dry, 6 mL) and DIPEA (190 mg, 1.47 mmol) was added. The reaction mixture was stirred for 1.5 h at RT and *tert*-butyl piperazine-1-carboxylate (**131**, 274 mg, 1.47 mmol) diluted with DIPEA (80 mg, 0.61 mmol) in DMF (dry, 4 mL) was added. The mixture was stirred for additional 20 h at RT. DCM (50 mL) was added and the organic phase was washed 4 times with H<sub>2</sub>O (50 mL) and dried over MgSO<sub>4</sub>. The solvent was evaporated under reduced pressure and the crude product was purified by column chromatography on silica (cyclohexane/EtOAc 4:1 → 1:1 → 1:3).

**Yield:** 613 mg (1.07 mmol, 87%), colorless solid.

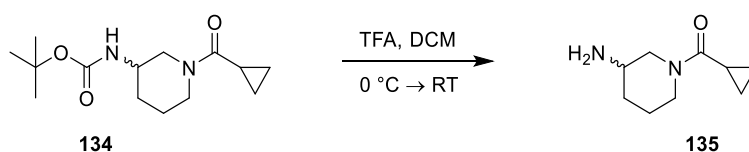
- **TLC:** R<sub>f</sub> = 0.73 (SiO<sub>2</sub>, cyclohexane/EtOAc, 1:1).
- **C<sub>34</sub>H<sub>45</sub>N<sub>3</sub>O<sub>5</sub>:** (575.74), [575.34].
- **<sup>1</sup>H-NMR (500 MHz, CDCl<sub>3</sub>, 300 K):** δ = 7.76 (d, <sup>3</sup>J = 7.4 Hz, 2H, H-4-, H-5-Fmoc), 7.64–7.57 (m, 2H, H-1-, H-8-Fmoc), 7.40 (t, <sup>3</sup>J = 7.4 Hz, 2H, H-3-, H-6-Fmoc), 7.31 (t, <sup>3</sup>J = 7.5 Hz, 2H, H-2-, H-7-Fmoc), 5.69 (d, <sup>3</sup>J = 8.5 Hz, 1H, NHCOO), 4.68–4.55 (m, 1H, NHCHCO), 4.41–4.31 (m, 2H, OCH<sub>2</sub>), 4.22 (t, <sup>3</sup>J = 7.2 Hz, 1H, H-9-Fmoc), 3.71–3.23 (m, 8H, CH<sub>2</sub>-2-, CH<sub>2</sub>-3-, CH<sub>2</sub>-5-, CH<sub>2</sub>-6-piperazine), 1.79–1.53 (m, 7H, NHCHCH<sub>2</sub>CH<sub>2</sub>, H-2<sub>eq</sub>-, H-3<sub>eq</sub>-, H-4<sub>eq</sub>-, H-5<sub>eq</sub>-, H-6<sub>eq</sub>-cyclohexyl), 1.48 (s, 9H, C(CH<sub>3</sub>)<sub>3</sub>), 1.31–1.04 (m, 6H, H-1-, H-3<sub>ax</sub>-, H-4<sub>ax</sub>-, H-5<sub>ax</sub>-cyclohexyl, NHCHCH<sub>2</sub>CH<sub>2</sub>), 0.90–0.80 (m, 2H, H-2<sub>ax</sub>-, H-6<sub>ax</sub>-cyclohexyl) ppm.
- **<sup>13</sup>C-NMR (126 MHz, CDCl<sub>3</sub>, 300 K):** δ = 170.8, 156.1, 154.6, 144.0, 143.9, 141.4, 127.8, 127.2, 125.3, 120.1, 80.6, 67.1, 51.0, 47.3, 45.6, 42.1, 37.6, 33.5, 33.2, 32.7, 30.9, 28.5, 26.7, 26.4 ppm.
- **MS (ESI pos.):** m/z (%) = 520.28 (100) ([M-Boc+2Na]<sup>+</sup>, calcd. 520.26), 598.32 (89) ([M+Na]<sup>+</sup>, calcd. 598.33), 576.35 (21) ([M+H]<sup>+</sup>, calcd. 576.35).

***rac-tert-Butyl (1-(cyclopropanecarbonyl)piperidin-3-yl)carbamate (134, SR149)***

Cyclopropanecarboxylic acid (**98**, 215 mg, 2.50 mmol) and HATU (1.14 g, 3.00 mmol) were dissolved in DMF (dry, 7 mL) and DIPEA (387 mg, 3.00 mmol) was added. The reaction mixture was stirred for 1.5 h at RT and *rac-tert-butyl* piperidin-3-ylcarbamate (**133**, 600 mg, 3.00 mmol) dissolved in DMF (dry, 5 mL) was added. The mixture was stirred for additional 20 h at RT. DCM (100 mL) was added and the organic phase was washed 4 times with H<sub>2</sub>O (100 mL), once with NH<sub>4</sub>Cl (sat. 100 mL) and dried over MgSO<sub>4</sub>. The solvent was evaporated under reduced pressure and the crude product was purified using column chromatography on silica (cyclohexane/EtOAc 1:9).

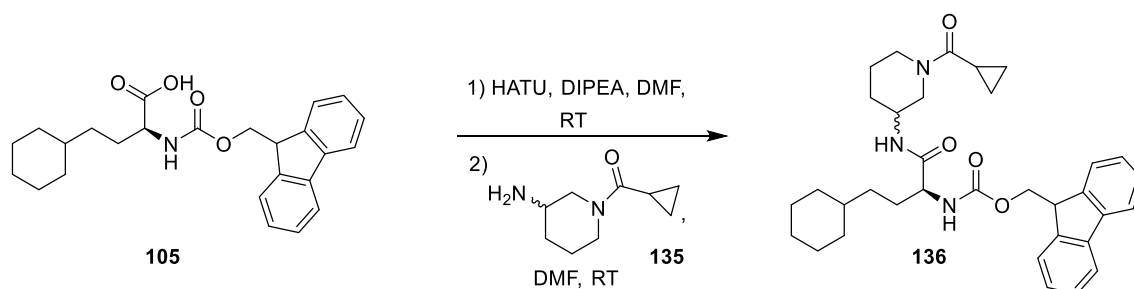
**Yield:** 636 mg (2.37 mmol, 95%), colorless solid.

- **TLC:** R<sub>f</sub> = 0.56 (SiO<sub>2</sub>, cyclohexane/EtOAc, 1:9, ninhydrin).
- **C<sub>14</sub>H<sub>24</sub>N<sub>2</sub>O<sub>3</sub>:** (268.35), [268.18].
- **<sup>1</sup>H-NMR (500 MHz, CDCl<sub>3</sub>, 300 K):** δ = 4.73–4.54 (m, 1H, NH), 4.05–2.84 (m, 5H, CH-3-, CH<sub>2</sub>-2-, CH<sub>2</sub>-6-piperidine), 1.97–1.86 (m, 1H, CH cyclopropyl), 1.81–1.49 (m, 4H, CH<sub>2</sub>-4-, CH<sub>2</sub>-5 piperidine), 1.42 (s, 9H, C(CH<sub>3</sub>)<sub>3</sub>), 1.01–0.89 (m, 2H, (CH<sub>A</sub>H<sub>B</sub>)<sub>2</sub> cyclopropyl), 0.80–0.66 (m, 2H, (CH<sub>A</sub>H<sub>B</sub>)<sub>2</sub> cyclopropyl) ppm.
- **<sup>13</sup>C-NMR (126 MHz, CDCl<sub>3</sub>, 300 K):** δ = 172.7, 155.3, 79.7, 50.4, 46.9, 42.7, 30.3, 28.8, 22.5, 11.0, 7.7 ppm.
- **MS (ESI pos.):** m/z (%) = 307.17 (23) ([M+K]<sup>+</sup>, calcd. 307.27), 291.20 (100) ([M+Na]<sup>+</sup>, calcd. 291.17), 269.21 (5) ([M+H]<sup>+</sup>, calcd. 269.19), 169.12 (32) ([M-Boc+H]<sup>+</sup>, calcd. 169.14).

***rac-(3-Aminopiperidin-1-yl)(cyclopropyl)methanone (135, SR151)***

*rac-tert-Butyl* (1-(cyclopropanecarbonyl)piperidin-3-yl)carbamate (**134**, 430 mg, 1.60 mmol) was dissolved in DCM (10 mL) cooled to 0 °C and TFA (2 mL) was added dropwise. The mixture was stirred for 1 h allowing to warm to RT. The solvent was removed under reduced pressure and the residue was dissolved in MeOH. The mixture was cooled to 5 °C, K<sub>2</sub>CO<sub>3</sub> (3.6 g, 26.0 mmol) was added and stirred for 10 min. The solid was filtered off and the solvent was removed under reduced pressure. The quantitatively obtained crude product was used without further purification in the next step.

**(9H-Fluoren-9-yl)methyl ((S)-4-cyclohexyl-1-(((SR)-1-(cyclopropanecarbonyl)piperidin-3-yl)amino)-1-oxobutan-2-yl)carbamate (136, SR153)**

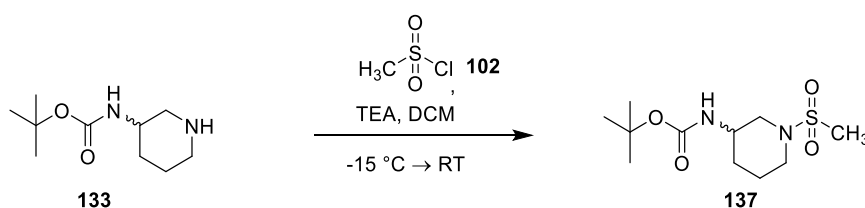


(S)-2-(((9H-Fluoren-9-yl)methoxy)carbonyl)amino)-4-cyclohexylbutanoic acid (**105**, 500 mg, 1.23 mmol) and HATU (560 mg, 1.47 mmol) were dissolved in DMF (dry, 10 mL) and DIPEA (190 mg, 1.47 mmol) was added. The reaction mixture was stirred for 1.5 h at RT and *rac*-(3-aminopiperidin-1-yl)(cyclopropyl)methanone (**135**, 248 mg, 1.47 mmol) dissolved in DMF (dry, 5 mL) was added. The mixture was stirred for additional 20 h at RT. EtOAc (100 mL) was added and the organic phase was washed 4 times with H<sub>2</sub>O (50 mL) and dried over MgSO<sub>4</sub>. The solvent was evaporated under reduced pressure and the crude product was purified using column chromatography on silica (cyclohexane/EtOAc 1:3 → 1:9).

**Yield:** 553 mg (0.992 mmol, 81%), colorless solid.

- **TLC:** R<sub>f</sub> = 0.37 (SiO<sub>2</sub>, cyclohexane/EtOAc, 1:3).
- **C<sub>34</sub>H<sub>43</sub>N<sub>3</sub>O<sub>4</sub>:** (557.72), [557.33].
- **<sup>1</sup>H-NMR (400 MHz, DMSO-d<sub>6</sub>, 300 K):** (mixture of diastereomers) δ = 7.96–7.80 (m, 3H, CONHCH, H-4-, H-5-Fmoc), 7.77–7.68 (m, 2H, H-1-, H-8-Fmoc), 7.46–7.37 (m, 3H, NHCOO, H-3-, H-6-Fmoc), 7.32 (t, <sup>3</sup>J = 7.4 Hz, 2H, H-2-, H-7-Fmoc), 4.33–4.13 (m, 3H, NHCHCO, OCH<sub>2</sub>), 4.09–3.78 (m, 2H, H-9-Fmoc, CH piperidine), 3.76–3.47 (m, 2H, CH<sub>2</sub>-2 piperidine), 3.39–3.05 (m, 2H, CH<sub>2</sub>-6 piperidine), 2.00–1.29 (m, 12H, CH<sub>2</sub>-5-, CH<sub>2</sub>-4 piperidine, CH cyclopropyl, NHCHCH<sub>2</sub>CH<sub>2</sub>, H-2<sub>eq</sub>-, H-3<sub>eq</sub>-, H-4<sub>eq</sub>-, H-5<sub>eq</sub>-, H-6<sub>eq</sub>-cyclohexyl), 1.27–1.03 (m, 6H, H-1-, H-3<sub>ax</sub>-, H-4<sub>ax</sub>-, H-5<sub>ax</sub>-cyclohexyl, NHCHCH<sub>2</sub>CH<sub>2</sub>), 0.91–0.77 (m, 2H, H-2<sub>ax</sub>-, H-6<sub>ax</sub>-cyclohexyl), 0.76–0.53 (m, 4H, CH(CH<sub>2</sub>)<sub>2</sub> cyclopropyl) ppm.
- **<sup>13</sup>C-NMR (101 MHz, DMSO-d<sub>6</sub>, 300 K):** (mixture of diastereomers) δ = 171.0, 170.9, 152.0 (2x), 143.9, 143.8, 140.7 (2x), 138.6, 127.6, 127.0, 125.3, 120.1 (2x), 65.5, 46.6, 36.8, 33.0, 32.9, 32.7, 32.6, 26.1, 25.8 (2x), 10.4, 6.8 ppm.
- **MS (ESI pos.):** m/z (%) = 580.43 (100) ([M+Na]<sup>+</sup>, calcd. 580.32).

***rac*-tert-Butyl (1-(methylsulfonyl)piperidin-3-yl)carbamate (137, SR148)**



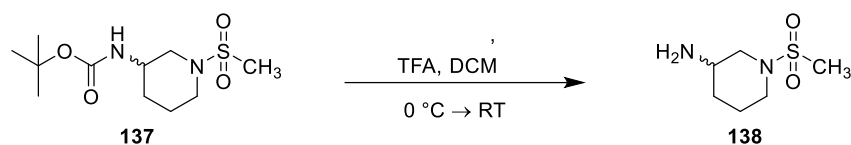
*rac*-tert-Butyl piperidin-3-ylcarbamate (**133**, 801 mg, 4.00 mmol) was dissolved in DCM (dry, 20 mL) and triethylamine (405 mg, 4.00 mmol) was added. The solution was cooled to -15 °C and methanesulfonyl chloride (**102**, 687 mg, 6.00 mmol) was added dropwise. The mixture was stirred for 6 h at RT. The reaction

mixture was acidified with  $\text{NH}_4\text{Cl}$  (sat., 3 mL) and extracted 3 times with DCM. The separated organic phase was washed 3 times with  $\text{H}_2\text{O}$  (20 mL) and dried over  $\text{MgSO}_4$ . The solvent was evaporated under reduced pressure to obtain a colorless solid.

**Yield:** 1.08 mg (3.88 mmol, 97%), colorless solid.

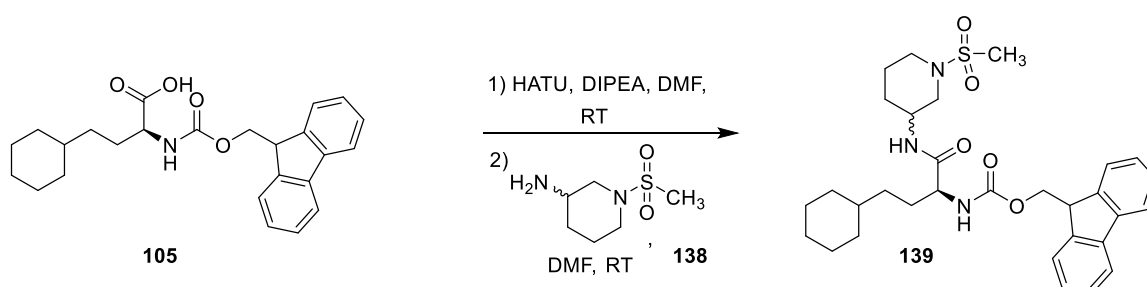
- **TLC:**  $R_f = 0.63$  ( $\text{SiO}_2$ , cyclohexane/EtOAc, 1:20, ninhydrin).
- **$\text{C}_{11}\text{H}_{22}\text{N}_2\text{O}_4\text{S}$ :** (278.37), [278.13].
- **$^1\text{H-NMR}$  (500 MHz,  $\text{CDCl}_3$ , 300 K):**  $\delta = 4.95\text{--}4.78$  (m, 1H, NH), 3.89–3.74 (m, 1H, CH piperidine), 3.72–2.95 (m, 4H,  $\text{CH}_2$ -2-,  $\text{CH}_2$ -6-piperidine), 2.77 (s, 3H,  $\text{SO}_2\text{CH}_3$ ), 1.88–1.57 (m, 4H,  $\text{CH}_2$ -4-,  $\text{CH}_2$ -5-piperidine), 1.43 (s, 9H,  $\text{C}(\text{CH}_3)_3$ ) ppm.
- **$^{13}\text{C-NMR}$  (126 MHz,  $\text{CDCl}_3$ , 300 K):**  $\delta = 155.0, 79.8, 50.8, 46.3, 45.6, 35.2, 29.2, 28.5, 22.1$  ppm.
- **MS (ESI neg.):**  $m/z$  (%) = 323.08 (84) ( $[\text{M}+\text{EtOH}-\text{H}]^-$ , calcd. 323.16), 313.06 (100) ( $[\text{M}+\text{Cl}]^-$ , calcd. 313.58), 162.95 (67) ( $[\text{M}_{\text{fr.}}]^-$ , calcd. 162.95), 160.92 (60) ( $[\text{M}_{\text{fr.}}-\text{H}]^-$ , calcd. 160.94).

***rac*-1-(Methylsulfonyl)piperidin-3-amine (138, SR150)**



*rac*-*tert*-Butyl (1-(methylsulfonyl)piperidin-3-yl)carbamate (**137**, 450 mg, 1.62 mmol) was dissolved in DCM (10 mL) cooled to 0 °C and TFA (2 mL) was added dropwise. The mixture was stirred for 1 h allowing to warm to RT. The solvent was removed under reduced pressure and the residue was dissolved in MeOH. The mixture was cooled to 5 °C,  $\text{K}_2\text{CO}_3$  (3.6 g, 26.0 mmol) was added and stirred for 10 min. The solid was filtered off and the solvent was removed under reduced pressure. The quantitatively obtained crude product was used without further purification in the next step.

**(9*H*-Fluoren-9-yl)methyl ((*S*)-4-cyclohexyl-1-(((*SR*)-1-(methylsulfonyl)piperidin-3-yl)amino)-1-oxobutan-2-yl)carbamate (139, SR244)**

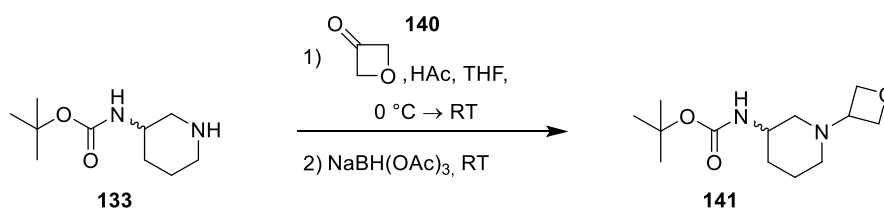


(*S*)-2-(((9*H*-Fluoren-9-yl)methoxy)carbonyl)amino-4-cyclohexylbutanoic acid (**105**, 500 mg, 1.23 mmol) and HATU (560 mg, 1.47 mmol) were dissolved in DMF (dry, 10 mL) and DIPEA (190 mg, 1.47 mmol) was added. The reaction mixture was stirred for 1.5 h at RT and *rac*-1-(methylsulfonyl)piperidin-3-amine (**138**, 262 mg, 1.47 mmol) dissolved in DMF (dry, 5 mL) was added. The mixture was stirred for additional 20 h at RT.  $\text{H}_2\text{O}$  (50 mL) was added and the resulting precipitate was filtered off, washed with  $\text{H}_2\text{O}$  and dried in a vacuum oven.

**Yield:** 655 mg (1.15 mmol, 94%), colorless solid.

- **TLC:**  $R_f = 0.44$  (SiO<sub>2</sub>, cyclohexane/EtOAc, 1:3).
- **C<sub>31</sub>H<sub>41</sub>N<sub>3</sub>O<sub>5</sub>S:** (567.74), [567.28].
- **<sup>1</sup>H-NMR (500 MHz, DMSO-d<sub>6</sub>, 300 K):** (mixture of diastereomers)  $\delta = 7.94$  (d,  $^3J = 7.4$  Hz, 1H, CONHCH), 7.89 (d,  $^3J = 7.5$  Hz, 2H, H-4-, H-5-Fmoc), 7.76–7.70 (m, 2H, H-1-, H-8-Fmoc), 7.46 (dd,  $^3J = 8.3, 3.0$  Hz, 1H, NHCOO), 7.42 (t,  $^3J = 7.5$  Hz, 2H, H-3-, H-6-Fmoc), 7.32 (td,  $^3J = 7.5, 3.4$  Hz, 2H, H-2-, H-7-Fmoc), 4.31–4.17 (m, 3H, NHCHCO, OCH<sub>2</sub>), 3.99–3.90 (m, 1H, H-9-Fmoc), 3.75–3.67 (m, 1H, CH piperidine), 3.51–3.39 (m, 1H, CH<sub>A</sub>H<sub>B</sub>-2 piperidine), 3.37–3.27 (m, 1H, CH<sub>A</sub>H<sub>B</sub>-2 piperidine), 2.87–2.82 (m, 3H, CH<sub>3</sub>), 2.81–2.73 (m, 1H, CH<sub>A</sub>H<sub>B</sub>-6 piperidine), 2.56–2.49 (m, 1H, CH<sub>A</sub>H<sub>B</sub>-6 piperidine), 1.83–1.69 (m, 2H, CH<sub>2</sub>-5 piperidine), 1.68–1.45 (m, 8H, CH<sub>2</sub>-4 piperidine, NHCHCH<sub>A</sub>H<sub>B</sub>CH<sub>2</sub>, H-2<sub>eq</sub>-, H-3<sub>eq</sub>-, H-4<sub>eq</sub>-, H-5<sub>eq</sub>-, H-6<sub>eq</sub>-cyclohexyl), 1.42–1.27 (m, 1H, NHCHCH<sub>A</sub>H<sub>B</sub>CH<sub>2</sub>), 1.26–1.05 (m, 6H, H-1-, H-3<sub>ax</sub>-, H-4<sub>ax</sub>-, H-5<sub>ax</sub>-cyclohexyl, NHCHCH<sub>2</sub>CH<sub>2</sub>), 0.90–0.77 (m, 2H, H-2<sub>ax</sub>-, H-6<sub>ax</sub>-cyclohexyl) ppm.
- **<sup>13</sup>C-NMR (126 MHz, DMSO-d<sub>6</sub>, 300 K):** (mixture of diastereomers)  $\delta = 170.7$  (2x), 155.9 (2x), 143.9, 143.8, 140.7 (2x), 127.6, 127.0, 125.4, 120.1, 65.6, 54.8, 54.7, 49.6, 49.4, 46.7, 45.4, 45.1, 45.0, 36.8 (2x), 34.6, 34.2, 33.1, 32.9 (2x), 32.7, 32.6, 29.7, 28.9, 28.6, 26.2, 25.8 (2x), 23.0, 22.9 ppm.
- **MS (ESI pos.):**  $m/z$  (%) = 586.32 (100) ([M+H]<sup>+</sup>, calcd. 586.29), 346.21 (62) ([M-Fmoc+H]<sup>+</sup>, calcd. 346.22).

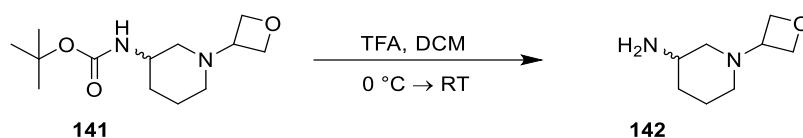
***rac-tert-Butyl (1-(oxetan-3-yl)piperidin-3-yl)carbamate (141, SR168)***



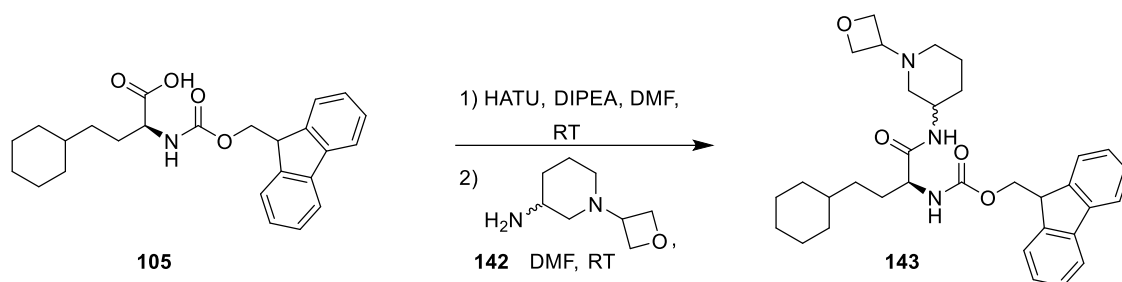
*rac-tert-Butyl piperidin-3-ylcarbamate (133, 400 mg, 2.00 mmol)* was dissolved in THF (dry, 10 mL) and oxetan-3-one (**140**, 107  $\mu$ L, 1.66 mmol) was added at 0 °C. The mixture was stirred for 1.5 h and allowed to warm to RT. Sodium triacetoxyborohydride (708 mg, 3.33 mmol) was added and the suspension was stirred for additional 20 h at RT. The reaction was quenched with NaHCO<sub>3</sub> (sat., 30 mL) and the solvent was evaporated under reduced pressure. The residue was dissolved in EtOAc (30 mL), H<sub>2</sub>O (30 mL) was added and extracted 4 times with EtOAc (30 mL). The organic phase was dried over MgSO<sub>4</sub>. The solvent was evaporated under reduced pressure and the crude product was purified using column chromatography on silica (cyclohexane/EtOAc 1:20 + 1% TEA).

**Yield:** 240 mg (0.937 mmol, 47%), colorless solid.

- **TLC:**  $R_f = 0.20$  (SiO<sub>2</sub>, cyclohexane/EtOAc + 1% TEA, 1:20, ninhydrin).
- **C<sub>13</sub>H<sub>24</sub>N<sub>2</sub>O<sub>3</sub>:** (256.34), [256.18].
- **<sup>1</sup>H-NMR (500 MHz, CDCl<sub>3</sub>, 300 K):**  $\delta = 5.16$ –4.92 (m, 1H, NH), 4.66–4.50 (m, 4H, 2xCH<sub>2</sub> oxetane), 3.82–3.69 (m, 1H, CH piperidine), 3.41 (p,  $^3J = 6.4$  Hz, 1H, CH oxetane), 2.47–1.83 (m, 4H, CH<sub>2</sub>-2-, CH<sub>2</sub>-6-piperidine), 1.81–1.33 (m, 4H, CH<sub>2</sub>-4-, CH<sub>2</sub>-5-piperidine), 1.43 (s, 9H, CH<sub>3</sub>) ppm.
- **<sup>13</sup>C-NMR (126 MHz, CDCl<sub>3</sub>, 300 K):**  $\delta = 155.2, 79.3, 75.9, 59.1, 55.2, 50.2, 45.8, 29.6, 28.6, 21.9$  ppm.
- **MS (ESI neg.):**  $m/z$  (%) = 255.20 (100) ([M-H]<sup>-</sup>, calcd. 255.17).

***rac*-1-(Oxetan-3-yl)piperidin-3-amine (142, SR199)**

*rac*-*tert*-Butyl (1-(oxetan-3-yl)piperidin-3-yl)carbamate (**141**, 350 mg, 1.37 mmol) was dissolved in DCM (10 mL) cooled to 0 °C and TFA (2 mL) was added dropwise. The mixture was stirred for 1 h allowing to warm to RT. The solvent was removed under reduced pressure and the residue was dissolved in EtOH. The mixture was cooled to 5 °C, K<sub>2</sub>CO<sub>3</sub> (3.6 g, 26.0 mmol) was added and stirred for 10 min. The solid was filtered off and the solvent was removed under reduced pressure. The quantitatively obtained crude product was used without further purification in the next step.

***(9H-Fluoren-9-yl)methyl ((S)-4-cyclohexyl-1-(((SR)-1-(oxetan-3-yl)piperidin-3-yl)amino)-1-oxobutan-2-yl)carbamate (143, SR200)***

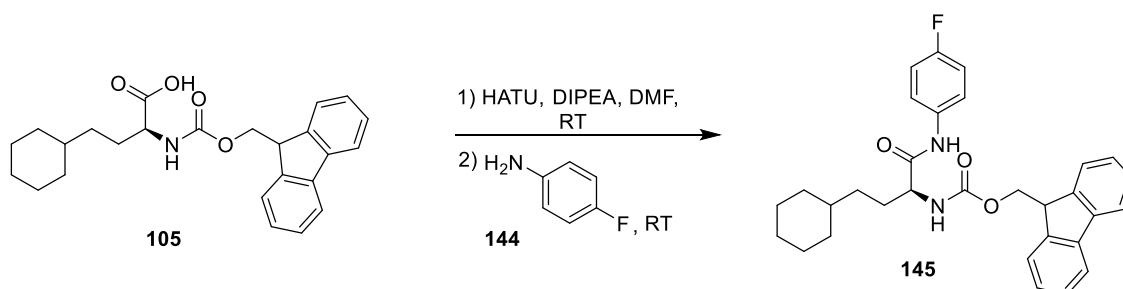
(*S*)-2-(((9*H*-Fluoren-9-yl)methoxy)carbonyl)amino-4-cyclohexylbutanoic acid (**105**, 463 mg, 1.14 mmol) and HATU (432 mg, 1.36 mmol) were dissolved in DMF (dry, 4 mL) and DIPEA (147 mg, 1.36 mmol) was added. The reaction mixture was stirred for 1.5 h at RT and *rac*-1-(oxetan-3-yl)piperidin-3-amine (**142**, 213 mg, 1.36 mmol) dissolved in DMF (dry, 4 mL) was added. The mixture was stirred for additional 4 h at RT. DCM (50 mL) was added and the organic phase was washed 4 times with H<sub>2</sub>O (50 mL) and dried over MgSO<sub>4</sub>. The solvent was evaporated under reduced pressure and the crude product was purified by column chromatography on silica (cyclohexane/EtOAc 1:1 → 1:20 → EtOAc).

**Yield:** 595 mg (1.09 mmol, 96%), colorless solid.

- **TLC:** R<sub>f</sub> = 0.20 (SiO<sub>2</sub>, cyclohexane/EtOAc, 1:20).
- **C<sub>33</sub>H<sub>43</sub>N<sub>3</sub>O<sub>4</sub>:** (545.71), [545.33].
- **<sup>1</sup>H-NMR (500 MHz, DMSO-*d*<sub>6</sub>, 300 K):** (mixture of diastereomers) δ = 7.89 (d, <sup>3</sup>J = 7.6 Hz, 2H, H-4-, H-5-Fmoc), 7.78–7.69 (m, 3H, CONHCH, H-1-, H-8-Fmoc), 7.47–7.38 (m, 3H, NHCOO, H-3-, H-6-Fmoc), 7.31 (t, <sup>3</sup>J = 7.4 Hz, 2H, H-2-, H-7-Fmoc), 4.52–4.43 (m, 2H, CH(CH<sub>A</sub>H<sub>B</sub>)<sub>2</sub> oxetane), 4.41–4.31 (m, 2H, CH(CH<sub>A</sub>H<sub>B</sub>)<sub>2</sub> oxetane), 4.30–4.17 (m, 3H, NHCHCO, OCH<sub>2</sub>), 3.96–3.87 (m, 1H, H-9-Fmoc), 3.76–3.66 (m, 1H, CH piperidine), 3.40–3.28 (m, 3H, CH<sub>2</sub>-2 piperidine, CH oxetane), 2.55–2.32 (m, 2H, CH<sub>2</sub>-6 piperidine), 1.92–1.39 (m, 11H, CH<sub>2</sub>-4-, CH<sub>2</sub>-5-piperidine, NHCHCH<sub>2</sub>, H-2<sub>eq</sub><sup>-</sup>, H-3<sub>eq</sub><sup>-</sup>, H-4<sub>eq</sub><sup>-</sup>, H-5<sub>eq</sub><sup>-</sup>, H-6<sub>eq</sub>-cyclohexyl), 1.31–1.04 (m, 6H, H-1-, H-3<sub>ax</sub><sup>-</sup>, H-4<sub>ax</sub><sup>-</sup>, H-5<sub>ax</sub>-cyclohexyl, NHCHCH<sub>A</sub>H<sub>B</sub>CH<sub>2</sub>), 0.91–0.76 (m, 2H, H-2<sub>ax</sub><sup>-</sup>, H-6<sub>ax</sub>-cyclohexyl) ppm.

- **$^{13}\text{C}$ -NMR (126 MHz, DMSO- $d_6$ , 300 K):** (mixture of diastereomers)  $\delta$  = 171.3, 171.2, 155.9 (2x), 143.9, 143.8, 140.7, 127.6, 127.0, 125.3 (2x), 120.1, 74.6 (3x), 74.5, 65.6 (2x), 58.4 (2x), 54.8, 54.4, 54.3, 49.2, 46.7, 45.1, 38.3, 36.8, 36.7, 33.0, 32.9, 32.7 (2x), 29.7, 29.6, 29.5, 26.2, 25.8, 22.9 ppm.
- **MS (ESI pos.):**  $m/z$  (%) = 546.31 (100) ( $[\text{M}+\text{H}]^+$ , calcd. 546.34).

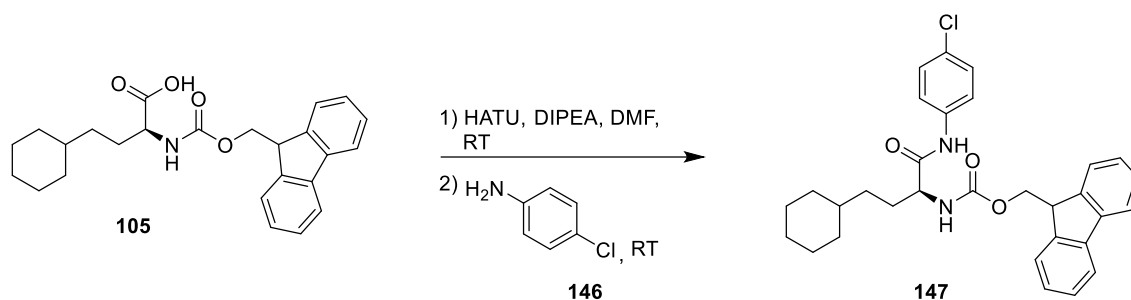
**(S)-(9H-Fluoren-9-yl)methyl (4-cyclohexyl-1-((4-fluorophenyl)amino)-1-oxobutan-2-yl)carbamate (145, SR340)**



(S)-2-(((9H-Fluoren-9-yl)methoxy)carbonyl)amino-4-cyclohexylbutanoic acid (**105**, 400 mg, 0.982 mmol) and HATU (448 mg, 1.18 mmol) were dissolved in DMF (dry, 10 mL) and DIPEA (152 mg, 1.18 mmol) was added. The reaction mixture was stirred for 1 h at RT and 4-fluoroaniline (**144**, 112  $\mu\text{L}$ , 1.18 mmol) was added. The mixture was stirred for additional 24 h at RT. DCM (150 mL) was added and the organic phase was washed 4 times with  $\text{H}_2\text{O}$  (150 mL) and dried over  $\text{MgSO}_4$ . The solvent was evaporated under reduced pressure and the crude product was recrystallized from acetone.

**Yield:** 438 mg (0.875 mmol, 89%), colorless solid.

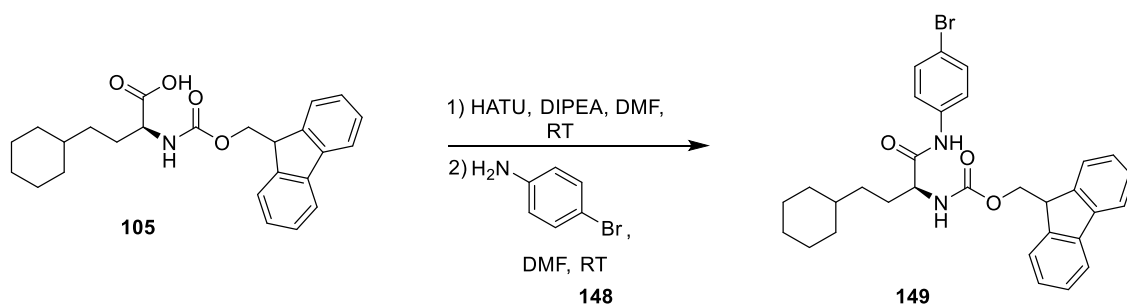
- **TLC:**  $R_f$  = 0.26 ( $\text{SiO}_2$ , cyclohexane/EtOAc, 4:1).
- **$\text{C}_{31}\text{H}_{33}\text{FN}_2\text{O}_3$ :** (500.60), [500.25].
- **$^1\text{H}$ -NMR (600 MHz, DMSO- $d_6$ , 300 K):**  $\delta$  = 10.06 (s, 1H, NH phenyl), 7.89 (d,  $^3J$  = 7.6 Hz, 2H, H-4-, H-5-Fmoc), 7.74 (t,  $^3J$  = 7.6 Hz, 2H, H-3-, H-6-Fmoc), 7.66–7.60 (m, 3H, NHCOO, H-2-, H-6-phenyl), 7.41 (td,  $^3J$  = 7.5, 3.3 Hz, 2H, H-1-, H-8-Fmoc), 7.32 (td,  $^3J$  = 7.5, 3.2 Hz, 2H, H-2-, H-7-Fmoc), 7.14 (t,  $^3J$  = 8.9 Hz, 2H, H-3-, H-5-phenyl), 4.32–4.18 (m, 3H,  $\text{OCH}_2$ ,  $\text{NHCHCO}$ ), 4.12–4.02 (m, 1H, H-9-Fmoc), 1.75–1.55 (m, 7H,  $\text{NHCHCH}_2\text{CH}_2$ , H-2 $_{\text{eq}}$ , H-3 $_{\text{eq}}$ , H-4 $_{\text{eq}}$ , H-5 $_{\text{eq}}$ , H-6 $_{\text{eq}}$ -cyclohexyl), 1.33–1.26 (m, 1H, H-1 cyclohexyl), 1.25–1.07 (m, 5H, H-3 $_{\text{ax}}$ , H-4 $_{\text{ax}}$ , H-5 $_{\text{ax}}$ -cyclohexyl,  $\text{NHCHCH}_2\text{CH}_2$ ), 0.90–0.79 (m, 2H, H-2 $_{\text{ax}}$ , H-6 $_{\text{ax}}$ -cyclohexyl) ppm.
- **$^{13}\text{C}$ -NMR (150 MHz, DMSO- $d_6$ , 300 K):**  $\delta$  = 171.0, 158.0 ( $^1J_{\text{CF}}$  = 241.9 Hz), 156.0, 143.8, 143.7, 140.7, 135.3, 127.6, 127.0, 125.3, 120.9, 120.0 ( $^3J_{\text{CF}}$  = 8.1 Hz), 115.2 ( $^2J_{\text{CF}}$  = 22.3 Hz), 65.6, 55.6, 46.6, 36.8, 33.1, 32.8, 32.6, 29.3, 26.1, 25.7 (2x) ppm.
- **MS (ESI pos.):**  $m/z$  (%) = 523.23 (52) ( $[\text{M}+\text{Na}]^+$ , calcd. 523.24), 501.27 (47) ( $[\text{M}+\text{H}]^+$ , calcd. 501.26), 279.25 (25) ( $[\text{M}-\text{Fmoc}+\text{H}]^+$ , calcd. 279.25), 179.28 (100) ( $[\text{M}_{\text{fr}}+\text{H}]^+$ , calcd. 179.29).

**(S)-2-(((9H-Fluoren-9-yl)methyl (1-((4-chlorophenyl)amino)-4-cyclohexyl-1-oxobutan-2-yl)carbamate (147, SR327)**

(S)-2-(((9H-Fluoren-9-yl)methoxy)carbonyl)amino)-4-cyclohexylbutanoic acid (**105**, 400 mg, 0.982 mmol) and HATU (448 mg, 1.18 mmol) were dissolved in DMF (dry, 10 mL) and DIPEA (152 mg, 1.18 mmol) was added. The reaction mixture was stirred for 1 h at RT and 4-chloroaniline (**146**, 150 mg, 1.18 mmol) was added. The mixture was stirred for additional 20 h at RT. DCM (100 mL) was added and the organic phase was washed 4 times with H<sub>2</sub>O (100 mL) and dried over MgSO<sub>4</sub>. The solvent was evaporated under reduced pressure and the crude product was purified using column chromatography on silica (cyclohexane/EtOAc, 4:1 → 1:1 → 1:3).

**Yield:** 439 mg (0.849 mmol, 86%), colorless solid.

- **TLC:** R<sub>f</sub> = 0.87 (SiO<sub>2</sub>, cyclohexane/EtOAc, 1:1).
- **C<sub>31</sub>H<sub>33</sub>ClN<sub>2</sub>O<sub>3</sub>:** (517.06), [516.22].
- **<sup>1</sup>H-NMR (250 MHz, DMSO-d<sub>6</sub>, 300 K):** δ = 10.14 (s, 1H, NH phenyl), 7.89 (d, <sup>3</sup>J = 7.4 Hz, 2H, H-4-, H-5-Fmoc), 7.74–7.59 (m, 5H, H-3-, H-6-Fmoc, NHCOO, H-2-, H-6-phenyl), 7.46–7.26 (m, 6H, H-1-, H-2-, H-7-, H-8-Fmoc, H-3-, H-5-phenyl), 4.32–4.17 (m, 3H, OCH<sub>2</sub>, NHCHCO), 4.15–4.03 (m, 1H, H-9-Fmoc), 1.78–1.52 (m, 7H, NHCHCH<sub>2</sub>CH<sub>2</sub>, H-2<sub>eq</sub>-, H-3<sub>eq</sub>-, H-4<sub>eq</sub>-, H-5<sub>eq</sub>-, H-6<sub>eq</sub>-cyclohexyl), 1.35–1.04 (m, 6H, H-1-, H-3<sub>ax</sub>-, H-4<sub>ax</sub>-, H-5<sub>ax</sub>-cyclohexyl, NHCHCH<sub>2</sub>CH<sub>2</sub>), 0.96–0.75 (m, 2H, H-2<sub>ax</sub>-, H-6<sub>ax</sub>-cyclohexyl) ppm.
- **<sup>13</sup>C-NMR (126 MHz, CDCl<sub>3</sub>, 300 K):** δ = 170.2, 156.8, 143.9, 141.4, 136.2, 129.6, 129.1, 128.0, 127.3, 125.1, 121.4, 120.2, 67.4, 56.2, 47.2, 37.6, 33.4, 33.3, 29.8, 29.6, 27.1, 26.6, 26.4 ppm.
- **MS (ESI pos.):** m/z (%) = 539.23 (58) ([M+Na]<sup>+</sup>, calcd. 539.21), 517.26 (100) ([M+H]<sup>+</sup>, calcd. 517.23), 295.21 (23) ([M-Fmoc+H]<sup>+</sup>, calcd. 295.16), 179.29 (95) ([M<sub>fr.</sub>+H]<sup>+</sup>, calcd. 179.09).

**(S)-2-(((9H-Fluoren-9-yl)methyl (1-((4-bromophenyl)amino)-4-cyclohexyl-1-oxobutan-2-yl)carbamate (149, SR337)**

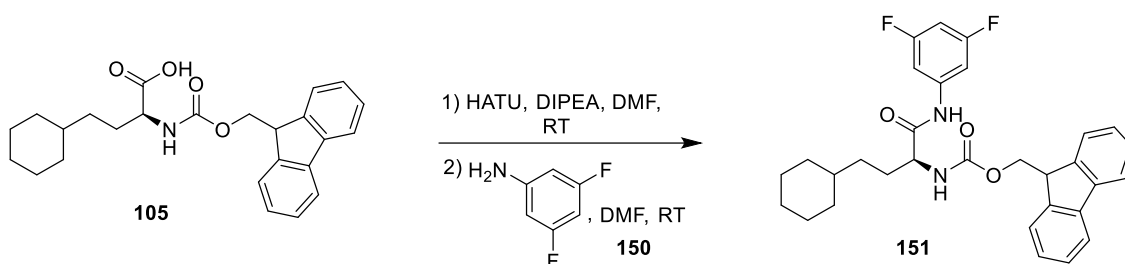


(*S*)-2-((((9*H*-Fluoren-9-yl)methoxy)carbonyl)amino)-4-cyclohexylbutanoic acid (**105**, 400 mg, 0.982 mmol) and HATU (448 mg, 1.18 mmol) were dissolved in DMF (dry, 6 mL) and DIPEA (152 mg, 1.18 mmol) was added. The reaction mixture was stirred for 1 h at RT and 4-bromoaniline (**148**, 203 mg, 1.18 mmol) dissolved in DMF (dry, 4 mL) was added. The mixture was stirred for additional 3 d at RT. DCM (150 mL) was added and the organic phase was washed 4 times with H<sub>2</sub>O (150 mL) and dried over MgSO<sub>4</sub>. The solvent was evaporated under reduced pressure and the crude product was purified using column chromatography on silica (cyclohexane/EtOAc 4:1 → 1:1 → 1:3 → 1:20). The product was further recrystallized from acetone.

**Yield:** 487 mg (0.867 mmol, 88%), colorless solid.

- **TLC:** R<sub>f</sub> = 0.36 (SiO<sub>2</sub>, cyclohexane/EtOAc, 4:1).
- **C<sub>31</sub>H<sub>33</sub>BrN<sub>2</sub>O<sub>3</sub>:** (561.51), [560.17].
- **<sup>1</sup>H-NMR (600 MHz, DMSO-d<sub>6</sub>, 300 K):** δ = 10.15 (s, 1H, NH 4-bromophenyl), 7.89 (d, <sup>3</sup>J = 7.6 Hz, 2H, H-4-, H-5-Fmoc), 7.74 (t, <sup>3</sup>J = 7.6 Hz, 2H, H-3-, H-6-Fmoc), 7.66 (d, <sup>3</sup>J = 7.9 Hz, 1H, NHCOO), 7.58 (d, <sup>3</sup>J = 8.7 Hz, 2H, H-3-, H-5-phenyl), 7.48 (d, <sup>3</sup>J = 8.7 Hz, 2H, H-2-, H-6-phenyl), 7.44–7.38 (m, 2H, H-1-, H-8-Fmoc), 7.34–7.29 (m, 2H, H-2-, H-7-Fmoc), 4.32–4.20 (m, 3H, OCH<sub>2</sub>, NHCHCO), 4.12–4.06 (m, 1H, H-9-Fmoc), 1.76–1.56 (m, 7H, NHCHCH<sub>2</sub>CH<sub>2</sub>, H-2<sub>eq</sub>-, H-3<sub>eq</sub>-, H-4<sub>eq</sub>-, H-5<sub>eq</sub>-, H-6<sub>eq</sub>-cyclohexyl), 1.33–1.25 (m, 1H, H-1 cyclohexyl), 1.24–1.06 (m, 5H, H-3<sub>ax</sub>-, H-4<sub>ax</sub>-, H-5<sub>ax</sub>-cyclohexyl, NHCHCH<sub>2</sub>CH<sub>2</sub>), 0.91–0.80 (m, 2H, H-2<sub>ax</sub>-, H-6<sub>ax</sub>-cyclohexyl) ppm.
- **<sup>13</sup>C-NMR (150 MHz, DMSO-d<sub>6</sub>, 300 K):** δ = 170.3, 155.0, 142.8, 142.7, 139.7, 137.3, 130.5, 126.6, 126.0, 124.3, 120.1, 119.0, 113.8, 64.6, 54.7, 45.6, 35.8, 32.1, 31.8, 31.6, 28.2, 25.1, 24.7 (2x) ppm.
- **MS (ESI pos.):** *m/z* (%) = 563.17 (16) ([M+H]<sup>+</sup>, calcd. 563.18), 561.17 (15) ([M+H]<sup>+</sup>, calcd. 561.18), 179.29 (100) ([M<sub>fr.</sub>+H]<sup>+</sup>, calcd. 179.09).

**(*S*)-(9*H*-Fluoren-9-yl)methyl (4-cyclohexyl-1-((3,5-difluorophenyl)amino)-1-oxobutan-2-yl)carbamate (**151**, SR338)**



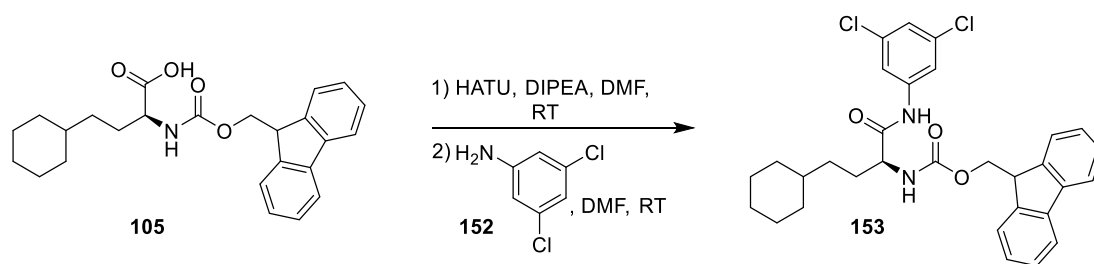
(*S*)-2-((((9*H*-Fluoren-9-yl)methoxy)carbonyl)amino)-4-cyclohexylbutanoic acid (**105**, 400 mg, 0.982 mmol) and HATU (448 mg, 1.18 mmol) were dissolved in DMF (dry, 6 mL) and DIPEA (152 mg, 1.18 mmol) was added. The reaction mixture was stirred for 1 h at RT and 3,5-difluoroaniline (**150**, 152 mg, 1.18 mmol) dissolved in DMF (dry, 4 mL) was added. The mixture was stirred for additional 3 d at RT. DCM (150 mL) was added and the organic phase was washed 4 times with H<sub>2</sub>O (150 mL) and dried over MgSO<sub>4</sub>. The solvent was evaporated under reduced pressure and the crude product was purified using column chromatography on silica (cyclohexane/EtOAc 4:1 → 1:1 → 1:3 → 1:20). The product was further recrystallized from acetone.

**Yield:** 410 mg (0.791 mmol, 81%), colorless solid.

- **TLC:** R<sub>f</sub> = 0.37 (SiO<sub>2</sub>, cyclohexane/EtOAc, 4:1).
- **C<sub>31</sub>H<sub>32</sub>F<sub>2</sub>N<sub>2</sub>O<sub>3</sub>:** (518.59), [518.24].

- **<sup>1</sup>H-NMR (600 MHz, DMSO-d<sub>6</sub>, 300 K):**  $\delta$  = 10.41 (s, 1H, NH phenyl), 7.89 (d, <sup>3</sup>J = 7.4 Hz, 2H, H-4-, H-5-Fmoc), 7.76–7.69 (m, 3H, H-1-, H-8-Fmoc, NHCOO), 7.44–7.39 (m, 2H, H-3-, H-6-Fmoc), 7.37–7.29 (m, 4H, H-2-, H-7-Fmoc, H-2-, H-6-phenyl), 6.96–6.86 (m, 1H, H-4 phenyl), 4.33–4.17 (m, 3H, OCH<sub>2</sub>, NHCHCO), 4.10–4.03 (m, 1H, H-9-Fmoc), 1.75–1.54 (m, 7H, NHCHCH<sub>2</sub>CH<sub>2</sub>, H-2<sub>eq</sub><sup>-</sup>, H-3<sub>eq</sub><sup>-</sup>, H-4<sub>eq</sub><sup>-</sup>, H-5<sub>eq</sub><sup>-</sup>, H-6<sub>eq</sub>-cyclohexyl), 1.35–1.25 (m, 1H, H-1 cyclohexyl), 1.24–1.05 (m, 5H, H-3<sub>ax</sub><sup>-</sup>, H-4<sub>ax</sub><sup>-</sup>, H-5<sub>ax</sub><sup>-</sup> cyclohexyl, NHCHCH<sub>2</sub>CH<sub>2</sub>), 0.91–0.80 (m, 2H, H-2<sub>ax</sub><sup>-</sup>, H-6<sub>ax</sub>-cyclohexyl) ppm.
- **<sup>13</sup>C-NMR (150 MHz, DMSO-d<sub>6</sub>, 300 K):**  $\delta$  = 172.5, 171.9, 162.4 (<sup>1</sup>J<sub>CF</sub> = 243.5 Hz), 162.3 (<sup>1</sup>J<sub>CF</sub> = 243.5 Hz), 156.1, 143.8, 143.7, 141.5, 141.4, 140.7, 127.6, 127.0, 125.2, 120.0, 102.0 (<sup>2</sup>J<sub>CF</sub> = 28.9 Hz), 98.5 (<sup>2</sup>J<sub>CF</sub> = 28.9 Hz), 65.6, 55.8, 46.6, 36.8, 33.1, 32.8, 32.6, 29.0, 26.1, 25.7 (2x) ppm.
- **MS (ESI pos.):** *m/z* (%) = 541.21 (16) ([M+Na]<sup>+</sup>, calcd. 541.23), 519.18 (22) ([M+H]<sup>+</sup>, calcd. 519.25), 297.20 (11) ([M-Fmoc+H]<sup>+</sup>, calcd. 297.18), 179.30 (100) ([M<sub>fr.</sub>+H]<sup>+</sup>, calcd. 179.09).

**(S)-(9H-Fluoren-9-yl)methyl (4-cyclohexyl-1-((3,5-dichlorophenyl)amino)-1-oxobutan-2-yl)carbamate (153, SR334)**

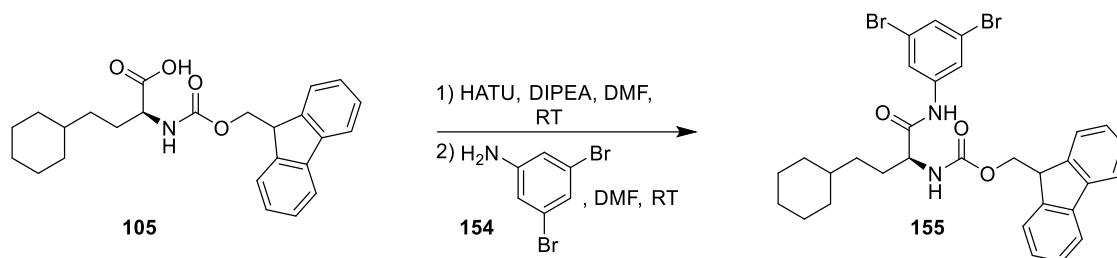


(S)-2-(((9H-Fluoren-9-yl)methoxy)carbonyl)amino-4-cyclohexylbutanoic acid (**105**, 400 mg, 0.982 mmol) and HATU (448 mg, 1.18 mmol) were dissolved in DMF (dry, 8 mL) and DIPEA (152 mg, 1.18 mmol) was added. The reaction mixture was stirred for 1 h at RT and 3,5-dichloroaniline (**152**, 191 mg, 1.18 mmol) was added. The mixture was stirred for additional 24 h at RT. DCM (150 mL) was added and the organic phase was washed with brine (100 mL), 3 times with H<sub>2</sub>O (150 mL) and dried over MgSO<sub>4</sub>. The solvent was evaporated under reduced pressure and the crude product was purified using column chromatography on silica (cyclohexane/EtOAc 4:1 → 1:1 → 1:3). The product was further recrystallized from MeOH.

**Yield:** 285 mg (0.553 mmol, 56%), colorless solid.

- **TLC:** R<sub>f</sub> = 0.45 (SiO<sub>2</sub>, cyclohexane/EtOAc, 4:1).
- **C<sub>31</sub>H<sub>32</sub>Cl<sub>2</sub>N<sub>2</sub>O<sub>3</sub>:** (551.50), [550.18].
- **<sup>1</sup>H-NMR (500 MHz, DMSO-d<sub>6</sub>, 300 K):**  $\delta$  = 10.38 (s, 1H, NH phenyl), 7.89 (d, <sup>3</sup>J = 7.6 Hz, 2H, H-4-, H-5-Fmoc), 7.76–7.71 (m, 3H, H-1-, H-8-Fmoc, NHCOO), 7.69 (d, <sup>4</sup>J = 1.8 Hz, 2H, H-2-, H-6-phenyl), 7.41 (t, <sup>3</sup>J = 7.5 Hz, 2H, H-3-, H-6-Fmoc), 7.32 (t, <sup>3</sup>J = 7.5 Hz, 2H, H-2-, H-7-Fmoc), 7.28 (t, <sup>4</sup>J = 1.7 Hz, 1H, H-4-phenyl), 4.33–4.12 (m, 3H, OCH<sub>2</sub>, NHCHCO), 4.08–4.01 (m, 1H, H-9-Fmoc), 1.76–1.55 (m, 7H, NHCHCH<sub>2</sub>CH<sub>2</sub>, H-2<sub>eq</sub><sup>-</sup>, H-3<sub>eq</sub><sup>-</sup>, H-4<sub>eq</sub><sup>-</sup>, H-5<sub>eq</sub><sup>-</sup>, H-6<sub>eq</sub>-cyclohexyl), 1.34–1.24 (m, 1H, H-1 cyclohexyl), 1.23–1.05 (m, 5H, H-3<sub>ax</sub><sup>-</sup>, H-4<sub>ax</sub><sup>-</sup>, H-5<sub>ax</sub>-cyclohexyl, NHCHCH<sub>2</sub>CH<sub>2</sub>), 0.90–0.78 (m, 2H, H-2<sub>ax</sub><sup>-</sup>, H-6<sub>ax</sub>-cyclohexyl) ppm.
- **<sup>13</sup>C-NMR (126 MHz, DMSO-d<sub>6</sub>, 300 K):**  $\delta$  = 172.0, 156.1, 143.8 (2x), 141.2, 140.7, 134.1, 127.6, 127.0, 125.3 (2x), 122.5, 120.1 (2x), 117.3, 65.6, 55.9, 46.7, 36.8, 33.2, 32.9, 32.6, 29.0, 26.1, 25.8 (2x) ppm.
- **MS (ESI pos.):** *m/z* (%) = 573.17 (12) ([M+Na]<sup>+</sup>, calcd. 573.13), 551.20 (18) ([M+H]<sup>+</sup>, calcd. 551.19), 179.17 (100) ([M<sub>fr.</sub>+H]<sup>+</sup>, calcd. 179.09).

**(S)-(9H-Fluoren-9-yl)methyl (4-cyclohexyl-1-((3,5-dibromophenyl)amino)-1-oxobutan-2-yl)carbamate (155, SR339)**

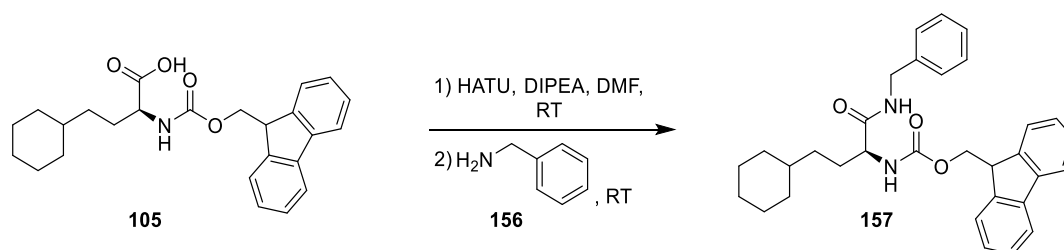


(S)-2-(((9H-Fluoren-9-yl)methoxy)carbonyl)amino-4-cyclohexylbutanoic acid (**105**, 400 mg, 0.982 mmol) and HATU (448 mg, 1.18 mmol) were dissolved in DMF (dry, 6 mL) and DIPEA (152 mg, 1.18 mmol) was added. The reaction mixture was stirred for 1 h at RT and 3,5-dibromoaniline (**154**, 296 mg, 1.18 mmol) dissolved in DMF (dry, 4 mL) was added. The mixture was stirred for additional 20 h at RT. DCM (150 mL) was added and the organic phase was washed 4 times with H<sub>2</sub>O (150 mL) and dried over MgSO<sub>4</sub>. The solvent was evaporated under reduced pressure and the crude product was purified using column chromatography on silica (cyclohexane/EtOAc 4:1 → 1:1).

**Yield:** 404 mg (0.631 mmol, 64%), colorless solid.

- **TLC:** R<sub>f</sub> = 0.43 (SiO<sub>2</sub>, cyclohexane/EtOAc, 4:1).
- **C<sub>31</sub>H<sub>32</sub>Br<sub>2</sub>N<sub>2</sub>O<sub>3</sub>:** (640.41), [638.08].
- **<sup>1</sup>H-NMR (600 MHz, DMSO-d<sub>6</sub>, 300 K):** δ = 10.31 (s, 1H, NH phenyl), 7.91–7.85 (m, 4H, H-2-, H-6-phenyl, H-4-, H-5-Fmoc), 7.76–7.68 (m, 3H, H-1-, H-8-Fmoc, NHCOO), 7.50–7.48 (m, 1H, H-4-phenyl), 7.43–7.39 (m, 2H, H-3-, H-6-Fmoc), 7.32 (t, <sup>3</sup>J = 7.4 Hz, 2H, H-2-, H-7-Fmoc), 4.34–4.19 (m, 3H, OCH<sub>2</sub>, NHCHCO), 4.07–4.00 (m, 1H, H-9-Fmoc), 1.75–1.56 (m, 7H, NHCHCH<sub>2</sub>CH<sub>2</sub>, H-2<sub>eq</sub>-, H-3<sub>eq</sub>-, H-4<sub>eq</sub>-, H-5<sub>eq</sub>-, H-6<sub>eq</sub>-cyclohexyl), 1.33–1.25 (m, 1H, H-1 cyclohexyl), 1.23–1.06 (m, 5H, H-3<sub>ax</sub>-, H-4<sub>ax</sub>-, H-5<sub>ax</sub>-cyclohexyl, NHCHCH<sub>2</sub>CH<sub>2</sub>), 0.90–0.80 (m, 2H, H-2<sub>ax</sub>-, H-6<sub>ax</sub>-cyclohexyl) ppm.
- **<sup>13</sup>C-NMR (150 MHz, DMSO-d<sub>6</sub>, 300 K):** δ = 171.9, 156.1, 143.8, 143.7, 141.5, 141.4, 140.7, 127.8, 127.6, 127.0, 125.2, 122.3, 120.5, 120.0, 65.6, 55.9, 46.6, 36.8, 33.1, 32.8, 32.6, 28.9, 26.1, 25.7 (2x) ppm.
- **MS (ESI neg.):** m/z (%) = 675.20 (8) ([M+Cl]<sup>-</sup>, calcd. 675.53), 417.23 (100) ([M-Fmoc+H]<sup>-</sup>, calcd. 417.00).

**(S)-(9H-Fluoren-9-yl)methyl (1-(benzylamino)-4-cyclohexyl-1-oxobutan-2-yl)carbamate (157, SR74)**



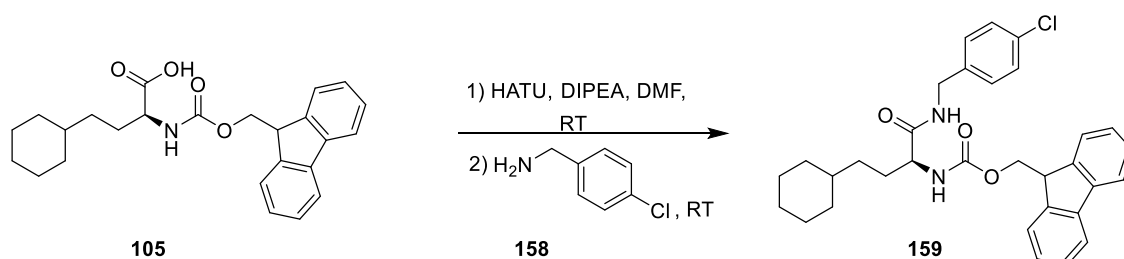
(S)-2-(((9H-Fluoren-9-yl)methoxy)carbonyl)amino-4-cyclohexylbutanoic acid (**105**, 400 mg, 1.18 mmol) and HATU (448 mg, 1.18 mmol) were dissolved in DMF (dry, 10 mL) and DIPEA (152 mg, 1.18 mmol) was added. The reaction mixture was stirred for 1.5 h at RT and phenylmethanamine (**156**, 126 mg, 1.18 mmol)

was added. The mixture was stirred for additional 24 h at RT. DCM (50 mL) was added and the organic phase was washed 5 times with H<sub>2</sub>O (20 mL) and dried over MgSO<sub>4</sub>. The solvent was evaporated under reduced pressure and the crude product was purified using column chromatography on silica (cyclohexane/EtOAc 1:4 → EtOH).

**Yield:** 373 mg (0.751 mmol, 76%), colorless solid.

- **TLC:** R<sub>f</sub> = 0.83 (SiO<sub>2</sub>, cyclohexane/EtOAc, 1:3).
- **C<sub>32</sub>H<sub>36</sub>N<sub>2</sub>O<sub>3</sub>:** (496.64), [496.27].
- **<sup>1</sup>H-NMR (500 MHz, DMSO-d<sub>6</sub>, 300 K):** δ = 8.41 (t, <sup>3</sup>J = 5.9 Hz, 1H, CONHCH<sub>2</sub>), 7.89 (d, <sup>3</sup>J = 7.5 Hz, 2H, H-4-, H-5-Fmoc), 7.77–7.70 (m, 2H, H-1-, H-8-Fmoc), 7.50 (d, <sup>3</sup>J = 8.2 Hz, 1H, NHCOO), 7.42 (t, <sup>3</sup>J = 7.5 Hz, 2H, H-3-, H-6-Fmoc), 7.35–7.18 (m, 7H, H-2-, H-3-, H-4-, H-5-, H-6-benzyl, H-2-, H-7-Fmoc), 4.37–4.16 (m, 5H, OCH<sub>2</sub>, NHCHCO, CH<sub>2</sub>-benzyl), 4.02–3.94 (m, 1H, H-9-Fmoc), 1.73–1.50 (m, 7H, NHCHCH<sub>2</sub>CH<sub>2</sub>, H-2<sub>eq</sub>-, H-3<sub>eq</sub>-, H-4<sub>eq</sub>-, H-5<sub>eq</sub>-, H-6<sub>eq</sub>-cyclohexyl), 1.28–1.05 (m, 6H, H-1-, H-3<sub>ax</sub>-, H-4<sub>ax</sub>-, H-5<sub>ax</sub>-cyclohexyl, NHCHCH<sub>2</sub>CH<sub>2</sub>), 0.90–0.75 (m, 2H, H-2<sub>ax</sub>-, H-6<sub>ax</sub>-cyclohexyl) ppm.
- **<sup>13</sup>C-NMR (126 MHz, DMSO-d<sub>6</sub>, 300 K):** δ = 172.0, 156.0, 143.9, 143.8, 140.7, 139.5, 128.2, 127.6, 127.1, 127.0, 126.7, 125.3, 120.1, 65.6, 55.0, 46.7, 42.0, 36.7, 33.0, 32.0, 32.7, 29.4, 26.2, 25.8 (2x) ppm.
- **MS (ESI pos.):** m/z (%) = 519.23 (100) ([M+Na]<sup>+</sup>, calcd. 519.26), 520.24 (34) ([M+Na]<sup>+</sup>, calcd. 520.28).

**(S)-2-(((9H-Fluoren-9-yl)methoxy)carbonyl)amino)-4-cyclohexylbutanoic acid (**105**, SR75)**



(S)-2-(((9H-Fluoren-9-yl)methoxy)carbonyl)amino)-4-cyclohexylbutanoic acid (**105**, 400 mg, 0.982 mmol) and HATU (448 mg, 1.18 mmol) were dissolved in DMF (dry, 10 mL) and DIPEA (152 mg, 1.18 mmol) was added. The reaction mixture was stirred for 1.5 h at RT and (4-chlorophenyl)methanamine (**158**, 167 mg, 1.18 mmol) was added. The mixture was stirred for additional 20 h at RT. DCM (50 mL) was added and the organic phase was washed 3 times with H<sub>2</sub>O (30 mL) and dried over MgSO<sub>4</sub>. The solvent was evaporated under reduced pressure and the crude product was purified by column chromatography on silica (cyclohexane/EtOAc 8:1 → 1:1 → EtOAc).

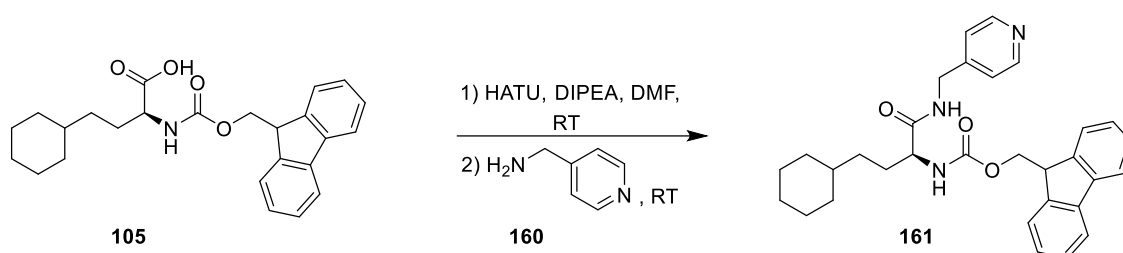
**Yield:** 350 mg (0.659 mmol, 67%), colorless solid.

- **TLC:** R<sub>f</sub> = 0.51 (SiO<sub>2</sub>, cyclohexane/EtOAc, 8:1).
- **C<sub>32</sub>H<sub>35</sub>ClN<sub>2</sub>O<sub>3</sub>:** (531.08), [530.23].
- **<sup>1</sup>H-NMR (500 MHz, DMSO-d<sub>6</sub>, 300 K):** δ = 8.45 (t, <sup>3</sup>J = 5.7 Hz, 1H, CONHCH<sub>2</sub>), 7.89 (d, <sup>3</sup>J = 7.5 Hz, 2H, H-4-, H-5-Fmoc), 7.77–7.70 (m, 2H, H-1-, H-8-Fmoc), 7.50 (d, <sup>3</sup>J = 8.0 Hz, 1H, NHCOO), 7.41 (t, <sup>3</sup>J = 7.5 Hz, 2H, H-3-, H-6-Fmoc), 7.38–7.22 (m, 6H, H-2-, H-7-Fmoc, H-2-, H-3-, H-5-, H-6-benzyl), 4.35–4.13 (m, 5H, OCH<sub>2</sub>, NHCHCO, CH<sub>2</sub>-benzyl), 3.99–3.92 (m, 1H, H-9-Fmoc), 1.72–1.47 (m, 7H,

NHCHCH<sub>2</sub>CH<sub>2</sub>, H-2<sub>eq</sub>-, H-3<sub>eq</sub>-, H-4<sub>eq</sub>-, H-5<sub>eq</sub>-, H-6<sub>eq</sub>-cyclohexyl), 1.25–1.02 (m, 6H, H-1-, H-3<sub>ax</sub>-, H-4<sub>ax</sub>-, H-5<sub>ax</sub>-cyclohexyl, NHCHCH<sub>2</sub>CH<sub>2</sub>), 0.89–0.75 (m, 2H, H-2<sub>ax</sub>-, H-6<sub>ax</sub>-cyclohexyl) ppm.

- **<sup>13</sup>C-NMR (126 MHz, DMSO-d<sub>6</sub>, 300 K):** δ = 172.1, 156.0, 143.9, 143.8, 140.7, 138.6, 131.3, 129.0, 128.1, 127.6, 127.1, 127.0, 125.3, 120.1, 65.6, 55.0, 46.7, 41.4, 36.7, 33.0, 32.9, 32.6, 29.4, 26.2, 25.8 (2x) ppm.
- **MS (ESI pos.):** *m/z* (%) = 553.21 (33) ([M+Na]<sup>+</sup>, calcd. 553.22), 531.25 (100) ([M+H]<sup>+</sup>, calcd. 531.24), 309.17 (35) ([M-Fmoc+H]<sup>+</sup>, calcd. 309.18), 179.29 (69) ([M<sub>fr</sub>+H]<sup>+</sup>, calcd. 179.29).

**(S)-(9H-Fluoren-9-yl)methyl (4-cyclohexyl-1-oxo-1-((pyridin-4-ylmethyl)amino)butan-2-yl)carbamate (161, SR86)**

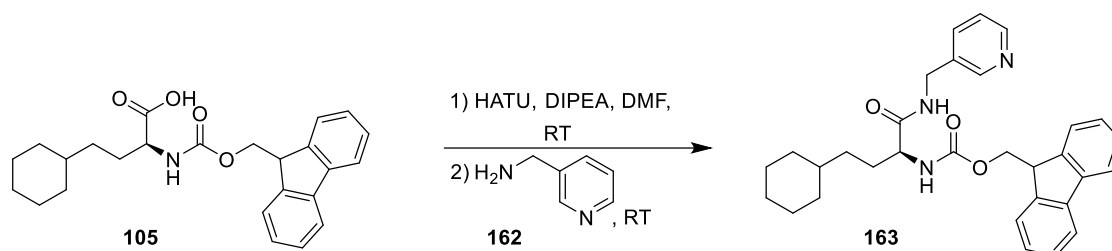


(S)-2-(((9H-Fluoren-9-yl)methoxy)carbonyl)amino-4-cyclohexylbutanoic acid (**105**, 500 mg, 1.23 mmol) and HATU (560 mg, 1.47 mmol) were dissolved in DMF (dry, 10 mL) and DIPEA (190 mg, 1.47 mmol) was added. The reaction mixture was stirred for 1.5 h at RT and pyridin-4-ylmethanamine (**160**, 159 mg, 1.47 mmol) was added. The mixture was stirred for additional 20 h at RT. DCM (100 mL) was added and the organic phase was washed 5 times with H<sub>2</sub>O (50 mL) and dried over MgSO<sub>4</sub>. The solvent was evaporated under reduced pressure and the crude product was triturated with cyclohexane/DCM (1:1).

**Yield:** 501 mg (1.01 mmol, 82%), colorless solid.

- **TLC:** R<sub>f</sub> = 0.27 (SiO<sub>2</sub>, cyclohexane/EtOAc, 1:20).
- **C<sub>31</sub>H<sub>35</sub>N<sub>3</sub>O<sub>3</sub>:** (497.63), [497.27].
- **<sup>1</sup>H-NMR (500 MHz, DMSO-d<sub>6</sub>, 300 K):** δ = 8.54 (t, <sup>3</sup>J = 5.9 Hz, 1H, CONHCH<sub>2</sub>), 8.46 (d, <sup>3</sup>J = 5.7 Hz, 2H, H-3-, H-5-picoline), 7.89 (d, <sup>3</sup>J = 7.5 Hz, 2H, H-4-, H-5-Fmoc), 7.77–7.71 (m, 2H, H-1-, H-8-Fmoc), 7.57 (d, <sup>3</sup>J = 8.3 Hz, 1H, NHCOO), 7.41 (t, <sup>3</sup>J = 7.5 Hz, 2H, H-3-, H-6-Fmoc), 7.31 (t, <sup>3</sup>J = 7.5 Hz, 2H, H-2-, H-7-Fmoc), 7.23 (d, <sup>3</sup>J = 5.7 Hz, 2H, H-2-, H-6-picoline), 4.36–4.18 (m, 5H, OCH<sub>2</sub>, NHCHCO, CH<sub>2</sub>-picoline), 4.02–3.94 (m, 1H, H-9-Fmoc), 1.75–1.51 (m, 7H, NHCHCH<sub>2</sub>CH<sub>2</sub>, H-2<sub>eq</sub>-, H-3<sub>eq</sub>-, H-4<sub>eq</sub>-, H-5<sub>eq</sub>-, H-6<sub>eq</sub>-cyclohexyl), 1.27–1.05 (m, 6H, H-1-, H-3<sub>ax</sub>-, H-4<sub>ax</sub>-, H-5<sub>ax</sub>-cyclohexyl, NHCHCH<sub>2</sub>CH<sub>2</sub>), 0.90–0.76 (m, 2H, H-2<sub>ax</sub>-, H-6<sub>ax</sub>-cyclohexyl) ppm.
- **<sup>13</sup>C-NMR (126 MHz, DMSO-d<sub>6</sub>, 300 K):** δ = 172.4, 156.1, 149.4, 148.5, 143.9, 143.8, 140.7 (2x), 127.6, 127.0, 125.3, 122.1, 120.1, 65.6, 55.0, 46.7, 41.1, 36.7, 33.1, 32.9, 32.7, 29.2, 26.4, 26.2, 25.8 (2x) ppm.
- **MS (ESI pos.):** *m/z* (%) = 498.29 (100) ([M+H]<sup>+</sup>, calcd. 498.28).

**(S)-(9H-Fluoren-9-yl)methyl (4-cyclohexyl-1-oxo-1-((pyridin-3-ylmethyl)amino)butan-2-yl)carbamate (163, SR87)**

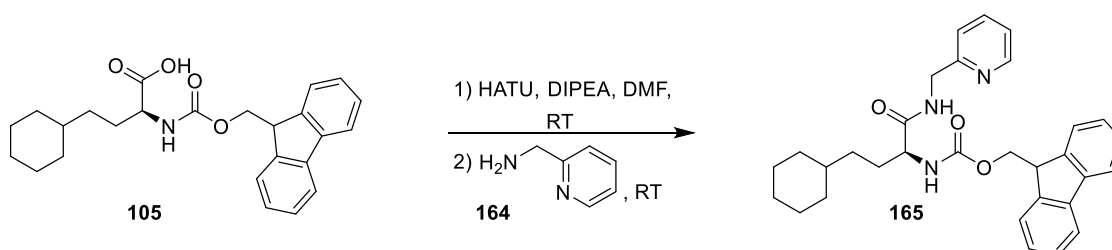


(S)-2-(((9H-Fluoren-9-yl)methoxy)carbonyl)amino-4-cyclohexylbutanoic acid (**105**, 500 mg, 1.23 mmol) and HATU (560 mg, 1.47 mmol) were dissolved in DMF (dry, 10 mL) and DIPEA (190 mg, 1.47 mmol) was added. The reaction mixture was stirred for 1.5 h at RT and pyridin-3-ylmethanamine (**162**, 159 mg, 1.47 mmol) was added. The mixture was stirred for additional 20 h at RT. DCM (100 mL) was added and the organic phase was washed 5 times with H<sub>2</sub>O (50 mL) and dried over MgSO<sub>4</sub>. The solvent was evaporated under reduced pressure and the crude product was triturated with cyclohexane/DCM (1:1).

**Yield:** 384 mg (0.77 mmol, 63%), colorless solid.

- **TLC:** R<sub>f</sub> = 0.36 (SiO<sub>2</sub>, cyclohexane/EtOAc, 1:20).
- **C<sub>31</sub>H<sub>35</sub>N<sub>3</sub>O<sub>3</sub>:** (497.63), [497.27].
- **<sup>1</sup>H-NMR (500 MHz, DMSO-d<sub>6</sub>, 300 K):** δ = 8.50 (t, <sup>3</sup>J = 5.7 Hz, 1H, CONHCH<sub>2</sub>), 8.47 (s, 1H, H-2 picoline), 8.46–8.40 (m, 1H, H-4 picoline), 7.89 (d, <sup>3</sup>J = 7.5 Hz, 2H, H-4-, H-5-Fmoc), 7.77–7.70 (m, 2H, H-1-, H-8-Fmoc), 7.63 (d, <sup>3</sup>J = 7.9 Hz, 1H, H-6 picoline), 7.53 (d, <sup>3</sup>J = 8.0 Hz, 1H, NHCOO), 7.41 (t, <sup>3</sup>J = 7.5 Hz, 2H, H-3-, H-6-Fmoc), 7.36–7.26 (m, 3H, H-5 picoline, H-2-, H-7-Fmoc), 4.37–4.14 (m, 5H, OCH<sub>2</sub>, NHCHCO, CH<sub>2</sub>-picoline), 3.99–3.90 (m, 1H, H-9 Fmoc), 1.72–1.47 (m, 7H, NHCHCH<sub>2</sub>CH<sub>2</sub>, H-2<sub>eq</sub>-, H-3<sub>eq</sub>-, H-4<sub>eq</sub>-, H-5<sub>eq</sub>-, H-6<sub>eq</sub>-cyclohexyl), 1.25–1.04 (m, 6H, H-1-, H-3<sub>ax</sub>-, H-4<sub>ax</sub>-, H-5<sub>ax</sub>-cyclohexyl, NHCHCH<sub>2</sub>CH<sub>2</sub>), 0.88–0.74 (m, 2H, H-2<sub>ax</sub>-, H-6<sub>ax</sub>-cyclohexyl) ppm.
- **<sup>13</sup>C-NMR (126 MHz, DMSO-d<sub>6</sub>, 300 K):** δ = 172.2, 156.0, 148.7, 148.0, 143.9, 143.8, 140.7 (2x), 135.0, 134.9, 127.6, 127.0, 125.4, 125.3, 123.4, 120.1, 65.6, 55.0, 46.7, 36.7, 33.0, 32.9, 32.6, 29.3, 26.3, 26.2, 25.8, 25.7 ppm.
- **MS (ESI pos.):** m/z (%) = 498.30 (100) ([M+H]<sup>+</sup>, calcd. 498.28).

**(S)-(9H-Fluoren-9-yl)methyl (4-cyclohexyl-1-oxo-1-((pyridin-2-ylmethyl)amino)butan-2-yl)carbamate (165, SR88)**



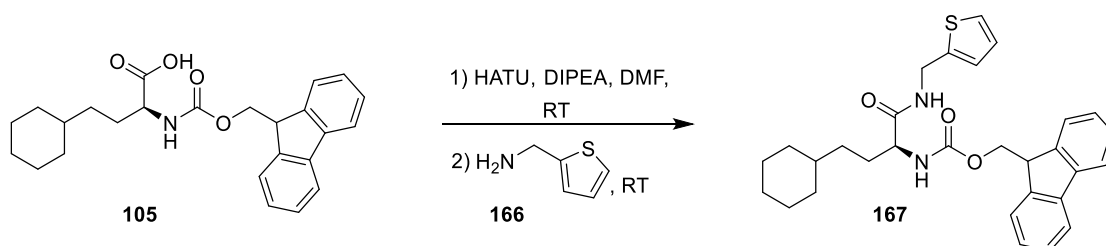
(S)-2-(((9H-Fluoren-9-yl)methoxy)carbonyl)amino-4-cyclohexylbutanoic acid (**105**, 500 mg, 1.23 mmol) and HATU (560 mg, 1.47 mmol) were dissolved in DMF (dry, 10 mL) and DIPEA (190 mg, 1.47 mmol) was added. The reaction mixture was stirred for 1.5 h at RT and pyridin-2-ylmethanamine (**164**, 159 mg,

1.47 mmol) was added. The mixture was stirred for additional 20 h at RT. DCM (100 mL) was added and the organic phase was washed 5 times with H<sub>2</sub>O (50 mL) and dried over MgSO<sub>4</sub>. The solvent was evaporated under reduced pressure and the crude product was triturated with cyclohexane/DCM (1:1).

**Yield:** 495 mg (1.00 mmol, 81%), colorless solid.

- **TLC:** R<sub>f</sub> = 0.31 (SiO<sub>2</sub>, cyclohexane/EtOAc, 1:3).
- **C<sub>31</sub>H<sub>35</sub>N<sub>3</sub>O<sub>3</sub>:** (497.63), [497.27].
- **<sup>1</sup>H-NMR (500 MHz, DMSO-d<sub>6</sub>, 300 K):** δ = 8.50 (t, <sup>3</sup>J = 5.8 Hz, 1H, CONHCH<sub>2</sub>), 8.48–8.45 (m, 1H, H-4 picoline), 7.89 (d, <sup>3</sup>J = 7.6 Hz, 2H, H-4-, H-5-Fmoc), 7.77–7.68 (m, 3H, H-5 picoline, H-1-, H-8-Fmoc), 7.55 (d, <sup>3</sup>J = 8.1 Hz, 1H, NHCOO), 7.41 (t, <sup>3</sup>J = 7.6 Hz, 2H, H-3-, H-6-Fmoc), 7.35–7.20 (m, 4H, H-4-, H-6-picoline, H-2-, H-7-Fmoc), 4.37 (d, <sup>3</sup>J = 5.6 Hz, 2H, CH<sub>2</sub>-picoline), 4.34–4.18 (m, 3H, OCH<sub>2</sub>, NHCHCO), 4.04–3.96 (m, 1H, H-9-Fmoc), 1.76–1.50 (m, 7H, NHCHCH<sub>2</sub>CH<sub>2</sub>, H-2<sub>eq</sub>-, H-3<sub>eq</sub>-, H-4<sub>eq</sub>-, H-5<sub>eq</sub>-, H-6<sub>eq</sub>-cyclohexyl), 1.28–1.05 (m, 6H, H-1-, H-3<sub>ax</sub>-, H-4<sub>ax</sub>-, H-5<sub>ax</sub>-cyclohexyl, NHCHCH<sub>2</sub>CH<sub>2</sub>), 0.90–0.77 (m, 2H, H-2<sub>ax</sub>-, H-6<sub>ax</sub>-cyclohexyl) ppm.
- **<sup>13</sup>C-NMR (126 MHz, DMSO-d<sub>6</sub>, 300 K):** δ = 172.3, 158.5, 156.0, 148.7, 143.9, 143.8, 140.7, 136.6, 127.6, 127.0, 125.3, 122.1, 120.8, 120.1, 65.6, 55.0, 46.7, 44.1, 36.8, 33.1, 32.9, 32.7, 29.3, 26.2, 25.8 (2x) ppm.
- **MS (ESI pos.):** m/z (%) = 498.29 (100) ([M+H]<sup>+</sup>, calcd. 498.28).

**(S)-(9H-Fluoren-9-yl)methyl (4-cyclohexyl-1-oxo-1-((thiophen-2-ylmethyl)amino)butan-2-yl)carbamate (167, SR85)**



(S)-2-(((9H-Fluoren-9-yl)methoxy)carbonyl)amino-4-cyclohexylbutanoic acid (**105**, 500 mg, 1.23 mmol) and HATU (560 mg, 1.47 mmol) were dissolved in DMF (dry, 10 mL) and DIPEA (190 mg, 1.47 mmol) was added. The reaction mixture was stirred for 1.5 h at RT and thiophen-2-ylmethanamine (**166**, 113 mg, 1.47 mmol) was added. The mixture was stirred for additional 20 h at RT. DCM (100 mL) was added and the organic phase was washed 5 times with H<sub>2</sub>O (50 mL) and dried over MgSO<sub>4</sub>. The solvent was evaporated under reduced pressure and the crude product was triturated with cyclohexane/DCM (1:1).

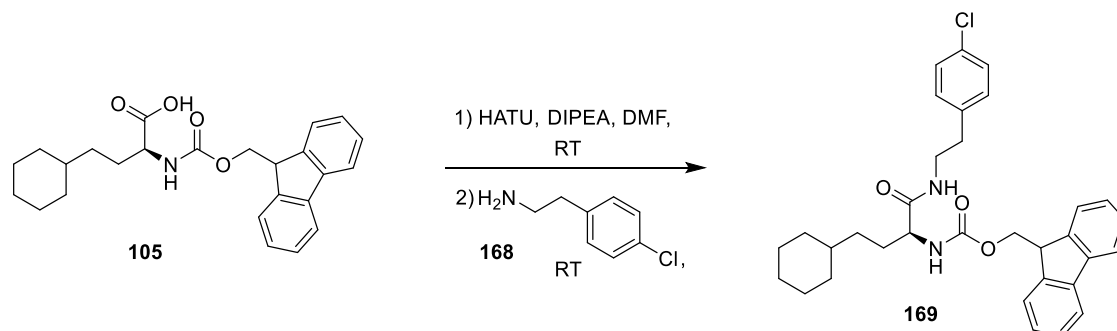
**Yield:** 468 mg (0.931 mmol, 76%), colorless solid.

- **TLC:** R<sub>f</sub> = 0.86 (SiO<sub>2</sub>, cyclohexane/EtOAc, 1:1).
- **C<sub>30</sub>H<sub>34</sub>N<sub>2</sub>O<sub>3</sub>S:** (502.67), [502.23].
- **<sup>1</sup>H-NMR (500 MHz, DMSO-d<sub>6</sub>, 300 K):** δ = 8.51 (t, <sup>3</sup>J = 5.7 Hz, 1H, CONHCH<sub>2</sub>), 7.89 (d, <sup>3</sup>J = 7.5 Hz, 2H, H-4-, H-5-Fmoc), 7.77–7.70 (m, 2H, H-1-, H-8-Fmoc), 7.49 (d, <sup>3</sup>J = 8.3 Hz, 1H, NHCOO), 7.42 (t, <sup>3</sup>J = 7.5 Hz, 2H, H-3-, H-6-Fmoc), 7.38–7.35 (m, 1H, H-5 thiophene), 7.32 (t, <sup>3</sup>J = 7.5 Hz, 2H, H-2-, H-7-Fmoc), 6.98–6.90 (m, 2H, H-3-, H-4-thiophene), 4.59–4.34 (m, 2H, OCH<sub>2</sub>), 4.33–4.15 (m, 3H, NHCHCO, CH<sub>2</sub>-thiophene), 4.00–3.90 (m, 1H, H-9 Fmoc), 1.71–1.47 (m, 7H, NHCHCH<sub>2</sub>CH<sub>2</sub>, H-2<sub>eq</sub>-, H-

3<sub>eq</sub><sup>-</sup>, H-4<sub>eq</sub><sup>-</sup>, H-5<sub>eq</sub><sup>-</sup>, H-6<sub>eq</sub>-cyclohexyl), 1.27–1.04 (m, 6H, H-1-, H-3<sub>ax</sub><sup>-</sup>, H-4<sub>ax</sub><sup>-</sup>, H-5<sub>ax</sub>-cyclohexyl, NHCHCH<sub>2</sub>CH<sub>2</sub>), 0.89–0.76 (m, 2H, H-2<sub>ax</sub><sup>-</sup>, H-6<sub>ax</sub>-cyclohexyl) ppm.

- **<sup>13</sup>C-NMR (126 MHz, DMSO-d<sub>6</sub>, 300 K):** δ = 171.8, 155.9, 143.9, 143.8, 142.5, 140.7, 127.6, 127.0, 126.6, 125.4, 125.2, 125.0, 120.1, 65.6, 54.8, 46.7, 37.2, 36.7, 33.0, 32.9, 32.6, 29.4, 26.2, 25.8 (2x) ppm.
- **MS (ESI pos.):** *m/z* (%) = 525.22 (100) ([M+Na]<sup>+</sup>, calcd. 525.22).

**(S)-2-(((9H-Fluoren-9-yl)methyl (1-((4-chlorophenethyl)amino)-4-cyclohexyl-1-oxobutan-2-yl)carbamate (169, SR57)**



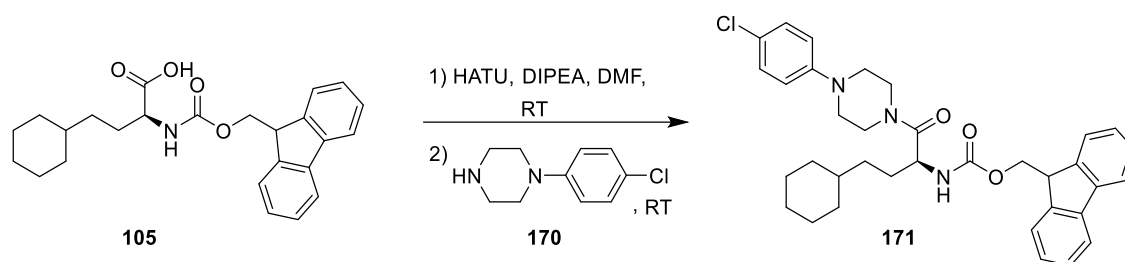
(S)-2-(((9H-Fluoren-9-yl)methoxy)carbonyl)amino-4-cyclohexylbutanoic acid (**105**, 500 mg, 1.23 mmol) and HATU (560 mg, 1.47 mmol) were dissolved in DMF (dry, 10 mL) and DIPEA (190 mg, 1.47 mmol) was added. The reaction mixture was stirred for 1.5 h at RT and 2-(4-chlorophenyl)ethanamine (**168**, 229 mg, 1.47 mmol) was added. The mixture was stirred for additional 20 h at RT. DCM (50 mL) was added and the organic phase was washed 5 times with H<sub>2</sub>O (20 mL) and dried over MgSO<sub>4</sub>. The solvent was evaporated under reduced pressure and the crude product was purified using column chromatography on silica (DCM/MeOH 10:1).

**Yield:** 418 mg (0.767 mmol, 62%), colorless solid.

- **TLC:** R<sub>f</sub> = 0.89 (SiO<sub>2</sub>, cyclohexane/EtOAc, 1:1).
- **C<sub>33</sub>H<sub>37</sub>ClN<sub>2</sub>O<sub>3</sub>:** (545.11), [544.25].
- **<sup>1</sup>H-NMR (500 MHz, CDCl<sub>3</sub>, 300 K):** δ = 7.76 (d, <sup>3</sup>J = 7.5 Hz, 2H, H-4-, H-5-Fmoc), 7.56 (d, <sup>3</sup>J = 7.5 Hz, 2H, H-1-, H-8-Fmoc), 7.40 (t, <sup>3</sup>J = 7.5 Hz, 2H, H-3-, H-6-Fmoc), 7.30 (t, <sup>3</sup>J = 7.5 Hz, 2H, H-2-, H-7-Fmoc), 7.22 (d, <sup>3</sup>J = 8.4 Hz, 2H, H-3-, H-5-phenyl), 7.07 (d, <sup>3</sup>J = 8.4 Hz, 2H, H-2-, H-6-phenyl), 5.95 (s, 1H, NHCOO), 5.24 (d, <sup>3</sup>J = 7.8 Hz, 1H, CONHCH<sub>2</sub>), 4.47–4.27 (m, 2H, OCH<sub>2</sub>), 4.22 (t, <sup>3</sup>J = 6.9 Hz, 1H, NHCHCO), 4.08–3.99 (m, 1H, H-9-Fmoc), 3.60–3.30 (m, 2H, NHCH<sub>2</sub>CH<sub>2</sub>), 2.83–2.64 (m, 2H, NHCH<sub>2</sub>CH<sub>2</sub>), 1.91–1.46 (m, 7H, NHCHCH<sub>2</sub>CH<sub>2</sub>, H-2<sub>eq</sub><sup>-</sup>, H-3<sub>eq</sub><sup>-</sup>, H-4<sub>eq</sub><sup>-</sup>, H-5<sub>eq</sub><sup>-</sup>, H-6<sub>eq</sub>-cyclohexyl), 1.35–1.02 (m, 6H, H-1-, H-3<sub>ax</sub><sup>-</sup>, H-4<sub>ax</sub><sup>-</sup>, H-5<sub>ax</sub>-cyclohexyl, NHCHCH<sub>2</sub>CH<sub>2</sub>), 0.95–0.73 (m, 2H, H-2<sub>ax</sub><sup>-</sup>, H-6<sub>ax</sub>-cyclohexyl) ppm.
- **<sup>13</sup>C-NMR (126 MHz, CDCl<sub>3</sub>, 300 K):** δ = 171.9, 156.3, 143.9, 141.4, 137.2, 132.5, 130.2, 128.8, 127.9, 127.2, 125.1, 120.1, 67.2, 55.5, 47.3, 40.5, 37.6, 35.1, 33.4, 33.3, 33.1, 30.2, 26.7, 26.4 ppm.
- **MS (ESI pos.):** *m/z* (%) = 511.18 (100) (M-Cl+2H)<sup>+</sup>, calcd. 511.30).



**(S)-(9H-Fluoren-9-yl)methyl (1-(4-(4-chlorophenyl)piperazin-1-yl)-4-cyclohexyl-1-oxobutan-2-yl)carbamate (171, SR105)**

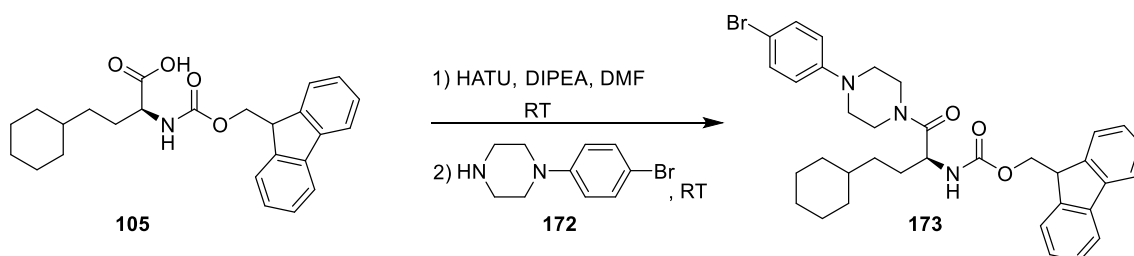


(S)-2-(((9H-Fluoren-9-yl)methoxy)carbonyl)amino-4-cyclohexylbutanoic acid (**105**, 500 mg, 1.23 mmol) and HATU (560 mg, 1.47 mmol) were dissolved in DMF (dry, 10 mL) and DIPEA (190 mg, 1.47 mmol) was added. The reaction mixture was stirred for 1.5 h at RT and 1-(4-(4-chlorophenyl)piperazine) (**170**, 290 mg, 1.47 mmol) was added. The mixture was stirred for additional 24 h at RT. DCM (50 mL) was added and the organic phase was washed 5 times with H<sub>2</sub>O (50 mL) and dried over MgSO<sub>4</sub>. The solvent was evaporated under reduced pressure and the crude product was triturated with cyclohexane/DCM (1:1).

**Yield:** 651 mg (1.11 mmol, 91%), colorless solid.

- **TLC:** R<sub>f</sub> = 0.68 (SiO<sub>2</sub>, cyclohexane/EtOAc, 1:1).
- **C<sub>35</sub>H<sub>40</sub>ClN<sub>3</sub>O<sub>3</sub>:** (586.16), [585.28].
- **<sup>1</sup>H-NMR (500 MHz, DMSO-d<sub>6</sub>, 300 K):** δ = 7.88 (d, <sup>3</sup>J = 7.5 Hz, 2H, H-4-, H-5-Fmoc), 7.72 (dd, <sup>3</sup>J = 7.6, 3.5 Hz, 2H, H-1-, H-8-Fmoc), 7.63 (d, <sup>3</sup>J = 8.3 Hz, 1H, NHCOO), 7.40 (dt, <sup>3</sup>J = 7.6, 3.1 Hz, 2H, H-3-, H-6-Fmoc), 7.30 (t, <sup>3</sup>J = 7.4 Hz, 2H, H-2-, H-7-Fmoc), 7.24 (d, <sup>3</sup>J = 9.0 Hz, 2H, H-3-, H-5-phenyl), 6.94 (d, <sup>3</sup>J = 9.0 Hz, 2H, H-2-, H-6-phenyl), 4.46–4.36 (m, 1H, NHCHCO), 4.32–4.17 (m, 3H, OCH<sub>2</sub>, H-9 Fmoc), 3.72–3.44 (m, 4H, CH<sub>2</sub>-2-, CH<sub>2</sub>-6-piperazine), 3.17–2.99 (m, 4H, CH<sub>2</sub>-3-, CH<sub>2</sub>-5-piperazine), 1.71–1.48 (m, 7H, NHCHCH<sub>2</sub>CH<sub>2</sub>, H-2<sub>eq</sub>-, H-3<sub>eq</sub>-, H-4<sub>eq</sub>-, H-5<sub>eq</sub>-, H-6<sub>eq</sub>- cyclohexyl), 1.30–1.02 (m, 6H, H-1-, H-3<sub>ax</sub>-, H-4<sub>ax</sub>-, H-5<sub>ax</sub>-cyclohexyl, NHCHCH<sub>2</sub>CH<sub>2</sub>), 0.91–0.75 (m, 2H, H-2<sub>ax</sub>-, H-6<sub>ax</sub>-cyclohexyl) ppm.
- **<sup>13</sup>C-NMR (126 MHz, DMSO-d<sub>6</sub>, 300 K):** δ = 170.1, 155.9, 149.5, 143.8, 140.7, 128.7, 127.6, 127.0, 125.3, 122.7, 120.1, 117.3, 65.6, 50.7, 48.6, 48.1, 46.7, 44.6, 41.2, 37.0, 32.9, 32.7, 29.0, 26.4, 26.2, 25.8 (2x) ppm.
- **MS (ESI pos.):** m/z (%) = 586.20 (9) (M+H)<sup>+</sup>, calcd. 586.29), 364.23 (100) ([M-Fmoc+2H]<sup>+</sup>, calcd. 364.22), 295.22 (93) ([M<sub>fr.</sub>]<sup>+</sup>, calcd. 295.07).

**(S)-(9H-Fluoren-9-yl)methyl (1-(4-(4-bromophenyl)piperazin-1-yl)-4-cyclohexyl-1-oxobutan-2-yl)carbamate (173, SR106)**

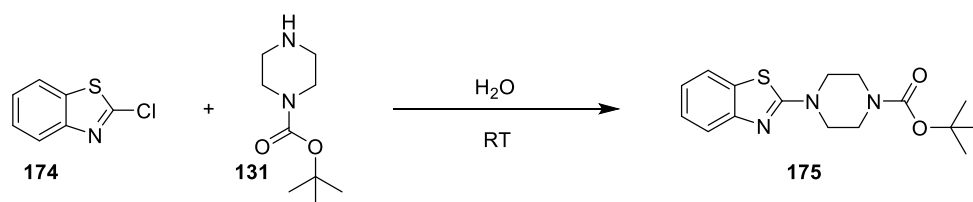


(*S*)-2-(((9*H*-Fluoren-9-yl)methoxy)carbonyl)amino)-4-cyclohexylbutanoic acid (**105**, 500 mg, 1.23 mmol) and HATU (560 mg, 1.47 mmol) were dissolved in DMF (dry, 10 mL) and DIPEA (190 mg, 1.47 mmol) was added. The reaction mixture was stirred for 1.5 h at RT and 1-(4-bromophenyl)piperazine (**172**, 355 mg, 1.47 mmol) was added. The mixture was stirred for additional 24 h at RT. DCM (50 mL) was added and the organic phase was washed 5 times with H<sub>2</sub>O (50 mL) and dried over MgSO<sub>4</sub>. The solvent was evaporated under reduced pressure and the crude product was triturated with cyclohexane/DCM (1:1).

**Yield:** 610 mg (0.97 mmol, 79%), colorless solid.

- **TLC:** R<sub>f</sub> = 0.79 (SiO<sub>2</sub>, cyclohexane/EtOAc, 1:1).
- **C<sub>35</sub>H<sub>40</sub>BrN<sub>3</sub>O<sub>3</sub>:** (630.61), [629.23].
- **<sup>1</sup>H-NMR (500 MHz, DMSO-d<sub>6</sub>, 300 K):** δ = 7.88 (d, <sup>3</sup>J = 7.6 Hz, 2H, H-4-, H-5-Fmoc), 7.72 (dd, <sup>3</sup>J = 7.4, 3.4 Hz, 2H, H-1-, H-8-Fmoc), 7.63 (d, <sup>3</sup>J = 8.3 Hz, 1H, NHCOO), 7.40 (dt, <sup>3</sup>J = 7.4, 3.0 Hz, 2H, H-3-, H-6-Fmoc), 7.35 (d, <sup>3</sup>J = 9.0 Hz, 2H, H-3-, H-5-phenyl), 7.30 (t, <sup>3</sup>J = 7.4 Hz, 2H, H-2-, H-7-Fmoc), 6.89 (d, <sup>3</sup>J = 9.0 Hz, 2H, H-2-, H-6-phenyl), 4.45–4.37 (m, 1H, NHCHCO), 4.31–4.17 (m, 3H, OCH<sub>2</sub>, H-9 Fmoc), 3.69–3.45 (m, 4H, CH<sub>2</sub>-2-, CH<sub>2</sub>-6-piperazine), 3.17–2.99 (m, 4H, CH<sub>2</sub>-3-, CH<sub>2</sub>-5-piperazine), 1.69–1.48 (m, 7H, NHCHCH<sub>2</sub>CH<sub>2</sub>, H-2<sub>eq</sub>-, H-3<sub>eq</sub>-, H-4<sub>eq</sub>-, H-5<sub>eq</sub>-, H-6<sub>eq</sub>-cyclohexyl), 1.28–1.03 (m, 6H, H-1-, H-3<sub>ax</sub>-, H-4<sub>ax</sub>-, H-5<sub>ax</sub>-cyclohexyl, NHCHCH<sub>2</sub>CH<sub>2</sub>), 0.91–0.74 (m, 2H, H-2<sub>ax</sub>-, H-6<sub>ax</sub>-cyclohexyl) ppm.
- **<sup>13</sup>C-NMR (126 MHz, DMSO-d<sub>6</sub>, 300 K):** δ = 170.1, 155.9, 149.5, 143.8, 140.7, 131.5, 127.6, 127.0, 125.3, 120.1, 117.7, 110.5, 65.6, 50.7, 48.4, 47.9, 46.7, 44.6, 41.2, 37.0, 32.9, 32.7, 29.0, 26.2, 25.8 (2x) ppm.
- **MS (ESI pos.):** *m/z* (%) = 632.27 (22) ([M+H]<sup>+</sup>, calcd. 632.23), 408.20 (41) ([M-Fmoc+2H]<sup>+</sup>, calcd. 408.17), 339.11 (100) ([M<sub>fr.</sub>]<sup>+</sup>, calcd. 339.02).

#### *tert*-Butyl 4-(benzo[*d*]thiazol-2-yl)piperazine-1-carboxylate (**175**, SR117)



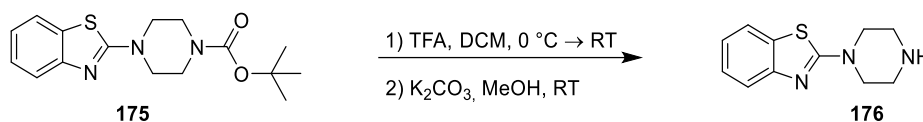
2-Chlorobenzo[*d*]thiazole (**174**, 170 mg, 1.00 mmol) and *tert*-butyl piperazine-1-carboxylate (**131**, 373 mg, 2.00 mmol) were suspended in H<sub>2</sub>O (2 mL) and stirred for 5 d at RT. The precipitate was dissolved in EtOAc, the aqueous phase was extracted 3 times with EtOAc (50 mL) and dried over MgSO<sub>4</sub>. The solvent was evaporated under reduced pressure and the crude product was purified using column chromatography on silica (cyclohexane/EtOAc 20:1 → EtOAc).

**Yield:** 282 mg (0.884 mmol, 88%), colorless solid.

- **TLC:** R<sub>f</sub> = 0.81 (SiO<sub>2</sub>, cyclohexane/EtOAc, 1:1).
- **C<sub>16</sub>H<sub>21</sub>N<sub>3</sub>O<sub>2</sub>S:** (319.42), [319.14].
- **<sup>1</sup>H-NMR (500 MHz, CDCl<sub>3</sub>, 300 K):** δ = 7.61 (d, <sup>3</sup>J = 7.8 Hz, 1H, H-7 benzothiazole), 7.56 (d, <sup>3</sup>J = 7.8 Hz, 1H, H-4 benzothiazole), 7.30 (dt, <sup>3</sup>J = 7.8, 1.3 Hz, 1H, H-6 benzothiazole), 7.09 (dt, <sup>3</sup>J = 7.8, 1.2 Hz, 1H, H-5 benzothiazole), 3.64–3.54 (m, 8H, CH<sub>2</sub>-2-, CH<sub>2</sub>-3-, CH<sub>2</sub>-5-, CH<sub>2</sub>-6-piperazine), 1.49 (s, 9H, C(CH<sub>3</sub>)<sub>3</sub>) ppm.

- **$^{13}\text{C}$ -NMR (126 MHz,  $\text{CDCl}_3$ , 300 K):**  $\delta$  = 168.8, 154.7, 152.7, 130.8, 126.2, 121.8, 120.9, 119.4, 80.6, 48.3, 43.4, 28.5 ppm.
- **MS (ESI pos.):**  $m/z$  (%) = 342.18 (65) ( $[\text{M}+\text{Na}]^+$ , calcd. 342.13), 320.24 (36) ( $[\text{M}+\text{H}]^+$ , calcd. 320.15), 264.19 (100) ( $[\text{M}-\text{Boc}+\text{EtOH}]^+$ , calcd. 264.12), 220.08 (61) ( $[\text{M}-\text{Boc}+\text{H}]^+$ , calcd. 220.09).

### 2-(Piperazin-1-yl)benzo[d]thiazole (**176**, SR120)

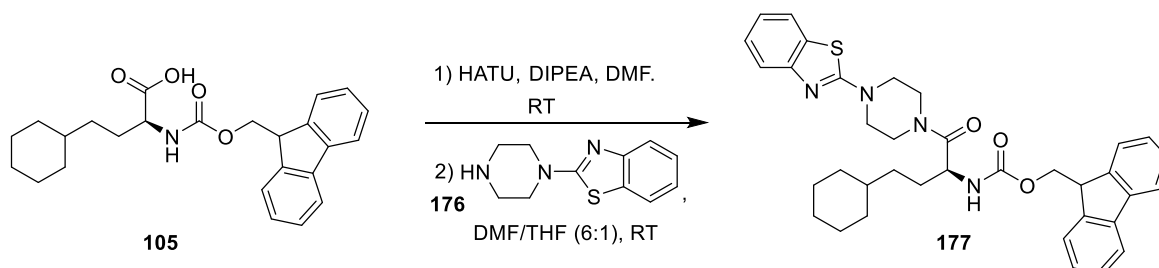


*tert*-Butyl 4-(benzo[d]thiazol-2-yl)piperazine-1-carboxylate (**175**, 365 mg, 1.14 mmol) was dissolved in DCM (15 mL), cooled to 0 °C and TFA (2 mL) was added. The mixture was stirred for 3 h at RT and the solvent was removed under reduced pressure. The crude product was dissolved in MeOH,  $\text{K}_2\text{CO}_3$  (3.6 g, 26.0 mmol) was added and stirred for additional 5 min at 5 °C. The mixture was filtered and the solvent was removed under reduced pressure.  $\text{H}_2\text{O}$  was added and the aqueous phase was extracted 3 times with EtOAc (50 mL). The organic phase was dried over  $\text{MgSO}_4$  and the solvent was evaporated under reduced pressure to obtain the product.

**Yield:** 246 mg (1.12 mmol, quant.), colorless solid.

- **TLC:**  $R_f$  = 0.51 ( $\text{SiO}_2$ , cyclohexane/EtOAc, 20:1).
- **$\text{C}_{11}\text{H}_{13}\text{N}_3\text{S}$ :** (219.30), [219.08].
- **$^1\text{H}$ -NMR (500 MHz,  $\text{DMSO}-d_6$ , 300 K):**  $\delta$  = 7.74 (d,  $^3J$  = 7.9 Hz, 1H, H-7 benzothiazole), 7.44 (d,  $^3J$  = 7.9 Hz, 1H, H-4 benzothiazole), 7.26 (dt,  $^3J$  = 7.9, 1.3 Hz, 1H, H-6 benzothiazole), 7.05 (dt,  $^3J$  = 7.9, 1.1 Hz, 1H, H-5 benzothiazole), 3.51–3.43 (m, 4H,  $\text{CH}_2$ -2-,  $\text{CH}_2$ -6-piperazine), 2.86–2.74 (m, 4H,  $\text{CH}_2$ -3-,  $\text{CH}_2$ -5-piperazine) ppm.
- **$^{13}\text{C}$ -NMR (126 MHz,  $\text{DMSO}-d_6$ , 300 K):**  $\delta$  = 168.4, 152.2, 130.2, 125.9, 121.1, 121.0, 118.5, 49.3, 45.0 ppm.
- **MS (ESI pos.):**  $m/z$  (%) = 220.10 (100) ( $[\text{M}+\text{H}]^+$ , calcd. 220.09).

### (*S*)-(9*H*-Fluoren-9-yl)methyl (1-(4-(benzo[d]thiazol-2-yl)piperazin-1-yl)-4-cyclohexyl-1-oxobutan-2-yl)carbamate (**177**, SR122)



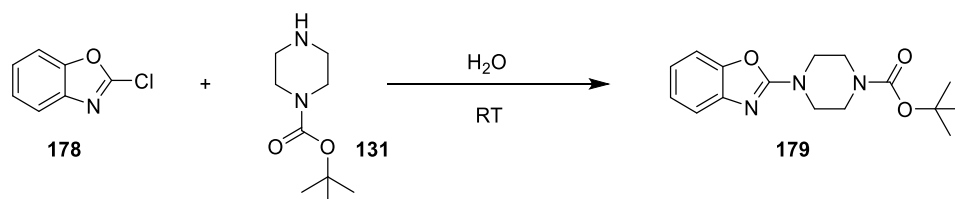
(*S*)-2-(((9*H*-Fluoren-9-yl)methoxy)carbonyl)amino)-4-cyclohexylbutanoic acid (**105**, 500 mg, 1.23 mmol) and HATU (560 mg, 1.47 mmol) were dissolved in DMF (dry, 6 mL) and DIPEA (190 mg, 1.47 mmol) was added. The reaction mixture was stirred for 1.5 h at RT and 2-(piperazin-1-yl)benzo[d]thiazole (**176**, 260 mg, 1.19 mmol) diluted in DMF/THF mixture (dry, 7 mL, 6:1) was added. The mixture was stirred for additional

20 h at RT. DCM (50 mL) was added and the organic phase was washed 5 times with H<sub>2</sub>O (50 mL) and dried over MgSO<sub>4</sub>. The solvent was evaporated under reduced pressure and the crude product was purified using column chromatography on silica (DCM/MeOH 10:1).

**Yield:** 466 mg (0.766 mmol, 62%), colorless solid.

- **TLC:** R<sub>f</sub> = 0.96 (SiO<sub>2</sub>, DCM/MeOH 10:1).
- **C<sub>36</sub>H<sub>40</sub>N<sub>4</sub>O<sub>3</sub>S:** (608.79), [608.28].
- **<sup>1</sup>H-NMR (400 MHz, DMSO-d<sub>6</sub>, 300 K):** δ = 7.91–7.85 (m, 2H, H-4-, H-5-Fmoc), 7.79 (d, <sup>3</sup>J = 7.6 Hz, 1H, H-7 benzothiazole), 7.73 (dd, <sup>3</sup>J = 7.7, 3.5 Hz, 2H, H-1-, H-8-Fmoc), 7.64 (d, <sup>3</sup>J = 8.2 Hz, 1H, NHCOO), 7.48 (d, <sup>3</sup>J = 7.6 Hz, 1H, H-4 benzothiazole), 7.44–7.40 (m, 2H, H-3-, H-6-Fmoc), 7.35–7.26 (m, 3H, H-2-, H-7-Fmoc, H-6 benzothiazole), 7.13–7.06 (m, 1H, H-5 benzothiazole), 4.47–4.38 (m, 1H, NHCHCO), 4.32–4.18 (m, 3H, OCH<sub>2</sub>, H-9-Fmoc), 3.74–3.46 (m, 8H, CH<sub>2</sub>-2-, CH<sub>2</sub>-3-, CH<sub>2</sub>-5-, CH<sub>2</sub>-6-piperazine), 1.71–1.51 (m, 7H, NHCHCH<sub>2</sub>CH<sub>2</sub>, H-2<sub>eq</sub>-, H-3<sub>eq</sub>-, H-4<sub>eq</sub>-, H-5<sub>eq</sub>-, H-6<sub>eq</sub>-cyclohexyl), 1.27–1.04 (m, 6H, H-1-, H-3<sub>ax</sub>-, H-4<sub>ax</sub>-, H-5<sub>ax</sub>-cyclohexyl, NHCHCH<sub>2</sub>CH<sub>2</sub>), 0.92–0.77 (m, 2H, H-2<sub>ax</sub>-, H-6<sub>ax</sub>-cyclohexyl) ppm.
- **<sup>13</sup>C-NMR (126 MHz, DMSO-d<sub>6</sub>, 300 K):** δ = 173.3, 168.1, 168.0, 152.3, 143.9, 130.4, 127.3 (2x), 126.0, 124.6, 123.9, 121.4 (2x), 121.2, 120.0, 118.7, 67.8, 50.4, 47.1, 40.9, 37.1, 33.0, 32.9, 32.7, 32.6, 32.1, 26.2, 25.8 (2x) ppm.
- **MS (ESI pos.):** m/z (%) = 387.24 (100) ([M-Fmoc+H]<sup>+</sup>, calcd. 387.23).

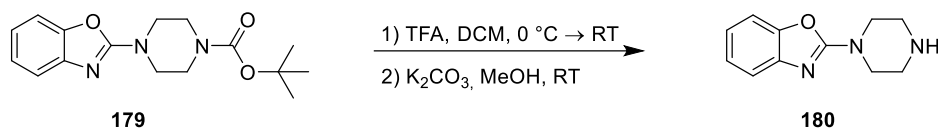
***tert*-Butyl 4-(benzo[d]oxazol-2-yl)piperazine-1-carboxylate (179, SR118)**



2-Chlorobenzo[d]oxazole (**178**, 153 mg, 1.00 mmol) and *tert*-butyl piperazine-1-carboxylate (**131**, 373 mg, 2.00 mmol) were suspended in H<sub>2</sub>O (2 mL) and stirred for 3 d at RT. The precipitate was dissolved in EtOAc, the aqueous phase was extracted 3 times with EtOAc (50 mL) and dried over MgSO<sub>4</sub>. The solvent was removed under reduced pressure to obtain the product.

**Yield:** 303 mg (0.999 mmol, quant.), colorless solid.

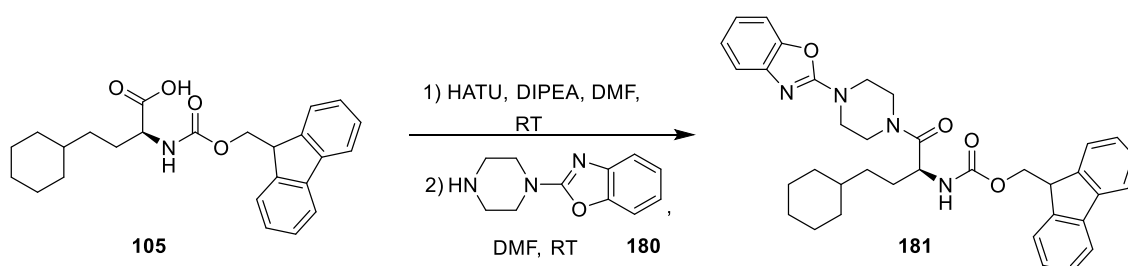
- **TLC:** R<sub>f</sub> = 0.67 (SiO<sub>2</sub>, cyclohexane/EtOAc, 1:1).
- **C<sub>16</sub>H<sub>21</sub>N<sub>3</sub>O<sub>3</sub>:** (303.36), [303.16].1
- **<sup>1</sup>H-NMR (500 MHz, CDCl<sub>3</sub>, 300 K):** δ = 7.36 (d, <sup>3</sup>J = 7.7 Hz, 1H, H-7 benzoxazole), 7.25 (d, <sup>3</sup>J = 7.7 Hz, 1H, H-4 benzoxazole), 7.17 (t, <sup>3</sup>J = 7.7 Hz, 1H, H-6 benzoxazole), 7.03 (t, <sup>3</sup>J = 7.7 Hz, 1H, H-5 benzoxazole), 3.71–3.36 (m, 4H, CH<sub>2</sub>-2-, CH<sub>2</sub>-6-piperazine), 3.60–3.51 (m, 4H, CH<sub>2</sub>-3-, CH<sub>2</sub>-5-piperazine), 1.48 (s, 9H, C(CH<sub>3</sub>)<sub>3</sub>) ppm.
- **<sup>13</sup>C-NMR (126 MHz, CDCl<sub>3</sub>, 300 K):** δ = 162.1, 154.7, 148.9, 143.0, 124.2, 121.1, 116.6, 108.9, 80.5, 45.5, 43.3, 28.5 ppm.
- **MS (ESI pos.):** m/z (%) = 304.25 (14) ([M+H]<sup>+</sup>, calcd. 304.17), 248.20 (100) ([M<sub>fr.</sub>+2H]<sup>+</sup>, calcd. 248.11), 204.12 (49) ([M-Boc+2H]<sup>+</sup>, calcd. 204.12).

**2-(Piperazin-1-yl)benzo[d]oxazole (180, SR121)**

*tert*-Butyl 4-(benzo[d]oxazol-2-yl)piperazine-1-carboxylate (**179**, 500 mg, 1.65 mmol) was dissolved in DCM (15 mL), cooled to 0 °C and TFA (2 mL) was added. The mixture was stirred for 3 h at RT and the solvent was removed under reduced pressure. The crude product was dissolved in MeOH, K<sub>2</sub>CO<sub>3</sub> (3.6 g, 25.96 mmol) was added and stirred for additional 5 min at 5 °C. The mixture was filtered and the solvent was removed under reduced pressure. H<sub>2</sub>O was added and the aqueous phase was extracted 3 times with EtOAc (50 mL). The organic phase was dried over MgSO<sub>4</sub> and the solvent was evaporated under reduced pressure to obtain the product.

**Yield:** 298 mg (1.47 mmol, 89%), yellowish solid.

- **TLC:** R<sub>f</sub> = 0.17 (SiO<sub>2</sub>, DCM/MeOH, 10:1).
- **C<sub>11</sub>H<sub>13</sub>N<sub>3</sub>O:** (203.24), [203.11].
- **<sup>1</sup>H-NMR (250 MHz, CDCl<sub>3</sub>, 300 K):** δ = 7.36 (d, <sup>3</sup>J = 7.7 Hz, 1H, H-7 benzoxazole), 7.26 (d, <sup>3</sup>J = 7.7 Hz, 1H, H-4 benzoxazole), 7.17 (dt, <sup>3</sup>J = 7.7, 1.1 Hz, 1H, H-6 benzoxazole), 7.04 (dt, <sup>3</sup>J = 7.7, 1.1 Hz, 1H, H-5 benzoxazole), 3.89–3.65 (m, 4H, CH<sub>2</sub>-2-, CH<sub>2</sub>-6-piperazine), 3.17–2.96 (m, 4H, CH<sub>2</sub>-3-, CH<sub>2</sub>-5-piperazine) ppm.
- **MS (ESI pos.):** *m/z* (%) = 204. 23 (100) ([M+H]<sup>+</sup>, calcd. 204.11).

**(S)-(9H-Fluoren-9-yl)methyl (1-(4-(benzo[d]oxazol-2-yl)piperazin-1-yl)-4-cyclohexyl-1-oxobutan-2-yl)carbamate (181, SR123)**

(S)-2-(((9H-Fluoren-9-yl)methoxy)carbonyl)amino-4-cyclohexylbutanoic acid (**105**, 500 mg, 1.23 mmol) and HATU (560 mg, 1.47 mmol) were dissolved in DMF (dry, 6 mL) and DIPEA (190 mg, 1.47 mmol) was added. The reaction mixture was stirred for 1.5 h at RT and 2-(piperazin-1-yl)benzo[d]oxazole (**180**, 298 mg, 1.47 mmol) diluted in DMF (dry, 6 mL) was added. The mixture was stirred for additional 20 h at RT. DCM (50 mL) was added and the organic phase was washed 5 times with H<sub>2</sub>O (50 mL) and dried over MgSO<sub>4</sub>. The solvent was evaporated under reduced pressure and the crude product was purified using column chromatography on silica (DCM/MeOH 10:1).

**Yield:** 571 mg (0.964 mmol, 79%), colorless solid.

- **TLC:** R<sub>f</sub> = 0.94 (SiO<sub>2</sub>, DCM/MeOH 10:1).
- **C<sub>36</sub>H<sub>40</sub>N<sub>4</sub>O<sub>4</sub>:** (592.73), [592.30].

- **$^1\text{H-NMR}$  (400 MHz, DMSO- $d_6$ , 300 K):**  $\delta$  = 7.91–7.84 (m, 2H, H-4-, H-5-Fmoc), 7.79–7.69 (m, 2H, H-1-, H-8-Fmoc), 7.63 (d,  $^3J$  = 8.2 Hz, 1H, NHCOO), 7.45–7.36 (m, 3H, H-3-, H-6-Fmoc, H-7 benzoxazole), 7.35–7.27 (m, 3H, H-2-, H-7-Fmoc, H-4 benzoxazole), 7.17 (t,  $^3J$  = 7.5 Hz, 1H, H-6 benzoxazole), 7.04 (t,  $^3J$  = 7.5 Hz, 1H, H-5 benzoxazole), 4.48–4.39 (m, 1H, NHCHCO), 4.33–4.18 (m, 3H, OCH<sub>2</sub>, H-9 Fmoc), 3.76–3.40 (m, 8H, CH<sub>2</sub>-2-, CH<sub>2</sub>-3-, CH<sub>2</sub>-5-, CH<sub>2</sub>-6-piperazine), 1.71–1.50 (m, 7H, NHCHCH<sub>2</sub>CH<sub>2</sub>, H-2<sub>eq</sub>-, H-3<sub>eq</sub>-, H-4<sub>eq</sub>-, H-5<sub>eq</sub>-, H-6<sub>eq</sub>-cyclohexyl), 1.27–1.04 (m, 6H, H-1-, H-3<sub>ax</sub>-, H-4<sub>ax</sub>-, H-5<sub>ax</sub>-cyclohexyl, NHCHCH<sub>2</sub>CH<sub>2</sub>), 0.92–0.77 (m, 2H, H-2<sub>ax</sub>-, H-6<sub>ax</sub>-cyclohexyl) ppm.
- **$^{13}\text{C-NMR}$  (101 MHz, DMSO- $d_6$ , 300 K):**  $\delta$  = 170.5, 161.6, 155.9, 148.3, 143.8 (2x), 142.8, 140.7, 127.6, 127.0, 125.3, 124.0, 120.7, 116.0, 109.0, 65.6, 50.8, 46.7, 37.0, 32.9, 32.7, 28.9, 26.1, 25.8, 25.7 ppm.
- **MS (ESI pos.):**  $m/z$  (%) = 371.09 (100) ([M-Fmoc+2H]<sup>+</sup>, calcd. 371.25).

#### 8.4.5 Fmoc deprotections

The amines (**184-216**, **Table 21**), used in the amide-coupling reaction in **Section 8.4.6**, were freshly prepared directly before coupling to the acid following a general method: The corresponding Fmoc-protected amine (1.2 eq) was dissolved in dry DMF and piperidine 20% was added. The mixture was stirred for 1 h at RT, and DCM or EtOAc was added. The organic phase was washed 5 times with H<sub>2</sub>O and dried over MgSO<sub>4</sub>. The solvent was evaporated under reduced pressure, and the crude product (quantitative) was used without further purification.

**Table 21.** Summary of amines prepared by Fmoc deprotection.

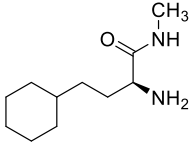
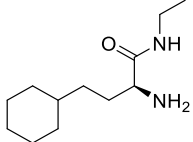
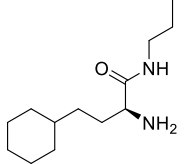
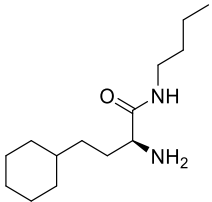
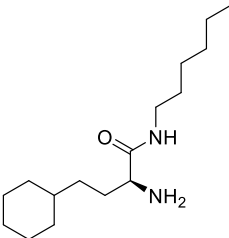
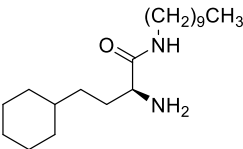
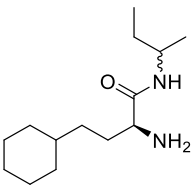
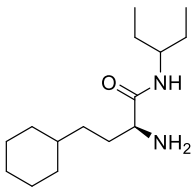
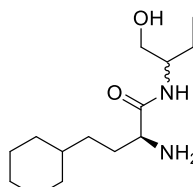
<p><b>(S)-2-Amino-4-cyclohexyl-N-methylbutanamide (184)</b></p> 	<p><b>(S)-2-Amino-4-cyclohexyl-N-ethylbutanamide (185)</b></p> 	<p><b>(S)-2-Amino-4-cyclohexyl-N-propylbutanamide (186)</b></p> 
<p><b>(S)-2-Amino-N-butyl-4-cyclohexylbutanamide (187)</b></p> 	<p><b>(S)-2-Amino-4-cyclohexyl-N-hexylbutanamide (188)</b></p> 	<p><b>(S)-2-Amino-4-cyclohexyl-N-decylbutanamide (189)</b></p> 
<p><b>(S)-2-Amino-N-((SR)-sec-butyl)-4-cyclohexylbutanamide (190)</b></p> 	<p><b>(S)-2-Amino-4-cyclohexyl-N-(pentan-3-yl)butanamide (191)</b></p> 	<p><b>(S)-2-Amino-4-cyclohexyl-N-((SR)-1-hydroxybutan-2-yl)butanamide (192)</b></p> 

Table 21. (continued)

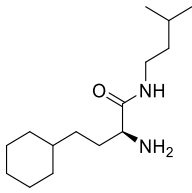
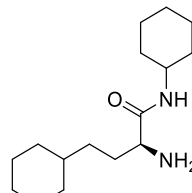
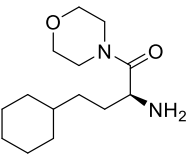
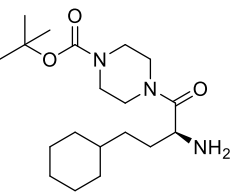
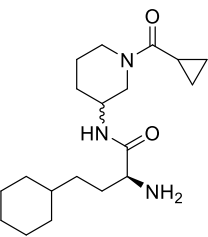
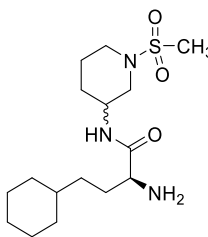
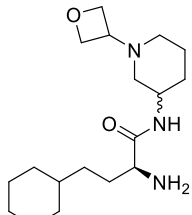
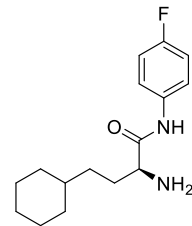
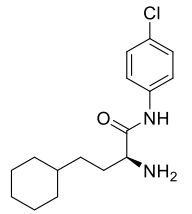
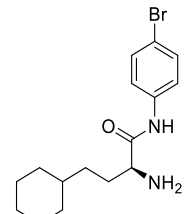
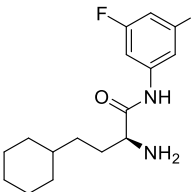
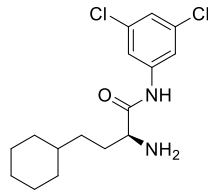
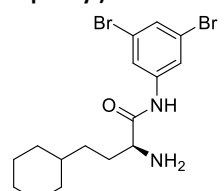
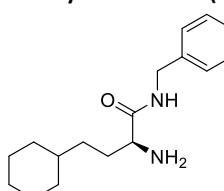
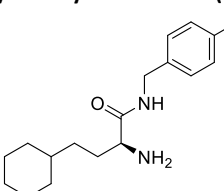
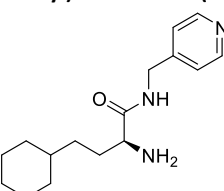
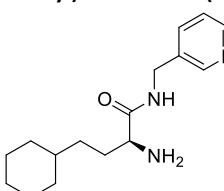
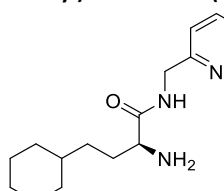
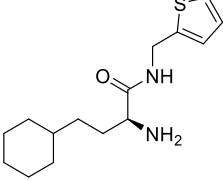
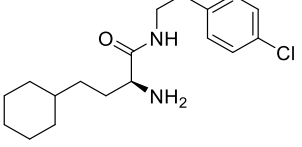
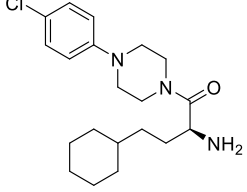
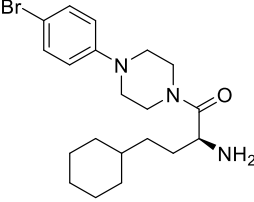
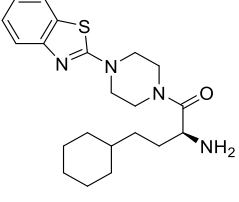
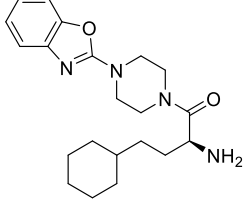
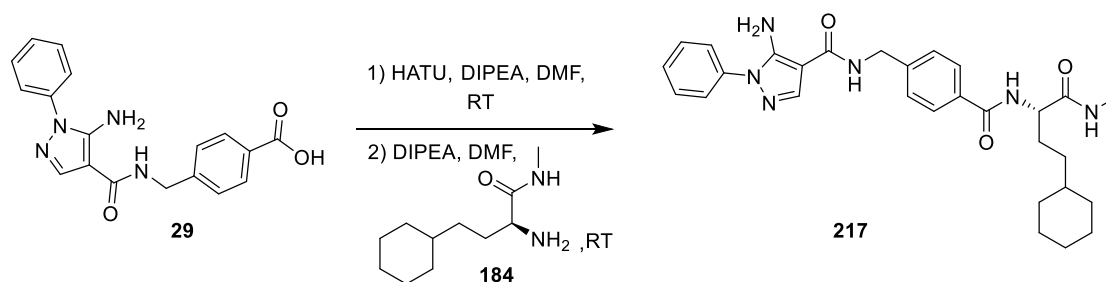
<p><b>(S)-2-Amino-4-cyclohexyl-N-isopentylbutanamide (193)</b></p> 	<p><b>(S)-2-Amino-N,4-dicyclohexylbutanamide (194)</b></p> 	<p><b>(S)-2-Amino-4-cyclohexyl-1-morpholinobutan-1-one (195)</b></p> 
<p><b>tert-Butyl (S)-4-(2-amino-4-cyclohexylbutanoyl)piperazine-1-carboxylate (196)</b></p> 	<p><b>(S)-2-Amino-4-cyclohexyl-N-((SR)-1-(cyclopropanecarbonyl)piperidin-3-yl)butanamide (197)</b></p> 	<p><b>(S)-2-Amino-4-cyclohexyl-N-((SR)-1-(methylsulfonyl)piperidin-3-yl)butanamide (198)</b></p> 
<p><b>(S)-2-Amino-4-cyclohexyl-N-((RS)-1-(oxetan-3-yl)piperidin-3-yl)butanamide (199)</b></p> 	<p><b>(S)-2-Amino-4-cyclohexyl-N-(4-fluorophenyl)butanamide (200)</b></p> 	<p><b>(S)-2-Amino-N-(4-chlorophenyl)-4-cyclohexylbutanamide (201)</b></p> 
<p><b>(S)-2-Amino-N-(4-bromophenyl)-4-cyclohexylbutanamide (202)</b></p> 	<p><b>(S)-2-Amino-4-cyclohexyl-N-(3,5-difluorophenyl)butanamide (203)</b></p> 	<p><b>(S)-2-Amino-4-cyclohexyl-N-(3,5-dichlorophenyl)butanamide (204)</b></p> 
<p><b>(S)-2-Amino-4-cyclohexyl-N-(3,5-dibromophenyl)butanamide (205)</b></p> 	<p><b>(S)-2-Amino-N-benzyl-4-cyclohexylbutanamide (206)</b></p> 	<p><b>(S)-2-Amino-N-(4-chlorobenzyl)-4-cyclohexylbutanamide (207)</b></p> 
<p><b>(S)-2-Amino-4-cyclohexyl-N-(pyridin-4-ylmethyl)butanamide (208)</b></p> 	<p><b>(S)-2-Amino-4-cyclohexyl-N-(pyridin-3-ylmethyl)butanamide (209)</b></p> 	<p><b>(S)-2-Amino-4-cyclohexyl-N-(pyridin-2-ylmethyl)butanamide (210)</b></p> 

Table 21. (continued)

<p>(S)-2-Amino-4-cyclohexyl-N-(thiophen-2-ylmethyl)butanamide (<b>211</b>)</p> 	<p>(S)-2-Amino-N-(4-chlorophenethyl)-4-cyclohexylbutanamide (<b>212</b>)</p> 	<p>(S)-2-Amino-1-(4-(4-chlorophenyl)piperazin-1-yl)-4-cyclohexylbutan-1-one (<b>213</b>)</p> 
<p>(S)-2-Amino-1-(4-(4-bromophenyl)piperazin-1-yl)-4-cyclohexylbutan-1-one (<b>214</b>)</p> 	<p>(S)-2-Amino-1-(4-(benzo[d]thiazol-2-yl)piperazin-1-yl)-4-cyclohexylbutan-1-one (<b>215</b>)</p> 	<p>(S)-2-Amino-1-(4-(benzo[d]oxazol-2-yl)piperazin-1-yl)-4-cyclohexylbutan-1-one (<b>216</b>)</p> 

#### 8.4.6 Synthesis of final compounds

##### (S)-5-Amino-N-(4-((4-cyclohexyl-1-(methylamino)-1-oxobutan-2-yl)carbamoyl)benzyl)-1-phenyl-1H-pyrazole-4-carboxamide (**217**, SR41)



4-((5-Amino-1-phenyl-1H-pyrazole-4-carboxamido)methyl)benzoic acid (**29**, 100 mg, 0.297 mmol) and HATU (136 mg, 0.357 mmol) were dissolved in DMF (5 mL) and DIPEA (58 mg, 0.45 mmol) was added. The solution was stirred for 2 h at RT and (S)-2-amino-4-cyclohexyl-N-methylbutanamide (**184**, 71 mg, 0.36 mmol), diluted in DMF (5 mL) and DIPEA (58 mg, 0.45 mmol), was added. The mixture was stirred for 20 h at RT. DCM (50 mL) was added and the organic phase was washed 5 times with H<sub>2</sub>O (20 mL) and dried over MgSO<sub>4</sub>. The solvent was evaporated under reduced pressure and the crude product was purified using column chromatography on silica (DCM/MeOH 20:1 → 10:1 → EtOH).

**Yield:** 90 mg (0.17 mmol, 59%), yellowish solid.

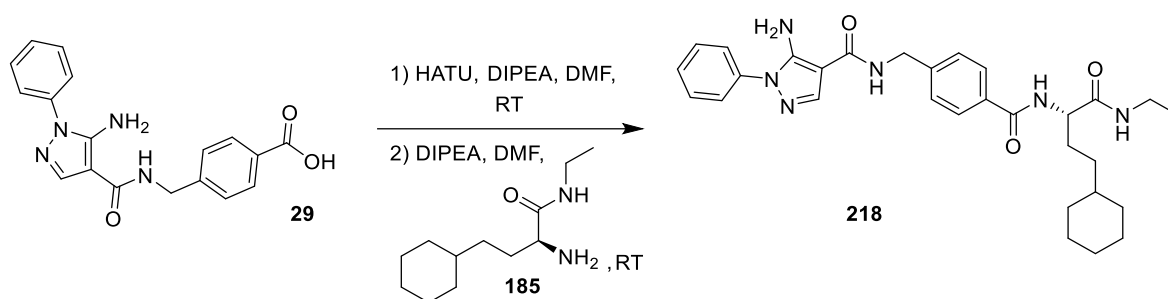
- **TLC:**  $R_f = 0.38$  (SiO<sub>2</sub>, EtOAc/MeOH 10:1).
- **C<sub>29</sub>H<sub>36</sub>N<sub>6</sub>O<sub>3</sub>:** (516.63), [516.28].
- **HPLC:**  $t_R = 13.91$  min.
- **<sup>1</sup>H-NMR (500 MHz, DMSO-d<sub>6</sub>, 300 K):**  $\delta = 8.51$  (t,  $^3J = 6.0$  Hz, 1H, CONHCH<sub>2</sub>), 8.33 (d,  $^3J = 8.1$  Hz, 1H, CONHCHCO), 7.96 (s, 1H, pyrazole), 7.89–7.84 (m, 3H, CONHCH<sub>3</sub>, H-3-, H-5-benzyl), 7.60–7.49 (m, 4H, H-2-, H-3-, H-5-, H-6-phenyl), 7.42–7.33 (m, 3H, H-4 phenyl, H-2-, H-6-benzyl), 6.38 (s, 2H, NH<sub>2</sub>),



4.47 (d,  $^3J = 6.0$  Hz, 2H, CH<sub>2</sub> benzyl), 4.38–4.30 (m, 1H, NHCHCONH), 2.58 (d,  $^3J = 4.6$  Hz, 3H, CH<sub>3</sub>), 1.81–1.72 (m, 1H, NHCHCH<sub>A</sub>H<sub>B</sub>CH<sub>2</sub>), 1.71–1.54 (m, 6H, NHCHCH<sub>A</sub>H<sub>B</sub>CH<sub>2</sub>, H-2<sub>eq</sub><sup>-</sup>, H-3<sub>eq</sub><sup>-</sup>, H-4<sub>eq</sub><sup>-</sup>, H-5<sub>eq</sub><sup>-</sup>, H-6<sub>eq</sub><sup>-</sup>-cyclohexyl), 1.28–1.03 (m, 6H, H-1-, H-3<sub>ax</sub><sup>-</sup>, H-4<sub>ax</sub><sup>-</sup>, H-5<sub>ax</sub><sup>-</sup>-cyclohexyl, NHCHCH<sub>2</sub>CH<sub>2</sub>), 0.90–0.76 (m, 2H, H-2<sub>ax</sub><sup>-</sup>, H-6<sub>ax</sub><sup>-</sup>-cyclohexyl) ppm.

- **<sup>13</sup>C-NMR (126 MHz, DMSO-d<sub>6</sub>, 300 K):**  $\delta = 172.3, 166.1, 164.2, 149.2, 143.6, 138.4, 138.2, 132.6, 129.4, 127.6, 127.1, 126.8, 123.1, 97.4, 53.6, 41.3, 36.8, 33.4, 32.9, 32.7, 29.2, 26.2, 25.8$  (2x), 25.6 ppm.
- **MS (ESI pos.):**  $m/z$  (%) = 517.20 (100) ([M+H]<sup>+</sup>, calcd. 517.29), 486.17 (87) ([M<sub>fr.(I)}</sub>]<sup>+</sup>, calcd. 486.25), 319.09 (56) ([M<sub>fr.(II)}</sub>]<sup>+</sup>, calcd. 319.25).
- **HRMS (FTMS ++ p MALDI):**  $m/z = 539.2742$  [M+Na]<sup>+</sup>, calcd. for [C<sub>29</sub>H<sub>36</sub>N<sub>6</sub>NaO<sub>3</sub>]<sup>+</sup> = 539.2747.

**(S)-5-Amino-N-(4-((4-cyclohexyl-1-(ethylamino)-1-oxobutan-2-yl)carbamoyl)benzyl)-1-phenyl-1H-pyrazole-4-carboxamide (218, SR43)**



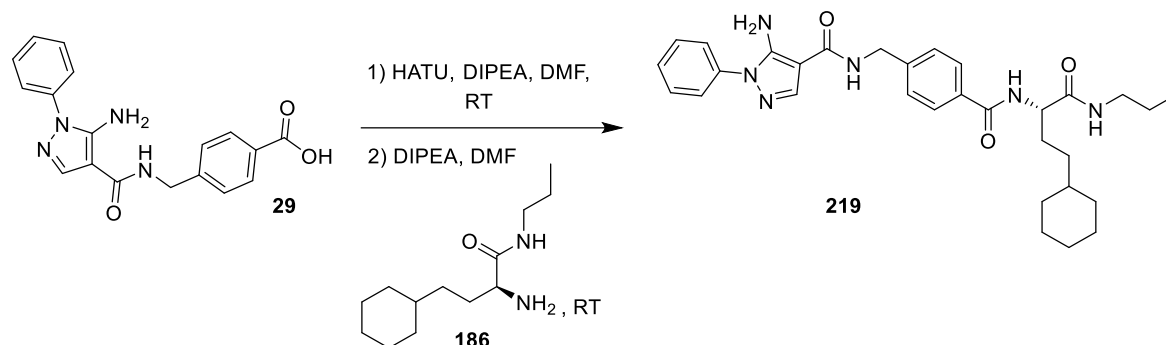
4-((5-Amino-1-phenyl-1H-pyrazole-4-carboxamido)methyl)benzoic acid (**29**, 100 mg, 0.297 mmol) and HATU (136 mg, 0.357 mmol) were dissolved in DMF (8 mL) and DIPEA (81 mg, 0.62 mmol) was added. The solution was stirred for 2.5 h at RT and (S)-2-amino-4-cyclohexyl-N-ethylbutanamide (**185**, 76 mg, 0.36 mmol), diluted in DMF (7 mL) and DIPEA (42 mg, 0.33 mmol), was added. The mixture was stirred for 3 d at RT. DCM (50 mL) was added and the organic phase was washed 5 times with H<sub>2</sub>O (20 mL) and dried over MgSO<sub>4</sub>. The solvent was evaporated under reduced pressure and the crude product was purified using column chromatography on silica (DCM/MeOH: 20:1 → 10:1 → EtOH).

**Yield:** 82 mg (0.16 mmol, 52%), yellowish solid.

- **TLC:** R<sub>f</sub> = 0.25 (SiO<sub>2</sub>, DCM/MeOH 20:1).
- **C<sub>30</sub>H<sub>38</sub>N<sub>6</sub>O<sub>3</sub>:** (530.66), [530.30].
- **HPLC:** t<sub>R</sub> = 14.41 min.
- **<sup>1</sup>H-NMR (500 MHz, CDCl<sub>3</sub>, 300 K):**  $\delta = 7.75$  (s, 1H, pyrazole), 7.68 (d,  $^3J = 8.2$  Hz, 2H, H-3-, H-5-benzyl), 7.57–7.47 (m, 4H, H-2-, H-3-, H-5-, H-6-phenyl), 7.42–7.36 (m, 1H, H-4-phenyl), 7.29 (d,  $^3J = 8.2$  Hz, 2H, H-2-, H-6-benzyl), 7.08 (d,  $^3J = 8.0$  Hz, 1H, NHCHCO), 6.67–6.55 (m, 2H, NHCH<sub>2</sub>C<sub>Ar</sub>, NHCH<sub>2</sub>CH<sub>3</sub>), 5.55 (br s, 2H, NH<sub>2</sub>), 4.63–4.51 (m, 3H, CH<sub>2</sub> benzyl, NHCHCO), 3.36–3.17 (m, 2H, NHCH<sub>2</sub>CH<sub>3</sub>), 1.98–1.88 (m, 1H, NHCHCH<sub>A</sub>H<sub>B</sub>CH<sub>2</sub>), 1.81–1.57 (m, 6H, NHCHCH<sub>A</sub>H<sub>B</sub>CH<sub>2</sub>, H-2<sub>eq</sub><sup>-</sup>, H-3<sub>eq</sub><sup>-</sup>, H-4<sub>eq</sub><sup>-</sup>, H-5<sub>eq</sub><sup>-</sup>, H-6<sub>eq</sub><sup>-</sup>-cyclohexyl), 1.33–1.05 (m, 9H, H-1-, H-3<sub>ax</sub><sup>-</sup>, H-4<sub>ax</sub><sup>-</sup>, H-5<sub>ax</sub><sup>-</sup>-cyclohexyl, NHCHCH<sub>2</sub>CH<sub>2</sub>, CH<sub>3</sub>), 0.92–0.78 (m, 2H, H-2<sub>ax</sub><sup>-</sup>, H-6<sub>ax</sub><sup>-</sup>-cyclohexyl) ppm.
- **<sup>13</sup>C-NMR (126 MHz, CDCl<sub>3</sub>, 300 K):**  $\delta = 171.8, 167.2, 164.8, 149.0, 143.0, 137.8, 137.7$  (2x), 133.0, 129.9, 128.2, 127.6, 123.9, 98.0, 54.1, 42.6, 37.7, 34.6, 33.4, 33.3 (2x), 30.3, 26.7, 26.4, 14.8 (2x) ppm.
- **MS (ESI pos.):**  $m/z$  (%) = 531.23 (100) ([M+H]<sup>+</sup>, calcd. 531.31).

- **HRMS (FTMS + p MALDI):**  $m/z = 531.3063$   $[M+H]^+$ , calcd. for  $[C_{30}H_{39}N_6O_3]^+ = 531.3078$ .

**(S)-5-Amino-N-(4-((4-cyclohexyl-1-oxo-1-(propylamino)butan-2-yl)carbamoyl)benzyl)-1-phenyl-1H-pyrazole-4-carboxamide (219, SR61)**



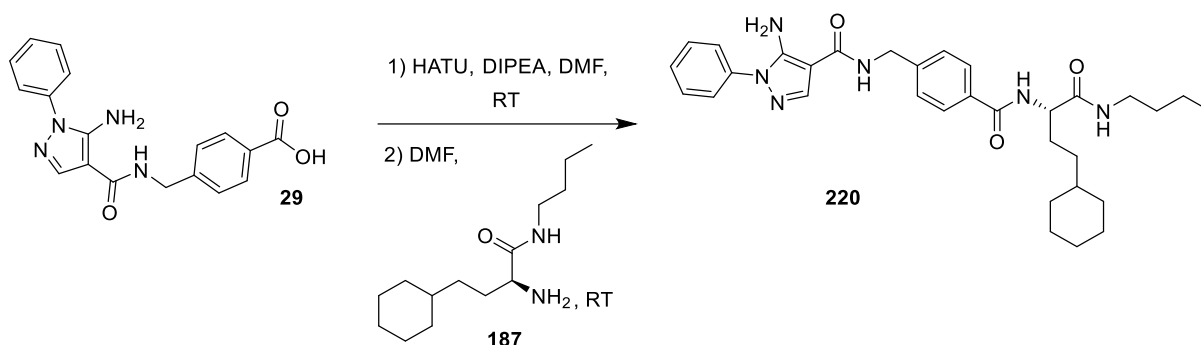
4-((5-Amino-1-phenyl-1H-pyrazole-4-carboxamido)methyl)benzoic acid (**29**, 100 mg, 0.297 mmol) and HATU (152 mg, 0.400 mmol) were dissolved in DMF (5 mL) and DIPEA (58 mg, 0.45 mmol) was added. The solution was stirred for 1.5 h at RT and (S)-2-amino-4-cyclohexyl-N-propylbutanamide (**186**, 81 mg, 0.36 mmol), diluted in DMF (5 mL) and DIPEA (58 mg, 0.45 mmol), was added. The mixture was stirred for 20 h at RT. DCM (100 mL) was added and the organic phase was washed 5 times with H<sub>2</sub>O (20 mL) and dried over MgSO<sub>4</sub>. The solvent was evaporated under reduced pressure and the crude product was purified using column chromatography on silica (DCM/MeOH 20:1).

**Yield:** 121 mg (0.222 mmol, 75%), yellowish solid.

- **TLC:**  $R_f = 0.17$  (SiO<sub>2</sub>, DCM/MeOH 20:1).
- **C<sub>31</sub>H<sub>40</sub>N<sub>6</sub>O<sub>3</sub>:** (544.69), [544.32].
- **HPLC:**  $t_R = 14.92$  min.
- **<sup>1</sup>H-NMR (500 MHz, DMSO-d<sub>6</sub>, 300 K):**  $\delta = 8.55\text{--}8.47$  (m, 1H, NHCH<sub>2</sub>C<sub>Ar</sub>), 8.28 (d,  $^3J = 8.1$  Hz, 1H, NHCHCO), 7.98 (s, 1H, pyrazole), 7.92 (t,  $^3J = 5.7$  Hz, 1H, NHCH<sub>2</sub>CH<sub>2</sub>), 7.85 (d,  $^3J = 8.3$  Hz, 2H, H-3-, H-5-benzyl), 7.59–7.49 (m, 4H, H-2-, H-3-, H-5-, H-6-phenyl), 7.41–7.31 (m, 3H, H-4 phenyl, H-2-, H-6-benzyl), 6.38 (br s, 2H, NH<sub>2</sub>), 4.49–4.43 (m, 2H, CH<sub>2</sub> benzyl), 4.39–4.32 (m, 1H, NHCHCO), 3.10–2.93 (m, 2H, NHCH<sub>2</sub>CH<sub>2</sub>), 1.81–1.71 (m, 1H, NHCHCH<sub>A</sub>H<sub>B</sub>CH<sub>2</sub>), 1.70–1.55 (m, 6H, NHCHCH<sub>A</sub>H<sub>B</sub>CH<sub>2</sub>, H-2<sub>eq</sub>-, H-3<sub>eq</sub>-, H-4<sub>eq</sub>-, H-5<sub>eq</sub>-, H-6<sub>eq</sub>-cyclohexyl), 1.40 (sext,  $^3J = 7.3$  Hz, 2H, NHCH<sub>2</sub>CH<sub>2</sub>), 1.28–1.04 (m, 6H, H-1-, H-3<sub>ax</sub>-, H-4<sub>ax</sub>-, H-5<sub>ax</sub>-cyclohexyl, NHCHCH<sub>2</sub>CH<sub>2</sub>), 0.90–0.77 (m, 5H, H-2<sub>ax</sub>-, H-6<sub>ax</sub>-cyclohexyl, CH<sub>3</sub>) ppm.
- **<sup>13</sup>C-NMR (126 MHz, DMSO-d<sub>6</sub>, 300 K):**  $\delta = 171.7, 166.0, 164.2, 149.2, 143.6, 141.4, 138.4, 138.2, 132.7, 129.4, 127.6, 127.1, 127.0, 126.8$  (2x), 123.1, 97.4, 53.6, 41.3, 36.8, 33.3, 32.9, 32.7, 29.4, 26.2, 25.8 (2x), 22.3, 11.4 ppm.
- **MS (ESI pos.):**  $m/z$  (%) = 545.32 (100) ( $[M+H]^+$ , calcd. 545.33), 486.27 (30) ( $[M_{fr.}]^+$ , calcd. 486.25).

**HRMS (FTMS + p MALDI):**  $m/z = 545.3222$   $[M+H]^+$ , calcd. for  $[C_{31}H_{41}N_6O_3]^+ = 545.3240$ .

**(S)-5-Amino-N-(4-((1-(butylamino)-4-cyclohexyl-1-oxobutan-2-yl)carbamoyl)benzyl)-1-phenyl-1H-pyrazole-4-carboxamide (220, SR59)**

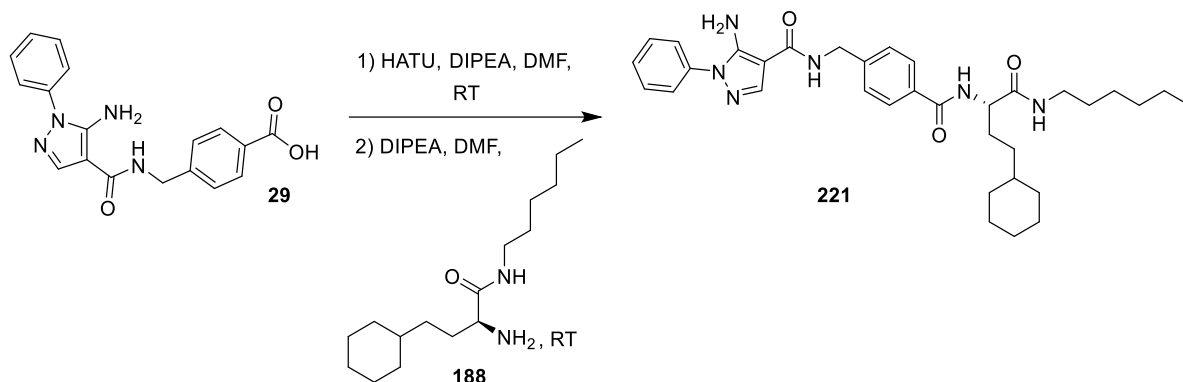


4-((5-Amino-1-phenyl-1H-pyrazole-4-carboxamido)methyl)benzoic acid (**29**, 100 mg, 0.297 mmol) and HATU (136 mg, 0.357 mmol) were dissolved in DMF (5 mL) and DIPEA (46 mg, 0.36 mmol) was added. The solution was stirred for 1.5 h at RT and (S)-2-amino-4-cyclohexyl-N-butylbutanamide (**187**, 120 mg, 0.500 mmol) diluted in DMF (5 mL), was added. The mixture was stirred for 3 d at RT. DCM (50 mL) was added and the organic phase was washed 5 times with H<sub>2</sub>O (20 mL) and dried over MgSO<sub>4</sub>. The solvent was evaporated under reduced pressure and the crude product was purified using column chromatography on silica (DCM/MeOH 20:1).

**Yield:** 140 mg (0.251 mmol, 85%), colorless solid.

- **TLC:** R<sub>f</sub> = 0.30 (SiO<sub>2</sub>, DCM/MeOH 20:1).
- **C<sub>32</sub>H<sub>42</sub>N<sub>6</sub>O<sub>3</sub>:** (558.71), [558.33].
- **HPLC:** t<sub>R</sub> = 15.50 min.
- **<sup>1</sup>H-NMR (500 MHz, DMSO-d<sub>6</sub>, 300 K):** δ = 8.51 (t, <sup>3</sup>J = 6.1 Hz, 1H, NHCH<sub>2</sub>C<sub>Ar</sub>), 8.27 (d, <sup>3</sup>J = 8.0 Hz, 1H, NHCHCO), 7.98 (s, 1H, pyrazole), 7.91 (t, <sup>3</sup>J = 5.1 Hz, 1H, NHCH<sub>2</sub>CH<sub>2</sub>), 7.85 (d, <sup>3</sup>J = 8.1 Hz, 2H, H-3-, H-5-benzyl), 7.61–7.48 (m, 4H, H-2-, H-3-, H-5-, H-6-phenyl), 7.42–7.35 (m, 3H, H-4-phenyl, H-2-, H-6-benzyl), 6.38 (br s, 2H, NH<sub>2</sub>), 4.47 (d, <sup>3</sup>J = 6.0 Hz, 2H, CH<sub>2</sub> benzyl), 4.39–4.31 (m, 1H, NHCHCO), 3.14–2.97 (m, 2H, NHCH<sub>2</sub>CH<sub>2</sub>), 1.80–1.71 (m, 1H, NHCHCH<sub>A</sub>H<sub>B</sub>CH<sub>2</sub>), 1.70–1.55 (m, 6H, NHCHCH<sub>A</sub>H<sub>B</sub>CH<sub>2</sub>, H-2<sub>eq</sub>-, H-3<sub>eq</sub>-, H-4<sub>eq</sub>-, H-5<sub>eq</sub>-, H-6<sub>eq</sub>-cyclohexyl), 1.42–1.33 (m, 2H, NHCH<sub>2</sub>CH<sub>2</sub>), 1.31–1.04 (m, 8H, H-1-, H-3<sub>ax</sub>-, H-4<sub>ax</sub>-, H-5<sub>ax</sub>-cyclohexyl, NHCHCH<sub>2</sub>CH<sub>2</sub>, CH<sub>2</sub>CH<sub>3</sub>), 0.91–0.77 (m, 5H, H-2<sub>ax</sub>-, H-6<sub>ax</sub>-cyclohexyl, CH<sub>3</sub>) ppm.
- **<sup>13</sup>C-NMR (126 MHz, DMSO-d<sub>6</sub>, 300 K):** δ = 171.6, 166.0, 164.2, 149.2, 143.6, 138.4, 138.2, 132.7, 129.4, 127.6, 127.1, 126.8, 123.1, 97.4, 53.6, 41.3, 38.1, 36.8, 33.3, 32.9, 32.7, 31.2, 29.4, 26.2, 25.8 (2x), 19.5, 13.7 ppm.
- **MS (ESI neg.):** m/z (%) = 557.47 (100) ([M-H]<sup>-</sup>, calcd. 557.31), 603.44 (41) ([M+EtO]<sup>-</sup>, calcd. 603.36).
- **HRMS (FTMS + p MALDI):** m/z = 581.3211 [M+Na]<sup>+</sup>, calcd. for [C<sub>32</sub>H<sub>42</sub>N<sub>6</sub>NaO<sub>3</sub>]<sup>+</sup> = 581.3216.

**(S)-5-Amino-N-(4-((4-cyclohexyl-1-(hexylamino)-1-oxobutan-2-yl)carbamoyl)benzyl)-1-phenyl-1H-pyrazole-4-carboxamide (221, SR81)**

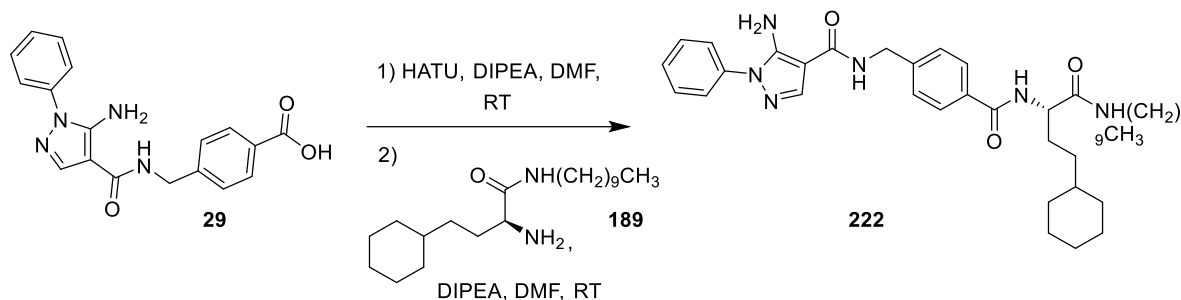


4-((5-Amino-1-phenyl-1H-pyrazole-4-carboxamido)methyl)benzoic acid (**29**, 150 mg, 0.446 mmol) and HATU (203 mg, 0.535 mmol) were dissolved in DMF (5 mL) and DIPEA (87 mg, 0.67 mmol) was added. The solution was stirred for 1.5 h at RT and (S)-2-amino-4-cyclohexyl-N-hexylbutanamide (**188**, 144 mg, 0.535 mmol), diluted in DMF (5 mL) and DIPEA (87 mg, 0.67 mmol), was added. The mixture was stirred for 20 h at RT. EtOAc (50 mL) was added and the organic phase was washed 4 times with H<sub>2</sub>O (20 mL) and dried over MgSO<sub>4</sub>. The solvent was evaporated under reduced pressure and the crude product was purified using column chromatography on silica (cyclohexane/EtOAc 1:1 → 1:6 → EtOAc).

**Yield:** 206 mg (0.351 mmol, 79%), colorless solid.

- **TLC:** R<sub>f</sub> = 0.33 (SiO<sub>2</sub>, cyclohexane/EtOAc 1:6).
- **C<sub>34</sub>H<sub>46</sub>N<sub>6</sub>O<sub>3</sub>:** (568.77), [586.36].
- **HPLC:** t<sub>R</sub> = 16.70 min.
- **<sup>1</sup>H-NMR (500 MHz, DMSO-d<sub>6</sub>, 300 K):** δ = 8.52 (t, <sup>3</sup>J = 6.1 Hz, 1H, NHCH<sub>2</sub>C<sub>Ar</sub>), 8.28 (d, <sup>3</sup>J = 8.1 Hz, 1H, NHCHCO), 7.99 (s, 1H, pyrazole), 7.92 (t, <sup>3</sup>J = 5.6 Hz, 1H, NHCH<sub>2</sub>CH<sub>2</sub>), 7.86 (d, <sup>3</sup>J = 8.3 Hz, 2H, H-3-, H-5-benzyl), 7.60–7.49 (m, 4H, H-2-, H-3-, H-5-, H-6-phenyl), 7.41–7.35 (m, 3H, H-4-phenyl, H-2-, H-6-benzyl), 6.39 (br s, 2H, NH<sub>2</sub>), 4.47 (d, 2H, <sup>3</sup>J = 5.9 Hz, CH<sub>2</sub> benzyl), 4.39–4.31 (m, 1H, NHCHCO), 3.16–3.06 (m, 1H, NHCH<sub>A</sub>H<sub>B</sub>CH<sub>2</sub>-hexyl), 3.04–2.94 (m, 1H, NHCH<sub>A</sub>H<sub>B</sub>CH<sub>2</sub>-hexyl), 1.81–1.55 (m, 7H, NHCHCH<sub>2</sub>, H-2<sub>eq</sub>-, H-3<sub>eq</sub>-, H-4<sub>eq</sub>-, H-5<sub>eq</sub>-, H-6<sub>eq</sub>-cyclohexyl), 1.43–1.32 (m, 2H, NHCH<sub>2</sub>CH<sub>2</sub>-hexyl), 1.31–1.04 (m, 12H, CH<sub>2</sub>-3-, CH<sub>2</sub>-4-, CH<sub>2</sub>-5-NH-decyl, NHCHCH<sub>2</sub>CH<sub>2</sub>, H-1-, H-3<sub>ax</sub>-, H-4<sub>ax</sub>-, H-5<sub>ax</sub>-cyclohexyl), 0.91–0.77 (m, 5H, CH<sub>3</sub>, H-2<sub>ax</sub>-, H-6<sub>ax</sub>-cyclohexyl) ppm.
- **<sup>13</sup>C-NMR (126 MHz, DMSO-d<sub>6</sub>, 300 K):** δ = 171.6, 166.0, 164.2, 149.2, 143.6, 138.4, 138.3, 132.7, 129.4, 127.6, 127.1, 126.8, 123.1, 97.4, 53.6, 41.3, 38.4, 36.8, 33.3, 32.9, 32.7, 31.0, 29.4, 29.0, 26.2, 26.0, 25.8 (2x), 22.1, 13.9 ppm.
- **MS (ESI pos.):** m/z (%) = 587.38 (48) ([M+H]<sup>+</sup>, calcd. 587.37), 486.27 (13) ([M<sub>fr.(I)}</sub>]<sup>+</sup>, calcd. 486.25), 190.35 (100) ([M<sub>fr.(II)}</sub>+Na]<sup>+</sup>, calcd. 190.13).
- **HRMS (FTMS + p MALDI):** m/z = 609.3523 [M+Na]<sup>+</sup>, calcd. for [C<sub>34</sub>H<sub>46</sub>N<sub>6</sub>NaO<sub>3</sub>]<sup>+</sup> = 609.3529.

**(S)-5-Amino-N-(4-((4-cyclohexyl-1-(decylamino)-1-oxobutan-2-yl)carbamoyl)benzyl)-1-phenyl-1H-pyrazole-4-carboxamide (222, SR73)**

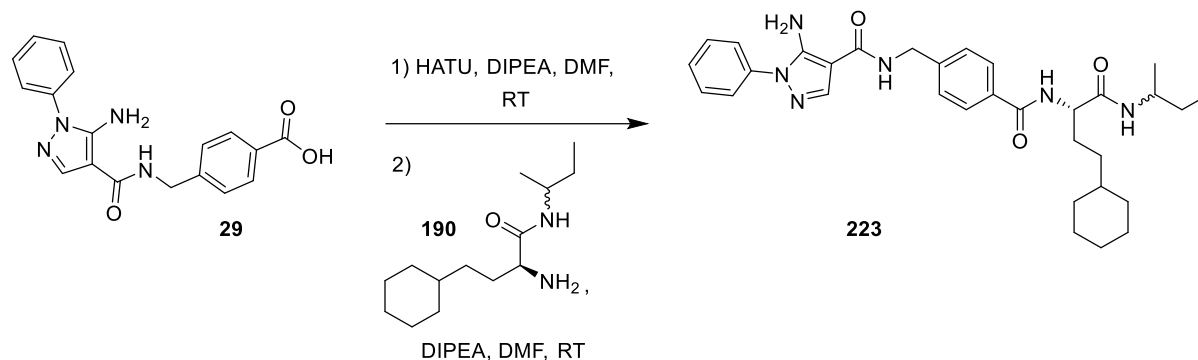


4-((5-Amino-1-phenyl-1H-pyrazole-4-carboxamido)methyl)benzoic acid (**29**, 200 mg, 0.595 mmol) and HATU (280 mg, 0.736 mmol) were dissolved in DMF (5 mL) and DIPEA (115 mg, 0.893 mmol) was added. The solution was stirred for 2 h at RT and (S)-2-amino-4-cyclohexyl-N-decylbutanamide (**189**, 239 mg, 0.736 mmol), diluted in DMF (5 mL) and DIPEA (115 mg, 0.893 mmol), was added. The mixture was stirred for 20 h at RT. DCM (100 mL) was added and the organic phase was washed 5 times with H<sub>2</sub>O (20 mL) and dried over MgSO<sub>4</sub>. The solvent was evaporated under reduced pressure and the crude product was purified using column chromatography on silica (cyclohexane/EtOAc 1:6 → EtOAc).

**Yield:** 217 mg (0.338 mmol, 57%), colorless solid.

- **TLC:** R<sub>f</sub> = 0.41 (SiO<sub>2</sub>, cyclohexane/EtOAc 1:6).
- **C<sub>38</sub>H<sub>54</sub>N<sub>6</sub>O<sub>3</sub>:** (642.87), [642.43].
- **HPLC:** t<sub>R</sub> = 20.95 min.
- **<sup>1</sup>H-NMR (500 MHz, DMSO-d<sub>6</sub>, 300 K):** δ = 8.51 (t, <sup>3</sup>J = 5.9 Hz, 1H, NHCH<sub>2</sub>C<sub>Ar</sub>), 8.27 (d, <sup>3</sup>J = 8.0 Hz, 1H, NHCHCO), 7.98 (s, 1H, pyrazole), 7.91 (t, <sup>3</sup>J = 5.6 Hz, 1H, NHCH<sub>2</sub>CH<sub>2</sub>), 7.85 (d, <sup>3</sup>J = 8.3 Hz, 2H, H-3-, H-5-benzyl), 7.59–7.50 (m, 4H, H-2-, H-3-, H-5-, H-6-phenyl), 7.41–7.35 (m, 3H, H-4 phenyl, H-2-, H-6-benzyl), 6.38 (br s, 2H, NH<sub>2</sub>), 4.47 (d, 2H, <sup>3</sup>J = 5.9 Hz, CH<sub>2</sub> benzyl), 4.39–4.31 (m, 1H, NHCHCO), 3.16–3.06 (m, 1H, NHCH<sub>A</sub>H<sub>B</sub>CH<sub>2</sub>-decyl), 3.03–2.94 (m, 1H, NHCH<sub>A</sub>H<sub>B</sub>CH<sub>2</sub>-decyl), 1.80–1.71 (m, 1H, NHCHCH<sub>A</sub>H<sub>B</sub>CH<sub>2</sub>), 1.70–1.55 (m, 6H, NHCHCH<sub>A</sub>H<sub>B</sub>CH<sub>2</sub>, H-2<sub>eq</sub>-, H-3<sub>eq</sub>-, H-4<sub>eq</sub>-, H-5<sub>eq</sub>-, H-6<sub>eq</sub>-cyclohexyl), 1.44–1.33 (m, 2H, NHCH<sub>A</sub>H<sub>B</sub>CH<sub>2</sub>-decyl), 1.32–1.03 (m, 20H, CH<sub>2</sub>-3-, CH<sub>2</sub>-4-, CH<sub>2</sub>-5-, CH<sub>2</sub>-6-, CH<sub>2</sub>-7-, CH<sub>2</sub>-8-, CH<sub>2</sub>-9-NH-decyl, NHCHCH<sub>2</sub>CH<sub>2</sub>, H-1-, H-3<sub>ax</sub>-, H-4<sub>ax</sub>-, H-5<sub>ax</sub>-cyclohexyl), 0.90–0.77 (m, 5H, CH<sub>3</sub>, H-2<sub>ax</sub>-, H-6<sub>ax</sub>-cyclohexyl) ppm.
- **<sup>13</sup>C-NMR (126 MHz, DMSO-d<sub>6</sub>, 300 K):** δ = 171.6, 166.0, 164.2, 149.2, 143.6, 138.4, 138.3, 132.7, 129.4, 127.6, 127.1, 126.8, 123.1, 97.4, 53.7, 41.3, 38.4, 36.8, 33.3, 32.9, 32.8, 31.3, 29.4, 29.1, 29.0 (2x), 28.8 (2x), 26.3, 26.2, 25.8 (2x), 22.1, 14.0 ppm.
- **MS (ESI pos.):** m/z (%) = 643.46 (96) ([M+H]<sup>+</sup>, calcd. 643.44), 486.33 (25) ([M<sub>fr.(I)}</sub>]<sup>+</sup>, calcd. 486.25), 190.35 (100) ([M<sub>fr.(II)}</sub>+Na]<sup>+</sup>, calcd. 190.13).
- **HRMS (FTMS + p MALDI):** m/z = 665.4169 [M+Na]<sup>+</sup>, calcd. for [C<sub>38</sub>H<sub>54</sub>N<sub>6</sub>NaO<sub>3</sub>]<sup>+</sup> = 466.4155.

**5-Amino-N-(4-(((S)-1-(((SR)-sec-butyl)amino)-4-cyclohexyl-1-oxobutan-2-yl)carbamoyl)benzyl)-1-phenyl-1H-pyrazole-4-carboxamide (223, SR63)**

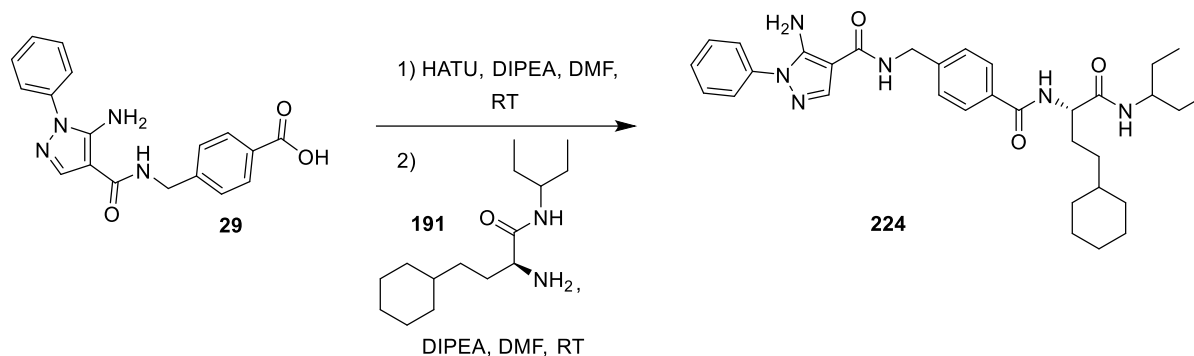


4-(((5-Amino-1-phenyl-1H-pyrazole-4-carboxamido)methyl)benzoic acid (**29**, 150 mg, 0.446 mmol) and HATU (240 mg, 0.631 mmol) were dissolved in DMF (5 mL) and DIPEA (87 mg, 0.67 mmol) was added. The solution was stirred for 2 h at RT and (S)-2-amino-N-(((SR)-sec-butyl)-4-cyclohexylbutanamide (**190**, 81 mg, 0.36 mmol), diluted in DMF (5 mL) and DIPEA (87 mg, 0.67 mmol), was added. The mixture was stirred for 20 h at RT. DCM (50 mL) was added and the organic phase was washed 5 times with H<sub>2</sub>O (20 mL) and dried over MgSO<sub>4</sub>. The solvent was evaporated under reduced pressure and the crude product was purified using column chromatography on silica (DCM/MeOH 20:1).

**Yield:** 155 mg (0.277 mmol, 78%), colorless solid.

- **TLC:**  $R_f = 0.19$  (SiO<sub>2</sub>, DCM/MeOH 20:1).
- **C<sub>32</sub>H<sub>42</sub>N<sub>6</sub>O<sub>3</sub>:** (558.71), [558.33].
- **HPLC:** (mixture of diastereomeres)  $t_R = 15.46$  min.
- **<sup>1</sup>H-NMR (500 MHz, DMSO-d<sub>6</sub>, 300 K):** (mixture of diastereomeres)  $\delta = 8.51$  (t,  $^3J = 5.9$  Hz, 1H, NHCH<sub>2</sub>C<sub>Ar</sub>), 8.25 (d,  $^3J = 8.1$  Hz, 0.5H, NHCHCO), 8.22 (d,  $^3J = 8.1$  Hz, 0.5H, NHCHCO), 7.98 (s, 1H, pyrazole), 7.85 (d,  $^3J = 8.0$  Hz, 2H, H-3-, H-5-benzyl), 7.74 (d,  $^3J = 8.2$  Hz, 0.5H, NHCH(CH<sub>3</sub>)CH<sub>2</sub>CH<sub>3</sub>), 7.70 (d,  $^3J = 8.2$  Hz, 0.5H, NHCH(CH<sub>3</sub>)CH<sub>2</sub>CH<sub>3</sub>), 7.59–7.49 (m, 4H, H-2-, H-3-, H-5-, H-6-phenyl), 7.41–7.34 (m, 3H, H-4 phenyl, H-2-, H-6-benzyl), 6.38 (br s, 2H, NH<sub>2</sub>), 4.47 (d,  $^3J = 5.8$  Hz, 2H, CH<sub>2</sub> benzyl), 4.40–4.32 (m, 1H, NHCHCO), 3.67 (sext,  $^3J = 6.7$  Hz, 1H, NHCHCH<sub>3</sub>), 1.78–1.55 (m, 7H, NHCHCH<sub>2</sub>CH<sub>2</sub>, H-2<sub>eq</sub>-, H-3<sub>eq</sub>-, H-4<sub>eq</sub>-, H-5<sub>eq</sub>-, H-6<sub>eq</sub>-cyclohexyl), 1.43–1.32 (m, 2H, CH<sub>2</sub>CH<sub>3</sub>), 1.28–1.08 (m, 6H, H-1-, H-3<sub>ax</sub>-, H-4<sub>ax</sub>-, H-5<sub>ax</sub>-cyclohexyl, NHCHCH<sub>2</sub>CH<sub>2</sub>), 1.02 (d,  $^3J = 6.7$ , 1.5H, CHCH<sub>3</sub>), 1.00 (d,  $^3J = 6.7$ , 1.5H, CHCH<sub>3</sub>), 0.88–0.77 (m, 5H, H-2<sub>ax</sub>-, H-6<sub>ax</sub>-cyclohexyl, CH<sub>2</sub>CH<sub>3</sub>) ppm.
- **<sup>13</sup>C-NMR (126 MHz, DMSO-d<sub>6</sub>, 300 K):** (mixture of diastereomeres)  $\delta = 171.7$ , 165.9 (2x), 164.2, 149.2, 143.6, 138.4, 138.2, 132.7, 129.4, 127.5, 127.1, 126.8, 123.1, 97.4, 53.6 (2x), 45.7 (2x), 41.3, 36.8, 33.3, 33.0, 32.7, 29.7, 29.4, 28.8 (2x), 26.2, 25.8 (2x), 20.3 (2x), 10.5, 10.4 ppm.
- **MS (ESI pos.):**  $m/z$  (%) = 581.39 (100) ([M+Na]<sup>+</sup>, calcd. 581.32).
- **HRMS (FTMS + p MALDI):**  $m/z = 581.3209$  [M+Na]<sup>+</sup>, calcd. for [C<sub>32</sub>H<sub>42</sub>N<sub>6</sub>NaO<sub>3</sub>]<sup>+</sup> = 581.3216.

**(S)-5-Amino-N-(4-((4-cyclohexyl-1-oxo-1-(pentan-3-ylamino)butan-2-yl)carbamoyl)benzyl)-1-phenyl-1H-pyrazole-4-carboxamide (224, SR65)**

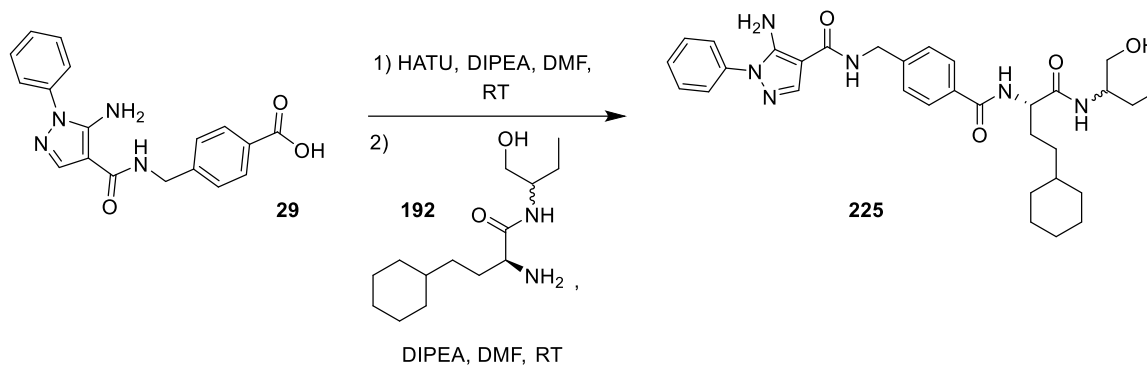


4-((5-Amino-1-phenyl-1H-pyrazole-4-carboxamido)methyl)benzoic acid (**29**, 150 mg, 0.446 mmol) and HATU (204 mg, 0.535 mmol) were dissolved in DMF (5 mL) and DIPEA (87 mg, 0.67 mmol) was added. The solution was stirred for 2 h at RT and (S)-2-amino-4-cyclohexyl-N-(pentan-3-yl)butanamide (**191**, 136 mg, 0.535 mmol), diluted in DMF (5 mL) and DIPEA (87 mg, 0.67 mmol), was added. The mixture was stirred for 20 h at RT. DCM (50 mL) was added and the organic phase was washed 5 times with H<sub>2</sub>O (20 mL) and dried over MgSO<sub>4</sub>. The solvent was evaporated under reduced pressure and the crude product was purified using column chromatography on silica (DCM/MeOH 20:1).

**Yield:** 148 mg (0.258 mmol, 58%), yellowish solid.

- **TLC:**  $R_f = 0.20$  (SiO<sub>2</sub>, DCM/MeOH 20:1).
- **C<sub>33</sub>H<sub>44</sub>N<sub>6</sub>O<sub>3</sub>:** (572.74), [572.35].
- **HPLC:**  $t_R = 15.90$  min.
- **<sup>1</sup>H-NMR (500 MHz, CDCl<sub>3</sub>, 300 K):**  $\delta = 7.76$  (s, 1H, pyrazole), 7.67 (d,  $^3J = 8.2$  Hz, 2H, H-3-, H-5-benzyl), 7.56–7.46 (m, 4H, H-2-, H-3-, H-5-, H-6-phenyl), 7.38 (t,  $^3J = 7.2$  Hz, 1H, H-4-phenyl), 7.29 (d,  $^3J = 8.2$  Hz, 2H, H-2-, H-6-benzyl), 7.15 (d,  $^3J = 7.9$  Hz, 1H, NHCHCO), 6.66 (t,  $^3J = 5.9$  Hz, 1H, NHCH<sub>2</sub>C<sub>Ar</sub>), 6.33 (d,  $^3J = 9.0$  Hz, 1H, NHCH(CH<sub>A</sub>H<sub>B</sub>CH<sub>3</sub>)<sub>2</sub>), 5.52 (s, 2H, NH<sub>2</sub>), 4.65–4.51 (m, 3H, CH<sub>2</sub> benzyl, NHCHCO), 3.78–3.68 (m, 1H, NHCH(CH<sub>A</sub>H<sub>B</sub>CH<sub>3</sub>)<sub>2</sub>), 2.00–1.88 (m, 1H, NHCHCH<sub>A</sub>H<sub>B</sub>CH<sub>2</sub>), 1.82–1.72 (m, 1H, NHCHCH<sub>A</sub>H<sub>B</sub>CH<sub>2</sub>), 1.71–1.59 (m, 5H, H-2<sub>eq</sub>-, H-3<sub>eq</sub>-, H-4<sub>eq</sub>-, H-5<sub>eq</sub>-, H-6<sub>eq</sub>-cyclohexyl), 1.58–1.44 (m, 2H, NHCH(CH<sub>A</sub>H<sub>B</sub>CH<sub>3</sub>)<sub>2</sub>), 1.43–1.05 (m, 8H, NHCH(CH<sub>A</sub>H<sub>B</sub>CH<sub>3</sub>)<sub>2</sub>, H-1-, H-3<sub>ax</sub>-, H-4<sub>ax</sub>-, H-5<sub>ax</sub>-cyclohexyl, NHCHCH<sub>A</sub>H<sub>B</sub>CH<sub>2</sub>), 0.93–0.78 (m, 8H, H-2<sub>ax</sub>-, H-6<sub>ax</sub>-cyclohexyl, NHCH(CH<sub>A</sub>H<sub>B</sub>CH<sub>3</sub>)<sub>2</sub> ppm.
- **<sup>13</sup>C-NMR (126 MHz, DMSO-d<sub>6</sub>, 300 K):**  $\delta = 171.7, 167.1, 164.8, 149.0, 142.9, 137.8, 137.7, 133.0, 129.9, 128.2, 127.6$  (2x), 123.9, 98.0, 54.3, 52.5, 42.6, 37.7, 33.4 (2x), 33.2, 30.4, 27.5 (2x), 26.7, 26.4, 10.5, 10.4 ppm.
- **MS (ESI pos.):**  $m/z$  (%) = 573.27 (100) ([M+H]<sup>+</sup>, calcd. 573.36), 486.20 (61) ([M<sub>fr.</sub>]<sup>+</sup>, calcd. 486.25).
- **HRMS (FTMS + p MALDI):**  $m/z = 573.3540$  [M+H]<sup>+</sup>, calcd. for [C<sub>33</sub>H<sub>45</sub>N<sub>6</sub>O<sub>3</sub>]<sup>+</sup> = 573.3553.

**5-Amino-N-(4-(((S)-4-cyclohexyl-1-(((SR)-1-hydroxybutan-2-yl)amino)-1-oxobutan-2-yl)carbamoyl)benzyl)-1-phenyl-1H-pyrazole-4-carboxamide (225, SR103)**



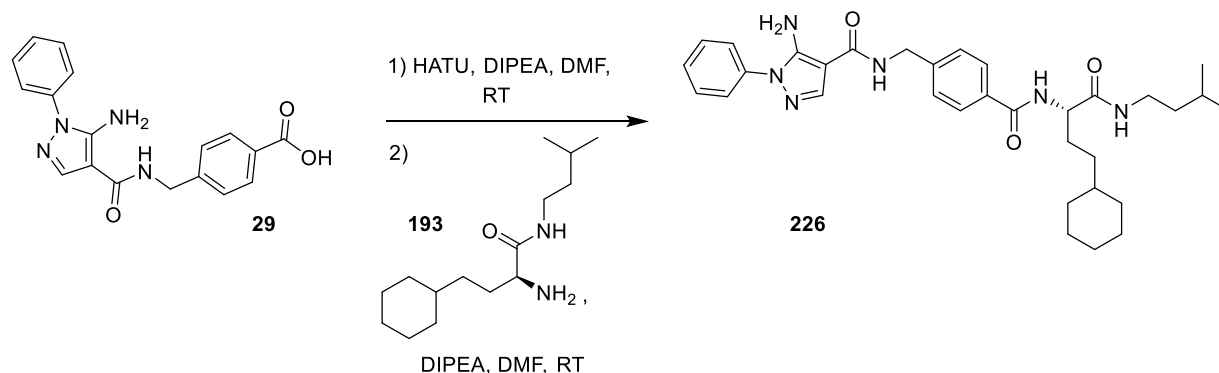
4-(((5-Amino-1-phenyl-1H-pyrazole-4-carboxamido)methyl)benzoic acid (**29**, 200 mg, 0.595 mmol) and HATU (280 mg, 0.736 mmol) were dissolved in DMF (5 mL) and DIPEA (115 mg, 0.893 mmol) was added. The solution was stirred for 1.5 h at RT and (*S*)-2-amino-4-cyclohexyl-*N*-(((*SR*)-1-hydroxybutan-2-yl)butanamide (**192**, 189 mg, 0.714 mmol), diluted in DMF (5 mL) and DIPEA (115 mg, 0.893 mmol), was added. The mixture was stirred for 20 h at RT. DCM (50 mL) was added and the organic phase was washed 5 times with H<sub>2</sub>O (20 mL) and dried over MgSO<sub>4</sub>. The solvent was evaporated under reduced pressure and the crude product was purified by flashcolumn chromatography on silica (cyclohexane/EtOAc 1:20).

**Yield:** 166 mg (0.289 mmol, 49%), colorless solid.

- **TLC:**  $R_f = 0.76$  (SiO<sub>2</sub>, EtOAc/MeOH 10:1).
- **C<sub>32</sub>H<sub>42</sub>N<sub>6</sub>O<sub>3</sub>:** (574.71), [574.33].
- **HPLC:** (mixture of diastereomeres)  $t_R = 13.78, 14.08$  min.
- **<sup>1</sup>H-NMR (500 MHz, DMSO-d<sub>6</sub>, 300 K):** (mixture of diastereomeres)  $\delta = 8.52$  (t,  $^3J = 6.1$  Hz, 1H, NHCH<sub>2</sub>C<sub>Ar</sub>), 8.30 (d,  $^3J = 8.1$  Hz, 0.7H, NHCHCO), 8.25 (d,  $^3J = 8.1$  Hz, 0.3H, NHCHCO), 7.99 (s, 1H, pyrazole), 7.85 (d,  $^3J = 8.3$  Hz, 2H, H-3-, H-5-benzyl), 7.68 (d,  $^3J = 8.5$  Hz, 0.3H, NHCH(CH<sub>2</sub>)<sub>2</sub>), 7.60–7.49 (m, 4.7H, H-2-, H-3-, H-5-, H-6-phenyl, NHCH(CH<sub>2</sub>)<sub>2</sub>), 7.42–7.33 (m, 3H, H-4 phenyl, H-2-, H-6-benzyl), 6.38 (br s, 2H, NH<sub>2</sub>), 4.65–4.58 (m, 1H, OH), 4.47 (d,  $^3J = 5.9$  Hz, 2H, CH<sub>2</sub> benzyl), 4.45–4.34 (m, 1H, NHCHCO), 3.66–3.56 (m, 1H, NHCH(CH<sub>2</sub>)<sub>2</sub>), 3.40–3.30 (m, 1H, NHCHCH<sub>A</sub>H<sub>B</sub>OH), 3.29–3.20 (m, 1H, NHCHCH<sub>A</sub>H<sub>B</sub>OH), 1.81–1.53 (m, 8H, NHCHCH<sub>2</sub>CH<sub>2</sub>CH, H-1-, H-2<sub>eq</sub>-, H-3<sub>eq</sub>-, H-4<sub>eq</sub>-, H-5<sub>eq</sub>-, H-6<sub>eq</sub>-cyclohexyl), 1.36–1.04 (m, 7H, NHCHCH<sub>2</sub>CH<sub>3</sub>, NHCHCH<sub>2</sub>CH<sub>2</sub>, H-3<sub>ax</sub>-, H-4<sub>ax</sub>-, H-5<sub>ax</sub>-cyclohexyl), 0.90–0.77 (m, 5H, H-2<sub>ax</sub>-, H-6<sub>ax</sub>-cyclohexyl, CH<sub>3</sub>) ppm.
- **<sup>13</sup>C-NMR (126 MHz, DMSO-d<sub>6</sub>, 300 K):** (mixture of diastereomeres)  $\delta = 171.7, 166.0, 165.9, 164.2, 149.2, 143.6, 138.4, 138.3, 132.7, 129.4, 127.6, 127.5, 127.1, 126.8, 123.1, 97.4, 63.0$  (2x), 53.8, 53.7, 52.2 (2x), 41.4, 36.9, 36.8, 33.3, 33.2, 33.0, 32.8, 29.7, 29.4, 26.4, 26.2, 25.8 (2x), 23.7, 10.4 (2x) ppm.
- **MS (ESI pos.):**  $m/z$  (%) = 575.17 (100) ([M+H]<sup>+</sup>, calcd. 575.34), 486.08 (33) ([M<sub>fr.(I)}</sub>]<sup>+</sup>, calcd. 486.25), 319.04 (12) ([M<sub>fr.(II)}</sub>]<sup>+</sup>, calcd. 319.12).
- **HRMS (FTMS + p MALDI):**  $m/z = 597.3173$  [M+Na]<sup>+</sup>, calcd. for [C<sub>32</sub>H<sub>42</sub>N<sub>6</sub>NaO<sub>4</sub>]<sup>+</sup> = 597.3165.



**(S)-5-Amino-N-(4-((4-cyclohexyl-1-(isopentylamino)-1-oxobutan-2-yl)carbamoyl)benzyl)-1-phenyl-1H-pyrazole-4-carboxamide (226, SR68)**

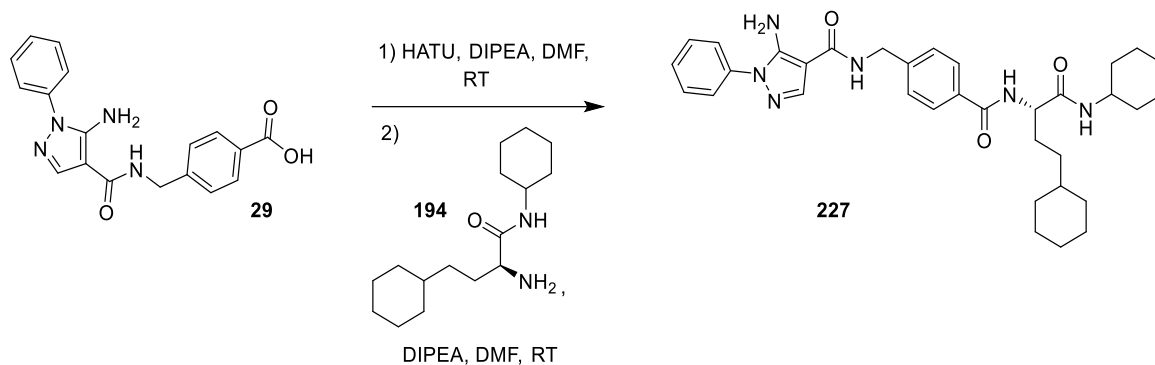


4-((5-Amino-1-phenyl-1H-pyrazole-4-carboxamido)methyl)benzoic acid (**29**, 200 mg, 0.595 mmol) and HATU (272 mg, 0.714 mmol) were dissolved in DMF (5 mL) and DIPEA (115 mg, 0.893 mmol) was added. The solution was stirred for 1 h at RT and (S)-2-amino-4-cyclohexyl-N-isopentylbutanamide (**193**, 182 mg, 0.714 mmol), diluted in DMF (5 mL) and DIPEA (115 mg, 0.893 mmol), was added. The mixture was stirred for 20 h at RT. EtOAc (100 mL) was added and the organic phase was washed 5 times with H<sub>2</sub>O (20 mL) and dried over MgSO<sub>4</sub>. The solvent was evaporated under reduced pressure and the crude product was purified using column chromatography on silica (cyclohexane/EtOAc 1:1 → 1:6 → EtOAc).

**Yield:** 327 mg (0.571 mmol, 96%), colorless solid.

- **TLC:** R<sub>f</sub> = 0.41 (SiO<sub>2</sub>, cyclohexane/EtOAc 1:6).
- **C<sub>33</sub>H<sub>44</sub>N<sub>6</sub>O<sub>3</sub>:** (572.74), [572.35].
- **HPLC:** t<sub>R</sub> = 16.02 min.
- **<sup>1</sup>H-NMR (500 MHz, DMSO-d<sub>6</sub>, 300 K):** δ = 8.52 (t, <sup>3</sup>J = 6.1 Hz, 1H, NHCH<sub>2</sub>C<sub>Ar</sub>), 8.27 (d, <sup>3</sup>J = 8.0 Hz, 1H, NHCHCO), 7.99 (s, 1H, pyrazole), 7.90 (t, <sup>3</sup>J = 5.6 Hz, 1H, NHCH<sub>2</sub>CH<sub>2</sub>), 7.85 (d, <sup>3</sup>J = 8.3 Hz, 2H, H-3-, H-5-benzyl), 7.59–7.49 (m, 4H, H-2-, H-3-, H-5-, H-6-phenyl), 7.41–7.35 (m, 3H, H-4 phenyl, H-2-, H-6-benzyl), 6.38 (br s, 2H, NH<sub>2</sub>), 4.47 (d, <sup>3</sup>J = 6.0 Hz, 2H, CH<sub>2</sub> benzyl), 4.38–4.31 (m, 1H, NHCHCO), 3.16–2.99 (m, 2H, NHCH<sub>2</sub>CH<sub>2</sub>), 1.80–1.71 (m, 1H, NHCHCH<sub>A</sub>H<sub>B</sub>CH<sub>2</sub>), 1.70–1.52 (m, 6H, NHCHCH<sub>A</sub>H<sub>B</sub>CH<sub>2</sub>, H-2<sub>eq</sub>-, H-3<sub>eq</sub>-, H-4<sub>eq</sub>-, H-5<sub>eq</sub>-, H-6<sub>eq</sub>-cyclohexyl), 1.33–1.03 (m, 9H, NHCH<sub>2</sub>CH<sub>2</sub>, CH<sub>3</sub>CHCH<sub>3</sub>, H-1-, H-3<sub>ax</sub>-, H-4<sub>ax</sub>-, H-5<sub>ax</sub>-cyclohexyl, NHCHCH<sub>2</sub>CH<sub>2</sub>), 0.90–0.79 (m, 8H, H-2<sub>ax</sub>-, H-6<sub>ax</sub>-cyclohexyl, CH<sub>3</sub>CHCH<sub>3</sub>) ppm.
- **<sup>13</sup>C-NMR (126 MHz, DMSO-d<sub>6</sub>, 300 K):** δ = 171.6, 166.0, 164.2, 149.2, 143.6, 138.4, 138.2, 132.7, 129.4, 127.6, 127.1, 126.8, 123.1, 97.4, 53.6, 41.3, 38.1, 36.8, 36.7, 33.3, 32.9, 32.7, 29.3, 26.2, 25.8 (2x), 25.1, 22.4 (2x) ppm.
- **MS (ESI pos.):** m/z (%) = 573.38 (100) ([M+H]<sup>+</sup>, calcd. 573.35), 486.30 (26) ([M<sub>fr.(11)</sub>]<sup>+</sup>, calcd. 486.25), 319.22 (22) ([M<sub>fr.(11)</sub>]<sup>+</sup>, calcd. 319.12).
- **HRMS (FTMS + p MALDI):** m/z = 573.3530 [M+H]<sup>+</sup>, calcd. for [C<sub>33</sub>H<sub>45</sub>N<sub>6</sub>O<sub>3</sub>]<sup>+</sup> = 573.3548.

**(S)-5-Amino-N-(4-((4-cyclohexyl-1-(cyclohexylamino)-1-oxobutan-2-yl)carbamoyl)benzyl)-1-phenyl-1H-pyrazole-4-carboxamide (227, SR69)**

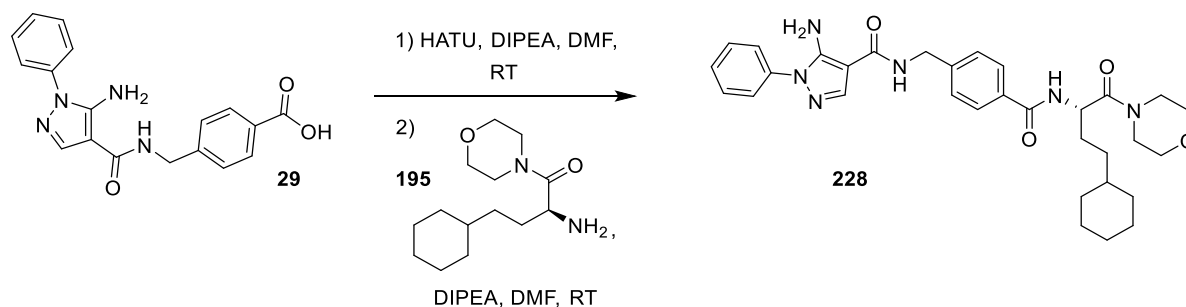


4-((5-Amino-1-phenyl-1H-pyrazole-4-carboxamido)methyl)benzoic acid (**29**, 200 mg, 0.595 mmol) and HATU (280 mg, 0.736 mmol) were dissolved in DMF (5 mL) and DIPEA (115 mg, 0.893 mmol) was added. The solution was stirred for 1 h at RT and (S)-2-amino-N,4-dicyclohexylbutanamide (**194**, 159 mg, 0.714 mmol), diluted in DMF (5 mL) and DIPEA (115 mg, 0.893 mmol), was added. The mixture was stirred for 20 h at RT. EtOAc (100 mL) was added and the organic phase was washed 4 times with H<sub>2</sub>O (50 mL), once with an aqueous NaCl solution (sat., 50 mL) and dried over MgSO<sub>4</sub>. The solvent was evaporated under reduced pressure and the crude product was purified using column chromatography on silica (cyclohexane/EtOAc 2:3 → 1:6 → EtOAc).

**Yield:** 138 mg (0.236 mmol, 40%), colorless solid.

- **TLC:**  $R_f = 0.38$  (SiO<sub>2</sub>, cyclohexane/EtOAc 1:6).
- **C<sub>34</sub>H<sub>44</sub>N<sub>6</sub>O<sub>3</sub>:** (584.75), [584.35].
- **HPLC:**  $t_R = 16.27$  min.
- **<sup>1</sup>H-NMR (500 MHz, DMSO-d<sub>6</sub>, 300 K):**  $\delta = 8.52$  (t,  $^3J = 6.0$  Hz, 1H, NHCH<sub>2</sub>C<sub>Ar</sub>), 8.24 (d,  $^3J = 8.2$  Hz, 1H, NHCHCO), 7.99 (s, 1H, pyrazole), 7.89–7.78 (m, 3H, NH-cyclohexyl, H-3-, H-5-benzyl), 7.60–7.49 (m, 4H, H-2-, H-3-, H-5-, H-6-phenyl), 7.42–7.30 (m, 3H, H-4 phenyl, H-2-, H-6-benzyl), 6.39 (br s, 2H, NH<sub>2</sub>), 4.48 (d,  $^3J = 6.0$  Hz, 2H, CH<sub>2</sub> benzyl), 4.42–4.33 (m, 1H, NHCHCO), 3.61–3.47 (m, 1H, NHCH cyclohexyl), 1.78–1.48 (m, 12H, NHCHCH<sub>2</sub>CH<sub>2</sub>, H-2<sub>eq</sub>-, H-3<sub>eq</sub>-, H-4<sub>eq</sub>-, H-5<sub>eq</sub>-, H-6<sub>eq</sub>-cyclohexyl, H-2<sub>eq</sub>-, H-3<sub>eq</sub>-, H-4<sub>eq</sub>-, H-5<sub>eq</sub>-, H-6<sub>eq</sub>-NH-cyclohexyl), 1.33–1.03 (m, 11H, H-1-, H-3<sub>ax</sub>-, H-4<sub>ax</sub>-, H-5<sub>ax</sub>-cyclohexyl, NHCHCH<sub>2</sub>CH<sub>2</sub>, H-2<sub>ax</sub>-, H-3<sub>ax</sub>-, H-4<sub>ax</sub>-, H-5<sub>ax</sub>-, H-6<sub>ax</sub>-NH-cyclohexyl), 0.90–0.76 (m, 2H, H-2<sub>ax</sub>-, H-6<sub>ax</sub>-cyclohexyl) ppm.
- **<sup>13</sup>C-NMR (126 MHz, DMSO-d<sub>6</sub>, 300 K):**  $\delta = 170.8, 165.9, 164.1, 149.2, 143.6, 138.4, 138.3, 132.7, 129.4, 127.5, 127.1, 127.0, 126.8$  (2x), 123.1, 97.4, 53.5, 47.5, 41.3, 36.8, 33.2, 33.0, 32.7, 32.4, 32.3, 29.6, 26.2, 25.8 (2x), 25.2, 24.6, 24.5 ppm.
- **MS (ESI pos.):**  $m/z$  (%) = 585.25 (100) ([M+H]<sup>+</sup>, calcd. 585.36), 486.16 (80) ([M<sub>fr.</sub>]<sup>+</sup>, calcd. 486.25).
- **HRMS (FTMS + p MALDI):**  $m/z$  607.3360 [M+Na]<sup>+</sup>, calcd. for [C<sub>34</sub>H<sub>44</sub>N<sub>6</sub>NaO<sub>3</sub>]<sup>+</sup> = 607.3376.

**(S)-5-Amino-N-(4-((4-cyclohexyl-1-morpholino-1-oxobutan-2-yl)carbamoyl)benzyl)-1-phenyl-1H-pyrazole-4-carboxamide (228, SR141)**

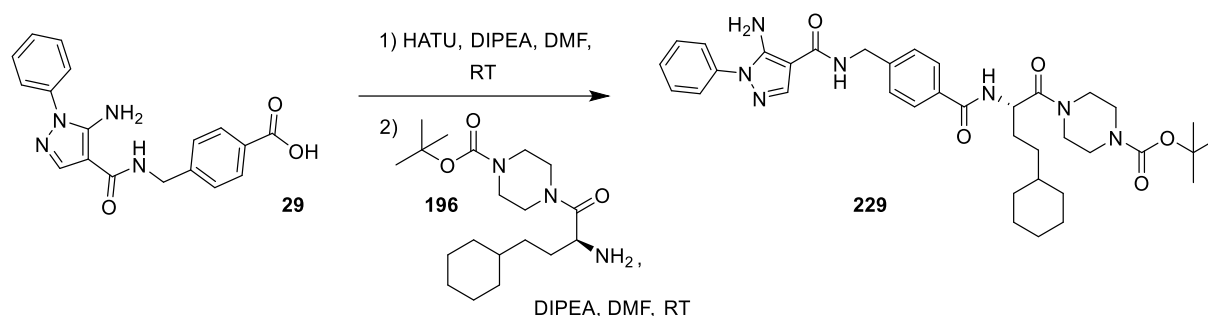


4-((5-Amino-1-phenyl-1H-pyrazole-4-carboxamido)methyl)benzoic acid (**29**, 200 mg, 0.595 mmol) and HATU (280 mg, 0.736 mmol) were dissolved in DMF (5 mL) and DIPEA (115 mg, 0.893 mmol) was added. The solution was stirred for 1.5 h at RT and (S)-2-amino-4-cyclohexyl-1-morpholinobutan-1-one (**195**, 182 mg, 0.714 mmol), diluted in DMF (5 mL) and DIPEA (115 mg, 0.893 mmol), was added. The mixture was stirred for 20 h at RT. DCM (50 mL) was added and the organic phase was washed 5 times with H<sub>2</sub>O (20 mL) and dried over MgSO<sub>4</sub>. The solvent was evaporated under reduced pressure and the crude product was purified using flashcolumn chromatography on silica (cyclohexane/EtOAc 1:1 → 1:10).

**Yield:** 90 mg (0.157 mmol, 26%), colorless solid.

- **TLC:** R<sub>f</sub> = 0.27 (cyclohexane/EtOAc 1:10).
- **C<sub>32</sub>H<sub>40</sub>N<sub>6</sub>O<sub>4</sub>:** (572.70), [572.31].
- **HPLC:** t<sub>R</sub> = 14.55 min.
- **<sup>1</sup>H-NMR (500 MHz, DMSO-d<sub>6</sub>, 300 K):** δ = 8.54 (d, <sup>3</sup>J = 8.1 Hz, 1H, NHCHCO), 8.52 (t, <sup>3</sup>J = 6.1 Hz, 1H, NHCH<sub>2</sub>C<sub>Ar</sub>), 7.99 (s, 1H, pyrazole), 7.86 (d, <sup>3</sup>J = 8.3 Hz, 2H, H-3-, H-5-benzyl), 7.59–7.55 (m, 2H, H-2-, H-6-phenyl), 7.52 (t, <sup>3</sup>J = 7.9 Hz, 2H, H-3-, H-5-phenyl), 7.41–7.35 (m, 3H, H-4 phenyl, H-2-, H-6-benzyl), 6.38 (br s, 2H, NH<sub>2</sub>), 4.86–4.78 (m, 1H, NHCHCO), 4.47 (d, <sup>3</sup>J = 5.9 Hz, 2H, CH<sub>2</sub> benzyl), 3.61–3.39 (m, 8H, CH<sub>2</sub>-2-, CH<sub>2</sub>-3-, CH<sub>2</sub>-5-, CH<sub>2</sub>-6-morpholine), 1.77–1.55 (m, 7H, NHCHCH<sub>2</sub>CH<sub>2</sub>, H-2<sub>eq</sub>-, H-3<sub>eq</sub>-, H-4<sub>eq</sub>-, H-5<sub>eq</sub>-, H-6<sub>eq</sub>-cyclohexyl), 1.27–1.05 (m, 6H, H-1-, H-3<sub>ax</sub>-, H-4<sub>ax</sub>-, H-5<sub>ax</sub>-cyclohexyl, NHCHCH<sub>2</sub>CH<sub>2</sub>), 0.90–0.78 (m, 2H, H-2<sub>ax</sub>-, H-6<sub>ax</sub>-cyclohexyl) ppm.
- **<sup>13</sup>C-NMR (126 MHz, DMSO-d<sub>6</sub>, 300 K):** δ = 170.1, 165.9, 164.2, 149.2, 143.7, 138.4, 138.2, 132.4, 129.4, 127.6, 127.1, 126.9, 123.1, 97.4, 66.2, 49.3, 45.6, 42.0, 41.3, 37.0, 33.1, 32.9, 32.7, 28.8, 26.2, 25.8 (2x) ppm.
- **MS (ESI pos.):** m/z (%) = 573.33 (51) ([M+H]<sup>+</sup>, calcd. 573.32), 486.28 (23) ([M<sub>fr.(I)}</sub>]<sup>+</sup>, calcd. 486.25), 190.35 (100) ([M<sub>fr.(II)}</sub>+Na]<sup>+</sup>, calcd. 190.13).
- **HRMS (FTMS + p MALDI):** m/z = 595.2997 [M+Na]<sup>+</sup>, calcd. for [C<sub>32</sub>H<sub>40</sub>N<sub>6</sub>NaO<sub>4</sub>]<sup>+</sup> = 595.3009.

**(S)-tert-Butyl 4-(2-(4-((5-amino-1-phenyl-1H-pyrazole-4-carboxamido)methyl)benzamido)-4-cyclohexylbutanoyl)piperazine-1-carboxylate (229, SR142)**

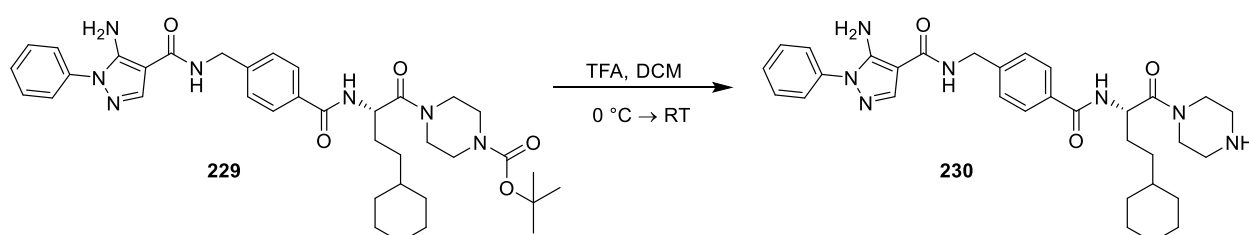


4-((5-Amino-1-phenyl-1H-pyrazole-4-carboxamido)methyl)benzoic acid (**29**, 200 mg, 0.595 mmol) and HATU (280 mg, 0.736 mmol) were dissolved in DMF (8 mL) and DIPEA (115 mg, 0.893 mmol) was added. The solution was stirred for 1.5 h at RT (*S*)-tert-butyl 4-(2-amino-4-cyclohexylbutanoyl)piperazine-1-carboxylate (**196**, 252 mg, 0.714 mmol), diluted in DMF (8 mL) and DIPEA (115 mg, 0.893 mmol), was added. The mixture was stirred for 20 h at RT. DCM (50 mL) was added and the organic phase was washed 5 times with H<sub>2</sub>O (20 mL) and dried over MgSO<sub>4</sub>. The solvent was evaporated under reduced pressure and the crude product was purified using flashcolumn chromatography on silica (cyclohexane/EtOAc 1:1 → 1:20 → EtOAc).

**Yield:** 138 mg (0.205 mmol, 35%), colorless solid.

- **TLC:**  $R_f = 0.58$  (EtOAc/MeOH 10:1).
- **C<sub>37</sub>H<sub>49</sub>N<sub>7</sub>O<sub>4</sub>:** (671.83), [671.38].
- **HPLC:**  $t_R = 16.40$  min.
- **<sup>1</sup>H-NMR (500 MHz, DMSO-d<sub>6</sub>, 300 K):**  $\delta = 8.58\text{--}8.47$  (m, 2H, NHCHCO, NHCH<sub>2</sub>C<sub>Ar</sub>), 7.98 (s, 1H, pyrazole), 7.85 (d, <sup>3</sup>*J* = 8.2 Hz, 2H, H-3-, H-5-benzyl), 7.59–7.49 (m, 4H, H-2-, H-3-, H-5-, H-6-phenyl), 7.41–7.32 (m, 3H, H-4 phenyl, H-2-, H-6-benzyl), 6.38 (br s, 2H, NH<sub>2</sub>), 4.87–4.79 (m, 1H, NHCHCO), 4.47 (d, <sup>3</sup>*J* = 5.9 Hz, 2H, CH<sub>2</sub> benzyl), 3.64–3.18 (m, 8H, CH<sub>2</sub> piperazine), 1.77–1.54 (m, 7H, NHCHCH<sub>2</sub>CH<sub>2</sub>, H-2<sub>eq</sub>-, H-3<sub>eq</sub>-, H-4<sub>eq</sub>-, H-5<sub>eq</sub>-, H-6<sub>eq</sub>-cyclohexyl), 1.40 (s, 9H, C(CH<sub>3</sub>)<sub>3</sub>), 1.28–1.05 (m, 6H, H-1-, H-3<sub>ax</sub>-, H-4<sub>ax</sub>-, H-5<sub>ax</sub>-cyclohexyl, NHCHCH<sub>2</sub>CH<sub>2</sub>), 0.91–0.78 (m, 2H, H-2<sub>ax</sub>-, H-6<sub>ax</sub>-cyclohexyl) ppm.
- **<sup>13</sup>C-NMR (126 MHz, DMSO-d<sub>6</sub>, 300 K):**  $\delta = 170.2, 165.9, 164.2, 153.8, 149.2, 143.7, 138.4, 138.2, 132.4, 129.4, 127.6, 127.1, 126.8, 123.1, 97.4, 79.2, 59.8, 49.5, 44.7, 41.4, 41.3, 38.2, 37.0, 33.1, 32.9, 32.7, 28.8, 28.0, 26.2, 25.8$  (2x) ppm.
- **MS (ESI pos.):**  $m/z$  (%) = 672.42 (24) ([M-H]<sup>+</sup>, calcd. 672.42), 486.26 (11) ([M<sub>fr.(l)}</sub>]<sup>+</sup>, calcd. 486.26), 190.36 (100) ([M<sub>fr.(l)}</sub>+Na]<sup>+</sup>, calcd. 6190.13).
- **HRMS (FTMS + p MALDI):**  $m/z = 694.3688$  [M+Na]<sup>+</sup>, calcd. for [C<sub>37</sub>H<sub>49</sub>N<sub>7</sub>NaO<sub>5</sub>]<sup>+</sup> = 694.3693.

**(S)-5-Amino-N-(4-((4-cyclohexyl-1-oxo-1-(piperazin-1-yl)butan-2-yl)carbamoyl)benzyl)-1-phenyl-1H-pyrazole-4-carboxamide (230, SR154)**

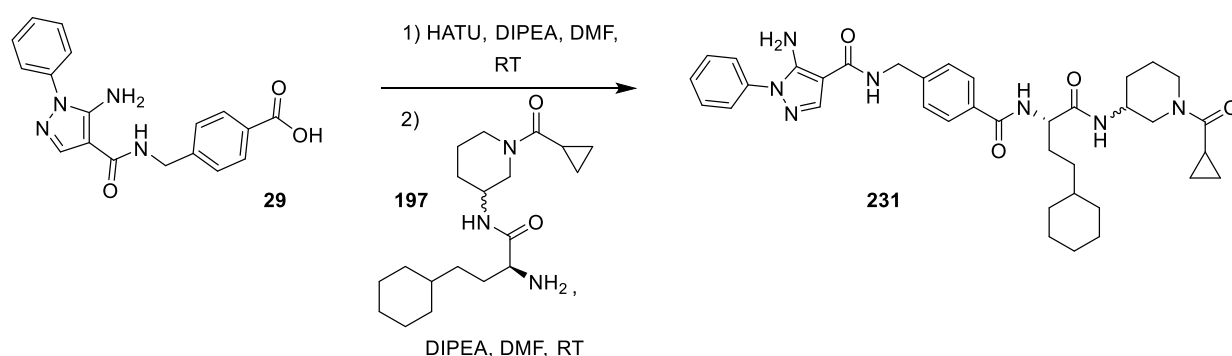


(*S*)-*tert*-Butyl-4-(2-(4-((5-amino-1-phenyl-1*H*-pyrazole-4-carboxamido)methyl)benzamido)-4-cyclohexylbutanoyl)piperazine-1-carboxylate (**229**, 80 mg, 0.12 mmol) was dissolved in DCM (10 mL) and cooled to 0 °C. TFA (2 mL) was added dropwise and the mixture was stirred for 1.5 h at RT. The solvent was removed under reduced pressure and the crude product was dissolved in MeOH. The mixture was cooled to 5 °C and neutralized with K<sub>2</sub>CO<sub>3</sub> (3.6 g, 26.0 mmol). After 10 min of stirring, the mixture was filtrated and the solvent was removed under reduced pressure. The crude product was purified using column chromatography on silica (cyclohexane/EtOAc 1:9 → EtOAc → EtOH+1% TEA).

**Yield:** 35 mg (0.061 mmol, 51%), colorless solid.

- **TLC:** R<sub>f</sub> = 0.04 (EtOAc/MeOH 10:1).
- **C<sub>37</sub>H<sub>49</sub>N<sub>7</sub>O<sub>4</sub>:** (671.83), [671.38].
- **HPLC:** t<sub>R</sub> = 10.10 min.
- **<sup>1</sup>H-NMR (500 MHz, DMSO-d<sub>6</sub>, 300 K):** δ = 8.56 (t, <sup>3</sup>J = 8.2 Hz, 1H, NHCHCO), 8.50 (t, <sup>3</sup>J = 8.2 Hz 2H, NHCH<sub>2</sub>C<sub>Ar</sub>), 8.00 (s, 1H, pyrazole), 7.84 (d, <sup>3</sup>J = 8.2 Hz, 2H, H-3-, H-5-benzyl), 7.60–7.49 (m, 4H, H-2-, H-3-, H-5-, H-6-phenyl), 7.41–7.34 (m, 3H, H-4 phenyl, H-2-, H-6-benzyl), 6.38 (br s, 2H, NH<sub>2</sub>), 4.88–4.76 (m, 1H, NHCHCO), 4.46 (d, <sup>3</sup>J = 5.9 Hz, 2H, CH<sub>2</sub> benzyl), 3.64–3.45 (m, 4H, CH<sub>2</sub>-2-, CH<sub>2</sub>-6-piperazine), 2.47–2.29 (m, 4H, CH<sub>2</sub>-3-, CH<sub>2</sub>-5-piperazine), 1.76–1.54 (m, 7H, NHCHCH<sub>2</sub>CH<sub>2</sub>, H-2<sub>eq</sub>-, H-3<sub>eq</sub>-, H-4<sub>eq</sub>-, H-5<sub>eq</sub>-, H-6<sub>eq</sub>-cyclohexyl), 1.29–1.04 (m, 7H, NH piperazine, H-1-, H-3<sub>ax</sub>-, H-4<sub>ax</sub>-, H-5<sub>ax</sub>-cyclohexyl, NHCHCH<sub>2</sub>CH<sub>2</sub>), 0.90–0.77 (m, 2H, H-2<sub>ax</sub>-, H-6<sub>ax</sub>-cyclohexyl) ppm.
- **<sup>13</sup>C-NMR (126 MHz, DMSO-d<sub>6</sub>, 300 K):** δ = 169.8, 165.8, 164.2, 149.2, 143.7, 138.5, 138.3, 132.4, 129.4, 127.6, 127.1, 126.9, 123.1, 97.4, 51.3, 50.8, 44.9, 41.5, 41.3, 37.0, 33.1, 32.9, 32.7, 30.4, 29.0, 28.9, 26.2, 25.8 (2x) ppm.
- **MS (ESI pos.):** *m/z* (%) = 572.43 (100) ([M+H]<sup>+</sup>, calcd. 572.34).
- **HRMS (FTMS + p MALDI):** *m/z* = 572.3328 [M+H]<sup>+</sup>, calcd. for [C<sub>32</sub>H<sub>42</sub>N<sub>7</sub>O<sub>3</sub>]<sup>+</sup> = 572.3344.

**5-Amino-N-(4-(((*S*)-4-cyclohexyl-1-(((*SR*)-1-(cyclopropanecarbonyl)piperidin-3-yl)amino)-1-oxobutan-2-yl)carbamoyl)benzyl)-1-phenyl-1*H*-pyrazole-4-carboxamide (**231**, SR160)**

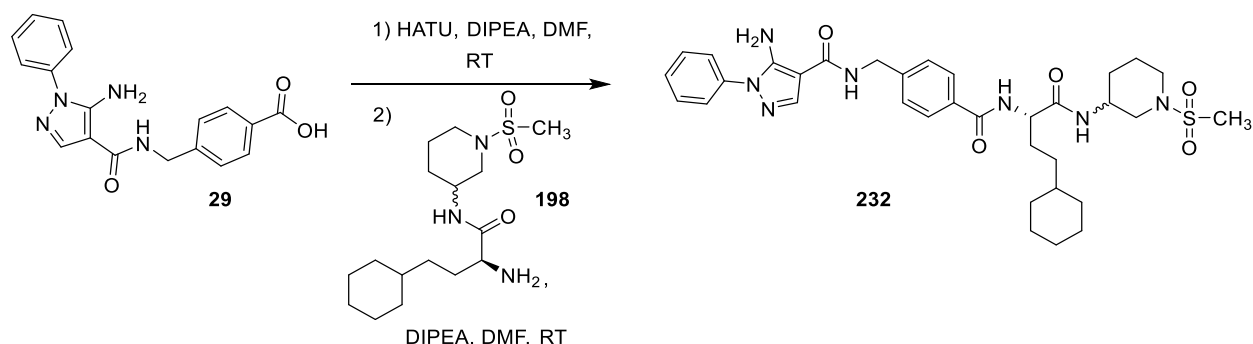


4-((5-Amino-1-phenyl-1*H*-pyrazole-4-carboxamido)methyl)benzoic acid (**29**, 200 mg, 0.595 mmol) and HATU (280 mg, 0.736 mmol) were dissolved in DMF (5 mL) and DIPEA (115 mg, 0.893 mmol) was added. The solution was stirred for 1.5 h at RT and (*S*)-2-amino-4-cyclohexyl-*N*-((*SR*)-1-(cyclopropanecarbonyl)piperidin-3-yl)butanamide (**197**, 240 mg, 0.714 mmol), diluted in DMF (5 mL) and DIPEA (115 mg, 0.893 mmol), was added. The mixture was stirred for 20 h at RT. DCM (50 mL) was added and the organic phase was washed 5 times with H<sub>2</sub>O (20 mL) and dried over MgSO<sub>4</sub>. The solvent was evaporated under reduced pressure and the crude product was triturated with cyclohexane/EtOAc (1:1).

**Yield:** 120 mg (0.184 mmol, 31%), colorless solid.

- **TLC:**  $R_f = 0.21$  ( $\text{SiO}_2$ , EtOAc/MeOH 10:1).
- **$\text{C}_{37}\text{H}_{47}\text{N}_7\text{O}_4$ :** (653.81), [653.37].
- **HPLC:** (mixture of diastereomers)  $t_R = 14.28, 14.51$  min.
- **$^1\text{H-NMR}$  (500 MHz,  $\text{DMSO-d}_6$ , 300 K):** (mixture of diastereomers)  $\delta = 8.52$  (t,  $^3J = 6.1$  Hz, 1H,  $\text{NHCH}_2\text{C}_{\text{Ar}}$ ), 8.30 (d,  $^3J = 8.1$  Hz, 1H,  $\text{NHCHCO}$ ), 8.07–7.88 (m, 2H,  $\text{NHCH}$  piperidine, pyrazole), 7.85 (d,  $^3J = 8.3$  Hz, 2H, H-3-, H-5-benzyl), 7.60–7.49 (m, 4H, H-2-, H-3-, H-5-, H-6-phenyl), 7.43–7.34 (m, 3H, H-4 phenyl, H-2-, H-6-benzyl), 6.38 (br s, 2H,  $\text{NH}_2$ ), 4.53–4.31 (m, 3H,  $\text{CH}_2$  benzyl,  $\text{NHCHCO}$ ), 4.20–3.46 (m, 3H, CH piperidine,  $\text{CH}_A\text{H}_B$ -2 piperidine), 3.27–3.01 (m, 1H,  $\text{CH}_A\text{H}_B$ -2 piperidine), 2.76–2.56 (m, 1H,  $\text{CH}_A\text{H}_B$ -6 piperidine), 2.54–2.45 (m, 1H,  $\text{CH}_A\text{H}_B$ -6 piperidine), 2.02–1.31 (m, 12H,  $\text{CH}_2$ -4-,  $\text{CH}_2$ -5-piperidine,  $\text{NHCHCH}_2$ , H-2 $_{\text{eq}}$ -, H-3 $_{\text{eq}}$ -, H-4 $_{\text{eq}}$ -, H-5 $_{\text{eq}}$ -, H-6 $_{\text{eq}}$ -cyclohexyl, CH cyclopropyl), 1.30–1.02 (m, 6H, H-1-, H-3 $_{\text{ax}}$ -, H-4 $_{\text{ax}}$ -, H-5 $_{\text{ax}}$ -cyclohexyl,  $\text{NHCHCH}_2\text{CH}_2$ ), 0.92–0.77 (m, 2H, H-2 $_{\text{ax}}$ -, H-6 $_{\text{ax}}$ -cyclohexyl), 0.92–0.77 (m, 4H,  $\text{CH}_2$  cyclopropyl) ppm.
- **$^{13}\text{C-NMR}$  (126 MHz,  $\text{DMSO-d}_6$ , 300 K):** (mixture of diastereomers)  $\delta = 172.0, 171.4, 171.0, 170.9, 166.1, 164.1, 149.2, 143.6, 138.4, 138.2, 132.7, 132.6, 129.4, 127.6, 127.1, 126.8, 123.1, 97.4, 53.4, 49.0, 46.1, 45.9, 45.1, 41.8, 41.3, 36.9, 33.5, 33.3, 33.0, 32.7, 29.9, 29.7, 29.4, 29.3, 26.2, 25.8$  (2x), 24.1, 22.5, 10.4, 10.3, 7.0, 6.8 ppm.
- **MS (ESI neg.):**  $m/z$  (%) = 652.31 (100) ( $[\text{M-H}]^-$ , calcd. 652.36).
- **HRMS (FTMS + p MALDI):**  $m/z = 692.3311$   $[\text{M+K}]^+$ , calcd. for  $[\text{C}_{37}\text{H}_{47}\text{KN}_7\text{O}_4]^+ = 692.3321$ .

**5-Amino-N-(4-(((S)-4-cyclohexyl-1-(((SR)-1-(methylsulfonyl)piperidin-3-yl)amino)-1-oxobutan-2-yl)carbamoyl)benzyl)-1-phenyl-1H-pyrazole-4-carboxamide (232, SR159)**



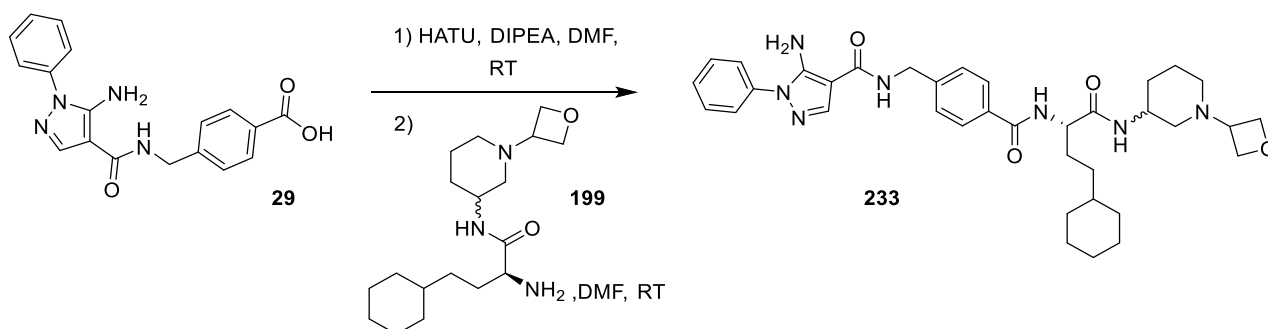
4-(((5-Amino-1-phenyl-1H-pyrazole-4-carboxamido)methyl)benzoic acid (**29**, 200 mg, 0.595 mmol) and HATU (280 mg, 0.736 mmol) were dissolved in DMF (5 mL) and DIPEA (115 mg, 0.893 mmol) was added. The solution was stirred for 1.5 h at RT and (S)-2-amino-4-cyclohexyl-N-(((SR)-1-(methylsulfonyl)piperidin-3-yl)butanamide (**198**, 247 mg, 0.714 mmol), diluted in DMF (5 mL) and DIPEA (115 mg, 0.893 mmol), was added. The mixture was stirred for 20 h at RT. DCM (50 mL) was added and the organic phase was washed 5 times with  $\text{H}_2\text{O}$  (20 mL) and dried over  $\text{MgSO}_4$ . The solvent was evaporated under reduced pressure and the crude product was triturated with cyclohexane/EtOAc (1:1).

**Yield:** 78 mg (0.11 mmol, 19%), colorless solid.

- **TLC:**  $R_f = 0.14$  ( $\text{SiO}_2$ , cyclohexane/EtOAc 1:3).
- **$\text{C}_{34}\text{H}_{45}\text{N}_7\text{O}_5\text{S}$ :** (663.83), [663.32].
- **HPLC:** (mixture of diastereomers)  $t_R = 14.12, 14.41$  min.

- **<sup>1</sup>H-NMR (500 MHz, DMSO-d<sub>6</sub>, 300 K):** (mixture of diastereomeres)  $\delta$  = 8.52 (t, <sup>3</sup>J = 6.0 Hz, 1H, NHCH<sub>2</sub>C<sub>Ar</sub>), 8.32 (d, <sup>3</sup>J = 8.1 Hz, 1H, NHCHCO), 8.03 (d, <sup>3</sup>J = 7.5 Hz, 1H, NHCH piperidine), 7.99 (s, 1H, pyrazole), 7.85 (d, <sup>3</sup>J = 8.4 Hz, 2H, H-3-, H-5-benzyl), 7.60–7.49 (m, 4H, H-2-, H-3-, H-5-, H-6-phenyl), 7.42–7.34 (m, 3H, H-4 phenyl, H-2-, H-6-benzyl), 6.38 (br s, 2H, NH<sub>2</sub>), 4.47 (d, <sup>3</sup>J = 6.0 Hz, 2H, CH<sub>2</sub> benzyl), 4.44–4.35 (m, 1H, NHCHCO), 3.78–3.67 (m, 1H, CH piperidine), 3.53–3.40 (m, 1H, CH<sub>A</sub>H<sub>B</sub>-2 piperidine), 3.37–3.28 (m, 1H, CH<sub>A</sub>H<sub>B</sub>-2 piperidine), 2.87–2.82 (m, 3H, CH<sub>3</sub>), 2.81–2.71 (m, 1H, CH<sub>A</sub>H<sub>B</sub>-6 piperidine), 2.58–2.51 (m, 1H, CH<sub>A</sub>H<sub>B</sub>-6 piperidine), 1.85–1.46 (m, 10H, CH<sub>2</sub>-4-, CH<sub>2</sub>-5-piperidine, NHCHCH<sub>A</sub>H<sub>B</sub>, H-2<sub>eq</sub>-, H-3<sub>eq</sub>-, H-4<sub>eq</sub>-, H-5<sub>eq</sub>-, H-6<sub>eq</sub>-cyclohexyl), 1.45–1.30 (m, 1H, NHCHCH<sub>A</sub>H<sub>B</sub>), 1.29–1.04 (m, 6H, H-1-, H-3<sub>ax</sub>-, H-4<sub>ax</sub>-, H-5<sub>ax</sub>-cyclohexyl, NHCHCH<sub>2</sub>CH<sub>2</sub>), 0.90–0.77 (m, 2H, H-2<sub>ax</sub>-, H-6<sub>ax</sub>-cyclohexyl) ppm.
- **<sup>13</sup>C-NMR (126 MHz, DMSO-d<sub>6</sub>, 300 K):** (mixture of diastereomeres)  $\delta$  = 171.7, 166.1 (2x), 164.1, 149.2, 143.6, 138.4, 138.2, 132.7, 129.4, 127.6, 127.1, 126.8, 123.1, 97.4, 53.6, 53.5, 49.6, 49.4, 45.4, 45.2, 45.1, 41.3, 36.8 (2x), 34.3 (2x), 33.3, 32.9 (2x), 32.7 (2x), 29.5, 29.0, 28.7, 26.2, 25.8 (2x), 23.0 (2x) ppm.
- **MS (ESI neg.):** *m/z* (%) = 662.27 (100) ([M-H]<sup>-</sup>, calcd. 662.31), 698.30 (50) ([M+Cl]<sup>-</sup>, calcd. 698.77).
- **HRMS (FTMS + p MALDI):** *m/z* = 702.2830 [M+K]<sup>+</sup>, calcd. for [C<sub>34</sub>H<sub>45</sub>KN<sub>7</sub>O<sub>5</sub>S]<sup>+</sup> = 702.2840.

**5-Amino-N-(4-(((S)-4-cyclohexyl-1-(((SR)-1-(oxetan-3-yl)piperidin-3-yl)amino)-1-oxobutan-2-yl)carbamoyl)benzyl)-1-phenyl-1H-pyrazole-4-carboxamide (233, SR202)**



4-((5-Amino-1-phenyl-1H-pyrazole-4-carboxamido)methyl)benzoic acid (**29**, 233 mg, 0.692 mmol) and HATU (316 mg, 0.830 mmol) were dissolved in DMF (5 mL) and DIPEA (134 mg, 1.038 mmol) was added. The solution was stirred for 1 h at RT and (S)-2-amino-4-cyclohexyl-N-(((SR)-1-(oxetan-3-yl)piperidin-3-yl)butanamide (**199**, 268 mg, 0.830 mmol), diluted in DMF (5 mL), was added. The mixture was stirred for 20 h at RT. DCM (50 mL) was added and the organic phase was washed 5 times with H<sub>2</sub>O (20 mL) and dried over MgSO<sub>4</sub>. The solvent was evaporated under reduced pressure and the crude product was purified using column chromatography on silica (cyclohexane/EtOAc 1:20 → EtOAc → EtOH).

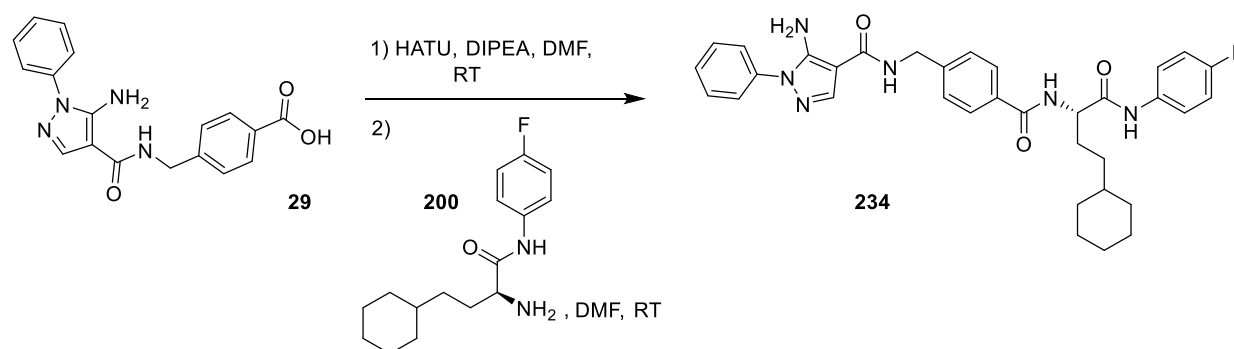
**Yield:** 175 mg (0.273 mmol, 39%), colorless solid.

- **TLC:** R<sub>f</sub> = 0.16 (SiO<sub>2</sub>, EtOAc/MeOH 10:1).
- **C<sub>36</sub>H<sub>47</sub>N<sub>7</sub>O<sub>4</sub>:** (641.80), [641.37].
- **HPLC:** (mixture of diastereomeres) t<sub>R</sub> = 10.36 min.
- **<sup>1</sup>H-NMR (500 MHz, DMSO-d<sub>6</sub>, 300 K):** (mixture of diastereomeres)  $\delta$  = 8.60 (t, <sup>3</sup>J = 5.9 Hz, 1H, NHCH<sub>2</sub>C<sub>Ar</sub>), 8.40 (d, <sup>3</sup>J = 8.2 Hz, 1H, NHCHCO), 8.02 (s, 1H, pyrazole), 7.91 (d, <sup>3</sup>J = 7.9 Hz, 1H, NHCH piperidine), 7.85 (dd, <sup>3</sup>J = 8.5, 1.9 Hz, 2H, H-3-, H-5-benzyl), 7.59–7.49 (m, 4H, H-2-, H-3-, H-5-, H-6-phenyl), 7.41–7.35 (m, 3H, H-4 phenyl, H-2-, H-6-benzyl), 6.38 (br s, 2H, NH<sub>2</sub>), 4.53–4.44 (m, 4H, CH<sub>2</sub>

benzyl,  $\text{CH}(\text{CH}_A\text{H}_B)_2$  oxetane), 4.43–4.31 (m, 3H,  $\text{NHCHCO}$ ,  $\text{CH}(\text{CH}_A\text{H}_B)_2$  oxetane), 3.76–3.67 (m, 1H, CH piperidine), 3.48–3.26 (m, 3H,  $\text{CH}_2$ -2 piperidine, CH-oxetane), 2.55–2.46 (m, 1H,  $\text{CH}_A\text{H}_B$ -6 piperidine), 2.45–2.35 (m, 1H,  $\text{CH}_A\text{H}_B$ -6 piperidine), 1.89–1.54 (m, 10H,  $\text{CH}_2$ -4-,  $\text{CH}_2$ -5-piperidine,  $\text{NHCHCH}_A\text{H}_B$ , H-2<sub>eq</sub>-, H-3<sub>eq</sub>-, H-4<sub>eq</sub>-, H-5<sub>eq</sub>-, H-6<sub>eq</sub>-cyclohexyl), 1.51–1.38 (m, 1H,  $\text{NHCHCH}_A\text{H}_B$ ), 1.31–1.04 (m, 6H, H-1-, H-3<sub>ax</sub>-, H-4<sub>ax</sub>-, H-5<sub>ax</sub>-cyclohexyl,  $\text{NHCHCH}_2\text{CH}_2$ ), 0.89–0.77 (m, 2H, H-2<sub>ax</sub>-, H-6<sub>ax</sub>-cyclohexyl) ppm.

- **$^{13}\text{C}$ -NMR (126 MHz, DMSO- $d_6$ , 300 K):** (mixture of diastereomers)  $\delta$  = 171.3 (2x), 166.1 (2x), 164.2, 149.2, 143.7, 143.6, 138.5, 138.3, 132.7 (2x), 129.4, 127.6, 127.1, 126.8, 123.1, 97.5, 74.7, 74.6, 58.4, 54.4 (2x), 53.7, 53.6, 49.2, 45.2 (2x), 41.3, 36.8 (2x), 33.3, 33.0, 32.7, 29.7, 29.5, 29.4, 26.2, 25.8 (2x), 23.0, 29.9 ppm.
- **MS (ESI pos.):**  $m/z$  (%) = 642.51 (100) ( $[\text{M}-\text{H}]^+$ , calcd. 642.38).
- **HRMS (FTMS + p MALDI):**  $m/z$  = 642.3760  $[\text{M}+\text{H}]^+$ , calcd. for  $[\text{C}_{36}\text{H}_{48}\text{N}_7\text{O}_4]^+$  = 642.3762.

**(S)-5-Amino-N-(4-((4-cyclohexyl-1-((4-fluorophenyl)amino)-1-oxobutan-2-yl)carbamoyl)benzyl)-1-phenyl-1H-pyrazole-4-carboxamide (234, SR348)**



4-((1-Phenyl-1H-pyrazole-4-carboxamido)methyl)benzoic acid (**29**, 200 mg, 0.595 mmol) and HATU (271 mg, 0.714 mmol) were dissolved in DMF (dry, 6 mL) and DIPEA (92 mg, 0.71 mmol) was added. The solution was stirred for 1 h at RT and (S)-2-amino-4-cyclohexyl-N-(4-fluorophenyl)butanamide (**200**, 270 mg, 0.714 mmol), dissolved in DMF (dry, 6 mL), was added. The reaction was stirred for additional 4 d at RT. DCM (150 mL) was added, the organic phase was washed 4 times with  $\text{H}_2\text{O}$  (150 mL) and dried over  $\text{MgSO}_4$ . The solvent was removed under reduced pressure and the crude product was purified using column chromatography on silica (cyclohexane/EtOAc 1:1  $\rightarrow$  1:3  $\rightarrow$  1:20). The product was recrystallized from acetone.

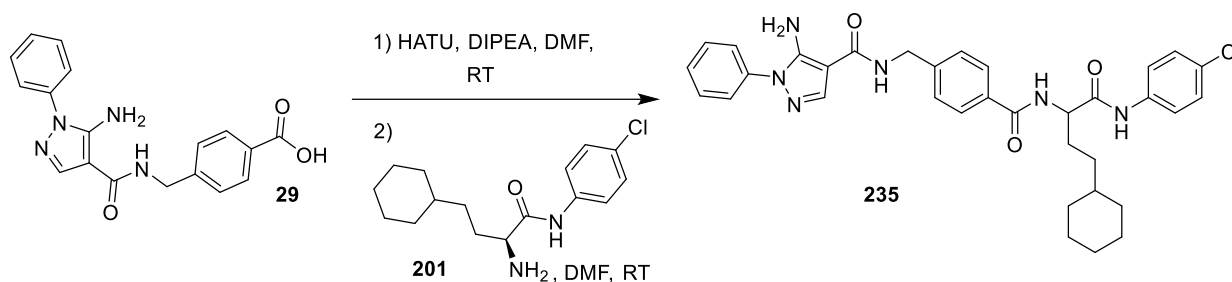
**Yield:** 149 mg (0.250 mmol, 42%), colorless solid.

- **TLC:**  $R_f$  = 0.73 ( $\text{SiO}_2$ , cyclohexane/EtOAc 1:3).
- **$\text{C}_{34}\text{H}_{37}\text{FN}_6\text{O}_3$ :** (598.69), [596.29].
- **HPLC:**  $t_R$  = 16.09 min.
- **$^1\text{H}$ -NMR (600 MHz, DMSO- $d_6$ , 300 K):**  $\delta$  = 10.15 (s, 1H, NH F-phenyl), 8.57–8.44 (m, 2H,  $\text{NHCH}_2\text{C}_{Ar}$ ,  $\text{NHCHCO}$ ), 7.99 (s, 1H, pyrazole), 7.89 (d,  $^3J$  = 7.5 Hz, 2H, H-3-, H-5-benzyl), 7.68–7.48 (m, 6H, H-2-, H-3-, H-5-, H-6-phenyl, H-2-, H-6-F-phenyl), 7.43–7.35 (m, 3H, H-4-phenyl, H-2-, H-6-benzyl), 7.14 (t,  $^3J$  = 8.1 Hz, 2H, H-3-, H-5-F-phenyl), 6.37 (br s, 2H,  $\text{NH}_2$ ), 4.56–4.43 (m, 3H,  $\text{CH}_2$  benzyl,  $\text{NHCHCO}$ ), 1.88–1.75 (m, 2H,  $\text{NHCHCH}_2$ ), 1.73–1.56 (m, 5H, H-2<sub>eq</sub>-, H-3<sub>eq</sub>-, H-4<sub>eq</sub>-, H-5<sub>eq</sub>-, H-6<sub>eq</sub>-cyclohexyl), 1.39–1.30 (m, 1H, H-1 cyclohexyl), 1.28–1.05 (m, 5H,  $\text{NHCHCH}_2\text{CH}_2$ , H-3<sub>ax</sub>-, H-4<sub>ax</sub>-, H-5<sub>ax</sub>-cyclohexyl), 0.92–0.81 (m, 2H, H-2<sub>ax</sub>-, H-6<sub>ax</sub>-cyclohexyl) ppm.



- **$^{13}\text{C-NMR}$  (150 MHz, DMSO- $d_6$ , 300 K):**  $\delta$  = 171.0, 166.3, 164.1, 157.9 ( $^1J_{\text{CF}}$  = 240.8 Hz), 149.2, 143.6, 138.3, 138.2, 135.4, 132.5, 129.3, 127.6, 127.0, 126.8, 123.1, 121.0 ( $^3J_{\text{CF}}$  = 7.9 Hz), 115.2 ( $^2J_{\text{CF}}$  = 22.3 Hz), 97.4, 54.5, 41.3, 36.8, 33.3, 32.8, 32.7, 29.1, 26.1, 25.8 (2x) ppm.
- **MS (ESI pos.):**  $m/z$  (%) = 619.20 (13) ( $[\text{M}+\text{Na}]^+$ , calcd. 619.28), 597.20 (100) ( $[\text{M}+\text{H}]^+$ , calcd. 597.31), 486.19 (99) ( $[\text{M}_{\text{fr.}(i)}]^+$ , calcd. 486.25), 458.21 (16) ( $[\text{M}_{\text{fr.}(ii)}]^+$ , calcd. 458.26), 319.04 (28) ( $[\text{M}_{\text{fr.}(iii)}]^+$ , calcd. 319.12).
- **HRMS (FTMS + p MALDI):**  $m/z$  = 619.2816  $[\text{M}+\text{Na}]^+$ , calcd. for  $[\text{C}_{34}\text{H}_{37}\text{FN}_6\text{NaO}_3]^+$  = 619.2809.

**5-Amino-N-(4-((1-((4-chlorophenyl)amino)-4-cyclohexyl-1-oxobutan-2-yl)carbamoyl)benzyl)-1-phenyl-1H-pyrazole-4-carboxamide (235, SR332)**

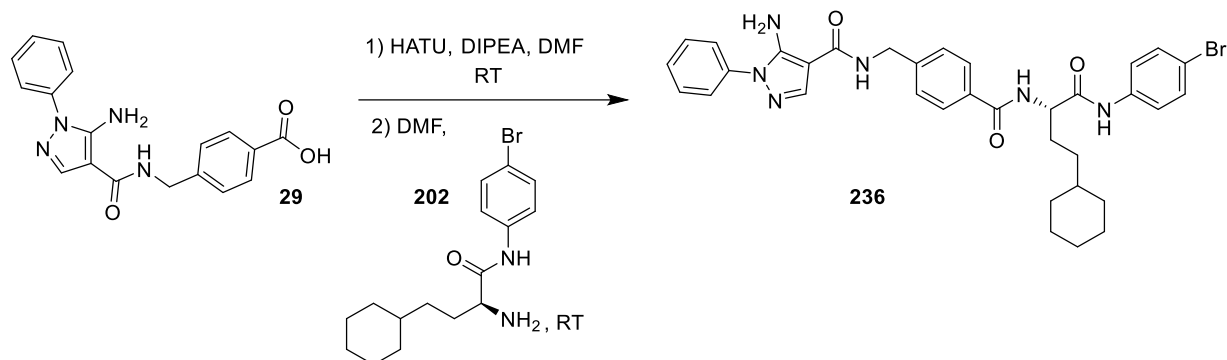


4-((1-Phenyl-1H-pyrazole-4-carboxamido)methyl)benzoic acid (**29**, 185 mg, 0.551 mmol) and HATU (251 mg, 0.661 mmol) were dissolved in DMF (dry, 10 mL) and DIPEA (85 mg, 0.661 mmol) was added. The solution was stirred for 1 h at RT and (S)-2-amino-N-(4-chlorophenyl)-4-cyclohexyl-butanamide (**201**, 195 mg, 0.661 mmol), dissolved in DMF (dry, 8 mL), was added. The reaction was stirred for additional 2 d at RT. DCM (100 mL) was added, the organic phase was washed 4 times with H<sub>2</sub>O (100 mL) and dried over MgSO<sub>4</sub>. The solvent was removed under reduced pressure and the crude product was purified using column chromatography on silica (cyclohexane/EtOAc 1:1 → 1:3 → 1:20).

**Yield:** 91 mg (0.148 mmol, 27%), colorless solid.

- **TLC:**  $R_f$  = 0.40 (SiO<sub>2</sub>, cyclohexane/EtOAc 1:3).
- **C<sub>34</sub>H<sub>37</sub>ClN<sub>6</sub>O<sub>3</sub>:** (613.15), [612.26].
- **HPLC:**  $t_R$  = 16.82 min.
- **$^1\text{H-NMR}$  (500 MHz, DMSO- $d_6$ , 300 K):**  $\delta$  = 10.26 (s, 1H, NH Cl-phenyl), 8.60–8.48 (m, 2H, NHCH<sub>2</sub>C<sub>Ar</sub>, NHCHCO), 7.99 (s, 1H, pyrazole), 7.88 (d,  $^3J$  = 8.0 Hz, 2H, H-3-, H-5-benzyl), 7.65 (d,  $^3J$  = 8.6 Hz, 2H, H-2-, H-6-Cl-phenyl), 7.60–7.49 (m, 4H, H-2-, H-3-, H-5-, H-6-phenyl), 7.44–7.31 (m, 5H, H-4 phenyl, H-2-, H-6-benzyl, H-3-, H-5-Cl-phenyl), 6.38 (br s, 2H, NH<sub>2</sub>), 4.56–4.42 (m, 3H, CH<sub>2</sub> benzyl, NHCHCO), 1.88–1.75 (m, 2H, NHCHCH<sub>2</sub>), 1.73–1.55 (m, 5H, H-2<sub>eq</sub>-, H-3<sub>eq</sub>-, H-4<sub>eq</sub>-, H-5<sub>eq</sub>-, H-6<sub>eq</sub>-cyclohexyl), 1.40–1.29 (m, 1H, H-1 cyclohexyl), 1.28–1.04 (m, 5H, NHCHCH<sub>2</sub>CH<sub>2</sub>, H-3<sub>ax</sub>-, H-4<sub>ax</sub>-, H-5<sub>ax</sub>-cyclohexyl), 0.92–0.79 (m, 2H, H-2<sub>ax</sub>-, H-6<sub>ax</sub>-cyclohexyl) ppm.
- **$^{13}\text{C-NMR}$  (126 MHz, DMSO- $d_6$ , 300 K):**  $\delta$  = 171.4, 166.4, 164.2, 149.2, 143.7, 138.4, 138.2, 138.0, 132.4, 129.4, 128.6, 127.7, 127.1, 126.8, 123.1, 120.8, 97.4, 54.7, 41.3, 36.9, 33.4, 32.9, 32.7, 29.1, 26.1, 25.8 (2x) ppm.
- **MS (ESI pos.):**  $m/z$  (%) = 613.21 (76) ( $[\text{M}+\text{H}]^+$ , calcd. 613.27), 486.20 (100) ( $[\text{M}_{\text{fr.}}]^+$ , calcd. 486.26).
- **HRMS (FTMS + p MALDI):**  $m/z$  = 613.2684  $[\text{M}+\text{H}]^+$ , calcd. for  $[\text{C}_{34}\text{H}_{38}\text{ClN}_6\text{O}_3]^+$  = 613.2694.

**(S)-5-Amino-N-(4-((1-((4-bromophenyl)amino)-4-cyclohexyl-1-oxobutan-2-yl)carbamoyl)benzyl)-1-phenyl-1H-pyrazole-4-carboxamide (236, SR343)**

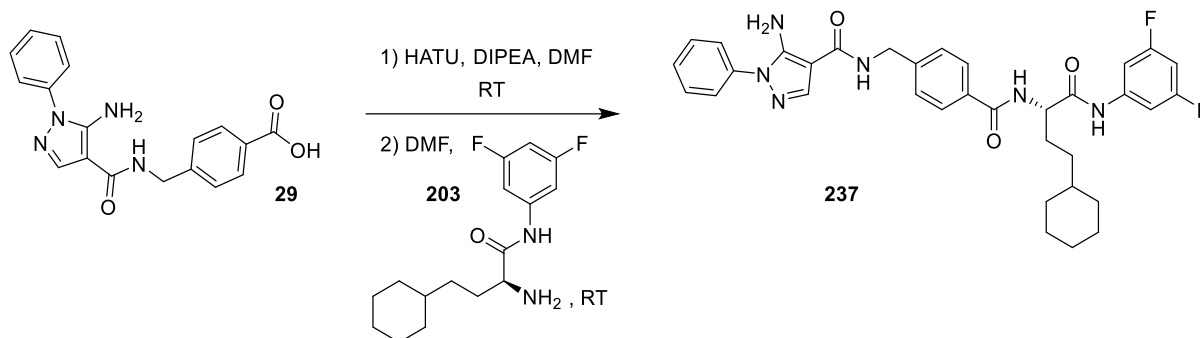


4-((1-Phenyl-1H-pyrazole-4-carboxamido)methyl)benzoic acid (**29**, 200 mg, 0.595 mmol) and HATU (271 mg, 0.714 mmol) were dissolved in DMF (dry, 6 mL) and DIPEA (92 mg, 0.71 mmol) was added. The solution was stirred for 1 h at RT and (S)-2-amino-N-(4-bromophenyl)-4-cyclohexylbutanamide (**202**, 204 mg, 0.600 mmol), dissolved in DMF (dry, 6 mL), was added. The reaction was stirred for additional 20 h at RT. DCM (150 mL) was added, the organic phase was washed 4 times with H<sub>2</sub>O (150 mL) and dried over MgSO<sub>4</sub>. The solvent was removed under reduced pressure and the crude product was purified using column chromatography on silica (cyclohexane/EtOAc 1:1 → 1:3 → 1:20). The product was recrystallized from acetone.

**Yield:** 69 mg (0.105 mmol, 18%), colorless solid.

- **TLC:** R<sub>f</sub> = 0.17 (SiO<sub>2</sub>, cyclohexane/EtOAc 1:1).
- **C<sub>34</sub>H<sub>37</sub>BrN<sub>6</sub>O<sub>3</sub>:** (657.60), [656.21].
- **HPLC:** t<sub>R</sub> = 17.02 min.
- **<sup>1</sup>H-NMR (600 MHz, DMSO-d<sub>6</sub>, 300 K):** δ = 10.23 (s, 1H, NH Br-phenyl), 8.55–8.48 (m, 2H, NHCH<sub>2</sub>C<sub>Ar</sub>, NHCHCO), 7.98 (s, 1H, pyrazole), 7.88 (d, <sup>3</sup>J = 8.2 Hz, 2H, H-3-, H-5-benzyl), 7.60 (d, <sup>3</sup>J = 9.0 Hz, 2H, H-3-, H-5-Br-phenyl), 7.57 (d, <sup>3</sup>J = 7.8 Hz, 2H, H-2-, H-6-phenyl), 7.52 (t, <sup>3</sup>J = 8.0 Hz, 2H, H-3-, H-5-phenyl), 7.48 (d, <sup>3</sup>J = 9.0 Hz, 2H, H-2-, H-6-Br-phenyl), 7.41–7.37 (m, 3H, H-4 phenyl, H-2-, H-6-benzyl), 6.37 (br s, 2H, NH<sub>2</sub>), 4.54–4.46 (m, 3H, CH<sub>2</sub> benzyl, NHCHCO), 1.87–1.75 (m, 2H, NHCHCH<sub>2</sub>), 1.72–1.55 (m, 5H, H-2<sub>eq</sub>-, H-3<sub>eq</sub>-, H-4<sub>eq</sub>-, H-5<sub>eq</sub>-, H-6<sub>eq</sub>-cyclohexyl), 1.37–1.29 (m, 1H, H-1 cyclohexyl), 1.28–1.06 (m, 5H, NHCHCH<sub>2</sub>CH<sub>2</sub>, H-3<sub>ax</sub>-, H-4<sub>ax</sub>-, H-5<sub>ax</sub>-cyclohexyl), 0.92–0.81 (m, 2H, H-2<sub>ax</sub>-, H-6<sub>ax</sub>-cyclohexyl) ppm.
- **<sup>13</sup>C-NMR (75 MHz, DMSO-d<sub>6</sub>, 300 K):** δ = 171.4, 166.5, 164.2, 149.2, 143.7, 138.4, 138.2, 132.4, 131.5, 129.4, 127.7, 127.1, 126.8, 123.1, 121.2, 114.8, 97.4, 54.7, 41.3, 36.9, 33.4, 32.9, 32.7, 29.1, 26.1, 25.8 (2x) ppm.
- **MS (ESI pos.):** m/z (%) = 681.14 (15) ([M+Na]<sup>+</sup>, calcd. 681.20), 659.14 (41) ([M+H]<sup>+</sup>, calcd. 659.22), 486.19 (100) ([M<sub>fr.(I)}</sub>]<sup>+</sup>, calcd. 486.25), 392.00 (60) ([M<sub>fr.(II)}</sub>]<sup>+</sup>, calcd. 392.24), 324.21 (57) ([M<sub>fr.(III)}</sub>]<sup>+</sup>, calcd. 324.10).
- **HRMS (FTMS + p MALDI):** m/z = 679.2019 [M+Na]<sup>+</sup>, calcd. for [C<sub>34</sub>H<sub>37</sub>BrN<sub>6</sub>NaO<sub>3</sub>]<sup>+</sup> = 679.2008.

**(S)-5-Amino-N-(4-((4-cyclohexyl-1-((3,5-difluorophenyl)amino)-1-oxobutan-2-yl)carbamoyl)benzyl)-1-phenyl-1H-pyrazole-4-carboxamide (237, SR344)**

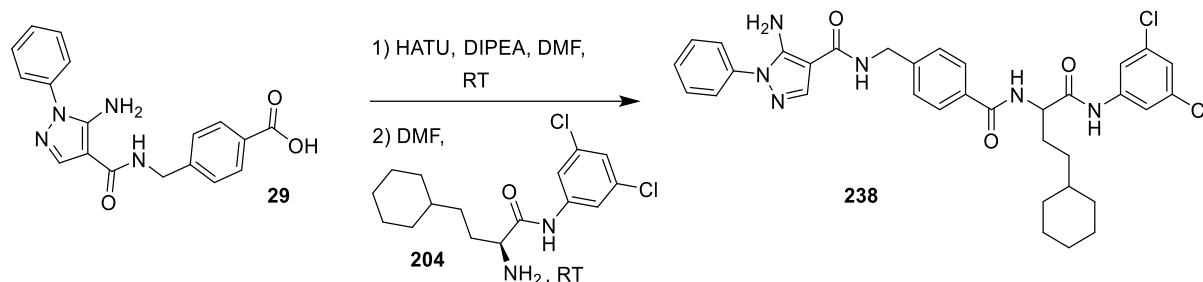


4-((1-Phenyl-1H-pyrazole-4-carboxamido)methyl)benzoic acid (**29**, 200 mg, 0.595 mmol) and HATU (271 mg, 0.714 mmol) were dissolved in DMF (dry, 6 mL) and DIPEA (92 mg, 0.71 mmol) was added. The solution was stirred for 1 h at RT and (S)-2-amino-4-cyclohexyl-N-(3,5-difluorophenyl)butanamide (**203**, 178 mg, 0.600 mmol), dissolved in DMF (dry, 6 mL), was added. The reaction was stirred for additional 20 h at RT. DCM (150 mL) was added, the organic phase was washed 4 times with H<sub>2</sub>O (150 mL) and dried over MgSO<sub>4</sub>. The solvent was removed under reduced pressure and the crude product was purified using column chromatography on silica (cyclohexane/EtOAc 1:1 → 1:3 → 1:20). The crude product was recrystallized from acetone.

**Yield:** 202 mg (0.329 mmol, 55%), colorless solid.

- **TLC:** R<sub>f</sub> = 0.19 (SiO<sub>2</sub>, cyclohexane/EtOAc 1:1).
- **C<sub>34</sub>H<sub>36</sub>F<sub>2</sub>N<sub>6</sub>O<sub>3</sub>:** (614.68), [614.28].
- **HPLC:** t<sub>R</sub> = 16.74 min.
- **<sup>1</sup>H-NMR (600 MHz, DMSO-d<sub>6</sub>, 300 K):** δ = 10.50 (s, 1H, NH F-phenyl), 8.58 (d, <sup>3</sup>J = 7.4 Hz, 1H, NHCHCO), 8.48 (t, <sup>3</sup>J = 5.9 Hz, 1H, NHCH<sub>2</sub>C<sub>Ar</sub>), 8.00 (s, 1H, pyrazole), 7.90 (d, <sup>3</sup>J = 8.2 Hz, 2H, H-3-, H-5-benzyl), 7.58 (d, <sup>3</sup>J = 7.9 Hz, 2H, H-2-, H-6-phenyl), 7.53 (t, <sup>3</sup>J = 8.0 Hz, 2H, H-3-, H-5-phenyl), 7.43–7.34 (m, 5H, H-4 phenyl, H-2-, H-6-benzyl, H-2-, H-6-F-phenyl), 6.91 (tt, <sup>3</sup>J = 9.2, 2.0 Hz, 1H, H-4-F-phenyl), 6.38 (br s, 2H, NH<sub>2</sub>), 4.53–4.46 (m, 3H, CH<sub>2</sub> benzyl, NHCHCO), 1.88–1.77 (m, 2H, NHCHCH<sub>2</sub>), 1.74–1.57 (m, 5H, H-2<sub>eq</sub>-, H-3<sub>eq</sub>-, H-4<sub>eq</sub>-, H-5<sub>eq</sub>-, H-6<sub>eq</sub>-cyclohexyl), 1.40–1.32 (m, 1H, H-1 cyclohexyl), 1.29–1.07 (m, 5H, NHCHCH<sub>2</sub>CH<sub>2</sub>, H-3<sub>ax</sub>-, H-4<sub>ax</sub>-, H-5<sub>ax</sub>-cyclohexyl), 0.92–0.82 (m, 2H, H-2<sub>ax</sub>-, H-6<sub>ax</sub>-cyclohexyl) ppm.
- **<sup>13</sup>C-NMR (75 MHz, DMSO-d<sub>6</sub>, 300 K):** δ = 171.9, 166.5, 164.2, 162.5 (<sup>1</sup>J<sub>CF</sub> = 243.3 Hz), 162.3 (<sup>1</sup>J<sub>C-F</sub> = 243.3 Hz), 149.2, 143.8, 141.8 (<sup>2</sup>J<sub>CF</sub> = 13.7 Hz), 138.4, 138.2, 132.3, 129.4, 127.7, 127.1, 126.8, 123.1, 102.1 (<sup>2</sup>J<sub>CF</sub> = 19.3 Hz), 102.0 (<sup>2</sup>J<sub>CF</sub> = 19.3 Hz), 98.4 (<sup>2</sup>J<sub>CF</sub> = 26.3 Hz), 97.4, 54.8, 41.3, 36.9, 33.4, 32.9, 32.7, 28.9, 26.1, 25.8 (2x) ppm.
- **MS (ESI pos.):** m/z (%) = 615.26 (100) ([M-H]<sup>+</sup>, calcd. 615.28), 486.11 (69) ([M<sub>fr.</sub>]<sup>+</sup>, calcd. 486.25).
- **HRMS (FTMS + p MALDI):** m/z = 615.2887 [M+H]<sup>+</sup>, calcd. for [C<sub>34</sub>H<sub>37</sub>F<sub>2</sub>N<sub>6</sub>O<sub>3</sub>]<sup>+</sup> = 615.2895, 637.2710 [M+Na]<sup>+</sup>, calcd. for [C<sub>34</sub>H<sub>36</sub>F<sub>2</sub>N<sub>6</sub>NaO<sub>3</sub>]<sup>+</sup> = 637.2709.

**5-Amino-N-(4-((4-cyclohexyl-1-((3,5-dichlorophenyl)amino)-1-oxobutan-2-yl)carbamoyl)benzyl)-1-phenyl-1H-pyrazole-4-carboxamide (238, SR336)**

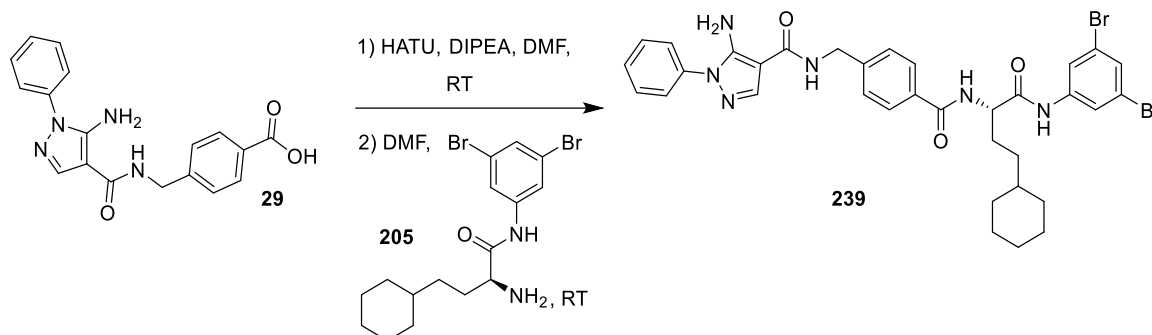


4-((1-Phenyl-1H-pyrazole-4-carboxamido)methyl)benzoic acid (**29**, 140 mg, 0.417 mmol) and HATU (190 mg, 0.500 mmol) were dissolved in DMF (dry, 6 mL) and DIPEA (65 mg, 0.50 mmol) was added. The solution was stirred for 1 h at RT and (*S*)-2-amino-4-cyclohexyl-*N*-(3,5-dichlorophenyl)butanamide (**204**, 165 mg, 0.500 mmol), dissolved in DMF (dry, 6 mL), was added. The reaction was stirred for additional 20 h at RT. DCM (100 mL) was added, the organic phase was washed 4 times with H<sub>2</sub>O (100 mL) and dried over MgSO<sub>4</sub>. The solvent was removed under reduced pressure and the crude product was purified using column chromatography on silica (cyclohexane/EtOAc 1:1 → 1:20 → EtOAc). The product was further recrystallized from acetone.

**Yield:** 97 mg (0.150 mmol, 32%), colorless solid.

- **TLC:** R<sub>f</sub> = 0.48 (SiO<sub>2</sub>, cyclohexane/EtOAc 1:3).
- **C<sub>34</sub>H<sub>36</sub>Cl<sub>2</sub>N<sub>6</sub>O<sub>3</sub>:** (647.59), [646.22].
- **HPLC:** t<sub>R</sub> = 18.27 min.
- **<sup>1</sup>H-NMR (500 MHz, DMSO-d<sub>6</sub>, 300 K):** δ = 10.49 (s, 1H, NH Cl-phenyl), 8.60 (d, <sup>3</sup>J = 7.3 Hz, 1H, NHCHCO), 8.53 (t, <sup>3</sup>J = 6.1 Hz, 1H, NHCH<sub>2</sub>C<sub>Ar</sub>), 7.99 (s, 1H, pyrazole), 7.88 (d, <sup>3</sup>J = 8.3 Hz, 2H, H-3-, H-5-benzyl), 7.71 (d, <sup>4</sup>J = 1.9 Hz, 2H, H-2-, H-6-Cl-phenyl), 7.58–7.49 (m, 4H, H-2-, H-3-, H-5-, H-6-phenyl), 7.42–7.36 (m, 3H, H-4 phenyl, H-2-, H-6-benzyl), 7.28 (t, <sup>4</sup>J = 1.9 Hz, 1H, H-4-Cl-phenyl), 6.39 (br s, 2H, NH<sub>2</sub>), 4.51–4.23 (m, 3H, CH<sub>2</sub> benzyl, NHCHCO), 1.88–1.75 (m, 2H, NHCHCH<sub>2</sub>), 1.73–1.55 (m, 5H, H-2<sub>eq</sub>-, H-3<sub>eq</sub>-, H-4<sub>eq</sub>-, H-5<sub>eq</sub>-, H-6<sub>eq</sub>-cyclohexyl), 1.39–1.30 (m, 1H, H-1 cyclohexyl), 1.28–1.05 (m, 5H, NHCHCH<sub>2</sub>CH<sub>2</sub>, H-3<sub>ax</sub>-, H-4<sub>ax</sub>-, H-5<sub>ax</sub>-cyclohexyl), 0.91–0.80 (m, 2H, H-2<sub>ax</sub>-, H-6<sub>ax</sub>-cyclohexyl) ppm.
- **<sup>13</sup>C-NMR (126 MHz, DMSO-d<sub>6</sub>, 300 K):** δ = 172.0, 166.6, 164.2, 149.2, 143.8, 141.3, 138.4, 138.2, 134.1, 132.3, 129.4, 127.7, 127.1, 126.8, 123.1, 122.5, 117.3, 97.4, 54.9, 41.3, 36.9, 33.4, 32.9, 32.7, 28.8, 26.1, 25.8 (2x) ppm.
- **MS (ESI pos.):** m/z (%) = 647.13 (4) ([M+H]<sup>+</sup>, calcd. 647.23), 354.99 (19) ([M<sub>fr.(I)}</sub>)<sup>+</sup>, calcd. 355.10), 329.02 (100) ([M<sub>fr.(II)}</sub>)<sup>+</sup>, calcd. 329.10).
- **HRMS (FTMS + p MALDI):** m/z = 669.2099 [M+Na]<sup>+</sup>, calcd. for [C<sub>34</sub>H<sub>36</sub>Cl<sub>2</sub>N<sub>6</sub>NaO<sub>3</sub>]<sup>+</sup> = 669.2124.

**(S)-5-Amino-N-(4-((4-cyclohexyl-1-((3,5-dibromophenyl)amino)-1-oxobutan-2-yl)carbamoyl)benzyl)-1-phenyl-1H-pyrazole-4-carboxamide (239, SR347)**

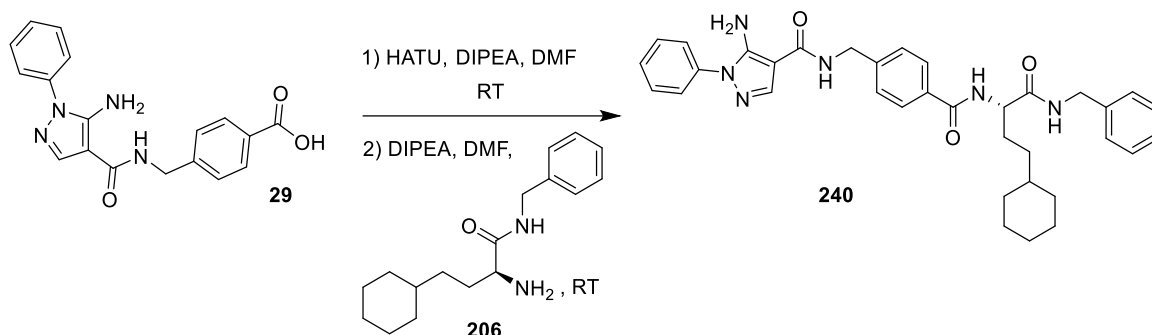


4-((1-Phenyl-1H-pyrazole-4-carboxamido)methyl)benzoic acid (**29**, 200 mg, 0.595 mmol) and HATU (271 mg, 0.714 mmol) were dissolved in DMF (dry, 6 mL) and DIPEA (92 mg, 0.71 mmol) was added. The solution was stirred for 1 h at RT and (S)-2-amino-4-cyclohexyl-N-(3,5-dibromophenyl)butanamide (**205**, 251 mg, 0.600 mmol), dissolved in DMF (dry, 6 mL), was added. The reaction was stirred for additional 4 d at RT. DCM (150 mL) was added, the organic phase was washed 4 times with H<sub>2</sub>O (150 mL) and dried over MgSO<sub>4</sub>. The solvent was removed under reduced pressure and the crude product was purified using column chromatography on silica (cyclohexane/EtOAc 1:1 → 1:3 → 1:20). The product was further recrystallized from acetone.

**Yield:** 79 mg (0.11 mmol, 18%), colorless solid.

- **TLC:** R<sub>f</sub> = 0.67 (SiO<sub>2</sub>, cyclohexane/EtOAc 1:3).
- **C<sub>34</sub>H<sub>36</sub>Br<sub>2</sub>N<sub>6</sub>O<sub>3</sub>:** (736.50), [734.12].
- **HPLC:** t<sub>R</sub> = 18.81 min.
- **<sup>1</sup>H-NMR (600 MHz, DMSO-d<sub>6</sub>, 300 K):** δ = 10.39 (s, 1H, NH Br-phenyl), 8.57 (d, <sup>3</sup>J = 7.6 Hz, 1H, NHCHCO), 8.51 (t, <sup>3</sup>J = 5.6 Hz, 1H, NHCH<sub>2</sub>C<sub>Ar</sub>), 7.99 (s, 1H, pyrazole), 7.92–7.84 (m, 4H, H-3-, H-5-benzyl, H-2-, H-6-Br-phenyl), 7.60–7.48 (m, 5H, H-4-Br-phenyl, H-2-, H-3-, H-5-, H-6-phenyl), 7.42–7.35 (m, 3H, H-4 phenyl, H-2-, H-6-benzyl), 6.37 (br s, 2H, NH<sub>2</sub>), 4.52–4.42 (m, 3H, CH<sub>2</sub> benzyl, NHCHCO), 1.88–1.75 (m, 2H, NHCHCH<sub>2</sub>), 1.72–1.55 (m, 5H, H-2<sub>eq</sub>-, H-3<sub>eq</sub>-, H-4<sub>eq</sub>-, H-5<sub>eq</sub>-, H-6<sub>eq</sub>-cyclohexyl), 1.38–1.30 (m, 1H, H-1 cyclohexyl), 1.27–1.06 (m, 5H, NHCHCH<sub>2</sub>CH<sub>2</sub>, H-3<sub>ax</sub>-, H-4<sub>ax</sub>-, H-5<sub>ax</sub>-cyclohexyl), 0.91–0.81 (m, 2H, H-2<sub>ax</sub>-, H-6<sub>ax</sub>-cyclohexyl) ppm.
- **<sup>13</sup>C-NMR (75 MHz, DMSO-d<sub>6</sub>, 300 K):** δ = 171.9, 166.5, 164.1, 149.2, 143.8, 141.6, 138.4, 138.2, 132.3, 129.4, 127.8, 127.7, 127.1, 126.8, 123.1, 122.3, 120.5, 97.4, 54.9, 41.3, 36.9, 33.4, 32.8, 32.7, 28.8, 26.1, 25.8 (2x) ppm.
- **MS (ESI pos.):** m/z (%) = 737.14 (84) ([M+H]<sup>+</sup>, calcd. 737.13), 486.21 (100) ([M<sub>fr.</sub>]<sup>+</sup>, calcd. 486.25).
- **HRMS (FTMS + p MALDI):** m/z = 737.1271 [M+H]<sup>+</sup>, calcd. for [C<sub>34</sub>H<sub>37</sub>Br<sub>2</sub>N<sub>6</sub>O<sub>3</sub>]<sup>+</sup> = 737.1273.

**(S)-5-Amino-N-(4-((1-(benzylamino)-4-cyclohexyl-1-oxobutan-2-yl)carbamoyl)benzyl)-1-phenyl-1H-pyrazole-4-carboxamide (240, SR83)**

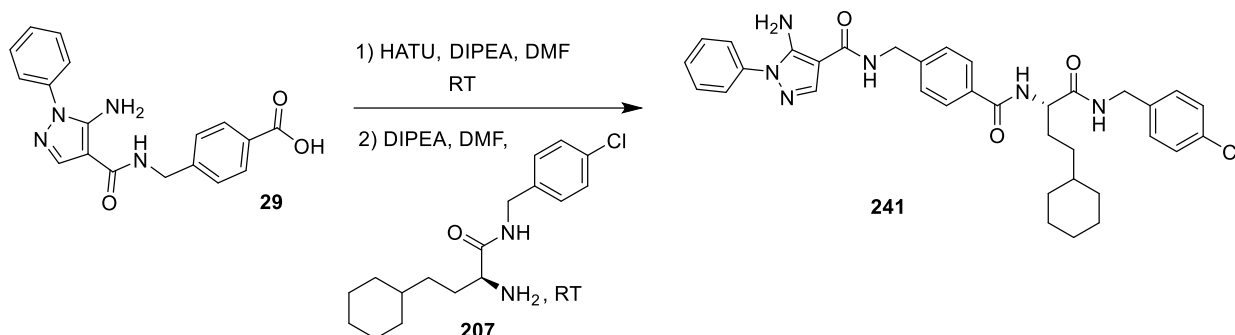


4-((5-Amino-1-phenyl-1H-pyrazole-4-carboxamido)methyl)benzoic acid (**29**, 150 mg, 0.446 mmol) and HATU (203 mg, 0.535 mmol) were dissolved in DMF (5 mL) and DIPEA (87 mg, 0.67 mmol) was added. The solution was stirred for 1.5 h at RT and (S)-2-amino-N-benzyl-4-cyclohexylbutanamide (**206**, 147 mg, 0.535 mmol), diluted in DMF (5 mL) and DIPEA (87 mg, 0.67 mmol, 1.5 eq), was added. The mixture was stirred for 20 h at RT. DCM (50 mL) was added and the organic phase was washed 3 times with H<sub>2</sub>O (20 mL) and dried over MgSO<sub>4</sub>. The solvent was evaporated under reduced pressure the crude product was triturated with cyclohexane/EtOAc (1:1).

**Yield:** 202 mg (0.341 mmol, 76%), colorless solid.

- **TLC:** R<sub>f</sub> = 0.67 (SiO<sub>2</sub>, EtOAc/MeOH 10:1).
- **C<sub>35</sub>H<sub>40</sub>N<sub>6</sub>O<sub>3</sub>:** (592.73), [592.32].
- **HPLC:** t<sub>R</sub> = 15.56 min.
- **<sup>1</sup>H-NMR (500 MHz, DMSO-d<sub>6</sub>, 300 K):** δ = 8.70 (t, <sup>3</sup>J = 6.1 Hz, 1H, NH benzyl). 8.62 (t, <sup>3</sup>J = 6.0 Hz, 1H, NHCH<sub>2</sub>C benzyl-CO), 8.49 (d, <sup>3</sup>J = 8.1 Hz, 1H, NHCHCO), 8.07 (s, 1H, pyrazole), 7.88 (d, <sup>3</sup>J = 8.3 Hz, 2H, H-3-, H-5-benzyl-CO), 7.59–7.49 (m, 4H, H-2-, H-3-, H-5-, H-6-phenyl), 7.41–7.35 (m, 3H, H-4 phenyl, H-2-, H-6-benzyl-CO), 7.31–7.35 (m, 5H, H-2-, H-3-, H-4-, H-5-, H-6-benzyl), 6.37 (br s, 2H, NH<sub>2</sub>), 4.49–4.38 (m, 3H, CH<sub>2</sub> benzyl-CO, NHCHCO), 4.33–4.22 (m, 2H, CH<sub>2</sub> benzyl), 1.86–1.53 (m, 7H, NHCHCH<sub>2</sub>, H-2<sub>eq</sub>-, H-3<sub>eq</sub>-, H-4<sub>eq</sub>-, H-5<sub>eq</sub>-, H-6<sub>eq</sub>-cyclohexyl), 1.33–1.03 (m, 6H, NHCHCH<sub>2</sub>CH<sub>2</sub>, H-1-, H-3<sub>ax</sub>-, H-4<sub>ax</sub>-, H-5<sub>ax</sub>-cyclohexyl), 0.88–0.75 (m, 2H, H-2<sub>ax</sub>-, H-6<sub>ax</sub>-cyclohexyl) ppm.
- **<sup>13</sup>C-NMR (126 MHz, DMSO-d<sub>6</sub>, 300 K):** δ = 172.1, 166.1, 164.2, 149.2, 143.7, 139.6, 138.6, 138.3, 132.6, 129.4, 128.2, 127.6, 127.1, 126.8, 126.7, 123.1, 97.5, 53.9, 42.0, 41.3, 36.8, 33.3, 32.9, 32.7, 29.2, 26.2, 25.8 (2x) ppm.
- **MS (MALDI pos.):** m/z (%) = 614.8 (100) ([M+Na]<sup>+</sup>, calcd. 615.31), 592.86 (55) ([M]<sup>+</sup>, calcd. 592.32).
- **HRMS (FTMS + p MALDI):** m/z = 631.2784 [M+K]<sup>+</sup>, calcd. for [C<sub>35</sub>H<sub>40</sub>KN<sub>6</sub>O<sub>3</sub>]<sup>+</sup> = 631.2799.

**(S)-5-Amino-N-(4-((1-((4-chlorobenzyl)amino)-4-cyclohexyl-1-oxobutan-2-yl)carbamoyl)benzyl)-1-phenyl-1H-pyrazole-4-carboxamide (241, SR82)**

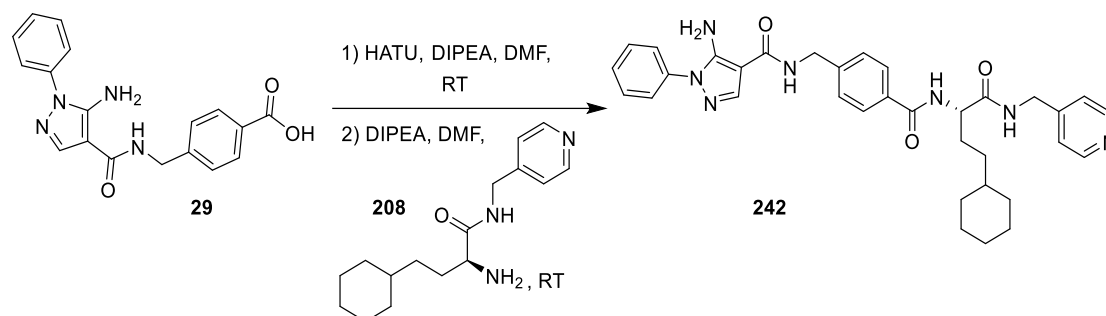


4-((5-Amino-1-phenyl-1H-pyrazole-4-carboxamido)methyl)benzoic acid (**29**, 200 mg, 0.595 mmol) and HATU (280 mg, 0.736 mmol) were dissolved in DMF (5 mL) and DIPEA (115 mg, 0.893 mmol) was added. The solution was stirred for 1.5 h at RT and (S)-2-amino-N-(4-chlorobenzyl)-4-cyclohexylbutanamide (**207**, 221 mg, 0.736 mmol), diluted in DMF (5 mL) and DIPEA (115 mg, 0.893 mmol), was added. The mixture was stirred for 20 h at RT. EtOAc (100 mL) was added and the organic phase was washed 4 times with H<sub>2</sub>O (20 mL) and dried over MgSO<sub>4</sub>. The solvent was evaporated under reduced pressure and the crude product was purified using column chromatography on silica (cyclohexane/EtOAc 1:1 → 1:4 → 1:7 → EtOAc).

**Yield:** 203 mg (0.324 mmol, 54%), colorless solid.

- **TLC:** R<sub>f</sub> = 0.66 (SiO<sub>2</sub>, EtOAc/MeOH 10:1).
- **C<sub>35</sub>H<sub>39</sub>ClN<sub>6</sub>O<sub>3</sub>:** (627.18), [626.28].
- **HPLC:** t<sub>R</sub> = 16.06 min.
- **<sup>1</sup>H-NMR (500 MHz, DMSO-d<sub>6</sub>, 300 K):** δ = 8.57–8.44 (m, 2H, NHCH<sub>2</sub>C<sub>Ar</sub>, NHCH<sub>2</sub> Cl-benzyl), 8.39 (d, <sup>3</sup>J = 7.9 Hz, 1H, NHCHCO), 8.00 (s, 1H, pyrazole), 7.88 (d, <sup>3</sup>J = 8.3 Hz, 2H, H-3-, H-5-benzyl), 7.61–7.49 (m, 4H, H-2-, H-3-, H-5-, H-6-phenyl), 7.42–7.33 (m, 5H, H-4 phenyl, H-2-, H-6-benzyl, H-3-, H-5-Cl-benzyl), 7.28 (d, <sup>3</sup>J = 8.4 Hz, 2H, H-2-, H-6-Cl-benzyl) 6.39 (br s, 2H, NH<sub>2</sub>), 4.48 (d, <sup>3</sup>J = 6.0 Hz, 2H, CH<sub>2</sub> benzyl), 4.44–4.37 (m, 1H, NHCHCO), 4.27 (d, <sup>3</sup>J = 6.3 Hz, 2H, CH<sub>2</sub> Cl-benzyl) 1.86–1.53 (m, 7H, NHCHCH<sub>2</sub>, H-2<sub>eq</sub>-, H-3<sub>eq</sub>-, H-4<sub>eq</sub>-, H-5<sub>eq</sub>-, H-6<sub>eq</sub>-cyclohexyl), 1.28–1.04 (m, 6H, NHCHCH<sub>2</sub>CH<sub>2</sub>, H-1-, H-3<sub>ax</sub>-, H-4<sub>ax</sub>-, H-5<sub>ax</sub>-cyclohexyl), 0.90–0.73 (m, 2H, H-2<sub>ax</sub>-, H-6<sub>ax</sub>-cyclohexyl) ppm.
- **<sup>13</sup>C-NMR (126 MHz, DMSO-d<sub>6</sub>, 300 K):** δ = 172.1, 166.3, 164.2, 149.2, 143.6, 138.7, 138.4, 138.2, 132.6, 131.2, 129.4, 129.0, 128.2, 127.7, 127.1, 126.8, 123.1, 97.4, 53.8, 41.4, 36.7, 33.3, 32.9, 32.7, 29.1, 26.2, 25.8 ppm.
- **MS (ESI pos.):** m/z (%) = 627.35 (100) ([M+H]<sup>+</sup>, calcd. 627.29), 486.25 (23) ([M<sub>fr.(l)}</sub>]<sup>+</sup>, calcd. 486.25).
- **HRMS (FTMS + p MALDI):** m/z = 649.2661 [M+Na]<sup>+</sup>, calcd. for [C<sub>35</sub>H<sub>39</sub>ClN<sub>6</sub>NaO<sub>3</sub>]<sup>+</sup> = 649.2670.

**(S)-5-Amino-N-(4-((4-cyclohexyl-1-oxo-1-((pyridin-4-ylmethyl)amino)butan-2-yl)carbamoyl)benzyl)-1-phenyl-1H-pyrazole-4-carboxamide (242, SR92)**



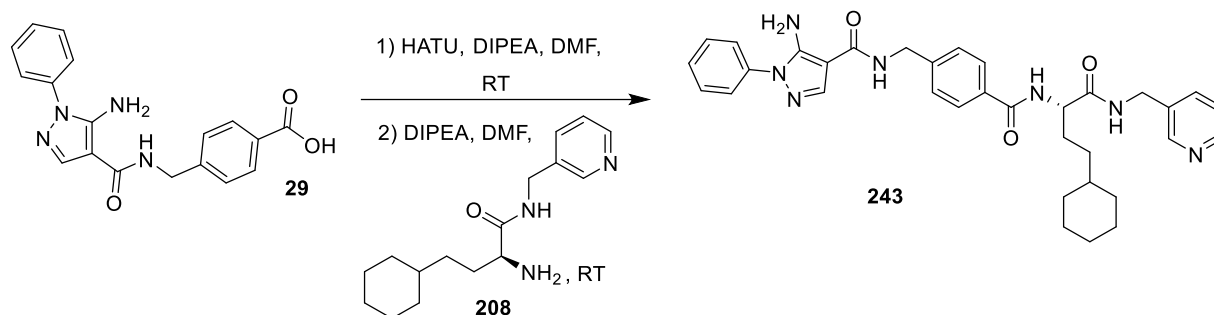
4-((5-Amino-1-phenyl-1H-pyrazole-4-carboxamido)methyl)benzoic acid (**29**, 200 mg, 0.595 mmol) and HATU (280 mg, 0.736 mmol) were dissolved in DMF (5 mL) and DIPEA (115 mg, 0.893 mmol) was added. The solution was stirred for 1.5 h at RT and (S)-2-amino-4-cyclohexyl-N-(pyridin-4-ylmethyl)butanamide (**208**, 202 mg, 0.736 mmol), diluted in DMF (5 mL) and DIPEA (115 mg, 0.893 mmol), was added. The mixture was stirred for 20 h at RT. DCM (50 mL) was added and the organic phase was washed 5 times with H<sub>2</sub>O (20 mL) and dried over MgSO<sub>4</sub>. The solvent was evaporated under reduced pressure and the crude product was purified using column chromatography on silica (EtOAc/MeOH 10:1).

**Yield:** 153 mg (0.258 mmol, 43%), colorless solid.

- **TLC:**  $R_f = 0.21$  (SiO<sub>2</sub>, EtOAc/MeOH 10:1).
- **C<sub>34</sub>H<sub>39</sub>N<sub>7</sub>O<sub>3</sub>:** (593.72), [593.31].
- **HPLC:**  $t_R = 10.54$  min.
- **<sup>1</sup>H-NMR (300 MHz, DMSO-d<sub>6</sub>, 300 K):**  $\delta = 8.58$  (t,  $^3J = 5.8$  Hz, 1H, NHCH<sub>2</sub> pyridine), 8.53–8.46 (m, 3H, NHCH<sub>2</sub> benzyl, H-2-, H-6-pyridine), 8.41 (d,  $^3J = 7.6$  Hz, 1H, NHCHCO), 7.98 (s, 1H, pyrazole), 7.88 (d,  $^3J = 8.5$  Hz, 2H, H-3-, H-5-benzyl), 7.60–7.48 (m, 4H, H-2-, H-3-, H-5-, H-6-phenyl), 7.43–7.33 (m, 3H, H-4 phenyl, H-2-, H-6-benzyl), 7.27–7.23 (m, 2H, H-3-, H-5-pyridine), 6.37 (s, 2H, NH<sub>2</sub>), 4.51–4.37 (m, 3H, CH<sub>2</sub> benzyl, NHCHCO), 4.31 (d,  $^3J = 5.9$  Hz, 2H, CH<sub>2</sub> pyridine), 1.90–1.55 (m, 7H, NHCHCH<sub>2</sub>, H-2<sub>eq</sub>-, H-3<sub>eq</sub>-, H-4<sub>eq</sub>-, H-5<sub>eq</sub>-, H-6<sub>eq</sub>-cyclohexyl), 1.35–1.06 (m, 6H, NHCHCH<sub>2</sub>CH<sub>2</sub>, H-1-, H-3<sub>ax</sub>-, H-4<sub>ax</sub>-, H-5<sub>ax</sub>-cyclohexyl), 0.94–0.75 (m, 2H, H-2<sub>ax</sub>-, H-6<sub>ax</sub>-cyclohexyl) ppm.
- **<sup>13</sup>C-NMR (75 MHz, DMSO-d<sub>6</sub>, 300 K):**  $\delta = 172.3, 166.4, 164.1, 149.4, 149.2, 148.6, 143.6, 138.4, 138.2, 132.6, 129.4, 127.6, 127.1, 126.8, 123.1, 122.0, 97.4, 53.8, 41.3, 41.1, 36.7, 33.3, 32.9, 32.7, 28.9, 26.1, 25.8$  (2x) ppm.
- **MS (ESI pos.):**  $m/z$  (%) = 594.35 (100) ([M+H]<sup>+</sup>, calcd. 594.32), 297.81 (35) ([M<sub>fr</sub>+Na]<sup>+</sup>, calcd. 297.18).
- **HRMS (FTMS + p MALDI):**  $m/z = 594.3188$  [M+H]<sup>+</sup>, calcd. for [C<sub>34</sub>H<sub>40</sub>N<sub>7</sub>O<sub>3</sub>]<sup>+</sup> = 594.3193.



**(S)-5-Amino-N-(4-((4-cyclohexyl-1-oxo-1-((pyridin-3-ylmethyl)amino)butan-2-yl)carbamoyl)benzyl)-1-phenyl-1H-pyrazole-4-carboxamide (243, SR93)**

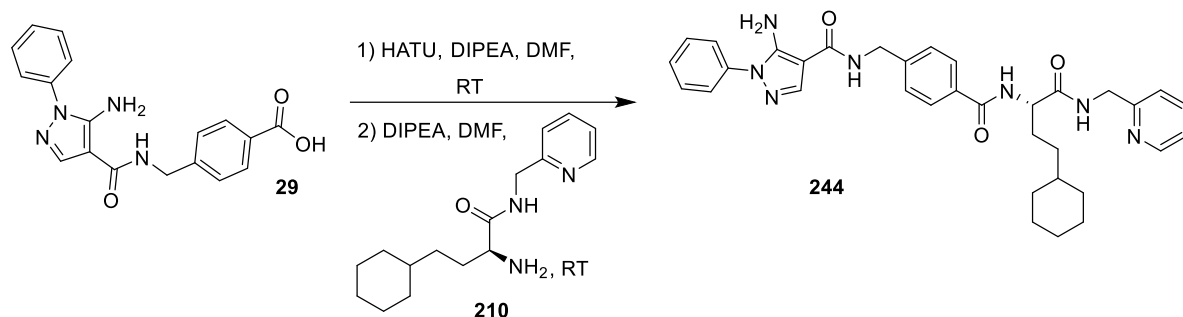


4-((5-Amino-1-phenyl-1H-pyrazole-4-carboxamido)methyl)benzoic acid (**29**, 150 mg, 0.446 mmol) and HATU (203 mg, 0.535 mmol) were dissolved in DMF (5 mL) and DIPEA (87 mg, 0.67 mmol) was added. The solution was stirred for 1.5 h at RT and (S)-2-amino-4-cyclohexyl-N-(pyridin-3-ylmethyl)butanamide (**208**, 147 mg, 0.535 mmol), diluted in DMF (5 mL) and DIPEA (87 mg, 0.67 mmol), was added. The mixture was stirred for 20 h at RT. DCM (50 mL) was added and the organic phase was washed 5 times with H<sub>2</sub>O (20 mL) and dried over MgSO<sub>4</sub>. The solvent was evaporated under reduced pressure the crude product was purified using column chromatography on silica (EtOAc/MeOH 10:1).

**Yield:** 64 mg (0.11 mmol, 24%), colorless solid.

- **TLC:** R<sub>f</sub> = 0.18 (SiO<sub>2</sub>, EtOAc/MeOH 10:1).
- **C<sub>34</sub>H<sub>39</sub>N<sub>7</sub>O<sub>3</sub>:** (593.72), [593.31].
- **HPLC:** t<sub>R</sub> = 10.98 min.
- **<sup>1</sup>H-NMR (300 MHz, DMSO-d<sub>6</sub>, 300 K):** δ = 8.57–8.45 (m, 3H, NHCH<sub>2</sub> pyridine, NHCH<sub>2</sub> benzyl, H-2 pyridine), 8.43 (dd, <sup>3</sup>J = 4.8, 1.4 Hz, 1H, H-6 pyridine), 8.38 (d, <sup>3</sup>J = 7.9 Hz, 1H, NHCHCO), 7.98 (s, 1H, pyrazole), 7.87 (d, <sup>3</sup>J = 8.3 Hz, 2H, H-3-, H-5-benzyl), 7.65 (dt, <sup>3</sup>J = 7.8, 1.9 Hz, 1H, H-5 pyridine), 7.60–7.49 (m, 4H, H-2-, H-3-, H-5-, H-6-phenyl), 7.43–7.30 (m, 4H, H-4 phenyl, H-2-, H-6-benzyl, H-4 pyridine), 6.37 (s, 2H, NH<sub>2</sub>), 4.48 (d, <sup>3</sup>J = 6.0 Hz, 2H, CH<sub>2</sub> benzyl), 4.45–4.35 (m, 1H, NHCHCO), 4.31 (d, <sup>3</sup>J = 5.9 Hz, 2H, CH<sub>2</sub> pyridine), 1.89–1.53 (m, 7H, NHCHCH<sub>2</sub>, H-2<sub>eq</sub>-, H-3<sub>eq</sub>-, H-4<sub>eq</sub>-, H-5<sub>eq</sub>-, H-6<sub>eq</sub>-cyclohexyl), 1.32–1.03 (m, 6H, NHCHCH<sub>2</sub>CH<sub>2</sub>, H-1-, H-3<sub>ax</sub>-, H-4<sub>ax</sub>-, H-5<sub>ax</sub>-cyclohexyl), 0.94–0.74 (m, 2H, H-2<sub>ax</sub>-, H-6<sub>ax</sub>-cyclohexyl) ppm.
- **<sup>13</sup>C-NMR (75 MHz, DMSO-d<sub>6</sub>, 300 K):** δ = 172.1, 166.3, 164.1, 149.2, 148.6, 148.0, 143.6, 138.4, 138.2, 135.0, 134.9, 132.6, 129.4, 127.6, 127.1, 126.8, 123.3, 123.1, 97.4, 53.8, 41.3, 36.7, 33.3, 32.9, 32.6, 29.0, 26.1, 25.8, 25.7 ppm.
- **MS (ESI pos.):** k m/z (%) = 594.37 (100) ([M+H]<sup>+</sup>, calcd. 594.13), 319.16 (11) ([M<sub>fr.(1)}</sub>]<sup>+</sup>, calcd. 319.12), 297.79 (64) ([M<sub>fr.(1)}</sub>+Na]<sup>+</sup>, calcd. 297.17).
- **HRMS (FTMS + p MALDI):** m/z = 616.3010 [M+Na]<sup>+</sup>, calcd. for [C<sub>34</sub>H<sub>39</sub>N<sub>7</sub>NaO<sub>3</sub>]<sup>+</sup> = 616.3012.

**(S)-5-Amino-N-(4-((4-cyclohexyl-1-oxo-1-((pyridin-2-ylmethyl)amino)butan-2-yl)carbamoyl)benzyl)-1-phenyl-1H-pyrazole-4-carboxamide (244, SR94)**

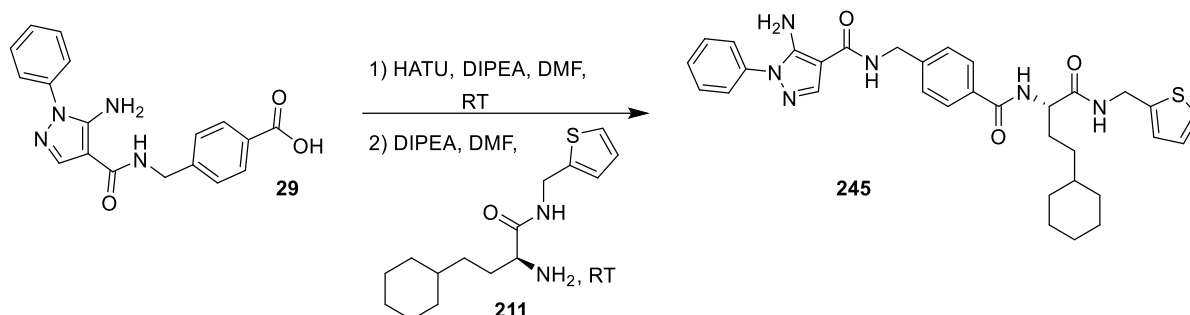


4-((5-Amino-1-phenyl-1H-pyrazole-4-carboxamido)methyl)benzoic acid (**29**, 200 mg, 0.595 mmol) and HATU (280 mg, 0.736 mmol) were dissolved in DMF (5 mL) and DIPEA (115 mg, 0.893 mmol) was added. The solution was stirred for 1.5 h at RT and (S)-2-amino-4-cyclohexyl-N-(pyridin-2-ylmethyl)butanamide (**210**, 202 mg, 0.736 mmol), diluted in DMF (5 mL) and DIPEA (115 mg, 0.893 mmol), was added. The mixture was stirred for 20 h at RT. DCM (50 mL) was added and the organic phase was washed 5 times with H<sub>2</sub>O (20 mL) and dried over MgSO<sub>4</sub>. The solvent was evaporated under reduced pressure and the crude product was purified using column chromatography on silica (EtOAc/MeOH 10:1).

**Yield:** 183 mg (0.308 mmol, 52%), colorless solid.

- **TLC:**  $R_f = 0.34$  (SiO<sub>2</sub>, EtOAc/MeOH 10:1).
- **C<sub>34</sub>H<sub>39</sub>N<sub>7</sub>O<sub>3</sub>:** (593.72), [593.31].
- **HPLC:**  $t_R = 12.45$  min.
- **<sup>1</sup>H-NMR (500 MHz, DMSO-d<sub>6</sub>, 300 K):**  $\delta = 8.58$  (t,  $^3J = 5.9$  Hz, 1H, NHCH<sub>2</sub> pyridine), 8.52 (t,  $^3J = 6.1$  Hz, 1H, NHCH<sub>2</sub> benzyl), 8.49–8.46 (m, 1H, H-6 pyridine), 8.43 (d,  $^3J = 7.9$  Hz, 1H, NHCHCO), 7.99 (s, 1H, pyrazole), 7.88 (d,  $^3J = 8.2$  Hz, 2H, H-3-, H-5-benzyl), 7.74 (dt,  $^3J = 7.7$ , 1.8 Hz, 1H, H-4 pyridine), 7.59–7.49 (m, 4H, H-2-, H-3-, H-5-, H-6-phenyl), 7.42–7.36 (m, 3H, H-4 phenyl, H-2-, H-6-benzyl), 7.29 (d,  $^3J = 7.8$  Hz, 1H, H-3 pyridine), 7.26–7.22 (m, 1H, H-5 pyridine), 6.38 (s, 2H, NH<sub>2</sub>), 4.50–4.41 (m, 3H, CH<sub>2</sub> benzyl, NHCHCO), 4.37 (d,  $^3J = 6.1$  Hz, 2H, CH<sub>2</sub> pyridine), 1.90–1.55 (m, 7H, NHCHCH<sub>2</sub>, H-2<sub>eq</sub>-, H-3<sub>eq</sub>-, H-4<sub>eq</sub>-, H-5<sub>eq</sub>-, H-6<sub>eq</sub>-cyclohexyl), 1.30–1.05 (m, 6H, NHCHCH<sub>2</sub>CH<sub>2</sub>, H-1-, H-3<sub>ax</sub>-, H-4<sub>ax</sub>-, H-5<sub>ax</sub>-cyclohexyl), 0.89–0.78 (m, 2H, H-2<sub>ax</sub>-, H-6<sub>ax</sub>-cyclohexyl) ppm.
- **<sup>13</sup>C-NMR (126 MHz, DMSO-d<sub>6</sub>, 300 K):**  $\delta = 172.2, 166.3, 164.1, 158.7, 149.2, 148.8, 143.6, 138.2, 136.7, 132.6, 129.4, 127.6, 127.1, 126.8, 123.1, 122.0, 120.7, 97.4, 53.8, 44.4, 41.3, 36.8, 33.4, 32.9, 32.7, 29.0, 26.2, 25.8$  (2x) ppm.
- **MS (ESI pos.):**  $m/z$  (%) = 594.37 (100) ([M+H]<sup>+</sup>, calcd. 594.32).
- **HRMS (FTMS + p MALDI):**  $m/z = 616.3007$  [M+Na]<sup>+</sup>, calcd. for [C<sub>34</sub>H<sub>39</sub>N<sub>7</sub>NaO<sub>3</sub>]<sup>+</sup> = 616.3012.

**(S)-5-Amino-N-(4-((4-cyclohexyl-1-oxo-1-((thiophen-2-ylmethyl)amino)butan-2-yl)carbamoyl)benzyl)-1-phenyl-1H-pyrazole-4-carboxamide (245, SR97)**

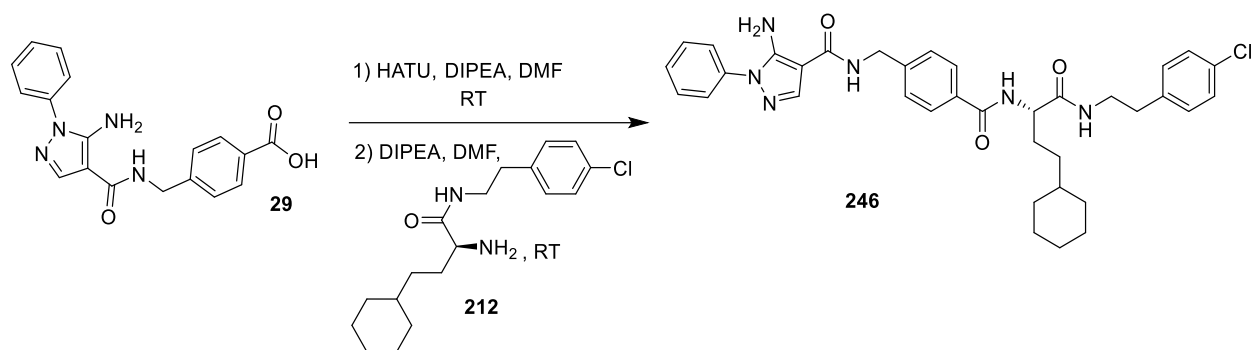


4-((5-Amino-1-phenyl-1H-pyrazol-4-yl)carbamoyl)benzoic acid (**29**, 200 mg, 0.595 mmol) and HATU (280 mg, 0.736 mmol) were dissolved in DMF (5 mL) and DIPEA (115 mg, 0.893 mmol) was added. The solution was stirred for 1.5 h at RT and (S)-2-amino-4-cyclohexyl-N-(thiophen-2-ylmethyl)butanamide (**211**, 370 mg, 0.736 mmol), diluted in DMF (5 mL) and DIPEA (115 mg, 0.893 mmol), was added. The mixture was stirred for 20 h at RT. DCM (50 mL) was added and the organic phase was washed 5 times with H<sub>2</sub>O (20 mL) and dried over MgSO<sub>4</sub>. The solvent was evaporated under reduced pressure the crude product was triturated with cyclohexane/DCM (1:1).

**Yield:** 111 mg (0.185 mmol, 31%), colorless solid.

- **TLC:** R<sub>f</sub> = 0.67 (SiO<sub>2</sub>, EtOAc/MeOH 10:1).
- **C<sub>33</sub>H<sub>38</sub>N<sub>6</sub>O<sub>3</sub>S:** (598.76), [598.27].
- **HPLC:** t<sub>R</sub> = 15.33 min.
- **<sup>1</sup>H-NMR (500 MHz, DMSO-d<sub>6</sub>, 300 K):** δ = 8.58 (t, <sup>3</sup>J = 5.9 Hz, 1H, NH benzyl), 8.52 (t, <sup>3</sup>J = 6.1 Hz, 1H, NHCH<sub>2</sub> thiophene), 8.36 (d, <sup>3</sup>J = 8.1 Hz, 1H, NHCHCO), 7.99 (s, 1H, pyrazole), 7.87 (d, <sup>3</sup>J = 8.3 Hz, 2H, H-3-, H-5-benzyl), 7.59–7.50 (m, 4H, H-2-, H-3-, H-5-, H-6-phenyl), 7.41–7.32 (m, 4H, H-4 phenyl, H-2-, H-6-benzyl, H-5 thiophene), 6.97–6.92 (m, 2H, H-3-, H-4-thiophene), 6.38 (br s, 2H, NH<sub>2</sub>), 4.53–4.35 (m, 5H, CH<sub>2</sub> benzyl, CH<sub>2</sub> thiophene, NHCHCO), 1.85–1.75 (m, 1H, NHCHCH<sub>A</sub>H<sub>B</sub>CH<sub>2</sub>), 1.74–1.55 (m, 6H, NHCHCH<sub>A</sub>H<sub>B</sub>CH<sub>2</sub>, H-2<sub>eq</sub>-, H-3<sub>eq</sub>-, H-4<sub>eq</sub>-, H-5<sub>eq</sub>-, H-6<sub>eq</sub>-cyclohexyl), 1.28–1.04 (m, 6H, NHCHCH<sub>2</sub>CH<sub>2</sub>, H-1-, H-3<sub>ax</sub>-, H-4<sub>ax</sub>-, H-5<sub>ax</sub>-cyclohexyl), 0.89–0.76 (m, 2H, H-2<sub>ax</sub>-, H-6<sub>ax</sub>-cyclohexyl) ppm.
- **<sup>13</sup>C-NMR (126 MHz, DMSO-d<sub>6</sub>, 300 K):** δ = 171.8, 166.1, 164.2, 149.2, 143.6, 142.6, 138.4, 138.2, 132.6, 129.4, 127.6, 127.1, 126.8, 126.6, 125.2, 125.0, 123.1, 97.4, 53.6, 41.4, 37.2, 36.8, 33.3, 32.9, 32.7, 29.2, 26.2, 25.8 (2x) ppm.
- **MS (MALDI pos.):** m/z (%) = 620.76 (100) ([M+Na]<sup>+</sup>, calcd. 621.26), 598.79 (52) ([M]<sup>+</sup>, calcd. 598.27).
- **HRMS (FTMS + p MALDI):** m/z = 599.2781 [M+H]<sup>+</sup>, calcd. for [C<sub>33</sub>H<sub>39</sub>N<sub>6</sub>O<sub>3</sub>S]<sup>+</sup> = 599.2799.

**(S)-5-Amino-N-(4-((1-((4-chlorophenethyl)amino)-4-cyclohexyl-1-oxobutan-2-yl)carbamoyl)benzyl)-1-phenyl-1H-pyrazole-4-carboxamide (246, SR72)**

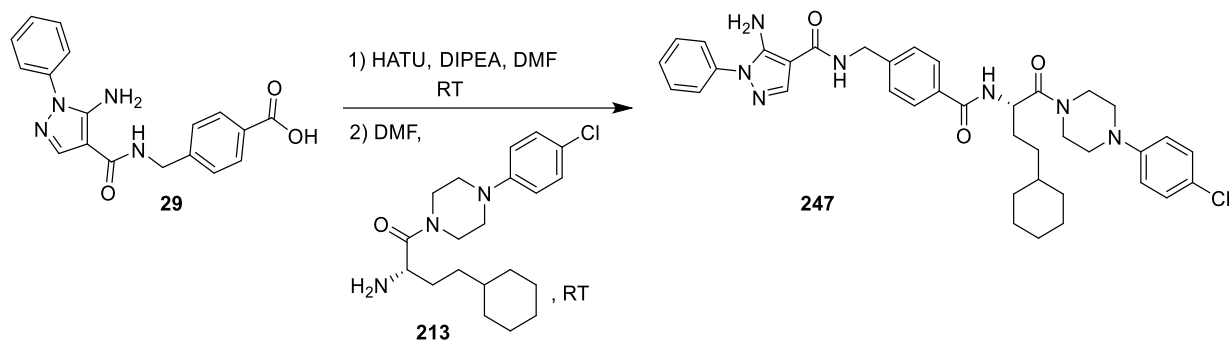


4-((5-Amino-1-phenyl-1H-pyrazole-4-carboxamido)methyl)benzoic acid (**29**, 200 mg, 0.595 mmol) and HATU (280 mg, 0.736 mmol) were dissolved in DMF (5 mL) and DIPEA (115 mg, 0.893 mmol) was added. The solution was stirred for 2 h at RT and (S)-2-amino-N-(4-chlorophenethyl)-4-cyclohexylbutanamide (**212**, 238 mg, 0.736 mmol), diluted in DMF (5 mL) and DIPEA (115 mg, 0.893 mmol), was added. The mixture was stirred for 20 h at RT. EtOAc (100 mL) was added and the organic phase was washed 5 times with H<sub>2</sub>O (20 mL) and dried over MgSO<sub>4</sub>. The solvent was evaporated under reduced pressure and the crude product was purified using column chromatography on silica (cyclohexane/EtOAc 1:6 → EtOAc).

**Yield:** 250 mg (0.390 mmol, 66%), yellowish solid.

- **TLC:**  $R_f = 0.22$  (SiO<sub>2</sub>, cyclohexane/EtOAc 1:6).
- **C<sub>36</sub>H<sub>41</sub>ClN<sub>6</sub>O<sub>3</sub>:** (641.20), [640.29].
- **HPLC:**  $t_R = 16.32$  min.
- **<sup>1</sup>H-NMR (500 MHz, DMSO-d<sub>6</sub>, 300 K):**  $\delta = 8.52$  (t,  $^3J = 6.1$  Hz, 1H, NHCH<sub>2</sub>C<sub>Ar</sub>), 8.27 (d,  $^3J = 8.0$  Hz, 1H, NHCHCO), 8.01–7.94 (m, 2H, pyrazole, NHCH<sub>2</sub>CH<sub>2</sub>), 7.85 (d,  $^3J = 8.3$  Hz, 2H, H-3-, H-5-benzyl), 7.60–7.49 (m, 4H, H-2-, H-3-, H-5-, H-6-phenyl), 7.42–7.35 (m, 3H, H-4 phenyl, H-2-, H-6-benzyl), 6.39 (br s, 2H, NH<sub>2</sub>), 4.48 (d,  $^3J = 6.1$  Hz, 2H, CH<sub>2</sub> benzyl), 4.35–4.27 (m, 1H, NHCHCO), 3.41–3.32 (m, 1H, NHCH<sub>A</sub>CH<sub>B</sub>CH<sub>2</sub>), 3.28–3.20 (m, 1H, NHCH<sub>A</sub>CH<sub>B</sub>CH<sub>2</sub>), 2.71 (t, 2H,  $^3J = 7.0$  Hz, NHCH<sub>2</sub>CH<sub>2</sub>), 1.69–1.53 (m, 7H, NHCHCH<sub>2</sub>CH<sub>2</sub>, H-2<sub>eq</sub>-, H-3<sub>eq</sub>-, H-4<sub>eq</sub>-, H-5<sub>eq</sub>-, H-6<sub>eq</sub>-cyclohexyl), 1.28–1.01 (m, 6H, NHCHCH<sub>2</sub>CH<sub>2</sub>, H-1-, H-3<sub>ax</sub>-, H-4<sub>ax</sub>-, H-5<sub>ax</sub>-cyclohexyl), 0.89–0.73 (m, 2H, H-2<sub>ax</sub>-, H-6<sub>ax</sub>-cyclohexyl) ppm.
- **<sup>13</sup>C-NMR (126 MHz, DMSO-d<sub>6</sub>, 300 K):**  $\delta = 171.8, 166.0, 164.2, 149.2, 143.6, 138.4$  (2x), 138.3, 132.6, 130.7, 130.6, 129.4, 128.1, 127.6, 127.1, 126.8, 123.1, 97.4, 53.7, 41.3, 36.9, 34.3, 33.3, 32.9, 32.7, 29.3, 26.2, 25.9, 25.8 ppm.
- **MS (ESI pos.):**  $m/z$  (%) = 641.34 (29) ([M+H]<sup>+</sup>, calcd. 641.30), 486.23 (10) ([M<sub>fr.(1)}</sub>]<sup>+</sup>, calcd. 486.25), 190.35 (100) ([M<sub>fr.(1)}</sub>+Na]<sup>+</sup>, calcd. 190.13).
- **HRMS (FTMS + p MALDI):**  $m/z = 663.2821$  [M+Na]<sup>+</sup>, calcd. for [C<sub>36</sub>H<sub>41</sub>ClN<sub>6</sub>NaO<sub>3</sub>]<sup>+</sup> = 663.2821.

**(S)-5-Amino-N-(4-((1-(4-chlorophenyl)piperazin-1-yl)-4-cyclohexyl-1-oxobutan-2-yl)carbamoyl)benzyl)-1-phenyl-1H-pyrazole-4-carboxamide (247, SR108)**

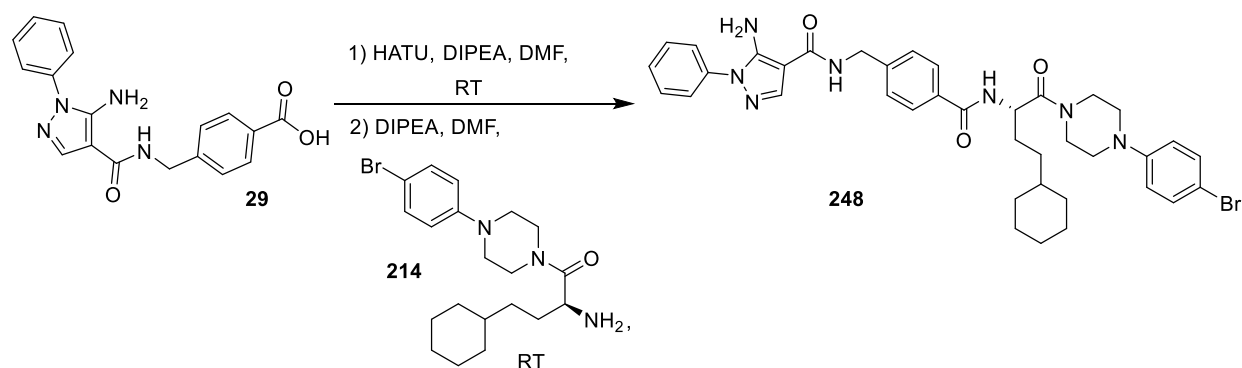


4-((5-Amino-1-phenyl-1H-pyrazole-4-carboxamido)methyl)benzoic acid (**29**, 200 mg, 0.595 mmol) and HATU (280 mg, 0.736 mmol) were dissolved in DMF (5 mL) and DIPEA (115 mg, 0.893 mmol) was added. The solution was stirred for 1.5 h at RT and (S)-2-amino-1-(4-(4-chlorophenyl)piperazin-1-yl)-4-cyclohexylbutan-1-one (**213**, 279 mg, 0.768 mmol), diluted in DMF (5 mL), was added. The mixture was stirred for 5 d at RT. DCM (50 mL) was added and the organic phase was washed 4 times with H<sub>2</sub>O (20 mL) and dried over MgSO<sub>4</sub>. The solvent was evaporated under reduced pressure and the crude product was purified using column chromatography on silica (cyclohexane/EtOAc 1:10 → 1:20 → EtOAc).

**Yield:** 99 mg (0.15 mmol, 24%), yellowish solid.

- **TLC:** R<sub>f</sub> = 0.45 (SiO<sub>2</sub>, cyclohexane/EtOAc 1:20).
- **C<sub>38</sub>H<sub>44</sub>ClN<sub>7</sub>O<sub>3</sub>:** (682.25), [682.25].
- **HPLC:** t<sub>R</sub> = 17.40 min.
- **<sup>1</sup>H-NMR (600 MHz, DMSO-d<sub>6</sub>, 300 K):** δ = 8.55 (d, <sup>3</sup>J = 8.1 Hz, 1H, NHCHCO), 8.49 (t, <sup>3</sup>J = 5.8 Hz, 1H, NHCH<sub>2</sub>C<sub>Ar</sub>), 7.98 (s, 1H, pyrazole), 7.86 (d, <sup>3</sup>J = 8.1 Hz, 2H, H-3-, H-5-benzyl), 7.57 (d, <sup>3</sup>J = 7.9 Hz, 2H, H-2-, H-6-phenyl), 7.53 (t, <sup>3</sup>J = 7.6 Hz, 2H, H-3-, H-5-phenyl), 7.41–7.35 (m, 3H, H-4 phenyl, H-2-, H-6-benzyl), 7.23 (d, <sup>3</sup>J = 8.8 Hz, 2H, H-3-, H-5-Cl-phenyl), 6.95 (d, <sup>3</sup>J = 8.4 Hz, 2H, H-2-, H-6-Cl-phenyl), 6.37 (br s, 2H, NH<sub>2</sub>), 4.92–4.85 (m, 1H, NHCHCO), 4.47 (d, <sup>3</sup>J = 5.8 Hz, 2H, CH<sub>2</sub> benzyl), 3.77–3.54 (m, 4H, CH<sub>2</sub>-2-, CH<sub>2</sub>-6-piperazine), 3.23–3.02 (m, 4H, CH<sub>2</sub>-3-, CH<sub>2</sub>-5-piperazine), 1.80–1.55 (m, 7H, NHCHCH<sub>2</sub>CH<sub>2</sub>, H-2<sub>eq</sub>-, H-3<sub>eq</sub>-, H-4<sub>eq</sub>-, H-5<sub>eq</sub>-, H-6<sub>eq</sub>-cyclohexyl), 1.29–1.04 (m, 6H, H-1-, H-3<sub>ax</sub>-, H-4<sub>ax</sub>-, H-5<sub>ax</sub>-cyclohexyl, NHCHCH<sub>2</sub>CH<sub>2</sub>), 0.90–0.79 (m, 2H, H-2<sub>ax</sub>-, H-6<sub>ax</sub>-cyclohexyl) ppm.
- **<sup>13</sup>C-NMR (150 MHz, DMSO-d<sub>6</sub>, 300 K):** δ = 170.0, 165.8, 164.1, 149.5, 149.2, 143.6, 138.3, 138.2, 132.4, 129.3, 128.6, 127.5, 127.0, 126.8, 123.1, 122.8, 117.2, 97.4, 49.3, 48.5, 48.0, 44.6, 41.3, 36.9, 33.1, 32.8, 32.7, 28.8, 26.3, 26.1, 25.7 (2x) ppm.
- **MS (ESI pos.):** m/z (%) = 682.40 (93) ([M+H]<sup>+</sup>, calcd. 682.33), 486.28 (41) ([M<sub>fr.(I)}</sub>]<sup>+</sup>, calcd. 486.25), 392.26 (31) ([M<sub>fr.(II)}</sub>+Na]<sup>+</sup>, calcd. 392.23), 324.26 (100) ([M<sub>fr.(III)}</sub>+Na]<sup>+</sup>, calcd. 324.18).
- **HRMS (FTMS + p MALDI):** m/z = 704.3092 [M+Na]<sup>+</sup>, calcd. for [C<sub>38</sub>H<sub>44</sub>ClN<sub>7</sub>NaO<sub>3</sub>]<sup>+</sup> = 704.3092.

**(S)-5-Amino-N-(4-((1-(4-(4-bromophenyl)piperazin-1-yl)-4-cyclohexyl-1-oxobutan-2-yl)carbamoyl)benzyl)-1-phenyl-1H-pyrazole-4-carboxamide (248, SR111)**

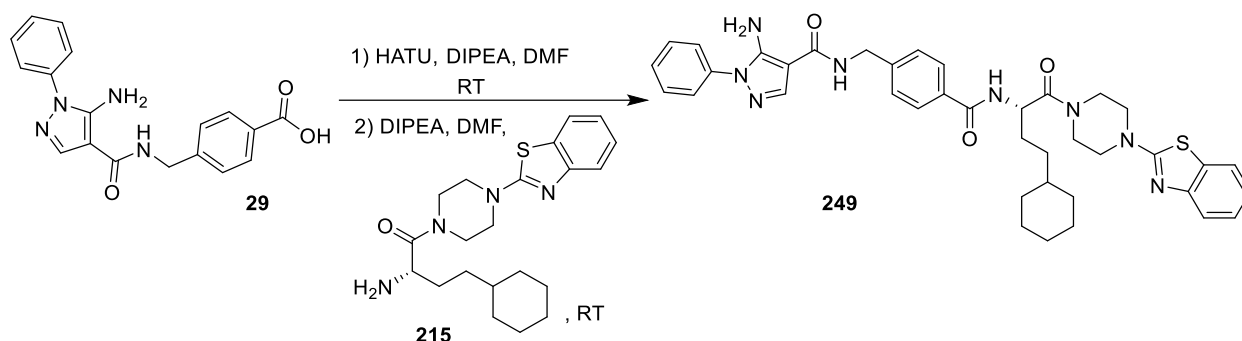


4-((5-Amino-1-phenyl-1H-pyrazole-4-carboxamido)methyl)benzoic acid (**29**, 200 mg, 0.595 mmol) and HATU (280 mg, 0.736 mmol) were dissolved in DMF (5 mL) and DIPEA (115 mg, 0.893 mmol) was added. The solution was stirred for 1.5 h at RT and (S)-2-amino-1-(4-(4-bromophenyl)piperazin-1-yl)-4-cyclohexylbutan-1-one (**214**, 290 mg, 0.714 mmol), diluted in DMF (5 mL) and DIPEA (115 mg, 0.893 mmol), was added. The mixture was stirred for 20 h at RT. DCM (50 mL) was added and the organic phase was washed 5 times with H<sub>2</sub>O (20 mL) and dried over MgSO<sub>4</sub>. The solvent was evaporated under reduced pressure and the crude product was purified using column chromatography on silica (cyclohexane/EtOAc 10:1 → 1-3 → 1:20 → EtOAc).

**Yield:** 277 mg (0.381 mmol, 64%), colorless solid.

- **TLC:**  $R_f = 0.48$  (SiO<sub>2</sub>, cyclohexane/EtOAc 1:20).
- **C<sub>38</sub>H<sub>44</sub>BrN<sub>7</sub>O<sub>3</sub>:** (726.71), [725.27].
- **HPLC:**  $t_R = 17.58$  min.
- **<sup>1</sup>H-NMR (500 MHz, DMSO-d<sub>6</sub>, 300 K):**  $\delta = 8.57$  (d,  $^3J = 8.0$  Hz, 1H, NHCHCO), 8.51 (t,  $^3J = 6.0$  Hz, 1H, NHCH<sub>2</sub>C<sub>Ar</sub>), 7.99 (s, 1H, pyrazole), 7.86 (d,  $^3J = 8.3$  Hz, 2H, H-3-, H-5-benzyl), 7.61–7.48 (m, 4H, H-2-, H-3-, H-5-, H-6-phenyl), 7.43–7.31 (m, 5H, H-4 phenyl, H-2-, H-6-benzyl, H-3-, H-5-Br-phenyl), 6.90 (d,  $^3J = 9.1$  Hz, 2H, H-2-, H-6-Br-phenyl), 6.39 (br s, 2H, NH<sub>2</sub>), 4.92–4.85 (m, 1H, NHCHCO), 4.47 (d,  $^3J = 5.9$  Hz, 2H, CH<sub>2</sub> benzyl), 3.76–3.51 (m, 4H, CH<sub>2</sub>-2-, CH<sub>2</sub>-6-piperazine), 3.24–3.01 (m, 4H, CH<sub>2</sub>-3-, CH<sub>2</sub>-5-piperazine), 1.81–1.54 (m, 7H, NHCHCH<sub>2</sub>CH<sub>2</sub>, H-2<sub>eq</sub>-, H-3<sub>eq</sub>-, H-4<sub>eq</sub>-, H-5<sub>eq</sub>-, H-6<sub>eq</sub>-cyclohexyl), 1.29–1.03 (m, 6H, H-1-, H-3<sub>ax</sub>-, H-4<sub>ax</sub>-, H-5<sub>ax</sub>-cyclohexyl, NHCHCH<sub>2</sub>CH<sub>2</sub>), 0.91–0.78 (m, 2H, H-2<sub>ax</sub>-, H-6<sub>ax</sub>-cyclohexyl) ppm.
- **<sup>13</sup>C-NMR (126 MHz, DMSO-d<sub>6</sub>, 300 K):**  $\delta = 170.0, 165.9, 164.2, 149.9, 149.2, 143.7, 138.4, 138.2, 132.4, 131.6, 129.4, 127.6, 127.1, 126.8, 123.1, 117.7, 110.5, 97.4, 49.4, 48.4, 47.9, 44.6, 41.3, 37.0, 33.2, 32.9, 32.7, 28.9, 26.2, 25.8$  (2x) ppm.
- **MS (ESI pos.):**  $m/z$  (%) = 728.43 (91) ([M+H]<sup>+</sup>, calcd. 728.28), 486.33 (84) ([M<sub>fr.(I)}</sub>]<sup>+</sup>, calcd. 486.25), 241.24 (100) ([M<sub>fr.(II)}</sub>+2H]<sup>+</sup>, calcd. 241.04), 267.14 (73) ([M<sub>fr.(III)}</sub>]<sup>+</sup>, calcd. 267.01), 458.37 (19) ([M<sub>fr.(IV)}</sub>]<sup>+</sup>, calcd. 458.37).
- **HRMS (FTMS + p MALDI):**  $m/z = 750.2548$  [M+Na]<sup>+</sup>, calcd. for [C<sub>38</sub>H<sub>44</sub>BrN<sub>7</sub>NaO<sub>3</sub>]<sup>+</sup> = 750.2566, 766.2304 [M+K]<sup>+</sup>, calcd. for [C<sub>38</sub>H<sub>44</sub>BrN<sub>7</sub>KO<sub>3</sub>]<sup>+</sup> = 766.2306.

**(S)-5-Amino-N-(4-((1-(4-(benzo[d]thiazol-2-yl)piperazin-1-yl)-4-cyclohexyl-1-oxobutan-2-yl)carbamoyl)benzyl)-1-phenyl-1H-pyrazole-4-carboxamide (249, SR126)**

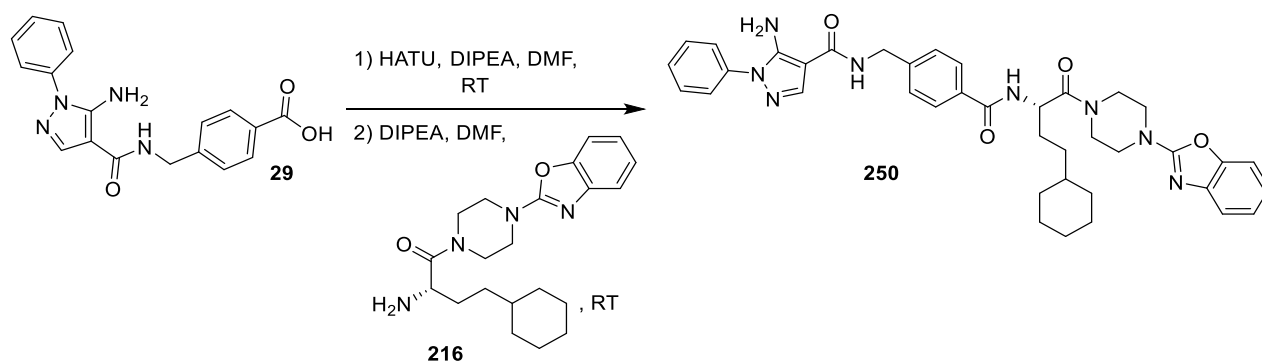


4-((5-Amino-1-phenyl-1H-pyrazole-4-carboxamido)methyl)benzoic acid (**29**, 200 mg, 0.595 mmol) and HATU (280 mg, 0.736 mmol) were dissolved in DMF (5 mL) and DIPEA (115 mg, 0.893 mmol) was added. The solution was stirred for 2 h at RT and (S)-2-amino-1-(4-(benzo[d]thiazol-2-yl)piperazin-1-yl)-4-cyclohexylbutan-1-one (**215**, 276 mg, 0.714 mmol), diluted in DMF (5 mL) and DIPEA (115 mg, 0.893 mmol), was added. The mixture was stirred for 3 h at RT. DCM (50 mL) was added and the organic phase was washed 5 times with H<sub>2</sub>O (20 mL) and dried over MgSO<sub>4</sub>. The solvent was evaporated under reduced pressure and the crude product was purified using flashcolumn chromatography on silica (cyclohexane/EtOAc 1:1 → 1:20).

**Yield:** 315 mg (0.447 mmol, 75%), colorless solid.

- **TLC:** R<sub>f</sub> = 0.48 (cyclohexane/EtOAc 1:20).
- **C<sub>39</sub>H<sub>44</sub>N<sub>8</sub>O<sub>3</sub>S:** (704.88), [704.33].
- **HPLC:** t<sub>R</sub> = 16.64 min.
- **<sup>1</sup>H-NMR (400 MHz, DMSO-d<sub>6</sub>, 300 K):** δ = 8.58 (d, <sup>3</sup>J = 8.0 Hz, 1H, NHCHCO), 8.50 (t, <sup>3</sup>J = 6.0 Hz, 1H, NHCH<sub>2</sub>), 7.98 (s, 1H, pyrazole), 7.87 (d, <sup>3</sup>J = 8.3 Hz, 2H, H-3-, H-5-benzyl), 7.77 (d, <sup>3</sup>J = 7.9 Hz, 1H, H-7 benzothiazole), 7.60–7.44 (m, 5H, H-2-, H-3-, H-5-, H-6-phenyl, H-4 benzothiazole), 7.42–7.33 (m, 3H, H-4 phenyl, H-2-, H-6-benzyl), 7.28 (t, <sup>3</sup>J = 7.8 Hz, 1H, H-6 benzothiazole), 7.08 (t, <sup>3</sup>J = 7.8 Hz, 1H, H-5 benzothiazole), 6.37 (br s, 2H, NH<sub>2</sub>), 4.95–4.85 (m, 1H, NHCHCO), 4.47 (d, <sup>3</sup>J = 5.9 Hz, 2H, CH<sub>2</sub> benzyl), 3.86–3.44 (m, 8H, piperazine), 1.83–1.53 (m, 7H, NHCHCH<sub>2</sub>CH<sub>2</sub>, H-2<sub>eq</sub>-, H-3<sub>eq</sub>-, H-4<sub>eq</sub>-, H-5<sub>eq</sub>-, H-6<sub>eq</sub>-cyclohexyl), 1.30–1.02 (m, 6H, H-1-, H-3<sub>ax</sub>-, H-4<sub>ax</sub>-, H-5<sub>ax</sub>-cyclohexyl, NHCHCH<sub>2</sub>CH<sub>2</sub>), 0.92–0.77 (m, 2H, H-2<sub>ax</sub>-, H-6<sub>ax</sub>-cyclohexyl) ppm.
- **<sup>13</sup>C-NMR (101 MHz, DMSO-d<sub>6</sub>, 300 K):** δ = 170.3, 168.1, 165.9, 164.1, 152.3, 149.2, 143.7, 138.4, 138.2, 132.4, 130.4, 129.4, 127.6, 127.1, 126.8, 123.1, 121.4, 121.2, 118.7, 97.4, 49.5, 48.1, 47.7, 44.6, 44.3, 41.3, 37.0, 33.1, 32.9, 32.7, 28.8, 26.1, 25.8 (2x) ppm.
- **MS (MALDI pos.):** m/z (%) = 704.35 (100) ([M]<sup>+</sup>, calcd. 704.33), 705.36 (39) ([M]<sup>+</sup>, calcd. 705.33), 726.32 (22) ([M+Na-H]<sup>+</sup>, calcd. 726.31), 727.32 (14) ([M+Na-H]<sup>+</sup>, calcd. 727.31).
- **HRMS (FTMS + p MALDI):** m/z = 705.3327 [M+H]<sup>+</sup>, calcd. for [C<sub>39</sub>H<sub>48</sub>N<sub>8</sub>O<sub>3</sub>S]<sup>+</sup> = 705.3330.

**(S)-5-Amino-N-(4-((1-(4-(benzo[d]oxazol-2-yl)piperazin-1-yl)-4-cyclohexyl-1-oxobutan-2-yl)carbamoyl)benzyl)-1-phenyl-1H-pyrazole-4-carboxamide (250, SR127)**



4-((5-Amino-1-phenyl-1H-pyrazole-4-carboxamido)methyl)benzoic acid (**29**, 200 mg, 0.595 mmol) and HATU (280 mg, 0.736 mmol) were dissolved in DMF (5 mL) and DIPEA (115 mg, 0.893 mmol) was added. The solution was stirred for 1.5 h at RT and (S)-2-amino-1-(4-(benzo[d]oxazol-2-yl)piperazin-1-yl)-4-cyclohexylbutan-1-one (**216**, 265 mg, 0.714 mmol), diluted in DMF (5 mL) and DIPEA (115 mg, 0.893 mmol), was added. The mixture was stirred for 3 h at RT. DCM (50 mL) was added and the organic phase was washed 5 times with H<sub>2</sub>O (20 mL) and dried over MgSO<sub>4</sub>. The solvent was evaporated under reduced pressure and the crude product was purified by flashcolumn chromatography on silica (cyclohexane/EtOAc 1:1 → 1:20).

**Yield:** 247 mg (0.359 mmol, 60%), yellowish solid.

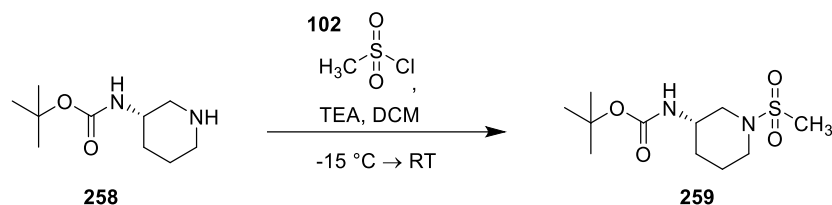
- **TLC:**  $R_f = 0.38$  (cyclohexane/EtOAc 1:20).
- **C<sub>39</sub>H<sub>44</sub>N<sub>8</sub>O<sub>4</sub>:** (688.82), [688.35].
- **HPLC:**  $t_R = 16.08$  min.
- **<sup>1</sup>H-NMR (400 MHz, DMSO-d<sub>6</sub>, 300 K):**  $\delta = 8.58$  (d,  $^3J = 7.9$  Hz, 1H, NHCHCO), 8.50 (t,  $^3J = 6.0$  Hz, 1H, NHCH<sub>2</sub>), 7.98 (s, 1H, pyrazole), 7.87 (d,  $^3J = 8.3$  Hz, 2H, H-3-, H-5-benzyl), 7.60–7.48 (m, 4H, H-2-, H-3-, H-5-, H-6-phenyl), 7.44–7.35 (m, 4H, H-4 phenyl, H-2-, H-6-benzyl, H-7 benzoxazole), 7.30 (d,  $^3J = 7.7$  Hz, 1H, H-4 benzoxazole), 7.16 (t,  $^3J = 7.7$  Hz, 1H, H-6 benzoxazole), 7.03 (t,  $^3J = 7.7$  Hz, 1H, H-5 benzoxazole), 6.37 (br s, 2H, NH<sub>2</sub>), 4.95–4.85 (m, 1H, NHCHCO), 4.47 (d,  $^3J = 5.9$  Hz, 2H, CH<sub>2</sub> benzyl), 3.86–3.49 (m, 8H, piperazine), 1.82–1.53 (m, 7H, NHCHCH<sub>2</sub>CH<sub>2</sub>, H-2<sub>eq</sub>-, H-3<sub>eq</sub>-, H-4<sub>eq</sub>-, H-5<sub>eq</sub>-, H-6<sub>eq</sub>-cyclohexyl), 1.32–1.02 (m, 6H, H-1-, H-3<sub>ax</sub>-, H-4<sub>ax</sub>-, H-5<sub>ax</sub>-cyclohexyl, NHCHCH<sub>2</sub>CH<sub>2</sub>), 0.95–0.77 (m, 2H, H-2<sub>ax</sub>-, H-6<sub>ax</sub>-cyclohexyl) ppm.
- **<sup>13</sup>C-NMR (101 MHz, DMSO-d<sub>6</sub>, 300 K):**  $\delta = 170.3, 165.9, 164.1, 161.6, 149.2, 148.4, 143.7, 142.8, 138.4, 138.2, 132.4, 129.4, 127.6, 127.1, 126.8, 124.0, 123.1, 120.7, 116.0, 109.0, 97.4, 49.5, 44.3, 41.3, 37.0, 33.1, 32.9, 32.7, 28.8, 26.2, 25.8$  (2x) ppm.
- **MS (MALDI pos.):**  $m/z$  (%) = 688.63 (100) ([M]<sup>+</sup>, calcd. 688.35), 689.64 (51) ([M]<sup>+</sup>, calcd. 689.35), 710.58 (8) ([M+Na-H]<sup>+</sup>, calcd. 726.31), 712.58 (6) ([M+Na-H]<sup>+</sup>, calcd. 712.58).
- **HRMS (FTMS + p MALDI):**  $m/z = 689.3544$  [M+H]<sup>+</sup>, calcd. for [C<sub>39</sub>H<sub>45</sub>N<sub>8</sub>O<sub>4</sub>]<sup>+</sup> = 689.3558.



## 8.5 Experimental part of Chapter 5

### 8.5.1 Synthesis of intermediates

#### *tert*-Butyl (*S*)-(1-(methanesulfonyl)piperidin-3-yl)carbamate (**259**, SR228)

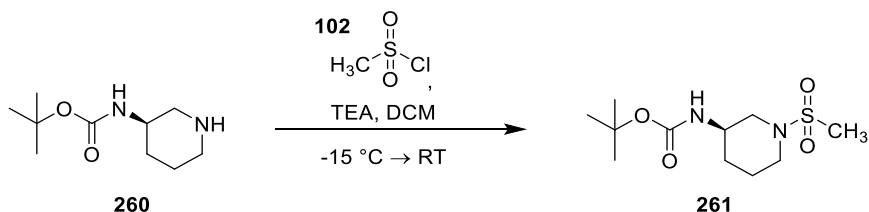


*tert*-Butyl (*S*)-piperidin-3-ylcarbamate (**258**, 801 mg, 4.00 mmol) was dissolved in DCM (dry, 20 mL) and TEA (405 mg, 4.00 mmol) was added. The solution was cooled to  $-15\text{ }^\circ\text{C}$  and methanesulfonyl chloride (**102**, 687 mg, 6.00 mmol) was added dropwise. The mixture was stirred for 20 h at RT. The reaction mixture was acidified with  $\text{NH}_4\text{Cl}$  (sat., 3 mL) and extracted 3 times with DCM. The organic phase was separated and washed 2 times with  $\text{H}_2\text{O}$  (20 mL) and dried over  $\text{MgSO}_4$ . The solvent was evaporated under reduced pressure to obtain a colorless solid.

**Yield:** 1.03 g (3.71 mmol, 93%), colorless solid.

- **TLC:**  $R_f = 0.63$  ( $\text{SiO}_2$ , cyclohexane/EtOAc, 1:20, ninhydrin).
- **$\text{C}_{11}\text{H}_{22}\text{N}_2\text{O}_4\text{S}$ :** (278.37), [278.13].
- **$^1\text{H-NMR}$  (250 MHz,  $\text{CDCl}_3$ , 300 K):**  $\delta = 6.95$  (d,  $^3J = 7.5$  Hz, 1H, NH), 3.58–3.46 (m, 1H, CH piperidine) 3.40–3.01 (m, 2H,  $\text{CH}_2$ -2 piperidine), 2.85 (s, 3H,  $\text{SO}_2\text{CH}_3$ ), 2.71–2.57 (m, 1H,  $\text{CH}_A\text{H}_B$ -6 piperidine), 2.47–2.35 (m, 1H,  $\text{CH}_A\text{H}_B$ -6 piperidine), 1.84–1.67 (m, 2H,  $\text{CH}_2$ -4 piperidine), (s, 9H,  $\text{C}(\text{CH}_3)_3$ ), 1.59–1.11 (m, 2H,  $\text{CH}_2$ -5 piperidine) ppm.
- **$^{13}\text{C-NMR}$  (126 MHz,  $\text{CDCl}_3$ , 300 K):**  $\delta = 155.0, 79.8, 50.8, 46.3, 45.6, 35.2, 29.2, 28.5, 22.1$  ppm.
- **MS (ESI neg.):**  $m/z$  (%) = 323.15 (100) ( $[\text{M}+\text{EtOH}-\text{H}]^-$ , calcd. 323.16), 313.13 (39) ( $[\text{M}+\text{Cl}]^-$ , calcd. 313.58).

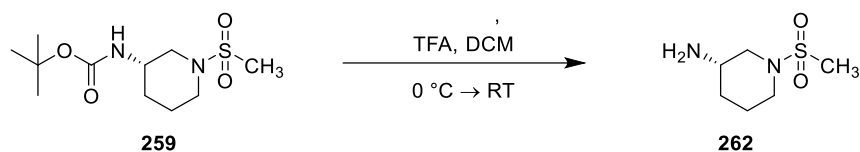
#### *tert*-Butyl (*R*)-(1-(methanesulfonyl)piperidin-3-yl)carbamate (**261**, SR229)



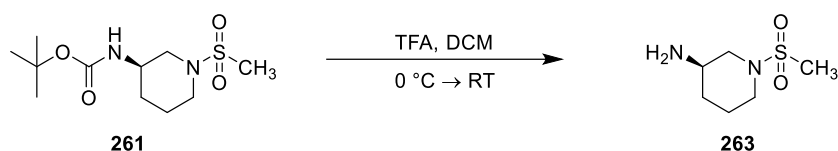
The synthesis of *tert*-butyl (*R*)-(1-(methanesulfonyl)piperidin-3-yl)carbamate (**261**) was performed analogously to compound **259**. The starting material was *tert*-butyl (*R*)-piperidin-3-ylcarbamate (**260**, 801 mg, 4.00 mmol).

**Yield:** 915 mg (3.29 mmol, 97%), light brownish solid.

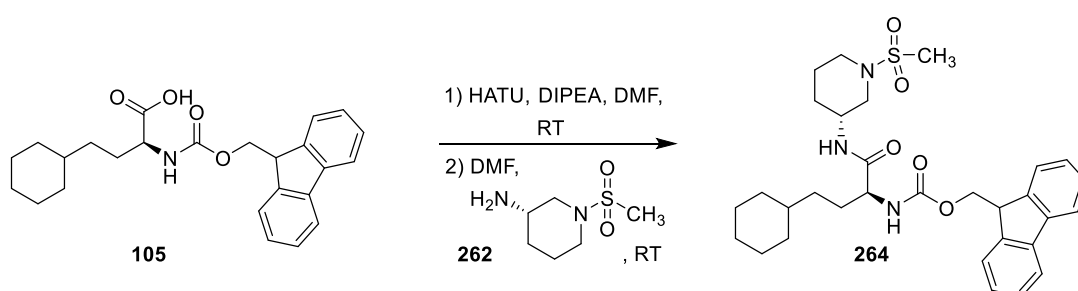
The analytical data are in accordance with compound **259**.

**(S)-1-(Methylsulfonyl)piperidin-3-amine (262, SR234)**

*tert*-Butyl (*S*)-1-(methylsulfonyl)piperidin-3-ylcarbamate (**259**, 420 mg, 1.51 mmol) was dissolved in DCM (dry, 10 mL), cooled to 0 °C and TFA (2 mL) was added dropwise. The mixture was stirred for 2 h and thereby warmed to RT. The solvent was removed in vacuo and the residue was dissolved in 20 mL MeOH. The mixture was then cooled to 5 °C, K<sub>2</sub>CO<sub>3</sub> (3.58 g, 26.0 mmol) was added and stirred for additional 10 min. The solid was filtered off and the solvent was removed under reduced pressure. The crude product was obtained in quantitative yield and used without further purification in the next step.

**(R)-1-(Methylsulfonyl)piperidin-3-amine (263, SR235)**

The synthesis of (*R*)-1-(methylsulfonyl)piperidin-3-amine (**263**) was performed analogously to compound **262**. The starting material was *tert*-butyl (*R*)-1-(methylsulfonyl)piperidin-3-ylcarbamate (**261**, 420 mg, 1.51 mmol). The crude product was obtained in quantitative yield and used without further purification in the next step.

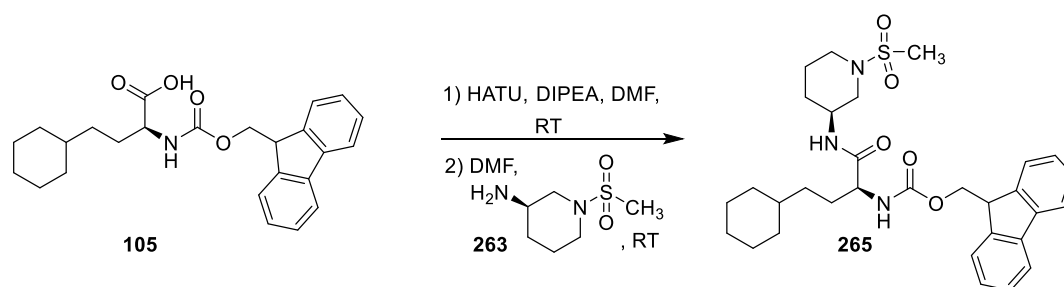
**(9*H*-Fluoren-9-yl)methyl ((S)-4-cyclohexyl-1-(((R)-1-(methylsulfonyl)piperidin-3-yl)amino)-1-oxobutan-2-yl)carbamate (264, SR236)**

(*S*)-2-(((9*H*-Fluoren-9-yl)methoxy)carbonyl)amino)-4-cyclohexylbutanoic acid (**105**, 500 mg, 1.23 mmol) and HATU (560 mg, 1.47 mmol) were dissolved in DMF (dry, 10 mL) and DIPEA (190 mg, 1.47 mmol) was added. The reaction mixture was stirred for 1.5 h at RT and (*S*)-1-(methylsulfonyl)piperidin-3-amine (**262**, 262 mg, 1.47 mmol) dissolved in DMF (dry, 3 mL) was added. The mixture was stirred for additional 20 h at RT. H<sub>2</sub>O (50 mL) was added and the resulting precipitate was filtered off, washed with H<sub>2</sub>O and dried in a vacuum oven.

**Yield:** 663 mg (1.17 mmol, 95%), colorless solid.

- **TLC:**  $R_f = 0.76$  ( $\text{SiO}_2$ , EtOAc/MeOH, 9:1).
- **$\text{C}_{31}\text{H}_{41}\text{N}_3\text{O}_5\text{S}$ :** (567.74), [567.28].
- **$^1\text{H-NMR}$  (500 MHz, DMSO- $d_6$ , 300 K):**  $\delta = 7.91\text{--}7.78$  (m, 4H, H-1-, H-4-, H-5-, H-8-Fmoc), 7.76–7.70 (m, 2H, H-1-, H-8-Fmoc), 7.46–7.59 (m, 1H, NHCOO), 7.41 (td,  $^3J = 7.4, 1.2$  Hz, 2H, H-3-, H-6-Fmoc), 7.34 (td,  $^3J = 7.4, 1.2$  Hz, 2H, H-2-, H-7-Fmoc), 6.66 (d,  $^3J = 8.5$  Hz, 1H, CONHCH), 4.32–4.18 (m, 3H, NHCHCO, OCH<sub>2</sub>), 3.92–3.84 (m, 1H, H-9 Fmoc), 3.78–3.66 (m, 1H, CH piperidine), 3.56–3.22 (m, 2H, CH<sub>2</sub>-2 piperidine), 2.84 (s, 3H, CH<sub>3</sub>), 2.85–2.74 (m, 1H, CH<sub>A</sub>H<sub>B</sub>-6 piperidine), 2.67–2.49 (m, 1H, CH<sub>A</sub>H<sub>B</sub>-6 piperidine), 1.86–1.31 (m, 11H, CH<sub>2</sub>-4-, CH<sub>2</sub>-5-piperidine, NHCHCH<sub>2</sub>CH<sub>2</sub>, H-2<sub>eq</sub>-, H-3<sub>eq</sub>-, H-4<sub>eq</sub>-, H-5<sub>eq</sub>-, H-6<sub>eq</sub>-cyclohexyl), 1.28–1.04 (m, 6H, H-1-, H-3<sub>ax</sub>-, H-4<sub>ax</sub>-, H-5<sub>ax</sub>-cyclohexyl, NHCHCH<sub>2</sub>CH<sub>2</sub>), 0.90–0.74 (m, 2H, H-2<sub>ax</sub>-, H-6<sub>ax</sub>-cyclohexyl) ppm.
- **$^{13}\text{C-NMR}$  (126 MHz, DMSO- $d_6$ , 300 K):**  $\delta = 174.6, 172.1, 156.8$  (2x), 143.9, 143.8, 140.7 (2x), 128.9, 127.7, 127.3, 123.9, 121.4, 120.0, 61.8, 54.6, 54.5, 49.5, 49.4, 45.4 (2x), 45.0, 44.6, 37.0, 36.8, 34.3, 34.2, 32.9 (2x), 32.8, 32.7, 32.6, 32.4, 29.8, 28.9, 28.7, 26.2 (2x), 25.7, 22.9, 22.7 ppm.
- **MS (ESI pos.):**  $m/z$  (%) = 590.34 (100) ( $[\text{M}+\text{Na}]^+$ , calcd. 590.27).

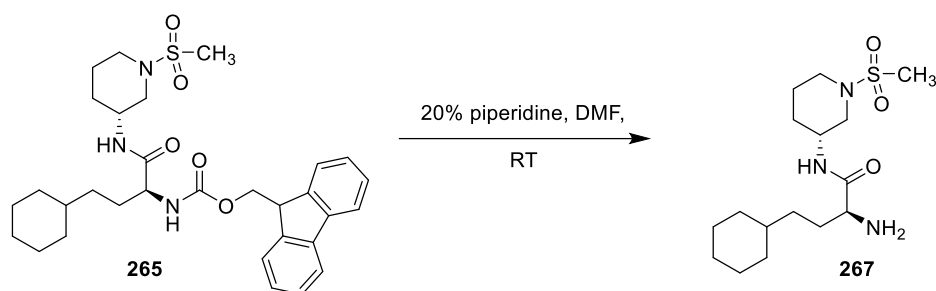
**(9H-Fluoren-9-yl)methyl ((S)-4-cyclohexyl-1-(((S)-1-(methylsulfonyl)piperidin-3-yl)amino)-1-oxobutan-2-yl)carbamate (265, SR237)**



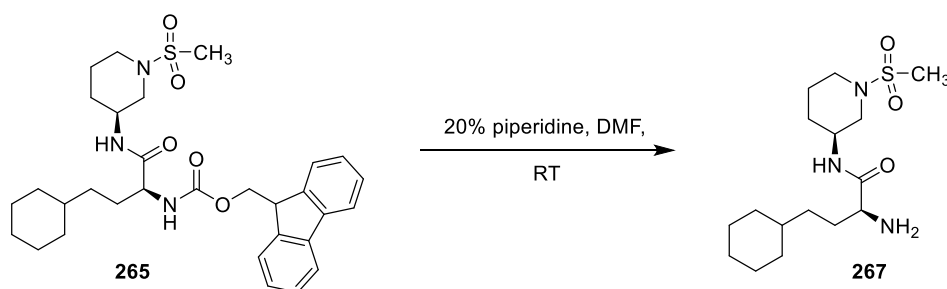
The synthesis of (9H-Fluoren-9-yl)methyl ((S)-4-cyclohexyl-1-(((S)-1-(methylsulfonyl)piperidin-3-yl)amino)-1-oxobutan-2-yl)carbamate (**265**) was performed analogously to compound **264**. The starting material was (S)-1-(methylsulfonyl)piperidin-3-amine (**263**, 262 mg, 1.47 mmol).

**Yield:** 655 mg (1.15 mmol, 94%), light brownish solid.

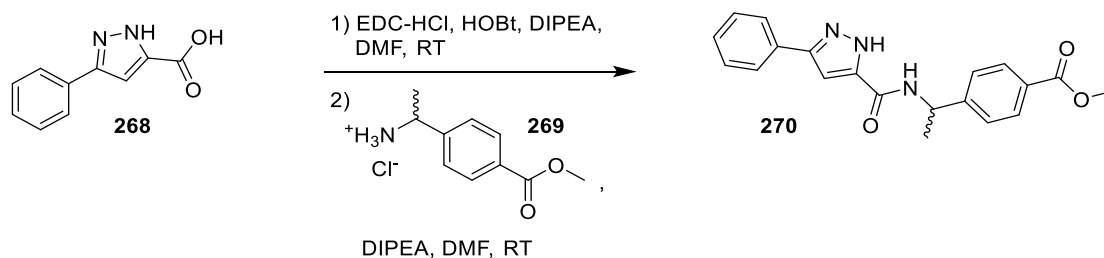
- **TLC:**  $R_f = 0.76$  ( $\text{SiO}_2$ , EtOAc/MeOH, 9:1).
- **$\text{C}_{31}\text{H}_{41}\text{N}_3\text{O}_5\text{S}$ :** (567.74), [567.28].
- **$^1\text{H-NMR}$  (500 MHz, DMSO- $d_6$ , 300 K):**  $\delta = 7.92\text{--}7.73$  (m, 4H, H-1-, H-4-, H-5-, H-8-Fmoc), 7.46–7.59 (m, 1H, NHCOO), 7.42–7.31 (m, 4H, H-2-, H-3-, H-6-, H-7-Fmoc), 6.65 (d,  $^3J = 8.5$  Hz, 1H, CONHCH), 4.33–4.22 (m, 3H, NHCHCO, OCH<sub>2</sub>), 3.89–3.82 (m, 1H, H-9 Fmoc), 3.78–3.66 (m, 1H, CH piperidine), 3.53–3.25 (m, 2H, CH<sub>2</sub>-2 piperidine), 2.85 (s, 3H, CH<sub>3</sub>), 2.89–2.71 (m, 1H, CH<sub>A</sub>H<sub>B</sub>-6 piperidine), 2.64–2.47 (m, 1H, CH<sub>A</sub>H<sub>B</sub>-6 piperidine), 1.82–1.69 (m, 2H, CH<sub>2</sub>-5 piperidine), 1.68–1.28 (m, 9H, CH<sub>2</sub>-4 piperidine, NHCHCH<sub>2</sub>CH<sub>2</sub>, H-2<sub>eq</sub>-, H-3<sub>eq</sub>-, H-4<sub>eq</sub>-, H-5<sub>eq</sub>-, H-6<sub>eq</sub>-cyclohexyl), 1.26–1.02 (m, 6H, H-1-, H-3<sub>ax</sub>-, H-4<sub>ax</sub>-, H-5<sub>ax</sub>-cyclohexyl, NHCHCH<sub>2</sub>CH<sub>2</sub>), 0.90–0.74 (m, 2H, H-2<sub>ax</sub>-, H-6<sub>ax</sub>-cyclohexyl) ppm.
- **$^{13}\text{C-NMR}$  (126 MHz, DMSO- $d_6$ , 300 K):**  $\delta = 174.6, 172.1, 156.8, 143.9, 140.6, 140.4, 128.9, 127.7, 127.3, 123.9, 121.4, 120.0, 61.8, 54.7$  (2x), 49.6, 49.5, 45.4, 45.3, 45.1, 44.6, 36.9, 36.8, 34.4, 34.3, 32.9 (2x), 32.8, 32.7 (2x), 32.3, 29.8, 28.9, 28.8, 26.1 (2x), 25.8, 23.0, 22.9 ppm.
- **MS (ESI pos.):**  $m/z$  (%) = 590.34 (100) ( $[\text{M}+\text{H}]^+$ , calcd. 590.27), 346.22 (38) ( $[\text{M-Fmoc}+\text{H}]^+$ , calcd. 346.22).

**(S)-2-Amino-4-cyclohexyl-N-((R)-1-(methylsulfonyl)piperidin-3-yl)butanamide (266)**

The synthesis of (S)-2-amino-4-cyclohexyl-N-((R)-1-(methylsulfonyl)piperidin-3-yl) (266) was performed according to the general procedure for Fmoc deprotections (Section 8.4.5). The starting material was (9H-fluoren-9-yl)methyl ((S)-4-cyclohexyl-1-(((R)-1-(methylsulfonyl)piperidin-3-yl)amino)-1-oxobutan-2-yl)carbamate (264, 835 mg, 1.47 mmol). The amine was freshly prepared prior to the synthesis of 294.

**(S)-2-Amino-4-cyclohexyl-N-((S)-1-(methylsulfonyl)piperidin-3-yl)butanamide (267)**

The synthesis of (S)-2-amino-4-cyclohexyl-N-((S)-1-(methylsulfonyl)piperidin-3-yl) (267) was performed according to the general procedure for Fmoc deprotections (Section 8.4.5). The starting material was (9H-fluoren-9-yl)methyl ((S)-4-cyclohexyl-1-(((S)-1-(methylsulfonyl)piperidin-3-yl)amino)-1-oxobutan-2-yl)carbamate (265, 406 mg, 0.716 mmol). The amine was freshly prepared prior to the synthesis of 295.

**Methyl 4-(1-(3-phenyl-1H-pyrazole-5-carboxamido)ethyl)benzoate (270, SR254)**

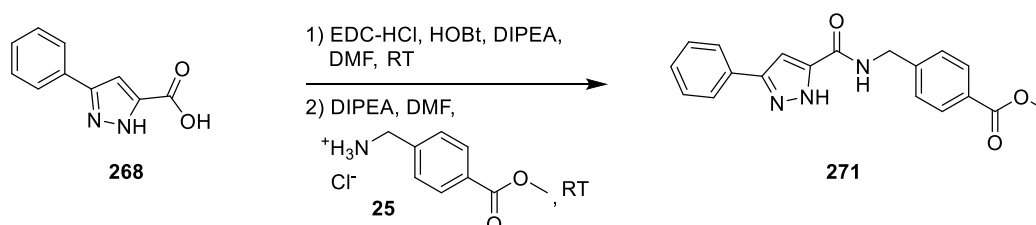
3-Phenyl-1H-pyrazole-5-carboxylic acid (268, 1.00 g, 5.314 mmol), HOBT (862 mg, 6.38 mmol) and EDC-HCl (1.22 g, 6.38 mmol) were dissolved in DMF (dry, 10 mL) and DIPEA (1.03 g, 7.97 mmol) was added. The mixture was stirred for 1.5 h at RT and a solution of methyl 4-(1-aminoethyl)benzoate hydrochloride (269, 1.38 g, 6.38 mmol) dissolved in DMF (dry, 10 mL) and DIPEA (1.03 g, 7.97 mmol) was added. The reaction mixture was stirred for additional 20 h at RT. DCM (100 mL) and H<sub>2</sub>O (200 mL) were added and the aqueous phase was extracted 2 times with DCM (50 mL). The organic phase was separated, dried over MgSO<sub>4</sub> and

the solvent was removed under reduced pressure. The crude product was purified using column chromatography on silica (cyclohexane/EtOAc 1:1 → 1:3).

**Yield:** 1.606 g (4.80 mmol, 90%), colorless solid.

- **TLC:**  $R_f = 0.29$  (SiO<sub>2</sub>, cyclohexane/EtOAc 1:1).
- **C<sub>20</sub>H<sub>19</sub>N<sub>3</sub>O<sub>3</sub>:** (349.38), [349.14].
- **<sup>1</sup>H-NMR (500 MHz, DMSO-d<sub>6</sub>, 300 K):**  $\delta = 7.94$  (d, <sup>3</sup> $J = 8.5$  Hz, 2H, H-3-, H-5-benzyl), 7.58 (d, <sup>3</sup> $J = 6.9$  Hz, 2H, H-2-, H-6-phenyl), 7.41 (d, <sup>3</sup> $J = 8.3$  Hz, 2H, H-2-, H-6-benzyl), 7.38–7.30 (m, 4H, H-3-, H-4-, H-5-phenyl), 7.06 (s, 1H, CH pyrazole), 5.35 (p, <sup>3</sup> $J = 7.4$  Hz, 1H, CHCH<sub>3</sub>), 3.88 (s, 3H, CO<sub>2</sub>CH<sub>3</sub>), 1.56 (d, <sup>3</sup> $J = 7.0$  Hz, 3H, CHCH<sub>3</sub>) ppm.
- **<sup>13</sup>C-NMR (126 MHz, DMSO-d<sub>6</sub>, 300 K):**  $\delta = 167.1, 161.4, 148.6, 146.2, 130.1, 129.2$  (2x), 128.9, 126.3, 126.2, 125.7, 103.4, 52.3, 48.7, 22.1 ppm.
- **MS (ESI neg.):**  $m/z$  (%) = 348.11 (100) ([M-H]<sup>-</sup>, calcd. 348.13), 697.20 (24) ([2M-H]<sup>-</sup>, calcd. 697.27).

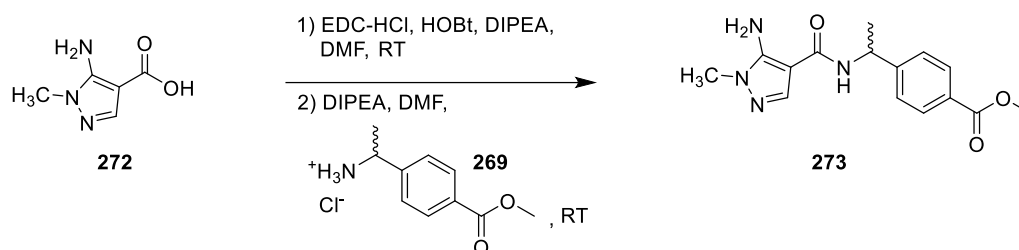
**Methyl 4-((3-phenyl-1H-pyrazole-5-carboxamido)methyl)benzoate (271, SR271)**



3-Phenyl-1H-pyrazole-5-carboxylic acid (**268**, 500 mg, 2.66 mmol), HOBT (431 mg, 3.19 mmol) and EDC-HCl (611 mg, 3.19 mmol) were dissolved in DMF (dry, 10 mL) and DIPEA (512 mg, 3.99 mmol) was added. The mixture was stirred for 1 h at RT and a solution of methyl 4-(aminomethyl)benzoate hydrochloride (**25**, 688 mg, 3.19 mmol) dissolved in DMF (dry, 15 mL) and DIPEA (512 mg, 3.99 mmol) was added. The reaction mixture was stirred for additional 20 h at RT. DCM (150 mL) was added and the organic phase was washed 4 times with H<sub>2</sub>O (150 mL). The organic phase was separated, dried over MgSO<sub>4</sub> and the solvent was removed under reduced pressure. The crude product was precipitated from cyclohexane.

**Yield:** 711 mg (2.12 mmol, 80%), colorless solid.

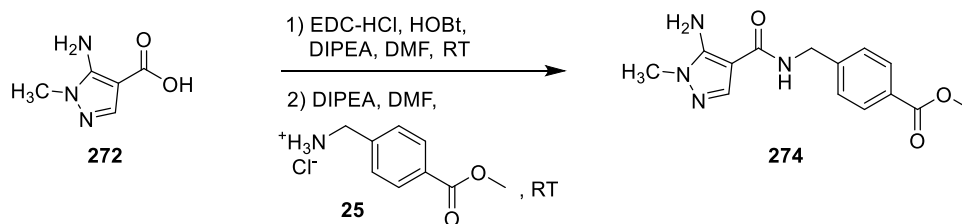
- **TLC:**  $R_f = 0.70$  (SiO<sub>2</sub>, cyclohexane/EtOAc 1:3).
- **C<sub>19</sub>H<sub>17</sub>N<sub>3</sub>O<sub>3</sub>:** (335.36), [335.13].
- **<sup>1</sup>H-NMR (600 MHz, DMSO-d<sub>6</sub>, 300 K):**  $\delta = 13.70$  (s, 1H, NH pyrazole), 9.22–8.73 (s, 1H, CONH), 7.93 (d, <sup>3</sup> $J = 8.1$  Hz, 2H, H-3-, H-5-benzyl), 7.80 (d, <sup>3</sup> $J = 7.3$  Hz, 2H, H-2-, H-6-benzyl), 7.51–7.42 (m, 4H, H-2-, H-3-, H-5-, H-6-phenyl), 7.39–7.32 (m, 1H, H-4 phenyl), 4.60–4.48 (m, 2H, CH<sub>2</sub>), 3.84 (s, 3H, CH<sub>3</sub>) ppm.
- **<sup>13</sup>C-NMR (150 MHz, DMSO-d<sub>6</sub>, 300 K):**  $\delta = 166.1, 161.8, 147.7, 145.4, 140.8, 129.2$  (2x), 128.9, 128.1, 127.3, 125.2, 102.5, 52.0, 41.8 ppm.
- **MS (ESI neg.):**  $m/z$  (%) = 334.07 (100) ([M-H]<sup>-</sup>, calcd. 334.12).

**Methyl 4-((1-(5-amino-1-methyl-1H-pyrazole-4-carboxamido)ethyl)benzoate (273, SR269)**

5-Amino-1-methyl-1H-pyrazole-4-carboxylic acid (**272**, 436 mg, 3.09 mmol), HOBT (501 mg, 3.71 mmol) and EDC-HCl (711 mg, 3.71 mmol) were dissolved in DMF (dry, 8 mL) and DIPEA (600 mg, 4.64 mmol) was added. The mixture was stirred for 1 h at RT and a solution of methyl 4-(1-aminoethyl)benzoate hydrochloride (**269**, 800 mg, 3.71 mmol) dissolved in DMF (dry, 7 mL) and DIPEA (600 mg, 4.64 mmol) was added. The reaction mixture was stirred for additional 20 h at RT DCM (100 mL) was added, the organic phase was washed 4 times with H<sub>2</sub>O (50 mL) and once with a NaCl solution (sat., 50 mL). The organic phase was separated, dried over MgSO<sub>4</sub> and the solvent was removed under reduced pressure. The crude product was precipitated from cyclohexane.

**Yield:** 632 mg (2.09 mmol, 68%), colorless solid.

- **TLC:**  $R_f = 0.20$  (SiO<sub>2</sub>, cyclohexan/EtOAc 1:3).
- **C<sub>15</sub>H<sub>18</sub>N<sub>4</sub>O<sub>3</sub>:** (302.33), [302.14].
- **<sup>1</sup>H-NMR (600 MHz, DMSO-d<sub>6</sub>, 300 K):**  $\delta = 8.25\text{--}7.68$  (m, 4H, H-2-, H-3-, H-5-, H-6-benzyl), 7.65–7.28 (m, 2H, CH pyrazole, CONH), 6.11 (s, 2H, NH<sub>2</sub>), 5.30–4.95 (m, 1H, CHCH<sub>3</sub>), 3.83 (s, 3H, CO<sub>2</sub>CH<sub>3</sub>), 3.50 (s, 3H, NCH<sub>3</sub>), 1.43 (s, 3H, CHCH<sub>3</sub>) ppm.
- **<sup>13</sup>C-NMR (150 MHz, DMSO-d<sub>6</sub>, 300 K):**  $\delta = 166.1, 163.4, 151.2, 149.4, 136.3, 129.2, 127.8, 126.2, 96.7, 52.0, 47.2, 33.8, 22.1$  ppm.
- **MS (ESI neg.):**  $m/z$  (%) = 301.14 (100) ([M-H]<sup>-</sup>, calcd. 301.13), 347.06 (35) ([M-H+EtOH]<sup>-</sup>, calcd. 347.17).

**Methyl 4-((5-amino-1-methyl-1H-pyrazole-4-carboxamido)methyl)benzoate (274, SR270)**

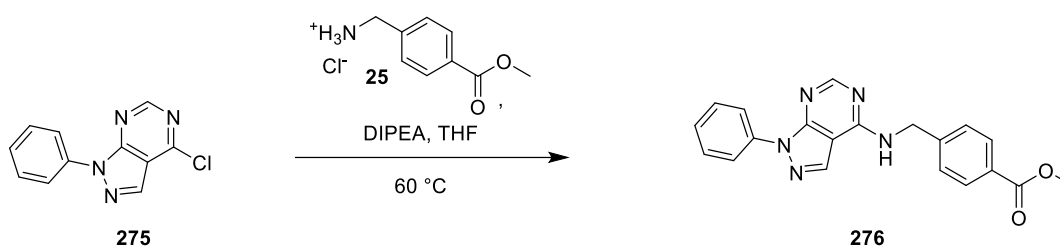
5-Amino-1-methyl-1H-pyrazole-4-carboxylic acid (**272**, 500 mg, 3.54 mmol), HOBT (574 mg, 4.25 mmol) and EDC-HCl (815 mg, 4.25 mmol) were dissolved in DMF (dry, 10 mL) and DIPEA (687 mg, 5.31 mmol) was added. The mixture was stirred for 1 h at RT and a solution of methyl 4-(aminomethyl)benzoate hydrochloride (**25**, 857 mg, 4.25 mmol) dissolved in DMF (dry, 10 mL) and DIPEA (687 mg, 5.31 mmol) was added. The reaction mixture was stirred for additional 20 h at RT. DCM (100 mL) was added, the organic phase was washed 4 times with H<sub>2</sub>O (100 mL), and once with brine (100 mL). The organic phase was

separated, dried over  $\text{MgSO}_4$  and the solvent was removed under reduced pressure. The crude product was precipitated from cyclohexane.

**Yield:** 722 mg (2.50 mmol, 71%), colorless solid.

- **TLC:**  $R_f = 0.25$  ( $\text{SiO}_2$ , cyclohexane/EtOAc 1:3).
- **$\text{C}_{14}\text{H}_{16}\text{N}_4\text{O}_3$ :** (288.30), [288.12].
- **$^1\text{H-NMR}$  (600 MHz,  $\text{DMSO-d}_6$ , 300 K):**  $\delta = 8.32$  (t,  $^3J = 5.9$  Hz, 1H, CONH), 7.92 (d,  $^3J = 8.1$  Hz, 2H, H-3-, H-5-benzyl), 7.68 (s, 1H, CH pyrazole), 7.41 (d,  $^3J = 8.1$  Hz, 2H, H-2-, H-6-benzyl), 6.16 (s, 2H,  $\text{NH}_2$ ), 4.45 (d,  $^3J = 6.1$  Hz, 2H,  $\text{CH}_2$ ), 3.84 (s, 3H,  $\text{CO}_2\text{CH}_3$ ), 3.51 (s, 3H,  $\text{NCH}_3$ ) ppm.
- **$^{13}\text{C-NMR}$  (150 MHz,  $\text{DMSO-d}_6$ , 300 K):**  $\delta = 166.1, 164.1, 149.4, 146.1, 136.1, 129.2, 128.0, 127.2, 96.7, 52.0, 41.3, 33.9$  ppm.
- **MS (ESI pos.):**  $m/z$  (%) = 289.03 (100) ( $[\text{M}+\text{H}]^+$ , calcd. 289.13).

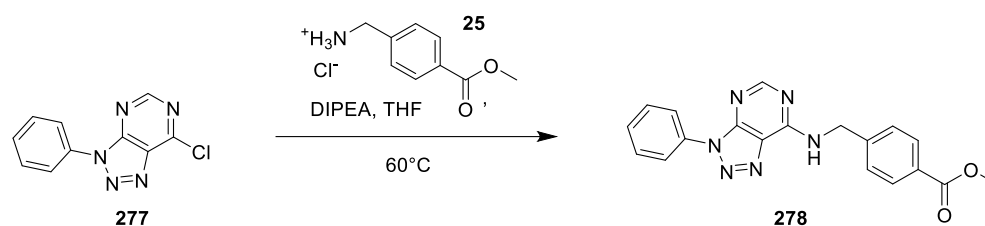
**Methyl 4-(((1-phenyl-1H-pyrazolo[3,4-d]pyrimidin-4-yl)amino)methyl)benzoate (276, SR286)**



4-Chloro-1-phenyl-1H-pyrazolo[3,4-d]pyrimidine (**275**, 250 mg, 1.08 mmol) was diluted in THF (dry, 10 mL) and DIPEA (140 mg, 1.08 mmol) was added. In a separate flask methyl 4-(aminomethyl)benzoate hydrochloride (**25**, 219 mg, 1.08 mmol) and DIPEA (140 mg, 1.08 mmol) were dissolved in THF (dry, 10 mL) and stirred at RT for 5 min. The latter suspension was added to the first solution and the mixture was heated to 60 °C for 20 h. EtOAc (150 mL) was added and the organic phase was washed 3 times with  $\text{H}_2\text{O}$  (50 mL). The organic phase was separated, dried over  $\text{MgSO}_4$  and the solvent was removed under reduced pressure. The crude product was purified using column chromatography on silica (cyclohexane/EtOAc 10:1).

**Yield:** 358 mg (0.996 mmol, 92%), colorless solid.

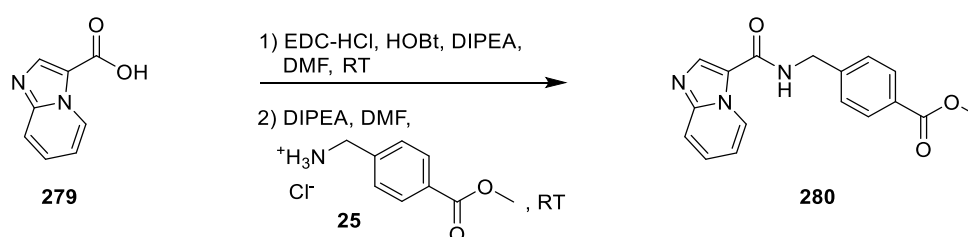
- **TLC:**  $R_f = 0.59$  ( $\text{SiO}_2$ , cyclohexane/EtOAc 1:1).
- **$\text{C}_{20}\text{H}_{17}\text{N}_5\text{O}_2$ :** (359.38), [359.14].
- **$^1\text{H-NMR}$  (400 MHz,  $\text{DMSO-d}_6$ , 300 K):**  $\delta = 9.07$  (t,  $^3J = 5.6$  Hz, 1H, NH), 8.45 (s, 1H, pyrimidine), 8.38 (s, 1H, pyrazole), 8.20 (d,  $^3J = 8.1$  Hz, 2H, H-3-, H-5-benzyl), 7.95 (d,  $^3J = 8.1$  Hz, 2H, H-2-, H-6-phenyl), 7.59–7.49 (m, 4H, H-2-, H-6-benzyl, H-3-, H-5-phenyl), 7.35 (t,  $^3J = 7.3$  Hz, 1H, H-4 phenyl), 4.88 (d,  $^3J = 5.8$  Hz, 2H,  $\text{CH}_2$ ) 3.84 (s, 3H,  $\text{CH}_3$ ) ppm.
- **$^{13}\text{C-NMR}$  (150 MHz,  $\text{DMSO-d}_6$ , 300 K):**  $\delta = 166.0, 156.4$  (2x), 152.8, 144.8, 138.9, 133.7, 129.3 (2x), 129.1, 127.5, 126.1, 120.6, 101.8, 52.2, 42.9 ppm.
- **MS (ESI pos.):**  $m/z$  (%) = 359.89 (100) ( $[\text{M}-\text{H}]^+$ , calcd. 360.15).

**Methyl 4-(((3-phenyl-3H-[1,2,3]triazolo[4,5-d]pyrimidin-7-yl)amino)methyl)benzoate (278, SR287)**

7-Chloro-3-phenyl-3H-[1,2,3]triazolo[4,5-d]pyrimidine (**277**, 250 mg, 1.08 mmol) was diluted in THF (dry, 10 mL) and DIPEA (140 mg, 1.08 mmol) was added. In a separate flask methyl 4-(aminomethyl)benzoate hydrochloride (**25**, 218 mg, 1.08 mmol) and DIPEA (140 mg, 1.08 mmol) were dissolved in THF (dry, 10 mL) and stirred at RT for 5 min. This suspension was then added to the first solution and the mixture was heated to 60 °C for 20 h. EtOAc (150 mL) was added and the organic phase was washed 3 times with H<sub>2</sub>O (50 mL). The organic phase was separated, dried over MgSO<sub>4</sub> and the solvent was removed under reduced pressure. The crude product was precipitated from cyclohexane.

**Yield:** 324 mg (0.899 mmol, 83%), colorless solid.

- **TLC:** R<sub>f</sub> = 0.72 (SiO<sub>2</sub>, cyclohexane/EtOAc 1:1).
- **C<sub>19</sub>H<sub>16</sub>N<sub>6</sub>O<sub>2</sub>:** (360.37), [360.13].
- **<sup>1</sup>H-NMR (600 MHz, DMSO-d<sub>6</sub>, 300 K):** (mixture of rotamers): δ = 9.73 (t, <sup>3</sup>J = 6.1 Hz, 0.8H, NH), 9.35 (t, <sup>3</sup>J = 7.0 Hz, 0.2H, NH), 8.47 (s, 0.8H, pyrimidine), 8.43 (s, 0.2H, pyrimidine), 8.15 (d, <sup>3</sup>J = 7.9 Hz, 1.6H, H-3-, H-5-benzyl), 8.15 (d, <sup>3</sup>J = 7.9 Hz, 0.4H, H-3-, H-5-benzyl), 7.92 (d, <sup>3</sup>J = 7.9 Hz, 2H, H-2-, H-6-phenyl), 7.66 (t, <sup>3</sup>J = 7.9 Hz, 2H, H-3-, H-5-phenyl), 7.58–7.49 (m, 3H, H-2-, H-6-benzyl, H-4 phenyl), 5.32 (d, <sup>3</sup>J = 7.0 Hz, 0.4H, CH<sub>2</sub>), 4.88 (d, <sup>3</sup>J = 6.1 Hz, 1.6H, CH<sub>2</sub>), 3.83 (s, 3H, CH<sub>3</sub>) ppm.
- **<sup>13</sup>C-NMR (150 MHz, DMSO-d<sub>6</sub>, 300 K):** (mixture of rotamers) δ = 166.0, 157.4, 157.0, 154.5, 148.1, 144.5, 135.7, 129.6, 129.4, 129.3, 128.5, 128.3, 127.4, 124.8, 121.5, 121.4, 52.0, 43.0 ppm.
- **MS (ESI neg.):** m/z (%) = 359.05 (100) ([M-H]<sup>-</sup>, calcd. 359.12).

**Methyl 4-((imidazo[1,2-a]pyridine-3-carboxamido)methyl)benzoate (280, SR280)**

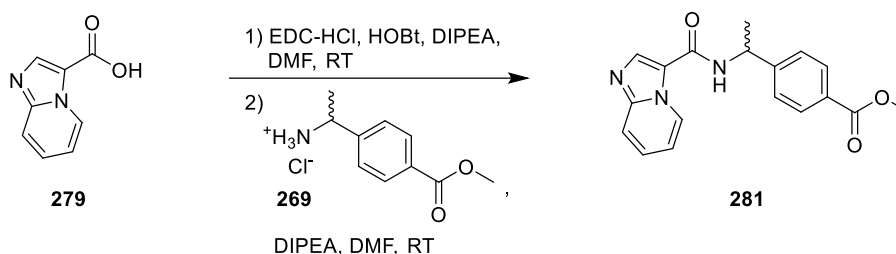
Imidazo[1,2-a]pyridine-3-carboxylic acid (**279**, 500 mg, 3.08 mmol), HOBT (500 mg, 3.70 mmol) and EDC-HCl (709 mg, 3.70 mmol) were dissolved in DMF (dry, 8 mL) and DIPEA (598 mg, 4.63 mmol) was added. The mixture was stirred for 1 h at RT and a solution of methyl 4-(aminomethyl)benzoate hydrochloride (**25**, 789 mg, 3.91 mmol) dissolved in DMF (dry, 7 mL), DMSO (dry, 3 mL) and DIPEA (598 mg, 4.63 mmol) was added. The reaction mixture was stirred for additional 20 h at RT DCM (200 mL) was added, the organic phase was washed 4 times with H<sub>2</sub>O (150 mL). The organic phase was separated, dried over MgSO<sub>4</sub> and the solvent was removed under reduced pressure. The crude product was dissolved in DCM and precipitated with cyclohexane.



**Yield:** 837 mg (2.71 mmol, 88%), colorless solid.

- **TLC:**  $R_f = 0.26$  (SiO<sub>2</sub>, cyclohexane/EtOAc 1:3).
- **C<sub>17</sub>H<sub>15</sub>N<sub>3</sub>O<sub>3</sub>:** (309.32), [309.11].
- **<sup>1</sup>H-NMR (600 MHz, DMSO-d<sub>6</sub>, 300 K):**  $\delta = 9.47$  (d,  $^3J = 7.0$  Hz, 1H, CH-5 imidazo[1,2-*a*]pyridine), 9.13 (t,  $^3J = 5.8$  Hz, 1H, NH), 8.42 (s, 1H, CH-2 imidazo[1,2-*a*]pyridine), 7.93 (d,  $^3J = 8.2$  Hz, 2H, H-3-, H-5-benzyl), 7.72 (d,  $^3J = 9.2$  Hz, 1H, CH-8 imidazo[1,2-*a*]pyridine), 7.49 (d,  $^3J = 8.0$  Hz, 2H, H-2-, H-6-benzyl), 7.46 (t,  $^3J = 7.7$  Hz, 1H, CH-7 imidazo[1,2-*a*]pyridine), 7.11 (t,  $^3J = 6.9$  Hz, 1H, CH-6 imidazo[1,2-*a*]pyridine), 4.60 (d,  $^3J = 5.8$  Hz, 2H, CH<sub>2</sub>), 3.83 (s, 3H, CH<sub>3</sub>) ppm.
- **<sup>13</sup>C-NMR (150 MHz, DMSO-d<sub>6</sub>, 300 K):**  $\delta = 166.1, 160.2, 146.9, 145.3, 136.9, 129.3, 128.2, 127.5, 127.4, 126.9, 117.9, 117.2, 113.8, 52.0, 41.6$  ppm.
- **MS (ESI neg.):**  $m/z$  (%) = 308.09 (100) ([M-H]<sup>-</sup>, calcd. 308.10).

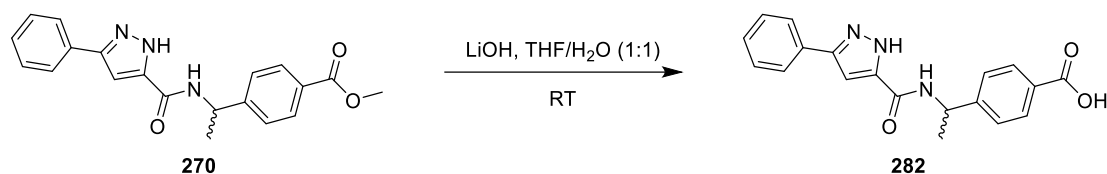
**Methyl 4-(1-(imidazo[1,2-*a*]pyridine-3-carboxamido)ethyl)benzoate (281, SR269)**



5-Amino-1-methyl-1*H*-pyrazole-4-carboxylic acid (**279**, 251 mg, 1.55 mmol), HOBT (209 mg, 1.85 mmol) and EDC-HCl (296 mg, 1.854 mmol) were dissolved in DMF (dry, 8 mL) and DIPEA (300 mg, 2.32 mmol) was added. The mixture was stirred for 1 h at RT and a solution of methyl 4-(1-aminoethyl)benzoate hydrochloride (**269**, 400 mg, 3.71 mmol) dissolved in DMF (dry, 7 mL), DMSO (dry, 5 mL) and DIPEA (300 mg, 2.32 mmol) was added. The reaction mixture was stirred for additional 20 h at RT, then DCM (150 mL) was added and the organic phase washed 4 times with H<sub>2</sub>O (100 mL). The organic phase was separated, dried over MgSO<sub>4</sub> and the solvent was removed under reduced pressure. The crude product was purified using column chromatography on silica (cyclohexane/EtOAc 1:10).

**Yield:** 365 mg (1.13 mmol, 73%), yellowish solid.

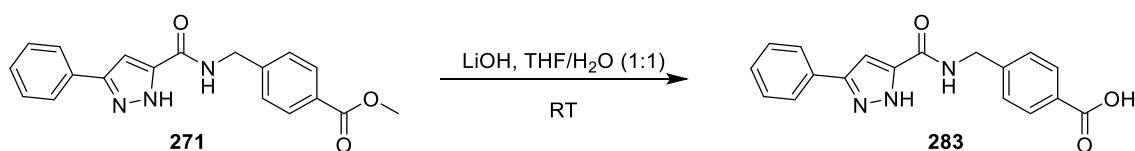
- **TLC:**  $R_f = 0.31$  (SiO<sub>2</sub>, cyclohexane/EtOAc 1:3).
- **C<sub>18</sub>H<sub>17</sub>N<sub>3</sub>O<sub>3</sub>:** (323.35), [323.13].
- **<sup>1</sup>H-NMR (600 MHz, DMSO-d<sub>6</sub>, 300 K):**  $\delta = 9.40$  (d,  $^3J = 7.2$  Hz, 1H, CH-5 imidazo[1,2-*a*]pyridine), 8.88 (d,  $^3J = 7.6$  Hz, 1H, NH), 8.51 (s, 1H, CH-2 imidazo[1,2-*a*]pyridine), 7.93 (d,  $^3J = 8.3$  Hz, 2H, H-3-, H-5-benzyl), 7.70 (d,  $^3J = 8.9$  Hz, 1H, CH-8 imidazo[1,2-*a*]pyridine), 7.55 (d,  $^3J = 8.1$  Hz, 2H, H-2-, H-6-benzyl), 7.44 (t,  $^3J = 7.6$  Hz, 1H, CH-7 imidazo[1,2-*a*]pyridine), 7.08 (t,  $^3J = 6.9$  Hz, 1H, CH-6 imidazo[1,2-*a*]pyridine), 5.27 (p,  $^3J = 7.2$  Hz, 1H, CHCH<sub>3</sub>), 3.83 (s, 3H, OCH<sub>3</sub>), 1.52 (d,  $^3J = 7.1$  Hz, 3H, CHCH<sub>3</sub>) ppm.
- **<sup>13</sup>C-NMR (150 MHz, DMSO-d<sub>6</sub>, 300 K):**  $\delta = 166.1, 159.5, 150.4, 146.9, 137.1, 129.3, 128.1, 127.5, 126.9, 126.3, 117.9, 117.2, 113.8, 52.0, 47.7, 21.9$  ppm.
- **MS (ESI neg.):**  $m/z$  (%) = 322.08 (100) ([M-H]<sup>-</sup>, calcd. 322.12).

**4-(1-(3-Phenyl-1H-pyrazole-5-carboxamido)ethyl)benzoic acid (282, SR259)**

Methyl 4-(1-(3-phenyl-1H-pyrazole-5-carboxamido)ethyl)benzoate (**270**, 200 mg, 0.572 mmol) was dissolved in a mixture of THF/H<sub>2</sub>O (10 mL, 1:1) and LiOH·H<sub>2</sub>O (69 mg, 2.86 mmol) was added. The suspension was stirred for 24 h at RT and then acidified with HCl (aq., 10 mL, 1 M). The precipitate was filtered, washed with H<sub>2</sub>O and dried under reduced pressure in a vacuum oven.

**Yield:** 178 mg (0.531 mmol, 93%), colorless solid.

- **TLC:**  $R_f = 0.33$  (SiO<sub>2</sub>, cyclohexan/EtOAc 1:3).
- **C<sub>19</sub>H<sub>17</sub>N<sub>3</sub>O<sub>3</sub>:** (335.36), [335.13].
- **<sup>1</sup>H-NMR (600 MHz, DMSO-d<sub>6</sub>, 300 K):**  $\delta = 13.95\text{--}12.45$  (m, 2H, NH pyrazole, COOH), 8.72 (s, 1H, CONH), 7.91 (d, <sup>3</sup> $J = 8.2$  Hz, 2H, H-3-, H-5-benzyl), 7.80 (d, <sup>3</sup> $J = 7.6$  Hz, 2H, H-2-, H-6-phenyl), 7.52 (d, <sup>3</sup> $J = 8.2$  Hz, 2H, H-2-, H-6-benzyl), 7.46 (t, <sup>3</sup> $J = 7.6$  Hz, 2H, H-3-, H-5-phenyl), 7.35 (t, <sup>3</sup> $J = 7.5$  Hz, 1H, H-4 phenyl), 7.19 (s, 1H, CH pyrazole), 5.21 (p, <sup>3</sup> $J = 7.1$  Hz, 1H, CHCH<sub>3</sub>), 1.56 (d, <sup>3</sup> $J = 7.1$  Hz, 3H, CHCH<sub>3</sub>) ppm.
- **<sup>13</sup>C-NMR (150 MHz, DMSO-d<sub>6</sub>, 300 K):**  $\delta = 168.1, 150.7, 148.6, 146.2, 130.4, 103.2, 129.9, 129.1, 127.3, 126.2, 125.2, 103.6, 47.8, 21.8$  ppm.
- **MS (ESI neg.):**  $m/z$  (%) = 334.10 (100) ([M-H]<sup>-</sup>, calcd. 334.12), 370.05 (22) [M+Cl]<sup>-</sup>, calcd. 370.58).

**4-((3-Phenyl-1H-pyrazole-5-carboxamido)methyl)benzoic acid (283, SR273)**

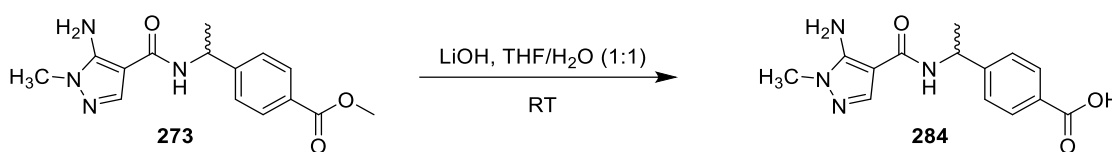
Methyl 4-((3-phenyl-1H-pyrazole-5-carboxamido)methyl)benzoate (**271**, 600 mg, 1.79 mmol) was dissolved in a mixture of THF/H<sub>2</sub>O (10 mL, 1:1) and LiOH·H<sub>2</sub>O (214 mg, 8.95 mmol) was added. The suspension was stirred for 24 h at RT and then acidified with HCl (aq., 10 mL, 1 M). The precipitate was filtered, washed with H<sub>2</sub>O and dried under reduced pressure in a vacuum oven.

**Yield:** 544 mg (1.69 mmol, 95%), colorless solid.

- **TLC:**  $R_f = 0.30$  (SiO<sub>2</sub>, cyclohexane/EtOAc 1:3).
- **C<sub>18</sub>H<sub>15</sub>N<sub>3</sub>O<sub>3</sub>:** (321.33), [321.11].
- **<sup>1</sup>H-NMR (600 MHz, DMSO-d<sub>6</sub>, 300 K):**  $\delta = 13.70\text{--}12.68$  (m, 2H, NH pyrazole, COOH), 8.95 (s, 1H, CONH), 7.91 (d, <sup>3</sup> $J = 8.0$  Hz, 2H, H-3-, H-5-benzyl), 7.80 (d, <sup>3</sup> $J = 7.6$  Hz, 2H, H-2-, H-6-phenyl), 7.50–7.41 (m, 4H, H-3-, H-5-phenyl, H-2-, H-6-benzyl), 7.36 (t, <sup>3</sup> $J = 7.6$  Hz, 1H, H-4 phenyl), 7.17 (s, 1H, CH pyrazole), 4.54 (d, <sup>3</sup> $J = 6.2$  Hz, 2H, CH<sub>2</sub>) ppm.
- **<sup>13</sup>C-NMR (150 MHz, DMSO-d<sub>6</sub>, 300 K):**  $\delta = 167.2, 157.0, 147.7, 144.8, 140.8, 129.4, 129.3, 129.0, 128.2, 127.2$  (2x), 125.2, 102.5, 41.8 ppm.

- **MS (ESI neg.):**  $m/z$  (%) = 320.10 (100) ( $[M-H]^-$ , calcd. 320.10), 356.08 (56) ( $[M+Cl]^-$ , calcd. 356.56).

#### 4-(1-(5-Amino-1-methyl-1H-pyrazole-4-carboxamido)ethyl)benzoic acid (**284**, SR274)

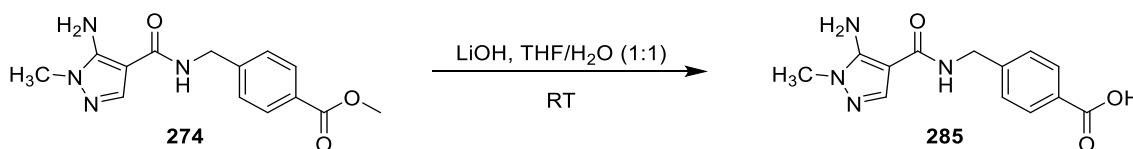


Methyl 4-(1-(5-amino-1-methyl-1H-pyrazole-4-carboxamido)ethyl)benzoate (**273**, 500 mg, 1.65 mmol) was dissolved in a mixture of THF/H<sub>2</sub>O (10 mL, 1:1) and LiOHxH<sub>2</sub>O (198 mg, 8.27 mmol) was added. The solvent was removed under reduced pressure. The crude product was triturated with DCM/H<sub>2</sub>O (1:1), filtered, washed with H<sub>2</sub>O and dried under reduced pressure in a vacuum oven.

**Yield:** 368 mg (1.28 mmol, 77%), colorless solid

- **TLC:**  $R_f$  = 0.13 (SiO<sub>2</sub>, DCM/MeOH 10:1).
- **C<sub>14</sub>H<sub>16</sub>N<sub>4</sub>O<sub>3</sub>:** (288.30), [288.12].
- **<sup>1</sup>H-NMR (600 MHz, DMSO-d<sub>6</sub>, 300 K):**  $\delta$  = 12.83 (br s, 1H, COOH), 8.06 (d, <sup>3</sup>J = 7.9 Hz, 1H, CONH), 7.89 (d, <sup>3</sup>J = 7.9 Hz, H-3-, H-5-benzyl), 7.78 (s, 1H, CH pyrazole), 7.44 (d, <sup>3</sup>J = 8.0 Hz, H-2-, H-6-benzyl), 6.11 (br s, 2H, NH<sub>2</sub>), 5.13 (p, <sup>3</sup>J = 7.3 Hz, 1H, CONHCH), 3.50 (s, 3H, NCH<sub>3</sub>), 1.43 (d, <sup>3</sup>J = 7.2 Hz, 3H, CHCH<sub>3</sub>) ppm.
- **<sup>13</sup>C-NMR (150 MHz, DMSO-d<sub>6</sub>, 300 K):**  $\delta$  = 167.2, 163.4, 150.7, 149.5, 136.3, 129.3, 129.0, 126.1, 96.7, 47.2, 33.9, 22.1 ppm.
- **MS (ESI neg.):**  $m/z$  (%) = 287.10 (100) ( $[M-H]^-$ , calcd. 287.29), 243.12 (20) ( $[M-COOH]^-$ , calcd. 243.12).

#### 4-((5-Amino-1-methyl-1H-pyrazole-4-carboxamido)methyl)benzoic acid (**285**, SR272)



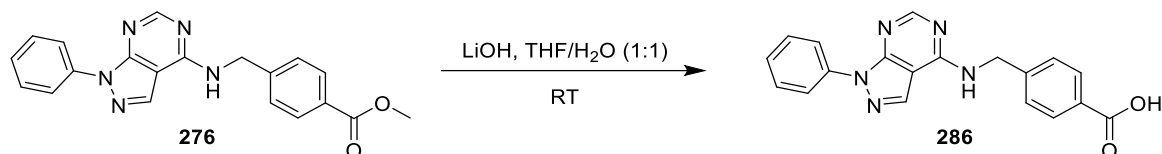
Methyl 4-((5-amino-1-methyl-1H-pyrazole-4-carboxamido)methyl)benzoate (**274**, 600 mg, 2.08 mmol) was dissolved in a mixture of THF/H<sub>2</sub>O (10 mL, 1:1) and LiOHxH<sub>2</sub>O (249 mg, 10.4 mmol) was added. The suspension was stirred for 24 h at RT and then acidified with HCl (aq., 10 mL, 1 M). The precipitate was filtered, washed with H<sub>2</sub>O and dried under reduced pressure in a vacuum oven.

**Yield:** 504 mg (1.84 mmol, 88%), colorless solid.

- **TLC:**  $R_f$  = 0.08 (SiO<sub>2</sub>, cyclohexane/EtOAc 1:3).
- **C<sub>13</sub>H<sub>14</sub>N<sub>4</sub>O<sub>3</sub>:** (274.28), [274.11].
- **<sup>1</sup>H-NMR (600 MHz, DMSO-d<sub>6</sub>, 300 K):**  $\delta$  = 8.50–8.44 (m, 1H, CONH), 7.90 (d, <sup>3</sup>J = 8.2 Hz, 2H, H-3-, H-5-benzyl), 7.84 (s, 1H, pyrazole), 7.39 (d, <sup>3</sup>J = 8.2 Hz, 2H, H-2-, H-6-benzyl), 6.34–4.64 (m, 3H, COOH, NH<sub>2</sub>), 4.47–4.42 (m, 2H, CH<sub>2</sub>), 3.55 (s, 3H, NCH<sub>3</sub>) ppm.
- **<sup>13</sup>C-NMR (150 MHz, DMSO-d<sub>6</sub>, 300 K):**  $\delta$  = 167.2, 163.8, 149.6, 145.5, 135.7, 129.4, 129.2, 127.1, 97.0, 41.4, 33.8 ppm.

- **MS (ESI neg.):**  $m/z$  (%) = 273.08 (100) ( $[M-H]^-$ , calcd. 273.10), 309.07 (47) ( $[M+Cl]^-$ , calcd. 308.53), 229.11 (28) ( $[M-COOH]^-$ , calcd. 229.11).

#### 4-(((1-Phenyl-1H-pyrazolo[3,4-d]pyrimidin-4-yl)amino)methyl)benzoic acid (**286**, SR297)

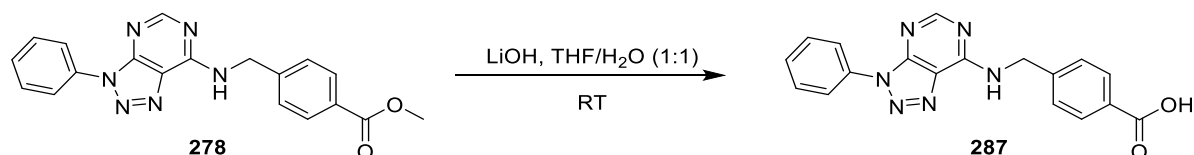


Methyl 4-(((1-phenyl-1H-pyrazolo[3,4-d]pyrimidin-4-yl)amino)methyl)benzoate (**276**, 500 mg, 1.39 mmol) was dissolved in a mixture of THF/H<sub>2</sub>O (20 mL, 1:1) and LiOHxH<sub>2</sub>O (166 mg, 6.96 mmol) was added. The suspension was stirred for 4 d at RT and then acidified with HCl (aq., 10 mL, 1 M). The precipitate was filtered, washed with H<sub>2</sub>O and dried under reduced pressure in a vacuum oven.

**Yield:** 455 mg (1.32 mmol, 95%), colorless solid.

- **TLC:**  $R_f$  = 0.02 (SiO<sub>2</sub>, cyclohexane/EtOAc 1:10).
- **C<sub>19</sub>H<sub>15</sub>N<sub>5</sub>O<sub>2</sub>:** (345.35), [345.12].
- **<sup>1</sup>H-NMR (300 MHz, DMSO-d<sub>6</sub>, 300 K):**  $\delta$  = 13.41–12.35 (br s, 1H, COOH), 9.16 (t, <sup>3</sup> $J$  = 6.1 Hz, 1H, NH), 8.48 (s, 1H, pyrimidine), 8.38 (s, 1H, pyrazole), 8.19 (d, <sup>3</sup> $J$  = 7.8 Hz, 2H, H-3-, H-5-benzyl), 7.92 (d, <sup>3</sup> $J$  = 8.3 Hz, 2H, H-2-, H-6-phenyl), 7.60–7.45 (m, 4H, H-2-, H-6-benzyl, H-3-, H-5-phenyl), 7.34 (tt, <sup>3</sup> $J$  = 7.4, 1.1 Hz, 1H, H-4 phenyl), 4.86 (d, <sup>3</sup> $J$  = 5.9 Hz, 2H, CH<sub>2</sub>) ppm.
- **<sup>13</sup>C-NMR (75 MHz, DMSO-d<sub>6</sub>, 300 K):**  $\delta$  = 167.1, 156.4 (2x), 152.8, 144.3, 138.9, 133.8, 129.5, 129.1 (2x), 127.4, 126.2, 120.7, 101.9, 43.1 ppm.
- **MS (ESI neg.):**  $m/z$  (%) = 344.04 (100) ( $[M-H]^-$ , calcd. 344.10).

#### 4-(((3-Phenyl-3H-[1,2,3]triazolo[4,5-d]pyrimidin-7-yl)amino)methyl)benzoic acid (**287**, SR298)



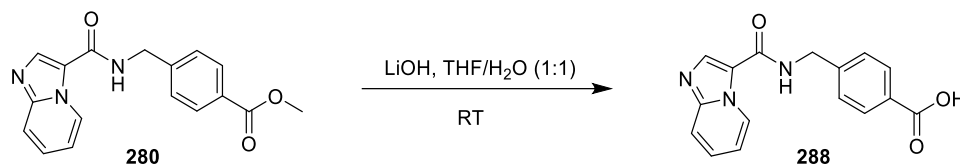
Methyl 4-(((3-phenyl-3H-[1,2,3]triazolo[4,5-d]pyrimidin-7-yl)amino)methyl)benzoate (**278**, 290 mg, 0.81 mmol) was dissolved in a mixture of THF/H<sub>2</sub>O (20 mL, 1:1) and LiOHxH<sub>2</sub>O (96 mg, 4.03 mmol) was added. The suspension was stirred for 4 d at RT and then acidified with HCl (aq., 10 mL, 1 M). The precipitate was filtered, washed with H<sub>2</sub>O and dried under reduced pressure in a vacuum oven.

**Yield:** 231 mg (0.667 mmol, 83%), colorless solid.

- **TLC:**  $R_f$  = 0.60 (SiO<sub>2</sub>, cyclohexane /EtOAc 1:10).
- **C<sub>18</sub>H<sub>14</sub>N<sub>6</sub>O<sub>2</sub>:** (346.34), [346.12].
- **<sup>1</sup>H-NMR (300 MHz, DMSO-d<sub>6</sub>, 300 K):** (mixture of rotamers)  $\delta$  = 12.86 (s, 1H, COOH), 9.81–9.60 (m, 0.8H, NH), 9.42–9.26 (m, 0.2H, NH), 8.56–8.37 (m, 1H, pyrimidine), 8.15 (d, <sup>3</sup> $J$  = 8.1 Hz, 2H, H-3-, H-5-benzyl), 7.91 (d, <sup>3</sup> $J$  = 7.8 Hz, 2H, H-2-, H-6-phenyl), 7.73–7.37 (m, 5H, H-3-, H-4-, H-5-phenyl, H-2-, H-6-benzyl), 5.39–5.25 (m, 0.4H, CH<sub>2</sub>), 4.97–4.77 (m, 1.6H, CH<sub>2</sub>) ppm.

- **$^{13}\text{C}$ -NMR (75 MHz, DMSO- $d_6$ , 300 K):** (mixture of rotamers)  $\delta = 167.1, 157.5, 154.5, 148.1, 144.0, 135.8, 129.6, 129.4, 128.5, 127.3, 127.2, 124.9, 121.4, 43.1$  ppm.
- **MS (ESI neg.):**  $m/z$  (%) = 345.07 (100) ( $[\text{M}-\text{H}]^-$ , calcd. 345.11).

#### 4-((Imidazo[1,2-*a*]pyridine-3-carboxamido)methyl)benzoic acid (**288**, SR282)

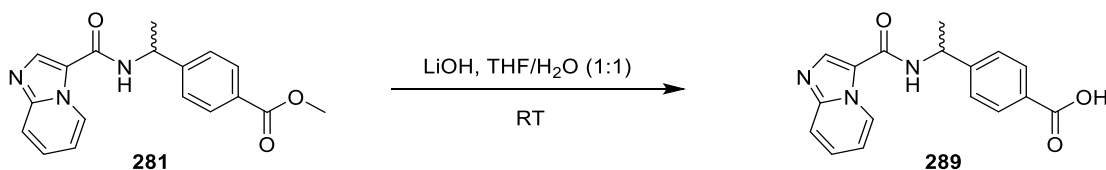


Methyl 4-((imidazo[1,2-*a*]pyridine-3-carboxamido)methyl)benzoate (**280**, 600 mg, 1.94 mmol) was dissolved in a mixture of THF/ $\text{H}_2\text{O}$  (20 mL, 1:1) and  $\text{LiOH}\cdot\text{H}_2\text{O}$  (232 mg, 9.70 mmol) was added. The suspension was stirred for 3 d at RT and then acidified with HCl (aq., 10 mL, 1 M). The precipitate was filtered, washed with  $\text{H}_2\text{O}$  and dried under reduced pressure in a vacuum oven.

**Yield:** 367 mg (1.24 mmol, 64%), yellowish solid.

- **TLC:**  $R_f = 0.02$  ( $\text{SiO}_2$ , cyclohexane/EtOAc 1:10).
- **$\text{C}_{16}\text{H}_{13}\text{N}_3\text{O}_3$ :** (295.29), [295.10].
- **$^1\text{H}$ -NMR (300 MHz, DMSO- $d_6$ , 300 K):**  $\delta = 9.89$  (t,  $^3J = 5.9$  Hz, 1H, NH), 9.69 (d,  $^3J = 7.0$  Hz, 1H, CH-5 imidazo[1,2-*a*]pyridine), 9.03 (s, 1H, CH-2 imidazo[1,2-*a*]pyridine), 8.08–7.67 (m, 4H, H-3-, H-5-benzyl, CH-8-, CH-7-imidazo[1,2-*a*]pyridine), 7.58–7.45 (m, 3H, H-2-, H-6-benzyl, CH-6 imidazo[1,2-*a*]pyridine), 4.59 (d,  $^3J = 5.8$  Hz, 2H,  $\text{CH}_2$ ) ppm.
- **$^{13}\text{C}$ -NMR (75 MHz, DMSO- $d_6$ , 300 K):**  $\delta = 167.1, 158.7, 144.1, 141.5, 133.3, 129.5, 129.4, 129.2, 127.7, 127.4, 118.8, 117.4, 113.5, 41.8$  ppm.
- **MS (ESI neg.):**  $m/z$  (%) = 294.10 (100) ( $[\text{M}-\text{H}]^-$ , calcd. 294.09).

#### 4-(1-(Imidazo[1,2-*a*]pyridine-3-carboxamido)ethyl)benzoic acid (**289**, SR296)



Methyl 4-(1-(imidazo[1,2-*a*]pyridine-3-carboxamido)ethyl)benzoate (**281**, 337 mg, 1.04 mmol) was dissolved in a mixture of THF/ $\text{H}_2\text{O}$  (20 mL, 1:1) and  $\text{LiOH}\cdot\text{H}_2\text{O}$  (125 mg, 5.21 mmol) was added. The suspension was stirred for 4 d at RT and then acidified with HCl (aq., 10 mL, 1 M). The precipitate was filtered, washed with  $\text{H}_2\text{O}$  and dried under reduced pressure in a vacuum oven.

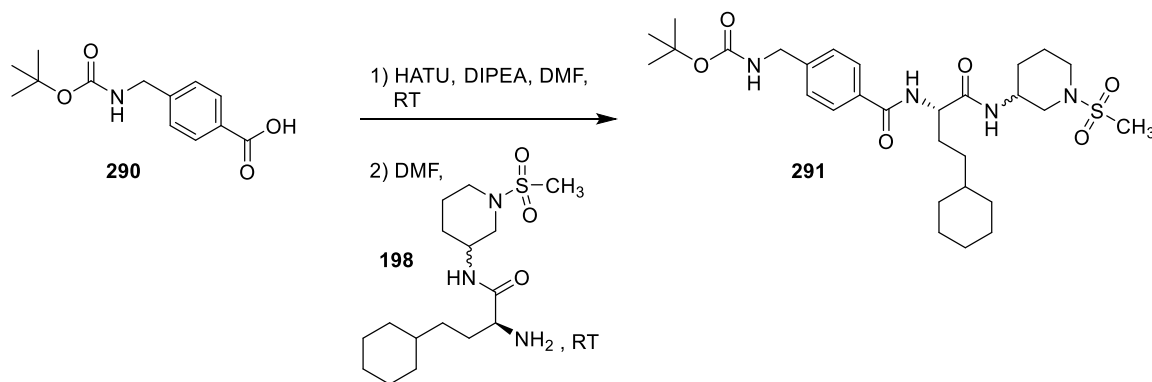
**Yield:** 308 mg (0.996 mmol, 96%), yellowish solid.

- **TLC:**  $R_f = 0.07$  ( $\text{SiO}_2$ , cyclohexane/EtOAc 1:3).
- **$\text{C}_{17}\text{H}_{15}\text{N}_3\text{O}_3$ :** (309.32), [309.11].
- **$^1\text{H}$ -NMR (300 MHz, DMSO- $d_6$ , 300 K):**  $\delta = 12.85$  (s, 1H, COOH), 9.41 (d,  $^3J = 7.1$  Hz, 1H, CH-5 imidazo[1,2-*a*]pyridine), 8.93 (d,  $^3J = 7.7$  Hz, 1H, NH), 8.55 (s, 1H, CH-2 imidazo[1,2-*a*]pyridine), 7.91 (d,  $^3J = 8.3$  Hz, 2H, H-3-, H-5-benzyl), 7.71 (d,  $^3J = 9.0$  Hz, 1H, CH-8 imidazo[1,2-*a*]pyridine) 7.53 (d,

$^3J = 8.3$  Hz, 2H, H-2-, H-6-benzyl), 7.45 (t,  $^3J = 7.7$  Hz, 1H, CH-7 imidazo[1,2-*a*]pyridine), 7.09 (t,  $^3J = 7.0$  Hz, 1H, CH-6 imidazo[1,2-*a*]pyridine), 5.26 (p,  $^3J = 7.3$  Hz, 1H, CHCH<sub>3</sub>), 1.52 (d,  $^3J = 7.1$  Hz, 3H, CHCH<sub>3</sub>) ppm.

- **$^{13}\text{C-NMR}$  (75 MHz, DMSO-*d*<sub>6</sub>, 300 K):**  $\delta = 167.2, 159.5, 150.4, 146.8, 137.0, 129.5, 129.3, 127.6, 127.1, 126.2, 118.0, 117.2, 113.9, 47.8, 22.0$  ppm.
- **MS (ESI neg.):**  $m/z$  (%) = 308.12 (100) ([M-H]<sup>-</sup>, calcd. 308.10).

***tert*-Butyl 4-(((*S*)-4-cyclohexyl-1-(((*SR*)-1-(methylsulfonyl)piperidin-3-yl)amino)-1-oxobutan-2-yl)carbamoyl)benzyl)carbamate (**291**, SR313)**

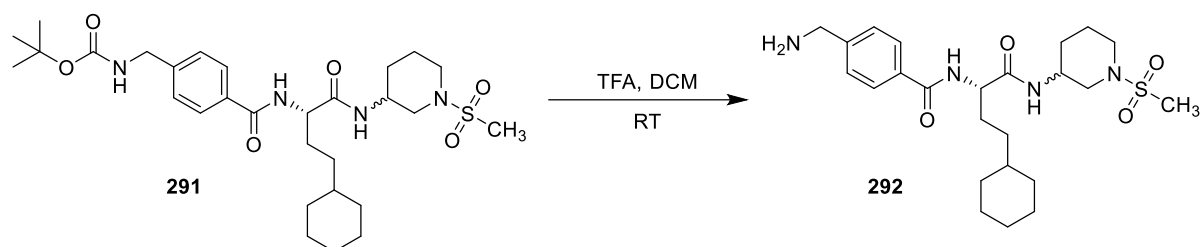


4-(((*tert*-Butoxycarbonyl)amino)methyl)benzoic acid (**290**, 598 mg, 2.38 mmol) and HATU (1.09 g, 2.86 mmol) were dissolved in DMF (12 mL) and DIPEA (396 mg, 2.86 mmol) was added. The solution was stirred for 1.5 h at RT and (*S*)-2-amino-4-cyclohexyl-*N*-(((*SR*)-1-(methylsulfonyl)piperidin-3-yl)butanamide (**198**, 987 mg, 2.86 mmol), diluted in DMF (8 mL), was added. The mixture was stirred for 3 d at RT. DCM (150 mL) was added and the organic phase was washed 4 times with H<sub>2</sub>O (100 mL) and dried over MgSO<sub>4</sub>. The solvent was evaporated under reduced pressure and the crude product was purified using flashcolumn chromatography on silica (cyclohexane/EtOAc 1:1 → 1:10 → EtOAc).

**Yield:** 628 mg (1.09 mmol, 46%), yellowish solid.

- **TLC:**  $R_f = 0.17$  (SiO<sub>2</sub>, cyclohexane/EtOAc 1:3).
- **C<sub>29</sub>H<sub>46</sub>N<sub>4</sub>O<sub>6</sub>S:** (578.31), [578.77].
- **$^1\text{H-NMR}$  (300 MHz, DMSO-*d*<sub>6</sub>, 300 K):** (mixture of diastereomers)  $\delta = 8.86$  (s, 1H, NHCH<sub>2</sub>), 8.39–8.29 (d,  $^3J = 8.0$  Hz, 1H, NHCHCO), 7.99 (d,  $^3J = 7.6$  Hz, 1H, NHCH piperidine), 7.83 (d,  $^3J = 8.2$  Hz, 2H, H-3-, H-5-benzyl), 7.44 (t,  $^3J = 6.2$  Hz, 1H, NHCOO), 7.80 (d,  $^3J = 8.2$  Hz, 2H, H-2-, H-6-benzyl), 4.46–4.31 (m, 1H, CH<sub>2</sub>, NHCHCO), 4.17 (d,  $^3J = 6.2$  Hz, 2H, CH<sub>2</sub> benzyl), 3.80–3.65 (m, 1H, CH piperidine), 3.54–3.27 (m, 2H, CH<sub>2</sub>-2 piperidine), 2.85 (s, 3H, SO<sub>2</sub>CH<sub>3</sub>), 2.81–2.71 (m, 1H, CH<sub>A</sub>H<sub>B</sub>-6 piperidine), 2.60–2.54 (m, 1H, CH<sub>A</sub>H<sub>B</sub>-6 piperidine), 1.85–1.05 (m, 27H, CH<sub>2</sub>-4-, CH<sub>2</sub>-5-piperidine, NHCHCH<sub>2</sub>, CH-1-, CH<sub>2</sub>-2-, CH<sub>2</sub>-3-, CH<sub>2</sub>-4-, CH<sub>2</sub>-5-, CH<sub>2</sub>-6-cyclohexyl, NHCHCH<sub>2</sub>CH<sub>2</sub>, (CH<sub>3</sub>)<sub>3</sub>), 0.94–0.76 (m, 2H, H-2<sub>ax</sub>, H-6<sub>ax</sub> cyclohexyl) ppm.
- **$^{13}\text{C-NMR}$  (75 MHz, DMSO-*d*<sub>6</sub>, 300 K):** (mixture of diastereomers)  $\delta = 171.6, 166.1, 155.8, 143.5, 132.6, 127.5, 126.5, 77.9, 53.6, 49.6, 45.4, 45.2, 43.1, 38.2, 36.8, 34.4, 33.3, 32.9, 32.7, 29.4, 28.9, 26.1, 25.8$  (2x), 23.0 ppm.
- **MS (ESI pos.):**  $m/z$  (%) = 579.31 (100) ([M+H]<sup>+</sup>, calcd. 579.32), 601.29 (63) ([M+Na]<sup>+</sup>, calcd. 601.30).

**4-(Aminomethyl)-N-((S)-4-cyclohexyl-1-(((SR)-1-(methylsulfonyl)piperidin-3-yl)amino)-1-oxobutan-2-yl)benzamide (292, SR322)**

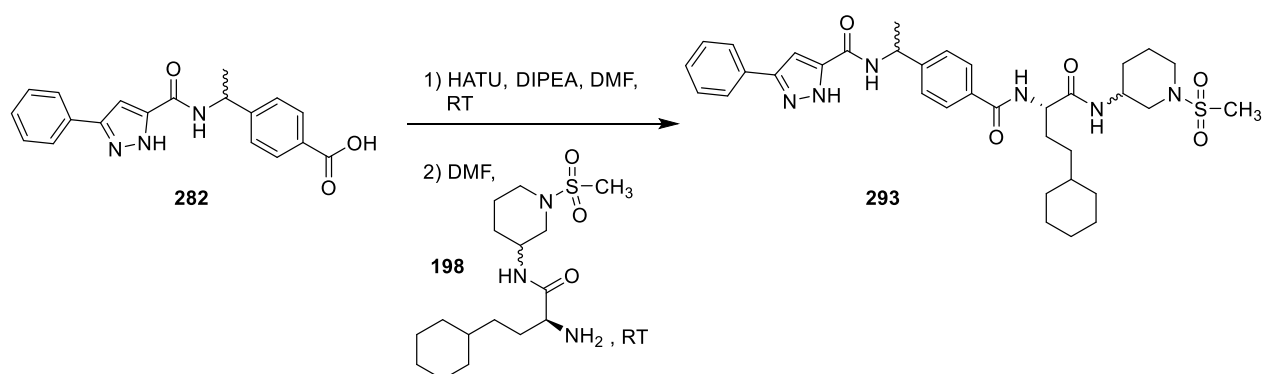


*tert*-Butyl 4-(((*S*)-4-cyclohexyl-1-(((*SR*)-1-(methylsulfonyl)piperidin-3-yl)amino)-1-oxobutan-2-yl)carbamoyl)benzyl carbamate (**291**, 350 mg, 0.605 mmol) was dissolved in DCM (10 mL) and cooled to 0 °C. TFA (2 mL) was added dropwise and the mixture was stirred for 30 min at RT. The solvent was removed under reduced pressure and the crude product was dissolved in MeOH. The mixture was cooled to 5 °C and neutralized with K<sub>2</sub>CO<sub>3</sub> (3.6 g, 26.0 mmol). After 10 min of stirring, the mixture was filtrated and the solvent was removed under reduced pressure. The crude product was used without further purification.

**Yield:** 290 mg (0.605 mmol, quant.), yellowish solid.

### 8.5.2 Synthesis of final compounds

**N-((SR)-1-(4-(((S)-4-Cyclohexyl-1-(((SR)-1-(methylsulfonyl)piperidin-3-yl)amino)-1-oxobutan-2-yl)carbamoyl)phenyl)ethyl)-3-phenyl-1H-pyrazole-5-carboxamide carboxamide (293, SR262)**



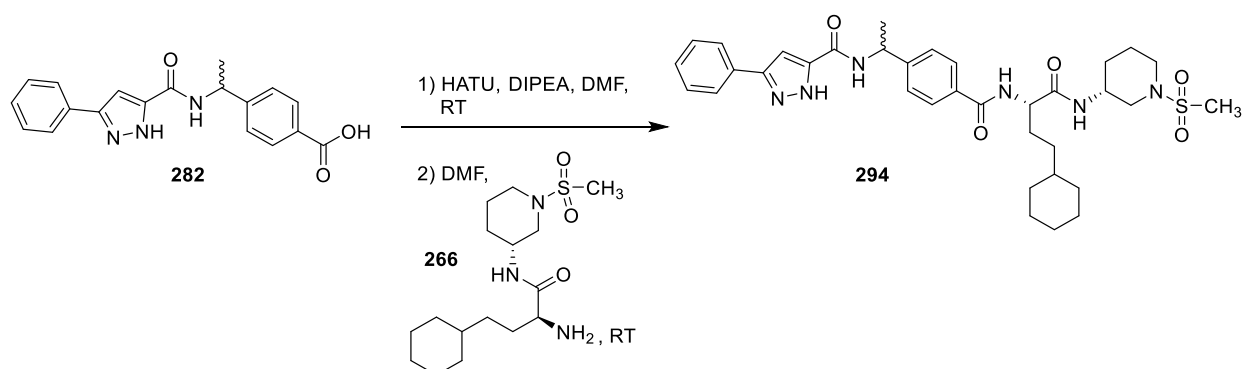
4-(1-(3-Phenyl-1*H*-pyrazole-5-carboxamido)ethyl)benzoic acid (**282**, 200 mg, 0.597 mmol) and HATU (309 mg, 0.716 mmol) were dissolved in DMF (5 mL) and DIPEA (105 mg, 0.716 mmol) was added. The solution was stirred for 1.5 h at RT and (*S*)-2-amino-4-cyclohexyl-*N*-((*SR*)-1-(methylsulfonyl)piperidin-3-yl)butanamide (**198**, 281 mg, 0.716 mmol), diluted in DMF (5 mL), was added. The mixture was stirred for 20 h at RT. DCM (100 mL) was added and the organic phase was washed 4 times with H<sub>2</sub>O (100 mL) and dried over MgSO<sub>4</sub>. The solvent was evaporated under reduced pressure and the crude product was purified using flashcolumn chromatography on silica (cyclohexane/EtOAc 1:3 → EtOAc).

**Yield:** 89 mg (0.13 mmol, 30%), colorless solid.

- **TLC:** R<sub>f</sub> = 0.70 (SiO<sub>2</sub>, EtOAc/MeOH 1:10).
- **C<sub>35</sub>H<sub>46</sub>N<sub>6</sub>O<sub>5</sub>S:** (662.84), [662.33].

- **HPLC:** (mixture of diastereomers)  $t_{R,1} = 14.75$  min;  $t_{R,2} = 15.02$  min.
- **$^1\text{H-NMR}$  (400 MHz, DMSO- $d_6$ , 300 K):** (mixture of diastereomers)  $\delta = 13.64$  (br s, 1H, H-1 pyrazole), 8.97–8.76 (m, 0.4H,  $\text{NHCHC}_{Ar}$ ), 8.66–8.45 (m, 0.6H,  $\text{NHCHC}_{Ar}$ ), 8.30 (d,  $^3J = 7.6$  Hz, 1H,  $\text{NHCHCO}$ ), 8.04–7.93 (m, 1H,  $\text{NHCH}$  piperidine), 7.89–7.82 (m, 2H, H-3-, H-5-benzyl), 7.80 (d,  $^3J = 7.2$  Hz, 2H, H-2-, H-6-phenyl), 7.54–7.29 (m, 5.4H, H-3-, H-4-, H-5-phenyl, H-2-, H-6-benzyl, CH pyrazol), 7.06 (s, 0.6H, CH pyrazol), 5.20 (p,  $^3J = 7.6$  Hz, 1H,  $\text{CH}_3\text{CH}$ ), 4.45–4.33 (m, 1H,  $\text{NHCHCO}$ ), 3.81–3.66 (m, 1H, CH piperidine), 3.54–3.40 (m, 1H,  $\text{CH}_A\text{H}_B$ -2 piperidine), 3.39–3.27 (m, 1H,  $\text{CH}_A\text{H}_B$ -2 piperidine), 2.85 (s, 3H,  $\text{SO}_2\text{CH}_3$ ), 2.81–2.70 (m, 1H,  $\text{CH}_A\text{H}_B$ -6 piperidine), 2.59–2.51 (m, 1H,  $\text{CH}_A\text{H}_B$ -6 piperidine), 1.85–1.46 (m, 13H,  $\text{CH}_2$ -4-,  $\text{CH}_2$ -5-piperidine,  $\text{NHCHCH}_A\text{H}_B$ , H-2 $_{eq^-}$ , H-3 $_{eq^-}$ , H-4 $_{eq^-}$ , H-5 $_{eq^-}$ , H-6 $_{eq^-}$ -cyclohexyl,  $\text{CHCH}_3$ ), 1.44–1.31 (m, 1H,  $\text{NHCHCH}_A\text{H}_B$ ), 1.29–1.05 (m, 6H, H-1-, H-3 $_{ax^-}$ , H-4 $_{ax^-}$ , H-5 $_{ax^-}$ -cyclohexyl,  $\text{NHCHCH}_2\text{CH}_2$ ), 0.92–0.72 (m, 2H, H-2 $_{ax^-}$ , H-6 $_{ax^-}$ -cyclohexyl) ppm.
- **$^{13}\text{C-NMR}$  (101 MHz, DMSO- $d_6$ , 300 K):** (mixture of diastereomers)  $\delta = 171.6, 166.2, 161.9, 147.7, 144.9, 132.7, 129.1, 128.8, 127.9, 127.7, 127.6, 126.0, 125.4, 102.8, 53.5, 53.4, 49.6, 49.4, 45.4, 45.2, 45.1, 36.8, 34.4, 33.3$  (2x), 32.9 (2x), 32.7, 29.4, 28.9, 28.7, 26.1, 25.8 (2x), 23.0 (2x), 22.0 (2x) ppm.
- **MS (ESI neg.):**  $m/z$  (%) = 707.29 (93) ( $[\text{M}+\text{EtOH}-\text{H}]^-$ , calcd. 707.36), 661.29 (100) ( $[\text{M}-\text{H}]^-$ , calcd. 661.32), 418.17 (30) ( $[\text{M}_{fr.}+\text{EtOH}-\text{H}]^-$ , calcd. 418.23), 372.19 (42) ( $[\text{M}_{fr.}]^-$ , calcd. 372.20).
- **HRMS (FTMS + p MALDI):**  $m/z = 685.3138$   $[\text{M}+\text{Na}]^+$ , calcd. for  $[\text{C}_{35}\text{H}_{46}\text{N}_6\text{NaO}_5\text{S}]^+ = 685.3148$ .

***N*-((*SR*)-1-(4-(((*S*)-4-Cyclohexyl-1-(((*R*)-1-(methylsulfonyl)piperidin-3-yl)amino)-1-oxobutan-2-yl)carbamoyl)phenyl)ethyl)-3-phenyl-1*H*-pyrazole-5-carboxamide (**294**, *SR264*)**



(*SR*)-4-(1-(3-Phenyl-1*H*-pyrazole-5-carboxamido)ethyl)benzoic acid (**282**, 200 mg, 0.597 mmol) and HATU (309 mg, 0.716 mmol) were dissolved in DMF (5 mL) and DIPEA (105 mg, 0.716 mmol) was added. The solution was stirred for 1.5 h at RT and (*S*)-2-amino-4-cyclohexyl-*N*-((*R*)-1-(methylsulfonyl)piperidin-3-yl)butanamide (**266**, 281 mg, 0.716 mmol), diluted in DMF (5 mL), was added. The mixture was stirred for 20 h at RT. DCM (100 mL) was added and the organic phase was washed 4 times with  $\text{H}_2\text{O}$  (100 mL) and dried over  $\text{MgSO}_4$ . The solvent was evaporated under reduced pressure and the crude product was purified using flashcolumn chromatography on silica (cyclohexane/EtOAc 1:1  $\rightarrow$  1:3  $\rightarrow$  1:20).

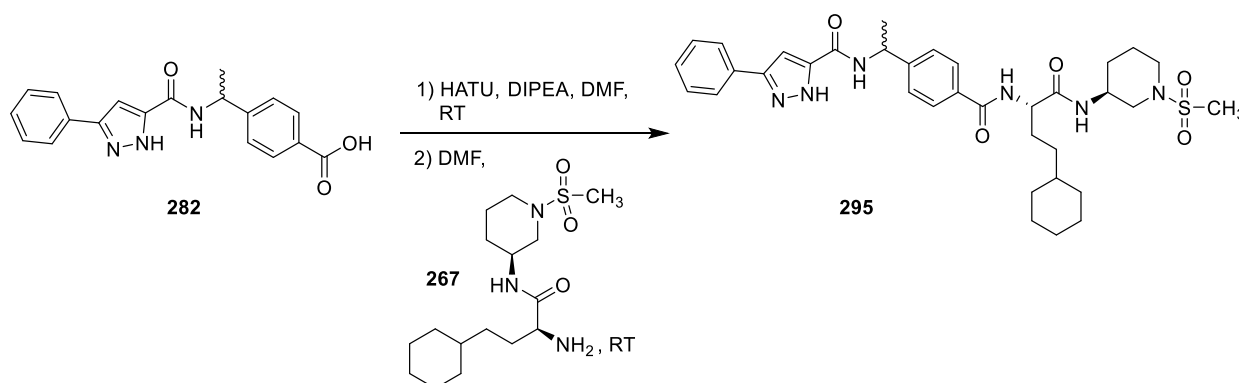
**Yield:** 102 mg (0.154 mmol, 34%), colorless solid.

- **TLC:**  $R_f = 0.63$  ( $\text{SiO}_2$ , EtOAc/MeOH 1:10).
- **$\text{C}_{35}\text{H}_{46}\text{N}_6\text{O}_5\text{S}$ :** (662.84), [662.33].
- **HPLC:** (mixture of diastereomers)  $t_R = 14.73$  min.



- **$^1\text{H-NMR}$  (600 MHz, DMSO- $d_6$ , 300 K):** (mixture of diastereomers)  $\delta$  = 13.68–13.56 (m, 1H, H-1 pyrazole), 8.94–8.82 (m, 0.4H,  $\text{NHCHC}_{\text{Ar}}$ ), 8.63–8.51 (m, 0.6H,  $\text{NHCHC}_{\text{Ar}}$ ), 8.35–8.26 (m, 1H,  $\text{NHCHCO}$ ), 7.99 (d,  $^3J$  = 7.9 Hz, 1H,  $\text{NHCH}$  piperidine), 7.88–7.81 (m, 2H, H-3-, H-5-benzyl), 7.79 (d,  $^3J$  = 7.7 Hz, 2H, H-2-, H-6-phenyl), 7.51–7.29 (m, 5.4H, H-3-, H-4-, H-5-phenyl, H-2-, H-6-benzyl, CH pyrazole), 7.06 (s, 0.6H, CH pyrazole), 5.20 (p,  $^3J$  = 7.4 Hz, 1H,  $\text{CH}_3\text{CH}$ ), 4.44–4.36 (m, 1H,  $\text{NHCHCO}$ ), 3.76–3.67 (m, 1H, CH piperidine), 3.46–3.41 (m, 1H,  $\text{CH}_\text{A}\text{H}_\text{B}$ -2 piperidine), 3.34–3.27 (m, 1H,  $\text{CH}_\text{A}\text{H}_\text{B}$ -2 piperidine), 2.84 (s, 3H,  $\text{SO}_2\text{CH}_3$ ), 2.80–2.77 (m, 1H,  $\text{CH}_\text{A}\text{H}_\text{B}$ -6 piperidine), 2.58–2.51 (m, 1H,  $\text{CH}_\text{A}\text{H}_\text{B}$ -6 piperidine), 1.84–1.33 (m, 14H,  $\text{CH}_2$ -4-,  $\text{CH}_2$ -5-piperidine,  $\text{NHCHCH}_2$ , H-2 $_{\text{eq}}$ -, H-3 $_{\text{eq}}$ -, H-4 $_{\text{eq}}$ -, H-5 $_{\text{eq}}$ -, H-6 $_{\text{eq}}$ -cyclohexyl,  $\text{CHCH}_3$ ), 1.30–1.05 (m, 6H, H-1-, H-3 $_{\text{ax}}$ -, H-4 $_{\text{ax}}$ -, H-5 $_{\text{ax}}$ -cyclohexyl,  $\text{NHCHCH}_2\text{CH}_2$ ), 0.90–0.77 (m, 2H, H-2 $_{\text{ax}}$ -, H-6 $_{\text{ax}}$ -cyclohexyl) ppm.
- **$^{13}\text{C-NMR}$  (150 MHz, DMSO- $d_6$ , 300 K):** (mixture of diastereomers)  $\delta$  = 171.6, 166.1, 160.7, 148.2, 147.8, 143.4, 132.6, 129.0 (2x), 127.5, 125.9, 125.3 (2x), 125.0, 102.1, 53.4, 49.4, 45.3, 45.1, 45.0, 36.8, 34.3, 33.2, 32.9, 32.6, 29.4, 28.6, 26.1, 25.8, 23.0, 21.9 (2x) ppm.
- **MS (ESI neg.):**  $m/z$  (%) = 707.32 (48) ( $[\text{M}+\text{EtOH}-\text{H}]^-$ , calcd. 707.36), 661.31 (41) ( $[\text{M}-\text{H}]^-$ , calcd. 661.32), 418.19 (57) ( $[\text{M}_{\text{fr.}}+\text{EtOH}-\text{H}]^-$ , calcd. 418.23), 372.19 (100) ( $[\text{M}_{\text{fr.}}]^-$ , calcd. 372.20).
- **HRMS (FTMS + p MALDI):**  $m/z$  = 685.3144  $[\text{M}+\text{Na}]^+$ , calcd. for  $[\text{C}_{35}\text{H}_{46}\text{N}_6\text{NaO}_5\text{S}]^+$  = 685.3148.

***N-((SR)-1-(4-(((S)-4-Cyclohexyl-1-(((S)-1-(methylsulfonyl)piperidin-3-yl)amino)-1-oxobutan-2-yl)carbamoyl)phenyl)ethyl)-3-phenyl-1H-pyrazole-5-carboxamide (295, SR265)***



4-(1-(3-Phenyl-1H-pyrazole-5-carboxamido)ethyl)benzoic acid (**282**, 200 mg, 0.597 mmol) and HATU (272 mg, 0.716 mmol) were dissolved in DMF (5 mL) and DIPEA (93 mg, 0.72 mmol) was added. The solution was stirred for 1.5 h at RT and (*S*)-2-amino-4-cyclohexyl-*N*-((*S*)-1-(methylsulfonyl)piperidin-3-yl)butanamide (**267**, 248 mg, 0.716 mmol), diluted in DMF (5 mL), was added. The mixture was stirred for 20 h at RT. DCM (100 mL) was added and the organic phase was washed 4 times with  $\text{H}_2\text{O}$  (100 mL) and dried over  $\text{MgSO}_4$ . The solvent was evaporated under reduced pressure and the crude product was purified using flashcolumn chromatography on silica (cyclohexane/EtOAc 1:1  $\rightarrow$  1:3  $\rightarrow$  1:20).

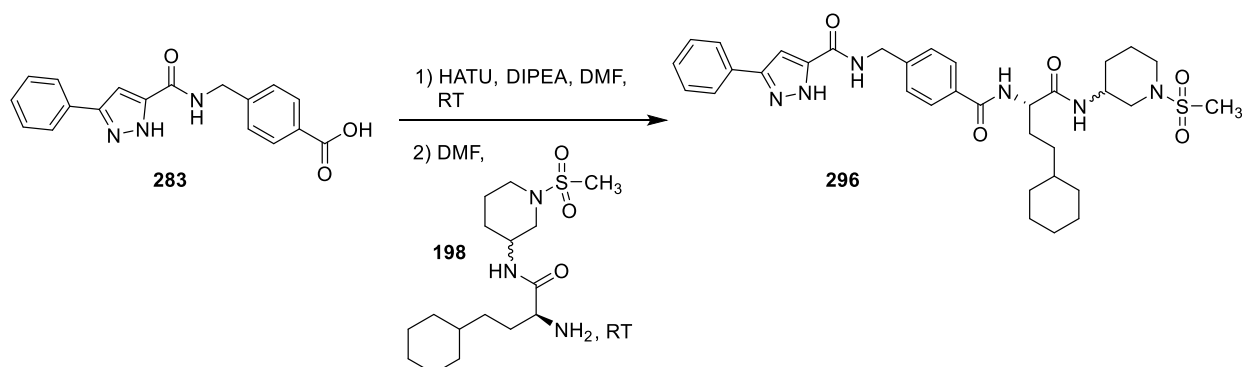
**Yield:** 121 mg (0.183 mmol, 41%), colorless solid.

- **TLC:**  $R_f$  = 0.07 ( $\text{SiO}_2$ , cyclohexane/EtOAc 1:3).
- **$\text{C}_{35}\text{H}_{46}\text{N}_6\text{O}_5\text{S}$ :** (662.84), [662.33].
- **HPLC:** (mixture of diastereomers)  $t_R$  = 15.01 min.
- **$^1\text{H-NMR}$  (600 MHz, DMSO- $d_6$ , 300 K):** (mixture of diastereomers)  $\delta$  = 13.66–13.57 (m, 1H, H-1 pyrazol), 8.88 (d,  $^3J$  = 8.0 Hz, 0.4H,  $\text{NHCHC}_{\text{Ar}}$ ), 8.56 (d,  $^3J$  = 8.4 Hz, 0.6H,  $\text{NHCHC}_{\text{Ar}}$ ), 8.34–8.27 (m, 1H,  $\text{NHCHCO}$ ), 8.03–7.96 (m, 1H,  $\text{NHCH}$  piperidine), 7.89–7.82 (m, 2H, H-3-, H-5-benzyl), 7.80 (d,  $^3J$  = 7.6

Hz, 2H, H-2-, H-6-phenyl), 7.52–7.42 (m, 4H, H-3-, H-5-phenyl, H-2-, H-6-benzyl), 7.40–7.30 (m, 1.4H, H-4 phenyl, CH pyrazole), 7.06 (s, 0.6H, CH pyrazole), 5.20 (p,  $^3J = 7.3$  Hz, 1H, CH<sub>3</sub>CH), 4.39 (q,  $^3J = 8.0$  Hz, 1H, NHCHCO), 3.77–3.67 (m, 1H, CH piperidine), 3.52–3.46 (m, 1H, CH<sub>A</sub>H<sub>B</sub>-2 piperidine), 3.37–3.31 (m, 1H, CH<sub>A</sub>H<sub>B</sub>-2 piperidine), 2.85 (s, 3H, SO<sub>2</sub>CH<sub>3</sub>), 2.78–2.71 (m, 1H, CH<sub>A</sub>H<sub>B</sub>-6 piperidine), 2.56–2.49 (m, 1H, CH<sub>A</sub>H<sub>B</sub>-6 piperidine), 1.81–1.46 (m, 13H, CH<sub>2</sub>-4-, CH<sub>2</sub>-5-piperidine, NHCHCH<sub>A</sub>H<sub>B</sub>, H-2<sub>eq</sub>-, H-3<sub>eq</sub>-, H-4<sub>eq</sub>-, H-5<sub>eq</sub>-, H-6<sub>eq</sub>-cyclohexyl, CHCH<sub>3</sub>), 1.39–1.30 (m, 1H, NHCHCH<sub>A</sub>H<sub>B</sub>), 1.28–1.04 (m, 6H, H-1-, H-3<sub>ax</sub>-, H-4<sub>ax</sub>-, H-5<sub>ax</sub>-cyclohexyl, NHCHCH<sub>2</sub>CH<sub>2</sub>), 0.89–0.79 (m, 2H, H-2<sub>ax</sub>-, H-6<sub>ax</sub>-cyclohexyl) ppm.

- **<sup>13</sup>C-NMR (150 MHz, DMSO-d<sub>6</sub>, 300 K):** (mixture of diastereomers)  $\delta = 171.6, 166.1, 161.0, 148.2, 147.8, 143.5, 132.6, 129.1, 128.8, 128.4, 127.5, 125.9, 125.8, 125.4, 125.0, 102.8, 102.2, 53.5, 49.5, 47.7, 45.3, 45.2, 36.8, 34.4, 33.2, 32.9, 32.7, 29.4, 28.9, 26.1, 25.8, 25.7, 23.0, 21.9$  ppm.
- **MS (ESI neg.):**  $m/z$  (%) = 707.35 (71) ([M+EtOH-H]<sup>-</sup>, calcd. 707.36), 661.26 (100) ([M-H]<sup>-</sup>, calcd. 661.31), 372.24 (65) ([M<sub>fr.</sub>]<sup>-</sup>, calcd. 372.20).
- **HRMS (FTMS + p MALDI):**  $m/z = 685.3140$  [M+Na]<sup>+</sup>, calcd. for [C<sub>35</sub>H<sub>46</sub>N<sub>6</sub>NaO<sub>5</sub>S]<sup>+</sup> = 685.3148.

***N*-(4-(((*S*)-4-Cyclohexyl-1-(((*S*R)-1-(methylsulfonyl)piperidin-3-yl)amino)-1-oxobutan-2-yl)carbamoyl)benzyl)-3-phenyl-1H-pyrazole-5-carboxamide (296, SR275)**



4-((3-Phenyl-1H-pyrazole-5-carboxamido)methyl)benzoic acid (**283**, 200 mg, 0.622 mmol) and HATU (284 mg, 0.747 mmol) were dissolved in DMF (5 mL) and DIPEA (96 mg, 0.75 mmol) was added. The solution was stirred for 1.5 h at RT and (*S*)-2-amino-4-cyclohexyl-*N*-(((*S*R)-1-(methylsulfonyl)piperidin-3-yl)butanamide (**198**, 258 mg, 0.747 mmol), diluted in DMF (5 mL), was added. The mixture was stirred for 20 h at RT. DCM (100 mL) was added and the organic phase was washed 4 times with H<sub>2</sub>O (100 mL) and dried over MgSO<sub>4</sub>. The solvent was evaporated under reduced pressure and the crude product was purified using flashcolumn chromatography on silica (cyclohexane/EtOAc 1:1 → 1:3 → 1:20 → EtOAc).

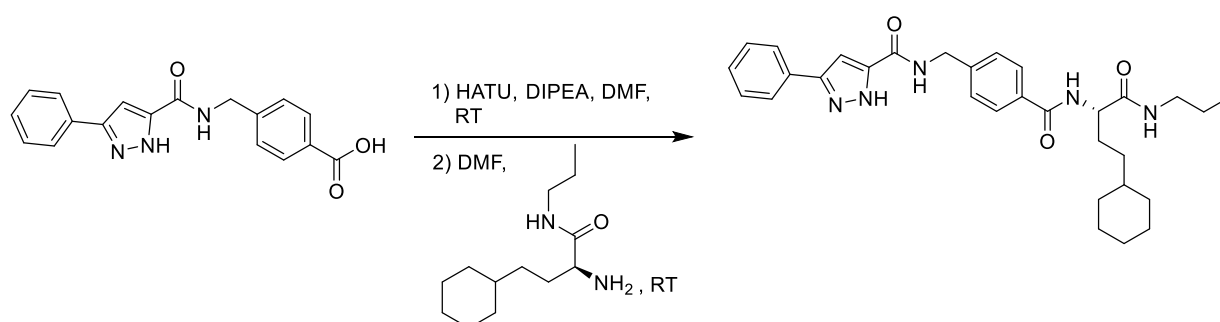
**Yield:** 113 mg (0.174 mmol, 28%), colorless solid.

- **TLC:**  $R_f = 0.44$  (SiO<sub>2</sub>, cyclohexane/ EtOAc 1:10).
- **C<sub>34</sub>H<sub>44</sub>N<sub>6</sub>O<sub>5</sub>S:** (648.82), [648.31].
- **HPLC:** (mixture of diastereomers)  $t_{R,1} = 14.60$  min;  $t_{R,2} = 14.98$  min.
- **<sup>1</sup>H-NMR (600 MHz, DMSO-d<sub>6</sub>, 300 K):** (mixture of diastereomers)  $\delta = 13.68$  (br s, 1H, H-1 pyrazole), 8.86 (br s, 1H, NHCH<sub>2</sub>), 8.32 (d,  $^3J = 8.0$  Hz, 1H, NHCHCO), 8.01 (d,  $^3J = 7.6$  Hz, 1H, NHCH piperidine), 7.91–7.71 (m, 4H, H-3-, H-5-benzyl, H-2-, H-6-phenyl), 7.54–7.29 (m, 5H, H-3-, H-4-, H-5-phenyl, H-2-, H-6-benzyl), 7.12 (br s, 1H, CH pyrazole), 4.60–4.32 (m, 3H, CH<sub>2</sub> benzyl, NHCHCO), 3.82–3.64 (m, 1H, CH piperidine), 3.55–3.41 (m, 1H, CH<sub>A</sub>H<sub>B</sub>-2 piperidine), 3.37–3.24 (m, 1H, CH<sub>A</sub>H<sub>B</sub>-2 piperidine),

2.85 (s, 3H, SO<sub>2</sub>CH<sub>3</sub>), 2.82–2.70 (m, 1H, CH<sub>A</sub>H<sub>B</sub>-6 piperidine), 2.60–2.53 (m, 1H, CH<sub>A</sub>H<sub>B</sub>-6 piperidine), 1.85–1.46 (m, 10H, CH<sub>2</sub>-4-, CH<sub>2</sub>-5-piperidine, NHCHCH<sub>A</sub>H<sub>B</sub>, H-2<sub>eq</sub>-, H-3<sub>eq</sub>-, H-4<sub>eq</sub>-, H-5<sub>eq</sub>-, H-6<sub>eq</sub>-cyclohexyl), 1.44–1.31 (m, 1H, NHCHCH<sub>A</sub>H<sub>B</sub>), 1.26–1.02 (m, 6H, H-1-, H-3<sub>ax</sub>-, H-4<sub>ax</sub>-, H-5<sub>ax</sub>-cyclohexyl, NHCHCH<sub>2</sub>CH<sub>2</sub>), 0.90–0.76 (m, 2H, H-2<sub>ax</sub>-, H-6<sub>ax</sub>-cyclohexyl) ppm.

- **<sup>13</sup>C-NMR (150 MHz, DMSO-d<sub>6</sub>, 300 K):** (mixture of diastereomers) δ = 171.6, 166.0, 162.1, 149.5, 143.9, 132.7, 128.9, 127.5, 126.9, 125.2, 102.9, 53.6, 53.4, 49.5, 49.4, 45.3, 45.3, 45.2, 45.1, 41.8, 36.8, 34.4, 34.3, 33.2, 32.9, 32.6, 29.4, 28.9, 28.6, 26.1, 25.7, 22.9 ppm.
- **MS (ESI neg.):** *m/z* (%) = 647.22 (100) ([M-H]<sup>-</sup>, calcd. 647.30).
- **HRMS (FTMS + p MALDI):** *m/z* = 671.2980 [M+Na]<sup>+</sup>, calcd. for [C<sub>34</sub>H<sub>44</sub>N<sub>6</sub>NaO<sub>5</sub>S]<sup>+</sup> = 671.2992.

**(S)-N-(4-((4-Cyclohexyl-1-oxo-1-(propylamino)butan-2-yl)carbamoyl)benzyl)-3-phenyl-1H-pyrazole-5-carboxamide (297, SR278)**



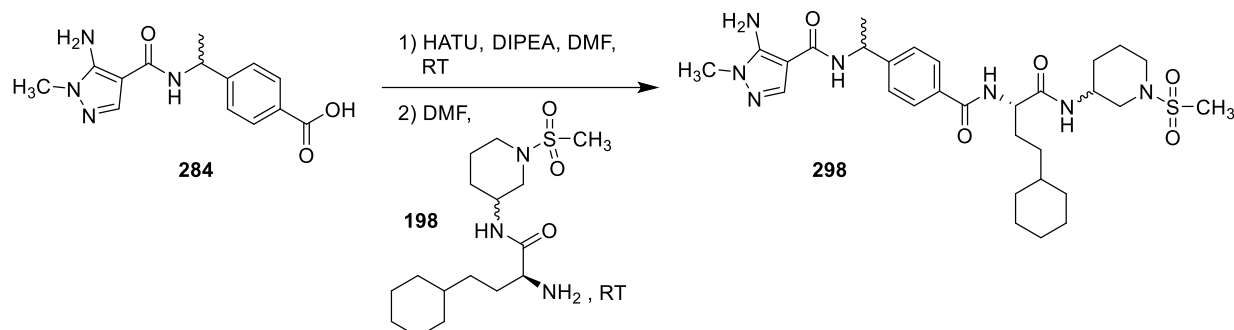
4-((3-Phenyl-1H-pyrazole-5-carboxamido)methyl)benzoic acid (**283**, 200 mg, 0.622 mmol) and HATU (284 mg, 0.747 mmol) were dissolved in DMF (5 mL) and DIPEA (96 mg, 0.75 mmol) was added. The solution was stirred for 1.5 h at RT (S)-2-amino-4-cyclohexyl-N-propylbutanamide (**186**, 169 mg, 0.747 mmol), diluted in DMF (5 mL), was added. The mixture was stirred for 20 h at RT. DCM (100 mL) was added and the organic phase was washed 4 times with H<sub>2</sub>O (150 mL), once with a NaCl solution (sat., 50 mL) and dried over MgSO<sub>4</sub>. The solvent was evaporated under reduced pressure and the crude product was precipitated from EtOAc.

**Yield:** 197mg (0.372 mmol, 60%), colorless solid.

- **TLC:** R<sub>f</sub> = 0.34 (SiO<sub>2</sub>, cyclohexane/ EtOAc 1:3).
- **C<sub>31</sub>H<sub>39</sub>N<sub>5</sub>O<sub>3</sub>:** (529.67), [529.31].
- **HPLC:** t<sub>R</sub> = 15.23 min.
- **<sup>1</sup>H-NMR (250 MHz, DMSO-d<sub>6</sub>, 300 K):** (mixture of rotamers) δ = 13.67 (s, 1H, H-1 pyrazole), 9.18–9.02 (m, 0.4H, NHCH<sub>2</sub>Ar), 8.89–8.73 (m, 0.6H, NHCH<sub>2</sub>Ar), 8.26 (d, <sup>3</sup>J = 7.9 Hz, 1H, NHCHCO), 7.98–7.71 (m, 5H, NHCH<sub>2</sub>CH<sub>2</sub>, H-3-, H-5-benzyl, H-2-, H-6-phenyl), 7.55–7.25 (m, 5.4H, H-3-, H-4-, H-5-phenyl, H-2-, H-6-benzyl, CH pyrazole), 7.09 (s, 0.6H, CH pyrazole), 4.60–4.42 (m, 2H, CH<sub>2</sub> benzyl), 4.41–4.28 (m, 1H, NHCHCO), 3.15–2.90 (m, 2H, NHCH<sub>2</sub>CH<sub>2</sub>), 1.80–1.51 (m, 7H, NHCHCH<sub>2</sub>, H-2<sub>eq</sub>-, H-3<sub>eq</sub>-, H-4<sub>eq</sub>-, H-5<sub>eq</sub>-, H-6<sub>eq</sub>-cyclohexyl), 1.40 (sext., <sup>3</sup>J = 7.3 Hz, 2H, NHCH<sub>2</sub>CH<sub>2</sub>), 1.28–1.04 (m, 6H, H-1-, H-3<sub>ax</sub>-, H-4<sub>ax</sub>-, H-5<sub>ax</sub>-cyclohexyl, NHCHCH<sub>2</sub>CH<sub>2</sub>), 0.92–0.72 (m, 5H, CH<sub>3</sub>, H-2<sub>ax</sub>-, H-6<sub>ax</sub>-cyclohexyl) ppm.
- **<sup>13</sup>C-NMR (126 MHz, DMSO-d<sub>6</sub>, 300 K):** (mixture of rotamers) δ = 171.7, 166.0, 161.8, 147.7, 143.5, 143.3, 132.7, 129.1, 128.8, 128.5, 127.6, 126.9, 125.3, 125.1, 102.8, 53.7, 41.8, 36.8, 33.3, 32.9, 32.7, 29.4, 26.2, 25.8 (2x), 22.3, 11.4 ppm.
- **MS (ESI neg.):** *m/z* (%) = 528.14 (100) ([M-H]<sup>-</sup>, calcd. 528.30).

- **HRMS (FTMS + p MALDI):**  $m/z$  552.2922  $[M+Na]^+$ , calcd. for  $[C_{31}H_{39}N_5NaO_3]^+$  = 552.2945.

**5-Amino-N-((SR)-1-(4-(((S)-4-cyclohexyl-1-((SR)-1-(methylsulfonyl)piperidin-3-yl)amino)-1-oxobutan-2-yl)carbamoyl)phenyl)ethyl)-1-methyl-1H-pyrazole-4-carboxamide (298, SR277)**

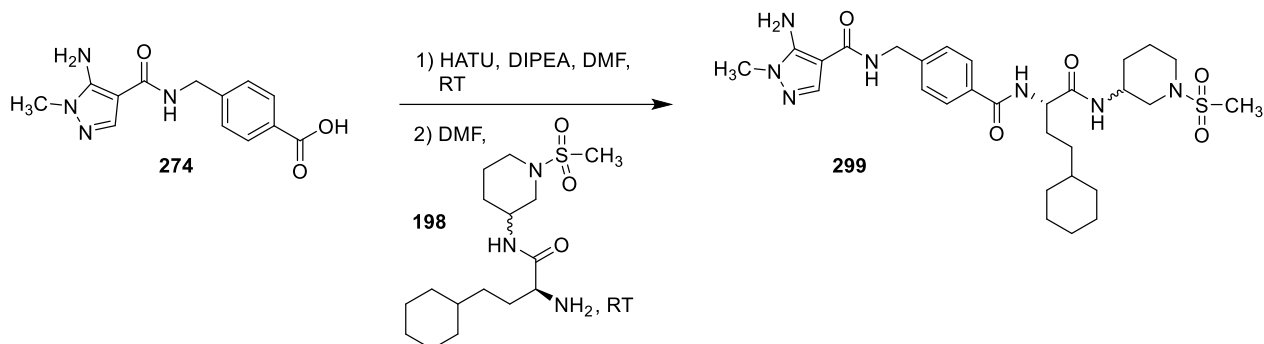


4-(1-(5-Amino-1-methyl-1H-pyrazole-4-carboxamido)ethyl)benzoic acid (**284**, 125 mg, 0.404 mmol) and HATU (184 mg, 0.485 mmol) were dissolved in DMF (5 mL) and DIPEA (63 mg, 0.40 mmol) was added. The solution was stirred for 1.5 h at RT (*S*)-2-amino-4-cyclohexyl-N-((*SR*)-1-(methylsulfonyl)piperidin-3-yl)butanamide (**198**, 168 mg, 0.485 mmol), diluted in DMF (5 mL) was added. The mixture was stirred for 20 h at RT. DCM (100 mL) was added and the organic phase was washed 3 times with H<sub>2</sub>O (100 mL), once with a NaCl solution (sat., 50 mL) and dried over MgSO<sub>4</sub>. The solvent was evaporated under reduced pressure and the crude product was purified using flashcolumn chromatography on silica (cyclohexane/EtOAc 1:1 → EtOAc → EtOAc/MeOH 10:1).

**Yield:** 162 mg (0.263 mmol, 65%), colorless solid.

- **TLC:**  $R_f$  = 0.24 (SiO<sub>2</sub>, EtOAc/MeOH 10:1).
- **C<sub>30</sub>H<sub>45</sub>N<sub>7</sub>O<sub>5</sub>S:** (615.79), [615.32].
- **HPLC:** (mixture of diastereomers)  $t_{R,1}$  = 13.06 min;  $t_{R,2}$  = 13.35 min.
- **<sup>1</sup>H-NMR (600 MHz, DMSO-d<sub>6</sub>, 300 K):** (mixture of diastereomers)  $\delta$  = 8.28 (d,  $^3J$  = 8.1 Hz, 1H, NHCHCO), 8.02 (d,  $^3J$  = 7.8 Hz, 1H, NHCHCH<sub>3</sub>), 7.99 (d,  $^3J$  = 8.0 Hz, 1H, NHCH piperidine), 7.82 (dt,  $^3J$  = 8.4, 2.6 Hz, 2H, H-3-, H-5-benzyl), 7.77 (s, 1H, CH pyrazole), 7.40 (d,  $^3J$  = 8.4 Hz, 2H, H-2-, H-6-benzyl), 6.10 (s, 2H, NH<sub>2</sub>), 5.11 (p,  $^3J$  = 7.3 Hz, 1H, CHCH<sub>3</sub>), 4.43–4.35 (m, 1H, NHCHCO), 3.80–3.68 (m, 1H, CH piperidine), 3.52–3.47 (m, 1H, CH<sub>A</sub>H<sub>B</sub>-2 piperidine), 3.49 (s, 3H, NCH<sub>3</sub>), 3.46–3.42 (m, 1H, CH<sub>A</sub>H<sub>B</sub>-2 piperidine), 2.86–2.68 (m, 4H, SO<sub>2</sub>CH<sub>3</sub>, CH<sub>A</sub>H<sub>B</sub>-6 piperidine), 2.57–2.48 (m, 1H, CH<sub>A</sub>H<sub>B</sub>-6 piperidine), 1.84–1.48 (m, 10H, CH<sub>2</sub>-4-, CH<sub>2</sub>-5-piperidine, NHCHCH<sub>A</sub>H<sub>B</sub>, H-2<sub>eq</sub>-, H-3<sub>eq</sub>-, H-4<sub>eq</sub>-, H-5<sub>eq</sub>-, H-6<sub>eq</sub>-cyclohexyl), 1.42 (d,  $^3J$  = 7.1 Hz, 3H, CHCH<sub>3</sub>), 1.45–1.30 (m, 1H, NHCHCH<sub>A</sub>H<sub>B</sub>), 1.28–1.05 (m, 6H, H-1-, H-3<sub>ax</sub>-, H-4<sub>ax</sub>-, H-5<sub>ax</sub>-cyclohexyl, NHCHCH<sub>2</sub>CH<sub>2</sub>), 0.92–0.78 (m, 2H, H-2<sub>ax</sub>-, H-6<sub>ax</sub>-cyclohexyl) ppm.
- **<sup>13</sup>C-NMR (150 MHz, DMSO-d<sub>6</sub>, 300 K):** (mixture of diastereomers)  $\delta$  = 171.6 (2x), 166.2, 166.1, 163.4, 149.4, 148.9, 136.2, 132.4, 127.4, 125.7, 113.7, 96.7, 53.5, 53.4, 49.5, 49.4, 49.2, 47.1, 45.4 (2x), 45.2, 45.1, 36.9, 36.8, 34.4, 34.3, 33.8, 33.2, 32.9, 32.6, 29.4, 28.9, 28.6, 26.1 (2x), 26.1 (2x), 25.8 (2x), 25.7, 23.0 (2x), 22.3, 22.2 ppm.
- **MS (ESI pos.):**  $m/z$  (%) = 616.22 (100) ( $[M+H]^+$ , calcd. 616.33), 438.14 (37) ( $[M_{fr.}]^+$ , calcd. 438.25).
- **HRMS (FTMS + p MALDI):**  $m/z$  638.3092  $[M+Na]^+$ , calcd. for  $[C_{30}H_{45}N_7NaO_5S]^+$  = 638.3101.

**5-Amino-N-(4-(((S)-4-cyclohexyl-1-(((SR)-1-(methylsulfonyl)piperidin-3-yl)amino)-1-oxobutan-2-yl)carbamoyl)benzyl)-1-methyl-1H-pyrazole-4-carboxamide (299, SR276)**

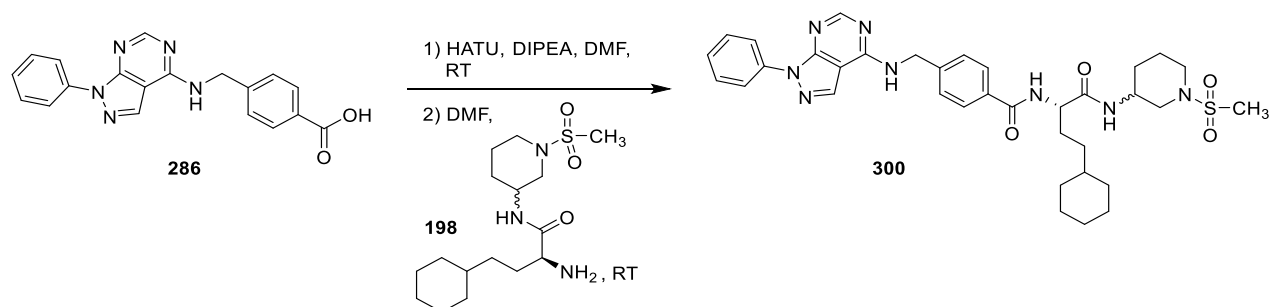


4-((5-Amino-1-methyl-1H-pyrazole-4-carboxamido)methyl)benzoic acid (**274**, 200 mg, 0.729 mmol) and HATU (333 mg, 0.875 mmol) were dissolved in DMF (5 mL) and DIPEA (113 mg, 0.875 mmol) was added. The solution was stirred for 1.5 h at RT (*S*)-2-amino-4-cyclohexyl-*N*-((*SR*)-1-(methylsulfonyl)piperidin-3-yl)butanamide (**198**, 302 mg, 0.875 mmol), diluted in DMF (5 mL), was added. The mixture was stirred for 20 h at RT. DCM (100 mL) was added and the organic phase was washed 4 times with H<sub>2</sub>O (100 mL) and dried over MgSO<sub>4</sub>. The solvent was evaporated under reduced pressure and the crude product was triturated with EtOAc/cyclohexane (1:1) and recrystallized from DCM.

**Yield:** 281 mg (0.467 mmol, 64%), colorless solid.

- **TLC:** R<sub>f</sub> = 0.37 (SiO<sub>2</sub>, DCM/MeOH 10:1).
- **C<sub>29</sub>H<sub>43</sub>N<sub>7</sub>O<sub>5</sub>S:** (601.76), [601.30].
- **HPLC:** (mixture of diastereomers) t<sub>R,1</sub> = 12.73 min; t<sub>R,2</sub> = 13.04 min.
- **<sup>1</sup>H-NMR (300 MHz, DMSO-d<sub>6</sub>, 300 K):** (mixture of diastereomers) δ = 8.35–8.24 (m, 2H, NHCH<sub>2</sub>C<sub>Ar</sub>, NHCHCO), 8.01 (d, <sup>3</sup>J = 7.6 Hz, 1H, NHCH piperidine), 7.83 (d, <sup>3</sup>J = 7.2 Hz, 2H, H-3-, H-5-benzyl), 7.68 (s, 1H, CH pyrazole), 7.36–7.28 (m, 2H, H-2-, H-6-benzyl), 6.15 (s, 2H, NH<sub>2</sub>), 4.46–4.35 (m, 3H, CH<sub>2</sub> benzyl, NHCHCO), 3.77–3.67 (m, 1H, CH piperidine), 3.51 (s, 3H, CH<sub>3</sub> pyrazole), 3.50–3.40 (m, 1H, CH<sub>A</sub>H<sub>B-2</sub> piperidine), 3.36–3.28 (m, 1H, CH<sub>A</sub>H<sub>B-2</sub> piperidine), 2.90–2.71 (m, 4H, CH<sub>3</sub>, CH<sub>A</sub>H<sub>B-6</sub> piperidine), 2.58–2.47 (m, 1H, CH<sub>A</sub>H<sub>B-6</sub> piperidine), 1.82–1.48 (m, 10H, CH<sub>2</sub>-4-, CH<sub>2</sub>-5-piperidine, NHCHCH<sub>A</sub>H<sub>B</sub>, H-2<sub>eq</sub>-, H-3<sub>eq</sub>-, H-4<sub>eq</sub>-, H-5<sub>eq</sub>-, H-6<sub>eq</sub>-cyclohexyl), 1.45–1.31 (m, 1H, NHCHCH<sub>A</sub>H<sub>B</sub>), 1.28–1.03 (m, 6H, H-1-, H-3<sub>ax</sub>-, H-4<sub>ax</sub>-, H-5<sub>ax</sub>-cyclohexyl, NHCHCH<sub>2</sub>CH<sub>2</sub>), 0.90–0.79 (m, 2H, H-2<sub>ax</sub>-, H-6<sub>ax</sub>-cyclohexyl) ppm.
- **<sup>13</sup>C-NMR (75 MHz, DMSO-d<sub>6</sub>, 300 K):** (mixture of diastereomers) δ = 171.6 (2x), 166.1 (2x), 164.1, 149.4, 143.8, 136.1, 132.6, 132.5, 127.5, 127.0, 126.7, 126.6, 96.7, 53.5, 53.4, 49.6, 49.4, 45.4, 45.2, 45.1, 41.2, 36.8, 34.4, 34.3, 33.9, 33.2, 32.9, 32.8, 32.7, 32.6, 29.4, 28.9, 28.6, 26.1, 25.8 (2x), 23.0, 22.9 ppm.
- **MS (ESI neg.):** m/z (%) = 646.16 (39) ([M+EtOH-H]<sup>-</sup>, calcd. 646.33), 600.19 (100) ([M-H]<sup>-</sup>, calcd. 600-29).
- **HRMS (FTMS + p MALDI):** m/z = 624.2950 [M+Na]<sup>+</sup>, calcd. for [C<sub>29</sub>H<sub>43</sub>N<sub>7</sub>NaO<sub>5</sub>S]<sup>+</sup> = 624.2944.

***N*-((*S*)-4-Cyclohexyl-1-(((*SR*)-1-(methylsulfonyl)piperidin-3-yl)amino)-1-oxobutan-2-yl)-4-(((1-phenyl-1*H*-pyrazolo[3,4-*d*]pyrimidin-4-yl)amino)methyl)benzamide (**300**, *SR300*)**

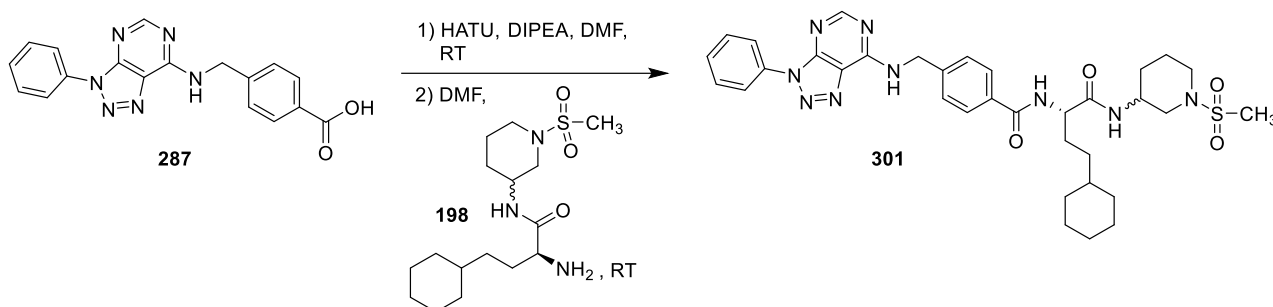


4-(((1-Phenyl-1*H*-pyrazolo[3,4-*d*]pyrimidin-4-yl)amino)methyl)benzoic acid (**286**, 200 mg, 0.579 mmol) and HATU (264 mg, 0.695 mmol) were dissolved in DMF (5 mL) and DIPEA (90 mg, 0.70 mmol) was added. The solution was stirred for 1.5 h at RT and (*S*)-2-amino-4-cyclohexyl-*N*-((*SR*)-1-(methylsulfonyl)piperidin-3-yl)butanamide (**198**, 240 mg, 0.695 mmol), diluted in DMF (5 mL), was added. The mixture was stirred for 20 h at RT. DCM (150 mL) was added and the organic phase was washed 5 times with H<sub>2</sub>O (100 mL) and dried over MgSO<sub>4</sub>. The solvent was evaporated under reduced pressure and the crude product was triturated with EtOAc/cyclohexane (1:1) and recrystallized from DCM.

**Yield:** 125 mg (0.185 mmol, 32%), colorless solid.

- **TLC:**  $R_f = 0.21$  (SiO<sub>2</sub>, cyclohexane/EtOAc 1:10).
- **C<sub>34</sub>H<sub>44</sub>N<sub>8</sub>O<sub>4</sub>S:** (672.84), [672.32].
- **HPLC:** (mixture of diastereomers)  $t_{R,1} = 15.90$  min;  $t_{R,2} = 16.22$  min.
- **<sup>1</sup>H-NMR (300 MHz, DMSO-*d*<sub>6</sub>, 300 K):** (mixture of diastereomers)  $\delta = 9.03$  (t,  $^3J = 5.8$  Hz, 1H, NHCH<sub>2</sub>C<sub>Ar</sub>), 8.45 (s, 1H, pyrimidine), 8.38 (s, 1H, pyrazole), 8.31 (d,  $^3J = 8.0$  Hz, 1H, NHCHCO), 8.19 (d,  $^3J = 8.0$  Hz, 2H, H-3-, H-5-benzyl), 8.00 (d,  $^3J = 7.6$  Hz, 1H, NHCH piperidine), 7.86 (d,  $^3J = 7.8$  Hz, 2H, H-2-, H-6-phenyl), 7.55 (t,  $^3J = 7.8$  Hz, 2H, H-3-, H-5-phenyl), 7.45 (d,  $^3J = 8.0$  Hz, 2H, H-2-, H-6-benzyl), 7.34 (t,  $^3J = 7.6$  Hz, 1H, H-4 phenyl), 4.84 (d,  $^3J = 5.8$  Hz, 2H, CH<sub>2</sub> benzyl), 4.46–4.34 (m, 1H, NHCHCO), 3.79–3.64 (m, 1H, CH piperidine), 3.53–3.40 (m, 1H, CH<sub>A</sub>H<sub>B-2</sub> piperidine), 3.37–3.23 (m, 1H, CH<sub>A</sub>H<sub>B-2</sub> piperidine), 2.84 (s, 3H, CH<sub>3</sub>), 2.83–2.69 (m, 1H, CH<sub>A</sub>H<sub>B-6</sub> piperidine), 2.59–2.41 (m, 1H, CH<sub>A</sub>H<sub>B-6</sub> piperidine), 1.86–1.32 (m, 11H, CH<sub>2</sub>-4-, CH<sub>2</sub>-5-piperidine, NHCHCH<sub>2</sub>, H-2<sub>eq</sub><sup>-</sup>, H-3<sub>eq</sub><sup>-</sup>, H-4<sub>eq</sub><sup>-</sup>, H-5<sub>eq</sub><sup>-</sup>, H-6<sub>eq</sub><sup>-</sup>-cyclohexyl), 1.30–1.01 (m, 6H, H-1-, H-3<sub>ax</sub><sup>-</sup>, H-4<sub>ax</sub><sup>-</sup>, H-5<sub>ax</sub><sup>-</sup>-cyclohexyl, NHCHCH<sub>2</sub>CH<sub>2</sub>), 0.95–0.72 (m, 2H, H-2<sub>ax</sub><sup>-</sup>, H-6<sub>ax</sub><sup>-</sup>-cyclohexyl) ppm.
- **<sup>13</sup>C-NMR (150 MHz, DMSO-*d*<sub>6</sub>, 300 K):** (mixture of diastereomers)  $\delta = 171.6, 166.1, 156.4, 152.9, 142.4, 138.9, 133.7, 132.9, 129.1, 127.7, 127.0, 126.1, 120.7, 101.8, 53.4, 49.5, 49.4, 45.3, 45.2, 45.1, 43.0, 36.8, 34.4, 34.3, 33.2, 32.9, 32.6, 29.4, 28.6, 26.1, 25.7, 22.9$  ppm.
- **MS (ESI pos.):**  $m/z$  (%) = 673.25 (100) ([M+H]<sup>+</sup>, calcd. 673.33), 494.98 (26) ([M<sub>fr.</sub>]<sup>+</sup>, calcd. 495.28).
- **HRMS (FTMS + p MALDI):**  $m/z = 695.3099$  [M+Na]<sup>+</sup>, calcd. for [C<sub>35</sub>H<sub>44</sub>N<sub>8</sub>NaO<sub>4</sub>S]<sup>+</sup> = 695.3104.

***N*-((*S*)-4-Cyclohexyl-1-(((*SR*)-1-(methylsulfonyl)piperidin-3-yl)amino)-1-oxobutan-2-yl)-4-(((3-phenyl-3*H*-[1,2,3]triazolo[4,5-*d*]pyrimidin-7-yl)amino)methyl)benzamide (**301**, *SR301*)**

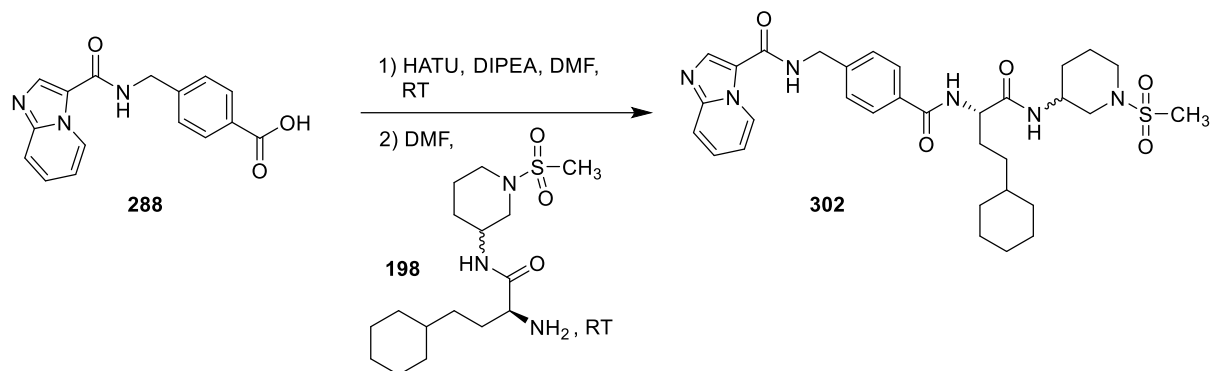


4-(((3-Phenyl-3*H*-[1,2,3]triazolo[4,5-*d*]pyrimidin-7-yl)amino)methyl)benzoic acid (**287**, 200 mg, 0.577 mmol) and HATU (263 mg, 0.693 mmol) were dissolved in DMF (5 mL) and DIPEA (90 mg, 0.693 mmol) was added. The solution was stirred for 1.5 h at RT and (*S*)-2-amino-4-cyclohexyl-*N*-((*SR*)-1-(methylsulfonyl)piperidin-3-yl)butanamide (**198**, 239 mg, 0.693 mmol), diluted in DMF (5 mL), was added. The mixture was stirred for 20 h at RT. DCM (150 mL) was added and the organic phase was washed 5 times with H<sub>2</sub>O (150 mL) and dried over MgSO<sub>4</sub>. The solvent was evaporated under reduced pressure and the crude product was triturated with EtOAc/cyclohexane (1:1) and recrystallized from DCM.

**Yield:** 51 mg (0.075 mmol, 13%), colorless solid.

- **TLC:**  $R_f = 0.20$  (SiO<sub>2</sub>, cyclohexane/EtOAc 1:10).
- **C<sub>34</sub>H<sub>43</sub>N<sub>9</sub>O<sub>4</sub>S:** (673.83), [673.32].
- **HPLC:** (mixture of diastereomers)  $t_{R,1} = 15.97$  min;  $t_{R,2} = 16.27$  min.
- **<sup>1</sup>H-NMR (400 MHz, DMSO-*d*<sub>6</sub>, 300 K):** (mixture of diastereomers/ rotamers)  $\delta = 9.77$ – $9.63$  (m, 1H, NH) 8.56–8.39 (m, 2H, NHCHCO, CH pyrimidine), 8.22–8.09 (m, 3H, NHCH piperidine, H-3-, H-5-benzyl), 7.72–7.60 (m, 2H, H-2-, H-6-phenyl), 7.58–7.39 (m, 3H, H-3-, H-4, H-5-phenyl), 7.32 (d, 2H,  $^3J = 7.5$  Hz, H-2-, H-6-benzyl), 4.84 (d,  $^3J = 5.6$  Hz, 2H, CH<sub>2</sub>), 3.89–3.10 (m, 4H, CH piperidine, CH<sub>2</sub>-2 piperidine, NHCHCO), 2.95–2.79 (m, 5H, CH<sub>3</sub>, CH<sub>2</sub>-6-piperidine), 1.87–1.38 (m, 12H, CH<sub>2</sub>-4-, CH<sub>2</sub>-5-piperidine, NHCHCH<sub>2</sub>, H-1-, H-2<sub>eq</sub>-, H-3<sub>eq</sub>-, H-4<sub>eq</sub>-, H-5<sub>eq</sub>-, H-6<sub>eq</sub>-cyclohexyl), 1.30–1.03 (m, 5H, H-3<sub>ax</sub>-, H-4<sub>ax</sub>-, H-5<sub>ax</sub>-cyclohexyl, NHCHCH<sub>2</sub>CH<sub>2</sub>), 0.94–0.76 (m, 2H, H-2<sub>ax</sub>-, H-6<sub>ax</sub>-cyclohexyl).
- **MS (ESI pos.):**  $m/z$  (%) = 696.30 (100) ([M+Na]<sup>+</sup>, calcd. 696.31).
- **HRMS (FTMS + p MALDI):**  $m/z$  696.3054 [M+Na]<sup>+</sup>, calcd. for [C<sub>34</sub>H<sub>43</sub>N<sub>9</sub>NaO<sub>4</sub>S]<sup>+</sup> = 696.3056.

***N*-4-(((*S*)-4-Cyclohexyl-1-(((*SR*)-1-(methylsulfonyl)piperidin-3-yl)amino)-1-oxobutan-2-yl)carbamoyl)benzyl)imidazo[1,2-*a*]pyridine-3-carboxamide (**302**, SR302)**



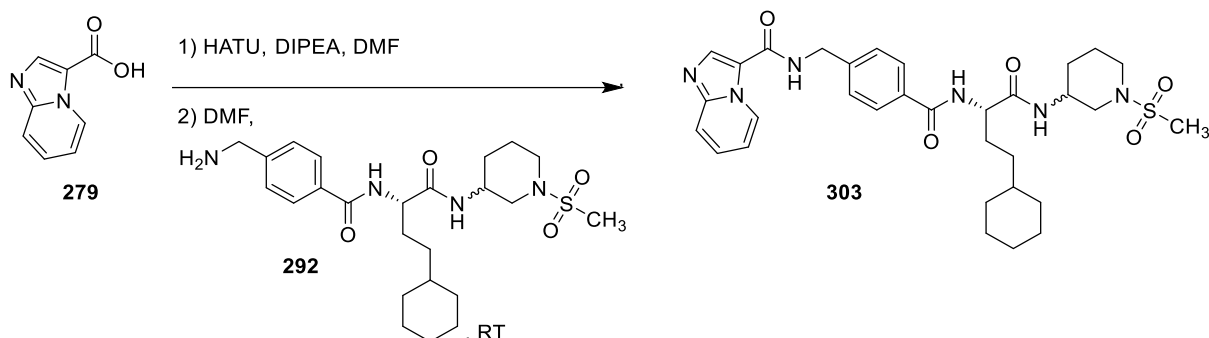
4-((Imidazo[1,2-*a*]pyridine-3-carboxamido)methyl)benzoic acid (**288**, 200 mg, 0.677 mmol) and HATU (309 mg, 0.813 mmol) were dissolved in DMF (5 mL) and DIPEA (105 mg, 0.813 mmol) was added. The solution was stirred for 1.5 h at RT and (*S*)-2-amino-4-cyclohexyl-*N*-((*SR*)-1-(methylsulfonyl)piperidin-3-yl)butanamide (**198**, 281 mg, 0.813 mmol), diluted in DMF (5 mL), was added. The mixture was stirred for 20 h at RT. DCM (150 mL) was added and the organic phase was washed 5 times with H<sub>2</sub>O (150 mL) and dried over MgSO<sub>4</sub>. The solvent was evaporated under reduced pressure and the crude product was purified using column chromatography on silica (EtOAc/MeOH 10:1).

**Yield:** 48 mg (0.077 mmol, 11%), colorless solid.

- **TLC:**  $R_f = 0.19$  (SiO<sub>2</sub>, EtOAc/MeOH 10:1).
- **C<sub>32</sub>H<sub>42</sub>N<sub>6</sub>O<sub>5</sub>S:** (622.78), [622.29].
- **HPLC:** (mixture of diastereomers)  $t_{R,1} = 11.75$  min;  $t_{R,2} = 12.02$  min.
- **<sup>1</sup>H-NMR (300 MHz, DMSO-*d*<sub>6</sub>, 300 K):** (mixture of diastereomers)  $\delta = 9.47$  (d,  $^3J = 7.0$  Hz, 1H, NHCHCO), 9.09 (t,  $^3J = 6.1$  Hz, 1H, NHCH<sub>2</sub>C<sub>Ar</sub>), 8.40 (s, 1H, CH-2 imidazo[1,2-*a*]pyridine), 8.31 (d,  $^3J = 8.0$  Hz, 1H, CH-5 imidazo[1,2-*a*]pyridine), 8.00 (d,  $^3J = 7.5$  Hz, 1H, NHCH piperidine), 7.85 (d,  $^3J = 8.3$  Hz, 2H, H-3-, H-5-benzyl), 7.72 (d,  $^3J = 9.0$  Hz, 1H, CH-8 imidazo[1,2-*a*]pyridine), 7.51–7.31 (m, 3H, H-2-, H-6-benzyl, CH-6 imidazo[1,2-*a*]pyridine), 7.12 (td,  $^3J = 6.9, 1.3$  Hz, 1H, CH-7 imidazo[1,2-*a*]pyridine), 4.57 (d,  $^3J = 6.1$  Hz, 2H, CH<sub>2</sub> benzyl), 4.45–4.33 (m, 1H, NHCHCO), 3.79–3.65 (m, 1H, CH piperidine), 3.53–3.37 (m, 1H, CH<sub>A</sub>H<sub>B</sub>-2 piperidine), 3.36–3.25 (m, 1H, CH<sub>A</sub>H<sub>B</sub>-2 piperidine), 2.85 (s, 3H, CH<sub>3</sub>), 2.83–2.70 (m, 1H, CH<sub>A</sub>H<sub>B</sub>-6 piperidine), 2.59–2.41 (m, 1H, CH<sub>A</sub>H<sub>B</sub>-6 piperidine), 1.88–1.31 (m, 11H, CH<sub>2</sub>-4-, CH<sub>2</sub>-5-piperidine, NHCHCH<sub>2</sub>, H-2<sub>eq</sub>-, H-3<sub>eq</sub>-, H-4<sub>eq</sub>-, H-5<sub>eq</sub>-, H-6<sub>eq</sub>-cyclohexyl), 1.29–1.00 (m, 6H, H-1-, H-3<sub>ax</sub>-, H-4<sub>ax</sub>-, H-5<sub>ax</sub>-cyclohexyl, NHCHCH<sub>2</sub>CH<sub>2</sub>), 0.93–0.71 (m, 2H, H-2<sub>ax</sub>-, H-6<sub>ax</sub>-cyclohexyl) ppm.
- **<sup>13</sup>C-NMR (75 MHz, DMSO-*d*<sub>6</sub>, 300 K):** (mixture of diastereomers)  $\delta = 171.7, 166.1, 160.2, 146.9, 143.0, 136.9, 132.8, 127.6$  (2x), 127.0, 126.9, 118.0, 117.3, 113.9, 107.0, 53.6, 53.4, 49.4, 45.4, 45.2, 45.1, 41.6, 36.8, 34.4, 34.3, 33.3, 32.9, 32.7, 29.4, 28.6, 26.1 (2x), 25.8, 23.0 ppm.
- **MS (ESI neg.):**  $m/z$  (%) = 667.29 (100) ([M+EtOH-H]<sup>-</sup>, calcd. 667.32), 621.30 (94) ([M-H]<sup>-</sup>, calcd. 621.28), 361.24 (48) ([M<sub>fr.</sub>+EtOH+H]<sup>-</sup>, calcd. 361.24).
- **HRMS (FTMS + p MALDI):**  $m/z$  645.2801 [M+Na]<sup>+</sup>, calcd. for [C<sub>32</sub>H<sub>42</sub>N<sub>7</sub>NaO<sub>5</sub>S]<sup>+</sup> = 645.2835.



***N*-(4-(((*S*)-4-Cyclohexyl-1-(((*SR*)-1-(methylsulfonyl)piperidin-3-yl)amino)-1-oxobutan-2-yl)carbamoyl)benzyl)imidazo[1,2-*a*]pyridine-3-carboxamide (303, SR353)**

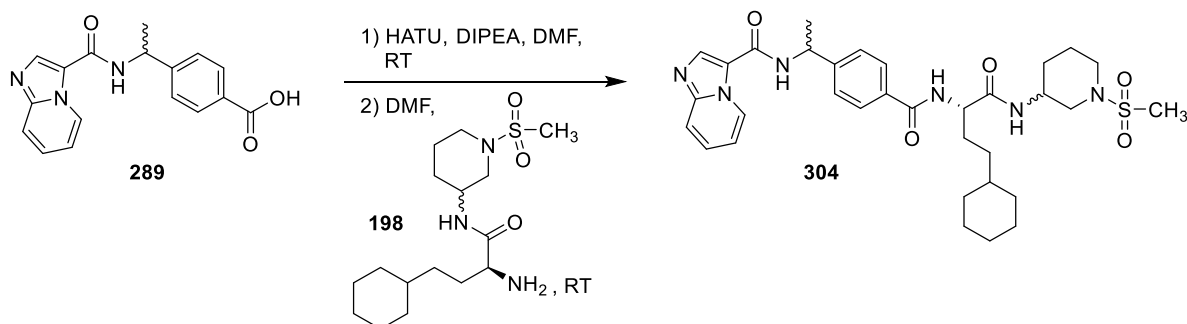


Imidazo[1,2-*a*]pyridine-3-carboxylic acid (**279**, 42 mg, 0.26 mmol) and HATU (119 mg, 0.313 mmol) were dissolved in DMF (8 mL) and DIPEA (40 mg, 0.31 mmol) was added. The solution was stirred for 1.5 h at RT and 4-(aminomethyl)-*N*-(((*S*)-4-cyclohexyl-1-(((*SR*)-1-(methylsulfonyl)piperidin-3-yl)amino)-1-oxobutan-2-yl)benzamide (**292**, 150 mg, 0.313 mmol), diluted in DMF (7 mL), was added. The mixture was stirred for 20 h at RT and H<sub>2</sub>O (100 mL) was added. The precipitate was filtered off and the crude product was purified by column chromatography on silica (EtOAc → EtOAc/MeOH 10:1 → EtOH).

**Yield:** 141 mg (0.227 mmol, 87%), colorless solid.

The analytical data are in accordance with compound **302**.

***N*-(((*SR*)-1-(4-(((*S*)-4-Cyclohexyl-1-(((*SR*)-1-(methylsulfonyl)piperidin-3-yl)amino)-1-oxobutan-2-yl)carbamoyl)phenyl)ethyl)imidazo[1,2-*a*]pyridine-3-carboxamide (304, SR360)**



4-(1-(imidazo[1,2-*a*]pyridine-3-carboxamido)ethyl)benzoic acid (**289**, 200 mg, 0.647 mmol) and HATU (295 mg, 0.776 mmol) were dissolved in DMF (6 mL) and DIPEA (100 mg, 0.776 mmol) was added. The solution was stirred for 1.5 h at RT and (*S*)-2-amino-4-cyclohexyl-*N*-(((*SR*)-1-(methylsulfonyl)piperidin-3-yl)butanamide (**198**, 268 mg, 0.776 mmol), diluted in DMF (6 mL), was added. The mixture was stirred for 20 h at RT. DCM (100 mL) was added and the organic phase was washed 4 times with H<sub>2</sub>O (100 mL) and dried over MgSO<sub>4</sub>. The solvent was evaporated under reduced pressure and the crude product was purified using column chromatography on silica (hexane/EtOAc 1:1 → EtOAc → EtOAc/MeOH 10:1).

**Yield:** 209 mg (0.328 mmol, 51%), colorless solid.

- **TLC:** R<sub>f</sub> = 0.20 (SiO<sub>2</sub>, EtOAc/MeOH 10:1).
- **C<sub>33</sub>H<sub>44</sub>N<sub>6</sub>O<sub>5</sub>S:** (636.80), [636.31].

- **HPLC:** (mixture of diastereomers)  $t_{R,1} = 13.44$  min;  $t_{R,2} = 13.72$  min.
- **$^1\text{H-NMR}$  (600 MHz, DMSO- $d_6$ , 300 K):** (mixture of diastereomers)  $\delta = 9.41$  (d,  $^3J = 6.9$  Hz, 1H, NHCHCO), 8.84 (d,  $^3J = 7.9$  Hz, 1H, NHCHC<sub>Ar</sub>), 8.49 (d,  $^4J = 1.5$  Hz, 1H, CH-2 imidazo[1,2-*a*]pyridine), 8.30 (d,  $^3J = 8.1$  Hz, 1H, CH-5 imidazo[1,2-*a*]pyridine), 7.99 (d,  $^3J = 7.5$  Hz, 1H, NHCH piperidine), 7.85 (dt,  $^3J = 8.3, 3.0$  Hz, 2H, H-3-, H-5-benzyl), 7.70 (dt,  $^3J = 9.0, 1.1$  Hz, 1H, CH-8-imidazo[1,2-*a*]pyridine), 7.49 (d,  $^3J = 8.3$  Hz, 2H, H-2-, H-6-benzyl) 7.44 (ddd,  $^3J = 9.0, 6.8, 1.3$  Hz, 1H, CH-6 imidazo[1,2-*a*]pyridine), 7.08 (td,  $^3J = 6.9, 1.1$  Hz, 1H, CH-7 imidazo[1,2-*a*]pyridine), 5.25 (p,  $^3J = 7.2$  Hz, 1H, CHCH<sub>3</sub>), 4.43–4.36 (m, 1H, NHCHCO), 3.76–3.69 (m, 1H, CH piperidine), 3.51–3.41 (m, 1H, CH<sub>A</sub>H<sub>B</sub>-2 piperidine), 3.36–3.29 (m, 1H, CH<sub>A</sub>H<sub>B</sub>-2 piperidine), 2.84 (s, 3H, SO<sub>2</sub>CH<sub>3</sub>), 2.79–2.71 (m, 1H, CH<sub>A</sub>H<sub>B</sub>-6 piperidine), 2.57–2.52 (m, 1H, CH<sub>A</sub>H<sub>B</sub>-6 piperidine), 1.84–1.55 (m, 10H, CH<sub>2</sub>-4-, CH<sub>A</sub>H<sub>B</sub>-5-piperidine, NHCHCH<sub>2</sub>, H-2<sub>eq</sub>-, H-3<sub>eq</sub>-, H-4<sub>eq</sub>-, H-5<sub>eq</sub>-, H-6<sub>eq</sub>-cyclohexyl), 1.52 (d,  $^3J = 7.1$  Hz, 3H, CHCH<sub>3</sub>), 1.44–1.31 (m, 1H, CH<sub>A</sub>H<sub>B</sub>-5 piperidine), 1.28–1.06 (m, 6H, H-1-, H-3<sub>ax</sub>-, H-4<sub>ax</sub>-, H-5<sub>ax</sub>-cyclohexyl, NHCHCH<sub>2</sub>CH<sub>2</sub>), 0.89–0.77 (m, 2H, H-2<sub>ax</sub>-, H-6<sub>ax</sub>-cyclohexyl) ppm.
- **$^{13}\text{C-NMR}$  (150 MHz, DMSO- $d_6$ , 300 K):** (mixture of diastereomers)  $\delta = 171.6, 166.1, 159.4, 148.2, 146.9, 137.0, 132.7, 127.6, 127.5, 126.9, 125.8, 118.0, 117.2, 113.8, 53.5, 53.4, 49.6, 49.4, 47.7, 45.4, 45.2, 45.1, 36.8$  (2x), 34.4, 34.3, 33.2, 32.9, 32.6, 29.4, 28.9, 28.6, 26.1, 25.8, 25.7, 23.0 (2x), 22.2, 22.1 ppm.
- **MS (ESI pos.):**  $m/z$  (%) = 637.50 (100) ([M+H]<sup>+</sup>, calcd. 637.32), 459.31 (60) ([M<sub>fr.</sub>]<sup>+</sup>, calcd. 459.24).
- **HRMS (FTMS + p MALDI):**  $m/z$  637.3173 [M+H]<sup>+</sup>, calcd. for [C<sub>33</sub>H<sub>45</sub>N<sub>6</sub>O<sub>5</sub>S]<sup>+</sup> = 637.3172.

## 8.6 Results selectivity profiling

**Table 22.** Selectivity screening results compounds of Chapter 3 and Chapter 4

DiscoverX Gene Symbol	Entrez Gene symbol	33 (SR318), % of control at 1 $\mu\text{M}$	35 (SR321), % of control at 100 nM	218 (SR43), % of control at 1 $\mu\text{M}$	242 (SR92), % of control at 100 nM
AAK1	AAK1	97	100	82	100
ABL1(E255K)-phosphorylated	ABL1(E255K)-phosphorylated	100	92	77	83
ABL1(F317I)-nonphosphorylated	ABL1(F317I)-nonphosphorylated	73	100	100	100
ABL1(F317I)-phosphorylated	ABL1(F317I)-phosphorylated	100	100	81	90
ABL1(F317L)-nonphosphorylated	ABL1(F317L)-nonphosphorylated	100	100	75	100
ABL1(F317L)-phosphorylated	ABL1(F317L)-phosphorylated	96	82	95	70
ABL1(H396P)-nonphosphorylated	ABL1	99	98	56	92
ABL1(H396P)-phosphorylated	ABL1(H396P)-phosphorylated	100	99	95	86
ABL1(M351T)-phosphorylated	ABL1(M351T)-phosphorylated	91	100	89	91
ABL1(Q252H)-nonphosphorylated	ABL1	81	100	28	81
ABL1(Q252H)-phosphorylated	ABL1(Q252H)-phosphorylated	99	98	74	79
ABL1(T315I)-nonphosphorylated	ABL1(T315I)-nonphosphorylated	86	80	100	77

Table 22. (continued)

DiscoverX Gene Symbol	Entrez Gene symbol	33 (SR318), % of control at 1 $\mu$ M	35 (SR321), % of control at 100 nM	218 (SR43), % of control at 1 $\mu$ M	242 (SR92), % of control at 100 nM
ABL1(T315I)-phosphorylated	ABL1(T315I)-phosphorylated	100	100	94	83
ABL1(Y253F)-phosphorylated	ABL1(Y253F)-phosphorylated	100	98	80	90
ABL1-nonphosphorylated	ABL1	62	93	8.8	86
ABL1-phosphorylated	ABL1-phosphorylated	86	88	70	69
ABL2	ABL2	100	87	68	75
ACVR1	ACVR1	100	100	92	100
ACVR1B	ACVR1B	100	100	100	88
ACVR2A	ACVR2A	100	83	100	66
ACVR2B	ACVR2B	100	96	100	74
ACVRL1	ACVRL1	100	100	77	100
ADCK3	ADCK3	100	100	92	88
ADCK4	ADCK4	94	100	100	100
AKT1	AKT1	79	100	99	100
AKT2	AKT2	100	100	96	99
AKT3	AKT3	100	97	100	88
ALK	ALK	100	100	100	94
ALK(C1156Y)	ALK(C1156Y)	95	100	86	100
ALK(L1196M)	ALK(L1196M)	100	100	82	100
AMPK-alpha1	AMPK-alpha1	100	100	57	100
AMPK-alpha2	AMPK-alpha2	96	100	100	100
ANKK1	ANKK1	100	100	100	95
ARK5	ARK5	100	100	100	96
ASK1	ASK1	100	91	94	100
ASK2	ASK2	100	100	100	100
AURKA	AURKA	95	100	89	92
AURKB	AURKB	100	95	84	94
AURKC	AURKC	100	100	100	100
AXL	AXL	100	95	100	100
BIKE	BIKE	100	100	100	100
BLK	BLK	100	100	94	100
BMPR1A	BMPR1A	78	100	100	79
BMPR1B	BMPR1B	100	92	77	100
BMPR2	BMPR2	100	100	79	100
BMX	BMX	100	75	86	31
BRAF	BRAF	100	100	82	87
BRAF(V600E)	BRAF(V600E)	100	100	80	100
BRK	BRK	100	97	100	100
BRSK1	BRSK1	100	100	100	100
BRSK2	BRSK2	89	100	100	100

**Table 22.** (continued)

DiscoverX Gene Symbol	Entrez Gene symbol	33 (SR318), % of control at 1 $\mu$ M	35 (SR321), % of control at 100 nM	218 (SR43), % of control at 1 $\mu$ M	242 (SR92), % of control at 100 nM
BTK	BTK	100	100	100	100
BUB1	BUB1	100	100	87	93
CAMK1	CAMK1	92	100	82	79
CAMK1B	CAMK1B	100	79	100	63
CAMK1D	CAMK1D	92	100	84	100
CAMK1G	CAMK1G	100	100	100	100
CAMK2A	CAMK2A	100	100	84	85
CAMK2B	CAMK2B	100	96	91	77
CAMK2D	CAMK2D	100	100	100	100
CAMK2G	CAMK2G	100	100	100	100
CAMK4	CAMK4	100	100	79	100
CAMKK1	CAMKK1	100	100	100	100
CAMKK2	CAMKK2	100	100	100	100
CASK	CASK	100	100	84	100
CDC2L1	CDC2L1	99	100	100	100
CDC2L2	CDC2L2	100	100	100	90
CDC2L5	CDC2L5	100	100	82	100
CDK11	CDK11	100	96	100	85
CDK2	CDK2	100	96	100	90
CDK3	CDK3	100	100	100	100
CDK4	CDK4	100	96	91	95
CDK4-cyclinD1	CDK4-cyclinD1	100	100	100	96
CDK4-cyclinD3	CDK4-cyclinD3	100	100	100	84
CDK5	CDK5	100	88	78	100
CDK7	CDK7	100	100	66	96
CDK8	CDK8	100	97	100	100
CDK9	CDK9	100	100	100	100
CDKL1	CDKL1	100	80	93	86
CDKL2	CDKL2	100	100	85	100
CDKL3	CDKL3	100	100	100	87
CDKL5	CDKL5	100	100	95	93
CHEK1	CHEK1	100	100	87	97
CHEK2	CHEK2	100	100	100	100
CIT	CIT	100	86	100	93
CLK1	CLK1	90	96	77	80
CLK2	CLK2	100	100	71	100
CLK3	CLK3	92	100	92	94
CLK4	CLK4	93	100	100	100
CSF1R	CSF1R	100	100	90	100
CSF1R-autoinhibited	CSF1R-autoinhibited	100	100	87	100

**Table 22.** (continued)

DiscoverX Gene Symbol	Entrez Gene symbol	33 (SR318), % of control at 1 $\mu$ M	35 (SR321), % of control at 100 nM	218 (SR43), % of control at 1 $\mu$ M	242 (SR92), % of control at 100 nM
CSK	CSK	100	100	86	88
CSNK1A1	CSNK1A1	100	99	78	87
CSNK1A1L	CSNK1A1L	100	94	100	100
CSNK1D	CSNK1D	100	100	100	100
CSNK1E	CSNK1E	100	100	89	87
CSNK1G1	CSNK1G1	100	100	86	100
CSNK1G2	CSNK1G2	100	96	93	84
CSNK1G3	CSNK1G3	94	100	94	99
CSNK2A1	CSNK2A1	100	94	97	87
CSNK2A2	CSNK2A2	91	88	86	78
CTK	CTK	100	100	75	100
DAPK1	DAPK1	100	100	89	100
DAPK2	DAPK2	100	98	77	84
DAPK3	DAPK3	100	92	82	87
DCAMKL1	DCAMKL1	98	100	74	83
DCAMKL2	DCAMKL2	100	100	100	100
DCAMKL3	DCAMKL3	100	100	81	100
DDR1	DDR1	3	100	0.9	41
DDR2	DDR2	31	100	9.4	71
DLK	DLK	100	100	72	100
DMPK	DMPK	100	83	100	100
DMPK2	DMPK2	100	99	100	82
DRAK1	DRAK1	88	100	97	100
DRAK2	DRAK2	100	100	100	96
DYRK1A	DYRK1A	100	99	79	90
DYRK1B	DYRK1B	65	100	57	71
DYRK2	DYRK2	100	100	86	84
EGFR	EGFR	100	100	93	100
EGFR(E746-A750del)	EGFR(E746-A750del)	89	100	100	100
EGFR(G719C)	EGFR(G719C)	92	96	98	100
EGFR(G719S)	EGFR(G719S)	93	80	100	91
EGFR(L747-E749del, A750P)	EGFR(L747-E749del, A750P)	100	100	97	95
EGFR(L747-S752del, P753S)	EGFR(L747-S752del, P753S)	100	100	95	69
EGFR(L747-T751del,Sins)	EGFR(L747-T751del,Sins)	81	100	100	81
EGFR(L858R)	EGFR(L858R)	100	100	98	100
EGFR(L858R,T790M)	EGFR(L858R,T790M)	72	95	99	88
EGFR(L861Q)	EGFR(L861Q)	67	100	100	100
EGFR(S752-I759del)	EGFR(S752-I759del)	49	99	97	100
EGFR(T790M)	EGFR(T790M)	100	97	100	91

**Table 22.** (continued)

DiscoverX Gene Symbol	Entrez Gene symbol	33 (SR318), % of control at 1 $\mu$ M	35 (SR321), % of control at 100 nM	218 (SR43), % of control at 1 $\mu$ M	242 (SR92), % of control at 100 nM
EIF2AK1	EIF2AK1	90	95	100	100
EPHA1	EPHA1	100	100	11	93
EPHA2	EPHA2	100	80	85	43
EPHA3	EPHA3	97	91	100	87
EPHA4	EPHA4	100	70	75	100
EPHA5	EPHA5	100	92	87	100
EPHA6	EPHA6	100	88	82	100
EPHA7	EPHA7	100	86	98	80
EPHA8	EPHA8	100	95	84	99
EPHB1	EPHB1	100	89	96	84
EPHB2	EPHB2	100	100	96	100
EPHB3	EPHB3	100	79	80	100
EPHB4	EPHB4	100	95	79	100
EPHB6	EPHB6	72	100	70	93
ERBB2	ERBB2	100	100	97	100
ERBB3	ERBB3	100	100	85	100
ERBB4	ERBB4	100	100	100	100
ERK1	ERK1	100	93	98	81
ERK2	ERK2	100	93	88	100
ERK3	ERK3	100	100	100	91
ERK4	ERK4	100	100	94	100
ERK5	ERK5	74	100	100	100
ERK8	ERK8	100	100	86	100
ERN1	ERN1	100	94	82	86
FAK	FAK	100	100	100	99
FER	FER	100	98	92	69
FES	FES	100	100	64	100
FGFR1	FGFR1	100	100	100	100
FGFR2	FGFR2	80	100	100	100
FGFR3	FGFR3	100	100	100	100
FGFR3(G697C)	FGFR3	100	100	23	100
FGFR4	FGFR4	100	100	100	100
FGR	FGR	100	95	78	95
FLT1	FLT1	100	100	100	95
FLT3	FLT3	99	87	92	100
FLT3(D835H)	FLT3(D835H)	100	100	80	80
FLT3(D835V)	FLT3(D835V)	100	88	100	90
FLT3(D835Y)	FLT3	100	100	0	100
FLT3(ITD)	FLT3(ITD)	100	100	100	100
FLT3(ITD,D835V)	FLT3(ITD,D835V)	100	100	100	84

Table 22. (continued)

DiscoverX Gene Symbol	Entrez Gene symbol	33 (SR318), % of control at 1 $\mu$ M	35 (SR321), % of control at 100 nM	218 (SR43), % of control at 1 $\mu$ M	242 (SR92), % of control at 100 nM
FLT3(ITD,F691L)	FLT3(ITD,F691L)	100	100	84	97
FLT3(K663Q)	FLT3	100	100	0	99
FLT3(N841I)	FLT3(N841I)	100	88	100	89
FLT3(R834Q)	FLT3	100	100	62	100
FLT3-autoinhibited	FLT3-autoinhibited	77	100	88	83
FLT4	FLT4	100	100	80	77
FRK	FRK	100	77	100	79
FYN	FYN	100	86	100	73
GAK	GAK	93	100	100	100
GCN2(Kin.Dom.2,S808G)	GCN2(Kin.Dom.2,S808G)	100	100	100	87
GRK1	GRK1	100	94	89	100
GRK2	GRK2	100	100	100	83
GRK3	GRK3	100	100	100	93
GRK4	GRK4	100	100	100	100
GRK7	GRK7	100	100	69	91
GSK3A	GSK3A	88	100	100	100
GSK3B	GSK3B	100	100	77	100
HASPIN	HASPIN	100	100	98	100
HCK	HCK	100	100	64	100
HIPK1	HIPK1	100	99	65	89
HIPK2	HIPK2	100	100	72	100
HIPK3	HIPK3	100	88	80	92
HIPK4	HIPK4	100	100	100	100
HPK1	HPK1	94	100	100	100
HUNK	HUNK	100	100	98	100
ICK	ICK	92	79	94	93
IGF1R	IGF1R	100	100	100	83
IKK-alpha	IKK-alpha	100	100	97	100
IKK-beta	IKK-beta	100	100	80	100
IKK-epsilon	IKK-epsilon	74	78	79	73
INSR	INSR	95	100	97	85
INSRR	INSRR	100	100	100	100
IRAK1	IRAK1	100	100	90	98
IRAK3	IRAK3	100	100	87	100
IRAK4	IRAK4	80	100	97	100
ITK	ITK	100	100	90	91
JAK1(JH1domain-catalytic)	JAK1(JH1domain-catalytic)	100	100	100	100
JAK1(JH2domain-pseudokinase)	JAK1(JH2domain-pseudokinase)	100	89	79	78
JAK2(JH1domain-catalytic)	JAK2(JH1domain-catalytic)	85	100	83	100

**Table 22.** (continued)

DiscoverX Gene Symbol	Entrez Gene symbol	33 (SR318), % of control at 1 $\mu$ M	35 (SR321), % of control at 100 nM	218 (SR43), % of control at 1 $\mu$ M	242 (SR92), % of control at 100 nM
JAK3(JH1domain-catalytic)	JAK3(JH1domain-catalytic)	100	100	90	100
JNK1	JNK1	74	99	72	80
JNK2	JNK2	80	85	95	88
JNK3	JNK3	65	100	94	99
KIT	KIT	7.7	100	38	100
KIT(A829P)	KIT	81	100	67	100
KIT(D816H)	KIT(D816H)	100	78	85	60
KIT(D816V)	KIT(D816V)	100	100	98	94
KIT(L576P)	KIT	28	100	53	100
KIT(V559D)	KIT	3	100	24	100
KIT(V559D,T670I)	KIT(V559D,T670I)	100	100	93	100
KIT(V559D,V654A)	KIT(V559D,V654A)	93	100	100	100
KIT-autoinhibited	KIT-autoinhibited	97	100	75	92
LATS1	LATS1	100	100	79	82
LATS2	LATS2	100	97	67	93
LCK	LCK	90	100	94	74
LIMK1	LIMK1	100	100	96	100
LIMK2	LIMK2	100	100	95	81
LKB1	LKB1	84	100	18	100
LOK	LOK	100	100	62	100
LRRK2	LRRK2	100	57	82	44
LRRK2(G2019S)	LRRK2(G2019S)	100	100	87	100
LTK	LTK	100	100	69	100
LYN	LYN	100	100	96	89
LZK	LZK	100	100	92	100
MAK	MAK	100	100	63	100
MAP3K1	MAP3K1	100	65	70	69
MAP3K15	MAP3K15	100	84	100	69
MAP3K2	MAP3K2	100	100	84	100
MAP3K3	MAP3K3	100	100	66	84
MAP3K4	MAP3K4	98	100	11	100
MAP4K2	MAP4K2	100	100	81	99
MAP4K3	MAP4K3	100	78	100	72
MAP4K4	MAP4K4	100	81	100	67
MAP4K5	MAP4K5	100	88	100	73
MAPKAPK2	MAPKAPK2	100	100	100	100
MAPKAPK5	MAPKAPK5	100	100	81	97
MARK1	MARK1	97	100	100	100
MARK2	MARK2	100	100	100	100
MARK3	MARK3	100	94	83	100



**Table 22.** (continued)

DiscoverX Gene Symbol	Entrez Gene symbol	33 (SR318), % of control at 1 $\mu$ M	35 (SR321), % of control at 100 nM	218 (SR43), % of control at 1 $\mu$ M	242 (SR92), % of control at 100 nM
MARK4	MARK4	99	98	100	100
MAST1	MAST1	100	88	100	93
MEK1	MEK1	100	89	80	85
MEK2	MEK2	100	93	77	89
MEK3	MEK3	100	100	80	78
MEK4	MEK4	100	100	100	100
MEK5	MEK5	100	73	79	94
MEK6	MEK6	100	79	98	90
MELK	MELK	100	80	100	98
MERTK	MERTK	93	100	62	91
MET	MET	100	100	94	77
MET(M1250T)	MET(M1250T)	100	76	100	91
MET(Y1235D)	MET(Y1235D)	93	100	77	90
MINK	MINK	100	97	98	100
MKK7	MKK7	100	100	100	100
MKNK1	MKNK1	100	98	100	82
MKNK2	MKNK2	88	100	100	100
MLCK	MLCK	100	92	100	100
MLK1	MLK1	100	100	98	85
MLK2	MLK2	100	87	100	100
MLK3	MLK3	95	100	100	72
MRCKA	MRCKA	100	100	100	100
MRCKB	MRCKB	100	100	100	100
MST1	MST1	100	100	73	100
MST1R	MST1R	100	100	64	86
MST2	MST2	100	100	100	100
MST3	MST3	100	100	87	100
MST4	MST4	100	93	100	100
MTOR	MTOR	100	100	100	86
MUSK	MUSK	100	100	100	100
MYLK	MYLK	95	100	80	91
MYLK2	MYLK2	94	100	100	87
MYLK4	MYLK4	31	100	96	100
MYO3A	MYO3A	100	98	69	83
MYO3B	MYO3B	94	100	77	95
NDR1	NDR1	100	93	88	100
NDR2	NDR2	100	20	87	24
NEK1	NEK1	100	58	94	57
NEK10	NEK10	89	100	56	100
NEK11	NEK11	100	100	69	100

**Table 22.** (continued)

DiscoverX Gene Symbol	Entrez Gene symbol	33 (SR318), % of control at 1 $\mu$ M	35 (SR321), % of control at 100 nM	218 (SR43), % of control at 1 $\mu$ M	242 (SR92), % of control at 100 nM
NEK2	NEK2	100	100	92	96
NEK3	NEK3	96	100	72	94
NEK4	NEK4	88	100	99	79
NEK5	NEK5	100	100	100	91
NEK6	NEK6	100	83	81	100
NEK7	NEK7	94	97	96	100
NEK9	NEK9	100	100	100	100
NIK	NIK	100	90	100	100
NIM1	NIM1	98	70	75	64
NLK	NLK	55	100	59	100
OSR1	OSR1	100	91	98	83
p38-alpha	p38-alpha	0	100	1.5	89
p38-beta	p38-beta	0	100	3.4	32
p38-delta	p38-delta	100	100	67	100
p38-gamma	p38-gamma	100	100	70	100
PAK1	PAK1	80	92	98	79
PAK2	PAK2	86	100	100	100
PAK3	PAK3	100	100	50	100
PAK4	PAK4	97	100	91	85
PAK6	PAK6	100	100	81	76
PAK7	PAK7	99	100	94	97
PCK1	PCK1	100	100	93	100
PCK2	PCK2	92	100	100	100
PCK3	PCK3	100	100	100	100
PDGFRA	PDGFRA	94	92	91	75
PDGFRB	PDGFRB	100	100	70	100
PDPK1	PDPK1	82	100	91	100
PFCDPK1(P.falci parum)	PFCDPK1(P.falci parum)	98	100	90	95
PFPK5(P.falci parum)	PFPK5(P.falci parum)	100	100	86	100
PFTAIRE2	PFTAIRE2	100	77	100	88
PFTK1	PFTK1	100	100	98	100
PHKG1	PHKG1	85	100	100	87
PHKG2	PHKG2	100	100	80	83
PIK3C2B	PIK3C2B	88	86	100	83
PIK3C2G	PIK3C2G	85	100	63	98
PIK3CA	PIK3CA	100	100	100	100
PIK3CA(C420R)	PIK3CA(C420R)	98	85	100	93
PIK3CA(E542K)	PIK3CA(E542K)	64	74	84	62
PIK3CA(E545A)	PIK3CA(E545A)	100	100	100	100
PIK3CA(E545K)	PIK3CA(E545K)	81	68	70	54

**Table 22.** (continued)

DiscoverX Gene Symbol	Entrez Gene symbol	33 (SR318), % of control at 1 $\mu$ M	35 (SR321), % of control at 100 nM	218 (SR43), % of control at 1 $\mu$ M	242 (SR92), % of control at 100 nM
PIK3CA(H1047L)	PIK3CA(H1047L)	100	86	100	91
PIK3CA(H1047Y)	PIK3CA(H1047Y)	97	100	92	100
PIK3CA(I800L)	PIK3CA(I800L)	52	70	84	59
PIK3CA(M1043I)	PIK3CA(M1043I)	100	68	85	93
PIK3CA(Q546K)	PIK3CA(Q546K)	82	67	80	62
PIK3CB	PIK3CB	72	100	100	83
PIK3CD	PIK3CD	100	100	100	87
PIK3CG	PIK3CG	84	95	100	100
PIK4CB	PIK4CB	82	77	79	98
PIKFYVE	PIKFYVE	100	65	99	70
PIM1	PIM1	89	100	88	91
PIM2	PIM2	88	100	100	100
PIM3	PIM3	90	100	87	96
PIP5K1A	PIP5K1A	100	100	100	100
PIP5K1C	PIP5K1C	100	90	100	75
PIP5K2B	PIP5K2B	100	96	91	86
PIP5K2C	PIP5K2C	100	99	100	92
PKAC-alpha	PKAC-alpha	88	100	82	100
PKAC-beta	PKAC-beta	97	100	100	100
PKMYT1	PKMYT1	100	77	100	75
PKN1	PKN1	100	100	96	99
PKN2	PKN2	100	100	92	99
PKNB(M.tuberculosis)	PKNB(M.tuberculosis)	100	100	91	77
PLK1	PLK1	89	93	88	86
PLK2	PLK2	100	100	84	92
PLK3	PLK3	99	100	85	88
PLK4	PLK4	92	96	75	91
PRKCD	PRKCD	100	100	100	100
PRKCE	PRKCE	100	88	66	74
PRKCH	PRKCH	93	100	100	94
PRKCI	PRKCI	100	100	99	100
PRKCQ	PRKCQ	100	100	92	92
PRKD1	PRKD1	100	100	77	100
PRKD2	PRKD2	100	100	100	100
PRKD3	PRKD3	100	99	93	100
PRKG1	PRKG1	100	100	94	97
PRKG2	PRKG2	100	89	100	89
PRKR	PRKR	100	64	100	60
PRKX	PRKX	100	100	96	100
PRP4	PRP4	100	100	82	93

**Table 22.** (continued)

DiscoverX Gene Symbol	Entrez Gene symbol	33 (SR318), % of control at 1 $\mu$ M	35 (SR321), % of control at 100 nM	218 (SR43), % of control at 1 $\mu$ M	242 (SR92), % of control at 100 nM
PYK2	PYK2	100	93	100	100
QSK	QSK	87	76	100	100
RAF1	RAF1	100	99	96	100
RET	RET	100	89	95	93
RET(M918T)	RET(M918T)	89	100	82	80
RET(V804L)	RET(V804L)	99	100	83	90
RET(V804M)	RET(V804M)	100	100	75	99
RIOK1	RIOK1	100	100	100	91
RIOK2	RIOK2	100	100	92	100
RIOK3	RIOK3	99	100	99	100
RIPK1	RIPK1	100	89	90	73
RIPK2	RIPK2	100	97	100	65
RIPK4	RIPK4	88	58	67	83
RIPK5	RIPK5	100	100	52	84
ROCK1	ROCK1	100	100	64	100
ROCK2	ROCK2	100	100	65	94
ROS1	ROS1	96	100	96	71
RPS6KA4(Kin.Dom.1-N-terminal)	RPS6KA4(Kin.Dom.1-N-terminal)	100	83	100	74
RPS6KA4(Kin.Dom.2-C-terminal)	RPS6KA4(Kin.Dom.2-C-terminal)	100	90	69	87
RPS6KA5(Kin.Dom.1-N-terminal)	RPS6KA5(Kin.Dom.1-N-terminal)	90	100	100	100
RPS6KA5(Kin.Dom.2-C-terminal)	RPS6KA5(Kin.Dom.2-C-terminal)	100	82	93	76
RSK1(Kin.Dom.1-N-terminal)	RSK1(Kin.Dom.1-N-terminal)	100	100	91	100
RSK1(Kin.Dom.2-C-terminal)	RSK1(Kin.Dom.2-C-terminal)	100	100	100	100
RSK2(Kin.Dom.1-N-terminal)	RSK2(Kin.Dom.1-N-terminal)	100	100	97	100
RSK2(Kin.Dom.2-C-terminal)	RSK2(Kin.Dom.2-C-terminal)	100	100	80	100
RSK3(Kin.Dom.1-N-terminal)	RSK3(Kin.Dom.1-N-terminal)	100	100	88	100
RSK3(Kin.Dom.2-C-terminal)	RSK3(Kin.Dom.2-C-terminal)	83	96	85	100
RSK4(Kin.Dom.1-N-terminal)	RSK4(Kin.Dom.1-N-terminal)	95	100	90	100
RSK4(Kin.Dom.2-C-terminal)	RSK4(Kin.Dom.2-C-terminal)	29	92	85	92
S6K1	S6K1	100	96	86	73
SBK1	SBK1	89	100	86	100
SGK	SGK	100	100	63	100
SgK110	SgK110	100	100	93	99
SGK2	SGK2	100	95	74	74
SGK3	SGK3	100	92	95	100
SIK	SIK	100	91	90	100

**Table 22.** (continued)

DiscoverX Gene Symbol	Entrez Gene symbol	33 (SR318), % of control at 1 $\mu$ M	35 (SR321), % of control at 100 nM	218 (SR43), % of control at 1 $\mu$ M	242 (SR92), % of control at 100 nM
SIK2	SIK2	96	100	100	100
SLK	SLK	100	100	93	89
SNARK	SNARK	100	100	99	100
SNRK	SNRK	100	100	100	100
SRC	SRC	87	100	88	100
SRMS	SRMS	100	93	100	86
SRPK1	SRPK1	100	95	65	73
SRPK2	SRPK2	100	100	79	45
SRPK3	SRPK3	100	100	100	100
STK16	STK16	93	100	74	100
STK33	STK33	100	87	90	93
STK35	STK35	100	100	100	100
STK36	STK36	95	100	90	98
STK39	STK39	100	100	100	56
SYK	SYK	100	100	100	73
TAK1	TAK1	100	89	74	81
TAOK1	TAOK1	100	96	93	92
TAOK2	TAOK2	100	89	100	83
TAOK3	TAOK3	100	99	97	89
TBK1	TBK1	88	100	69	91
TEC	TEC	100	94	87	80
TESK1	TESK1	100	100	100	91
TGFBR1	TGFBR1	100	89	98	100
TGFBR2	TGFBR2	100	100	86	100
TIE1	TIE1	100	100	100	100
TIE2	TIE2	92	100	100	72
TLK1	TLK1	90	100	92	100
TLK2	TLK2	100	100	100	73
TNIK	TNIK	83	100	95	99
TNK1	TNK1	100	88	86	100
TNK2	TNK2	100	100	90	88
TNNI3K	TNNI3K	100	79	100	71
TRKA	TRKA	100	100	69	97
TRKB	TRKB	100	100	87	100
TRKC	TRKC	100	100	92	90
TRPM6	TRPM6	100	94	100	70
TSSK1B	TSSK1B	100	94	100	97
TSSK3	TSSK3	100	100	98	100
TTK	TTK	100	91	100	79
TXK	TXK	100	100	100	100

**Table 22.** (continued)

DiscoverX Gene Symbol	Entrez Gene symbol	33 (SR318), % of control at 1 $\mu$ M	35 (SR321), % of control at 100 nM	218 (SR43), % of control at 1 $\mu$ M	242 (SR92), % of control at 100 nM
TYK2(JH1domain-catalytic)	TYK2(JH1domain-catalytic)	78	100	91	90
TYK2(JH2domain-pseudokinase)	TYK2(JH2domain-pseudokinase)	100	100	90	97
TYRO3	TYRO3	100	100	95	99
ULK1	ULK1	100	100	100	100
ULK2	ULK2	100	100	68	96
ULK3	ULK3	100	100	90	99
VEGFR2	VEGFR2	81	97	85	80
VPS34	VPS34	100	100	100	100
VRK2	VRK2	100	100	100	83
WEE1	WEE1	100	97	96	75
WEE2	WEE2	100	100	95	100
WNK1	WNK1	100	100	100	97
WNK2	WNK2	89	100	100	100
WNK3	WNK3	100	100	100	100
WNK4	WNK4	100	100	100	100
YANK1	YANK1	95	76	100	100
YANK2	YANK2	85	100	100	100
YANK3	YANK3	100	100	100	100
YES	YES	100	100	82	100
YSK1	YSK1	93	81	96	86
YSK4	YSK4	89	89	86	71
ZAK	ZAK	8.8	100	9.4	100
ZAP70	ZAP70	89	100	91	100

**Table 23.** Selectivity screening results compounds of Chapter 5

DiscoverX Gene Symbol	Entrez Gene symbol	298 (SR277), % of control at 100 nM	300 (SR300), % of control at 1 $\mu$ M	301 (SR301), % of control at 100 nM	302 (SR302), % of control at 1 $\mu$ M	304 (SR360), % of control at 100 nM
AAK1	AAK1	96	85	90	98	100
ABL1(E255K)-phosphorylated	ABL1(E255K)-phosphorylated	100	74	87	77	83
ABL1(F317I)-nonphosphorylated	ABL1(F317I)-nonphosphorylated	99	100	88	45	100
ABL1(F317I)-phosphorylated	ABL1(F317I)-phosphorylated	100	95	95	55	90
ABL1(F317L)-nonphosphorylated	ABL1(F317L)-nonphosphorylated	79	88	100	1.2	82
ABL1(F317L)-phosphorylated	ABL1(F317L)-phosphorylated	87	96	91	13	81
ABL1(H396P)-nonphosphorylated	ABL1	82	92	99	12	92
ABL1(H396P)-phosphorylated	ABL1(H396P)-phosphorylated	100	97	100	35	100
ABL1(M351T)-phosphorylated	ABL1(M351T)-phosphorylated	100	100	100	35	99

**Table 23.** (continued)

DiscoverX Gene Symbol	Entrez Gene symbol	298 (SR277), % of control at 100 nM	300 (SR300), % of control at 1 $\mu$ M	301 (SR301), % of control at 100 nM	302 (SR302), % of control at 1 $\mu$ M	304 (SR360), % of control at 100 nM
ABL1(Q252H)-nonphosphorylated	ABL1	70	68	89	2.1	68
ABL1(Q252H)-phosphorylated	ABL1(Q252H)-phosphorylated	100	94	95	69	96
ABL1(T315I)-nonphosphorylated	ABL1(T315I)-nonphosphorylated	64	100	100	92	100
ABL1(T315I)-phosphorylated	ABL1(T315I)-phosphorylated	100	100	100	100	100
ABL1(Y253F)-phosphorylated	ABL1(Y253F)-phosphorylated	99	100	84	100	100
ABL1-nonphosphorylated	ABL1	68	80	88	3.9	74
ABL1-phosphorylated	ABL1-phosphorylated	94	74	82	27	100
ABL2	ABL2	100	84	100	23	96
ACVR1	ACVR1	97	100	88	100	100
ACVR1B	ACVR1B	84	87	94	100	100
ACVR2A	ACVR2A	69	100	68	100	100
ACVR2B	ACVR2B	84	100	83	100	100
ACVRL1	ACVRL1	100	66	97	100	100
ADCK3	ADCK3	64	86	97	98	99
ADCK4	ADCK4	100	100	100	77	100
AKT1	AKT1	97	93	100	93	100
AKT2	AKT2	97	87	100	80	87
AKT3	AKT3	97	74	86	100	100
ALK	ALK	100	100	100	100	100
ALK(C1156Y)	ALK(C1156Y)	96	100	100	90	100
ALK(L1196M)	ALK(L1196M)	100	99	100	89	100
AMPK-alpha1	AMPK-alpha1	100	100	100	100	91
AMPK-alpha2	AMPK-alpha2	100	100	100	100	100
ANKK1	ANKK1	100	100	80	100	100
ARK5	ARK5	94	98	100	99	100
ASK1	ASK1	93	100	100	91	90
ASK2	ASK2	100	100	100	95	100
AURKA	AURKA	100	100	100	100	95
AURKB	AURKB	90	100	100	100	89
AURKC	AURKC	100	94	78	100	93
AXL	AXL	88	98	79	87	96
BIKE	BIKE	100	86	84	100	95
BLK	BLK	100	100	100	71	77
BMPR1A	BMPR1A	83	66	90	91	96
BMPR1B	BMPR1B	98	100	91	92	98
BMPR2	BMPR2	100	100	100	100	100
BMX	BMX	35	94	79	100	67

**Table 23.** (continued)

DiscoverX Gene Symbol	Entrez Gene symbol	298 (SR277), % of control at 100 nM	300 (SR300), % of control at 1 $\mu$ M	301 (SR301), % of control at 100 nM	302 (SR302), % of control at 1 $\mu$ M	304 (SR360), % of control at 100 nM
BRAF	BRAF	85	100	81	11	100
BRAF(V600E)	BRAF(V600E)	100	100	100	2.9	92
BRK	BRK	89	100	76	100	100
BRSK1	BRSK1	100	100	100	100	100
BRSK2	BRSK2	72	100	79	100	86
BTK	BTK	100	100	100	100	100
BUB1	BUB1	100	100	100	100	100
CAMK1	CAMK1	89	95	96	100	100
CAMK1B	CAMK1B	100	77	100	81	100
CAMK1D	CAMK1D	100	93	97	100	100
CAMK1G	CAMK1G	90	100	92	94	90
CAMK2A	CAMK2A	74	100	100	100	100
CAMK2B	CAMK2B	90	100	100	100	94
CAMK2D	CAMK2D	93	96	93	99	100
CAMK2G	CAMK2G	97	100	94	100	100
CAMK4	CAMK4	100	70	98	75	95
CAMKK1	CAMKK1	90	100	88	100	100
CAMKK2	CAMKK2	90	100	78	100	100
CASK	CASK	100	90	100	89	100
CDC2L1	CDC2L1	100	100	100	91	100
CDC2L2	CDC2L2	99	87	87	93	100
CDC2L5	CDC2L5	100	100	100	100	100
CDK11	CDK11	67	99	90	97	77
CDK2	CDK2	100	100	100	100	99
CDK3	CDK3	100	100	82	97	100
CDK4	CDK4	100	100	91	99	100
CDK4-cyclinD1	CDK4-cyclinD1	100	100	100	100	100
CDK4-cyclinD3	CDK4-cyclinD3	100	91	100	99	100
CDK5	CDK5	81	100	94	100	92
CDK7	CDK7	100	79	100	96	80
CDK8	CDK8	100	92	100	100	100
CDK9	CDK9	97	100	87	91	100
CDKL1	CDKL1	72	100	71	100	100
CDKL2	CDKL2	100	100	100	100	100
CDKL3	CDKL3	75	94	96	81	91
CDKL5	CDKL5	98	92	100	100	100
CHEK1	CHEK1	100	100	100	100	100
CHEK2	CHEK2	86	100	100	81	84
CIT	CIT	65	91	98	89	89
CLK1	CLK1	81	100	87	88	100



**Table 23.** (continued)

DiscoverX Gene Symbol	Entrez Gene symbol	298 (SR277), % of control at 100 nM	300 (SR300), % of control at 1 $\mu$ M	301 (SR301), % of control at 100 nM	302 (SR302), % of control at 1 $\mu$ M	304 (SR360), % of control at 100 nM
CLK2	CLK2	81	100	100	100	100
CLK3	CLK3	99	100	85	100	100
CLK4	CLK4	99	94	85	100	100
CSF1R	CSF1R	100	90	100	92	98
CSF1R-autoinhibited	CSF1R-autoinhibited	100	100	100	100	100
CSK	CSK	92	98	91	100	100
CSNK1A1	CSNK1A1	100	76	99	100	84
CSNK1A1L	CSNK1A1L	93	100	100	100	100
CSNK1D	CSNK1D	93	100	96	97	100
CSNK1E	CSNK1E	100	100	100	91	86
CSNK1G1	CSNK1G1	100	100	100	95	90
CSNK1G2	CSNK1G2	100	100	82	95	99
CSNK1G3	CSNK1G3	100	100	100	98	100
CSNK2A1	CSNK2A1	100	97	94	81	93
CSNK2A2	CSNK2A2	96	81	85	100	100
CTK	CTK	100	97	100	100	48
DAPK1	DAPK1	83	96	92	100	100
DAPK2	DAPK2	81	100	90	100	100
DAPK3	DAPK3	74	100	88	100	100
DCAMKL1	DCAMKL1	100	95	100	100	100
DCAMKL2	DCAMKL2	98	90	95	89	100
DCAMKL3	DCAMKL3	99	84	87	99	100
DDR1	DDR1	0.4	0	89	0.1	0.3
DDR2	DDR2	8.4	7.7	100	0.4	1.9
DLK	DLK	100	100	100	91	100
DMPK	DMPK	84	72	100	100	95
DMPK2	DMPK2	100	100	99	100	100
DRAK1	DRAK1	100	89	100	72	78
DRAK2	DRAK2	83	100	100	90	80
DYRK1A	DYRK1A	88	90	87	100	100
DYRK1B	DYRK1B	100	100	100	68	37
DYRK2	DYRK2	100	94	100	95	80
EGFR	EGFR	100	96	100	100	98
EGFR(E746-A750del)	EGFR(E746-A750del)	100	89	100	83	100
EGFR(G719C)	EGFR(G719C)	100	87	86	86	74
EGFR(G719S)	EGFR(G719S)	89	92	72	91	77
EGFR(L747-E749del, A750P)	EGFR(L747-E749del, A750P)	98	100	93	100	86
EGFR(L747-S752del, P753S)	EGFR(L747-S752del, P753S)	83	100	66	100	100

**Table 23.** (continued)

DiscoverX Gene Symbol	Entrez Gene symbol	298 (SR277), % of control at 100 nM	300 (SR300), % of control at 1 $\mu$ M	301 (SR301), % of control at 100 nM	302 (SR302), % of control at 1 $\mu$ M	304 (SR360), % of control at 100 nM
EGFR(L747-T751del,Sins)	EGFR(L747-T751del,Sins)	100	57	94	85	61
EGFR(L858R)	EGFR(L858R)	100	100	100	100	93
EGFR(L858R,T790M)	EGFR(L858R,T790M)	95	59	84	84	100
EGFR(L861Q)	EGFR(L861Q)	100	54	100	59	100
EGFR(S752-I759del)	EGFR(S752-I759del)	100	79	100	54	69
EGFR(T790M)	EGFR(T790M)	100	91	100	100	100
EIF2AK1	EIF2AK1	100	97	81	100	100
EPHA1	EPHA1	96	100	95	100	100
EPHA2	EPHA2	58	100	100	79	82
EPHA3	EPHA3	77	99	75	100	100
EPHA4	EPHA4	95	88	76	98	100
EPHA5	EPHA5	98	100	96	100	100
EPHA6	EPHA6	87	97	100	100	100
EPHA7	EPHA7	94	100	98	100	100
EPHA8	EPHA8	100	100	100	98	100
EPHB1	EPHB1	100	85	100	100	100
EPHB2	EPHB2	85	100	87	100	98
EPHB3	EPHB3	83	100	91	100	100
EPHB4	EPHB4	100	100	96	100	100
EPHB6	EPHB6	100	76	100	87	100
ERBB2	ERBB2	100	86	100	100	100
ERBB3	ERBB3	100	88	100	100	99
ERBB4	ERBB4	81	100	61	100	100
ERK1	ERK1	100	100	89	100	96
ERK2	ERK2	97	100	90	100	86
ERK3	ERK3	100	100	94	100	100
ERK4	ERK4	100	100	96	100	100
ERK5	ERK5	100	100	94	91	100
ERK8	ERK8	100	100	100	86	100
ERN1	ERN1	96	96	100	100	83
FAK	FAK	96	100	100	100	100
FER	FER	75	88	86	100	100
FES	FES	91	100	87	100	100
FGFR1	FGFR1	82	100	91	100	98
FGFR2	FGFR2	100	100	97	78	96
FGFR3	FGFR3	89	100	100	100	100
FGFR3(G697C)	FGFR3	82	99	83	89	100
FGFR4	FGFR4	100	100	100	100	100
FGR	FGR	88	84	88	100	100

**Table 23.** (continued)

DiscoverX Gene Symbol	Entrez Gene symbol	298 (SR277), % of control at 100 nM	300 (SR300), % of control at 1 $\mu$ M	301 (SR301), % of control at 100 nM	302 (SR302), % of control at 1 $\mu$ M	304 (SR360), % of control at 100 nM
FLT1	FLT1	100	100	86	100	100
FLT3	FLT3	85	98	82	100	100
FLT3(D835H)	FLT3(D835H)	100	67	94	93	61
FLT3(D835V)	FLT3(D835V)	100	100	89	100	100
FLT3(D835Y)	FLT3	100	100	93	100	100
FLT3(ITD)	FLT3(ITD)	100	91	80	100	100
FLT3(ITD,D835V)	FLT3(ITD,D835V)	100	74	100	90	100
FLT3(ITD,F691L)	FLT3(ITD,F691L)	100	100	100	100	85
FLT3(K663Q)	FLT3	100	100	94	100	85
FLT3(N841I)	FLT3(N841I)	91	100	99	100	100
FLT3(R834Q)	FLT3	100	100	94	100	100
FLT3-autoinhibited	FLT3-autoinhibited	98	79	97	85	100
FLT4	FLT4	100	76	81	100	100
FRK	FRK	86	100	60	42	100
FYN	FYN	84	100	56	90	100
GAK	GAK	97	90	95	79	100
GCN2(Kin.Dom.2,S808G)	GCN2(Kin.Dom.2,S808G)	100	91	100	100	100
GRK1	GRK1	100	100	94	97	100
GRK2	GRK2	100	60	72	81	100
GRK3	GRK3	100	97	100	100	100
GRK4	GRK4	100	94	100	100	74
GRK7	GRK7	100	100	100	100	100
GSK3A	GSK3A	97	88	100	43	100
GSK3B	GSK3B	100	100	100	100	99
HASPIN	HASPIN	100	89	100	9.5	62
HCK	HCK	100	92	100	100	92
HIPK1	HIPK1	100	90	100	96	98
HIPK2	HIPK2	100	100	100	100	100
HIPK3	HIPK3	100	100	100	100	95
HIPK4	HIPK4	100	100	100	100	100
HPK1	HPK1	100	85	100	100	100
HUNK	HUNK	100	100	100	100	100
ICK	ICK	100	91	100	100	98
IGF1R	IGF1R	81	100	100	100	100
IKK-alpha	IKK-alpha	100	100	100	100	100
IKK-beta	IKK-beta	100	100	100	100	100
IKK-epsilon	IKK-epsilon	64	96	73	100	100
INSR	INSR	100	92	100	92	100
INSRR	INSRR	100	94	100	81	100

**Table 23.** (continued)

DiscoverX Gene Symbol	Entrez Gene symbol	298 (SR277), % of control at 100 nM	300 (SR300), % of control at 1 $\mu$ M	301 (SR301), % of control at 100 nM	302 (SR302), % of control at 1 $\mu$ M	304 (SR360), % of control at 100 nM
IRAK1	IRAK1	100	94	100	97	100
IRAK3	IRAK3	100	91	100	100	84
IRAK4	IRAK4	100	73	100	83	100
ITK	ITK	100	100	100	100	100
JAK1(JH1domain-catalytic)	JAK1(JH1domain-catalytic)	96	100	100	95	100
JAK1(JH2domain-pseudokinase)	JAK1(JH2domain-pseudokinase)	100	100	89	100	100
JAK2(JH1domain-catalytic)	JAK2(JH1domain-catalytic)	100	82	100	75	97
JAK3(JH1domain-catalytic)	JAK3(JH1domain-catalytic)	100	100	100	100	100
JNK1	JNK1	88	82	85	85	80
JNK2	JNK2	92	94	83	92	86
JNK3	JNK3	100	89	100	100	75
KIT	KIT	100	83	89	16	94
KIT(A829P)	KIT	100	100	100	35	100
KIT(D816H)	KIT(D816H)	100	76	68	73	100
KIT(D816V)	KIT(D816V)	80	98	100	82	100
KIT(L576P)	KIT	69	98	78	40	100
KIT(V559D)	KIT	89	92	93	8.5	91
KIT(V559D,T670I)	KIT(V559D,T670I)	95	79	100	100	100
KIT(V559D,V654A)	KIT(V559D,V654A)	89	99	100	75	79
KIT-autoinhibited	KIT-autoinhibited	100	100	100	100	99
LATS1	LATS1	100	77	100	100	100
LATS2	LATS2	100	100	100	100	100
LCK	LCK	85	83	100	35	100
LIMK1	LIMK1	100	94	100	100	100
LIMK2	LIMK2	100	100	100	99	100
LKB1	LKB1	100	79	100	76	96
LOK	LOK	100	100	100	100	97
LRRK2	LRRK2	41	100	51	99	100
LRRK2(G2019S)	LRRK2(G2019S)	100	100	100	100	100
LTK	LTK	100	100	100	100	85
LYN	LYN	94	100	96	83	90
LZK	LZK	100	100	100	100	100
MAK	MAK	100	84	100	100	88
MAP3K1	MAP3K1	100	100	81	100	77
MAP3K15	MAP3K15	100	100	74	69	84
MAP3K2	MAP3K2	100	90	100	77	100
MAP3K3	MAP3K3	100	87	100	96	100
MAP3K4	MAP3K4	79	99	75	86	98

**Table 23.** (continued)

DiscoverX Gene Symbol	Entrez Gene symbol	298 (SR277), % of control at 100 nM	300 (SR300), % of control at 1 $\mu$ M	301 (SR301), % of control at 100 nM	302 (SR302), % of control at 1 $\mu$ M	304 (SR360), % of control at 100 nM
MAP4K2	MAP4K2	100	100	100	89	100
MAP4K3	MAP4K3	70	100	75	100	100
MAP4K4	MAP4K4	75	100	66	100	100
MAP4K5	MAP4K5	82	100	76	100	96
MAPKAPK2	MAPKAPK2	100	100	100	100	74
MAPKAPK5	MAPKAPK5	100	100	100	95	100
MARK1	MARK1	72	100	74	100	90
MARK2	MARK2	100	100	100	100	100
MARK3	MARK3	46	100	100	100	79
MARK4	MARK4	65	100	71	100	95
MAST1	MAST1	86	100	100	100	100
MEK1	MEK1	100	100	100	94	100
MEK2	MEK2	100	100	90	100	100
MEK3	MEK3	100	100	85	95	100
MEK4	MEK4	100	100	100	84	100
MEK5	MEK5	98	91	100	100	100
MEK6	MEK6	75	100	67	100	54
MELK	MELK	95	100	100	67	33
MERTK	MERTK	100	88	91	100	71
MET	MET	68	100	68	100	100
MET(M1250T)	MET(M1250T)	80	100	87	100	100
MET(Y1235D)	MET(Y1235D)	91	100	98	99	100
MINK	MINK	100	100	85	100	77
MKK7	MKK7	100	90	100	100	100
MKNK1	MKNK1	82	100	86	99	100
MKNK2	MKNK2	100	97	100	100	75
MLCK	MLCK	100	85	100	100	57
MLK1	MLK1	100	100	90	100	100
MLK2	MLK2	70	100	73	100	94
MLK3	MLK3	75	89	92	94	100
MRCKA	MRCKA	100	100	100	100	100
MRCKB	MRCKB	100	95	90	99	100
MST1	MST1	100	100	100	100	90
MST1R	MST1R	100	85	97	100	99
MST2	MST2	97	100	95	100	91
MST3	MST3	94	97	100	87	100
MST4	MST4	100	100	92	86	100
MTOR	MTOR	100	96	100	95	100
MUSK	MUSK	95	100	100	90	100
MYLK	MYLK	100	96	100	89	100

**Table 23.** (continued)

DiscoverX Gene Symbol	Entrez Gene symbol	298 (SR277), % of control at 100 nM	300 (SR300), % of control at 1 $\mu$ M	301 (SR301), % of control at 100 nM	302 (SR302), % of control at 1 $\mu$ M	304 (SR360), % of control at 100 nM
MYLK2	MYLK2	84	94	90	100	100
MYLK4	MYLK4	94	98	100	100	100
MYO3A	MYO3A	96	100	97	100	96
MYO3B	MYO3B	100	66	100	96	60
NDR1	NDR1	97	100	83	99	79
NDR2	NDR2	35	100	24	100	97
NEK1	NEK1	43	100	51	88	52
NEK10	NEK10	100	93	100	18	100
NEK11	NEK11	100	100	100	100	100
NEK2	NEK2	92	100	100	100	99
NEK3	NEK3	100	96	100	90	100
NEK4	NEK4	100	74	100	77	89
NEK5	NEK5	79	100	95	92	100
NEK6	NEK6	77	100	86	100	91
NEK7	NEK7	97	100	88	100	100
NEK9	NEK9	100	100	100	100	100
NIK	NIK	100	99	83	90	100
NIM1	NIM1	92	93	60	87	100
NLK	NLK	100	96	100	72	100
OSR1	OSR1	100	92	100	100	97
p38-alpha	p38-alpha	100	1.5	100	0	29
p38-beta	p38-beta	89	20	100	3.4	70
p38-delta	p38-delta	100	87	100	100	94
p38-gamma	p38-gamma	100	98	100	99	100
PAK1	PAK1	86	79	100	89	100
PAK2	PAK2	84	69	100	76	97
PAK3	PAK3	96	100	100	100	77
PAK4	PAK4	90	100	100	100	100
PAK6	PAK6	100	97	100	99	100
PAK7	PAK7	100	96	100	100	100
PCK1	PCK1	100	100	100	100	100
PCK2	PCK2	71	100	86	90	100
PCK3	PCK3	100	84	100	85	100
PDGFRA	PDGFRA	100	100	91	89	100
PDGFRB	PDGFRB	100	100	86	100	100
PDPK1	PDPK1	93	97	99	100	100
PFCDPK1(P.falciparum)	PFCDPK1(P.falciparum)	95	79	100	80	63
PFPK5(P.falciparum)	PFPK5(P.falciparum)	100	100	100	100	88
PFTAIRE2	PFTAIRE2	78	100	74	100	100

**Table 23.** (continued)

DiscoverX Gene Symbol	Entrez Gene symbol	298 (SR277), % of control at 100 nM	300 (SR300), % of control at 1 $\mu$ M	301 (SR301), % of control at 100 nM	302 (SR302), % of control at 1 $\mu$ M	304 (SR360), % of control at 100 nM
PFTK1	PFTK1	99	100	100	100	100
PHKG1	PHKG1	81	89	87	86	100
PHKG2	PHKG2	91	100	100	100	100
PIK3C2B	PIK3C2B	83	100	95	100	100
PIK3C2G	PIK3C2G	97	87	81	94	69
PIK3CA	PIK3CA	90	100	98	100	99
PIK3CA(C420R)	PIK3CA(C420R)	100	88	89	88	100
PIK3CA(E542K)	PIK3CA(E542K)	91	80	64	73	100
PIK3CA(E545A)	PIK3CA(E545A)	100	100	100	100	100
PIK3CA(E545K)	PIK3CA(E545K)	77	79	53	86	98
PIK3CA(H1047L)	PIK3CA(H1047L)	73	100	76	92	100
PIK3CA(H1047Y)	PIK3CA(H1047Y)	100	90	100	100	100
PIK3CA(I800L)	PIK3CA(I800L)	77	100	44	54	100
PIK3CA(M1043I)	PIK3CA(M1043I)	76	91	87	100	73
PIK3CA(Q546K)	PIK3CA(Q546K)	82	95	60	85	100
PIK3CB	PIK3CB	80	81	81	77	100
PIK3CD	PIK3CD	61	87	91	100	99
PIK3CG	PIK3CG	100	100	85	100	85
PIK4CB	PIK4CB	100	100	100	87	91
PIKFYVE	PIKFYVE	80	81	61	100	100
PIM1	PIM1	90	96	95	100	100
PIM2	PIM2	77	97	88	100	100
PIM3	PIM3	99	88	100	89	100
PIP5K1A	PIP5K1A	100	100	100	100	85
PIP5K1C	PIP5K1C	73	100	85	100	100
PIP5K2B	PIP5K2B	100	74	100	100	100
PIP5K2C	PIP5K2C	100	100	100	100	100
PKAC-alpha	PKAC-alpha	100	95	100	100	100
PKAC-beta	PKAC-beta	95	100	92	100	100
PKMYT1	PKMYT1	60	92	74	100	100
PKN1	PKN1	100	100	98	100	100
PKN2	PKN2	100	67	95	100	100
PKNB(M.tuberculosis)	PKNB(M.tuberculosis)	100	91	90	100	100
PLK1	PLK1	100	56	80	86	82
PLK2	PLK2	100	96	99	100	91
PLK3	PLK3	100	89	100	93	100
PLK4	PLK4	100	92	82	100	89
PRKCD	PRKCD	67	100	80	100	92
PRKCE	PRKCE	100	93	63	77	100
PRKCH	PRKCH	100	97	79	100	100

**Table 23.** (continued)

DiscoverX Gene Symbol	Entrez Gene symbol	298 (SR277), % of control at 100 nM	300 (SR300), % of control at 1 $\mu$ M	301 (SR301), % of control at 100 nM	302 (SR302), % of control at 1 $\mu$ M	304 (SR360), % of control at 100 nM
PRKCI	PRKCI	100	100	100	100	100
PRKCQ	PRKCQ	86	76	90	80	100
PRKD1	PRKD1	99	74	91	89	100
PRKD2	PRKD2	77	100	92	100	100
PRKD3	PRKD3	100	100	100	91	100
PRKG1	PRKG1	87	100	95	100	100
PRKG2	PRKG2	78	100	79	100	100
PRKR	PRKR	46	72	55	100	100
PRKX	PRKX	100	100	100	100	89
PRP4	PRP4	52	82	60	100	74
PYK2	PYK2	99	79	94	95	100
QSK	QSK	99	100	78	65	100
RAF1	RAF1	80	100	70	21	91
RET	RET	81	100	87	100	100
RET(M918T)	RET(M918T)	100	100	93	97	100
RET(V804L)	RET(V804L)	100	93	83	100	96
RET(V804M)	RET(V804M)	100	100	82	100	100
RIOK1	RIOK1	100	100	54	100	88
RIOK2	RIOK2	97	100	99	85	100
RIOK3	RIOK3	100	85	88	100	98
RIPK1	RIPK1	100	100	94	98	100
RIPK2	RIPK2	84	100	59	100	100
RIPK4	RIPK4	93	88	100	91	100
RIPK5	RIPK5	100	77	80	100	98
ROCK1	ROCK1	100	84	93	100	100
ROCK2	ROCK2	100	98	100	100	100
ROS1	ROS1	68	93	91	100	97
RPS6KA4(Kin.Dom.1-N-terminal)	RPS6KA4(Kin.Dom.1-N-terminal)	79	100	86	100	100
RPS6KA4(Kin.Dom.2-C-terminal)	RPS6KA4(Kin.Dom.2-C-terminal)	100	100	91	95	95
RPS6KA5(Kin.Dom.1-N-terminal)	RPS6KA5(Kin.Dom.1-N-terminal)	96	91	81	100	100
RPS6KA5(Kin.Dom.2-C-terminal)	RPS6KA5(Kin.Dom.2-C-terminal)	100	100	95	100	95
RSK1(Kin.Dom.1-N-terminal)	RSK1(Kin.Dom.1-N-terminal)	90	94	100	100	94
RSK1(Kin.Dom.2-C-terminal)	RSK1(Kin.Dom.2-C-terminal)	92	100	100	87	100
RSK2(Kin.Dom.1-N-terminal)	RSK2(Kin.Dom.1-N-terminal)	100	100	100	91	100
RSK2(Kin.Dom.2-C-terminal)	RSK2(Kin.Dom.2-C-terminal)	100	90	100	100	96
RSK3(Kin.Dom.1-N-terminal)	RSK3(Kin.Dom.1-N-terminal)	100	83	100	96	98



**Table 23.** (continued)

DiscoverX Gene Symbol	Entrez Gene symbol	298 (SR277), % of control at 100 nM	300 (SR300), % of control at 1 $\mu$ M	301 (SR301), % of control at 100 nM	302 (SR302), % of control at 1 $\mu$ M	304 (SR360), % of control at 100 nM
RSK3(Kin.Dom.2-C-terminal)	RSK3(Kin.Dom.2-C-terminal)	83	96	100	100	97
RSK4(Kin.Dom.1-N-terminal)	RSK4(Kin.Dom.1-N-terminal)	100	92	100	84	100
RSK4(Kin.Dom.2-C-terminal)	RSK4(Kin.Dom.2-C-terminal)	96	99	100	77	100
S6K1	S6K1	100	90	100	100	100
SBK1	SBK1	96	85	82	79	100
SGK	SGK	100	100	100	98	100
SgK110	SgK110	84	100	100	100	52
SGK2	SGK2	94	100	100	84	100
SGK3	SGK3	100	100	83	100	100
SIK	SIK	91	99	100	100	98
SIK2	SIK2	100	100	86	92	100
SLK	SLK	79	89	100	100	100
SNARK	SNARK	100	100	100	100	100
SNRK	SNRK	100	93	81	100	98
SRC	SRC	96	88	94	96	100
SRMS	SRMS	100	100	98	100	100
SRPK1	SRPK1	88	68	78	100	92
SRPK2	SRPK2	100	100	34	100	39
SRPK3	SRPK3	100	100	100	100	74
STK16	STK16	100	86	100	100	94
STK33	STK33	82	88	84	92	43
STK35	STK35	100	100	100	100	100
STK36	STK36	100	97	97	98	96
STK39	STK39	100	86	100	73	100
SYK	SYK	71	73	88	100	100
TAK1	TAK1	100	92	100	100	84
TAOK1	TAOK1	100	100	100	99	100
TAOK2	TAOK2	100	93	93	96	100
TAOK3	TAOK3	100	100	100	100	93
TBK1	TBK1	75	85	88	100	100
TEC	TEC	100	100	100	100	100
TESK1	TESK1	94	100	100	100	100
TGFBR1	TGFBR1	98	100	100	100	100
TGFBR2	TGFBR2	100	86	93	99	96
TIE1	TIE1	100	97	100	97	100
TIE2	TIE2	78	100	73	100	100
TLK1	TLK1	69	100	94	100	100
TLK2	TLK2	88	86	82	100	100

**Table 23.** (continued)

DiscoverX Gene Symbol	Entrez Gene symbol	298 (SR277), % of control at 100 nM	300 (SR300), % of control at 1 $\mu$ M	301 (SR301), % of control at 100 nM	302 (SR302), % of control at 1 $\mu$ M	304 (SR360), % of control at 100 nM
TNIK	TNIK	100	91	45	98	97
TNK1	TNK1	92	92	96	100	93
TNK2	TNK2	100	97	91	100	100
TNNI3K	TNNI3K	69	100	63	100	100
TRKA	TRKA	100	100	100	98	100
TRKB	TRKB	100	91	100	92	100
TRKC	TRKC	100	93	86	100	100
TRPM6	TRPM6	100	100	96	100	100
TSSK1B	TSSK1B	97	85	85	100	81
TSSK3	TSSK3	91	95	100	92	100
TTK	TTK	88	92	91	100	96
TXK	TXK	74	100	77	100	94
TYK2(JH1domain-catalytic)	TYK2(JH1domain-catalytic)	100	58	99	49	100
TYK2(JH2domain-pseudokinase)	TYK2(JH2domain-pseudokinase)	100	100	100	100	93
TYRO3	TYRO3	100	100	90	98	100
ULK1	ULK1	100	100	100	100	100
ULK2	ULK2	100	100	100	100	100
ULK3	ULK3	98	87	99	87	100
VEGFR2	VEGFR2	100	92	85	81	100
VPS34	VPS34	100	100	100	100	100
VRK2	VRK2	100	86	91	69	100
WEE1	WEE1	75	100	72	100	100
WEE2	WEE2	94	100	100	100	100
WNK1	WNK1	100	100	100	99	100
WNK2	WNK2	100	100	100	100	100
WNK3	WNK3	100	100	85	83	100
WNK4	WNK4	100	100	100	89	100
YANK1	YANK1	98	90	57	99	97
YANK2	YANK2	80	100	65	100	100
YANK3	YANK3	100	83	100	100	100
YES	YES	100	92	98	100	100
YSK1	YSK1	100	94	90	90	40
YSK4	YSK4	100	94	92	83	90
ZAK	ZAK	79	76	89	38	74
ZAP70	ZAP70	100	100	100	92	100

## 9 Abbreviations

- AcOH: acetic acid  
 aq: aqueous  
 ATP: adenosine triphosphate  
 ax: axial  
 BCR-ABL: breakpoint cluster region - abelson tyrosine-protein kinase  
 Boc: *tert*-butyloxycarbonyl  
 Boc<sub>2</sub>O: di-*tert*-butyl dicarbonate  
 BRET: bioluminescence resonance energy transfer  
 calcd.: calculated  
 CDI: 1,1'-carbonyldiimidazole  
 CDK: cyclin-dependent kinase  
 compd.: compound  
 conc.: concentrated  
 COPD: chronic obstructive pulmonary disease  
 COSY: homonuclear correlation spectroscopy  
 COX: cyclooxygenase  
 CRP: c-reactive protein  
 δ: chemical shift (in ppm) or delta  
 ΔT: heating  
 ΔT<sub>m</sub>: differences in the melting temperature  
 d: doublet (NMR) or day(s)  
 DCC: *N,N'*-dicyclohexylcarbodiimide  
 DCM: dichloromethane  
 DDR: discoidin domain receptor  
 DEPT: distortionless enhancement by polarization transfer  
 DIPEA: *N,N*-diisopropylethylamine  
 DMF: *N,N*-dimethylformamide  
 DMSO: dimethylsulfoxide  
 DNA: deoxyribonucleic acid  
 DSF: differential scanning fluorimetry  
 DUSP10: dual specificity protein phosphatase 10  
 ED<sub>50</sub>: median effective dose  
 EDC-HCl: 1-ethyl-3-(3-dimethylaminopropyl)carbodiimid-hydrochloride  
 EGFR: epidermal growth factor receptor  
 Et<sub>2</sub>O: ethoxyethane  
 EtOAc: ethyl acetate  
 EtOH: ethanol  
 EPHA2: ephrin type-A receptor 2  
 eq: equivalents or equatorial  
 ERK1/2: extracellular signal-regulated kinase 1/2  
 ESI: electron spray ionization  
 et al.: (lat.) et alii or et aliae  
 FDA: U. S. Food and Drug Administration  
 Fmoc: fluorenylmethoxycarbonyl  
 FTMS: fourier-transform mass spectrometry  
 fr. = fragment  
 ΔG: Gibbs free energy or binding affinity  
 GK: gatekeeper  
 HAc: acetic acid  
 HATU: *N*-[(dimethylamino)-1*H*-1,2,3-triazolo-[4,5-*b*]pyridin-1-ylmethylene]-*N*-methylmethanaminium hexafluorophosphate *N*-oxide  
 HCl: hydrochloric acid  
 HLM: human liver microsomes  
 HMBC: heteronuclear multiple bond correlation  
 HOBt: 1-hydroxybenzotriazole  
 HPLC: high performance liquid chromatography  
 HRI/II: hydrophobic region 1/2  
 HRMS: high resolution mass spectrometry  
 Hsp27: heat shock protein 27  
 HSQC: heteronuclear single quantum coherence  
 h: hour(s)  
 IL: interleukin  
 IR: insulin receptor  
*J*: coupling constant (in Hz)  
 K<sub>d</sub>: dissociation constant  
 K<sub>i</sub>: inhibitory constant  
 KIT: mast/stem cell growth factor receptor  
 KOtBu: potassium *tert*-butoxide  
 LC: liquid chromatography  
 LiOH: lithium hydroxide  
 IC<sub>50</sub>: half maximal inhibitory concentration  
 lit.: literature  
 LPS: lipopolysaccharide  
 M: molarity (in mol/L)  
 MALDI: matrix-assisted laser desorption/ionization  
 MAPK: mitogene activated protein kinase  
 MEK1/2: dual specificity mitogen-activated protein kinase kinase 1/2  
 MeOH: methanol  
 min: minute(s)  
 MK2: map kinase-activated protein kinase 2  
 MS: mass spectrometry  
 MW: microwave  
 MYLK4: myosin light chain kinase family member 4  
 n: number of repeats  
 N: equivalent concentration or normality (in mol/L)  
 NaOH: sodium hydroxide  
 NaBH(OAc)<sub>3</sub>: sodium triacetoxymethylborohydride  
 NDR2: nuclear Dbf2-related kinase 2  
 NFκB: nuclear factor kappa-light-chain-enhancer of activated B cells  
 NMR: nuclear magnetic resonance  
 PDB: protein data bank  
 PDGFR: platelet-derived growth factor receptors  
 ppm: parts per million  
 PTC: phase transfer catalyst  
 q: quartet (NMR)  
 p: quintet  
 quant.: quantitative  
 rac: racemic  
 R<sub>f</sub>: retention factor  
 rpm: rounds per minute  
 RSK4: ribosomal protein S6 kinase alpha-6  
 RT: room temperature  
 RTK: receptor tyrosine kinase  
 s: singlet (NMR)  
 S: standard selectivity score  
 SAR: structure-activity relationship  
 sat.: saturated  
 SD: standard deviation  
 SEM: standard error of the mean  
 sept: septet  
 SEM: standard error of mean  
 sext: sextet  
 SLK: STE20-like kinase  
 STK: serine/threonine-protein kinase  
 t: triplet (NMR)  
 t<sub>R</sub>: retention time  
 TEA: trimethylamine  
 TEBA: benzyltriethylammonium chloride  
 TFA: trifluoroacetic acid  
 THF: tetrahydrofurane  
 TLC: thin-layer chromatography  
 TMS: trimethylsilyl  
 TNF-α: tumor necrosis factor alpha  
 TRKA/B/C: tropomyosin receptor kinases A/B/C  
 UV/Vis: ultraviolet and visible light  
 ZAK: leucine zipper- and sterile alpha motif kinase

## 10 References

1. Bononi, A.; Agnoletto, C.; De Marchi, E.; Marchi, S.; Patergnani, S.; Bonora, M.; Giorgi, C.; Missiroli, S.; Poletti, F.; Rimessi, A.; Pinton, P. Protein kinases and phosphatases in the control of cell fate. *Enzyme Res* **2011**, 2011, 329098-329098.
2. Manning, G.; Whyte, D. B.; Martinez, R.; Hunter, T.; Sudarsanam, S. The Protein Kinase Complement of the Human Genome. *Science* **2002**, 298, 1912.
3. Fabbro, D.; Cowan-Jacob, S. W.; Moebitz, H. Ten things you should know about protein kinases: IUPHAR Review 14. *Br J Pharmacol* **2015**, 172, 2675-2700.
4. Zheng, J.; Trafny, E. A.; Knighton, D. R.; Xuong, N.; Taylor, S. S.; Ten Eyck, L. F.; Sowadski, J. M. 2.2 A refined crystal structure of the catalytic subunit of cAMP-dependent protein kinase complexed with MnATP and a peptide inhibitor. *Acta Crystallographica Section D* **1993**, 49, 362-365.
5. Taylor, S. S.; Knighton, D. R.; Zheng, J.; Eyck, L. F. T.; Sowadski, J. M. Structural Framework for the Protein Kinase Family. *Annual Review of Cell Biology* **1992**, 8, 429-462.
6. Roskoski, R. Classification of small molecule protein kinase inhibitors based upon the structures of their drug-enzyme complexes. *Pharmacological Research* **2016**, 103, 26-48.
7. Johnson, L. N.; Lewis, R. J. Structural Basis for Control by Phosphorylation. *Chemical Reviews* **2001**, 101, 2209-2242.
8. Nolen, B.; Taylor, S.; Ghosh, G. Regulation of Protein Kinases: Controlling Activity through Activation Segment Conformation. *Molecular Cell* **2004**, 15, 661-675.
9. Kornev, A. P.; Haste, N. M.; Taylor, S. S.; Eyck, L. F. T. Surface comparison of active and inactive protein kinases identifies a conserved activation mechanism. *Proc Natl Acad Sci U S A* **2006**, 103, 17783-17788.
10. Kornev, A. P.; Taylor, S. S. Dynamics-Driven Allostery in Protein Kinases. *Trends Biochem Sci* **2015**, 40, 628-647.
11. Ten Eyck, L. F.; Taylor, S. S.; Kornev, A. P. Conserved spatial patterns across the protein kinase family. *Biochimica et Biophysica Acta (BBA) - Proteins and Proteomics* **2008**, 1784, 238-243.
12. Taylor, S. S.; Kornev, A. P. Protein kinases: evolution of dynamic regulatory proteins. *Trends Biochem Sci* **2011**, 36, 65-77.
13. Kornev, A. P.; Taylor, S. S.; Ten Eyck, L. F. A Helix Scaffold for the Assembly of Active Protein Kinases. *Proc. Natl. Acad. Sci. U. S. A.* **2008**, 105, 14377.
14. Huse, M.; Kuriyan, J. The conformational plasticity of protein kinases. *Cell* **2002**, 109, 275.
15. Noble, M. E. M.; Endicott, J. A.; Johnson, L. N. Protein Kinase Inhibitors: Insights into Drug Design from Structure. *Science* **2004**, 303, 1800-1805.
16. Tong, M.; Seeliger, M. A. Targeting Conformational Plasticity of Protein Kinases. *ACS Chem Biol* **2015**, 10, 190-200.
17. Kar, G.; Keskin, O.; Gursoy, A.; Nussinov, R. Allostery and population shift in drug discovery. *Current Opinion in Pharmacology* **2010**, 10, 715-722.
18. Bhullar, K. S.; Lagarón, N. O.; McGowan, E. M.; Parmar, I.; Jha, A.; Hubbard, B. P.; Rupasinghe, H. P. V. Kinase-targeted cancer therapies: progress, challenges and future directions. *Mol Cancer* **2018**, 17, 48-48.
19. Cohen, P. Protein kinases — the major drug targets of the twenty-first century? *Nature Reviews Drug Discovery* **2002**, 1, 309-315.
20. Fabbro, D.; Cowan-Jacob, S. W.; Möbitz, H.; Martiny-Baron, G. Targeting Cancer with Small-Molecular-Weight Kinase Inhibitors. In *Kinase Inhibitors: Methods and Protocols*, Kuster, B., Ed. Humana Press: Totowa, NJ, 2012; pp 1-34.
21. Hanahan, D.; Weinberg, R. A. The Hallmarks of Cancer. *Cell* **2000**, 100, 57-70.
22. Hunter, T. Signaling & 2000 and Beyond. *Cell* **2000**, 100, 113-127.
23. Blume-Jensen, P.; Hunter, T. Oncogenic kinase signalling. *Nature* **2001**, 411, 355-365.
24. Schindler, T.; Bornmann, W.; Pellicena, P.; Miller, W. T.; Clarkson, B.; Kuriyan, J. Structural Mechanism for STI-571 Inhibition of Abelson Tyrosine Kinase. *Science* **2000**, 289, 1938-1942.
25. Kantarjian, H. M.; Fojo, T.; Mathisen, M.; Zwelling, L. A. Cancer drugs in the United States: Justum Pretium—the just price. *J Clin Oncol* **2013**, 31, 3600-3604.
26. Roskoski, R. Properties of FDA-approved small molecule protein kinase inhibitors. *Pharmacological Research* **2019**, 144, 19-50.
27. Knapp, S.; Sundström, M. Recently targeted kinases and their inhibitors—the path to clinical trials. *Current Opinion in Pharmacology* **2014**, 17, 58-63.
28. Fedorov, O.; Müller, S.; Knapp, S. The (un)targeted cancer kinome. *Nature Chemical Biology* **2010**, 6, 166-169.
29. Henrik, M.; Wolfgang, J.; Sandra, W. C.-J. Expanding the Opportunities for Modulating Kinase Targets with Allosteric Approaches. *Current Topics in Medicinal Chemistry* **2017**, 17, 59-70.
30. Cowan-Jacob, S. W.; Jahnke, W.; Knapp, S. Novel approaches for targeting kinases: allosteric inhibition, allosteric activation and pseudokinases. *Future Medicinal Chemistry* **2014**, 6, 541-561.
31. Müller, S.; Chaikuad, A.; Gray, N. S.; Knapp, S. The ins and outs of selective kinase inhibitor development. *Nature Chemical Biology* **2015**, 11, 818-821.
32. Liu, Q.; Sabnis, Y.; Zhao, Z.; Zhang, T.; Buhrlage, S. J.; Jones, L. H.; Gray, N. S. Developing irreversible inhibitors of the protein kinase cysteinome. *Chemistry & biology* **2013**, 20, 146-159.
33. Chaikuad, A.; Koch, P.; Laufer, S. A.; Knapp, S. The Cysteinome of Protein Kinases as a Target in Drug Development. *Angewandte Chemie International Edition* **2018**, 57, 4372-4385.
34. Knight, Z. A.; Shokat, K. M. Features of Selective Kinase Inhibitors. *Chemistry & Biology* **2005**, 12, 621-637.

35. Berman, H. M.; Westbrook, J.; Feng, Z.; Gilliland, G.; Bhat, T. N.; Weissig, H.; Shindyalov, I. N.; Bourne, P. E. The Protein Data Bank. *Nucleic Acids Res* **2000**, *28*, 235-242.
36. Vijayan, R. S. K.; He, P.; Modi, V.; Duong-Ly, K. C.; Ma, H.; Peterson, J. R.; Dunbrack, R. L.; Levy, R. M. Conformational Analysis of the DFG-Out Kinase Motif and Biochemical Profiling of Structurally Validated Type II Inhibitors. *Journal of Medicinal Chemistry* **2015**, *58*, 466-479.
37. Davis, M. I.; Hunt, J. P.; Herrgard, S.; Ciceri, P.; Wodicka, L. M.; Pallares, G.; Hocker, M.; Treiber, D. K.; Zarrinkar, P. P. Comprehensive analysis of kinase inhibitor selectivity. *Nat. Biotechnol.* **2011**, *29*, 1046.
38. Bishop, A. C.; Ubersax, J. A.; Petsch, D. T.; Matheos, D. P.; Gray, N. S.; Blethrow, J.; Shimizu, E.; Tsien, J. Z.; Schultz, P. G.; Rose, M. D.; Wood, J. L.; Morgan, D. O.; Shokat, K. M. A chemical switch for inhibitor-sensitive alleles of any protein kinase. *Nature* **2000**, *407*, 395-401.
39. Zou, H. Y.; Li, Q.; Engstrom, L. D.; West, M.; Appleman, V.; Wong, K. A.; McTigue, M.; Deng, Y.-L.; Liu, W.; Brooun, A.; Timofeevski, S.; McDonnell, S. R. P.; Jiang, P.; Falk, M. D.; Lappin, P. B.; Affolter, T.; Nichols, T.; Hu, W.; Lam, J.; Johnson, T. W.; Smeal, T.; Charest, A.; Fantin, V. R. PF-06463922 is a potent and selective next-generation ROS1/ALK inhibitor capable of blocking crizotinib-resistant ROS1 mutations. *Proceedings of the National Academy of Sciences* **2015**, *112*, 3493-3498.
40. Basit, S.; Ashraf, Z.; Lee, K.; Latif, M. First macrocyclic 3rd-generation ALK inhibitor for treatment of ALK/ROS1 cancer: Clinical and designing strategy update of lorlatinib. *European Journal of Medicinal Chemistry* **2017**, *134*, 348-356.
41. Tao, Z.-F.; Wang, L.; Stewart, K. D.; Chen, Z.; Gu, W.; Bui, M.-H.; Merta, P.; Zhang, H.; Kovar, P.; Johnson, E.; Park, C.; Judge, R.; Rosenberg, S.; Sowin, T.; Lin, N.-H. Structure-Based Design, Synthesis, and Biological Evaluation of Potent and Selective Macrocyclic Checkpoint Kinase 1 Inhibitors. *Journal of Medicinal Chemistry* **2007**, *50*, 1514-1527.
42. Zhao, Z.; Wu, H.; Wang, L.; Liu, Y.; Knapp, S.; Liu, Q.; Gray, N. S. Exploration of type II binding mode: A privileged approach for kinase inhibitor focused drug discovery? *ACS Chem Biol* **2014**, *9*, 1230-1241.
43. Goldstein, D. M.; Gray, N. S.; Zarrinkar, P. P. High-throughput kinase profiling as a platform for drug discovery. *Nature Reviews Drug Discovery* **2008**, *7*, 391-397.
44. Karaman, M. W.; Herrgard, S.; Treiber, D. K.; Gallant, P.; Atteridge, C. E.; Campbell, B. T.; Chan, K. W.; Ciceri, P.; Davis, M. I.; Edeen, P. T.; Faraoni, R.; Floyd, M.; Hunt, J. P.; Lockhart, D. J.; Milanov, Z. V.; Morrison, M. J.; Pallares, G.; Patel, H. K.; Pritchard, S.; Wodicka, L. M.; Zarrinkar, P. P. A quantitative analysis of kinase inhibitor selectivity. *Nature Biotechnology* **2008**, *26*, 127-132.
45. Cowan-Jacob, S. W. Structural biology of protein tyrosine kinases. *Cellular and Molecular Life Sciences CMLS* **2006**, *63*, 2608-2625.
46. Liu, Y.; Gray, N. S. Rational design of inhibitors that bind to inactive kinase conformations. *Nat. Chem. Biol.* **2006**, *2*, 358.
47. Zhang, J.; Yang, P. L.; Gray, N. S. Targeting cancer with small molecule kinase inhibitors. *Nature Reviews Cancer* **2009**, *9*, 28-39.
48. Zuccotto, F.; Ardini, E.; Casale, E.; Angiolini, M. Through the "Gatekeeper Door": Exploiting the Active Kinase Conformation. *Journal of Medicinal Chemistry* **2010**, *53*, 2681-2694.
49. Wentsch, H. K.; Walter, N. M.; Bührmann, M.; Mayer-Wrangowski, S.; Rauh, D.; Zaman, G. J. R.; Willemsen-Seegers, N.; Buijsman, R. C.; Henning, M.; Dauch, D.; Zender, L.; Laufer, S. Optimized Target Residence Time: Type I Inhibitors for p38 $\alpha$  MAP Kinase with Improved Binding Kinetics through Direct Interaction with the R-Spine. *Angewandte Chemie International Edition* **2017**, *56*, 5363-5367.
50. Wood, E. R.; Truesdale, A. T.; McDonald, O. B.; Yuan, D.; Hassell, A.; Dickerson, S. H.; Ellis, B.; Pennisi, C.; Horne, E.; Lackey, K.; Alligood, K. J.; Rusnak, D. W.; Gilmer, T. M.; Shewchuk, L. A Unique Structure for Epidermal Growth Factor Receptor Bound to GW572016 (Lapatinib). *Relationships among Protein Conformation, Inhibitor Off-Rate, and Receptor Activity in Tumor Cells* **2004**, *64*, 6652-6659.
51. Axten, J. M.; Medina, J. R.; Feng, Y.; Shu, A.; Romeril, S. P.; Grant, S. W.; Li, W. H.; Heerding, D. A.; Minthorn, E.; Mencken, T.; Atkins, C.; Liu, Q.; Rabindran, S.; Kumar, R.; Hong, X.; Goetz, A.; Stanley, T.; Taylor, J. D.; Sigethy, S. D.; Tomberlin, G. H.; Hassell, A. M.; Kahler, K. M.; Shewchuk, L. M.; Gampe, R. T. Discovery of 7-methyl-5-(1-([3-(trifluoromethyl)phenyl]acetyl)-2,3-dihydro-1H-indol-5-yl)-7H-pyrrolo[2,3-d]pyrimidin-4-amine (GSK2606414), a potent and selective first-in-class inhibitor of protein kinase R (PKR)-like endoplasmic reticulum kinase (PERK). *J Med Chem* **2012**, *55*, 7193-207.
52. Wang, H.; Blais, J.; Ron, D.; Cardozo, T. Structural Determinants of PERK Inhibitor Potency and Selectivity. *Chemical Biology & Drug Design* **2010**, *76*, 480-495.
53. Buchanan, S. G.; Hendle, J.; Lee, P. S.; Smith, C. R.; Bounaud, P. Y.; Jessen, K. A.; Tang, C. M.; Huser, N. H.; Felce, J. D.; Froning, K. J.; Peterman, M. C.; Aubol, B. E.; Gessert, S. F.; Sauder, J. M.; Schwinn, K. D.; Russell, M.; Rooney, I. A.; Adams, J.; Leon, B. C.; Do, T. H.; Blaney, J. M.; Sprengeler, P. A.; Thompson, D. A.; Smyth, L.; Pelletier, L. A.; Atwell, S.; Holme, K.; Wasserman, S. R.; Emtage, S.; Burley, S. K.; Reich, S. H. SGX523 is an exquisitely selective, ATP-competitive inhibitor of the MET receptor tyrosine kinase with antitumor activity in vivo. *Mol Cancer Ther* **2009**, *8*, 3181-90.
54. Guimarães, C. R. W.; Rai, B. K.; Munchhof, M. J.; Liu, S.; Wang, J.; Bhattacharya, S. K.; Buckbinder, L. Understanding the impact of the p-loop conformation on kinase selectivity. *J. Chem. Inf. Model.* **2011**, *51*, 1199.
55. Rahul, P. G.; Anuseema, B.; Mangesh, V. D.; Gaurao, V. D.; Abhay, T. S. p38 Mitogen-Activated Protein Kinase Inhibitors: A Review on Pharmacophore Mapping and QSAR Studies. *Current Topics in Medicinal Chemistry* **2013**, *13*, 1015-1035.
56. Chaikwad, A.; M C Tacconi, E.; Zimmer, J.; Liang, Y.; Gray, N. S.; Tarsounas, M.; Knapp, S. A unique inhibitor binding site in ERK1/2 is associated with slow binding kinetics. *Nature Chemical Biology* **2014**, *10*, 853-860.
57. Over, B.; Wetzels, S.; Grütter, C.; Nakai, Y.; Renner, S.; Rauh, D.; Waldmann, H. Natural-product-derived fragments for fragment-based ligand discovery. *Nature Chemistry* **2013**, *5*, 21-28.
58. Tomita, N.; Hayashi, Y.; Suzuki, S.; Oomori, Y.; Aramaki, Y.; Matsushita, Y.; Iwatani, M.; Iwata, H.; Okabe, A.; Awazu, Y.; Isono, O.; Skene, R. J.; Hosfield, D. J.; Miki, H.; Kawamoto, T.; Hori, A.; Baba, A. Structure-based discovery of cellular-active allosteric inhibitors of FAK. *Bioorganic & Medicinal Chemistry Letters* **2013**, *23*, 1779-1785.

59. Heinrich, T.; Grädler, U.; Böttcher, H.; Blukat, A.; Shutes, A. Allosteric IGF-1R Inhibitors. *ACS Medicinal Chemistry Letters* **2010**, *1*, 199-203.
60. Goodwin, N. C.; Cianchetta, G.; Burgoon, H. A.; Healy, J.; Mabon, R.; Strobel, E. D.; Allen, J.; Wang, S.; Hamman, B. D.; Rawlins, D. B. Discovery of a Type III Inhibitor of LIM Kinase 2 That Binds in a DFG-Out Conformation. *ACS Medicinal Chemistry Letters* **2015**, *6*, 53-57.
61. Wu, P.; Clausen, M. H.; Nielsen, T. E. Allosteric small-molecule kinase inhibitors. *Pharmacology & Therapeutics* **2015**, *156*, 59-68.
62. Hashemzadeh, S.; Ramezani, F.; Rafii-Tabar, H. Study of Molecular Mechanism of the Interaction Between MEK1/2 and Trametinib with Docking and Molecular Dynamic Simulation. *Interdisciplinary Sciences: Computational Life Sciences* **2019**, *11*, 115-124.
63. Roskoski, R. Allosteric MEK1/2 inhibitors including cobimetanib and trametinib in the treatment of cutaneous melanomas. *Pharmacological Research* **2017**, *117*, 20-31.
64. Shang, J.; Lu, S.; Jiang, Y.; Zhang, J. Allosteric modulators of MEK1: drug design and discovery. *Chemical Biology & Drug Design* **2016**, *88*, 485-497.
65. Coit, D. G.; Thompson, J. A.; Algazi, A.; Andtbacka, R.; Bichakjian, C. K.; Carson, W. E.; Daniels, G. A.; DiMaio, D.; Fields, R. C.; Fleming, M. D.; Gastman, B.; Gonzalez, R.; Guild, V.; Johnson, D.; Joseph, R. W.; Lange, J. R.; Martini, M. C.; Materin, M. A.; Olszanski, A. J.; Ott, P.; Gupta, A. P.; Ross, M. I.; Salama, A. K.; Skitzki, J.; Swetter, S. M.; Tanabe, K. K.; Torres-Roca, J. F.; Trisal, V.; Urist, M. M.; McMillian, N.; Engh, A. NCCN Guidelines Insights: Melanoma, Version 3.2016. **2016**, *14*, 945.
66. Larkin, J.; Ascierto, P. A.; Dréno, B.; Atkinson, V.; Liskay, G.; Maio, M.; Mandalà, M.; Demidov, L.; Stryakovsky, D.; Thomas, L.; de la Cruz-Merino, L.; Dutriaux, C.; Garbe, C.; Sovak, M. A.; Chang, I.; Choong, N.; Hack, S. P.; McArthur, G. A.; Ribas, A. Combined Vemurafenib and Cobimetanib in BRAF-Mutated Melanoma. *New England Journal of Medicine* **2014**, *371*, 1867-1876.
67. Bagal, S. K.; Omoto, K.; Blakemore, D. C.; Bungay, P. J.; Bilsland, J. G.; Clarke, P. J.; Corbett, M. S.; Cronin, C. N.; Cui, J. J.; Dias, R.; Flanagan, N. J.; Greasley, S. E.; Grimley, R.; Johnson, E.; Fengas, D.; Kitching, L.; Kraus, M. L.; McAlpine, I.; Nagata, A.; Waldron, G. J.; Warmus, J. S. Discovery of Allosteric, Potent, Subtype Selective, and Peripherally Restricted TrkA Kinase Inhibitors. *Journal of Medicinal Chemistry* **2019**, *62*, 247-265.
68. Furuya, N.; Momose, T.; Katsuno, K.; Fushimi, N.; Muranaka, H.; Handa, C.; Ozawa, T.; Kinoshita, T. The juxtamembrane region of TrkA kinase is critical for inhibitor selectivity. *Bioorganic & Medicinal Chemistry Letters* **2017**, *27*, 1233-1236.
69. Su, H.-P.; Rickert, K.; Burlein, C.; Narayan, K.; Bukhtiyarova, M.; Hurzy, D. M.; Stump, C. A.; Zhang, X.; Reid, J.; Krasowska-Zoladek, A.; Tummala, S.; Shipman, J. M.; Kornienko, M.; Lemaire, P. A.; Krosky, D.; Heller, A.; Achab, A.; Chamberlin, C.; Saradjian, P.; Sauvagnat, B.; Yang, X.; Ziebell, M. R.; Nickbarg, E.; Sanders, J. M.; Bilodeau, M. T.; Carroll, S. S.; Lumb, K. J.; Soisson, S. M.; Henze, D. A.; Cooke, A. J. Structural characterization of nonactive site, TrkA-selective kinase inhibitors. *Proceedings of the National Academy of Sciences* **2017**, *114*, E297-E306.
70. Vandana, L.; Indraneel, G. New Directions in Targeting Protein Kinases: Focusing Upon True Allosteric and Bivalent Inhibitors. *Current Pharmaceutical Design* **2012**, *18*, 2936-2945.
71. Zhang, J.; Adrián, F. J.; Jahnke, W.; Cowan-Jacob, S. W.; Li, A. G.; Iacob, R. E.; Sim, T.; Powers, J.; Dierks, C.; Sun, F.; Guo, G.-R.; Ding, Q.; Okram, B.; Choi, Y.; Wojciechowski, A.; Deng, X.; Liu, G.; Fendrich, G.; Strauss, A.; Vajpai, N.; Grzesiek, S.; Tuntland, T.; Liu, Y.; Bursulaya, B.; Azam, M.; Manley, P. W.; Engen, J. R.; Daley, G. Q.; Warmuth, M.; Gray, N. S. Targeting Bcr–Abl by combining allosteric with ATP-binding-site inhibitors. *Nature* **2010**, *463*, 501-506.
72. Nagar, B.; Hantschel, O.; Young, M. A.; Scheffzek, K.; Veach, D.; Bornmann, W.; Clarkson, B.; Superti-Furga, G.; Kuriyan, J. Structural Basis for the Autoinhibition of c-Abl Tyrosine Kinase. *Cell* **2003**, *112*, 859-871.
73. Pendergast, A. M.; Witte, O. N. Role of the ABL oncogene tyrosine kinase activity in human leukaemia. *Baillière's Clinical Haematology* **1987**, *1*, 1001-1020.
74. Adrián, F. J.; Ding, Q.; Sim, T.; Velentza, A.; Sloan, C.; Liu, Y.; Zhang, G.; Hur, W.; Ding, S.; Manley, P.; Mestan, J.; Fabbro, D.; Gray, N. S. Allosteric inhibitors of Bcr–abl–dependent cell proliferation. *Nature Chemical Biology* **2006**, *2*, 95-102.
75. Schneider, R.; Becker, C.; Simard, J. R.; Getlik, M.; Bohlke, N.; Janning, P.; Rauh, D. Direct Binding Assay for the Detection of Type IV Allosteric Inhibitors of Abl. *Journal of the American Chemical Society* **2012**, *134*, 9138-9141.
76. Nagar, B.; Hantschel, O.; Seeliger, M.; Davies, J. M.; Weis, W. I.; Superti-Furga, G.; Kuriyan, J. Organization of the SH3-SH2 Unit in Active and Inactive Forms of the c-Abl Tyrosine Kinase. *Molecular Cell* **2006**, *21*, 787-798.
77. Fang, Z.; Grütter, C.; Rauh, D. Strategies for the Selective Regulation of Kinases with Allosteric Modulators: Exploiting Exclusive Structural Features. *ACS Chem. Biol.* **2013**, *8*, 58.
78. Eadie, L. N.; Saunders, V. A.; Branford, S.; White, D. L.; Hughes, T. P. The new allosteric inhibitor asciminib is susceptible to resistance mediated by ABCB1 and ABCG2 overexpression in vitro. *Oncotarget* **2018**, *9*, 13423-13437.
79. Schoepfer, J.; Jahnke, W.; Berellini, G.; Buonamici, S.; Cotesta, S.; Cowan-Jacob, S. W.; Dodd, S.; Drueckes, P.; Fabbro, D.; Gabriel, T.; Groell, J.-M.; Grotzfeld, R. M.; Hassan, A. Q.; Henry, C.; Iyer, V.; Jones, D.; Lombardo, F.; Loo, A.; Manley, P. W.; Pellé, X.; Rummel, G.; Salem, B.; Warmuth, M.; Wylie, A. A.; Zoller, T.; Marzinzik, A. L.; Furet, P. Discovery of Asciminib (ABL001), an Allosteric Inhibitor of the Tyrosine Kinase Activity of BCR-ABL1. *Journal of Medicinal Chemistry* **2018**, *61*, 8120-8135.
80. Jeffrey, P. D.; Russo, A. A.; Polyak, K.; Gibbs, E.; Hurwitz, J.; Massagué, J.; Pavletich, N. P. Mechanism of CDK activation revealed by the structure of a cyclinA-CDK2 complex. *Nature* **1995**, *376*, 313-320.
81. Roskoski, R. Cyclin-dependent protein serine/threonine kinase inhibitors as anticancer drugs. *Pharmacological Research* **2019**, *139*, 471-488.
82. Christodoulou, M. S.; Caporuscio, F.; Restelli, V.; Carlino, L.; Cannazza, G.; Costanzi, E.; Citti, C.; Lo Presti, L.; Pisani, P.; Battistutta, R.; Broggin, M.; Passarella, D.; Rastelli, G. Probing an Allosteric Pocket of CDK2 with Small Molecules. *ChemMedChem* **2017**, *12*, 33-41.

83. Mariaule, G.; Belmont, P. Cyclin-Dependent Kinase Inhibitors as Marketed Anticancer Drugs: Where Are We Now? A Short Survey. *Molecules* **2014**, *19*, 14366-14382.
84. Betzi, S.; Alam, R.; Martin, M.; Lubbers, D. J.; Han, H.; Jakkraj, S. R.; Georg, G. I.; Schönbrunn, E. Discovery of a Potential Allosteric Ligand Binding Site in CDK2. *ACS Chem. Biol.* **2011**, *6*, 492.
85. Rettenmaier, T. J.; Sadowsky, J. D.; Thomsen, N. D.; Chen, S. C.; Doak, A. K.; Arkin, M. R.; Wells, J. A. A small-molecule mimic of a peptide docking motif inhibits the protein kinase PDK1. *Proc Natl Acad Sci U S A* **2014**, *111*, 18590-18595.
86. Biondi, R. M.; Cheung, P. C.; Casamayor, A.; Deak, M.; Currie, R. A.; Alessi, D. R. Identification of a pocket in the PDK1 kinase domain that interacts with PIF and the C-terminal residues of PKA. *EMBO J* **2000**, *19*, 979-988.
87. Bobkova, E. V.; Weber, M. J.; Xu, Z.; Zhang, Y.-L.; Jung, J.; Blume-Jensen, P.; Northrup, A.; Kunapuli, P.; Andersen, J. N.; Kariv, I. Discovery of PDK1 kinase inhibitors with a novel mechanism of action by ultrahigh throughput screening. *J Biol Chem* **2010**, *285*, 18838-18846.
88. Converso, A.; Hartingh, T.; Garbaccio, R. M.; Tasber, E.; Rickert, K.; Fraley, M. E.; Yan, Y.; Kreatsoulas, C.; Stirdivant, S.; Drakas, B.; Walsh, E. S.; Hamilton, K.; Buser, C. A.; Mao, X.; Abrams, M. T.; Beck, S. C.; Tao, W.; Lobell, R.; Sepp-Lorenzino, L.; Zugay-Murphy, J.; Sardana, V.; Munshi, S. K.; Jezequel-Sur, S. M.; Zuck, P. D.; Hartman, G. D. Development of thioquinazolinones, allosteric Chk1 kinase inhibitors. *Bioorganic & Medicinal Chemistry Letters* **2009**, *19*, 1240-1244.
89. Vanderpool, D.; Johnson, T. O.; Ping, C.; Bergqvist, S.; Alton, G.; Phonephaly, S.; Rui, E.; Luo, C.; Deng, Y.-L.; Grant, S.; Quenzer, T.; Margosiak, S.; Register, J.; Brown, E.; Ermolieff, J. Characterization of the CHK1 Allosteric Inhibitor Binding Site. *Biochemistry* **2009**, *48*, 9823-9830.
90. Hartnett, J. C.; Barnett, S. F.; Bilodeau, M. T.; Defeo-Jones, D.; Hartman, G. D.; Huber, H. E.; Jones, R. E.; Kral, A. M.; Robinson, R. G.; Wu, Z. Optimization of 2,3,5-trisubstituted pyridine derivatives as potent allosteric Akt1 and Akt2 inhibitors. *Bioorganic & Medicinal Chemistry Letters* **2008**, *18*, 2194-2197.
91. Siu, T.; Li, Y.; Nagasawa, J.; Liang, J.; Tehrani, L.; Chua, P.; Jones, R. E.; Defeo-Jones, D.; Barnett, S. F.; Robinson, R. G. The design and synthesis of potent and cell-active allosteric dual Akt 1 and 2 inhibitors devoid of hERG activity. *Bioorganic & Medicinal Chemistry Letters* **2008**, *18*, 4191-4194.
92. Bjune, K.; Sundvold, H.; Leren, T. P.; Naderi, S. MK-2206, an allosteric inhibitor of AKT, stimulates LDLR expression and LDL uptake: A potential hypocholesterolemic agent. *Atherosclerosis* **2018**, *276*, 28-38.
93. Huang, B. X.; Newcomer, K.; Kevala, K.; Barnaeva, E.; Zheng, W.; Hu, X.; Patnaik, S.; Southall, N.; Marugan, J.; Ferrer, M.; Kim, H.-Y. Identification of 4-phenylquinolin-2(1H)-one as a specific allosteric inhibitor of Akt. *Sci Rep* **2017**, *7*, 11673-11673.
94. Ahad, A. M.; Zuohe, S.; Du-Cuny, L.; Moses, S. A.; Zhou, L. L.; Zhang, S.; Powis, G.; Meuillet, E. J.; Mash, E. A. Development of sulfonamide AKT PH domain inhibitors. *Bioorganic & medicinal chemistry* **2011**, *19*, 2046-2054.
95. Kim, D.; Sun, M.; He, L.; Zhou, Q.-H.; Chen, J.; Sun, X.-M.; Bepler, G.; Sebti, S. M.; Cheng, J. Q. A small molecule inhibits Akt through direct binding to Akt and preventing Akt membrane translocation. *J Biol Chem* **2010**, *285*, 8383-8394.
96. Ranieri, C.; Di Tommaso, S.; Loconte, D. C.; Grossi, V.; Sanese, P.; Bagnulo, R.; Susca, F. C.; Forte, G.; Peserico, A.; De Luisi, A.; Bartuli, A.; Selicorni, A.; Melis, D.; Lerone, M.; Praticò, A. D.; Abbadessa, G.; Yu, Y.; Schwartz, B.; Ruggieri, M.; Simone, C.; Resta, N. In vitro efficacy of ARQ 092, an allosteric AKT inhibitor, on primary fibroblast cells derived from patients with PIK3CA-related overgrowth spectrum (PROS). *Neurogenetics* **2018**, *19*, 77-91.
97. Zhang, X.; Gureasko, J.; Shen, K.; Cole, P. A.; Kuriyan, J. An Allosteric Mechanism for Activation of the Kinase Domain of Epidermal Growth Factor Receptor. *Cell* **2006**, *125*, 1137-1149.
98. Lu, X.; Yu, L.; Zhang, Z.; Ren, X.; Smaill, J. B.; Ding, K. Targeting EGFR L858R/T790M and EGFR L858R/T790M/C797S resistance mutations in NSCLC: Current developments in medicinal chemistry. *Medicinal Research Reviews* **2018**, *38*, 1550-1581.
99. Jia, Y.; Yun, C.-H.; Park, E.; Ercan, D.; Manuia, M.; Juarez, J.; Xu, C.; Rhee, K.; Chen, T.; Zhang, H.; Palakurthi, S.; Jang, J.; Lelais, G.; DiDonato, M.; Bursulaya, B.; Michellys, P.-Y.; Epple, R.; Marsilje, T. H.; McNeill, M.; Lu, W.; Harris, J.; Bender, S.; Wong, K.-K.; Jänne, P. A.; Eck, M. J. Overcoming EGFR(T790M) and EGFR(C797S) resistance with mutant-selective allosteric inhibitors. *Nature* **2016**, *534*, 129-132.
100. Caporuscio, F.; Tinivella, A.; Restelli, V.; Semrau, M. S.; Pinzi, L.; Storici, P.; Broggin, M.; Rastelli, G. Identification of small-molecule EGFR allosteric inhibitors by high-throughput docking. *Future Medicinal Chemistry* **2018**, *10*, 1545-1553.
101. Carlino, L.; Christodoulou, M. S.; Restelli, V.; Caporuscio, F.; Foschi, F.; Semrau, M. S.; Costanzi, E.; Tinivella, A.; Pinzi, L.; Lo Presti, L.; Battistutta, R.; Storici, P.; Broggin, M.; Passarella, D.; Rastelli, G. Structure-Activity Relationships of Hexahydrocyclopenta[c]quinoline Derivatives as Allosteric Inhibitors of CDK2 and EGFR. *ChemMedChem* **2018**, *13*, 2627-2634.
102. Liu, H.; Liang, H.; Meng, H.; Deng, X.; Zhang, X.; Lai, L. A novel allosteric inhibitor that prevents IKK $\beta$  activation. *MedChemComm* **2018**, *9*, 239-243.
103. Roskoski, R. A historical overview of protein kinases and their targeted small molecule inhibitors. *Pharmacological Research* **2015**, *100*, 1-23.
104. Jabbour, E.; Parikh, S. A.; Kantarjian, H.; Cortes, J. Chronic myeloid leukemia: mechanisms of resistance and treatment. *Hematol Oncol Clin North Am* **2011**, *25*, 981-v.
105. Corbin, A. S.; Rosée, P. L.; Stoffregen, E. P.; Druker, B. J.; Deininger, M. W. Several Bcr-Abl kinase domain mutants associated with imatinib mesylate resistance remain sensitive to imatinib. *Blood* **2003**, *101*, 4611-4614.
106. Ohanian, M.; Cortes, J.; Kantarjian, H.; Jabbour, E. Tyrosine kinase inhibitors in acute and chronic leukemias. *Expert Opinion on Pharmacotherapy* **2012**, *13*, 927-938.
107. Gibbons, D. L.; Pricl, S.; Kantarjian, H.; Cortes, J.; Quintás-Cardama, A. The rise and fall of gatekeeper mutations? The BCR-ABL1 T315I paradigm. *Cancer* **2012**, *118*, 293-299.
108. Potashman, M. H.; Duggan, M. E. Covalent Modifiers: An Orthogonal Approach to Drug Design. *Journal of Medicinal Chemistry* **2009**, *52*, 1231-1246.

109. Miller, R. M.; Paavilainen, V. O.; Krishnan, S.; Serafimova, I. M.; Taunton, J. Electrophilic fragment-based design of reversible covalent kinase inhibitors. *Journal of the American Chemical Society* **2013**, *135*, 5298-5301.
110. Zhao, Z.; Liu, Q.; Bliven, S.; Xie, L.; Bourne, P. E. Determining Cysteines Available for Covalent Inhibition Across the Human Kinome. *Journal of Medicinal Chemistry* **2017**, *60*, 2879-2889.
111. Singh, J.; Petter, R. C.; Kluge, A. F. Targeted covalent drugs of the kinase family. *Current Opinion in Chemical Biology* **2010**, *14*, 475-480.
112. Cross, D. A. E.; Ashton, S. E.; Ghiorghiu, S.; Eberlein, C.; Nebhan, C. A.; Spitzler, P. J.; Orme, J. P.; Finlay, M. R. V.; Ward, R. A.; Mellor, M. J.; Hughes, G.; Rahi, A.; Jacobs, V. N.; Red Brewer, M.; Ichihara, E.; Sun, J.; Jin, H.; Ballard, P.; Al-Kadhimi, K.; Rowlinson, R.; Klinowska, T.; Richmond, G. H. P.; Cantarini, M.; Kim, D.-W.; Ranson, M. R.; Pao, W. AZD9291, an irreversible EGFR TKI, overcomes T790M-mediated resistance to EGFR inhibitors in lung cancer. *Cancer discovery* **2014**, *4*, 1046-1061.
113. Rosell, R.; Moran, T.; Queralt, C.; Porta, R.; Cardenal, F.; Camps, C.; Majem, M.; Lopez-Vivanco, G.; Isla, D.; Provencio, M.; Insa, A.; Massuti, B.; Gonzalez-Larriba, J. L.; Paz-Ares, L.; Bover, I.; Garcia-Campelo, R.; Moreno, M. A.; Catot, S.; Rolfo, C.; Reguart, N.; Palmero, R.; Sánchez, J. M.; Bastus, R.; Mayo, C.; Bertran-Alamillo, J.; Molina, M. A.; Sanchez, J. J.; Taron, M. Screening for Epidermal Growth Factor Receptor Mutations in Lung Cancer. *New England Journal of Medicine* **2009**, *361*, 958-967.
114. Li, D.; Ambrogio, L.; Shimamura, T.; Kubo, S.; Takahashi, M.; Chirieac, L. R.; Padera, R. F.; Shapiro, G. I.; Baum, A.; Himmelsbach, F.; Rettig, W. J.; Meyerson, M.; Solca, F.; Greulich, H.; Wong, K. K. BIBW2992, an irreversible EGFR/HER2 inhibitor highly effective in preclinical lung cancer models. *Oncogene* **2008**, *27*, 4702-4711.
115. Ninomiya, T.; Takigawa, N.; Ichihara, E.; Ochi, N.; Murakami, T.; Honda, Y.; Kubo, T.; Minami, D.; Kudo, K.; Tanimoto, M.; Kiura, K. Afatinib Prolongs Survival Compared with Gefitinib in an Epidermal Growth Factor Receptor-Driven Lung Cancer Model. *Molecular Cancer Therapeutics* **2013**, *12*, 589-597.
116. Keating, G. M. Afatinib: A Review in Advanced Non-Small Cell Lung Cancer. *Targeted Oncology* **2016**, *11*, 825-835.
117. Akinleye, A.; Furqan, M.; Adekunle, O. Ibrutinib and Indolent B-Cell Lymphomas. *Clinical Lymphoma, Myeloma and Leukemia* **2014**, *14*, 253-260.
118. Pan, Z.; Scheerens, H.; Li, S.-J.; Schultz, B. E.; Sprengeler, P. A.; Burrill, L. C.; Mendonca, R. V.; Sweeney, M. D.; Scott, K. C. K.; Grothaus, P. G.; Jeffery, D. A.; Spoerke, J. M.; Honigberg, L. A.; Young, P. R.; Dalrymple, S. A.; Palmer, J. T. Discovery of Selective Irreversible Inhibitors for Bruton's Tyrosine Kinase. *ChemMedChem* **2007**, *2*, 58-61.
119. Yver, A. Osimertinib (AZD9291) a science-driven, collaborative approach to rapid drug design and development. *Annals of Oncology* **2016**, *27*, 1165-1170.
120. Deeks, E. D. Neratinib: First Global Approval. *Drugs* **2017**, *77*, 1695-1704.
121. Adaptive Randomization of Neratinib in Early Breast Cancer. *New England Journal of Medicine* **2016**, *375*, 1591-1594.
122. Tsou, H.-R.; Overbeek-Klumpers, E. G.; Hallett, W. A.; Reich, M. F.; Floyd, M. B.; Johnson, B. D.; Michalak, R. S.; Nilakantan, R.; Discafani, C.; Golas, J.; Rabindran, S. K.; Shen, R.; Shi, X.; Wang, Y.-F.; Upeslaci, J.; Wissner, A. Optimization of 6,7-Disubstituted-4-(arylamino)quinoline-3-carbonitriles as Orally Active, Irreversible Inhibitors of Human Epidermal Growth Factor Receptor-2 Kinase Activity. *Journal of Medicinal Chemistry* **2005**, *48*, 1107-1131.
123. Ramalingam, S. S.; O'Byrne, K.; Boyer, M.; Mok, T.; Jänne, P. A.; Zhang, H.; Liang, J.; Taylor, I.; Sbar, E. I.; Paz-Ares, L. Dacomitinib versus erlotinib in patients with EGFR-mutated advanced nonsmall-cell lung cancer (NSCLC): pooled subset analyses from two randomized trials. *Annals of Oncology* **2016**, *27*, 423-429.
124. Wu, Y.-L.; Cheng, Y.; Zhou, X.; Lee, K. H.; Nakagawa, K.; Niho, S.; Tsuji, F.; Linke, R.; Rosell, R.; Corral, J.; Migliorino, M. R.; Pluzanski, A.; Sbar, E. I.; Wang, T.; White, J. L.; Nadanaciva, S.; Sandin, R.; Mok, T. S. Dacomitinib versus gefitinib as first-line treatment for patients with EGFR-mutation-positive non-small-cell lung cancer (ARCHER 1050): a randomised, open-label, phase 3 trial. *The Lancet Oncology* **2017**, *18*, 1454-1466.
125. Serafimova, I. M.; Pufall, M. A.; Krishnan, S.; Duda, K.; Cohen, M. S.; Maglathlin, R. L.; McFarland, J. M.; Miller, R. M.; Frödin, M.; Taunton, J. Reversible targeting of noncatalytic cysteines with chemically tuned electrophiles. *Nature chemical biology* **2012**, *8*, 471-476.
126. Forster, M.; Chaikuad, A.; Bauer, S. M.; Holstein, J.; Robers, M. B.; Corona, C. R.; Gehringer, M.; Pfaffenrot, E.; Ghoreschi, K.; Knapp, S.; Laufer, S. A. Selective JAK3 Inhibitors with a Covalent Reversible Binding Mode Targeting a New Induced Fit Binding Pocket. *Cell Chem Biol* **2016**, *23*, 1335-1340.
127. Fabbro, D. 25 Years of Small Molecular Weight Kinase Inhibitors: Potentials and Limitations. *Mol. Pharmacol.* **2015**, *87*, 766.
128. Gorre, M. E.; Mohammed, M.; Ellwood, K.; Hsu, N.; Paquette, R.; Rao, P. N.; Sawyers, C. L. Clinical Resistance to STI-571 Cancer Therapy Caused by BCR-ABL Gene Mutation or Amplification. *Science* **2001**, *293*, 876-880.
129. Blencke, S.; Zech, B.; Engkvist, O.; Greff, Z.; Órfi, L.; Horváth, Z.; Kéri, G.; Ullrich, A.; Daub, H. Characterization of a Conserved Structural Determinant Controlling Protein Kinase Sensitivity to Selective Inhibitors. *Chemistry & Biology* **2004**, *11*, 691-701.
130. Cools, J.; Stover, E. H.; Boulton, C. L.; Gotlib, J.; Legare, R. D.; Amaral, S. M.; Curley, D. P.; Duclos, N.; Rowan, R.; Kutok, J. L.; Lee, B. H.; Williams, I. R.; Coutre, S. E.; Stone, R. M.; DeAngelo, D. J.; Marynen, P.; Manley, P. W.; Meyer, T.; Fabbro, D.; Neuberg, D.; Weisberg, E.; Griffin, J. D.; Gilliland, D. G. PKC412 overcomes resistance to imatinib in a murine model of FIP1L1-PDGFR $\beta$ -induced myeloproliferative disease. *Cancer Cell* **2003**, *3*, 459-469.
131. Cools, J.; Mentens, N.; Furet, P.; Fabbro, D.; Clark, J. J.; Griffin, J. D.; Marynen, P.; Gilliland, D. G. Prediction of Resistance to Small Molecule FLT3 Inhibitors. *Implications for Molecularly Targeted Therapy of Acute Leukemia* **2004**, *64*, 6385-6389.
132. Fletcher, J. A.; Rubin, B. P. KIT Mutations in GIST. *Current Opinion in Genetics & Development* **2007**, *17*, 3-7.
133. Katayama, R.; Shaw, A. T.; Khan, T. M.; Mino-Kenudson, M.; Solomon, B. J.; Halmos, B.; Jessop, N. A.; Wain, J. C.; Yeo, A. T.; Benes, C.; Drew, L.; Saeh, J. C.; Crosby, K.; Sequist, L. V.; Iafrate, A. J.; Engelman, J. A. Mechanisms of acquired crizotinib resistance in ALK-rearranged lung Cancers. *Sci Transl Med* **2012**, *4*, 120ra17-120ra17.



134. Daub, H.; Specht, K.; Ullrich, A. Strategies to overcome resistance to targeted protein kinase inhibitors. *Nature Reviews Drug Discovery* **2004**, *3*, 1001-1010.
135. Kobayashi, S.; Boggon, T. J.; Dayaram, T.; Jänne, P. A.; Kocher, O.; Meyerson, M.; Johnson, B. E.; Eck, M. J.; Tenen, D. G.; Halmos, B. EGFR Mutation and Resistance of Non-Small-Cell Lung Cancer to Gefitinib. *New England Journal of Medicine* **2005**, *352*, 786-792.
136. Müller, S.; Ackloo, S.; Arrowsmith, C. H.; Bauser, M.; Baryza, J. L.; Blagg, J.; Böttcher, J.; Bountra, C.; Brown, P. J.; Bunnage, M. E.; Carter, A. J.; Damerell, D.; Dötsch, V.; Drewry, D. H.; Edwards, A. M.; Edwards, J.; Elkins, J. M.; Fischer, C.; Frye, S. V.; Gollner, A.; Grimshaw, C. E.; Ijzerman, A.; Hanke, T.; Hartung, I. V.; Hitchcock, S.; Howe, T.; Hughes, T. V.; Laufer, S.; Li, V. M. J.; Liras, S.; Marsden, B. D.; Matsui, H.; Mathias, J.; O'Hagan, R. C.; Owen, D. R.; Pande, V.; Rauh, D.; Rosenberg, S. H.; Roth, B. L.; Schneider, N. S.; Scholten, C.; Singh Saikatendu, K.; Simeonov, A.; Takizawa, M.; Tse, C.; Thompson, P. R.; Treiber, D. K.; Viana, A. Y. I.; Wells, C. I.; Willson, T. M.; Zuercher, W. J.; Knapp, S.; Mueller-Fahrnow, A. Donated chemical probes for open science. *eLife* **2018**, *7*, e34311.
137. Han, J.; Lee, J.; Bibbs, L.; Ulevitch, R. A MAP kinase targeted by endotoxin and hyperosmolarity in mammalian cells. *Science* **1994**, *265*, 808-811.
138. Freshney, N. W.; Rawlinson, L.; Guesdon, F.; Jones, E.; Cowley, S.; Hsuan, J.; Saklatvala, J. Interleukin-1 activates a novel protein kinase cascade that results in the phosphorylation of hsp27. *Cell* **1994**, *78*, 1039-1049.
139. Rouse, J.; Cohen, P.; Trigon, S.; Morange, M.; Alonso-Llamazares, A.; Zamanillo, D.; Hunt, T.; Nebreda, A. R. A novel kinase cascade triggered by stress and heat shock that stimulates MAPKAP kinase-2 and phosphorylation of the small heat shock proteins. *Cell* **1994**, *78*, 1027-1037.
140. Lee, J. C.; Laydon, J. T.; McDonnell, P. C.; Gallagher, T. F.; Kumar, S.; Green, D.; McNulty, D.; Blumenthal, M. J.; Heys, J. R.; Landvatter, S. W.; Strickler, J. E.; McLaughlin, M. M.; Siemens, I. R.; Fisher, S. M.; Livi, G. P.; White, J. R.; Adams, J. L.; Young, P. R. A protein kinase involved in the regulation of inflammatory cytokine biosynthesis. *Nature* **1994**, *372*, 739.
141. Jiang, Y.; Chen, C.; Li, Z.; Guo, W.; Gegner, J. A.; Lin, S.; Han, J. Characterization of the Structure and Function of a New Mitogen-activated Protein Kinase (p38 $\beta$ ). *Journal of Biological Chemistry* **1996**, *271*, 17920-17926.
142. CUENDA, A.; GOEDERT, M.; CRAXTON, M.; JAKES, R.; COHEN, P. 13 Activation of the novel MAP kinase homologue SAPK4 by cytokines and cellular stresses is mediated by SKK3 (MKK6). *Biochemical Society Transactions* **1997**, *25*, S569-S569.
143. Goedert, M.; Cuenda, A.; Craxton, M.; Jakes, R.; Cohen, P. Activation of the novel stress-activated protein kinase SAPK4 by cytokines and cellular stresses is mediated by SKK3 (MKK6); comparison of its substrate specificity with that of other SAP kinases. *EMBO J* **1997**, *16*, 3563-3571.
144. Li, Z.; Jiang, Y.; Ulevitch, R. J.; Han, J. The Primary Structure of p38 $\gamma$ : A New Member of p38 Group of MAP Kinases. *Biochemical and Biophysical Research Communications* **1996**, *228*, 334-340.
145. Mertens, S.; Craxton, M.; Goedert, M. SAP kinase-3, a new member of the family of mammalian stress-activated protein kinases. *FEBS Letters* **1996**, *383*, 273-276.
146. Cuadrado, A.; Nebreda, A. R. Mechanisms and Functions of p38 MAPK Signalling. *Biochem. J.* **2010**, *429*, 403.
147. Ono, K.; Han, J. The p38 signal transduction pathway. Activation and function. *Cell. Signalling* **2000**, *12*, 1.
148. Cuenda, A.; Rousseau, S. p38 MAP-Kinases Pathway Regulation, Function and Role in Human Diseases. *Biochim. Biophys. Acta, Mol. Cell Res.* **2007**, *1773*, 1358.
149. Hale, K. K.; Trollinger, D.; Rihaneck, M.; Manthey, C. L. Differential Expression and Activation of p38 Mitogen-Activated Protein Kinase  $\alpha$ ,  $\beta$ ,  $\gamma$ , and  $\delta$  in Inflammatory Cell Lineages. *The Journal of Immunology* **1999**, *162*, 4246-4252.
150. Zervos, A. S.; Faccio, L.; Gatto, J. P.; Kyriakis, J. M.; Brent, R. Mxi2, a mitogen-activated protein kinase that recognizes and phosphorylates Max protein. *Proc Natl Acad Sci U S A* **1995**, *92*, 10531-10534.
151. Sanz, V.; Arozarena, I.; Crespo, P. Distinct carboxy-termini confer divergent characteristics to the mitogen-activated protein kinase p38 $\alpha$  and its splice isoform Mxi2. *FEBS Letters* **2000**, *474*, 169-174.
152. Sanz-Moreno, V.; Casar, B.; Crespo, P. p38 $\alpha$  isoform Mxi2 binds to extracellular signal-regulated kinase 1 and 2 mitogen-activated protein kinase and regulates its nuclear activity by sustaining its phosphorylation levels. *Mol Cell Biol* **2003**, *23*, 3079-3090.
153. Cargnello, M.; Roux, P. P. Activation and function of the MAPKs and their substrates, the MAPK-activated protein kinases. *Microbiol Mol Biol Rev* **2011**, *75*, 50-83.
154. Metz, K. S.; Deoudes, E. M.; Berginski, M. E.; Jimenez-Ruiz, I.; Aksoy, B. A.; Hammerbacher, J.; Gomez, S. M.; Phanstiel, D. H. Coral: Clear and Customizable Visualization of Human Kinome Data. *Cell Syst* **2018**, *7*, 347-350.e1.
155. Keshet, Y.; Seger, R. The MAP Kinase Signaling Cascades: A System of Hundreds of Components Regulates a Diverse Array of Physiological Functions. In *MAP Kinase Signaling Protocols: Second Edition*, Seger, R., Ed. Humana Press: Totowa, NJ, 2010; pp 3-38.
156. Roskoski, R. ERK1/2 MAP kinases: Structure, function, and regulation. *Pharmacological Research* **2012**, *66*, 105-143.
157. Avruch, J.; Khokhlatchev, A.; Kyriakis, J.; Luo, Z. J.; Tzivion, G.; Vavvas, D.; Zhang, X. Ras Activation of the Raf Kinase: Tyrosine Kinase Recruitment of the MAP Kinase Cascade. *Recent progress in hormone research* **2001**, *56*, 127-55.
158. Pylayeva-Gupta, Y.; Grabocka, E.; Bar-Sagi, D. RAS oncogenes: weaving a tumorigenic web. *Nat Rev Cancer* **2011**, *11*, 761-774.
159. Roskoski, R. RAF protein-serine/threonine kinases: Structure and regulation. *Biochemical and Biophysical Research Communications* **2010**, *399*, 313-317.
160. Zheng, C. F.; Guan, K. L. Properties of MEKs, the kinases that phosphorylate and activate the extracellular signal-regulated kinases. *Journal of Biological Chemistry* **1993**, *268*, 23933-23939.
161. Jain, R.; Watson, U.; Vasudevan, L.; Saini, D. K. Chapter Three - ERK Activation Pathways Downstream of GPCRs. In *International Review of Cell and Molecular Biology*, Shukla, A. K., Ed. Academic Press: 2018; Vol. 338, pp 79-109.

162. Sturgill, T. W.; Ray, L. B.; Erikson, E.; Maller, J. L. Insulin-stimulated MAP-2 kinase phosphorylates and activates ribosomal protein S6 kinase II. *Nature* **1988**, *334*, 715-718.
163. Wortzel, I.; Seger, R. The ERK Cascade: Distinct Functions within Various Subcellular Organelles. *Genes Cancer* **2011**, *2*, 195-209.
164. Steelman, L. S.; Chappell, W. H.; Abrams, S. L.; Kempf, R. C.; Long, J.; Laidler, P.; Mijatovic, S.; Maksimovic-Ivanic, D.; Stivala, F.; Mazzarino, M. C.; Donia, M.; Fagone, P.; Malaponte, G.; Nicoletti, F.; Libra, M.; Milella, M.; Tafuri, A.; Bonati, A.; Bäsecke, J.; Cocco, L.; Evangelisti, C.; Martelli, A. M.; Montalto, G.; Cervello, M.; McCubrey, J. A. Roles of the Raf/MEK/ERK and PI3K/PTEN/Akt/mTOR pathways in controlling growth and sensitivity to therapy-implications for cancer and aging. *Aging (Albany NY)* **2011**, *3*, 192-222.
165. Zeke, A.; Misheva, M.; Reményi, A.; Bogoyevitch, M. A. JNK Signaling: Regulation and Functions Based on Complex Protein-Protein Partnerships. *Microbiol Mol Biol Rev* **2016**, *80*, 793-835.
166. Bogoyevitch, M. A.; Ngoei, K. R. W.; Zhao, T. T.; Yeap, Y. Y. C.; Ng, D. C. H. c-Jun N-terminal kinase (JNK) signaling: Recent advances and challenges. *Biochimica et Biophysica Acta (BBA) - Proteins and Proteomics* **2010**, *1804*, 463-475.
167. Lawler, S.; Fleming, Y.; Goedert, M.; Cohen, P. Synergistic activation of SAPK1/JNK1 by two MAP kinase kinases *in vitro*. *Current Biology* **1998**, *8*, 1387-1391.
168. Raingeaud, J.; Whitmarsh, A. J.; Barrett, T.; Dérijard, B.; Davis, R. J. MKK3- and MKK6-regulated gene expression is mediated by the p38 mitogen-activated protein kinase signal transduction pathway. *Mol Cell Biol* **1996**, *16*, 1247-1255.
169. Wagner, E. F.; Nebreda, Á. R. Signal integration by JNK and p38 MAPK pathways in cancer development. *Nature Reviews Cancer* **2009**, *9*, 537-549.
170. Kato, Y.; Chao, T.-H.; Hayashi, M.; Tapping, R. I.; Lee, J.-D. Role of BMK1 in regulation of growth factor-induced cellular responses. *Immunologic Research* **2000**, *21*, 233-237.
171. Wang, X.; Finegan, K. G.; Robinson, A. C.; Knowles, L.; Khosravi-Far, R.; Hinchliffe, K. A.; Boot-Handford, R. P.; Tournier, C. Activation of extracellular signal-regulated protein kinase 5 downregulates FasL upon osmotic stress. *Cell Death & Differentiation* **2006**, *13*, 2099-2108.
172. Drew, B. A.; Burow, M. E.; Beckman, B. S. MEK5/ERK5 pathway: the first fifteen years. *Biochim Biophys Acta* **2012**, *1825*, 37-48.
173. Xu, B.-e.; Stippec, S.; Lenertz, L.; Lee, B.-H.; Zhang, W.; Lee, Y.-K.; Cobb, M. H. WNK1 Activates ERK5 by an MEKK2/3-dependent Mechanism. *Journal of Biological Chemistry* **2004**, *279*, 7826-7831.
174. Sun, W.; Wei, X.; Kesavan, K.; Garrington, T. P.; Fan, R.; Mei, J.; Anderson, S. M.; Gelfand, E. W.; Johnson, G. L. MEK kinase 2 and the adaptor protein Lad regulate extracellular signal-regulated kinase 5 activation by epidermal growth factor via Src. *Mol Cell Biol* **2003**, *23*, 2298-2308.
175. Chao, T.-H.; Hayashi, M.; Tapping, R. I.; Kato, Y.; Lee, J.-D. MEKK3 Directly Regulates MEK5 Activity as Part of the Big Mitogen-activated Protein Kinase 1 (BMK1) Signaling Pathway. *Journal of Biological Chemistry* **1999**, *274*, 36035-36038.
176. Garrington, T. P.; Ishizuka, T.; Papst, P. J.; Chayama, K.; Webb, S.; Yujiri, T.; Sun, W.; Sather, S.; Russell, D. M.; Gibson, S. B.; Keller, G.; Gelfand, E. W.; Johnson, G. L. MEKK2 gene disruption causes loss of cytokine production in response to IgE and c-Kit ligand stimulation of ES cell-derived mast cells. *EMBO J* **2000**, *19*, 5387-5395.
177. English, J. M.; Vanderbilt, C. A.; Xu, S.; Marcus, S.; Cobb, M. H. Isolation of MEK5 and Differential Expression of Alternatively Spliced Forms. *Journal of Biological Chemistry* **1995**, *270*, 28897-28902.
178. Zhou, G.; Bao, Z. Q.; Dixon, J. E. Components of a New Human Protein Kinase Signal Transduction Pathway. *Journal of Biological Chemistry* **1995**, *270*, 12665-12669.
179. Hayashi, M.; Tapping, R. I.; Chao, T.-H.; Lo, J.-F.; King, C. C.; Yang, Y.; Lee, J.-D. BMK1 Mediates Growth Factor-induced Cell Proliferation through Direct Cellular Activation of Serum and Glucocorticoid-inducible Kinase. *Journal of Biological Chemistry* **2001**, *276*, 8631-8634.
180. English, J. M.; Pearson, G.; Baer, R.; Cobb, M. H. Identification of Substrates and Regulators of the Mitogen-activated Protein Kinase ERK5 Using Chimeric Protein Kinases. *Journal of Biological Chemistry* **1998**, *273*, 3854-3860.
181. Kamakura, S.; Moriguchi, T.; Nishida, E. Activation of the Protein Kinase ERK5/BMK1 by Receptor Tyrosine Kinases: IDENTIFICATION AND CHARACTERIZATION OF A SIGNALING PATHWAY TO THE NUCLEUS. *Journal of Biological Chemistry* **1999**, *274*, 26563-26571.
182. Yang, C. C.; Ornatsky, O. I.; McDermott, J. C.; Cruz, T. F.; Prody, C. A. Interaction of myocyte enhancer factor 2 (MEF2) with a mitogen-activated protein kinase, ERK5/BMK1. *Nucleic Acids Res* **1998**, *26*, 4771-4777.
183. Kato, Y.; Kravchenko, V. V.; Tapping, R. I.; Han, J.; Ulevitch, R. J.; Lee, J. D. BMK1/ERK5 regulates serum-induced early gene expression through transcription factor MEF2C. *EMBO J* **1997**, *16*, 7054-7066.
184. Kasler, H. G.; Victoria, J.; Duramad, O.; Winoto, A. ERK5 is a novel type of mitogen-activated protein kinase containing a transcriptional activation domain. *Mol Cell Biol* **2000**, *20*, 8382-8389.
185. Hayashi, M.; Lee, J.-D. Role of the BMK1/ERK5 signaling pathway: lessons from knockout mice. *Journal of Molecular Medicine* **2004**, *82*, 800-808.
186. Zarubin, T.; Han, J. Activation and signaling of the p38 MAP kinase pathway. *Cell Research* **2005**, *15*, 11-18.
187. Lee, J. C.; Kumar, S.; Griswold, D. E.; Underwood, D. C.; Votta, B. J.; Adams, J. L. Inhibition of p38 MAP kinase as a therapeutic strategy. *Immunopharmacology* **2000**, *47*, 185.
188. Zhang, Y.; Neo, S. Y.; Han, J.; Yaw, L. P.; Lin, S.-C. RGS16 Attenuates Gαq-dependent p38 Mitogen-activated Protein Kinase Activation by Platelet-activating Factor. *Journal of Biological Chemistry* **1999**, *274*, 2851-2857.
189. Koul, H. K.; Pal, M.; Koul, S. Role of p38 MAP Kinase Signal Transduction in Solid Tumors. *Genes Cancer* **2013**, *4*, 342-359.
190. Cuevas, B. D.; Abell, A. N.; Johnson, G. L. Role of mitogen-activated protein kinase kinases in signal integration. *Oncogene* **2007**, *26*, 3159-3171.

191. Alonso, G.; Ambrosino, C.; Jones, M.; Nebreda, A. R. Differential Activation of p38 Mitogen-activated Protein Kinase Isoforms Depending on Signal Strength. *Journal of Biological Chemistry* **2000**, *275*, 40641-40648.
192. Brancho, D.; Tanaka, N.; Jaeschke, A.; Ventura, J.-J.; Kelkar, N.; Tanaka, Y.; Kyuuma, M.; Takeshita, T.; Flavell, R. A.; Davis, R. J. Mechanism of p38 MAP kinase activation in vivo. *Genes Dev* **2003**, *17*, 1969-1978.
193. Activation of the MAP kinase homologue RK requires the phosphorylation of Thr-180 and Tyr-182 and both residues are phosphorylated in chemically stressed KB cells. *FEBS Letters* **1995**, *364*, 223-228.
194. Hu, M. C.-T.; Wang, Y.-p.; Mikhail, A.; Qiu, W. R.; Tan, T.-H. Murine p38- $\delta$  Mitogen-activated Protein Kinase, a Developmentally Regulated Protein Kinase That Is Activated by Stress and Proinflammatory Cytokines. *Journal of Biological Chemistry* **1999**, *274*, 7095-7102.
195. Yoshioka, K. Scaffold Proteins in Mammalian MAP Kinase Cascades. *The Journal of Biochemistry* **2004**, *135*, 657-661.
196. Uhlik, M. T.; Abell, A. N.; Johnson, N. L.; Sun, W.; Cuevas, B. D.; Lobel-Rice, K. E.; Horne, E. A.; Dell'Acqua, M. L.; Johnson, G. L. Rac-MEKK3-MKK3 scaffolding for p38 MAPK activation during hyperosmotic shock. *Nature Cell Biology* **2003**, *5*, 1104-1110.
197. Yasuda, J.; Whitmarsh, A. J.; Cavanagh, J.; Sharma, M.; Davis, R. J. The JIP group of mitogen-activated protein kinase scaffold proteins. *Mol Cell Biol* **1999**, *19*, 7245-7254.
198. Whitmarsh, A. J. The JIP family of MAPK scaffold proteins. *Biochemical Society Transactions* **2006**, *34*, 828-832.
199. Ge, B.; Gram, H.; Di Padova, F.; Huang, B.; New, L.; Ulevitch, R. J.; Luo, Y.; Han, J. MAPKK-Independent Activation of p38 $\alpha$  Mediated by TAB1-Dependent Autophosphorylation of p38 $\alpha$ . *Science* **2002**, *295*, 1291-1294.
200. Salvador, J. M.; Mittelstadt, P. R.; Guszczynski, T.; Copeland, T. D.; Yamaguchi, H.; Appella, E.; Fornace, A. J.; Ashwell, J. D. Alternative p38 activation pathway mediated by T cell receptor-proximal tyrosine kinases. *Nature Immunology* **2005**, *6*, 390-395.
201. Ashwell, J. D. The many paths to p38 mitogen-activated protein kinase activation in the immune system. *Nature Reviews Immunology* **2006**, *6*, 532-540.
202. De Nicola, G. F.; Martin, E. D.; Chaikuad, A.; Bassi, R.; Clark, J.; Martino, L.; Verma, S.; Sicard, P.; Tata, R.; Atkinson, R. A.; Knapp, S.; Conte, M. R.; Marber, M. S. Mechanism and Consequence of the Autoactivation of p38 $\alpha$  Mitogen-Activated Protein Kinase Promoted by TAB1. *Nat. Struct. Mol. Biol.* **2013**, *20*, 1182.
203. Thapa, D.; Nichols, C.; Bassi, R.; Martin, E. D.; Verma, S.; Conte, M. R.; De Santis, V.; De Nicola, G. F.; Marber, M. S. TAB1-Induced Autoactivation of p38 $\alpha$  Mitogen-Activated Protein Kinase Is Crucially Dependent on Threonine 185. *Mol Cell Biol* **2018**, *38*, e00409-17.
204. Alam, M. S.; Gaida, M. M.; Debnath, S.; Tagad, H. D.; Miller Jenkins, L. M.; Appella, E.; Rahman, M. J.; Ashwell, J. D. Unique properties of TCR-activated p38 are necessary for NFAT-dependent T-cell activation. *PLoS Biol* **2018**, *16*, e2004111-e2004111.
205. Giardino Torchia, M. L.; Dutta, D.; Mittelstadt, P. R.; Guha, J.; Gaida, M. M.; Fish, K.; Barr, V. A.; Akpan, I. O.; Samelson, L. E.; Tagad, H. D.; Debnath, S.; Miller Jenkins, L. M.; Appella, E.; Ashwell, J. D. Intensity and duration of TCR signaling is limited by p38 phosphorylation of ZAP-70(T293) and destabilization of the signalosome. *Proc Natl Acad Sci U S A* **2018**, *115*, 2174-2179.
206. Moens, U.; Kostenko, S.; Sveinbjørnsson, B. The Role of Mitogen-Activated Protein Kinase-Activated Protein Kinases (MAPKAPKs) in Inflammation. *Genes (Basel)* **2013**, *4*, 101-133.
207. Enslin, H.; Davis, R. J. Regulation of MAP kinases by docking domains. *Biology of the Cell* **2001**, *93*, 5-14.
208. Tanoue, T.; Nishida, E. Molecular recognitions in the MAP kinase cascades. *Cellular Signalling* **2003**, *15*, 455-462.
209. Gaestel, M. Specificity of signaling from MAPKs to MAPKAPKs: kinases' tango nuevo. In *Front Biosci*, 2008; Vol. 13, pp 6050-6059.
210. Tanoue, T.; Adachi, M.; Moriguchi, T.; Nishida, E. A conserved docking motif in MAP kinases common to substrates, activators and regulators. *Nature Cell Biology* **2000**, *2*, 110-116.
211. Engel, K.; Kotlyarov, A.; Gaestel, M. Leptomycin B-sensitive nuclear export of MAPKAP kinase 2 is regulated by phosphorylation. *EMBO J* **1998**, *17*, 3363-3371.
212. Ben-Levy, R.; Hooper, S.; Wilson, R.; Paterson, H. F.; Marshall, C. J. Nuclear export of the stress-activated protein kinase p38 mediated by its substrate MAPKAP kinase-2. *Current Biology* **1998**, *8*, 1049-1057.
213. White, A.; Pargellis, C. A.; Studts, J. M.; Werneburg, B. G.; Farmer, B. T., 2nd. Molecular basis of MAPK-activated protein kinase 2:p38 assembly. *Proc Natl Acad Sci U S A* **2007**, *104*, 6353-6358.
214. Meng, W.; Swenson, L. L.; Fitzgibbon, M. J.; Hayakawa, K.; ter Haar, E.; Behrens, A. E.; Fulghum, J. R.; Lippke, J. A. Structure of Mitogen-activated Protein Kinase-activated Protein (MAPKAP) Kinase 2 Suggests a Bifunctional Switch That Couples Kinase Activation with Nuclear Export. *Journal of Biological Chemistry* **2002**, *277*, 37401-37405.
215. Soni, S.; Anand, P.; Padwad, Y. S. MAPKAPK2: the master regulator of RNA-binding proteins modulates transcript stability and tumor progression. *J Exp Clin Cancer Res* **2019**, *38*, 121-121.
216. Ronkina, N.; Kotlyarov, A.; Dittrich-Breiholz, O.; Kracht, M.; Hitti, E.; Milarski, K.; Askew, R.; Marusic, S.; Lin, L. L.; Gaestel, M.; Telliez, J. B. The mitogen-activated protein kinase (MAPK)-activated protein kinases MK2 and MK3 cooperate in stimulation of tumor necrosis factor biosynthesis and stabilization of p38 MAPK. *Mol Cell Biol* **2007**, *27*, 170-181.
217. Kostenko, S.; Moens, U. Heat shock protein 27 phosphorylation: kinases, phosphatases, functions and pathology. *Cellular and Molecular Life Sciences* **2009**, *66*, 3289-3307.
218. Kotlyarov, A.; Neining, A.; Schubert, C.; Eckert, R.; Birchmeier, C.; Volk, H.-D.; Gaestel, M. MAPKAP kinase 2 is essential for LPS-induced TNF- $\alpha$  biosynthesis. *Nature Cell Biology* **1999**, *1*, 94-97.
219. Neining, A.; Kontoyiannis, D.; Kotlyarov, A.; Winzen, R.; Eckert, R.; Volk, H.-D.; Holtmann, H.; Kollias, G.; Gaestel, M. MK2 Targets AU-rich Elements and Regulates Biosynthesis of Tumor Necrosis Factor and Interleukin-6 Independently at Different Post-transcriptional Levels. *Journal of Biological Chemistry* **2002**, *277*, 3065-3068.
220. Manke, I. A.; Nguyen, A.; Lim, D.; Stewart, M. Q.; Elia, A. E. H.; Yaffe, M. B. MAPKAP Kinase-2 Is a Cell Cycle Checkpoint Kinase that Regulates the G<sub>2</sub>/M Transition and S Phase Progression in Response to UV Irradiation. *Molecular Cell* **2005**, *17*, 37-48.

221. Roy, S.; Roy, S.; Rana, A.; Akhter, Y.; Hande, M. P.; Banerjee, B. The role of p38 MAPK pathway in p53 compromised state and telomere mediated DNA damage response. *Mutation Research/Genetic Toxicology and Environmental Mutagenesis* **2018**, *836*, 89-97.
222. Weber, H. O.; Ludwig, R. L.; Morrison, D.; Kotlyarov, A.; Gaestel, M.; Vousden, K. H. HDM2 phosphorylation by MAPKAP kinase 2. *Oncogene* **2005**, *24*, 1965-1972.
223. Johansen, C.; Vestergaard, C.; Kragballe, K.; Kollias, G.; Gaestel, M.; Iversen, L. MK2 regulates the early stages of skin tumor promotion. *Carcinogenesis* **2009**, *30*, 2100-2108.
224. Arthur, J. MSK activation and physiological roles. *Front Biosci* **2008**, *13*, 5866-5879.
225. Vermeulen, L.; Berghe, W. V.; Beck, I. M. E.; De Bosscher, K.; Haegeman, G. The versatile role of MSKs in transcriptional regulation. *Trends Biochem Sci* **2009**, *34*, 311-318.
226. Shin, M.-S.; Shinghirunusorn, P.; Sugishima, Y.; Nishimura, M.; Suzuki, S.; Koizumi, K.; Saiki, I.; Sakurai, H. Cross interference with TNF- $\alpha$ -induced TAK1 activation via EGFR-mediated p38 phosphorylation of TAK1-binding protein 1. *Biochimica et Biophysica Acta (BBA) - Molecular Cell Research* **2009**, *1793*, 1156-1164.
227. Richter, J. D.; Sonenberg, N. Regulation of cap-dependent translation by eIF4E inhibitory proteins. *Nature* **2005**, *433*, 477-480.
228. Shveygert, M.; Kaiser, C.; Bradrick, S. S.; Gromeier, M. Regulation of eukaryotic initiation factor 4E (eIF4E) phosphorylation by mitogen-activated protein kinase occurs through modulation of Mnk1-eIF4G interaction. *Mol Cell Biol* **2010**, *30*, 5160-5167.
229. Wendel, H.-G.; Silva, R. L. A.; Malina, A.; Mills, J. R.; Zhu, H.; Ueda, T.; Watanabe-Fukunaga, R.; Fukunaga, R.; Teruya-Feldstein, J.; Pelletier, J.; Lowe, S. W. Dissecting eIF4E action in tumorigenesis. *Genes Dev* **2007**, *21*, 3232-3237.
230. Hefner, Y.; Börsch-Haubold, A. G.; Murakami, M.; Wilde, J. I.; Pasquet, S.; Schieltz, D.; Ghomashchi, F.; Yates, J. R.; Armstrong, C. G.; Paterson, A.; Cohen, P.; Fukunaga, R.; Hunter, T.; Kudo, I.; Watson, S. P.; Gelb, M. H. Serine 727 Phosphorylation and Activation of Cytosolic Phospholipase A2 by MNK1-related Protein Kinases. *Journal of Biological Chemistry* **2000**, *275*, 37542-37551.
231. Sacconi, S.; Pantano, S.; Natoli, G. p38-dependent marking of inflammatory genes for increased NF- $\kappa$ B recruitment. *Nature Immunology* **2002**, *3*, 69-75.
232. Strahl, B. D.; Allis, C. D. The language of covalent histone modifications. *Nature* **2000**, *403*, 41-45.
233. Thomson, S.; Clayton, A. L.; Hazzalin, C. A.; Rose, S.; Barratt, M. J.; Mahadevan, L. C. The nucleosomal response associated with immediate-early gene induction is mediated via alternative MAP kinase cascades: MSK1 as a potential histone H3/HMG-14 kinase. *EMBO J* **1999**, *18*, 4779-4793.
234. Dolado, I.; Nebreda, A. Regulation of Tumorigenesis by p38 $\alpha$  MAP Kinase. In 2007; Vol. 20, pp 99-128.
235. Risco, A.; Cuenda, A. New Insights into the p38 $\gamma$  and p38 $\delta$  MAPK Pathways. *J Signal Transduct* **2012**, *2012*, 520289-520289.
236. Escós, A.; Risco, A.; Alsina-Beauchamp, D.; Cuenda, A. p38 $\gamma$  and p38 $\delta$  Mitogen Activated Protein Kinases (MAPKs), New Stars in the MAPK Galaxy. *Front Cell Dev Biol* **2016**, *4*, 31-31.
237. Hasegawa, M.; Cuenda, A.; Spillantini, M. G.; Thomas, G. M.; Buée-Scherrer, V.; Cohen, P.; Goedert, M. Stress-activated Protein Kinase-3 Interacts with the PDZ Domain of  $\alpha$ 1-Syntrophin: A MECHANISM FOR SPECIFIC SUBSTRATE RECOGNITION. *Journal of Biological Chemistry* **1999**, *274*, 12626-12631.
238. Hou, S.-W.; Zhi, H.-Y.; Pohl, N.; Loesch, M.; Qi, X.-M.; Li, R.-S.; Basir, Z.; Chen, G. PTPH1 dephosphorylates and cooperates with p38 $\gamma$  MAPK to increase ras oncogenesis through PDZ-mediated interaction. *Cancer research* **2010**, *70*, 2901-2910.
239. Sabio, G.; Cerezo-Guisado, M. I.; Del Reino, P.; Iñesta-Vaquera, F. A.; Rousseau, S.; Arthur, J. S. C.; Campbell, D. G.; Centeno, F.; Cuenda, A. p38 $\gamma$  regulates interaction of nuclear PSF and RNA with the tumour-suppressor hDlg in response to osmotic shock. *J Cell Sci* **2010**, *123*, 2596-2604.
240. Goedert, M.; Hasegawa, M.; Jakes, R.; Lawler, S.; Cuenda, A.; Cohen, P. Phosphorylation of microtubule-associated protein tau by stress-activated protein kinases. *FEBS Letters* **1997**, *409*, 57-62.
241. Feijoo, C.; Campbell, D. G.; Jakes, R.; Goedert, M.; Cuenda, A. Evidence that phosphorylation of the microtubule-associated protein Tau by SAPK4/p38 $\delta$  at Thr50 promotes microtubule assembly. *J Cell Sci* **2005**, *118*, 397-408.
242. Zhu, X.; Rottkamp, C. A.; Boux, H.; Takeda, A.; Perry, G.; Smith, M. A. Activation of p38 Kinase Links Tau Phosphorylation, Oxidative Stress, and Cell Cycle-Related Events in Alzheimer Disease. *Journal of Neuropathology & Experimental Neurology* **2000**, *59*, 880-888.
243. Parker, C. G.; Hunt, J.; Diener, K.; McGinley, M.; Soriano, B.; Keesler, G. A.; Bray, J.; Yao, Z.; Wang, X. S.; Kohno, T.; Lichenstein, H. S. Identification of Stathmin as a Novel Substrate for p38 Delta. *Biochemical and Biophysical Research Communications* **1998**, *249*, 791-796.
244. Sumara, G.; Formentini, I.; Collins, S.; Sumara, I.; Windak, R.; Bodenmiller, B.; Ramracheya, R.; Caille, D.; Jiang, H.; Platt, K. A.; Meda, P.; Aebersold, R.; Rorsman, P.; Ricci, R. Regulation of PKD by the MAPK p38delta in insulin secretion and glucose homeostasis. *Cell* **2009**, *136*, 235-248.
245. Knebel, A.; Haydon, C. E.; Morrice, N.; Cohen, P. Stress-induced regulation of eukaryotic elongation factor 2 kinase by SB 203580-sensitive and -insensitive pathways. *Biochem J* **2002**, *367*, 525-532.
246. Knebel, A.; Morrice, N.; Cohen, P. A novel method to identify protein kinase substrates: eEF2 kinase is phosphorylated and inhibited by SAPK4/p38delta. *EMBO J* **2001**, *20*, 4360-4369.
247. Nurmohamed, M. T.; Dijkmans, B. A. C. Efficacy, Tolerability and Cost Effectiveness of Disease-Modifying Antirheumatic Drugs and Biologic Agents in Rheumatoid Arthritis. *Drugs* **2005**, *65*, 661-694.
248. Kumar, S.; Jiang, M. S.; Adams, J. L.; Lee, J. C. Pyridinylimidazole compound sb203580 inhibits the activity but not the activation of p38 mitogen-activated protein kinase. *Biochem. Biophys. Res. Commun.* **1999**, *263*, 825.
249. Kumar, S.; Boehm, J.; Lee, J. C. p38 map kinases: Key signalling molecules as therapeutic targets for inflammatory diseases. *Nat. Rev. Drug Discovery* **2003**, *2*, 717.

250. Boehm, J. C.; Smietana, J. M.; Sorenson, M. E.; Garigipati, R. S.; Gallagher, T. F.; Sheldrake, P. L.; Bradbeer, J.; Badger, A. M.; Laydon, J. T.; Lee, J. C.; Hillegass, L. M.; Griswold, D. E.; Breton, J. J.; Chabot-Fletcher, M. C.; Adams, J. L. 1-Substituted 4-Aryl-5-pyridinylimidazoles: A New Class of Cytokine Suppressive Drugs with Low 5-Lipoxygenase and Cyclooxygenase Inhibitory Potency. *Journal of Medicinal Chemistry* **1996**, *39*, 3929-3937.
251. Gallagher, T. F.; Seibel, G. L.; Kassis, S.; Laydon, J. T.; Blumenthal, M. J.; Lee, J. C.; Lee, D.; Boehm, J. C.; Fier-Thompson, S. M.; Abt, J. W.; Soreson, M. E.; Smietana, J. M.; Hall, R. F.; Garigipati, R. S.; Bender, P. E.; Erhard, K. F.; Krog, A. J.; Hofmann, G. A.; Sheldrake, P. L.; McDonnell, P. C.; Kumar, S.; Young, P. R.; Adams, J. L. Regulation of stress-induced cytokine production by pyridinylimidazoles; inhibition of CSBP kinase. *Bioorg. Med. Chem.* **1997**, *5*, 49.
252. Adams, J. L.; Boehm, J. C.; Kassis, S.; Gorycki, P. D.; Webb, E. F.; Hall, R.; Sorenson, M.; Lee, J. C.; Ayrton, A.; Griswold, D. E.; Gallagher, T. F. Pyrimidinylimidazole inhibitors of CSBP/p38 kinase demonstrating decreased inhibition of hepatic cytochrome P450 enzymes. *Bioorg. Med. Chem. Lett.* **1998**, *8*, 3111.
253. Lisnock, J.; Tebben, A.; Frantz, B.; O'Neill, E. A.; Croft, G.; O'Keefe, S. J.; Li, B.; Hacker, C.; de Laszlo, S.; Smith, A.; Libby, B.; Liverton, N.; Hermes, J.; LoGrasso, P. Molecular Basis for p38 Protein Kinase Inhibitor Specificity. *Biochemistry* **1998**, *37*, 16573-16581.
254. Badger, A. M.; Bradbeer, J. N.; Votta, B.; Lee, J. C.; Adams, J. L.; Griswold, D. E. Pharmacological profile of SB 203580, a selective inhibitor of cytokine suppressive binding protein/p38 kinase, in animal models of arthritis, bone resorption, endotoxin shock and immune function. *J. Pharmacol. Exp. Ther.* **1996**, *279*, 1453.
255. Ma, X. L.; Kumar, S.; Gao, F.; Loudon, C. S.; Lopez, B. L.; Christopher, T. A.; Wang, C.; Lee, J. C.; Feuerstein, G. Z.; Yue, T.-L. Inhibition of p38 Mitogen-Activated Protein Kinase Decreases Cardiomyocyte Apoptosis and Improves Cardiac Function After Myocardial Ischemia and Reperfusion. *Circulation* **1999**, *99*, 1685-1691.
256. Montalban, A. G.; Boman, E.; Chang, C.-D.; Ceide, S. C.; Dahl, R.; Dalesandro, D.; Delaet, N. G. J.; Erb, E.; Ernst, J. T.; Gibbs, A.; Kahl, J.; Kessler, L.; Lundström, J.; Miller, S.; Nakanishi, H.; Roberts, E.; Saiah, E.; Sullivan, R.; Wang, Z.; Larson, C. J. The design and synthesis of novel  $\alpha$ -ketoamide-based p38 MAP kinase inhibitors. *Bioorganic & Medicinal Chemistry Letters* **2008**, *18*, 1772-1777.
257. Laufer, S. A.; Striegel, H.-G.; Wagner, G. K. Imidazole Inhibitors of Cytokine Release: Probing Substituents in the 2 Position. *Journal of Medicinal Chemistry* **2002**, *45*, 4695-4705.
258. Barancik, M.; Htun, P.; Strohm, C.; Kilian, S.; Schaper, W. Inhibition of the Cardiac p38-MAPK Pathway by SB203580 Delays Ischemic Cell Death. *Journal of Cardiovascular Pharmacology* **2000**, *35*, 474-483.
259. Jin, N.; Wang, Q.; Zhang, X.; Jiang, D.; Cheng, H.; Zhu, K. The selective p38 mitogen-activated protein kinase inhibitor, SB203580, improves renal disease in MRL/lpr mouse model of systemic lupus. *International Immunopharmacology* **2011**, *11*, 1319-1326.
260. Wilson, K. P.; McCaffrey, P. G.; Hsiao, K.; Pazhanisamy, S.; Galullo, V.; Bemis, G. W.; Fitzgibbon, M. J.; Caron, P. R.; Murcko, M. A.; Su, M. S. S. The structural basis for the specificity of pyridinylimidazole inhibitors of p38 MAP kinase. *Chem. Biol.* **1997**, *4*, 423.
261. Laufer, S. A.; Zimmermann, W.; Ruff, K. J. Tetrasubstituted Imidazole Inhibitors of Cytokine Release: Probing Substituents in the N-1 Position. *Journal of Medicinal Chemistry* **2004**, *47*, 6311-6325.
262. Ward, K. W.; Proksch, J. W.; Salyers, K. L.; Azzarano, L. M.; Morgan, J. A.; Roethke, T. J.; McSurdy-Freed, J. E.; Levy, M. A.; Smith, B. R. SB-242235, a selective inhibitor of p38 mitogen-activated protein kinase. I: Preclinical pharmacokinetics. *Xenobiotica* **2002**, *32*, 221-233.
263. Ward, K. W.; Proksch, J. W.; Gorycki, P. D.; Yu, C. P.; Ho, M. Y. K.; Bush, B. D.; Levy, M. A.; Smith, B. R. SB-242235, a selective inhibitor of p38 mitogen-activated protein kinase. II: In vitro and in vivo metabolism studies and pharmacokinetic extrapolation to man. *Xenobiotica* **2002**, *32*, 235-250.
264. Badger, A. M.; Griswold, D. E.; Kapadia, R.; Blake, S.; Swift, B. A.; Hoffman, S. J.; Stroup, G. B.; Webb, E.; Rieman, D. J.; Gowen, M.; Boehm, J. C.; Adams, J. L.; Lee, J. C. Disease-modifying activity of SB 242235, a selective inhibitor of p38 mitogen-activated protein kinase, in rat adjuvant-induced arthritis. *Arthritis & Rheumatism* **2000**, *43*, 175-183.
265. Pargellis, C.; Tong, L.; Churchill, L.; Cirillo, P. F.; Gilmore, T.; Graham, A. G.; Grob, P. M.; Hickey, E. R.; Moss, N.; Pav, S.; Regan, J. Inhibition of p38 map kinase by utilizing a novel allosteric binding site. *Nat. Struct. Biol.* **2002**, *9*, 268.
266. Kuma, Y.; Sabio, G.; Bain, J.; Shpiro, N.; Márquez, R.; Cuenda, A. BIRB796 Inhibits All p38 MAPK Isoforms in Vitro and in Vivo. *Journal of Biological Chemistry* **2005**, *280*, 19472-19479.
267. Regan, J.; Breitefelder, S.; Cirillo, P.; Gilmore, T.; Graham, A. G.; Hickey, E.; Klaus, B.; Madwed, J.; Moriaki, M.; Moss, N.; Pargellis, C.; Pav, S.; Proto, A.; Swinamer, A.; Tong, L.; Torcellini, C. Pyrazole Urea-Based Inhibitors of p38 MAP Kinase: From Lead Compound to Clinical Candidate. *Journal of Medicinal Chemistry* **2002**, *45*, 2994-3008.
268. Regan, J.; Pargellis, C. A.; Cirillo, P. F.; Gilmore, T.; Hickey, E. R.; Peet, G. W.; Proto, A.; Swinamer, A.; Moss, N. The kinetics of binding to p38MAP kinase by analogues of BIRB 796. *Bioorganic & Medicinal Chemistry Letters* **2003**, *13*, 3101-3104.
269. Branger, J.; van den Blink, B.; Weijer, S.; Madwed, J.; Bos, C. L.; Gupta, A.; Polmar, S. H.; Olszyna, D. P.; Hack, C. E.; van Deventer, S. J. H.; Peppelenbosch, M. P.; van der Poll, T. Antiinflammatory effects of a p38 mitogen activated protein kinase inhibitor during human endotoxemia. *J. Immunol.* **2002**, *168*, 4070.
270. Schreiber, S.; Feagan, B.; D'Haens, G.; Colombel, J. F.; Geboes, K.; Yurcov, M.; Isakov, V.; Golovenko, O.; Bernstein, C. N.; Ludwig, D.; Winter, T.; Meier, U.; Yong, C.; Steffgen, J. Oral p38 Mitogen-Activated Protein Kinase Inhibition With BIRB 796 for Active Crohn's Disease: A Randomized, Double-Blind, Placebo-Controlled Trial. *Clinical Gastroenterology and Hepatology* **2006**, *4*, 325-334.
271. Iwano, S.; Asaoka, Y.; Akiyama, H.; Takizawa, S.; Nobumasa, H.; Hashimoto, H.; Miyamoto, Y. A possible mechanism for hepatotoxicity induced by BIRB-796, an orally active p38 mitogen-activated protein kinase inhibitor. *Journal of Applied Toxicology* **2011**, *31*, 671-677.

272. Dominguez, C.; Powers, D. A.; Tamayo, N. p38 MAP kinase inhibitors: many are made, but few are chosen. *Curr. Opin. Drug Discovery Dev.* **2005**, *8*, 421.
273. GENOVESE, M. C.; COHEN, S. B.; WOFSY, D.; WEINBLATT, M. E.; FIRESTEIN, G. S.; BRAHN, E.; STRAND, V.; BAKER, D. G.; TONG, S. E. A 24-Week, Randomized, Double-Blind, Placebo-Controlled, Parallel Group Study of the Efficacy of Oral SCIO-469, a p38 Mitogen-activated Protein Kinase Inhibitor, in Patients with Active Rheumatoid Arthritis. *The Journal of Rheumatology* **2011**, *38*, 846-854.
274. Damjanov, N.; Kauffman, R. S.; Spencer-Green, G. T. Efficacy, pharmacodynamics, and safety of VX-702, a novel p38 MAPK inhibitor, in rheumatoid arthritis: Results of two randomized, double-blind, placebo-controlled clinical studies. *Arthritis & Rheumatism* **2009**, *60*, 1232-1241.
275. Weisman, M. A double-blind, placebo-controlled trial of VX-745, an oral p38 mitogen activated protein kinase (MAPK) inhibitor, in patients with rheumatoid arthritis (RA). **2002**.
276. Genovese, M. C. Inhibition of p38: Has the fat lady sung? *Arthritis & Rheumatism* **2009**, *60*, 317-320.
277. Scheltens, P.; Prins, N.; Lammertsma, A.; Yaqub, M.; Gouw, A.; Wink, A. M.; Chu, H.-M.; van Berckel, B. N. M.; Alam, J. An exploratory clinical study of p38 $\alpha$  kinase inhibition in Alzheimer's disease. *Ann Clin Transl Neurol* **2018**, *5*, 464-473.
278. Duffy, J. P.; Harrington, E. M.; Salituro, F. G.; Cochran, J. E.; Green, J.; Gao, H.; Bemis, G. W.; Evindar, G.; Galullo, V. P.; Ford, P. J.; Germann, U. A.; Wilson, K. P.; Bellon, S. F.; Chen, G.; Taslimi, P.; Jones, P.; Huang, C.; Pazhanisamy, S.; Wang, Y.-M.; Murcko, M. A.; Su, M. S. S. The Discovery of VX-745: A Novel and Selective p38 $\alpha$  Kinase Inhibitor. *ACS Medicinal Chemistry Letters* **2011**, *2*, 758-763.
279. Christie, J. D.; Vaslef, S.; Chang, P. K.; May, A. K.; Gunn, S. R.; Yang, S.; Hards, K.; Kahl, L.; Powley, W. M.; Lipson, D. A.; Bayliffe, A. I.; Lazaar, A. L. A Randomized Dose-Escalation Study of the Safety and Anti-Inflammatory Activity of the p38 Mitogen-Activated Protein Kinase Inhibitor Dilmapiomod in Severe Trauma Subjects at Risk for Acute Respiratory Distress Syndrome. *Critical Care Medicine* **2015**, *43*, 1859-1869.
280. Sarov-Blat, L.; Morgan, J. M.; Fernandez, P.; James, R.; Fang, Z.; Hurle, M. R.; Baidoo, C.; Willette, R. N.; Lepore, J. J.; Jensen, S. E.; Sprecher, D. L. Inhibition of p38 Mitogen-Activated Protein Kinase Reduces Inflammation After Coronary Vascular Injury in Humans. *Arteriosclerosis, Thrombosis, and Vascular Biology* **2010**, *30*, 2256-2263.
281. Anand, P.; Shenoy, R.; Palmer, J. E.; Baines, A. J.; Lai, R. Y. K.; Robertson, J.; Bird, N.; Ostfeld, T.; Chizh, B. A. Clinical trial of the p38 MAP kinase inhibitor dilmapiomod in neuropathic pain following nerve injury. *European Journal of Pain* **2011**, *15*, 1040-1048.
282. Millan, D. S.; Bunnage, M. E.; Burrows, J. L.; Butcher, K. J.; Dodd, P. G.; Evans, T. J.; Fairman, D. A.; Hughes, S. J.; Kilty, I. C.; Lemaitre, A.; Lewthwaite, R. A.; Mahnke, A.; Mathias, J. P.; Philip, J.; Smith, R. T.; Stefaniak, M. H.; Yeadon, M.; Phillips, C. Design and Synthesis of Inhaled p38 Inhibitors for the Treatment of Chronic Obstructive Pulmonary Disease. *Journal of Medicinal Chemistry* **2011**, *54*, 7797-7814.
283. Selness, S. R.; Devraj, R. V.; Devadas, B.; Walker, J. K.; Boehm, T. L.; Durley, R. C.; Shieh, H.; Xing, L.; Rucker, P. V.; Jerome, K. D.; Benson, A. G.; Marrufo, L. D.; Madsen, H. M.; Hitchcock, J.; Owen, T. J.; Christie, L.; Promo, M. A.; Hickory, B. S.; Alvira, E.; Naing, W.; Bleviss-Bal, R.; Messing, D.; Yang, J.; Mao, M. K.; Yalamanchili, G.; Vonder Embse, R.; Hirsch, J.; Saabye, M.; Bonar, S.; Webb, E.; Anderson, G.; Monahan, J. B. Discovery of PH-797804, a highly selective and potent inhibitor of p38 MAP kinase. *Bioorganic & Medicinal Chemistry Letters* **2011**, *21*, 4066-4071.
284. Xing, L.; Shieh, H. S.; Selness, S. R.; Devraj, R. V.; Walker, J. K.; Devadas, B.; Hope, H. R.; Compton, R. P.; Schindler, J. F.; Hirsch, J. L.; Benson, A. G.; Kurumbail, R. G.; Stegeman, R. A.; Williams, J. M.; Broadus, R. M.; Walden, Z.; Monahan, J. B. Structural Bioinformatics-Based Prediction of Exceptional Selectivity of p38 MAP Kinase Inhibitor PH-797804. *Biochemistry* **2009**, *48*, 6402-6411.
285. Hope, H. R.; Anderson, G. D.; Burnette, B. L.; Compton, R. P.; Devraj, R. V.; Hirsch, J. L.; Keith, R. H.; Li, X.; Mbalaviele, G.; Messing, D. M.; Saabye, M. J.; Schindler, J. F.; Selness, S. R.; Stillwell, L. I.; Webb, E. G.; Zhang, J.; Monahan, J. B. Anti-Inflammatory Properties of a Novel *N*-Phenyl Pyridinone Inhibitor of p38 Mitogen-Activated Protein Kinase: Preclinical-to-Clinical Translation. *Journal of Pharmacology and Experimental Therapeutics* **2009**, *331*, 882-895.
286. MacNee, W.; Allan, R. J.; Jones, I.; De Salvo, M. C.; Tan, L. F. Efficacy and safety of the oral p38 inhibitor PH-797804 in chronic obstructive pulmonary disease: a randomised clinical trial. *Thorax* **2013**, *68*, 738-745.
287. O'Donoghue, M. L.; Glaser, R.; Aylward, P. E.; Cavender, M. A.; Crisp, A.; Fox, K. A. A.; Laws, I.; Lopez-Sendon, J. L.; Steg, P. G.; Theroux, P.; Sabatine, M. S.; Morrow, D. A. Rationale and design of the Losmapimod To Inhibit p38 MAP kinase as a Therapeutic target and modify outcomes after an acute coronary syndrome trial. *American Heart Journal* **2015**, *169*, 622-630.e6.
288. O'Donoghue, M. L.; Glaser, R.; Cavender, M. A.; Aylward, P. E.; Bonaca, M. P.; Budaj, A.; Davies, R. Y.; Dellborg, M.; Fox, K. A. A.; Gutierrez, J. A. T.; Hamm, C.; Kiss, R. G.; Kovar, F.; Kuder, J. F.; Im, K. A.; Lepore, J. J.; Lopez-Sendon, J. L.; Ophuis, T. O.; Parkhomenko, A.; Shannon, J. B.; Spinar, J.; Tanguay, J.-F.; Ruda, M.; Steg, P. G.; Theroux, P.; Wiviott, S. D.; Laws, I.; Sabatine, M. S.; Morrow, D. A.; Investigators, f. t. L.-T. Effect of Losmapimod on Cardiovascular Outcomes in Patients Hospitalized With Acute Myocardial Infarction: A Randomized Clinical Trial. *JAMA* **2016**, *315*, 1591-1599.
289. Elkhawad, M.; Rudd, J. H. F.; Sarov-Blat, L.; Cai, G.; Wells, R.; Davies, L. C.; Collier, D. J.; Marber, M. S.; Choudhury, R. P.; Fayad, Z. A.; Tawakol, A.; Gleeson, F. V.; Lepore, J. J.; Davis, B.; Willette, R. N.; Wilkinson, I. B.; Sprecher, D. L.; Cheriyan, J. Effects of p38 Mitogen-Activated Protein Kinase Inhibition on Vascular and Systemic Inflammation in Patients With Atherosclerosis. *JACC: Cardiovascular Imaging* **2012**, *5*, 911-922.
290. Newby, L. K.; Marber, M. S.; Melloni, C.; Sarov-Blat, L.; Aberle, L. H.; Aylward, P. E.; Cai, G.; de Winter, R. J.; Hamm, C. W.; Heitner, J. F.; Kim, R.; Lerman, A.; Patel, M. R.; Tanguay, J.-F.; Lepore, J. J.; Al-Khalidi, H. R.; Sprecher, D. L.; Granger, C. B. Losmapimod, a novel p38 mitogen-activated protein kinase inhibitor, in non-ST-segment elevation myocardial infarction: a randomised phase 2 trial. *The Lancet* **2014**, *384*, 1187-1195.

291. Cheriyan, J.; Webb, A. J.; Sarov-Blat, L.; Elkhawad, M.; Wallace, S. M. L.; Mäki-Petäjä, K. M.; Collier, D. J.; Morgan, J.; Fang, Z.; Willette, R. N.; Lepore, J. J.; Cockcroft, J. R.; Sprecher, D. L.; Wilkinson, I. B. Inhibition of p38 Mitogen-Activated Protein Kinase Improves Nitric Oxide-Mediated Vasodilatation and Reduces Inflammation in Hypercholesterolemia. *Circulation* **2011**, *123*, 515-523.
292. Ostenfeld, T.; Krishen, A.; Lai, R. Y.; Bullman, J.; Green, J.; Anand, P.; Scholz, J.; Kelly, M. A Randomized, Placebo-controlled Trial of the Analgesic Efficacy and Safety of the p38 MAP Kinase Inhibitor, Losmapimod, in Patients With Neuropathic Pain From Lumbosacral Radiculopathy. *The Clinical Journal of Pain* **2015**, *31*, 283-293.
293. Marks-Konczalik, J.; Costa, M.; Robertson, J.; McKie, E.; Yang, S.; Pascoe, S. A post-hoc subgroup analysis of data from a six month clinical trial comparing the efficacy and safety of losmapimod in moderate-severe COPD patients with >2% and >2% blood eosinophils. *Respiratory Medicine* **2015**, *109*, 860-869.
294. Carter, L. presented at the American College of Rheumatology–Association of Rheumatology Health Professionals (ACR–ARHP) Annual Scientific Meeting, San Francisco, California, **2008**, Abstract 359
295. Kivitz, A. J. A Randomized, Placebo-Controlled Phase 2 Study of ARRY-797 in Patients with Osteoarthritis Pain Refractory to NSAID Treatment Showed Statistically Significant Improvements in WOMAC Pain and in Biomarkers of Bone and Cartilage Degradation ; Meeting: **2012** ACR/ARHP Annual Meeting.
296. Carter, L. Arry-797, a novel inhibitor of p38 mapk kinase: phase 1 pharmacokinetic and pharmacodynamic results. **2008**.
297. Muchir, A.; Wu, W.; Choi, J. C.; Iwata, S.; Morrow, J.; Homma, S.; Worman, H. J. Abnormal p38 $\alpha$  mitogen-activated protein kinase signaling in dilated cardiomyopathy caused by lamin A/C gene mutation. *Hum Mol Genet* **2012**, *21*, 4325-4333.
298. Remmers, A. E. presented at the American College of Rheumatology–Association of Rheumatology Health Professionals (ACR–ARHP) Annual Scientific Meeting, San Francisco, California, **2008**, Abstract 357.
299. Xing, L. Clinical candidates of small molecule p38 MAPK inhibitors for inflammatory diseases. *MAP Kinase* **2016**, *4*.
300. Tacke, F.; Luedde, T.; Trautwein, C. Inflammatory Pathways in Liver Homeostasis and Liver Injury. *Clinical Reviews in Allergy & Immunology* **2009**, *36*, 4-12.
301. Black, S.; Kushner, I.; Samols, D. C-reactive Protein. *Journal of Biological Chemistry* **2004**, *279*, 48487-48490.
302. Hammaker, D.; Firestein, G. S. "Go upstream, young man": lessons learned from the p38 saga. *Ann Rheum Dis* **2010**, *69* Suppl 1, i77-i82.
303. Arthur, J. S. C.; Ley, S. C. Mitogen-activated protein kinases in innate immunity. *Nature Reviews Immunology* **2013**, *13*, 679-692.
304. Wadgaonkar, R.; Pierce, J.; Somnay, K.; Damico, R.; Crow, M.; Collins, T.; Garcia, J. Regulation of c-Jun N-terminal Kinase and p38 Kinase Pathways in Endothelial Cells. *American journal of respiratory cell and molecular biology* **2004**, *31*, 423-31.
305. Cohen, P. Targeting protein kinases for the development of anti-inflammatory drugs. *Curr. Opin. Cell Biol.* **2009**, *21*, 317.
306. Fitzgerald, C. E.; Patel, S. B.; Becker, J. W.; Cameron, P. M.; Zaller, D.; Pikounis, V. B.; O'Keefe, S. J.; Scapin, G. Structural basis for p38 $\alpha$ MAP kinase quinazolinone and pyridol-pyrimidine inhibitor specificity. *Nat. Struct. Biol.* **2003**, *10*, 764.
307. Azevedo, R.; van Zeeland, M.; Raaijmakers, H.; Kazemier, B.; de Vlieg, J.; Oubrie, A. X-ray structure of p38[ $\alpha$ ] bound to TAK-715: comparison with three classic inhibitors. *Acta Crystallographica Section D* **2012**, *68*, 1041-1050.
308. Wroblewski, S. T.; Lin, S.; Hynes, J.; Wu, H.; Pitt, S.; Shen, D. R.; Zhang, R.; Gillooly, K. M.; Shuster, D. J.; McIntyre, K. W.; Doweyko, A. M.; Kish, K. F.; Tredup, J. A.; Duke, G. J.; Sack, J. S.; McKinnon, M.; Dodd, J.; Barrish, J. C.; Schieven, G. L.; Leftheris, K. Synthesis and SAR of new pyrrolo[2,1-f][1,2,4]triazines as potent p38 $\alpha$  MAP kinase inhibitors. *Bioorganic & Medicinal Chemistry Letters* **2008**, *18*, 2739-2744.
309. Heo, J.; Shin, H.; Lee, J.; Kim, T.; Inn, K.-S.; Kim, N.-J. Synthesis and biological evaluation of N-cyclopropylbenzamide-benzophenone hybrids as novel and selective p38 mitogen activated protein kinase (MAPK) inhibitors. *Bioorganic & Medicinal Chemistry Letters* **2015**, *25*, 3694-3698.
310. Martz, K. E.; Dorn, A.; Baur, B.; Schattel, V.; Goettert, M. I.; Mayer-Wrangowski, S. C.; Rauh, D.; Laufer, S. A. Targeting the Hinge Glycine Flip and the Activation Loop: Novel Approach to Potent p38 $\alpha$  Inhibitors. *Journal of Medicinal Chemistry* **2012**, *55*, 7862-7874.
311. Fischer, S.; Wentsch, H. K.; Mayer-Wrangowski, S. C.; Zimmermann, M.; Bauer, S. M.; Storch, K.; Niess, R.; Koeberle, S. C.; Grütter, C.; Boeckler, F. M.; Rauh, D.; Laufer, S. A. Dibenzosuberones as p38 Mitogen-Activated Protein Kinase Inhibitors with Low ATP Competitiveness and Outstanding Whole Blood Activity. *Journal of Medicinal Chemistry* **2013**, *56*, 241-253.
312. Koeberle, S. C.; Fischer, S.; Schollmeyer, D.; Schattel, V.; Grutter, C.; Rauh, D.; Laufer, S. A. Design, synthesis, and biological evaluation of novel disubstituted dibenzosuberones as highly potent and selective inhibitors of p38 mitogen activated protein kinase. *J. Med. Chem.* **2012**, *55*, 5868.
313. Walter, N. M.; Wentsch, H. K.; Buehrmann, M.; Bauer, S. M.; Doering, E.; Mayer-Wrangowski, S.; Sievers-Engler, A.; Willemsen-Seegers, N.; Zaman, G.; Buijsman, R.; Laemmerhofer, M.; Rauh, D.; Laufer, S. A. Design, Synthesis, and Biological Evaluation of Novel Type 1/2 p38  $\alpha$  MAP Kinase Inhibitors with Excellent Selectivity, High Potency, and Prolonged Target Residence Time by Interfering with the R-Spine. *Journal of Medicinal Chemistry* **2017**, *60*, 8027-8054.
314. Baur, B.; Storch, K.; Martz, K. E.; Goettert, M. I.; Richters, A.; Rauh, D.; Laufer, S. A. Metabolically Stable Dibenzo[b,e]oxepin-11(6H)-ones as Highly Selective p38 MAP Kinase Inhibitors: Optimizing Anti-Cytokine Activity in Human Whole Blood. *Journal of Medicinal Chemistry* **2013**, *56*, 8561-8578.
315. Karcher, S. C.; Laufer, S. A. Aza-Analogue Dibenzepinone Scaffolds as p38 Mitogen-Activated Protein Kinase Inhibitors: Design, Synthesis, and Biological Data of Inhibitors with Improved Physicochemical Properties. *Journal of Medicinal Chemistry* **2009**, *52*, 1778-1782.

316. Laufer, S. A.; Ahrens, G. M.; Karcher, S. C.; Hering, J. S.; Niess, R. Design, synthesis, and biological evaluation of phenylamino-substituted 6,11-dihydro-dibenzo[b,e]oxepin-11-ones and dibenzo[a,d]cycloheptan-5-ones: Novel p38 MAP kinase inhibitors. *J. Med. Chem.* **2006**, *49*, 7912.
317. Koeberle, S. C.; Romir, J.; Fischer, S.; Koeberle, A.; Schattel, V.; Albrecht, W.; Grütter, C.; Werz, O.; Rauh, D.; Stehle, T.; Laufer, S. A. Skepinone-I is a selective p38 mitogen-activated protein kinase inhibitor. *Nat. Chem. Biol.* **2012**, *8*, 141.
318. Jerome, K. D.; Rucker, P. V.; Xing, L.; Shieh, H. S.; Baldus, J. E.; Selness, S. R.; Letavic, M. A.; Braganza, J. F.; McClure, K. F. Continued exploration of the triazolopyridine scaffold as a platform for p38 MAP kinase inhibition. *Bioorganic & Medicinal Chemistry Letters* **2010**, *20*, 469-473.
319. Herberich, B.; Cao, G.-Q.; Chakrabarti, P. P.; Falsey, J. R.; Pettus, L.; Rzasa, R. M.; Reed, A. B.; Reichelt, A.; Sham, K.; Thaman, M.; Wurz, R. P.; Xu, S.; Zhang, D.; Hsieh, F.; Lee, M. R.; Syed, R.; Li, V.; Grosfeld, D.; Plant, M. H.; Henkle, B.; Sherman, L.; Middleton, S.; Wong, L. M.; Tasker, A. S. Discovery of Highly Selective and Potent p38 Inhibitors Based on a Phthalazine Scaffold. *Journal of Medicinal Chemistry* **2008**, *51*, 6271-6279.
320. Lumeras, W.; Caturla, F.; Vidal, L.; Esteve, C.; Balagué, C.; Orellana, A.; Domínguez, M.; Roca, R.; Huerta, J. M.; Godessart, N.; Vidal, B. Design, Synthesis, and Structure–Activity Relationships of Aminopyridine N-Oxides, a Novel Scaffold for the Potent and Selective Inhibition of p38 Mitogen Activated Protein Kinase. *Journal of Medicinal Chemistry* **2009**, *52*, 5531-5545.
321. Lumeras, W.; Vidal, L.; Vidal, B.; Balagué, C.; Orellana, A.; Maldonado, M.; Domínguez, M.; Segarra, V.; Caturla, F. 1,7-Naphthyridine 1-Oxides as Novel Potent and Selective Inhibitors of p38 Mitogen Activated Protein Kinase. *Journal of Medicinal Chemistry* **2011**, *54*, 7899-7910.
322. Wroblewski, S. T.; Lin, S.; Murali Dhar, T. G.; Dyckman, A. J.; Li, T.; Pitt, S.; Zhang, R.; Fan, Y.; Doweyko, A. M.; Tokarski, J. S.; Kish, K. F.; Kiefer, S. E.; Sack, J. S.; Newitt, J. A.; Witmer, M. R.; McKinnon, M.; Barrish, J. C.; Dodd, J. H.; Schieven, G. L.; Leftheris, K. The identification of novel p38 $\alpha$  isoform selective kinase inhibitors having an unprecedented p38 $\alpha$  binding mode. *Bioorg. Med. Chem. Lett.* **2013**, *23*, 4120.
323. Pettus, L. H.; Xu, S.; Cao, G.-Q.; Chakrabarti, P. P.; Rzasa, R. M.; Sham, K.; Wurz, R. P.; Zhang, D.; Middleton, S.; Henkle, B.; Plant, M. H.; Saris, C. J. M.; Sherman, L.; Wong, L. M.; Powers, D. A.; Tudor, Y.; Yu, V.; Lee, M. R.; Syed, R.; Hsieh, F.; Tasker, A. S. 3-Amino-7-phthalazinylbenzoxazoles as a Novel Class of Potent, Selective, and Orally Available Inhibitors of p38 $\alpha$  Mitogen-Activated Protein Kinase. *Journal of Medicinal Chemistry* **2008**, *51*, 6280-6292.
324. Wurz, R. P.; Pettus, L. H.; Xu, S.; Henkle, B.; Sherman, L.; Plant, M.; Miner, K.; McBride, H.; Wong, L. M.; Saris, C. J. M.; Lee, M. R.; Chmait, S.; Mohr, C.; Hsieh, F.; Tasker, A. S. Part 1: Structure–Activity Relationship (SAR) investigations of fused pyrazoles as potent, selective and orally available inhibitors of p38 $\alpha$  mitogen-activated protein kinase. *Bioorganic & Medicinal Chemistry Letters* **2009**, *19*, 4724-4728.
325. Pettus, L. H.; Wurz, R. P.; Xu, S.; Herberich, B.; Henkle, B.; Liu, Q.; McBride, H. J.; Mu, S.; Plant, M. H.; Saris, C. J. M.; Sherman, L.; Wong, L. M.; Chmait, S.; Lee, M. R.; Mohr, C.; Hsieh, F.; Tasker, A. S. Discovery and Evaluation of 7-Alkyl-1,5-bis-aryl-pyrazolopyridinones as Highly Potent, Selective, and Orally Efficacious Inhibitors of p38 $\alpha$  Mitogen-Activated Protein Kinase. Atomic coordinates and structure factors for crystal structure of compound 3d with p38 $\alpha$  can be accessed using PDB code 3LHJ. *Journal of Medicinal Chemistry* **2010**, *53*, 2973-2985.
326. Wurz, R. P.; Pettus, L. H.; Henkle, B.; Sherman, L.; Plant, M.; Miner, K.; McBride, H. J.; Wong, L. M.; Saris, C. J. M.; Lee, M. R.; Chmait, S.; Mohr, C.; Hsieh, F.; Tasker, A. S. Part 2: Structure–activity relationship (SAR) investigations of fused pyrazoles as potent, selective and orally available inhibitors of p38 $\alpha$  mitogen-activated protein kinase. *Bioorganic & Medicinal Chemistry Letters* **2010**, *20*, 1680-1684.
327. Herberich, B.; Jackson, C.; Wurz, R. P.; Pettus, L. H.; Sherman, L.; Liu, Q.; Henkle, B.; Saris, C. J. M.; Wong, L. M.; Chmait, S.; Lee, M. R.; Mohr, C.; Hsieh, F.; Tasker, A. S. Identification of triazolopyridazinones as potent p38 $\alpha$  inhibitors. *Bioorganic & Medicinal Chemistry Letters* **2012**, *22*, 1226-1229.
328. Soth, M.; Abbot, S.; Abubakari, A.; Arora, N.; Arzeno, H.; Billedeau, R.; Dewdney, N.; Durkin, K.; Frauchiger, S.; Ghate, M.; Goldstein, D. M.; Hill, R. J.; Kuglstatler, A.; Li, F.; Loe, B.; McCaleb, K.; McIntosh, J.; Papp, E.; Park, J.; Stahl, M.; Sung, M.-L.; Suttman, R.; Swinney, D. C.; Weller, P.; Wong, B.; Zecic, H.; Gabriel, T. 3-Amino-pyrazolo[3,4-d]pyrimidines as p38 $\alpha$  kinase inhibitors: Design and development to a highly selective lead. *Bioorganic & Medicinal Chemistry Letters* **2011**, *21*, 3452-3456.
329. Ahn, Y. M.; Clare, M.; Ensinger, C. L.; Hood, M. M.; Lord, J. W.; Lu, W. P.; Miller, D. F.; Patt, W. C.; Smith, B. D.; Vogeti, L.; Kaufman, M. D.; Petillo, P. A.; Wise, S. C.; Abendroth, J.; Chun, L.; Clark, R.; Feese, M.; Kim, H.; Stewart, L.; Flynn, D. L. Switch control pocket inhibitors of p38-map kinase. Durable type II inhibitors that do not require binding into the canonical atp hinge region. *Bioorg. Med. Chem. Lett.* **2010**, *20*, 5793.
330. Flynn, D. L. WO2004/061084.
331. Flynn, D. L. WO2007/008917.
332. Flynn, D. L. WO2008/0248548.
333. Swann, S. L.; Merta, P. J.; Kifle, L.; Groebe, D.; Sarris, K.; Hajduk, P. J.; Sun, C. Biochemical and biophysical characterization of unique switch pocket inhibitors of p38 $\alpha$ . *Bioorganic & Medicinal Chemistry Letters* **2010**, *20*, 5787-5792.
334. Moffett, K.; Konteatis, Z.; Nguyen, D.; Shetty, R.; Ludington, J.; Fujimoto, T.; Lee, K.-J.; Chai, X.; Namboodiri, H.; Karpusas, M.; Dorsey, B.; Guarnieri, F.; Bukhtiyarova, M.; Springman, E.; Michelotti, E. Discovery of a novel class of non-ATP site DFG-out state p38 inhibitors utilizing computationally assisted virtual fragment-based drug design (vFBDD). *Bioorganic & Medicinal Chemistry Letters* **2011**, *21*, 7155-7165.
335. Kooistra, A. J.; Kanev, G. K.; van Linden, O. P. J.; Leurs, R.; de Esch, I. J. P.; de Graaf, C. KLIFS: a structural kinase-ligand interaction database. *Nucleic Acids Res* **2016**, *44*, D365-D371.
336. van Linden, O. P. J.; Kooistra, A. J.; Leurs, R.; de Esch, I. J. P.; de Graaf, C. KLIFS: A Knowledge-Based Structural Database To Navigate Kinase–Ligand Interaction Space. *Journal of Medicinal Chemistry* **2014**, *57*, 249-277.



337. Getlik, M.; Grutter, C.; Simard, J. R.; Nguyen, H. D.; Robubi, A.; Aust, B.; van Otterlo, W. A.; Rauh, D. Structure-based design, synthesis and biological evaluation of N-pyrazole, N'-thiazole urea inhibitors of MAP kinase p38 $\alpha$ . *Eur. J. Med. Chem.* **2012**, *48*, 1.
338. Gaulton, A.; Hersey, A.; Nowotka, M.; Bento, A. P.; Chambers, J.; Mendez, D.; Mutowo, P.; Atkinson, F.; Bellis, L. J.; Cibrián-Uhalte, E.; Davies, M.; Dedman, N.; Karlsson, A.; Magariños, M. P.; Overington, J. P.; Papadatos, G.; Smit, I.; Leach, A. R. The ChEMBL database in 2017. *Nucleic Acids Res* **2016**, *45*, D945-D954.
339. Davies, M.; Nowotka, M.; Papadatos, G.; Dedman, N.; Gaulton, A.; Atkinson, F.; Bellis, L.; Overington, J. P. ChEMBL web services: streamlining access to drug discovery data and utilities. *Nucleic Acids Res* **2015**, *43*, W612-W620.
340. Petersen, L. K.; Blakskjær, P.; Chaikuad, A.; Christensen, A. B.; Dietvorst, J.; Holmkvist, J.; Knapp, S.; Kořínek, M.; Larsen, L. K.; Pedersen, A. E.; Røhm, S.; Sløk, F. A.; Hansen, N. J. V. Novel p38 $\alpha$  map kinase inhibitors identified from yocto reactor dna-encoded small molecule library. *MedChemComm* **2016**, *7*, 1332.
341. Goldstein, D. M.; Alfredson, T.; Bertrand, J.; Browner, M. F.; Clifford, K.; Dalrymple, S. A.; Dunn, J.; Freire-Moar, J.; Harris, S.; Labadie, S. S.; La Fargue, J.; Lapierre, J. M.; Larrabee, S.; Li, F.; Papp, E.; McWeeney, D.; Ramesha, C.; Roberts, R.; Rotstein, D.; San Pablo, B.; Sjogren, E. B.; So, O.-Y.; Talamas, F. X.; Tao, W.; Trejo, A.; Villasenor, A.; Welch, M.; Welch, T.; Weller, P.; Whiteley, P. E.; Young, K.; Zipfel, S. Discovery of S-[5-Amino-1-(4-fluorophenyl)-1H-pyrazol-4-yl]-[3-(2,3-dihydroxypropoxy)phenyl]methanone (RO3201195), an Orally Bioavailable and Highly Selective Inhibitor of p38 Map Kinase. *Journal of Medicinal Chemistry* **2006**, *49*, 1562-1575.
342. Cogan, D. A.; Aungst, R.; Breinlinger, E. C.; Fadra, T.; Goldberg, D. R.; Hao, M. H.; Kroe, R.; Moss, N.; Pargellis, C.; Qian, K. C.; Swinamer, A. D. Structure-based design and subsequent optimization of 2-tolyl-(1,2,3-triazol-1-yl-4-carboxamide) inhibitors of p38 MAP kinase. *Bioorganic & Medicinal Chemistry Letters* **2008**, *18*, 3251-3255.
343. Tamayo, N.; Liao, L.; Goldberg, M.; Powers, D.; Tudor, Y.-Y.; Yu, V.; Wong, L. M.; Henkle, B.; Middleton, S.; Syed, R.; Harvey, T.; Jang, G.; Hungate, R.; Dominguez, C. Design and synthesis of potent pyridazine inhibitors of p38 MAP kinase. *Bioorganic & Medicinal Chemistry Letters* **2005**, *15*, 2409-2413.
344. Natarajan, S. R.; Heller, S. T.; Nam, K.; Singh, S. B.; Scapin, G.; Patel, S.; Thompson, J. E.; Fitzgerald, C. E.; O'Keefe, S. J. p38 MAP kinase inhibitors. Part 6: 2-Arylpyridazin-3-ones as templates for inhibitor design. *Bioorganic & Medicinal Chemistry Letters* **2006**, *16*, 5809-5813.
345. Hartshorn, M. J.; Murray, C. W.; Cleasby, A.; Frederickson, M.; Tickle, I. J.; Jhoti, H. Fragment-Based Lead Discovery Using X-ray Crystallography. *Journal of Medicinal Chemistry* **2005**, *48*, 403-413.
346. Gill, A. L.; Frederickson, M.; Cleasby, A.; Woodhead, S. J.; Carr, M. G.; Woodhead, A. J.; Walker, M. T.; Congreve, M. S.; Devine, L. A.; Tisi, D.; O'Reilly, M.; Seavers, L. C. A.; Davis, D. J.; Curry, J.; Anthony, R.; Padova, A.; Murray, C. W.; Carr, R. A. E.; Jhoti, H. Identification of Novel p38 $\alpha$  MAP Kinase Inhibitors Using Fragment-Based Lead Generation. *Journal of Medicinal Chemistry* **2005**, *48*, 414-426.
347. Baldwin, I.; Bamborough, P.; Haslam, C. G.; Hunjan, S. S.; Longstaff, T.; Mooney, C. J.; Patel, S.; Quinn, J.; Somers, D. O. Kinase array design, back to front: Biaryl amides. *Bioorganic & Medicinal Chemistry Letters* **2008**, *18*, 5285-5289.
348. Hynes, J.; Wu, H.; Pitt, S.; Shen, D. R.; Zhang, R.; Schieven, G. L.; Gillooly, K. M.; Shuster, D. J.; Taylor, T. L.; Yang, X.; McIntyre, K. W.; McKinnon, M.; Zhang, H.; Marathe, P. H.; Doweiko, A. M.; Kish, K.; Kiefer, S. E.; Sack, J. S.; Newitt, J. A.; Barrish, J. C.; Dodd, J.; Leftheris, K. The discovery of (R)-2-(sec-butylamino)-N-(2-methyl-5-(methylcarbamoyl)phenyl) thiazole-5-carboxamide (BMS-640994)—A potent and efficacious p38 $\alpha$  MAP kinase inhibitor. *Bioorganic & Medicinal Chemistry Letters* **2008**, *18*, 1762-1767.
349. Liu, C.; Lin, J.; Pitt, S.; Zhang, R. F.; Sack, J. S.; Kiefer, S. E.; Kish, K.; Doweiko, A. M.; Zhang, H.; Marathe, P. H.; Trzaskos, J.; McKinnon, M.; Dodd, J. H.; Barrish, J. C.; Schieven, G. L.; Leftheris, K. Benzothiazole based inhibitors of p38 $\alpha$  MAP kinase. *Bioorganic & Medicinal Chemistry Letters* **2008**, *18*, 1874-1879.
350. Simard, J. R.; Getlik, M.; Grutter, C.; Schneider, R.; Wulfert, S.; Rauh, D. Fluorophore labeling of the glycine-rich loop as a method of identifying inhibitors that bind to active and inactive kinase conformations. *J. Am. Chem. Soc.* **2010**, *132*, 4152.
351. Eastwood, P.; González, J.; Gómez, E.; Vidal, B.; Caturla, F.; Roca, R.; Balagué, C.; Orellana, A.; Domínguez, M. Indolin-2-one p38 $\alpha$  inhibitors I: Design, profiling and crystallographic binding mode. *Bioorganic & Medicinal Chemistry Letters* **2011**, *21*, 4130-4133.
352. McClure, K. F.; Abramov, Y. A.; Laird, E. R.; Barberia, J. T.; Cai, W.; Carty, T. J.; Cortina, S. R.; Danley, D. E.; Dipesa, A. J.; Donahue, K. M.; Dombroski, M. A.; Elliott, N. C.; Gabel, C. A.; Han, S.; Hynes, T. R.; LeMotte, P. K.; Mansour, M. N.; Marr, E. S.; Letavic, M. A.; Pandit, J.; Ripin, D. B.; Sweeney, F. J.; Tan, D.; Tao, Y. Theoretical and Experimental Design of Atypical Kinase Inhibitors: Application to p38 MAP Kinase. *Journal of Medicinal Chemistry* **2005**, *48*, 5728-5737.
353. Mavunkel, B. J.; Chakravarty, S.; Perumattam, J. J.; Luedtke, G. R.; Liang, X.; Lim, D.; Xu, Y.-j.; Laney, M.; Liu, D. Y.; Schreiner, G. F.; Lewicki, J. A.; Dugar, S. Indole-based heterocyclic inhibitors of p38 $\alpha$  MAP kinase: designing a conformationally restricted analogue. *Bioorganic & Medicinal Chemistry Letters* **2003**, *13*, 3087-3090.
354. Medicinal Chemistry Approaches for the Inhibition of the p38 MAPK Pathway. In *Protein Kinases as Drug Targets*, pp 271-304.
355. Eastwood, P.; González, J.; Gómez, E.; Caturla, F.; Balagué, C.; Orellana, A.; Domínguez, M. Indolin-2-one p38 $\alpha$  inhibitors II: Lead optimisation. *Bioorganic & Medicinal Chemistry Letters* **2011**, *21*, 5270-5273.
356. Eastwood, P.; González, J.; Gómez, E.; Caturla, F.; Aguilar, N.; Mir, M.; Aiguadé, J.; Matassa, V.; Balagué, C.; Orellana, A.; Domínguez, M. Indolin-2-one p38 $\alpha$  inhibitors III: Bioisosteric amide replacement. *Bioorganic & Medicinal Chemistry Letters* **2011**, *21*, 6253-6257.
357. Hansen, M. H.; Blakskjær, P.; Petersen, L. K.; Hansen, T. H.; Højfeldt, J. W.; Gothelf, K. V.; Hansen, N. J. V. A Yoctoliter-Scale DNA Reactor for Small-Molecule Evolution. *Journal of the American Chemical Society* **2009**, *131*, 1322-1327.
358. Blakskjær, P.; Heitner, T.; Hansen, N. J. V. Fidelity by design: Yoctoreactor and binder trap enrichment for small-molecule DNA-encoded libraries and drug discovery. *Current Opinion in Chemical Biology* **2015**, *26*, 62-71.

359. Eid, S.; Turk, S.; Volkamer, A.; Rippmann, F.; Fulle, S. KinMap: a web-based tool for interactive navigation through human kinome data. *BMC Bioinformatics* **2017**, *18*, 16.
360. Uitdehaag, J. C. M.; Verkaar, F.; Alwan, H.; de Man, J.; Buijsman, R. C.; Zaman, G. J. R. A guide to picking the most selective kinase inhibitor tool compounds for pharmacological validation of drug targets. *Br J Pharmacol* **2012**, *166*, 858-876.
361. Kim, K.-Y.; Park, K.-I.; Kim, S.-H.; Yu, S.-N.; Park, S.-G.; Kim, Y. W.; Seo, Y.-K.; Ma, J.-Y.; Ahn, S.-C. Inhibition of Autophagy Promotes Salinomycin-Induced Apoptosis via Reactive Oxygen Species-Mediated PI3K/AKT/mTOR and ERK/p38 MAPK-Dependent Signaling in Human Prostate Cancer Cells. *Int J Mol Sci* **2017**, *18*, 1088.
362. Gu, L.; Tao, X.; Xu, Y.; Han, X.; Qi, Y.; Xu, L.; Yin, L.; Peng, J. Dioscin alleviates BDL- and DMN-induced hepatic fibrosis via Sirt1/Nrf2-mediated inhibition of p38 MAPK pathway. *Toxicology and Applied Pharmacology* **2016**, *292*, 19-29.
363. Fann, D. Y.-W.; Lim, Y.-A.; Cheng, Y.-L.; Lok, K.-Z.; Chunduri, P.; Baik, S.-H.; Drummond, G. R.; Dheen, S. T.; Sobey, C. G.; Jo, D.-G.; Chen, C. L.-H.; Arumugam, T. V. Evidence that NF- $\kappa$ B and MAPK Signaling Promotes NLRP Inflammasome Activation in Neurons Following Ischemic Stroke. *Molecular Neurobiology* **2018**, *55*, 1082-1096.
364. Crowley, N. A.; Bloodgood, D. W.; Hardaway, J. A.; Kendra, A. M.; McCall, J. G.; Al-Hasani, R.; McCall, N. M.; Yu, W.; Schools, Z. L.; Krashes, M. J.; Lowell, B. B.; Whistler, J. L.; Bruchas, M. R.; Kash, T. L. Dynorphin Controls the Gain of an Amygdalar Anxiety Circuit. *Cell Rep* **2016**, *14*, 2774-2783.
365. Liu, Z.; Wu, H.; Jiang, K.; Wang, Y.; Zhang, W.; Chu, Q.; Li, J.; Huang, H.; Cai, T.; Ji, H.; Yang, C.; Tang, N. MAPK-Mediated YAP Activation Controls Mechanical-Tension-Induced Pulmonary Alveolar Regeneration. *Cell Rep* **2016**, *16*, 1810-1819.
366. Kim, J.; Kong, J.; Chang, H.; Kim, H.; Kim, A. EGF induces epithelial-mesenchymal transition through phospho-Smad2/3-Snail signaling pathway in breast cancer cells. *Oncotarget* **2016**, *7*, 85021-85032.
367. Cao, L.; Chen, X.; Xiao, X.; Ma, Q.; Li, W. Resveratrol inhibits hyperglycemia-driven ROS-induced invasion and migration of pancreatic cancer cells via suppression of the ERK and p38 MAPK signaling pathways. *International Journal of Oncology* **2016**, *49*.
368. Li, X.; Dai, Y.; Yan, S.; Shi, Y.; Han, B.; Li, J.; Cha, L.; Mu, J. Down-regulation of lncRNA KCNQ10T1 protects against myocardial ischemia/reperfusion injury following acute myocardial infarction. *Biochemical and Biophysical Research Communications* **2017**, *491*, 1026-1033.
369. Sreekanth, G. P.; Chuncharunee, A.; Sirimontaporn, A.; Panaampon, J.; Noisakran, S.; Yenchitsomanus, P.-T.; Limjindaporn, T. SB203580 Modulates p38 MAPK Signaling and Dengue Virus-Induced Liver Injury by Reducing MAPKAPK2, HSP27, and ATF2 Phosphorylation. *PLoS one* **2016**, *11*, e0149486-e0149486.
370. Ni, H.-D.; Yao, M.; Huang, B.; Xu, L.-S.; Zheng, Y.; Chu, Y.-X.; Wang, H.-Q.; Liu, M.-J.; Xu, S.-J.; Li, H.-B. Glial activation in the periaqueductal gray promotes descending facilitation of neuropathic pain through the p38 MAPK signaling pathway. *Journal of Neuroscience Research* **2016**, *94*, 50-61.
371. Jin, X.; Mo, Q.; Zhang, Y.; Gao, Y.; Wu, Y.; Li, J.; Hao, X.; Ma, D.; Gao, Q.; Chen, P. The p38 MAPK inhibitor BIRB796 enhances the antitumor effects of VX680 in cervical cancer. *Cancer Biol Ther* **2016**, *17*, 566-576.
372. Charron, C. E.; Russell, P.; Ito, K.; Lea, S.; Kizawa, Y.; Brindley, C.; Singh, D. RV568, a narrow-spectrum kinase inhibitor with p38 MAPK- $\alpha$  and - $\gamma$  selectivity, suppresses COPD inflammation. *European Respiratory Journal* **2017**, *50*, 1700188.
373. Friedman Ohana, R.; Levin, S.; Wood, M. G.; Zimmerman, K.; Dart, M. L.; Schwinn, M. K.; Kirkland, T. A.; Hurst, R.; Uyeda, H. T.; Encell, L. P.; Wood, K. V. Improved Deconvolution of Protein Targets for Bioactive Compounds Using a Palladium Cleavable Chloroalkane Capture Tag. *ACS Chem Biol* **2016**, *11*, 2608-2617.
374. Meng, L.; Huang, Z. In silico-in vitro discovery of untargeted kinase-inhibitor interactions from kinase-targeted therapies: A case study on the cancer MAPK signaling pathway. *Computational Biology and Chemistry* **2018**, *75*, 196-204.
375. Frank, S. B.; Berger, P. L.; Ljungman, M.; Miranti, C. K. Human prostate luminal cell differentiation requires NOTCH3 induction by p38-MAPK and MYC. *J Cell Sci* **2017**, *130*, 1952-1964.
376. Guo, F.; He, X.-B.; Li, S.; Le, W. A Central Role for Phosphorylated p38 $\alpha$  in Linking Proteasome Inhibition-Induced Apoptosis and Autophagy. *Molecular Neurobiology* **2017**, *54*, 7597-7609.
377. Yamaguchi, R.; Sakamoto, A.; Yamamoto, T.; Ishimaru, Y.; Narahara, S.; Sugiuchi, H.; Yamaguchi, Y. Surfactant Protein D Inhibits Interleukin-12p40 Production by Macrophages Through the SIRP1/ROCK/ERK Signaling Pathway. *The American Journal of the Medical Sciences* **2017**, *353*, 559-567.
378. Sulen, A.; Gullaksen, S.-E.; Bader, L.; McClymont, D. W.; Skavland, J.; Gavasso, S.; Gjertsen, B. T. Signaling effects of sodium hydrosulfide in healthy donor peripheral blood mononuclear cells. *Pharmacological Research* **2016**, *113*, 216-227.
379. Phoomvuthisarn, P.; Cross, A.; Glennon-Alty, L.; Wright, H. L.; Edwards, S. W. The CDK inhibitor purvalanol A induces neutrophil apoptosis and increases the turnover rate of Mcl-1: potential role of p38-MAPK in regulation of Mcl-1 turnover. *Clin Exp Immunol* **2018**, *192*, 171-180.
380. Potthoff, S. A.; Stamer, S.; Grave, K.; Königshausen, E.; Sivritas, S. H.; Thieme, M.; Mori, Y.; Woznowski, M.; Rump, L. C.; Stegbauer, J. Chronic p38 mitogen-activated protein kinase inhibition improves vascular function and remodeling in angiotensin II-dependent hypertension. *J Renin Angiotensin Aldosterone Syst* **2016**, *17*, 1470320316653284.
381. Ahammed, S.; Kundu, D.; Mukherjee, N.; Ranu, B. C. Microwave Assisted Synthesis of Chalcogenides. *Current Microwave Chemistry* **2017**, *4*, 25-35.
382. Alam, J.; Blackburn, K.; Patrick, D. Neflamapimod: Clinical Phase 2b-Ready Oral Small Molecule Inhibitor of p38 alpha to Reverse Synaptic Dysfunction in Early Alzheimer's Disease. *Jpad-Journal of Prevention of Alzheimers Disease* **2017**, *4*, 273-278.
383. Alam, J. J. Promoting recovery of function in subject that has suffered a neurologic injury resulting from an acute ischemic stroke including thrombotic stroke or embolic stroke, comprises administering a composition comprising VX-745. US9427439-B1.
384. Davis, T.; Brook, A. J. C.; Rokicki, M. J.; Bagley, M. C.; Kipling, D. Evaluating the Role of p38 MAPK in the Accelerated Cell Senescence of Werner Syndrome Fibroblasts. *Pharmaceuticals* **2016**, *9*.

385. Fisher, D. A. C.; Miner, C.; Engle, E.; Hu, H.; Collins, T. B.; Zhou, A.; Allen, M. J.; Malkova, O.; Oh, S. T. Aberrant Cytokine Production in Myelofibrosis Is Not Rectified By Ruxolitinib and Is Differentially Sensitive to Inhibition of JAK/STAT, MAP Kinase, and NF kappa B Signaling. *Blood* **2018**, 132.
386. Goldsmith, C. S.; Kim, S. M.; Karunaratna, N.; Neuendorff, N.; Toussaint, L. G.; Earnest, D. J.; Bell-Pedersen, D. Inhibition of p38 MAPK activity leads to cell type-specific effects on the molecular circadian clock and time-dependent reduction of glioma cell invasiveness. *BMC Cancer* **2018**, 18.
387. Jie, Z.; Shen, S.; Zhao, X.; Xu, W.; Zhang, X.; Huang, B.; Tang, P.; Qin, A.; Fan, S.; Xie, Z. Activating -catenin/Pax6 axis negatively regulates osteoclastogenesis by selectively inhibiting phosphorylation of p38/MAPK. *Faseb Journal* **2019**, 33, 4236-4247.
388. Singh, R. K.; Diwan, M.; Dastidar, S. G.; Najmi, A. K. Differential effect of p38 and MK2 kinase inhibitors on the inflammatory and toxicity biomarkers in vitro. *Human & Experimental Toxicology* **2018**, 37, 521-531.
389. Su, B.-C.; Chen, J.-Y. Pharmacological inhibition of p38 potentiates antimicrobial peptide TP4-induced cell death in glioblastoma cells. *Molecular and Cellular Biochemistry* **2020**, 464, 1-9.
390. Al-Maghout, T.; Pelzl, L.; Sahu, I.; Sukkar, B.; Hosseinzadeh, Z.; Gutti, R.; Laufer, S.; Voelkl, J.; Pieske, B.; Gawaz, M.; Lang, F. P38 Kinase, SGK1 and NF-kappa B Dependent Up-Regulation of Na<sup>+</sup>/Ca<sup>2+</sup> Exchanger Expression and Activity Following TGF beta 1 Treatment of Megakaryocytes. *Cellular Physiology and Biochemistry* **2017**, 42, 2169-2181.
391. Cheng, F.; Twardowski, L.; Fehr, S.; Aner, C.; Schaeffeler, E.; Joos, T.; Knorpp, T.; Dorweiler, B.; Laufer, S.; Schwab, M.; Torzewski, M. Selective p38 alpha MAP kinase/MAPK14 inhibition in enzymatically modified LDL-stimulated human monocytes: implications for atherosclerosis. *Faseb Journal* **2017**, 31, 674-686.
392. Cisterna, B. A.; Vilos, C. Combined nanotherapy based on Cisplatin and MAPK, MEK/ERK inhibitors for colorectal cancer. *Molecular Biology of the Cell* **2018**, 29.
393. Guenthoer, P.; Fuchs, K.; Reischl, G.; Quintanilla-Martinez, L.; Gonzalez-Menendez, I.; Laufer, S.; Pichler, B. J.; Kneilling, M. Evaluation of the therapeutic potential of the selective p38 MAPK inhibitor Skepinone-L and the dual p38/JNK 3 inhibitor LN 950 in experimental K/BxN serum transfer arthritis. *Inflammopharmacology* **2019**, 27, 1217-1227.
394. Signoretto, E.; Laufer, S. A.; Lang, F. Stimulating Effect of Sclareol on Suicidal Death of Human Erythrocytes. *Cellular Physiology and Biochemistry* **2016**, 39, 554-564.
395. Taves, S.; Berta, T.; Liu, D.-L.; Gan, S.; Chen, G.; Kim, Y. H.; Van de Ven, T.; Laufer, S.; Ji, R.-R. Spinal inhibition of p38 MAPK kinase reduces inflammatory and neuropathic pain in male but not female mice: Sex-dependent microglial signaling in the spinal cord. *Brain Behavior and Immunity* **2016**, 55, 70-81.
396. Wentsch, H. K.; Walter, N. M.; Buehrmann, M.; Mayer-Wrangowski, S.; Rauh, D.; Zaman, G. J. R.; Willemsen-Seegers, N.; Buijsman, R. C.; Henning, M.; Dauch, D.; Zender, L.; Laufer, S. Optimized Target Residence Time: Type 11/2 Inhibitors for p38 MAP Kinase with Improved Binding Kinetics through Direct Interaction with the R-Spine. *Angewandte Chemie-International Edition* **2017**, 56, 5363-5367.
397. Werner, M.; Pace, S.; Czapka, A.; Jordan, P. M.; Gerstmeier, J.; Koeberle, A.; Werz, O. Communication between human macrophages and epithelial cancer cell lines dictates lipid mediator biosynthesis. *Cellular and molecular life sciences : CMLS* **2020**.
398. Hari, S. B.; Perera, B. G. K.; Ranjitkar, P.; Seeliger, M. A.; Maly, D. J. Conformation-Selective Inhibitors Reveal Differences in the Activation and Phosphate-Binding Loops of the Tyrosine Kinases Abl and Src. *ACS Chem Biol* **2013**, 8, 2734-2743.
399. Hari, Sanjay B.; Merritt, Ethan A.; Maly, Dustin J. Conformation-Selective ATP-Competitive Inhibitors Control Regulatory Interactions and Noncatalytic Functions of Mitogen-Activated Protein Kinases. *Chemistry & Biology* **2014**, 21, 628-635.
400. Buchdunger, E.; Zimmermann, J.; Mett, H.; Meyer, T. G.; Müller, M.; Druker, B. J.; Lydon, N. Inhibition of the abl protein-tyrosine kinase in vitro and in vivo by a 2-phenylaminopyrimidine derivative. *Cancer Res.* **1996**, 56, 100.
401. Druker, B. J.; Tamura, S.; Buchdunger, E.; Ohno, S.; Segal, G. M.; Fanning, S.; Zimmermann, J.; Lydon, N. B. Effects of a selective inhibitor of the abl tyrosine kinase on the growth of bcr-abl positive cells. *Nat. Med.* **1996**, 2, 561.
402. Röhm, S.; Berger, B.-T.; Schröder, M.; Chaikuad, A.; Winkel, R.; Hekking, K. F. W.; Benningshof, J. J. C.; Müller, G.; Tesch, R.; Kudolo, M.; Forster, M.; Laufer, S.; Knapp, S. Fast Iterative Synthetic Approach toward Identification of Novel Highly Selective p38 MAP Kinase Inhibitors. *Journal of Medicinal Chemistry* **2019**, 62, 10757-10782.
403. Bosc, N.; Meyer, C.; Bonnet, P. The use of novel selectivity metrics in kinase research. *BMC Bioinformatics* **2017**, 18, 17.
404. Vidyasagar, A.; Wilson, N. A.; Djamali, A. Heat shock protein 27 (HSP27): biomarker of disease and therapeutic target. *Fibrogenesis & Tissue Repair* **2012**, 5, 7.
405. Abisambra, J. F.; Blair, L. J.; Hill, S. E.; Jones, J. R.; Kraft, C.; Rogers, J.; Koren, J.; Jinwal, U. K.; Lawson, L.; Johnson, A. G.; Wilcock, D.; O'Leary, J. C.; Jansen-West, K.; Muschol, M.; Golde, T. E.; Weeber, E. J.; Banko, J.; Dickey, C. A. Phosphorylation Dynamics Regulate Hsp27-Mediated Rescue of Neuronal Plasticity Deficits in Tau Transgenic Mice. *The Journal of Neuroscience* **2010**, 30, 15374-15382.
406. Armstrong, S. C.; Delacey, M.; Ganote, C. E. Phosphorylation State of hsp27 and p38 MAPK During Preconditioning and Protein Phosphatase Inhibitor Protection of Rabbit Cardiomyocytes. *Journal of Molecular and Cellular Cardiology* **1999**, 31, 555-567.
407. Ciocca, D. R.; Calderwood, S. K. Heat shock proteins in cancer: diagnostic, prognostic, predictive, and treatment implications. *Cell Stress Chaperones* **2005**, 10, 86-103.
408. Tweedle, E. M.; Khattak, I.; Ang, C. W.; Nedjadi, T.; Jenkins, R.; Park, B. K.; Kalirai, H.; Dodson, A.; Azadeh, B.; Terlizzo, M.; Grabsch, H.; Mueller, W.; Myint, S.; Clark, P.; Wong, H.; Greenhalf, W.; Neoptolemos, J. P.; Rooney, P. S.; Costello, E. Low molecular weight heat shock protein HSP27 is a prognostic indicator in rectal cancer but not colon cancer. *Gut* **2010**, 59, 1501-1510.
409. Kang, S. H.; Kang, K. W.; Kim, K.-H.; Kwon, B.; Kim, S.-K.; Lee, H.-Y.; Kong, S.-Y.; Lee, E. S.; Jang, S.-G.; Yoo, B. C. Upregulated HSP27 in human breast cancer cells reduces Herceptin susceptibility by increasing Her2 protein stability. *BMC Cancer* **2008**, 8, 286-286.
410. Zegzouti, H.; Goueli, S. A. *Kinase Screening and Profiling: Methods and Protocols*. 2016.

411. Roehm, N. W.; Rodgers, G. H.; Hatfield, S. M.; Glasebrook, A. L. An improved colorimetric assay for cell proliferation and viability utilizing the tetrazolium salt XTT. *Journal of Immunological Methods* **1991**, *142*, 257-265.
412. Arrowsmith, C. H.; Audia, J. E.; Austin, C.; Baell, J.; Bennett, J.; Blagg, J.; Bountra, C.; Brennan, P. E.; Brown, P. J.; Bunnage, M. E.; Buser-Doepner, C.; Campbell, R. M.; Carter, A. J.; Cohen, P.; Copeland, R. A.; Cravatt, B.; Dahlin, J. L.; Dhanak, D.; Edwards, A. M.; Frederiksen, M.; Frye, S. V.; Gray, N.; Grimshaw, C. E.; Hepworth, D.; Howe, T.; Huber, K. V. M.; Jin, J.; Knapp, S.; Kotz, J. D.; Kruger, R. G.; Lowe, D.; Mader, M. M.; Marsden, B.; Mueller-Fahnow, A.; Müller, S.; O'Hagan, R. C.; Overington, J. P.; Owen, D. R.; Rosenberg, S. H.; Roth, B.; Ross, R.; Schapira, M.; Schreiber, S. L.; Shoichet, B.; Sundström, M.; Superti-Furga, G.; Taunton, J.; Toledo-Sherman, L.; Walpole, C.; Walters, M. A.; Willson, T. M.; Workman, P.; Young, R. N.; Zuercher, W. J. The promise and peril of chemical probes. *Nature chemical biology* **2015**, *11*, 536-541.
413. Blagg, J.; Workman, P. Choose and Use Your Chemical Probe Wisely to Explore Cancer Biology. *Cancer Cell* **2017**, *32*, 9-25.
414. Regan, J.; Capolino, A.; Cirillo, P. F.; Gilmore, T.; Graham, A. G.; Hickey, E.; Kroe, R. R.; Madwed, J.; Moriaki, M.; Nelson, R.; Pargellis, C. A.; Swinamer, A.; Torcellini, C.; Tsang, M.; Moss, N. Structure-Activity Relationships of the p38 $\alpha$  MAP Kinase Inhibitor 1-(5-tert-Butyl-2-p-tolyl-2H-pyrazol-3-yl)-3-[4-(2-morpholin-4-yl-ethoxy)naphthalen-1-yl]urea (BIRB 796). *Journal of Medicinal Chemistry* **2003**, *46*, 4676-4686.
415. Arai, T.; Ohno, M.; Inoue, H.; Hayashi, S.; Aoki, T.; Hirokawa, H.; Meguro, H.; Koga, Y.; Oshida, K.; Kainoh, M.; Suyama, K.; Kawai, H. Design and synthesis of novel p38 $\alpha$  MAP kinase inhibitors: Discovery of pyrazole-benzyl ureas bearing 2-morpholinopyrimidine moiety. *Bioorganic & Medicinal Chemistry Letters* **2012**, *22*, 5118-5122.
416. Nasiri, A. H.; Saxena, K.; Bats, J. W.; Nasiri, H. R.; Schwalbe, H. Biophysical investigation and conformational analysis of p38 $\alpha$  kinase inhibitor doramipimod and its analogues. *MedChemComm* **2016**, *7*, 1421-1428.
417. Dietrich, J.; Hulme, C.; Hurlley, L. H. The design, synthesis, and evaluation of 8 hybrid DFG-out allosteric kinase inhibitors: A structural analysis of the binding interactions of Gleevec<sup>®</sup>, Nexavar<sup>®</sup>, and BIRB-796. *Bioorganic & Medicinal Chemistry* **2010**, *18*, 5738-5748.
418. Sullivan, J. E.; Holdgate, G. A.; Campbell, D.; Timms, D.; Gerhardt, S.; Breed, J.; Breeze, A. L.; Bermingham, A.; Paupit, R. A.; Norman, R. A.; Embrey, K. J.; Read, J.; VanScyoc, W. S.; Ward, W. H. J. Prevention of MKK6-Dependent Activation by Binding to p38 $\alpha$  MAP Kinase. *Biochemistry* **2005**, *44*, 16475-16490.
419. Wong, D. J. L.; Robert, L.; Atefi, M. S.; Lassen, A.; Avarappatt, G.; Cerniglia, M.; Avramis, E.; Tsoi, J.; Foulad, D.; Graeber, T. G.; Comin-Anduix, B.; Samatar, A.; Lo, R. S.; Ribas, A. Antitumor activity of the ERK inhibitor SCH72984 [corrected] against BRAF mutant, NRAS mutant and wild-type melanoma. *Mol Cancer* **2014**, *13*, 194-194.
420. Morris, E. J.; Jha, S.; Restaino, C. R.; Dayananth, P.; Zhu, H.; Cooper, A.; Carr, D.; Deng, Y.; Jin, W.; Black, S.; Long, B.; Liu, J.; DiNunzio, E.; Windsor, W.; Zhang, R.; Zhao, S.; Angagaw, M. H.; Pinheiro, E. M.; Desai, J.; Xiao, L.; Shipps, G.; Hruza, A.; Wang, J.; Kelly, J.; Paliwal, S.; Gao, X.; Babu, B. S.; Zhu, L.; Daublain, P.; Zhang, L.; Lutterbach, B. A.; Pelletier, M. R.; Philippart, U.; Siliphaivanh, P.; Witter, D.; Kirschmeier, P.; Bishop, W. R.; Hicklin, D.; Gilliland, D. G.; Jayaraman, L.; Zawel, L.; Fawell, S.; Samatar, A. A. Discovery of a Novel ERK Inhibitor with Activity in Models of Acquired Resistance to BRAF and MEK Inhibitors. *Cancer Discovery* **2013**, *3*, 742-750.
421. Hatzivassiliou, G.; Liu, B.; O'Brien, C.; Spoerke, J. M.; Hoeflich, K. P.; Haverty, P. M.; Soriano, R.; Forrest, W. F.; Heldens, S.; Chen, H.; Toy, K.; Ha, C.; Zhou, W.; Song, K.; Friedman, L. S.; Amler, L. C.; Hampton, G. M.; Moffat, J.; Belvin, M.; Lackner, M. R. ERK Inhibition Overcomes Acquired Resistance to MEK Inhibitors. *Molecular Cancer Therapeutics* **2012**, *11*, 1143-1154.
422. Fedorov, O.; Niesen, F. H.; Knapp, S. Kinase inhibitor selectivity profiling using differential scanning fluorimetry. *Methods Mol. Biol.* **2012**, *795*, 109.
423. Kranz, J. K.; Schalk-Hihi, C. Chapter eleven - Protein Thermal Shifts to Identify Low Molecular Weight Fragments. In *Methods in Enzymology*, Kuo, L. C., Ed. Academic Press: 2011; Vol. 493, pp 277-298.
424. Pantoliano, M. W.; Petrella, E. C.; Kwasnoski, J. D.; Lobanov, V. S.; Myslik, J.; Graf, E.; Carver, T.; Asel, E.; Springer, B. A.; Lane, P.; Salemme, F. R. High-Density Miniaturized Thermal Shift Assays as a General Strategy for Drug Discovery. *Journal of Biomolecular Screening* **2001**, *6*, 429-440.
425. Bai, N.; Roder, H.; Dickson, A.; Karanicolas, J. Isothermal Analysis of ThermoFluor Data can readily provide Quantitative Binding Affinities. *Sci Rep* **2019**, *9*, 2650-2650.
426. Zhang, R.; Monsma, F. Fluorescence-based thermal shift assays. *Curr Opin Drug Discov Devel* **2010**, *13*, 389-402.
427. Machleidt, T.; Woodroffe, C. C.; Schwinn, M. K.; Méndez, J.; Robers, M. B.; Zimmerman, K.; Otto, P.; Daniels, D. L.; Kirkland, T. A.; Wood, K. V. Nanobret—a novel bret platform for the analysis of protein-protein interactions. *ACS Chem. Biol.* **2015**, *10*, 1797.
428. Vasta, J. D.; Corona, C. R.; Wilkinson, J.; Zimprich, C. A.; Hartnett, J. R.; Ingold, M. R.; Zimmerman, K.; Machleidt, T.; Kirkland, T. A.; Huwiler, K. G.; Ohana, R. F.; Slater, M.; Otto, P.; Cong, M.; Wells, C. I.; Berger, B. T.; Hanke, T.; Glas, C.; Ding, K.; Drewry, D. H.; Huber, K. V. M.; Willson, T. M.; Knapp, S.; Müller, S.; Meisenheimer, P. L.; Fan, F.; Wood, K. V.; Robers, M. B. Quantitative, wide-spectrum kinase profiling in live cells for assessing the effect of cellular atp on target engagement. *Cell Chem. Biol.* **2018**, *25*, 206.
429. Bagley, M. C.; Davis, T.; Dix, M. C.; Widdowson, C. S.; Kipling, D. Microwave-assisted synthesis of N-pyrazole ureas and the p38 $\alpha$  inhibitor BIRB 796 for study into accelerated cell ageing. *Organic & Biomolecular Chemistry* **2006**, *4*, 4158-4164.
430. Knorr, L. Einwirkung von Acetessigester auf Phenylhydrazin. *Berichte der deutschen chemischen Gesellschaft* **1883**, *16*, 2597-2599.
431. Ghosh, A. K.; Brindisi, M.; Sarkar, A. The Curtius Rearrangement: Applications in Modern Drug Discovery and Medicinal Chemistry. *ChemMedChem* **2018**, *13*, 2351-2373.
432. Ghosh, A. K.; Sarkar, A.; Brindisi, M. The Curtius rearrangement: mechanistic insight and recent applications in natural product syntheses. *Organic & Biomolecular Chemistry* **2018**, *16*, 2006-2027.
433. Batey, R. A.; Santhakumar, V.; Yoshina-Ishii, C.; Taylor, S. D. An efficient new protocol for the formation of unsymmetrical tri- and tetrasubstituted ureas. *Tetrahedron Letters* **1998**, *39*, 6267-6270.

434. The Curtius Reaction. In *Organic Reactions*, pp 337-449.
435. Padiya, K. J.; Gavade, S.; Kardile, B.; Tiwari, M.; Bajare, S.; Mane, M.; Gaware, V.; Varghese, S.; Harel, D.; Kurhade, S. Unprecedented "In Water" Imidazole Carbonylation: Paradigm Shift for Preparation of Urea and Carbamate. *Organic Letters* **2012**, 14, 2814-2817.
436. Das, J.; Moquin, R. V.; Dyckman, A. J.; Li, T.; Pitt, S.; Zhang, R.; Shen, D. R.; McIntyre, K. W.; Gillooly, K.; Doweiko, A. M.; Newitt, J. A.; Sack, J. S.; Zhang, H.; Kiefer, S. E.; Kish, K.; McKinnon, M.; Barrish, J. C.; Dodd, J. H.; Schieven, G. L.; Leftheris, K. 5-Amino-pyrazoles as potent and selective p38 $\alpha$  inhibitors. *Bioorganic & Medicinal Chemistry Letters* **2010**, 20, 6886-6889.
437. Jagath Reddy, G.; Sailaja, S.; Manjula, D.; Srinivasa Rao, K. A CLEAN AND RAPID SYNTHESIS OF 5-AMINOPYRAZOLE-4-CARBOXYLIC ACID ESTERS AND NITRILES USING MONTMORILLONITE K10. In *Heterocyclic Communications*, 2005; Vol. 11, p 385.
438. Heravi, M. M.; Nami, N.; Seifi, N.; Oskooie, H. A.; Hekmatshoar, R. Microwave-Assisted Synthesis of Substituted Pyrazoles and Pyrazolo [3, 4-d]thiopyrimidines. *Phosphorus, Sulfur, and Silicon and the Related Elements* **2006**, 181, 591-599.
439. Dykman, A. Preparation of aryl-substituted pyrazol-amide compounds useful as kinase inhibitors, US7396935B2. **2004**.
440. Basel, Y.; Hassner, A. Di-tert-butyl Dicarboxylate and 4-(Dimethylamino)pyridine Revisited. Their Reactions with Amines and Alcohols. *The Journal of Organic Chemistry* **2000**, 65, 6368-6380.
441. Sheehan, J. C.; Hess, G. P. A New Method of Forming Peptide Bonds. *Journal of the American Chemical Society* **1955**, 77, 1067-1068.
442. Carpino, L. A.; Imazumi, H.; Foxman, B. M.; Vela, M. J.; Henklein, P.; El-Faham, A.; Klose, J.; Bienert, M. Comparison of the Effects of 5- and 6-HOAt on Model Peptide Coupling Reactions Relative to the Cases for the 4- and 7-Isomers. *Organic Letters* **2000**, 2, 2253-2256.
443. Valeur, E.; Bradley, M. Amide bond formation: beyond the myth of coupling reagents. *Chemical Society Reviews* **2009**, 38, 606-631.
444. Carpino, L. A.; El-Faham, A. The diisopropylcarbodiimide/ 1-hydroxy-7-azabenzotriazole system: Segment coupling and stepwise peptide assembly. *Tetrahedron* **1999**, 55, 6813-6830.
445. Al-Warhi, T. I.; Al-Hazimi, H. M. A.; El-Faham, A. Recent development in peptide coupling reagents. *Journal of Saudi Chemical Society* **2012**, 16, 97-116.
446. Antonovics, I.; Young, G. T. Amino-acids and peptides. Part XXV. The mechanism of the base-catalysed racemisation of the p-nitrophenyl esters of acylpeptides. *Journal of the Chemical Society C: Organic* **1967**, 595-601.
447. König, W.; Geiger, R. [A new method for synthesis of peptides: activation of the carboxyl group with dicyclohexylcarbodiimide using 1-hydroxybenzotriazoles as additives]. *Chem Ber* **1970**, 103, 788-798.
448. Carpino, L. A.; El-Faham, A.; Minor, C. A.; Albericio, F. Advantageous applications of azabenzotriazole (triazolopyridine)-based coupling reagents to solid-phase peptide synthesis. *Journal of the Chemical Society, Chemical Communications* **1994**, 201-203.
449. Carpino, L. A. 1-Hydroxy-7-azabenzotriazole. An efficient peptide coupling additive. *Journal of the American Chemical Society* **1993**, 115, 4397-4398.
450. Gribble, G. W.; Ferguson, D. C. Reactions of sodium borohydride in acidic media. Selective reduction of aldehydes with sodium triacetoxyborohydride. *Journal of the Chemical Society, Chemical Communications* **1975**, 535-536.
451. Abdel-Magid, A. F.; Mehrman, S. J. A Review on the Use of Sodium Triacetoxyborohydride in the Reductive Amination of Ketones and Aldehydes. *Organic Process Research & Development* **2006**, 10, 971-1031.
452. Abdel-Magid, A. F.; Maryanoff, C. A.; Carson, K. G. Reductive amination of aldehydes and ketones by using sodium triacetoxyborohydride. *Tetrahedron Letters* **1990**, 31, 5595-5598.
453. Verma, S. K.; Acharya, B. N.; Kaushik, M. P. Chemospecific and ligand free CuI catalysed heterogeneous N-arylation of amines with diheteroaryl halides at room temperature. *Organic & Biomolecular Chemistry* **2011**, 9, 1324-1327.
454. Job, G. E.; Buchwald, S. L. Copper-Catalyzed Arylation of  $\beta$ -Amino Alcohols. *Organic Letters* **2002**, 4, 3703-3706.
455. Surry, D. S.; Buchwald, S. L. Biaryl Phosphane Ligands in Palladium-Catalyzed Amination. *Angewandte Chemie International Edition* **2008**, 47, 6338-6361.
456. Goldberg, I. Ueber Phenylirungen bei Gegenwart von Kupfer als Katalysator. *Berichte der deutschen chemischen Gesellschaft* **1906**, 39, 1691-1692.
457. Uday Kumar, R. Metal free amination of 2-chloroazoles in aqueous medium. *Tetrahedron letters* **2016**, v. 57, pp. 637-640-2016 v.57.
458. Day, E.; Waters, B.; Spiegel, K.; Alnadaf, T.; Manley, P. W.; Buchdunger, E.; Walker, C.; Jarai, G. Inhibition of collagen-induced discoidin domain receptor 1 and 2 activation by imatinib, nilotinib and dasatinib. *European Journal of Pharmacology* **2008**, 599, 44-53.
459. Richters, A.; Nguyen, H. D.; Phan, T.; Simard, J. R.; Grütter, C.; Engel, J.; Rauh, D. Identification of Type II and III DDR2 Inhibitors. *Journal of Medicinal Chemistry* **2014**, 57, 4252-4262.
460. Valiathan, R. R.; Marco, M.; Leitinger, B.; Kleer, C. G.; Fridman, R. Discoidin domain receptor tyrosine kinases: new players in cancer progression. *Cancer Metastasis Rev* **2012**, 31, 295-321.
461. Borza, C. M.; Pozzi, A. Discoidin domain receptors in disease. *Matrix Biology* **2014**, 34, 185-192.
462. Shrivastava, A.; Radziejewski, C.; Campbell, E.; Kovac, L.; McGlynn, M.; Ryan, T. E.; Davis, S.; Goldfarb, M. P.; Glass, D. J.; Lemke, G.; Yancopoulos, G. D. An Orphan Receptor Tyrosine Kinase Family Whose Members Serve as Nonintegrin Collagen Receptors. *Molecular Cell* **1997**, 1, 25-34.
463. Vogel, W.; Gish, G. D.; Alves, F.; Pawson, T. The Discoidin Domain Receptor Tyrosine Kinases Are Activated by Collagen. *Molecular Cell* **1997**, 1, 13-23.
464. Agarwal, G.; Smith, A. W.; Jones, B. Discoidin domain receptors: Micro insights into macro assemblies. *Biochimica et Biophysica Acta (BBA) - Molecular Cell Research* **2019**, 1866, 118496.

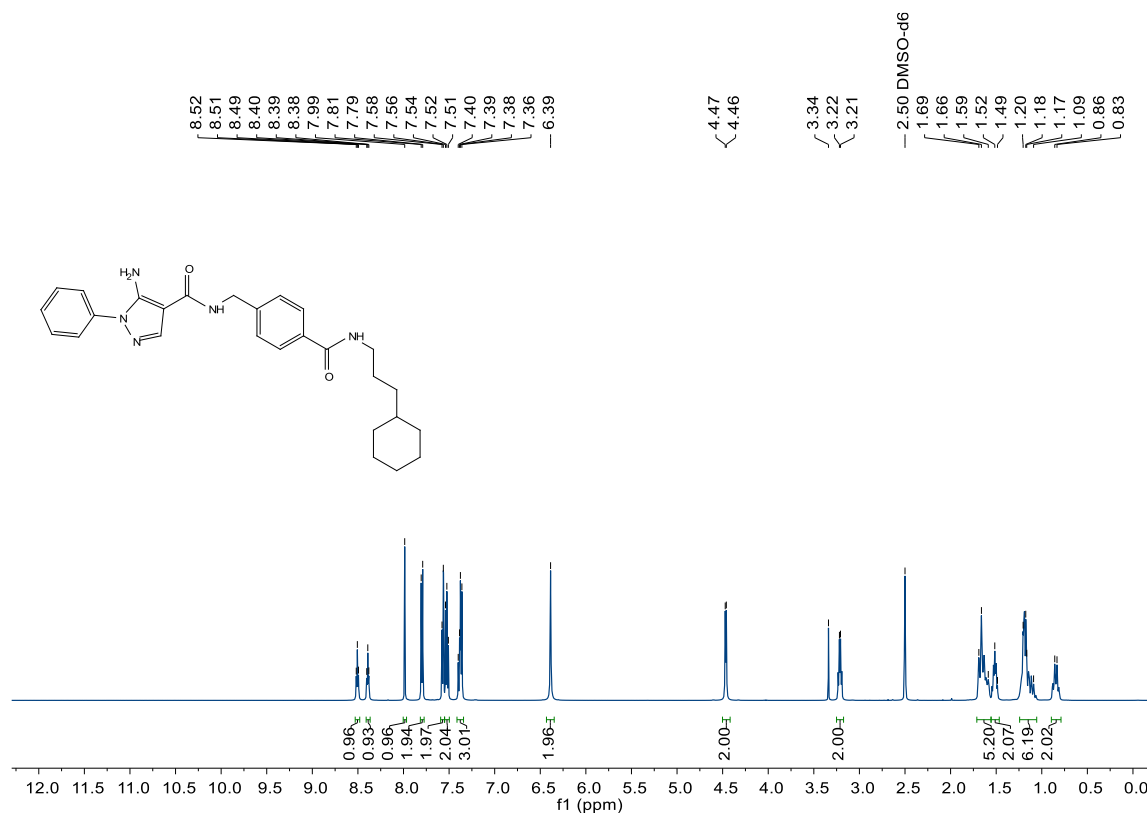
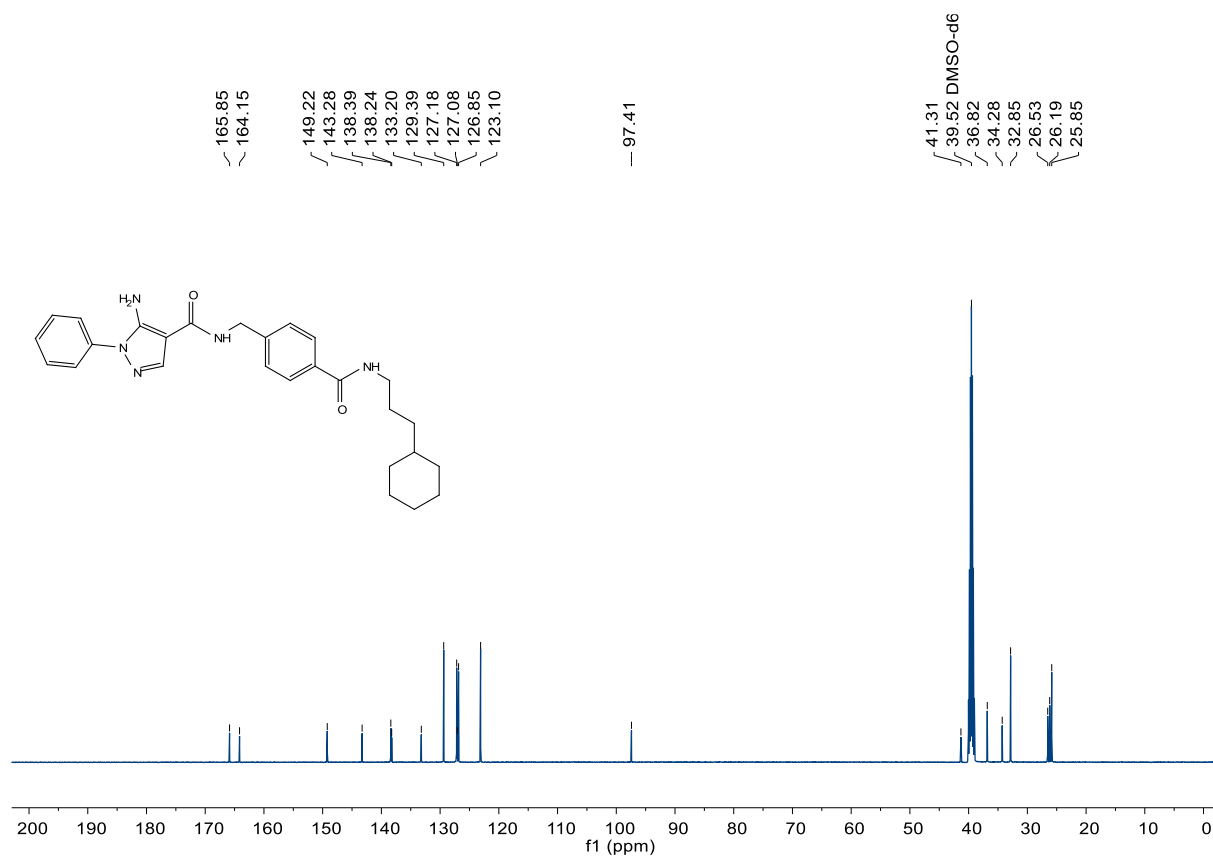
465. Leitinger, B. Chapter Two - Discoidin Domain Receptor Functions in Physiological and Pathological Conditions. In *International Review of Cell and Molecular Biology*, Jeon, K. W., Ed. Academic Press: 2014; Vol. 310, pp 39-87.
466. Alves, F.; Vogel, W.; Mossie, K.; Millauer, B.; Höfler, H.; Ullrich, A. Distinct structural characteristics of discoidin I subfamily receptor tyrosine kinases and complementary expression in human cancer. *Oncogene* **1995**, *10*, 609-618.
467. Fu, H.-L.; Sohail, A.; Valiathan, R. R.; Wasinski, B. D.; Kumarasiri, M.; Mahasenan, K. V.; Bernardo, M. M.; Tokmina-Roszyk, D.; Fields, G. B.; Mobashery, S.; Fridman, R. Shedding of discoidin domain receptor 1 by membrane-type matrix metalloproteinases. *J Biol Chem* **2013**, *288*, 12114-12129.
468. Leitinger, B. Molecular Analysis of Collagen Binding by the Human Discoidin Domain Receptors, DDR1 and DDR2: IDENTIFICATION OF COLLAGEN BINDING SITES IN DDR2. *Journal of Biological Chemistry* **2003**, *278*, 16761-16769.
469. Li, Y.; Lu, X.; Ren, X.; Ding, K. Small Molecule Discoidin Domain Receptor Kinase Inhibitors and Potential Medical Applications. *Journal of Medicinal Chemistry* **2015**, *58*, 3287-3301.
470. Xu, H.; Raynal, N.; Stathopoulos, S.; Myllyharju, J.; Farndale, R. W.; Leitinger, B. Collagen binding specificity of the discoidin domain receptors: binding sites on collagens II and III and molecular determinants for collagen IV recognition by DDR1. *Matrix Biol* **2011**, *30*, 16-26.
471. Fu, H.-L.; Valiathan, R. R.; Payne, L.; Kumarasiri, M.; Mahasenan, K. V.; Mobashery, S.; Huang, P.; Fridman, R. Glycosylation at Asn211 regulates the activation state of the discoidin domain receptor 1 (DDR1). *J Biol Chem* **2014**, *289*, 9275-9287.
472. Noordeen, N. A.; Carafoli, F.; Hohenester, E.; Horton, M. A.; Leitinger, B. A Transmembrane Leucine Zipper Is Required for Activation of the Dimeric Receptor Tyrosine Kinase DDR1. *Journal of Biological Chemistry* **2006**, *281*, 22744-22751.
473. Mihai, C.; Chotani, M.; Elton, T. S.; Agarwal, G. Mapping of DDR1 distribution and oligomerization on the cell surface by FRET microscopy. *J Mol Biol* **2009**, *385*, 432-445.
474. Yeung, D. A.; Shanker, N.; Sohail, A.; Weiss, B. A.; Wang, C.; Wellmerling, J.; Das, S.; Ganju, R. K.; Miller, J. L. C.; Herr, A. B.; Fridman, R.; Agarwal, G. Clustering, Spatial Distribution, and Phosphorylation of Discoidin Domain Receptors 1 and 2 in Response to Soluble Collagen I. *J Mol Biol* **2019**, *431*, 368-390.
475. Rammal, H.; Saby, C.; Magnien, K.; Van-Gulick, L.; Garnotel, R.; Buache, E.; El Btaouri, H.; Jeannesson, P.; Morjani, H. Discoidin Domain Receptors: Potential Actors and Targets in Cancer. *Frontiers in Pharmacology* **2016**, *7*.
476. Ikeda, K.; Wang, L.-H.; Torres, R.; Zhao, H.; Olaso, E.; Eng, F. J.; Labrador, P.; Klein, R.; Lovett, D.; Yancopoulos, G. D.; Friedman, S. L.; Lin, H. C. Discoidin Domain Receptor 2 Interacts with Src and Shc following Its Activation by Type I Collagen. *Journal of Biological Chemistry* **2002**, *277*, 19206-19212.
477. Wang, C.-Z.; Su, H.-W.; Hsu, Y.-C.; Shen, M.-R.; Tang, M.-J. A Discoidin Domain Receptor 1/SHP-2 Signaling Complex Inhibits  $\alpha 2\beta 1$ -Integrin-mediated Signal Transducers and Activators of Transcription 1/3 Activation and Cell Migration. *Molecular Biology of the Cell* **2006**, *17*, 2839-2852.
478. Das, S.; Ongusaha, P. P.; Yang, Y. S.; Park, J.-M.; Aaronson, S. A.; Lee, S. W. Discoidin Domain Receptor 1 Receptor Tyrosine Kinase Induces Cyclooxygenase-2 and Promotes Chemoresistance through Nuclear Factor- $\kappa$ B Pathway Activation. *Cancer Research* **2006**, *66*, 8123-8130.
479. Su, J.; Yu, J.; Ren, T.; Zhang, W.; Zhang, Y.; Liu, X.; Sun, T.; Lu, H.; Miyazawa, K.; Yao, L. Discoidin domain receptor 2 is associated with the increased expression of matrix metalloproteinase-13 in synovial fibroblasts of rheumatoid arthritis. *Molecular and Cellular Biochemistry* **2009**, *330*, 141.
480. Koo, D. H. H.; McFadden, C.; Huang, Y.; Abdulhussein, R.; Friese-Hamim, M.; Vogel, W. F. Pinpointing phosphotyrosine-dependent interactions downstream of the collagen receptor DDR1. *FEBS Letters* **2006**, *580*, 15-22.
481. Kumar, A.; Dutta Choudhury, M.; Ghosh, P.; Palit, P. Discoidin domain receptor 2: An emerging pharmacological drug target for prospective therapy against osteoarthritis. *Pharmacological Reports* **2019**, *71*, 399-408.
482. Yang, X.; Chen, L.; Xu, X.; Li, C.; Huang, C.; Deng, C.-X. TGF- $\beta$ /Smad3 Signals Repress Chondrocyte Hypertrophic Differentiation and Are Required for Maintaining Articular Cartilage. *Journal of Cell Biology* **2001**, *153*, 35-46.
483. Little, C. B.; Barai, A.; Burkhardt, D.; Smith, S. M.; Fosang, A. J.; Werb, Z.; Shah, M.; Thompson, E. W. Matrix metalloproteinase 13-deficient mice are resistant to osteoarthritic cartilage erosion but not chondrocyte hypertrophy or osteophyte development. *Arthritis Rheum* **2009**, *60*, 3723-3733.
484. Xu, L.; Peng, H.; Wu, D.; Hu, K.; Goldring, M. B.; Olsen, B. R.; Li, Y. Activation of the Discoidin Domain Receptor 2 Induces Expression of Matrix Metalloproteinase 13 Associated with Osteoarthritis in Mice. *Journal of Biological Chemistry* **2005**, *280*, 548-555.
485. Hanson, S. M.; Georghiou, G.; Thakur, M. K.; Miller, W. T.; Rest, J. S.; Chodera, J. D.; Seeliger, M. A. What Makes a Kinase Promiscuous for Inhibitors? *Cell Chem Biol* **2019**, *26*, 390-399.e5.
486. Murray, C. W.; Berdini, V.; Buck, I. M.; Carr, M. E.; Cleasby, A.; Coyle, J. E.; Curry, J. E.; Day, J. E. H.; Day, P. J.; Hearn, K.; Iqbal, A.; Lee, L. Y. W.; Martins, V.; Mortenson, P. N.; Munck, J. M.; Page, L. W.; Patel, S.; Roomans, S.; Smith, K.; Tamanini, E.; Saxty, G. Fragment-Based Discovery of Potent and Selective DDR1/2 Inhibitors. *ACS medicinal chemistry letters* **2015**, *6*, 798-803.
487. Liu, L.; Hussain, M.; Luo, J.; Duan, A.; Chen, C.; Tu, Z.; Zhang, J. Synthesis and biological evaluation of novel dasatinib analogues as potent DDR1 and DDR2 kinase inhibitors. *Chemical Biology & Drug Design* **2017**, *89*, 420-427.
488. Gao, M.; Duan, L.; Luo, J.; Zhang, L.; Lu, X.; Zhang, Y.; Zhang, Z.; Tu, Z.; Xu, Y.; Ren, X.; Ding, K. Discovery and Optimization of 3-(2-(Pyrazolo[1,5-a]pyrimidin-6-yl)ethynyl)benzamides as Novel Selective and Orally Bioavailable Discoidin Domain Receptor 1 (DDR1) Inhibitors. *Journal of Medicinal Chemistry* **2013**, *56*, 3281-3295.
489. Wang, Z.; Zhang, Y.; Pinkas, D. M.; Fox, A. E.; Luo, J.; Huang, H.; Cui, S.; Xiang, Q.; Xu, T.; Xun, Q.; Zhu, D.; Tu, Z.; Ren, X.; Brekken, R. A.; Bullock, A. N.; Liang, G.; Ding, K.; Lu, X. Design, Synthesis, and Biological Evaluation of 3-(Imidazo[1,2-a]pyrazin-3-ylethynyl)-4-isopropyl-N-(3-((4-methylpiperazin-1-yl)methyl)-5-(trifluoromethyl)phenyl)benzamide as a Dual Inhibitor of Discoidin Domain Receptors 1 and 2. *Journal of medicinal chemistry* **2018**, *61*, 7977-7990.

490. Kim, H.-G.; Tan, L.; Weisberg, E. L.; Liu, F.; Canning, P.; Choi, H. G.; Ezell, S. A.; Wu, H.; Zhao, Z.; Wang, J.; Mandinova, A.; Griffin, J. D.; Bullock, A. N.; Liu, Q.; Lee, S. W.; Gray, N. S. Discovery of a potent and selective DDR1 receptor tyrosine kinase inhibitor. *ACS Chem Biol* **2013**, *8*, 2145-2150.
491. Klein, R.; Silos-Santiago, I.; Smeyne, R. J.; Lira, S. A.; Brambilla, R.; Bryant, S.; Zhang, L.; Snider, W. D.; Barbacid, M. Disruption of the neurotrophin-3 receptor gene *trkC* eliminates Ia muscle afferents and results in abnormal movements. *Nature* **1994**, *368*, 249-251.
492. Smeyne, R. J.; Klein, R.; Schnapp, A.; Long, L. K.; Bryant, S.; Lewin, A.; Lira, S. A.; Barbacid, M. Severe sensory and sympathetic neuropathies in mice carrying a disrupted *Trk/NGF* receptor gene. *Nature* **1994**, *368*, 246-249.
493. Wang, Z.; Bian, H.; Bartual, S. G.; Du, W.; Luo, J.; Zhao, H.; Zhang, S.; Mo, C.; Zhou, Y.; Xu, Y.; Tu, Z.; Ren, X.; Lu, X.; Brekken, R. A.; Yao, L.; Bullock, A. N.; Su, J.; Ding, K. Structure-Based Design of Tetrahydroisoquinoline-7-carboxamides as Selective Discoidin Domain Receptor 1 (DDR1) Inhibitors. *Journal of medicinal chemistry* **2016**, *59*, 5911-5916.
494. Wang, Z.; Zhang, Y.; Bartual, S. G.; Luo, J.; Xu, T.; Du, W.; Xun, Q.; Tu, Z.; Brekken, R. A.; Ren, X.; Bullock, A. N.; Liang, G.; Lu, X.; Ding, K. Tetrahydroisoquinoline-7-carboxamide Derivatives as New Selective Discoidin Domain Receptor 1 (DDR1) Inhibitors. *ACS medicinal chemistry letters* **2017**, *8*, 327-332.
495. Zhu, D.; Huang, H.; Pinkas, D. M.; Luo, J.; Ganguly, D.; Fox, A. E.; Arner, E.; Xiang, Q.; Tu, Z.-C.; Bullock, A. N.; Brekken, R. A.; Ding, K.; Lu, X. 2-Amino-2,3-dihydro-1H-indene-5-carboxamide-Based Discoidin Domain Receptor 1 (DDR1) Inhibitors: Design, Synthesis, and in Vivo Antipancreatic Cancer Efficacy. *Journal of medicinal chemistry* **2019**, *62*, 7431-7444.
496. Richter, H.; Satz, A. L.; Bedoucha, M.; Buettelmann, B.; Petersen, A. C.; Harmeier, A.; Hermosilla, R.; Hochstrasser, R.; Burger, D.; Gsell, B.; Gasser, R.; Huber, S.; Hug, M. N.; Kocer, B.; Kuhn, B.; Ritter, M.; Rudolph, M. G.; Weibel, F.; Molina-David, J.; Kim, J.-J.; Santos, J. V.; Stihle, M.; Georges, G. J.; Bonfil, R. D.; Fridman, R.; Uhles, S.; Moll, S.; Faul, C.; Fornoni, A.; Prunotto, M. DNA-Encoded Library-Derived DDR1 Inhibitor Prevents Fibrosis and Renal Function Loss in a Genetic Mouse Model of Alport Syndrome. *ACS Chem Biol* **2019**, *14*, 37-49.
497. Artim, S. C.; Mendrola, J. M.; Lemmon, M. A. Assessing the range of kinase autoinhibition mechanisms in the insulin receptor family. *Biochem J* **2012**, *448*, 213-220.
498. Canning, P.; Tan, L.; Chu, K.; Lee, S. W.; Gray, N. S.; Bullock, A. N. Structural mechanisms determining inhibition of the collagen receptor DDR1 by selective and multi-targeted type II kinase inhibitors. *J Mol Biol* **2014**, *426*, 2457-2470.
499. Yeh, Y.-C.; Wu, C.-C.; Wang, Y.-K.; Tang, M.-J. DDR1 triggers epithelial cell differentiation by promoting cell adhesion through stabilization of E-cadherin. *Molecular Biology of the Cell* **2011**, *22*, 940-953.
500. Morales, C. P.; Souza, R. F.; Spechler, S. J. Hallmarks of cancer progression in Barrett's oesophagus. *The Lancet* **2002**, *360*, 1587-1589.
501. Chen, H.-R.; Yeh, Y.-C.; Liu, C.-Y.; Wu, Y.-T.; Lo, F.-Y.; Tang, M.-J.; Wang, Y.-K. DDR1 promotes E-cadherin stability via inhibition of integrin- $\beta$ 1-Src activation-mediated E-cadherin endocytosis. *Sci Rep* **2016**, *6*, 36336.
502. Kyriakis, J. M.; Avruch, J. Mammalian mapk signal transduction pathways activated by stress and inflammation: a 10-year update. *Physiol. Rev.* **2012**, *92*, 689.
503. Johnson, G. L.; Lapadat, R. Mitogen-activated protein kinase pathways mediated by erk, jnk, and p38 protein kinases. *Science* **2002**, *298*, 1911.
504. Hill, R. J.; Dabbagh, K.; Phippard, D.; Li, C.; Suttman, R. T.; Welch, M.; Papp, E.; Song, K. W.; Chang, K. C.; Leaffer, D.; Kim, Y. N.; Roberts, R. T.; Zabka, T. S.; Aud, D.; Dal, P. J.; Manning, A. M.; Peng, S. L.; Goldstein, D. M.; Wong, B. R. Pamapimod, a novel p38 mitogen-activated protein kinase inhibitor: preclinical analysis of efficacy and selectivity. *J. Pharmacol. Exp. Ther.* **2008**, *327*, 610.
505. David, M. G.; Tobias, G. Pathway to the Clinic: Inhibition of P38 MAP Kinase. A Review of Ten Chemotypes Selected for Development. *Current Topics in Medicinal Chemistry* **2005**, *5*, 1017-1029.
506. Caivano, M.; Rodriguez, C.; Cohen, P.; Alemany, S. 15-Deoxy- $\Delta$ 12,14-prostaglandin  $j_2$  regulates endogenous cot mapk kinase 1 activity induced by lipopolysaccharide. *J. Biol. Chem.* **2003**, *278*, 52124.
507. Stafford, M. J.; Morrice, N. A.; Pegg, M. W.; Cohen, P. Interleukin-1 stimulated activation of the cot catalytic subunit through the phosphorylation of thr290 and ser62. *FEBS Lett.* **2006**, *580*, 4010.
508. Kyriakis, J. M.; Avruch, J. Mammalian mitogen-activated protein kinase signal transduction pathways activated by stress and inflammation. *Physiol. Rev.* **2001**, *81*, 807.
509. O'Keefe, S. J.; Mudgett, J. S.; Cupo, S.; Parsons, J. N.; Chartrain, N. A.; Fitzgerald, C.; Chen, S.-L.; Lowitz, K.; Rasa, C.; Visco, D.; Luell, S.; Carballo-Jane, E.; Owens, K.; Zaller, D. M. Chemical Genetics Define the Roles of p38 $\alpha$  and p38 $\beta$  in Acute and Chronic Inflammation. *Journal of Biological Chemistry* **2007**, *282*, 34663-34671.
510. Silva, G.; Cunha, A.; Grégoire, I. P.; Seldon, M. P.; Soares, M. P. The antiapoptotic effect of heme oxygenase-1 in endothelial cells involves the degradation of p38 $\alpha$  mapk isoform. *J. Immunol.* **2006**, *177*, 1894.
511. Kuma, Y.; Campbell, D. G.; Cuenda, A. Identification of glycogen synthase as a new substrate for stress-activated protein kinase 2b/p38beta. *Biochem. J.* **2004**, *379*, 133.
512. John, H.; Jr; Katerina, L. Small Molecule p38 Inhibitors: Novel Structural Features and Advances from 2002-2005. *Current Topics in Medicinal Chemistry* **2005**, *5*, 967-985.
513. Goldstein, D. M.; Kuglstatter, A.; Lou, Y.; Soth, M. J. Selective p38 $\alpha$  inhibitors clinically evaluated for the treatment of chronic inflammatory disorders. *J. Med. Chem.* **2010**, *53*, 2345.
514. Astolfi, A.; Manfroni, G.; Cecchetti, V.; Barreca, M. L. A comprehensive structural overview of p38 $\alpha$  mitogen-activated protein kinase in complex with atp-site and non-atp-site binders. *ChemMedChem* **2018**, *13*, 7.
515. Koeberle, S. C.; Romir, J.; Fischer, S.; Koeberle, A.; Schattel, V.; Albrecht, W.; Grutter, C.; Werz, O.; Rauh, D.; Stehle, T.; Laufer, S. A. Skepinone-L is a selective p38 mitogen-activated protein kinase inhibitor. *Nat. Chem. Biol.* **2011**, *8*, 141.

516. Buchdunger, E., Zimmermann, Johann, Mett, Helmut, Meyer, Thomas George, Müller, Martin, Druker, Brian J., Lydon, Nicholas; . Inhibition of the Abl protein-tyrosine kinase in vitro and in vivo by a 2-phenylaminopyrimidine derivative. *Cancer research* **1996**, *56*, 100-104.
517. Khazak, V.; Astsaturov, I.; Serebriiskii, I. G.; Golemis, E. A. Selective raf inhibition in cancer therapy. *Expert Opin. Ther. Targets* **2007**, *11*, 1587.
518. Meyerowitz, J. G.; Weiss, W. A.; Gustafson, W. C. A new "angle" on kinase inhibitor design: prioritizing amphosteric activity above kinase inhibition. *Mol. Cell. Oncol.* **2015**, *2*, e975641.
519. Merck, E. Anfärbereagenzien für Dünnschicht- und Papier-Chromatographie, Darmstadt. **1970**.
520. Babij, N. R.; McCusker, E. O.; Whiteker, G. T.; Canturk, B.; Choy, N.; Creemer, L. C.; Amicis, C. V. D.; Hewlett, N. M.; Johnson, P. L.; Knobelsdorf, J. A.; Li, F.; Lorsbach, B. A.; Nugent, B. M.; Ryan, S. J.; Smith, M. R.; Yang, Q. NMR Chemical Shifts of Trace Impurities: Industrially Preferred Solvents Used in Process and Green Chemistry. *Organic Process Research & Development* **2016**, *20*, 661-667.
521. Bauer, S.; M Kubiak, J.; Rothbauer, U.; Laufer, S. *From Enzyme to Whole Blood: Sequential Screening Procedure for Identification and Evaluation of p38 MAPK Inhibitors*. 2015; Vol. 1360, p 123-148.
522. Carpino, L. A.; Mansour, E. M. E.; Cheng, C. H.; Williams, J. R.; MacDonald, R.; Knapczyk, J.; Carman, M.; Lopusinski, A. Polystyrene-based deblocking-scavenging agents for the 9-fluorenylmethoxycarbonyl amino-protecting group. *The Journal of Organic Chemistry* **1983**, *48*, 661-665.



## 11 Spectral data

Figure 59. Compound 33 (SR318),  $^1\text{H-NMR}$ , 500 MHz,  $\text{DMSO-d}_6$ Figure 60. Compound 33 (SR318),  $^{13}\text{C-NMR}$ , 126 MHz,  $\text{DMSO-d}_6$

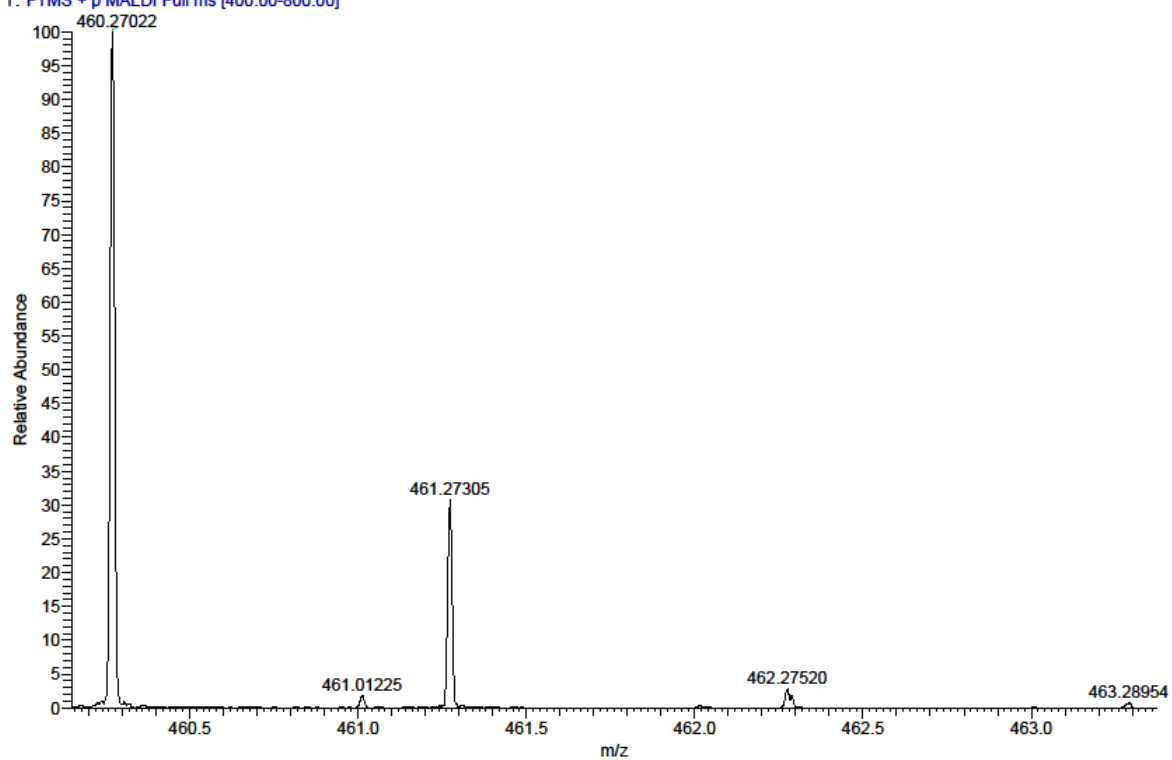
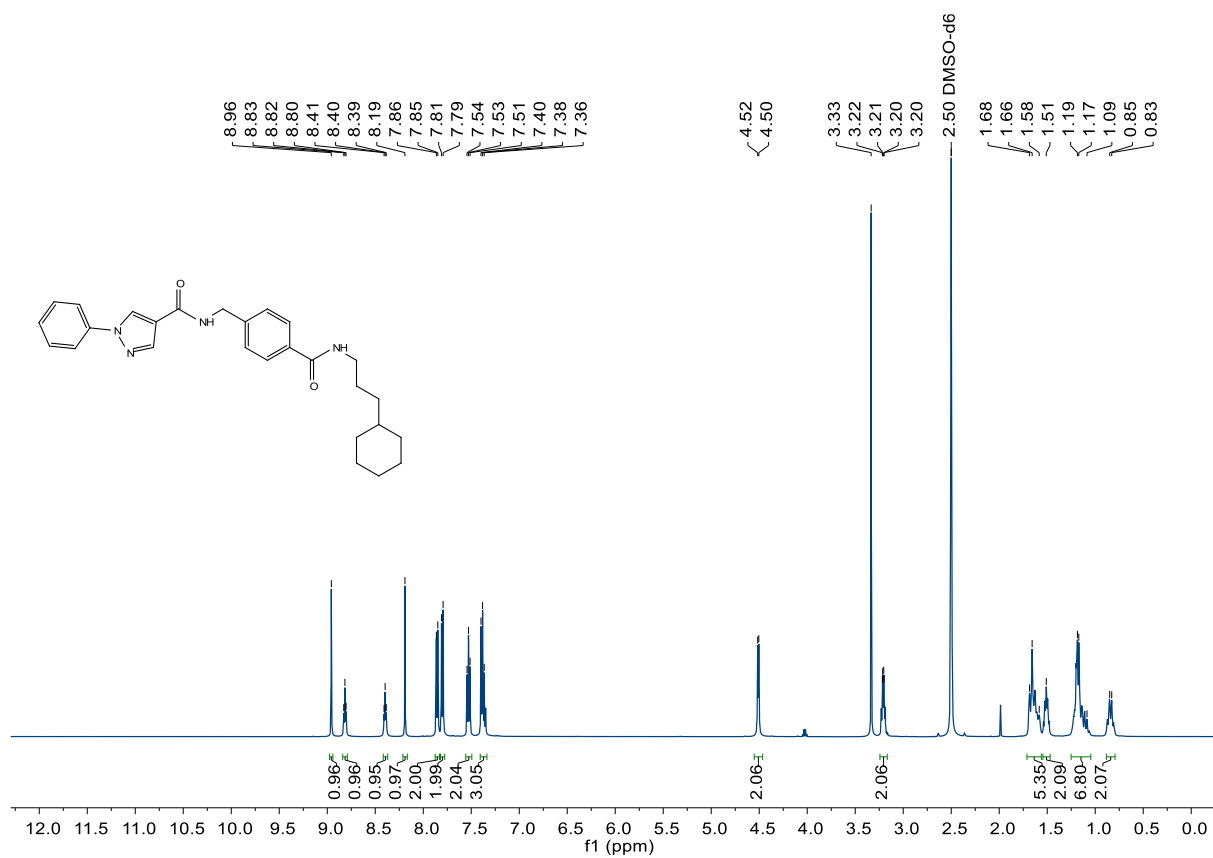
SR318\_F10 #1-13 RT: 0.00-1.33 AV: 13 NL: 6.10E5  
T: FTMS + p MALDI Full ms [400.00-800.00]

Figure 61. Compound 33 (SR318), HRMS (FTMS + p MALDI)

Figure 62. Compound 34 (SR329), <sup>1</sup>H-NMR, 500 MHz, DMSO-d<sub>6</sub>

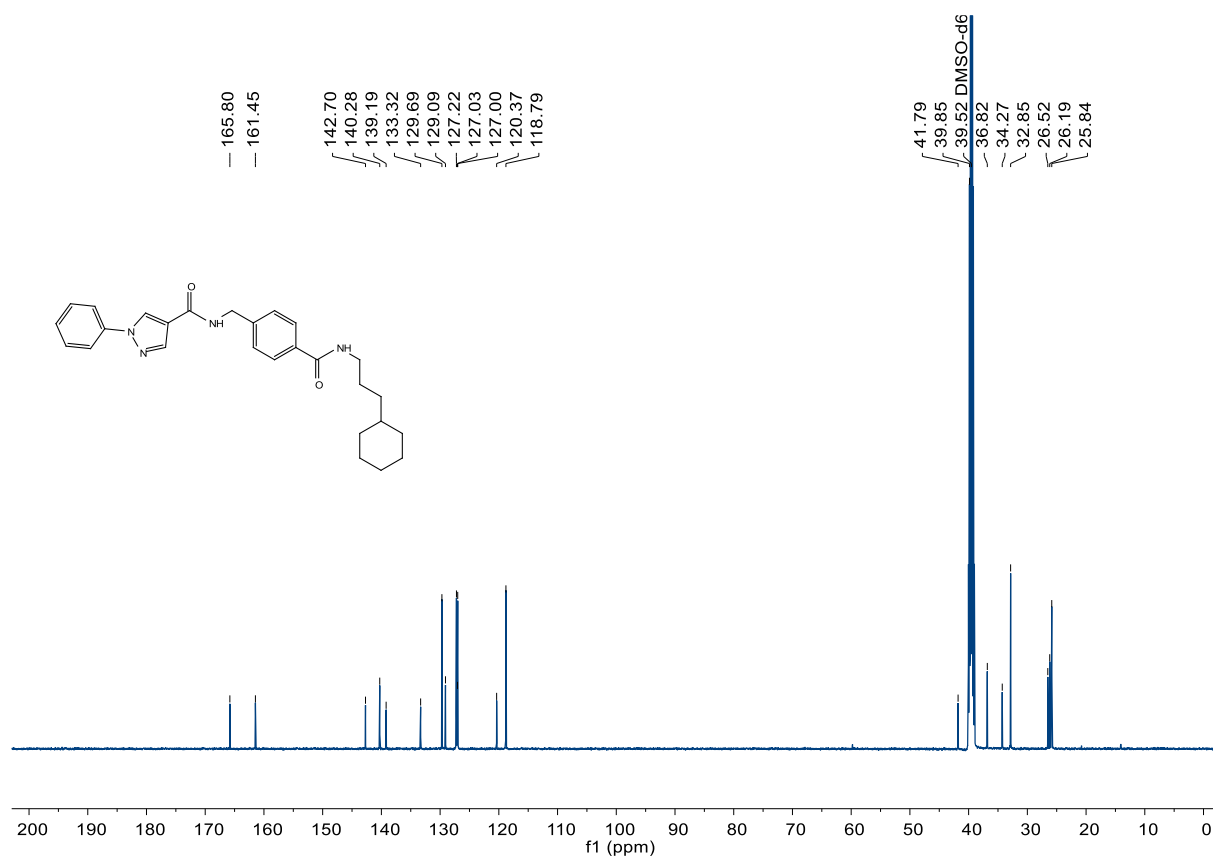


Figure 63. Compound 34 (SR329), <sup>13</sup>C-NMR, 126 MHz, DMSO-d<sub>6</sub>

C:\User\...\Knapp2018\180711\SR329\_F12

7/11/2018 5:11:35 PM

SR329 mit HCCA gemessen.

SR329\_F12 #1-11 RT: 0.00-1.01 AV: 11 NL: 2.55E5  
T: FTMS + p MALDI Full ms [400.00-800.00]

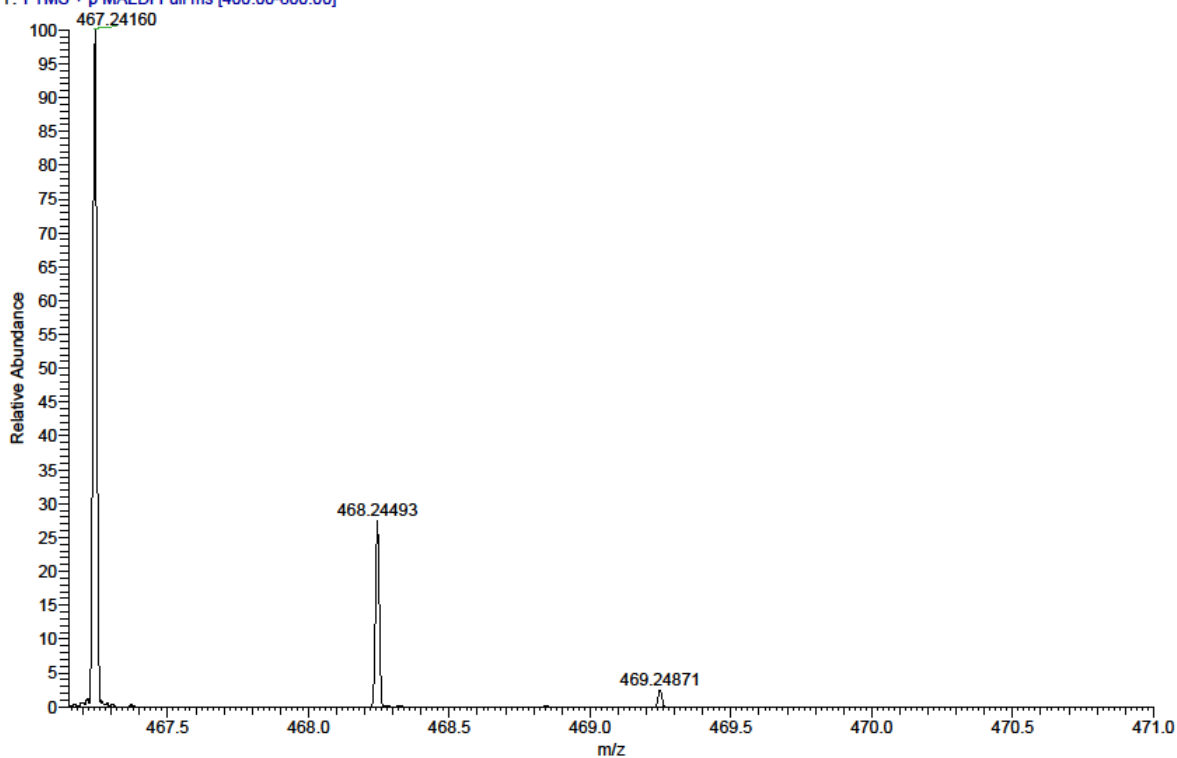


Figure 64. Compound 34 (SR329), HRMS (FTMS + p MALDI)

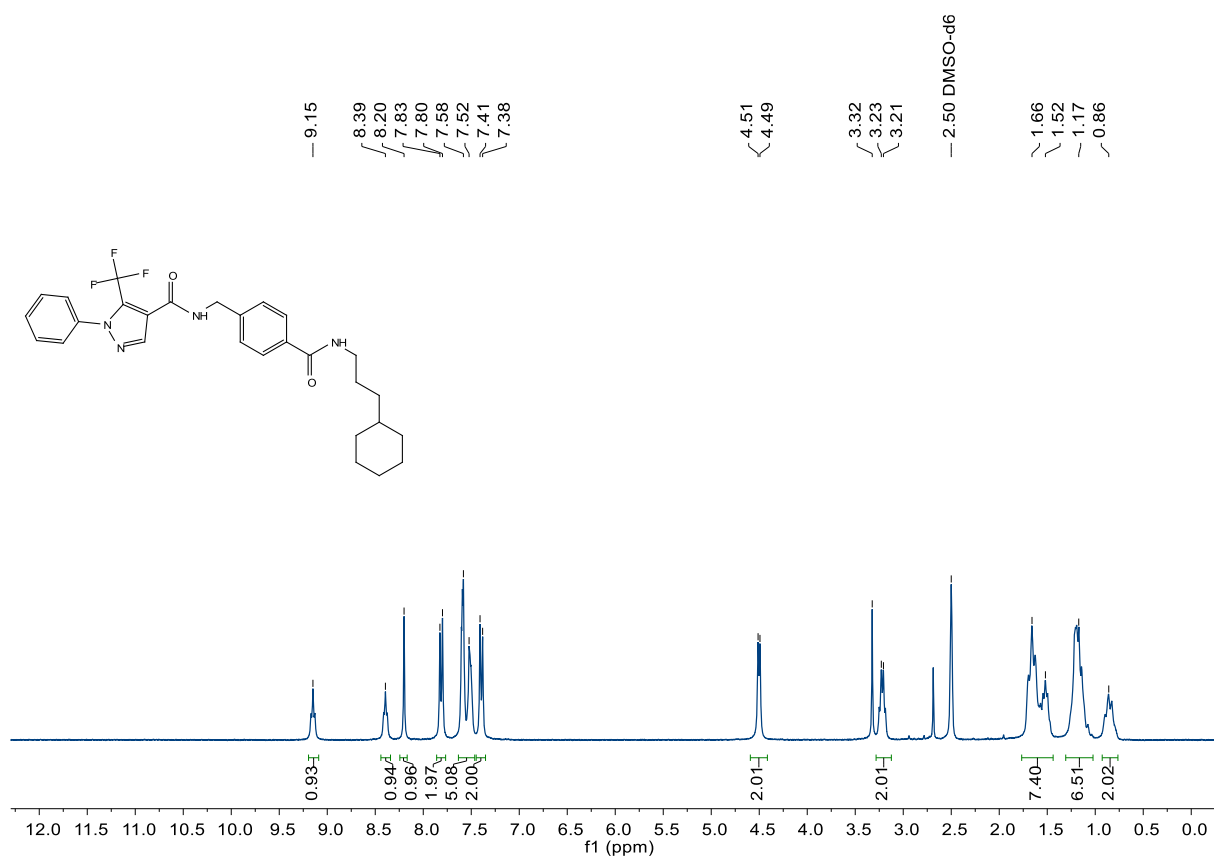


Figure 65. Compound 35 (SR321),  $^1\text{H-NMR}$ , 300 MHz,  $\text{DMSO-d}_6$

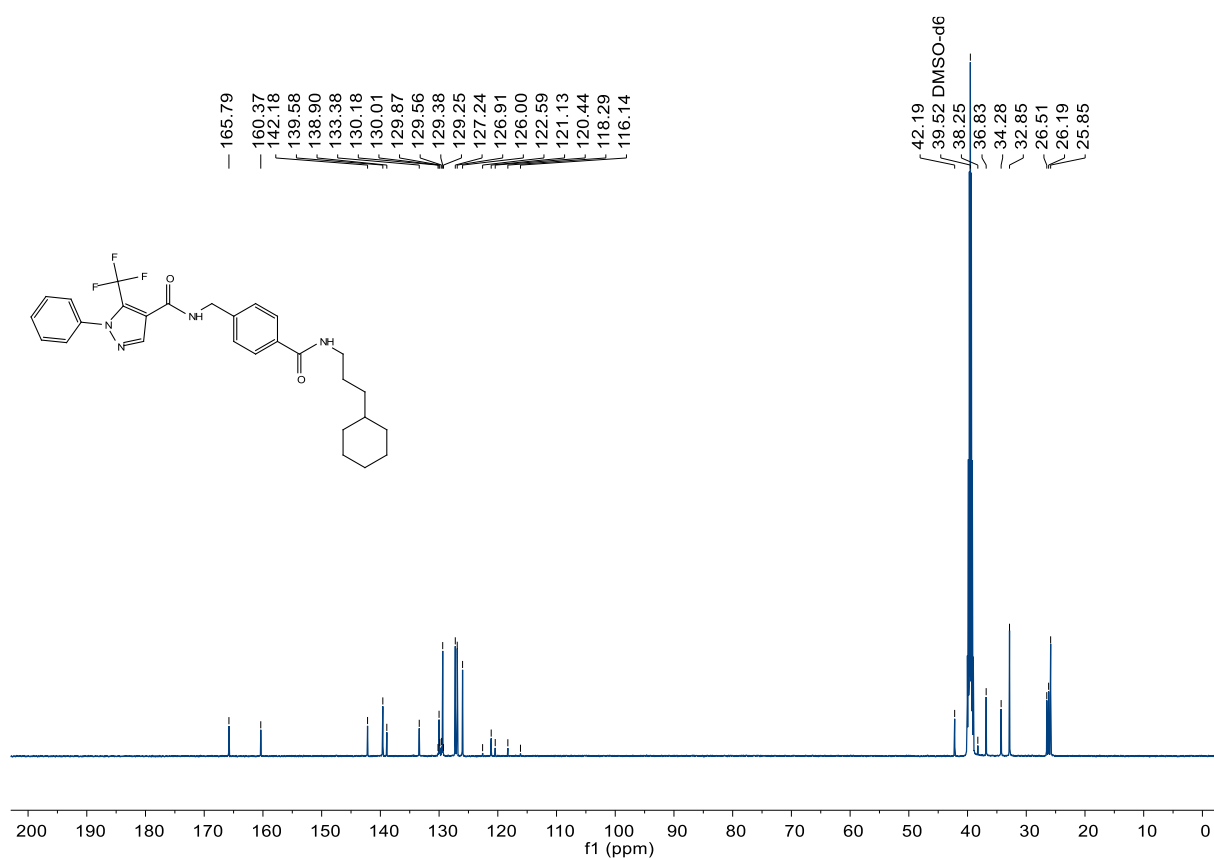


Figure 66. Compound 35 (SR321),  $^{13}\text{C-NMR}$ , 126 MHz,  $\text{DMSO-d}_6$

C:\User\...\Knapp2018\180711\SR321\_F11

7/11/2018 5:10:35 PM

SR321 mit HCCA gemessen.

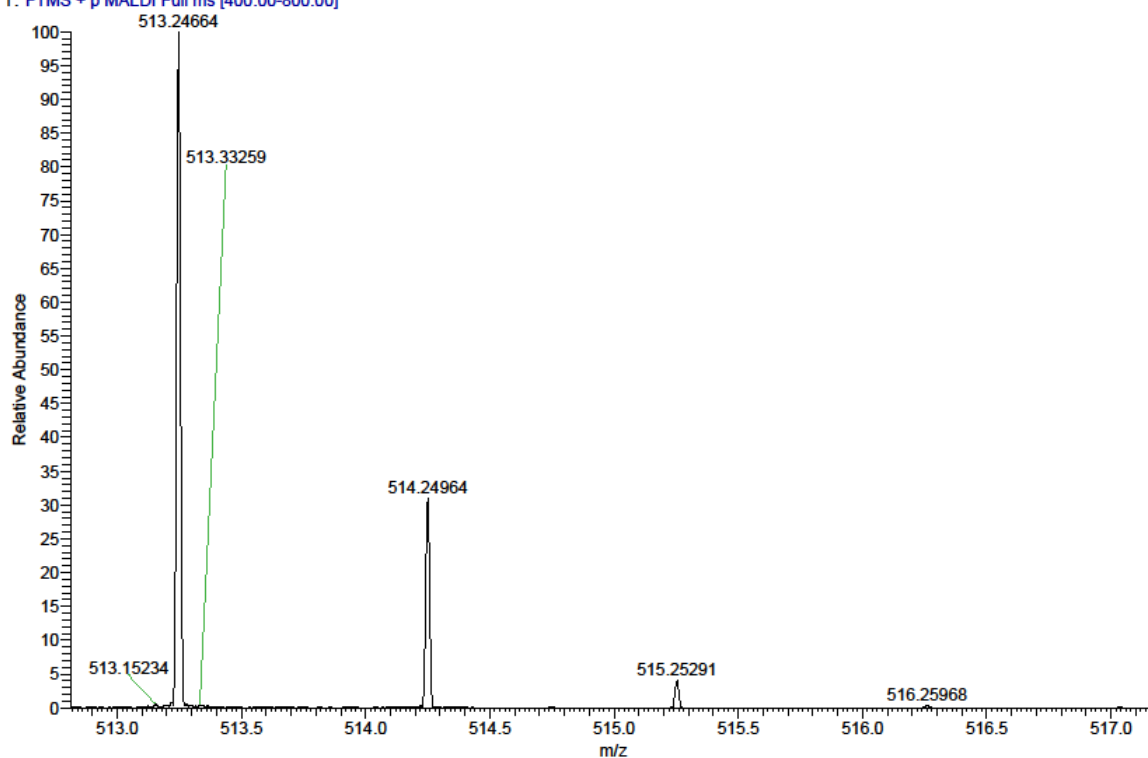
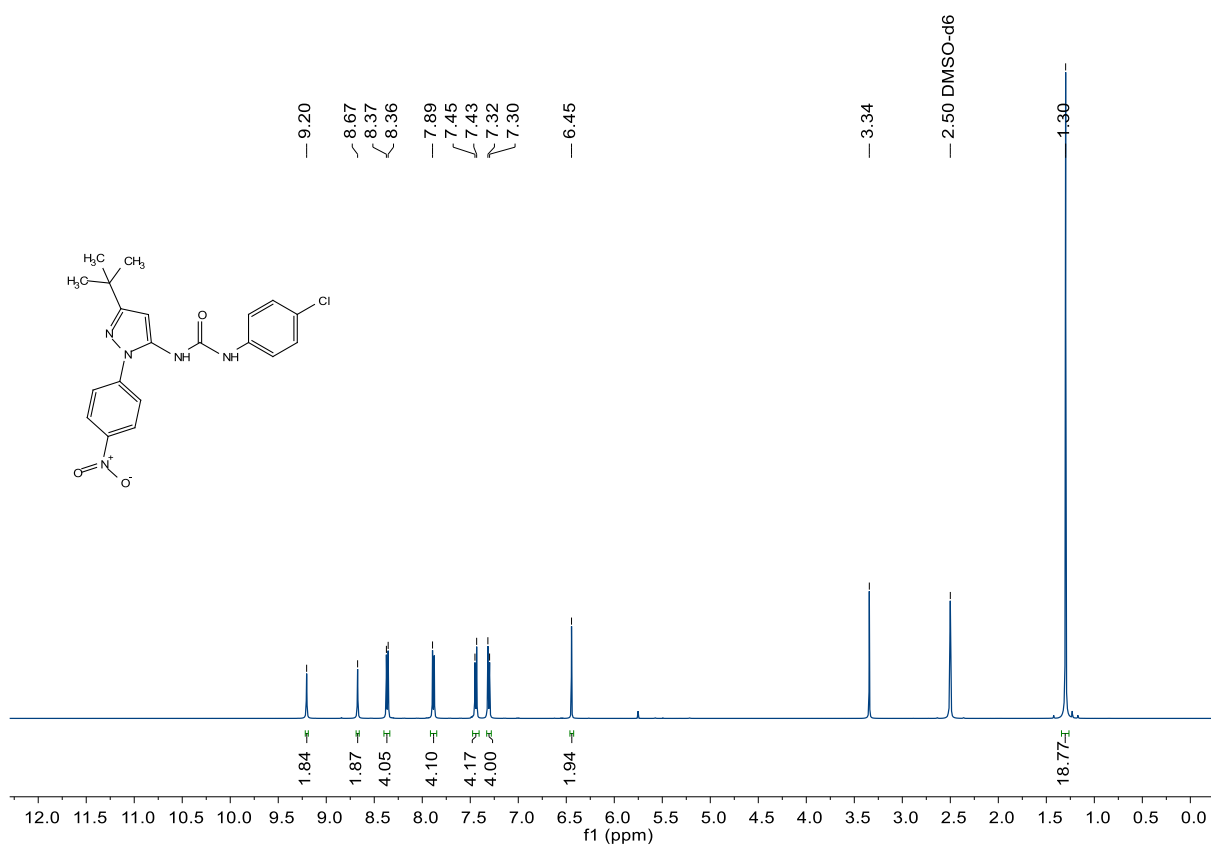
SR321\_F11 #1-5 RT: 0.00-0.29 AV: 5 NL: 7.93E6  
T: FTMS + p MALDI Full ms [400.00-800.00]

Figure 67. Compound 35 (SR321), HRMS (FTMS + p MALDI)

Figure 68. Compound 88 (SR225),  $^1\text{H-NMR}$ , 500 MHz,  $\text{DMSO-d}_6$

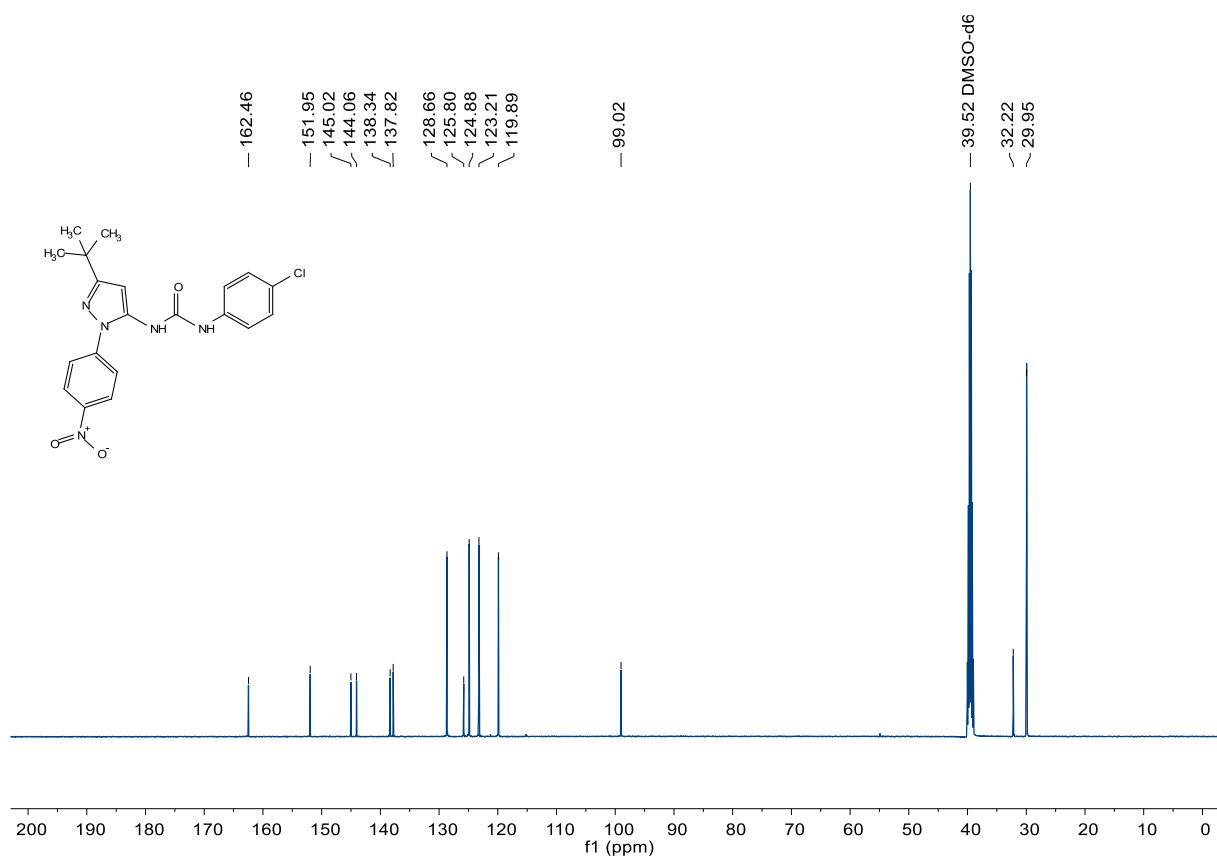


Figure 69. Compound 88 (SR225), <sup>13</sup>C-NMR, 126 MHz, DMSO-d<sub>6</sub>

C:\User\...Knapp\2019\190917\SR225\_A1

9/17/2019 10:44:04 AM

SR225 mit HCCA gemessen.

SR225\_A1 #1-9 RT: 0.01-1.06 AV: 9 NL: 1.87E5

T: FTMS + p MALDI Full ms [350.00-550.00]

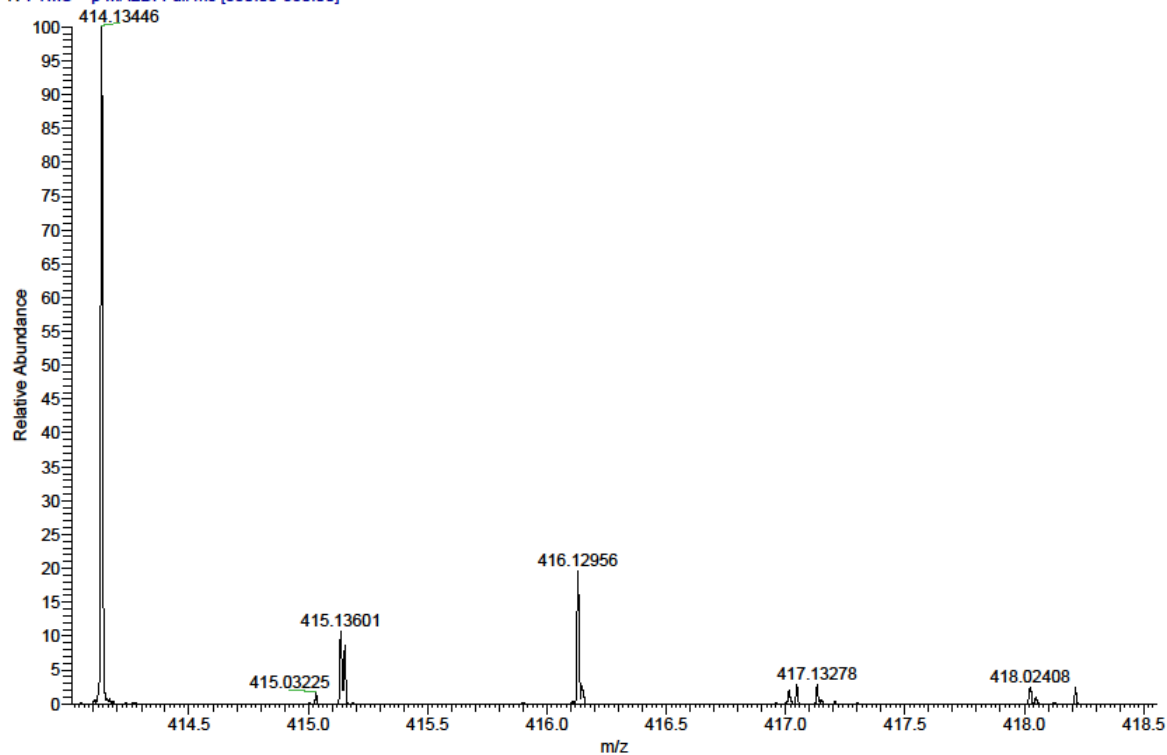


Figure 70. Compound 88 (SR225), HRMS (FTMS + p MALDI)

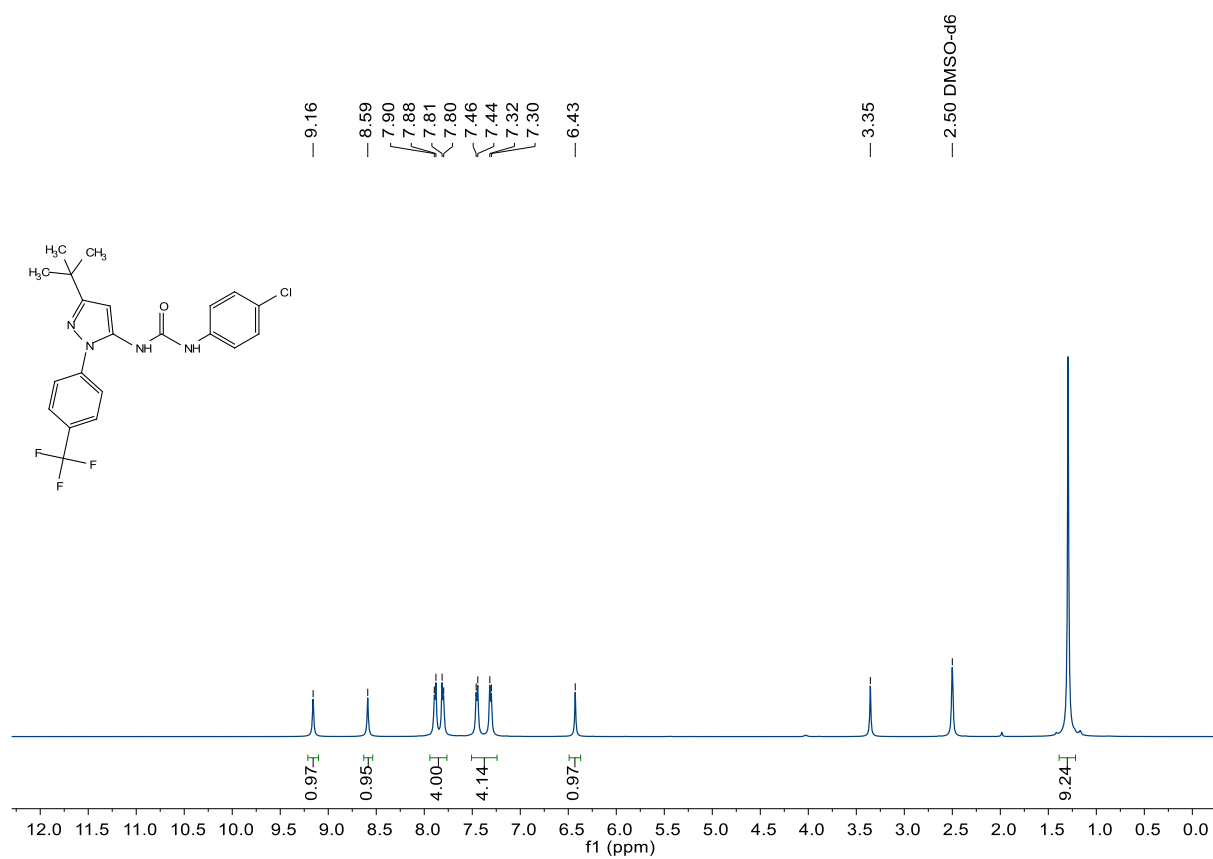


Figure 71. Compound 89 (SR238), <sup>1</sup>H-NMR, 500 MHz, DMSO-d<sub>6</sub>

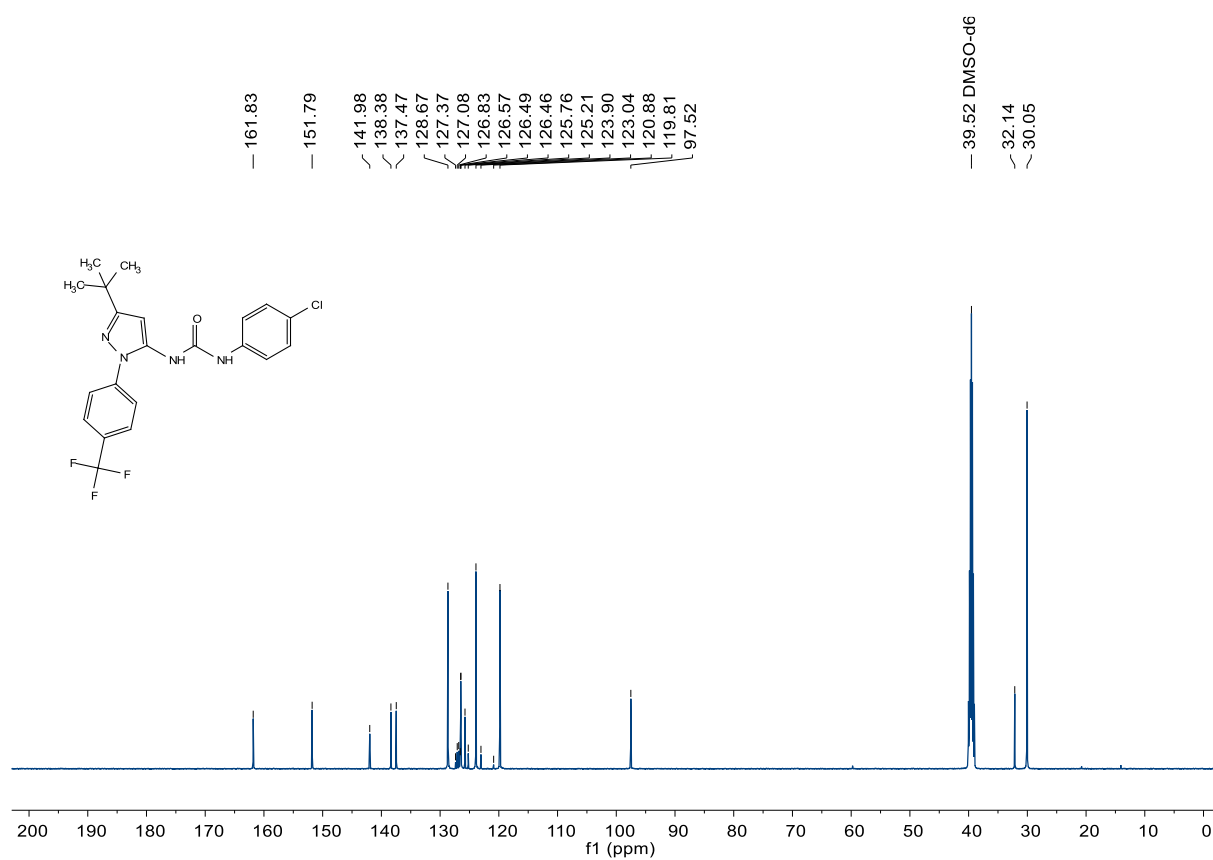


Figure 72. Compound 89 (SR238), <sup>13</sup>C-NMR, 126 MHz, DMSO-d<sub>6</sub>

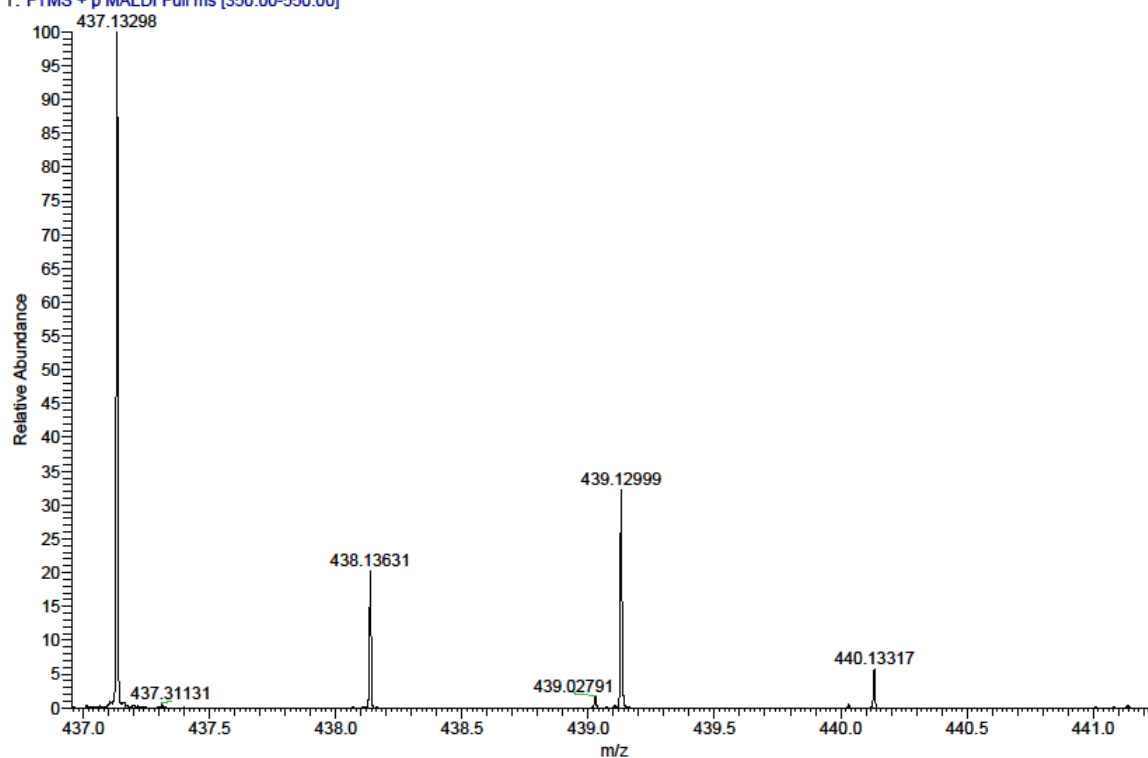
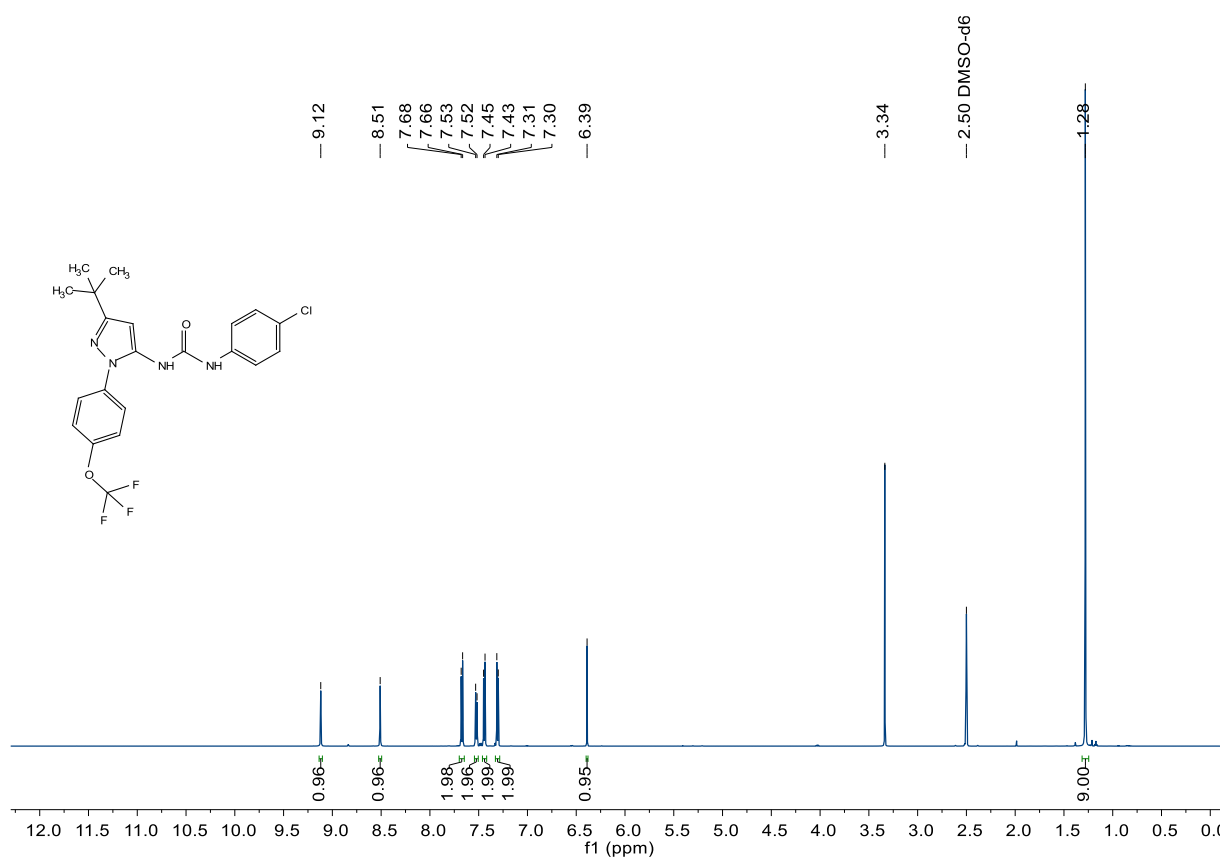
SR238\_A3 #1-10 RT: 0.00-1.19 AV: 10 NL: 4.11E5  
T: FTMS + p MALDI Full ms [350.00-550.00]

Figure 73. Compound 89 (SR238), HRMS (FTMS + p MALDI)

Figure 74. Compound 90 (SR239),  $^1\text{H-NMR}$ , 600 MHz,  $\text{DMSO-d}_6$



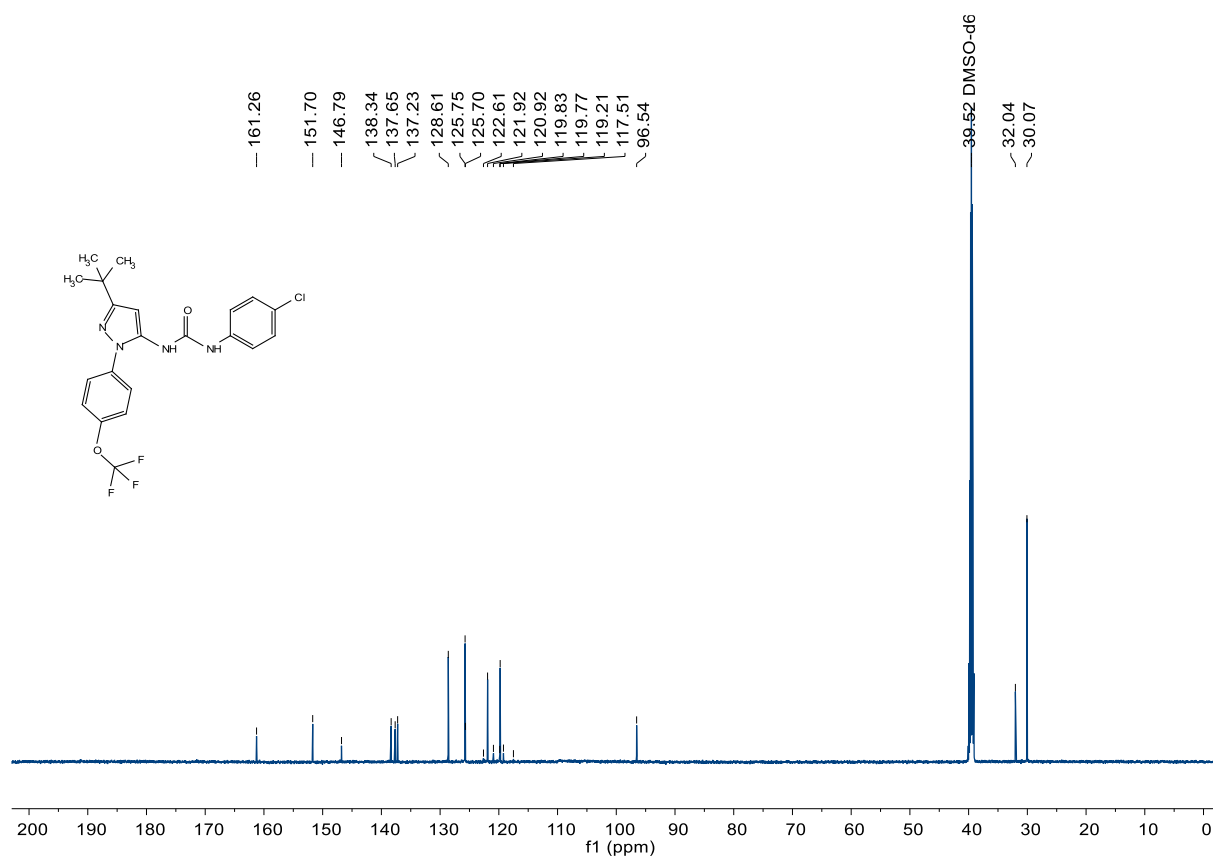


Figure 75. Compound 90 (SR239), <sup>13</sup>C-NMR, 126 MHz, DMSO-d<sub>6</sub>

C:\User\...\Knapp2019\190917\SR239\_A4

9/17/2019 10:48:51 AM

SR239 mit HCCA gemessen.

SR239\_A4 #9 RT: 1.16 AV: 1 NL: 3.37E6

T: FTMS + p MALDI Full ms [350.00-550.00]

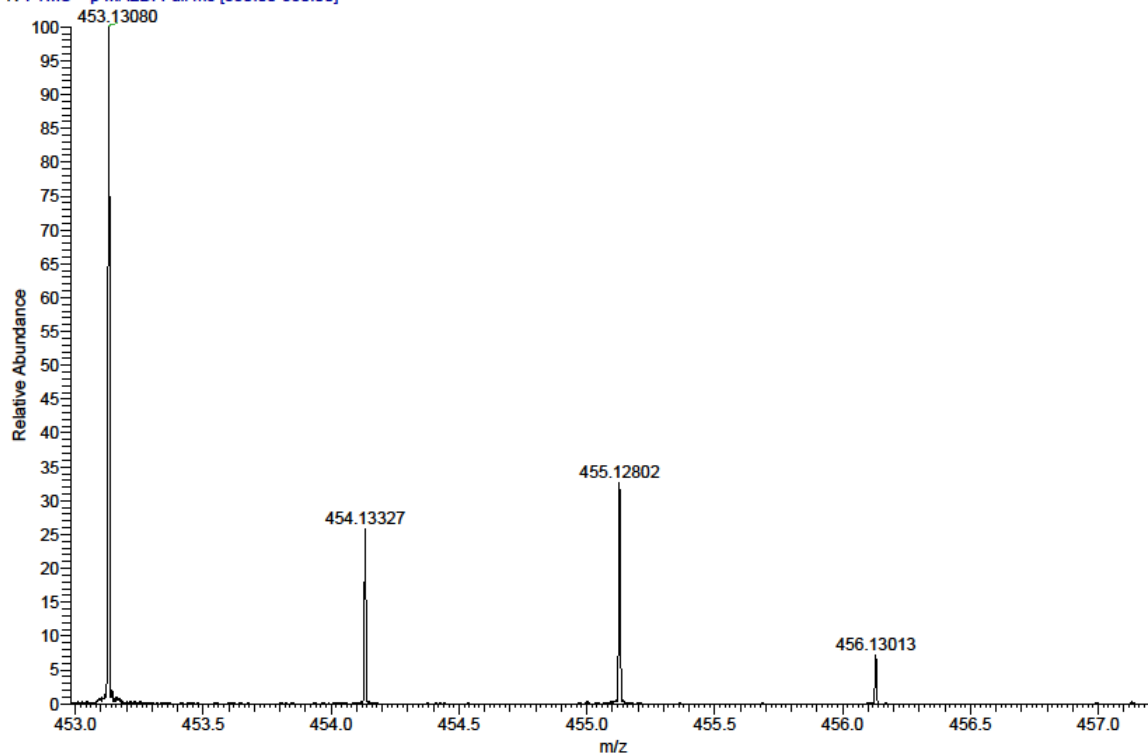
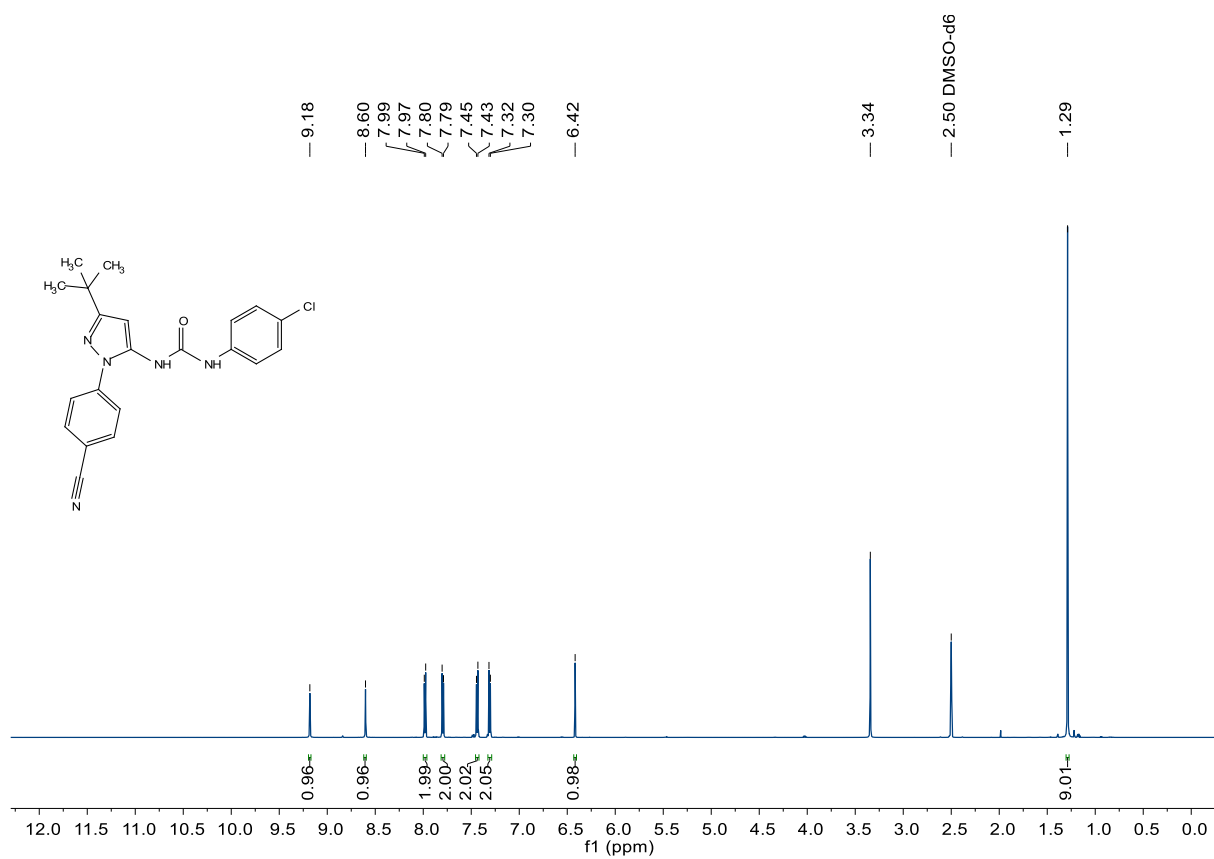
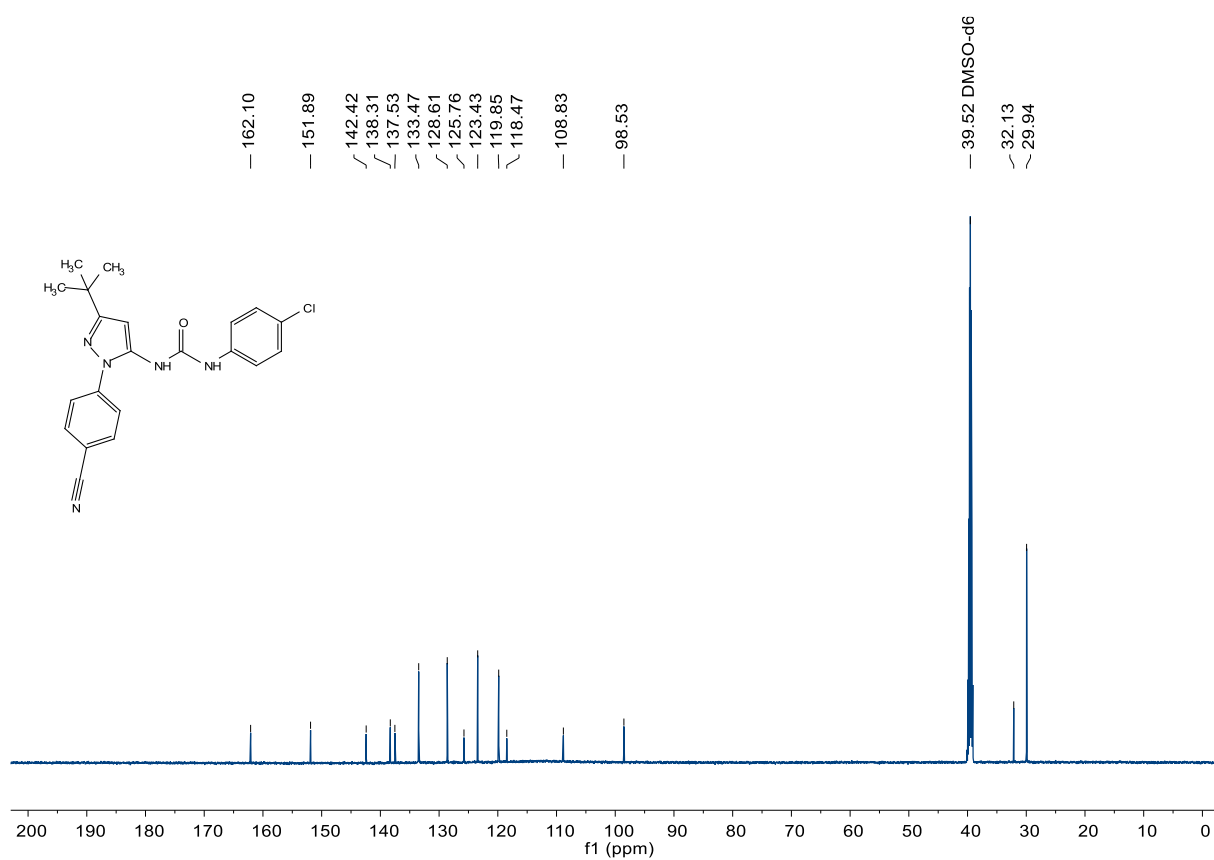


Figure 76. Compound 90 (SR239), HRMS (FTMS + p MALDI)



**Figure 77.** Compound 91 (SR240),  $^1\text{H-NMR}$ , 600 MHz,  $\text{DMSO-d}_6$



**Figure 78.** Compound 91 (SR240),  $^{13}\text{C-NMR}$ , 126 MHz,  $\text{DMSO-d}_6$

C:\User\...\Knapp2019\190917\SR240\_A5

9/17/2019 10:50:34 AM

SR240 mit HCCA gemessen.

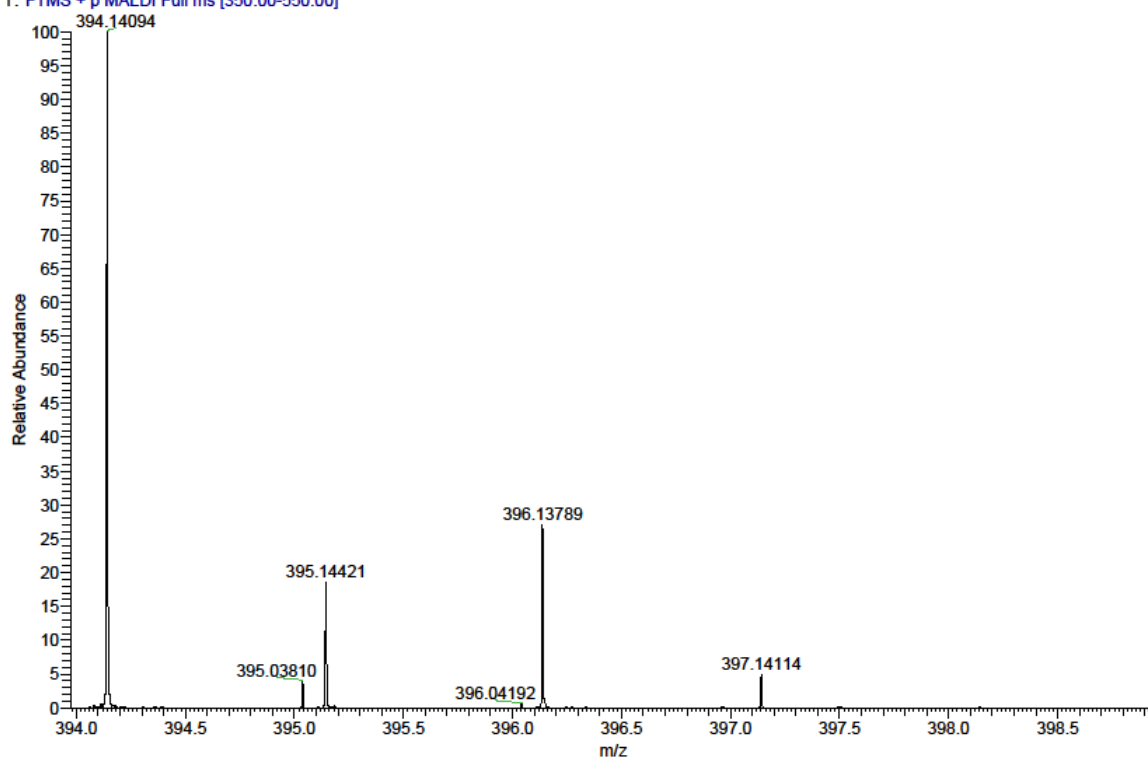
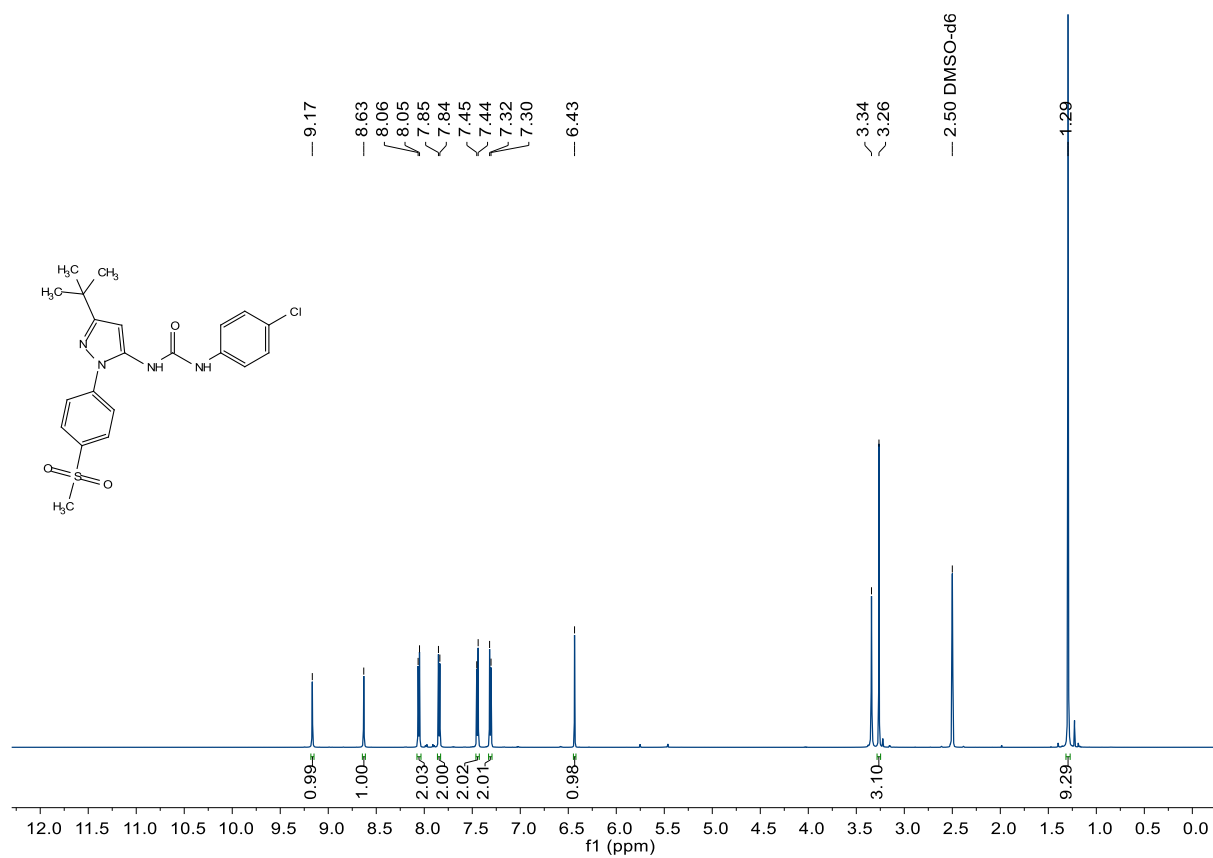
SR240\_A5 #1-9 RT: 0.00-1.18 AV: 9 NL: 1.66E5  
T: FTMS + p MALDI Full ms [350.00-550.00]

Figure 79. Compound 91 (SR240), HRMS (FTMS + p MALDI)

Figure 80. Compound 92 (SR245),  $^1\text{H-NMR}$ , 600 MHz,  $\text{DMSO-d}_6$

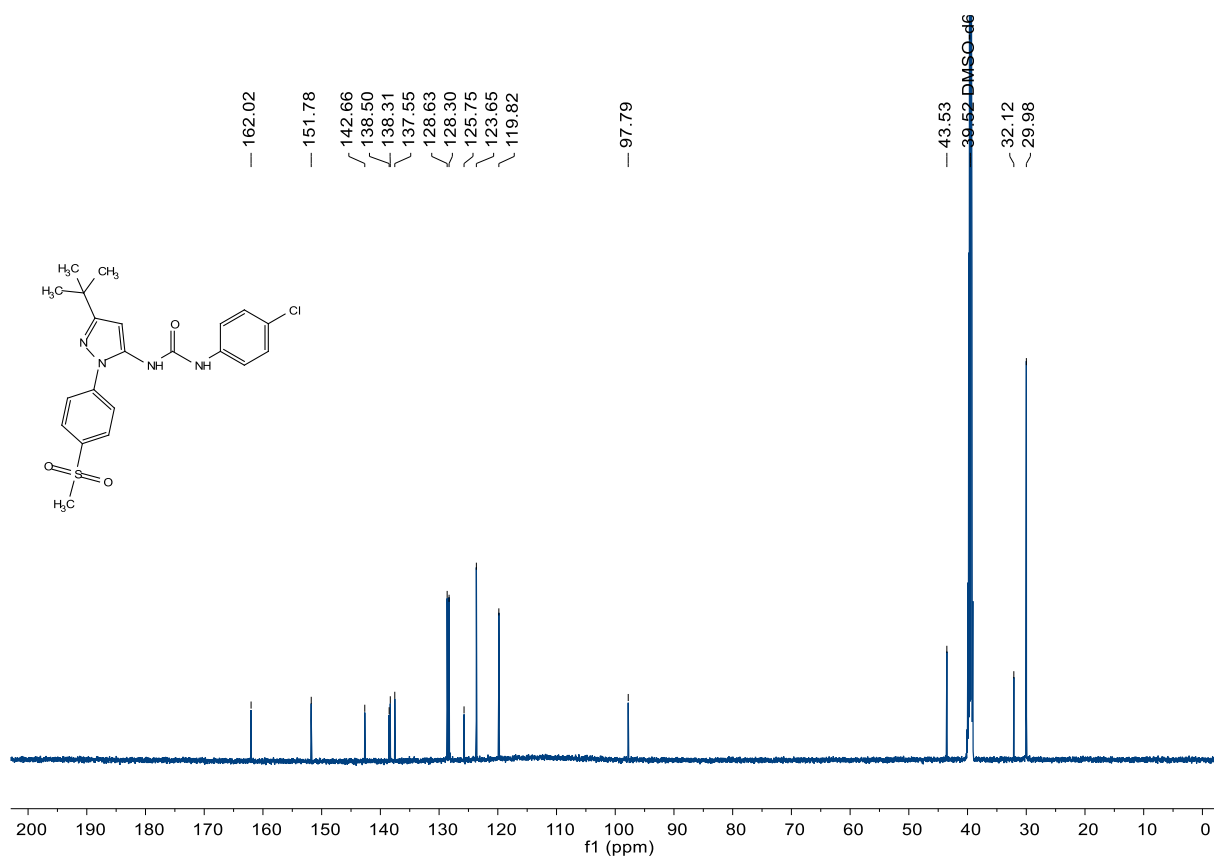


Figure 81. Compound 92 (SR245),  $^{13}\text{C}$ -NMR, 150 MHz,  $\text{DMSO-d}_6$

C:\User\...Knapp\2019\190917\SR245\_A6

9/17/2019 10:52:30 AM

SR245 mit HCCA gemessen.

SR245\_A6 #1-7 RT: 0.00-0.67 AV: 7 NL: 3.69E5

T: FTMS + p MALDI Full ms [350.00-550.00]

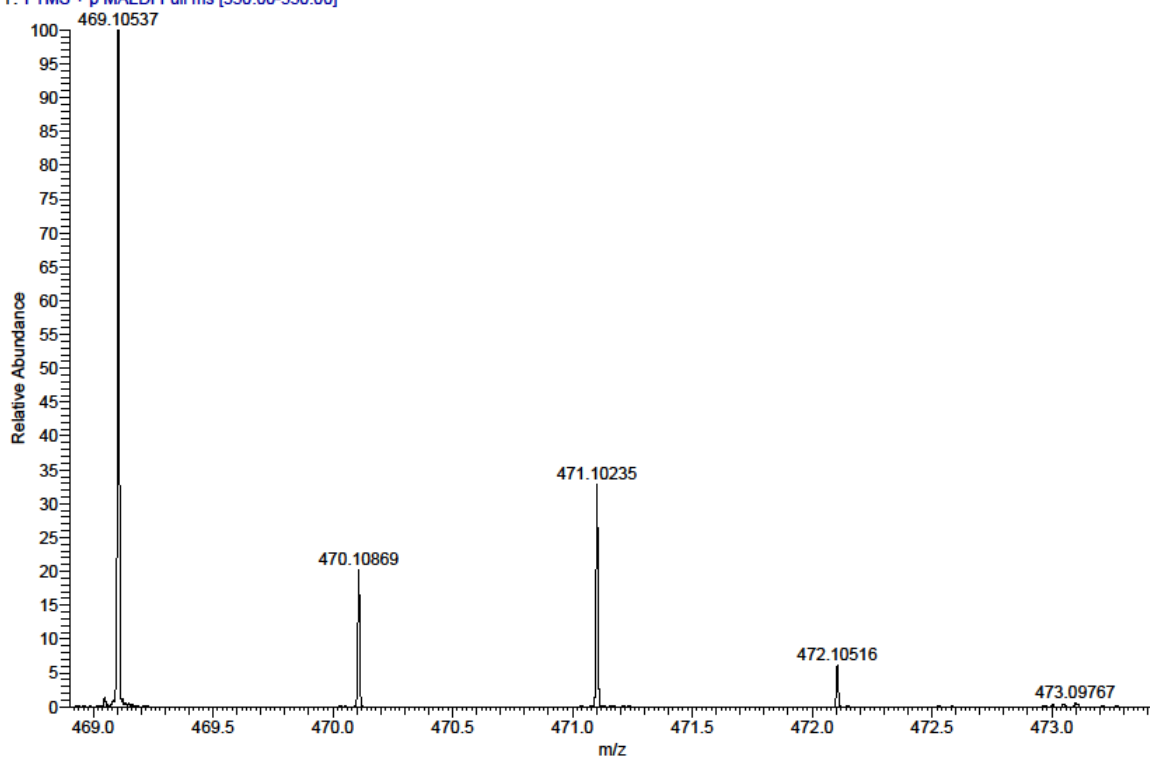


Figure 82. Compound 92 (SR245), HRMS (FTMS + p MALDI)

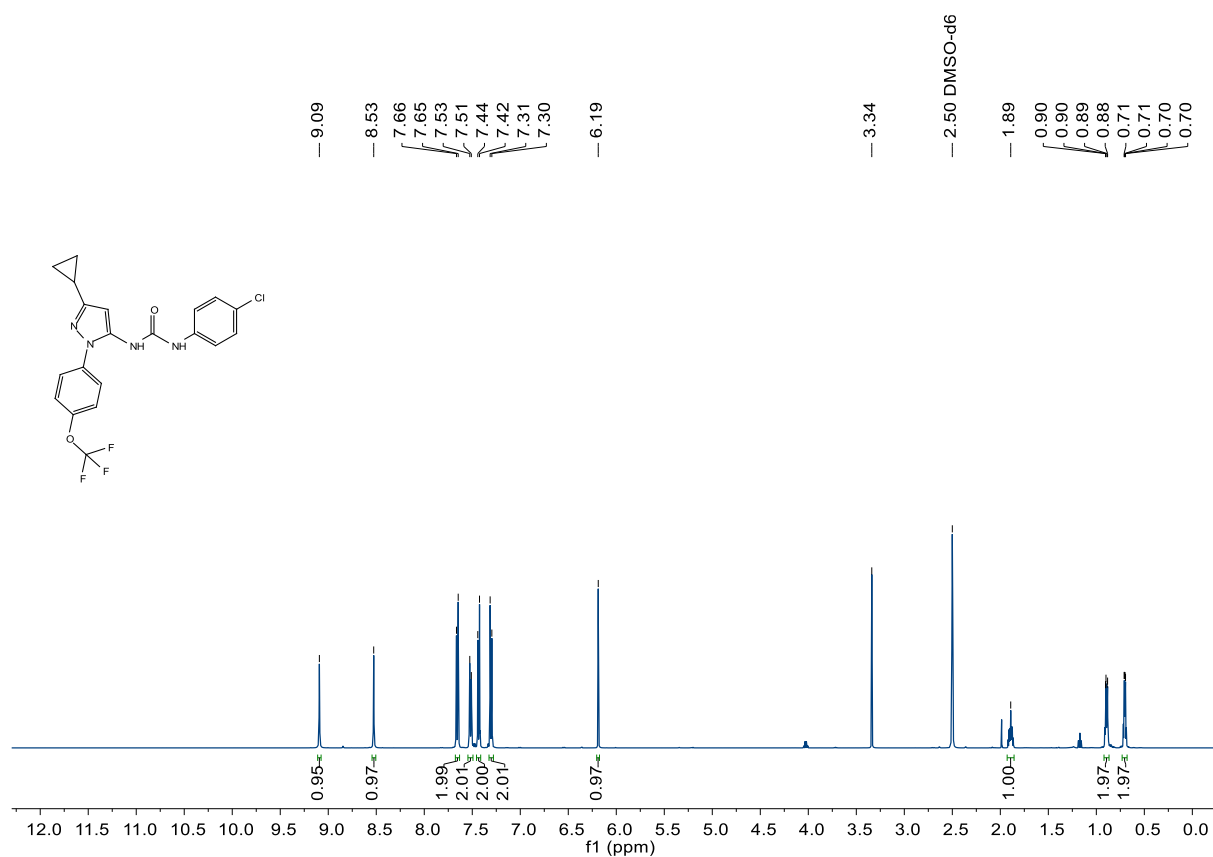


Figure 83. Compound 93 (SR258), <sup>1</sup>H-NMR, 500MHz, DMSO-d<sub>6</sub>

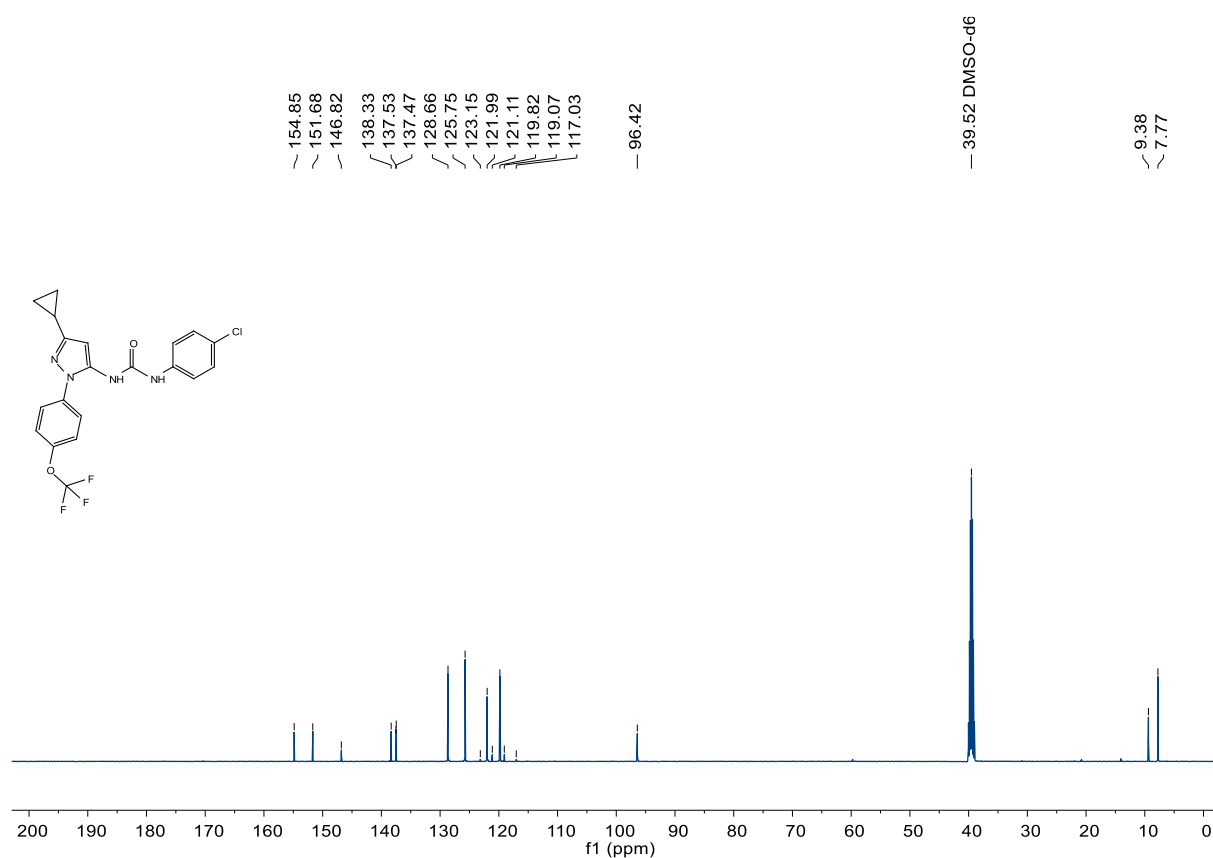


Figure 84. Compound 93 (SR258), <sup>13</sup>C-NMR, 126 MHz, DMSO-d<sub>6</sub>

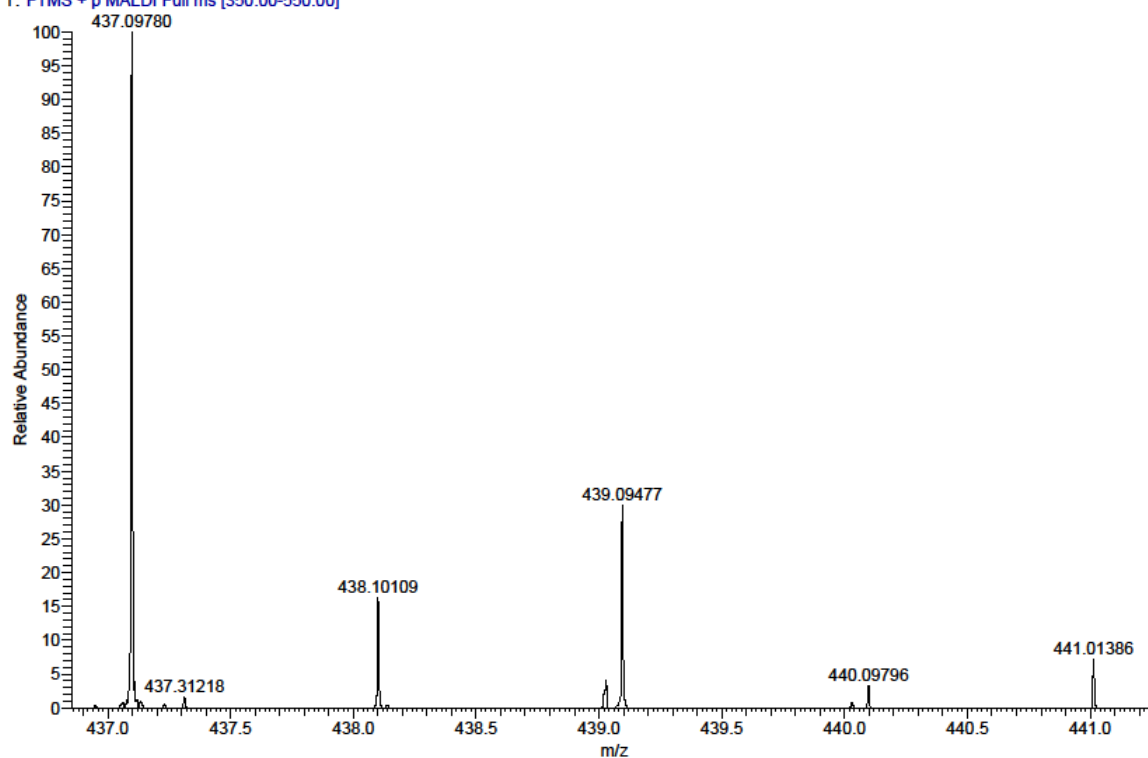
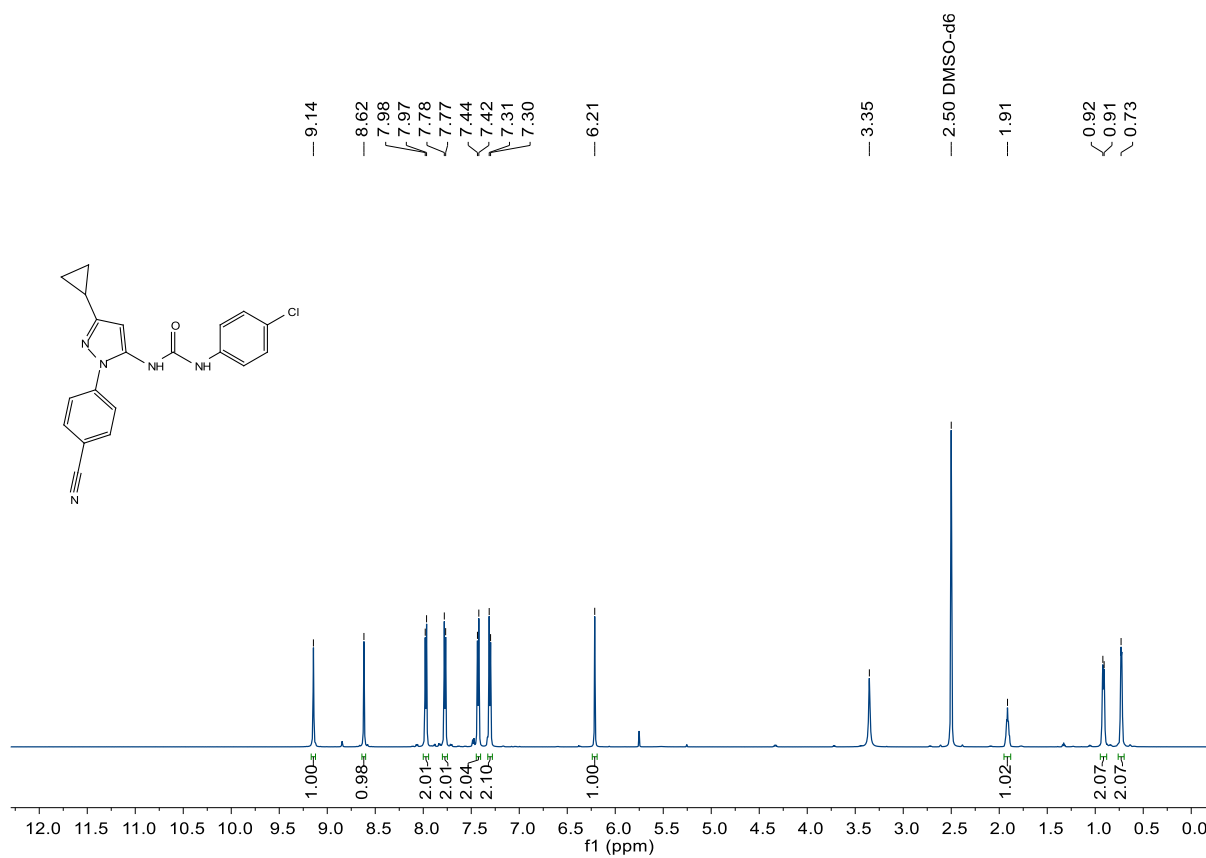
SR258\_A10 #1-4 RT: 0.00-0.34 AV: 4 NL: 1.60E5  
T: FTMS + p MALDI Full ms [350.00-550.00]

Figure 85. Compound 93 (SR258), HRMS (FTMS + p MALDI)

Figure 86. Compound 94 (SR261),  $^1\text{H-NMR}$ , 600 MHz,  $\text{DMSO-d}_6$

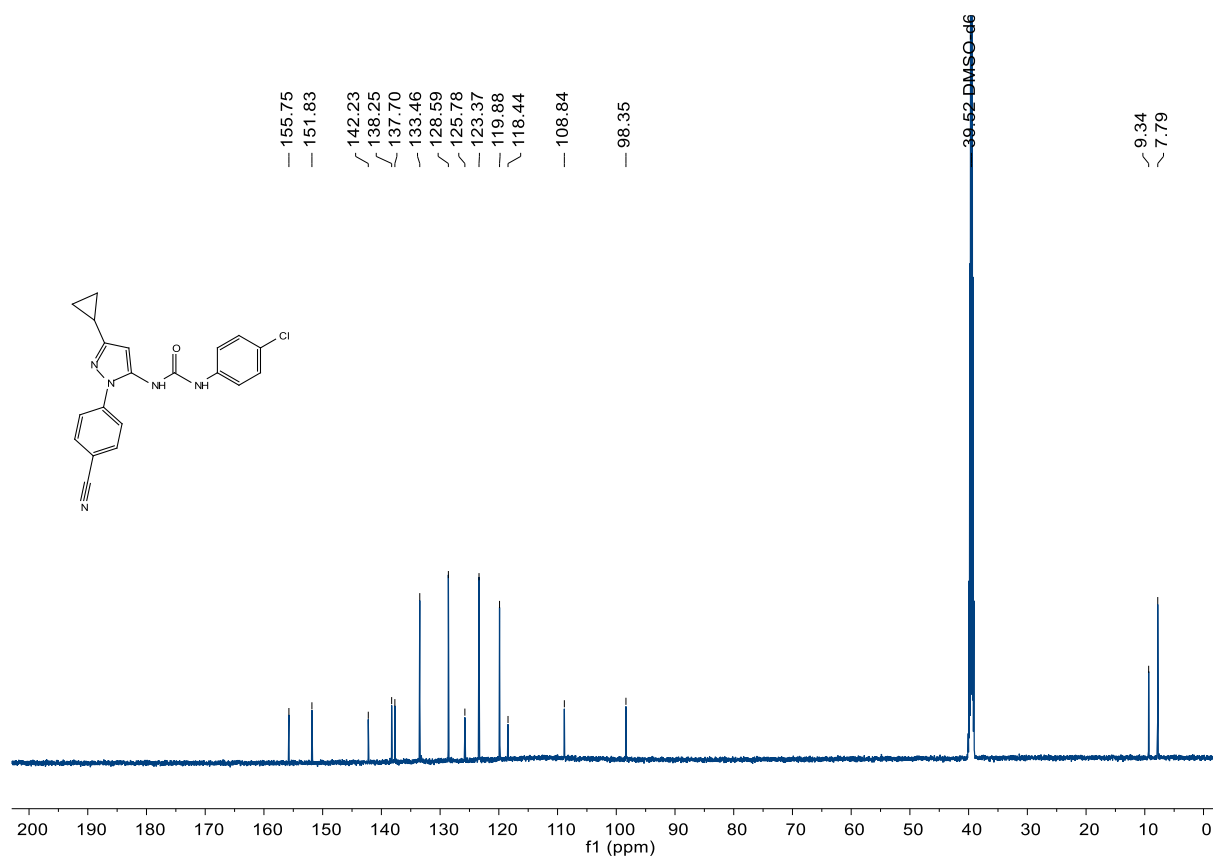


Figure 87. Compound 94 (SR261),  $^{13}\text{C-NMR}$ , 150 MHz,  $\text{DMSO-}d_6$

C:\User\...\Knapp2019\190917\SR261\_A11

9/17/2019 11:01:37 AM

SR261 mit HCCA gemessen.

SR261\_A11 #1-8 RT: 0.00-1.03 AV: 8 NL: 1.10E5  
T: FTMS + p MALDI Full ms [350.00-550.00]

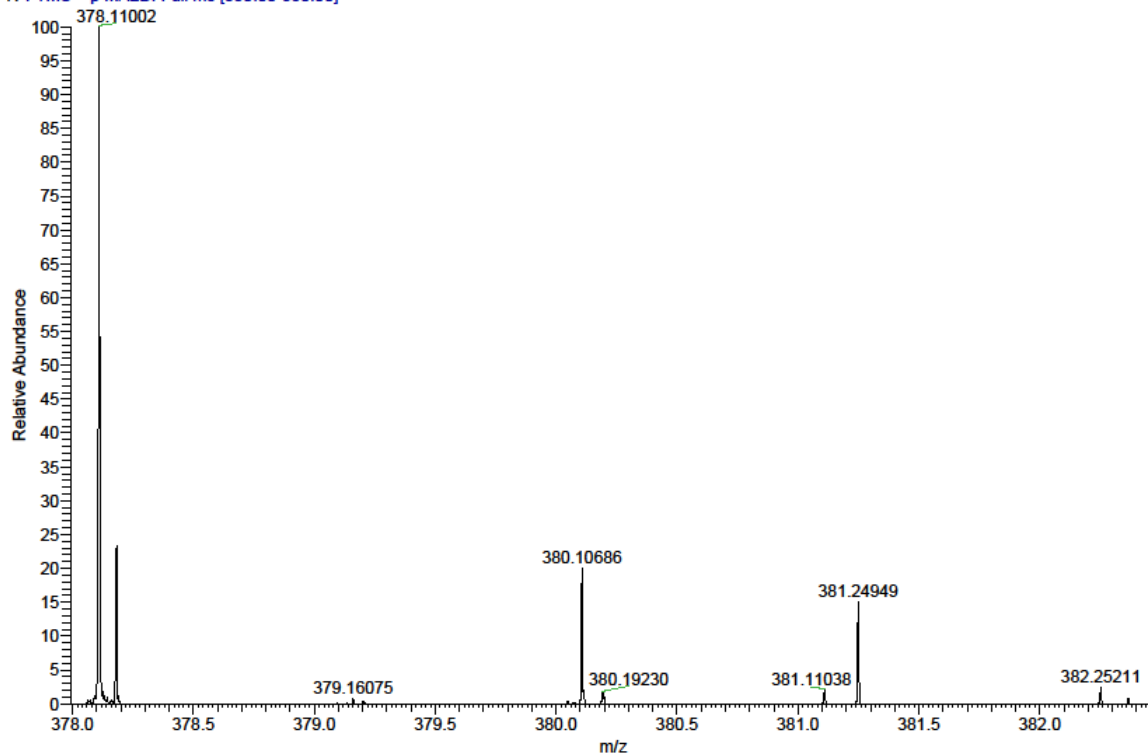


Figure 88. Compound 94 (SR261), HRMS (FTMS + p MALDI)

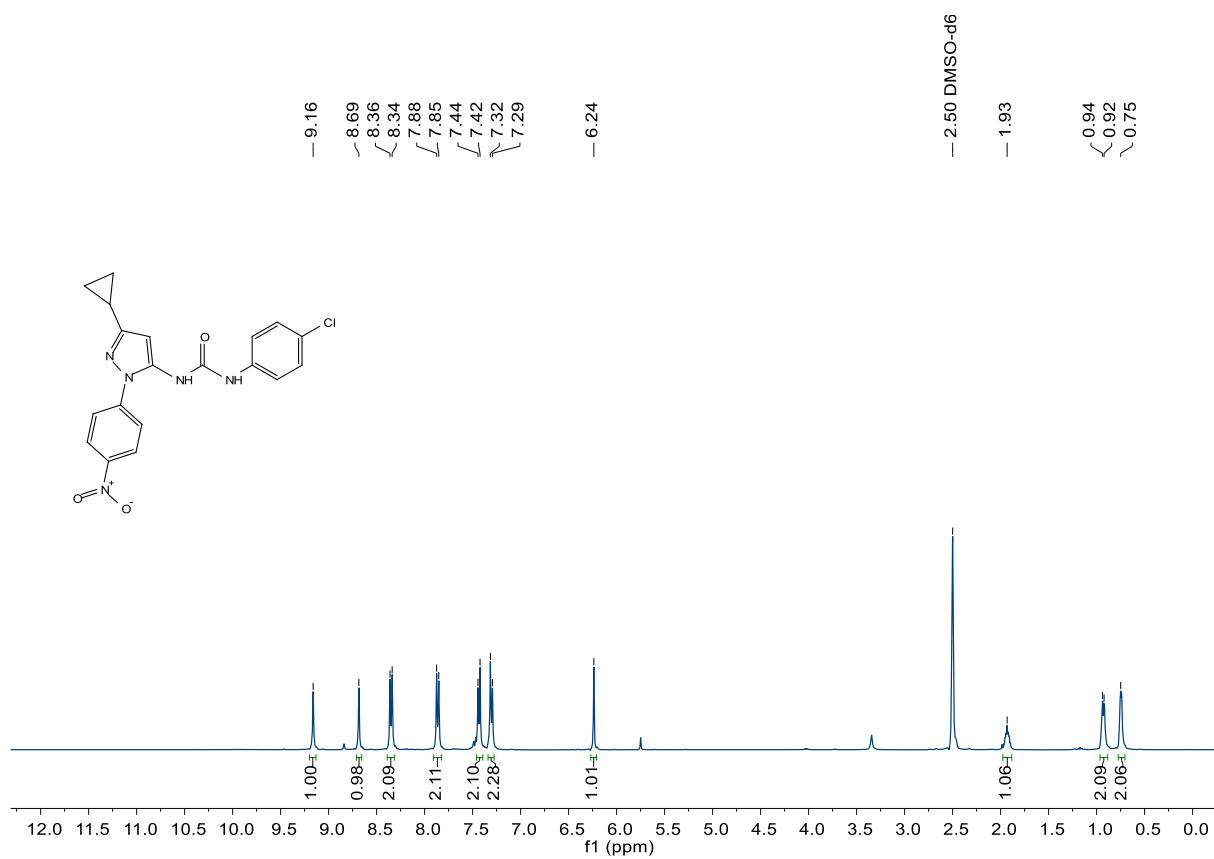


Figure 89. Compound 95 (SR263),  $^1\text{H-NMR}$ , 400 MHz,  $\text{DMSO-d}_6$

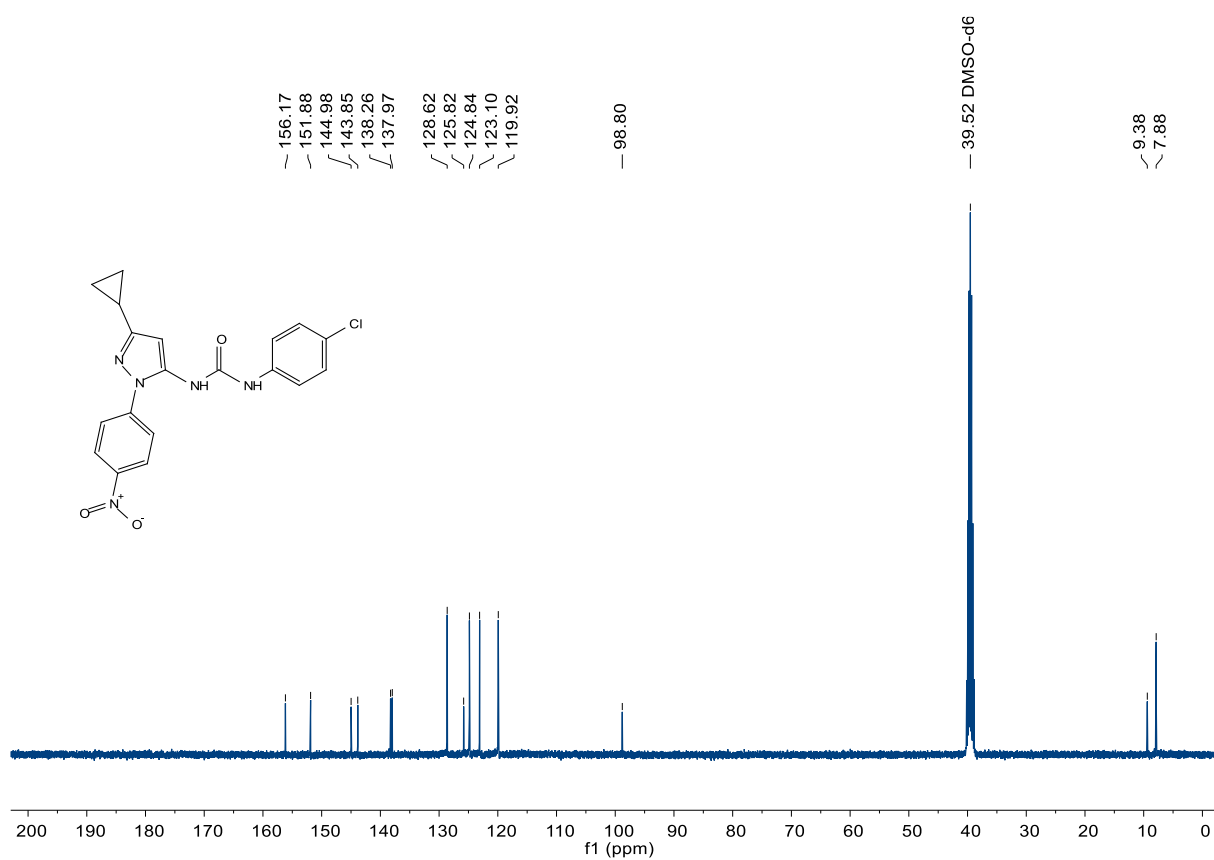


Figure 90. Compound 95 (SR263),  $^{13}\text{C-NMR}$ , 101 MHz,  $\text{DMSO-d}_6$



C:\User\...\Knapp\2019\190917\SR263\_A12

9/17/2019 11:04:51 AM

SR263 mit HCCA gemessen

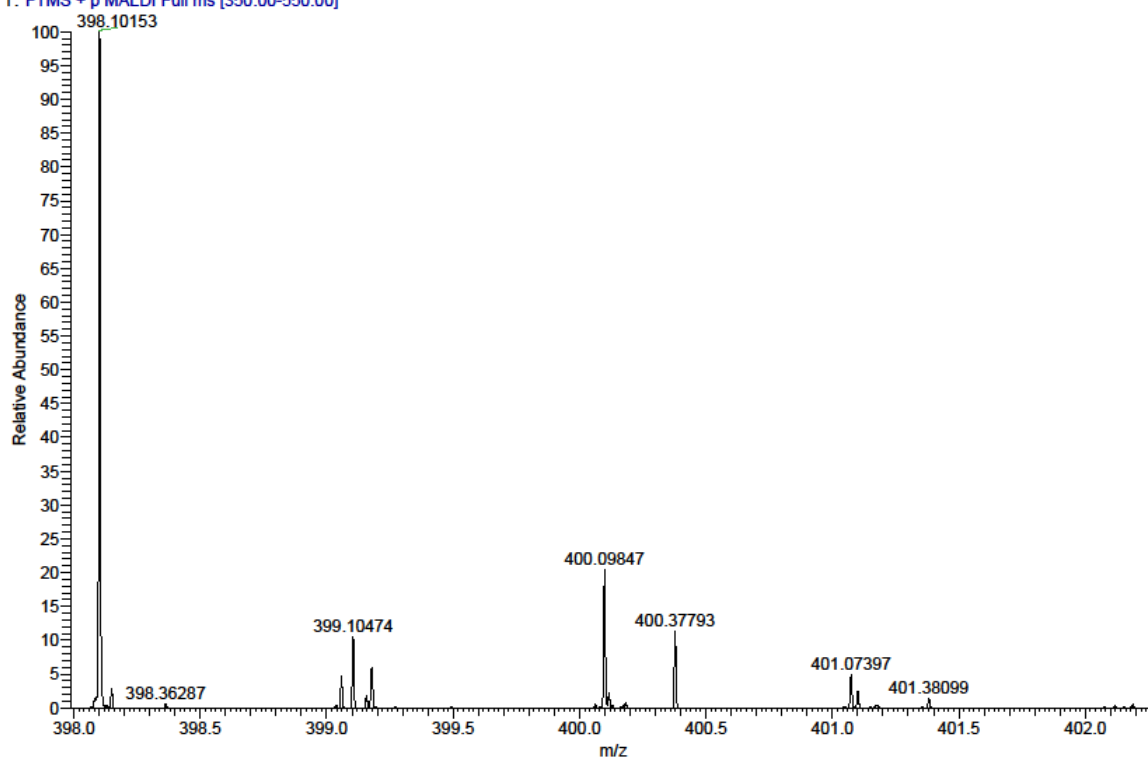
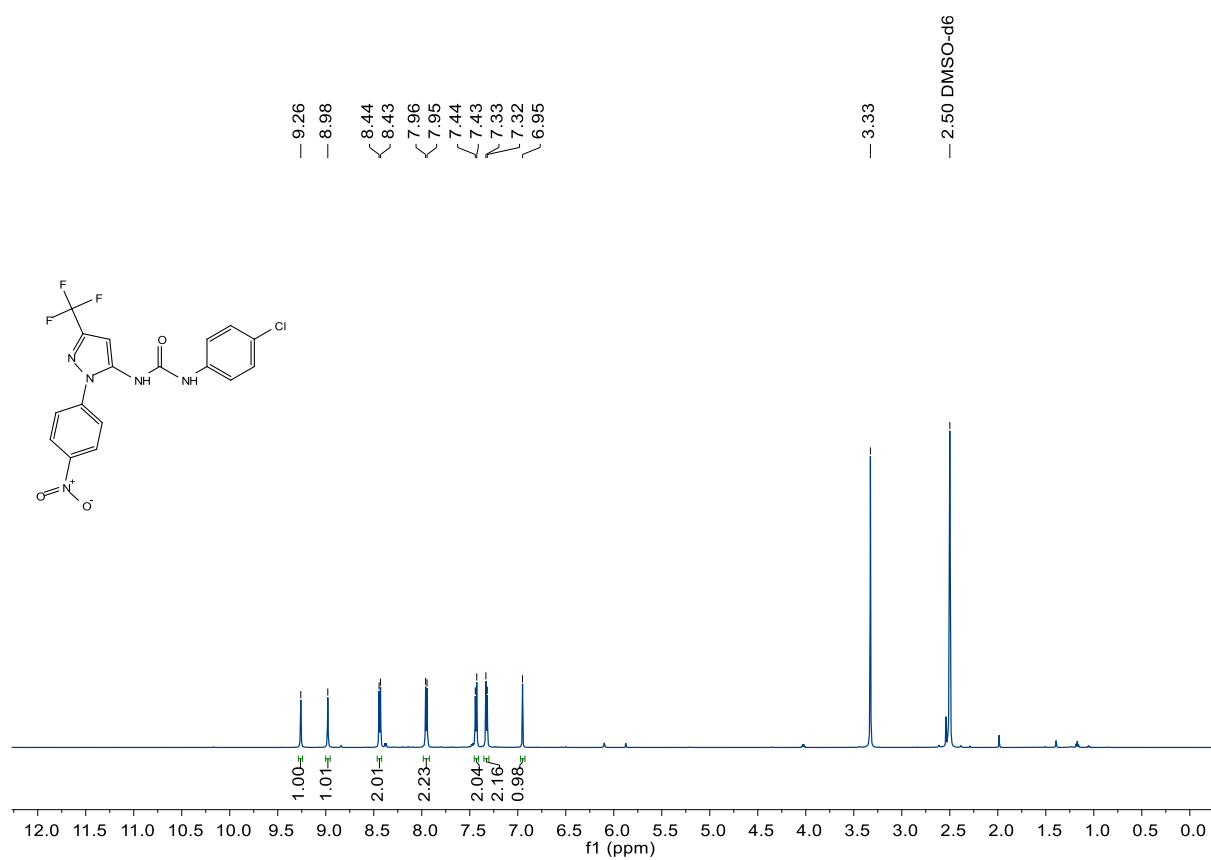
SR263\_A12 #1-20 RT: 0.00-2.82 AV: 20 NL: 9.68E4  
T: FTMS + p MALDI Full ms [350.00-550.00]

Figure 91. Compound 95 (SR263), HRMS (FTMS + p MALDI)

Figure 92. Compound 96 (SR266),  $^1\text{H-NMR}$ , 600 MHz,  $\text{DMSO-d}_6$

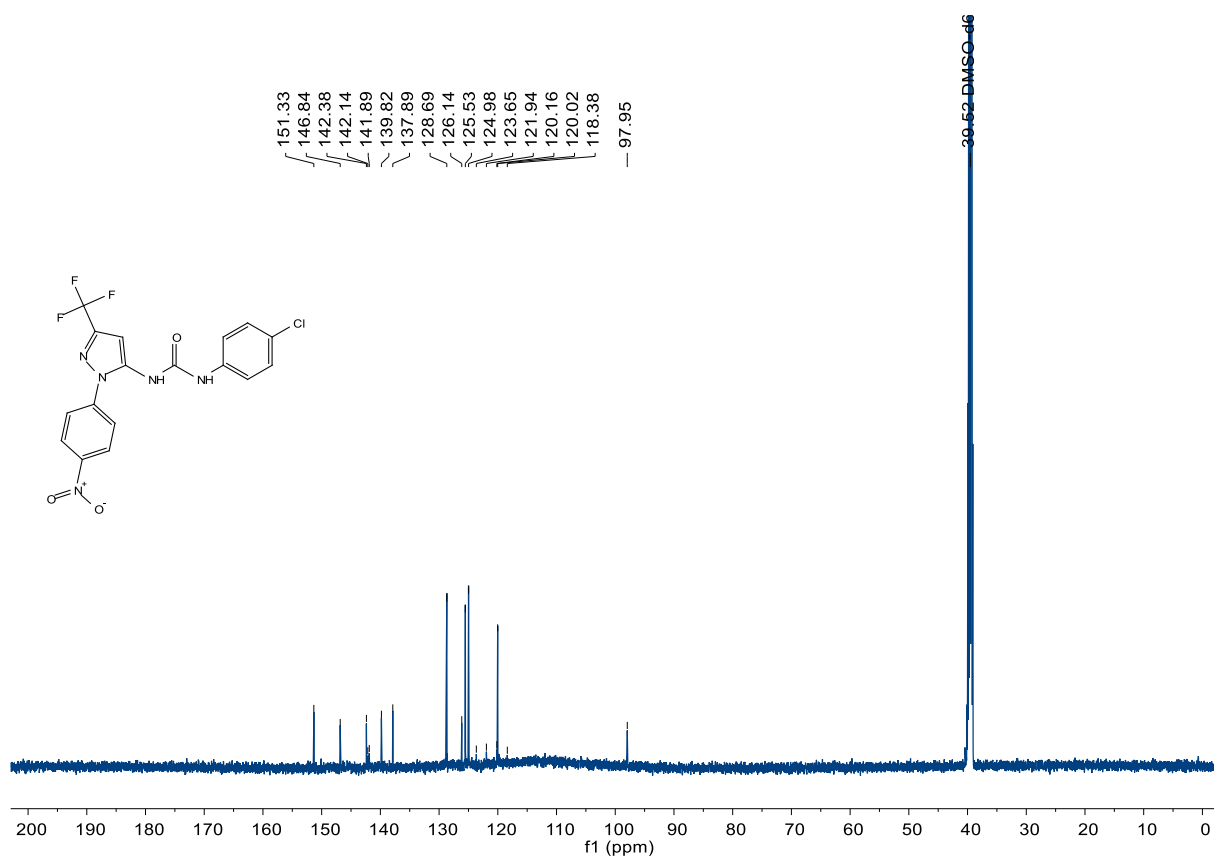


Figure 93. Compound 96 (SR266), <sup>13</sup>C-NMR, 150 MHz, DMSO-d<sub>6</sub>

C:\User\...Knapp\2019\190917\SR266\_B1

9/17/2019 11:59:21 AM

SR266 mit HCCA gemessen.

SR266\_B1 #1-20 RT: 0.00-2.81 AV: 20 NL: 9.97E4  
T: FTMS + p MALDI Full ms [350.00-550.00]

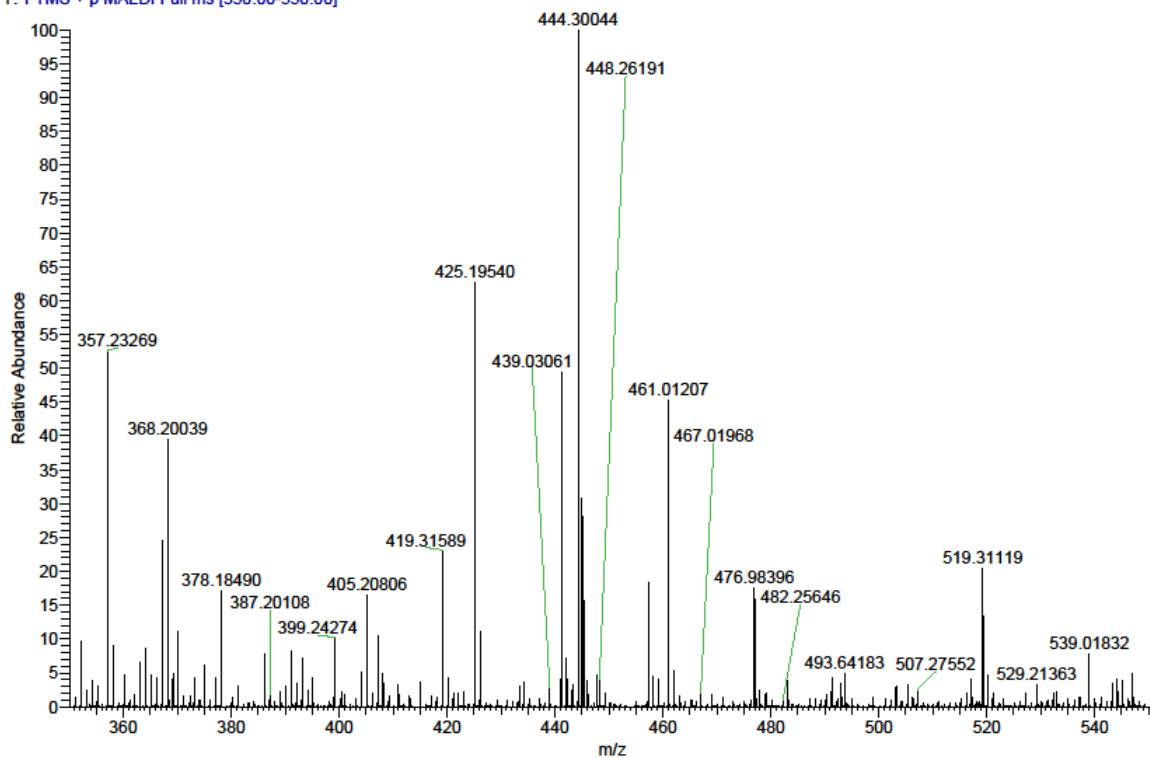


Figure 94. Compound 96 (SR266), HRMS (FTMS + p MALDI)

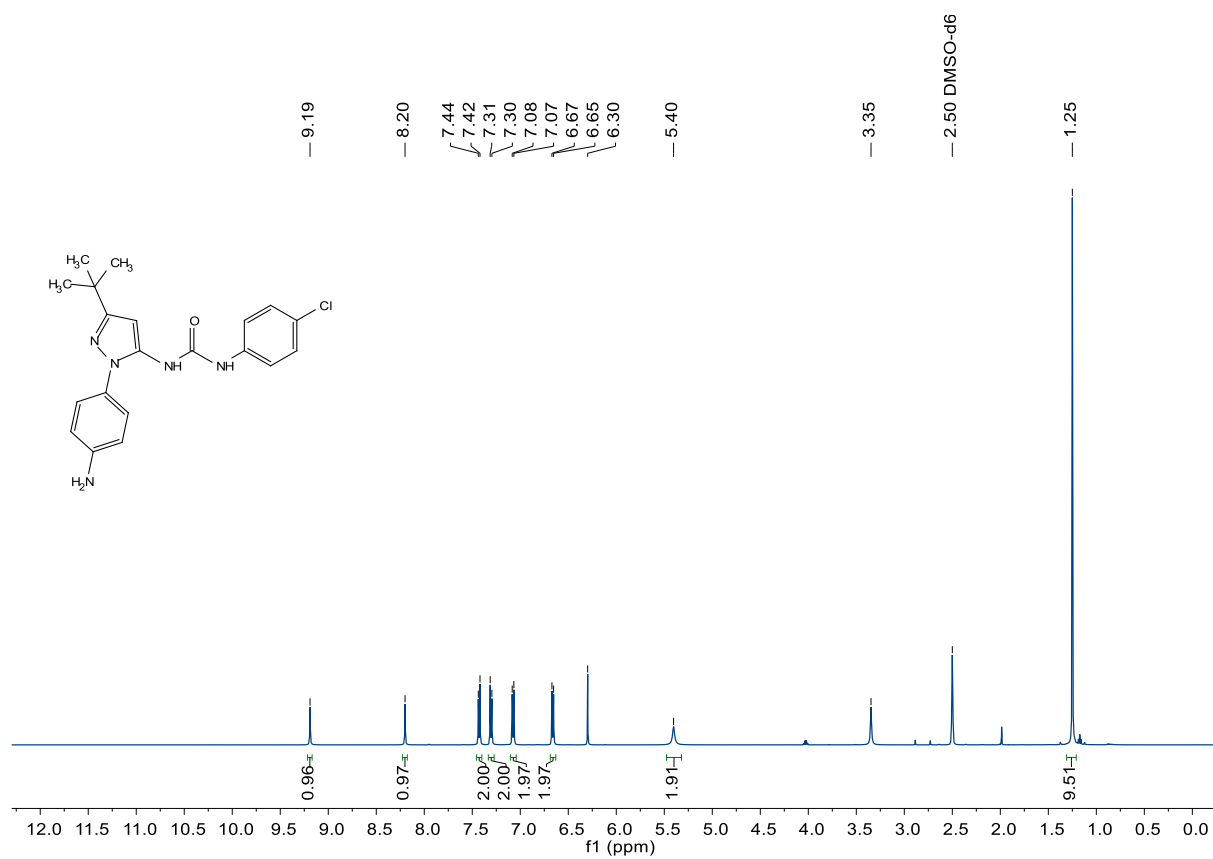


Figure 95. Compound 97 (SR226), <sup>1</sup>H-NMR, 1H, 500MHz, DMSO-d<sub>6</sub>

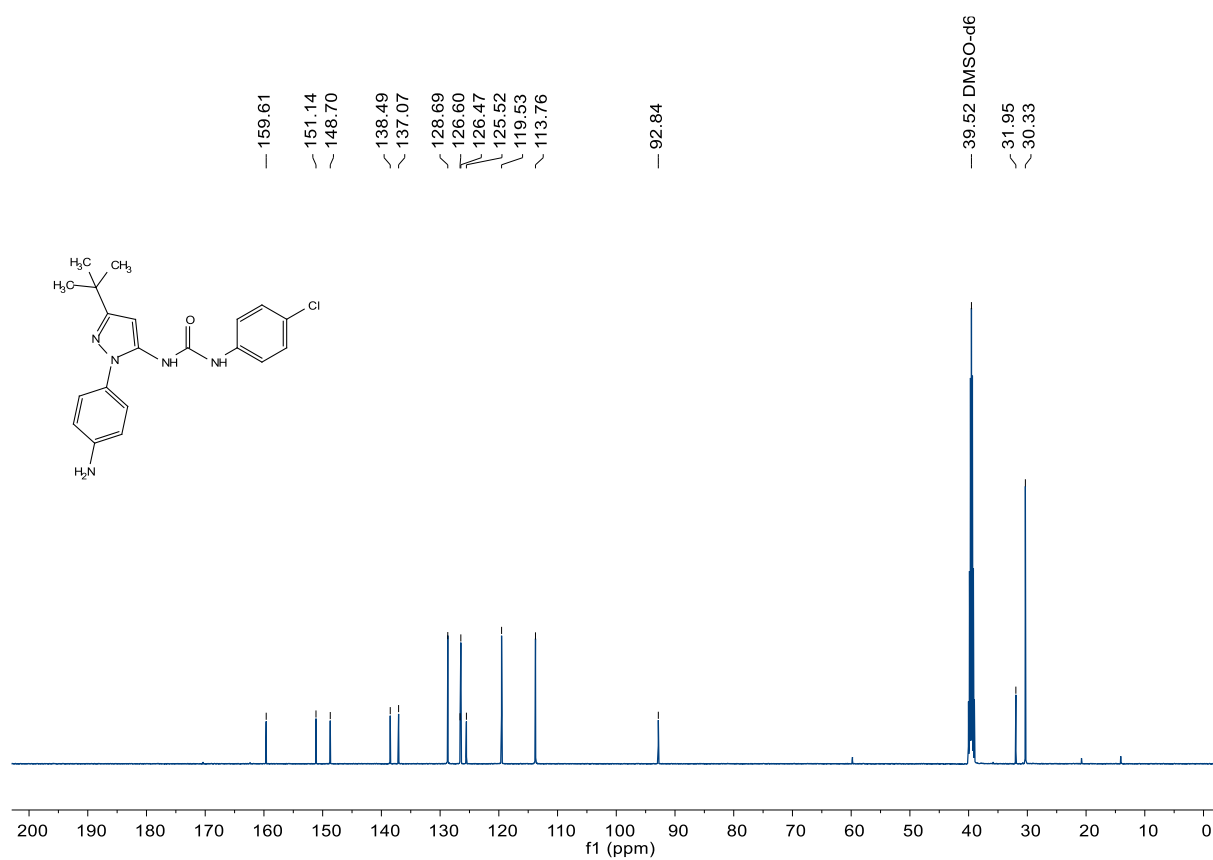


Figure 96. Compound 97 (SR226), <sup>13</sup>C-NMR, 126 MHz, DMSO-d<sub>6</sub>

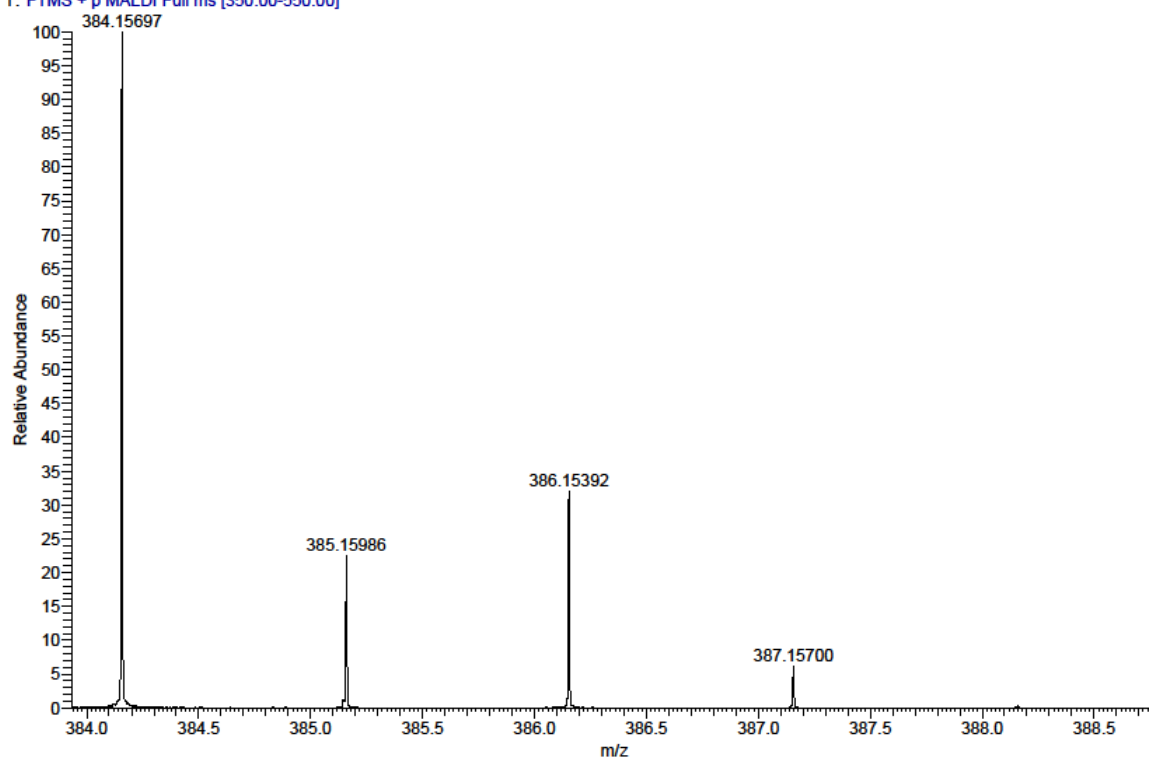
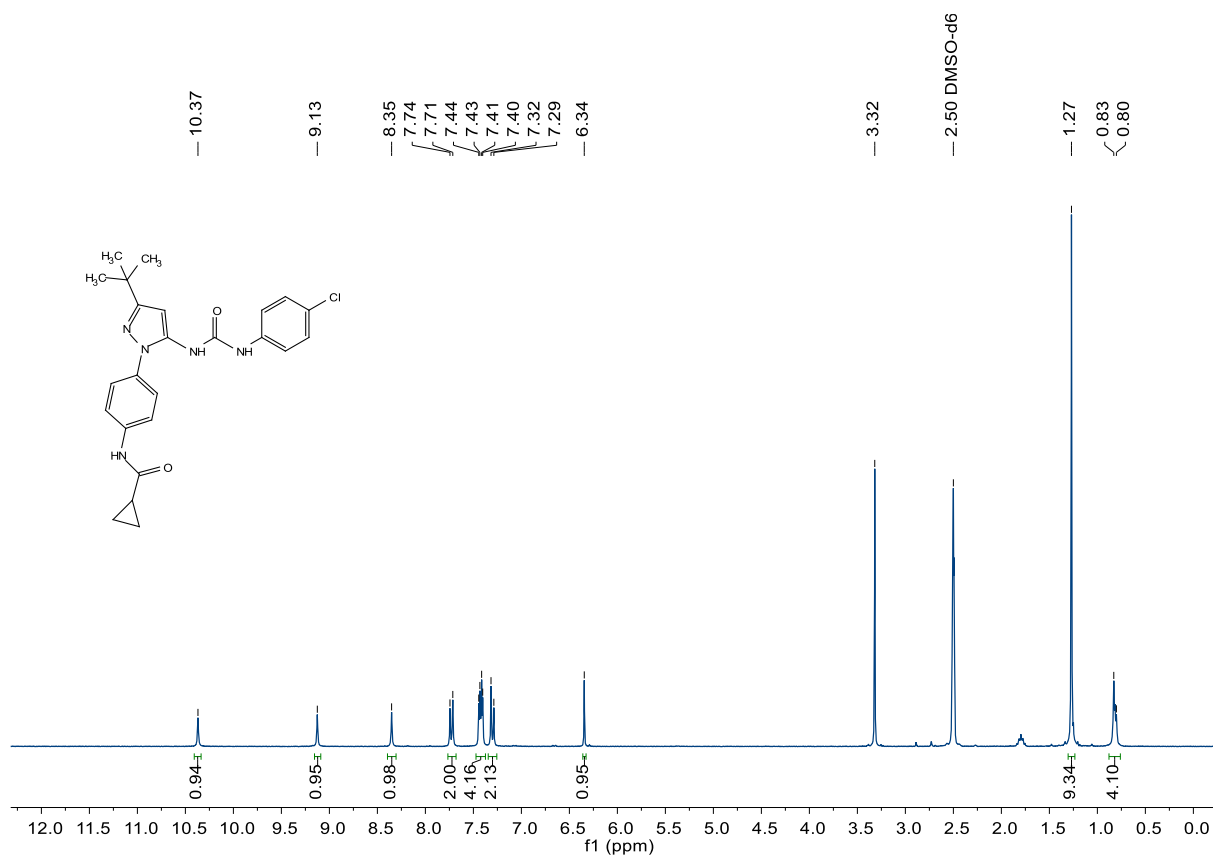
SR226\_A2 #1-4 RT: 0.00-0.35 AV: 4 NL: 2.22E6  
T: FTMS + p MALDI Full ms [350.00-550.00]

Figure 97. Compound 97 (SR226), HRMS (FTMS + p MALDI)

Figure 98. Compound 99 (SR246),  $^1\text{H-NMR}$ , 300 MHz,  $\text{DMSO-d}_6$

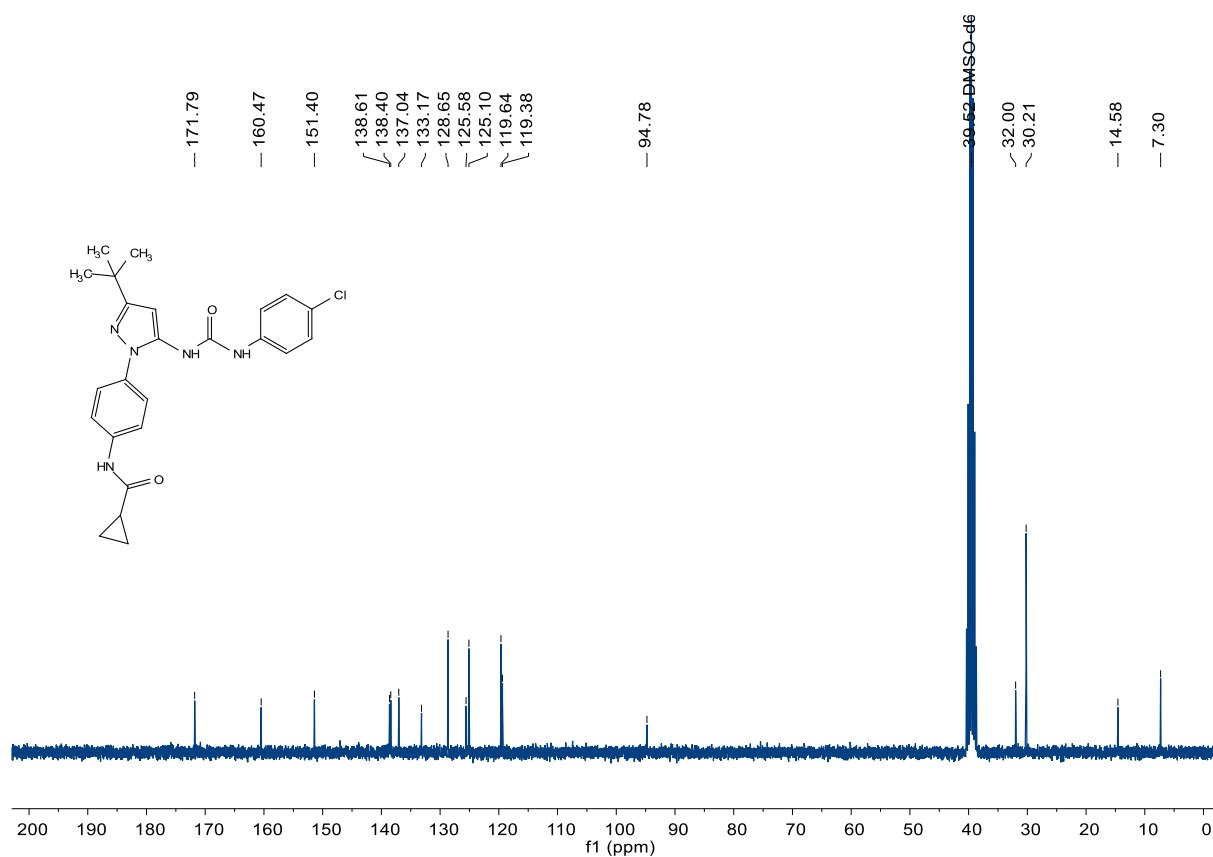


Figure 99. Compound 99 (SR246),  $^{13}\text{C-NMR}$ , 75 MHz,  $\text{DMSO-}d_6$

C:\User\...\Knapp\2019\190917\SR246\_A7

9/17/2019 10:54:10 AM

SR246 mit HCCA gemessen.

SR246\_A7 #7 RT: 0.72 AV: 1 NL: 6.20E6

T: FTMS + p MALDI Full ms [350.00-550.00]

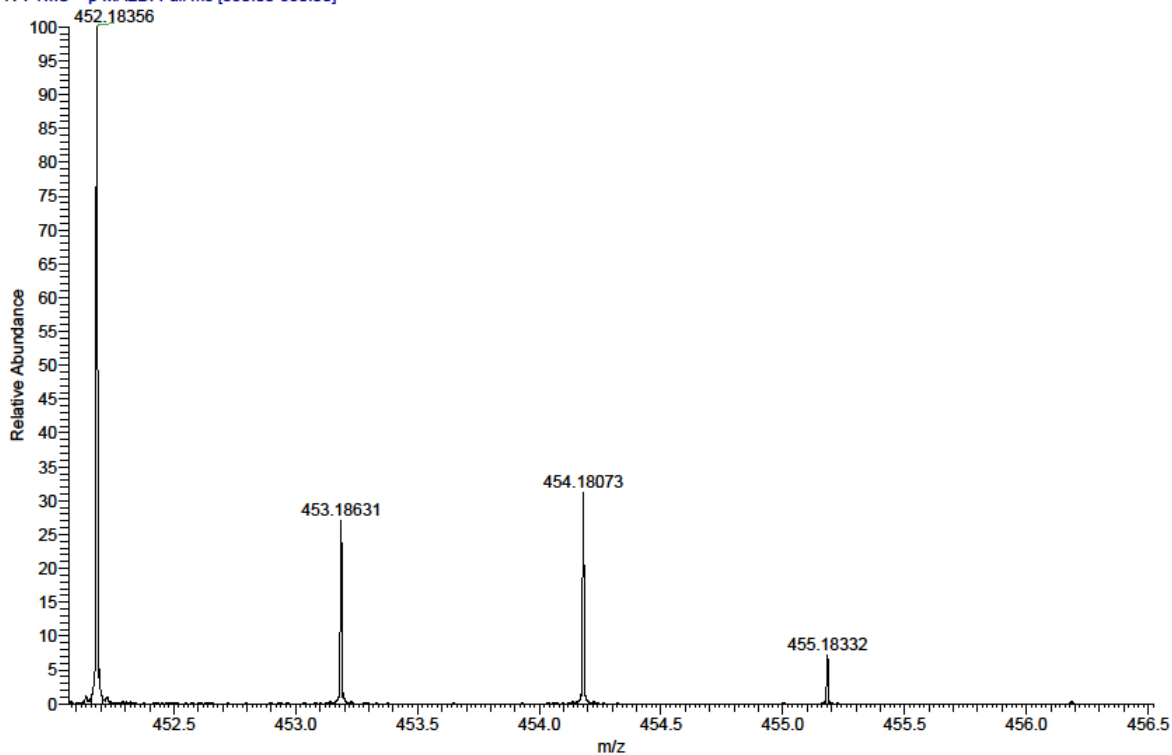


Figure 100. Compound 99 (SR246), HRMS (FTMS + p MALDI)

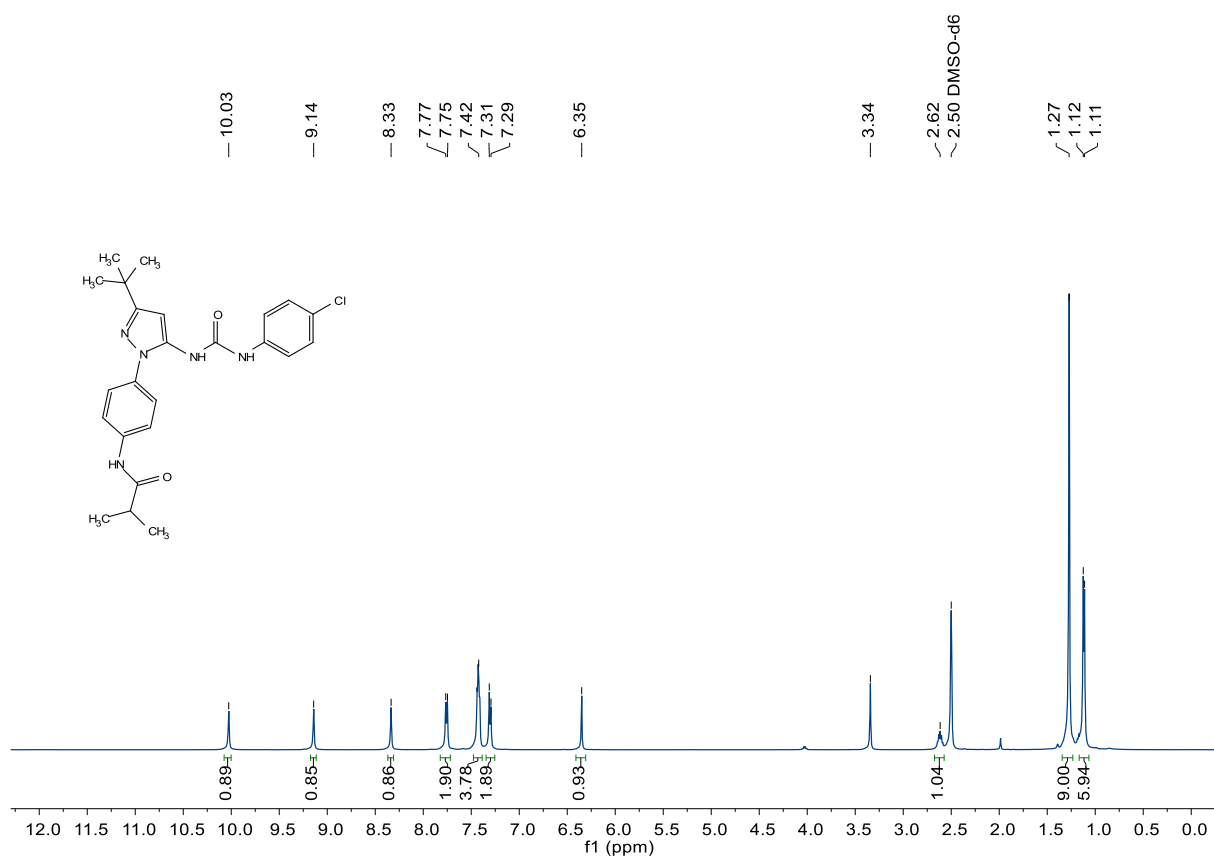


Figure 101. Compound 101 (SR253), <sup>1</sup>H-NMR, 500 MHz, DMSO-d<sub>6</sub>

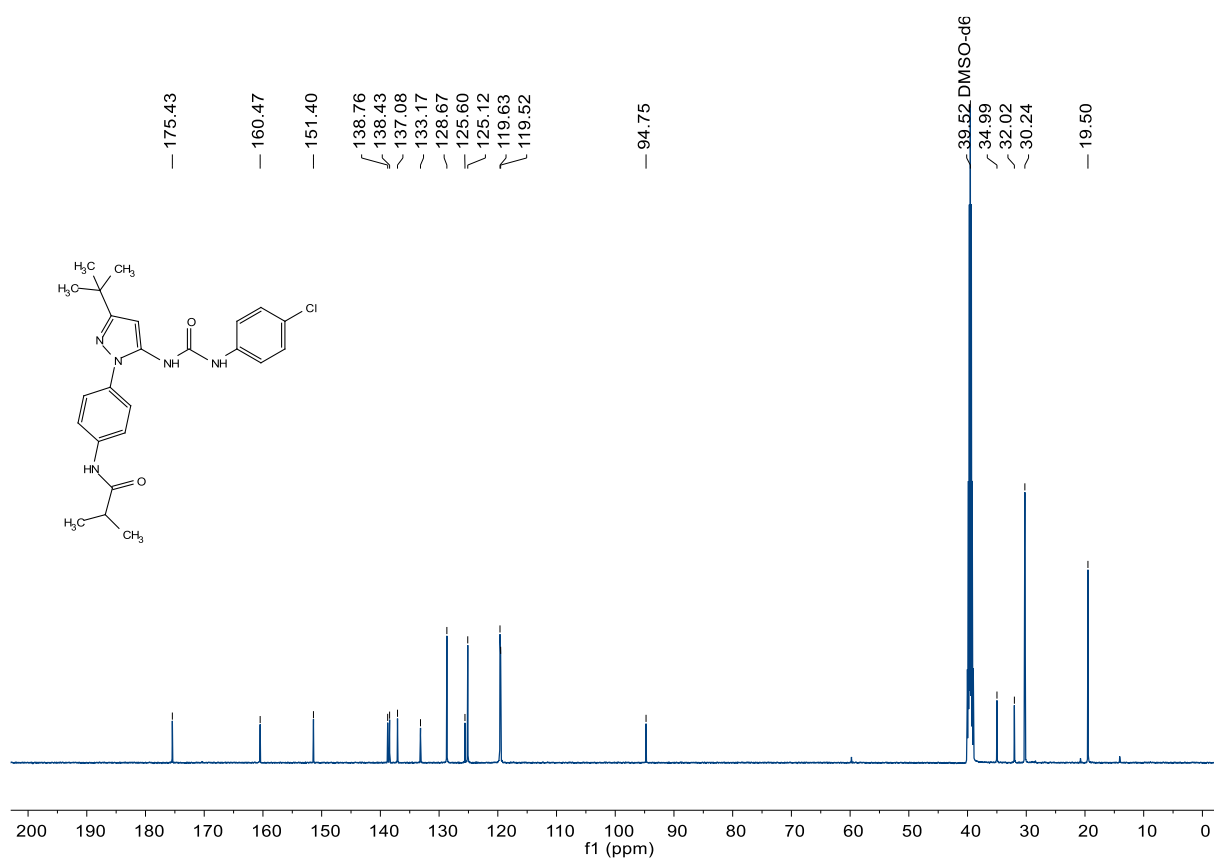


Figure 102. Compound 101 (SR253), <sup>13</sup>C-NMR, 126 MHz, DMSO-d<sub>6</sub>

C:\User\...\Knapp2019\190917\SR253\_A9

9/17/2019 10:57:34 AM

SR253 mit HCCA gemessen.

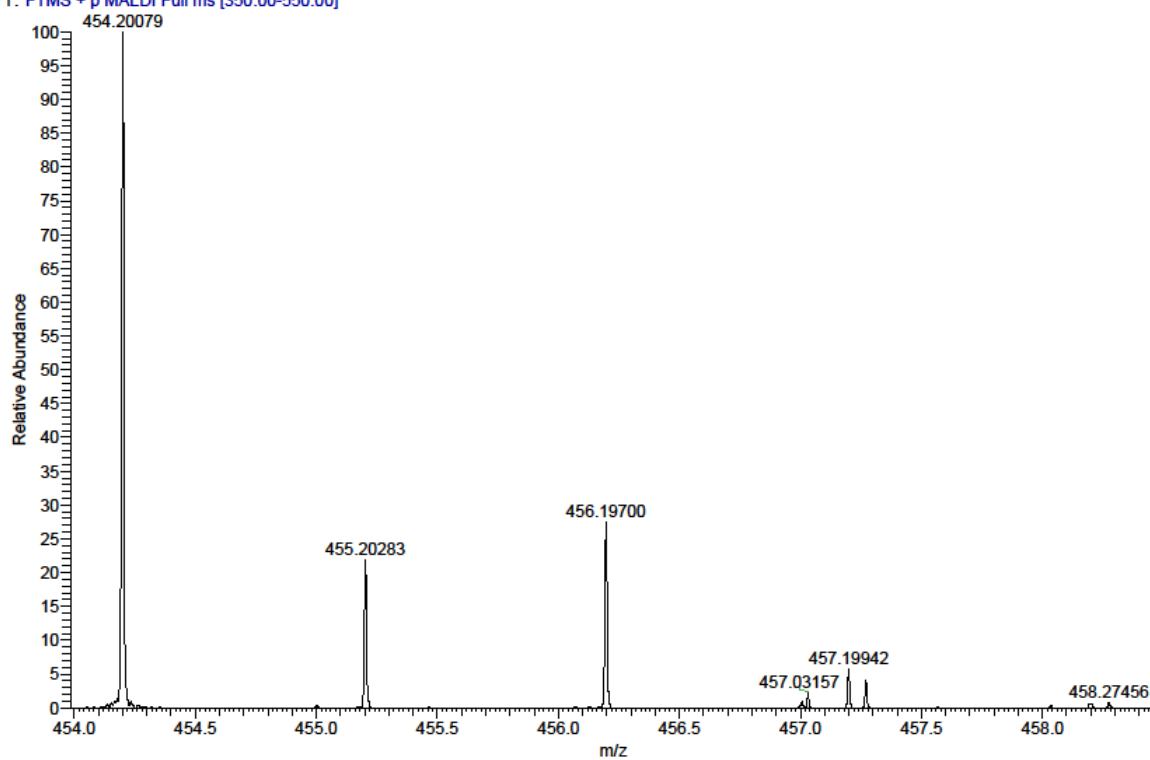
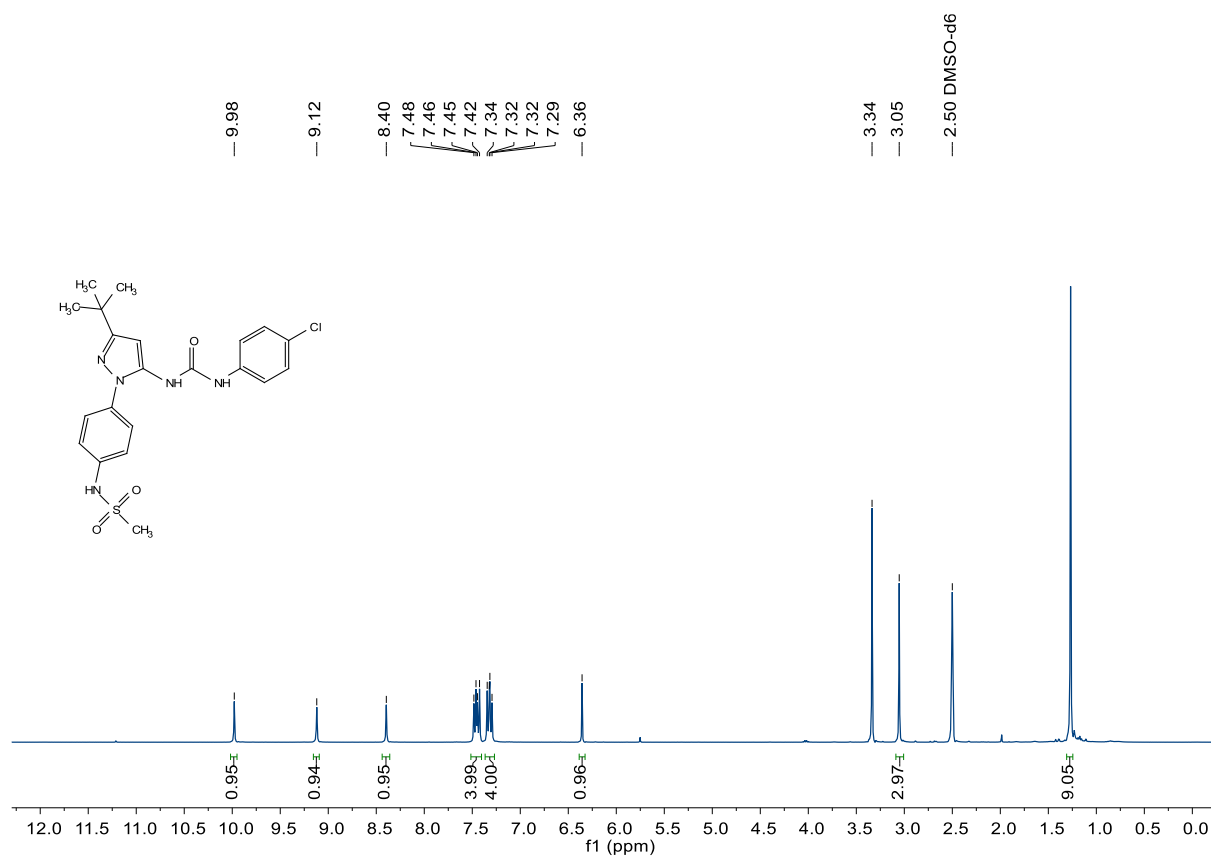
SR253\_A9 #1-9 RT: 0.00-1.26 AV: 9 NL: 3.04E5  
T: FTMS + p MALDI Full ms [350.00-550.00]

Figure 103. Compound 101 (SR253), HRMS (FTMS + p MALDI)

Figure 104. Compound 103 (SR249),  $^1\text{H-NMR}$ , 400 MHz,  $\text{DMSO-d}_6$

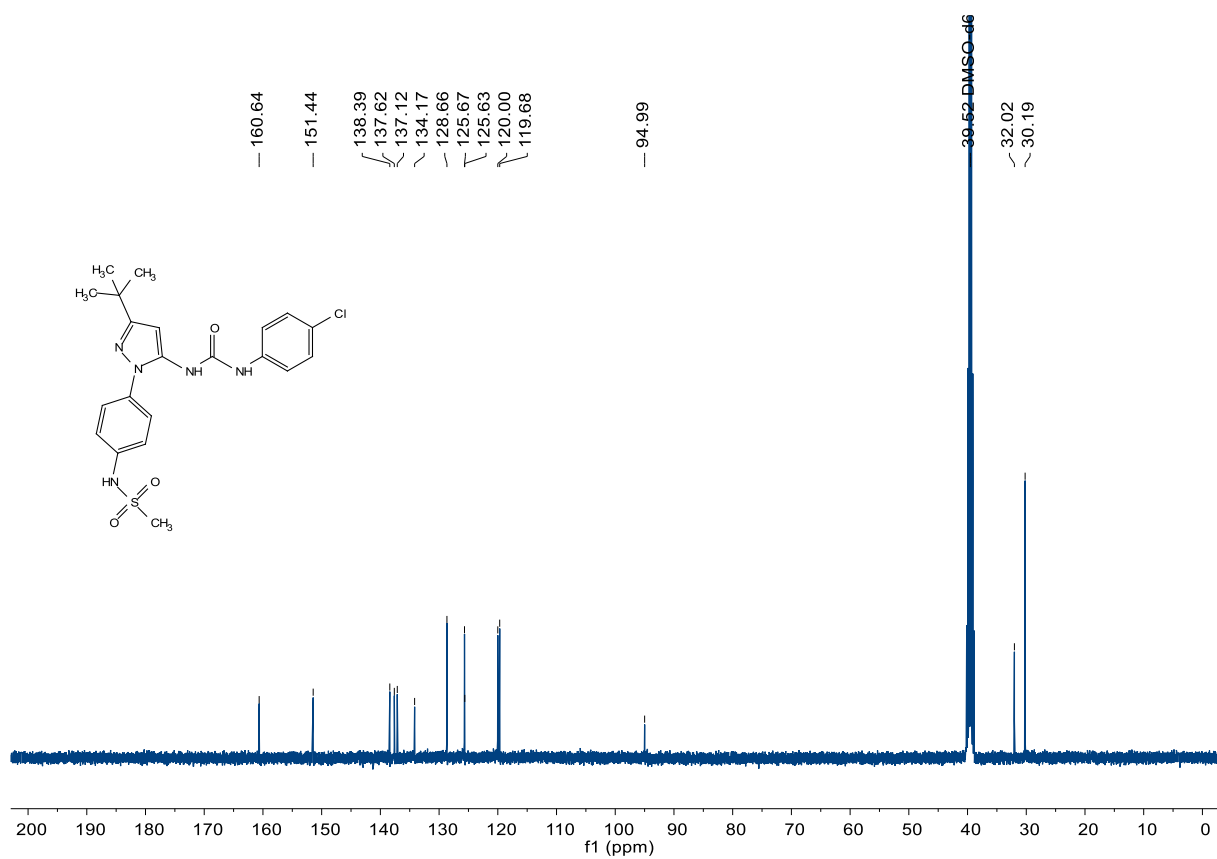


Figure 105. Compound 103 (SR249),  $^{13}\text{C}$ -NMR, 101 MHz,  $\text{DMSO-d}_6$

C:\User\...\Knapp\2019\190917\SR249\_A8

9/17/2019 10:55:39 AM

SR249 mit HCCA gemessen.

SR249\_A8 #9 RT: 1.04 AV: 1 NL: 1.56E6

T: FTMS + p MALDI Full ms [350.00-550.00]

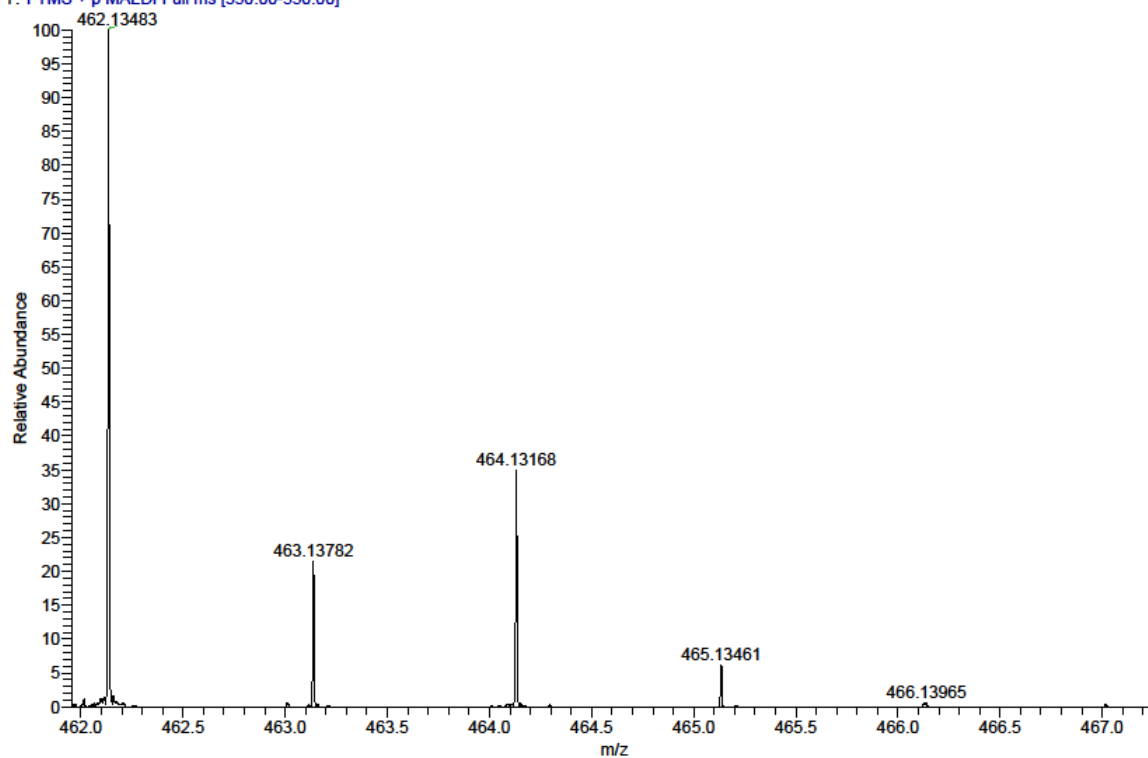


Figure 106. Compound 103 (SR249), HRMS (FTMS + p MALDI)



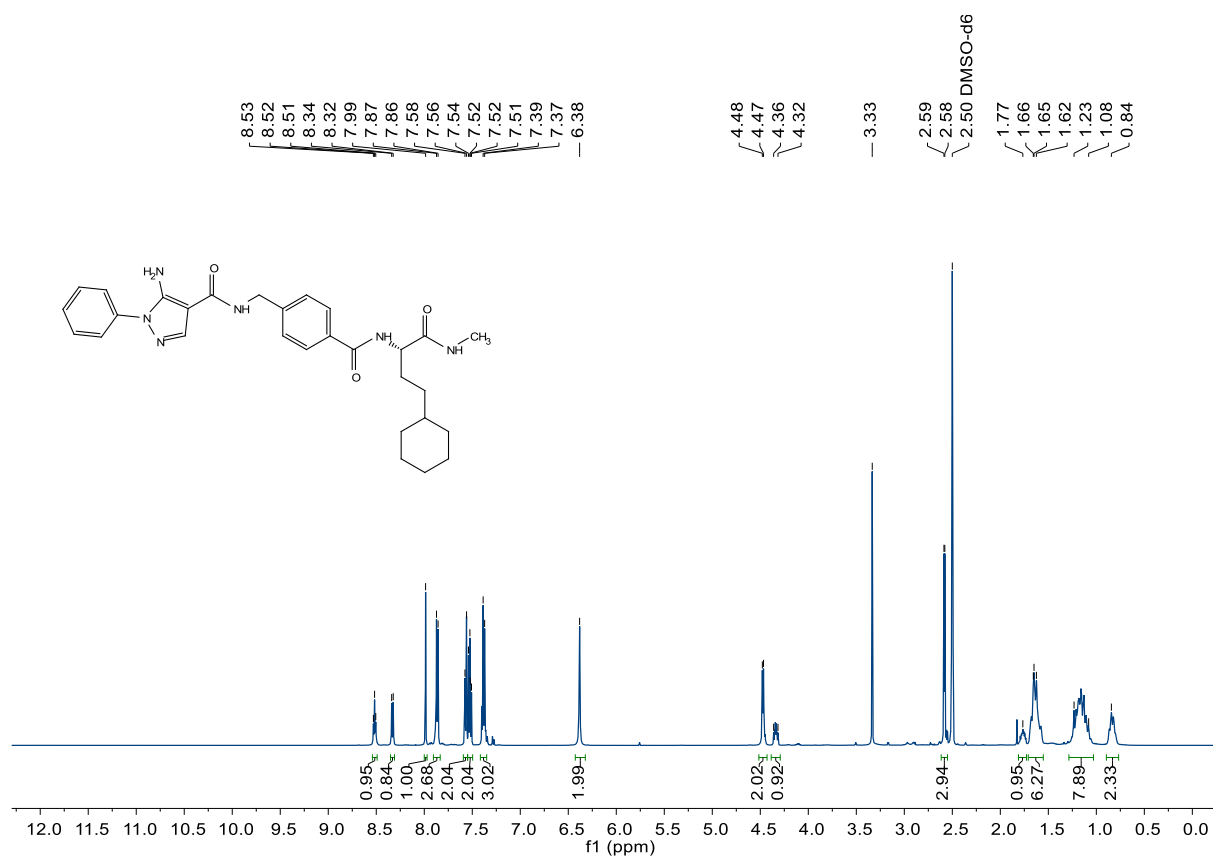


Figure 107. Compound 217 (SR41),  $^1\text{H-NMR}$ , 500 MHz,  $\text{DMSO-d}_6$

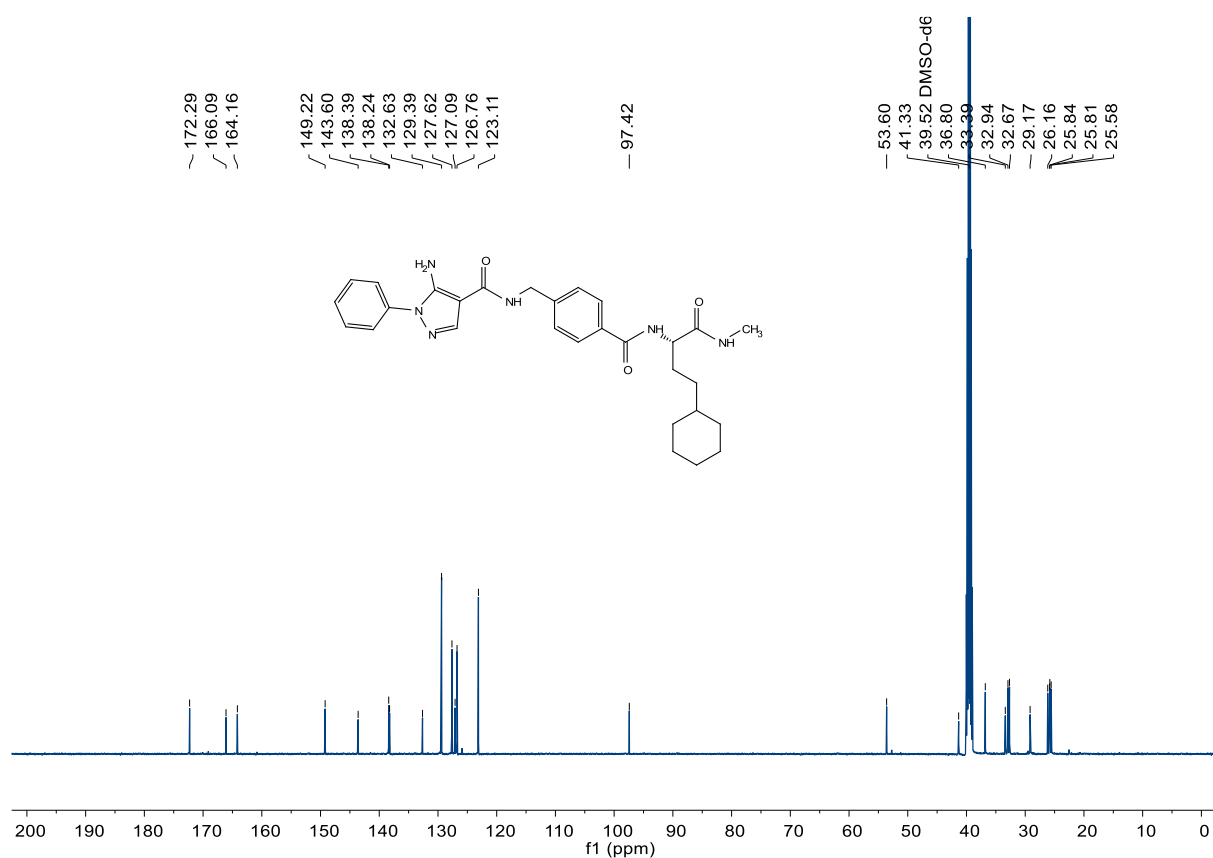


Figure 108. Compound 217 (SR41),  $^{13}\text{C-NMR}$ , 126 MHz,  $\text{DMSO-d}_6$

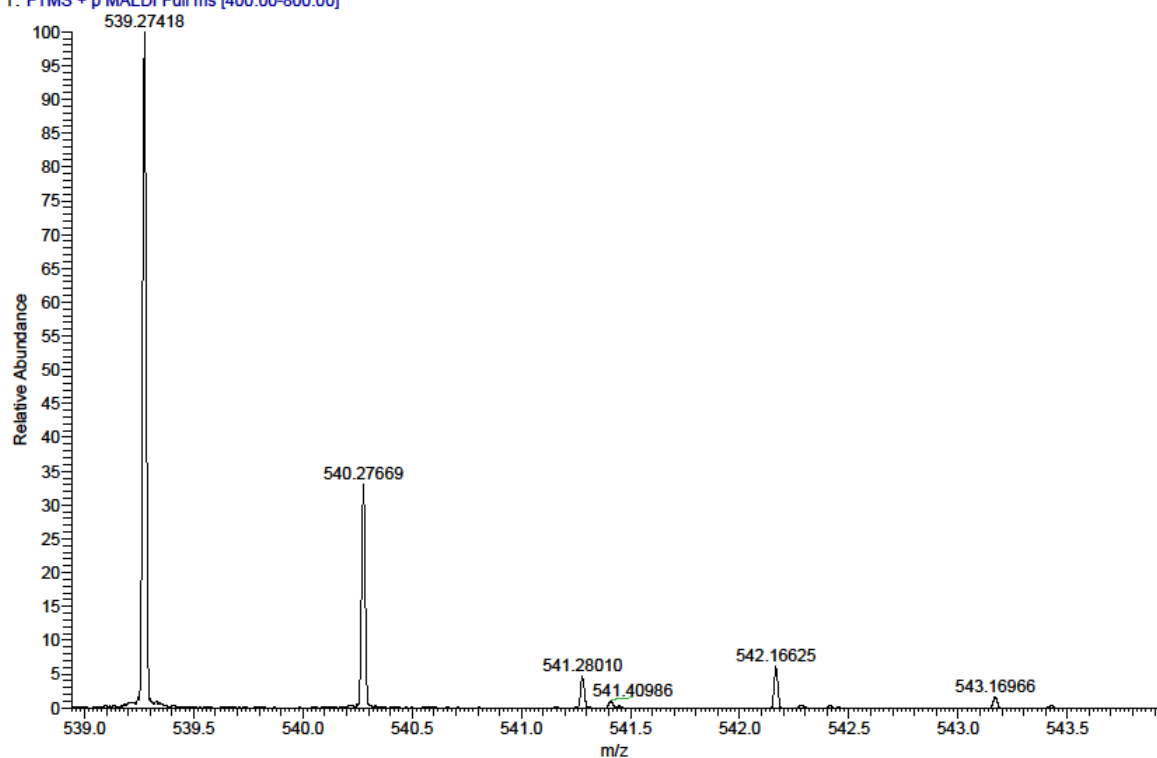
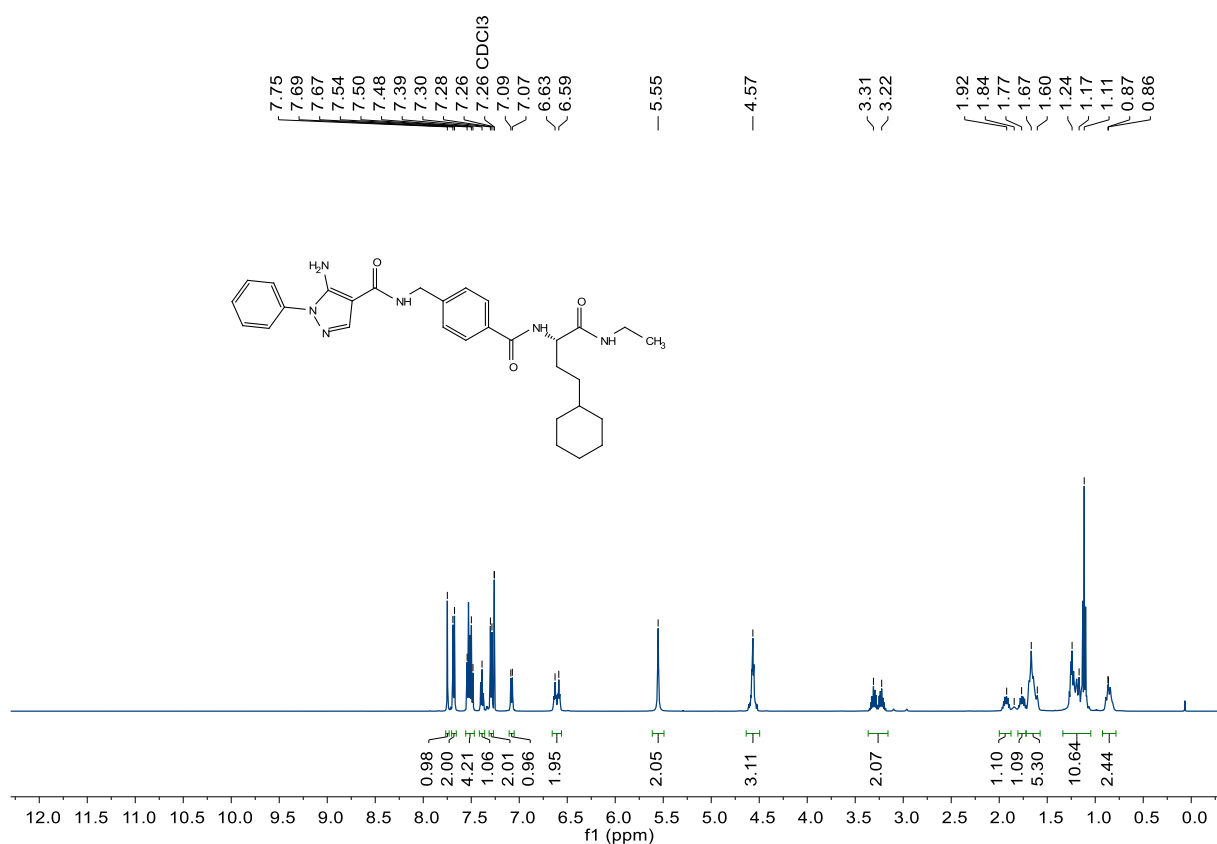
SR41\_G6 #1-8 RT: 0.01-0.59 AV: 8 NL: 9.00E6  
T: FTMS + p MALDI Full ms [400.00-800.00]

Figure 109. Compound 217 (SR41), HRMS (FTMS + p MALDI)

Figure 110. Compound 218 (SR43), <sup>1</sup>H-NMR, 500 MHz, CDCl<sub>3</sub>

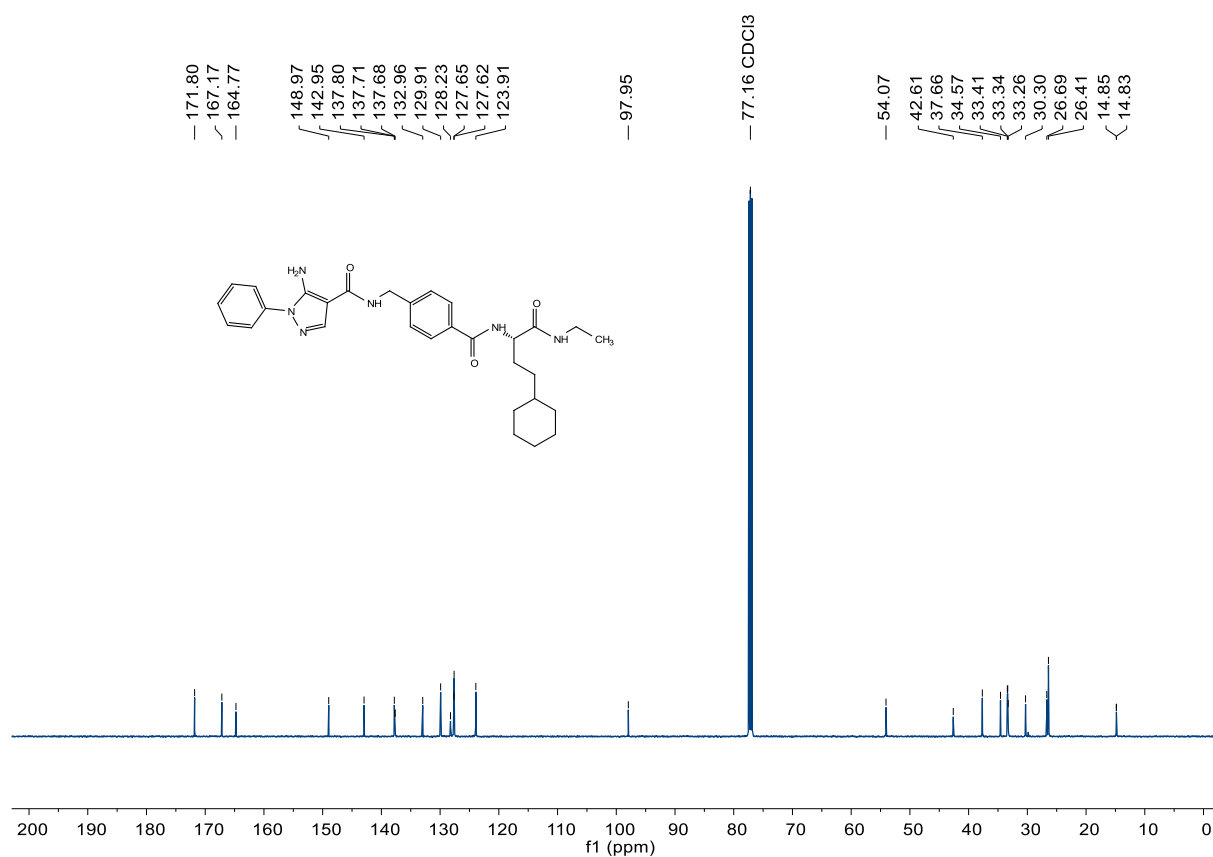


Figure 111. Compound 218 (SR43),  $^{13}\text{C-NMR}$ , 126 MHz,  $\text{CDCl}_3$

C:\User\...\Knapp\2018\180319\SR43\_C11

3/19/2018 2:08:22 PM

SR43 mit HCCA gemessen.

SR43\_C11 #1-3 RT: 0.02-0.26 AV: 3 NL: 2.43E5  
T: FTMS + p MALDI Full ms [500.00-800.00]

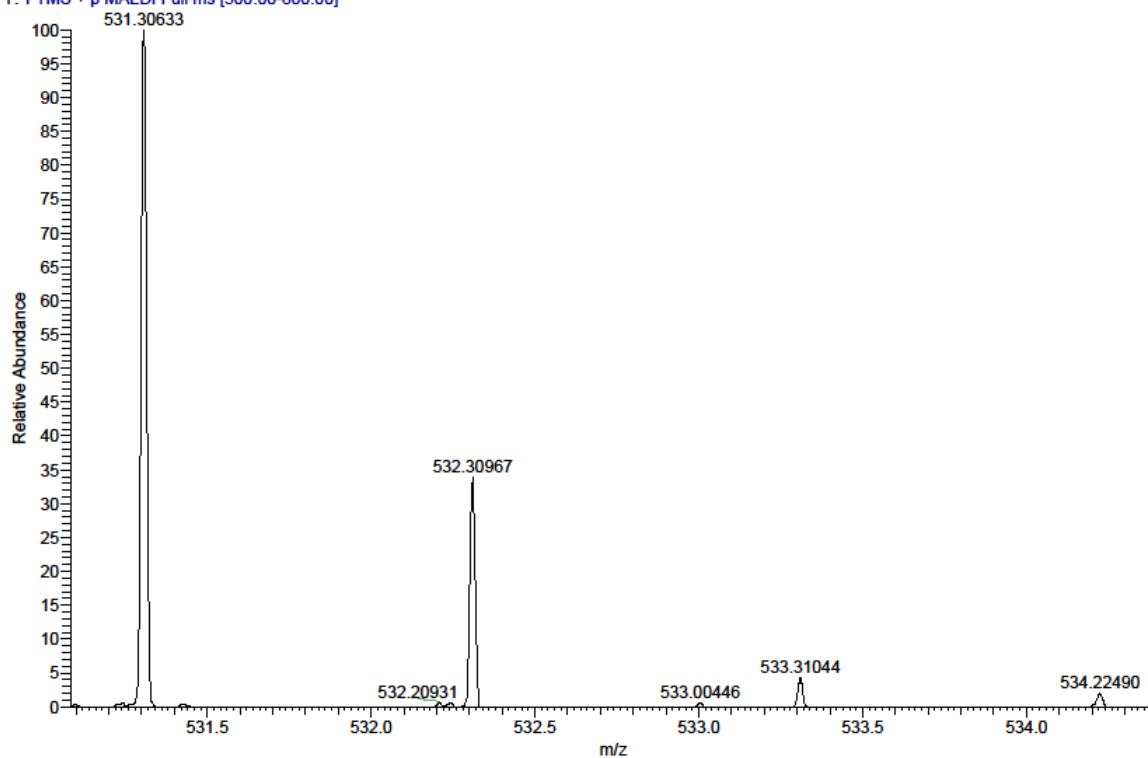


Figure 112. Compound 218 (SR43), HRMS (FTMS + p MALDI)

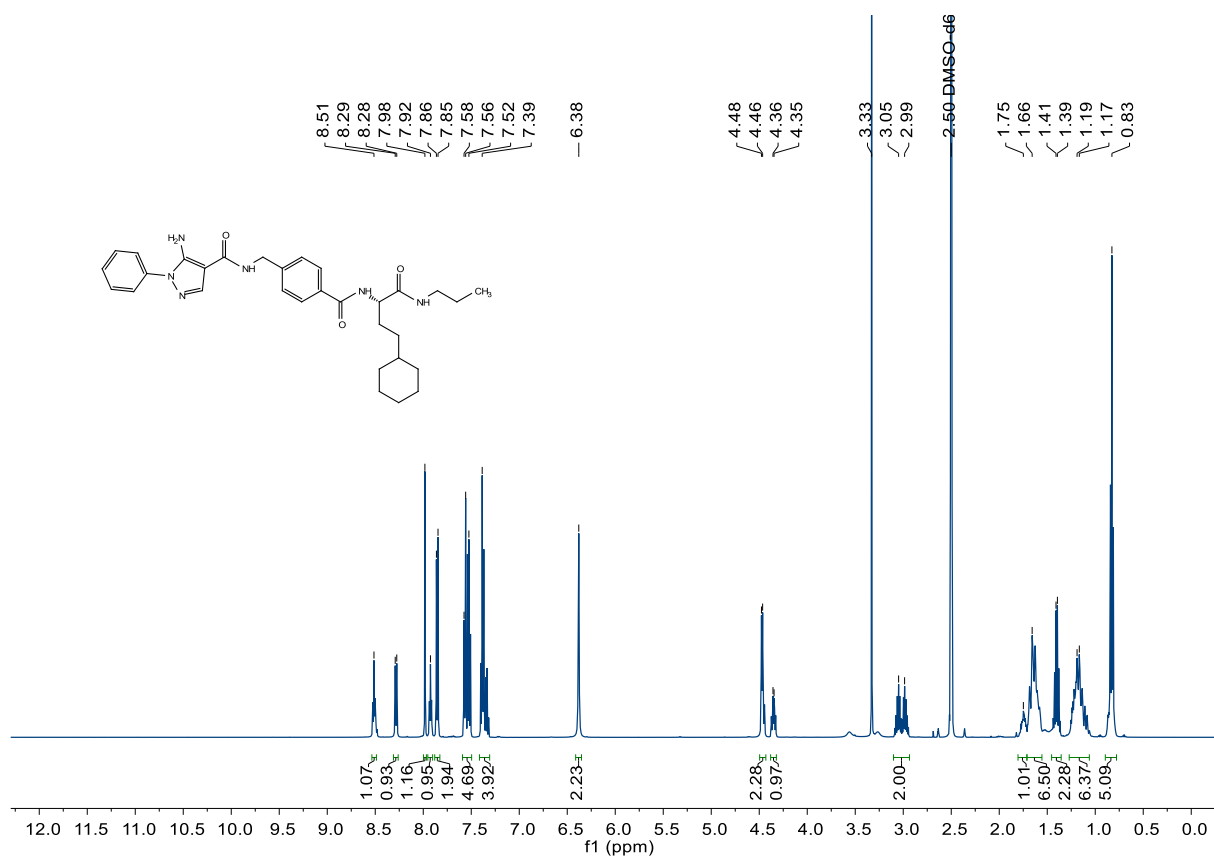


Figure 113. Compound 219 (SR61),  $^1\text{H-NMR}$ , 500 MHz,  $\text{DMSO-d}_6$

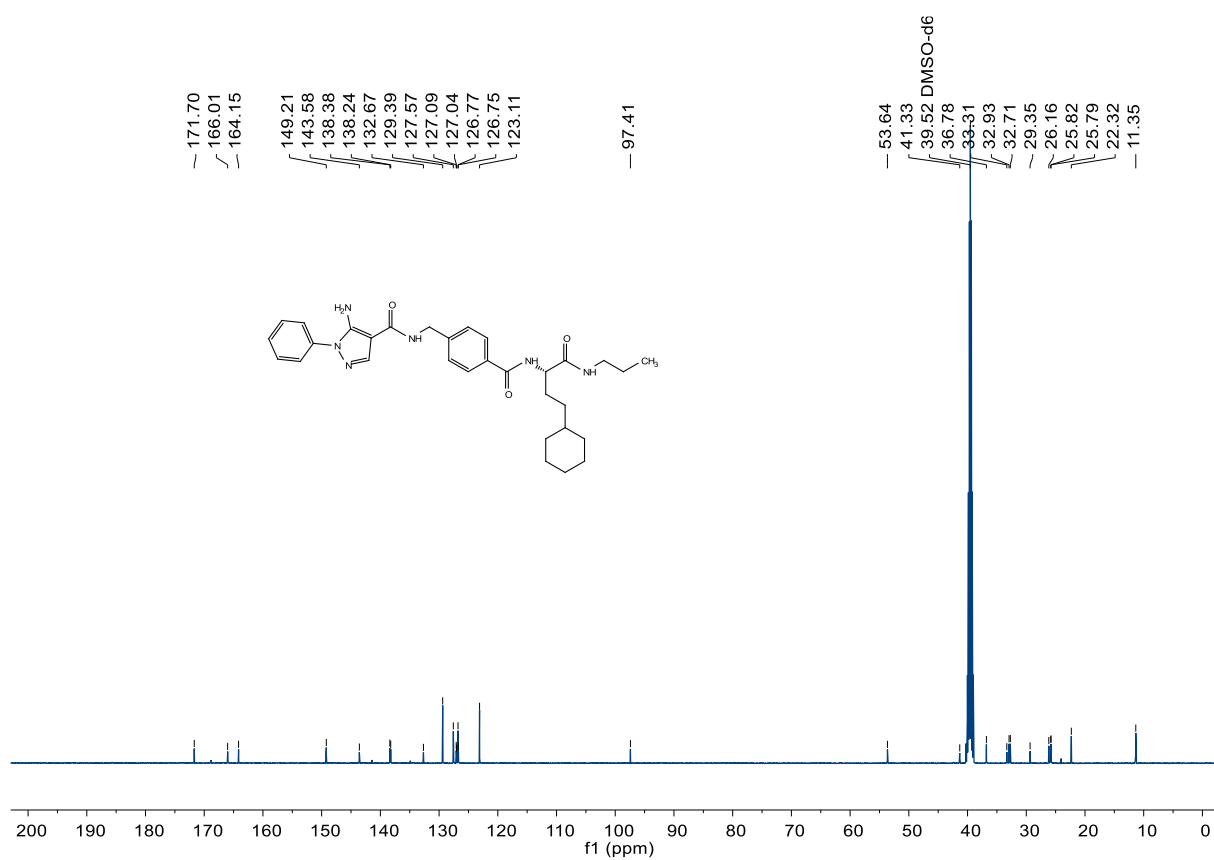


Figure 114. Compound 219 (SR61),  $^{13}\text{C-NMR}$ , 126 MHz,  $\text{DMSO-d}_6$

C:\User\...\Knapp2018\180711\SR61\_F5

7/11/2018 5:01:42 PM

SR61 mit HCCA gemessen.

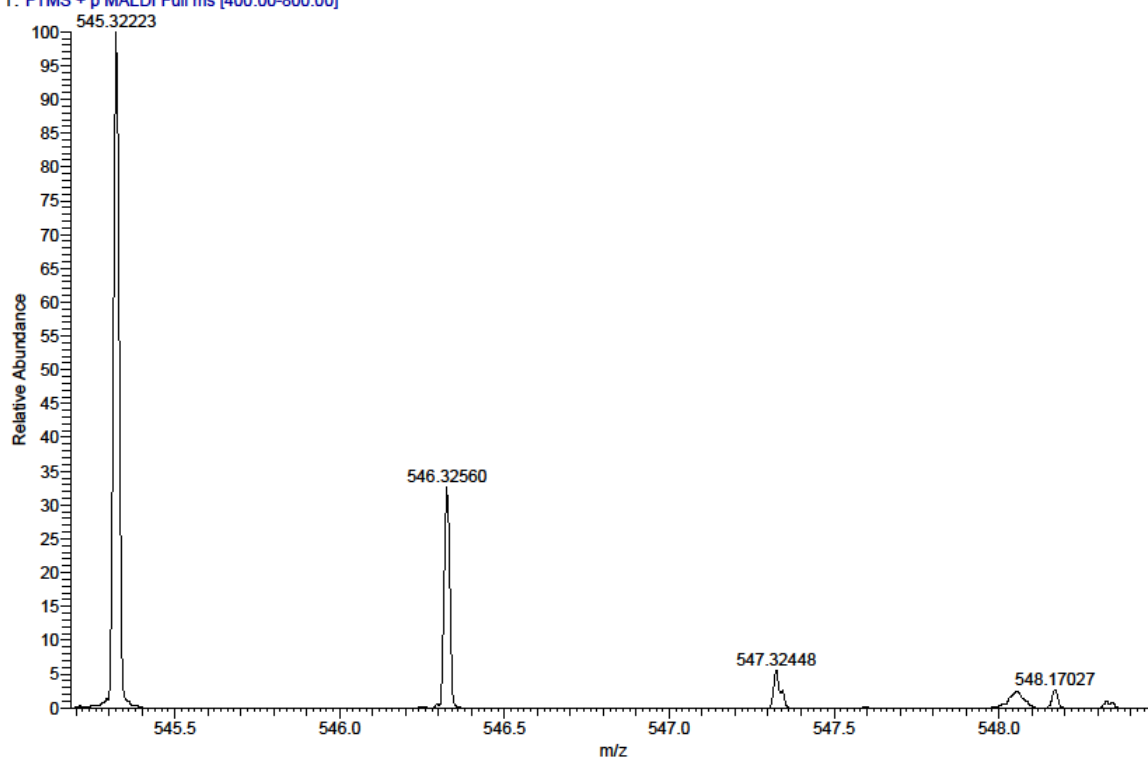
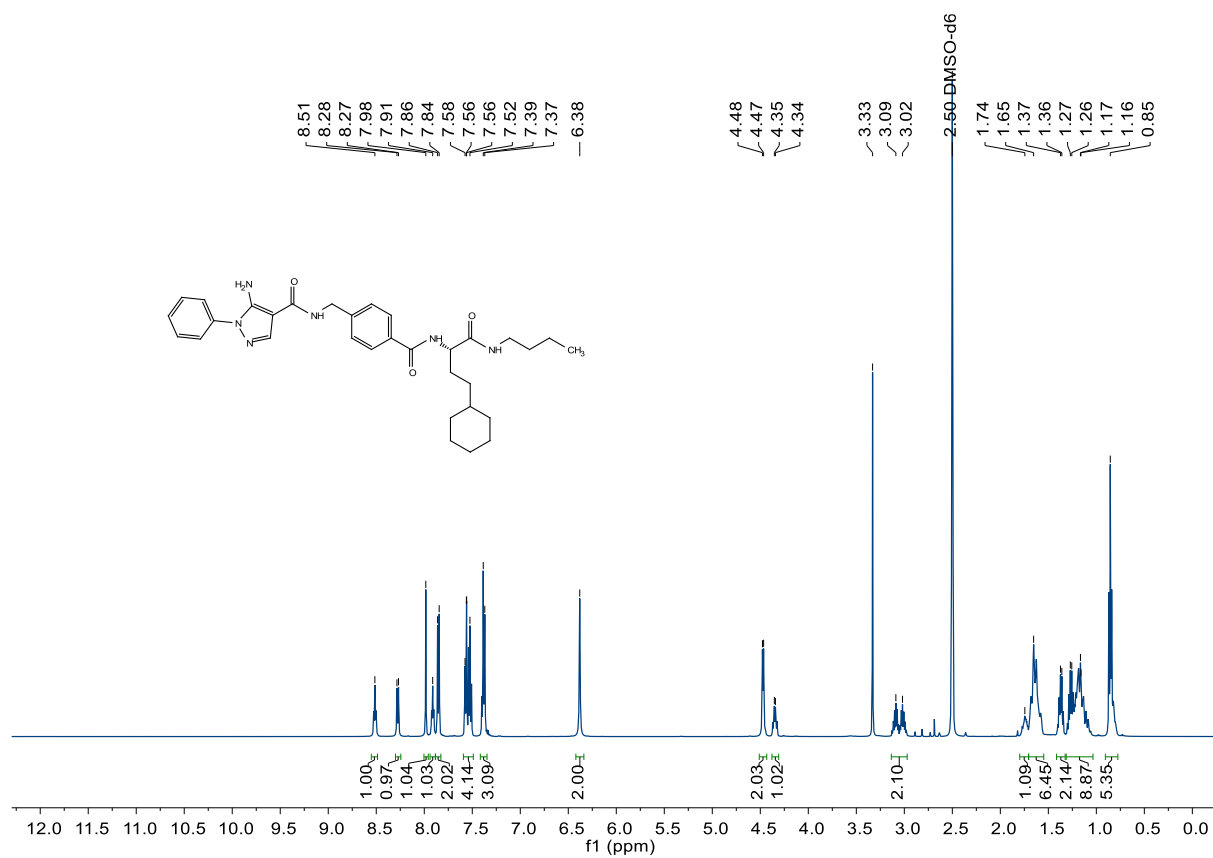
SR61\_F5 #1-7 RT: 0.01-0.66 AV: 7 NL: 4.23E5  
T: FTMS + p MALDI Full ms [400.00-800.00]

Figure 115. Compound 219 (SR61), HRMS (FTMS + p MALDI)

Figure 116. Compound 220 (SR59), <sup>1</sup>H-NMR, 500 MHz, DMSO-d<sub>6</sub>

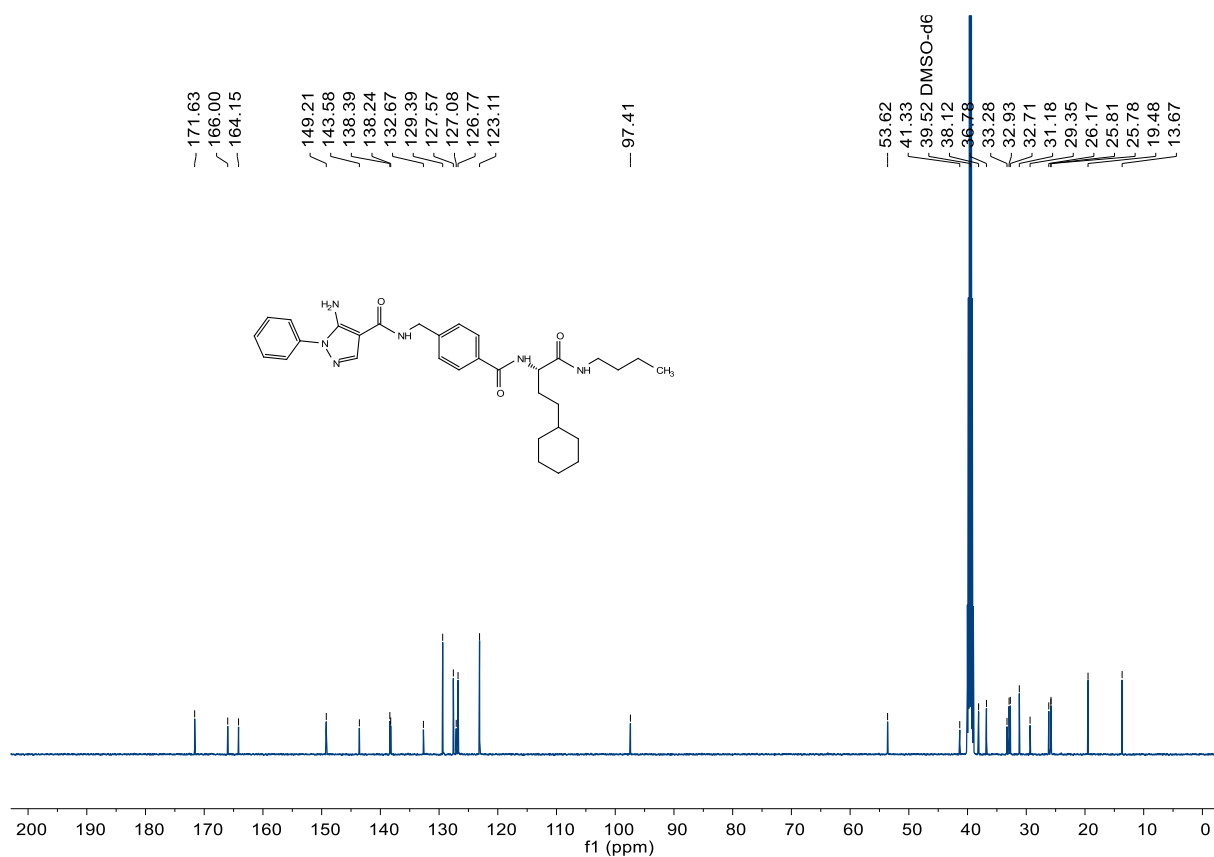


Figure 117. Compound 220 (SR59),  $^{13}\text{C-NMR}$ , 126 MHz,  $\text{DMSO-d}_6$

C:\User\...Knapp\2018\180308\SR59\_C4

3/8/2018 3:31:20 PM

SR59 mit HCCA gemessen.

SR59\_C4 #1-5 RT: 0.01-0.34 AV: 5 NL: 1.65E6

T: FTMS + p MALDI Full ms [500.00-800.00]

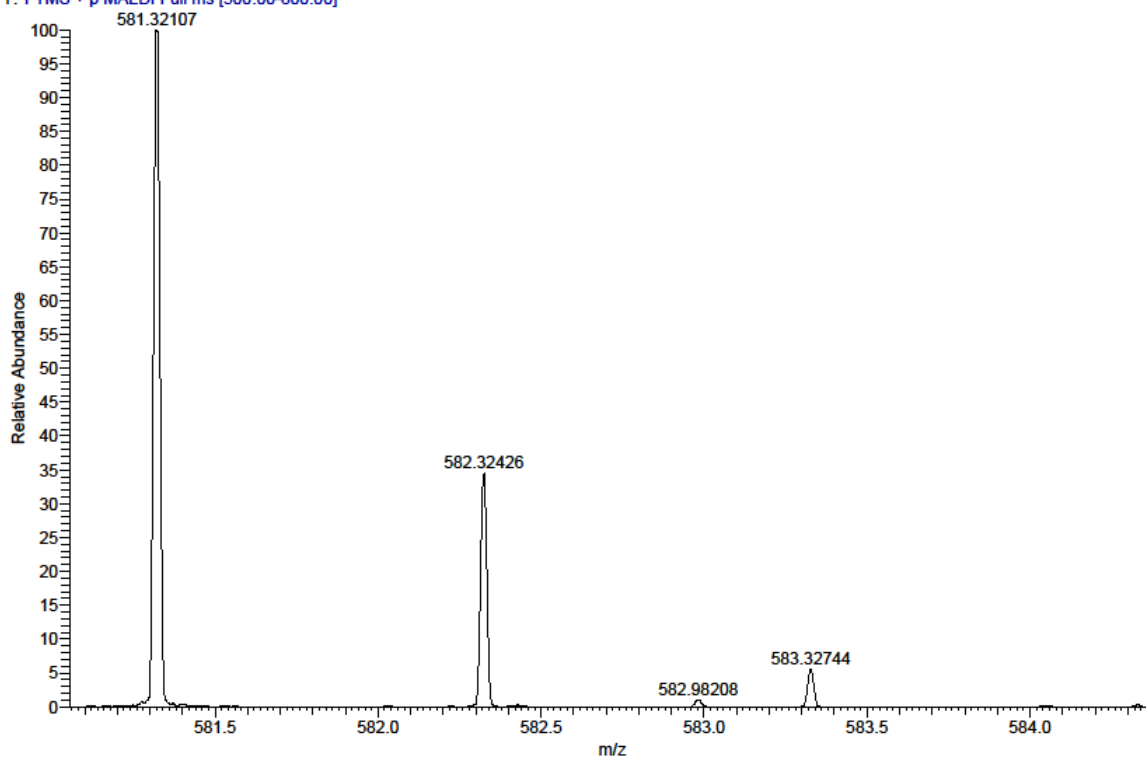


Figure 118. Compound 220 (SR59), HRMS (FTMS + p MALDI)

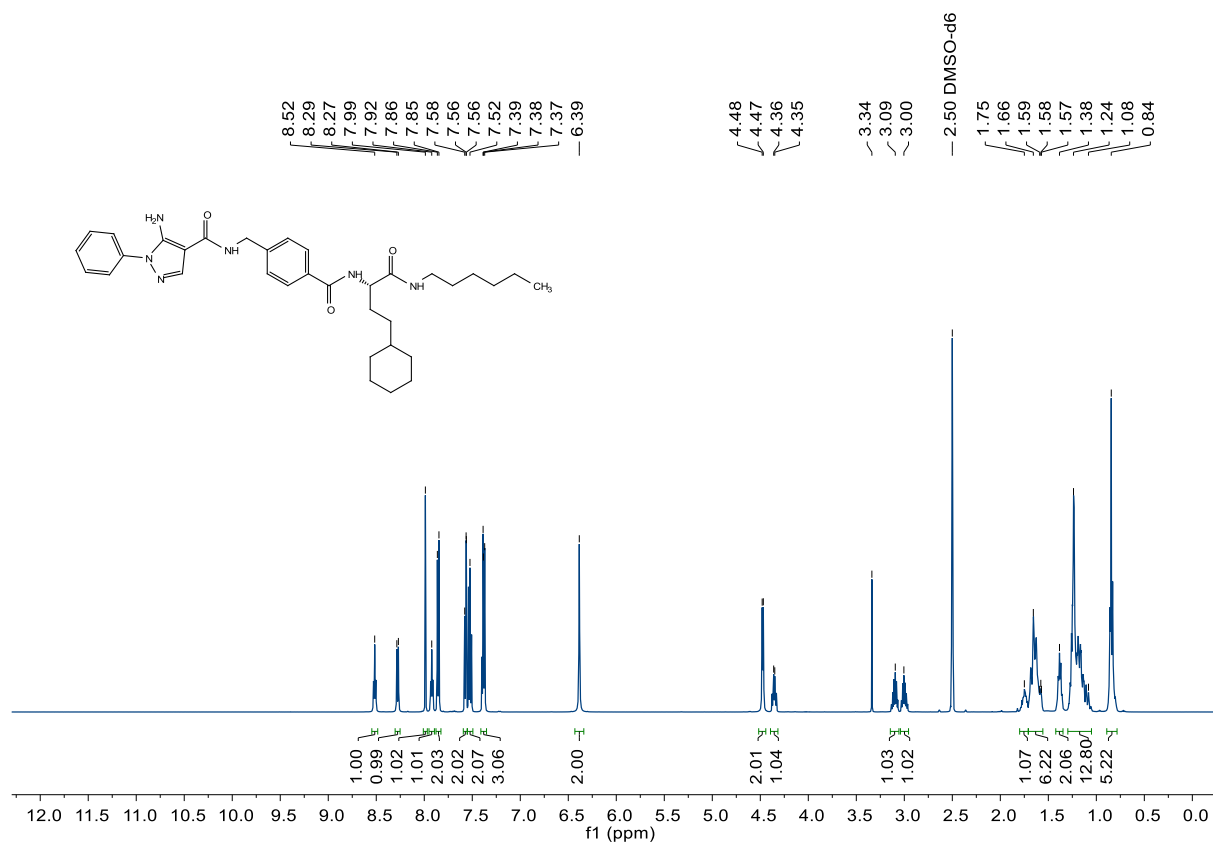


Figure 119. Compound 221 (SR81), <sup>1</sup>H-NMR, 500 MHz, DMSO-d<sub>6</sub>

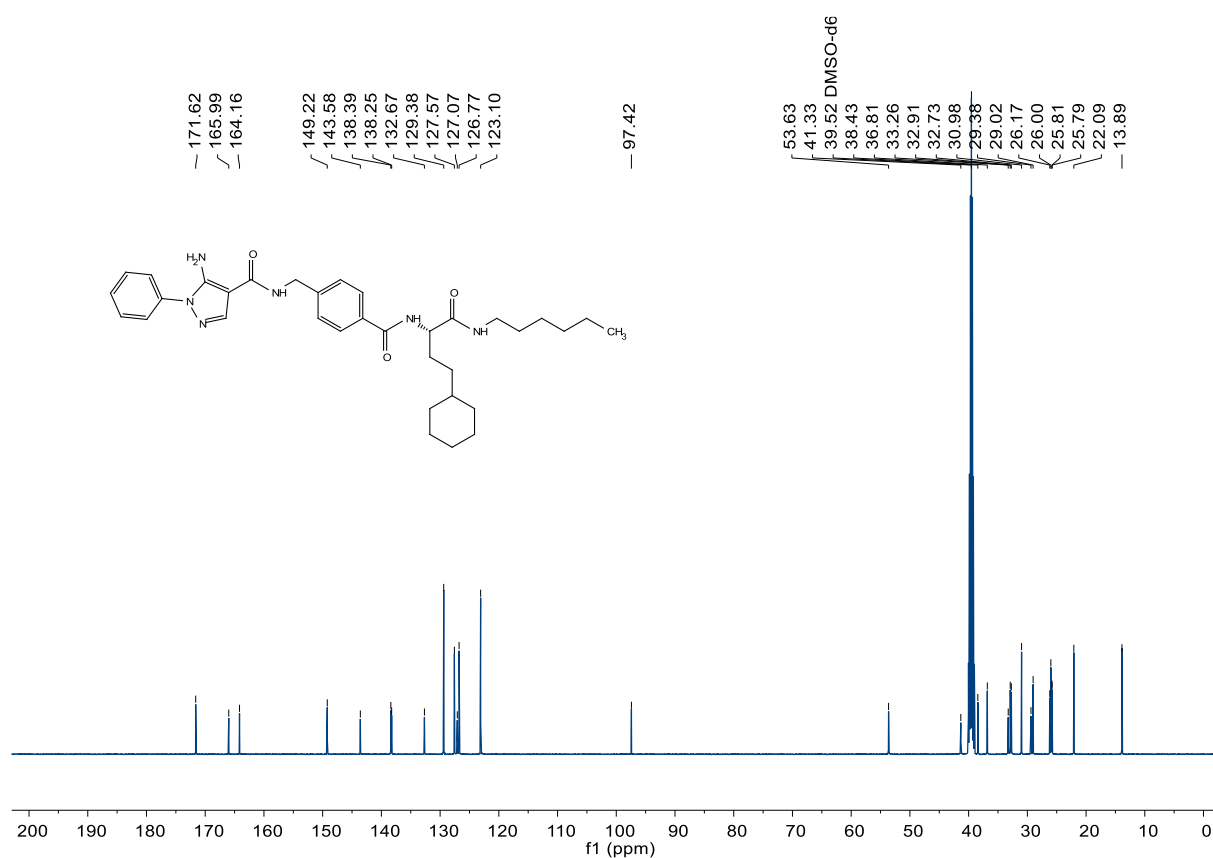


Figure 120. Compound 221 (SR81), <sup>13</sup>C-NMR, 126 MHz, DMSO-d<sub>6</sub>

SR81\_C7 #1-10 RT: 0.00-1.06 AV: 10 NL: 1.60E5  
T: FTMS + p MALDI Full ms [500.00-800.00]

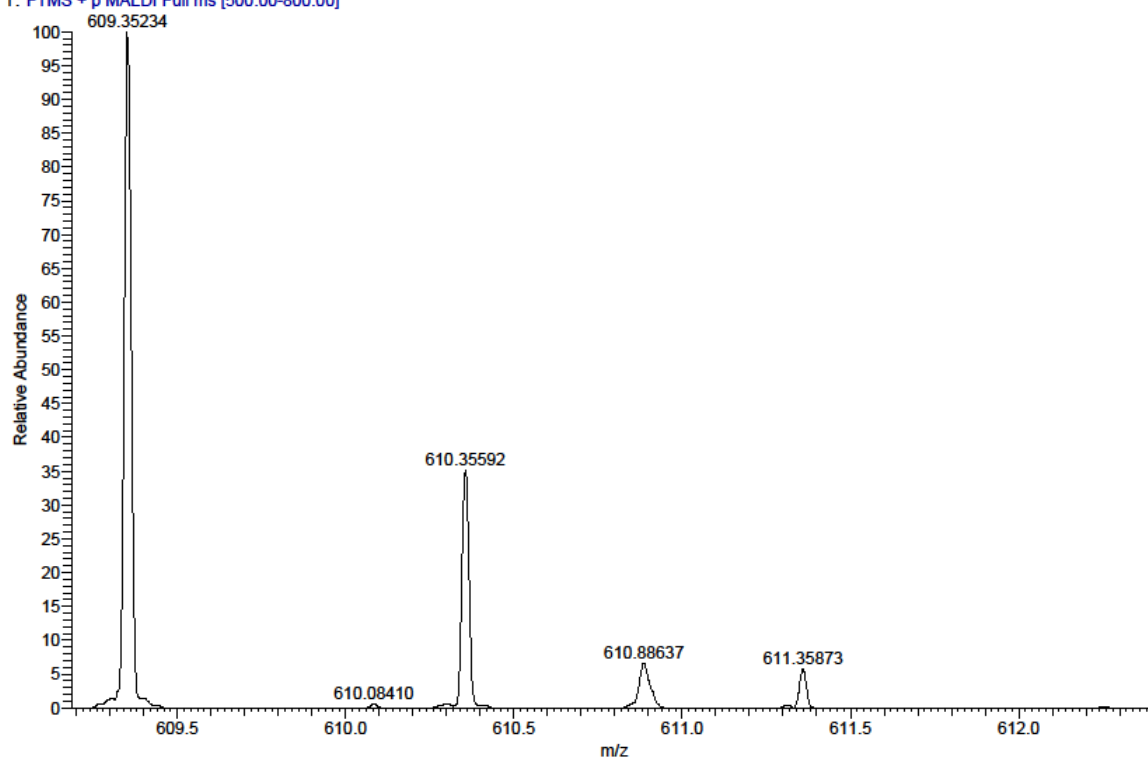


Figure 121. Compound 221 (SR81), HRMS (FTMS + p MALDI)

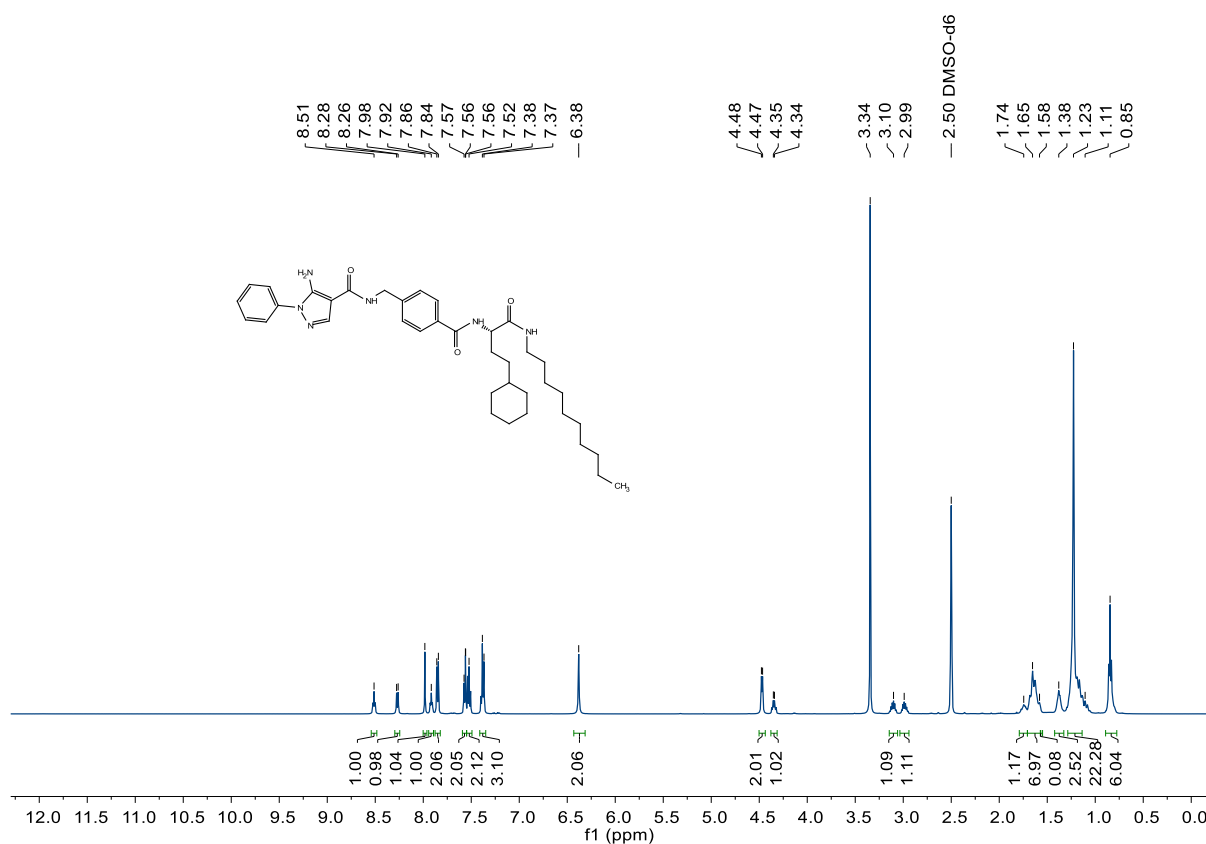


Figure 122. Compound 222 (SR73), <sup>1</sup>H-NMR, 500 MHz, DMSO-d<sub>6</sub>



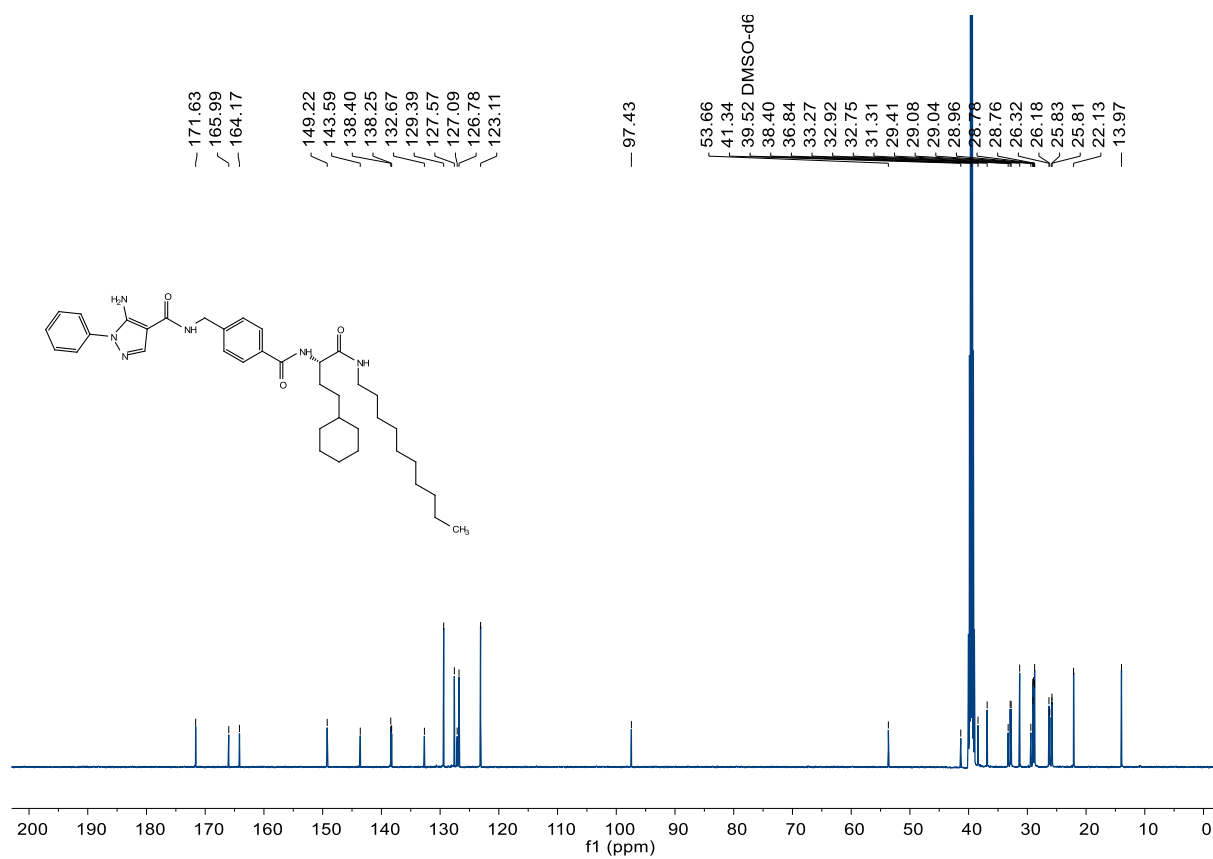


Figure 123. Compound 222 (SR73), <sup>13</sup>C-NMR, 126 MHz, DMSO-d<sub>6</sub>

C:\User\...\Knapp2018\180308\SR73\_C6

3/8/2018 3:34:20 PM

SR73 mit HCCA gemessen.

SR73\_C6 #1-4 RT: 0.00-0.29 AV: 4 NL: 3.58E5  
T: FTMS + p MALDI Full ms [500.00-800.00]

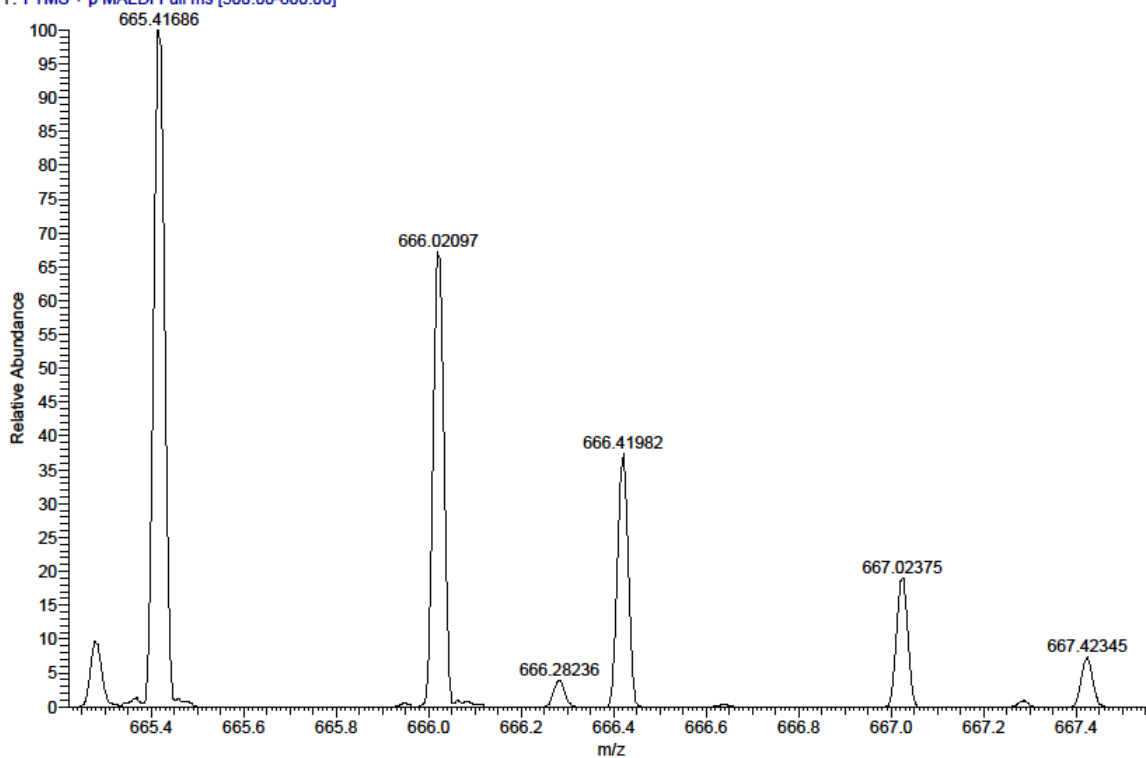


Figure 124. Compound 222 (SR73), HRMS (FTMS + p MALDI)

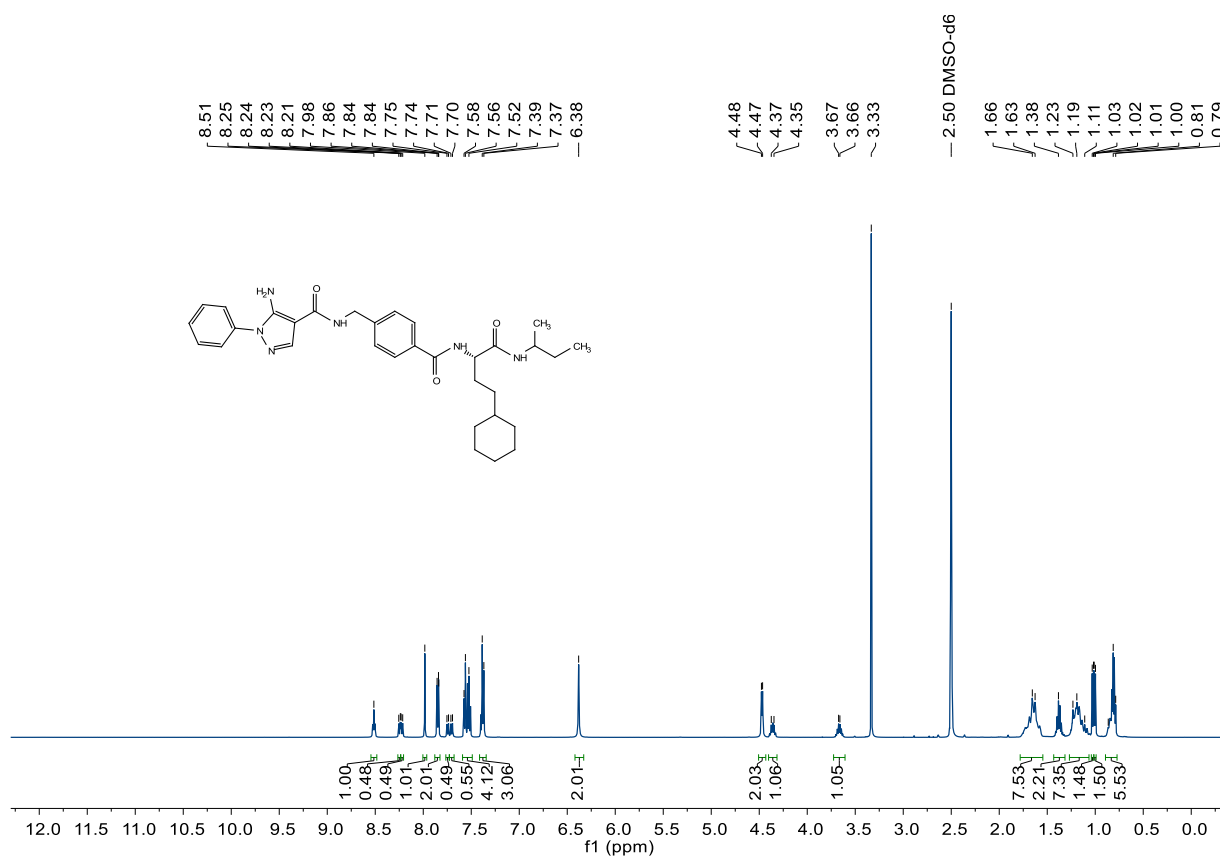


Figure 125. Compound 223 (SR63), <sup>1</sup>H-NMR, 500 MHz, DMSO-d<sub>6</sub>

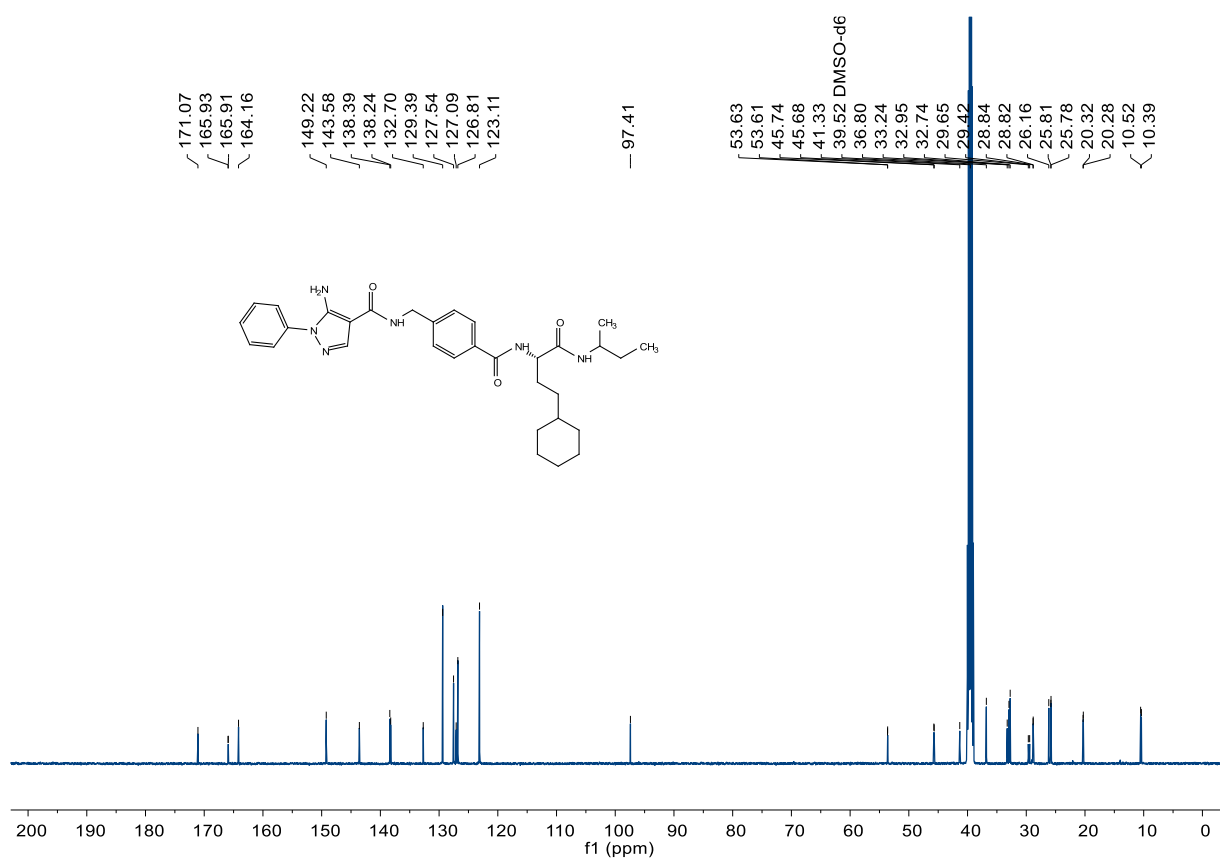
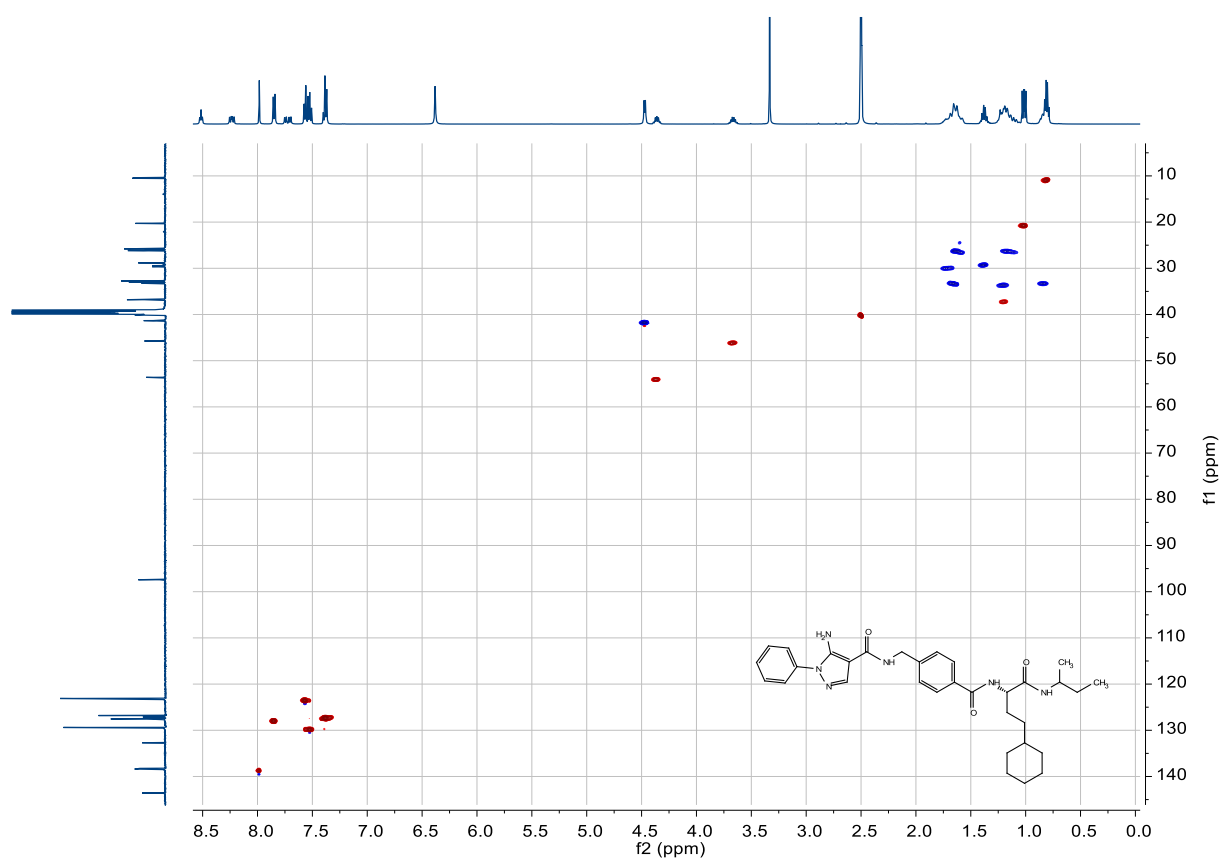
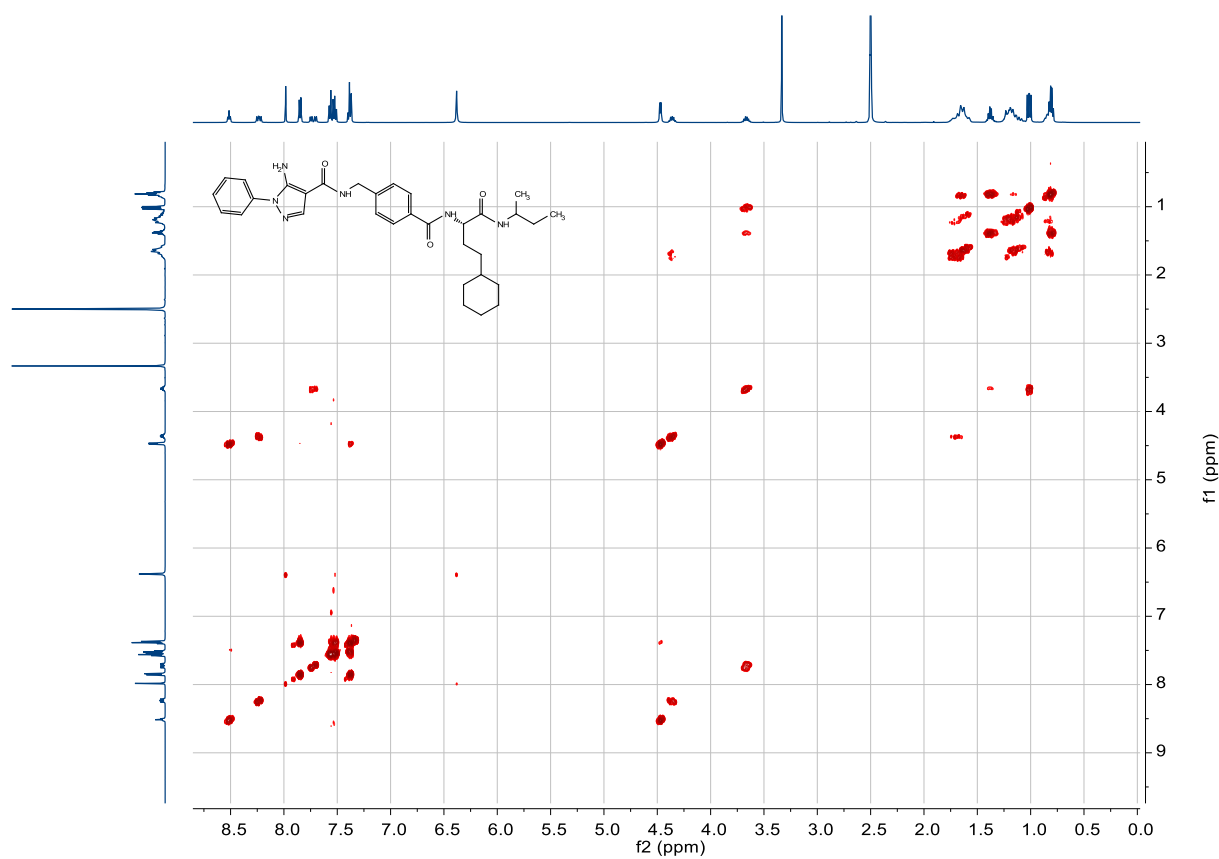


Figure 126. Compound 223 (SR63), <sup>13</sup>C-NMR, 126 MHz, DMSO-d<sub>6</sub>



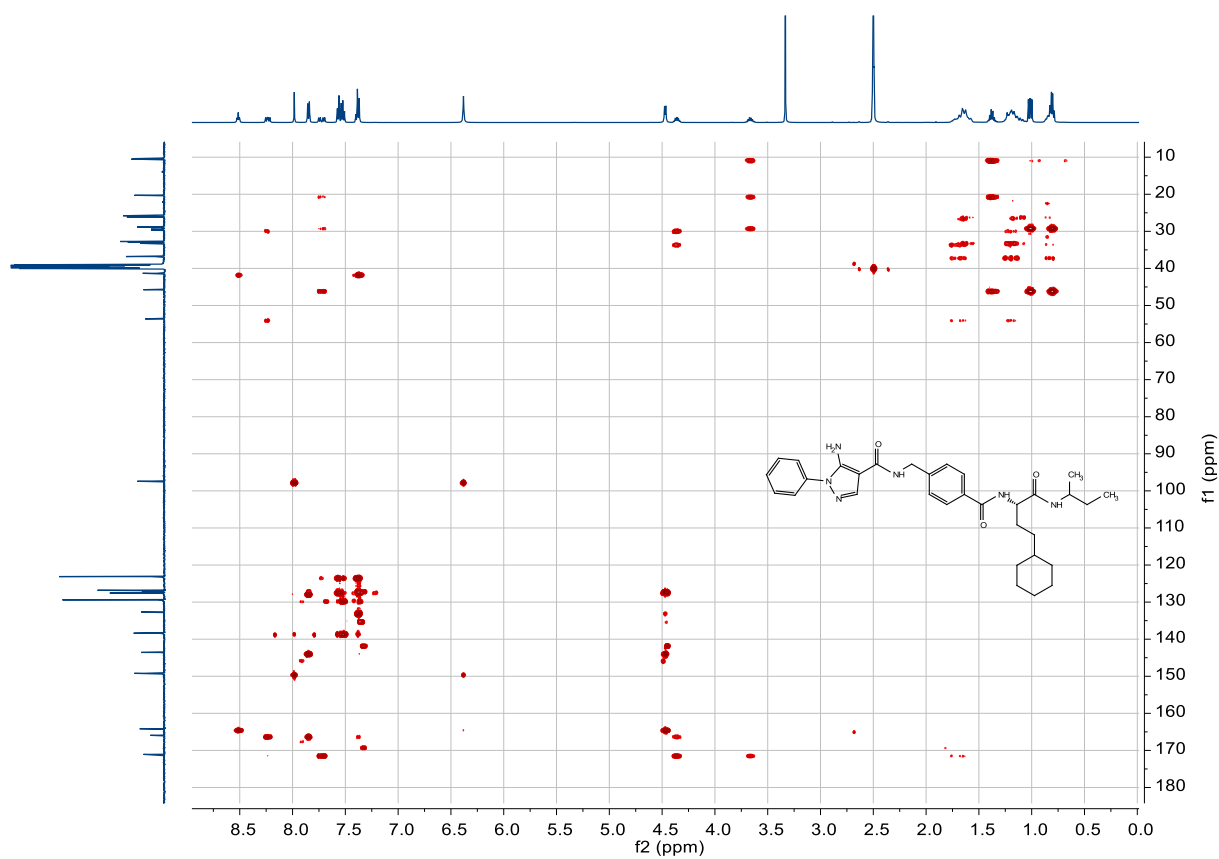


Figure 129. Compound **223** (SR63), HMBC, 500 MHz/ 126 MHz, DMSO- $d_6$

C:\User\...Knapp\2018\180711\SR63\_F6

7/11/2018 5:03:07 PM

SR63 mit HCCA gemessen.

SR63\_F6 #1-9 RT: 0.01-0.91 AV: 9 NL: 1.17E5

T: FTMS + p MALDI Full ms [400.00-800.00]

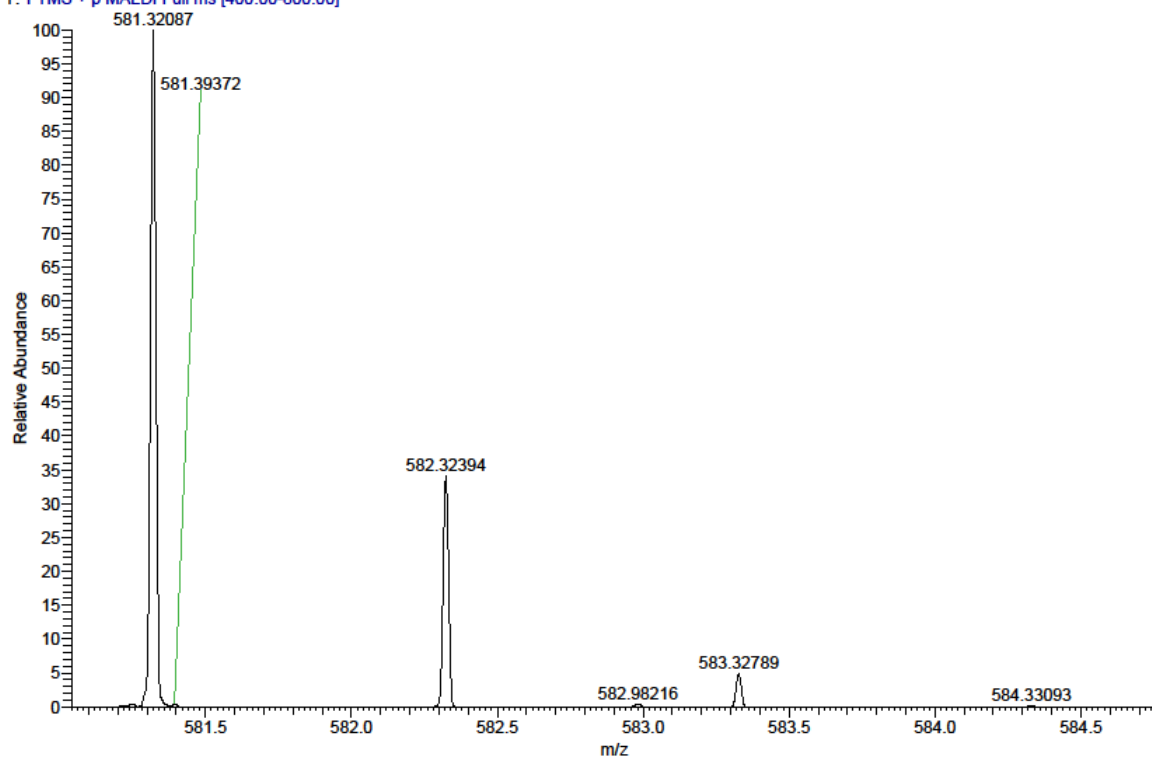


Figure 130. Compound **223** (SR63), HRMS (FTMS + p MALDI)

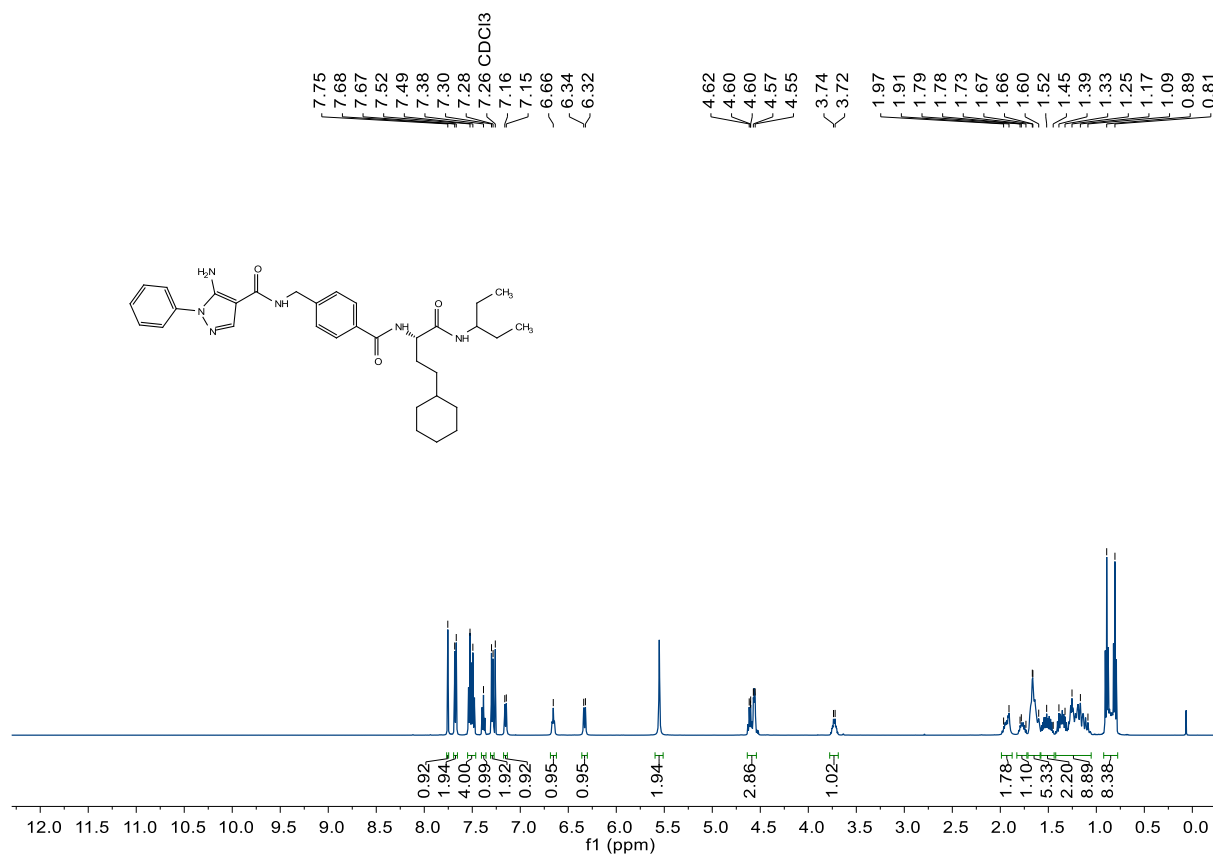


Figure 131. Compound 224 (SR65), <sup>1</sup>H-NMR, 500 MHz, DMSO-d<sub>6</sub>

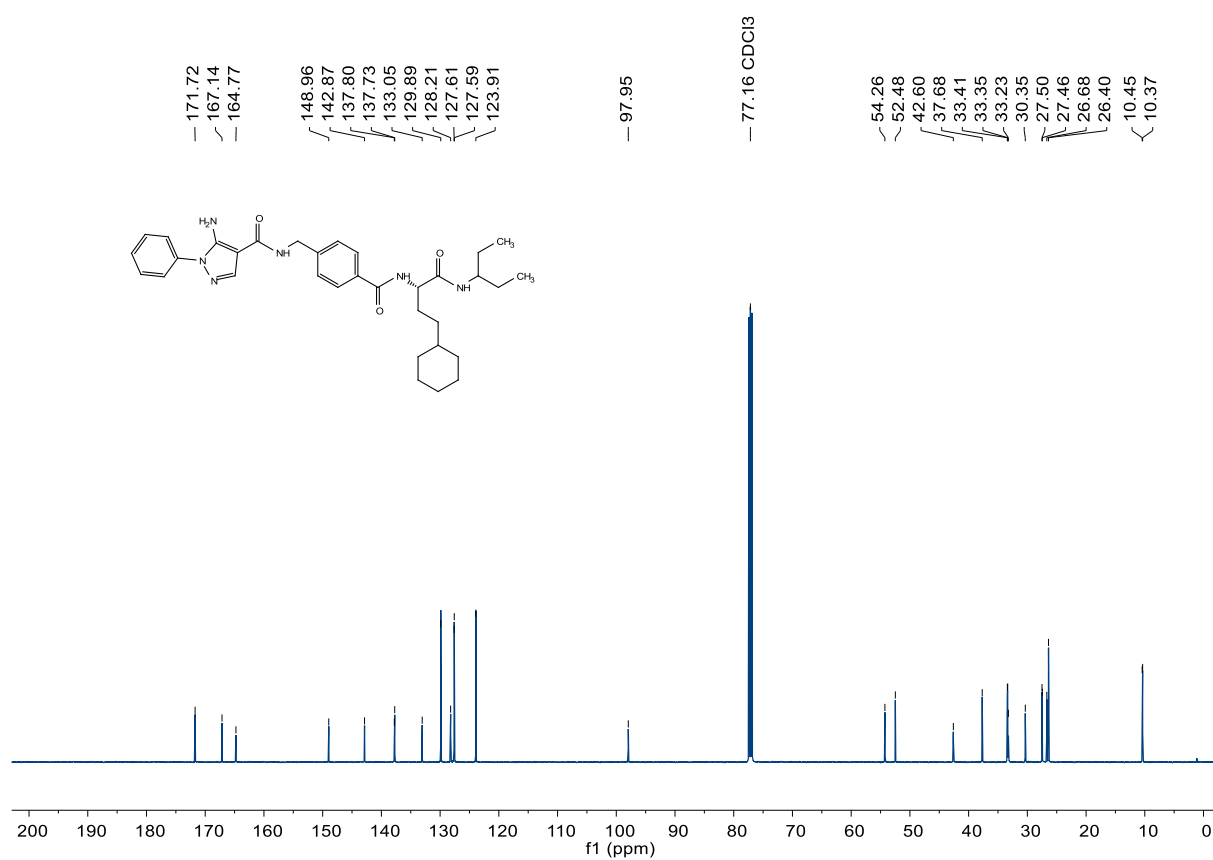
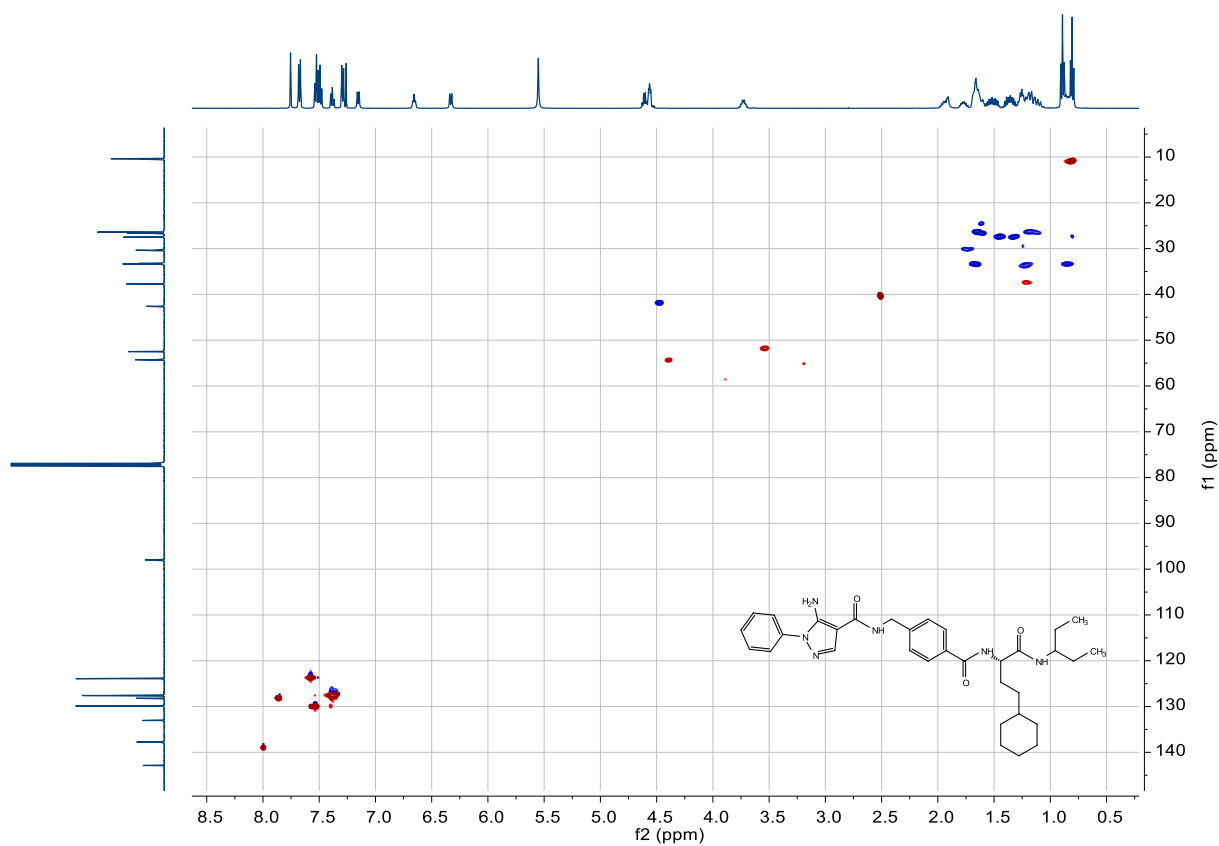
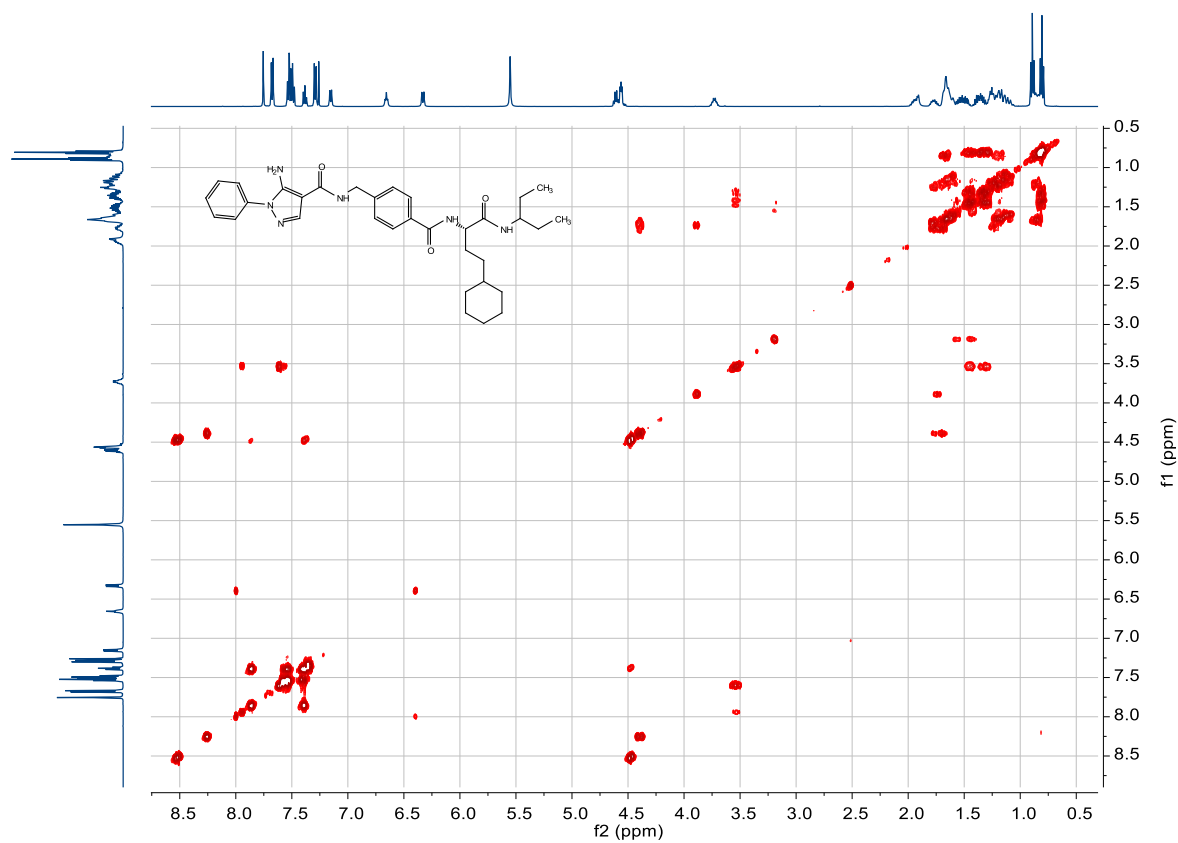


Figure 132. Compound 224 (SR65), <sup>13</sup>C-NMR, 126 MHz, DMSO-d<sub>6</sub>



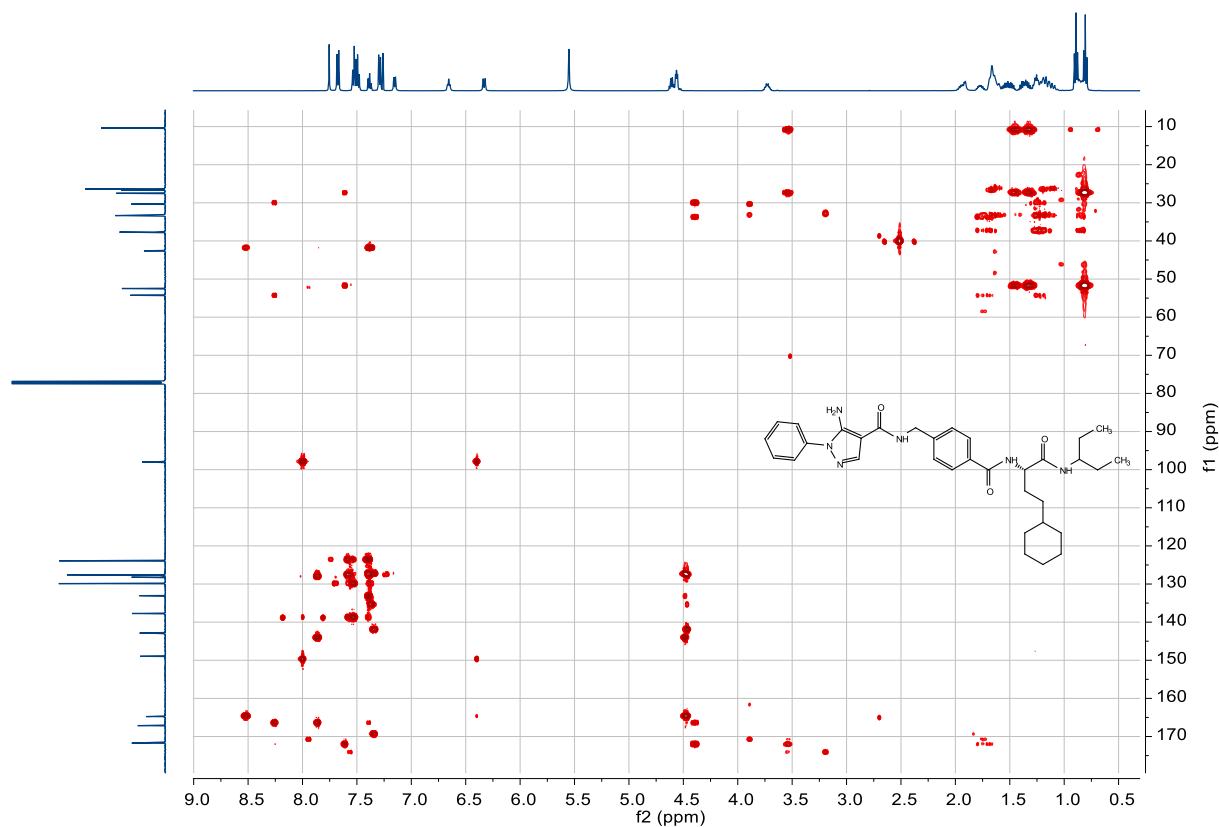


Figure 135. Compound 224 (SR65), HMBC, 500 MHz/ 126 MHz, DMSO- $d_6$

C:\User\...\Knapp\2018\180711\SR65\_G7

7/11/2018 5:21:49 PM

SR65 mit HCCA gemessen.

SR65\_G7 #1-6 RT: 0.01-0.43 AV: 6 NL: 4.15E6  
T: FTMS + p MALDI Full ms [400.00-800.00]

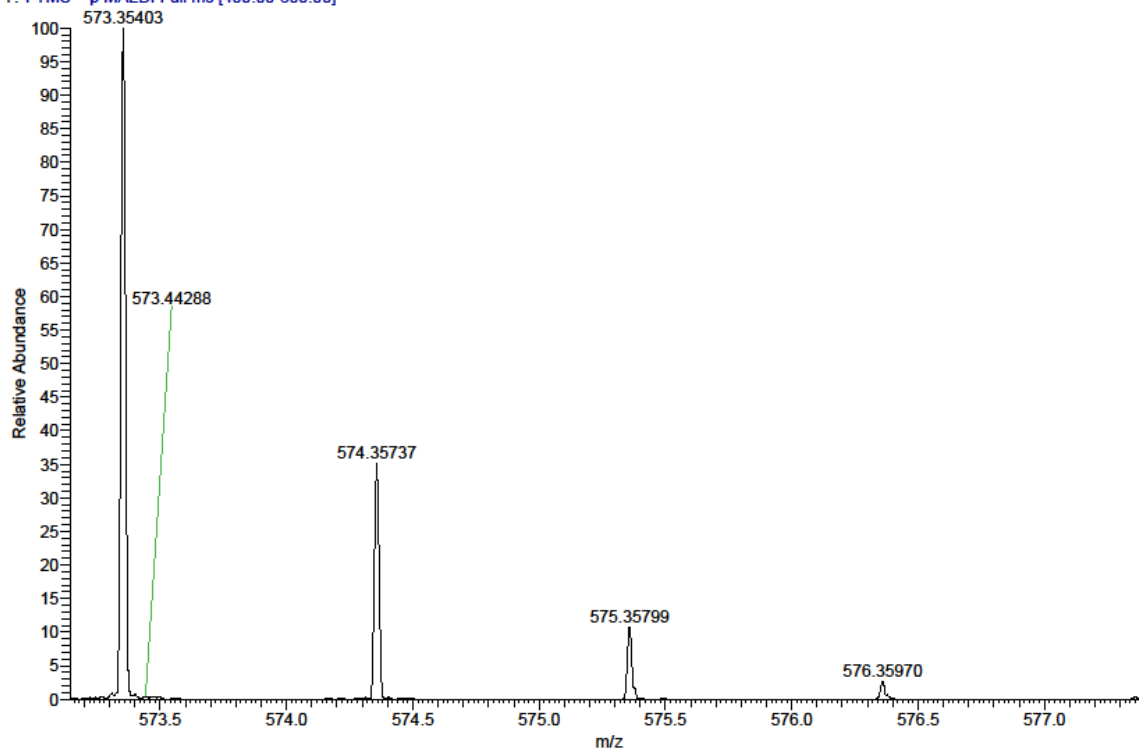


Figure 136. Compound 224 (SR65), HRMS (FTMS + p MALDI)

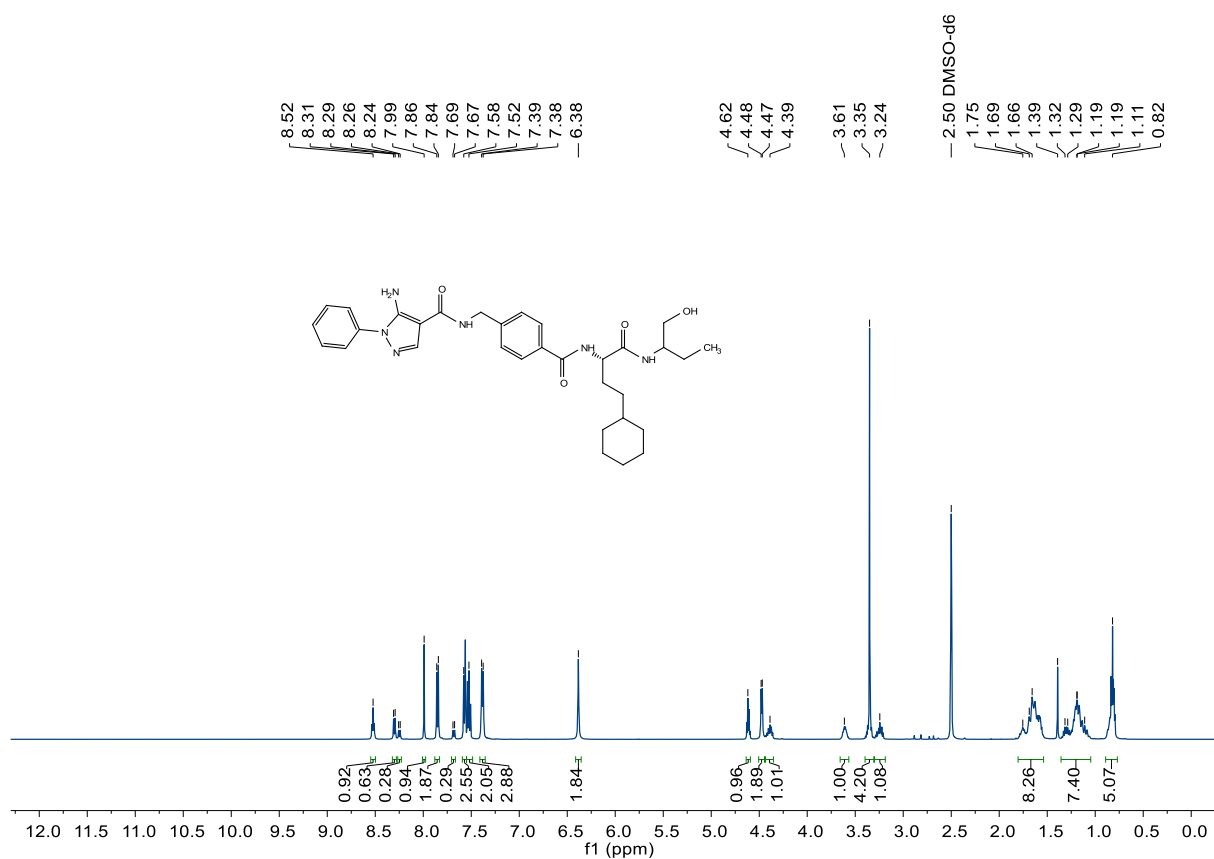


Figure 137. Compound 225 (SR103), <sup>1</sup>H-NMR, 500 MHz, DMSO-d<sub>6</sub>

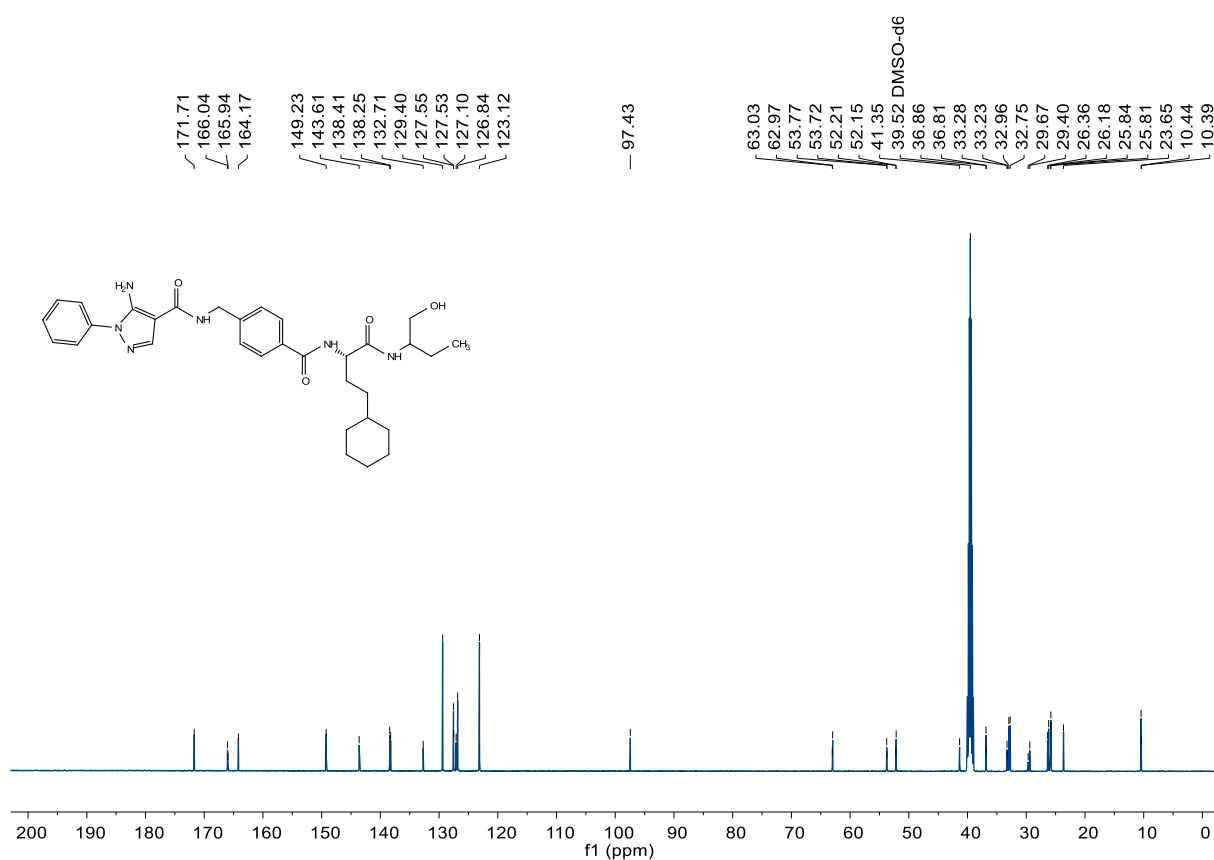


Figure 138. Compound 225 (SR103), <sup>13</sup>C-NMR, 126 MHz, DMSO-d<sub>6</sub>



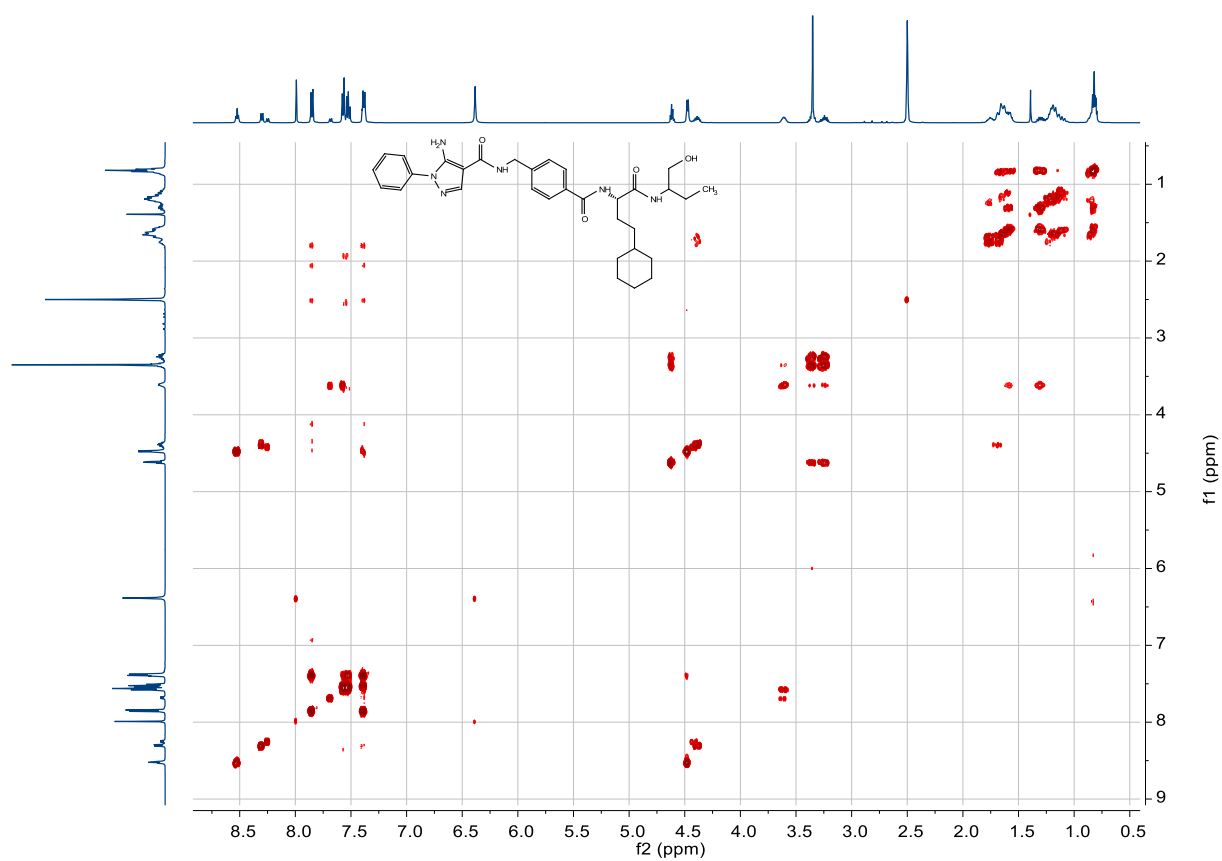


Figure 139. Compound 225 (SR103), COSY, 500 MHz, DMSO-*d*<sub>6</sub>

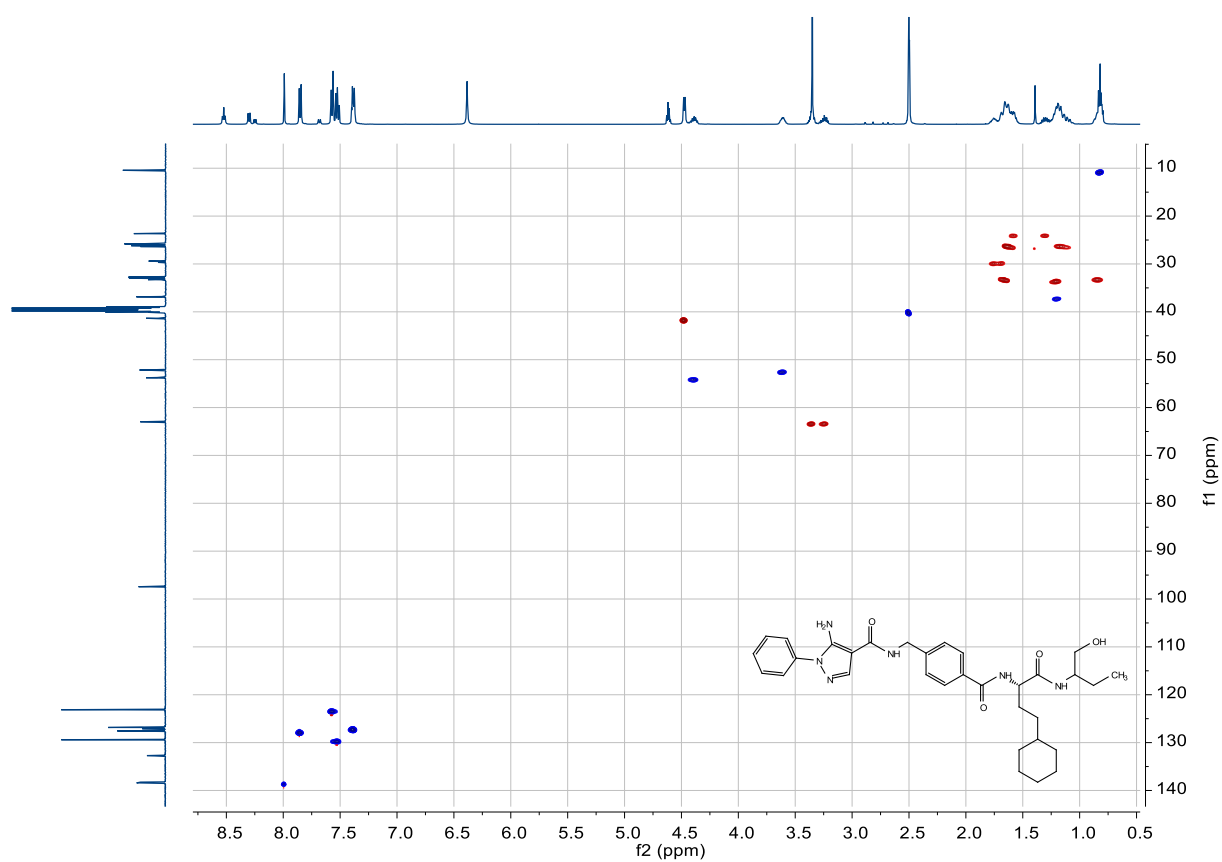


Figure 140. Compound 225 (SR103), HSQC, 500 MHz/ 126 MHz, DMSO-*d*<sub>6</sub>

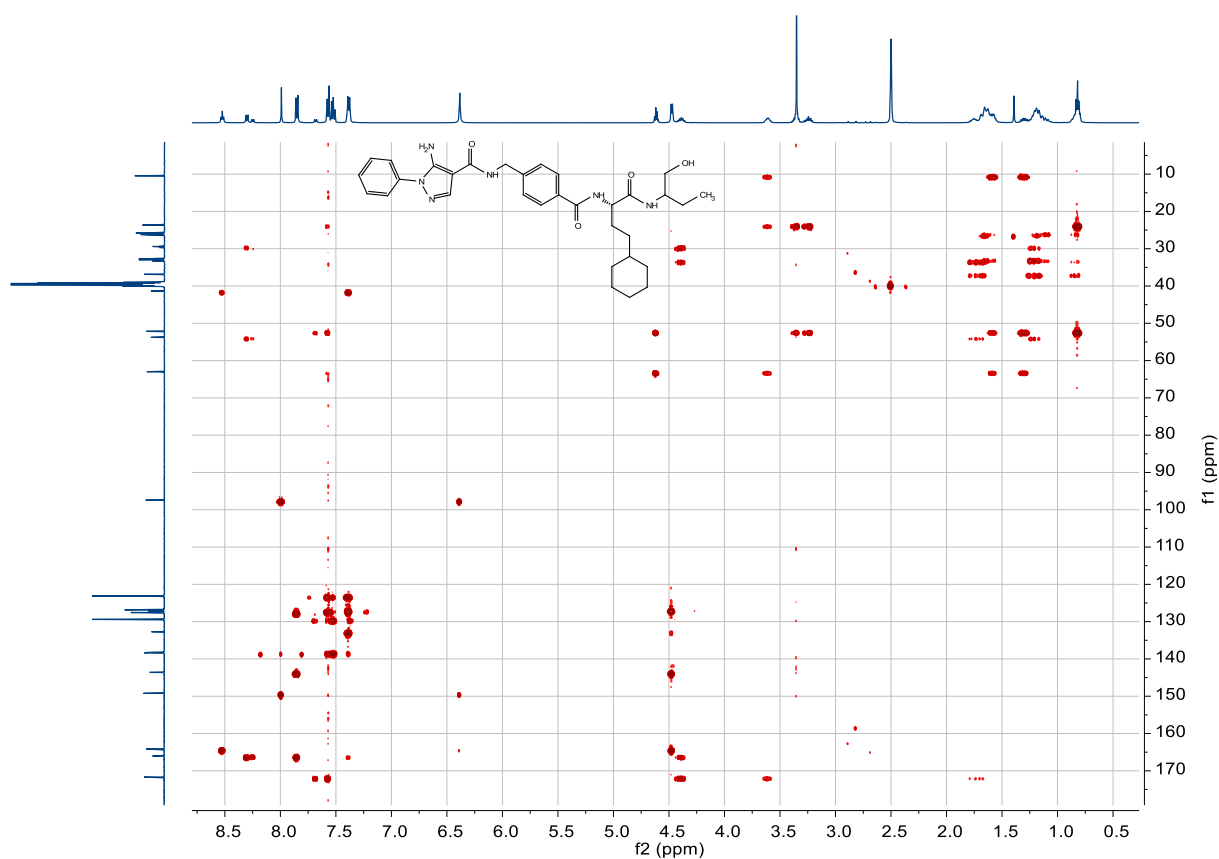


Figure 141. Compound 225 (SR103), HMBC, 500 MHz/ 126 MHz, DMSO- $d_6$

C:\User\...Knapp\2018\180921\SR103\_B1

9/21/2018 10:51:51 AM

SR103 mit HCCA gemessen.

SR103\_B1 #1-10 RT: 0.01-0.86 AV: 10 NL: 3.35E6

T: FTMS + p MALDI Full ms [400.00-750.00]

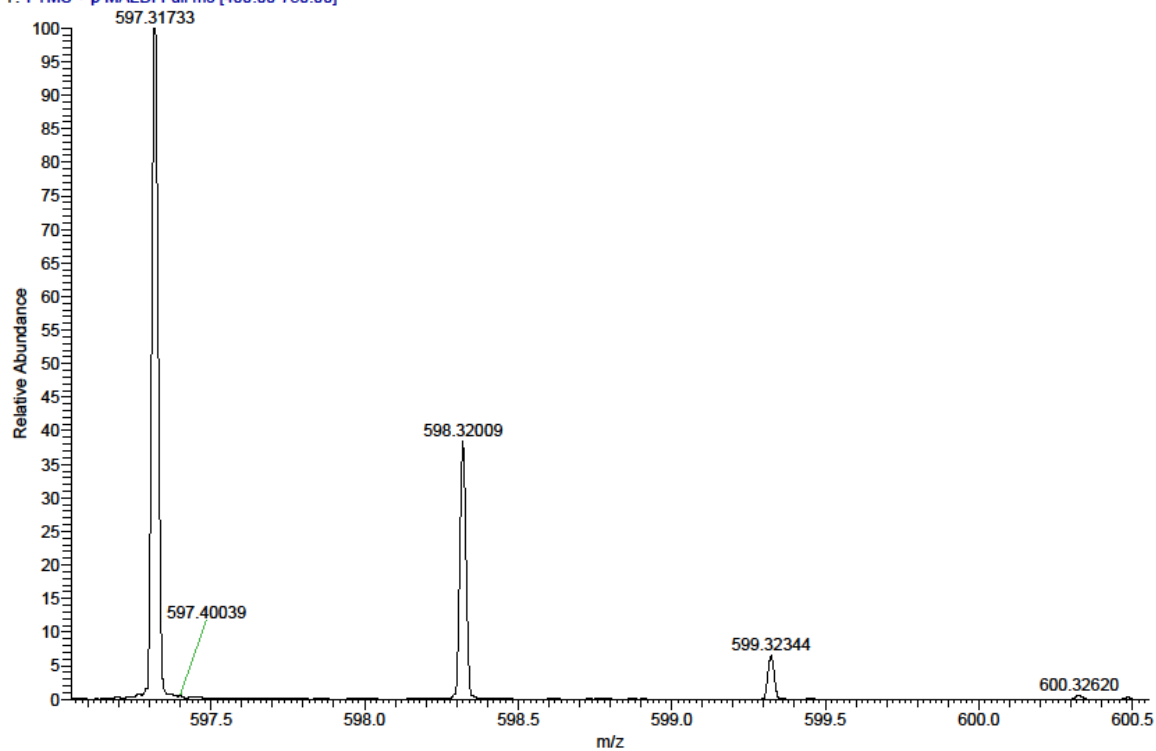


Figure 142. Compound 225 (SR103), HRMS (FTMS + p MALDI)

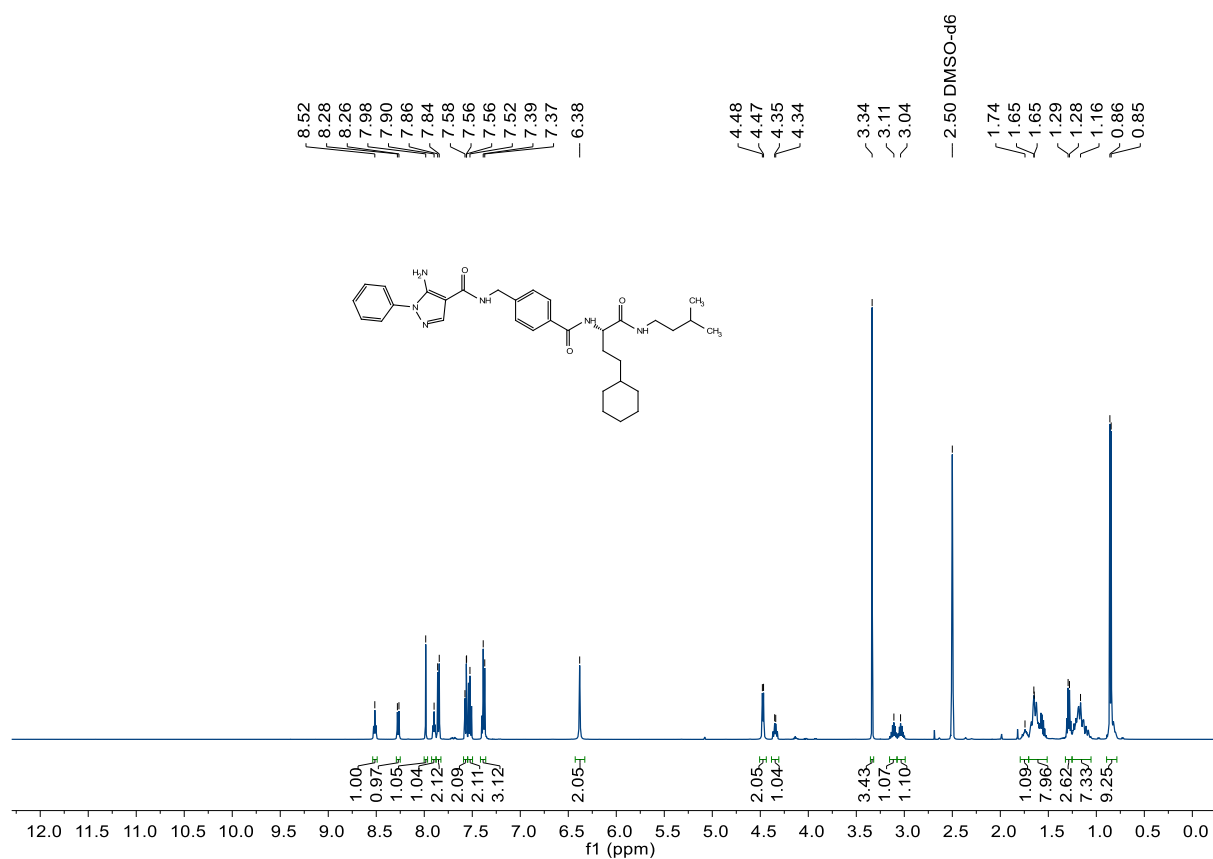


Figure 143. Compound 226 (SR68), <sup>1</sup>H-NMR, 500 MHz, DMSO-d<sub>6</sub>

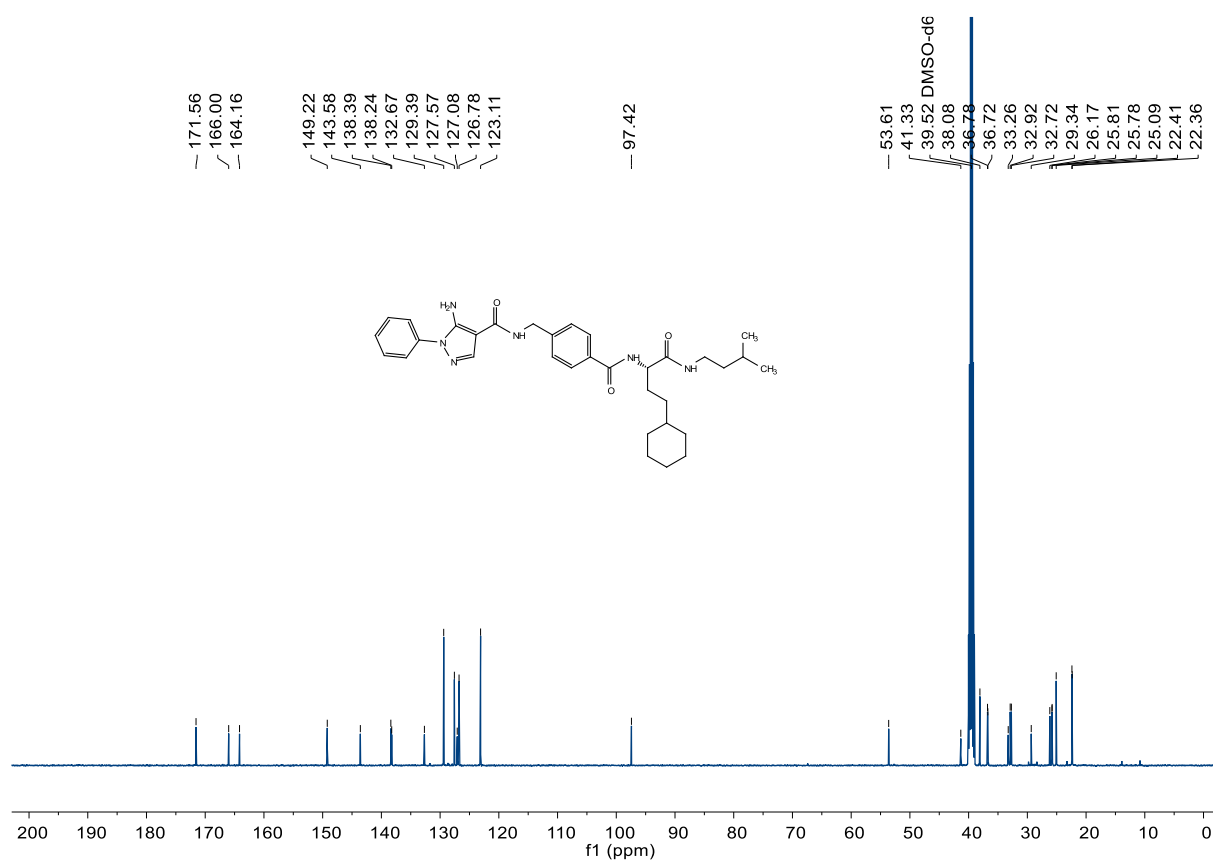
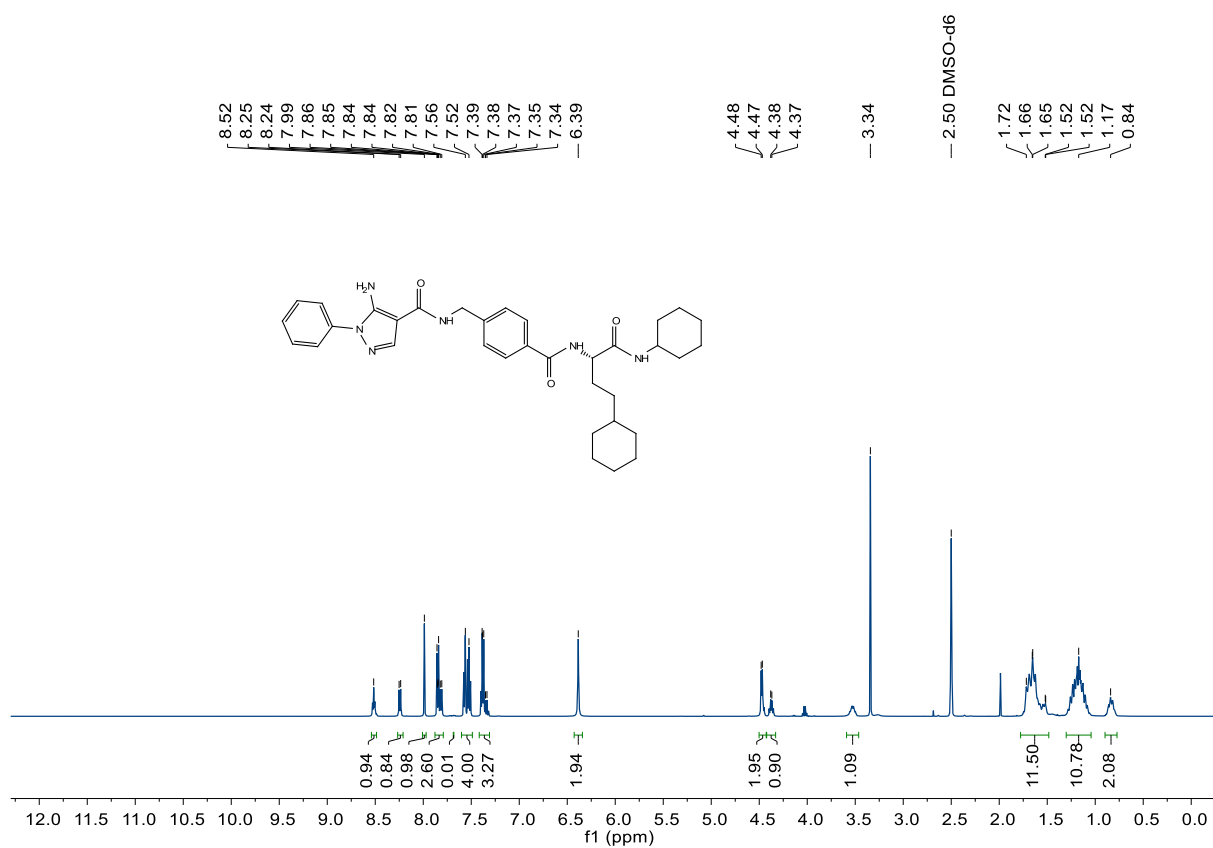
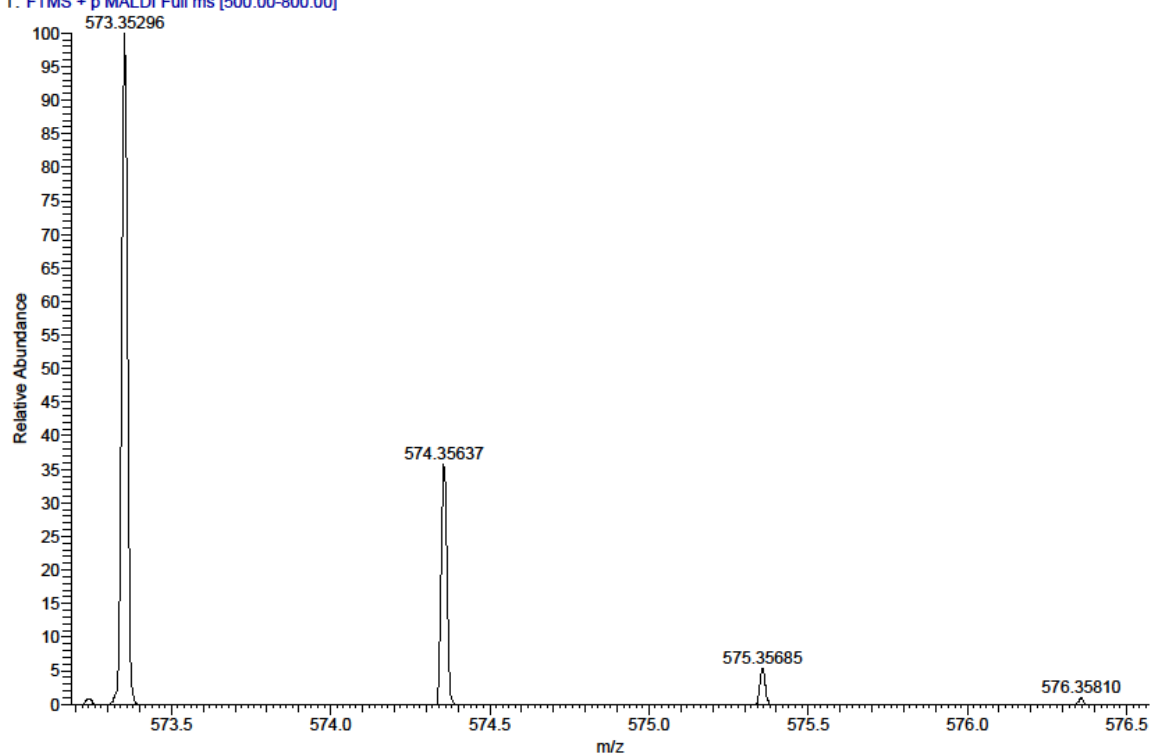


Figure 144. Compound 226 (SR68), <sup>13</sup>C-NMR, 126 MHz, DMSO-d<sub>6</sub>

SR68\_C12 #1-3 RT: 0.01-0.26 AV: 3 NL: 9.45E4  
T: FTMS + p MALDI Full ms [500.00-800.00]

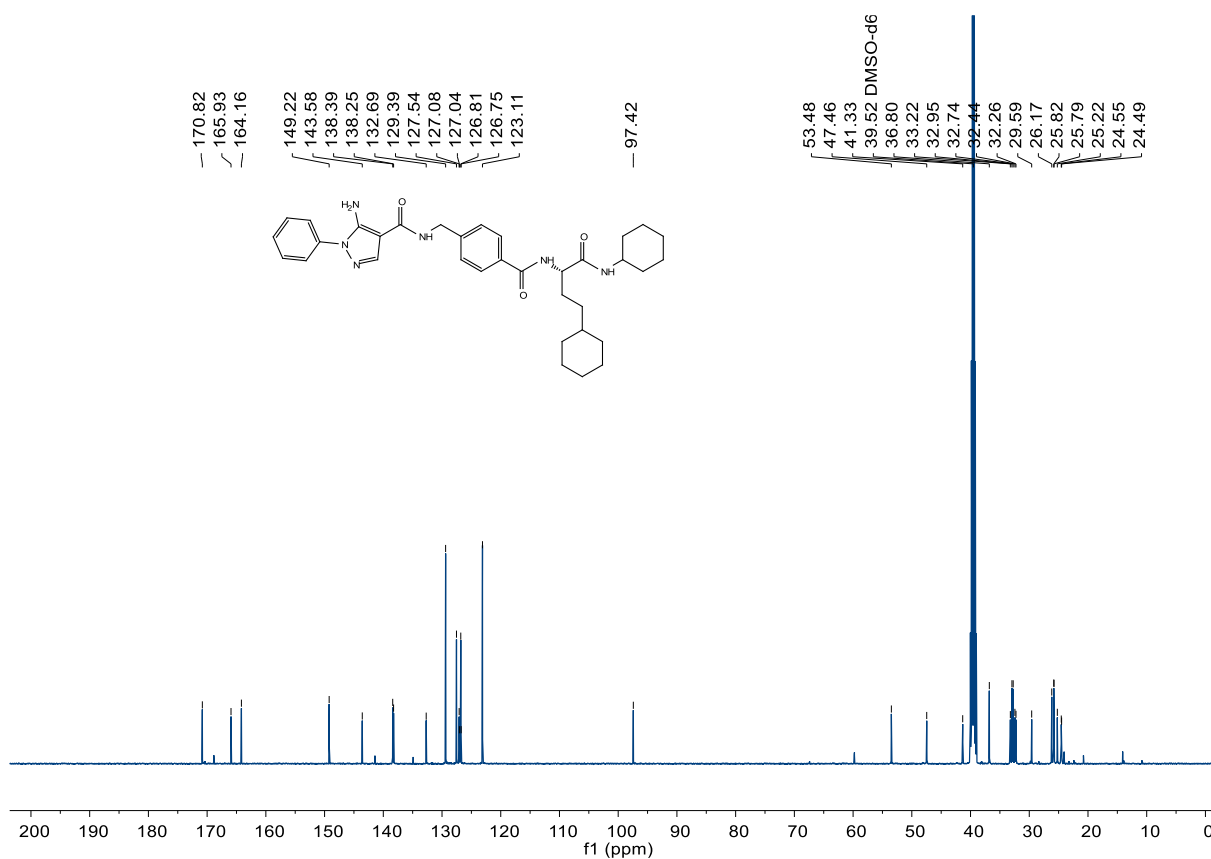


Figure 147. Compound 227 (SR69), <sup>13</sup>C-NMR, 126 MHz, DMSO-d<sub>6</sub>

C:\User\...\Knapp\2018\180921\SR69\_B3

9/21/2018 10:55:15 AM

SR69 mit HCCA gemessen.

SR69\_B3 #1-12 RT: 0.00-1.10 AV: 12 NL: 2.86E5  
T: FTMS + p MALDI Full ms [400.00-750.00]

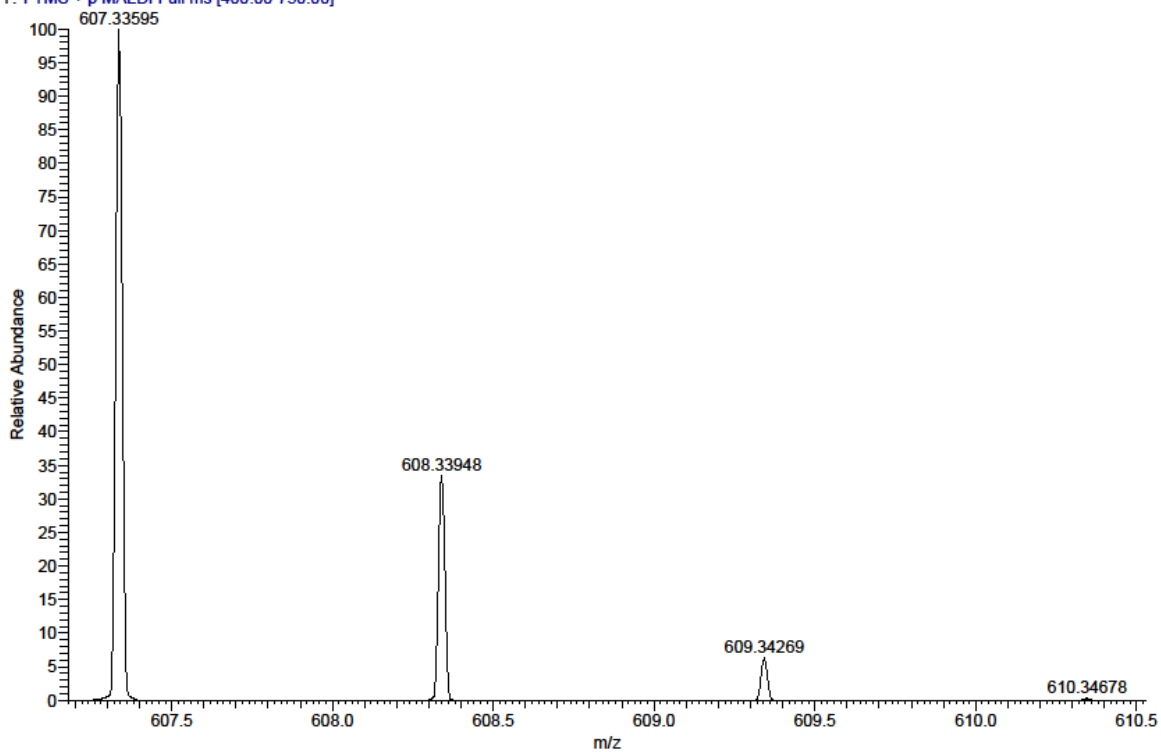


Figure 148. Compound 227 (SR69), HRMS (FTMS + p MALDI)

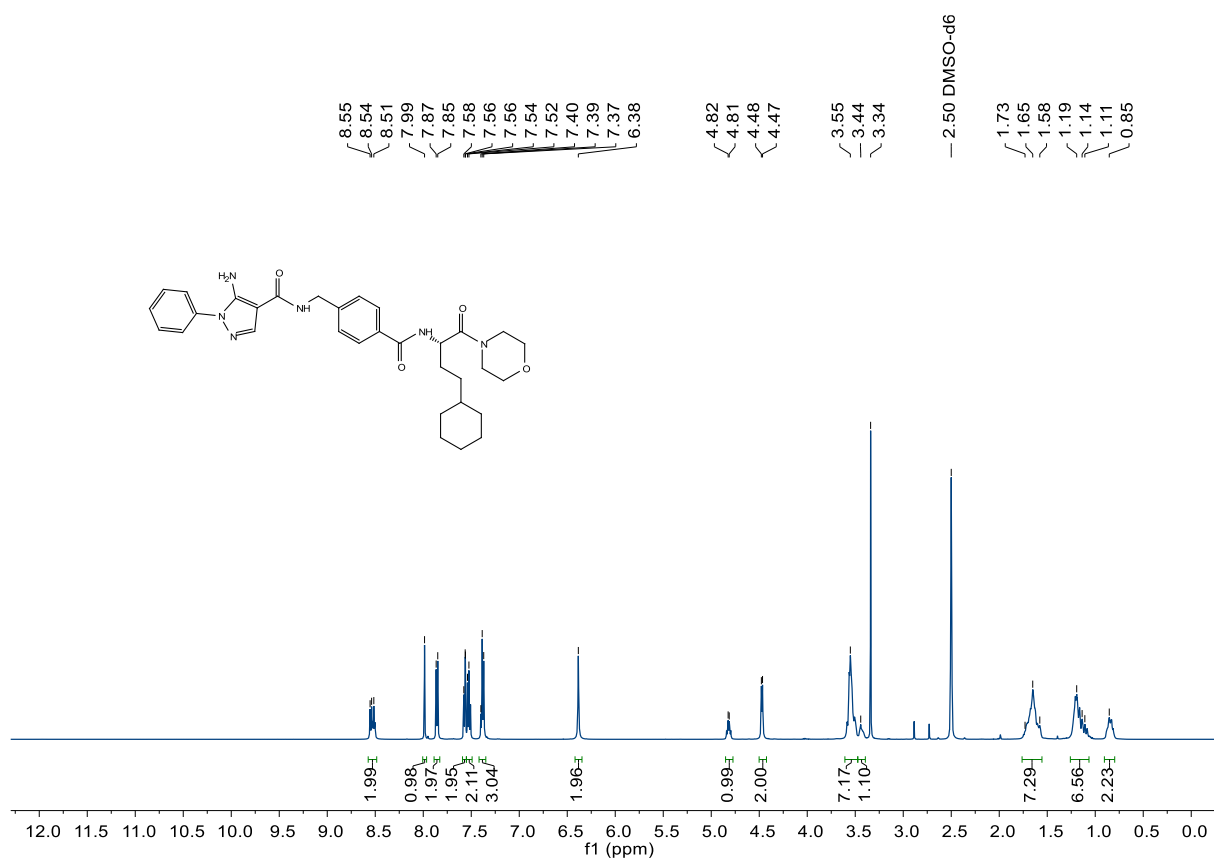


Figure 149. Compound 228 (SR141), <sup>1</sup>H-NMR, 500 MHz, DMSO-d<sub>6</sub>

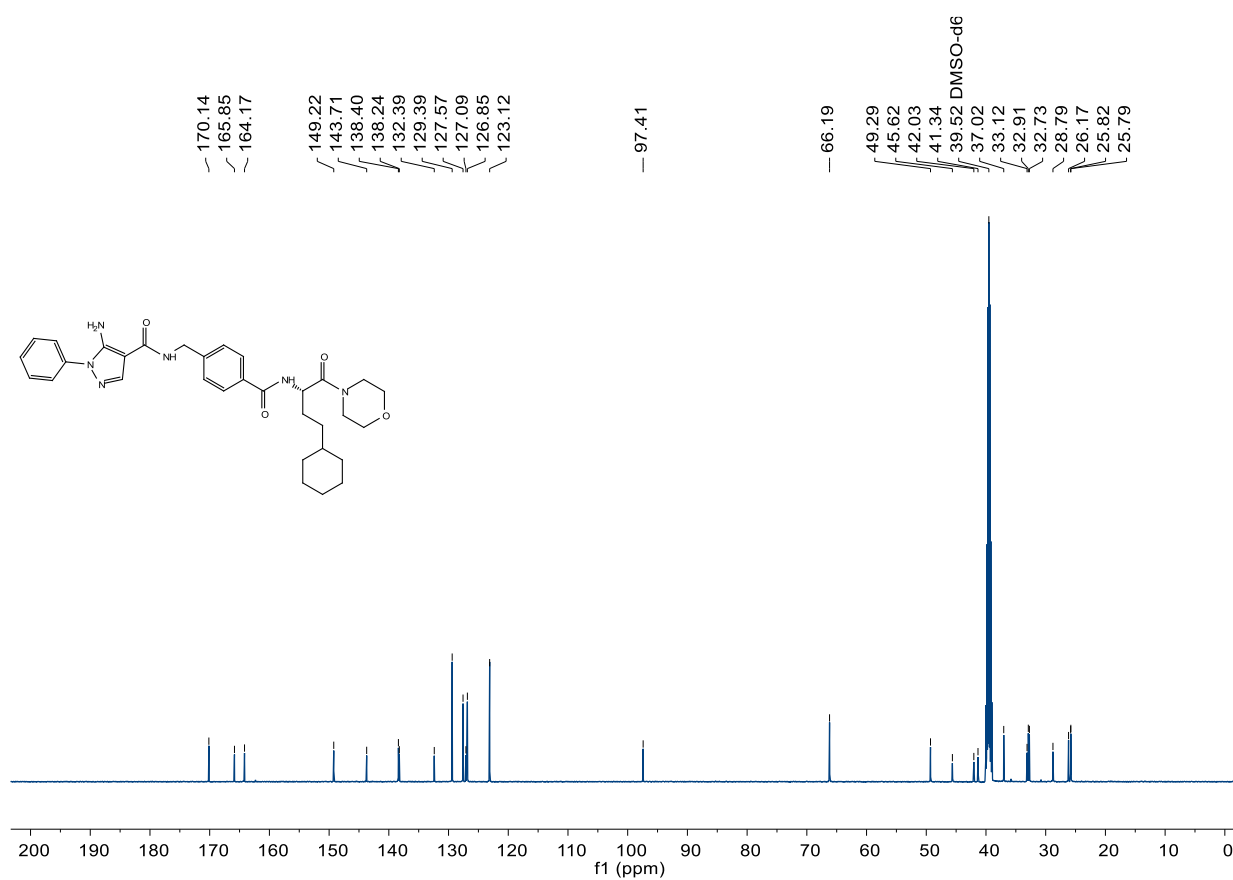


Figure 150. Compound 228 (SR141), <sup>13</sup>C-NMR, 126 MHz, DMSO-d<sub>6</sub>

C:\User\...\Knapp\2018\180308\SR141\_C5

3/8/2018 3:32:33 PM

SR141 mit HCCA gemessen.

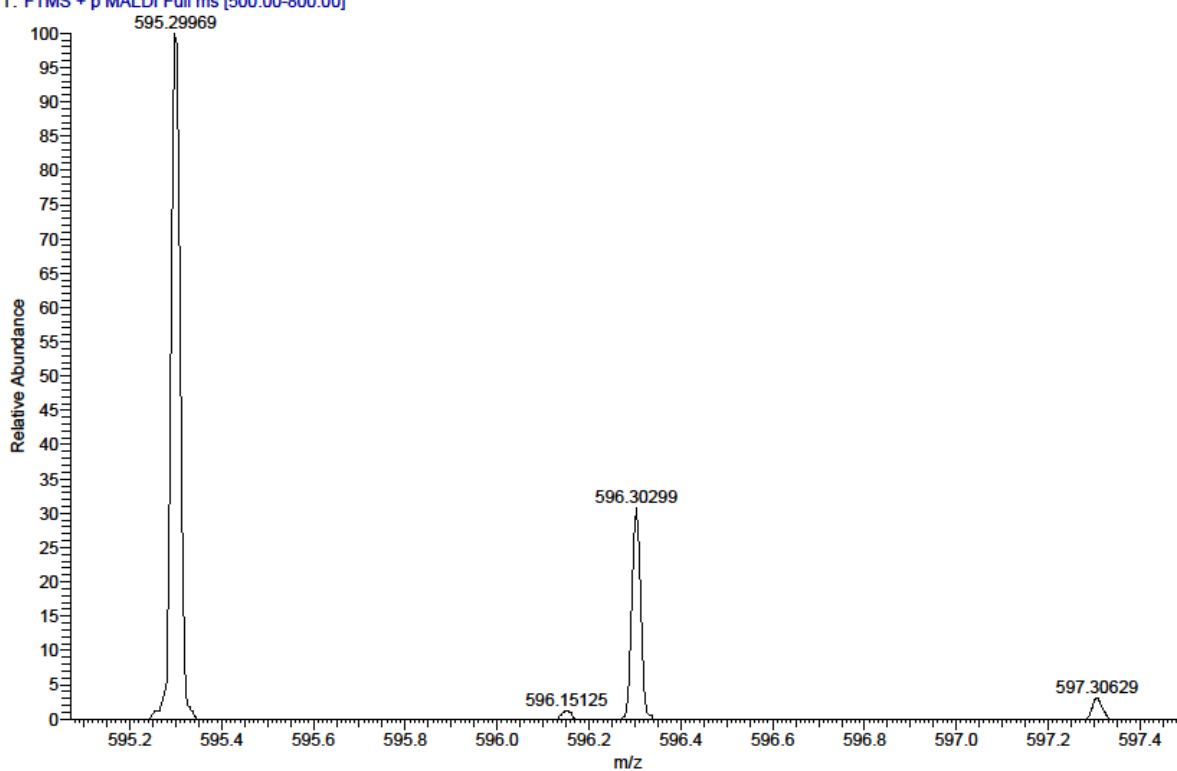
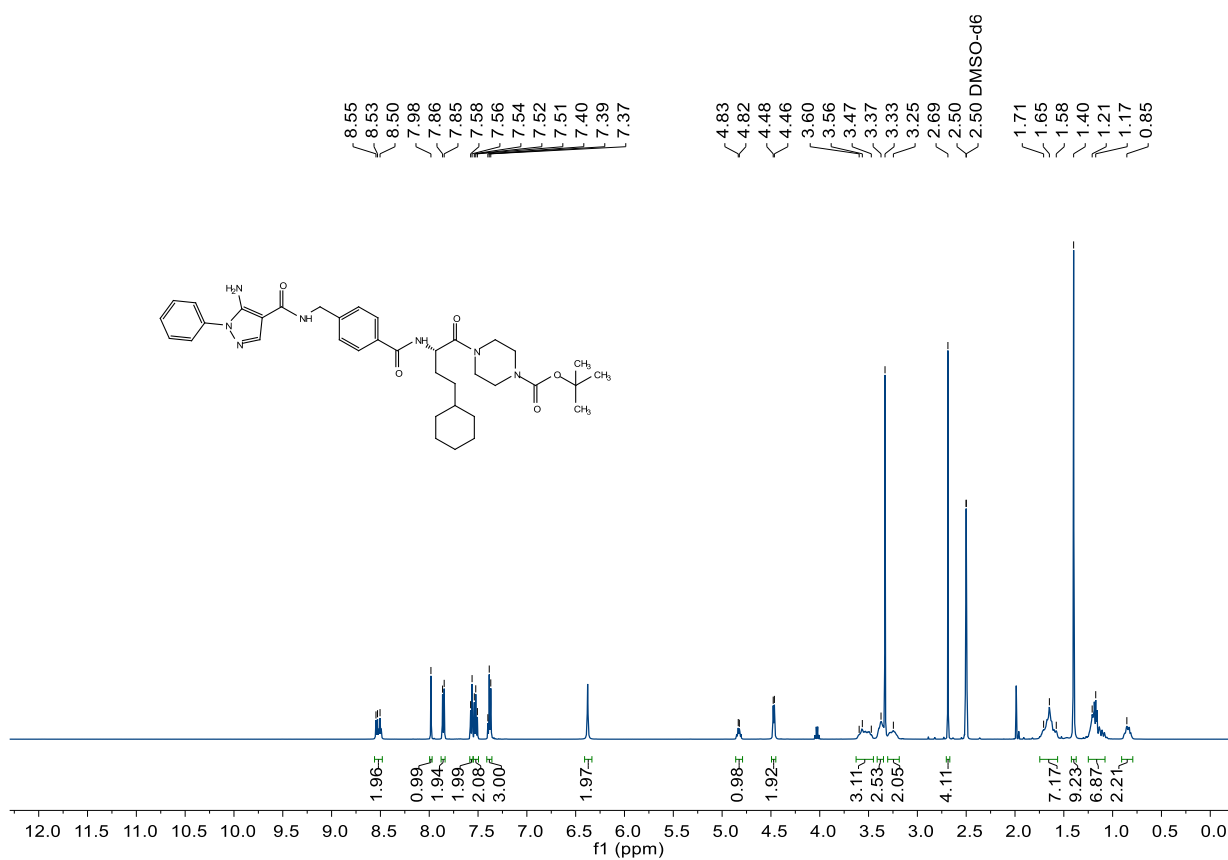
SR141\_C5 #1-8 RT: 0.01-0.84 AV: 8 NL: 3.49E4  
T: FTMS + p MALDI Full ms [500.00-800.00]

Figure 151. Compound 228 (SR141), HRMS (FTMS + p MALDI)

Figure 152. Compound 229 (SR142), <sup>1</sup>H-NMR, 500 MHz, DMSO-d<sub>6</sub>

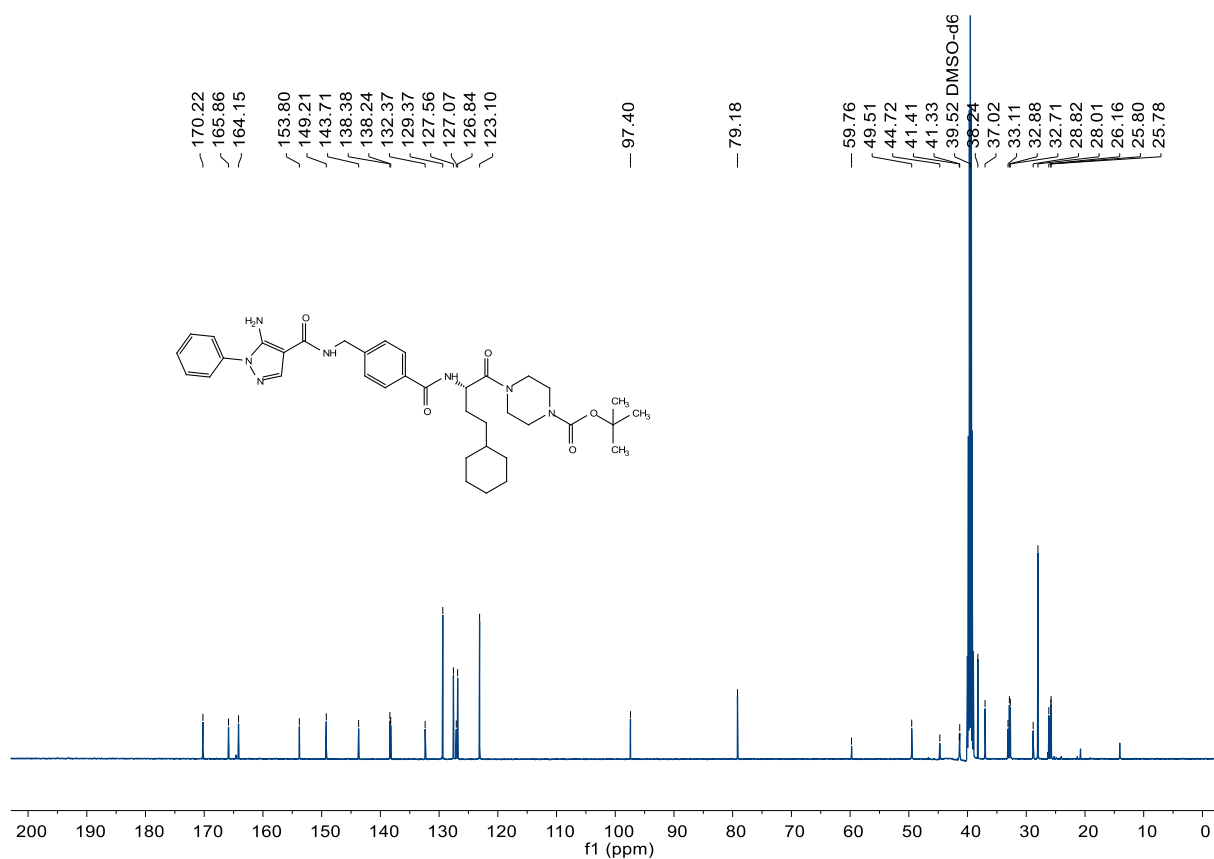


Figure 153. Compound 229 (SR142), <sup>13</sup>C-NMR, 126 MHz, DMSO-d<sub>6</sub>

C:\User\...Knapp\2018\180308\SR142\_C8

3/8/2018 3:37:32 PM

SR142 mit HCCA gemessen.

SR142\_C8 #1-8 RT: 0.01-0.70 AV: 8 NL: 1.23E5

T: FTMS + p MALDI Full ms [500.00-800.00]

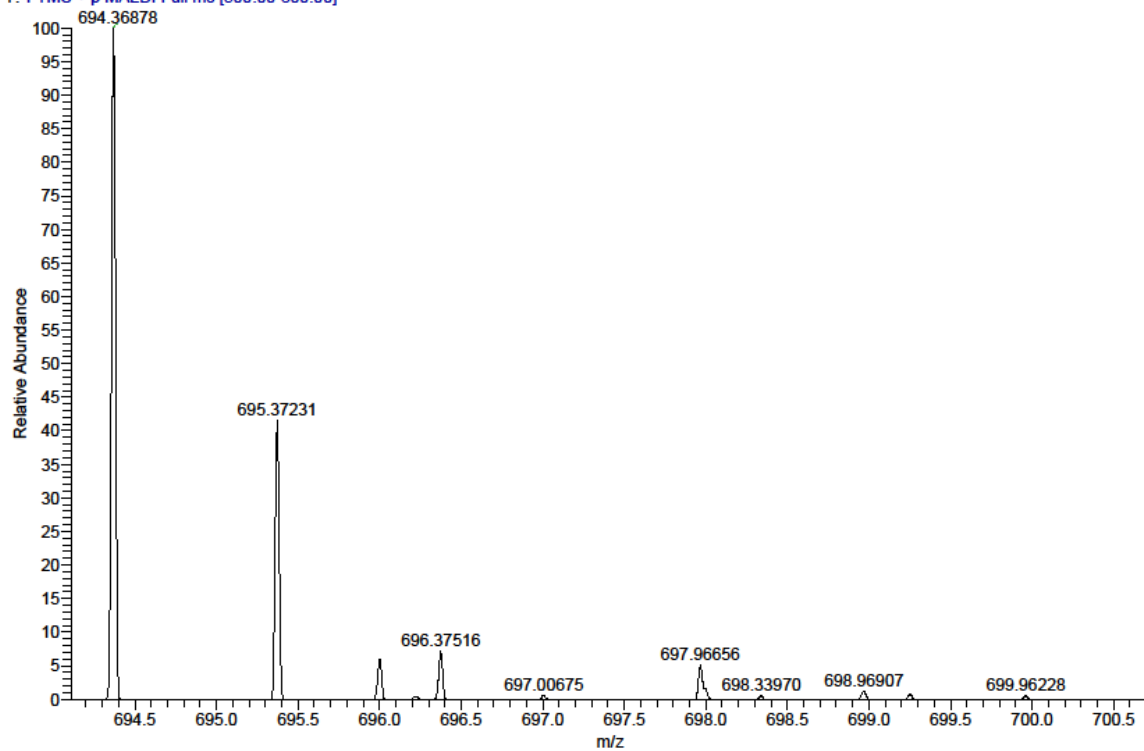


Figure 154. Compound 229 (SR142), HRMS (FTMS + p MALDI)



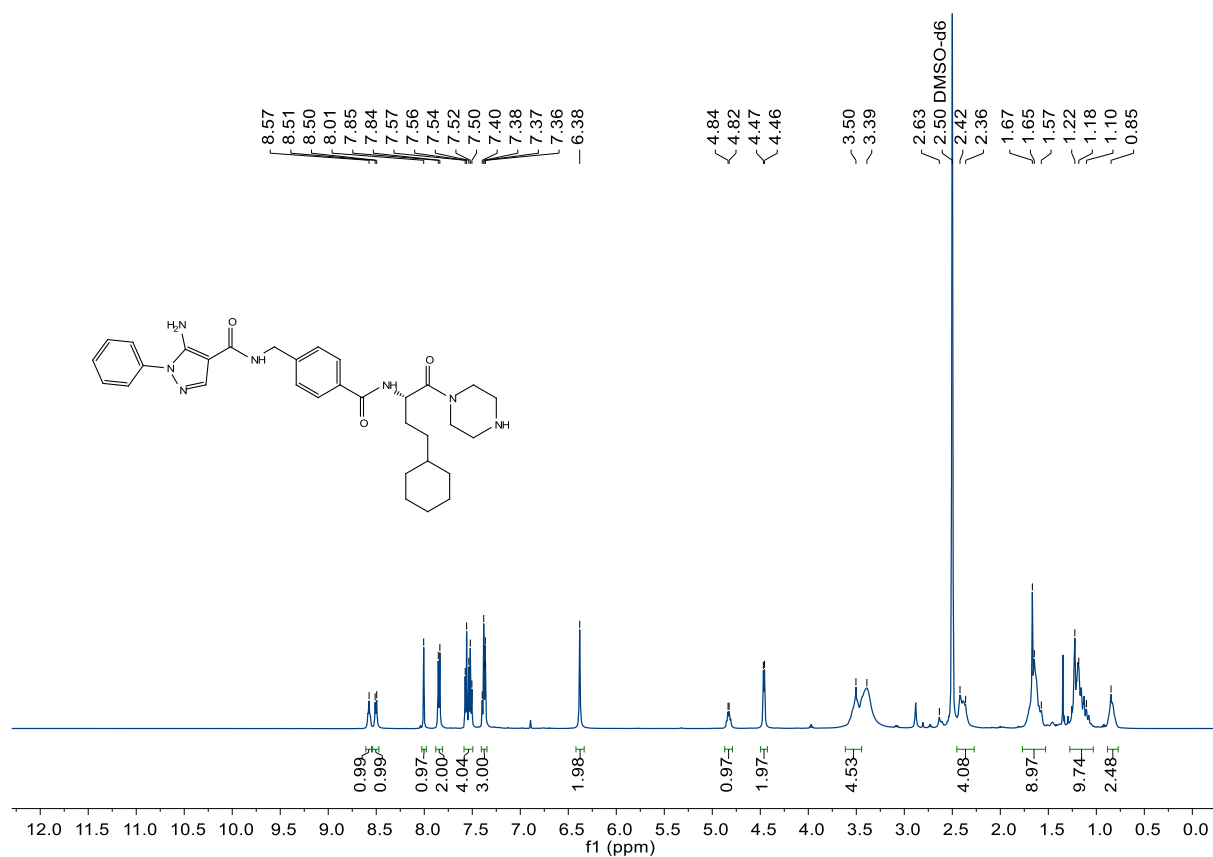


Figure 155. Compound 230 (SR154),  $^1\text{H-NMR}$ , 500 MHz,  $\text{DMSO-d}_6$

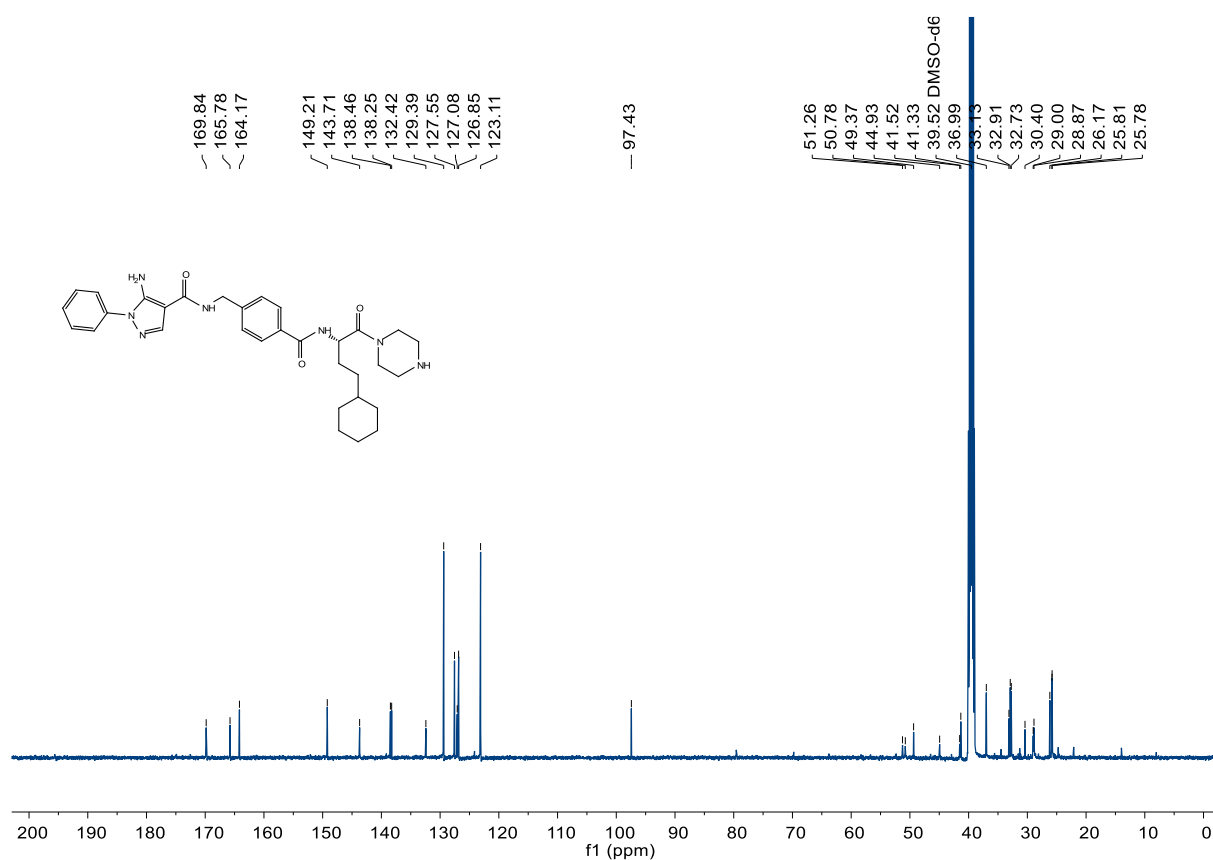


Figure 156. Compound 230 (SR154),  $^{13}\text{C-NMR}$ , 126 MHz,  $\text{DMSO-d}_6$

SR154\_D4 #1-20 RT: 0.00-2.27 AV: 20 NL: 2.14E4  
T: FTMS + p MALDI Full ms [500.00-800.00]

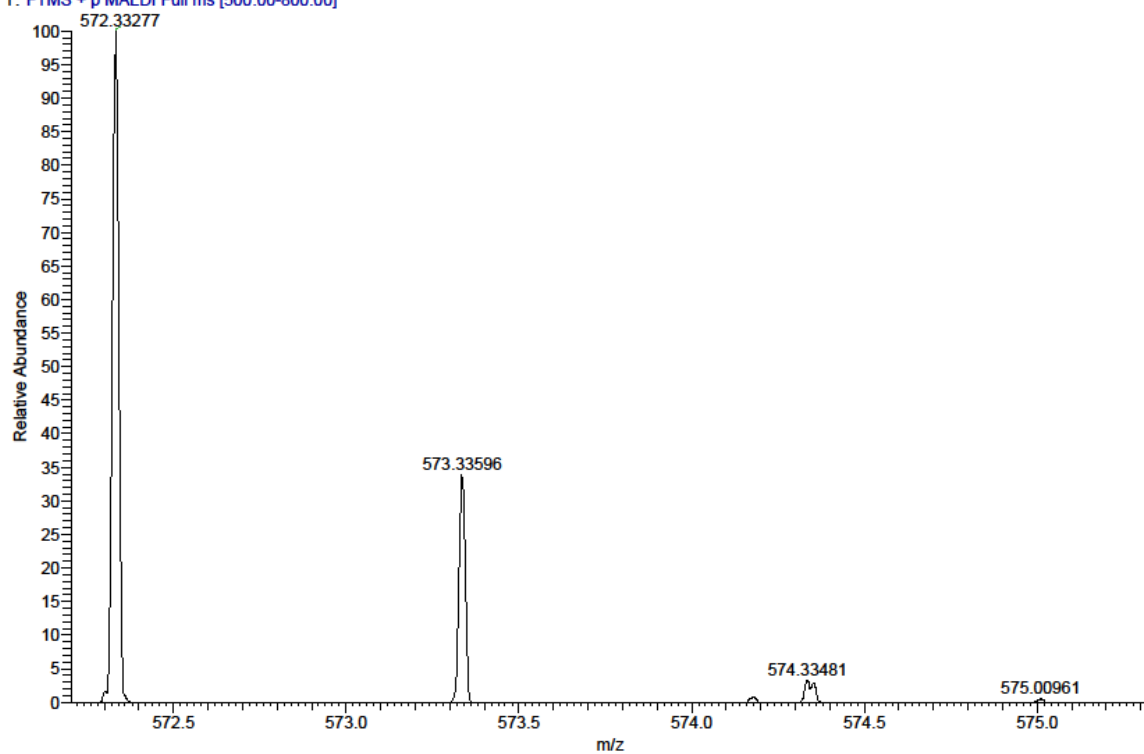


Figure 157. Compound 230 (SR154), HRMS (FTMS + p MALDI)

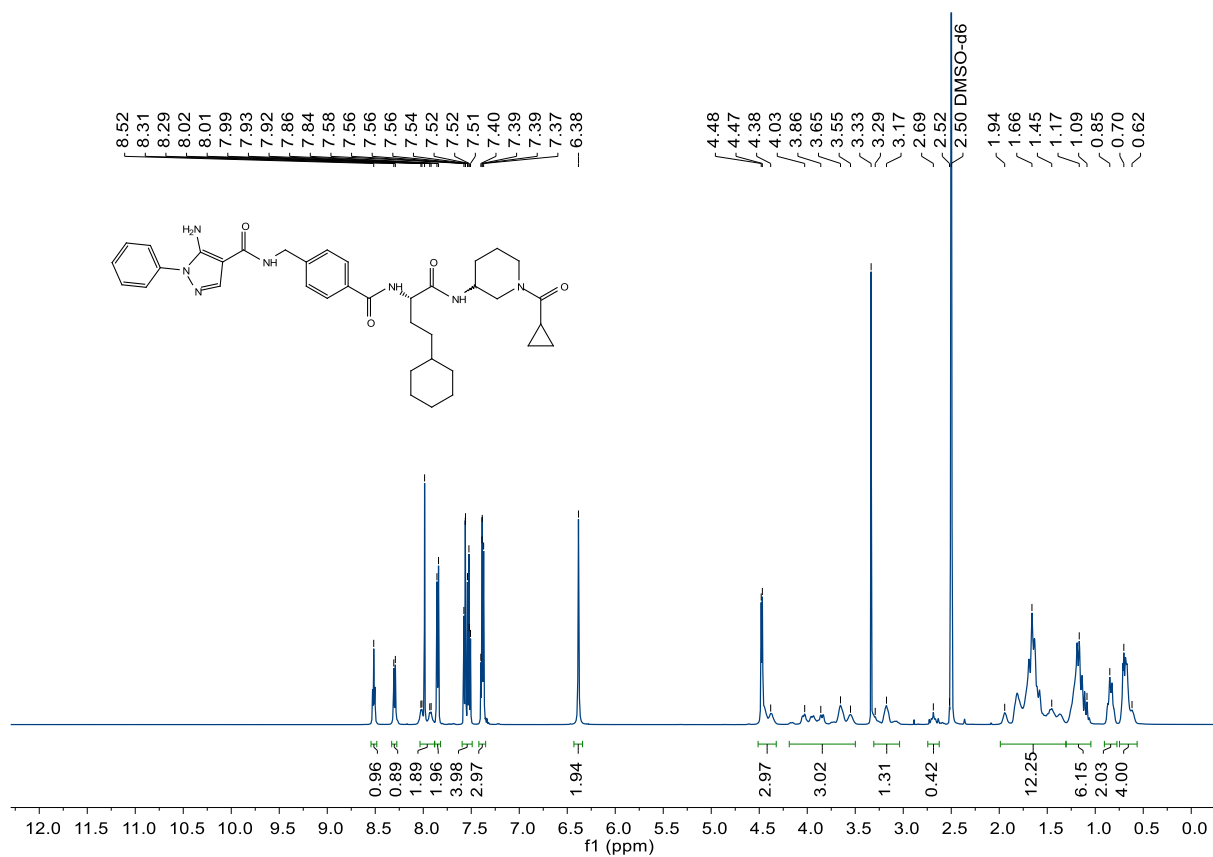


Figure 158. Compound 231 (SR160), <sup>1</sup>H-NMR, 500 MHz, DMSO-d<sub>6</sub>

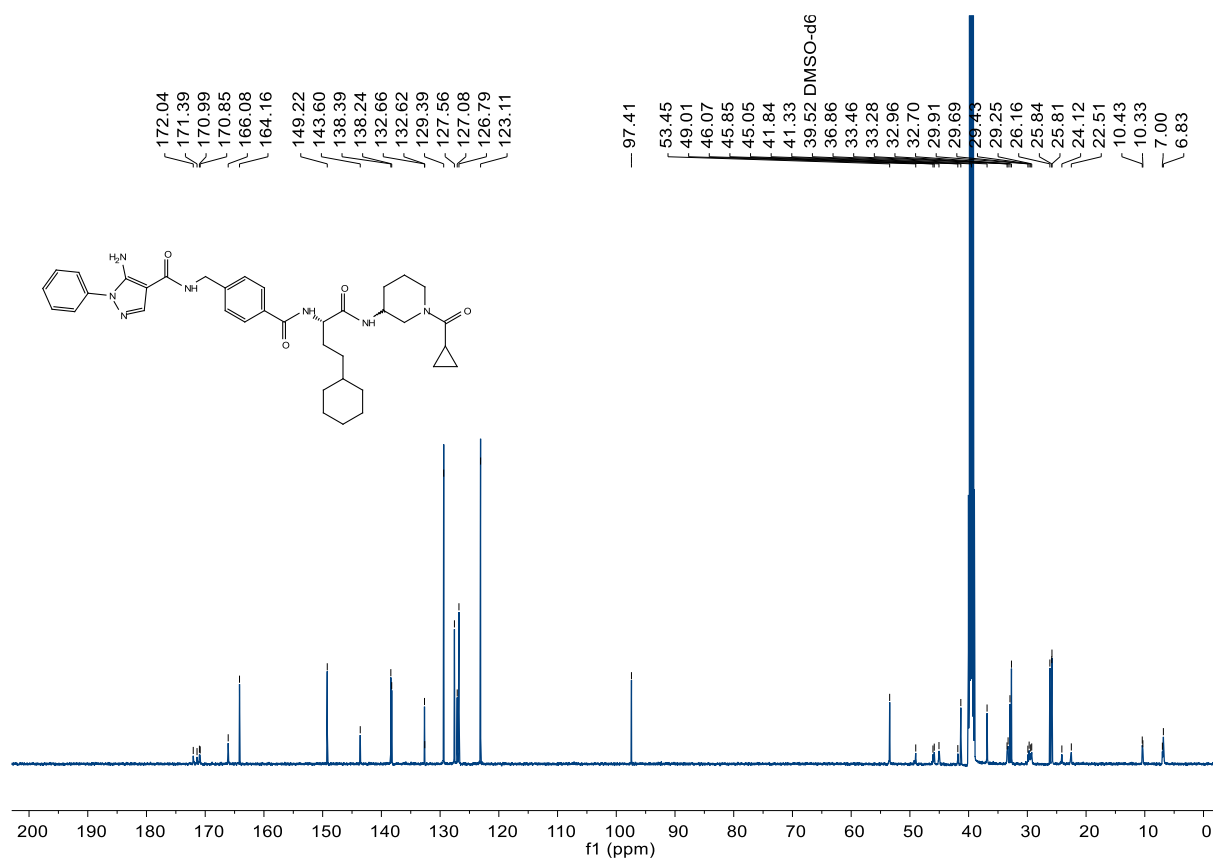


Figure 159. Compound 231 (SR160),  $^{13}\text{C}$ -NMR, 126 MHz,  $\text{DMSO-d}_6$

C:\User\...\Knapp2018\180319\SR160\_D6

3/19/2018 2:43:24 PM

SR160 mit HCCA gemessen.

SR160\_D6 #1-3 RT: 0.00-0.19 AV: 3 NL: 1.43E5  
T: FTMS + p MALDI Full ms [500.00-800.00]

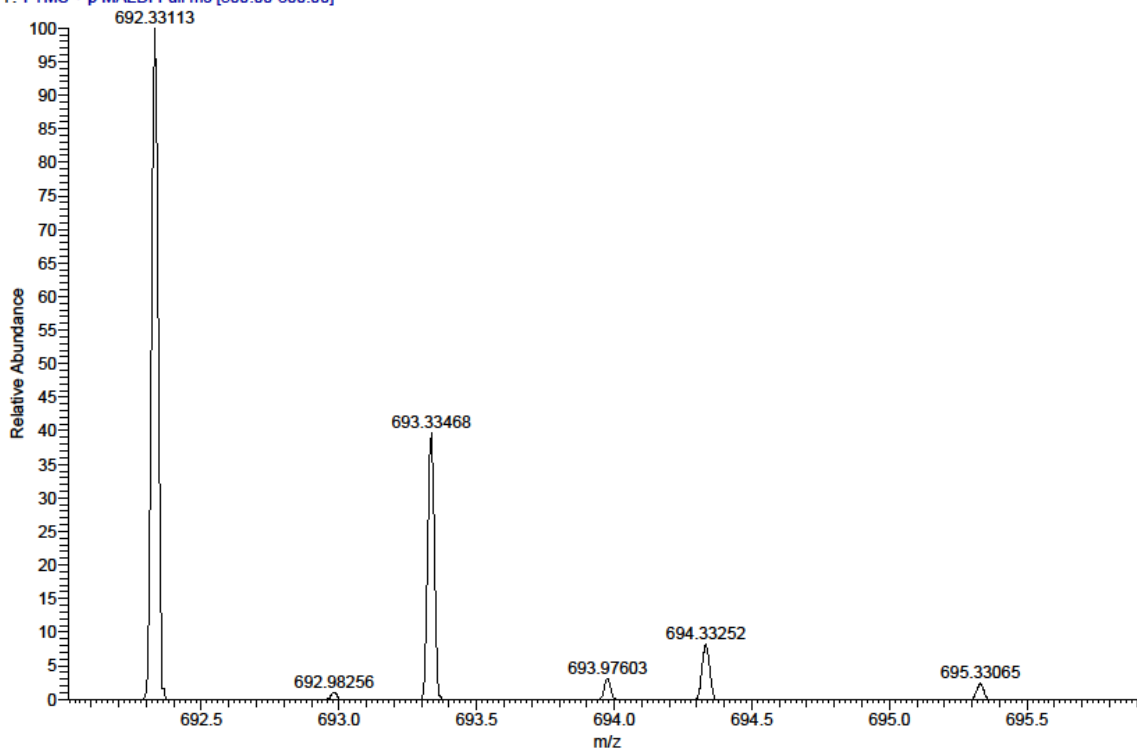


Figure 160. Compound 231 (SR160), HRMS (FTMS + p MALDI)

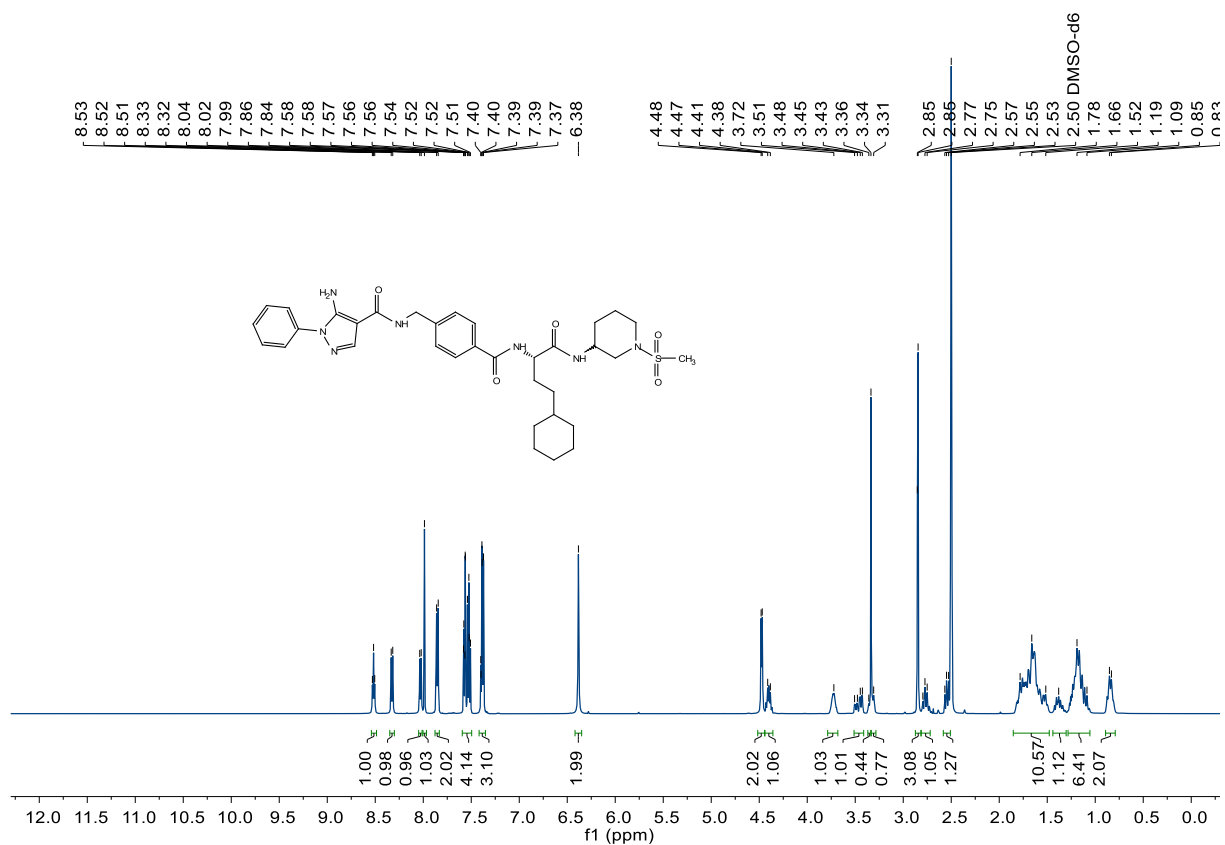


Figure 161. Compound 232 (SR159), <sup>1</sup>H-NMR, 500 MHz, DMSO-d<sub>6</sub>

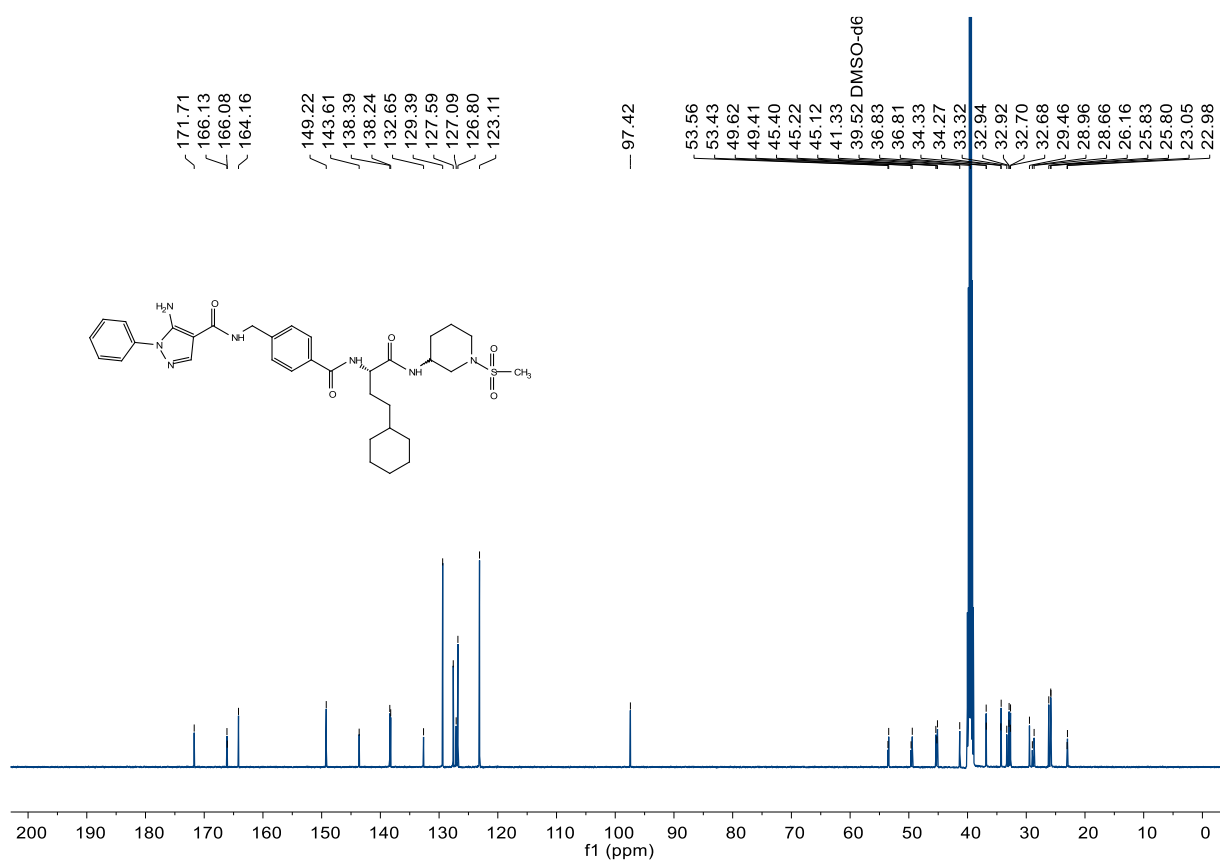


Figure 162. Compound 232 (SR159), <sup>13</sup>C-NMR, 126 MHz, DMSO-d<sub>6</sub>

C:\User\...\Knapp\2018\180319\SR159\_D5

3/19/2018 2:38:16 PM

SR159 mit HCCA gemessen.

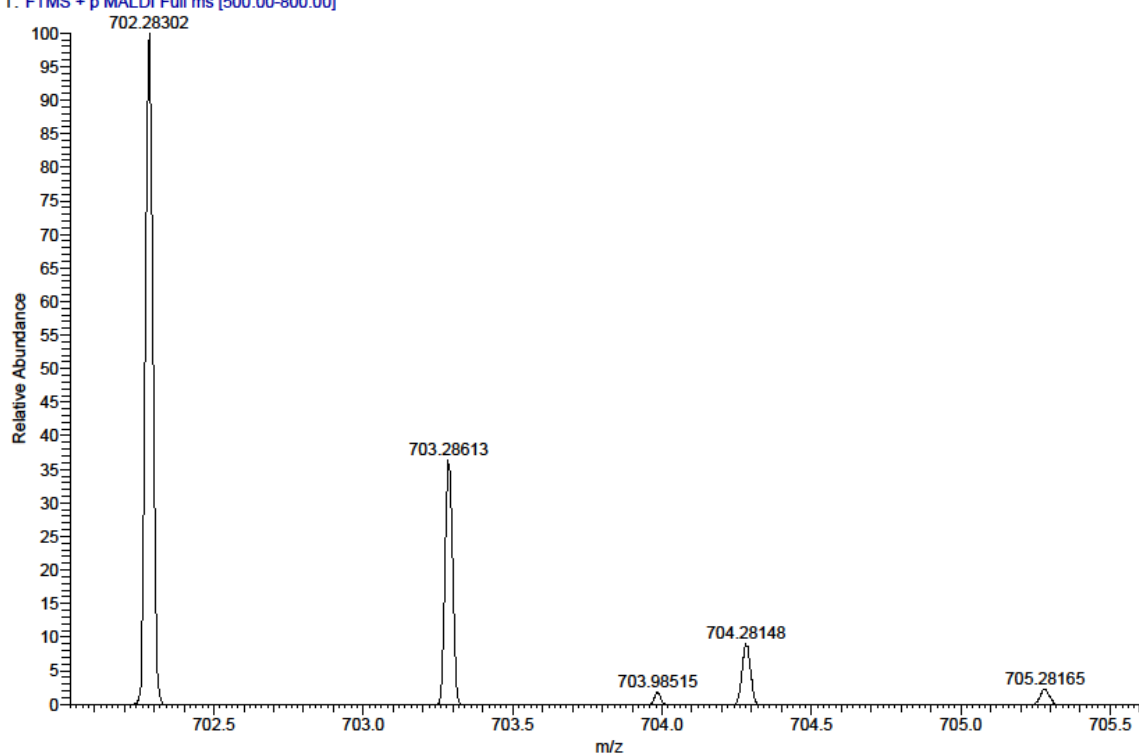
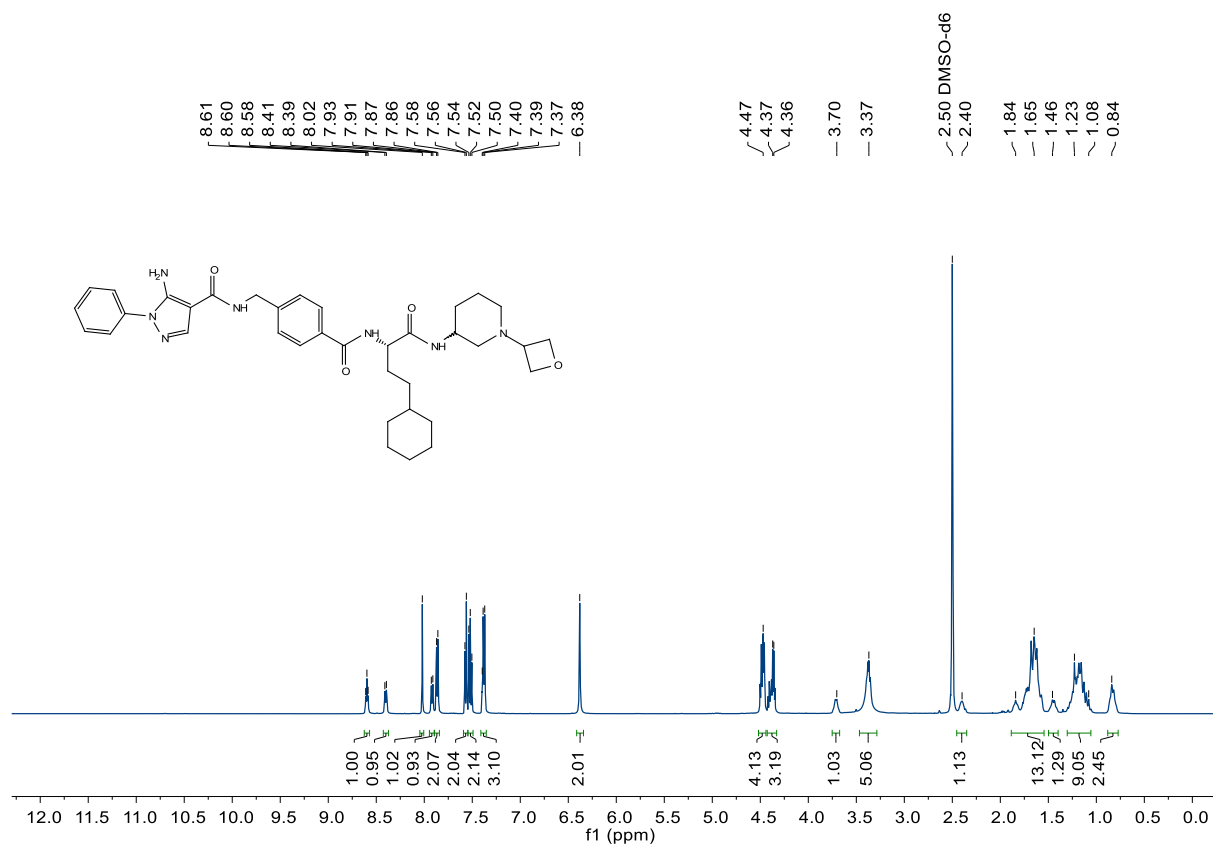
SR159\_D5 #1-3 RT: 0.01-0.25 AV: 3 NL: 8.75E4  
T: FTMS + p MALDI Full ms [500.00-800.00]

Figure 163. Compound 232 (SR159), HRMS (FTMS + p MALDI)

Figure 164. Compound 233 (SR202), <sup>1</sup>H-NMR, 500 MHz, DMSO-d<sub>6</sub>

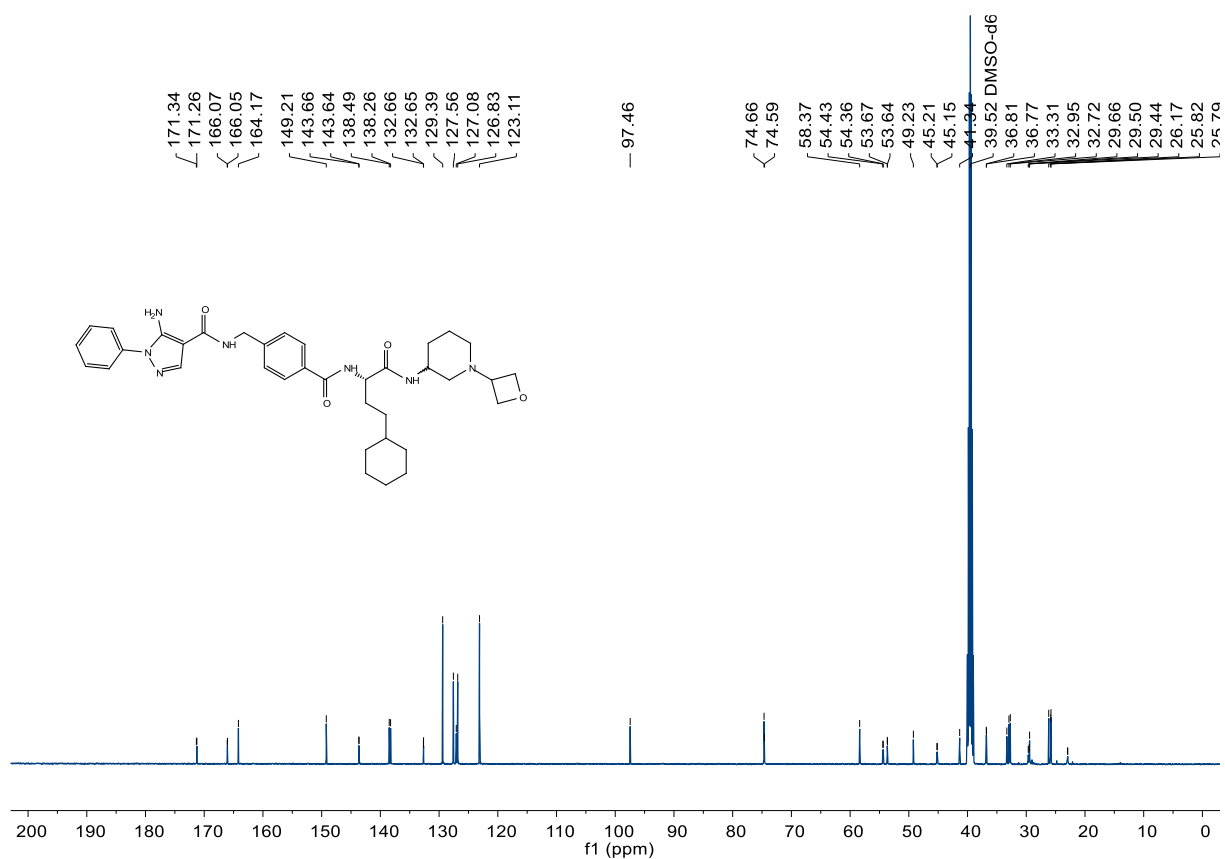


Figure 165. Compound 233 (SR202),  $^{13}\text{C}$ -NMR, 126 MHz,  $\text{DMSO-d}_6$

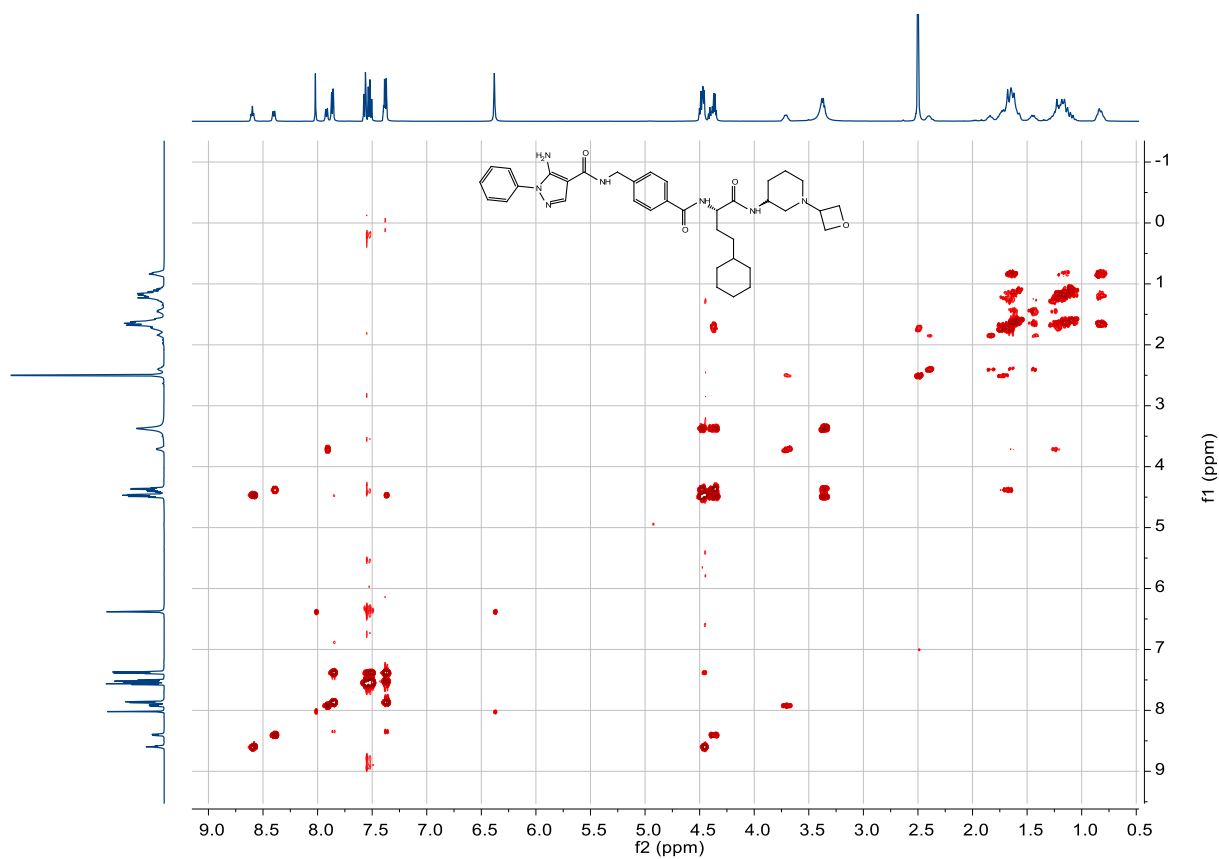


Figure 166. Compound 233 (SR202), COSY, 500 MHz,  $\text{DMSO-d}_6$

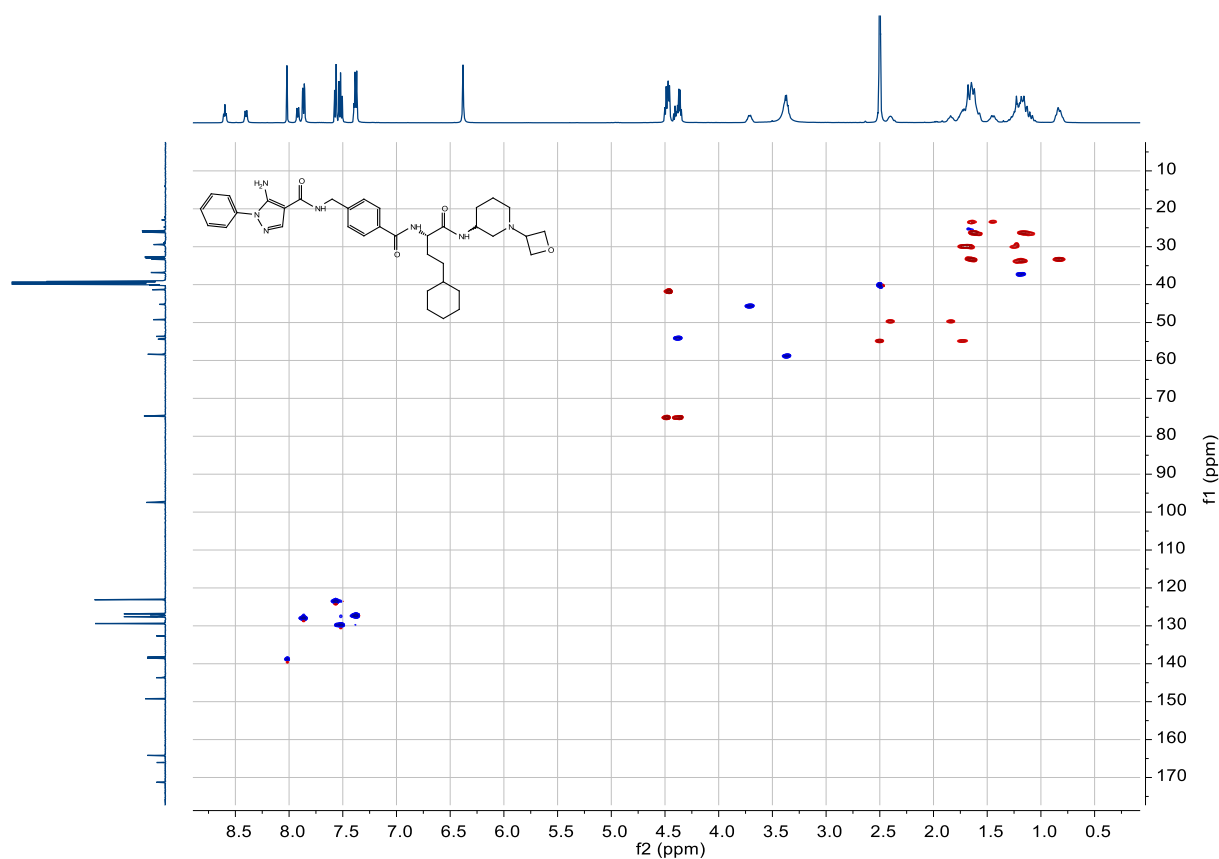


Figure 167. Compound 233 (SR202), HSQC, 500 MHz/ 126 MHz, DMSO-*d*<sub>6</sub>

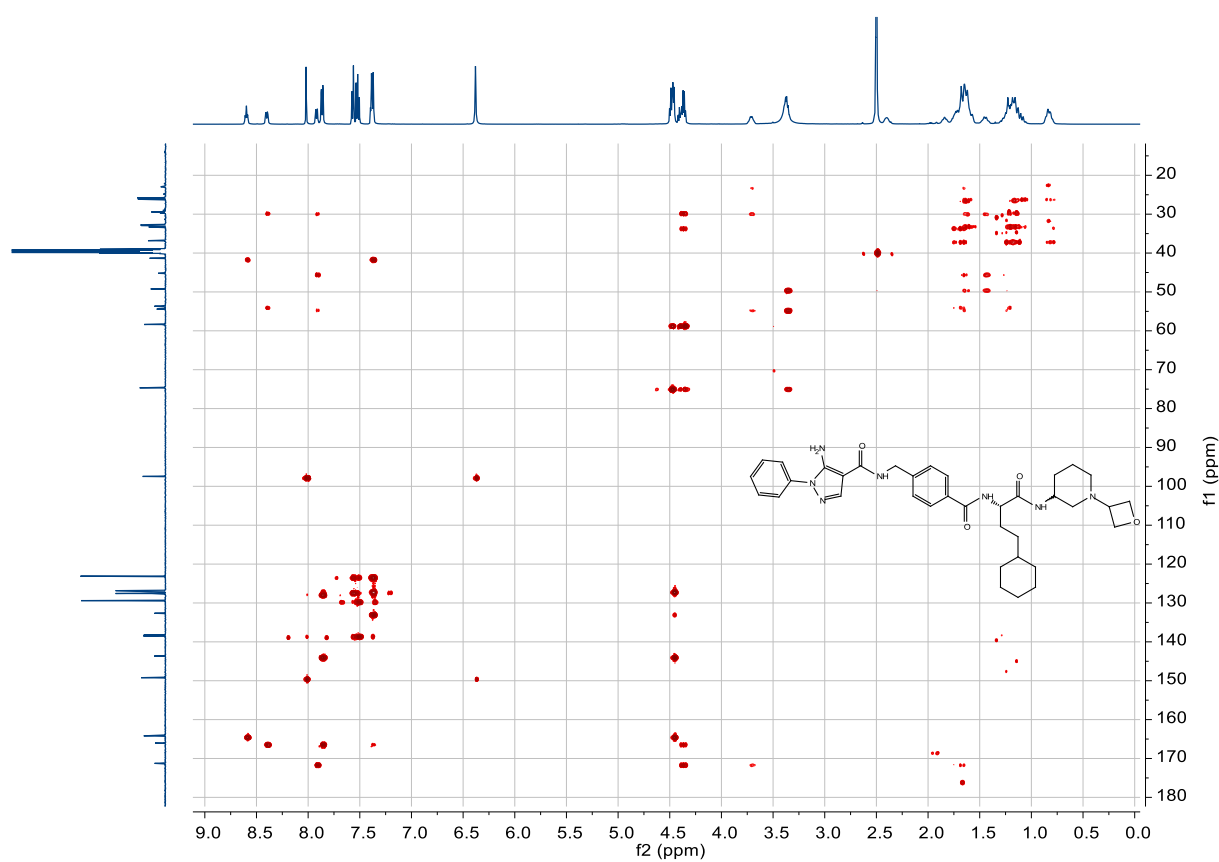
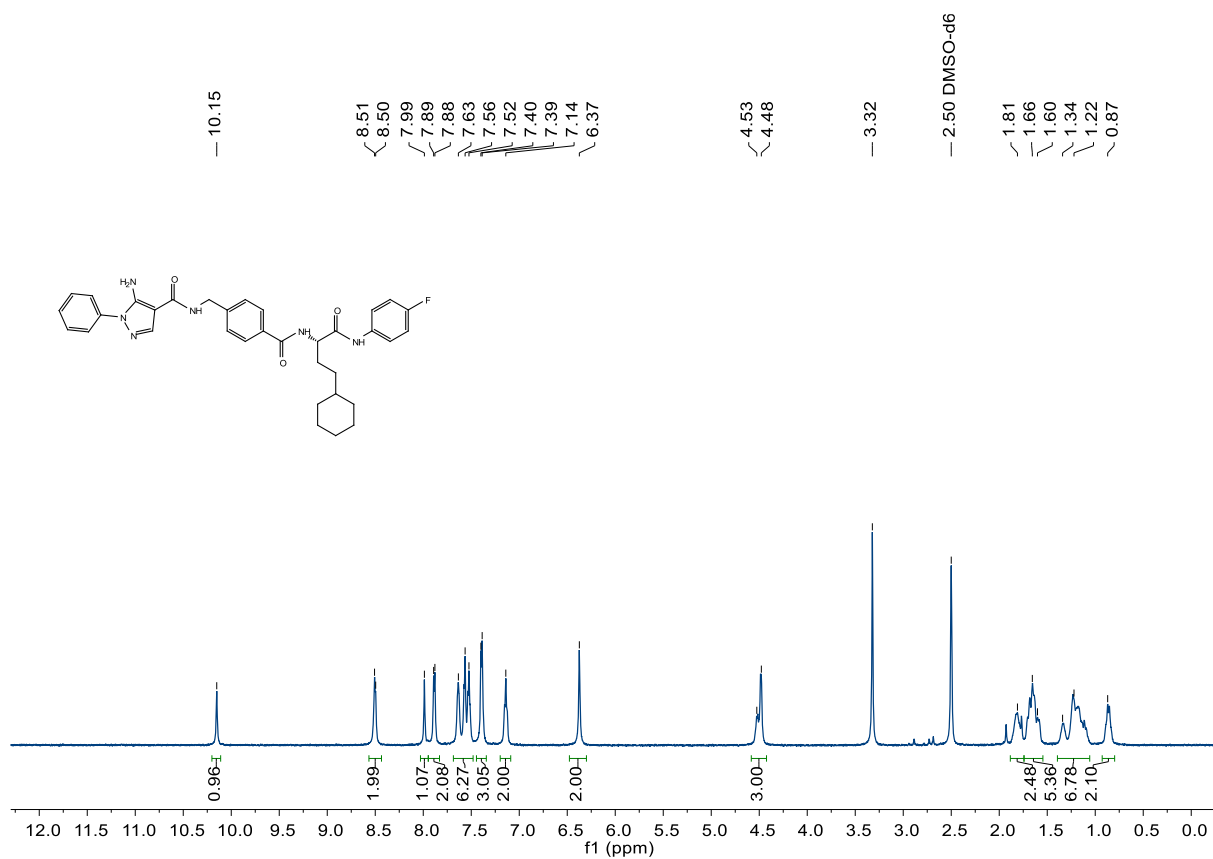
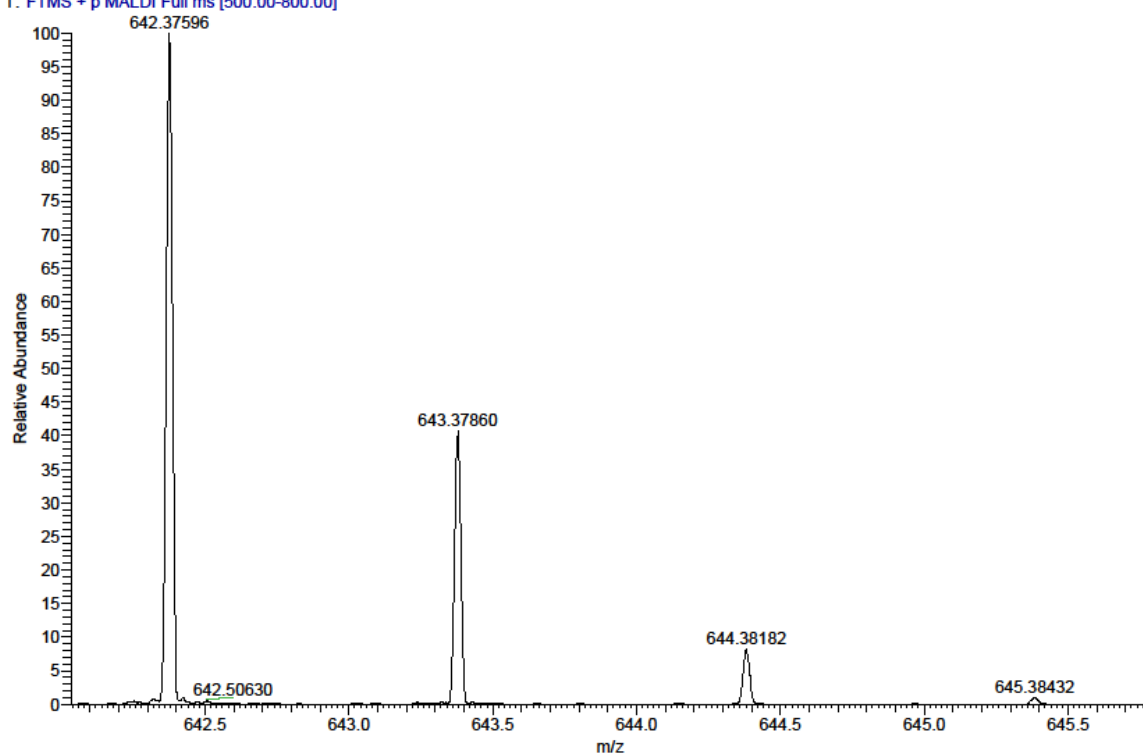


Figure 168. Compound 233 (SR202), HMBC, 500 MHz/ 126 MHz, DMSO-*d*<sub>6</sub>

SR202\_D7 #1-10 RT: 0.01-1.10 AV: 10 NL: 3.83E5  
T: FTMS + p MALDI Full ms [500.00-800.00]



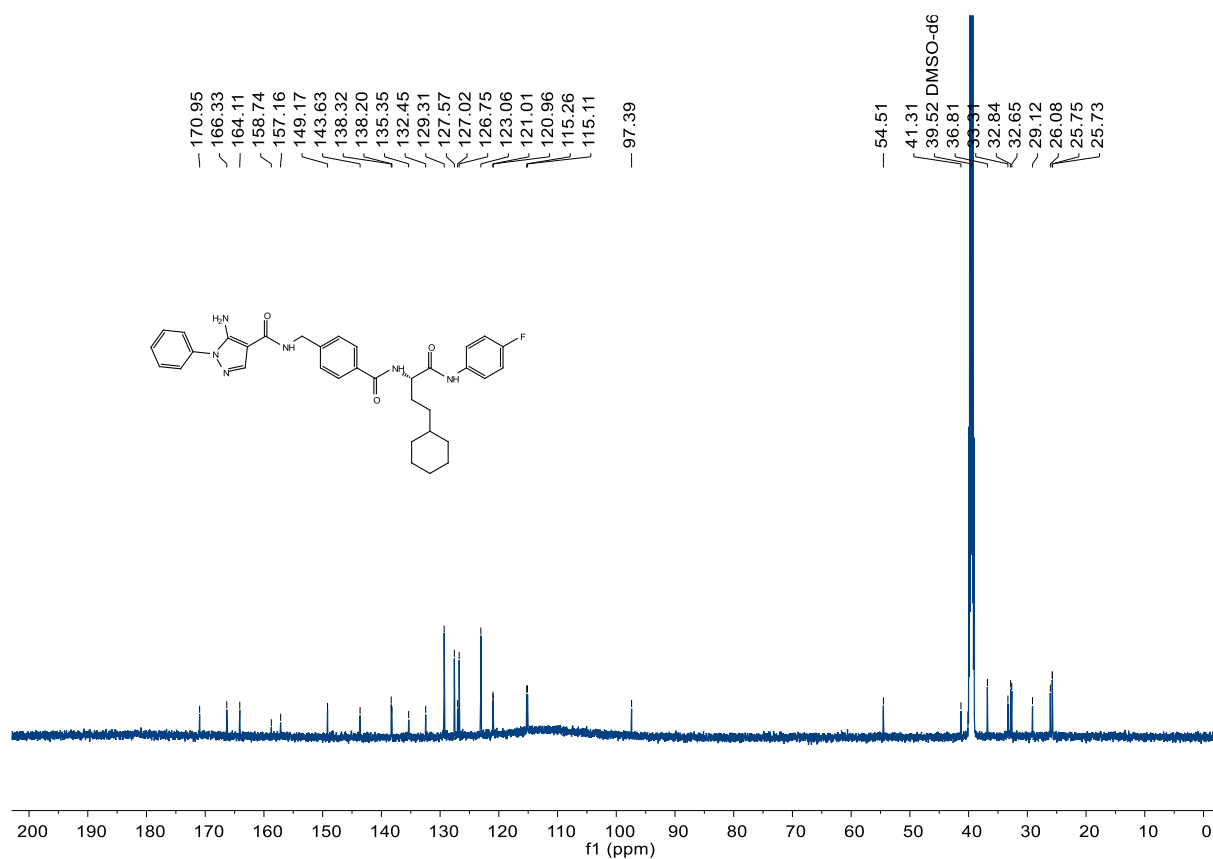


Figure 171. Compound 234 (SR348), <sup>13</sup>C-NMR, 150 MHz, DMSO-d<sub>6</sub>

C:\User\...\Knapp\2018\180711\SR348\_G4

7/11/2018 6:01:29 PM

SR348 mit HCCA gemessen, mehr Laserenergie

SR348\_G4#1-4 RT: 0.00-0.22 AV: 4 NL: 1.28E7  
T: FTMS + p MALDI Full ms [400.00-800.00]

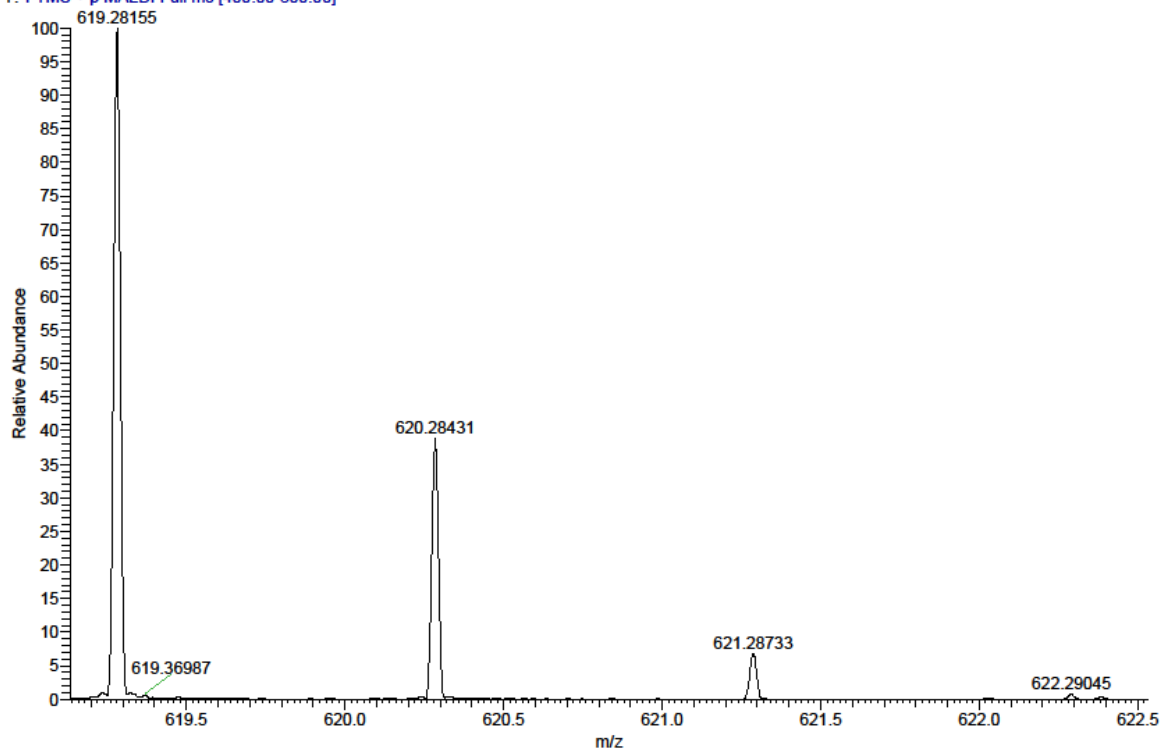


Figure 172. Compound 234 (SR348), HRMS (FTMS + p MALDI)

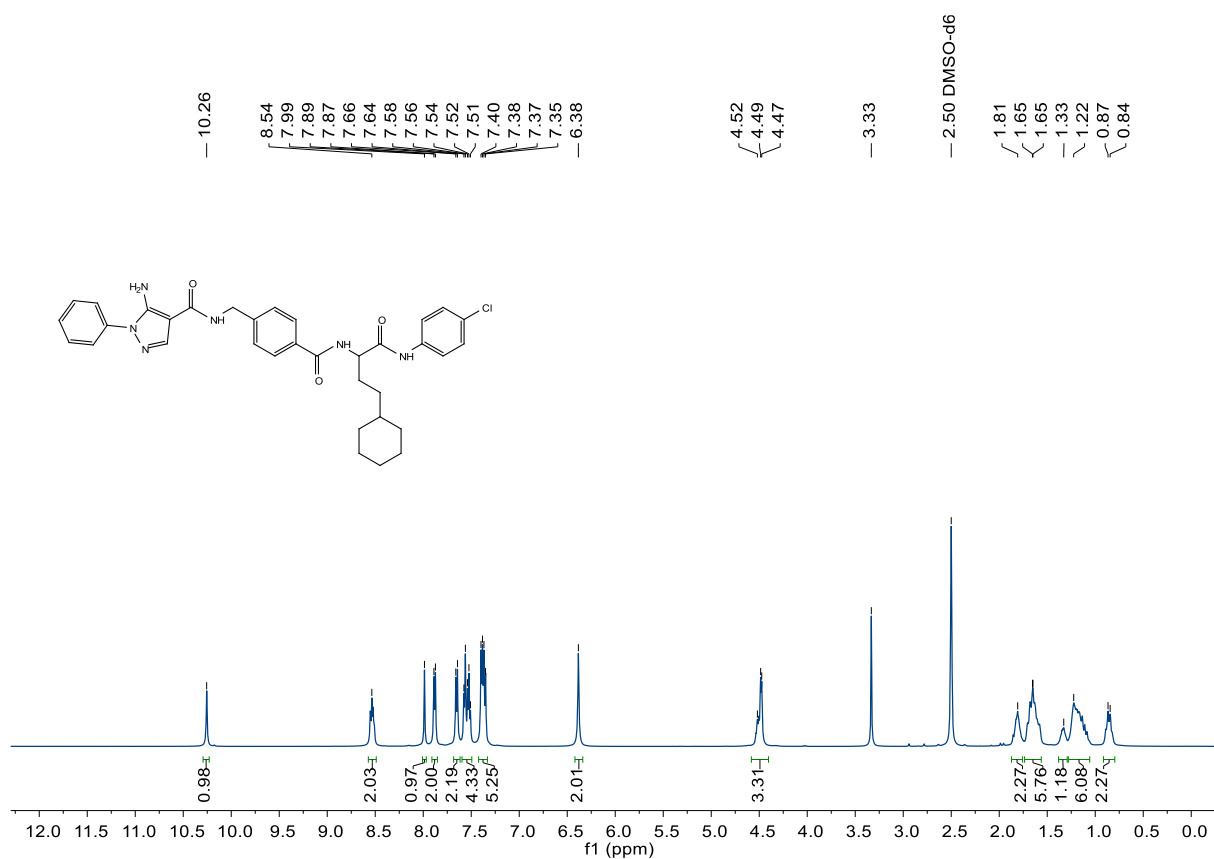


Figure 173. Compound 235 (SR332), <sup>1</sup>H-NMR, 500 MHz, DMSO-d<sub>6</sub>

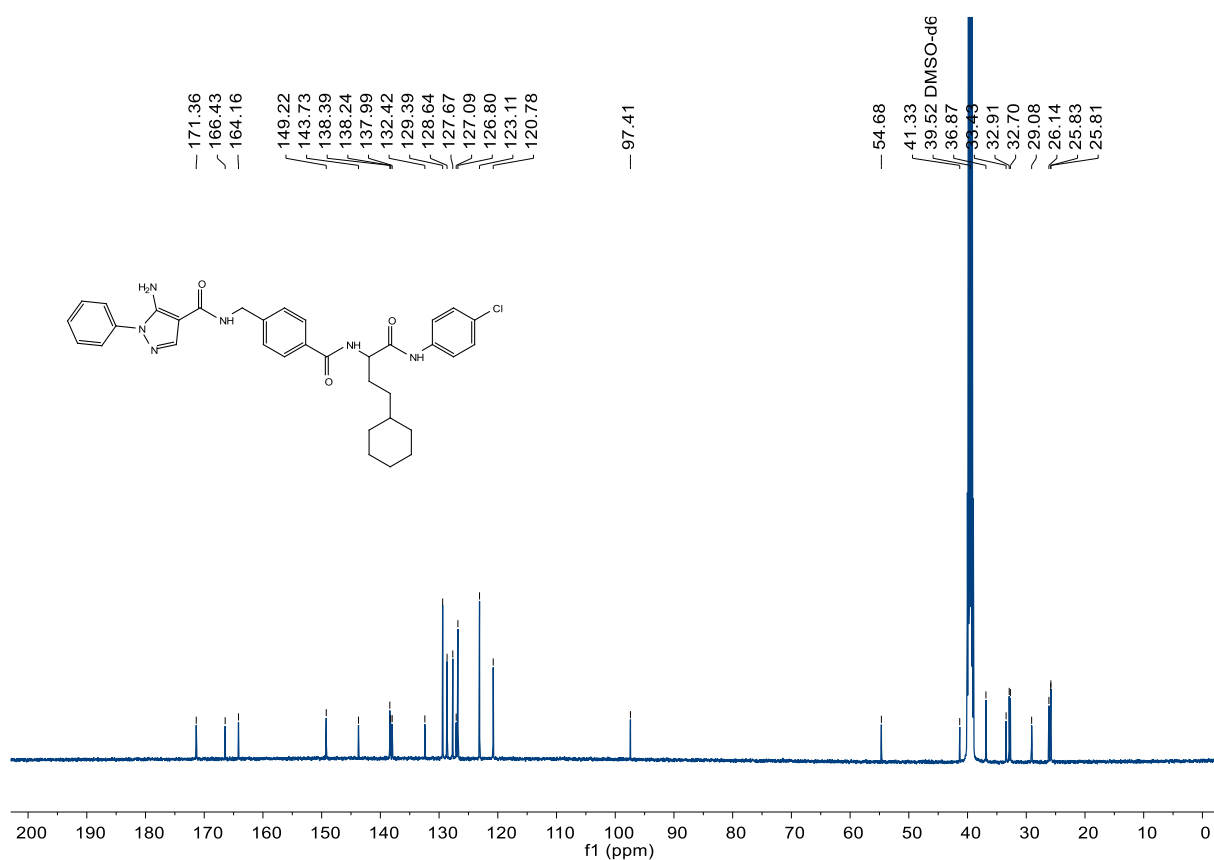


Figure 174. Compound 235 (SR332), <sup>13</sup>C-NMR, 126 MHz, DMSO-d<sub>6</sub>

C:\User\...\Knapp2018\180711\SR332\_G5

7/11/2018 5:19:42 PM

SR332 mit HCCA gemessen.

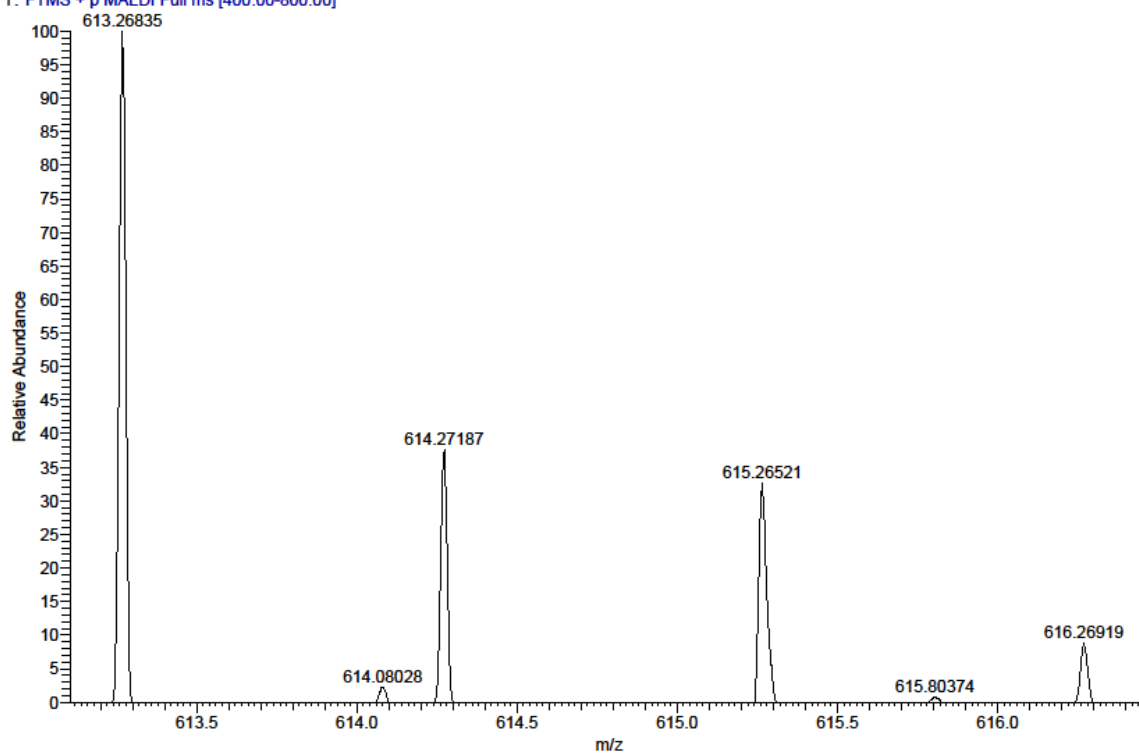
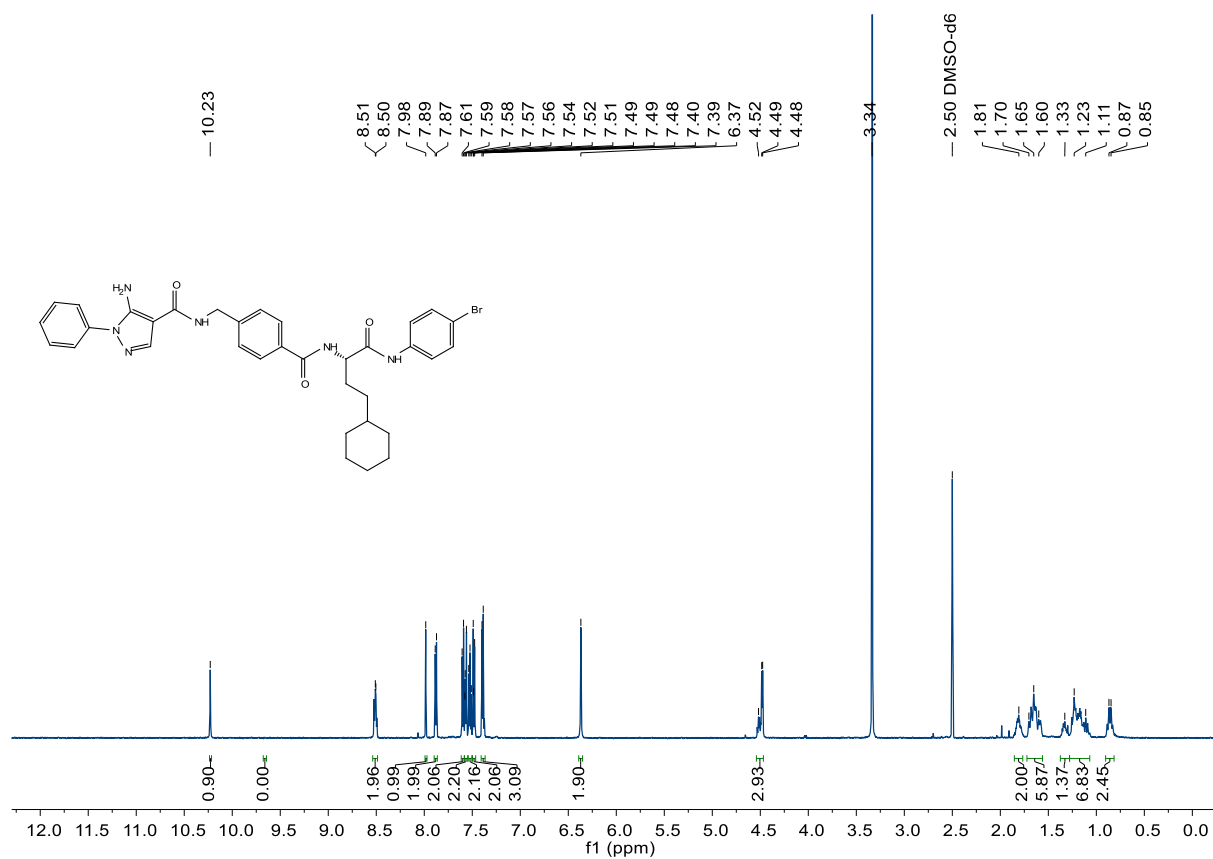
SR332\_G5 #1-5 RT: 0.00-0.35 AV: 5 NL: 4.91E4  
T: FTMS + p MALDI Full ms [400.00-800.00]

Figure 175. Compound 235 (SR332), HRMS (FTMS + p MALDI)

Figure 176. Compound 236 (SR343),  $^1\text{H-NMR}$ , 600 MHz,  $\text{DMSO-d}_6$

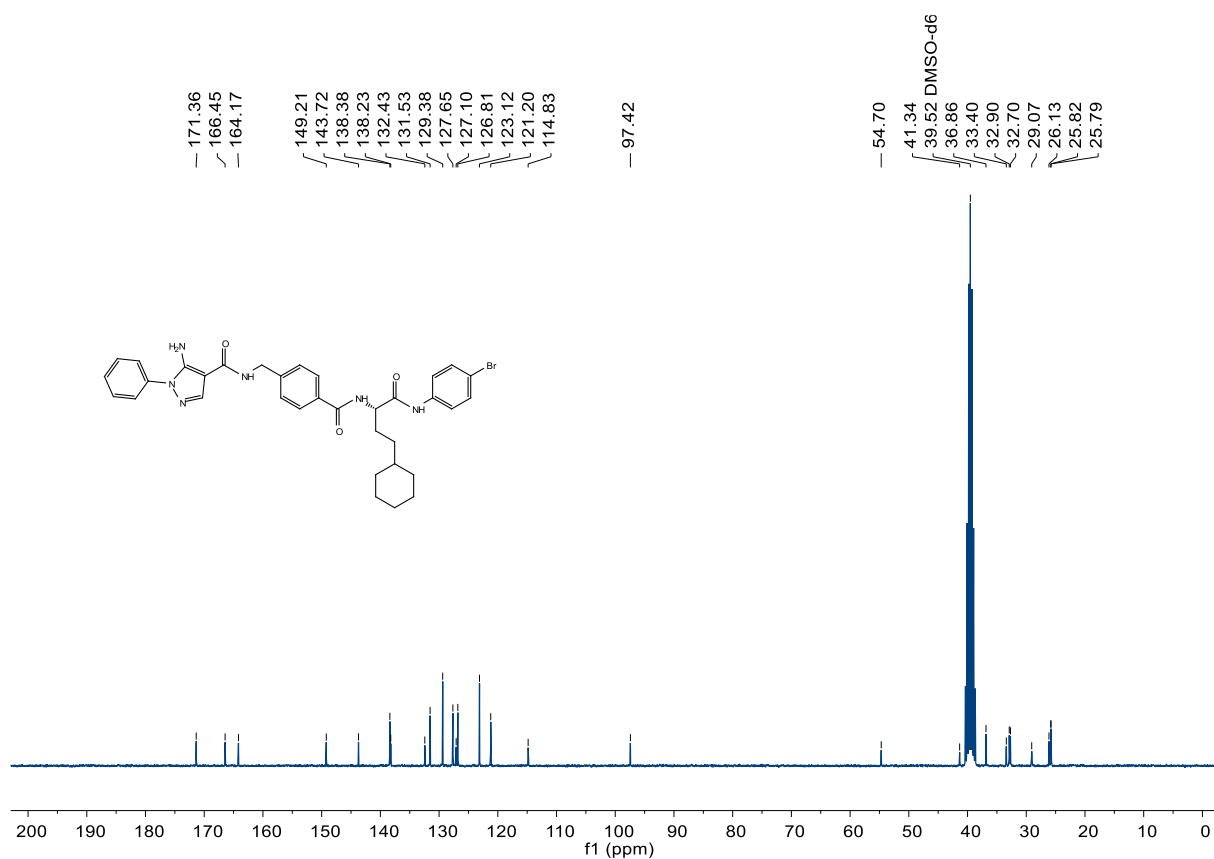


Figure 177. Compound 236 (SR343),  $^{13}\text{C-NMR}$ , 75 MHz,  $\text{DMSO-d}_6$

C:\User\...Knapp\2018\180711\SR343\_G1

7/11/2018 5:13:12 PM

SR343 mit HCCA gemessen.

SR343\_G1 #1-18 RT: 0.00-1.80 AV: 18 NL: 1.41E5

T: FTMS + p MALDI Full ms [400.00-800.00]

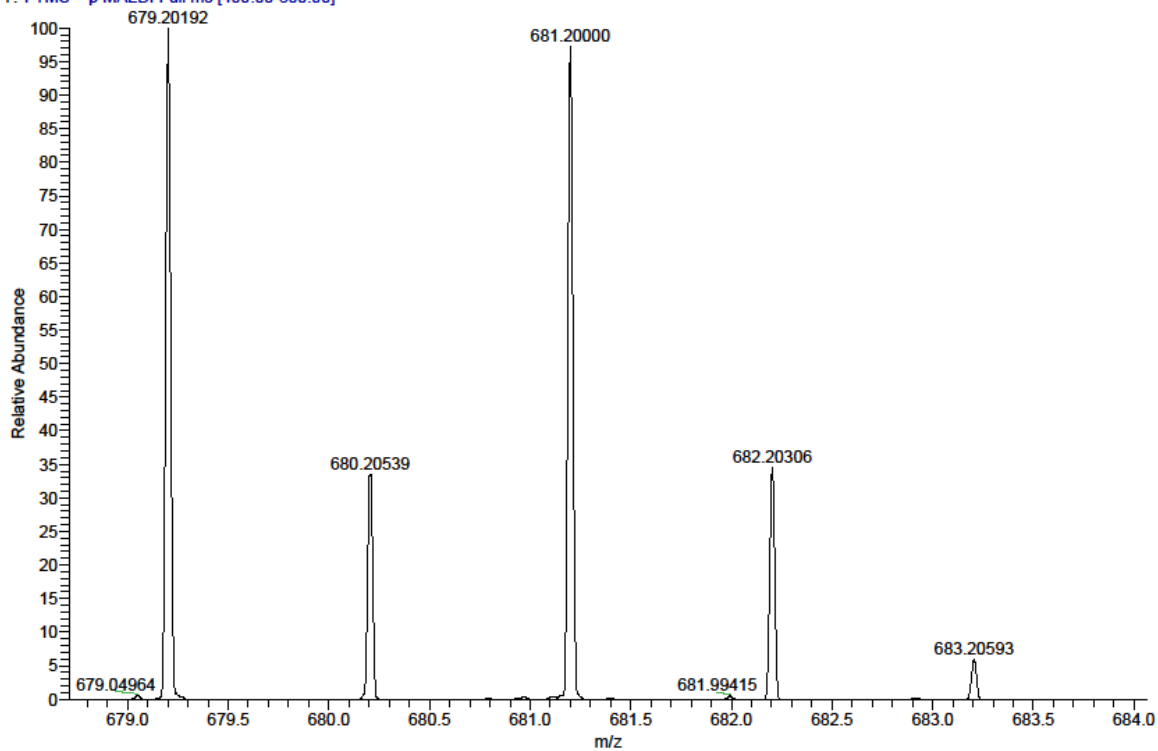
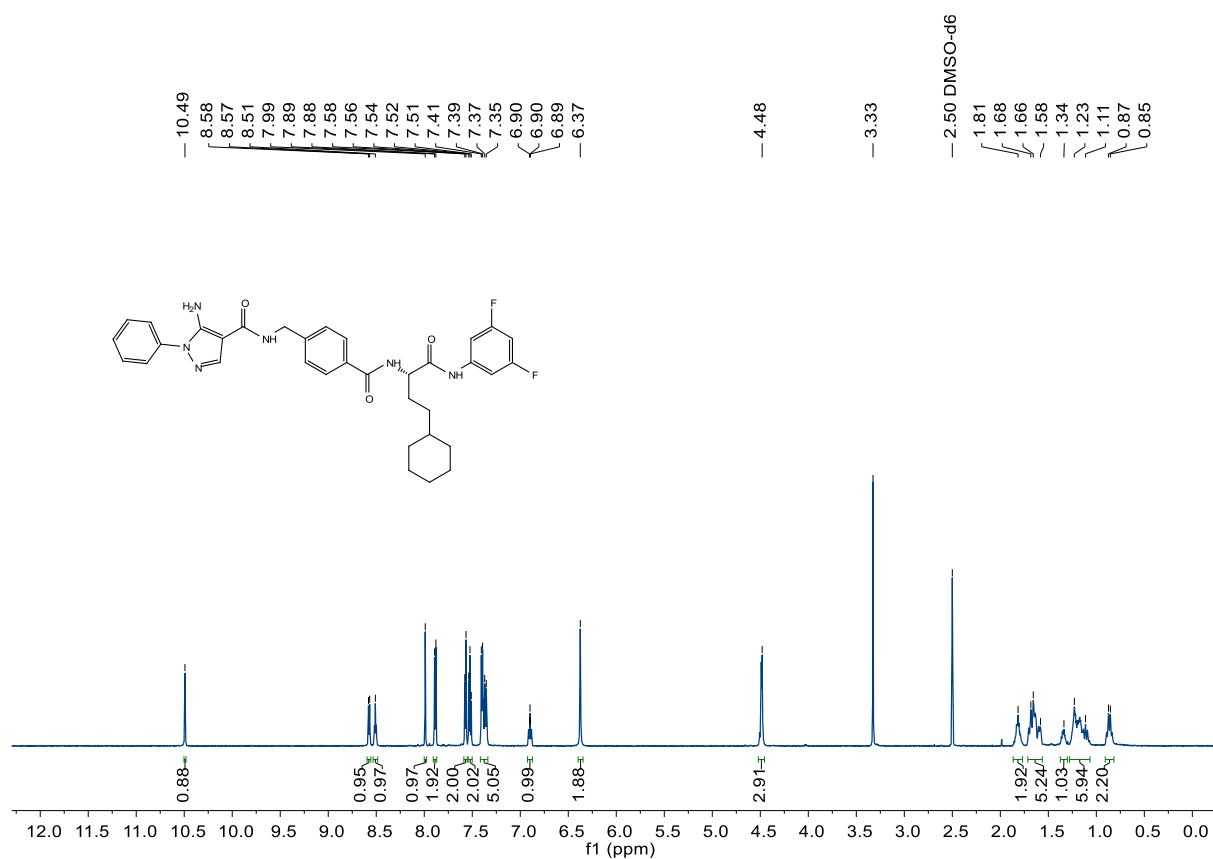
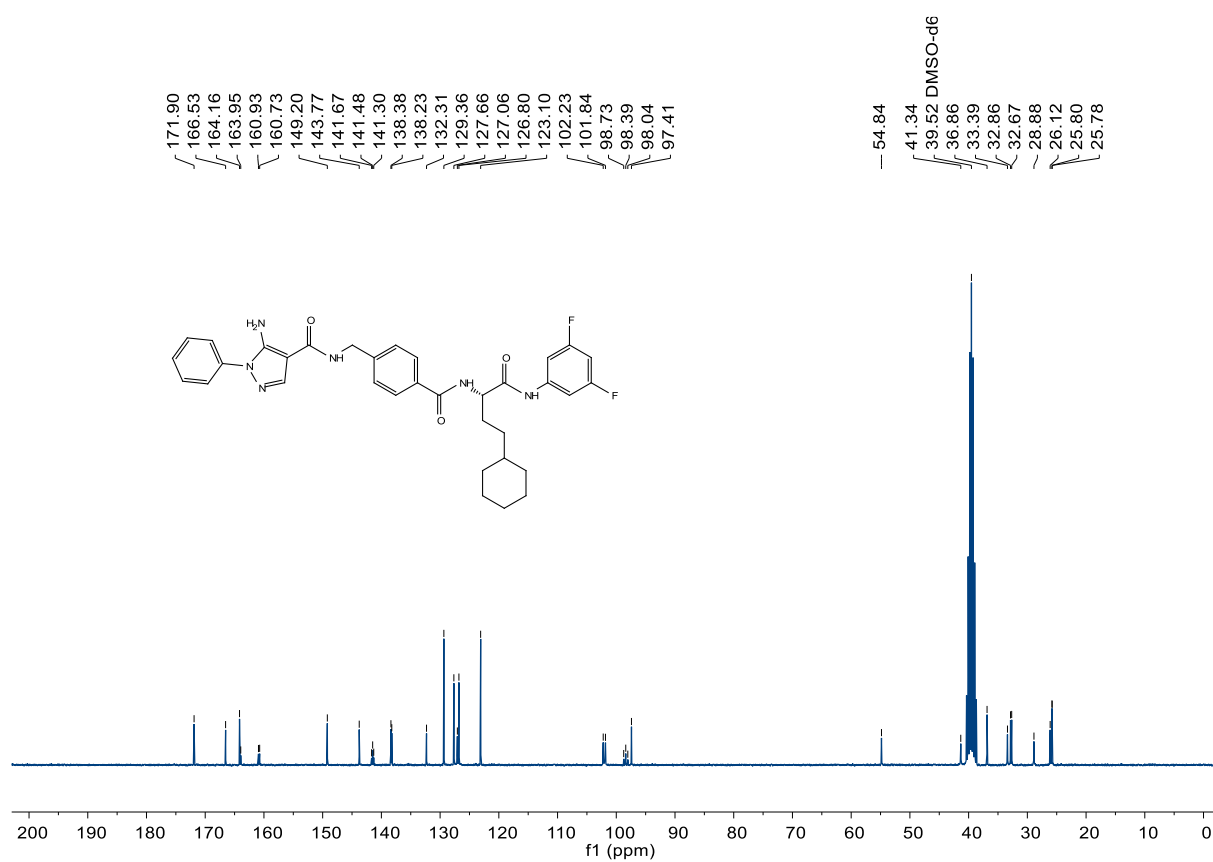


Figure 178. Compound 236 (SR343), HRMS (FTMS + p MALDI)



**Figure 179.** Compound **237** (SR344), <sup>1</sup>H-NMR, 600 MHz, DMSO-d<sub>6</sub>



**Figure 180.** Compound **237** (SR344), <sup>13</sup>C-NMR, 75 MHz, DMSO-d<sub>6</sub>

SR344\_G2 #1-4 RT: 0.00-0.25 AV: 4 NL: 1.20E6  
 T: FTMS + p MALDI Full ms [400.00-800.00]

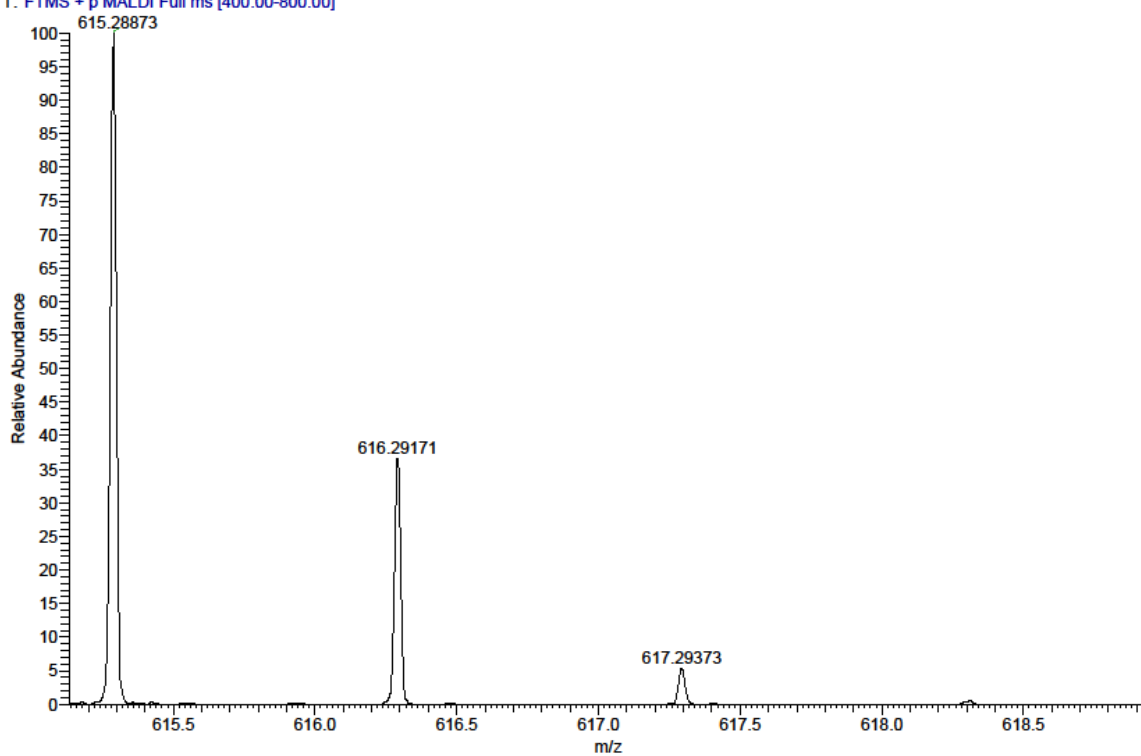


Figure 181. Compound 237 (SR344), HRMS (FTMS + p MALDI)

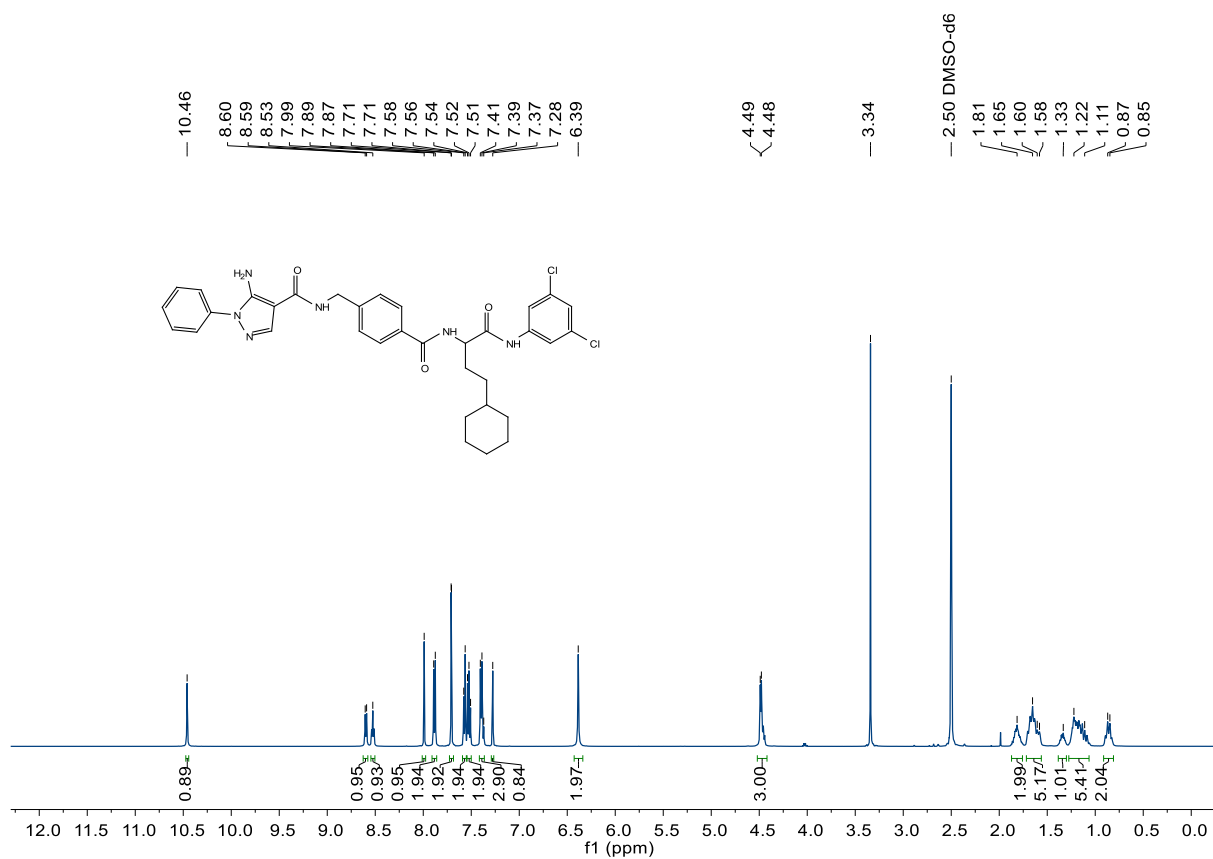


Figure 182. Compound 238 (SR336), <sup>1</sup>H-NMR, 500 MHz, DMSO-d<sub>6</sub>

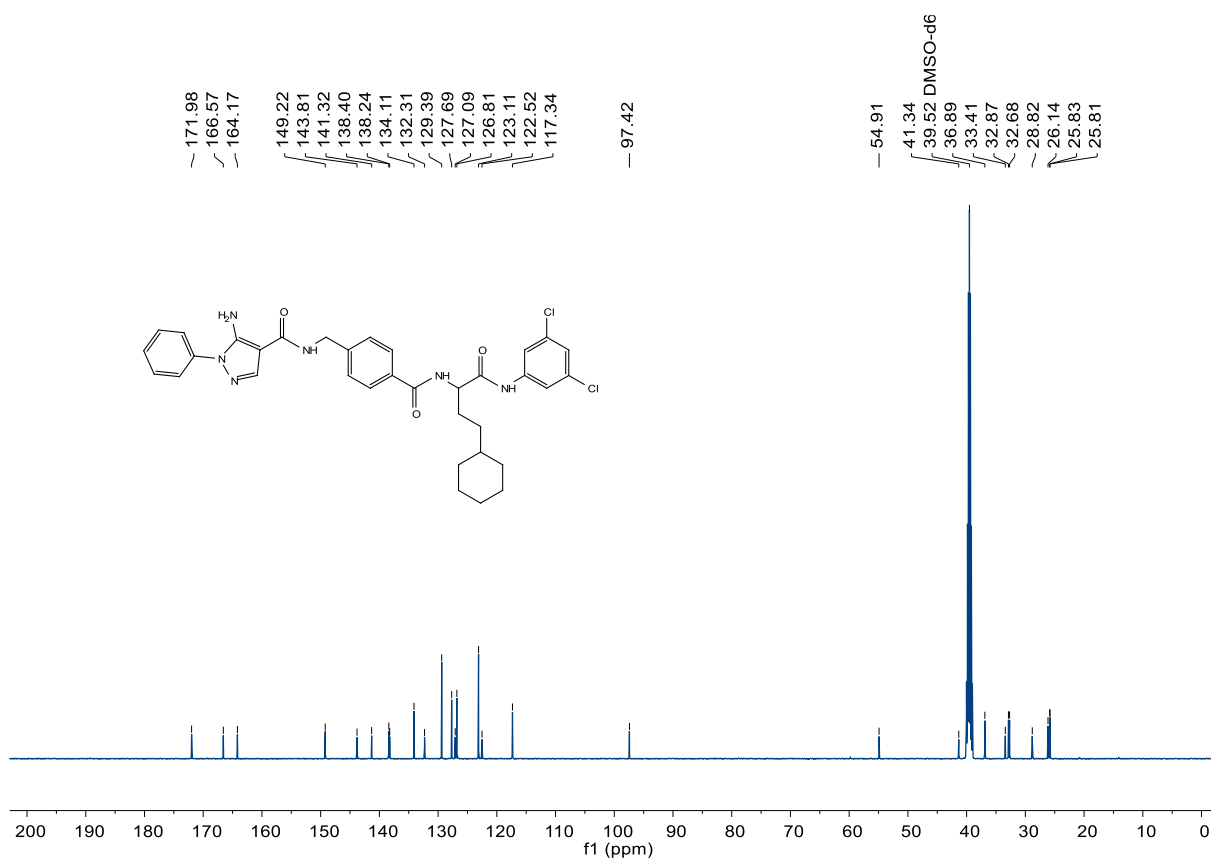


Figure 183. Compound 238 (SR336),  $^{13}\text{C-NMR}$ , 126 MHz,  $\text{DMSO-d}_6$

C:\User\...\Knapp\2018\180921\SR336\_A12

9/21/2018 10:50:49 AM

SR336 mit HCCA gemessen.

SR336\_A12 #1-6 RT: 0.01-0.53 AV: 6 NL: 5.85E4  
T: FTMS + p MALDI Full ms [400.00-750.00]

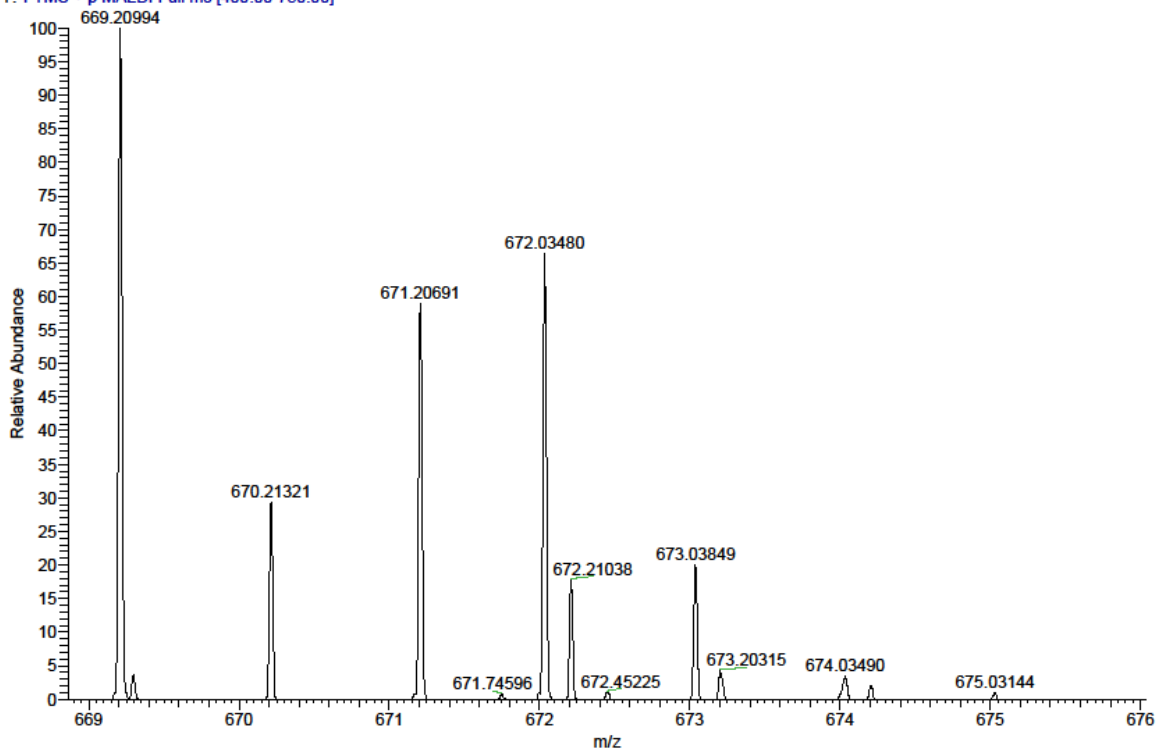


Figure 184. Compound 238 (SR336), HRMS (FTMS + p MALDI)

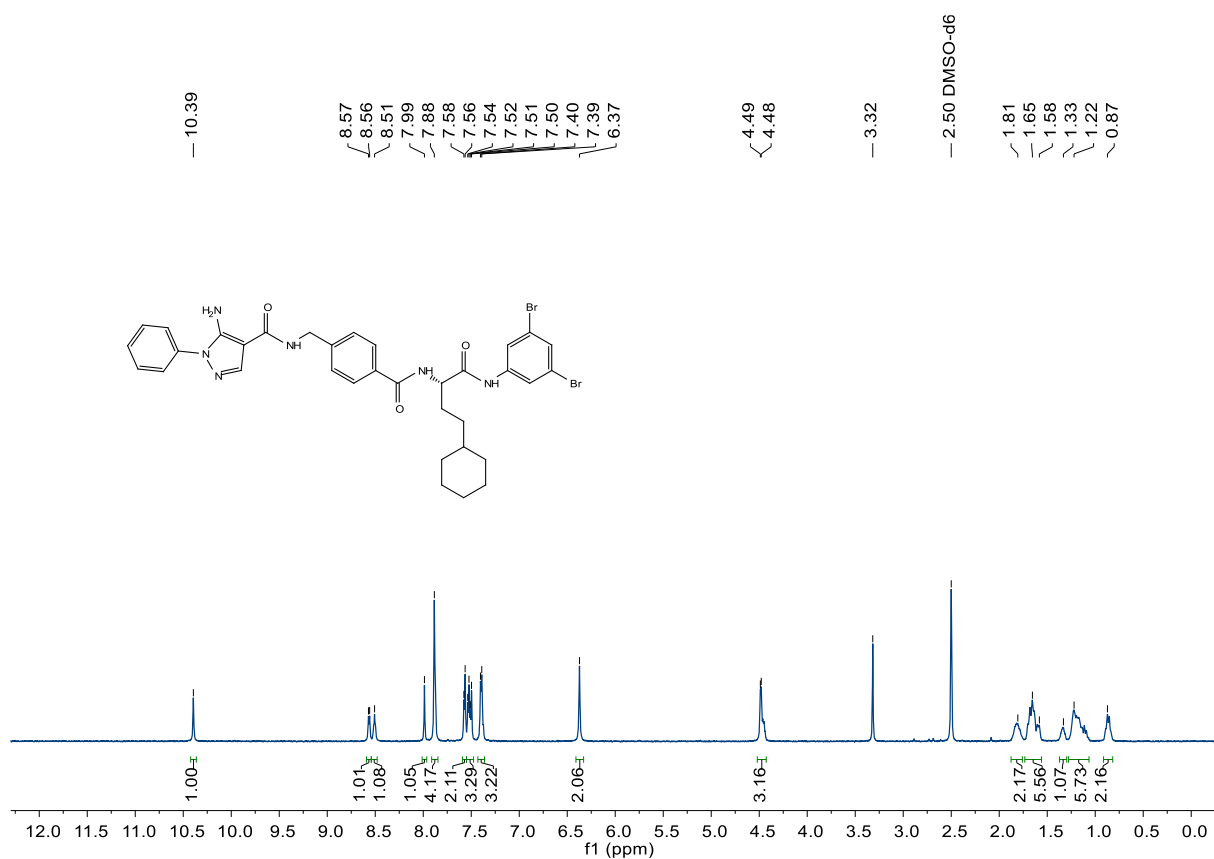


Figure 185. Compound 239 (SR347), <sup>1</sup>H-NMR, 600 MHz, DMSO-d<sub>6</sub>

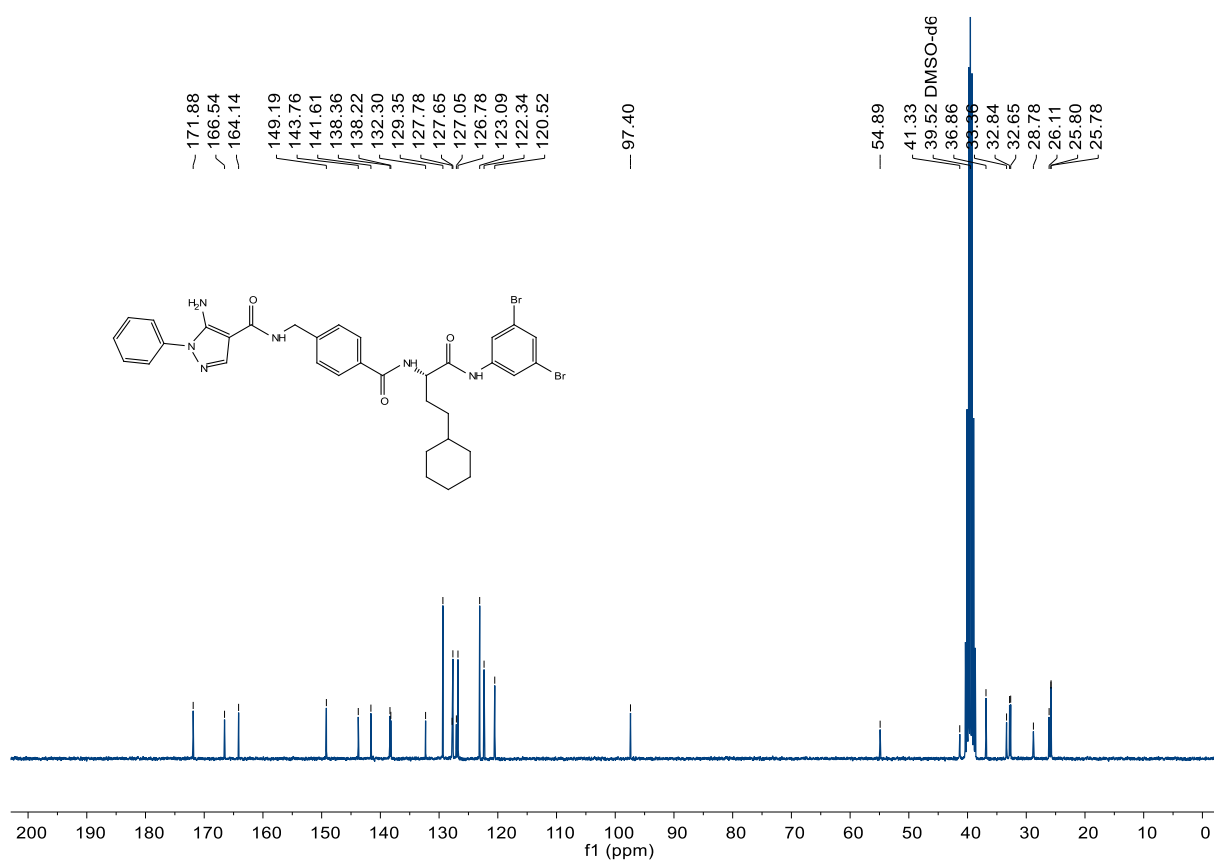


Figure 186. Compound 239 (SR347), <sup>13</sup>C-NMR, 75 MHz, DMSO-d<sub>6</sub>



C:\User\...\Knapp2018\180711\SR347\_G3

7/11/2018 5:16:27 PM

SR347 mit HCCA gemessen.

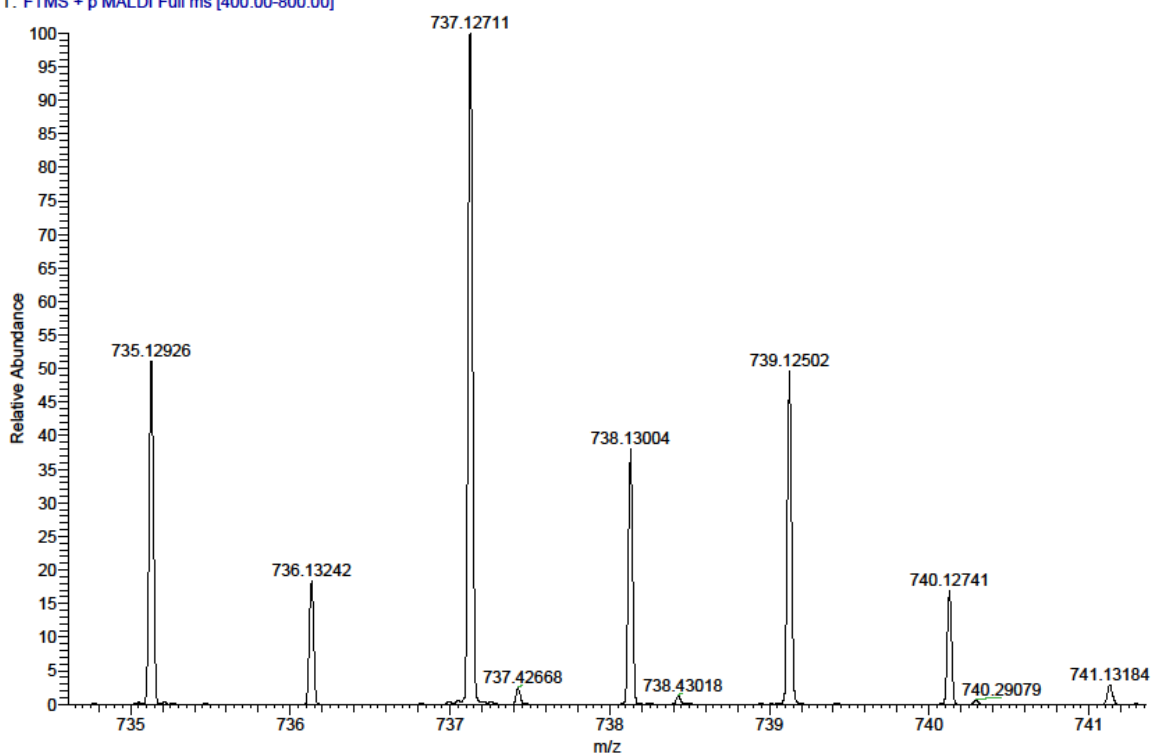
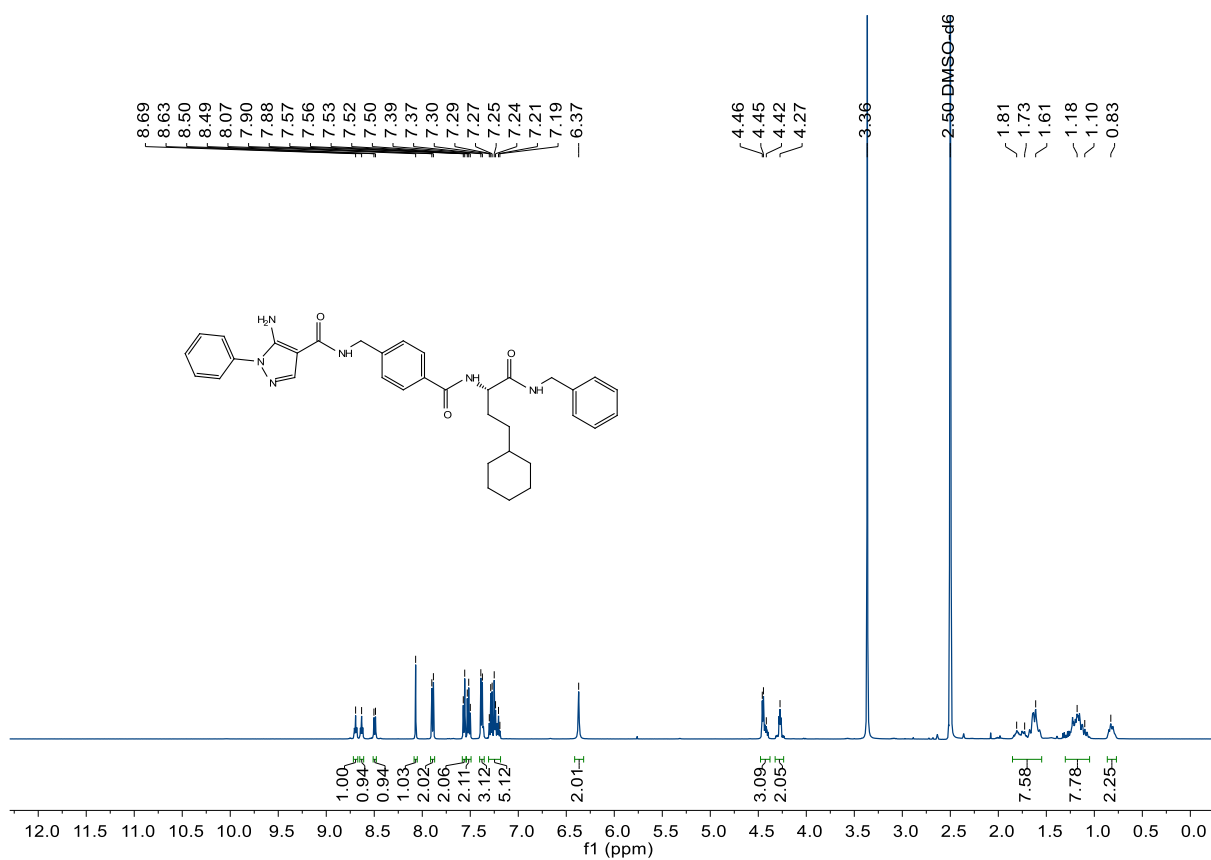
SR347\_G3 #1-11 RT: 0.00-1.00 AV: 11 NL: 7.48E5  
T: FTMS + p MALDI Full ms [400.00-800.00]

Figure 187. Compound 239 (SR347), HRMS (FTMS + p MALDI)

Figure 188. Compound 240 (SR83),  $^1\text{H-NMR}$ , 500 MHz,  $\text{DMSO-d}_6$

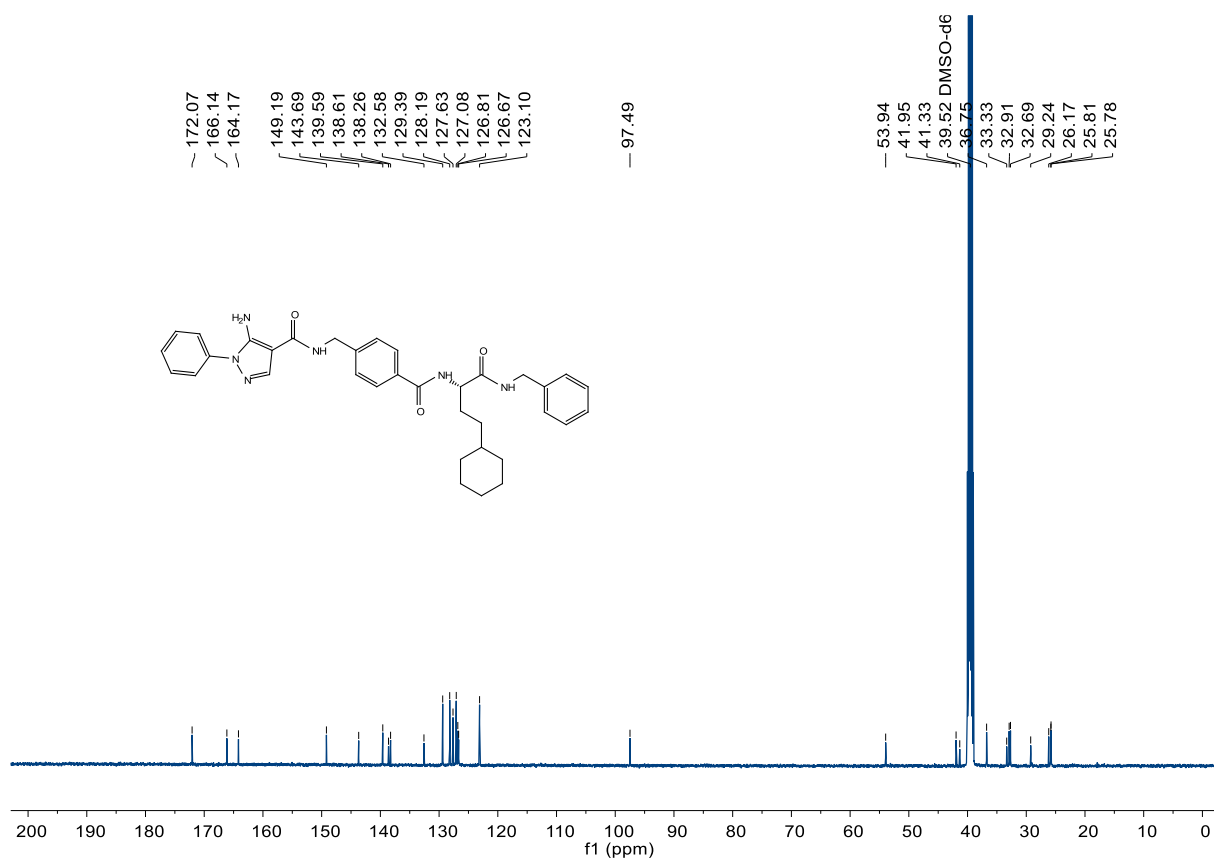


Figure 189. Compound 240 (SR83),  $^1\text{H-NMR}$ , 162 MHz,  $\text{DMSO-d}_6$

C:\User\...Knapp\2018\180319\SR83\_C10

3/19/2018 2:00:18 PM

SR83 mit HCCA gemessen.

SR83\_C10 #1-16 RT: 0.01-1.85 AV: 16 NL: 1.83E4

T: FTMS + p MALDI Full ms [500.00-800.00]

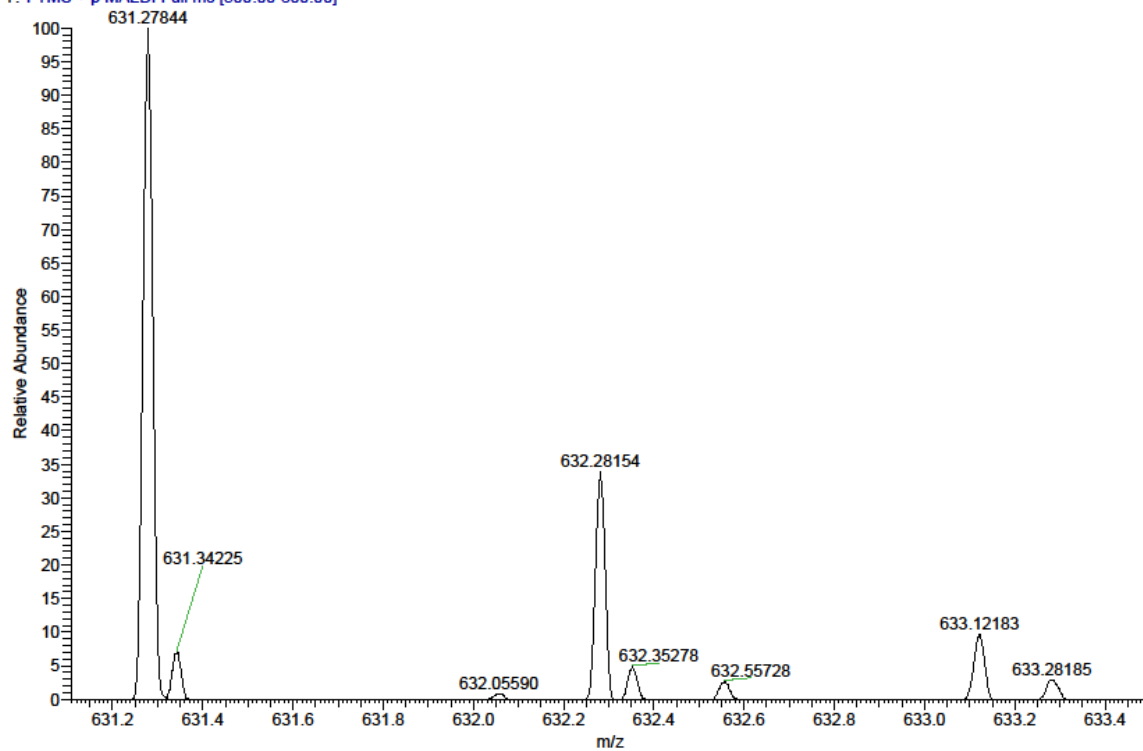


Figure 190. Compound 240 (SR83), HRMS (FTMS + p MALDI)

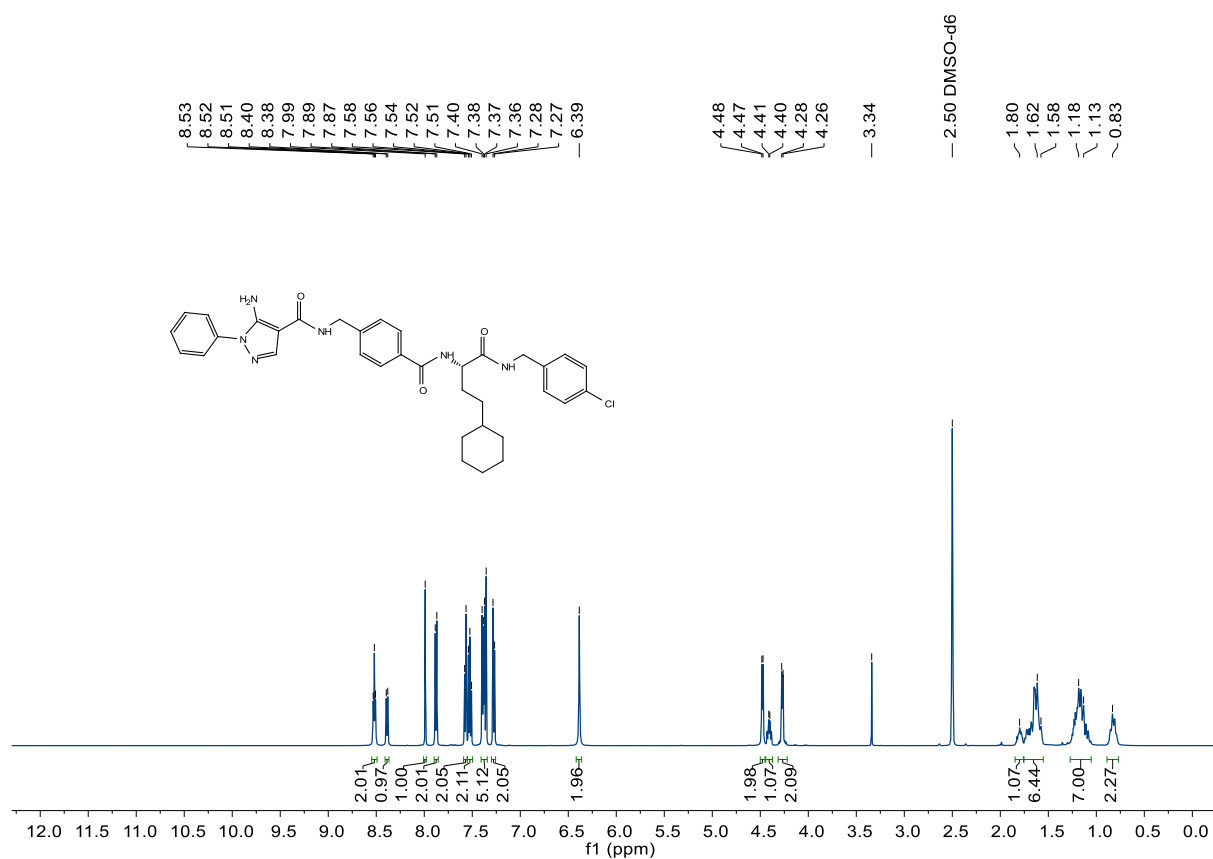


Figure 191. Compound 241 (SR82),  $^1\text{H-NMR}$ , 500 MHz,  $\text{DMSO-d}_6$

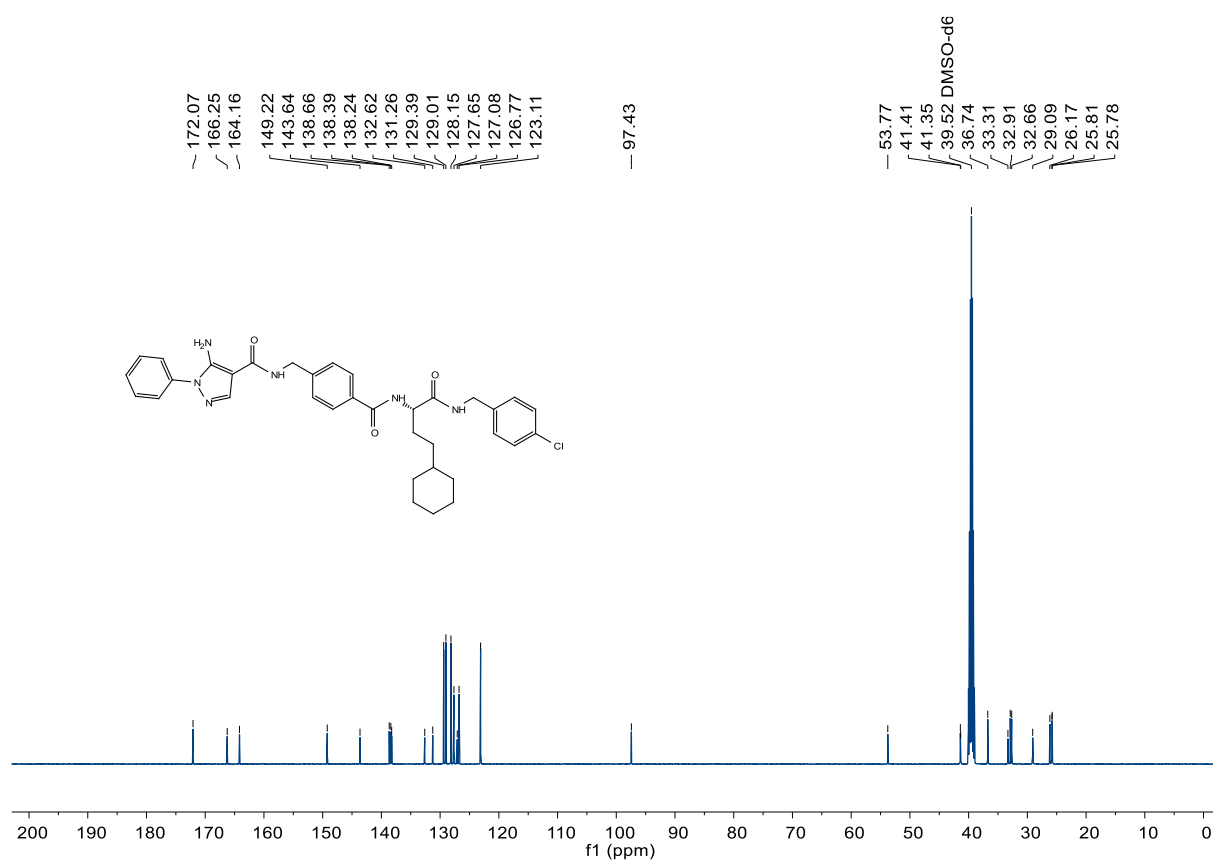


Figure 192. Compound 241 (SR82),  $^{13}\text{C-NMR}$ , 126 MHz,  $\text{DMSO-d}_6$

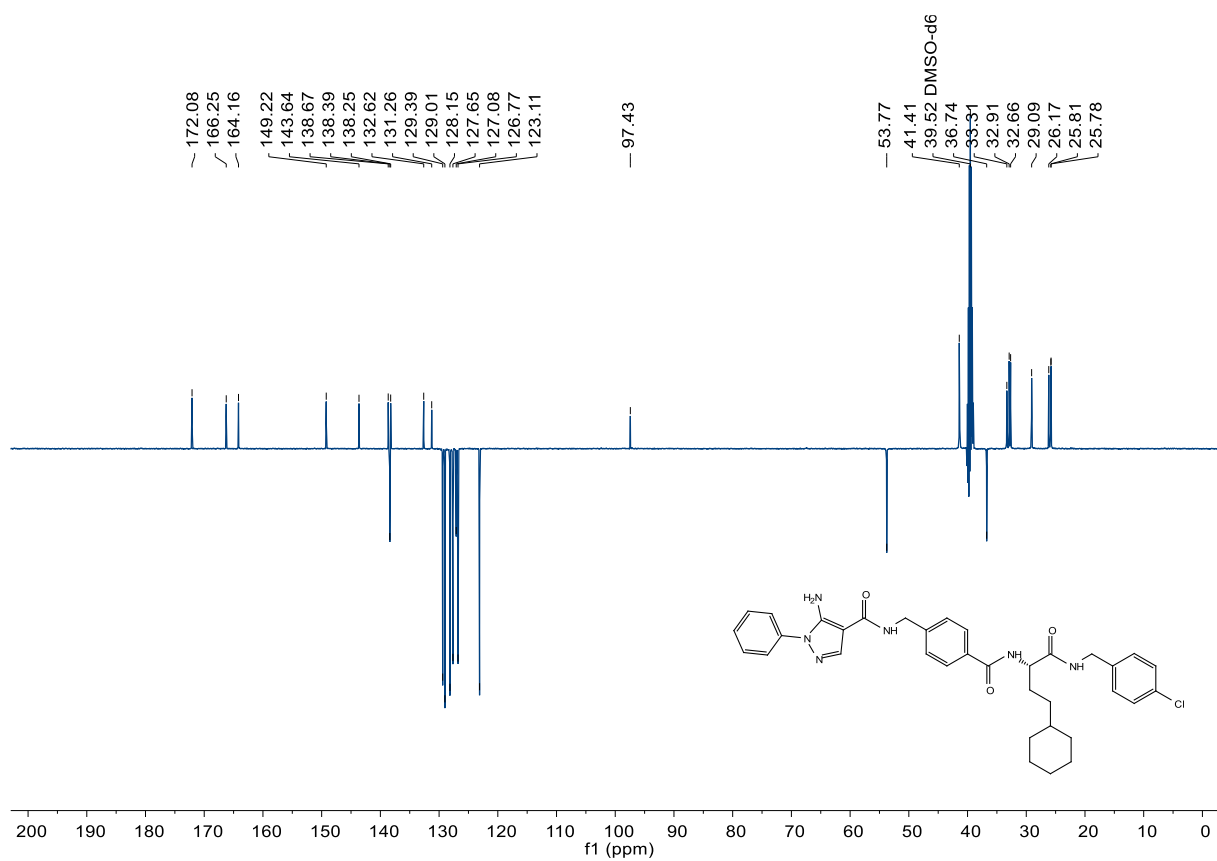


Figure 193. Compound 241 (SR82), DEPT, 126 MHz, DMSO- $d_6$

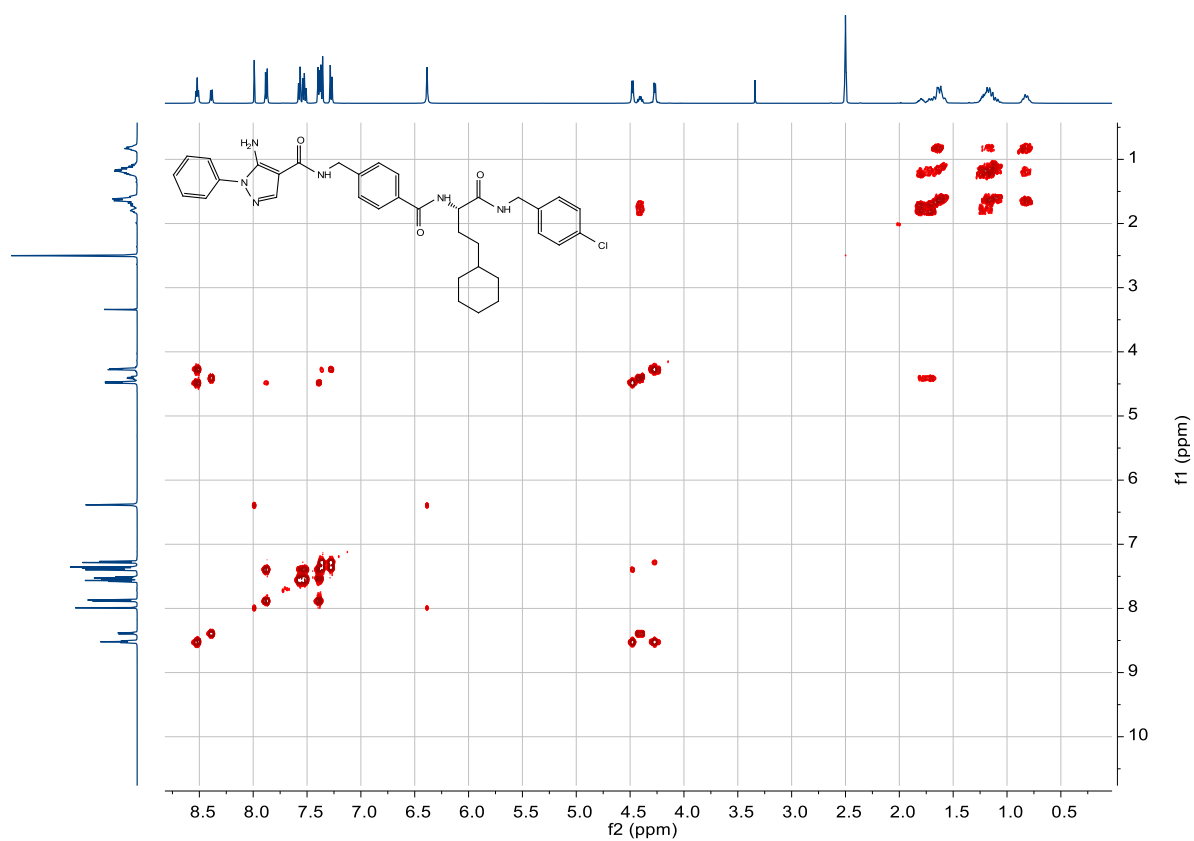


Figure 194. Compound 241 (SR82), COSY, 500 MHz, DMSO- $d_6$

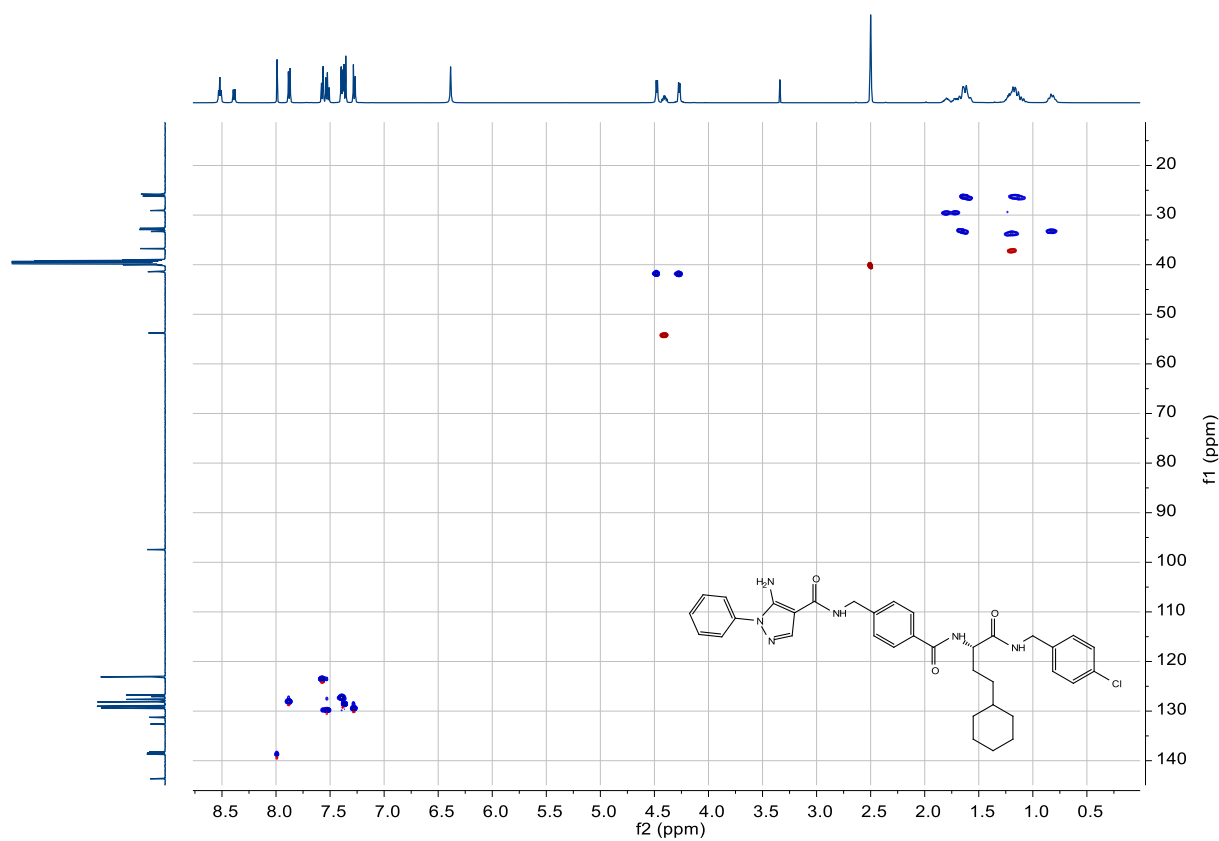


Figure 195. Compound 241 (SR82), HSQC, 500/ 126 MHz, DMSO-d<sub>6</sub>

C:\User\...\Knapp\2018\180319\SR82\_D1

3/19/2018 2:15:49 PM

SR82 mit HCCA gemessen.

SR82\_D1 #1-10 RT: 0.00-1.05 AV: 10 NL: 2.34E4  
T: FTMS + p MALDI Full ms [500.00-800.00]

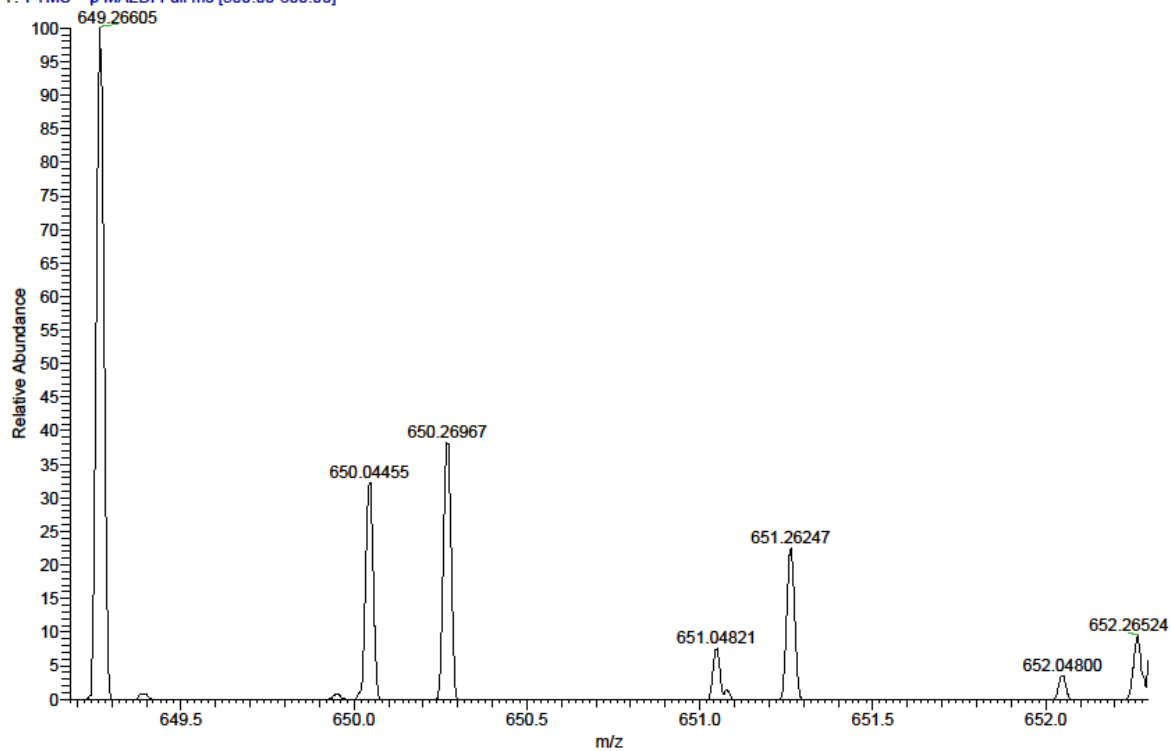


Figure 196. Compound 241 (SR82), HRMS (FTMS + p MALDI)

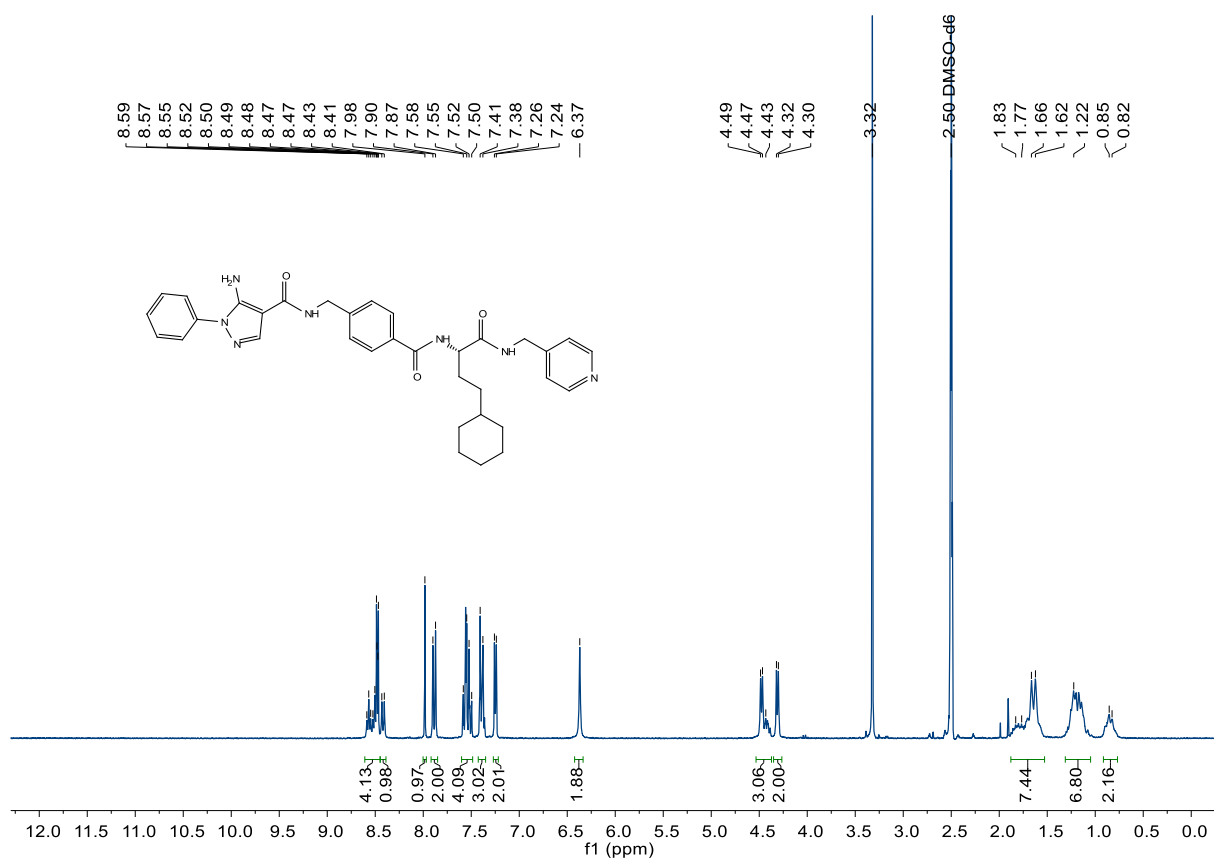


Figure 197. Compound 242 (SR92), <sup>1</sup>H-NMR, 300 MHz, DMSO-d<sub>6</sub>

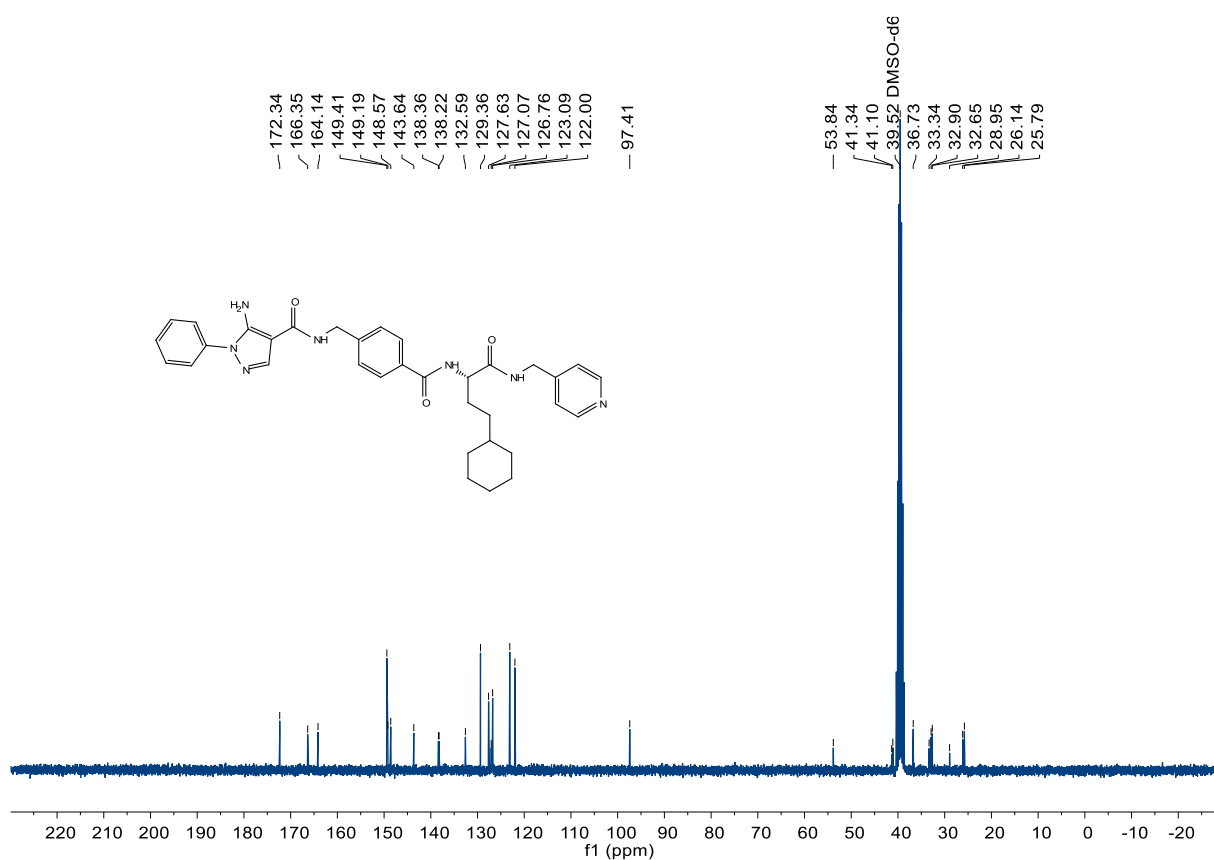
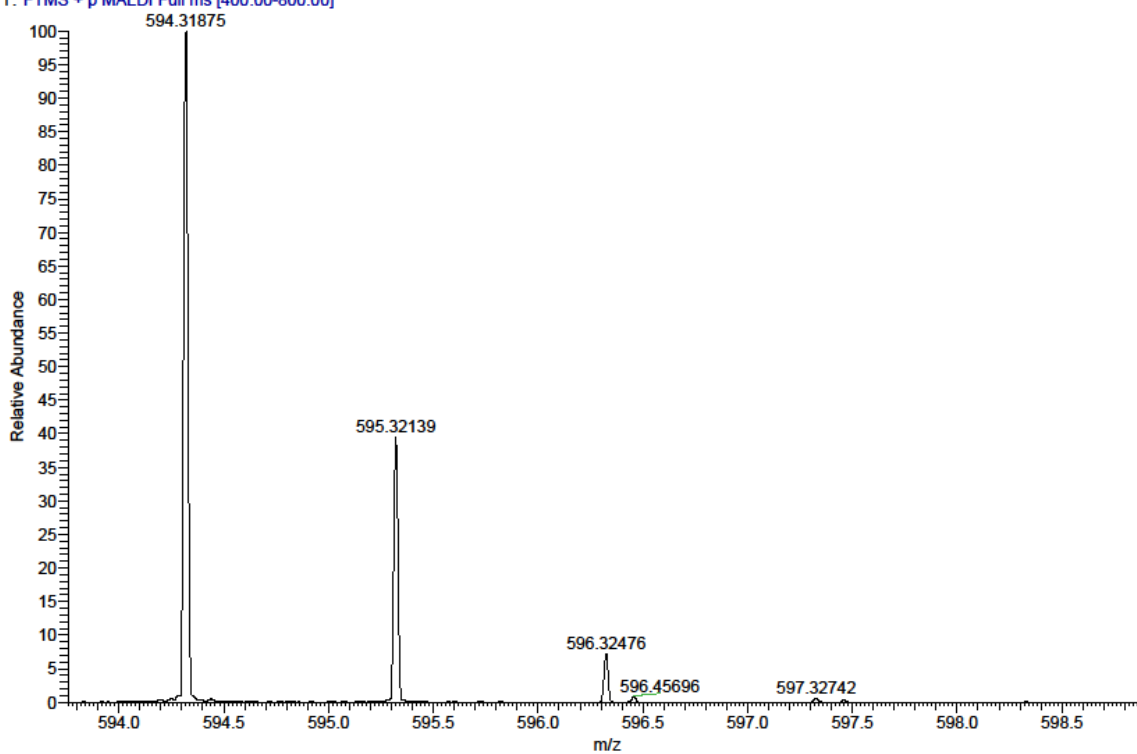
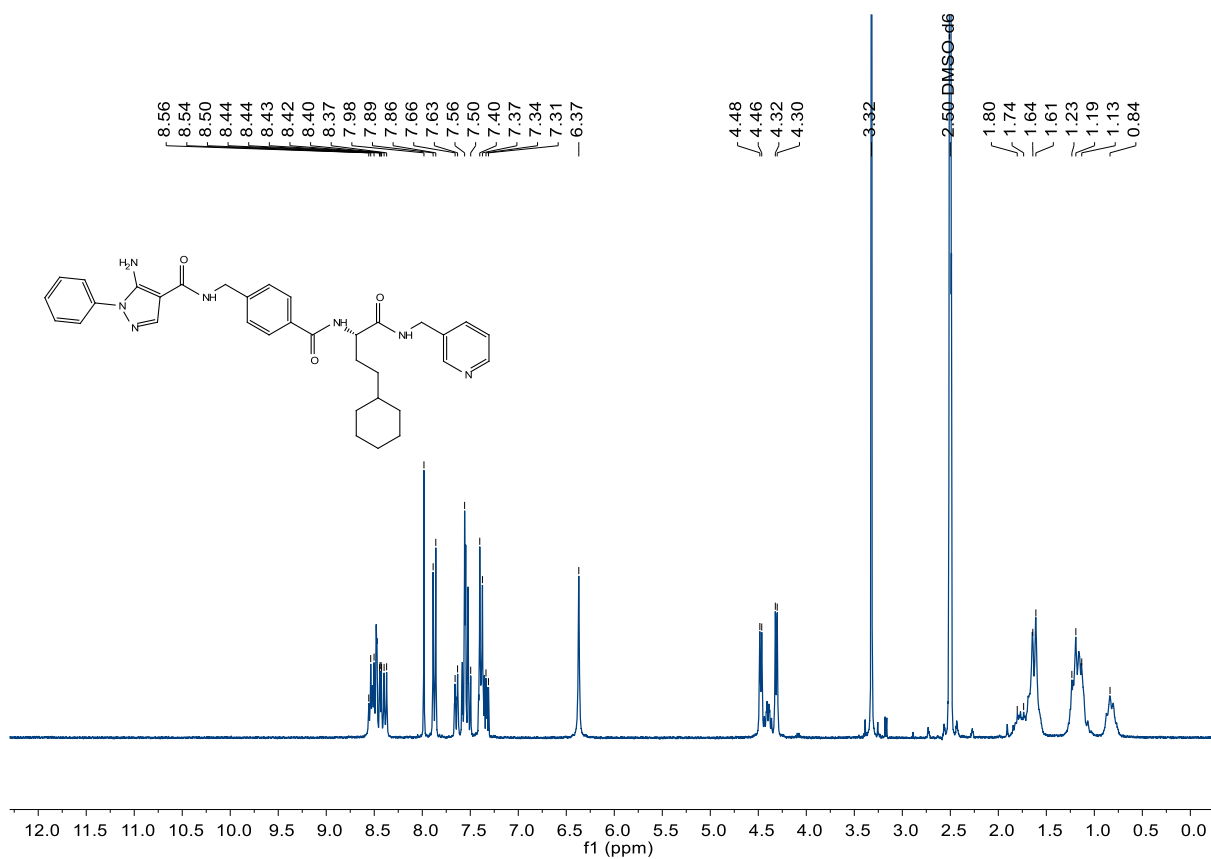


Figure 198. Compound 242 (SR92), <sup>13</sup>C-NMR, 75 MHz, DMSO-d<sub>6</sub>

C:\User\...\Knapp2018\180711\SR92\_F7

7/11/2018 5:04:46 PM

SR92 mit HCCA gemessen.

SR92\_F7 #1-5 RT: 0.00-0.29 AV: 5 NL: 1.85E7  
T: FTMS + p MALDI Full ms [400.00-800.00]**Figure 199.** Compound 242 (SR92), HRMS (FTMS + p MALDI)**Figure 200.** Compound 243 (SR93), <sup>1</sup>H-NMR, 300 MHz, DMSO-d<sub>6</sub>

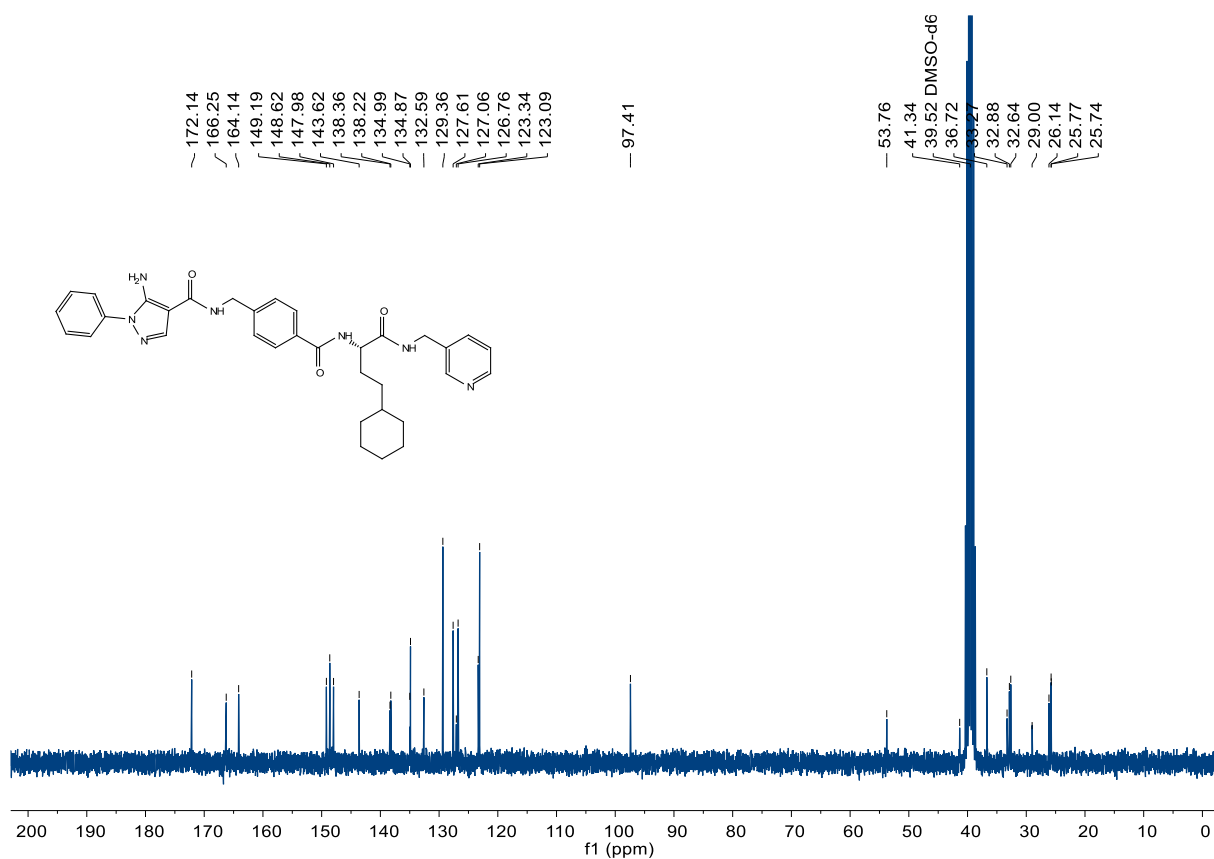


Figure 201. Compound 243 (SR93), <sup>13</sup>C-NMR, 75 MHz, DMSO-d<sub>6</sub>

C:\User\...Knapp\2018\180921\SR93\_B5

9/21/2018 10:58:31 AM

SR93 mit HCCA gemessen.

SR93\_B5 #1-11 RT: 0.01-0.94 AV: 11 NL: 9.56E5

T: FTMS + p MALDI Full ms [400.00-750.00]

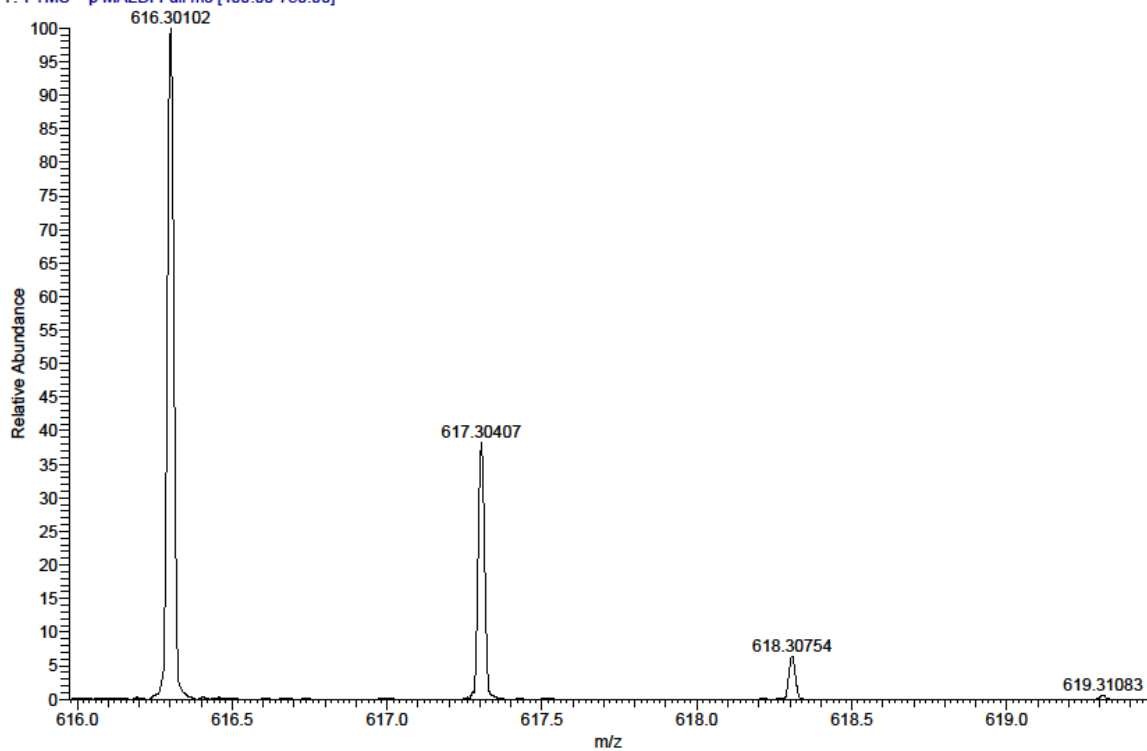
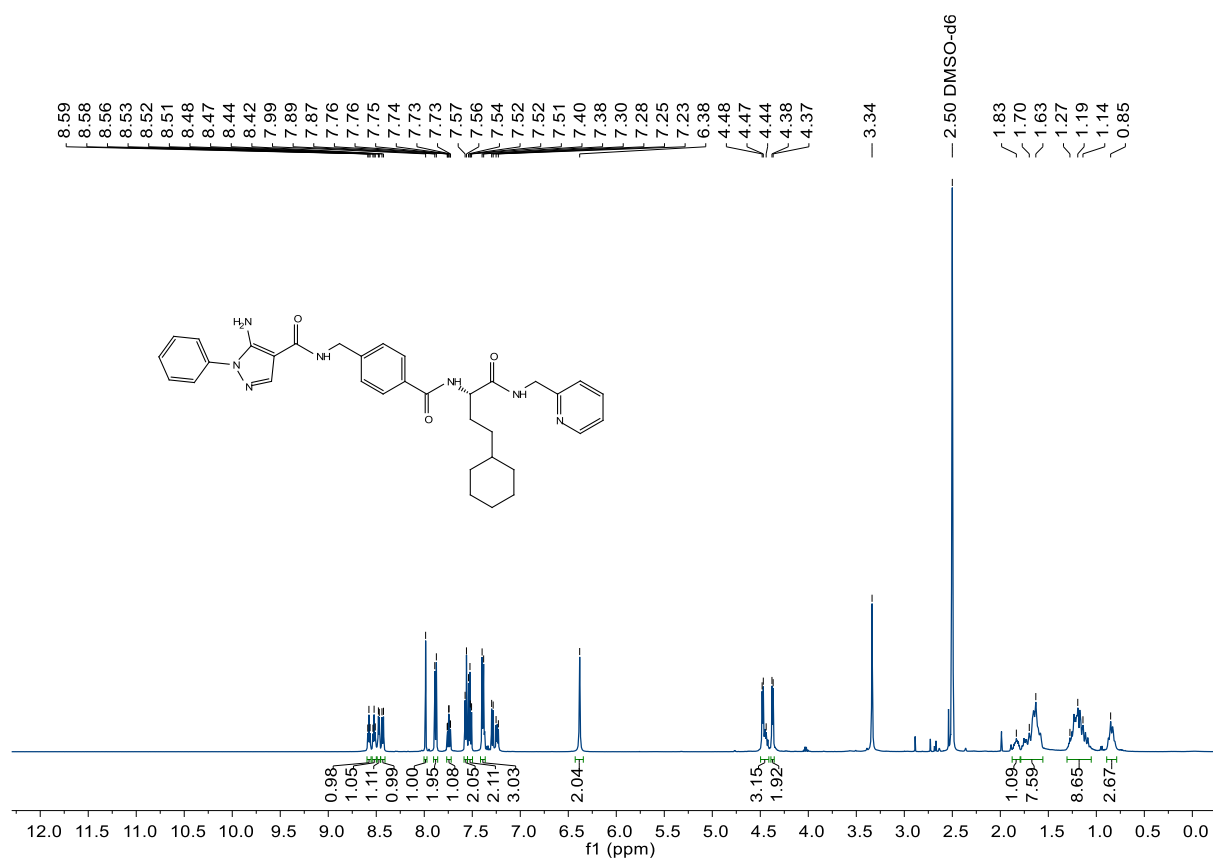
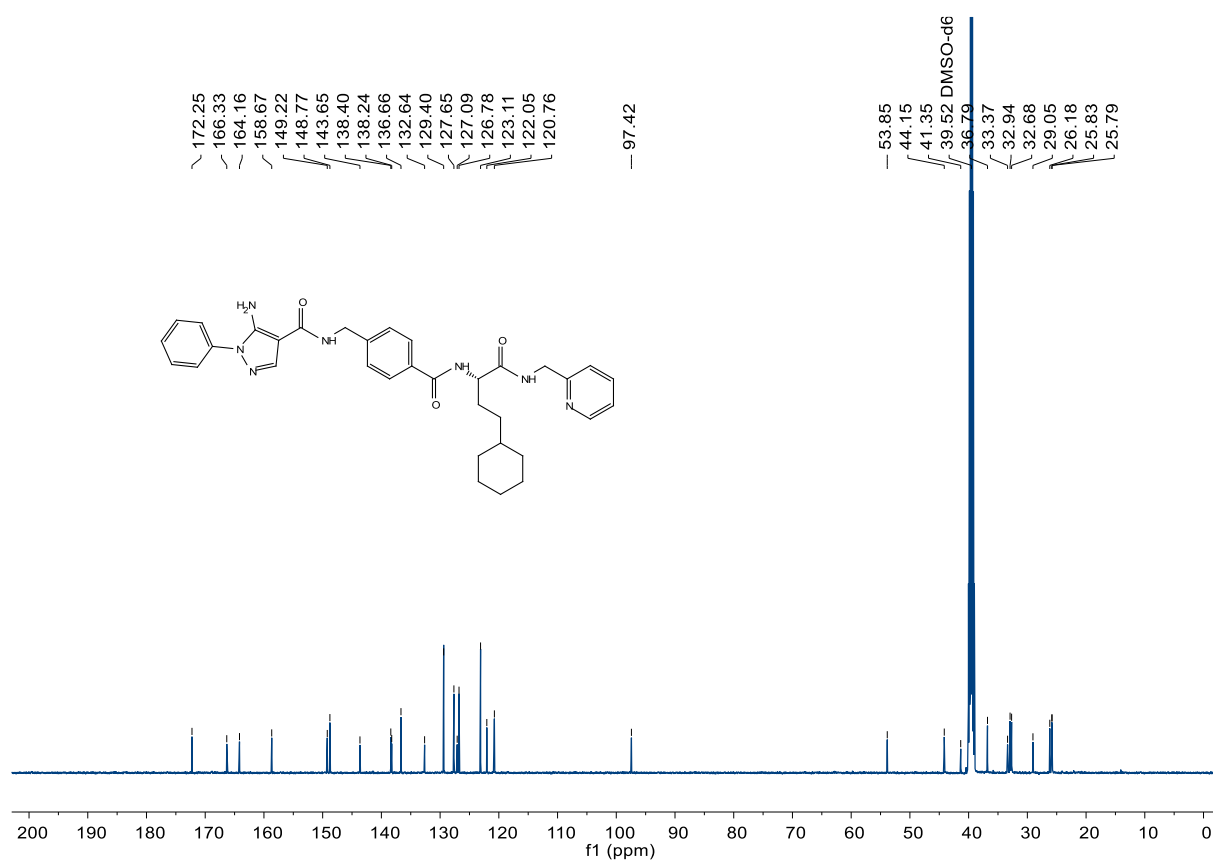


Figure 202. Compound 243 (SR93), HRMS (FTMS + p MALDI)





**Figure 203. Compound 244 (SR94),  $^1\text{H-NMR}$ , 500 MHz,  $\text{DMSO-d}_6$**



**Figure 204. Compound 244 (SR94),  $^{13}\text{C-NMR}$ , 126 MHz,  $\text{DMSO-d}_6$**

SR94\_B4 #1-9 RT: 0.01-0.73 AV: 9 NL: 3.86E5  
 T: FTMS + p MALDI Full ms [400.00-750.00]

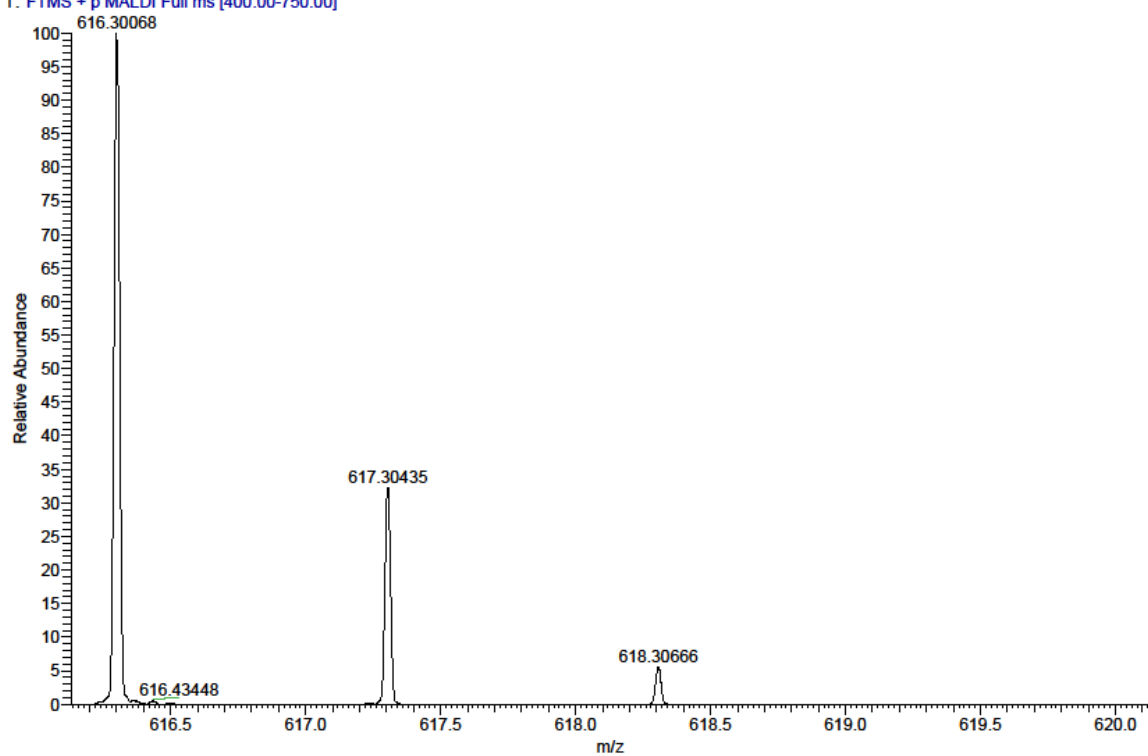


Figure 205. Compound 244 (SR94), HRMS (FTMS + p MALDI)

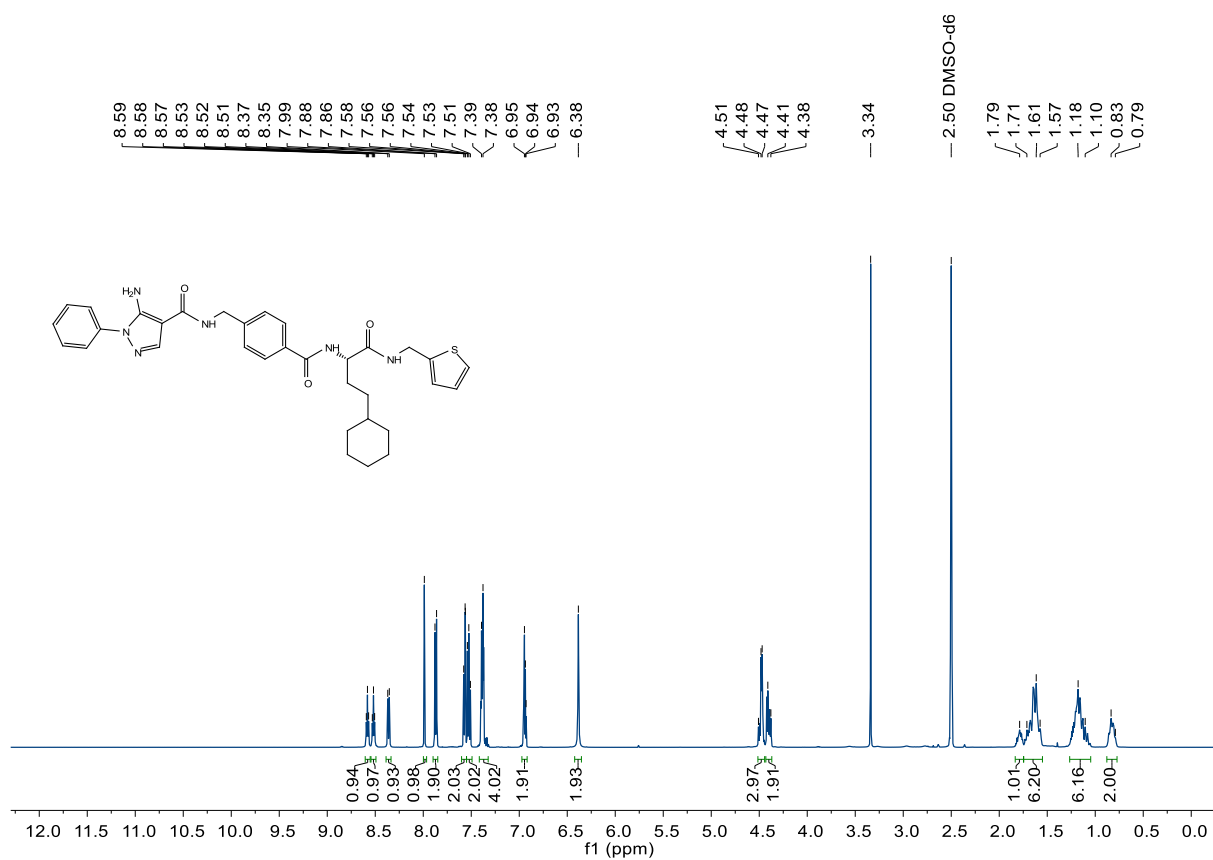


Figure 206. Compound 245 (SR97), <sup>1</sup>H-NMR, 500 MHz, DMSO-d<sub>6</sub>

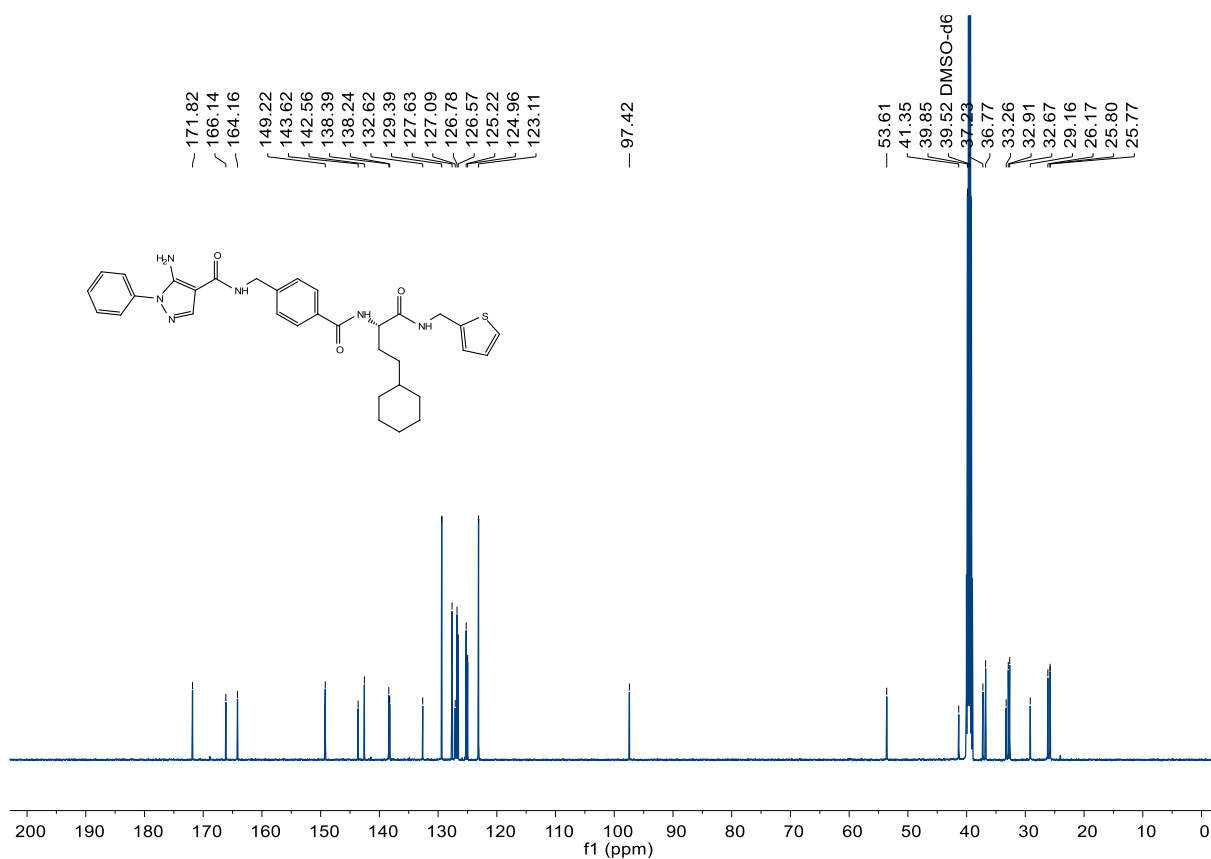


Figure 207. Compound 245 (SR97), <sup>13</sup>C-NMR, 126 MHz, DMSO-d<sub>6</sub>

C:\User\...\Knapp\2018\180308\SR97\_C1

3/8/2018 3:21:36 PM

SR97 mit HCCA gemessen.

SR97\_C1 #1-12 RT: 0.00-1.30 AV: 12 NL: 1.73E4  
T: FTMS + p MALDI Full ms [500.00-800.00]

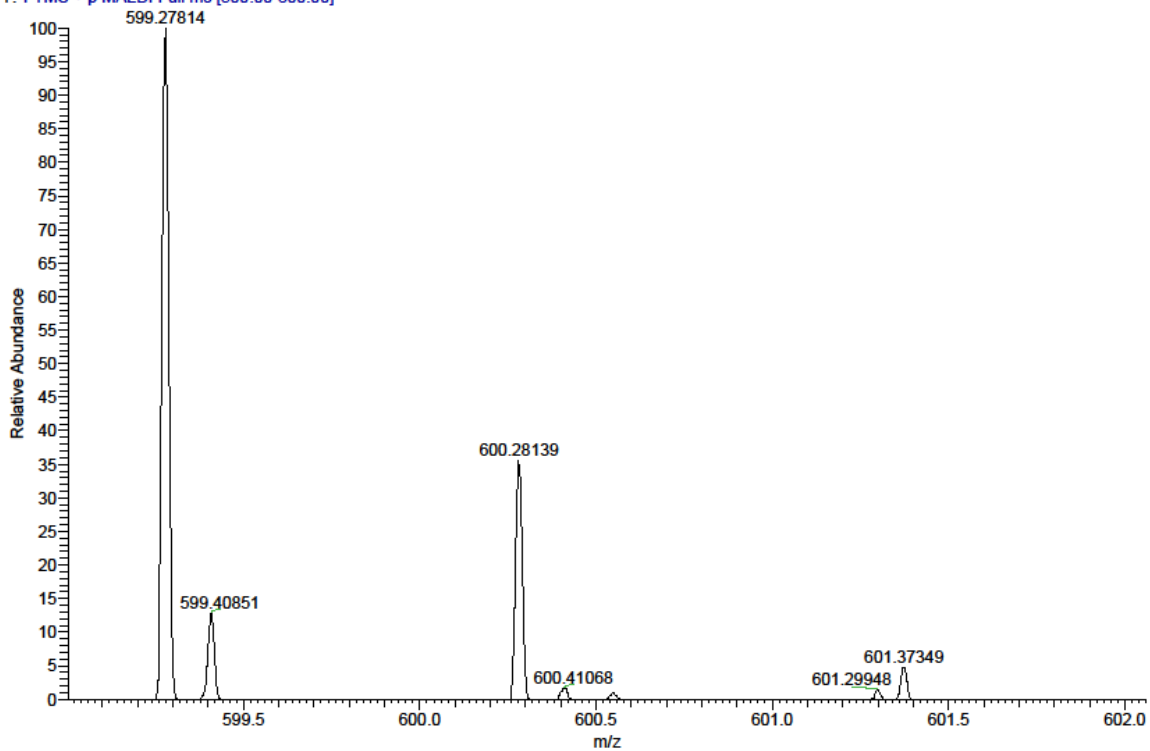


Figure 208. Compound 245 (SR97), HRMS (FTMS + p MALDI)

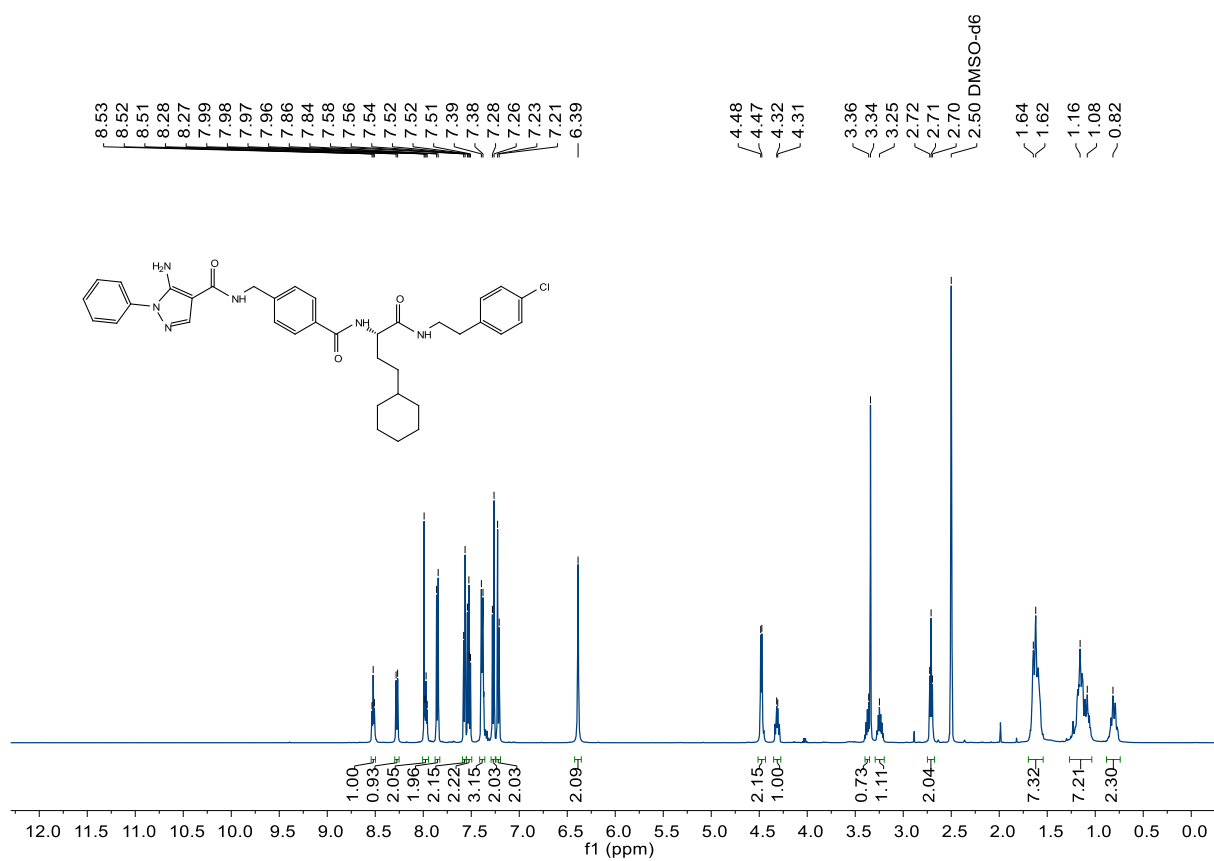


Figure 209. Compound 246 (SR72), <sup>1</sup>H-NMR, 500 MHz, DMSO-d<sub>6</sub>

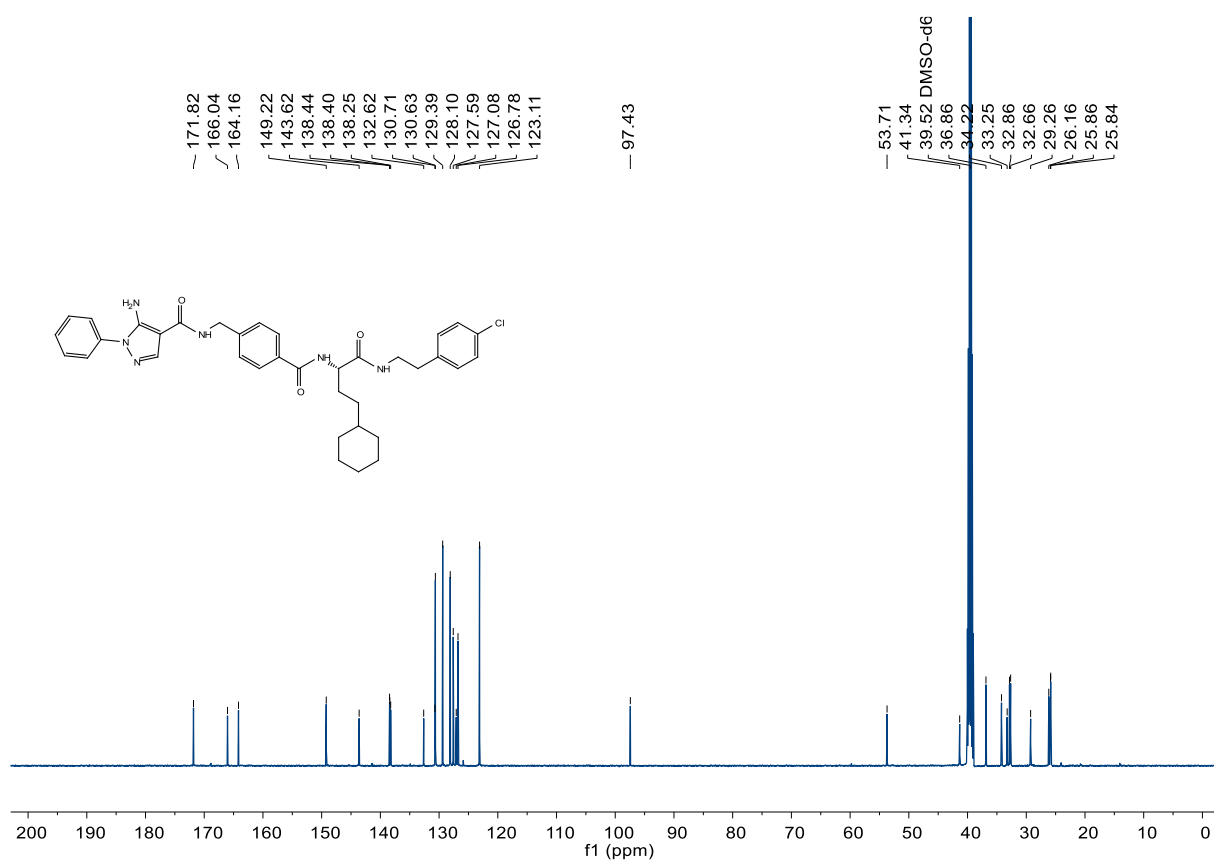


Figure 210. Compound 246 (SR72), <sup>13</sup>C-NMR, 126 MHz, DMSO-d<sub>6</sub>

C:\User\...\Knapp2018\180308\SR72\_C3

3/8/2018 3:29:11 PM

SR72 mit HCCA gemessen.

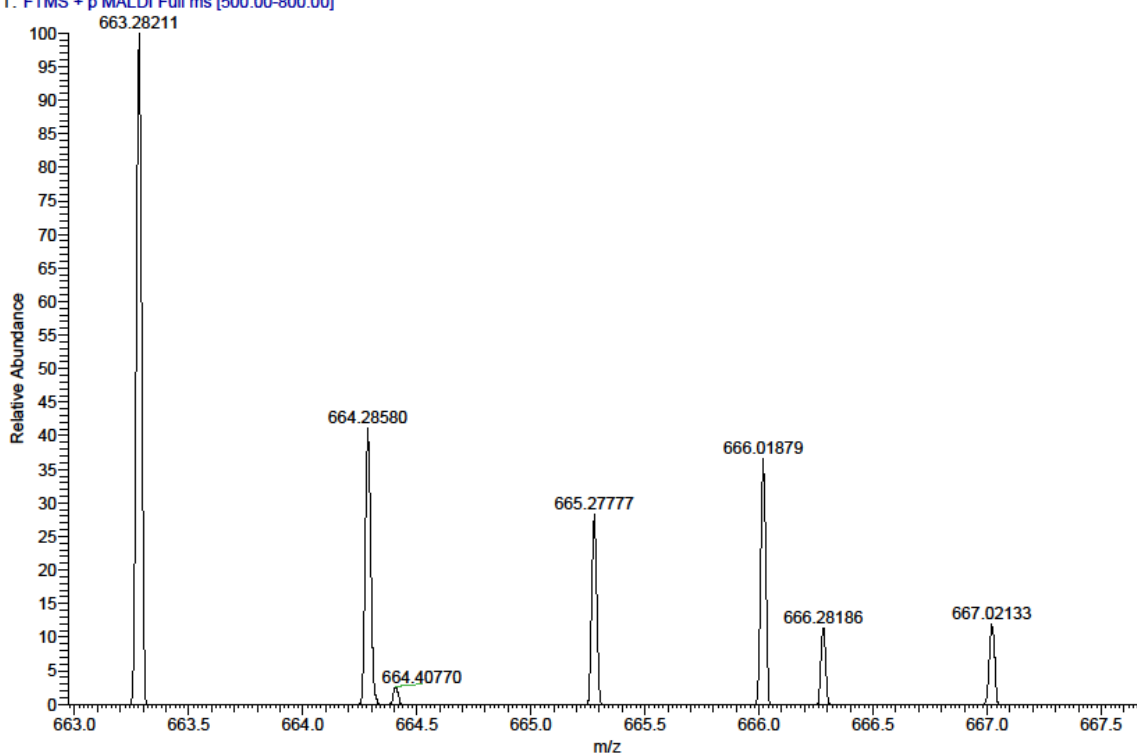
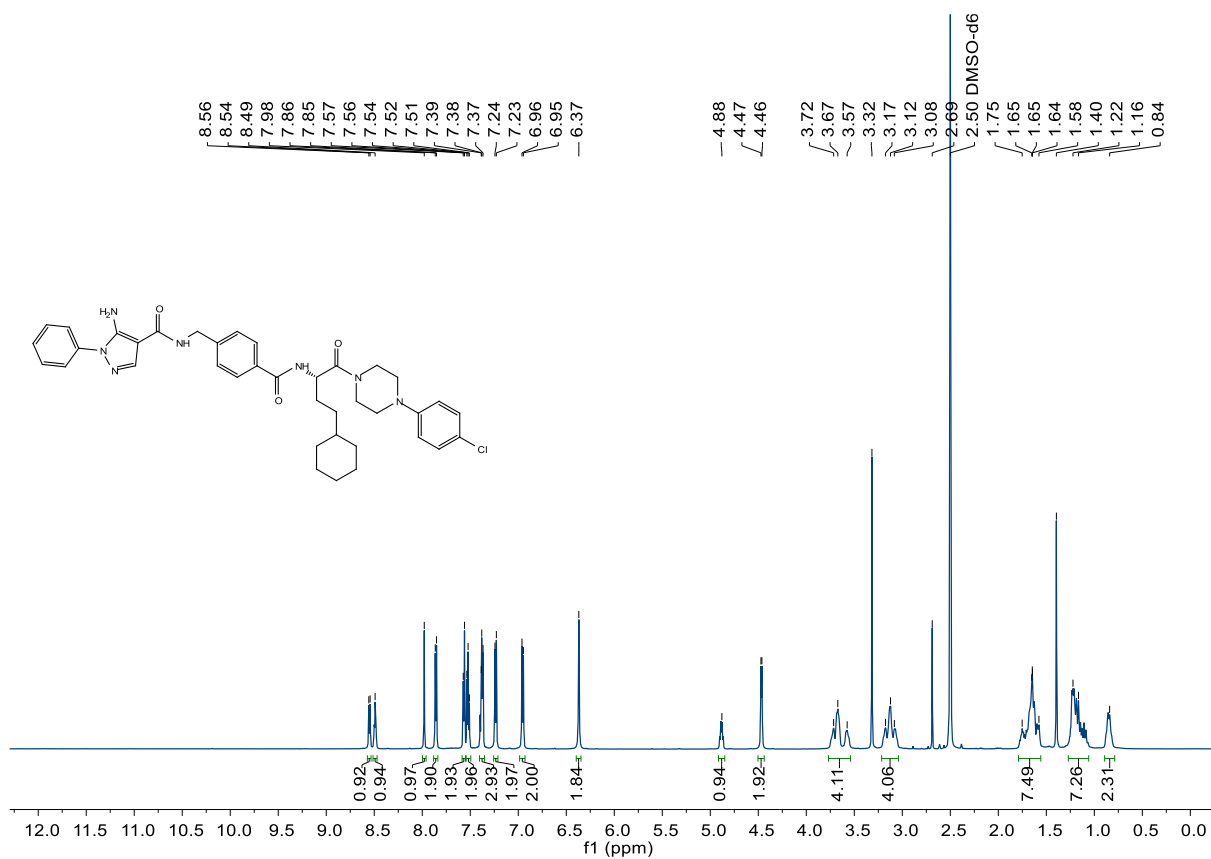
SR72\_C3 #1-13 RT: 0.01-1.44 AV: 13 NL: 1.88E4  
T: FTMS + p MALDI Full ms [500.00-800.00]

Figure 211. Compound 246 (SR72), HRMS (FTMS + p MALDI)

Figure 212. Compound 247 (SR108),  $^1\text{H-NMR}$ , 600 MHz,  $\text{DMSO-d}_6$

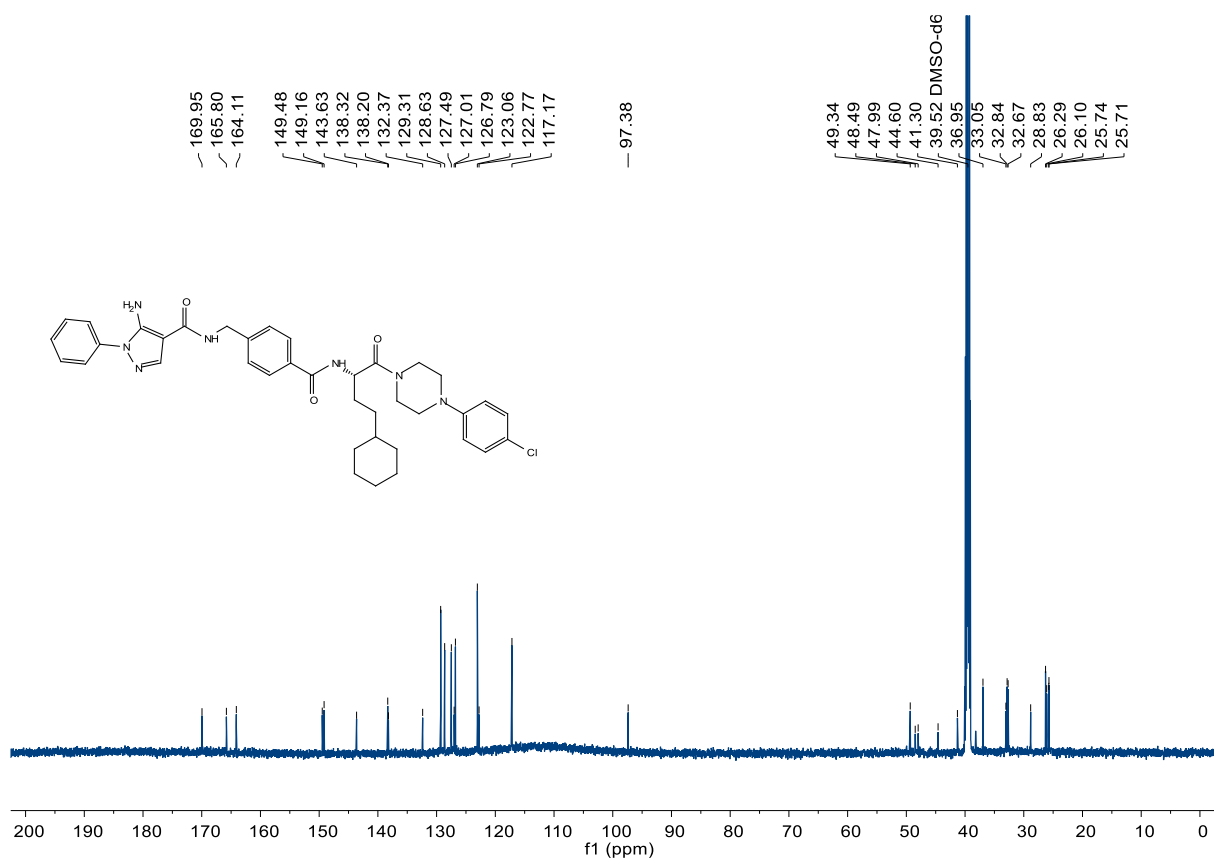


Figure 213. Compound 247 (SR108), <sup>13</sup>C-NMR, 150 MHz, DMSO-d<sub>6</sub>

C:\User\...Knapp\2018\180711\SR108\_F9

7/11/2018 5:06:36 PM

SR108 mit HCCA gemessen.

SR108\_F9 #1-14 RT: 0.00-1.37 AV: 14 NL: 1.21E5

T: FTMS + p MALDI Full ms [400.00-800.00]

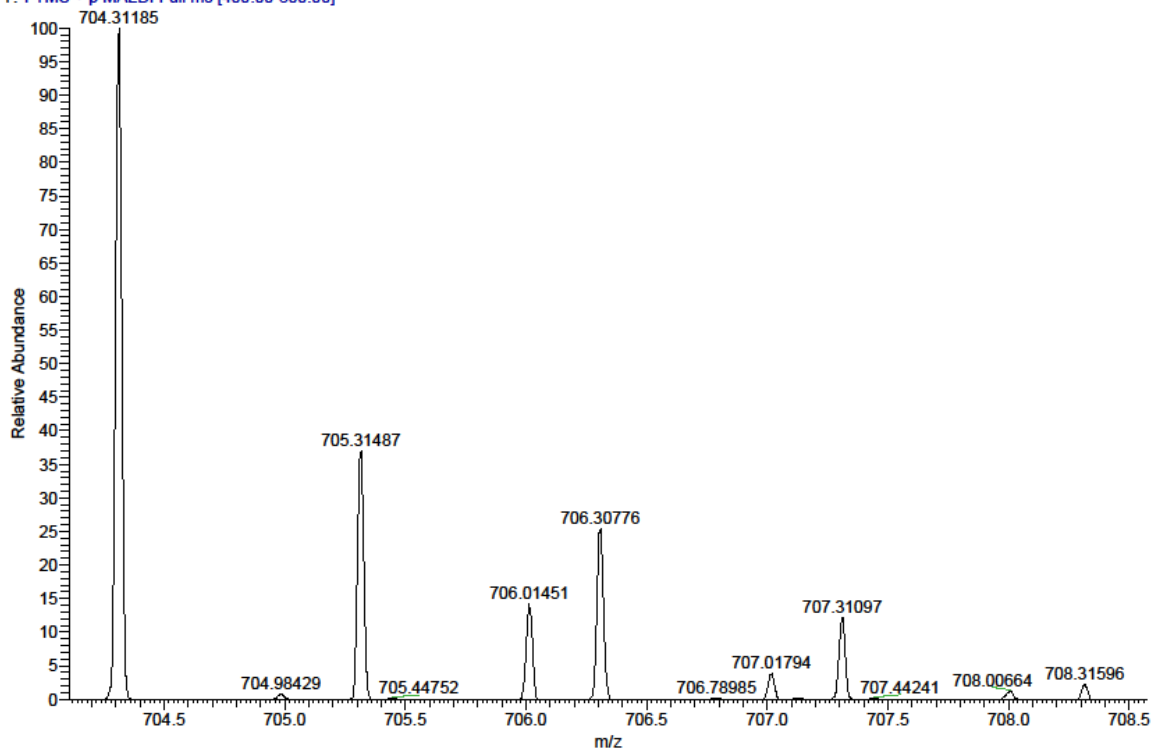
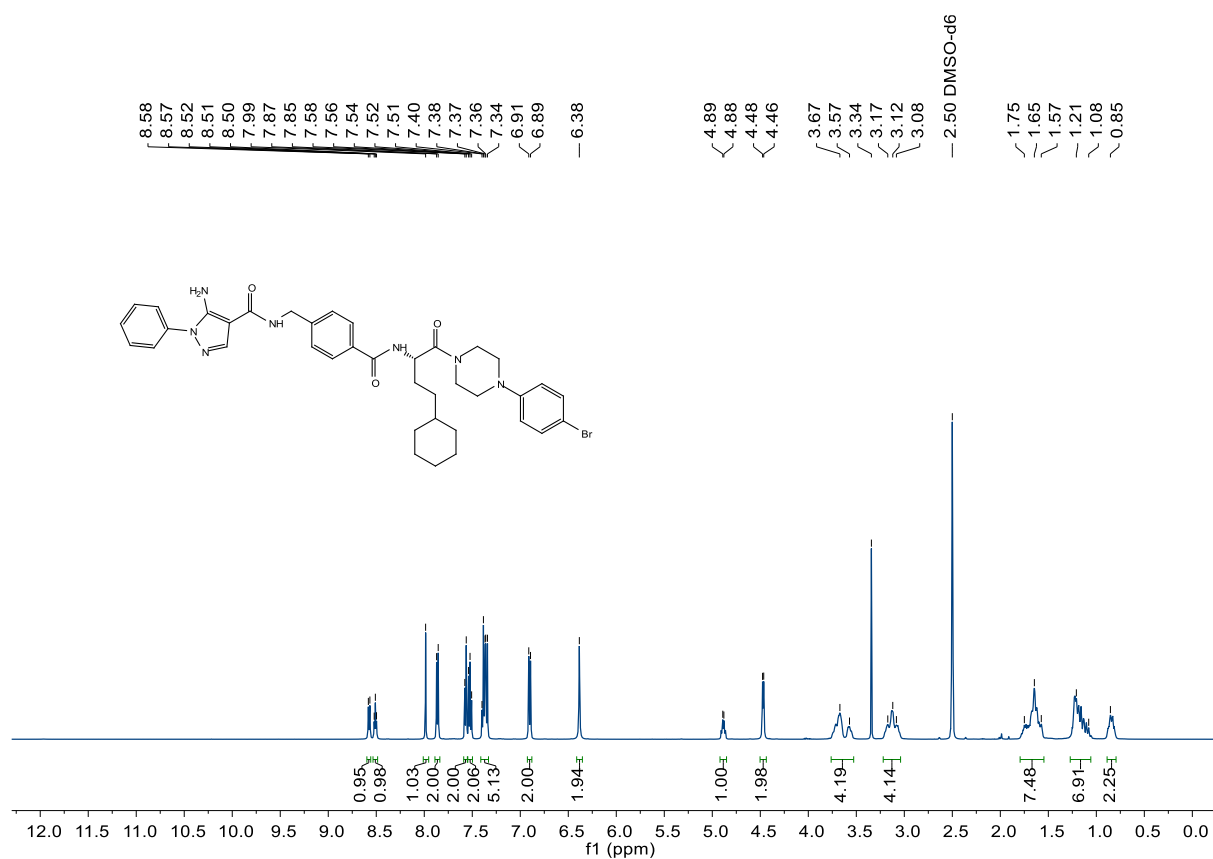
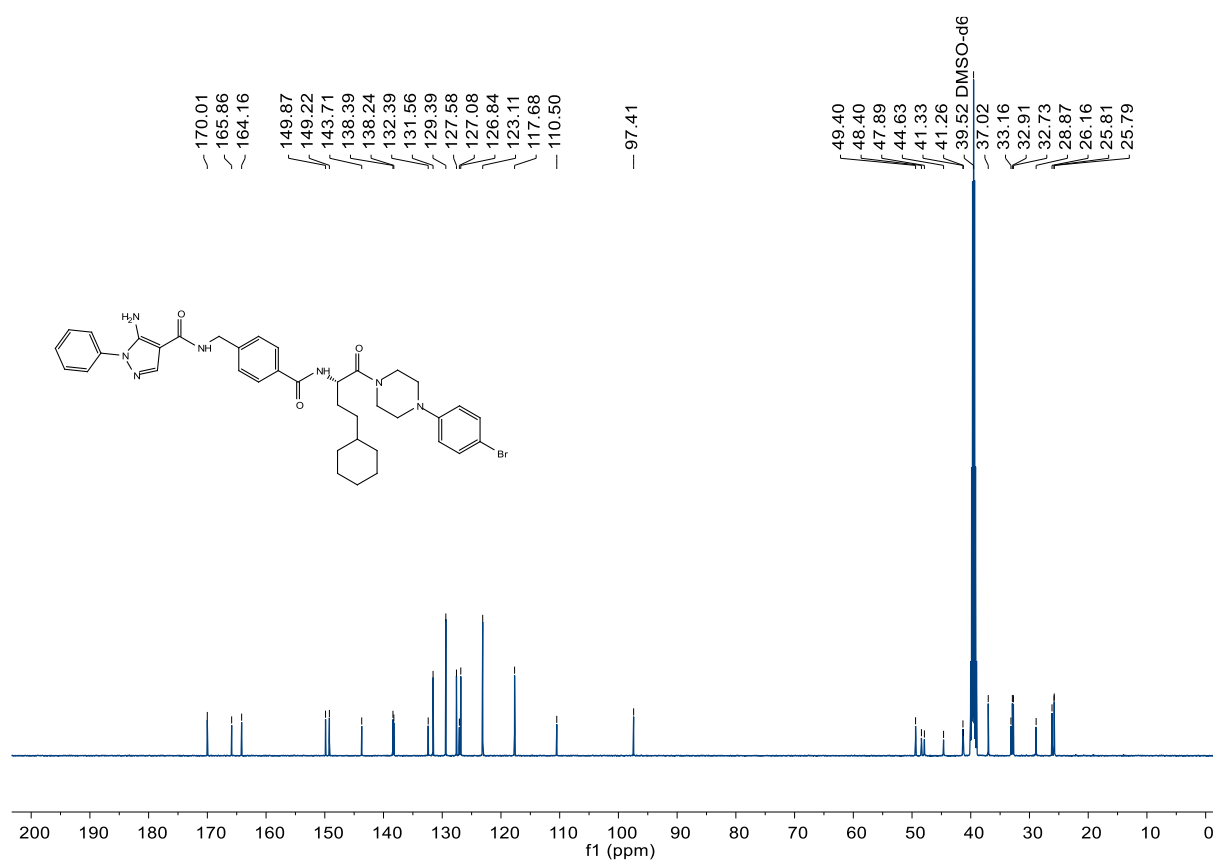


Figure 214. Compound 247 (SR108), HRMS (FTMS + p MALDI)



**Figure 215. Compound 248 (SR111),  $^1\text{H-NMR}$ , 500 MHz,  $\text{DMSO-d}_6$**



**Figure 216. Compound 248 (SR111),  $^{13}\text{C-NMR}$ , 126 MHz,  $\text{DMSO-d}_6$**

SR111\_C2 #1-20 RT: 0.01-2.32 AV: 20 NL: 1.43E3  
T: FTMS + p MALDI Full ms [500.00-800.00]

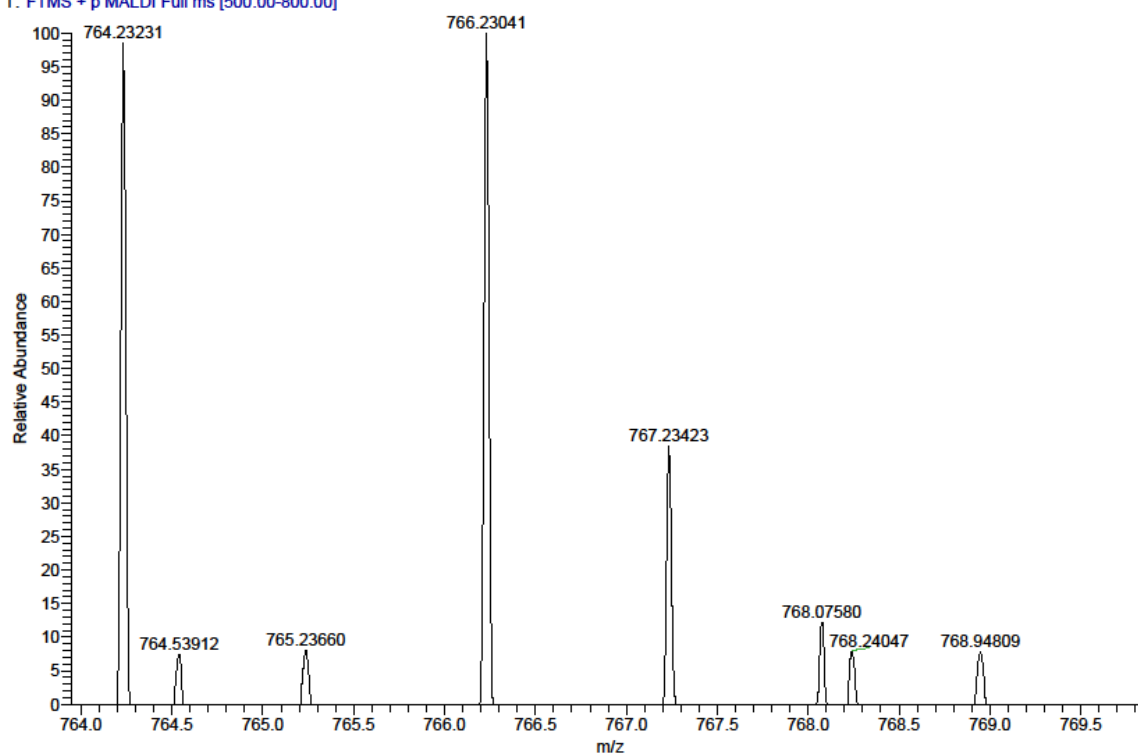


Figure 217. Compound 248 (SR111), HRMS (FTMS + p MALDI)

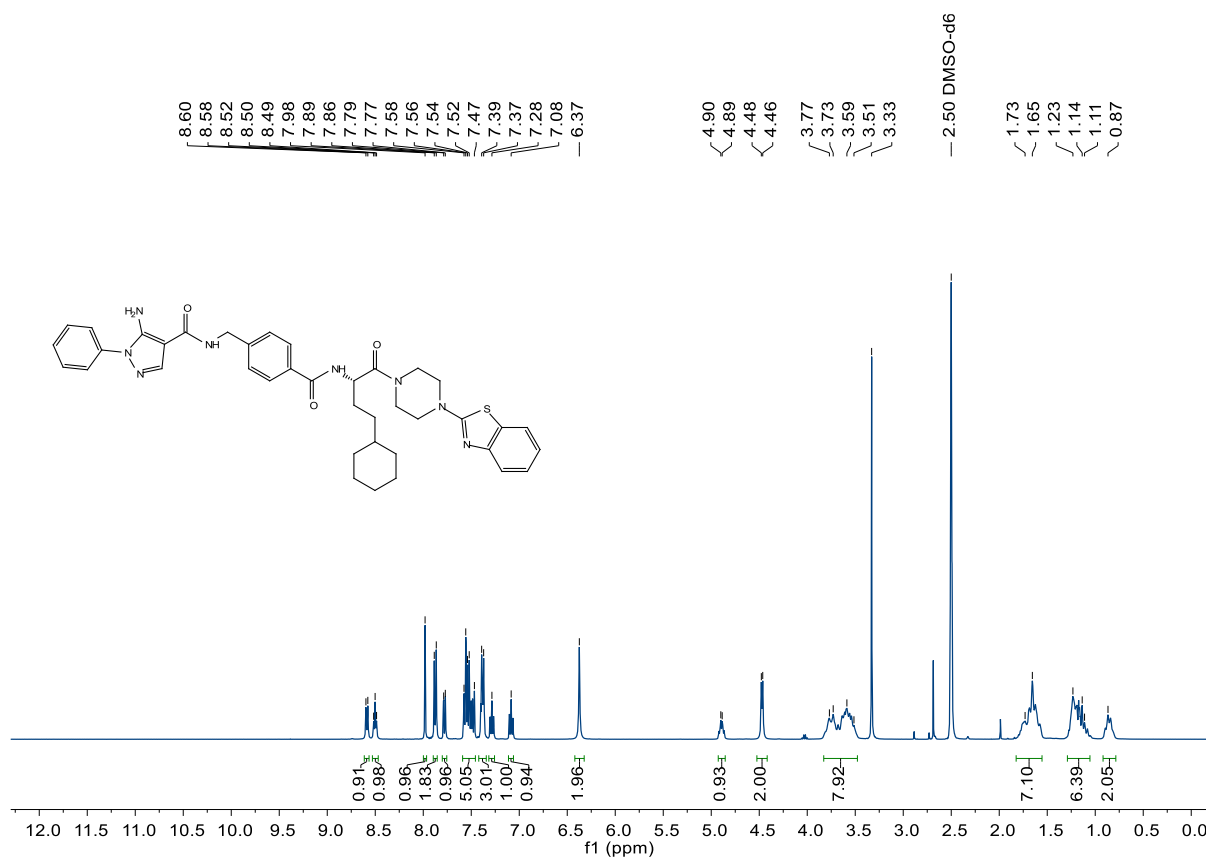


Figure 218. Compound 249 (SR126),  $^1\text{H-NMR}$ , 400 MHz,  $\text{DMSO-d}_6$



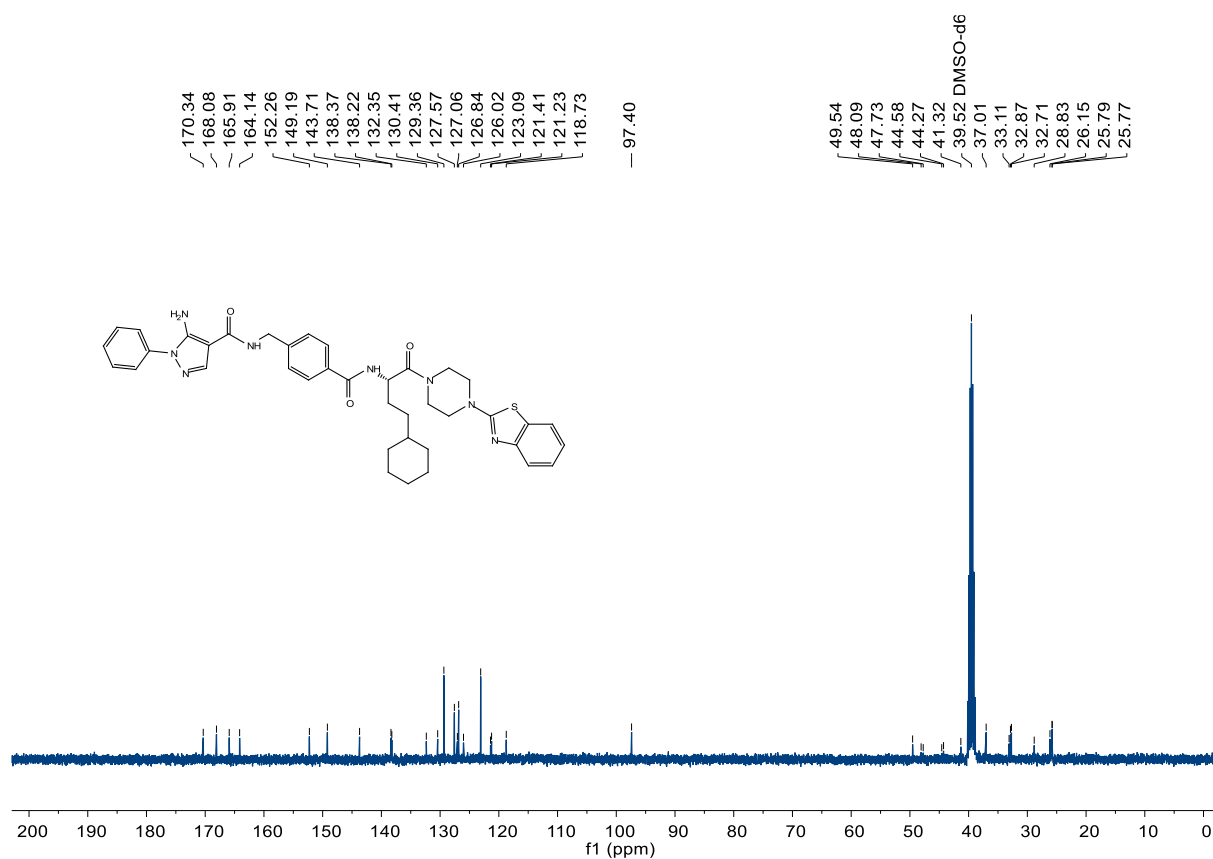


Figure 219. Compound 249 (SR126), <sup>13</sup>C-NMR, 101 MHz, DMSO-d<sub>6</sub>

C:\User\...\Knapp\2018\180319\SR126\_D2

3/19/2018 2:23:40 PM

SR126 mit HCCA gemessen.

SR126\_D2 #1-3 RT: 0.01-0.26 AV: 3 NL: 7.87E4  
T: FTMS + p MALDI Full ms [500.00-800.00]

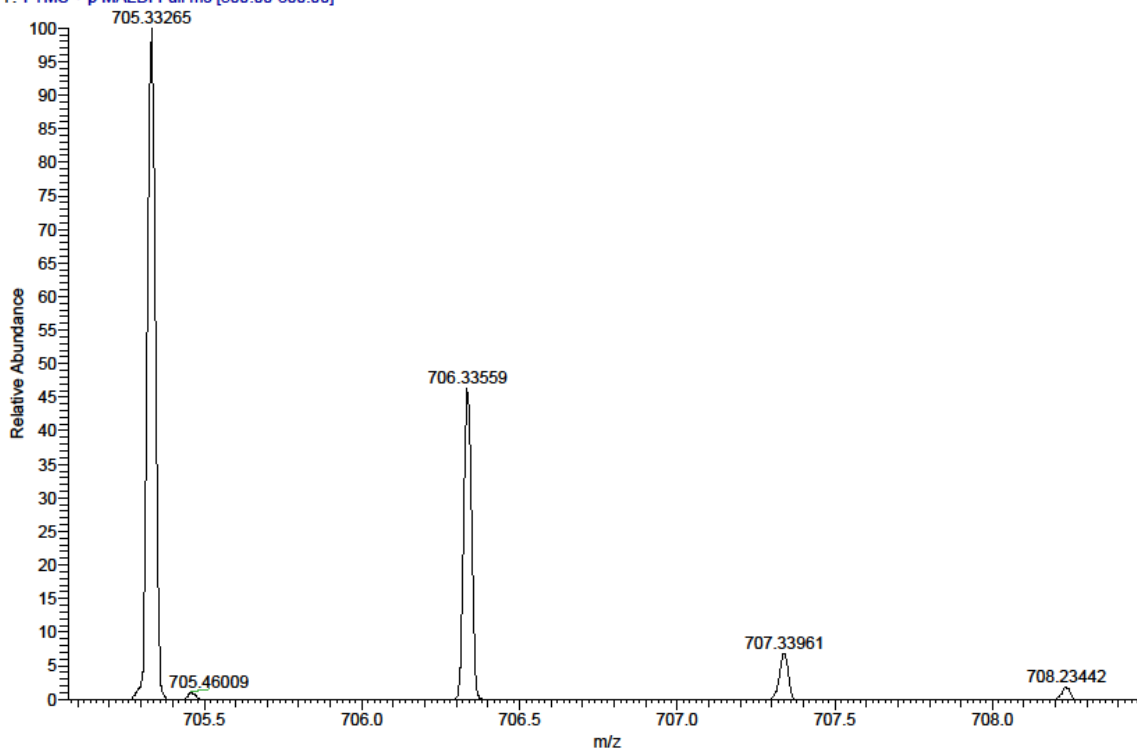


Figure 220. Compound 249 (SR126), HRMS (FTMS + p MALDI)

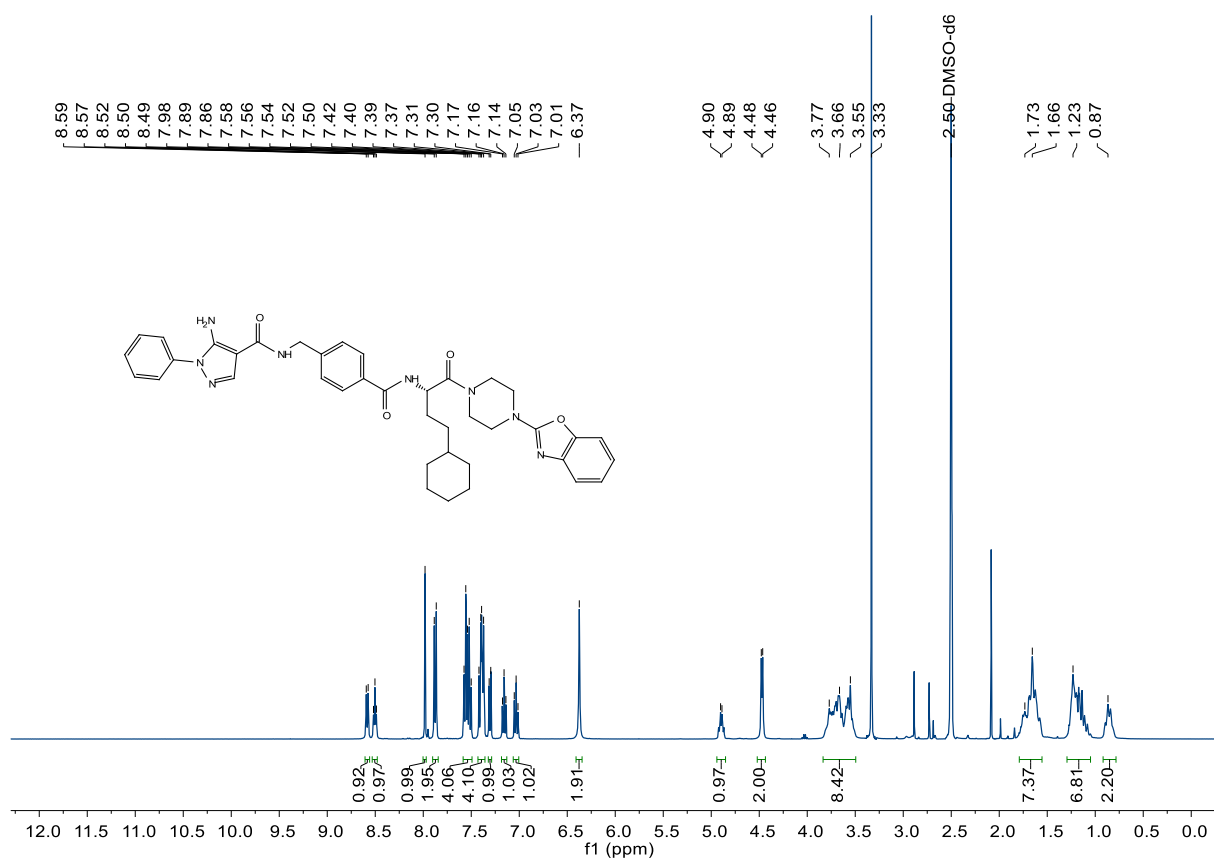


Figure 221. Compound 250 (SR127), <sup>1</sup>H-NMR, 400 MHz, DMSO-d<sub>6</sub>

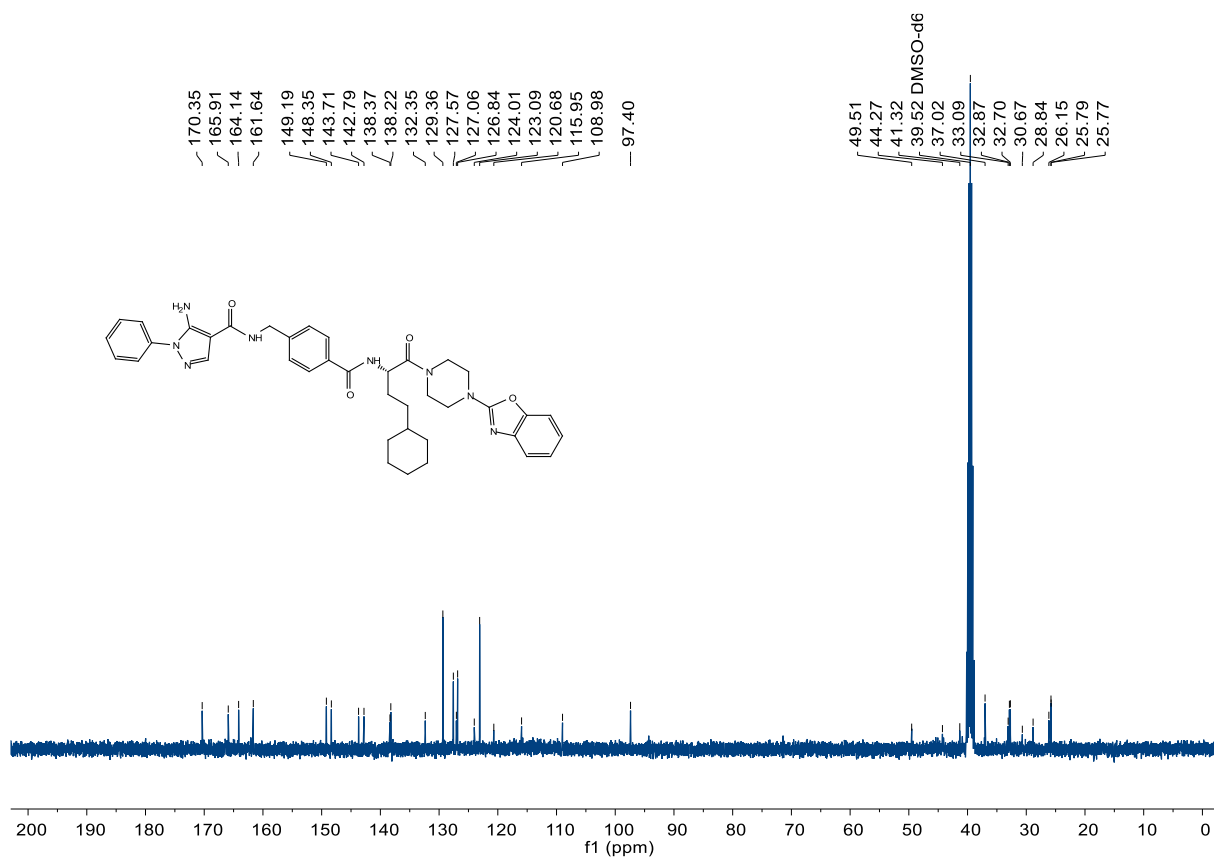


Figure 222. Compound 250 (SR127), <sup>13</sup>C-NMR, 101 MHz, DMSO-d<sub>6</sub>

C:\User\...\Knapp2018\180319\SR127\_D3

3/19/2018 2:27:20 PM

SR127 mit HCCA gemessen.

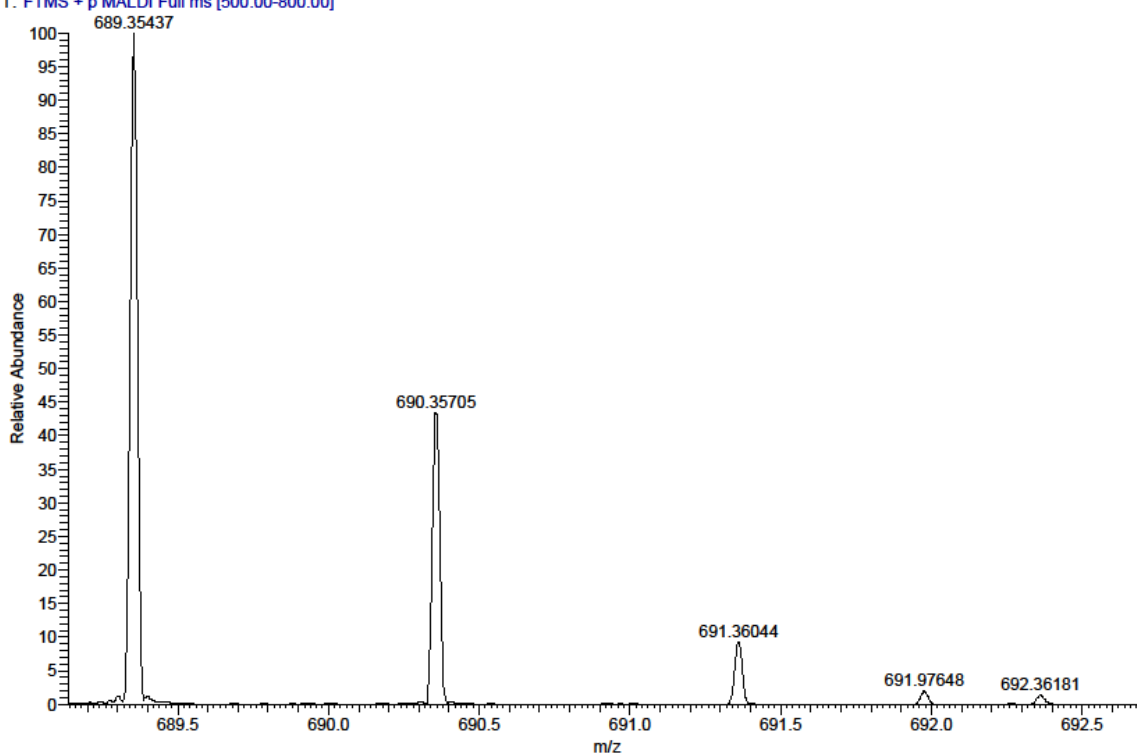
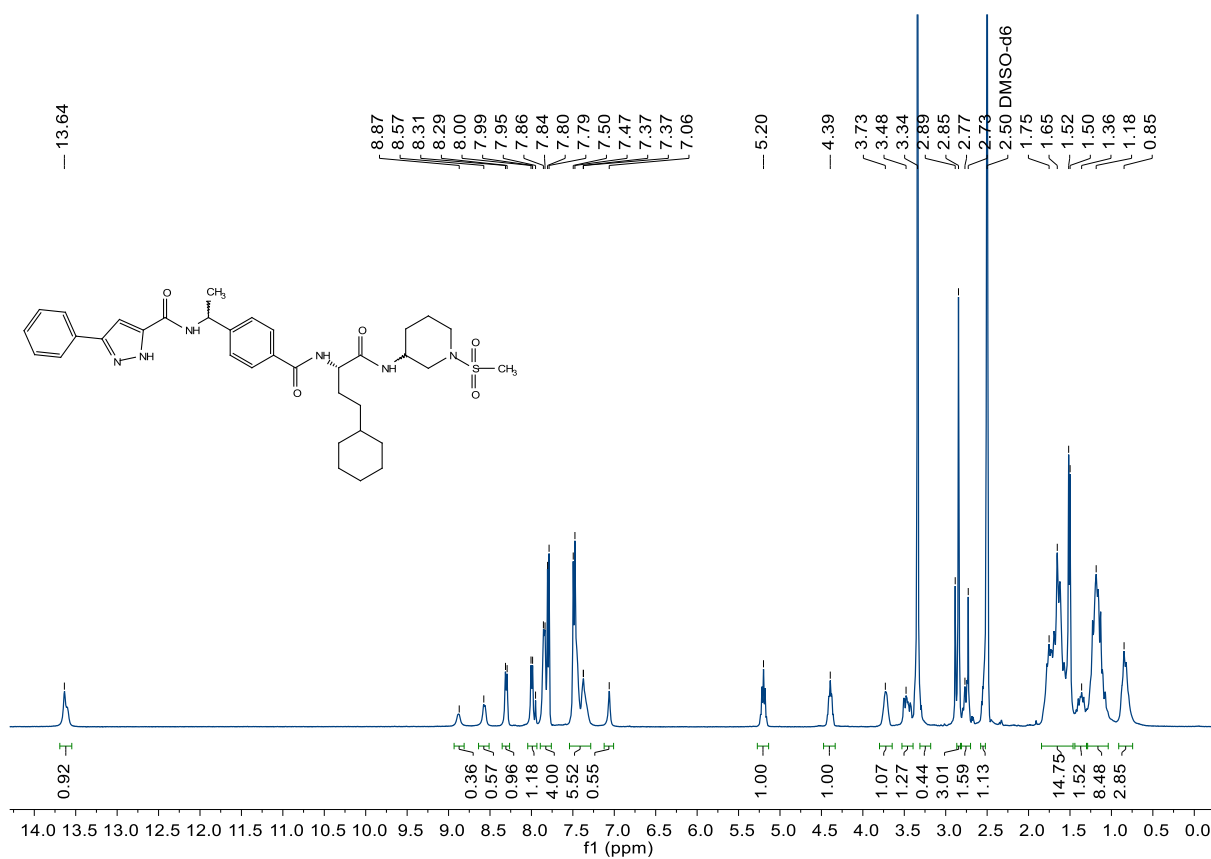
SR127\_D3 #1-4 RT: 0.01-0.38 AV: 4 NL: 8.89E5  
T: FTMS + p MALDI Full ms [500.00-800.00]

Figure 223. Compound 250 (SR127), HRMS (FTMS + p MALDI)

Figure 224. Compound 293 (SR262), <sup>1</sup>H-NMR, 600 MHz, DMSO-d<sub>6</sub>

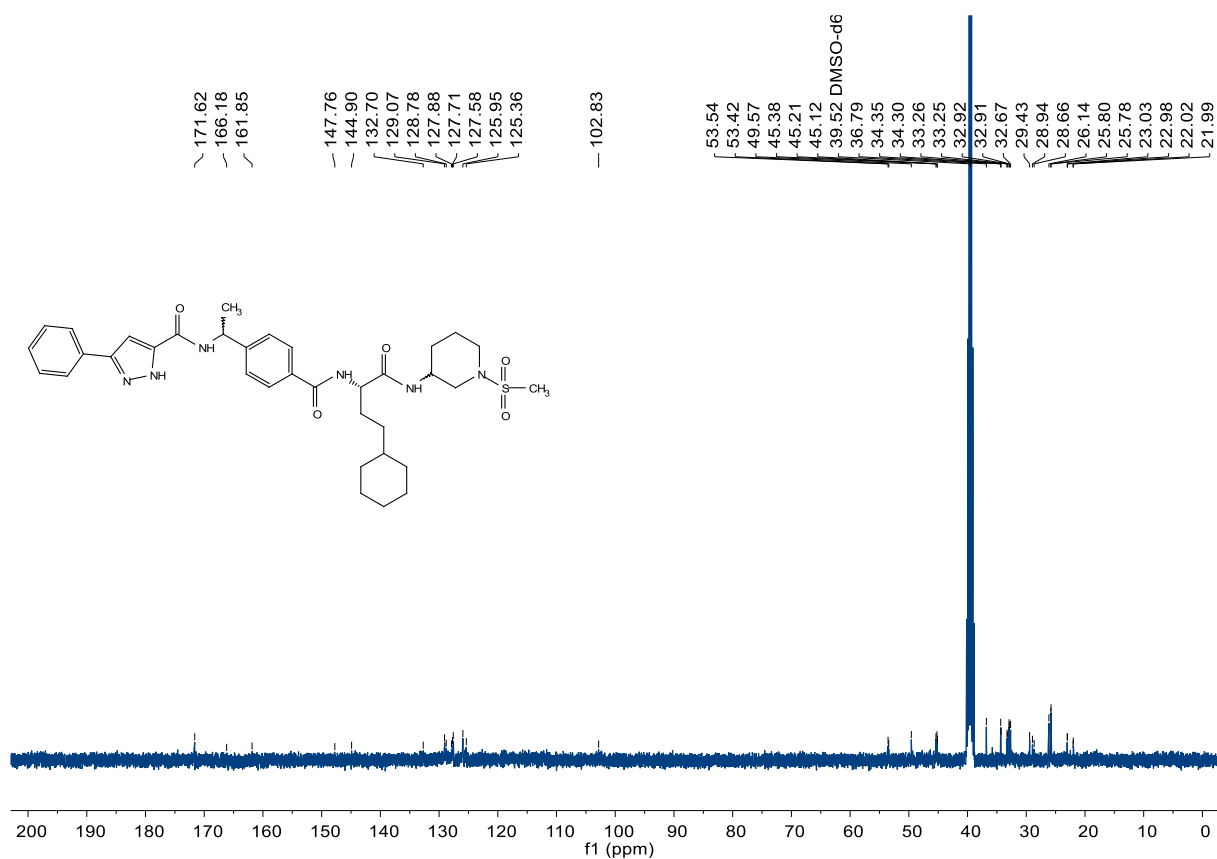


Figure 225. Compound 293 (SR262),  $^{13}\text{C}$ -NMR, 150 MHz,  $\text{DMSO-d}_6$

C:\User\...Knapp\2018\180921\SR262\_A9

9/21/2018 10:46:25 AM

SR262 mit HCCA gemessen.

SR262\_A9 #1-4 RT: 0.01-0.37 AV: 4 NL: 9.69E4

T: FTMS + p MALDI Full ms [450.00-750.00]

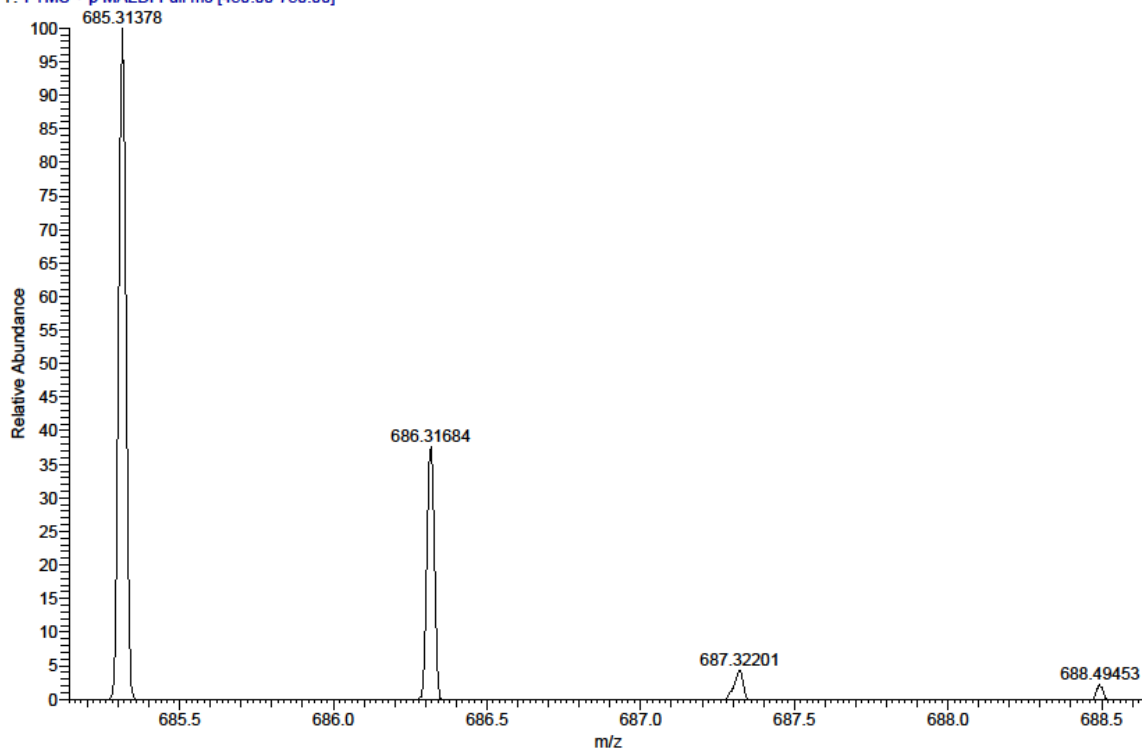


Figure 226. Compound 293 (SR262), HRMS (FTMS + p MALDI)

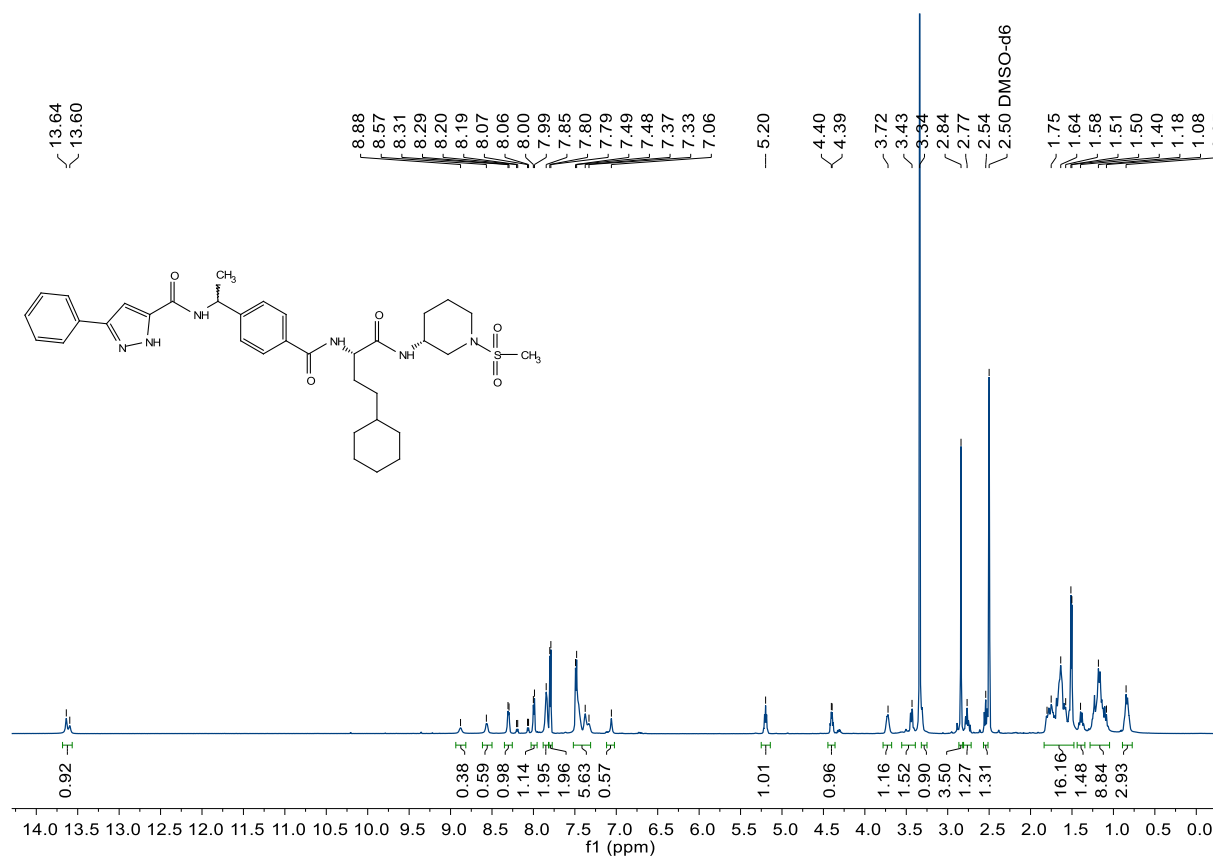


Figure 227. Compound 294 (SR264),  $^1\text{H-NMR}$ , 600 MHz,  $\text{DMSO-d}_6$

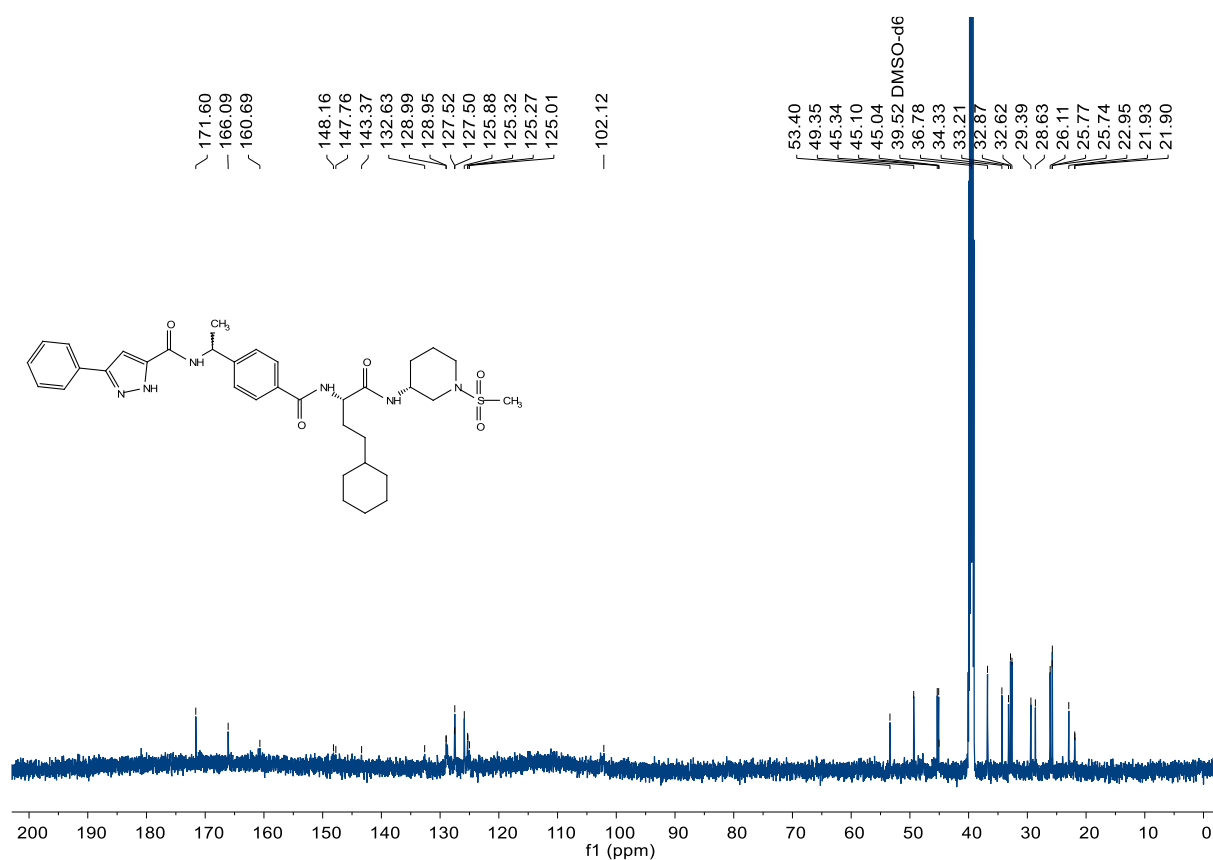
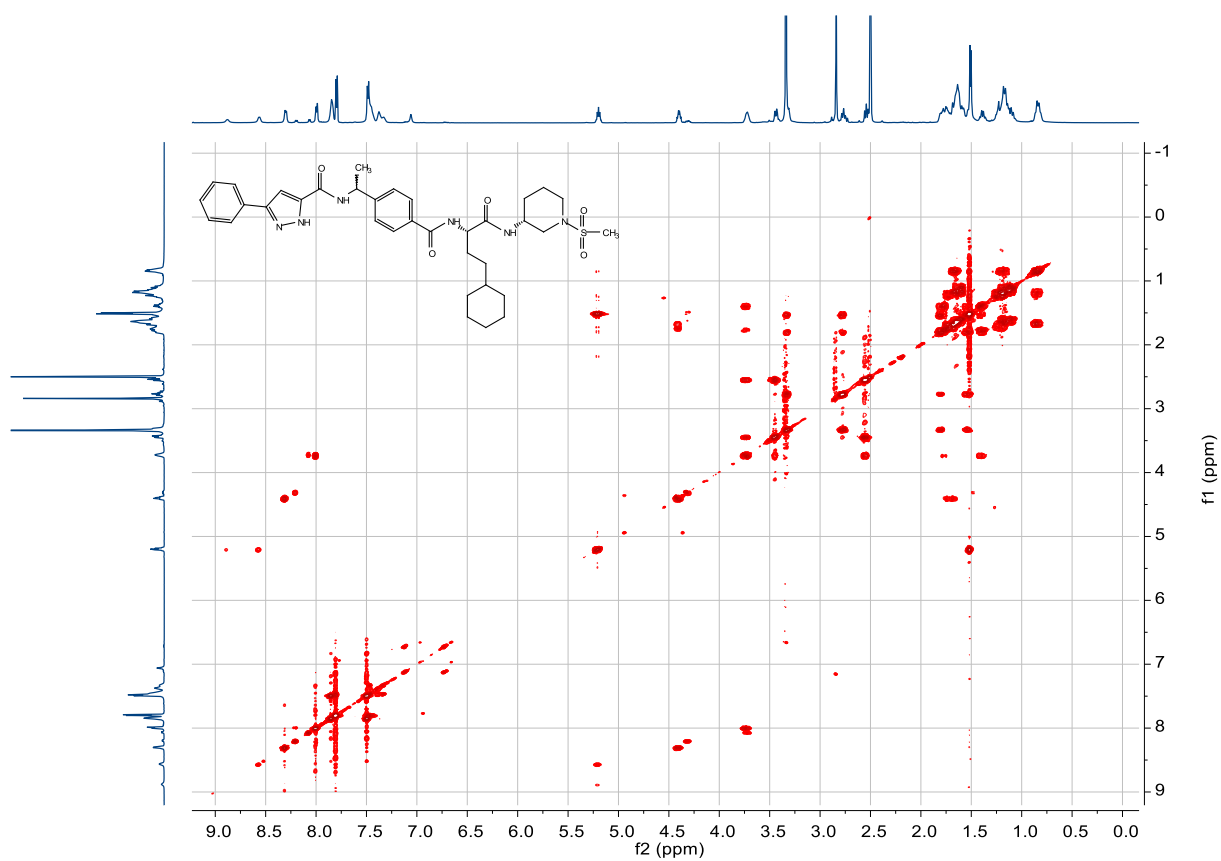
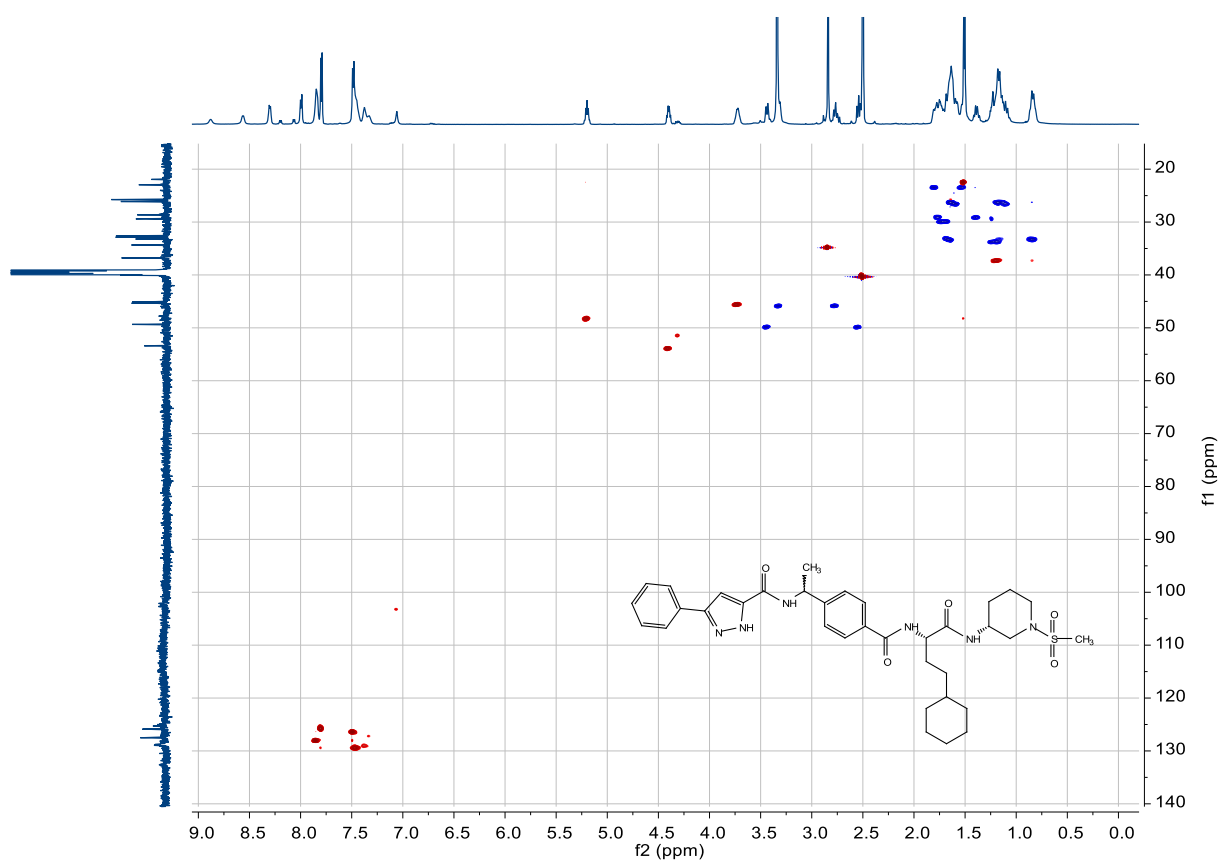


Figure 228. Compound 294 (SR264),  $^{13}\text{C-NMR}$ , 150 MHz,  $\text{DMSO-d}_6$

Figure 229. Compound 294 (SR264), COSY, 600MHz, DMSO-d<sub>6</sub>Figure 230. Compound 294 (SR264), HSQC, 600/ 150 MHz, DMSO-d<sub>6</sub>

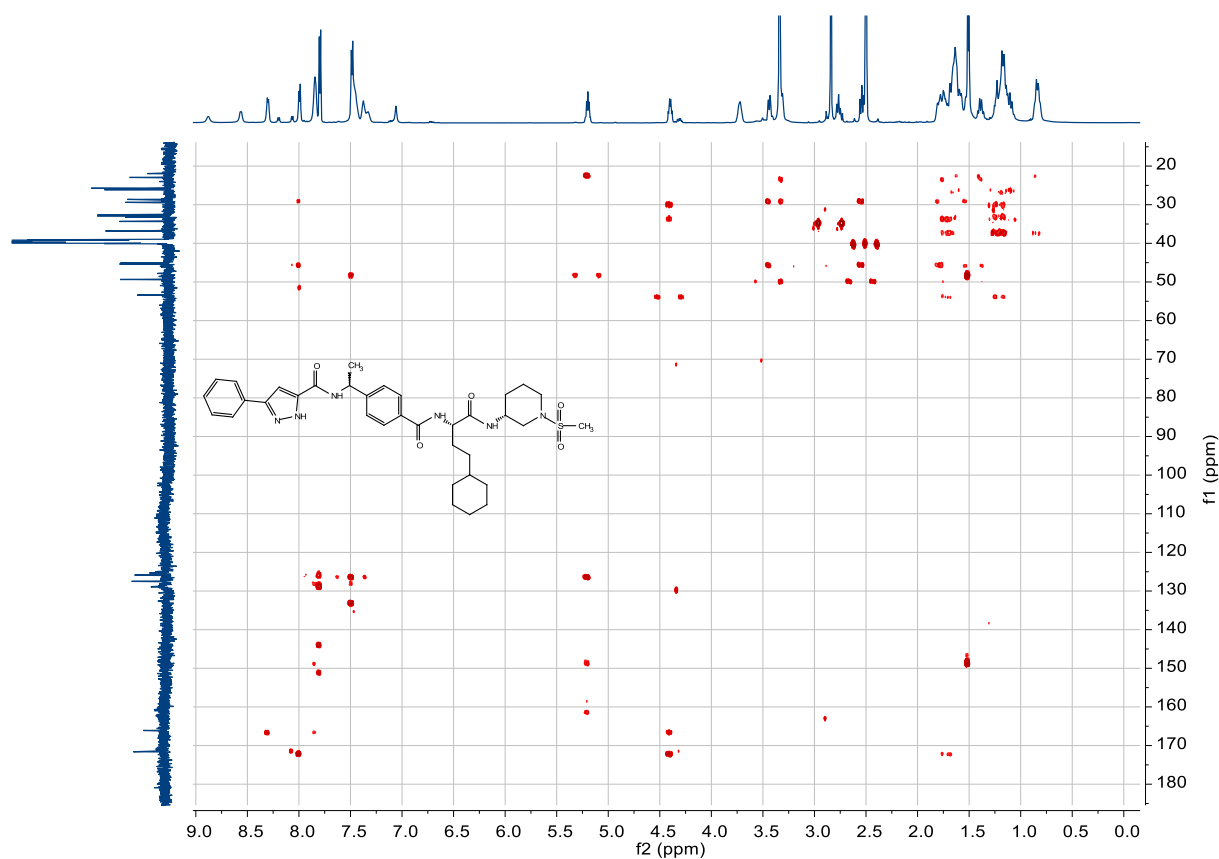


Figure 231. Compound 294 (SR264), HMBC, 600/ 150 MHz, DMSO-d<sub>6</sub>

C:\User\...\Knapp\2018\180921\SR264\_A10

9/21/2018 10:47:14 AM

SR264 mit HCCA gemessen.

SR264\_A10 #1-5 RT: 0.01-0.45 AV: 5 NL: 1.47E6  
T: FTMS + p MALDI Full ms [450.00-750.00]

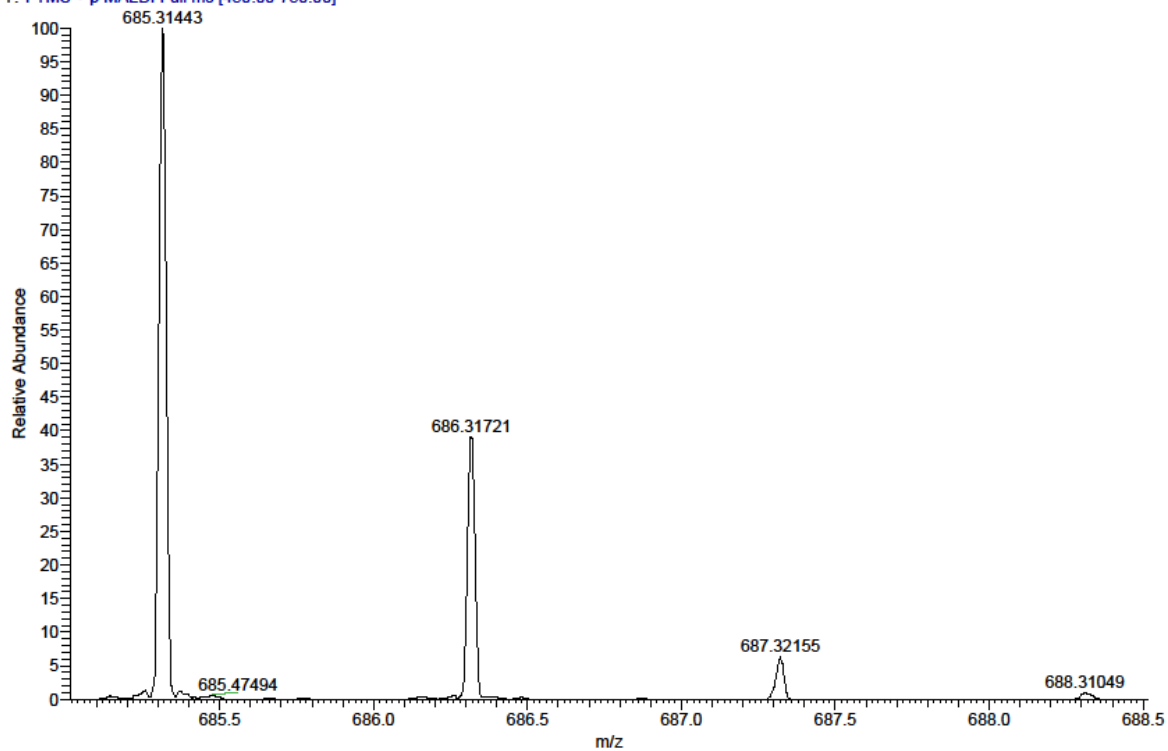
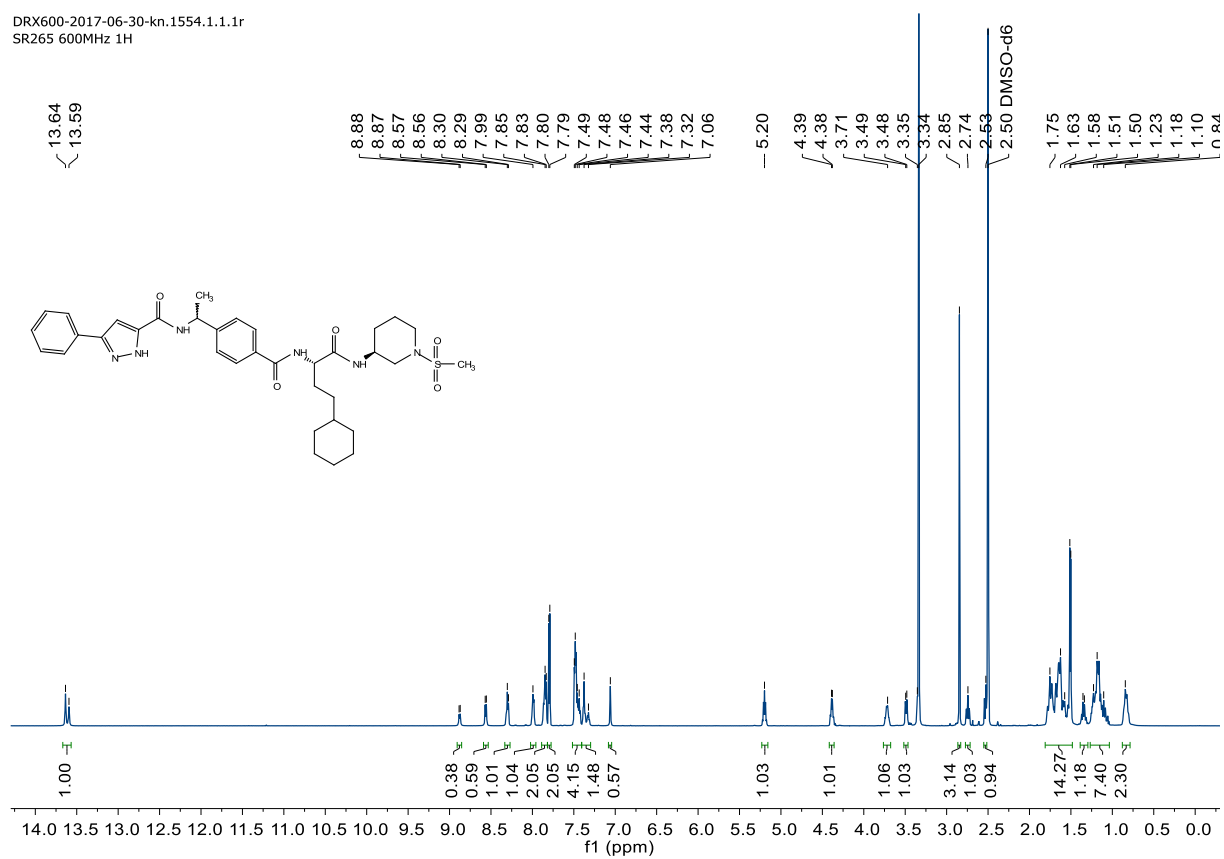
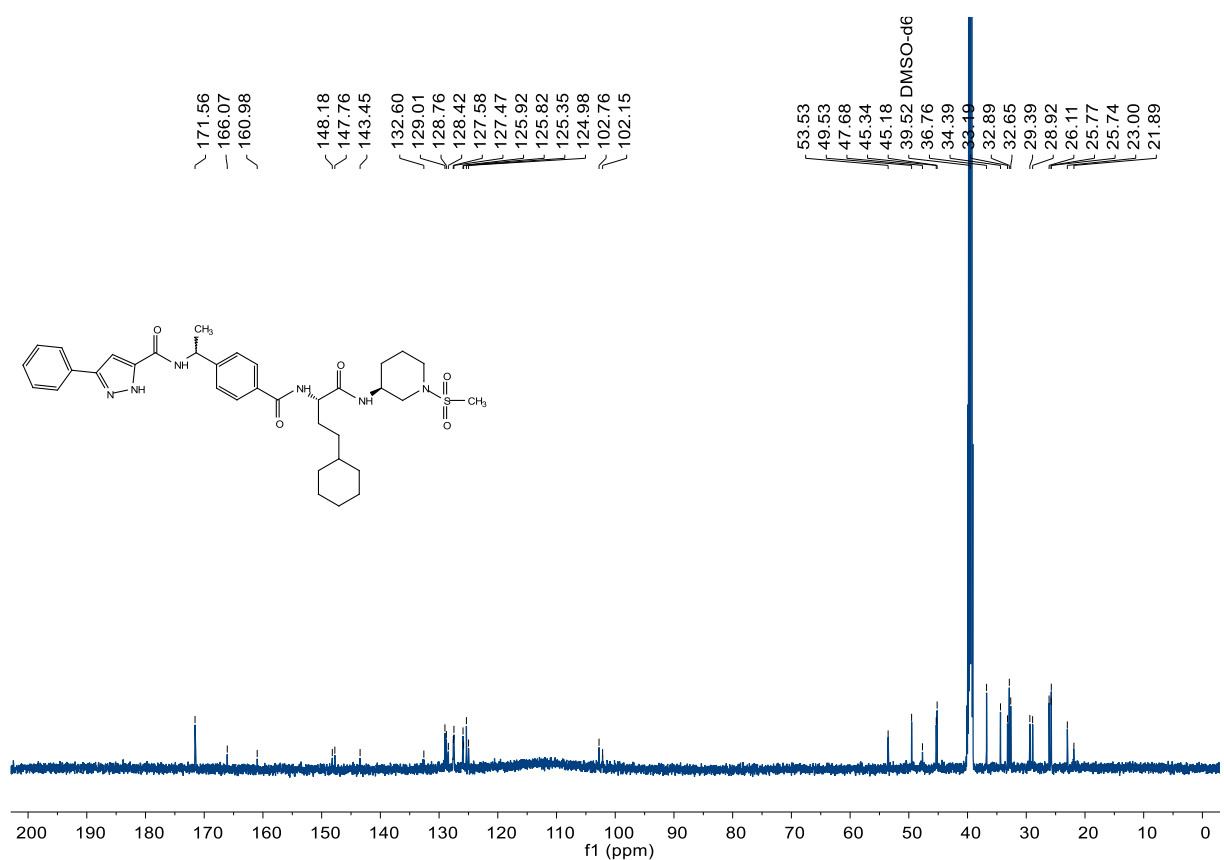


Figure 232. Compound 294 (SR264), HRMS (FTMS + p MALDI)

DRX600-2017-06-30-kn.1554.1.1.1r  
SR265 600MHz 1H

**Figure 233. Compound 295 (SR265), <sup>1</sup>H-NMR, 600 MHz, DMSO-d<sub>6</sub>**



**Figure 234. Compound 295 (SR265), <sup>13</sup>C-NMR, 150 MHz, DMSO-d<sub>6</sub>**



C:\User\...\Knapp\2018\180921\SR265\_A8

9/21/2018 10:43:38 AM

SR265 mit HCCA gemessen.

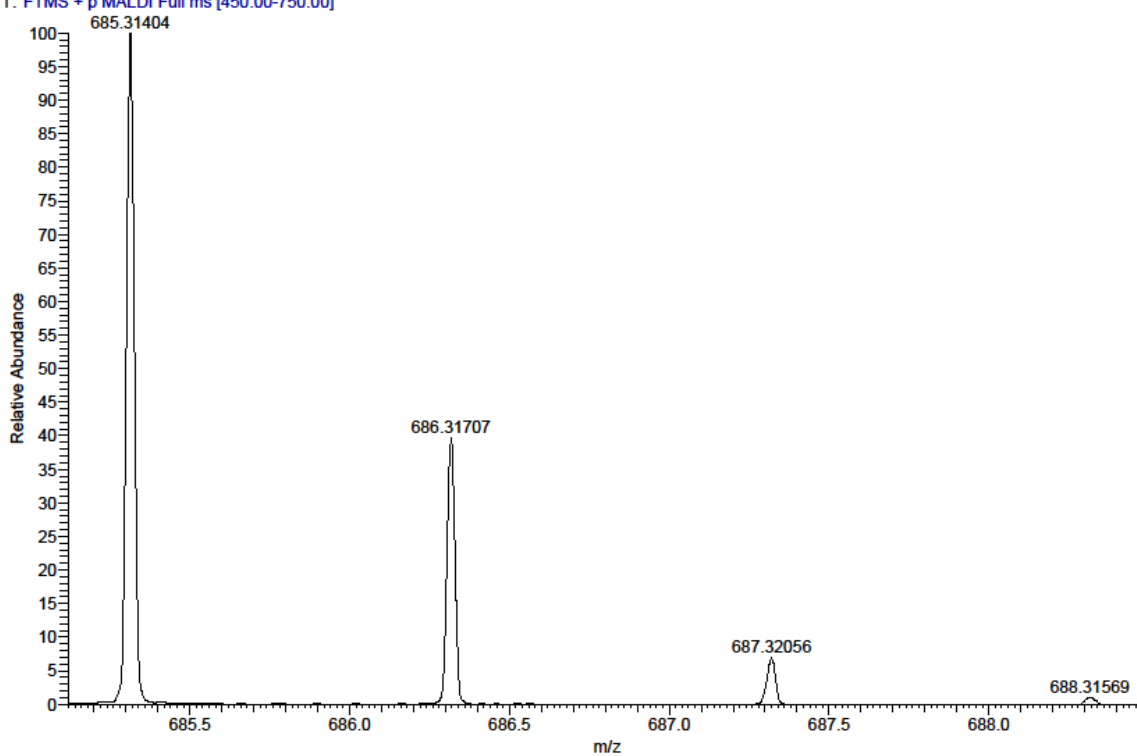
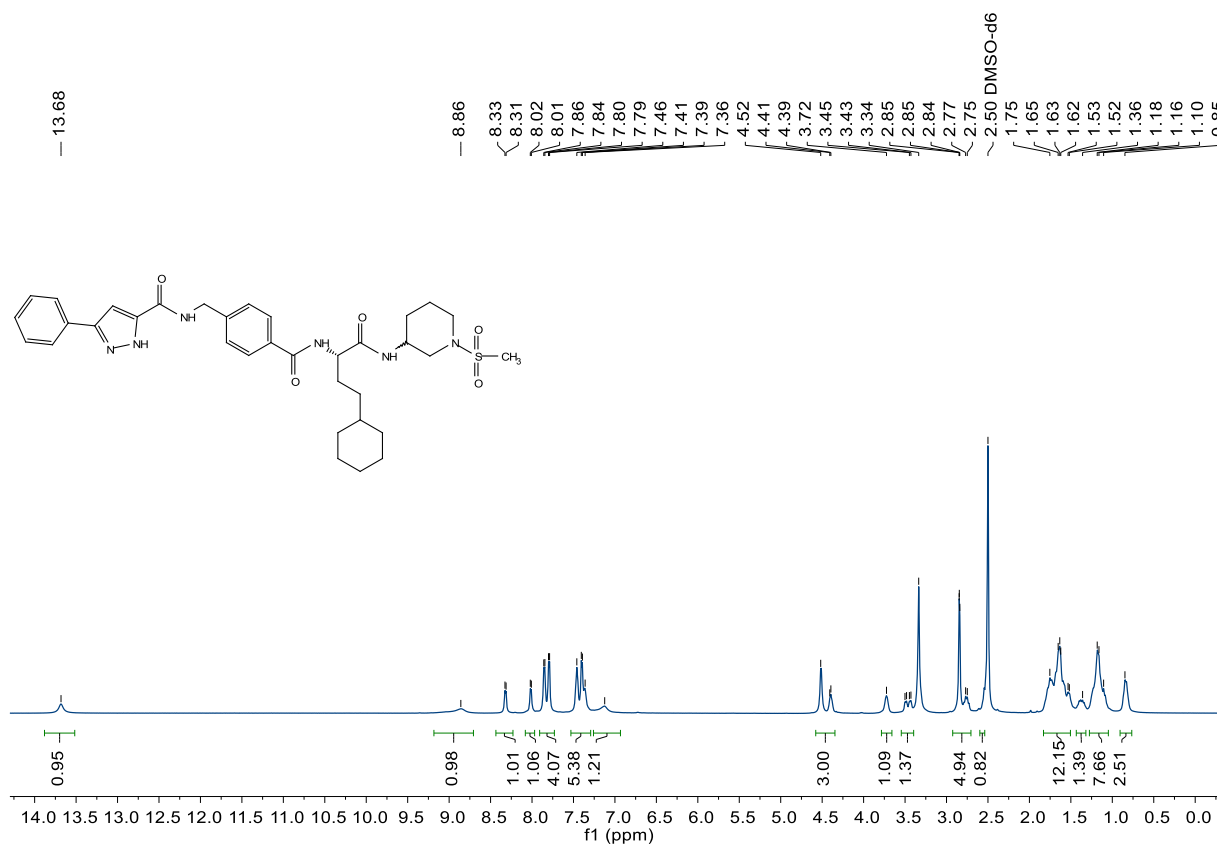
SR265\_A8 #1-13 RT: 0.01-1.38 AV: 13 NL: 1.11E6  
T: FTMS + p MALDI Full ms [450.00-750.00]

Figure 235. Compound 295 (SR265), HRMS (FTMS + p MALDI)

Figure 236. Compound 296 (SR275),  $^1\text{H-NMR}$ , 600 MHz,  $\text{DMSO-d}_6$

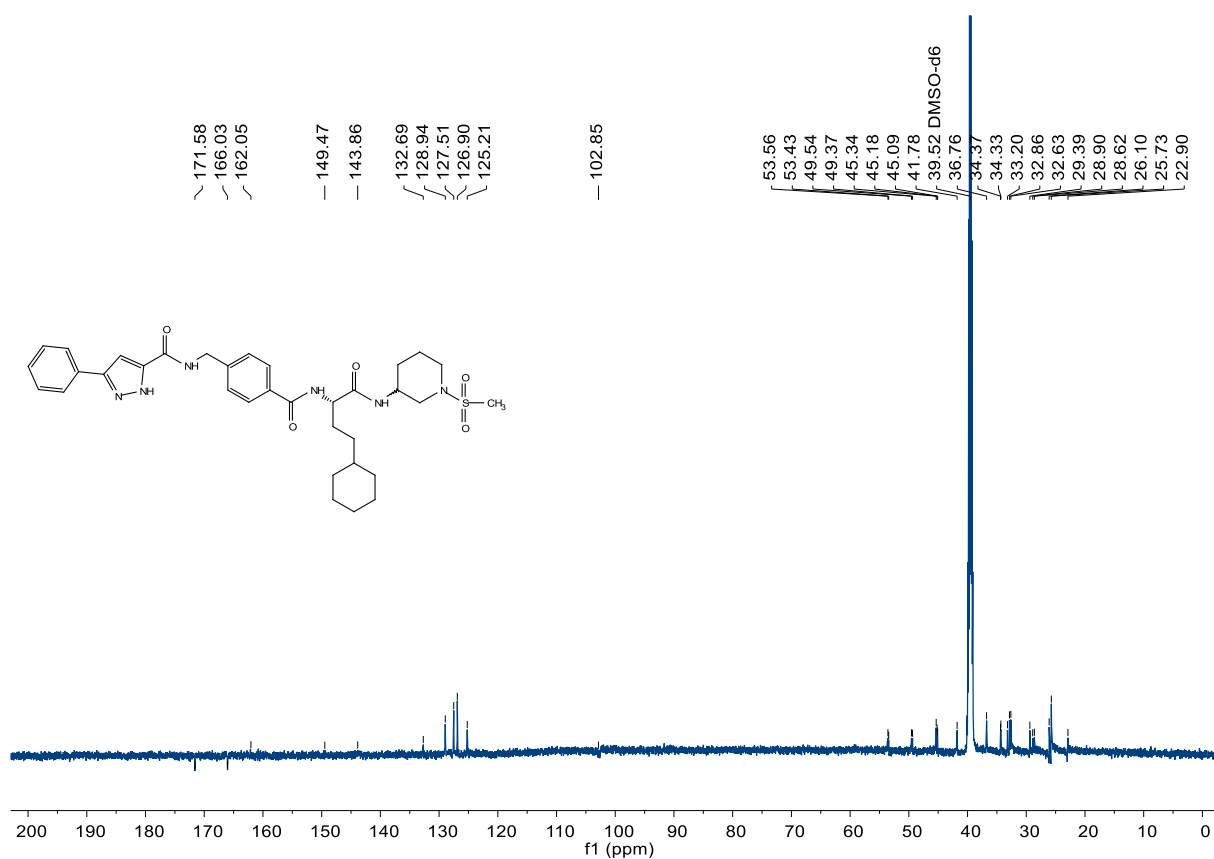


Figure 237. Compound 296 (SR275), <sup>13</sup>C-NMR, 150 MHz, DMSO-d<sub>6</sub>

C:\User\...Knapp\2018\180921\SR275\_A7

9/21/2018 10:42:19 AM

SR275 mit HCCA gemessen.

SR275\_A7 #1-4 RT: 0.00-0.37 AV: 4 NL: 1.32E5

T: FTMS + p MALDI Full ms [450.00-750.00]

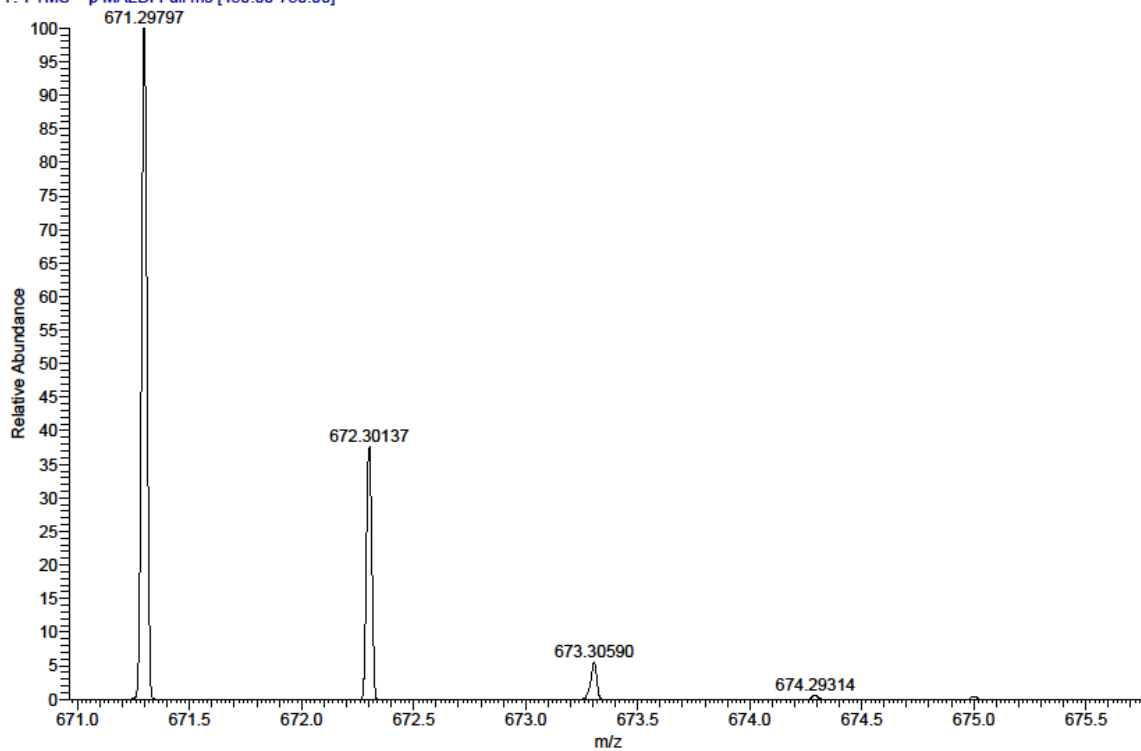


Figure 238. Compound 296 (SR275), HRMS (FTMS + p MALDI)

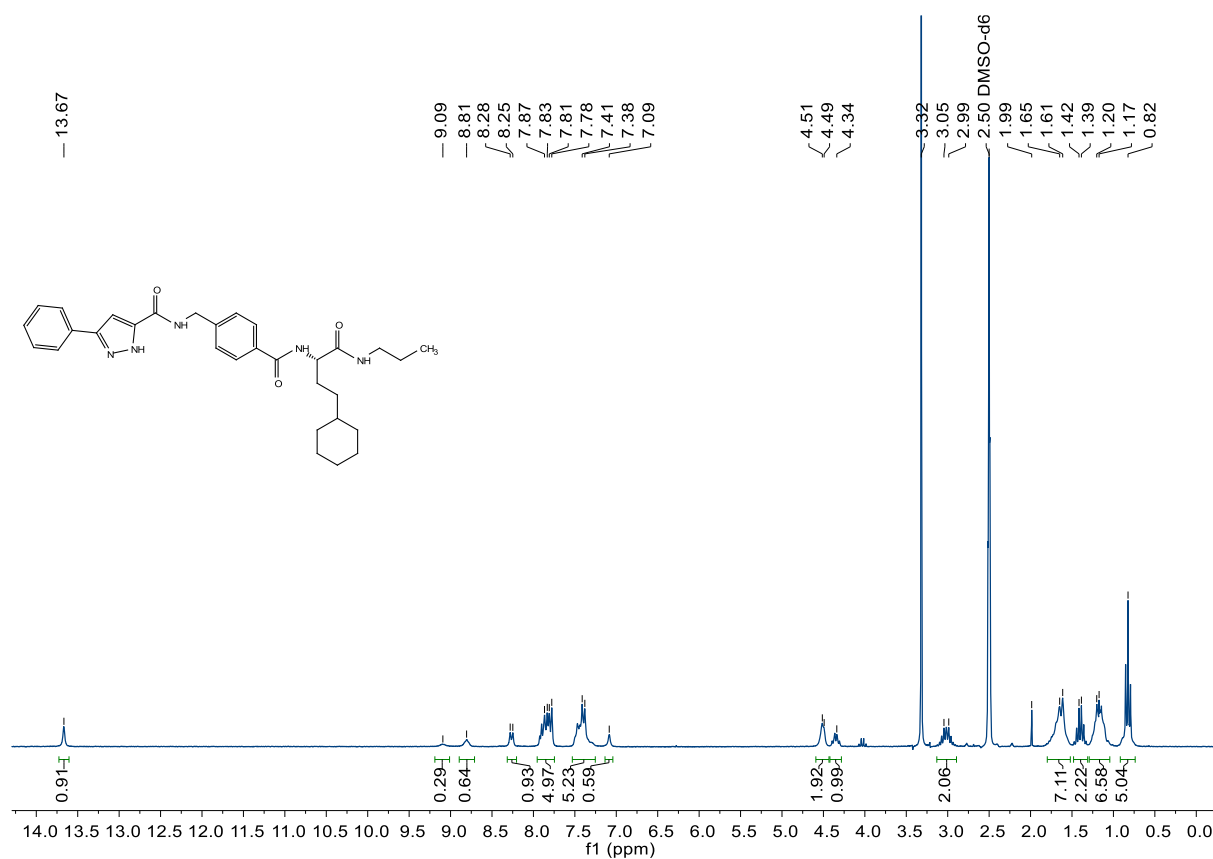


Figure 239. Compound 297 (SR278),  $^1\text{H-NMR}$ , 250 MHz,  $\text{DMSO-d}_6$

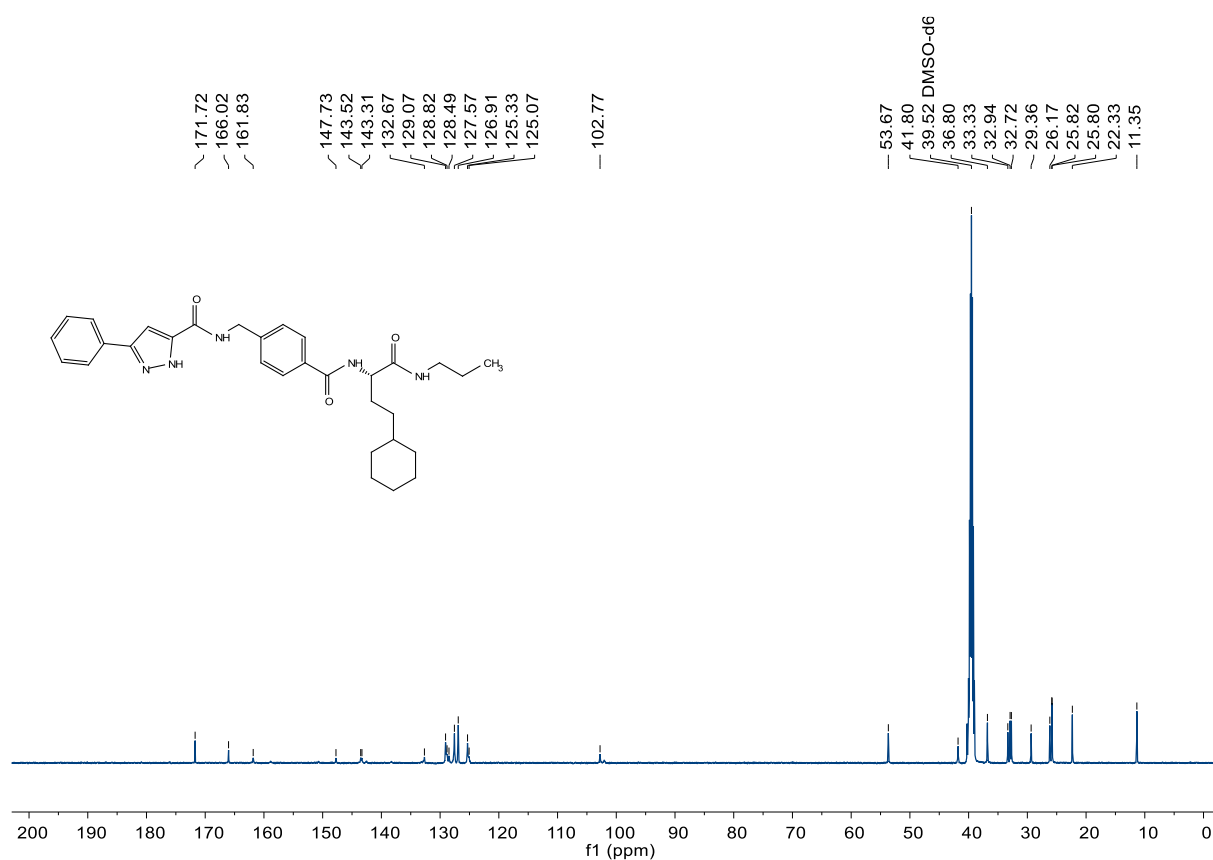


Figure 240. Compound 297 (SR278),  $^{13}\text{C-NMR}$ , 126 MHz,  $\text{DMSO-d}_6$

SR278\_A3 #1-5 RT: 0.01-0.50 AV: 5 NL: 8.30E4  
T: FTMS + p MALDI Full ms [450.00-750.00]

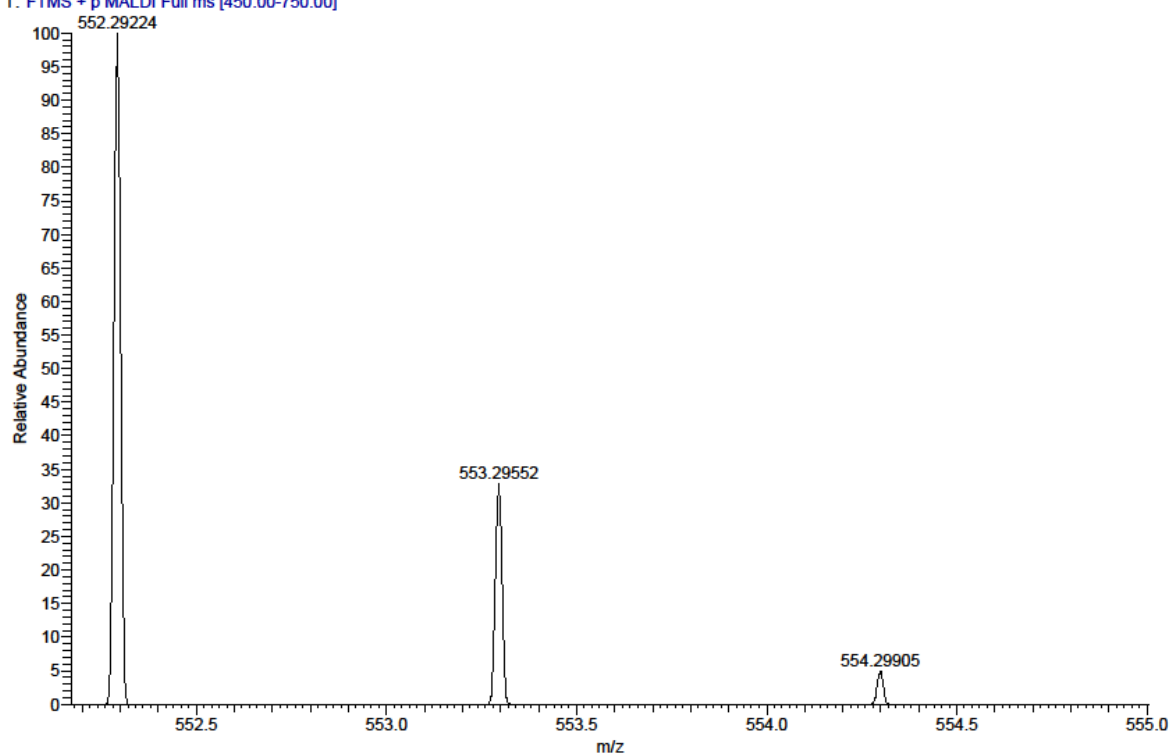


Figure 241. Compound 297 (SR278), HRMS (FTMS + p MALDI)

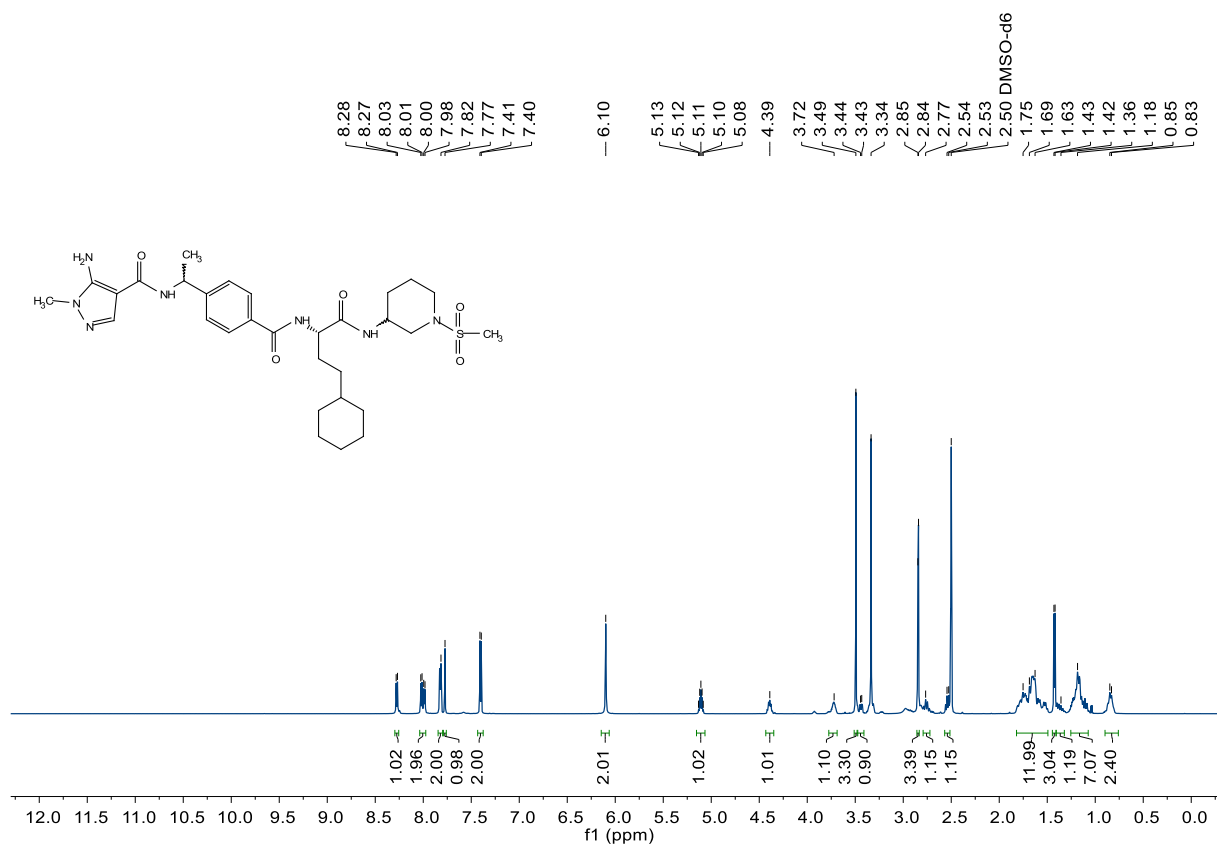


Figure 242. Compound 298 (SR277), <sup>1</sup>H-NMR, 600 MHz, DMSO-d<sub>6</sub>

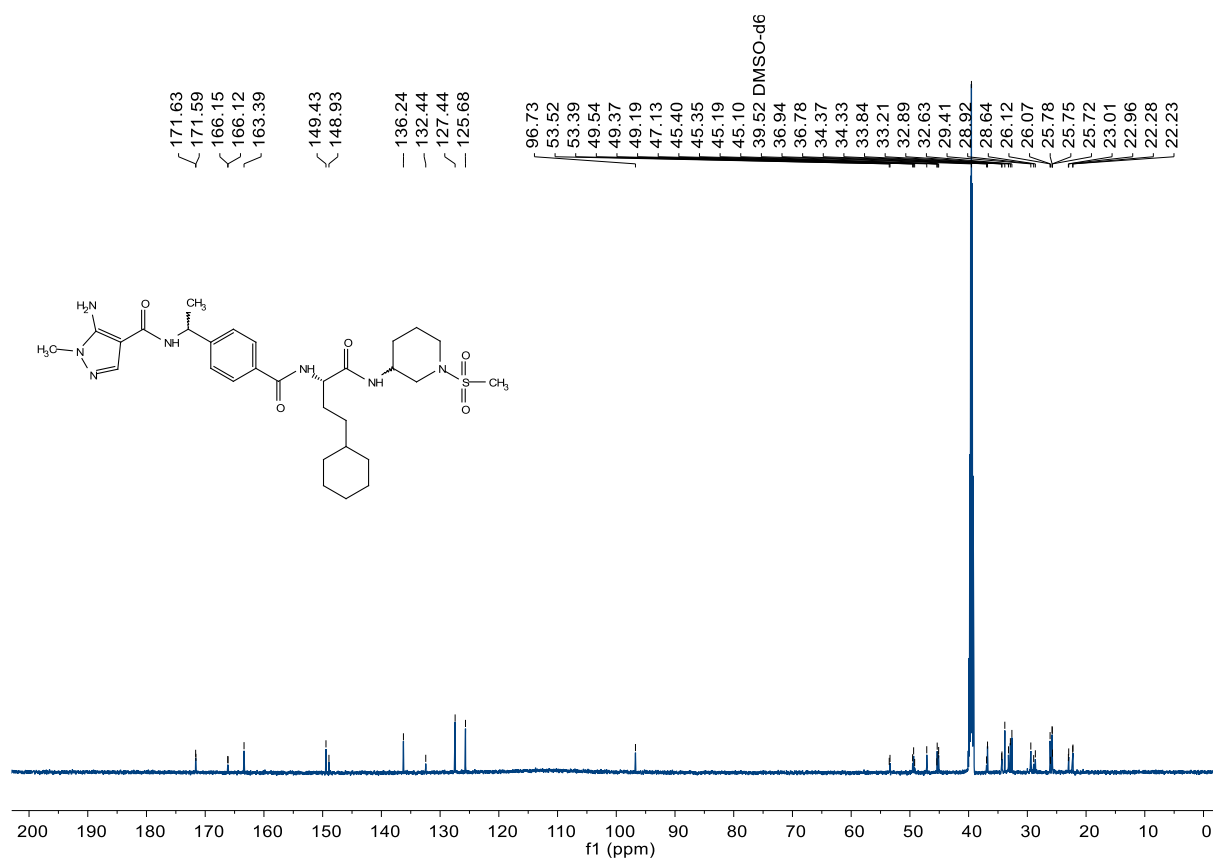


Figure 243. Compound 298 (SR277),  $^{13}\text{C-NMR}$ , 150 MHz,  $\text{DMSO-d}_6$

C:\User\...\Knapp\2018\180921\SR277\_A4

9/21/2018 10:38:56 AM

SR277 mit HCCA gemessen.

SR277\_A4 #1-4 RT: 0.01-0.37 AV: 4 NL: 6.39E4  
T: FTMS + p MALDI Full ms [450.00-750.00]

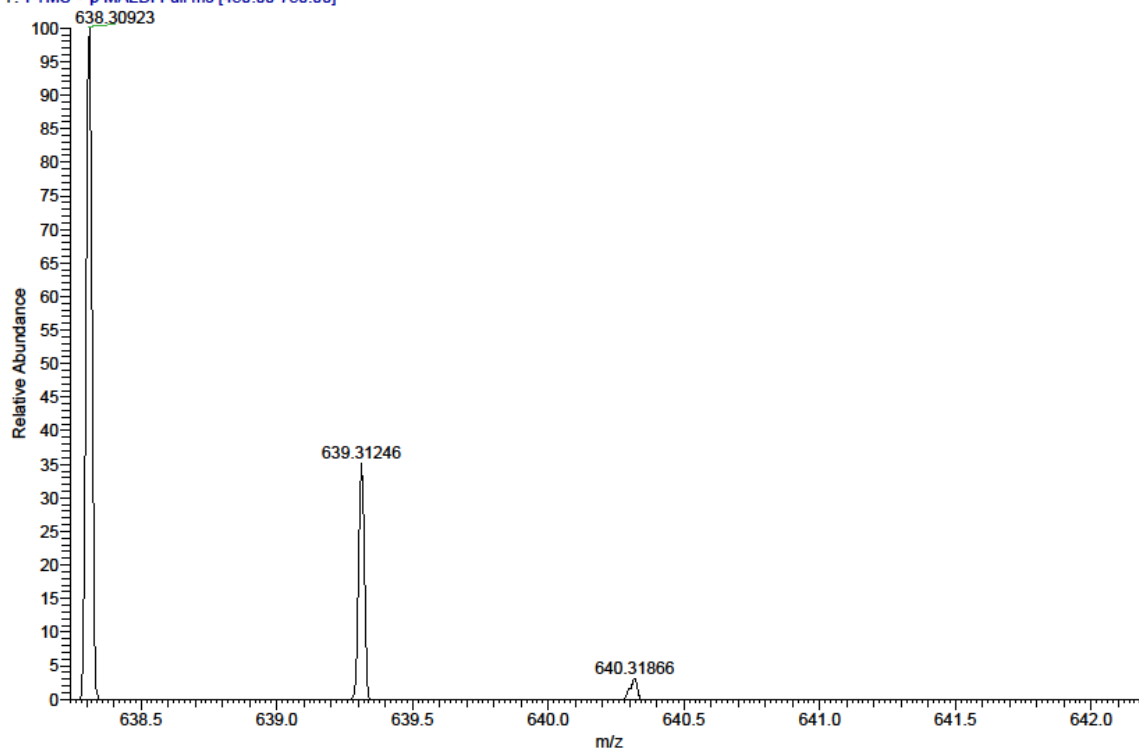


Figure 244. Compound 298 (SR277), HRMS (FTMS + p MALDI)

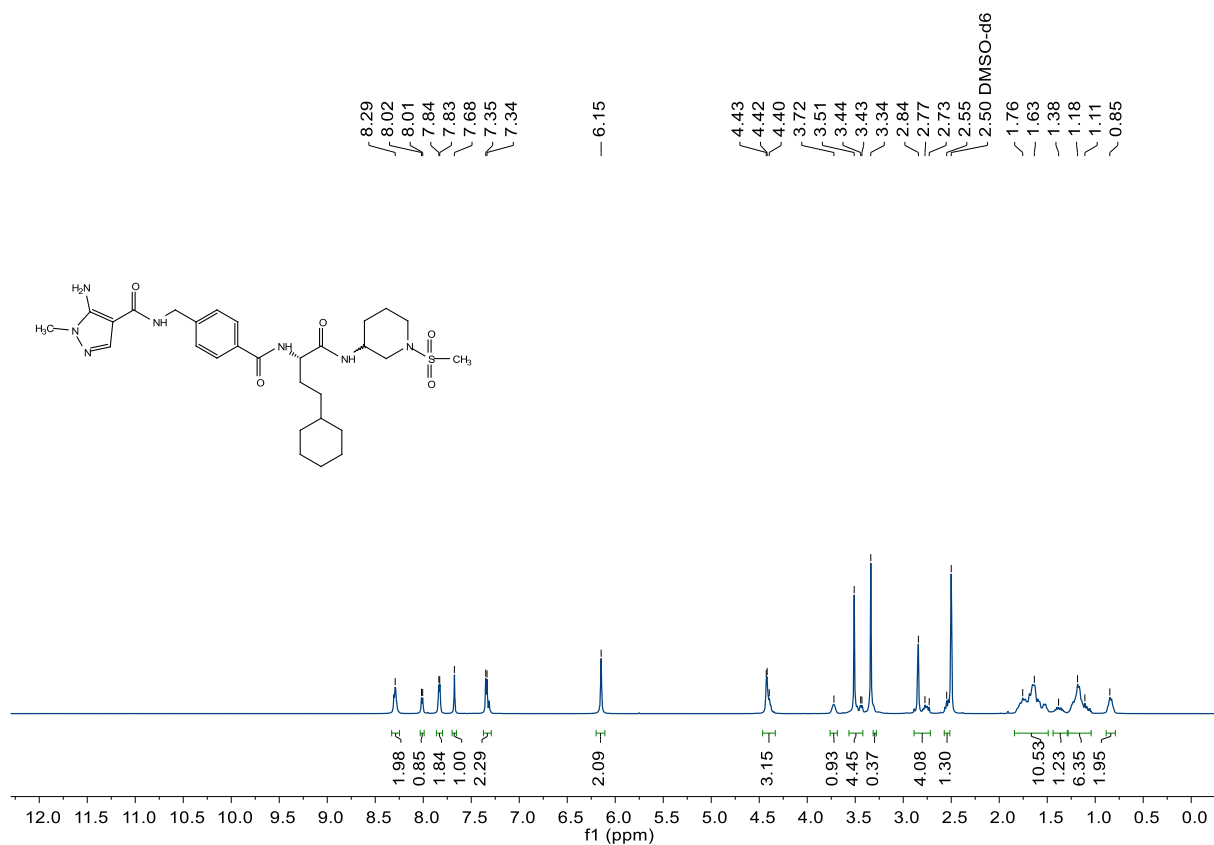


Figure 245. Compound 299 (SR276),  $^1\text{H-NMR}$ , 300 MHz,  $\text{DMSO-d}_6$

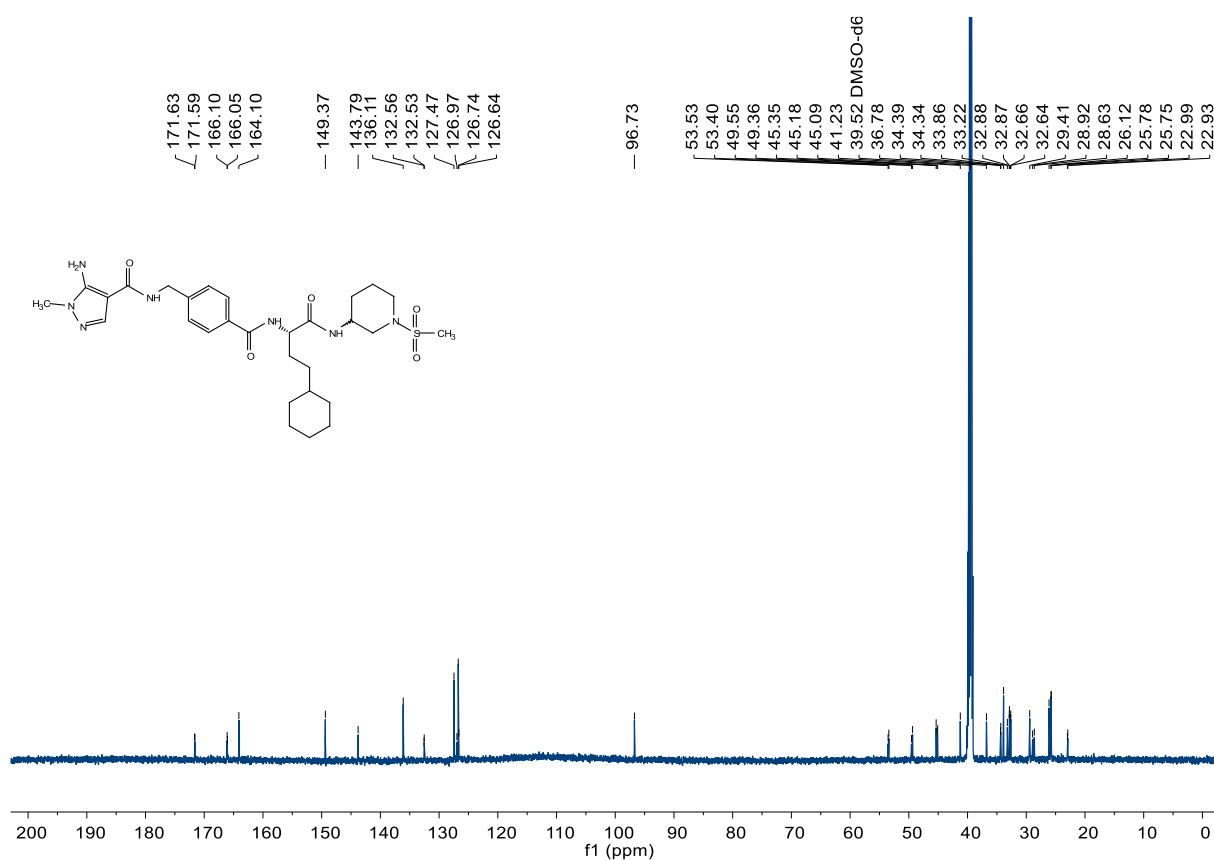
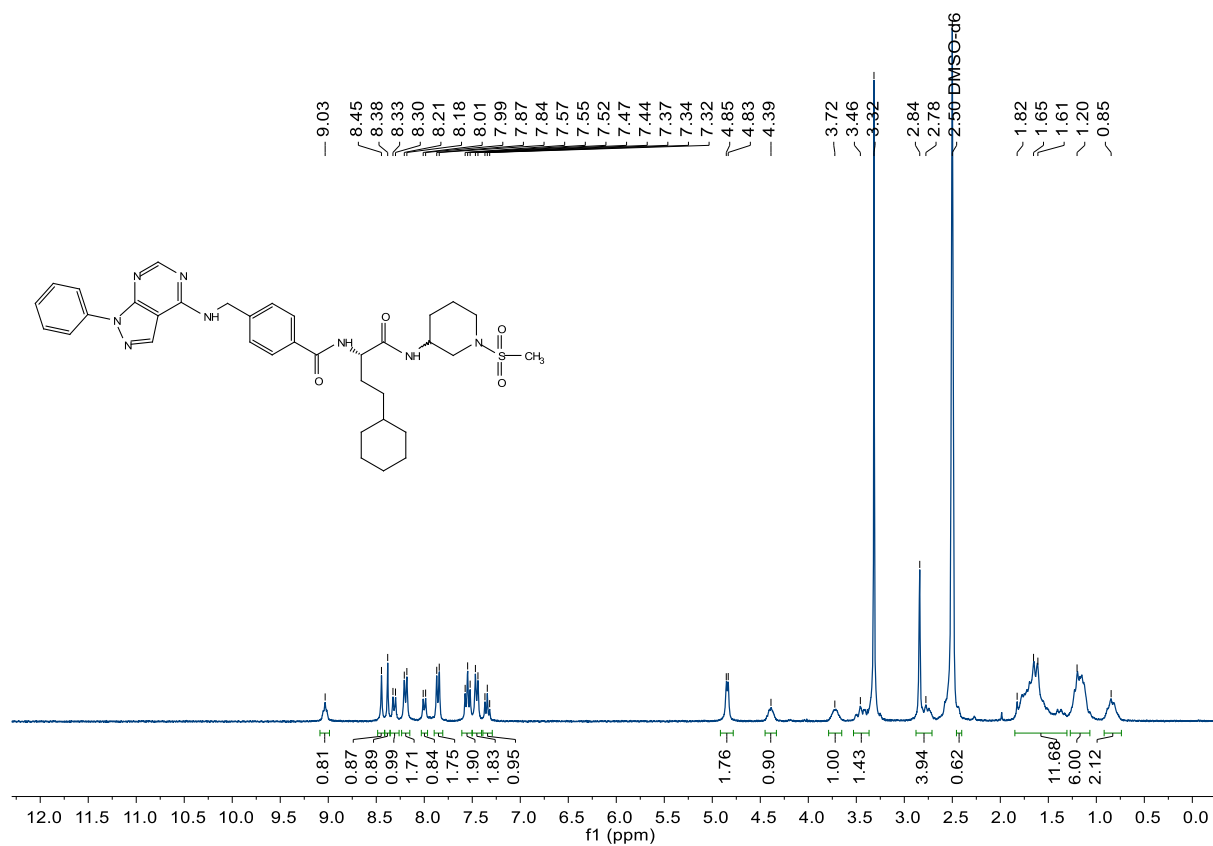
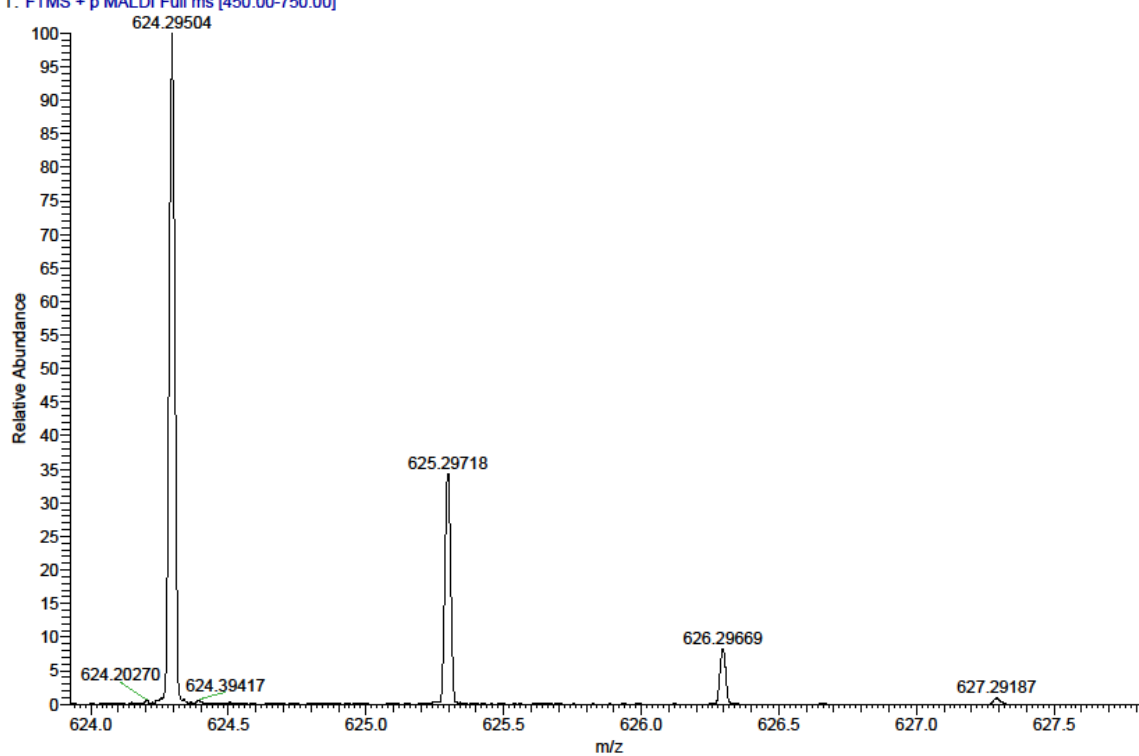


Figure 246. Compound 299 (SR276),  $^{13}\text{C-NMR}$ , 75 MHz,  $\text{DMSO-d}_6$

C:\User\...\Knapp\2018\180921\SR276\_A6

9/21/2018 10:41:05 AM

SR276 mit HCCA gemessen.

SR276\_A6 #6 RT: 0.51 AV: 1 NL: 5.29E7  
T: FTMS + p MALDI Full ms [450.00-750.00]

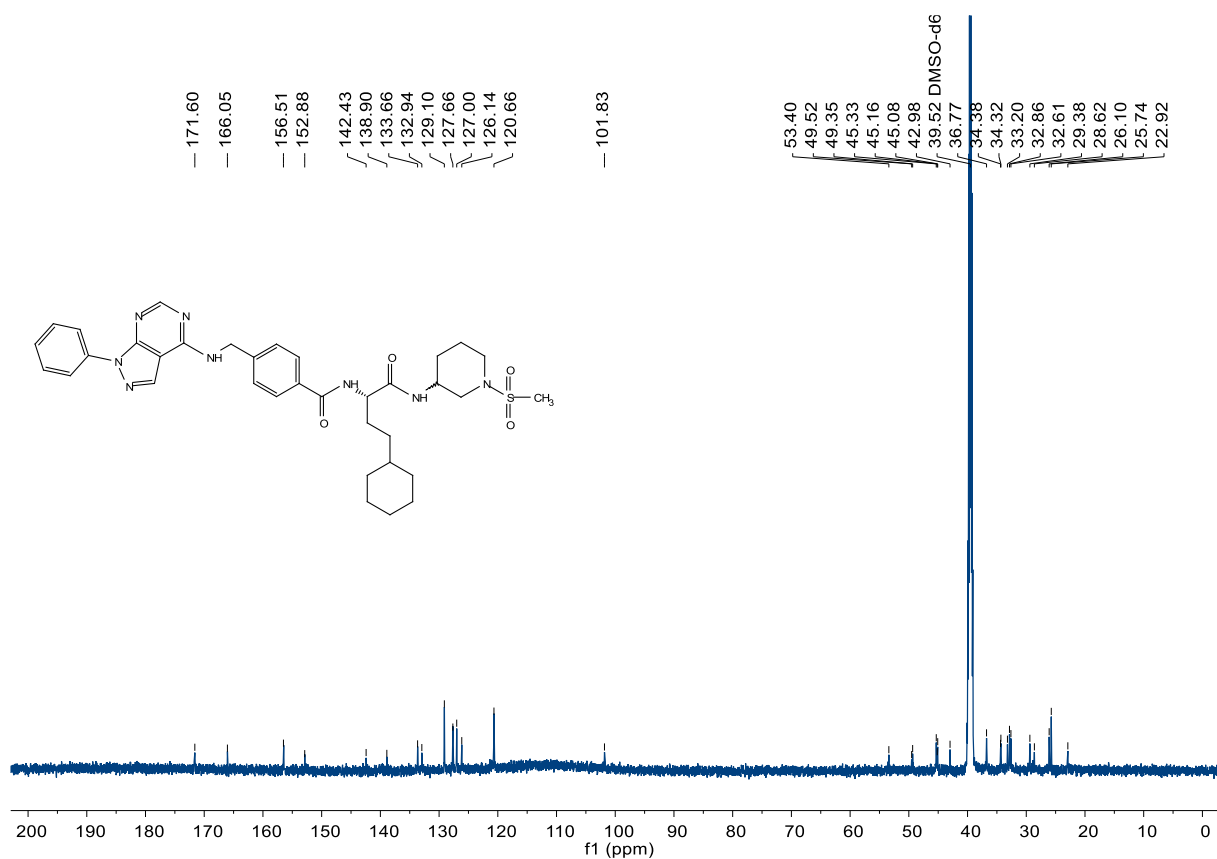


Figure 249. Compound 300 (SR300), <sup>1</sup>H-NMR, 75 MHz, DMSO-d<sub>6</sub>

C:\User\...Knapp\2018\180921\SR300\_A5

9/21/2018 10:40:02 AM

SR300 mit HCCA gemessen.

SR300\_A5 #1-5 RT: 0.01-0.39 AV: 5 NL: 3.00E6

T: FTMS + p MALDI Full ms [450.00-750.00]

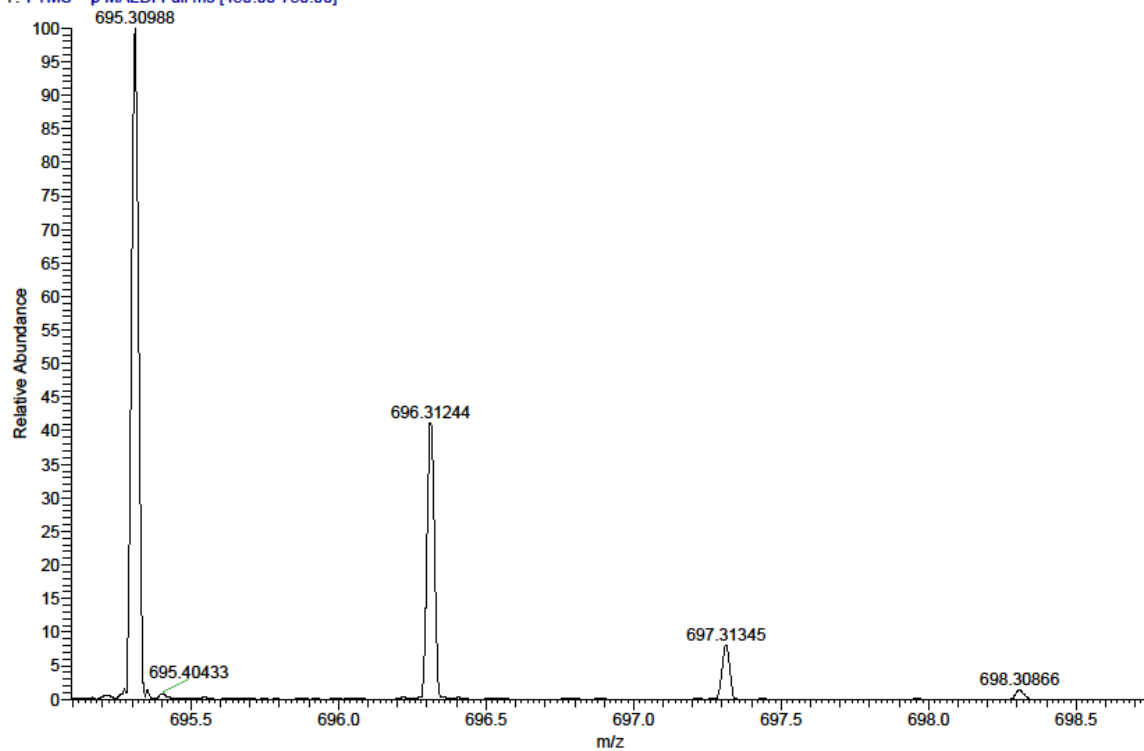


Figure 250. Compound 300 (SR300), HRMS (FTMS + p MALDI)



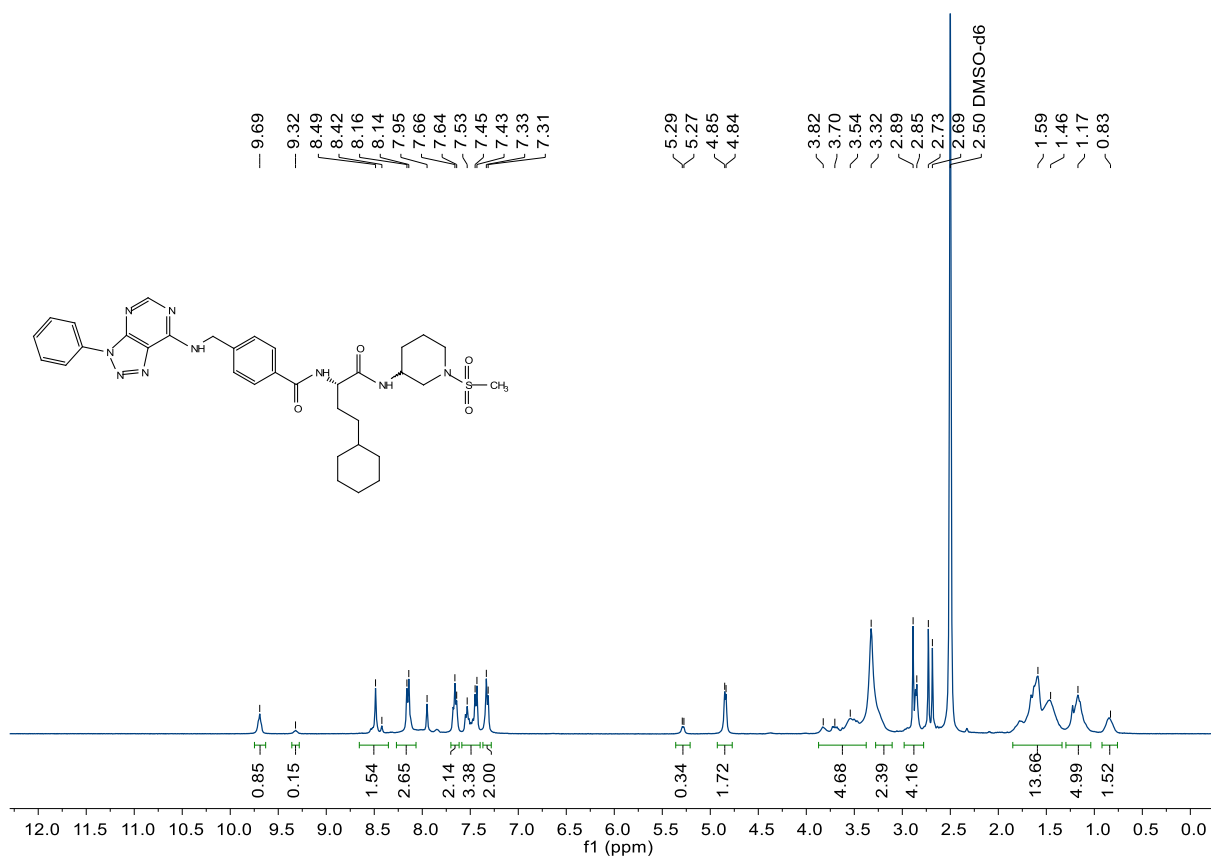


Figure 251. Compound 301 (SR301), <sup>1</sup>H-NMR, 400 MHz, DMSO-d<sub>6</sub>

C:\User\...\Knapp\2018\180921\SR301\_A2

9/21/2018 10:35:48 AM

SR301 mit HCCA gemessen.

SR301\_A2 #1-11 RT: 0.01-0.91 AV: 11 NL: 9.20E6  
T: FTMS + p MALDI Full ms [450.00-750.00]

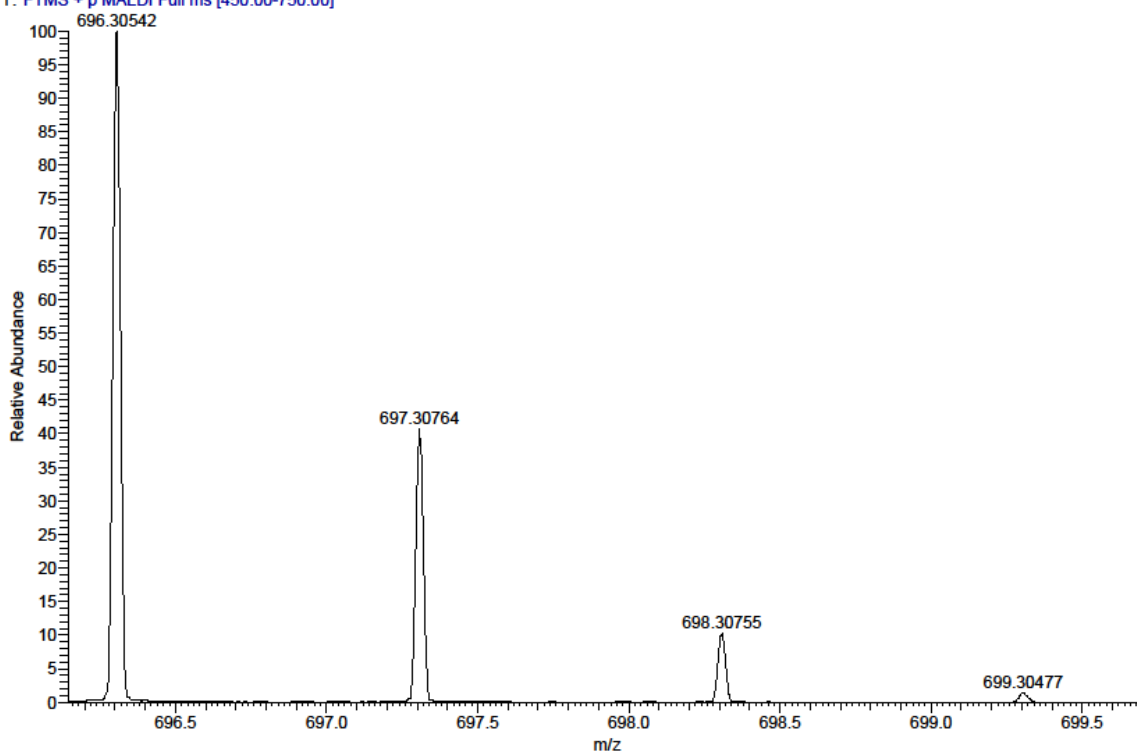


Figure 252. Compound 301 (SR301), HRMS (FTMS + p MALDI)

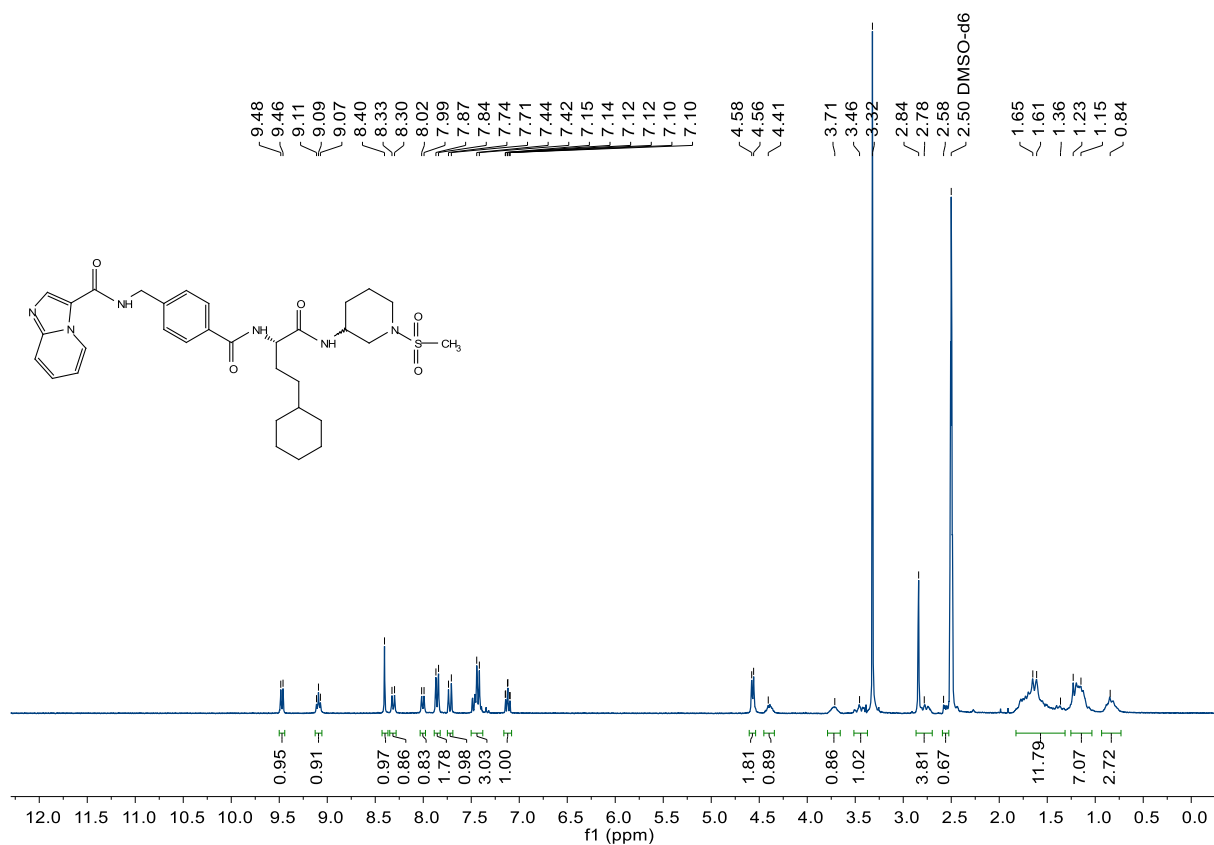


Figure 253. Compound 302 (SR302), <sup>1</sup>H-NMR, 300 MHz, DMSO-d<sub>6</sub>

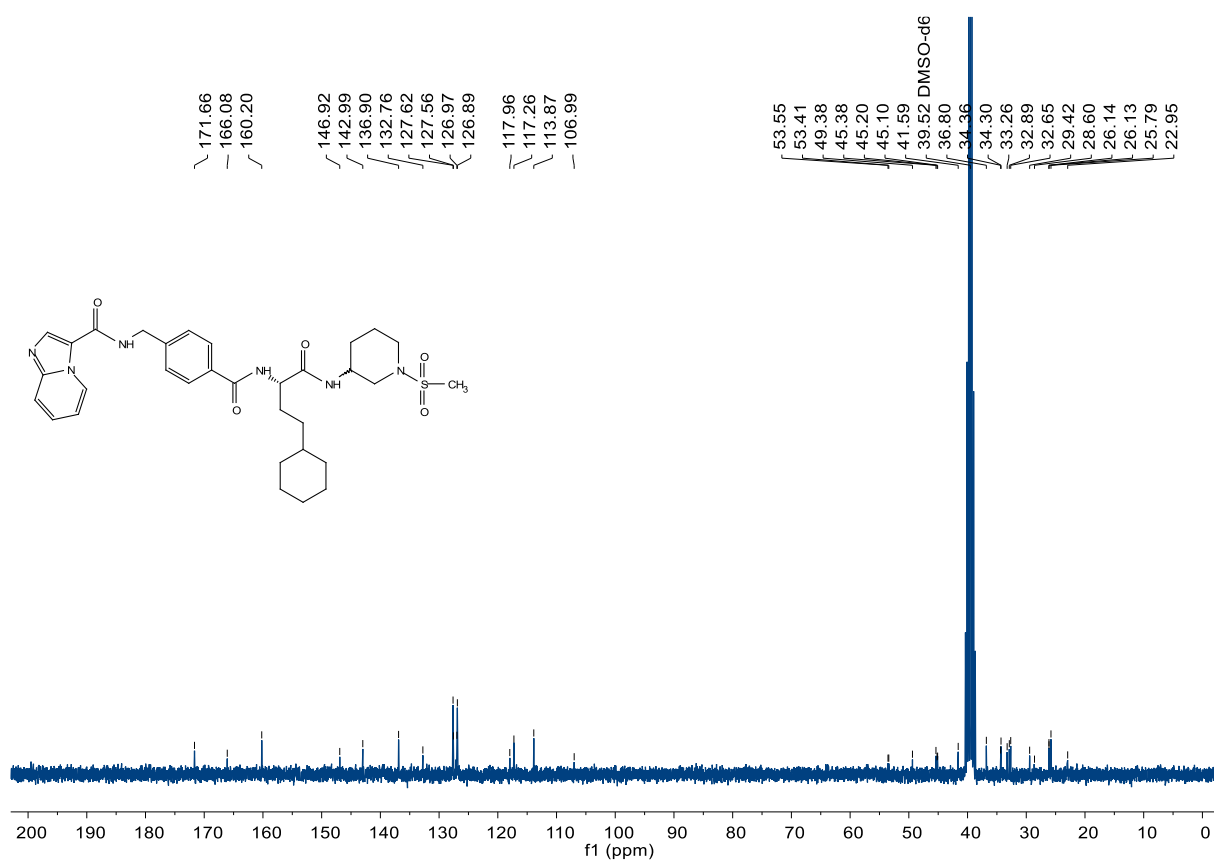


Figure 254. Compound 302 (SR302), <sup>13</sup>C-NMR, 75 MHz, DMSO-d<sub>6</sub>

C:\User\...Knapp\2018\180921\SR302\_A1

9/21/2018 10:34:58 AM

SR302 mit HCCA gemessen.

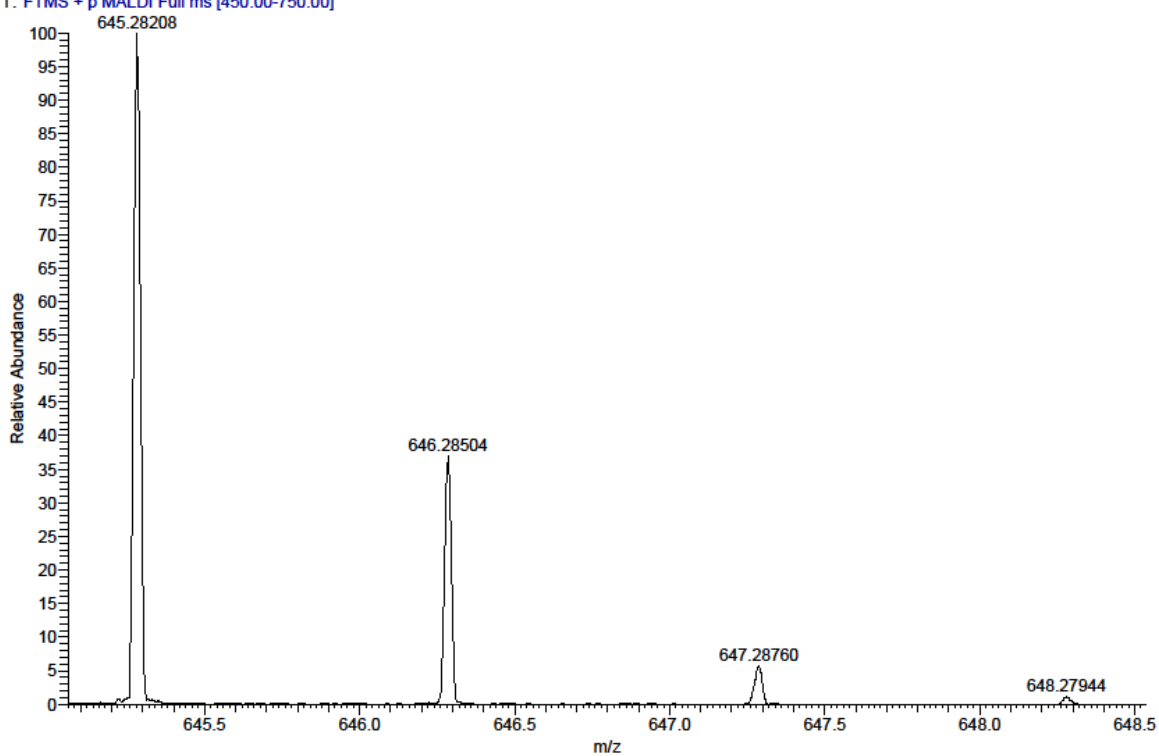
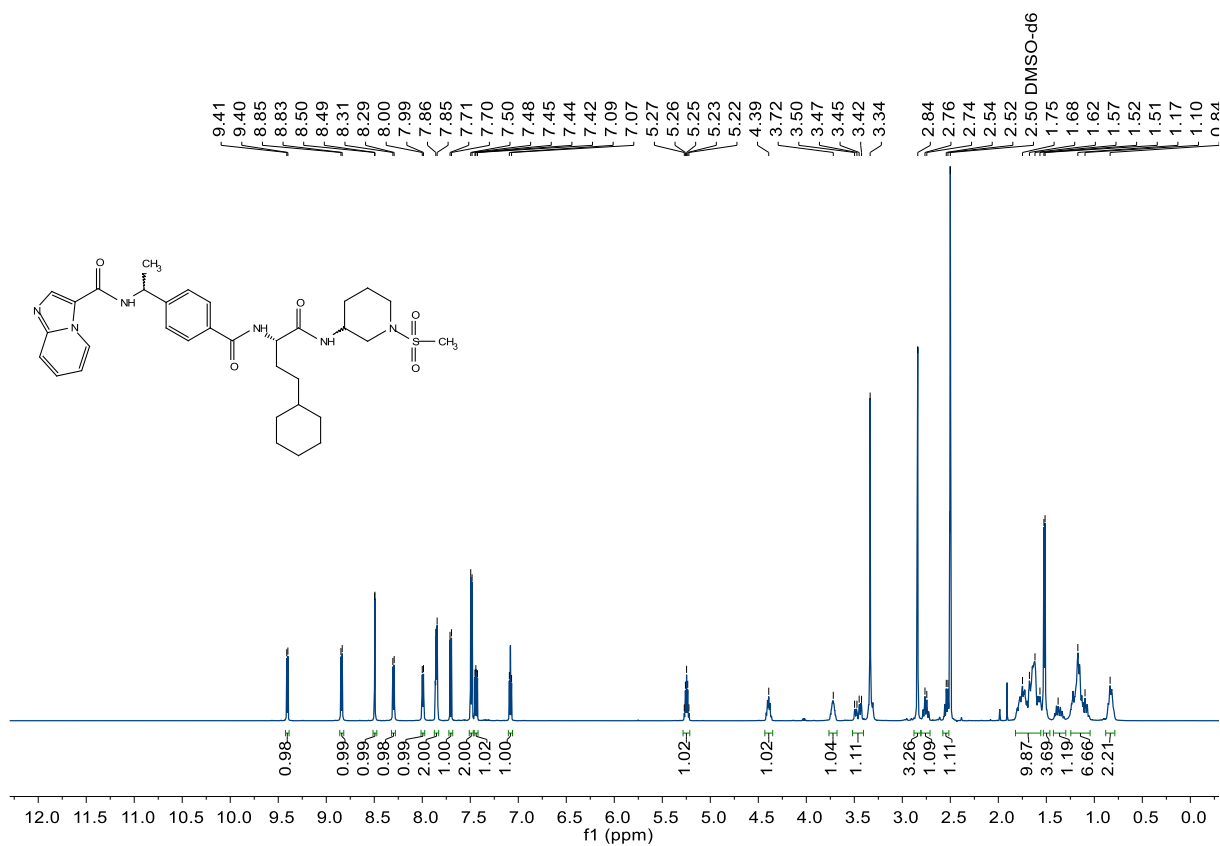
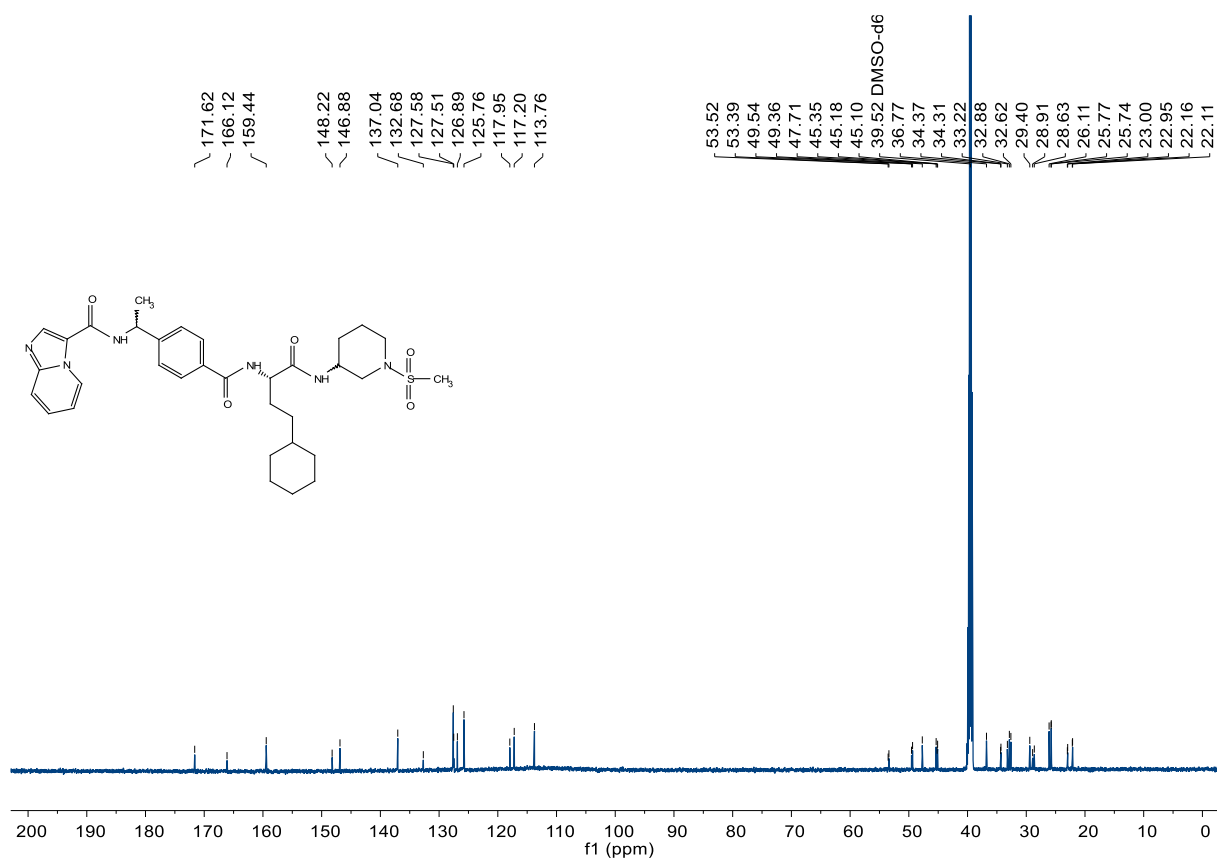
SR302\_A1 #1-6 RT: 0.00-0.43 AV: 6 NL: 7.09E6  
T: FTMS + p MALDI Full ms [450.00-750.00]

Figure 255. Compound 302 (SR302), HRMS (FTMS + p MALDI)

Figure 256. Compound 304 (SR360), <sup>1</sup>H-NMR, 600 MHz, DMSO-d<sub>6</sub>



**Figure 257.** Compound 304 (SR360),  $^{13}\text{C}$ -NMR, 150 MHz,  $\text{DMSO-d}_6$

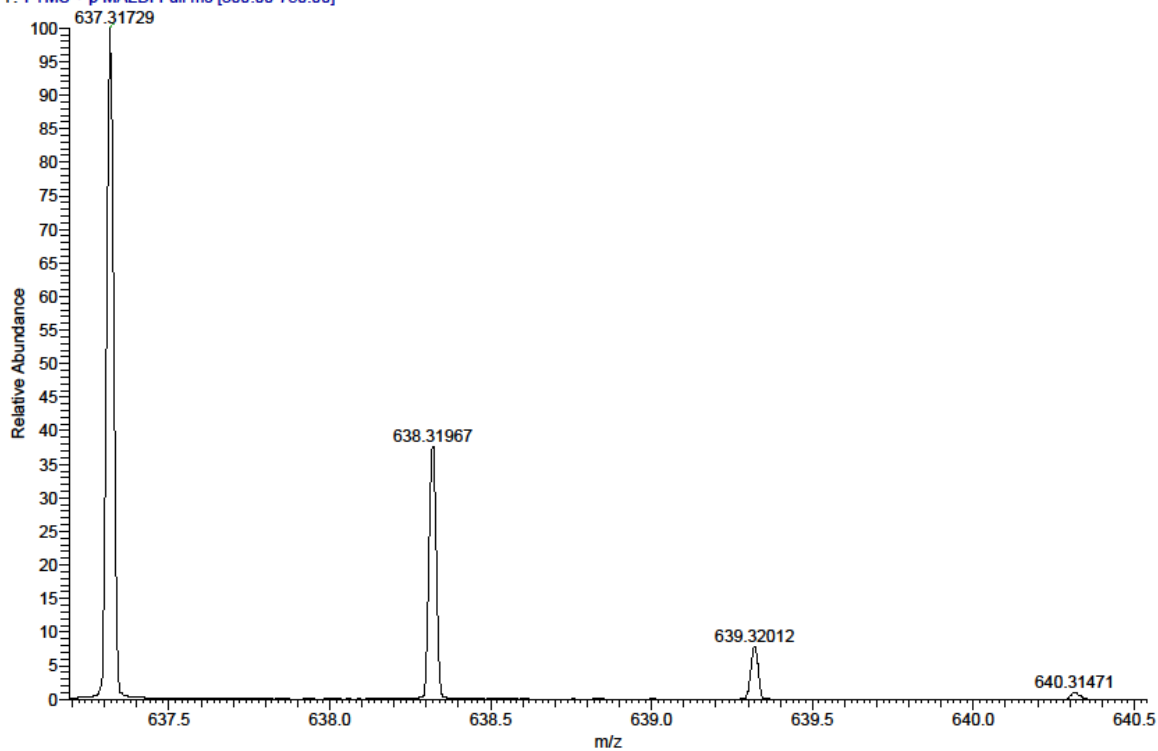
C:\User\...12019190215\SR360 42-53\_C2

2/15/2019 9:57:39 AM

SR360 42-53 mit HCCA gemessen.

SR360 42-53\_C2 #1-20 RT: 0.00-0.86 AV: 20 NL: 2.32E7

T: FTMS + p MALDI Full ms [300.00-750.00]



**Figure 258.** Compound 304 (SR360), HRMS (FTMS + p MALDI)

## **12 Acknowledgements**

First of all, I would like to thank Prof. Dr. Stefan Knapp for being the first member of his working group in Frankfurt, for the free creation of the topic and for the many helpful discussions. Helping to set up the laboratories in Frankfurt was a great experience for me and also allowed me to arrange my own workplace. I would also like to thank him for allowing me to participate in the open-science project of the Structural Genomics Consortium (SGC), the latter enabled me to build a variety of collaborations.

My very special thanks therefore go to my colleagues at the SGC in Frankfurt. Thanks to Apirat Chaikuad, Martin Schröder, Andreas Joerger, Deep Chatterjee and Sebastian Mathea for creating a variety of crystal structures without which my inhibitors could not have been optimized. I would like to thank Benedict-Tilman Berger for the cellular assay data and Martin Schröder, Deep Chatterjee and Andreas Krämer for providing the proteins and assisting with the thermal-shift assays. I thank Roberta Tesch for the *in silico* studies and her constant helpfulness. Furthermore, I would like to thank Susanne Müller-Knapp for her always nice support, especially for the DDR project.

Special thanks also go to Koen Hekking and his colleagues at Mercachem in the Netherlands for their collaboration and sharing of many compounds and data that have contributed to the development and publishing of a p38 probe. I would also like to thank the research group of Stefan Laufer at the University of Tübingen, Daniel Dauch at the University Hospital in Tübingen and Attila Reményi at the Research Centre for Natural Sciences in Hungary for their *in vitro* studies such as Western Blot analyses. Many thanks to Mark Bagley and his colleagues at the University of Sussex, UK, for their collaboration on the second p38 paper, and Christian Pohl of the Buchmann Institute for Molecular Life Sciences for the immunofluorescence studies.

At the University of Frankfurt I would like to thank the service unit mass spectrometry for the numerous measured mass spectra and especially Uwe Hener for his constant helpfulness. Many thanks to the NMR service department for the possibility to record my spectra on site. Without these analytical departments this work would not have been possible.

Finally, I would like to thank Andreas Joerger in particular for his competent lecturing skills, the quick review of my doctoral thesis and his constant helpfulness. Furthermore Many thanks to Fabian Acke and Thomas Hanke for their comments on the correction of my work. I would also like to thank Thomas Hanke and Francesco Greco for the excellent working atmosphere in the laboratory and on the other hand for their willingness to discuss, help and support in solving problems as well as all other colleagues of the working group.

## 13 Publications

(1) “Fast Iterative Synthetic Approach toward Identification of Novel Highly Selective p38 MAP Kinase Inhibitors.”

**Röhm S.**, Berger B.-T., Schröder M., Chaikuad A., Winkel R., Hekking K. F. W., Benningshof, J. J. C, Müller G., Tesch R., Kudolo M., Forster M., Laufer S., Knapp S.

**J. Med. Chem.** 2019, 62, 23, 10757-10782. DOI: 10.1021/acs.jmedchem.9b01227

Contribution: Wrote manuscript and contributed experimental data such as synthesis (SR-318 and SR-321) and analytical data. Created figures, schemes and tables (except for Figure 2, Figure 3 and Figure 4), design of journal cover.

(2) “Function, Structure and Topology of Protein Kinases.”

**Röhm, S.**, Krämer A., Knapp, S.

**Top. Med. Chem.** 2020, 97. DOI: 10.1007/7355\_2020\_97 (in press)

Contribution: Wrote book chapter and did literature research.

(3) “Novel p38 $\alpha$  MAP Kinase inhibitors identified from yoctoReactor DNA-encoded small molecule library.”

Petersen, L. K., Blakskjær P., Chaikuad, A., Christensen A. B., Dietvorst J., Holmkvist J., Knapp S., Kořínek, M., Larsen, L. K., Pedersen A. E., **Röhm, S.**, Sløk F. A., Hansen, N. J. V.

**Med. Chem. Comm.** 2016, 7, 1332–1339. DOI: 10.1039/C6MD00241B

Contribution: Analytical data of small-molecules investigated.

### Poster presentation and Abstract:

“VPC00628 derivatives aimed at targeting the P-loop/ $\alpha$ C pocket of p38 $\alpha$  provide a unique starting point for the development of selective DDR1 inhibitors”

9th Inhibitors of Protein Kinases Conference, 2017, Warschau (Polen).

## ***14 Curriculum Vitae***





## **15 Eidesstattliche Erklärung**

### **Erklärung**

Ich erkläre hiermit, dass ich mich bisher keiner Doktorprüfung im Mathematisch-Naturwissenschaftlichen Bereich unterzogen habe.

Frankfurt am Main, den .....

(Unterschrift)

### **Versicherung**

Ich erkläre hiermit, dass ich die vorgelegte Dissertation über

.....  
.....  
.....

selbständig angefertigt und mich anderer Hilfsmittel als der in ihr angegebenen nicht bedient habe, insbesondere, dass alle Entlehnungen aus anderen Schriften mit Angabe der betreffenden Schrift gekennzeichnet sind. Ich versichere, die Grundsätze der guten wissenschaftlichen Praxis beachtet, und nicht die Hilfe einer kommerziellen Promotions-vermittlung in Anspruch genommen zu haben.

Frankfurt am Main, den .....

(Unterschrift)